U.S. DEPARTMENT OF ENERGY

Office of ENERGY EFFICIENCY & RENEWABLE ENERGY

Advanced Engine and Fuel Technologies

2019 Annual Progress Report

Vehicle Technologies Office

(This page intentionally left blank)

Disclaimer

This report was prepared as an account of work sponsored by an agency of the United States government. Neither the United States government nor any agency thereof, nor any of their employees, makes any warranty, expressed or implied or assumes any legal liability or responsibility for the accuracy, completeness, or usefulness of any information, apparatus, product, or process disclosed or represents that its use would not infringe privately owned rights. Reference herein to any specific commercial product, process, or service by trade name, trademark, manufacturer, or otherwise does not necessarily constitute or imply its endorsement, recommendation, or favoring by the Unites States government or any agency thereof. The views and opinions of authors expressed herein do not necessarily state or reflect those of the United States government or any agency thereof.

Acknowledgements

We would like to express our sincere appreciation to Energetics and Oak Ridge National Laboratory for their technical and artistic contributions in preparing and publishing this report. In addition, we would like to thank all the participants for their contributions to the programs and all the authors who prepared the project abstracts that comprise this report.

Acronyms

List of Abbreviations, Definitions, and Nomenclature

0D, 0-D	zero-dimensional
1D, 1-D	one-dimensional
1-PE	1-phenylethanol
2CP	two-color pyrometry
2D	two-dimensional
25DMF	2,5-dimethylfuran
2-EP	2-ethylphenol
2M2B	2-methyl 2-butene
2-PE	2-phenylethanol
3D, 3-D	three-dimensional
3-EP	3-ethylphenol
4Comp	four-component surrogate fuel
4-EP	4-ethylphenol
A	ampere(s)
A30	Co-Optima gasoline blend containing 30% aromatics, by volume
AC	alternating current
A/C	air conditioning
ACEC	Advanced Combustion and Emission Control
ACEM	Advanced Cycle Efficiency Manager
ACI	advanced compression ignition
ACS	American Chemical Society
AEC	Advanced Engine Combustion
AFIDA	Advanced Fuel Ignition Delay Analyzer
AFR	air/fuel ratio
AFRstoich	stoichiometric air-fuel ratio
AHC	aromatic hydrocarbon
AHRR	apparent heat release rate
AI	auto-ignition
AISI	American Iron and Steel Institute
aka	also known as
AKI	anti-knock index
ALE	arbitrary Lagrangian–Eulerian
alk	alkane

ALK	Predominantly alkylate-containing Co-Optima gasoline blend
AMFI	additive mixing fuel injection (low-temperature gasoline combustion control system)
ANL	Argonne National Laboratory
APC	air per cylinder
Ar	argon
ARES	a rotational rheometer
aro	aromatic
ASI	after start of injection
ASME	American Society of Mechanical Engineers
ASOI, aSOI	after the start of injection
ASTM	ASTM International, formerly American Society for Testing and Materials
at.%	atomic percent
atdc	after top dead center
aTDC, ATDC	after top dead center
$aTDC_f$	after firing top dead center
atm	atmosphere(s)
Au	gold
a.u.	arbitrary units
AVFL	Advanced Vehicles/Fuels/Lubricants
AVL BOOST	internal combustion engine simulation software
AZ	Arizona
bara, bar-a, bar(a)	bar absolute
BDI	barrier discharge ignition
BET	Brunauer-Emmett-Teller
BETO	Bioenergy Technologies Office
BL	boundary layer
BMEP	brake mean effective pressure
BOB	blendstock for oxygenate blending
BP	bandpass
BSFC	brake specific fuel consumption
BTDC, bTDC	before top dead center
BTE	brake thermal efficiency
BTEX	benzene, toluene, ethylbenzene, and xylene
BTU	British thermal unit
BuOH	n-butanol
C	carbon

C	Celsius
C_0	small hydrocarbon
C1	hydrocarbon with one carbon atom
C2	hydrocarbon with two carbon atoms
C3	hydrocarbon with three carbon atoms
C4	hydrocarbon with four carbon atoms
C5	hydrocarbon with five carbon atoms
C6	hydrocarbon with six carbon atoms
C8	hydrocarbon with eight carbon atoms
C9	hydrocarbon with nine carbon atoms
C11	hydrocarbon with eleven carbon atoms
C18	hydrocarbon with eighteen carbon atoms
Ca	calcium
CA	California
CA	crank angle
CA10	crank angle at 10% mass fraction burned
CA50	crank angle at 50% mass fraction burned
CAC	charge air cooler
CAD	crank angle degree(s)
CB	carbon black
CB#1	custom blend gasoline-like fuel with higher ϕ-sensitivity, RON, and S than regular gasoline
CCD	charged coupled device
Cd	cadmium
CDA	cylinder deactivation
CDC	conventional diesel combustion
Ce	cerium
CeO_2	cerium dioxide
CERC	U.S.-China Clean Energy Research Center
CFA	grade no. 2-D S15 diesel emissions-certification fuel from Chevron-Phillips Chemical Co., batch A
CFB	No. 2 S15 emissions-certification diesel fuel
CFD	computational fluid dynamics
CFH	Central Fuel Hypothesis
CFR	Cooperative Fuel Research
CH_4	methane

C_2H_4	ethylene
C_2H_6	ethane
C_3H_8	propane
C_8H_{18}	octane
CHA	chabazite
CH_2O	formaldehyde
CHT	conjugate heat transfer
CI	compression ignition
CI	conversion inflection
CIERA	cavitation-induced erosion risk assessment
CLEERS	Crosscut Lean Exhaust Emissions Reduction Simulations
cm	centimeter(s)
cm^3	cubic centimeter(s)
CNG	compressed natural gas
CN	cetane number
CNN	convolutional neural networks
Co	cobalt
Co.	company
CO	Colorado
CO	carbon monoxide
CO_2	carbon dioxide
CONVERGE	computational fluid dynamics software package
Co-Optima	Co-Optimization of Fuels and Engines
Corp.	Corporation
CO-TPR	temperature-programmed reduction using CO as reducing gas
cP	centipoise
CPFR	constant pressure flow rig
CPU	central processing unit
CR, cr	compression ratio
CRADA	cooperative research and development agreement
CRC	Coordinating Research Council
crpm	cam revolutions per minute
C_{rr}	rolling resistance coefficient
cSt	centistoke(s)
CSU	Colorado State University
CT	Connecticut

CT	computed tomography
CTAB	cetyl trimethyl ammonium bromide
CTO	cesium titanates
Cu	copper
CUC	clean-up catalyst
Cu-CHA	copper chabazite
$Cu(OH)_2$	copper hydroxide
Cu/SAPO-34	copper/silicoaluminophosphate zeolite
CVCC	constant volume combustion chamber
d	day
Da	Damkohler number
dATDC	degrees above top dead center
DBE	double bond equivalent
DBI	diffused background illumination
DBI-EI	diffused back illumination extinction imaging
DC	District of Columbia
DC	direct current
DCCO	deceleration cylinder cut-off
DCPM	dicyclopentylmethane
DD13	Detroit Diesel baseline 13 liter engine
DD15	Detroit Diesel baseline 15 liter engine
DDI-PFS	double direct injection partial fuel stratification
deg	degree(s)
D-EGR	dedicated exhaust gas recirculation
DFI	ducted fuel injection
DFT	density functional theory
DI	direct injection
DIB	diisobutylene
DISI	direct injection spark ignition
DLC	diamond-like carbon
DISI	direct injection spark ignition
DMA	dynamic mechanical analysis
DOE	U.S. Department of Energy
DOHC	dual overhead camshaft
DOI, doi	digital object identifier
DRG	directed relation graph

DRIFTS	diffuse reflectance infrared Fourier transform spectroscopy
DS	down speed
DSC	differential scanning calorimetry
DSF	dynamic skip fire
DSL	dimpled stepped-lip
DSR	dynamic species reduction
E0	gasoline (neat)
E10	10% ethanol, 90% gasoline blend
E30	30% ethanol, 70% gasoline blend
E100	ethanol (neat)
E85	85% ethanol, 15% gasoline blend
EAL	Environmentally acceptable lubricants
EB25	25% by mass ethylbenzene, 75% by mass EEE
ECN	Engine Combustion Network
eDEAC, EDEAC	electrically actuated cylinder deactivation
EDS	energy-dispersive spectroscopy
EEE	certification gasoline
e.g.	*exempli gratia*, “for example”
EGAI	end-gas autoignition
EGR	exhaust gas recirculation
EHN	2-ethyl-hexylnitrate, a common diesel fuel ignition improver
EIHC	emissions index of unburned hydrocarbons
EO	engine-out
EOE	end of energizing
EOI	end of injection
EPA	Environmental Protection Agency
erpm	engine revolution(s) per minute
E_{stored}	accumulated stored energy in solid material
et al.	*et alii* (Latin, meaning *and others*)
etc.	*et cetera* (Latin, meaning *and the rest*)
ETH Zurich	Eidgenössische Technische Hochschule Zürich
EtOH	ethanol
EVC	exhaust valve closing
EVO	exhaust valve opening
Exp, exp	experiment; experimental
FACE	Fuels for Advanced Combustion Engines

FACE-F	Fuels for Advanced Combustion Engines – Gasoline F
FBP	final boiling point
Fe	iron
FE	fuel economy, fuel efficiency
FEA	finite element analysis
FEM	finite element method
FF	firing fraction
FFE	U.S. Environmental Protection Agency fuel economy highway driving cycle
FGF-LLNL	Fuels for Advanced Combustion Engines Gasoline F – Lawrence Livermore National Laborator
FIB	focused ion beam
FID	flame ionization detector
FPTF	fluid power test facility
FREI	Flames with Repetitive Extinction and Ignition
FSN	filter smoke number
ft	foot
ft-lb, ft·lb	foot pound(s)
FTE	freight ton efficiency
FTIR	Fourier-transform infrared spectroscopy
FTP	Federal Test Procedure
FTP-75	Federal Test Procedure
FY	Fiscal Year
g	gram(s)
G'	dynamic stiffness
gal	gallon
GBDI	groundless barrier discharge igniter
GCI	gasoline compression ignition
GC-MS	gas chromatograph – mass spectrometer
Gd	gadolinium
GDCI	gasoline direct injection compression ignition
GDI	gasoline direct injection; gasoline direct injector
GEN-V	Fifth generation
G EQN	G-Equation model
GF-5	Current lubricant specifications defining the performance level requirements in terms of engine tests
GF-6	Next lubricant specifications currently under development for higher fuel efficient performance

GM	General Motors
GPa	gigapascal(s)
GPF	gasoline particulate filter
GPU	graphic processing unit
GTDI	gasoline turbocharged direct injection
GTE	gas turbine efficiency
GW	George Washington University
h	hour(s)
H	high
^{1}H	protium, a hydrogen isotope
^{2}H	deuterium, a hydrogen isotope
H_2	diatomic hydrogen
H_2O	water
H_2O_2	hydrogen peroxide
HAADF-STEM	high-angle annular dard-field scanning transmission electron microscopy
H/C	hydrogen-to-carbon ratio
HC	hydrocarbon
HCCI	homogeneous charge compression ignition
HCl	hydrogen chloride
HD	heavy-duty
HDR	high dynamic range
HF	heat flux
HFIR	High Flux Isotope Reactor
H_2O	water
HO_2	hydroperoxyl radical
HOV, HoV	heat of vaporization
HP	high porosity
HPC	high-performance computing
hr	hour(s)
HR	heat release
HT	heat transfer
HT	high temperature
HWY	highway
HWFET	Highway Fuel Economy Test
Hz	Hertz
IBP	initial boiling point

i-BuOH, iBuOH	isobutanol
IC	internal combustion
ICE	internal combustion engine
ICEF	Internal Combustion Engine Fall Technical Conference
ICMOS	intensified complementary metal oxide semiconductor camera
ID	ignition delay
ID	identification
i.e.	*id est*, "that is"
IEEE	Institute of Electrical and Electronics Engineers
IL	ionic liquid
IL	Illinois
ILASS	Institute for Liquid Atomization and Spray Systems
IMEP	indicated mean effective pressure
IMEPg, $IMEP_g$	gross indicated mean effective pressure
IMEPn	net indicated mean effective pressure
in	inch(es)
IN	Indiana
Inc.	Incorporated
INCA	Integrated Calibration and Application tool (software)
i-PrOH, iPrOH	isopropanol
IQR	interquartile range
ISFC	indicated specific fuel combustion
ITE	indicated thermal efficiency
IVC	intake valve closing
IVO	intake valve opening
J	joule(s)
K	Kelvin
K	empirically determined coefficient that varies with operating conditions
Ka	Karlovitz number
keV	kiloelectron Volt(s)
kg	kilogram(s)
KH-RT	Kelvin Helmholtz–Rayleigh Taylor
kHz	kilohertz
KIVA	Fortran-based computational fluid dynamics software
kJ	kilojoule(s)
KLSA	knock limited spark advance

kPa	kilopascal(s)
kph	kilometer(s) per hour
kW	kilowatt(s)
kWh, kW-hr	kilowatt-hour(s)
KY	Kentucky
L, l	liter(s)
L	low
LA	Louisiana
LANL	Los Alamos National Laboratory
lbs., lbs	pounds
LD	light-duty
LED	light-emitting diode
LES	large eddy simulation
LESI	Lagrangian-Eulerian Spark-Ignition
LFS	laminar flame speed
LHV	lower heating value
Li	lithium
LIF	laser-induced fluorescence
LIVC	late intake valve closing
LLC	Limited Liability Company
LLNL	Lawrence Livermore National Laboratory
LNF	stock GM engine
LPG	liquefied petroleum gas
LSE	GM long-stroke engine
LSODE	Livermore Solver for Ordinary Differential Equations
LSPI	low speed pre-ignition
LSU	Louisiana State University
LT	low temperature
LTAT	low-temperature aftertreatment
LTC	low-temperature combustion
LTC-G	low-temperature combustion – gasoline
LTGC	low-temperature gasoline combustion
LTHR	low-temperature heat release
LTP	low-temperature plasma
LVF	liquid volume fraction
M	medium

m	meter(s)
m^2	square meter(s)
m^3	cubic meter(s)
MAF	mass air flow
MAP	manifold absolute pressure, manifold air pressure
MAPO	maximum amplitude pressure oscillation
MAT	mixture air temperature
MbH	mit beschränkter Haftung
MBT	maximum brake torque
MCCI	mixing-controlled compression ignition
MCE	multi-cylinder engine
MCM-41	Mobil Composition of Matter No. 41
MCP	multichannel plate
MD	medium-duty
MD	molecular dynamics
MD25	25 vol% methyl decanoate in CFB
MDPR	mean depth penetration rate
MEMS	micro-electromechanical system
MeOH	methanol
MER	molar expansion ratio
MFR	mass flow rate
Mg	magnesium
mg	milligram(s)
M/G	motor/generator
mi	mile(s)
MI	Michigan
min	minute(s)
MH	maximum torque
MKS	MKS Instruments
ml	milliliter(s)
ML	minimum torque
mm	millimeter(s)
MM	multimode
MMF	merit function
MOC	methane oxidation catalyst
mol	mole, molar

mol%	mole fraction
MON	motor octane number
MOU	memorandum of understanding
MPa	megapascal(s)
mPA	millipascal(s)
MPE	methylpropyl ether
mpg, MPG	mile(s) per gallon
mph	mile(s) per hour
MPI	Message Passing Interface
ms	millisecond(s)
MS	mail stop
MS	mass spectrometry
MW	megawatt(s)
MW	molecular weight
MY	model year
MZ-WSR	multizone well-stirred reactor
N	Newton(s) (unit of force)
N_2	diatomic nitrogen
N30	Co-Optima gasoline blend containing 30% naphthenes by volume
Na	sodium
NA	North America
NACV	North American Commercial Vehicle
NAP-XPS	near-ambient-pressure X-ray photoelectron spectroscopy
NC	North Carolina
n.d.	no date
N_E	electron density
NG	natural gas
NGC	next generation Cascadia: 2017 production Cascadia tractor
NH_3	ammonia
Ni	nickel
nm	nanometer(s)
N-m, Nm	Newton-meter(s)
NM	non-methane
NMEP	net mean effective pressure
NMHC	non-methane hydrocarbons
NMOG	non-methane organic gases

NMR	nuclear magnetic resonance spectroscopy
No.	Number
NO	nitric oxide
NO_x	oxides of nitrogen
NR	natural rubber
NREL	National Renewable Energy Laboratory
ns	nanosecond(s)
n/s	number per second
NSC	NO_x storage component (catalyst component)
NTC	negative temperature coefficient
Nu	Nusselt Number
NUIG	National University of Ireland, Galway
NVO	negative valve overlap
NY	New York
O	atomic oxygen
O_2	diatomic (molecular) oxygen
O_3	ozone
O30	Co-Optima gasoline blend containing 30% olefins by volume
OAC	oxygenated aromatic compound
O/C	oxygen-to-carbon ratio
OD	optical density
OEM	original equipment manufacturer
OH	hydroxyl radical
OH*	excited-state hydroxyl radical
OHC	oxidation half cycle
OI	octane index
OK	Oklahoma
ON/CR	octane number per compression ratio requirement
OP	operating point
ORC	organic Rankine cycle
ORNL	Oak Ridge National Laboratory
OSC	oxygen storage component (catalyst component)
OSP	oil-soluble polyalkylene glycol
P	phosphorus
P	pressure
PA	Pennsylvania

PACE	Partnership on Advanced Combustion Engines
PAG	polyalkylene glycol
PAH	polycyclic aromatic hydrocarbon
PAO	poly(alphaolefin)
PASS	Protection of Aftertreatment Systems from Sulfur
Pb	lead
P_c, Pc	compressed pressure
PC	pre-chamber
PCI	pre-chamber ignition
PCP	peak cylinder pressure
PCSI	pre-chamber spark ignition
PCV	positive crankcase ventilation
Pd	palladium
$PdAl_2O_3$	palladium aluminum oxide
PFI	port fuel injection
PFP	peak firing pressure
PFS	partial fuel stratification
PGM	platinum group metal
P-h	Pressure enthalpy
PHEV	plug-in hybrid electric vehicle
phr	part per hundred rubber
P_{in}	intake pressure
PIONA	paraffins, iso-paraffins, olefins, naphthenes, and aromatics
PLC	public limited company
PLIF	planar laser-induced fluorescence
PLII	planar laser-induced incandescence
PM	particulate matter
PMI	particulate mass index
PNA	passive NO_x adsorber
PNNL	Pacific Northwest National Laboratory
P.O.	Post Office
P2P	pin-to-pin
PPCI	partially premixed compression ignition
ppm	part(s) per million
ppmv	part(s) per million by volume
PRF	primary reference fuel

psi	pound(s) per square inch
PSM	particulate size mimic
PSU	Pennsylvania State University
Pt	platinum
PT, P-T	pressure–temperature
PTO	power take-off
PTS	Publications Tracking System
PTWA	plasma transfer wire arc
Pub	publication
PVD	physical vapor deposition
PVO	positive valve overlap
Q1	first quarter
Q4	fourth quarter
R^2	coefficient of determination: the proportion of the variance for a dependent variable that is explained by an independent variable or variables in a regression model
RANS	Reynolds-averaged Navier–Stokes
Rc, r_c	compression ratio
RCCI	reactivity-controlled compression ignition
RCM	rapid compression machine
R&D	research and development
RD387	real gasoline
RD5-87	research-grade regular E10 gasoline
RD5-87-A	research-grade regular E10 gasoline, AKI = 88, RON = 92.0
RD5-87-B	research-grade regular E10 gasoline, AKI = 87, RON = 90.6
RFF	roller finger follower
Rh	rhodium
RHC	reduction half cycle
RI	ringing intensity
RIF	representative interactive flamelet
RIF-ist	representative interactive flamelet – in situ tabulation
r/min	revolution(s) per minute
RM	rubber-maker
RMS	rubber-making silica
RNG	re-normalization group
RO_2	organic peroxy radicals
r_{OHC}	oxidation half cycle rate

ROHR, RoHR	rate of heat release
ROI	rate of injection
RON	research octane number
rpm, RPM	revolution(s) per minute
r-ratio	ratio of the half-cycle rates, r_{RHC}/r_{OHC}
r_{RHC}	reduction half cycle rate
RSD	rainbow schlieren deflectometry
s	second(s)
S	sensitivity
S	octane sensitivity (S = RON – MON)
S15	15 parts per million sulfur
S'_{min}	minimum torque from rheometer cure test
SACI	spark-assisted compression ignition
SAE	SAE International, formerly the Society of Automotive Engineers
SAGE	a combustion model that comes with the CONVERGE CFD software and includes detailed chemistry
S/B	stroke-to-bore ratio
sccm	standard cubic centimeter(s) per minute
SCE	single-cylinder engine
SCR	selective catalytic reduction
sec	second(s)
S-GDI	stoichiometric gasoline direct injection
Si	silicon
SI	spark ignition
SIDI	spark ignition direct injection
SINL	spatially integrated natural luminosity
s_L	laminar flame velocity
SMD	Sauter mean diameter
SNL	Sandia National Laboratories
SOE	start of energizing
SOI	start of injection
SOI2	start of the second injection for partial fuel stratification
SPI	stochastic pre-ignition
SPIE	the international society for optics and photonics, formerly known as the Society of Photographic Instrumentation Engineers
SS	steady state

SSZ-13	aluminosilicate zeolite
ST	spark timing
ST1	SuperTruck 1
ST2	SuperTruck 2
Std	standard
STLE	Society of Tribologists and Lubrication Engineers
SULEV	super ultra-low emission vehicle
SUNY	The State University of New York
SVTRIP	Stochastic Vehicle Trip Prediction, a software tool that can predict vehicle speed traces
t	time
T	temperature
T	incubation period
T	kg/T: measure of rolling resistance of tires
T25	25 vol% tri-propylene glycol mono-methyl ether in CFB
TAMU	Texas A&M University
TBBS	N-t-butyl-2-benzothiazole sulfenamide
TBC	thermal barrier coating
T_{BDC}	temperature at bottom dead center
T_c, Tc	compressed temperature
TC50	time at which 50% of cure has taken place
TC90	time at which 90% of cure has taken place
TCF	Technology Commercialization Fund
TCR	thermochemical recuperation
TDC	top dead center
TG	Co-Optima test gasoline
TGA	thermogravimetric analysis
THF	tetrahydrofuran
Ti	titanium
T_{in}	intake temperature
TN	Tennessee
TOF	turnover frequency
TOL	toluene
TP	two-phase
TPD	temperature programmed desorption
TPGME	tri(propylene glycol) methyl ether
TPI	transient plasma ignition

TPRF	toluene primary reference fuel
TR	time-resolved
TRL	technology readiness level
TSF	toluene standardization fuel
TWC	three-way catalyst
TX	Texas
u'	turbulent velocity fluctuation
UC Davis	University of California, Davis
UConn, UCONN	University of Connecticut
UDDS	Urban Dynamometer Driving Schedule
ug/hr	micrometer(s) per hour
UK	United Kingdom
UM	University of Michigan
U.S.	United States
USCAR	United States Council for Automotive Research LLC
U.S. DRIVE	United States Driving Research and Innovation for Vehicle efficiency and Energy sustainability
v	velocity
V	volt(s)
VA	Virginia
V/C	volume/control
VI	viscosity index
VN	vanadium nitride
vol%	percent by volume
vs.	versus
VSM	visible soot mass
VTO	Vehicle Technologies Office
W	Watt
WA	Washington
WCX	World Congress Experience, a conference of SAE International
WG	water gauge
WHR	waste heat recovery
WI	Wisconsin
WIMRC	Warwick Innovative Manufacturing Research Centre
wt%	weight of the component divided by total sample weight, multiplied by 100
W_{total}	total work required to reach material failure

XPS	X-ray photoelectron spectroscopy
Y_{N2}	mass fraction of nitrogen gas
YSI	yield sooting index
ZDDP	zinc dialkyldithiophosphate
Zero-RK	Zero-Order Reaction Kinetics combustion software package
ZSM-5	Zeolite Socony Mobil–5

List of Symbols

°	degree(s)
°aTDC, °ATDC	degree(s) after top dead center
°bTDC	degree(s) before top dead center
°C	degree(s) Celsius
°CA	crank angle degree(s)
°F	degree(s) Fahrenheit
ΔMW	change in molecular weight
γ	ratio of specific heats
Γ_{fa}	parameter that characterizes forced autoignition of the end gas
Γ_{hot}	parameter that characterizes “hot spot”
η_f	fuel-conversion efficiency (= work per cycle / chemical energy injected)
>	greater than
φ	angular position
λ	equivalence ratio (ratio of actual air-to-fuel ratio to stoichiometric air-to-fuel ratio)
λ	air excess ratio
<	less than
µ	micron
µg	microgram(s)
µL, µl	microliter(s)
µm	micrometer(s)
$\mu moleg^{-1}$	micromole(s) per gram
µs	microsecond(s)
%	percent
ϕ	fuel/air equivalence ratio
ϕ	fuel/air equivalence ratio

ϕ_m	fuel/charge-mass equivalence ratio (the same as ϕ, but the fuel is normalized by the total charge mass rather than only the air mass (Sjoberg II.5 definition: mass-based fuel-air equivalence ratio)
τ	residence time
τ_{main}	main ignition delay time (1 ms)
τ_{sim}	simulated period of time

Executive Summary

On behalf of the Vehicle Technologies Office of the U.S. Department of Energy, we are pleased to introduce the Fiscal Year (FY) 2019 Annual Progress Report for the Advanced Engine and Fuel Technologies Program. In support of the Vehicle Technology Office's goal for future U.S. economic growth, the Program focuses on early-stage research and development to improve understanding of combustion processes, fuel properties, and emissions control technologies, generating knowledge and insight necessary for industry to cost-effectively develop the next generation of engines and fuels.

One of the most promising and cost-effective approaches to improving the fuel economy of the U.S. vehicle fleet is to introduce the next generation of higher-efficiency, very-low-emission combustion engines that meet future federal emissions regulations into the passenger and commercial vehicle markets. Advanced fuel formulations that can incorporate non-petroleum-based blending agents could further enhance engine efficiency, reduce greenhouse gas emissions, and provide fuel diversification. Also, innovations in combustion, fuels, emissions control, air control, turbomachinery, and energy recovery could potentially increase fuel economy considerably compared to today's vehicles. The expected national economic, environmental, and energy security benefits from these next-generation engines and fuels would be significant inasmuch as the majority of vehicles sold over the next several decades will still include an engine.

The Program has set the following goals for passenger and commercial vehicle fuel economy improvements.

- By 2030, increase light-duty engine efficiency to demonstrate 35% improvement in passenger vehicle fuel economy (25% improvement from engine efficiency and 10% from fuel co-optimization) relative to a 2015 baseline vehicle, while meeting the U.S. Environmental Protection Agency Tier 3 Emission and Fuel Standards

- By 2030, improve heavy-duty engine efficiency by 35% relative to a 2009 baseline vehicle and identify cost-effective high-performance fuels that can further increase efficiency up to an additional 4%, while meeting prevailing U.S. Environmental Protection Agency emissions standards

The Program utilized advanced combustion processes to increase engine efficiency, resulting in a modeled passenger vehicle fuel economy improvement of 19.4% (over a Model Year 2015 baseline) in FY 2019.

This report highlights progress achieved by the Advanced Engine and Fuel Technologies Program during FY 2019. The nature, current focus, and recent progress of the Program are described together with summaries of National Laboratory, industry, and university projects that provide an overview of the exciting work being conducted to address critical technical barriers and challenges to commercializing the next generation of higher-efficiency engine, emissions control, and fuel technologies for passenger and commercial vehicles.

Gurpreet Singh, Program Manager Advanced Engine and Fuel Technologies Program
Vehicle Technologies Office

Gurpreet Singh
Program Manager
Advanced Engine and Fuel Technologies Program
Vehicle Technologies Office

Kenneth C. Howden
Technology Development Manager
Vehicle Technologies Office

Siddiq Khan
Technology Development Manager
Vehicle Technologies Office

Kevin Stork
Technology Development Manager
Vehicle Technologies Office

Michael Weismiller
Technology Development Manager
Vehicle Technologies Office

Table of Contents

List of Figures

List of Tables

Vehicle Technologies Office Overview

Vehicles move our national economy. Annually, vehicles transport 11 billion tons of freight—about $35 billion worth of goods each day[1]—and move people more than 3 trillion vehicle-miles.[2] Growing our economy requires transportation and transportation requires energy. The transportation sector accounts for approximately 30% of total U.S. energy needs[3] and 70% of U.S. petroleum consumption.[4] The average U.S. household spends over 15% of its total family expenditures on transportation, making it the most expensive spending category after housing.[5]

The Vehicle Technologies Office (VTO) has a comprehensive portfolio of early-stage research to enable industry to accelerate the development and widespread use of a variety of promising sustainable transportation technologies. The research pathways focus on fuel diversification, vehicle efficiency, energy storage, and mobility energy productivity that can improve the overall energy efficiency and efficacy of the transportation or mobility system. VTO leverages the unique capabilities and world-class expertise of the National Laboratory system to develop innovations in electrification, including advanced battery technologies; advanced combustion engines and fuels, including co-optimized systems; advanced materials for lighter-weight vehicle structures; and energy efficient mobility systems.

VTO is uniquely positioned to address early-stage challenges due to strategic public-private research partnerships with industry (e.g., U.S. DRIVE, 21st Century Truck Partnership) that leverage relevant expertise. These partnerships prevent duplication of effort, focus DOE research on critical R&D barriers, and accelerate progress. VTO focuses on research that industry does not have the technical capability to undertake on its own, usually due to a high degree of scientific or technical uncertainty, or that is too far from market realization to merit industry resources.

Annual Progress Report

As shown in the organization chart (below), VTO is organized by technology area: Batteries & Electrification R&D, Materials Technologies, Advanced Engine & Fuel R&D, Energy Efficient Mobility Systems, Technology Integration, and Analysis. Each year, VTO's technology areas prepare an Annual Progress Report (APR) that details progress and accomplishments during the fiscal year. VTO is pleased to submit this APR for Fiscal Year (FY) 2019. In this APR, each project active during FY 2019 describes work conducted in support of VTO's mission. Individual project descriptions in this APR detail funding, objectives, approach, results, and conclusions during FY 2019.

[1] Bureau of Transportation Statistics, U.S. Department of Transportation, Transportation Statistics Annual Report 2018, Table 4-1. https://www.bts.gov/tsar.
[2] Transportation Energy Data Book 37th Edition, Oak Ridge National Laboratory, 2019. Table 3.8 Shares of Highway Vehicle-Miles Traveled by Vehicle Type, 1970–2017.
[3] Ibid. Table 2.1. U.S. Consumption of Total Energy by End-use Sector, 1950–2018.
[4] Ibid. Table 1.12. U.S. Transportation Petroleum Use as a Percent of U.S. Petroleum Production, 2018.
[5] Ibid. Table 10.1 Average Annual Expenditures of Households by Income, 2016.

Organization Chart

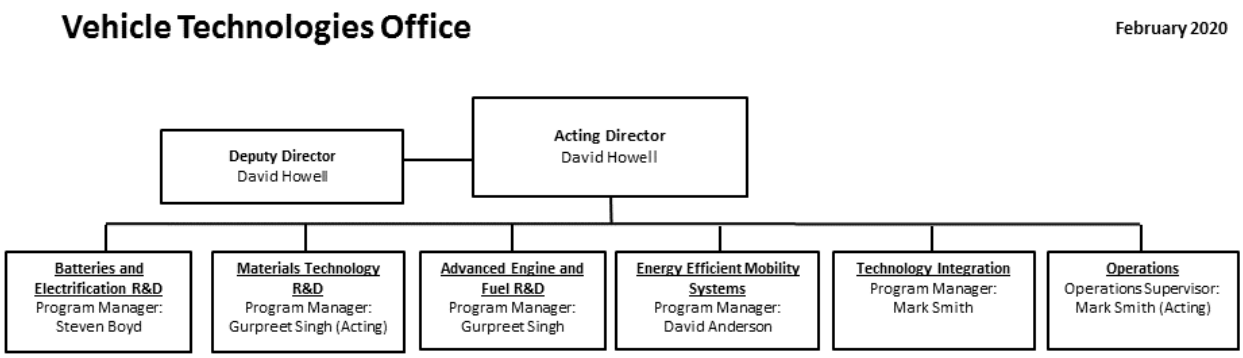

Advanced Engine and Fuel Technologies Program Overview

Introduction

The Advanced Engine and Fuel Technologies Program supports the Vehicle Technologies Office's goals of increasing domestic energy security through fuel diversification, improving vehicle efficiency and reducing emissions, and reducing vehicle initial and operating costs for consumers and businesses. The Program focuses on early-stage research and development (R&D) to improve understanding of the combustion processes, fuel properties, and emission control technologies while generating knowledge and insight necessary for industry to develop the next generation of engines and fuels.

The Program utilizes unique capabilities and expertise at the National Laboratories and collaborates closely with academia and industry to strengthen the knowledge base of the next generation of higher-efficiency, very-low-emissions combustion engines for passenger and commercial vehicles. In addition, a science-based understanding of how engine efficiency and emissions are affected by fuel properties, and conversely, how engines can be modified to take advantage of desirable fuel properties, could enable further efficiency improvements. The fundamental knowledge and new understanding developed by this Program can be used to co-optimize engines, fuels, and emission controls (exhaust aftertreatment). Market introduction of these co-optimized high-performance fuels and advanced engines that meet prevailing emissions regulations could expeditiously reduce petroleum use in U.S. highway transportation over the next several decades, during which time the Energy Information Administration reference case forecasts that the vast majority of vehicles sold will still include an engine.[6]

Goals

The Advanced Engine and Fuel Technologies Program sets the following goals for improvement of the fuel economy of passenger and commercial vehicles:

- By 2030, increase light-duty engine efficiency to demonstrate 35% improvement in passenger vehicle fuel economy (25% improvement from engine efficiency and 10% from fuel co-optimization) relative to a 2015 baseline vehicle, while meeting the U.S. Environmental Protection Agency Tier 3 Emission and Fuel Standards
- By 2030, improve heavy-duty engine efficiency by 35% relative to a 2009 baseline vehicle and identify cost-effective high-performance fuels that can further increase efficiency up to an additional 4%, while meeting prevailing U.S. Environmental Protection Agency emissions standards.

The Program utilized advanced combustion processes to increase engine efficiency, resulting in a modeled passenger vehicle fuel economy improvement of 19.4% (over a Model Year 2015 baseline) in Fiscal Year (FY) 2019.

The U.S. Environmental Protection Agency Tier 3 Bin 30 emissions standards for passenger vehicles would achieve a greater than 80% reduction in combined emissions of nitrogen oxides (NO_x) and non-methane organic gases and a 70% reduction in particulate matter (PM) emissions (to less than 3 mg/mi) compared to the previous Tier 2 Bin 5 standard. Future catalyst and emission control systems must be able to operate efficiently

[6] Energy Information Administration, *Annual Energy Outlook 2018*. Reference case scenario forecasts that even in 2050, over 96% of all highway transportation vehicles sold will still have internal combustion engines.

at the lower exhaust temperatures of advanced combustion engines (i.e., greater than 90% conversion of criteria pollutants at 150°C) to achieve these extremely low criteria pollutant emission levels.

Status of Current Technology

Gasoline and diesel internal combustion engines continue to be attractive options to power transportation vehicles, owing to significant advances in engine combustion, emission control, and fuel technologies that continue to increase the fuel efficiency of these engines and simultaneously reduce their exhaust emissions. Also, these engines can be readily adapted to use natural gas and biofuels such as ethanol and biodiesel. Integrated with hybrid and plug-in hybrid electric vehicle powertrains, these engines can be operated at fuel-efficient speed-load conditions. This next-generation hybrid engine–electric drivetrain could offer a cost-competitive and fuel-efficient powertrain as the U.S. transportation sector transitions to full electrification.

Spark-ignition (SI) gasoline engines power the majority of the U.S. light-duty vehicle fleet. They generally operate with stoichiometric combustion to allow the use of highly efficient and cost-effective three-way catalysts for emission control. Engine technology advances in recent years such as direct fuel injection, flexible valve timing and lift systems, improved combustion chamber design, and reduced mechanical friction losses are contributing to substantial improvements in gasoline engine efficiency. Boosted air handling and direct-injection fueling systems have enabled gasoline SI engine downsizing, which has been a major trend during the last decade, to improve light-duty vehicle fuel economy. Further efficiency improvement of downsized engines through higher compression ratios has been constrained by current fuel properties. Fuel autoignition, which causes engine knock, and low-speed pre-ignition, which can cause catastrophic engine failures, limit increasing compression ratio and efficiency of SI engines.

Lean-burn gasoline combustion engines have higher efficiencies but require lean-NO_x emission controls to meet the more stringent U.S. emissions regulations. Advances in lean-burn gasoline combustion and emission controls are critical for introducing this higher-efficiency technology in the U.S. market. Increased thermal efficiency can also be achieved with stoichiometric dilute combustion (i.e., high levels of exhaust gas recirculation). Remaining stoichiometric avoids the cost and complexity of lean aftertreatment systems, while still providing some of the benefits of reduced pumping losses, reduced heat transfer, and increased ratio of specific heats.

Achieving high efficiency in lean-burn and dilute gasoline engines depends on creating combustible mixtures near the spark plug and away from cylinder walls. A comprehensive understanding of the dynamics of fuel–air mixture preparation is required, including intake air flows and fuel sprays as well as their interactions with the combustion chamber surfaces over a wide operating range and generation of appropriate turbulence to enhance flame speed. Improved simulation tools are being developed for optimizing lean-burn and dilute systems over the wide range of potential intake systems, piston geometries, and injector designs. Also, robust, high-energy ignition systems and mixture control methods are being investigated to reduce combustion variability at lean or dilute, highly boosted conditions and achieve reliable ignition and combustion; examples include high-energy plugs, plasma, corona, and laser ignition systems.

Low-temperature combustion (LTC) strategies such as homogeneous charge compression ignition, pre-mixed charge compression ignition, and reactivity-controlled compression ignition exhibit high efficiency with very low levels of engine-out NO_x and PM emissions, thereby potentially reducing exhaust aftertreatment requirements. Significant R&D efforts have focused on air handling and conditioning of intake air, fuel–air mixing, fuel property impacts, combustion timing control, and transient response. Progress in LTC strategies continues to expand the operational range, covering speed and load combinations consistent with light- and heavy-duty drive cycles.

Multimode combustion strategies combine two operating modes to achieve overall higher efficiency compared to SI-only operation. Examples include (a) boosted spark ignition during starting and high-load operation to

meet cold-start emissions requirements and achieve suitable power density, and (b) LTC modes under low and medium loads for high efficiency. R&D efforts have focused on controlling transitions between the two operating modes, expanding the speed and load range during LTC, improving cold operation, and reducing combustion noise.

Diesel engines deliver fuel economies that are considerably higher than those of comparable SI engines. Key developments in combustion and emission controls have enabled manufacturers to achieve the mandated emissions levels and introduce new diesel-powered vehicles to the U.S. market. The U.S. Department of Energy (DOE) research has contributed to progress in all of these areas. However, diesels in passenger cars have had limited market penetration in the United States, primarily due to the cost of the fuel injection and emission control system components required to reduce emissions. The heavy-duty diesel is the most common engine for commercial vehicles because of its high efficiency and outstanding durability. Efficiency gains were modest in the early 2000s, when R&D efforts focused on meeting increasingly stringent heavy-duty engine criteria emissions standards while reducing fuel use and system cost. After the manufacturers met the U.S. Environmental Protection Agency 2010 emissions standards for NO_x and PM, efforts turned to further improving engine efficiency and system durability. Continued R&D to improve boosting and thermal management and to reduce and/or recover rejected thermal energy has resulted in current heavy-duty diesel engine efficiencies in the range of 43%–45%. Advanced combustion regimes and demonstrated waste heat recovery technologies can further improve overall engine efficiency to as high as 57%.

The Co-Optimization of Fuels and Engines ("Co-Optima") initiative, which kicked off in 2016, is a collaboration between the Advanced Engine and Fuel Technologies Program and the Bioenergy Technologies Office. A National Laboratory R&D consortium was formed to investigate the co-development of advanced fuels and engines, which offered a great opportunity to improve engine efficiency and diversify the fuel supply. Research focuses on identifying fuel properties that enable optimized engine performance and on developing a fuel-property-based approach that could provide the technical information needed to define future fuel requirements. Market introduction of advanced fuel and engine technologies can be accelerated by addressing the fuel property limitations and barriers to more efficient light-duty and heavy-duty engines. The market will define the best means to blend and provide these fuels.

Although NO_x and PM engine-out emissions are significantly lower for advanced LTC strategies and lean-burn technologies such as conventional and advanced diesel combustion strategies for light- and heavy-duty engines as well as lean-burn gasoline engines, further reductions are needed to meet future stringent regulations. Also, higher hydrocarbon and carbon monoxide emissions require additional controls, which are often a challenge with the low exhaust temperatures (about 150°C).

Selective catalytic reduction with urea as reducing agent (urea-SCR) technology has been used for NO_x control in Tier 3 light- and medium-duty vehicles, heavy-duty engines, and other diesel engine applications in the United States. All diesel vehicle manufacturers have adopted urea-SCR since it has a broader temperature range of effectiveness than competing means of NO_x reduction and allows the engine/emission control system to achieve higher fuel efficiency. Although urea-SCR is a relatively mature catalyst technology, more support research to aid formulation optimization and minimize degradation effects, such as hydrocarbon fouling, was conducted.

PM produced by direct-injection technology utilized for most advanced gasoline engines, although smaller in mass than diesel particulates, may still represent significant emissions in terms of particulate number counts. PM emissions from dilute combustion gasoline engines are not fully understood; their morphology and chemical composition are also affected by combustion. Research has been conducted to develop filtration systems (for smaller-diameter PM) that are durable and that introduce only low fuel economy penalties (generally caused by increased backpressure and the need to regenerate the filter).

Complex and precise engine and emission controls require sophisticated feedback systems employing new types of sensors. NO_x and PM sensors are under development and require additional advances to be cost-effective,

accurate, and reliable. Upcoming regulations with increased requirements for onboard diagnostics will be a challenge for manufacturers trying to bring advanced fuel-efficient solutions to market. Sensors and catalyst diagnostic approaches will be key elements of emission control research in the next few years.

Overall costs of current light- and medium-duty diesel engine systems remain higher than those of conventional gasoline systems. These costs are partly due to complex engine and exhaust gas recirculation systems and the catalyst expense and volume associated with urea-SCR systems and diesel particulate filters. Pragmatic research has substantially reduced the combined fuel penalty for SCR/diesel particulate filter systems, but further reductions are plausible. Another improvement being pursued is to pair NO_x trap technology with SCR catalysts. The advantage is that the SCR catalyst uses the NH_3 produced by the NO_x trap, so no urea injection is needed. Formulations and system geometries have been researched to reduce cost by reducing the overall precious metal content of the NO_x trap+SCR systems, making the systems more feasible for light-duty vehicles

Current Technical Focus Areas and Objectives

The Advanced Engine and Fuel Technologies Program supports early-stage R&D to improve the understanding of, and ability to manipulate, internal combustion engine combustion processes, generating knowledge and insight necessary for industry to develop the next generation of engines and fuels. The Program uses cutting-edge research to strengthen the knowledge base and technical expertise in high-efficiency, advanced combustion engines and fuels, leveraging unique facilities and capabilities at the National Laboratories and close collaboration with academia and industry.

The Program objectives are as follows:

- Accelerate the fundamental understanding of advanced combustion strategies that simultaneously show higher efficiencies and very low emissions, elucidating the effects of critical factors such as fuel spray characteristics, in-cylinder air motion, heat transfer, and others
- Develop science-based understanding of how engine efficiency and emissions are impacted by fuel properties and, conversely, how engines can be modified to take advantage of desirable fuel properties and control of emissions from co-optimized fuels/engines to meet future emissions regulations
- Reduce the fuel use penalty while improving the effectiveness and durability of emission control (exhaust aftertreatment) devices to enable advanced combustion strategies and high-performance fuels, as well as reduce the use of platinum group metals
- Develop precise and flexible engine controls, as well as sensors for control systems and engine diagnostics, to facilitate adjustments of parameters that allow advanced combustion engines to operate over a wider range of engine speed and load conditions
- Further advance engine technologies such as turbo-machinery, flexible valve systems, advanced combustion systems, and fuel system components to reduce parasitic and other losses to the environment, and incorporate waste heat recovery technologies to recover engine exhaust energy

The Program maintains close collaboration with industry through a number of working groups and teams to utilize these networks in identifying and addressing critical issues, setting goals, adjusting research priorities, and tracking progress. These working groups include a broad range of stakeholders representing vehicle and engine manufacturers, energy companies, biofuel producers, manufacturers of catalysts and emission control systems, fuel distributors and retailers, National Laboratories, and universities. The collaboration is conducted through numerous groups, including the Advanced Combustion and Emission Control Technical Team and the Driving Toward Net-Zero Carbon Fuels Tech Team of the U.S. DRIVE (Driving Research and Innovation for Vehicle efficiency and Energy Sustainability) Partnership and the Engine Powertrain Team of the 21st Century Truck Partnership. Additional collaboration is carried out under the Advanced Engine Combustion

Memorandum of Understanding and the Cross-Cut Lean Exhaust Emission Reduction Simulation (CLEERS) activity of the Advanced Engine Cross-Cut Team.

The Advanced Engine and Fuel Technologies Program focuses on the following research areas (Figure 1): combustion fundamentals, co-optimization of fuels and engines, alternative fuel engines, emission control R&D, high-efficiency engine technologies, lubricant technologies, and system-level efficiency improvement. Projects competitively selected and awarded through funding opportunity announcements are fully funded through the duration of the project in the year the funding is awarded. Directly funded work at the National Laboratories is subject to change based on annual appropriations.

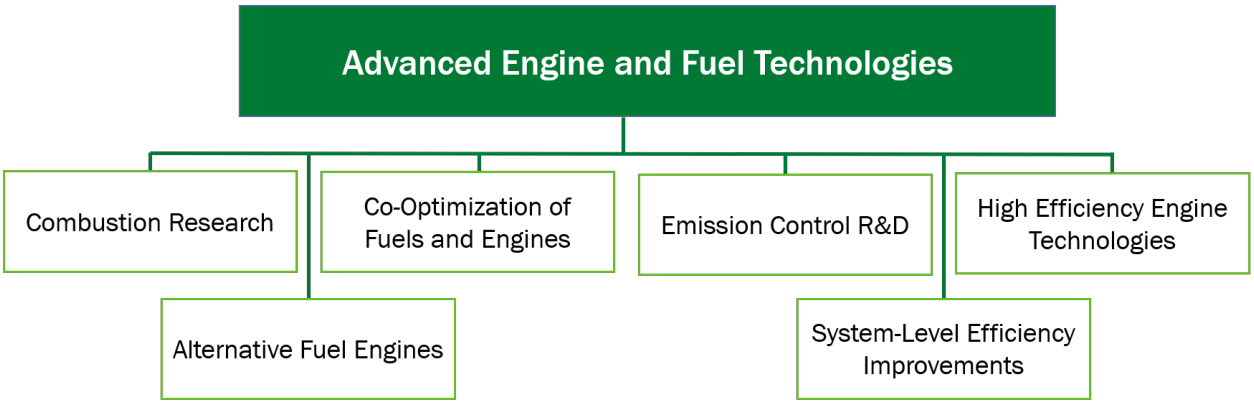

Figure 1 Research areas within the Advanced Engine and Fuel Technologies Program

Combustion Research

Combustion research activities focus on measuring, understanding, and modeling the physical and chemical processes that take place during combustion in an internal combustion engine. This is accomplished by leveraging the unique diagnostic tools, including advanced laser, high-intensity X-ray, and neutron-based measurements, to study fuel injection, air mixing, and combustion events. High-fidelity physical models of fuel injection, spray break-up, heat transfer, turbulence, and combustion phenomena are developed based on theory and measurements, as are detailed and accurate chemical kinetics models used to simulate surrogate fuels and determine their impacts on combustion efficiency and emissions. These models are needed for accurate numerical simulations of engine combustion. Simulations can allow for rapid iteration of design and diagnosing issues that are opaque to experimental measurements. High-throughput simulations have the potential to enable "virtual calibration," greatly reducing the development costs for new engines. However, attaining predictive accuracy from engine simulations remains one of the most challenging problems in engineering.

The Partnership to Advance Combustion Engines (PACE) National Laboratory consortium started in FY 2019. PACE is focused on utilizing the rapid growth in computing power and DOE investment in leadership class computing, including plans to deploy exascale (10^{18} floating point operations per second) computing in 2021. The vision for PACE is to combine unique experimental capabilities with leadership computing and emerging machine learning and artificial intelligence techniques to deliver predictive accuracy from engine simulations, enabling smarter engine design and breakthroughs in engine efficiency. The consortium model focuses the resources of six National Laboratory programs on common key barriers to efficiency in light-duty engines and creates a consolidated flagship effort that enhances engagement with industry.

Co-Optimization of Fuels and Engines

Early-stage research focuses on fuel property impacts on combustion to determine fuel characteristics that enable higher efficiency in advanced combustion strategies. Research topics include performance of tailored blend stocks, including bioderived, synthetic, and petroleum-based blend stocks. They are expected to increase

engine efficiency, specifically on advanced fuels that enable maximum performance of advanced conventional and kinetically controlled combustion strategies.

Alternative Fuel Engines

R&D activities focus on overcoming technical barriers to the implementation of alternative fuels. Fuels such as natural gas and drop-in biofuels frequently have technical barriers that impede their implementation in traditional engines. Work to overcome these barriers will include support for new alternative fuel engine offerings and evaluation of the emissions impact of novel alternative fuels.

Emission Control R&D

The lower exhaust temperatures of advanced internal combustion engines make conventional aftertreatment systems less effective. Research on exhaust aftertreatment systems for these advanced combustion engines will focus on catalyst technologies that are active at the lower exhaust temperatures, namely those that provide greater than 90% conversion efficiency at about 150°C. Early-stage fundamental research at the National Laboratories, in close collaboration with industry and academia, addresses barriers to achieving key performance metrics such as catalyst activity, selectivity, and durability. Research will also address cost-effectiveness by reducing the use of precious metals through single-atom catalysis and the development of alternatives to platinum group metals.

High-Efficiency Engine Technologies

Projects research and develop technologies for more efficient, clean, advanced engine/powertrain systems to improve passenger and commercial vehicle fuel economy.

System-Level Efficiency Improvement

R&D projects focus on system-level improvements to achieve vehicle performance targets. These include improving drivetrain efficiency and reducing aerodynamic drag and tire rolling resistance. For off-road vehicles, system-level efficiency improvements can also be accomplished with more efficient fluid power systems.

Technical Highlights

Combustion Research

Sandia National Laboratories is providing the scientific understanding needed to design, optimize, and calibrate the next generations of medium-duty diesel engines that comply with increasingly stringent pollutant emissions regulations while achieving thermal efficiencies exceeding 50%. In FY 2019, they (1) developed a conceptual model for turbulent flow evolution and vortex formation in stepped-lip combustion chambers, (2) identified combustion system design and/or operating parameters that are predicted to enhance vortex formation in stepped-lip combustion chambers for main injections starting near top dead center, (3) developed an experimental approach to study catalyst heating operation in the small-bore optical diesel engine and perform initial thermodynamic and high-speed imaging studies, and (4) began construction of the new medium-duty diesel research engine. (Busch, I.1)

Sandia National Laboratories conducted diesel combustion research in conjunction with combustion and flow modeling and simulation by Wisconsin Engine Research Consultants to develop a fundamental understanding of how in-cylinder controls can improve efficiency and reduce pollutant emissions of both conventional diesel and advanced low-temperature combustion; quantify the effects of fuel injection, mixing, and combustion processes on thermodynamic losses and pollutant emission formation; and improve computer modeling capabilities to accurately simulate these processes. In FY 2019, they (1) developed and applied diagnostics to quantify combustion-mode effects on heat transfer and efficiency; (2) used simulation predictions to guide and complement multiple-injection experiments; and (3) determined how mixing and jet interactions are affected by in-cylinder flows, the decay of spray-generated turbulence, large-scale structures, and/or entrainment wave effects on the bulk jet during the injection dwell. (Musculus, I.2)

Sandia National Laboratories is facilitating improvement of engine spray combustion modeling, accelerating the development of cleaner, more efficient engines and leading a multi-institution, international research effort on engine spray combustion called the Engine Combustion Network with a focus on diesel and gasoline sprays. In FY 2019, they (1) organized workshop activities for the Engine Combustion Network, including monthly web meetings, standards, and topic organization; (2) released comprehensive online Engine Combustion Network databases for diesel Spray D and Spray C; (3) investigated internal flow leading to a different rate of injection and mixture formation affecting diesel combustion; (4) developed a three-dimensional spray diagnostic for multi-hole gasoline direct-injection sprays, including liquid penetration and plume direction under cold-start and flash-boiling operation; and (5) characterized mixing and soot formation for multiple-injection sprays with wall impingement. (Pickett, I.3)

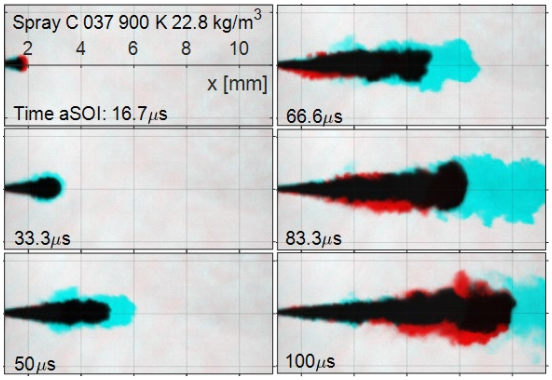

Figure 2 Overlaid, false-color long-distance microscopy images of Spray C #037 cooled (cyan, 90°C) and uncooled (red, 150°C) injectors. Overlapping regions are indicated in black, 900 K, 22.8 kg/m³, 0% oxygen gas. (Pickett, I.3)

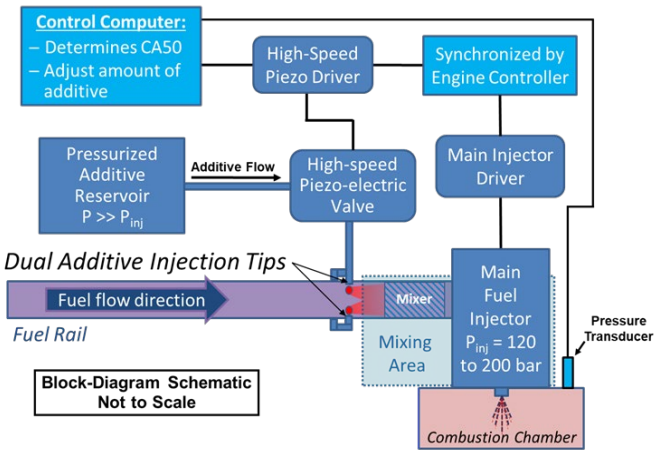

Figure 3 Block diagram of the additive-mixing fuel injection (Dec, I.4)

Low-temperature gasoline combustion (LTGC) engines have thermal efficiencies that meet or exceed those of diesel engines, giving them strong potential to improve internal combustion engine efficiency, reduce petroleum consumption, and lower CO_2 emissions. Sandia National Laboratories seeks to provide the fundamental understanding required to overcome technical barriers to LTGC engine development, as well as explore methods of exploiting this fundamental understanding to develop techniques that can overcome these barriers. In FY 2019, researchers conducted a range of experimental studies in the Sandia LTGC Engine Laboratory to further understand and demonstrate the capabilities of a new combustion-timing control method for LTGC engines, first introduced last year, called additive-mixing fuel injection. (Dec, I.4)

Sandia National Laboratories is working to achieve better understanding of ignition physical and chemical processes and use this information to develop more reliable engine simulation submodels. Relevant ignition processes include plasma formation from deposited electrical energy, plasma-to-flame transition, and flame kernel development. In FY 2019, researchers (1) evaluated the influence of ozone (O_3) addition on spark-assisted compression ignition strategies, (2) prototyped various pre-chamber and barrier discharge ignition systems, and (3) measured transient plasma ignition characteristics including potential O_3 formation. (Ekoto, I.5)

Argonne National Laboratory uses X-ray diagnostics of sprays to provide insight into the fundamentals of sprays and to generate quantitative data for development and validation of advanced injection simulations. In FY 2019, the research team (1) optimized the workflow for data analysis of X-ray tomography measurements of the internal flow passages of fuel injectors; (2) performed exploratory measurements using X-rays to probe the near-wall region of sprays impinging on surfaces, determined what measurement quantities are important

and feasible, and planned for the development of a built-for-purpose spray chamber for future spray–wall studies; and (3) completed first-of-their kind three-dimensional measurements of a cavitating diesel nozzle, including high-resolution measurements of the internal liquid and gas distributions. (Powell, I.6)

Fundamental data are needed to develop robust models that can be used to improve the understanding of the multiple physical and chemical processes that occur within combustion engines. Argonne National Laboratory is therefore using its rapid compression machine to acquire autoignition data at conditions representative of today's and future internal combustion engines and improve modeling capabilities. In FY 2019, researchers sought to quantify the autoignition behavior of binary olefin/aromatic blends with the aim of understanding and modeling chemical kinetic interactions. The team acquired autoignition data for binary blends of an iso-olefin, 2-methyl 2-butene, and an aromatic, covering wide ranges of temperatures, pressures, stoichiometries, and blending ratios. Researchers also improved previously developed scaling analyses to identify physical and chemical parameters that govern flame-driven compression ignition, with applications to mild ignition in rapid compression machines and to spark-assisted compression ignition in internal combustion engines. (Goldsborough, I.7)

Argonne National Laboratory is improving gasoline direct injection engine efficiency and expanding the tools to enable significant improvement of the current ignition technology. This project focuses on modeling conventional spark ignition as well non-conventional ignition technologies such as low-temperature plasma and pre-chamber ignition. In FY 2019, the project team (1) modeled a real low-temperature plasma ignition experiment and validated computational fluid dynamics results against experimental data, (2) explored low-temperature plasma ignition processes by evaluating the impact of plasma kinetics and fluid dynamics, (3) expanded low-temperature plasma studies to simulate advanced igniter geometries that are of interest to industry, and (4) planned future work to improve and expand conventional spark ignition models. (Scarcelli, I.8)

Researchers at Oak Ridge National Laboratory are using a thermodynamics-based approach to identify and pursue opportunities for improved efficiency in internal combustion engines. The specific combustion strategy is high dilution from exhaust gas recirculation for spark-ignited combustion enabled by fuel reforming through thermochemical recuperation. In FY 2019, researchers focused on the thermodynamics of consuming reformate in an engine, examining differences in the energy content of primary reforming products (H_2 and CO) between a 1st Law of Thermodynamics energy basis (enthalpy) and a 2nd Law of Thermodynamics basis

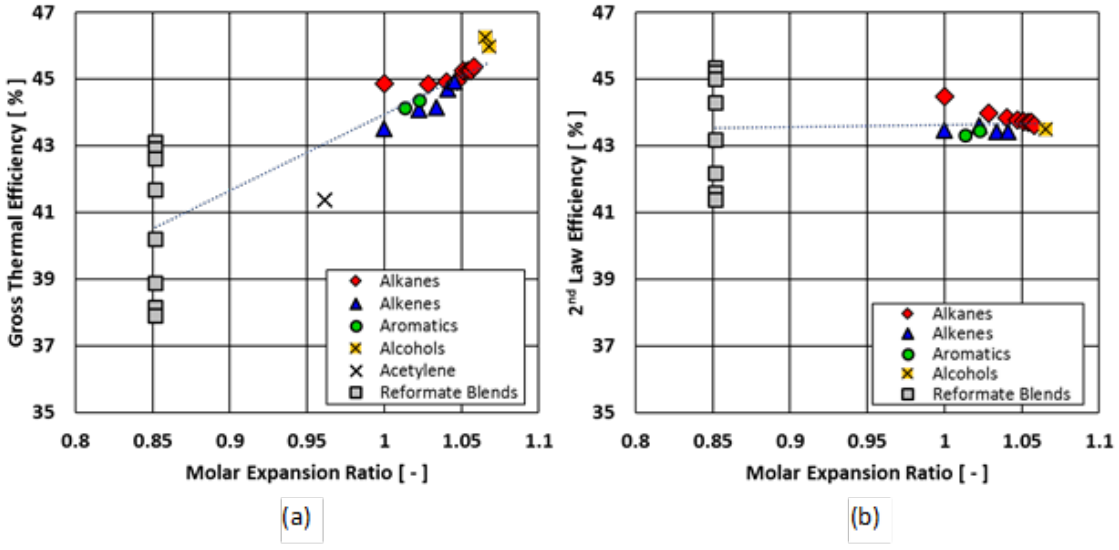

Figure 4 Simulated engine efficiency as a function of molar expansion ratio under stoichiometric conditions: (1) 1st Law of Thermodynamics basis and (b) 2nd Law of Thermodynamics basis (Syzbist, I.9)

(exergy)—a discrepancy that could be attributed to the molar expansion ratio. Oak Ridge National Laboratory completed an experimental investigation to improve understanding of molar expansion ratio's role in engine efficiency. (Szybist, I.9)

Oak Ridge National Laboratory is implementing high-fidelity neutron imaging capabilities using the High Flux Isotope Reactor (HFIR) and Spallation Neutron Source for advanced transportation research, with the specific objectives of improving design and control of complex advanced combustion systems and guiding model validation and input. The project's FY 2019 focus was to support improved fuel injector and spray models for predictive simulation. FY 2019 achievements include demonstrating neutron imaging of fuel injection in a dynamic capacity at the HFIR, showing the ability to both visualize and quantify internal injector dynamics, developing an approach to allow for quantitative measurement of "sub-pixel" displacement of the needle in a gasoline direct injector using ensemble neutron imaging of cyclic dynamic operation, developing a new experimental apparatus to enable dynamic imaging of all internal components of the Engine Combustion Network's Spray-G-style gasoline direct injector, and completing preliminary designs for a new spray chamber to enable imaging of spray impingement on a wall at various orientations. (Wissink, I.10)

Lawrence Livermore National Laboratory is developing predictive chemical kinetic models for gasoline, diesel, and next-generation fuels, as well as for fuel components used in surrogate fuels; combining component models into surrogate fuel models to represent real transportation fuels; and using these models to simulate advanced combustion strategies in engines. In FY 2019, it (1) developed fuel surrogate kinetic models with more representative components for real fuels to increase accuracy of autoignition predictions and to cover a range of real fuels; and (2) validated kinetic mechanisms over a range of temperature, pressure, and equivalence ratio conditions relevant to engine combustion. (Pitz, I.11)

Lawrence Livermore National Laboratory is advancing the state of the art in engine simulation through the development of fast and accurate models and working with industry partners to prove capability and impact of combustion chemistry software. In FY 2019, it (1) investigated the impact of reduced mechanisms on engine simulation results, (2) developed fast solvers for one-dimensional diffusion flames, and (3) released Zero-Order Reaction Kinetics software as open-source. (Whitesides, I.12)

Los Alamos National Laboratory is developing mathematical and computer algorithms and software to advance speed, accuracy, robustness, and range of applicability of FEARCE, an internal combustion engine modeling software, to be a more predictive computer code. In FY 2019, Los Alamos National Laboratory (1) developed a four-valve direct-injection, spark-ignition (DISI) engine system for validation of FEARCE, (2) validated progress of FEARCE on experimental data of the four-valve DISI engine; collaborated with Dr. Magnus Sjöberg of Sandia National Laboratories on the DISI setup and experimental data, (3) constructed systems to use Chemkin reactive chemistry software, (4) continued spray model development for both predictive spray break-up and subsequent droplet transport and droplet fate, and (5) continued the process of commercialization of FEARCE. (Carrington, I.13)

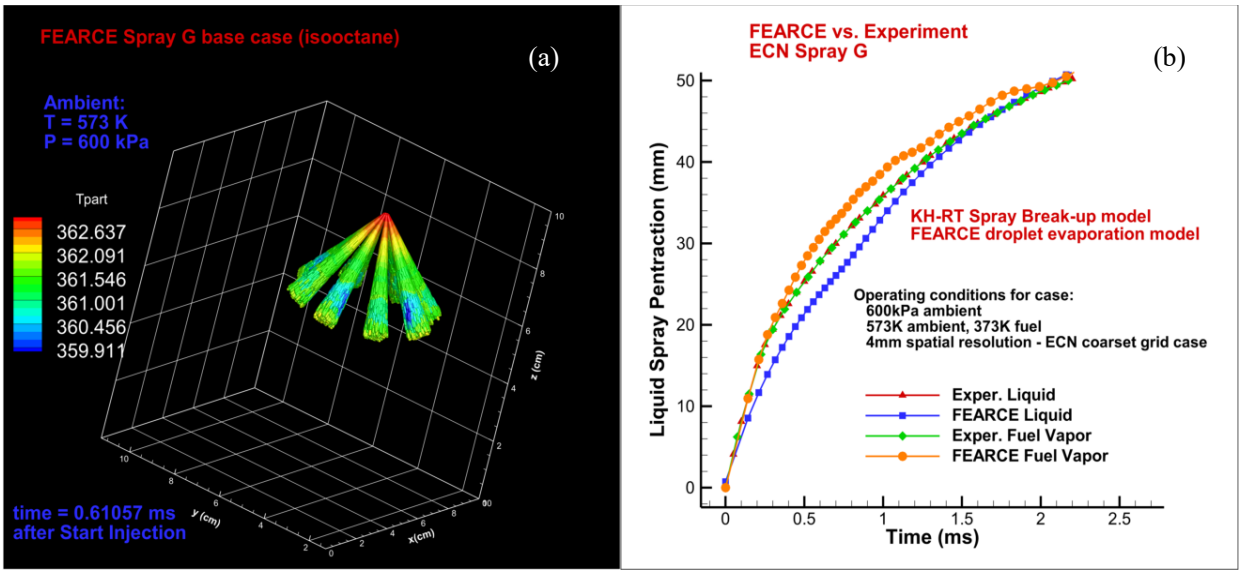

Figure 5 The Engine Combustion Network (ECN) Spray G case: injection of gasoline in quiescent nitrogen at 600 kPa, with (a) showing the Kelvin Helmholtz–Rayleigh Taylor (KH-RT) spray model and (b) showing the penetration depth of the liquid spray and vapor compared to ECN experimental data (Carrington, I.13)

Oak Ridge National Laboratory supported a multi-year collaborative effort using high-performance computing resources and graphic-processing-unit-enabled numerical solvers to evaluate the impact of increased simulation detail on the predictive accuracy and computational needs of computational fluid dynamics engine simulations. In FY 2019, it (1) refined the conjugate heat transfer modeling approach coupled with Reynolds-Averaged Navier–Stokes and large eddy simulation turbulence submodels, (2) evaluated the impact of these model refinements on predictive accuracy and computational requirements, and (3) adapted modeling tools for use on new high-performance computing resource and evaluated improvements in computational capabilities for engine simulation. (Edwards, I.14)

Argonne National Laboratory focused on fundamental understandings that inform advanced compression ignition use in a multimode operating strategy in FY 2019 to (1) evaluate advanced compression ignition control methodologies by utilizing static autoignition data and (2) develop an active pre-chamber ignition system for advanced compression ignition operation. (Rockstroh, I.15)

Argonne National Laboratory focused on developing the Nek5000 computational fluid dynamics platform into an effective exascale code for high-fidelity internal combustion engine simulations. This involves implementing the state-of-the-art submodels for combustion, spray, and ignition and validating against several benchmark engine experiments. These efforts will enable high-fidelity internal combustion engine simulations with minimal numerical inaccuracies. In FY 2019, the project (1) demonstrated the ability to quantitatively predict flow, including variability, under high-load and low-load conditions; (2) improved the capability of Nek5000 to model turbulent reacting flows; and (3) demonstrated the scalability of the engine simulations on leadership class machines. (Ameen, I.16)

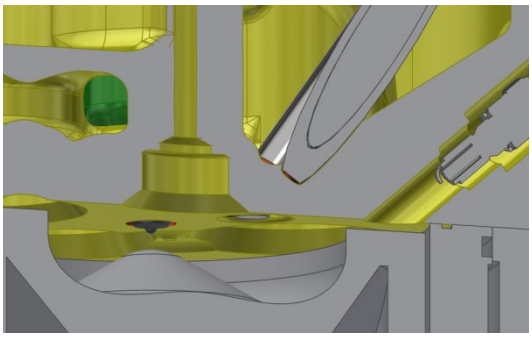

Figure 6 Cross-section view of single-cylinder heavy-duty Caterpillar research engine at Argonne National Laboratory (Kolodziej, I.17)

Argonne National Laboratory characterized the particulate emissions between diesel and gasoline mixing-controlled compression ignition combustion at high load and

demonstrated spark-ignition combustion as a possible solution to gasoline compression-ignition engine combustion stability at low load and idle in FY 2019 by (1) demonstrating low-load operation of a high-compression-ratio gasoline compression-ignition engine using knock-free spark-ignition combustion with good combustion stability and (2) measuring the particulate morphology of gasoline and diesel mixing-controlled compression ignition combustion at high load. (Kolodziej, I.17)

Argonne National Laboratory developed the cavitation-induced erosion risk assessment (CIERA) tool to allow for qualitative and quantitative predictions of erosion likelihood and severity. In FY 2019, it (1) developed and implemented a framework to quantify the incubation period, or time before material removal; (2) benchmarked the predictive capability of CIERA against standard approaches through comparison against available optical data from the literature; (3) identified best practices for predicting cavitation and erosion using the mixture modeling approach; (4) implemented representative interactive flamelet – in situ tabulation (RIF-ist) in the CONVERGE code; (5) performed extensive quantitative validation against gas jet flames followed by high-pressure spray flames; and (6) coupled the RIF-ist approach with detailed soot models and demonstrated prediction of slow-forming species and soot emissions. (Som, I.18)

Co-Optimization of Fuels and Engines

The U.S. Department of Energy (DOE) Co-Optimization of Fuels and Engines (Co-Optima) initiative is accelerating the introduction of efficient, clean, affordable, and scalable high-performance fuels and engines. FY 2019 marked the start of Co-Optima's second and final three-year phase. With boosted spark-ignition (SI) light-duty (LD) engine research completed in FY 2018, the initiative focused on LD multimode approaches that combine SI and other forms of combustion (e.g., advanced compression ignition [ACI]) to increase LD vehicle fuel economy. FY 2019 also marked the completion of much of the medium- and heavy-duty (MD/HD) mixing-controlled compression-ignition research and increased focus on MD/HD ACI combustion research. The Co-Optima initiative has provided new knowledge has spurred promising research directions and led to unanticipated observations—for example, established fuel properties predict performance for some ACI approaches but not others—that have been important for developing research plans for FY 2020 and beyond. Recent Co-Optima accomplishments have also significantly improved the state of the art in fuel kinetics and engine simulations. (Wagner, II,1)

Oak Ridge National Laboratory is studying how differing high-octane fuel formulations can be used to enable increased engine efficiency and estimating the magnitude of the effect that increased engine efficiency has on vehicle fuel economy. Researchers provide assessments of the potential benefits offered by improving gasoline octane ratings to support technoeconomic evaluations of potential future biofuel formulations in the United States, focusing on aspects of high-load, boosted spark ignition operation as a part of a multi-mode combustion strategy that utilizes advanced compression ignition at part-load conditions to improve efficiency. In FY 2019, the project (1) completed publication of the U.S. DRIVE (United States Driving Research and Innovation for Vehicle efficiency and Energy sustainability) Fuels Working Group High-Octane Fuels Study Report, (2) determined the relationship between fuel properties and the R factor for fuel economy calculation, and (3) initiated a study to examine whether boosted spark ignition operation at high loads and speeds is limited by motor octane rating rather than research octane rating. (Sluder, II.2)

Co-Optima's FY 2018 findings led to questions about ACI kinetics and the properties of the fuels used to study ACI. To address these questions, Oak Ridge National Laboratory (ORNL) partnered with General Motors Company to install a new single-cylinder engine that is capable of operating in a production-intent ACI combustion strategy. ORNL also partnered with Shell Global Solutions to develop a fuel matrix that is representative of fuels that are possible to make in a refinery (rather than using high concentrations of single-component fuels). In addition, the researchers developed an experimental matrix that allows them to see several fuel-specific differences at various engine operating conditions. (Szybist, II.3)

Figure 7 The new single-cylinder engine at ORNL, used to investigate multimode combustion for Co-Optima (Szybist, II.3)

Sandia National Laboratories is providing the science base needed to understand how emerging alternative fuels impact highly efficient direct-injection spark-ignition light-duty engines being developed by industry, elucidating how engine design and operation can be optimized for clean and efficient use of future fuels, and developing and applying advanced optical diagnostics for probing in-cylinder processes. In FY 2019, they (1) clarified why particulate matter index fails to predict engine-out soot particulate matter for boosted stratified-charge spark-ignition engine operation, (2) determined the octane requirement of a multimode engine that uses mixed-mode combustion at low to moderate loads, and (3) quantified the potential of a multimode engine to increase vehicle fuel economy. (Sjöberg, II.4)

To understand the effect of future renewable fuels on sprays, Sandia National Laboratories has acquired temporally and spatially resolved liquid volume fraction measurements of liquid plume position and dynamics for a range of fuels. The understanding provided by these unique datasets motivates the design and optimization of gasoline direct-injection systems that respond well to a wide variety of future renewable fuels. In FY 2019, researchers (1) developed a high-throughput facility and diagnostics for ensemble-average liquid volume fraction from computed tomography of high-speed extinction imaging, (2) completed a large database including more than a dozen fuels and operating conditions spanning intake flash-boiling to late injection, and (3) measured end-of-injection dribble and liquid film deposits on the injector for a range of conditions. (Pickett, II.5)

Engines using low-temperature gasoline combustion (LTGC) have the potential to reduce fuel costs and CO_2 emissions by 30% or more over current spark-ignition (SI) engines. It is critical to understand the effects of fuel properties on autoignition under LTGC-like conditions, including temperatures, pressures, and high dilution levels typical of these engines. In FY 2019, Sandia National Laboratories evaluated eight different fuels under well-premixed LTGC conditions with the same intake temperature. The research team found that the octane index gives a very poor correlation for the autoignition timing of naturally aspirated LTGC and that the lean mixtures used for LTGC were the biggest factor in causing the octane index to perform poorly for LTGC combustion. Researchers also evaluated a new custom fuel blend designed to improve LTGC performance compared to regular gasoline, finding that a fuel with properties similar to the blend would be better than regular gasoline for LTGC, SI, boosted-SI, or multimode LTGC-SI engines. (Dec, II.6)

Oak Ridge National Laboratory uses single-cylinder engine experiments to characterize potential fuel consumption benefits of various multimode advanced compression ignition (ACI) operating modes over state-of-the-art spark-ignited (SI) engines. In FY 2019, the project team (1) quantified the impact of fuel chemical function characteristics on spark-assisted and kinetically controlled compression ignition strategies focused on multimode operation, (2) demonstrated the performance of ACI strategies on a 12:1 compression ratio engine and the effect of the fuel choice on the maximum SI achievable load, and (3) quantified the trade-off between ACI and SI performance due to fuel chemistry effects on the required intake pressure and temperatures at a relatively low compression ratio with a wide range of Co-Optima core fuels. (Curran, II.7)

Oak Ridge National Laboratory sought clarity on the relationship between fuel properties and low-speed pre-ignition (LSPI). Downsized and turbocharged spark-ignited engines are greatly effective at improving fuel economy, but the increased specific outputs of these engines make them more prone to damaging phenomena such as LSPI. In FY 2019, the project team confirmed that LSPI number count is highly correlated to fuel–wall interaction, illustrated that lubricant effects are independent of only fuel–wall interaction, and developed a new engine platform to investigate fuel property effects on fuel–wall interactions relevant to LSPI. (Splitter, II.8)

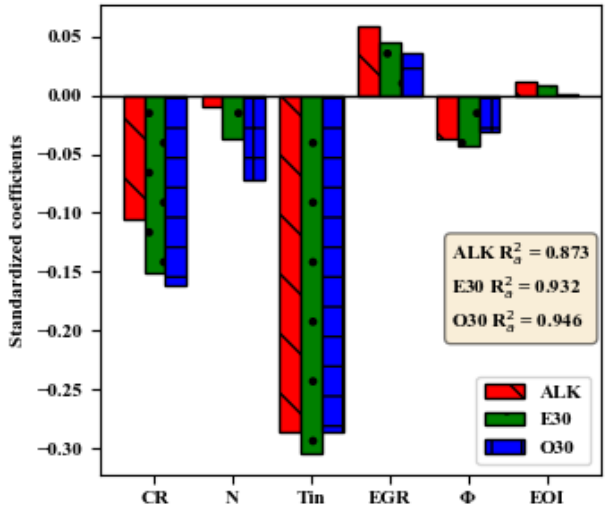

Figure 8 Impact of engine control parameters on the intake pressure requirement over all test conditions (Rockstroh, II.9)

Researchers at Argonne National Laboratory investigated five Co-Optima gasolines with different octane sensitivities. The purpose was to characterize the ignition delay behavior of the fuels over a range of engine-relevant conditions using experimental data from a rapid compression machine (RCM) and chemical kinetic simulation. The researchers successfully demonstrated the use of static autoignition delay data to generate fuel reactivity maps, which can be implemented in advanced compression ignition (ACI) engine control strategies for combustion phasing control in a multimode spark-ignition engine. Furthermore, the team investigated correlations between the engine control parameters and the thermodynamic state at the time of autoignition, ultimately correlating engine boost requirements to compressed pressure in an RCM over a range of intake temperatures and two equivalence ratios. In addition, the team completed a design of experiments study to correlate the engine control parameters on the ACI operating range in a multimode engine platform to distinguish fuel-specific effects on operating parameters. (Rockstroh, II.9)

Argonne National Laboratory is investigating how the physical properties of vehicle fuels affect the fuel injection process and the mechanisms of spray atomization. Researchers study the mixture formation in a spray chamber under conditions that mimic a gasoline direct-injection engine. The research team performed three-dimensional X-ray tomography measurements that quantify the near-nozzle fuel distributions under flash-boiling conditions for three alcohol fuel blends. With these same fuel blends, researchers performed ultra-small-angle X-ray scattering measurements to determine two-dimensional distributions of the near-nozzle surface area. Near-nozzle density and surface area were combined to build a map of the Sauter mean diameter in the near-nozzle spray atomization region. These experiments successfully quantified the near-nozzle fuel density distribution, surface area, and Sauter mean diameter of flash-boiling sprays across a range of fuel properties. (Powell, II.10)

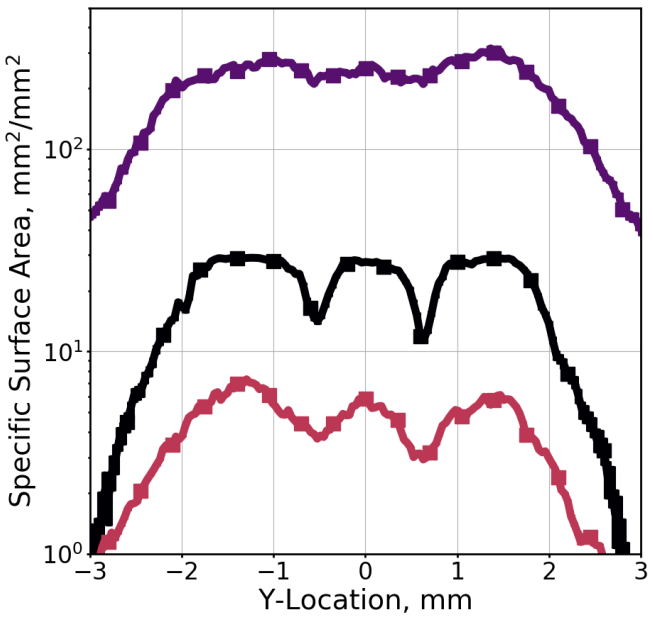

Figure 9 The surface area of fuel droplets as a function of position for three fuel blends at a distance 1 mm from the fuel injector (Powel, II.10)

Argonne National Laboratory identified the effects of fuel composition and engine intake conditions on combustion, autoignition, and knocking characteristics in FY 2019 by (1) developing a better understanding of the synergistic octane blending behavior of prenol in different base fuels, (2) investigating the correlation of a lean advanced compression ignition fuels rating metric on the Cooperative Fuel Research octane rating engine compared to modern advanced compression ignition multimode engines, and (3) creating a new test methodology to experimentally characterize the low-temperature chemistry of stoichiometric mixtures. (Kolodziej, II.11)

Argonne National Laboratory addresses challenges associated with measuring the autoignition properties of potential future fuels and fuel blends, interpreting their performance in combustion engines (in terms of knock and combustion phasing), and properly modeling their behavior in zero- and multi-dimensional simulation frameworks. This project acquired data for select high-performance fuels (i.e., isoalcohols) blended into a research-grade gasoline, covering a range of thermodynamic conditions and a range of blending levels. The team also acquired autoignition measurements for a representative ether, covering a range of thermodynamic conditions. (Goldsborough, II.12)

Sandia National Laboratories is developing advanced combustion strategies for mixing-controlled compression-ignition engines that are synergistic with renewable and/or unconventional fuels in a manner that enhances domestic energy security, economic competitiveness, and environmental quality. FY 2019 work aimed to determine the extent to which the use of oxygenated fuels, when combined with ducted fuel injection (DFI) and charge-gas dilution, can simultaneously lower the soot and nitrogen oxide (NO_x) emissions from mixing-controlled compression-ignition engines, as well as the corresponding impacts on other regulated emissions and efficiency. The research team concluded that employing DFI in combination with only 25 vol% of an oxygenated fuel can curtail in-cylinder soot incandescence by approximately two orders of magnitude for the two-duct configuration employed in this study. One order of magnitude comes from using DFI, and the second comes from blending with the oxygenated fuel. (Mueller, II.13)

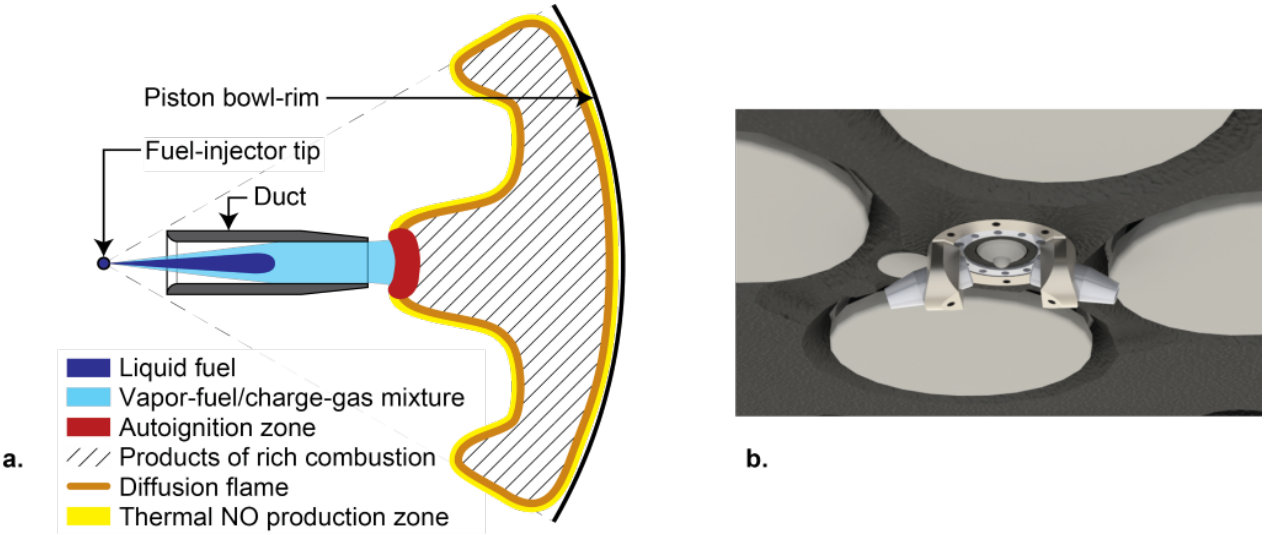

Figure 10 (a) Schematic of DFI with a single duct. (b) Rendering of the two-duct assembly installed in the optical engine. (Mueller, II.13)

National Renewable Energy Laboratory is developing experimental and simulation tools to characterize fuel ignition behavior in support of advanced combustion engine development; supporting the development of research fuels, surrogates, and blends, and related reduced kinetic mechanisms to further enable codevelopment of advanced combustion engines and high-performance fuels; linking bench-scale, constant-volume combustion-chamber-based fuel ignition measurements to single-cylinder research engine studies to enable rapid predictive feedback of engine performance for complex fuel blends; and developing

understanding of fuel chemical and physical properties that enable co-optimization of high-performance fuels and high-efficiency engines. In FY 2019, researchers (1) developed constant-volume combustion-chamber-based ignition delay measurements to quantify ϕ-sensitivity for fuels showing ϕ-sensitivity in published engine combustion studies and (2) supported development of a ϕ-sensitivity metric to apply to fuel screening for ACI and multimode strategies. (Zigler, II.14)

National Renewable Energy Laboratory is using a simple, straight quartz tube flow reactor connected to a dual gas chromatograph system to analyze autoignition products and soot precursor molecules to gain insight into skeletal reaction mechanisms. Researchers tested the ability of the flow reactor to observe ϕ-sensitivity using heptane and primary reference fuels by varying ϕ and residence time at low temperatures. It was determined that operation at elevated pressures is required to clearly observe ϕ-sensitivity; work is under way to increase operational pressure up to 10 bar. The project also measured methylpropyl ether autoignition in the flow reactor at two residence times to validate the kinetic mechanism. These data were used to improve a kinetic model that was developed at Massachusetts Institute of Technology. The researchers used flow reactor results in combination with quantum mechanical calculations to explain the differences in yield sooting index (an experimentally measured parameter for the sooting tendency of a molecule) values from the different isomers. (Fioroni, II.15)

Lawrence Berkeley National Laboratory is developing scenario co-optimization software as part of the Co-Optima effort. The co-optimizer gives experimentalists and computational scientists an easy-to-use optimizer that enables them to autonomously steer their laboratory experiments and to optimize the parameters in their simulation models, respectively. This project is adding new capabilities: bi-level optimization, constrained optimization, and the use of different types of surrogate models that steer experimentation and can be used to quantify the uncertainty of experimental outcomes across the experimental domain. In FY 2019, the team developed, verified, and demonstrated new bi-level optimization capabilities with surrogate modeling. The team also demonstrated the methods' efficiency and effectiveness on real engine data provided by Oak Ridge National Laboratory and National Renewable Energy Laboratory, as well as a simulation model from Lawrence Livermore National Laboratory. In addition, the project extended surrogate modeling capabilities to radial basis functions and demonstrated that surrogate model predictions are sensitive to outlier data, indicating that expert knowledge is needed when selecting data for training the surrogate. (Mueller, II.16)

Pacific Northwest National Laboratory seeks to advance understanding of the role of molecular-level solution structures, such as clustering, hydrogen-bonding networks, and crystallization, on fuel properties in a finished fuel. The research team is using nuclear magnetic resonance spectroscopic measurements and molecular dynamics simulations to develop predictive models that correlate molecular-level solution structures within fuel components to fuel properties and performance. During FY 2019 work, alcohol clusters and hydrogen-bonding networks for C1–C4 alcohols were observed in single-component surrogate fuels, as well as in gasoline. Researchers determined that alcohol concentration, the nature of the alcohol and of the fuel, and temperature influence the balance between cluster size and population and the extent of hydrogen-bonding network formation. (Bays, II.17)

As part of the Co-Optima initiative, Oak Ridge National Laboratory is using targeted flow reactor studies to evaluate the compatibility of Co-Optima candidate blendstocks with emissions control catalysts and identify opportunities for alternative emissions control strategies that make use of novel fuel chemistry. In FY 2019, the project team measured catalyst light-off for a series of binary, ternary, and quaternary blends of Co-Optima blendstocks to determine why fuel blends containing up to 30% of several different Co-Optima blendstocks all show similar catalyst light-off performance, even though the pure blendstocks have substantially different catalytic reactivity and surrogate blendstock for oxygenate blending (BOB) components. The team determined that aromatic constituents inhibit the catalytic reactivity of other fuel components, resulting in similar catalyst light-off temperatures for fuel blends containing similar levels of aromatics. (Pihl, II.18)

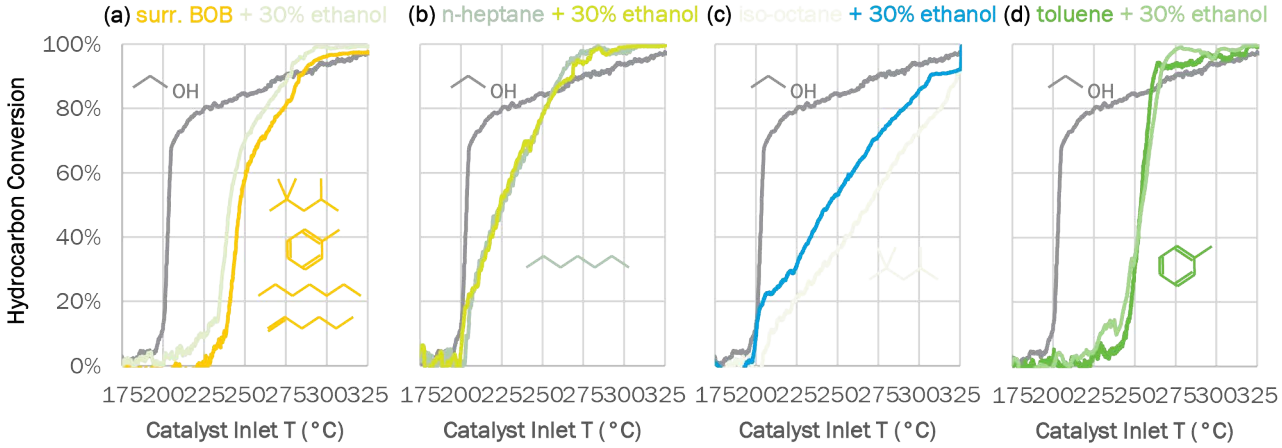

Figure 11 Hydrocarbon conversion vs. three-way catalyst inlet temperature under stoichiometric synthetic exhaust conditions for pure fuel components (dark lines) and 30% ethanol blends (light lines) with (a) a surrogate BOB containing 55% iso-octane, 25% toluene, 15% n-heptane, and 5% 1-hexene; (b) n-heptane; (c) iso-octane; and (d) toluene. The conversion of pure ethanol is denoted by the gray line in each chart, and the chemical structures of the fuel components in each experiment are shown within their respective charts. (Pihl, II.18)

Oak Ridge National Laboratory investigated the effects of fuel properties on particulate matter and gaseous emissions and how fuel property changes impact emissions across the potential range of air–fuel stratification modes. In FY 2019, it (1) quantified the impact of fuel aromatic content and fuel distillation curve on advanced compression ignition particulate matter mass emissions; (2) demonstrated how changes in the level of air–fuel stratification during advanced compression ignition combustion influence all forms of hydrocarbon emissions, including particulate matter and both oxygenated and non-oxygenated gaseous species; and (3) quantified the changes in hydrocarbon emission speciation as air–fuel stratification varies from fully premixed to highly stratified within potential advanced compression ignition modes of the multimode operating space. (DeBusk, II.19)

Lawrence Livermore National Laboratory is developing and improving chemical kinetic models for high-performance fuels and base fuels and using the models to simulate combustion properties at boosted spark ignition, advanced compression ignition, and mixing-controlled compression ignition engine conditions. In FY 2019, it (1) developed and improved chemical kinetic models for 5–7 high-performance fuels and base fuels for multimode, advanced compression ignition, and mixing-controlled compression ignition engine conditions so that the kinetic models accurately predict fuel behavior at engine conditions and (2) predicted sooting propensity behavior of mixing-controlled compression ignition blendstocks when blended into a diesel base fuel. (Pitz, II.20)

Lawrence Livermore National Laboratory is demonstrating new Co-Optima tools for stakeholders to evaluate a blendstock's potential with respect to market estimates. In FY 2019, it (1) assessed the validity of the Central

Fuel Hypothesis with respect to using the octane rating of a blendstock for oxygenate blending (BOB) to capture its blending performance with oxygenates and bio-derived hydrocarbons; (2) quantified the potential to optimize the BOB and finished fuel performance using a chemical kinetic model for the inputs to the boosted spark-ignition merit function, specifically, the research octane number and the octane sensitivity; (3) coordinated with the Co-Optima Fuel Properties Team to test the BOB and blendstock combinations found in the virtual fuel search to have the largest variation in the boosted spark-ignition merit score; and (4) validated the model octane predictions using new test data collected using the ASTM standard measurements for research octane number (D2699) and motor octane number (D2700). (McNenly, II.21)

To better understand fuel–engine interactions under different operating conditions, Argonne National Laboratory has developed computational fluid dynamics (CFD) models for four engine platforms that cover the full spectrum of multimode combustion. Recognizing that knock is a major bottleneck to achieving higher thermal efficiency in boosted spark-ignition combustion, the research team developed a new, more efficient model to study fuel effects on knock-limited spark advance and indicated thermal efficiency with knock constraint. To study the advanced compression ignition mode of combustion, researchers conducted a CFD study to reveal the correlation between mixture/thermal stratification and cylinder wall temperature and their impact on combustion phasing control. A computational framework using a hybrid combustion modeling strategy in CFD was developed for lean mixed-mode engine operation and was demonstrated to be able to capture pressure and heat release rate traces, as well as cyclic variability. The new computational model was then leveraged to investigate effects of NO_x chemistry and different fuel properties through sensitivity analysis. (Som, II.22)

The University of Alabama is accelerating deployment of co-optimized fuels and engines that will reduce fuel consumption, criterion pollutants, and greenhouse gas emissions. Specifically, it will acquire combustion measurements in a constant pressure flow rig with optical access and develop models to predict combustion characteristics based on known fuel and ambient conditions. In FY 2019, it (1) integrated time-resolved diagnostics systems to the test facility; (2) acquired simultaneous data at diesel conditions using over 400 injections in quick succession; and (3) analyzed rainbow schlieren deflectometry, OH* chemiluminescence, and two-color pyrometry data to describe the flame evolution process. (Agrawal, II.23)

The University of Michigan is developing new computational fluid dynamics tools to increase computational efficiency for multi-cycle simulations while maintaining accuracy by dynamic species reduction (DSR) during open valve events, thereby retaining the species of greatest importance to cyclic feedback effects. These tools will reduce the computational expense of a full-engine-cycle simulation with chemistry and allow the Co-Optima team to efficiently perform multi-cycle simulations to capture prior-cycle compositional and thermal effects while improving numerical accuracy. In FY 2019, the research team completed baseline simulations for DSR and completed and demonstrated the project's DSR model for two types of engine combustion conditions, observing good agreement with baseline simulations. (Middleton, II.24)

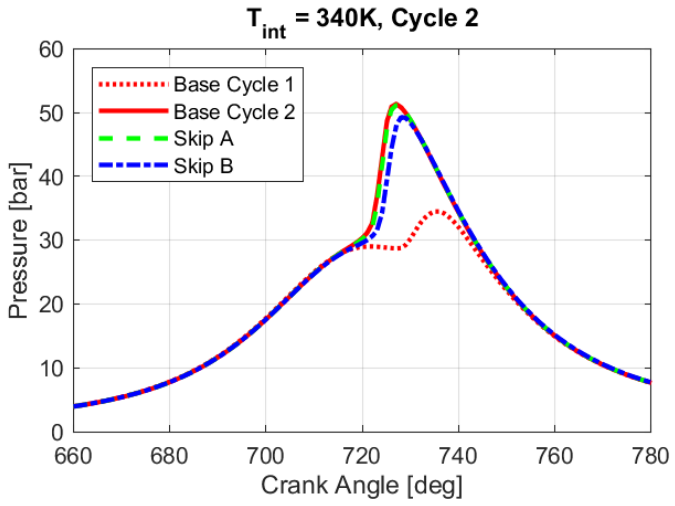

Figure 12 Second-cycle predictions for an advanced compression ignition engine operating condition, showing two configurations of DSR replicating the detailed baseline predictions (Middleton, II.24)

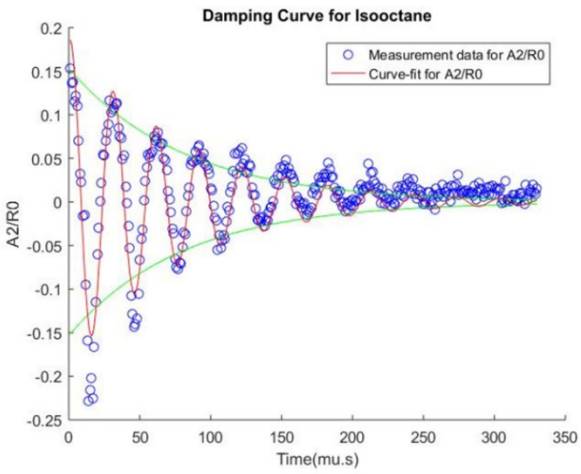

Figure 13 Sample damping curve for iso-octane. Data are used for physical property measurements, e.g., viscosity and surface tension. (Schoegl, II.25)

Louisiana State University, Texas A&M University, and the University of Connecticut have joined forces as part of the Co-Optima initiative, seeking to establish a foundation for small-volume, high-throughput fuel testing, where relevant fuel metrics are quantified in a micro-combustion experiment. The approach for micro-liter fuel characterization relies on cyclical combustion events within a heated micro-tube. This combustion mode is known as FREI (Flames with Repetitive Extinction and Ignition) and relies on self-excited instabilities that are sensitive to fuel properties. In FY 2019, the project team used micro-combustion tests at an intermediate pressure to demonstrate the existence of relevant combustion phenomena up to 10 bar. Researchers obtained new results showing the loss of an unstable combustion regime at diluted conditions, creating new pathways for fuel testing at high pressures. The project also quantified droplet oscillation to measure surface tension and viscosity with 20% accuracy. (Schoegl, II.25)

Yale University and The Pennsylvania State University are collaborating to gather and develop information that describes the effects of biofuel composition on soot formation. This project has defined a fundamental fuel property called yield sooting index (YSI) that quantifies the tendency of fuels to form particulates in combustion systems. The key advantage of YSI is that it enables high-throughput measurements with low sample volumes (<0.1 mL), which allowed over 50 biofuels to be tested in FY 2019. These measurements showed that properly chosen biofuels have the potential to reduce soot formation in internal combustion engines. Since YSI employs a well-defined laboratory-scale flame, the results can be simulated numerically. Simulations in FY 2019 validated detailed chemical kinetic mechanisms, identified key reaction pathways, and provided insight into the emissions characteristics of hypothetical fuels that have not yet been synthesized. (Pfefferle, II.26)

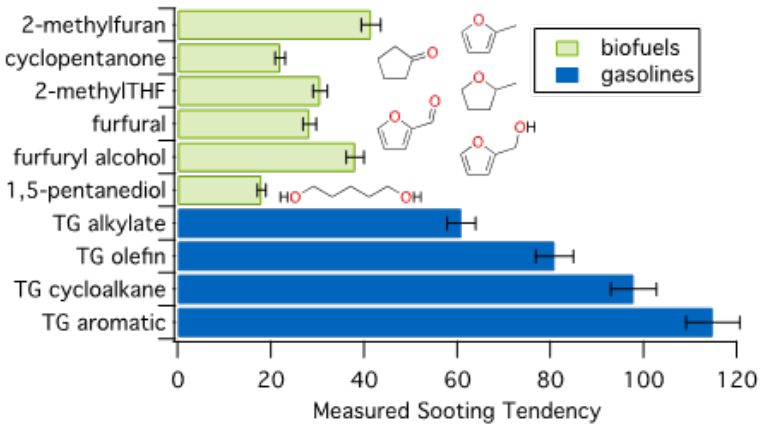

Figure 14 Sooting tendencies measured for several carbohydrate-derived biofuel molecules and for the Co-Optima test gasolines. A larger value corresponds to a sootier fuel. THF = tetrahydrofuran; TG = Co-Optima test gasoline. (Figure: Charles McEnally, Yale) (Pfefferle, II.26)

Alternative Fuel Engines

Colorado State University is addressing fundamental limitations to achieving diesel-like efficiencies in heavy-duty on-road natural gas engines. Its main project goal is to increase the peak torque efficiency. In FY 2019, it (1) designed, assembled, and tested an exhaust gas recirculation cart for cooperative fuel research engine testing; (2) demonstrated the effect of exhaust gas recirculation on flame speed and end-gas autoignition in the cooperative fuel research engine and rapid compression machine; (3) validated a reduced chemical kinetic

mechanism for use in engine and rapid compression machine modeling; and (4) completed CONVERGE and GT-Power models of the cooperative fuel research engine and validated with blind tests. (Olsen, III.1)

To enable highly efficient natural gas combustion engines, University of Minnesota Twin Cities is converting a small portion of the incoming methane-containing natural gas to more reactive, higher-molecular-weight hydrocarbons using a catalytic reaction called oxidative coupling of methane (OCM). These more reactive hydrocarbons created by the OCM process can influence combustion at low (<10%) concentrations in the intake air and can enable highly efficient natural gas engine combustion modes. In FY 2019, researchers (1) selected a Sr/La_2O_3 catalyst for all future project work based on its selectivity and conversion at low temperatures, (2) evaluated the short-contact-time reactor concept in both experiments and simulation, and (3) achieved the first budget period go/no-go milestone of greater than 10% methane conversion and 20% selectivity to C2 hydrocarbon products that may consist of ethane, ethylene, and acetylene. (Northrop, III.2)

Southwest Research Institute focused on improving the efficiency of a gasoline engine by using advanced petroleum and bio-derived fuels in a dedicated exhaust gas recirculation (D-EGR) engine in FY 2019 by (1) quantifying the impact of refinery fuel blending on hydrogen production in the dedicated cylinder of a D-EGR engine and (2) demonstrating a 25% reduction in petroleum consumption through a combination of D-EGR engine operation, optimized refinery fuel blending, and bio-derived fuel component addition. (Briggs, III.3)

Oak Ridge National Laboratory utilized the unique properties of propane to enable higher efficiency in direct injection engines in FY 2019 to (1) understand unique opportunities of propane for high compression ratio and dilution tolerance in stoichiometric spark-ignition operation with increased stroke and overexpansion, (2) quantify products and enthalpy balance of propane catalytic reforming over a range of temperature and space velocity conditions, and (3) develop a high-pressure fueling system to supply direct injection fuel rail pressure to the multi-cylinder engine. (Szybist, III.4)

Argonne National Laboratory, National Renewable Energy Laboratory, Oak Ridge National Laboratory, and Sandia National Laboratories are collaborating to investigate fundamental combustion processes for pre-chamber spark-ignition (PCSI) concepts to enable diesel-like efficiency in medium- and heavy-duty natural gas engines. This project involves early-stage research to achieve this efficiency by extending the lean dilution limit and/or exhaust gas recirculation dilution limit, as well as shortening burn duration, with integrated aftertreatment. The project has designed a modular PCSI system, sharing key design parameters and maintaining as much commonality as possible across bench-scale, single-cylinder engine (SCE), and multi-cylinder research engine platforms. Other FY 2019 activities include performing SCE simulations with CONVERGE computational fluid dynamics, modifying the Advanced Fuel Ignition Delay Analyzer to adapt a PCSI module in place of the existing piezoelectric diesel injector, modifying an existing direct-injection heavy-duty optical SCE for a natural gas PCSI to study pre-chamber output penetration to the main chamber and characterize flame propagation versus sequential autoignition, exploring a new approach to characterizing engine thermodynamics to provide insight on how

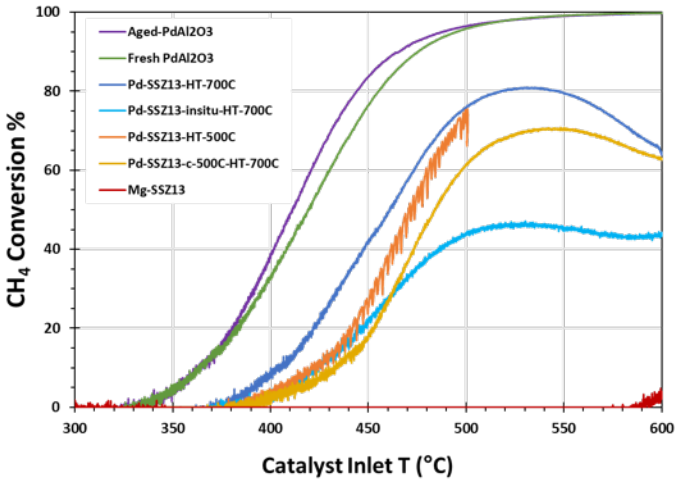

Figure 15 Methane oxidation catalyst light-off curve (figure: Melanie Debusk, Oak Ridge National Laboratory) (Zigler, III.5)

PCSI shifts the thermodynamic balances, and developing a new methane oxidation catalyst for lower-temperature conversion. (Zigler, III.5)

National Renewable Energy Laboratory is conducting early-stage research to understand fundamental challenges and potential for propane blends to support advanced compression ignition using direct injection. Laboratory researchers previously conducted scale experiments to understand how propane behaves with the high-pressure direct-injection fuel injector types required for injecting fuel during the compression stroke. FY 2019 research expanded these bench-scale injection control studies to span a range of fuel properties, including those of propane. The project also continued adapting the Advanced Fuel Ignition Delay Analyzer constant-volume combustion chamber platform to conduct experiments on propane blend ignition delay performance under advanced compression-ignition-relevant conditions. (Zigler, III.6)

Emission Control R&D

The Crosscut Lean Exhaust Emissions Reduction Simulations (CLEERS) activity supports development of improved computational tools and data for simulating realistic full-system performance of high-efficiency engines and associated emissions control systems. Oak Ridge National Laboratory (ORNL) coordinates CLEERS activities and collaborates across sectors to conduct focused measurement, analysis, and modeling activities aimed at developing the strategies, data sets, and device parameters needed for better models of catalytic emissions control devices. FY 2019 administrative efforts included organizing a CLEERS workshop and facilitating CLEERS focus group teleconferences. ORNL also supported the Advanced Combustion and Emissions Control Tech Team's Low-Temperature Aftertreatment Team in developing evaluation protocols for low-temperature catalysts and identifying future research directions. In addition, ORNL conducted extensive experiments to measure the impacts of exhaust gas composition and temperature on the storage and release of nitrous oxide (NO) on a Pd-exchanged zeolite passive NO_x adsorber material. Researchers developed and revised a conceptual mechanism to explain trends in both NO storage capacity and uptake rates. (Pihl, IV.1)

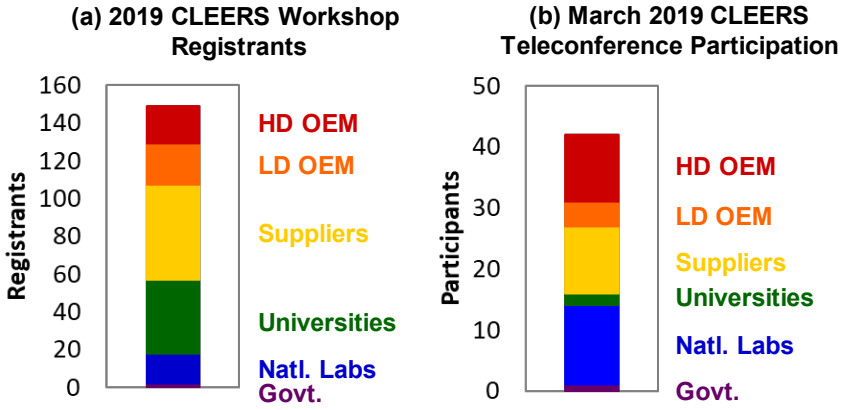

Figure 16 (a) 2019 CLEERS Workshop registrations and (b) March 2019 CLEERS teleconference participants by type of organization (HD – heavy-duty, LD – light-duty, OEM – original equipment manufacturer) (Pihl, IV.1)

Through the Crosscut Lean Exhaust Emissions Reduction Simulations initiative, Pacific Northwest National Laboratory supports fundamental research projects in four topic areas: selective catalytic reduction (SCR), passive NO_x (oxides of nitrogen) adsorbers (PNAs), multifunctional devices, and low-temperature aftertreatment (LTAT). Resources are shared among these efforts to allow for active response to current industrial needs. In FY 2019, the team (1) provided molecular insight toward the "mysterious" deactivation of Cu/SAPO-34 SCR catalysts, (2) achieved atomic Pd dispersion for Pd/SSZ-13-based PNAs, (3) published four low-temperature catalyst test protocols (Oxidation, Storage/Release, Three-Way Catalyst, and NH_3-SCR) in open literature, (4) discovered an approved method to enhance oxygen activation for improved low-temperature CO oxidation activity, and (5) developed a new technique to measure local permeability in multifunctional filters with zoned catalyst coatings. (Wang, IV.2)

Oak Ridge National Laboratory is (1) developing emissions control technologies that achieve >90% reduction of pollutants at low temperatures (<150°C) to enable fuel-efficient engines with low exhaust temperatures to meet new U.S. Environmental Protection Agency Tier 3 emissions, (2) identifying advancements in technologies that will enable commercialization of advanced combustion engine vehicles, and (3) advancing understanding of fundamental surface chemistry mechanisms that either enable or limit low-temperature emissions control. In FY 2019, researchers (1) synthesized a new class of novel supports to be investigated for improved durability and low-temperature oxidation; (2) demonstrated hydrocarbon trap functionality and durability of platinum-group-metal-free zeolite; (3) evaluated Pd/SSZ-13 (aluminosilicate zeolite) for passive NO_x adsorption and discovered a deactivation mechanism that occurs during evaluation as a single component; and (4) demonstrated the potential and durability of combining a non-platinum-group-metal zeolite, Pd/SSZ-13 PNA, and an oxidation catalyst to treat low-temperature emissions. (Toops, IV.3)

Oak Ridge National Laboratory is conducting research on an emissions control concept known as passive selective catalytic reduction. In FY 2019, the team (1) demonstrated a pathway for higher fuel efficiency with an improved passive selective catalytic reduction aftertreatment system architecture while meeting U.S. Environmental Protection Agency Tier 3 emissions levels, (2) identified potential strategies to reduce CO emissions during rich engine operation, and (3) procured and installed a MAHLE Jet Ignition engine as the engine platform for this project. (Prikhodko, IV.4)

Oak Ridge National Laboratory is conducting research and development to understand the fundamental chemistry of automotive catalysts, identify strategies for enabling self-diagnosing catalyst systems, and address critical barriers to market penetration. In FY 2019, researchers (1) determined a detailed model structure for fitting Cu-redox half-cycle kinetic parameters, (2) assembled selective catalytic reduction catalyst samples for analysis, and (3) built a reactor for performing transient response experiments. (Partridge, IV.5)

Pacific Northwest National Laboratory is developing protocols in collaboration with United States Council for Automotive Research to improve or optimize the properties of solid-state ammonia storage materials based on the information collected during the prior years. In FY 2019, the project focused on ways to develop experimental protocols to synthesize and quantify novel non-halide-containing materials to eliminate corrosive HCl generation observed in the metal halide ammine complexes. Three classes of novel materials were synthesized by a combination of co-precipitation, ion-exchange techniques, and solid-state synthesis: zeolite-based materials, amorphous oxides, and crystalline oxides. The team (1) achieved 10–15 wt% ammonia storage capacity in zeolite-based materials, (2) used a combination of metal doping and the Si/Al ratio to successfully decrease the temperature of ammonia release from 250°C to 150°C without loss of capacity, and (3) used ab initio and molecular dynamics simulations to identify the energetics of silicate, titano-silicate, and aluminosilicate materials. (Karkamkar, IV.6)

Pacific Northwest National Laboratory is developing a novel active selective catalytic reduction (SCR) phase that, when employed in the SCR on diesel particulate filter configuration, will enable improved passive soot oxidation capacity versus current SCR catalysts while retaining the necessary NO_x reduction performance efficiency to be attractive for the heavy-duty diesel application. In FY 2019, the team (1) demonstrated that coprecipitation of Mn with ZrO_2 or CeO_2 bulk oxide is the optimum method of selective catalytic oxidation (SCO)-phase synthesis, (2) demonstrated that 10 wt% Mn coprecipitated with 90% ZrO_2 is the near-optimum SCO-phase chemistry for NO oxidation activity and efficient Mn usage, (3) discovered that the active site for NO oxidation is the interface of Mn-dimer and ZrO_2, (4) demonstrated evidence of three separate pathways for SCR rate enhancement from inclusion of an SCO phase, (5) demonstrated improved low-temperature SCR performance and significantly increased NO_2 availability on the binary catalyst under SCR reaction conditions versus the SCR catalyst alone, and (6) discovered a unique ion-exchange aging mechanism that must be considered for accurate replication of field aging at the bench scale for SCR-SCO binary catalyst systems. (Rappe, IV.7)

Oak Ridge National Laboratory is addressing the challenges associated with emissions control compliance during vehicle cold start and transients encountered as a result of hybridization or low-temperature combustion. Key focuses include measuring the detailed exhaust chemistry during cold start of boosted spark-ignition, diesel, and hybrid spark-ignition engine platforms at engine out and downstream of relevant emissions control systems, including three-way catalysts and hydrocarbon (HC) traps. FY 2019 research aimed to characterize gasoline direct injection cold-start emissions using market-available vehicles, with a special focus on HC speciation upstream and downstream of the HC trap to study how different HC chemistry (e.g., functional group) affects the HC trap's effectiveness during cold start. Project researchers measured detailed gaseous emissions generated in the first 250 seconds of the cold-start Federal Test Procedure drive cycle on modern gasoline direct injection vehicles and determined the specific key molecular species contributing to total HC emissions. (Debusk, IV.8)

High Efficiency Engine Technologies

Volvo Group is working to develop and demonstrate an all new complete vehicle concept designed with an integrated approach to maximize freight efficiency. In FY 2019, the team (1) finalized a new cab interior concept design, (2) completed component and sub-system studies, and (3) completed aerodynamic optimization of the complete vehicle. (Amar, V.1)

Cummins Inc. is designing, developing, and demonstrating a very-high-efficiency engine optimized around the drive cycle that will yield a very high increase in vehicle freight efficiency compared to the 2009 baseline vehicle. In FY 2019, the project (1) demonstrated 50.3% brake thermal efficiency (BTE) of the new platform; (2) upfit the transmission integral 48 V, P2.5 mild hybrid system into the powertrain mule development truck; (3) fit engine waste heat recovery system components onto the 55% BTE development engine and began test cell development of the system; (4) identified a pathway to 55% BTE, considering the losses of the 50% BTE (engine only) system; (5) finalized the demonstrator vehicle outer body and began procurement; (6) confirmed the exceedance of the aerodynamic drag target for the demonstrator vehicle; (7) confirmed that the demonstrator vehicle's tire rolling resistance coefficient reduction will exceed the target; and (8) confirmed the weight target analytically for the demonstrator vehicle. (Dickson, V.2)

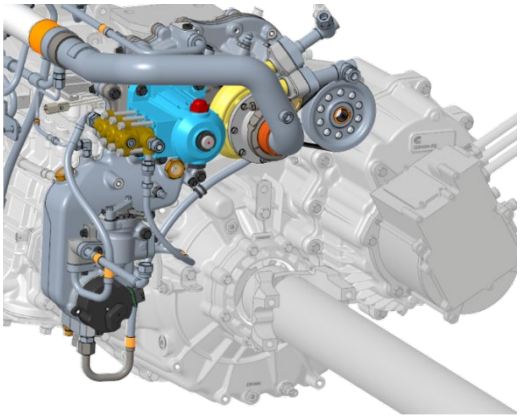

Figure 17 Transmission integral WHR turbine expander system. This system has begun rig testing and will be developed further in the test cell with integration into the mule vehicle in the first quarter of 2020 (Dickson, V.2)

Navistar, Inc., is researching, developing, and demonstrating a heavy-duty engine that can meet 2010 federal emissions standards and can achieve 55% brake thermal efficiency demonstrated in an operational engine at a 65-mph cruise point on a dynamometer. In FY 2019, the team (1) evaluated cylinder deactivation technology for fuel economy, (2) improved air system efficiency for the SuperTruck 2 engine, (3) investigated a novel fuel-system configuration to increase combustion burn rates, (4) identified an organic Rankine cycle waste heat recovery system that contributes to achieving 55% brake thermal efficiency, and (5) continued the gasoline compression ignition investigation at Argonne National Laboratory. (Zukouski, V.3)

Daimler Trucks North America is developing and demonstrating a greater than 100% improvement in overall freight efficiency on a heavy-duty Class 8 tractor-trailer measured in ton-miles per gallon. In FY 2019, the project (1) built and tested the A-sample integration vehicle on the road, (2) progressed from a 40% clay model into a single theme full-scale model in the design studio, (3) built and placed in a test cell an engine with a two-stage turbocharger and intercooled air system, (4) procured parts for waste heat recovery and set up parts into a test cell, and (5) selected concepts for major systems such as split cooling and the boost recoup motor location. (Villeneuve, V.4)

PACCAR Inc. is researching, developing, and demonstrating a Class 8 long-haul truck and trailer combination that can meet prevailing federal emissions standards and applicable safety and regulatory requirements. In FY 2019, the team (1) finalized the design for the vehicle cab and trailer aerodynamics, (2) completed the vehicle design for chassis and components, (3) defined the control system for hardware-in-loop and model-in-loop testing, (4) defined the powertrain architecture, (5) continued investigation of combustion recipe, and (6) finalized the engine design and combustion recipe and selected suppliers. (Hergart, V.5)

General Motors is developing and demonstrating a downsized, boosted, lean, low-temperature combustion (LTC) engine system capable of achieving 15%–17% fuel economy improvement relative to a contemporary naturally aspirated, stoichiometric combustion engine consistent with relevant emissions constraints. The project is focused on the integration and development of the engine as well as demonstration of the overall engine system performance potential over the Federal Test Procedure (FTP) drive cycles as well as the harsh conditions associated with real-world driving. In FY 2019, it (1) developed and demonstrated LTC engine calibration and control algorithms necessary for robust transient operation and LTC/spark-ignition combustion mode shifts with a prototype controller; (2) developed and demonstrated LTC engine calibration and control strategies necessary for robust operation over the hot FTP drive cycle consistent with stability objectives; (3) developed and demonstrated LTC engine calibration and control strategies necessary for robust operation over the hot FTP drive cycle consistent with fuel economy, engine-out emissions, and stability objectives; and (4) developed and demonstrated LTC engine calibration and control strategies necessary for robust operation over the cold FTP drive cycle consistent with fuel economy, engine-out emissions, and stability objectives. (Yun, V.6)

Delphi Technologies, PLC, is working to improve engine fuel efficiency by developing a production-feasible electrically actuated cylinder deactivation valve train that will enable internal combustion engines to employ an advanced combustion strategy known as dynamic skip fire. During FY 2019, the team (1) verified the deactivation roller finger follower and electrical actuators on a cylinder head function, (2) completed dynamics testing, (3) evaluated rocker arm load, (4) successfully completed 400 h durability testing, (5) used emission test data from a dynamic skip fire equipped vehicle to generate dyno testing points, (6) selected speed/loads to test the electronic deactivation hardware on the dynamometer, (7) determined the duration of each firing fraction used in each speed/load zone of vehicle test data that is covered by the selected speed/load test conditions for dynamometer testing, and (8) predicted 5.92% fuel economy gain compared to the baseline non-deactivation engine. (Roe, V.7)

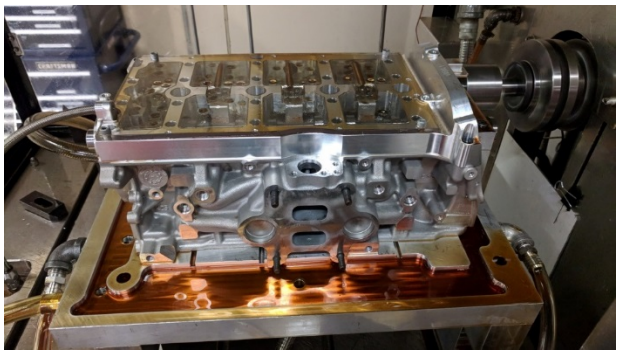

Figure 18 Durability test configuration (Roe, V.7)

HRL Laboratories, LLC, is increasing internal combustion engine efficiency and decreasing heat loss from the combustion chamber with temperature-following thermal barrier coatings. In FY 2019, the project (1) demonstrated scalable low-cost processes to coat valves, pistons, and port liners; (2) optimized temperature-following thermal barrier coating properties, including surface roughness, surface sealing, thermal conductivity, and heat capacity; (3) demonstrated durability of temperature-following thermal barrier coatings in engine tests; and (4) quantified efficiency gains achieved with thermal barrier coatings by simulation and experimental engine testing. (Schaedler, V.8)

Argonne National Laboratory is working to develop and demonstrate technologies that will achieve a 50% increase in freight efficiency over a 2016 baseline and will lead to the commercialization of clean vehicle solutions for medium-duty (MD) and heavy-duty (HD) trucks. In FY 2019, the project team (1) explored the ignition behavior of potential low-life-cycle-greenhouse-gas fuels to assess fuel properties; (2) defined the

engine requirements; (3) determined the choice and location of air-handling actuators and sensors; (4) explored the electrified MD powertrain architectures for a pickup and delivery van; (5) tested the baseline vehicle over selected duty cycles; (6) developed MD and HD route prediction algorithms; and (6) developed technologies for lightweight components, reduced aerodynamic drag, and low-rolling-resistance tires. (Freyermuth, V.9)

Lubricant Technologies

Ford Motor Company and Argonne National Laboratory have teamed to demonstrate the potential to reduce mechanical friction—a key factor in lost energy input—using advanced high-porosity (HP) plasma transfer wire arc (PTWA) coatings, surface finish, and design on the power cylinder system containing cylinder bore, piston rings, piston skirt, bearings and crankshaft, and advanced engine oils. This project developed (1) a process for depositing and honing HP PTWA coatings to achieve different porosity levels with improved surface finish on free-standing cylinder liners and engine blocks, (2) various techniques for characterizing coatings, (3) a method for achieving micro-polishing crankshaft journals, (4) a technique for depositing nano-composite vanadium nitride (VN)-Cu and VN-Ni coatings on piston rings and piston skirts, (5) a method for laboratory friction and wear assessment for generating a Stribeck curve, (6) a method for evaluating friction reduction potential of PTWA coatings and micro-polished journals using a motored cranktrain rig, and (7) a method for evaluating wear (durability) of PTWA coatings and ring coatings using a radiotracer method. (Gangopadhyay, VI.1)

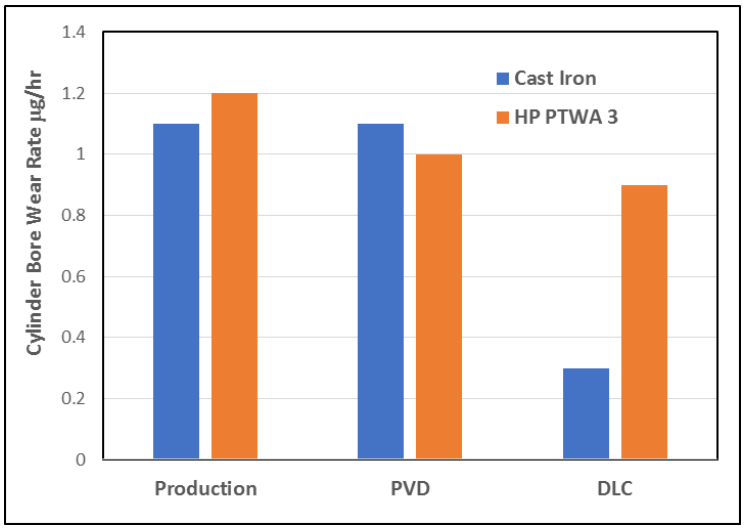

Figure 19 A comparison of cylinder bore wear rate between cast iron liner and HP PTWA 3 coating in contact with production, physical vapor deposition, and diamond-like carbon ring coatings (Gangopadhyay, VI.1)

George Washington University, GMC, and Valvoline New Product Development Lab are collaborating to develop prototype low- and ultra-low-viscosity oils and demonstrate that they improve fuel economy, as well as to develop surface materials technologies to maintain current durability for future engines using ultra-low-viscosity oils. For future vehicles, a 2018 platform engine with modern fuel-efficient technologies was used to measure vehicle performance and fuel efficiency. In FY 2019, the project team completed the design and fabrication of surface textures on the 2018 platform engine with fuel-efficient technologies incorporated. The textured parts were installed into the engine and tested on an engine dynamometer test to evaluate engine efficiency improvement using the 5W-30 baseline oil. In addition, microencapsulated friction modifiers were incorporated into an ultra-low-viscosity oil formulation and tested in an engine chassis dynamometer in a vehicle. (Hsu, VI.2)

System-Level Efficiency Improvement

PPG Industries, Inc., is developing sidewall compounds containing non-treated and treated Agilon® silica fillers to improve rolling resistance of tires, while taking into account other performance parameters relevant to non-tread tire components. The project team prepared two optimized silica prototypes and tested them in sidewall rubber compounds made with different variations of filler and curative loadings. Traditional performance parameters were determined, as well as parameters related to resistance to compound degradation. Results showed that functionalized silica technology can deliver the project goals by producing an improved overall compound performance balance, with relatively low hysteresis, while maintaining resistance to degradation. (Dos Santos, VII.1)

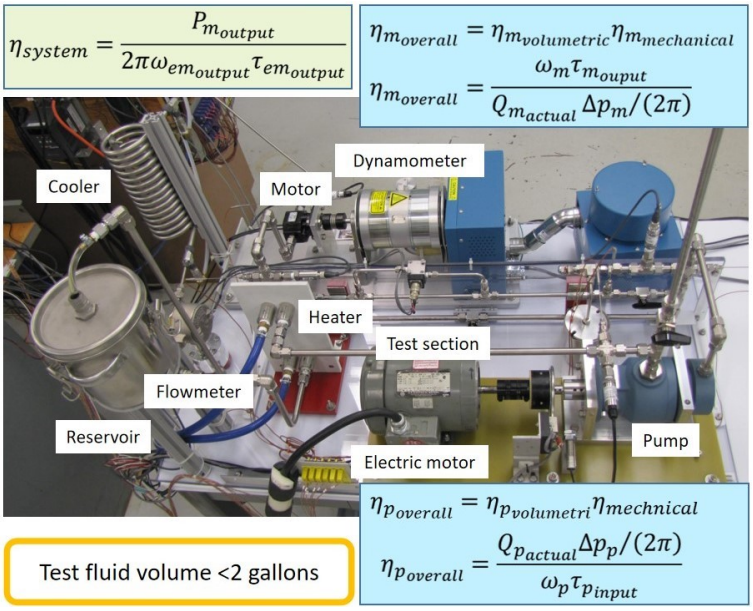

Figure 20 Test loop of the fluid power test facility (Fenske, VII.2)

A multilaboratory effort (Argonne National Laboratory, lead; Oak Ridge National Laboratory; and Pacific Northwest National Laboratory) is underway to develop high-performance hydraulic fluids and wear-resistant coatings to improve the efficiency, durability, and environmental compatibility of off-road hydraulic components. The project team has successfully developed binary and ternary composite base fluids from polyalphaolefin and different bioderived esters. The composite fluids exhibit superior rheological and frictional properties, as well as wear and scuffing protection capabilities, compared to fully formulated, commercially available fluids. The project has also developed catalyst coatings that demonstrate extreme resistance to wear under severe boundary conditions and significantly reduce friction over the uncoated test samples. In addition, the project completed the concept design, engineering design, and construction of an experimental fluid power test loop, as well as the integration of the loop with a data acquisition and control system. (Fenske, VII.2)

Oak Ridge National Laboratory is researching technologies to improve the energy efficiency of fluid power systems for off-road vehicles, focusing on development of eco-friendly additives for hydraulic fluids. In FY 2019, researchers (1) designed and synthesized candidate ionic liquids as eco-friendly additives for polyalkylene glycol and (2) demonstrated reduced toxicity of candidate ionic liquids and improved lubricating performance benchmarked against conventional additives. (Qu, VII.3)

This multilaboratory effort (Argonne National Laboratory, Oak Ridge National Laboratory, and Pacific Northwest National Laboratory) focuses on the development and evaluation of stable, energy-efficient fluids and additives that increase the efficiency and durability of components (pumps, valves, actuators, and motors) used in hydraulic fluid systems in off-road vehicles. In FY 2019, the project prepared a series of dendritic polymers that display good shear stabilities for their respective high molecular weights and demonstrated the polymers' superior viscosity index when a semi-crystalline segment is present. The team also demonstrated the efficient synthesis of polar co-polymers via controlled radical polymerization. In addition, the project achieved a multifunctional viscosity index improver that displayed comparable shear losses to the benchmark, but 5–7 times greater anti-wear properties. (Cosimbescu, VII.4)

The University of Minnesota is developing an efficient, compact, and smooth variable displacement propulsion motor to improve the efficiency of off-highway vehicles. During FY 2019, the project team constructed a comprehensive dynamic model of the variable displacement linkage motor (VDLM) that predicts all major energy losses and the torque ripple, as well as a novel kinematic model using an inverse cam design that prescribes the follower motion to generate the cam profile. A motor design code was developed that constructs the motor geometry from a given set of parameters, sizes links and bearings for the applied loads, and detects interference between components. Utilizing a multi-objective genetic algorithm, researchers also explored the design trade-offs between motor efficiency, size, and torque ripple, resulting in a solution with over 97% efficiency across the displacement range and 2.8% torque ripple at maximum displacement. Finally, the research team performed a detailed design of a single-cylinder prototype for the purpose of validating the mathematical models. (Van de Ven, VII.5)

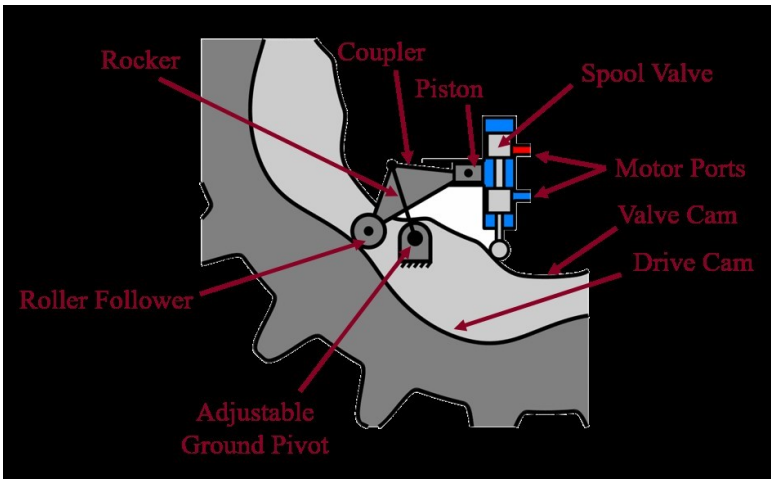

Figure 21 Diagram of the VDLM mechanism (Van de Ven, VII.5)

The University of Minnesota is developing a methodology for improving the efficiency of high-power off-road mobile machines that takes advantage of electrification without the need for very high power or costly electric components. The general idea is to develop a system architecture that marries the comparative advantages of hydraulic actuation and electrical actuation. As the project is in its first year, the primary objective was to establish the feasibility of the approach. Results indicated that, for all three representative machine platforms, the proposed system architecture can increase efficiency by approximately three times. A control algorithm has been developed that provides good position tracking despite switching in the pressure rails. A concept of tightly integrating an axial flux rotary electric motor with a radial ball piston pump/motor has been developed for use with the proposed system architecture. Preliminary analysis shows that this combination offers designs that can meet the desired efficiency and power density. (Li, VII.6)

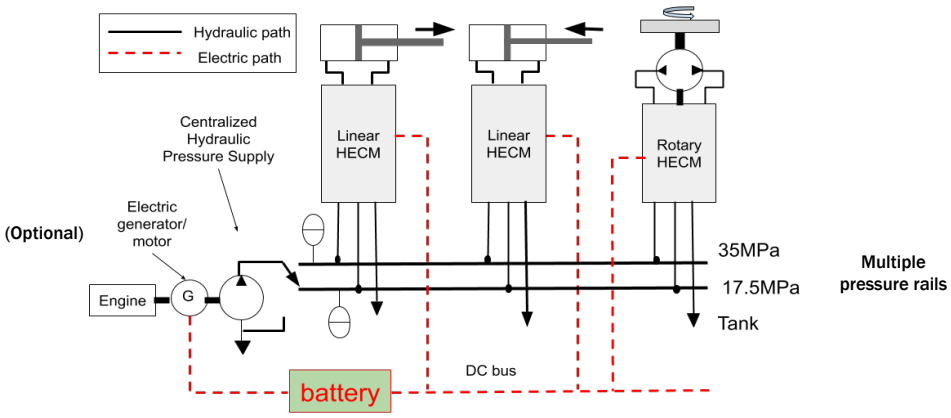

Figure 22 Hybrid hydraulic–electric architecture (HECM – hydraulic–electric control module) (Li, VII.6)

Purdue University seeks to introduce a new electro-hydraulic (EH) technology that drastically changes the current design approach of fluid power systems for off-road machines. This technology introduces a novel EH hybrid solution that benefits from both electric (ease of control) and fluid power (high power density) technologies. The approach includes simulations, prototype fabrication, and experimentation. FY 2019 activities included simulations aimed at design considerations for a four-quadrant EH hydraulic unit (the main energy conversion unit) and an individualized EH system (layout and control architecture for the usage of the EH unit to realize an individualized hydraulic drive). The project successfully formulated a design of a combined electric and hydraulic machine suitable for 15 kW actuation, with overall efficiency above 80% in the range of typical application. (Vacca, VII.7)

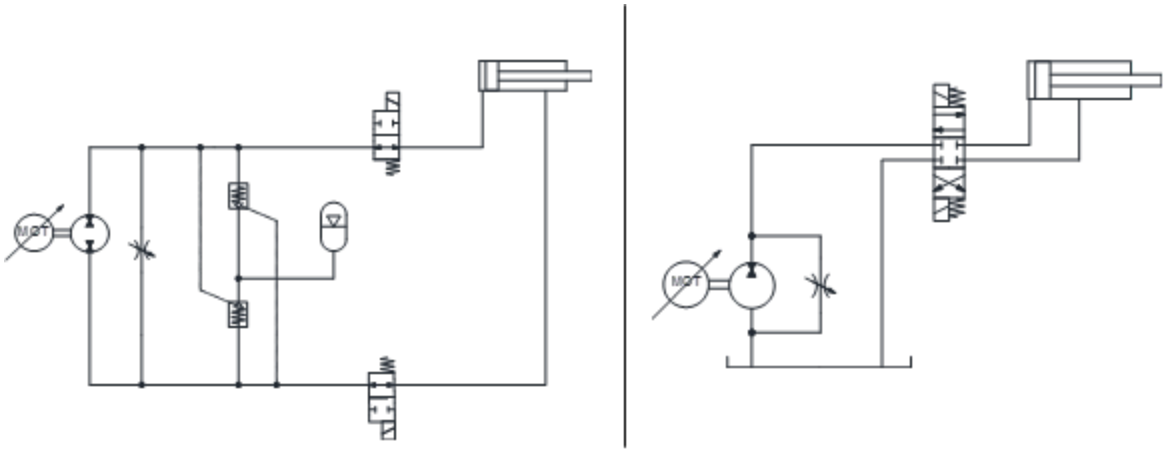

Figure 23 Proposed layouts for the EH system: closed center with accumulator (left); open center (right) (Vacca, VII.7)

Invention and Patent Disclosures

1. U.S. Patent No. 10,202,929 Issued: Dec, J.E., and R.F. Renzi. 2019. "Additive-Mixing Fuel-Injection System for Internal Combustion Engines." Issued February 12, 2019. (Dec, I.4)

2. U.S. Patent No. 10,138,855 Issued: Mueller, C.J. 2018. "Ducted Fuel Injection with Ignition Assist." Issued November 27, 2018. (Mueller, II.13)

3. U.S. Patent No. 10,161,626 Issued: Mueller, C.J. 2018. "Ducted Fuel Injection." Issued December 25, 2018. (Mueller, II.13)

4. U.S. Patent No. 10,371,689 Issued: McNenly, Matthew, Geoffrey Oxberry, Ahmed Ismail, Nicholas Killingsworth, and Daniel Flowers. 2019. "Ultra-Compact System for Characterization of Physical, Chemical and Ignition Properties of Fuels." Issued August 6, 2019. (McNenly, II.21)

5. U.S. Patent Number 10,427,137 Issued: Kyriakidou, Eleni, Todd J. Toops, Jae-Soon Choi, Michael J. Lance, and James E. Parks II. 2018. "Exhaust Treatment Catalysts with Enhanced Hydrothermal Stability and Low Temperature Activity." Issued October 1, 2019. (Toops, IV.3)

6. Invention Disclosure: Qu, J., H. Luo, and X. He. 2019. "Eco-Friendly Ionic Liquids as Lubricant Additives." ORNL Invention Disclosure #201904491. (Qu, VII.3)

7. U.S. Provisional Patent, Serial No. 62/801,137, Filed: Li, Perry Y. 2019. "Hybrid Hydraulic-Electric Actuation Architecture Hybrid." Filed February 5, 2019. (Li, VII.6)

I Combustion Research

I.1 Medium-Duty Diesel Combustion (Sandia National Laboratories)

Stephen Busch, Principal Investigator
Sandia National Laboratories
P.O. Box 969, MS 9053
Livermore, CA 94551-0969
E-mail: sbusch@sandia.gov

Michael Weismiller, DOE Technology Development Manager
U.S. Department of Energy
E-mail: Michael.Weismiller@ee.doe.gov

Start Date: October 1, 2018 End Date: September 30, 2019
Project Funding (FY19): $900,000 DOE share: $900,000 Non-DOE share: $0

Project Introduction

Faster combustion improves the efficiency of a diesel engine, and in medium-duty diesel engines, interactions between the fuel sprays and the piston bowl walls play a key role in determining heat release rates. Stepped-lip pistons can promote the formation of vortices that are correlated with faster, more efficient heat release, but this behavior is observed primarily for late injection timings at which the engine is not operating at its peak efficiency [1],[2],[3]. The project objectives were to explain the physical mechanisms responsible for this phenomenon, to identify measures that may enhance vortex formation, and to quantify the extent to which these measures may improve the engine's thermal efficiency.

Diesel exhaust aftertreatment systems effectively eliminate pollutants such as soot, nitrogen oxides, and unburned hydrocarbons, but only after their temperature reaches approximately 200°C. The goal of engine operation during the first minutes after a cold start is to quickly heat up the exhaust aftertreatment system while minimizing untreated pollutants. Catalyst heating operation involves multiple injections during the later stages of combustion to maximize exhaust temperature/enthalpy, and an effective catalyst heating strategy is critical for meeting increasingly strict pollutant emissions regulations. Because this mode of combustion is not well understood, efforts were devoted to developing an experimental methodology to provide initial insights into the mixture formation, combustion, and pollutant formation processes using thermodynamic measurements and high-speed imaging.

Finally, a new medium-duty diesel research engine was constructed to enable continued research into the aforementioned topics, as well as cutting-edge research into methods of reducing wall heat loss to improve efficiency.

Objectives

This project provides scientific understanding needed to design, optimize, and calibrate the next generations of medium-duty diesel engines that comply with increasingly stringent pollutant emissions regulations while achieving thermal efficiencies exceeding 50%.

Overall Objectives

- Develop conceptual models for spray-wall interactions, combustion, and pollutant formation in direct-injection diesel engines

- Provide scientific understanding of aspects of combustion chamber design that enable improvements in efficiency and/or reductions in pollutant emissions
- Develop conceptual models that describe fuel injection, mixture formation, combustion, and pollutant formation during catalyst heating operation.

Fiscal Year 2019 Objectives

- Develop a conceptual model for turbulent flow evolution and vortex formation in stepped-lip combustion chambers
- Identify combustion system design and/or operating parameters that are predicted to enhance vortex formation in stepped-lip combustion chambers for main injections starting near top dead center (TDC)
- Develop an experimental approach to study catalyst heating operation in the small-bore optical diesel engine, and perform initial thermodynamic and high-speed imaging studies
- Begin construction of the new medium-duty diesel research engine.

Approach

Analysis of experimental data leads to the hypothesis that promoting vortex formation will increase efficiency and reduce pollutant emissions in a diesel engine with stepped-lip pistons. Because the computational fluid dynamics (CFD) simulations (performed by Wisconsin Engine Research Consultants, a subcontractor) have demonstrated qualitative agreement with experimental results, the simulations are applied to identify combustion system operating and design parameters that may be expected to enhance vortex formation resulting from spray-wall interactions with stepped-lip pistons. The synthesis of the experimental and simulation results leads to a conceptual model for turbulent flow evolution in stepped-lip diesel combustion chambers.

A new experimental approach is developed to study catalyst heating operation and provide insight into mixture formation, ignition, combustion, and pollutant formation mechanisms. Thermodynamic measurements and high-speed optical and infrared imaging provide initial insights into this complex combustion regime and serve as a dataset for continued development of simulation capabilities.

A new medium-duty diesel research engine was constructed in 2019 to enable:

- Continued research into piston bowl geometry effects and catalyst heating operation
- Cutting-edge heat transfer research with low-thermal-mass coatings on combustion chamber surfaces.

Results

Key accomplishments:

- A new conceptual model describes the key phenomena responsible for the evolution of turbulent flow and the formation of toroidal vortices resulting from spray-wall interactions in the stepped-lip combustion chamber.
- The height of the squish region is identified as a key parameter to promote vortex formation for main injections starting near TDC. A dimpled stepped-lip (DSL) piston concept has been developed, and simulations predict it will enhance vortex action for main injections starting near TDC.
- For catalyst heating operation, experimental data indicate that the pilot and main injections are likely the most significant contributors to unburned hydrocarbon emissions in the exhaust.

Improving the efficiency of diesel engines requires fundamental understanding of the processes that govern fuel-air mixing rates. For engines with stepped-lip pistons, interactions between the fuel sprays and the piston bowl have dramatic effects on flow and mixing. Continued analysis of experimental and CFD simulation results has resulted in a conceptual model that describes key phenomena that drive the evolution of turbulent flow in a particular stepped-lip combustion chamber. Figure I.1.1 shows this model on a vertical plane containing a single spray axis. The figure depicts how the stepped-lip piston bowl geometry redirects the spray's outward, downward momentum and how shear in the boundary layer between the penetrating spray and the wall generates vorticity (local rotation of the flow).

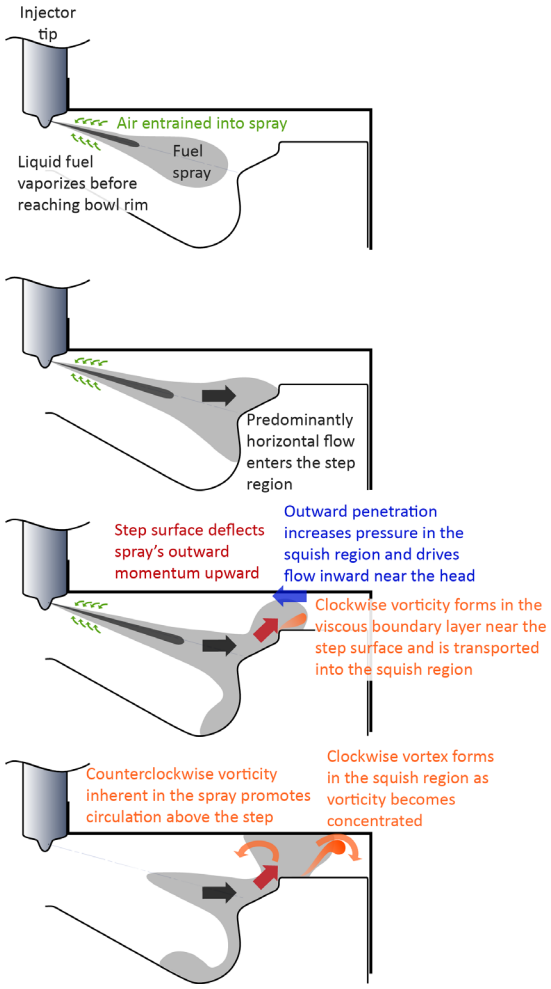

Figure I.1.1 Conceptual model describing the evolution of turbulent flow in a stepped-lip combustion chamber. Note that the effects of combustion are not considered in this version of the model.

The spray's momentum transports this vorticity to the squish region, where a toroidal vortex forms. At the same time, the outward penetration into the squish region creates an adverse pressure gradient that drives flow back inward near the cylinder head. This backflow, combined with the counterclockwise vorticity in the upper portion of the spray, results in a toroidal vortex above the step region.

This conceptual model applies to conditions for which the stepped-lip piston effectively creates vortices: at relatively late main injection timings. While injections starting near TDC advance the combustion phasing and improve the engine's efficiency, the strength and longevity of the toroidal vortices decrease, and the mixing-controlled portion of the combustion event becomes slower [4]. Thus, it is hypothesized that measures that

promote vortex formation for near-TDC injection timings will increase fuel-air mixing rates and therefore result in further efficiency improvements. A further CFD investigation focuses on whether combustion system operating and design parameters can promote vortex formation at the near-TDC injection timing. The only parameter predicted to achieve this is the space in the squish region (between the piston top and the cylinder head). A modified stepped-lip geometry is created to achieve this increase in squish region space; the resulting geometry is called a DSL piston and is shown in Figure I.1.2.

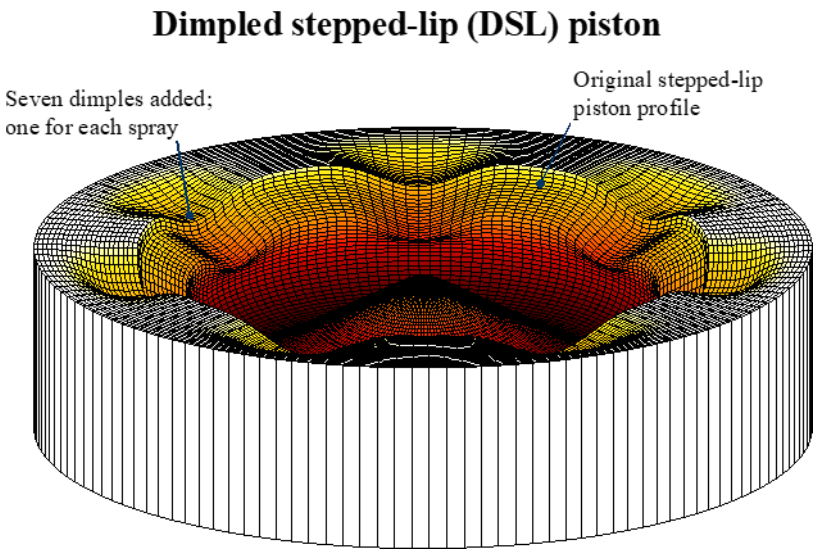

Figure I.1.2 The DSL piston. This design was created to test the hypothesis that increased space between the top piston surface and the cylinder head will promote vortex formation as the fuel sprays separate from the piston surface.

The effects of changing injection timing with the stepped-lip piston, as well as the effect of changing the bowl geometry on the flow structure, are visualized in Figure I.1.3. Toroidal vorticity is shown on a vertical cutting plane for a crank angle approximately 5 degrees after the end of the main injection. Interactions between the fuel spray and the piston bowl have strongly influenced the structure of the turbulent flow above the piston. The DSL piston effectively restores the rotational flow topology that is lost with the stepped-lip piston when the main injection timing is advanced to near TDC. Continued research efforts will be devoted to developing a DSL-like piston for the new medium-duty diesel engine to test the hypothesis that enhanced vortex formation will lead to thermal efficiency improvements.

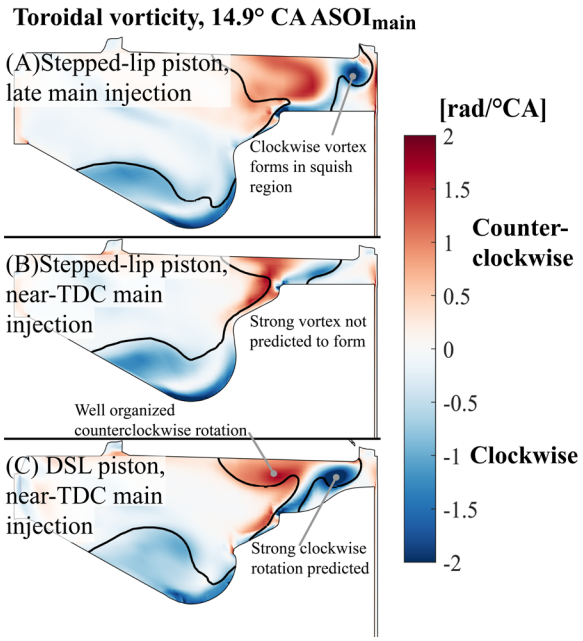

CA – crank angle; ASOI – after start of injection

Figure I.1.3 Toroidal vorticity (vorticity vector perpendicular to the page) for a vertical plane containing a spray axis. (A) Stepped-lip piston, main injection starting in the expansion stroke. (B) Stepped-lip piston, main injection starting near TDC. (C) DSL piston, main injection starting near TDC.

Fuel injection strategies for catalyst heating operation often include one or more pilot injections, a main injection, and one or more post injections. The variable quantity and timing of each injection event create an excessively large parameter space, so these initial studies are performed with a pilot-main-post injection strategy to provide insight into sources of unburned hydrocarbon emissions. The quantities and timings of each injection event are controlled as described in Table I.1.1.

Table I.1.1 Injection Timings and Quantities for Initial Study of Catalyst Heating Operation

Pilot timing	Pilot quantity	Main timing	Main quantity	Post timing	Post quantity
Fixed at 15 CAD ATDC	2 mg	Fixed at TDC	3, 5, 7 mg	Vary between 10–30 CAD ATDC	2, 4, 6 mg

CAD – crank angle degrees; ATDC – after top dead center

These various injection strategy calibrations are utilized in the running engine while maintaining a coolant temperature of 30°C. Unburned hydrocarbon emissions levels are measured, and Figure I.1.4 shows the emissions index of unburned hydrocarbons (EIHC) for each variation of post injection timing. EIHC levels are also shown for pilot-main injection strategies using dashed lines. While adding a post injection to a pilot-main injection strategy, the amount of unburned hydrocarbons per kilogram of fuel injected decreases. Regardless of injection strategy calibration, EIHC tends to increase as post injection timing is retarded. Increasing the main injection quantity typically reduces unburned hydrocarbons, particularly for late post injection timings.

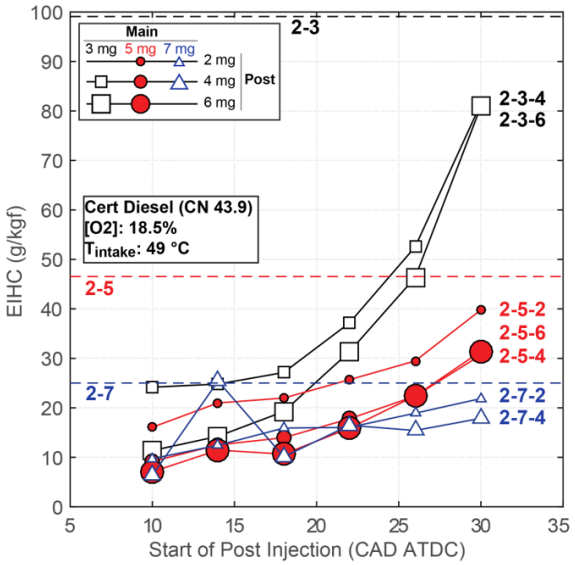

Figure I.1.4 EIHC as a function of the crank angle at which the post injection starts. Adding a post injection to a pilot-main injection strategy always decreases the mass of unburned hydrocarbons formed for the given fuel mass.

These results show that the pilot and main injections are significant sources of unburned hydrocarbons, and that the ability of a post injection to oxidize these hydrocarbons is diminished for late injection timings and small main injection quantities. Results from high-speed imaging experiments (not shown) suggest that combustion of the pilot and main takes place primarily within the piston bowl. Furthermore, early post injections can interact directly with the bowl contents, but late post injections are targeted above the bowl and are not observed to interact with the bowl contents. Thus, late post injections may be limited in their ability to reduce unburned hydrocarbon emissions.

Conclusions

The DSL piston design provides evidence that changes in piston geometry can enhance the formation of the vortices that form by interaction with the bowl surface. DSL-like piston designs will be developed to test the hypothesis that stronger vortices can increase heat release rates and, thereby, efficiency.

Experimental evidence suggests that the pilot and main injections are important sources of unburned hydrocarbon emissions in catalyst heating operation.

Key Publications

1. Busch, Stephen, Federico Perini, Rolf D. Reitz, and Eric Kurtz. N.D. “Effects of Stepped-lip Combustion System Design and Operating Parameters on Turbulent Flow Evolution in a Diesel Engine.” *SAE Journal of Engines*, in press.

2. Perini, Federico, Stephen Busch, Eric Kurtz, Alok Warey, Richard C. Peterson, and Rolf D. Reitz. 2019. “Limitations of Sector Mesh Geometry and Initial Conditions to Model Flow and Mixture Formation in Direct-Injection Diesel Engines.” *SAE Technical Paper* 2019-01-0204. DOI: https://doi.org/10.4271/2019-01-0204.

3. Perini, Federico, Stephen Busch, Kan Zha, Rolf D. Reitz, and Eric Kurtz. 2019. “Piston Bowl Geometry Effects on Combustion Development in a High-Speed Light-Duty Diesel Engine.” *SAE Technical Paper* 2019-24-0167. DOI: https://doi.org/10.4271/2019-24-0167.

References

1. Busch, Stephen, Kan Zha, Eric Kurtz, Alok Warey, and Richard C. Peterson. 2018. "Experimental and Numerical Studies of Bowl Geometry Impacts on Thermal Efficiency in a Light-Duty Diesel Engine." *SAE Technical Paper* 2018-01-0228. DOI: https://doi.org/10.4271/2018-01-0228.

2. Busch, Stephen, Kan Zha, Federico Perini, Rolf D. Reitz, Eric Kurtz, Alok Warey, and Richard C. Peterson. 2018. "Bowl Geometry Effects on Turbulent Flow Structure in a Direct Injection Diesel Engine." *SAE Technical Paper* 2018-01-1794. DOI: https://doi.org/10.4271/2018-01-1794.

3. Zha, Kan, Stephen Busch, Alok Warey, Richard C. Peterson, and Eric Kurtz. 2018. "A Study of Piston Geometry Effects on Late-Stage Combustion in a Light-Duty Optical Diesel Engine Using Combustion Image Velocimetry." *SAE Technical Paper* 2018-01-0230. DOI: https://doi.org/10.4271/2018-01-0230.

4. Busch, Stephen. 2018. "Light- and Medium-Duty Diesel Combustion." In *Advanced Combustion Engines and Fuels: 2018 Annual Progress Report*, 30–35. U.S. Department of Energy, Office of Energy Efficiency and Renewable Energy, Vehicle Technologies Office.

Acknowledgements

Ford Motor Company is acknowledged for their engineering support and for the loan of critical engine hardware for Sandia's new medium-duty diesel engine.

Sandia National Laboratories is a multimission laboratory managed and operated by National Technology and Engineering Solutions of Sandia, LLC, a wholly owned subsidiary of Honeywell International, Inc., for the U.S. Department of Energy's National Nuclear Security Administration under contract DE-NA-0003525.

SAND2019-13527 R

I.2 Heavy-Duty Diesel Combustion: Optical Engine Experiments and Modeling (Sandia National Laboratories)

Mark PB Musculus, Principal Investigator
Sandia National Laboratories
P.O. Box 969, MS 9053
Livermore, CA 94551-0969
E-mail: mpmuscu@sandia.gov

Michael Weismiller, DOE Technology Development Manager
U.S. Department of Energy
E-mail: Michael.Weismiller@ee.doe.gov

Start Date: October 1, 2018 End Date: September 30, 2019
Project Funding (FY19): $880,000 DOE share: $880,000 Non-DOE share: $0

Project Introduction

Regulatory drivers and market demands for lower pollutant emissions, lower carbon dioxide emissions, and lower fuel consumption motivate the development of cleaner and more fuel-efficient engine operating strategies. Most current production engines use a combination of both in-cylinder and exhaust emissions-control strategies to achieve these goals. The emissions and efficiency performance of in-cylinder strategies depend strongly on flow and mixing processes associated with fuel injection and heat losses.

Low heat transfer (HT) is desirable for increasing engine thermal efficiency and/or increasing exhaust temperatures to improve performance of turbocharging, exhaust emissions controls, and waste heat recovery. A large contributor to the higher thermal efficiency of advanced combustion modes is often a reduction in HT. For instance, reactivity-controlled compression ignition has achieved indicated thermal efficiencies as high as 59%, compared to 47% for conventional diesel, with HT losses reduced from 16% to 11% [1]. Even though the HT was responsible for much of the improvement in efficiency, the reduction was largely serendipitous, without direct design intention to reduce HT, which is generally difficult to achieve. Indeed, this year, in a new report of efforts to achieve 21st Century Truck Partnership goals for 50% or higher brake thermal efficiency, engineers from Cummins noted that HT is responsible for over 50% of the gap between theoretical and realized engine efficiency, making it "the largest area of opportunity, but also arguably the most difficult to impact" [2]. Different combustion modes have different spatio-temporal evolution of in-cylinder combustion/flows that affect HT, so to design combustion to minimize HT, it is important to understand how in-cylinder processes of different combustion modes affect HT.

Objectives

This project includes diesel combustion research at Sandia National Laboratories and combustion and flow modeling and simulation by Wisconsin Engine Research Consultants.

Overall Objectives

- Develop fundamental understanding of how in-cylinder controls can improve efficiency and reduce pollutant emissions of both conventional diesel and advanced low-temperature combustion
- Quantify the effects of fuel injection, mixing, and combustion processes on thermodynamic losses and pollutant emission formation
- Improve computer modeling capabilities to accurately simulate these processes.

Fiscal Year 2019 Objectives

- Develop and apply diagnostics to quantify combustion-mode effects on heat transfer and efficiency
- Use simulation predictions to guide and complement multiple-injection experiments
- Determine how mixing and jet interactions are affected by in-cylinder flows, the decay of spray-generated turbulence, large-scale structures, and/or entrainment wave effects on the bulk jet during the injection dwell.

Approach

This project uses an optically accessible, heavy-duty, direct-injection diesel engine (Figure I.2.1). For the HT measurements, 13 fast-acting (2.5 µs response time) surface thermocouples are installed into a round puck that is mounted into the cylinder wall, as shown in the photograph in the lower right of Figure I.2.1. The surface heat flux (HF) during combustion in the engine is derived from the transient temperature response of the cylinder-wall thermocouples. The piston crown has a cut-out in line with the thermocouples so that the thermocouples are directly exposed to impinging diesel jets and combustion. As shown in Figure I.2.1, two fueling options are available: (1) gasoline direct injection (GDI) using a Bosch side-injector mounted in the cylinder wall and (2) a centrally mounted Delphi DFI-1.5 common-rail diesel injector. The choice of injector(s) for the experiments depends on the combustion mode, as described in the results section.

For the results presented here, a window in place of one of the exhaust valves in the cylinder head provides imaging access to the squish region above the piston, as well as to a small portion of the piston bowl, in line with one of the diesel jet trajectories. A high-speed intensified complementary metal oxide semiconductor (ICMOS) camera equipped with a 310-nm bandpass (BP) filter images chemiluminescence emission from excited-state hydroxyl radicals (OH*), which are produced during combustion in relatively hot regions. Hence, the OH* imaging combined with thermocouple measurements shows the interaction between in-cylinder combustion and HT losses.

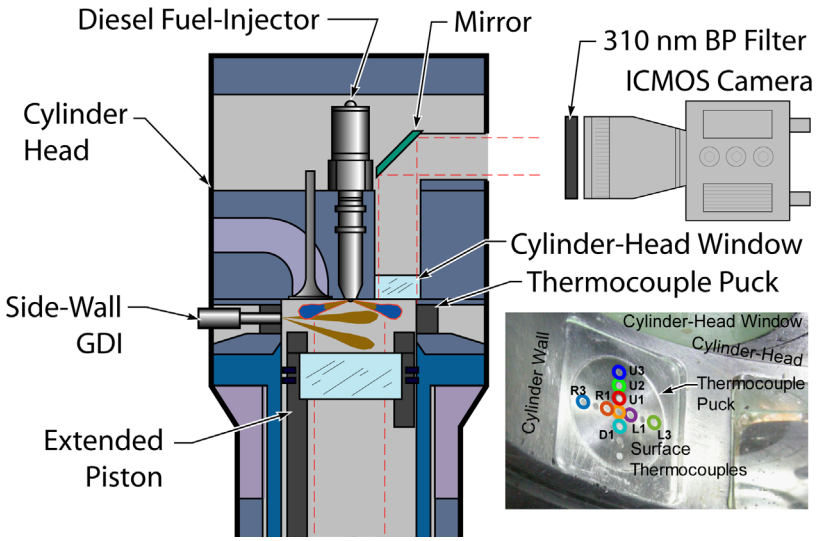

Figure I.2.1 Schematic showing the top half of the optical engine. Fueling options are a side-wall mounted GDI and a centrally located diesel fuel injector. The annotated photograph on the bottom right shows a round puck with surface thermocouples that is mounted in the cylinder wall. The camera position provides for imaging through the cylinder-head window.

Results

Figure I.2.2 shows results from a homogeneous-charge compression ignition (HCCI) type of operating condition, using a premixture of gasoline primary reference fuels (PRFs) n-heptane and iso-octane at a load of 4.8 bar gross indicated mean effective pressure (IMEPg). The GDI and diesel injectors were actuated near the beginning of the intake stroke to deliver iso-octane and n-heptane, respectively, in quantities with iso-octane at 57% of the total mixture (PRF57). With such early injection, the fuels were relatively homogeneous at ignition.

In Figure I.2.2, four key OH* chemiluminescence images at different crank angle degree (CAD) positions from one of the cycles show the progression of combustion. The measured HF for each of the thermocouples, as well as the apparent heat release rate (AHRR), is plotted above the images. In each of the images, the approximate location of key thermocouples is indicated by color-coded and labeled circles according to Figure I.2.1. From the perspective of the camera, thermocouples D1, T0, and U1–U3 are nearly along the camera line of sight so that they appear close together in the image.

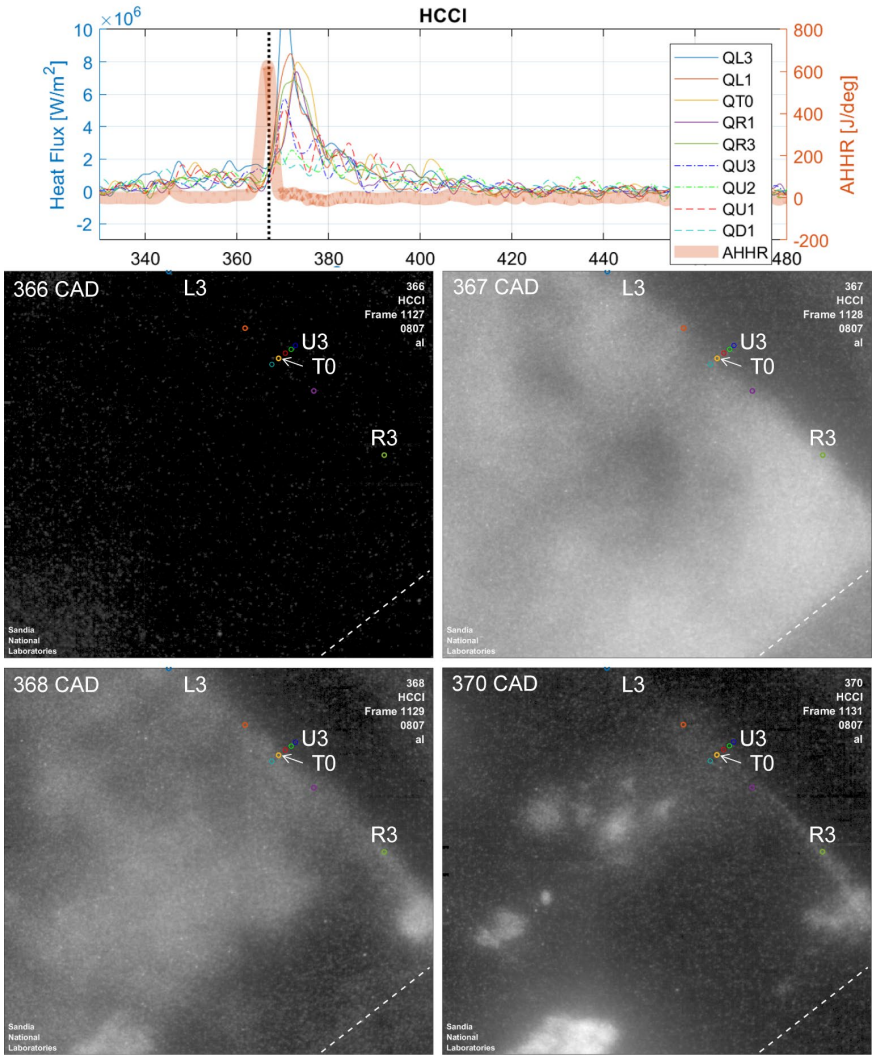

Figure I.2.2 AHRR and thermocouple HF measurements (top) and key OH* chemiluminescence images from one cycle of HCCI-type combustion. See Figure I.2.1 for physical locations of thermocouples, indicated by labels and color-coded circles.

In the plot at the top of Figure I.2.2, the HF generally increases slightly after low-temperature heat release near 346 CAD, though this is not visible in the images because no detectable OH* chemiluminescence is emitted during low-temperature heat release. Weak OH* chemiluminescence first appears at 366 CAD, near the peak AHRR. The OH* chemiluminescence quickly brightens at 367 CAD as HF of all thermocouples starts to increase, all at nearly the same time. OH* chemiluminescence quickly disappears after 368 CAD, near the end of the heat release, while the HF continues after combustion while hot gases are near the wall, such that the HF spikes are not as narrow nor in phase with the AHRR.

While the HF of all thermocouples can be characterized as increasing sharply at the onset of rapid combustion for the premixed conditions of Figure I.2.2, the characteristics are different for other combustion modes. Figure I.2.3 shows corresponding HF, AHRR, and key OH* chemiluminescence images for a conventional diesel combustion (CDC) condition, for which the diesel injector delivers n-heptane starting at 350 CAD and at a load of 4.3 bar IMEPg. The diesel injector is mounted in the cylinder head such that the trajectory of one of the jets is aligned with thermocouples D1, T0, and U1–U3 from the perspective of the camera. In Figure I.2.3, the luminosity recorded in the images includes not only OH* chemiluminescence but also some soot natural luminosity. Also, the energizing of the injector solenoid interferes with the HF measurements, appearing as a downward and then upward spike from 347 to 353 CAD.

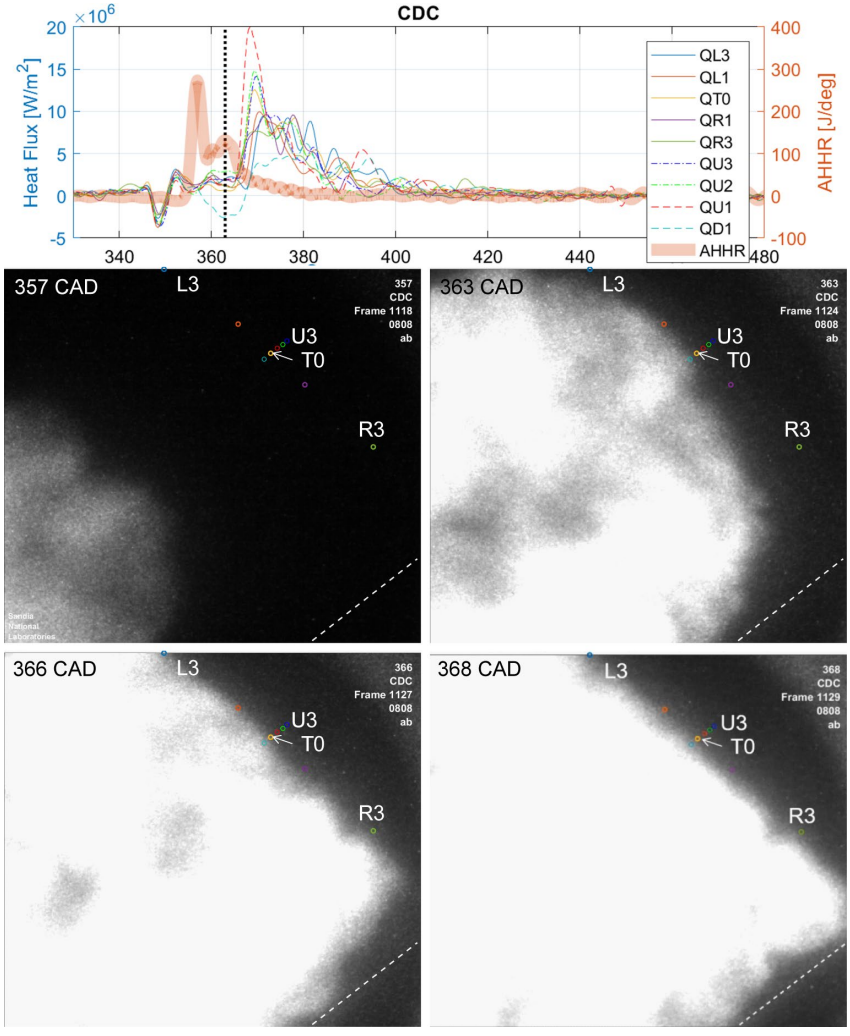

Figure I.2.3 AHRR and thermocouple HF measurements (top) and key OH* chemiluminescence images from one cycle of CDC. See Figure I.2.1 for physical locations of thermocouples, indicated by labels and color-coded circles.

For this operating condition, the ignition delay is relatively short, so a hot diffusion flame is established before the jet impinges on the wall where the thermocouples are located. Starting shortly after the start of combustion and after the injector solenoid energizing interference has ceased, the HF increases from 360 CAD to about 366 CAD, where it then increases more sharply. The OH* chemiluminescence images show that jet impingement on the wall occurs near 363 CAD, however. The low-level HF ahead of jet impingement (as indicated by OH* images) could be due in part to the pressure rise associated with combustion, radiative HT, or compression of the boundary layer ahead of the jet. After impingement, the thermocouples in line with the jet axis increase first, followed by thermocouples on either side of the jet, matching the spatial progression observed in the OH* chemiluminescence images as the jet impinges and flattens on the wall. However, there is a 3-degree crank-angle delay from impingement observed in the OH* chemiluminescence images to the rapid increase in HF. This also may be due to compression of the boundary layer ahead of the jet, or potentially to soot deposits for CDC conditions that may insulate the thermocouples for a short time.

A third operating condition, partially premixed compression ignition (PPCI), is shown in Figure I.2.4. This operating condition also uses n-heptane delivered by the diesel injector, but with an earlier start of injection at 335 CAD at a load of 4.0 bar IMEPg and with nitrogen dilution of the intake oxygen to 12.6% to simulate low-temperature combustion conditions using high exhaust gas recirculation. For this condition, the OH* chemiluminescence images show that ignition starts near the wall and quickly proceeds through the rest of the impinged jet, resulting in a narrow AHRR spike at the top of Figure I.2.4. Similar to the CDC condition, low-level HF precedes hot ignition, but in this case, it is more likely due to direct jet impingement on the wall, though some boundary layer compression may also contribute.

To explore the possible contribution of boundary layer compression to increased HF, simple scaling arguments are invoked. Figure I.2.5 shows a comparison of fired and motored HF for the CDC condition, with the shaded area indicating the difference in HF before jet impingement on the wall. Also shown in Figure I.2.5 are two different scalings of the motored HF according to two limiting scenarios, either one-dimensional (1-D) scaling of the boundary layer (BL) thickness according to the penetration distance of the jet, or isotropic scaling according to the volume of the penetrating jet. The effects of real three-dimensional fluid mechanics ahead of the jet that compress the boundary layer are expected to lie between these two extremes. Indeed, the measured HF lies between these two limits, suggesting that boundary layer compression may play an important role in local HT losses for operating conditions with jet impingement. However, other measurements in the literature in a constant-volume chamber did not observe a HF increase ahead of jet impingement [3], so this hypothesis needs to be revisited more carefully under fully non-reacting conditions where complications from combustion are not present.

Finally, in addition to the work on wall HF, the project continued simulation activities to develop insight into the interactions between multiple injections. Figure I.2.6 shows cross-sections of fuel, carbon monoxide (CO), and OH in a split-injection diesel jet as predicted by the simulations. The contributions to each of these quantities from the fuel of the two injections is separated in the plots. At the start of second-stage ignition, the simulations show that the second injection has mixed with first-injection residual jet to greatly increase local fuel concentration—the red color in the top fuel image, indicating high fuel concentration, is almost entirely from the second injection. Even so, products from first-stage ignition, such as CO, are primarily from first-injection fuel, again shown by the red color in the CO cross-sections. Importantly, the simulations therefore predict that the second-injection fuel is intimately mixed with first-stage ignition products of the first injection as the second-stage ignition commences. Later, after ignition, the OH cross-sections show that second-stage ignition products, such as OH, are primarily from the first-injection fuel. Even so, the simulations with a single injection show that the first injection would not ignite without the second injection. These simulation predictions provide guidance for planning what key measurements to include in fundamental experiments on mixing between injections and effects on ignition.

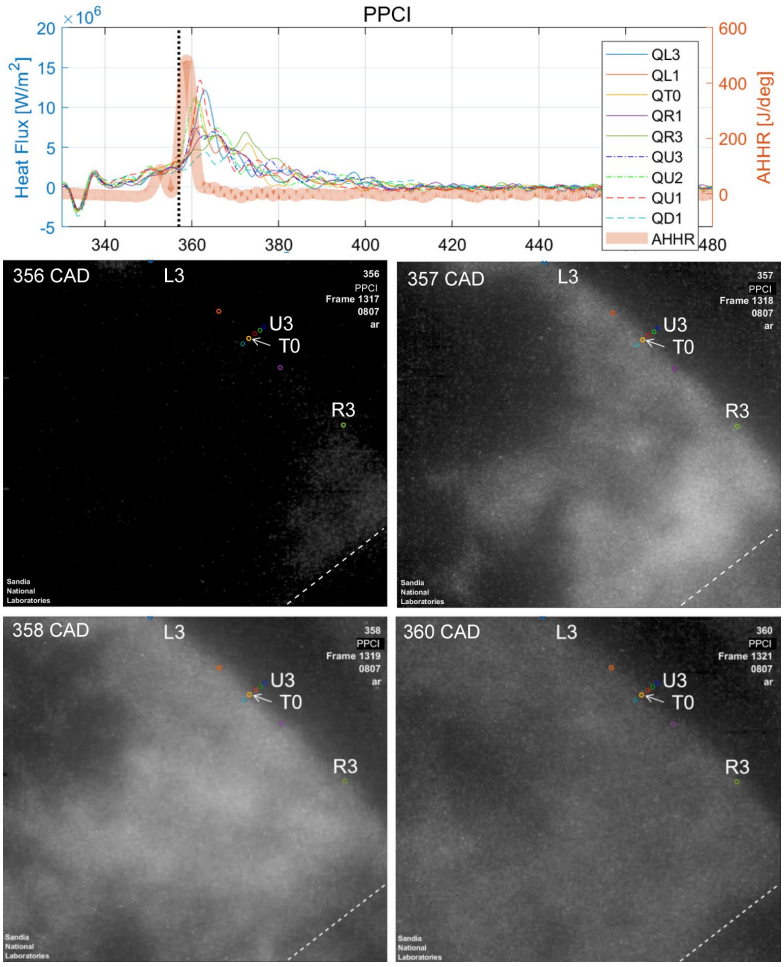

Figure I.2.4 AHRR and thermocouple HF measurements (top) and key OH* chemiluminescence images from one cycle of PPCI. See Figure I.1.1 for physical locations of thermocouples, indicated by labels and color-coded circles.

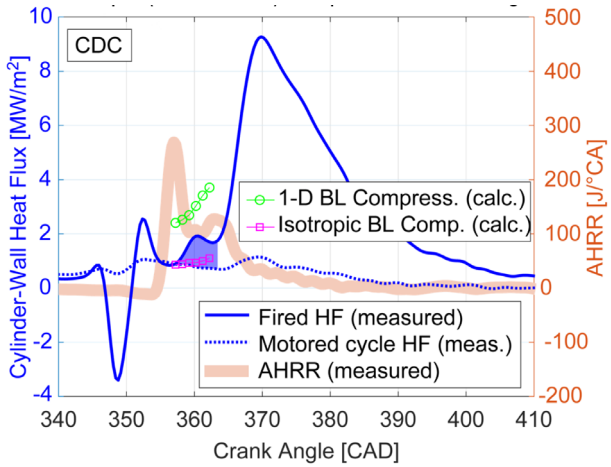

Figure I.2.5 Fired and motored thermocouple HF measurements and AHRR for CDC, with the shaded area indicating the difference between fired and motored HF ahead of jet impingement. Predictions from two simple scaling models are also included.

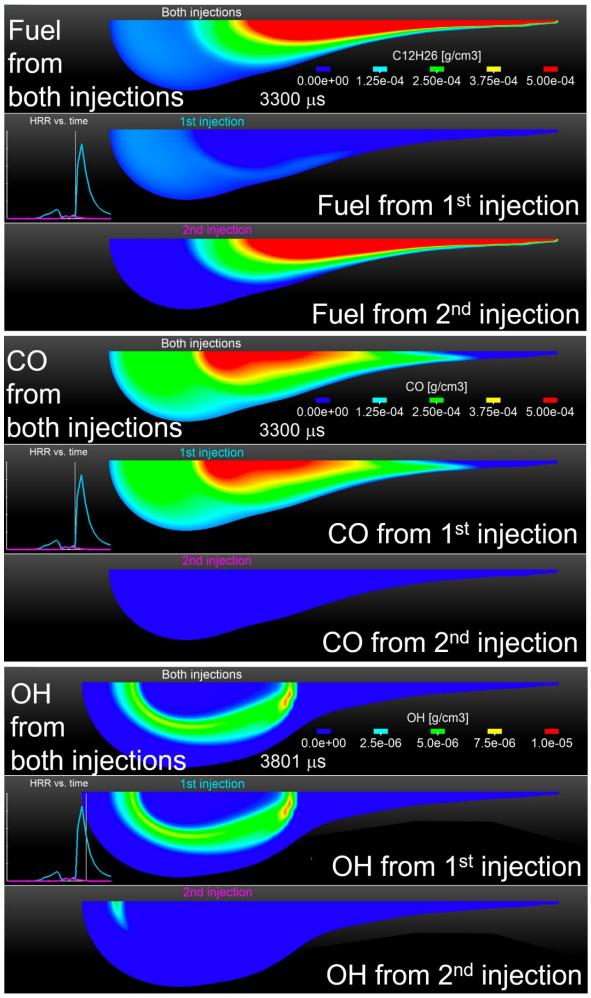

Figure I.2.6 Cross-sections of simulation-predicted fuel, CO, and OH according to the contributions of each injection of a split-injection diesel jet. Fuel and CO are at the start of second-stage ignition, and the OH is after the peak heat-release rate.

Conclusions

- Cylinder-wall heat flux measurements coupled with simultaneous OH* chemiluminescence imaging provide phenomenological insight into in-cylinder physical and chemical processes affecting heat transfer losses.
- Heat flux increases ahead of jet impingement for both CDC and low-temperature combustion, which is consistent with the hypothesis of boundary layer compression by penetrating jet, but further experiments are required to confirm the hypothesis.
- Future data analysis will provide similar insight into heat losses across multiple combustion modes.
- Split-injection simulations predict little displacement of the first-injection residual jet by the second injection, but much inter-jet mixing. Ignition products are from the first-injection fuel, but no ignition occurs without the second injection. These predictions help to guide experiments.

Key Publications/Presentations

1. Wissink, M.L., S.J. Curran, G. Roberts, M. PB Musculus, and C. Mounaïm-Rousselle. 2018. "Isolating the Effects of Reactivity Stratification in Reactivity-Controlled Compression Ignition with Iso-Octane and n-Heptane on a Light-Duty Multi-Cylinder Engine." *Int. J. Engine Research* 19 (9): 907–926.

2. Hessel, R., R. Reitz, and M. PB Musculus. 2019. "A Visual Investigation of CFD-Predicted In-Cylinder Mechanisms That Control First- and Second-Stage Ignition in Diesel Jets." SAE Technical Paper 2019-01-0543 (April).

3. Li, Z., G. Roberts, and M. PB Musculus. 2019. "Dilution and Injection Pressure Effects on Ignition and Onset of Soot at Threshold-Sooting Conditions by Simultaneous PAH-PLIF and Soot-PLII Imaging in a Heavy Duty Optical Diesel Engine." SAE Technical Paper 2019-01-0553 (April).

4. Qiu, L., R. Reitz, E. Eagle, and M. PB Musculus. 2019. "Investigation of Fuel Condensation Processes under Non-Reacting Conditions in an Optically-Accessible Engine." SAE Technical Paper 2019-01-0197.

5. Li, Z., and M. Musculus. 2018. "Multiple Injection Interactions on Ignition and Onset of Soot by Simultaneous PAH-PLIF and Soot-PLII Imaging." AEC Meeting (August), USCAR, Southfield, MI.

6. Musculus, M. 2018. "How Jets Get It All Mixed Up: Combustion Research Using Laser Diagnostics in Optical Engines at Sandia National Laboratories." Technical Seminar (November), UC Davis.

7. Li, Z., and M. Musculus. 2019. "Experimental Investigation of Cylinder-Wall Heat Flux under Five Combustion Modes: CDC, SIDI, HCCI, PPCI, RCCI." AEC Meeting (January), ORNL.

8. Musculus, M. 2019. "Comparison of Combustion Modes." Co-Optima 4th Annual All Hands Meeting (March), ORNL.

9. Musculus, M., D. Splitter, K. Kelly, C. Zhang, P. Miles, and R. Wagner. 2019. "The Benefits and Challenges of Pushing Engine BTE to Very High Levels (60%+): Where Is the Point of Diminishing Returns?" 21st Century Truck Partnership IC Powertrain Tech Team Meeting videoconference (April).

References

1. Splitter, D.A., R.M. Hanson, S.L. Kokjohn, and R.D. Reitz. 2011. "Reactivity Controlled Compression Ignition (RCCI) Heavy-Duty Engine Operation at Mid-and High-Loads with Conventional and Alternative Fuels." SAE Technical Paper 2011-01-0363.

2. Mohr, D., T. Shipp, and X. Lu. 2019. "The Thermodynamic Design, Analysis and Test of Cummins' Supertruck 2 50% Brake Thermal Efficiency Engine System." SAE Technical Paper 2019-01-0247.

3. Pickett, L., and J. López. 2005. "Jet-Wall Interaction Effects on Diesel Combustion and Soot Formation." SAE Technical Paper 2005-01-0921.

Acknowledgements

This research was sponsored by the U.S. Department of Energy's Office of Energy Efficiency and Renewable Energy. Optical engine experiments were conducted at the Combustion Research Facility, Sandia National Laboratories, Livermore, California. Sandia National Laboratories is a multi-mission laboratory managed and operated by National Technology and Engineering Solutions of Sandia, LLC, a wholly owned subsidiary of Honeywell International, Inc., for the U.S. Department of Energy's National Nuclear Security Administration under contract DE-NA0003525.

I.3 Spray Combustion and Soot Formation Cross-Cut Engine Research (Sandia National Laboratories)

Lyle M. Pickett, Principal Investigator
Sandia National Laboratories
P.O. Box 969, MS 9053
Livermore, CA 94551-9053
E-mail: LMPicke@sandia.gov

Michael Weismiller, DOE Technology Development Manager
U.S. Department of Energy
E-mail: Michael.Weismiller@ee.doe.gov

Start Date: October 1, 2018 End Date: September 30, 2019
Project Funding (FY19): $1,490,000 DOE share: $1,490,000 Non-DOE share: $0

Project Introduction

All future high-efficiency engines will have fuel sprayed directly into the engine cylinder. Engine developers agree that a major barrier to the rapid development and design of these clean, high-efficiency engines is the lack of accurate fuel spray computational fluid dynamics (CFD) models. The spray injection process largely determines the fuel–air mixture processes in the engine, which subsequently drive combustion and emissions in both direct-injection gasoline and diesel systems. More predictive spray combustion models will enable rapid design and optimization of future high-efficiency engines, providing more affordable vehicles and saving fuel.

Objectives

Overall Objectives

- Facilitate improvement of engine spray combustion modeling, accelerating the development of cleaner, more efficient engines
- Lead a multi-institution, international research effort on engine spray combustion called the Engine Combustion Network (ECN), with a focus on diesel and gasoline sprays.

Fiscal Year 2019 Objectives

- Organize workshop activities for the ECN, including monthly web meetings, standards, and topic organization
- Release comprehensive online ECN databases for diesel Spray D and Spray C (cavitating), including liquid penetration, vapor penetration, ignition, combustion, and soot formation processes
- Investigate internal flow leading to a different rate of injection (ROI) and mixture formation affecting diesel combustion
- Develop a three-dimensional spray diagnostic for multi-hole gasoline direct-injection sprays, including liquid penetration and plume direction under cold-start and flash-boiling operation
- Characterize mixing and soot formation for multiple-injection sprays with wall impingement.

Approach

The ECN, a multi-institution collaboration, has been established to accelerate the progression of predictive CFD modeling capabilities and leverage the expertise of the global spray research community. Having highly

vetted, quantitative datasets online [1] for both diesel and gasoline targets allows CFD models to be evaluated more critically and in a manner that has not happened to date. Productive CFD evaluation requires new experimental data with better quantification for the spray and the relevant boundary conditions, but the analysis also includes a working methodology to evaluate the capabilities of current modeling practices. Activities include the gathering of experimental and modeling results at target conditions to allow a side-by-side comparison and expert review of the current state of the art for diagnostics and engine modeling.

Experiments are performed in high-temperature, high-pressure spray facilities prepared to represent either diesel or gasoline engine conditions at the time of injection. Target conditions, such as the ECN diesel "Spray A" or "Spray D" operating condition, which uses an n-dodecane (single-component) fuel, or the gasoline "Spray G" operating condition for an eight-hole injector, are chosen as baseline conditions. Activities this year included construction of and experiments using transparent nozzles that match the geometry of the target fuel injector, development of diagnostics suited to a new high-throughput flow spray chamber, and experiments using multiple injections and with wall impingement to address combustion and soot formation dynamics. The topic of internal nozzle flow coupled to spray mixing is reviewed in this document. The references included discuss the other major objectives for this fiscal year and are available as a report.

Results

The project team constructed real-size, optically transparent nozzles to aid in understanding the initial conditions within a fuel injector, as well as how these conditions influence the spray delivery. The nozzles mount at the end of a modified solenoid-actuated ECN Spray A or Spray C/D injector body, as shown in Figure I.3.1. The transparent nozzles were machined and then hydroeroded to reach the same flow number, inlet rounding, and convergence as ECN Spray D. The transparent nozzles were clamped to metal injectors that had been ground flat just downstream of the usual metal needle-seat sealing surface [2],[3],[4].

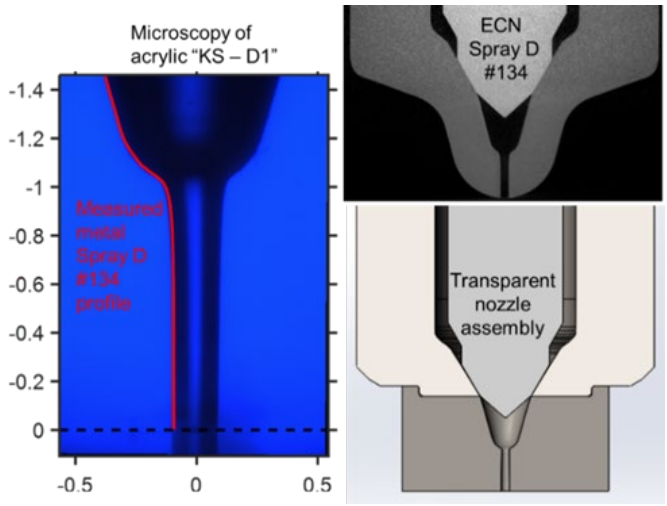

Figure I.3.1 Transparent nozzle construction and mounting for Spray D replicate

Visualization of fluid movement inside the nozzle at the beginning of injection led to a discovery about needle valve movement inside the injector, which ultimately is critical for CFD modeling approaches. At the left of Figure I.3.2 is shown high-speed imaging prior to the start of actual injection. The sac is initially full of liquid in this case, and as the needle begins to move, gas from the outside of the nozzle is pulled into the hole [2]. This result may be considered surprising because as the needle lifts open, high-pressure fuel should enter the sac and push liquid out of the hole, rather than the other way around. However, these observations led to further investigation of needle-movement measurements performed using X-ray diagnostics and confirmed by optical measurements within the nozzle [3], as shown in the middle of the figure. The indicated measurements are specifically for the movement of position N relative to the tip of the nozzle, as shown at the right of the

figure. The arrow in the figure shows that there is a displacement of the needle by approximately 5 µm well before (~100–200 µs) the actual start of injection. This feature is repeatable for different injectors and is within the resolution of the experiment. If this needle movement is applied directly as the needle lift within CFD, injection occurs much earlier than the actual start of injection. The ingestion of gas into the injector instead suggests that the gap at the needle-seat region, Position G, has not opened yet, and, in fact, the volume of the sac and hole must be increasing at first to draw gas inside the nozzle while contact at sealing surfaces remains.

To investigate the hypothesis that elasticity between injector components could cause an increase in volume as the needle moves and then opens, the project team performed finite element stress (FEA) analysis of the loaded injector, as shown at the right of Figure I.3.2. As a boundary condition, an axial force was applied to the needle to replicate the injector sealing force. To study the actual metal injector, the project used all steel components, not the hybrid version shown in Figure I.3.1 with both steel and acrylic. The upper end of the nozzle body was fixed to permit displacement/motion of the mating needle and nozzle pieces. The FEA simulations show the loaded state when the injector is fully closed and the reverse process to contact, but no load would represent the opening of the injector. FEA shows that the needle tip deforms approximately 3–4 µm axially relative to the tip or needle-seat datum, consistent with the measurement indicated by the arrow. The needle and nozzle both deform in the negative axial direction, but the needle moves more relative to the tip as it makes contact at the seat. Therefore, the bottom of the needle (Position N) is expected to move relative to the seat (Position G) as forces are relieved on the needle at the time of injection, ultimately causing an expansion of the volume in the sac and hole.

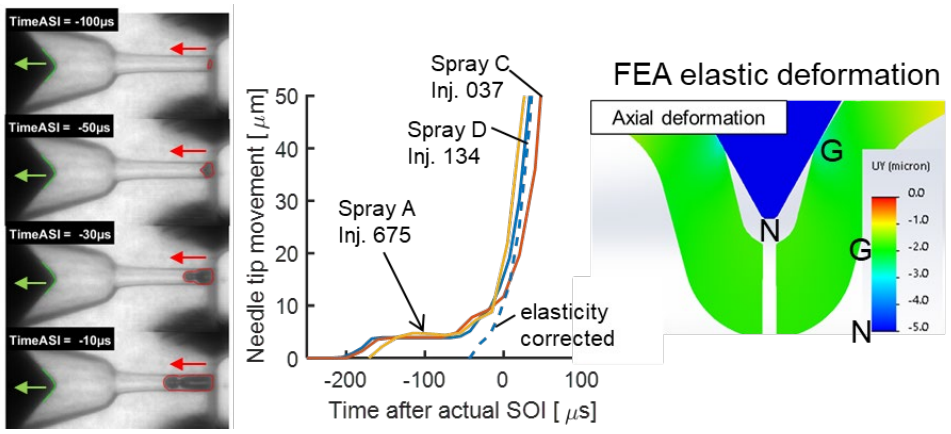

ASI – after start of injection; SOI – start of injection

Figure I.3.2 (left) Backlit imaging of the start of injection in the transparent Spray D replica with 1,000 bar injection pressure; (middle) measurement of needle tip movement N relative to nozzle tip by X-ray phase contrast imaging at Argonne National Laboratory, with data posted to the ECN website for Spray A, C, and D injectors [1]; (right) FEA predicting elastic deformation for metal injector components with needle valve in closed, loaded position

A key takeaway from these results is that the measured needle tip movement must be corrected for nozzle elasticity to represent the actual gap in the needle-seat region [2]. For example, the dashed line in Figure I.3.2 is the Spray D data corrected by 5 µm. This corrected profile is more appropriate for needle lift in internal flow CFD simulations and is recommended for use throughout the community.

While correct needle movement is important for accurate CFD simulations of internal flow, another important aspect is the initial gas–liquid state within the injector. The project studies using transparent nozzle visualization showed that gas is usually mixed into the injector at the end of injection [4]. Experimental results showed that the volume of gas in the sac after the needle closes depends upon the vessel gas pressure. Higher back pressure results in less cavitation and a smaller volume of ambient gas into the sac. However, a pressure decrease mimicking the expansion stroke causes the gas within the sac to expand significantly, proportional to the pressure decrease, while also evacuating liquid in front of the bubble. Because of the gas exchange and expansion, the sac may be significantly evacuated of liquid at the start of the next injection.

Utilizing the corrected needle-lift profile and the limiting condition of a completely evacuated sac, the project team performed CFD simulations of the needle movement while also considering very fine cell resolution in the needle-seat region to accurately model the restriction during startup of injection [2]. The resulting predictions of mass flow rate through the hole are shown in Figure I.3.3. The simulations show that gas injection leads liquid injection by approximately 10 µs; however, gas injection continues for the next 100 µs. Even after the hole mass flow rate (MFR) increases rapidly, a gas mixture dissolved into liquid is injected for a substantial time. By 125 µs ASI, the gas mass fraction decreases to near-zero levels, suggesting complete evacuation of gas from within the sac.

The shape of the ramp-up in MFR may be compared to the educated/virtual profile currently recommended for ECN Spray D simulations (at 100 MPa), as also plotted in Figure I.3.3. To adjust and evaluate the ramp-up MFR shapes, the educated ROI is time-shifted by 29 µs. The ramp-up slope for the educated ROI is consistent with the simulation MFR, neglecting the initial slower ramp. However, the educated ROI does not have the oscillations in ROI, which are related to the sac pressure oscillations. Such ROI oscillations may have a significant influence on the entire mixing field, particularly the onset of large-scale structures.

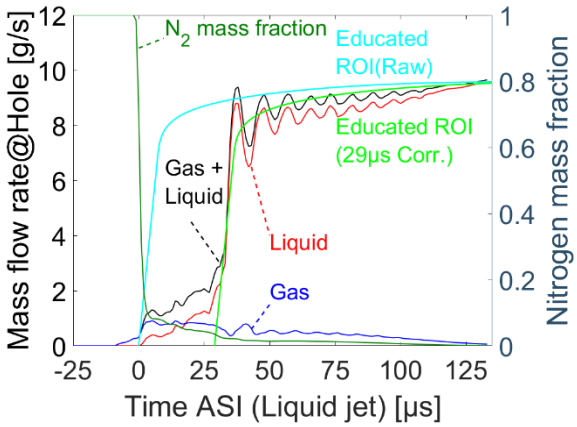

Figure I.3.3 MFR at the hole as a function of the time ASI of the liquid jet. MFR is recalculated as gas MFR and liquid MFR. Educated/virtual ECN ROIs are also shown for comparison. Nitrogen mass fraction for the fluid exiting the hole is indicated on the right axis.

Evidence that gas in the sac can alter the developing spray is found in high-speed microscopic imaging of Spray D and Spray C [7]. Figure I.3.4 compares the initial Spray C penetration with regular cooling of the injector to 90°C (in blue) and without cooling (approximately 150°C, in red). The images are rendered dark black where there is overlap between the two conditions. While timed to the same start of liquid injection, the cooler spray tends to penetrate more quickly. While the exact initial condition for the internal sac of the metal Spray C injector is unknown, it is expected that the hotter injector will have more gas in the sac. Having more gas within the injector, the ROI will ramp up more slowly, as indicated by Figure I.3.3.

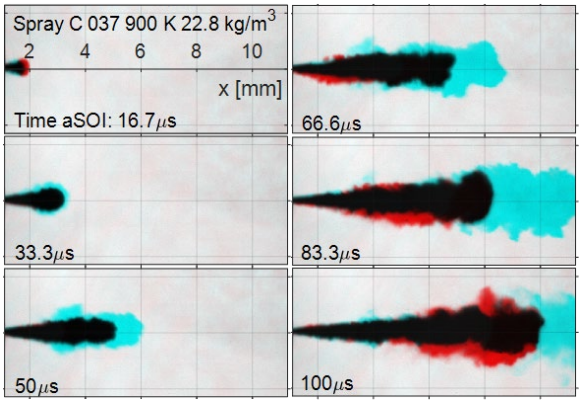

aSOI – after start of injection

Figure I.3.4 Overlaid, false-color long-distance microscopy images of Spray C #037 cooled (cyan, 90°C) and uncooled (red, 150°C) injectors. Overlapping regions are indicated in black. 900 K, 22.8 kg/m³, 0% oxygen gas.

A subtle difference in penetration of a few millimeters may not seem significant, but models of the jet penetration show that differences in the mixing field persist into the ignition region (and timings ASI), as shown in Figure I.3.5. Incorrect predictions of mixing, caused by inaccurate modeling of even the internal portions of the injector, may result in inaccurate combustion simulations.

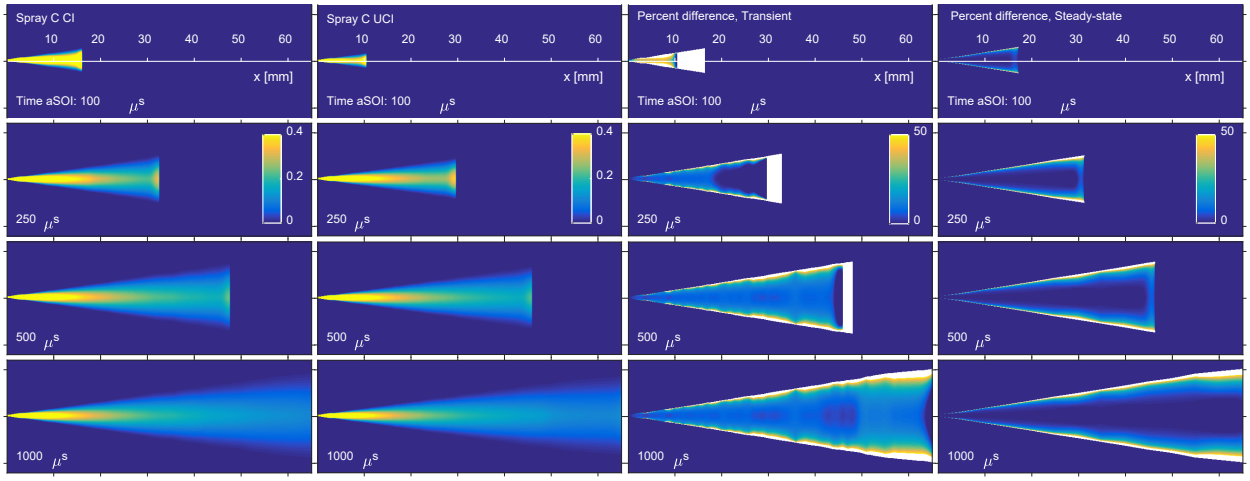

Figure I.3.5 One-dimensional modeled mixture fractions for Spray C cooled (CI) and uncooled (UCI) injectors using altered ROI and transient spreading angle models [7]. The percent difference color scale ranges from 0% to 50% (≥50% in white), and the mixture fraction ranges from 0 to 0.4.

Conclusions

Research in spray combustion this year has provided new information important for fuel sprays extending even inside the fuel injector. The ECN uses the diesel targets discussed, and the ECN community now uses the experimental data provided to improve CFD models that will be used to optimize future engine designs. Key activities for Fiscal Year 2019 included the following:

- Examination of internal nozzle flow using transparent nozzles, leading to discoveries about needle movement elasticity and gas exchange within the sac to create initial conditions with significant gas in the sac
- CFD simulations showing altered and slower ROI because of initial gas within the injector and more precise accounting for needle gap movement

- Near-field microscopy indicating clear differences in mixing and spray penetration, dependent upon the injector and the state of the sac, which persist to the timing of ignition and combustion.

Please see the references below for details about many other achievements/activities for Fiscal Year 2019.

Key Publications

See References [2],[3],[4],[5],[6] below.

References

1. Engine Combustion Network data archive. 2019. https://ecn.sandia.gov/.

2. Yasutomi, K., J. Manin, J. Hwang, L.M. Pickett, M. Arienti, S.A. Skeen, and S. Daly. 2019. "Diesel Injector Elasticity Effects on Internal Nozzle Flow." SAE 2019-01-2279.

3. Mitra, P., K. Matusik, D. Duke, P. Srivastava, K. Yasutomi, J. Manin, L.M. Pickett, C.F. Powell, M. Arienti, E. Baldwin, P.K. Senecal, and D. Schmidt. 2019. "Identification and Characterization of Steady Spray Conditions in Convergent, Single-Hole Diesel Injectors." SAE Technical Paper 2019-01-0281.

4. Abers, P.M., E. Cenker, J. Hwang, L.M. Pickett, and K. Yasutomi. 2019. "Effect of Pressure Cycling on Gas Exchange in a Transparent Fuel Injector." SAE Technical Paper 2019-01-2280.

5. Watanabe, N., N. Kurimoto, S.A. Skeen, E. Cenker, K. Yasutomi, and L.M. Pickett. 2019. "Ignition and Soot Formation/Oxidation Characteristics of Compositionally Unique International Diesel Blends." SAE Technical Paper 2019-01-0548.

6. Tagliante, F., T. Poinsot, L.M. Pickett, P. Pepiot, L.M. Malbec, G. Bruneaux, and C. Angelberger. 2019. "A Conceptual Model of the Flame Stabilization Mechanisms for a Lifted Diesel-Type Flame Based on Direct Numerical Simulation and Experiments." *Combustion and Flame* 201: 65–77.

7. Daly, S., E. Cenker, L.M. Pickett, and S.A. Skeen. 2018. "The Effects of Injector Temperature on Spray Characteristics in Heavy-Duty Diesel Sprays." *SAE Int.J.Engines* 11 (6): 879–891.

Acknowledgements

Scott A. Skeen is a coauthor of this report. We thank Hyung Sub Sim, Joonsik Hwang, Noud Maes, Koji Yasutomi, Naoki Watanabe, Shane Daly, Emre Cenker, Julien Manin, Lukas Weiss, Ioannis Karathanassis, Foivos Koukouvinis, Nathan Harry, Aaron Czeszynski, Tim Gilbertson, Alberto Garcia, Chris Ingwerson, Laurie Bell, David Cicone, and Nathan Prisbrey for their devoted research and support. Studies were performed at the Combustion Research Facility. Sandia National Laboratories is a multi-mission laboratory managed and operated by National Technology and Engineering Solutions for Sandia LLC, a wholly owned subsidiary of Honeywell International, Inc., for the U.S. Department of Energy's National Nuclear Security Administration under contract DE-NA0003525.

I.4 Low-Temperature Gasoline Combustion (LTGC) Engine Research (Sandia National Laboratories)

John E. Dec, Principal Investigator
Sandia National Laboratories
MS 9053, PO Box 969
Livermore, CA 94550
E-mail: jedec@sandia.gov

Michael Weismiller, DOE Technology Development Manager
U.S. Department of Energy
E-mail: Michael.Weismiller@ee.doe.gov

Start Date: October 1, 2018 End Date: September 30, 2019
Project Funding (FY19): $750,000 DOE share: $750,000 Non-DOE share: $0

Project Introduction

Improving the efficiency of internal combustion engines is critical for meeting global needs to reduce petroleum consumption and CO_2 emissions. Engines using low-temperature gasoline combustion (LTGC) (a superset of homogeneous-charge compression ignition [HCCI]) have a strong potential to contribute to these goals since their thermal efficiencies meet or exceed those of diesel engines. They also have very low NO_x and particulate emissions. LTGC can be applied either as a full-time operating strategy or, for light-duty engines, as part of a multimode combustion strategy in which the engine switches to conventional spark ignition at high loads. This multimode approach provides high efficiencies during LTGC operation at low and intermediate loads where light-duty engines operate most of the time and maintains high power density by switching to spark ignition for high loads. Full-time LTGC provides high efficiencies at all loads, as required for medium- and heavy-duty applications. LTGC engines have potential to cost less than diesels, and by providing medium- and heavy-duty engines that use gasoline with high efficiency, LTGC could help balance the demand for gasoline and diesel fuel, a problem that is expected to worsen if only conventional technologies are used. In all applications, LTGC allows gasoline to be used with high efficiency for better use of crude oil supplies and lower overall CO_2 production.

Although substantial progress has been made in understanding LTGC, several important aspects require additional research. In particular, rapid control of combustion timing remains a key technical barrier to the commercialization of these engines, and several studies related to this barrier were conducted at the Sandia LTGC Engine Laboratory in Fiscal Year (FY) 2019. The main effort in this area focused on further investigations and demonstrations of the potential of a new combustion-timing control method, first introduced last year, called additive-mixing fuel injection (AMFI), which can provide control over a wide range of conditions. A second effort involved developing a greater understanding of the use of partial fuel stratification (PFS) to control combustion timing. PFS has the advantage of providing near-instantaneous, next-cycle control but with a more limited control range than AMFI. However, the two techniques are synergistic, allowing them to be combined for more effective control of combustion timing.

Another technical barrier to practical LTGC engines involves low-load operation and combustion efficiency. The AMFI system provides a means to substantially improve low-load LTGC operation without the use of charge heating, and initial studies were conducted to determine the potential of this technique.

Finally, improved simulation tools are required to better understand LTGC and to optimize fuel-injection strategies and other parameters. Accordingly, we have continued our collaborations with the State University

of New York (SUNY)–Stony Brook to conduct computational fluid dynamics (CFD) simulations using large-eddy simulation (LES) to determine this technique's capability to predict PFS operation in LTGC engines.

Objectives

Overall Objectives

- Provide the fundamental understanding (science-base) required to overcome the technical barriers to the development of LTGC engines for light-duty and medium- and heavy-duty applications
- Explore methods of exploiting this fundamental understanding to develop practical techniques that can overcome these barriers to LTGC engines.

Fiscal Year 2019 Objectives

- Expand the understanding of the operating and control range for the new AMFI system
- Investigate the use of partial fuel stratification produced by double direct-injection PFS to control autoignition at naturally aspirated and low-boost conditions
- Collaborate with SUNY–Stony Brook to conduct CFD modeling to better understand the mixture formation with double direct-injection PFS
- Complete a study of the chemistry of ϕ-sensitivity, its relationship to octane sensitivity, and implications for fuel composition
- Continue collaborations with Lawrence Livermore National Laboratory to validate and improve kinetic models and surrogates.

Approach

Experimental studies were conducted in the Sandia LTGC Engine Laboratory using the all-metal single-cylinder LTGC research engine (displacement = 0.98 L). This facility allows operation over a wide range of conditions, and it has been designed to provide precise control of virtually all operating parameters, allowing well-characterized experiments. This LTGC research engine was derived from a Cummins B-series diesel, but the diesel piston was replaced with a custom LTGC piston having an open combustion chamber and a broad, shallow bowl. The compression ratio is 14:1 for all data presented in this report. The engine is equipped with a centrally located gasoline-type direct injector capable of 300 bar injection pressures supplied by General Motors. A research-grade E10 gasoline (gasoline blend with 10% ethanol) that is representative of regular-grade gasolines sold in the United States (called RD5-87) was used for these studies.

For improved control of combustion timing and improved operation at naturally aspirated and low-boost conditions, the engine's fueling system has been modified to include the AMFI system. This system doses the fuel with very small, but well-controlled, amounts of an ignition-enhancing additive each engine cycle, which provides robust control of autoignition timing and greatly reduces or even eliminates the need for charge heating. This new control system was first introduced last year, and it was found to work very well at the conditions investigated. Additional studies were conducted this year to understand the effects of other operating parameters, specifically charge temperature, higher intake-boost pressures, and exhaust gas recirculation (EGR), on the capabilities and benefits of the AMFI system. Based on understanding from previous works, the potential of combining additive mixing (AMFI) with controlled fuel stratification to improve low-load operation was also explored. Other previous works have shown that PFS has several potential benefits for higher-load LTGC, so studies were conducted on the use of PFS over a wide range of conditions for both non-additized fuel and additized fuel. These studies included an investigation of the ability of PFS to control combustion timing through a significant change in fueling rate. Additionally, we worked with collaborators at SUNY–Stony Brook to apply CFD with LES to a PFS sweep to determine the ability of these simulation tools to match experimental data.

Results

Control of combustion timing is perhaps the most challenging barrier to practical LTGC engines. Last year, we introduced a new, robust combustion-timing control technique with the inherent potential for control through rapid transients. This technique, called AMFI, can control combustion timing over a wide range, and it can also significantly reduce or even eliminate the heating/hot-residuals that are typically required to achieve autoignition in LTGC engines. The latter greatly simplifies the engine design, increases the power density, increases the thermal efficiency, and improves low-load operation.

Figure I.4.1 presents a block diagram schematic of the AMFI system. The system works by injecting very small amounts of an ignition-enhancing additive into the fuel to change the fuel's autoignition reactivity and thereby control the combustion timing (measured by the crank angle of the 50% burn point [CA50]) as the engine speed and load vary over the operating map. The additive used is 2-ethyl-hexylnitrate (EHN), a common diesel fuel ignition improver. The high-speed piezo-electric valve near the center of the block diagram schematic meters the tiny amounts of additive (~tenths to hundredths of a cubic millimeter) into the fuel each engine cycle. With these small amounts, it is estimated that a gallon-sized additive reservoir would only require refilling at service intervals of ~7,000 miles at a cost of ~$20, which is far less than the ~$150 savings in gasoline consumed over this same interval, compared to a conventional spark-ignition gasoline engine.

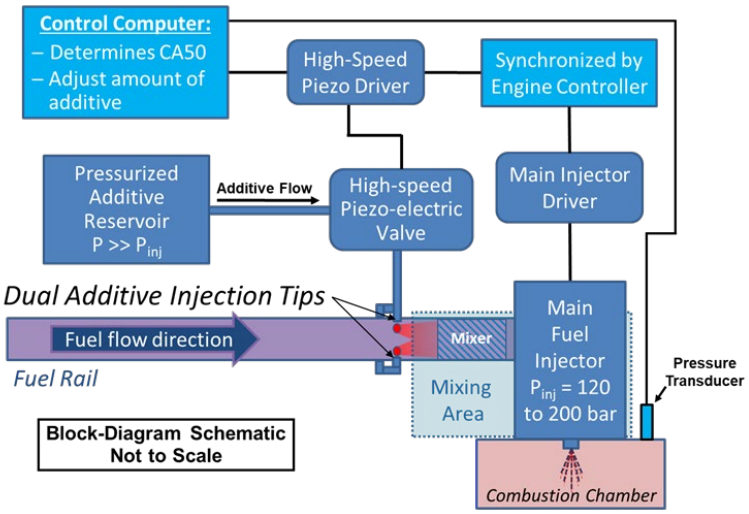

Figure I.4.1 Block diagram of the AMFI system

AMFI control of LTGC has been demonstrated for changes in fueling rate, engine speed, and low-boost operation [1]. In FY 2019, investigations of the potential of the AMFI system were expanded to include the effects of intake temperature (T_{in}), the performance of AMFI under higher-boost conditions requiring EGR, and the ability of the AMFI system to provide improved performance and CA50 control for low-load operation.

Figure I.4.2 shows that the AMFI system allows LTGC operation with no charge heating (T_{in} = 40°C) but that even modest increases in charge temperature can significantly reduce the amount of additive required to maintain the desired combustion stability criterion, ringing intensity (RI) = 3 MW/m^2 [2] in this case. The reduction in additive required is particularly large for the lowest equivalence ratio (ϕ) tested, ϕ = 0.36. Additionally, these results show that even if significant intake heating is applied, the additive remains effective and can still be used to precisely control CA50, as done for the higher T_{in} data points in Figure I.4.2.

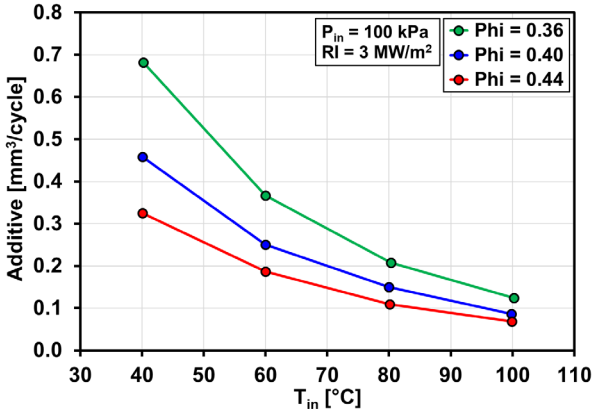

Figure I.4.2 Amount of additive required for intake temperatures (T_{in}) from 40 °C to 100 °C for ϕ = 0.36, 0.4, and 0.44. Additive amounts are those required to maintain RI = 3 MW/m^2. Intake pressure (P_{in}) = 1 bar; 1,200 rpm.

The ability of the AMFI system to control CA50 to maintain a constant RI = 5 MW/m^2 with changes in intake pressure (P_{in}) is shown in Figure I.4.3. Figure I.4.3(a) presents data from FY 2018 showing that the amount of additive required is reduced as the intake pressure is increased from 1.0 bar to 1.3 bar, representing moderate intake boosting. This occurs because the increased pressure enhances the autoignition [3], analogous to the effect of increased T_{in}. As the figure shows, the AMFI system can compensate for this by reducing the amount of additive supplied. However, extrapolating the additive data to higher P_{in} shows that the amount of additive required will go to zero as P_{in} is increased to about 1.4 bar, and at higher P_{in}, the fuel will be overly reactive even with no additive. For this reason, EGR is commonly used to reduce the reactivity of the charge at higher intake pressures (see for example Dec, et al. [3]). To determine whether the AMFI system can provide effective CA50 control at conditions using significant EGR, a new study was conducted in which P_{in} was increased to 1.6 bar and a relatively large amount of EGR, 48.3%, was used. This P_{in} was selected because it is well above the lowest P_{in} requiring EGR, and the amount of EGR used is well above the minimum required to prevent overly advanced combustion timing at this P_{in}, thus ensuring that the AMFI system was evaluated under conditions in which EGR has a large effect on autoignition. The results presented in Figure I.4.3(b) show that the AMFI system continues to work very well under these high-EGR conditions. As Figure I.4.3 shows, the AMFI system can compensate for changes in fueling rate (ϕ_m = 0.35, 0.37, and 0.39), and for each fueling rate, the CA50 can be adjusted by varying the amount of additive supplied. NO_x emissions remain far below the U.S. 2010 heavy-duty limit of 0.27 g/kWh for all data points. Furthermore, additional studies showed that even if the EGR rate varies, the amount of additive can be adjusted to compensate and maintain the desired CA50. This seamless tradeoff between additive and EGR indicates that the AMFI system should work well through transients in which amount and composition of the EGR are expected to vary.

Low-load operation is another important technical barrier to the commercialization of high-efficiency LTGC engines. Previous works have shown that obtaining good combustion efficiency at low loads requires the use of well-controlled fuel stratification [4]. Perhaps more importantly, for conventional LTGC operating strategies, it can be difficult to obtain enough heat from retained or rebreathed hot residuals to achieve autoignition at low loads. With the AMFI system, the additive enhances the autoignition reactions, but this effect alone is not sufficient for robust autoignition at low loads. However, the additive also makes the fuel ϕ-sensitive, meaning that richer regions in a stratified charge autoignite faster, even though they are cooler because of greater vaporization cooling from the larger amount of fuel. (Note that non-additized gasoline is not very ϕ-sensitive at naturally aspirated conditions [5].) Thus, with the AMFI system, stratifying the charge at low loads to improve combustion efficiency simultaneously enhances the autoignition, allowing robust autoignition with little or no heating and with only moderate amounts of additive.

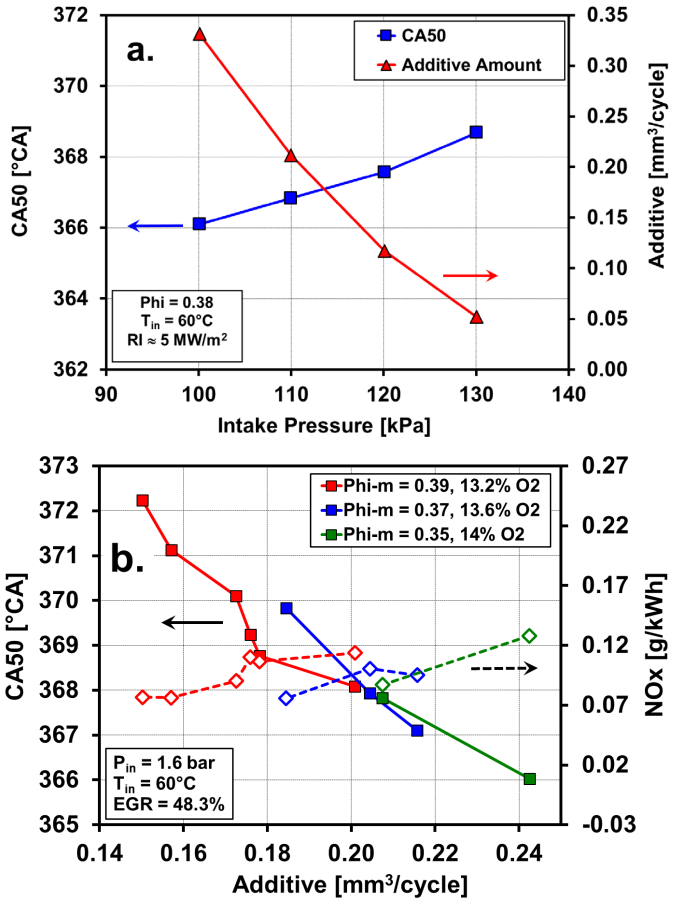

Figure I.4.3 (a) Amount of additive required to maintain RI = 5 MW/m² as P_{in} is increased from 1.0 bar to 1.3 bar at ϕ = 0.38. (b) CA50 and NO_x emissions vs. the amount of additive supplied for P_{in} = 1.6 bar with 48.3% EGR, for three fueling rates, ϕm = 0.35, 0.37, and 0.39 [5]. T_{in} = 60°C, 1,200 rpm.

This ability of the AMFI system to allow good low-load operation is demonstrated by the experimental results in Figure I.4.4. For these data, the T_{in} was held constant at a relatively low value of 60ºC, and the additive/fuel ratio was held constant at the amount required to get good autoignition for a well-mixed charge at ϕ = 0.32. The highest load shown, ϕ = 0.31, requires only mild charge stratification, and a start-of-injection (SOI) timing of 290 crank angle degrees (CAD) is used (i.e., 290 CAD after top dead center [TDC]-intake, or 70 CAD before TDC-compression), as shown in the Figure I.4.4 legend. As fueling is reduced to ϕ = 0.286, the combustion efficiency falls, causing the gross indicated mean effective pressure (IMEPg) to drop faster than the fueling rate; however, increasing the stratification by retarding the SOI to 305 CAD brings the combustion efficiency back, significantly increasing the IMEPg at ϕ = 0.286. As the fueling is further reduced, the SOI is progressively retarded in a series of steps to maintain good combustion efficiency, and the increased stratification also keeps CA50 in the range for good combustion stability with no adjustment of the amount of additive or the T_{in}, as the fueling is reduced down to the lowest load shown, IMEPg = 2.0 bar. At this load, the indicated thermal efficiency is still 37%, which is quite high compared to other combustion modes, and there is good potential for further improvement.

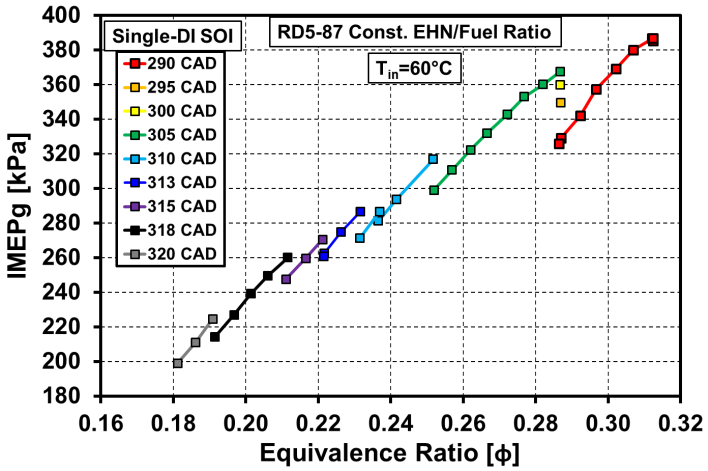

Figure I.4.4 Load (IMEPg) vs. fueling rate (ϕ) for stratified operation at low loads using a single direct injection (DI) at the SOI timings shown in the legend. T_{in} = 60°C, P_{in} = 1.0 bar, 1,200 rpm.

PFS is a technique that has several advantages for improving LTGC at higher loads if the fuel is sufficiently ϕ-sensitive. For this technique, an early fuel injection (SOI1), typically with an SOI = 60 CAD after TDC-intake, establishes a base fuel concentration, then a second injection at a variable time during the compression stroke (SOI2) produces a distribution of local equivalence ratios above the base ϕ. When the fuel is ϕ-sensitive, this ϕ distribution causes the autoignition to occur sequentially from the richest region to the leanest, which increases the combustion duration, reducing the peak heat release rate and, therefore, the maximum pressure rise rate. This has the advantages of (1) reducing the combustion noise or allowing a more advanced CA50 for higher efficiency at the same noise level, (2) allowing a higher fueling rate at the same CA50 without increasing noise or without inducing engine knock, or (3) various combinations of noise reduction, CA50 advancement, and increased load. PFS can also control CA50 because the richest regions produced by the PFS autoignite first, advancing the combustion timing compared to a well-mixed charge at the same global equivalence ratio. Figure I.4.5 illustrates this ability to control CA50 with PFS at a P_{in} of 1.3 bar, for which the RD5-87 gasoline is ϕ-sensitive. For an SOI2 = 200 CAD (early in the compression stroke), the charge is fairly well mixed, and CA50 is quite retarded (374 CAD = 14 CAD after TDC-compression). Then, as SOI2 is retarded to 325 CAD (late in the compression stroke), the amount of stratification increases substantially, advancing CA50 by about 8 CAD.

It is also important to develop simulation tools that can predict the behavior of LTGC combustion under stratified and partially stratified conditions in order to better optimize fuel injection strategies and other parameters. To this end, our collaboration partners at SUNY–Stony Brook have conducted CFD simulations using LES of LTGC with PFS in the engine under the same conditions used for the experimental data in Figure I.4.5. As the figure shows, the CFD-LES results match the experimental data well over the range of SOI2s investigated, giving confidence in the computational results. Future studies are planned using a matching optically accessible engine to verify the model's ability to correctly simulate fuel distributions under PFS conditions. Once validated, this simulation technique can provide a wealth of information about in-cylinder conditions that can be used to improve LTGC combustion but that would be difficult to measure experimentally.

The data in Figure I.4.5 show that PFS can adjust CA50 over a fairly wide range; furthermore, because the technique involves only changes in fuel injection, CA50 adjustments with PFS occur on the next engine cycle, making them essentially instantaneous.

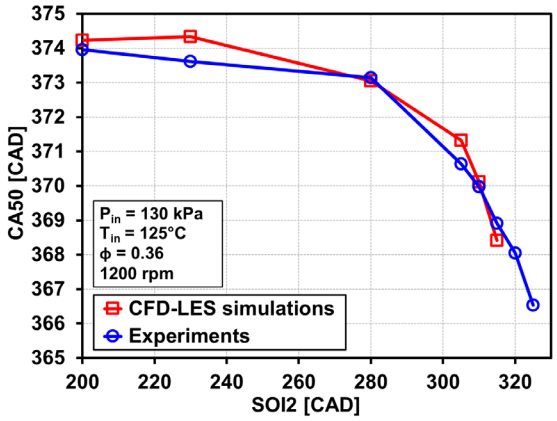

Figure I.4.5 A comparison between experimental measurements and CFD-LES simulations of CA50 as a function of SOI2 timing for PFS operation. For this typical PFS condition, the fuel was split 80/20 between SOI1 and SOI2. P_{in} = 1.3 bar, T_{in} = 125°C, ϕ = 0.36, 1,200 rpm. Both CA50 and SOI2 are CAD after TDC-intake.

To investigate the potential of PFS for transient control, the engine's fueling rate was varied from ϕ = 0.42 to ϕ = 0.32 in a series of steps using only PFS to maintain an acceptable CA50. Results for straight RD5-87 gasoline are shown by the red data points in Figure I.4.6. For this PFS-controlled load sweep, T_{in} was held constant at 152ºC, and as ϕ was reduced, the stratification was progressively increased by retarding SOI2 or increasing the fuel fraction in the second injection. The greater stratification increased the autoignition reactivity (see Figure I.4.5), compensating for the effect of the lower ϕ, to maintain good combustion stability. (For reference, this reduction in ϕ would have required T_{in} to be increased by about 23ºC if PFS had not been applied.) In addition to controlling CA50 for good combustion stability, carefully controlling the PFS kept NO_x below the U.S. 2010 heavy-duty (HD) limit, as shown on the right-hand axis of Figure I.4.6. These results show that PFS can provide near-instantaneous CA50 control through a transient, but its control range is more limited than that of the AMFI system. Therefore, it may be advantageous to combine the fast PFS control with AMFI control to extend the control range.

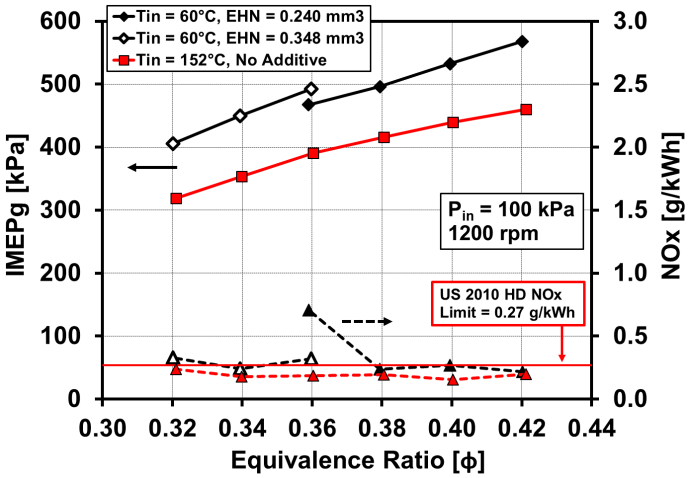

Figure I.4.6 Fueling rate (ϕ) sweeps using PFS to control CA50 for the straight E10 gasoline (red) and for EHN-additized E10 gasoline (black) with an adjustment in the amount of additive at ϕ = 0.36 to demonstrate combined PFS and AMFI control. T_{in} = 152°C for the straight fuel and 60°C for the additized fuel, P_{in} = 1.0 bar, 1,200 rpm.

The black data points in Figure I.4.6 show a fueling-rate sweep using PFS to control CA50 for EHN-additized fuel, combined with adjustment of the amount of additive at $\phi = 0.36$, as might be done using a combined AMFI-PFS control strategy. For these data, T_{in} was held constant at 60ºC, which increases the charge density compared to the straight fuel, so loads (IMEPg) are higher for a given ϕ, as can be seen in the figure. As with the straight fuel discussed above, stratification was increased as ϕ was reduced to maintain stable combustion. From $\phi = 0.42$ to $\phi = 0.38$, NO_x remains low, but at $\phi = 0.36$, NO_x emissions begin to rise. The amount of additive was then increased as shown in the legend, which allowed the amount of stratification to be reduced, decreasing NO_x emissions back to near the U.S. 2010 limit. Stratification alone was then used to maintain the CA50 as ϕ was reduced from 0.36 to 0.32.

Conclusions

- New investigations were conducted to further understand and demonstrate the capabilities of the AMFI combustion-timing control and operating system for LTGC engines, first introduced last year.
    - The AMFI system allows LTGC operation with little or no charge heating, but even modest increases in charge temperature greatly reduce the amount of additive required. The additive remains effective for precise CA50 control, even with significant charge heating.
    - Intake boost enhances autoignition, reducing the amount of additive required to achieve autoignition, and for $P_{in} \geq 1.4$ bar, EGR is required to prevent overly advanced combustion, even if no additive is supplied.
    - The AMFI system continues to provide precise CA50 control and control through changes in engine load, even when significant EGR is used at these higher boost pressures ($P_{in} \geq 1.4$ bar).
    - Adjusting the amount of additive can smoothly compensate for variations in EGR to obtain the desired CA50.
- Good LTGC operation was obtained for low loads down to IMEPg = 2 bar using the AMFI system combined with controlled fuel stratification. Additive amounts remain low because stratification enhances the effect of the additive in addition to improving low-load combustion efficiency.
- An extensive study of PFS over a wide range of conditions showed that PFS can provide near-instantaneous, next-cycle CA50 control for both non-additized and additized regular E10 gasoline. The CA50 control range is significant, but PFS must be combined with AMFI or another technique to obtain the full control authority required for LTGC engines.
- CFD-LES simulations of LTGC operation using PFS for CA50 control matched the experimental results well over a range of second-injection timings, showing the potential of CFD with LES to improve the understanding of in-cylinder processes in LTGC engines.
- PFS was demonstrated to be capable of providing CA50 control for a 24% reduction in fueling rate while maintaining NO_x below U.S. 2010 heavy-duty standards using straight E10 gasoline. An example of combined AMFI and PFS control through a load sweep was also presented.

Key Publications, Presentations, Awards, and Patents

1. Lopez-Pintor, D., J.E. Dec, and G.R. Gentz. 2019. “ϕ-Sensitivity for LTGC Engines: Understanding the Fundamentals and Tailoring Fuel Blends to Maximize this Property.” SAE Technical Paper 2019-01-0961, presented at the SAE 2019 World Congress. doi:10.4271/2019-01-0961.

2. Gentz, G.R., J. Dernotte, C. Ji, D. Lopez-Pintor, and J.E. Dec. 2019. "Combustion-Timing Control of Low-Temperature Gasoline Combustion (LTGC) Engines by Using Double Direct-Injections to Control Kinetic Rates." SAE Technical Paper 2019-01-1156, presented at the SAE 2019 World Congress. doi:10.4271/2019-01-1156.

3. Dec, J.E., G.R. Gentz, and D. Lopez-Pintor. 2019. "A Device for Rapid, Robust Combustion-Timing Control of LTGC Engines." Oral only presentation at the 2019 World Congress (April).

4. Sofianopoulos, A., M.R. Boldaji, B. Lawler, S. Mamalis, and J.E. Dec. 2019. "Effect of Engine Size, Speed, and Dilution Method on Thermal Stratification of Premixed HCCI Engines – A Large Eddy Simulation Study." *Int. J. Engine Research*, in press Nov. 2018, on-line publication available January 2019. doi:10.1177/1468087418820735.

5. Lopez-Pintor, D., J.E. Dec, and G.R. Gentz. 2019. "Understanding the Relationship between Octane Index and ϕ-Sensitivity for LTGC Engines." AEC Working Group Meeting (January).

6. Gentz, G.R., D. Lopez-Pintor, and J.E. Dec. 2019. "Investigating the Potential of Mixture Stratification for CA50 Control in an LTGC Engine." AEC Working Group Meeting (January).

7. Lopez-Pintor, D., J. Dec, and G.R. Gentz. 2019. "Evaluating a Custom Gasoline-Like Blend Designed to Improve ϕ-Sensitivity, RON and S." AEC Working Group Meeting (August).

8. Gentz, G.R., D. Lopez-Pintor, and J.E. Dec. 2019. "Mixture Stratification for CA50 Control of LTGC Engines with Reactivity-Enhanced and Non-Additized Gasoline." AEC Working Group Meeting (August).

9. Dec, J.E. 2019. "Low-Temperature Gasoline Combustion (LTGC) Engine Research." DOE Annual Merit Review, Office of Vehicle Technologies (June).

10. Invited Presentation at International Meeting: Dec, J.E., D. Lopez-Pintor, and G.R. Gentz. 2018. "ϕ-Sensitivity and ITHR – Key Fuel Properties for Advanced Compression Ignition Engines." SAE Co-Optimization of Fuels and Engines Symposium, Plymouth, MI (October 9–10).

11. Plenary Lecture at International Meeting: Dec, J.E. 2019. "Key Challenges and Solutions to Practical LTC-Gasoline Engines – Including a New Combustion-Timing Control Technique." Hyundai Engine Forum 2019, Hwaseong, S. Korea (July 4).

12. Lopez-Pintor, D. 2019. **Excellence in Oral Presentation Award** for SAE International Congress presentation of SAE Technical Paper 2019-01-1156.

13. **U.S. Patent No. 10,202,929 Issued**: Dec, J.E., and R.F. Renzi. 2019. "Additive-Mixing Fuel-Injection System for Internal Combustion Engines." (February 12).

References

1. Dec, J.E. 2018. "Low-Temperature Gasoline Combustion (LTGC) Engine Research." DOE Vehicle Technologies Office, Advanced Combustion Engines and Fuels, 2018 Annual Progress Report, report I.4, pp. 51–59. https://www.energy.gov/eere/vehicles/annual-progress-reports.

2. Eng, J.A. 2002. "Characterization of Pressure Waves in HCCI Combustion." SAE Technical Paper 2002-01-2859, doi:10.4271/2002-01-2859.

3. Dec, J.E., and Y. Yang. 2010. "Boosted HCCI for High Power without Engine Knock and with Ultra-Low NO_x Emissions – Using Conventional Gasoline." *SAE Int. J. Engines* 3 (1): 750–767. doi:10.4271/2010-01-1086.

4. Hwang, W., J.E. Dec, and M. Sjöberg. 2007. "Fuel Stratification for Low-Load Combustion: Performance & Fuel-PLIF Measurements." *SAE Transactions* 116 (3): 1437–1460. SAE paper 2007-01-4130, doi:10.4271/2007-01-4130.

5. Ji, C., J. Dec, J. Dernotte, and W. Cannella. 2014. "Effect of Ignition Improvers on the Combustion Performance of Regular Gasoline in an HCCI Engine." *SAE Int. J. Engines* 7 (2). doi:10.4271/2014-01-1282.

Acknowledgements

The author would like to thank post-doctoral researchers Dario Lopez-Pintor and Gerald Gentz for their significant contributions to the research reported here. The author is also grateful to Tim Gilbertson, Keith Penney, Aaron Czeszynski, and Alberto Garcia for their dedicated support of the LTGC Engine Laboratory.

Sandia National Laboratories is a multi-mission laboratory managed and operated by National Technology and Engineering Solutions of Sandia, LLC, a wholly owned subsidiary of Honeywell International, Inc., for the U.S. Department of Energy's National Nuclear Security Administration under contract DE-NA0003525.

I.5 Gasoline Combustion Fundamentals (Sandia National Laboratories)

Isaac W. Ekoto, Principal Investigator
Sandia National Laboratories
7011 East Avenue
Livermore, CA 94551
E-mail: iekoto@sandia.gov

Michael Weismiller, DOE Technology Development Manager
U.S. Department of Energy
E-mail: Michael.Weismiller@ee.doe.gov

Start Date: October 1, 2018 End Date: September 30, 2019
Project Funding (FY19): $930,000 DOE share: $930,000 Non-DOE share: $0

Project Introduction

Aggressive U.S. Department of Energy (DOE) Vehicle Technologies Office gasoline engine fuel economy and pollutant emissions targets can be met through some combination of reduced heat transfer, lower throttling losses, shorter combustion durations, lower combustion temperatures, improved mixture preparation, and higher compression ratios. Charge dilution by air or exhaust gas recirculation (EGR) is the most common method to achieve many of these benefits for low-power conditions, but the benefits of increased dilution are offset by poorer combustion stability. A major limitation of higher dilution levels is slow early burning rates with conventional inductor coil ignition systems. Advanced ignition technologies are needed to produce larger and more energetic ignition volumes while still performing well under elevated cylinder densities and charge motions. There is also opportunity for ignition systems to be an important source of radicals and heat that are used to tailor gasoline reactivity for advanced compression-ignition strategies. However, there is a lack of foundational understanding of igniter mechanisms for new technologies, which inhibits the development of production-ready systems.

Objectives

The objective is to achieve better understanding of ignition physical and chemical processes and use this information to develop more reliable engine simulation submodels. Relevant ignition processes include plasma formation from deposited electrical energy, plasma-to-flame transition, and flame kernel development. Experiments were performed in a single-cylinder research engine and ignition test vessels, each with optical access. In situ optical diagnostics and ex situ gas sampling measurements were used to elucidate important ignition process details. The project audience is automotive original equipment manufacturers, Tier 1 suppliers, and technology startups.

Overall Objectives

- Identify ignition technologies that enable effective combustion control for advanced gasoline engines
- Measure fundamental properties of ignition using advanced optical diagnostics
- Develop accurate and robust ignition process models for engine simulations.

Fiscal Year 2019 Objectives

- Evaluate the influence of ozone (O_3) addition on spark-assisted compression-ignition (SACI) strategies
- Prototype various pre-chamber and barrier discharge ignition systems
- Measure transient plasma ignition characteristics, including potential O_3 formation.

Approach

Research to characterize different ignition processes and associated engine combustion has leveraged experimental and numerical results from multiple partners. Prior to Fiscal Year (FY) 2019, the primary ignition technology investigated was transient plasma ignition (TPI), a form of low-temperature plasma formed by very-short-pulse, high-voltage electrical discharges. In FY 2019, additional ignition technologies evaluated included radio frequency corona and conventional inductor coil spark systems. Prototype igniters were also developed, such as barrier discharge igniters that augment radical formation, and plasma pre-chamber igniters that extend dilution tolerance limits without active fueling. In-house ignition test facilities were used to characterize thermal energy deposition, ignition volume, and radical formation for a range of electrode configurations. Impactful results were shared with Riccardo Scarcelli of Argonne National Laboratory, who modeled both the plasma discharge using non-equilibrium plasma solvers such as VizGlow or VizSpark and the associated transition to a sustained flame using the computational fluid dynamics solver, CONVERGE.

Methods to tailor fuel properties through the use of onboard generated O_3—a powerful oxidizing chemical agent generated through coronal discharges in intake air—for SACI combustion strategies were also explored. For these experiments, O_3 was seeded in the intake, and ignition was from a conventional sparkplug. Complementary rapid compression machine experiments at the PRISME Laboratory at the University of Orléans, France, were used to investigate the change in gasoline reactivity with O_3 addition.

Results

Performance and emissions characteristics for fuel-lean SACI combustion strategies with 30 ppm of added O_3 were explored in a single-cylinder, optically accessible, spray-guided research engine. End gas reactivity was previously found to increase with O_3 addition [1], but end gas autoignition still requires intake heating of 150°C or more for low-load operating conditions. For FY 2019 engine experiments, additional end gas thermal energy was supplied by the spark-initiated deflagration. Stratification helped to strengthen the deflagration but was also the primary source of nitrogen oxide (NO_x) emissions and thus had to be minimized. Intake pressure was fixed at 1.0 bar, and the intake temperature was kept at 80°C or lower. Engine load was varied between 1.5 bar and 5.5 bar indicated mean effective pressure (IMEP), and engine speed varied between 800 rpm and 1,600 rpm. Fuel stratification was achieved by a late-cycle injection of ~10%–25% of the total fuel and was used to maintain stable operation for the lowest loads. For each condition, spark timing, second start-of-injection timing, and fuel split between the main and second injection were optimized to maximize efficiency, with NO_x emissions held below 5 g/kg-fuel. Impactful results are as follows (see Figure I.5.1):

- Ozone addition decreased indicated specific fuel consumption (ISFC) by up to 9% across the map.
- Atomic oxygen initiated low-temperature heat release reactions in the end gas.
- End gas temperatures required for autoignition were reduced by up to 200 K with O_3 addition.
- Relative to stratified operation, homogeneous operation reduced NO_x emissions by an order of magnitude while maintaining comparable efficiency, albeit over a more limited load/speed range.

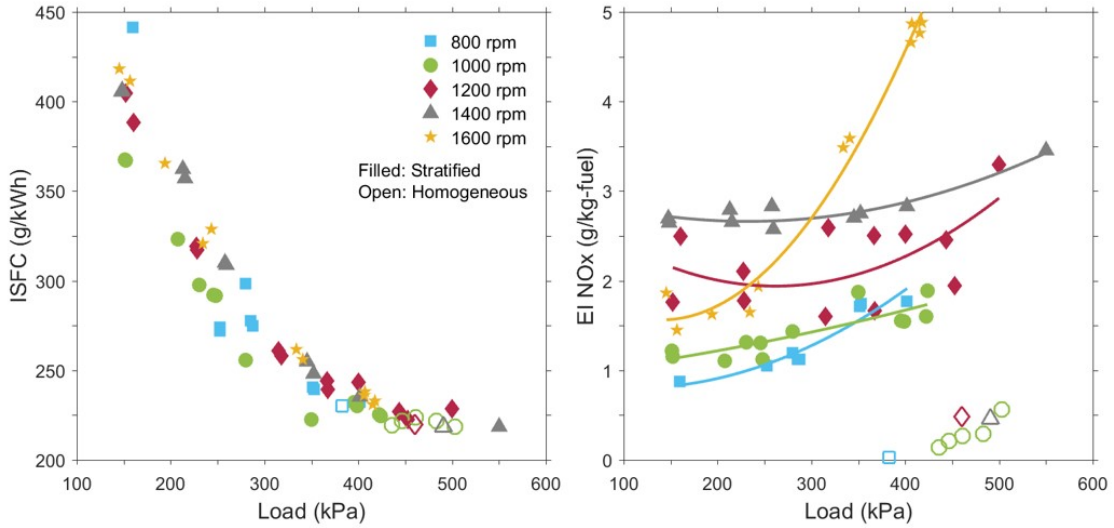

EI NO_x – emissions index of oxides of nitrogen

Figure I.5.1 Plots of ISFC and NO_x emissions as a function of load at engine speeds of 800–1,600 rpm for stratified and homogeneous SACI operation with intake-seeded O_3

A simplified analysis was developed to evaluate the end gas thermal energy deficit needed to initiate autoignition. As can be observed in Figure I.5.2(a), heat release rates from the initial spark deflagration were well matched, regardless of whether or not there was in-cylinder O_3. Accordingly, the increased thermal energy from the early deflagration was estimated from the integrated heat release up to the onset of low-temperature heat release, identified by the initial positive value in the profile difference. The green hatched area illustrates that the integrated energy is attributed exclusively to the early deflagration heat release.

- Ozone addition only influences end gas autoignition chemistry and not the deflagration.
- The energy deficit was greatest for higher engine speeds (i.e., shorter residence times) and lower loads (i.e., leaner and hence less reactive end gas mixtures).

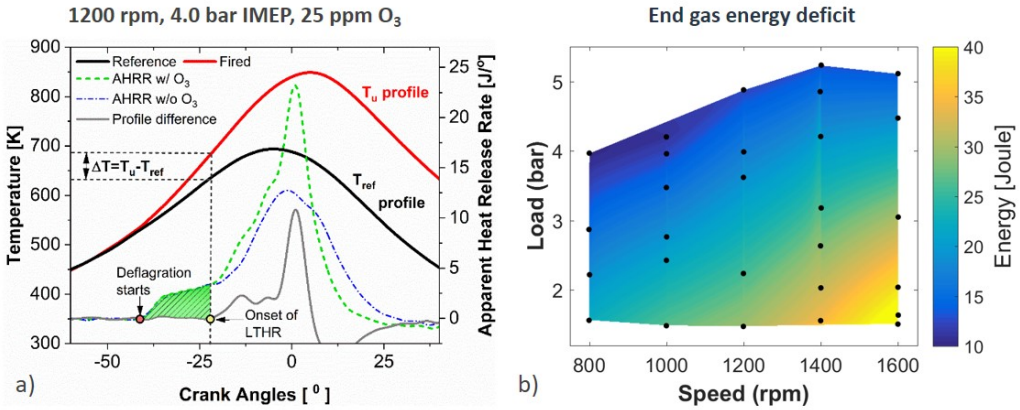

AHRR – apparent heat release rate

Figure I.5.2 (a) Schematic illustration of the heat release difference with and without O_3 addition and (b) the end gas energy deficit needed for optimal end gas autoignition estimated from the integrated heat release up to low-temperature heat release

To further reduce engine-out NO_x emissions, it is necessary to reduce or eliminate charge stratification. Doing this requires more robust ignition systems that can extend lean and dilute ignition limits while also promoting faster initial burn rates. These features likewise benefit more conventional combustion strategies by enabling greater dilution rates and shortening combustion durations. Accordingly, TPI ignition and early flame characteristics were investigated in an optically accessible ignition test vessel for near-atmospheric lean and EGR dilute propane/air mixtures. Transient plasma was generated using an available high-voltage (~35 kV), short-duration (~12 nanoseconds) pulse generator, with a ten-pulse burst discharged at 10 kHz. A wide-gap pin-to-pin (P2P) as well as partial and full barrier discharge igniter (BDI) configurations were evaluated. The first BDI had a flush-mounted and exposed anode tip, while the second had the tip covered by a high-dielectric-strength epoxy. Detailed schematics and images of igniter discharge characteristics are provided in Figure I.5.3. From these images it can be observed that P2P consistently produces twin streamers that bulge in the middle and connect at both electrodes, while both BDI configurations form luminous streamers around the insulator that produce large radical concentrations. High-speed schlieren imaging was used to characterize discharge streamer phenomena and estimate flame propagation rates. Flame propagation measurements were benchmarked against a similar operating point that used a high-energy inductive coil sparkplug (93 mJ).

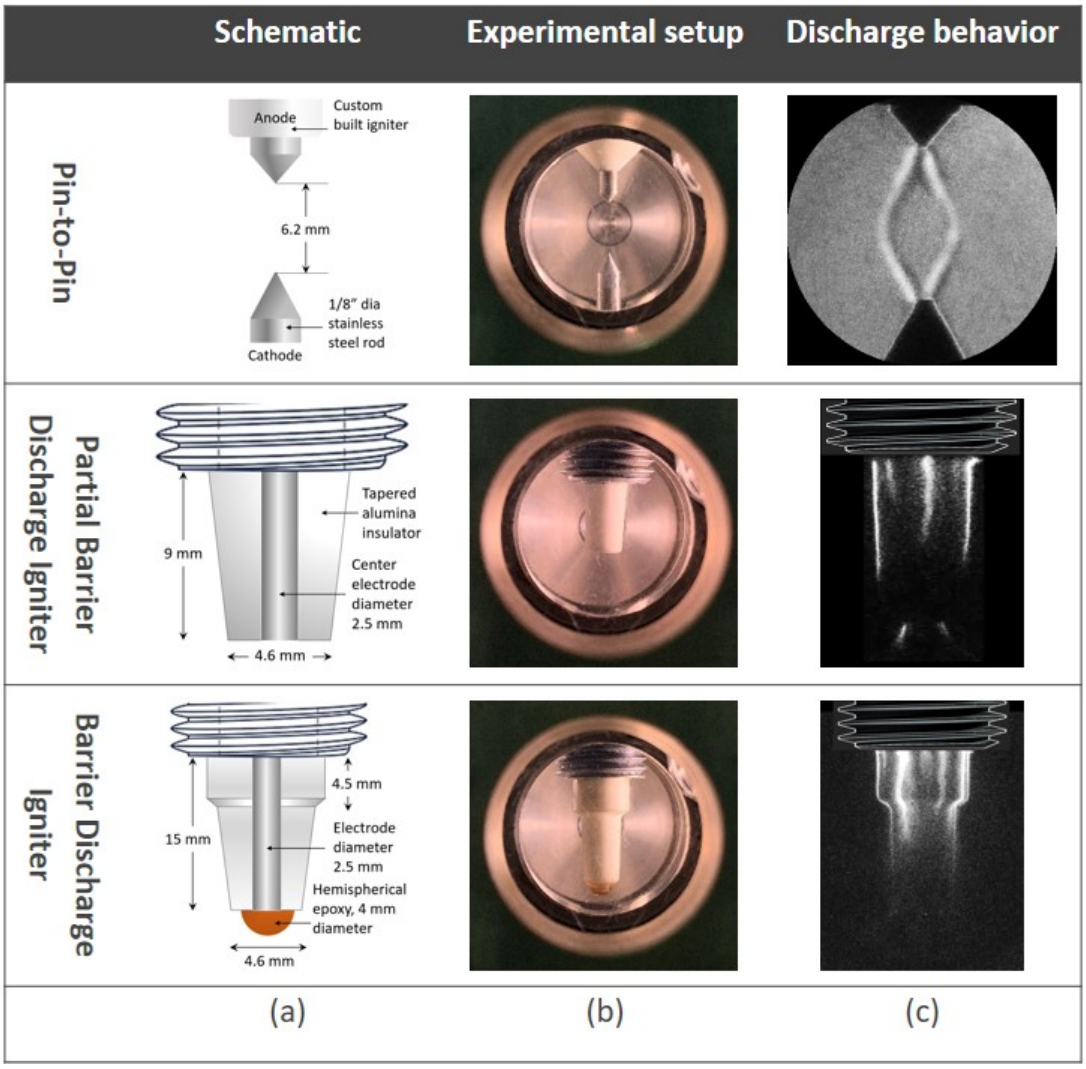

Figure I.5.3 (a) Schematic of the prototyped pin-to-pin (top), partial BDI (middle), and full BDI (bottom), with (b) corresponding images of the igniter in the ignition test vessel and (c) images of the discharge in air

Lean and EGR dilute ignition limits for spark ignition and TPI were measured as a function of discharge voltage and are plotted in Figure I.5.4; corresponding discharge energy for each pulse in the ten-pulse burst is also provided. The black vertical dashed line corresponds to the lean or dilute ignition limit for the inductive coil spark igniter. For each TPI igniter, the upper solid boundary represents the highest voltage possible without an associated transition to breakdown, while the lower dashed boundary corresponds to the lowest voltage where a sustained ignition kernel could be reliably achieved.

- Inductive spark equivalence ratio (ϕ) and EGR dilution ignition limits were 0.56 and 32%, respectively. These values were extended for all TPI, with the smallest gains for the P2P (0.52 and 36%), followed by the partial BDI (0.45 and 41%), and the largest ignition limit extension with the full BDI (0.41 and 45%).
- When five-pulse bursts were used for TPI, an ignition kernel would form but would not be sustained. These results indicate that the subsequent pulses provided expansion energy to the developing kernel.
- Both BDI configurations required larger discharge voltages (and hence energies) to achieve ignition but also had a wider range of acceptable discharge voltages for successful ignition.

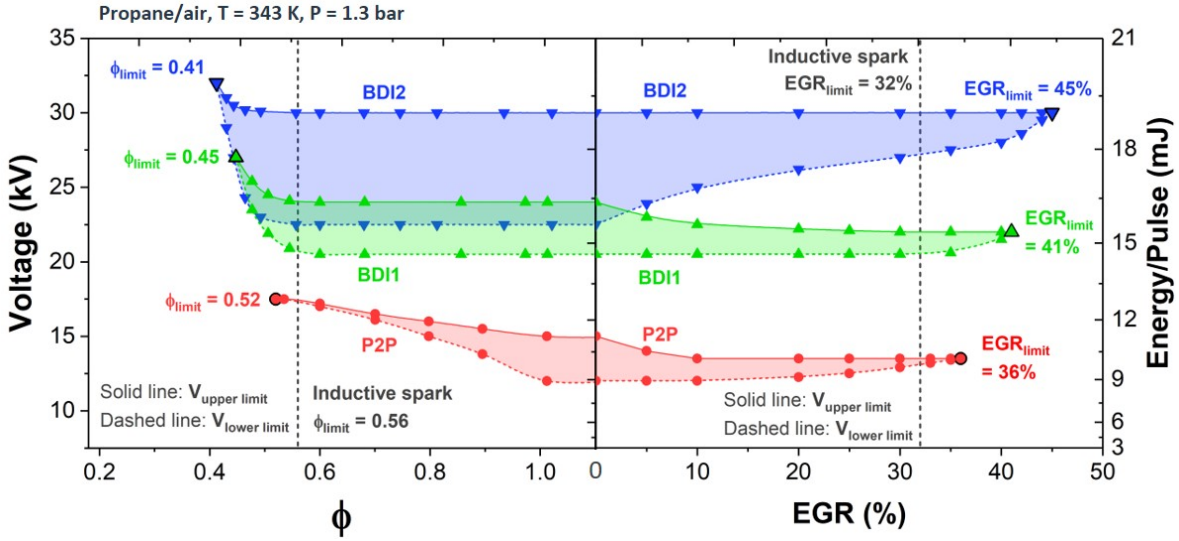

Figure I.5.4 Plots of lean and dilute ignition limits in quiescent propane/air mixtures for P2P, partial BDI, and full BDI as a function of discharge voltage for ten-pulse bursts at 10 kHz as well as corresponding inductive spark reference values

To evaluate the influence of TPI on burn rates under fuel-lean conditions, heat release traces for a fixed ϕ of 0.6 were calculated from high-speed pressure measurements, with traces for each igniter plotted in Figure I.5.5. Note that similar measurements were performed for multiple lean and dilute operating points. Flame kernel images at the 3% and 10% burn times are overlaid on the plot with the corresponding point in the heat release trace identified. For all TPI discharges, the discharge voltage was adjusted to the maximum value that still avoided inter-electrode breakdown.

- Relative to the spark igniter, total burn durations decreased by 27% for the P2P, 43% for the partial BDI, and 53% for the full BDI. The full BDI burn duration at ϕ = 0.6 was faster than for the spark at ϕ = 1.0.
- The 0 to 10% burn rates increased significantly relative to the spark ignition, by 70%, 96%, and 131%, respectively, for the P2P, partial BDI, and full BDI. Furthermore, peak BDI heat release rates were more than double the spark igniter peak values.

- Schlieren images of the ignition kernel at the 3% and 10% burn times illustrate substantially larger ignition kernel volumes for TPI relative to spark ignition, and a larger amount of flame front corrugation that likewise increases propagation speeds.

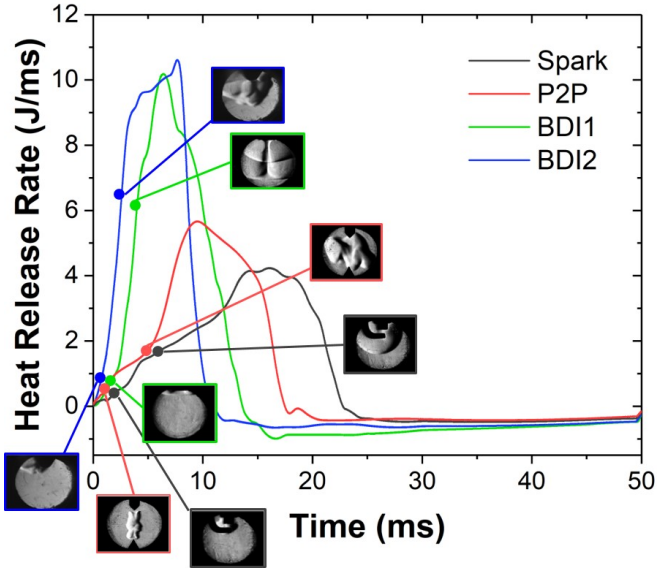

Figure I.5.5 Heat release rates for ignition at a fixed ϕ of 0.6 for the three TPI igniters and the inductive spark igniter evaluated. Images of the ignition volume at the 3% and 10% burn time are overlaid on the plot.

The final activity discussed in this report is the measurement of O_3 generated in the static ignition cell by full BDI discharges in air. The goal was to see if sufficient O_3 (up to 30 ppm) can be generated for the SACI strategy described earlier using only BDI discharges in the intake or early compression stroke. Hence, the fuel additive and enhanced ignition would be from the same source. For these experiments, air and varying amounts of EGR gases were used to fill the ignition test vessel at a range of pressures between 1 bar and 8 bar. A ten-discharge pulse burst at 10 kHz was performed for a range of total discharge energies. Total O_3 concentration in the cell at the end of the pulse burst was measured using an ultraviolet light absorption technique described in last year's report [2]. A contour plot of O_3 concentration for a half-liter displacement engine cylinder as a function of initial pressure and pulse burst discharge energy is provided in Figure I.5.6. Additional results were acquired to evaluate the influence of initial temperature and EGR concentration on O_3 yield but are not shown here for brevity.

- Ozone yield increased with higher discharge energy and lower ambient pressure. Both effects increased the reduced electric field, which in turn increased the plasma strength.
- For discharge energies above 130 mJ, a low pressure limit resulted from breakdown transition.
- For atmospheric-temperature air, 10–12 ppm O_3 was reliably generated from the ten-pulse burst, meaning three-pulse bursts should generate sufficient O_3 for the SACI strategy described earlier.
- Increased ambient temperatures and EGR addition decreased O_3 yields by more than half (not shown), which suggests additional engine tests are needed to verify performance.

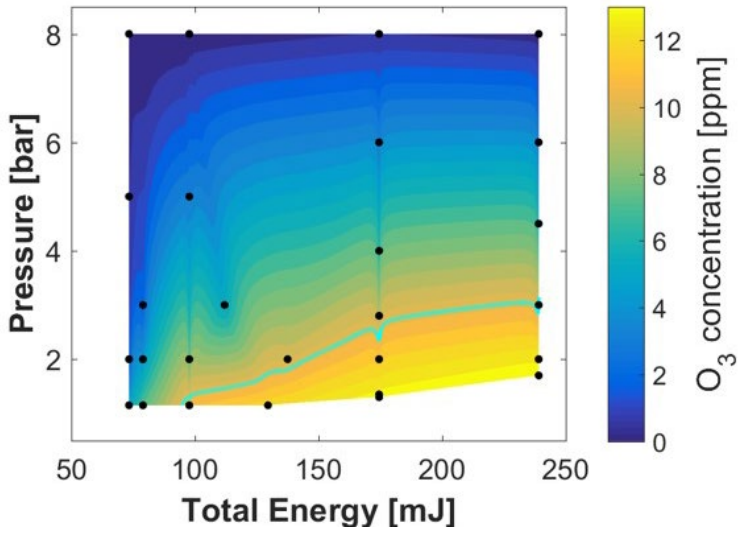

Figure I.5.6 Ozone yield from full BDI ten-pulse bursts in desiccated, atmospheric-temperature air as a function of initial pressure and discharge energy. Reported concentrations are corrected to match a 0.5-liter displacement engine cylinder. The cyan contour indicates the pressure and total energy combination required to produce 10 ppm of O_3.

Conclusions

A suite of experiments were performed to measure fundamental processes associated with active ignition and to evaluate how novel TPI technologies could be leveraged to enable clean and efficient modes of engine combustion that are not currently possible with conventional inductor coil ignition systems. The project has multiple National Laboratory, university, and industry partners, with data generated in our lab used to inform complementary simulation submodel development activities. Main conclusions are as follows:

- Ozone-addition SACI produced excellent efficiency for low-to-moderate engine loads and speeds, with NO_x emissions held below regulated exhaust levels for homogeneous charge mixtures. However, moderate stratification was needed for lower loads and higher speeds, which in turn increased NO_x emissions by an order of magnitude. It was concluded that stronger initial burn rates in lean mixtures need to be delivered by the ignition system.

- Large ignition volumes and reduced electrode heat losses for repetitively pulsed TPI led a factor of 2 increase in early flame burn rates relative to conventional spark ignition. Preliminary engine tests with BDI indicate these igniters likewise achieve faster early burn rates relative to conventional spark ignition.

- Ozone yields produced from full BDI pulse burst discharges were sufficient for the O_3-addition SACI strategy outlined above. Yields were found to increase with discharge voltage and decrease with higher ambient pressures, temperatures, and EGR dilution. Accordingly, the substitution of a conventional spark plug and coil with full BDI enables a combination of onboard tailoring of fuel reactivity for kinetically controlled combustion strategies and enhanced ignition.

Key Publications

1. Biswas, S., I. Ekoto, and R. Scarcelli. 2019. “Transient Plasma Ignition (TPI) for Automotive Applications.” Paper read at IAV Ignition Systems for Gasoline Engines - 4th International Conference, Berlin, Germany.

2. Biswas, S., and I. Ekoto. 2019. “Detailed Investigation into the Effect of Ozone Addition on Spark Assisted Compression Ignition Engine Performance and Emissions Characteristics.” SAE WCX, 2019-01-0966.

3. Biswas, S., and I. Ekoto. 2019. “Spark Assisted Compression Ignition Engine with Stratified Charge Combustion and Ozone Addition.” In 2019 JSAE/SAE Powertrains, Fuels and Lubricants International Meeting, Kyoto, Japan, 2019-01-2253.

4. Seignour, N., I. Ekoto, F. Foucher, and B. Moreau. 2019. “Measurements and Modeling of Ozone Enhanced Compression Ignition in a Rapid Compression Machine and Optically-Accessible Engine.” In 2019 JSAE/SAE Powertrains, Fuels and Lubricants International Meeting, Kyoto, Japan, 2019-01-2254.

References

1. Ekoto, I., and F. Foucher. 2018. “Mechanisms of Enhanced Reactivity with Ozone Addition for Advanced Compression Ignition.” *SAE International Journal of Fuels and Lubricants* 11 (4): 443–457. doi: https://doi.org/10.4271/2018-01-1249.

2. Ekoto, I. 2019. “Gasoline Combustion Fundamentals.” *Advanced Combustion Engines and Fuels 2018 Annual Progress Report*, U.S. Department of Energy, Vehicle Technologies Office, Washington, DC.

Acknowledgements

The work was performed at the Combustion Research Facility, Sandia National Laboratories, Livermore, California. Financial support was provided by the U.S. Department of Energy’s Vehicle Technologies Office. Sandia National Laboratories is a multi-mission laboratory managed and operated by National Technology and Engineering Solutions of Sandia, LLC, a wholly owned subsidiary of Honeywell International, Inc., for the U.S. Department of Energy's National Nuclear Security Administration under contract DE-NA0003525.

I.6 Fuel Injection and Spray Research Using X-Ray Diagnostics (Argonne National Laboratory)

Christopher F. Powell, Principal Investigator
Argonne National Laboratory
9700 S. Cass Avenue
Lemont, IL 60439
E-mail: powell@anl.gov

Michael Weismiller, DOE Technology Development Manager
U.S. Department of Energy
E-mail: Michael.Weismiller@ee.doe.gov

Start Date: October 1, 2018 End Date: September 30, 2019
Project Funding (FY19): $450,000 DOE share: $450,000 Non-DOE share: $0

Project Introduction

Fuel injection systems are one of the most important components in the design of combustion engines with high efficiency and low emissions. A detailed understanding of the fuel injection process and the mechanisms of spray atomization is needed to implement advanced combustion strategies with improved engine performance. X-ray diagnostics can provide unique data in the study of fuel injection; they are highly penetrative and can generate quantitative, unambiguous measurements of useful spray properties, even in the optically opaque region very near the nozzle. This project uses X-ray diagnostics of sprays to provide insight into the fundamentals of sprays and to generate quantitative data for development and validation of advanced injection simulations.

Objectives

Overall Objectives

- Utilize the unique capabilities of Argonne's Advanced Photon Source to improve the fundamental understanding of fuel injectors, the injection process, and fuel atomization and mixing
- Generate quantitative measurements of fuel injection under engine-relevant conditions, to be used to enable the development and validation of improved computational models of fuel injection
- Collaborate with injector manufacturers and engine designers, giving them access to our unique diagnostic tools, with the goal of improving their ability to build clean-burning, efficient engines.

Fiscal Year 2019 Objectives

- Optimize the workflow for data analysis of X-ray tomography measurements of the internal flow passages of fuel injectors
- Perform exploratory measurements using X-rays to probe the near-wall region of sprays impinging on surfaces; determine what measurement quantities are important and feasible, and plan for the development of a built-for-purpose spray chamber for future spray-wall studies
- Complete first-of-their kind three-dimensional (3D) measurements of a cavitating diesel nozzle, including high-resolution measurements of the internal liquid and gas distributions.

Approach

The aim of this project is to develop and perform high-precision measurements of fuel injection and sprays to further the development of accurate computational spray models. These measurements are performed at the Advanced Photon Source at Argonne National Laboratory. This source provides a very-high-flux beam of X-rays, enabling quantitative, time-resolved measurements of sprays with very high spatial resolution. The X-rays are used for five different measurement techniques: tomography to measure injector nozzle geometry, radiography to measure spray density, phase contrast imaging to acquire high-speed images, fluorescence to track atomic elements, and small-angle scattering to measure droplet size [1]. Each of these techniques complements other diagnostics by providing unique and useful information that cannot be obtained in other ways.

In the process of making these measurements, Argonne collaborates with industrial partners, including engine and fuel injection system manufacturers. Industry access to these diagnostics increases the understanding of the fundamental science behind their products. The group also collaborates with spray modelers to incorporate this previously unknown information about the spray formation region into new models. This leads to an improved understanding of the mechanisms of spray atomization and facilitates the development of fuel injection systems designed to improve efficiency and reduce pollutants.

In addition to measurements of injectors and sprays, the group explores other applications of X-ray diagnostics for combustion research. Measurements of cavitating flows provide unique data to improve the fundamental understanding of internal fuel flow and its role in spray atomization, as well as the relationship between injector geometry, cavitation, and nozzle damage. Recent measurements have also evaluated the use of X-rays as a diagnostic for shock tubes, natural gas injectors, and spark ignition. These new applications broaden the impact of the work and help to improve the fundamental understanding in other areas important to advanced combustion, including fundamental chemistry, gas jets, and ignition.

Results

Over the last several years, our group has developed and refined the process of making high-resolution scans of the internal flow passages of fuel injectors and delivering 3D models of their geometry to be used for computational fluid dynamics simulations. The main bottleneck to automated generation of a 3D injector geometry from X-ray data is the determination of the surface, a process called segmentation. In segmentation, the measured data is converted into a binary map that classifies each voxel as belonging to either injector metal or flow domain, accurately locating the metal surface at the transitions between these domains. The segmentation method itself relies heavily on user input, particularly the selection of value(s) of grayscale voxel intensity to be used as threshold(s) to distinguish between different materials. This can often be challenging in the presence of artifacts from reconstruction or noise from low-light conditions in dense or thick objects.

In Fiscal Year 2019, a significant effort was undertaken to streamline this process using an approach borrowed from biomedical applications using convolutional neural networks (CNN). As opposed to intensity-based thresholding, this approach relies on context in the image and hence is called semantic segmentation. A schematic of the algorithm used to generate the geometries using the CNN is shown in Figure I.6.1. The CNN approach requires training data that include both raw X-ray nozzle images as well as manually created 3D models of those nozzles. The CNN algorithm “learns” from the training data and can then accurately segment new nozzles based on the raw X-ray measurements. The algorithm streamlines a process that used to require about 30 man-hours into less than 30 minutes of processing, and little manual intervention. The accuracy of the new procedure has been documented in Tekawade et al. [2].

This innovation will enable us to greatly expand our capacity for generating fuel injector geometries. With this new capacity, a range of new experiments become possible, including broad surveys of many injectors, looking at manufacturing variability, tolerances, and erosion over time.

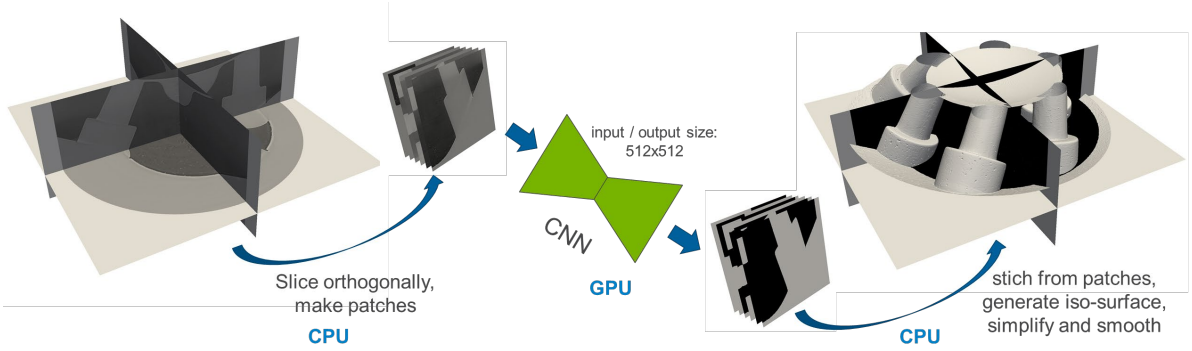

CPU – central processing unit; GPU – graphics processing unit

Figure I.6.1 Schematic overview of the algorithm that enables the new approach to 3D segmentation using a two-dimensional CNN architecture

In the next several years, much of our light-duty work will be focused on improving cold-start emissions. One significant problem during cold start is fuel impinging on walls, leading to elevated particulate levels. Because X-rays can make quantitative measurements in environments that are too optically dense for other diagnostics, they will be a useful tool for studying spray impingement. In Fiscal Year 2019, we performed several exploratory measurements of spray impingement. Figure I.6.2 shows the results from our first attempt, mapping the density distribution of a gasoline direct injection spray as it impinges on a wall. We are able to capture the density near the wall and track the motion of a wall film and rollup vortex. Other experiments have explored high-speed X-ray imaging and its ability to capture individual droplet collisions, splashing, and particle tracking. These first measurements are being used to test the feasibility and to prioritize the design features of a future spray chamber dedicated to X-ray measurements of impinging sprays. With the knowledge gained in 2019, we will design and fabricate a fit-for-purpose facility that enables quantitative measurements of spray/wall interactions, and ultimately unique data for the development and validation of improved computational simulations of the process.

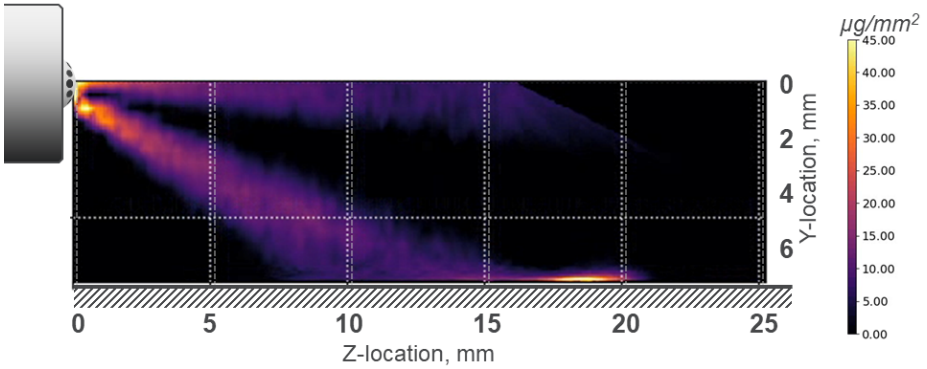

Figure I.6.2 Measurements of the average near-wall density field in a gasoline direct injection spray impinging on a wall

Manufacturing variations in the geometric features inside injectors, such as inlet corner sharpness and orifice diameter, can have a significant influence on the fuel flow inside the nozzle, causing cavitation or flow-separation near the nozzle walls. The occurrence of cavitation can not only lead to erosion in injectors, but can also have an impact on the downstream spray development. For this reason, internal flow is a major area of

fuel injection research. However, since steel nozzles are opaque to visible light, most research has been limited to either purpose-built transparent replicas or practical diesel injectors that have been modified for optical access. X-rays, however, are not limited by the opacity of a steel injector body, and we have taken advantage of this to quantify cavitation and flow separation inside steel nozzles.

In Fiscal Year 2019, X-ray tomography was used to build a time-averaged 3D map of the liquid and gas distributions inside the Engine Combustion Network "Spray C" single-hole diesel nozzle. This research nozzle is designed to promote cavitation and is an ideal candidate for this work. X-ray images of the flow through the nozzle were acquired as the injector fired and the nozzle was rotated. The resulting images were run through a computational tomography reconstruction, and the results are shown in Figure I.6.3. The regions of gas and liquid are clearly resolved, with a sharp, wrinkled boundary between them. The gas region is highly asymmetric, and its location and "thickness" correspond with the radius of the inlet corner that lies just upstream at the entrance to the nozzle.

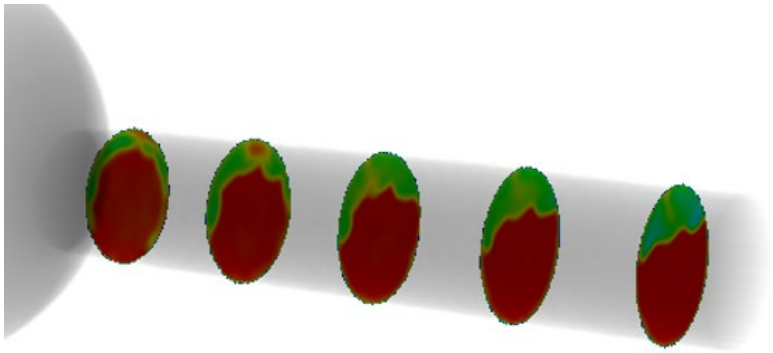

Figure I.6.3 Measurements of the average liquid (red) and gas (green) distribution inside a single-hole steel diesel injector

These measurements represent the first 3D measurements of injector cavitation in a round steel nozzle, operating at realistic diesel pressures with real fuel. The results have been shared with several computational simulation groups and are being used to improve the accuracy of cavitation and flow simulations.

Conclusions

X-ray diagnostics can reveal the flows inside fuel injectors as well as diagnose the mixing of fuel and air. Such measurements are not possible using other imaging techniques and represent a powerful data set for development and validation of computational models of fuel flow. This data is crucial for the development of accurate spray models and for the detailed understanding of spray behavior. Improvements to these models will speed the development of cleaner, more efficient engines.

Key Publications

1. Tekawade, Aniket, Brandon A. Sforzo, Katarzyna E. Matusik, Alan L. Kastengren, and Christopher F. Powell. 2019. "High-Fidelity Geometry Generation from CT Data Using Convolutional Neural Networks." Developments in X-Ray Tomography XII (September), Proceedings 11113, https://doi.org/10.1117/12.2540442, SPIE Optical Engineering + Applications, San Diego, CA.

2. Battistoni, M., S. Som, and C.F. Powell. 2019. "Highly Resolved Eulerian Simulations of Fuel Spray Transients in Single and Multi-Hole injectors: Nozzle Flow and Near-Exit Dynamics." *Fuel* 251 (September): 709–729, https://doi.org/10.1016/j.fuel.2019.04.076.

3. Sechenyh, Vitaliy, Daniel J. Duke, Andrew B. Swantek, Katarzyna E. Matusik, Alan L. Kastengren, Christopher F. Powell, Alberto Viera, Raul Payri, and Cyril Crua. 2019. "Quantitative Analysis of Dribble Volumes and Rates Using 3D Reconstruction of X-ray and DBI Images of Diesel Sprays." *International Journal of Engine Research* (July), https://doi.org/10.1177/1468087419860955.

4. Matusik, Katarzyna E., Brandon A. Sforzo, Hee Je Seong, Daniel J. Duke, Alan L. Kastengren, Jan Ilavsky, and Christopher F. Powell. 2019. "X-Ray Measurements of Fuel Spray Specific Surface Area and Sauter Mean Diameter for Cavitating and Non-Cavitating Diesel Sprays." *Atomization and Sprays* 29 (3): 199–216, doi:10.1615/AtomizSpr.2019030112.

5. Tekawade, A., P. Mitra, B.A. Sforzo, K.E. Matusik, A.L. Kastengren, D.P. Schmidt, and C.F. Powell. 2019. "A Comparison between CFD and 3D X-ray Diagnostics of Internal Flow in a Cavitating Diesel Injector Nozzle." 30th Annual Conference on Liquid Atomization and Spray Systems (May), Tempe, AZ.

6. Tekawade, A., B.A. Sforzo, K.E. Matusik, A.L. Kastengren, and C.F. Powell. 2019. "3D Imaging of Cavitating Flow in a Diesel Injector at Practical Conditions Using X-ray Micro-CT." 30th Annual Conference on Liquid Atomization and Spray Systems (May), Tempe, AZ.

7. Wallner, Thomas, Michael Pamminger, Riccardo Scarcelli, Christopher Powell, Severin Kamguia Simeu, Ron Reese, Asim Iqbal, Steven Wooldridge, and Brad Boyer. 2019. "Performance, Fuel Economy and Economic Assessment of a Combustion Concept Employing In-Cylinder Gasoline/NG Blending for Light-Duty Vehicle Applications." *International Journal of Engine Research* 12 (3): 271–289, https://doi.org/10.4271/03-12-03-0019.

8. Tzanetakis, T., Y. Pei, M. Traver, B. Sforzo, K. Matusik, A.L. Kastengren, and C.F. Powell. 2019. "Durability Study of a High Pressure Common Rail Fuel Injection System Using Lubricity Additive Dosed Gasoline-Like Fuel – Additional Cycle Runtime and Teardown Analysis." *SAE Int. J. Adv. & Curr. Prac. in Mobility* 1 (2): 654–674, https://doi.org/10.4271/2019-01-0263.

9. Mitra, P., E. Baldwin, K.E. Matusik, D. Duke, C.F. Powell, M. Arienti, L.M. Pickett, J. Manin, K. Yasutomi, P. Srivastava, P.K. Senecal, and D.P. Schmidt. 2019. "Identification and Characterization of Steady State Spray Conditions in Convergent, Single-Hole Diesel Injectors." SAE 2019 World Congress (April), Detroit, MI.

10. Seong, H., S. Choi, K.E. Matusik, A.L. Kastengren, and C.F. Powell. 2019. "3D Pore Analysis of Gasoline Particulate Filters Using X-ray Tomography: Impact of Coating and Ash-Loading." *Journal of Materials Science* (January), DOI 10.1007/s10853-018-03310-w.

11. Martinez, G.L., F. Poursadegh, G.M. Magnotti, K.E. Matusik, D.J. Duke, B.W. Knox, C.L. Genzale, C.F. Powell, and A.L. Kastengren. 2018. "Measurement of Sauter Mean Diameter in Diesel Sprays Using a Scattering-Absorption Measurement Ratio Technique." *International Journal of Engine Research* 20 (1): 6–19, https://doi.org/10.1177/1468087418819912.

12. Battistoni, Michele, Gina M. Magnotti, Caroline L. Genzale, Marco Arienti, Katarzyna E. Matusik, Daniel J. Duke, Jhoan Giraldo, Jan Ilavsky, Alan L. Kastengren, Christopher F. Powell, Pedro Marti-Aldaravi. 2018. "Experimental and Computational Investigation of Subcritical Near-Nozzle Spray Structure and Primary Atomization in the Engine Combustion Network Spray D." *SAE Int. J. Fuels Lubr.* (December), https://doi.org/10.4271/2018-01-0277.

13. Duke, Daniel J., Alan L. Kastengren, Katarzyna E. Matusik, and Christopher F. Powell. 2018. "Hard X-ray Fluorescence Spectroscopy of High Pressure Cavitating Fluids in Aluminum Nozzles." *International Journal of Multiphase Flow* 108 (November): 69–79.

References

1. Kastengren, A.L., and C.F. Powell. 2014. “Synchrotron X-Ray Techniques for Fluid Dynamics.” *Experiments in Fluids* 55 (February): 1686.

2. Tekawade, A., B.A. Sforzo, K.E. Matusik, A.L. Kastengren, and C.F. Powell. 2019. “High-Fidelity Geometry Generation from CT Data Using Convolutional Neural Networks.” Developments in X-Ray Tomography XII (September), Proceedings 11113, https://doi.org/10.1117/12.2540442, SPIE Optical Engineering + Applications, San Diego, CA.

Acknowledgements

The authors acknowledge Alan L. Kastengren, Brandon A. Sforzo, and Aniket Tekawade for their efforts as part of this work. Measurements were performed at the 7BM, 9ID, and 32ID beamlines of the Advanced Photon Source at Argonne National Laboratory. Use of the Advanced Photon Source is supported by the U.S. Department of Energy under Contract No. DEAC0206CH11357.

I.7 Rapid Compression Machine Studies to Understand Autoignition Fundamentals at Dilute Gasoline Conditions (Argonne National Laboratory)

S. Scott Goldsborough, Principal Investigator
Argonne National Laboratory
9700 S. Cass Avenue
Lemont, IL 60439
E-mail: Scott.Goldsborough@anl.gov

Michael Weismiller, DOE Technology Development Manager
U.S. Department of Energy
E-mail: Michael.Weismiller@ee.doe.gov

Start Date: October 1, 2018 End Date: September 30, 2019
Project Funding (FY19): $370,000 DOE share: $370,000 Non-DOE share: $0

Project Introduction

Accurate, predictive combustion models are necessary for the reliable design and control of next-generation engines able to meet mandated fuel economy and emissions standards, with associated reductions in development times and costs for new configurations [1]. The imprecision of available models prevents adoption of detailed simulation techniques within current design processes. Existing engineering-scale models can achieve satisfactory performance at some operating points; however, they are not sufficiently robust to cover complete ranges of conventional engine operation or to apply to novel/advanced combustion concepts. Therefore, there is a critical need to improve the understanding of the multiple physical and chemical processes that occur within combustion engines, including chemical ignition, fluid-chemistry interactions, and pollutant formation/decomposition. Advancing these understandings requires fundamental data that can be acquired, with sufficiently low experimental uncertainties, at conditions representative of engine combustion chambers. There is a particular lack of data to quantify the autoignition behavior of full-boiling-range fuels, to formulate robust multicomponent surrogate blends to replicate these fuels, and to develop/validate chemical kinetic models for individual constituents and blends. Moreover, there is a need to advance the capability to accurately estimate and reduce uncertainties in kinetic models of transportation fuels.

Objectives

Overall Objectives

- Acquire autoignition data using Argonne National Laboratory's rapid compression machine (RCM) at conditions representative of today's and future internal combustion engines, including high pressure (P = 15–80 bar), low-to-intermediate temperatures (T = 650 K–1,100 K), and a range of fuel loadings
- Improve understandings of advanced compression ignition phenomena and develop modeling capabilities for full-boiling-range fuels
- Collaborate with combustion researchers within the U.S. Department of Energy's Office of Vehicle Technologies and Basic Energy Sciences program to accurately quantify uncertainties in chemical kinetic models in order to improve their predictability for a range of fuels.

Fiscal Year 2019 Objectives

- Quantify the autoignition behavior of binary olefin/aromatic blends with the aim of understanding and modeling chemical kinetic interactions

- Improve scaling analysis for chemico-physical interpretations of flame-driven compression ignition for application to RCM data interpretation and advanced compression ignition in engines
- Further investigate non-ideal RCM operation using a higher-order computational fluid dynamics software.

Approach

RCMs are sophisticated experimental tools that can be employed to acquire fundamental insight into fuel ignition and pollutant formation chemistry, as well as fluid-chemistry interactions, especially at conditions that are relevant to advanced low-temperature combustion concepts as well as boosted spark-ignition strategies [2]. RCMs can create and maintain well-controlled, elevated temperature and pressure environments (e.g., T = 600 K–1,100 K, P = 5–80 bar) in which the chemically active period preceding autoignition can be monitored and probed via advanced in situ and ex situ diagnostics. The ability to utilize wide ranges of fuel and oxygen concentrations within RCMs, from ultra-lean to over-rich (e.g., ϕ = 0.2–2.0+), and spanning dilute to oxy-rich regimes (e.g., O_2 = 5% to >21%), offers specific advantages relative to other laboratory apparatuses such as shock tubes and flow reactors, where complications can arise under such conditions. Fuels' exothermic behavior at such conditions is not well characterized, even though the exothermic behavior is important for a range of combustion engine phenomena. Furthermore, the understanding of interdependent chemico-physical phenomena, such as "non-uniform ignition," that can occur at some conditions within RCMs is a topic of ongoing investigation within the combustion community, while interpretation of facility influences on datasets is also being addressed [3]. Combustion researchers are developing approaches to implementing novel diagnostics that can provide more rigorous constraints for model validation compared to integrated metrics such as ignition delay times, e.g., quantification of important radical and stable intermediates such as H_2O_2 and C_2H_4 [4],[5].

The project team is using Argonne National Laboratory's twin-piston RCM to acquire data necessary for a broad range of fuels, while making improvements to the facility's hardware and data analysis protocol to extend its capabilities and fidelity. Multidisciplinary collaborations are undertaken at Argonne National Laboratory and other U.S. laboratories, as well as with researchers at national and international institutions, including complementary RCM facilities.

Results

Key accomplishments for Fiscal Year 2019 include the following:

- Acquired autoignition data for binary blends of an iso-olefin, 2-methyl 2-butene (2M2B), and an aromatic, toluene (TOL), covering wide ranges of temperatures, pressures, stoichiometries, and blending ratios.
- Acquired additional RCM data for an E10 regular gasoline (gasoline blend with 10% ethanol) as part of the Coordinating Research Council Fuels for Advanced Combustion Engines Working Group's Advanced Vehicles/Fuels/Lubricants (AVFL) 31b project.
- Revised scaling analyses developed previously to identify physical and chemical parameters that govern flame-driven compression ignition, with applications to mild ignition in RCMs and to spark-assisted compression ignition in internal combustion engines.
- Initiated investigations using detailed, multidimensional reacting flow software (NEK5000) to understand impacts of non-ideal RCM operation.

Olefins and aromatics are important constituents of transportation-relevant fuels and are found in varying quantities in commercial gasoline. They also represent production routes for biomass to liquid transportation fuel. The presence of the C=C double bond in olefins gives these hydrocarbons advantageous characteristics. For instance, short-chain olefins have greater knock resistance than their saturated homologues. Olefins can

impart higher octane sensitivity (defined as research octane number minus motor octane number, RON – MON) to gasoline fuels, and thus can be used to displace aromatics in the fuel. At high concentrations, however, olefins can alter the fuel stability and promote the formation of gums, which are detrimental to injector hardware. In addition, olefins are important intermediates that form during combustion, and their generation can be a first step toward soot formation.

Extensive work has been undertaken to study the autoignition and combustion chemistry of linear olefins, with far fewer studies devoted to branched structures. The intent of this work was to follow on from Fiscal Year (FY) 2018 activities and contribute to fundamental understandings of how iso-olefins and aromatics interact during oxidation. Experimental measurements were conducted with binary blends of a representative iso-olefin, 2M2B, and a representative aromatic, TOL. The tests were performed over a temperature range of Tc = 700 K–1,000 K; a pressure range of Pc = 25 bar and 45 bar; ϕ = 0.5–2.0; and four blend ratios, from 3/0 (2M2B/TOL) to 0/3. Representative pressure–time histories are presented in Figure I.7.1a, while a summary of the measurements is depicted in Arrhenius format in Figure I.7.1b.

The data indicate that the chemical kinetic interactions are non-linear, where the reactivity appears to be dominated by 2M2B at the two intermediate blend levels (2/1 and 1/2), with TOL not significantly suppressing the autoignition chemistry. Collaborations are ongoing with Lawrence Livermore National Laboratory to model the chemical kinetics of these blends.

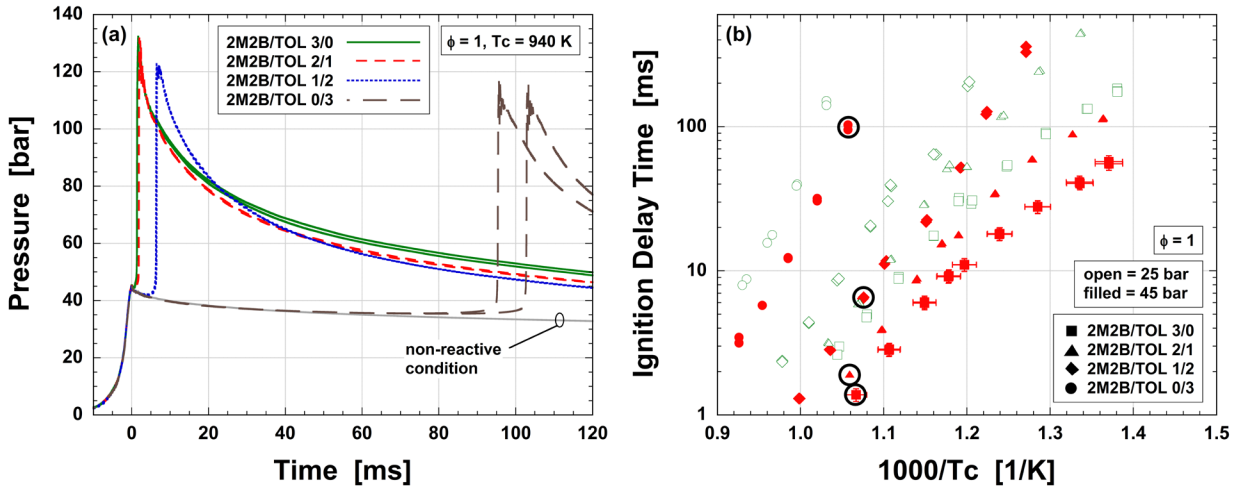

Figure I.7.1 Autoignition behavior of binary blends of 2M2B + TOL: (a) pressure–time histories at Tc = 940 K, Pc = 45 bar, ϕ = 1 highlight changes in fuel reactivity as TOL is added; (b) ignition delay times summarize, in Arrhenius format, the non-linear blending behavior of TOL, with conditions covering Tc = 700 K–1,000 K, Pc = 25 bar and 45 bar, and ϕ = 1. Two test shots are shown at each experimental condition, demonstrating very good repeatability of the measurements. Circles in (b) indicate the points where data are shown in (a).

Also in FY 2019, new experimental measurements were conducted with an E10 full-boiling-range gasoline as part of the Coordinating Research Council Fuels for Advanced Combustion Engines Working Group's AVFL31b project. The fuel matrix for that work utilizes 19 gasoline-type fuels of varying RON, sensitivity, and ethanol content formulated for Coordinating Research Council AVFL20 [6]. Fuel #1 (RON = 91, MON = 84.5) was used in the FY 2018 tests, with conditions selected for direct comparison against analogous measurements made at the Massachusetts Institute of Technology's Sloan Automotive Laboratory. Discrepancies noted between the datasets prompted the new set of measurements. Interpretation of the discrepancies is ongoing.

Another topic continued in FY 2019 was associated with the challenge of non-uniform ignition in RCMs. Flames and/or reaction fronts initiate at some conditions as a result of non-uniformities in the mixture (e.g.,

"hot spots"), thereby leading to compression heating of the reacting gas such that measured autoignition times are accelerated [2],[7]. The coupled physico-chemical behaviors that exist in the RCM reaction chamber are analogous to those during uncontrolled end gas compression ignition resulting from turbulent flame propagation in internal combustion engines, as well as those within advanced compression-ignition schemes such as spark-assisted compression ignition [8].

Extending work from FY 2018, scaling arguments were reformulated to characterize the competing processes of (a) "hot spot" quenching vs. ignition, (b) flame extinction vs. propagation, and (c) flame consumption/ forced autoignition vs. homogeneous ignition. The reformulated parameters were compared against an extensive data set of numerically simulated, "hot spot" initiated flames (using a one-dimensional reacting flow code [ASURF] [9]). Spherical symmetry was employed in the simulations using a centrally located "hot spot" to minimize the computational cost, while syngas blends (CO/H_2 = 80/20) with reliable kinetics and transport were used as the fuel. Lean fuel loadings of ϕ = 0.2 and 0.5 were employed to mimic experimental RCM data [10],[11]; these loadings are also representative of spark-assisted compression-ignition operation [8]. Wide ranges of temperature and pressure were covered (900 K–1,120 K, 1.5–15 bar), while the singular "hot spots" ranged in size from 0 mm to 2 mm with elevated temperatures of 1% to 90% greater than the surroundings, i.e., T′ = 1.01–1.90.

The parameters that characterize "hot spot" quenching (Γ_{hot}) and forced autoignition of the end gas (Γ_{fa}) are presented in Equations (Eqs.) (1) and (2), and their correlations with the simulation database are shown in Figure I.7.2a and Figure I.7.2b, respectively.

$$\Gamma_{hot} = \left[\mathcal{A}' - \left(n_f + n_O\right)'\right] \ln\left(\frac{1}{T'} + \left(1 - \frac{1}{T'}\right) \exp\left(-\frac{\mathrm{Nu}\,\bar{\gamma}\,\bar{\alpha}}{(r_{hot}/3)^2}\tau_{flame}\right)\right) \quad (1)$$

$$\Gamma_{fa} = -\left[\mathcal{A}_0(\gamma - 1) + \left(n_f + n_O\right)_0\right]\left(\frac{LHV^{\Delta}}{1 + LHV^{\Delta}}\right) \ln\left(1 - \frac{s_b^0\, A_{flame}}{3\, V}\left(\tau_{ig,bulk} - \tau_{flame}\right)\right) \quad (2)$$

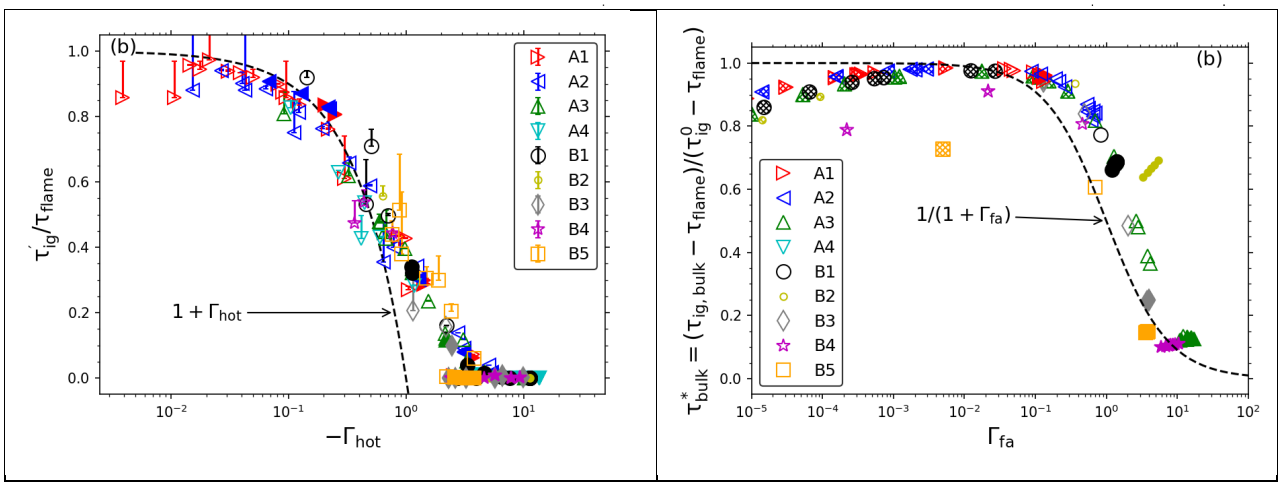

Figure I.7.2 Correlations from one-dimensional flame simulations [12] highlighting influence of (a) Γ_{hot} parameter on hot-spot quenching and (b) Γ_{fa} parameter on end-gas compression ignition.

A number of features of Γ_{hot} can be deduced from Eq. (1), where large values make it more probable for "hot spot" quenching to occur. The first bracketed term represents the kinetic sensitivity of the mixture, while the natural logarithm term represents the magnitude of heat loss, which is seen to be dependent on a normalized temperature gradient, heat transfer properties, and a timescale of the unperturbed chemical reactivity. Fuels that are thermally sensitive, i.e., with large $\mathcal{A}$, are more affected by heat loss, as are mixtures with high reaction orders (in this case, owing to density changes). For diffusively limited heat transport (as in the parametric simulations), the Nusselt number (Nu) is identically ⅓, but in engine scenarios, enhanced heat flow will increase Γ_{hot} through Nu. It is noted that mixtures with large γ and α can facilitate "hot spot" quenching,

while geometries with small r_{hot} do not have the capacity to retain heat. Finally, influences of T' are complex, as T' can influence the thermal sensitivity of the kinetics (via the Arrhenius number at T_{hot}, $\mathcal{A}'$) but can also lead to more rapid rates of heat loss. It should be noted that flame initiation is possible under conditions in which the "hot spot" thermally quenches, owing to radical generation that can occur early, but this feature is not captured in Eq. (1).

Important features of Γ_{fa} can be deduced from Eq. (2), where the first bracketed term again represents kinetic sensitivity, the second group the normalized heat addition due to the chemical energy release in the flame, and the third term the extent of flame consumption, or the product of the normalized compression heating rate and the time to bulk ignition. Eq. (2) indicates that thermally sensitive mixtures have a greater propensity for perturbation. Additionally, under conditions where the reaction order is high, such as for fuels with a negative-temperature-coefficient (NTC) region where RO_2 and HO_2 chemistry are important, the mixture can be sensitive to forced autoignition, even if it is thermally insensitive (i.e., small or even negative $\mathcal{A}_0$). The mixture heat capacity is also influential via γ, which can enhance or suppress chemical sensitivities. Next, when the chemical heat release is high, for instance, because of stoichiometric fuel loadings and low levels of dilution, or for low mixture heat capacities, there is a greater tendency for forced autoignition. When the normalized flame consumption is large, e.g., via high flame speeds (or enhanced by flame wrinkling), there can be a greater probability for forced autoignition. Finally, when the induction times are long, or the flame initiates early, there is more time available for the flame to perturbatively affect the reactivity of the end gas.

The scaling arguments are found to be useful since they indicate that experimental parameters have potential to suppress "hot spot"-initiated flame formation (e.g., via bath gases with high thermal diffusivity) or to avert flame compression of the end gas (e.g., via lean/diluted mixtures or bath gases with high heat capacity).

Finally, the project team used a detailed, multidimensional reacting flow software (NEK5000) to computationally investigate the development and evolution of non-idealities within the reaction chamber (e.g., "hot spots") that have potential to alter the measurements. For instance, unintended fluid and gas dynamics can result from operational issues such as piston asynchronicity, or turbulence generation/amplification during piston compression. These non-uniformities can alter the progress of chemical reaction and be observed as facility bias or as mild ignition. As discussed, past work has employed reduced-order scaling analyses and lower-order computational techniques, e.g., irrotational flow, Reynolds averaging. However, these formulations can alter interpretations of the calculations; therefore, a higher-order framework was pursued in this work. The current activity is ongoing in collaboration with ETH Zurich.

Conclusions

- Acquired autoignition data for binary blends of an iso-olefin, 2M2B, and an aromatic, TOL, covering wide ranges of temperatures, pressures, stoichiometries, and blending ratios
- Revised previously developed scaling analyses to identify physical and chemical parameters that govern flame-driven compression ignition, with applications to mild ignition in RCMs and to spark-assisted compression ignition in internal combustion engines
- Initiated investigations using higher-order, multidimensional reacting flow software (NEK5000) to understand impacts of non-ideal RCM operation.

Key Publications

1. Santner, J., and S.S. Goldsborough. 2019. "Hot-Spot Induced Mild Ignition: Numerical Simulation and Scaling Analysis." *Combustion and Flame* 209: 41–62.
2. Santner, J., and S.S. Goldsborough. 2019. "Mild Ignition: Experimental Observations and Numerical Predictions." 17th International Conference on Numerical Combustion, Aachen, Germany.

3. Goldsborough, S.S., C.E. Frouzakis, and Y.M. Wright. 2019. "Detailed Computational Investigation of Fluid Mechanical Behavior in Rapid Compression Machines." 17th International Conference on Numerical Combustion, Aachen, Germany.

4. Ure, A.D., S. Dooley, D. Kang, and S.S. Goldsborough. 2019. "A Chemical Functionality Approach towards the Formulation of a High Fidelity Surrogate Fuel for FACE Gasoline F." 11th U.S. Combustion Meeting, Pasadena, CA.

5. Mehl, M., D. Kang, S.S. Goldsborough, G. Kukkadapu, K. Zhang, S. Wagnon, W.J. Pitz, and C.K. Westbrook. 2019. "Experimental and Modeling Study of the Autoignition Behavior of a Standard Oxygenated Gasoline Fuel." 11th U.S. Combustion Meeting, Pasadena, CA.

6. Kang, D., A. Fridlyand, S.S. Goldsborough, M. Mehl, S. Wagnon, W.J. Pitz, and M.J. McNenly. 2019. "Impact of Ethanol Additions on Autoignition Characteristics of a Full Boiling Range Gasoline and Its Surrogates at Advanced Engine Conditions." 11th U.S. Combustion Meeting, Pasadena, CA.

7. Cheng, S., D. Kang, A. Fridlyand, S.S. Goldsborough, S. Wagnon, M.J. McNenly, M. Mehl, W.J. Pitz, and D. Vuilleumier. "Autoignition Behavior of Gasoline/Ethanol Blends at Engine-Relevant Conditions." Submitted to *Combustion and Flame* in 2019.

8. Waqas, M., S. Cheng, S.S. Goldsborough, T. Rockstroh, B. Johansson, and C.P. Kolodziej. 2019. "An Experimental and Numerical Investigation to Characterize the Low Temperature Heat Release (LTHR) in Stoichiometric and Lean Conditions." Submitted to International Combustion Symposium, Adelaide, Australia.

References

1. "Basic Research Needs for Clean and Efficient Combustion of 21st Century Transportation Fuels." U.S. Department of Energy, Office of Science (website). Accessed 2019. http://science.energy.gov/~/media/bes/pdf/reports/files/ctf_rpt.pdf.

2. Goldsborough, S.S., S. Hochgreb, G. Vanhove, M.S. Wooldridge, H.J. Curran, and C.-J. Sung. 2017. "Advances in Rapid Compression Machine Studies of Low- and Intermediate-Temperature Autoignition Phenomena." *Prog. Energy Combust. Sci.* 63: 1–78.

3. Goldsborough, S.S., and J. Santner. "Mining an Experimental Autoignition Database to Hierarchically Identify Facility Influences on the Measurements." In preparation.

4. Bahrini, C., O. Herbinet, P.-A. Glaude, C. Schoemaecker, C. Fittschen and F. Battin-Leclerc. 2012. "Quantification of Hydrogen Peroxide during the Low-Temperature Oxidation of Alkanes." *J. Am. Chem. Soc.* 139: 11944–11947.

5. Stranic, I., S.H. Pyun, D.F. Davidson, and R.K. Hanson. 2012. "Multi-Species Measurements in 1-Butanol Pyrolysis behind Reflected Shock Waves." *Combustion and Flame* 159: 3242–3250.

6. Sluder, C.S., D.E. Smith, M. Wissink, J.E. Anderson, T.G. Leone, and M.H. Shelby. 2017. "Effects of Octane Number, Sensitivity, Ethanol Content, and Engine Compression Ratio on GTDI Engine Efficiency, Fuel Economy and CO_2 Emissions: Final Report." Coordinating Research Council Report No. AVFL-20.

7. Fridlyand, A., S.S. Goldsborough, M. Al Rashidi, S.M. Sarathy, M. Mehl, and W.J. Pitz. 2019. "Low Temperature Autoignition of 5-Membered Ring Naphthenes: Effects of Substitution." *Combustion and Flame* 200: 387–404.

8. Sjoberg, M., and W. Zeng. 2016. "Combined Effects of Fuel and Dilution Type on Efficiency Gains of Lean Well-Mixed DISI Engine Operation with Enhanced Ignition and Intake Heating for Enabling Mixed-Mode Combustion." *SAE Int. J. Engines* 9: 750–767.

9. Chen, Z. 2008. PhD Dissertation, Princeton University.

10. Walton, S.M., X. He, B.T. Zigler, and M.S. Wooldridge. 2007. "An Experimental Investigation of the Ignition Properties of Hydrogen and Carbon Monoxide Mixtures for Syngas Turbine Applications." *Proc. Combust. Inst.* 31: 3147–3154.

11. Assanis, D., S.W. Wagnon, and M.S. Wooldridge. 2015. "An Experimental Study of Flame and Autoignition Interactions of Iso-Octane and Air Mixtures." *Combustion and Flame* 162 (4): 1214–1224.

12. Santner, J., and S.S. Goldsborough. 2019. "Hot-Spot Induced Mild Ignition: Numerical Simulation and Scaling Analysis." *Combustion and Flame* 209: 41–62.

Acknowledgements

Argonne National Laboratory performed this work under the auspices of the U.S. Department of Energy under Contract DE-AC02-06CH11357. Experimental measurements and analysis were conducted with the assistance of Dongil Kang, Song Cheng, Jake Tracey, and Monica Viz. Chemical kinetic modeling was conducted with the assistance of Scott Wagnon, Goutham Kukkadapu, William Pitz, and Russell Whitesides (Lawrence Livermore National Laboratory).

I.8 Development and Validation of Simulation Tools for Advanced Ignition Systems (Argonne National Laboratory)

Riccardo Scarcelli, Principal Investigator
Argonne National Laboratory
9700 S. Cass Avenue
Lemont, IL 60439
Email: rscarcelli@anl.gov

Michael Weismiller, DOE Technology Development Manager
U.S. Department of Energy
E-mail: Michael.Weismiller@ee.doe.gov

Start Date: October 1, 2016 End Date: September 30, 2023
Project Funding (FY19): $400,000 DOE share: $400,000 Non-DOE share: $0

Project Introduction

Due to the United States' heavy reliance on gasoline engines for automotive transportation, efficiency improvements of advanced gasoline direct injection (GDI) combustion concepts have the potential to dramatically reduce foreign oil consumption. However, combustion strategies such as stratified, dilute, and boosted operation present challenging conditions for conventional ignition systems, thereby limiting the attainable benefits of these advanced combustion concepts. Advanced ignition systems for GDI engines enable the continued use of conventional combustion systems (reducing cost/risk) while providing potentially substantial benefits to fuel economy. In-depth understanding of the ignition physics and advanced ignition models will aid the development of dilution-tolerant, high-efficiency, and low-emissions GDI combustion systems.

Objectives

This research project addresses the technological barrier of limited attainable GDI engine efficiency due to the lack of robust spark ignition dilute combustion technology and controls, which is essentially caused by:

- Limited understanding of advanced ignition mechanisms enabling high-efficiency GDI engines
- Limited availability of modeling tools to support the development of advanced ignition systems.

While the ultimate benefit is the improvement of GDI engine efficiency, the goal of this project is to expand the tools (knowledge and models) to enable significant improvement of the current ignition technology. This project focuses on modeling conventional spark ignition as well non-conventional ignition technologies such as low-temperature plasma (LTP) and pre-chamber ignition.

Fiscal Year (FY) 2019 Objectives

- Model a real LTP ignition experiment and validate computational fluid dynamics (CFD) results against experimental data
- Understand LTP ignition processes by evaluating the impact of plasma kinetics and fluid dynamics
- Expand LTP studies to simulate advanced igniter geometries that are of interest to industry
- Plan future work to improve and expand conventional spark ignition models.

Approach

This is a simulation effort that aims at improving the fundamental understanding of advanced ignition processes and building comprehensive models that can be leveraged to potentially simulate any ignition system of interest. Advanced diagnostics from project partners Sandia National Laboratories (SNL or Sandia) and Michigan Technological University are leveraged with the intent to enhance the fundamental understanding of ignition processes of conventional as well as non-conventional technologies and provide a dataset for model validation. High-fidelity thermal and non-thermal plasma simulations are carried out using the commercial solvers VizGlow/VizSpark through a collaboration with Esgee Technologies Inc. and University of Texas at Austin. The goal of these simulations is to provide proper understanding of the plasma properties as a result of the electrical discharge characteristics. The analysis of non-equilibrium plasma characteristics is carried out in collaboration with industry partners actively working in the field of LTP, such as Transient Plasma Systems and Tenneco (formerly Federal Mogul). The impact of LTP systems on engine combustion is being evaluated in collaboration with the University of Perugia. Novel ignition modeling capabilities are ultimately implemented into the CFD engine code CONVERGE that is largely used in the automotive industry.

The main tasks planned at Argonne National Laboratory are the following:

- Expand the capabilities of conventional spark ignition models to improve the predictive nature of these models at challenging (boosted, dilute, cold-start) engine operation
- Improve the fundamental understanding of non-conventional ignition technologies (LTP, pre-chamber ignition) that are being evaluated by the automotive industry
- Build and develop comprehensive models that can be used to simulate conventional as well as non-conventional ignition processes in internal combustion engines
- Use the developed models to guide the research and development of advanced ignition systems to achieve highly dilute and highly efficient combustion in GDI engines.

Results

Previously, during FY 2018, a pin-to-pin electrode geometry coupled with nanosecond high-voltage electrical discharge was simulated using the non-equilibrium plasma solver VizGlow. The comparison between Argonne simulations and Sandia experiments in terms of plasma chemical and thermal properties in the proximity of the positive electrode (anode) indicated a close quantitative agreement. An initial step was made to convey the improved LTP knowledge into the development of an LTP ignition model for CFD engine simulations. The information generated using VizGlow was used to initialize the post-discharge plasma characteristics in CONVERGE CFD, by a mixed deposition of plasma species and thermal energy. The LTP ignition mechanism showed substantial differences with respect to thermal ignition. The ignition process was the result of the local accumulation of active species that triggered the fuel kinetics above a certain threshold. However, simulation results could not be validated due to the absence of experimental data.

Major accomplishments in FY 2019 can be summarized as follows:

- LTP ignition simulations were performed and validated against experiments.
- Multi-pulse LTP discharge was simulated, and plasma properties were evaluated from pulse to pulse.
- In-depth analysis of the impact of plasma chemistry on LTP ignition was performed using detailed kinetics.
- LTP simulations were extended to advanced igniter geometries being evaluated by industry (groundless barrier discharge igniter [GBDI], Corona).
- Action items were defined to continue the development of conventional spark ignition models.

LTP Ignition Simulations Performed and Validated against Experiments

A real LTP ignition event tested at Sandia was simulated using VizGlow and subsequently CONVERGE. The VizGlow simulations used the detailed geometry of both the pin electrodes and voltage boundary conditions measured at Sandia. The model was calibrated to agree with experiments in terms of post-discharge plasma regime (glow or spark). VizGlow simulations identified the distribution of thermal (temperature) and chemical (atomic oxygen, O) plasma properties in the gap between the two pin electrodes. The post-discharge distribution was mapped into CONVERGE CFD, and the simulation of a multi-pulse discharge was carried out using the assumption that each pulse would provide the same amount of thermal/chemical energy deposition. Figure I.8.1 shows the comparison between optical data from Sandia and CFD simulations from Argonne. By applying the VizGlow output to CONVERGE, simulations could not reproduce the LTP ignition event. By enhancing the chemical properties (represented by O) by a factor of 10, simulations qualitatively agreed with experiments. This factor of 10 was shown to account for simplistic assumptions that can be summarized as follows:

- Subsequent pulses do not necessarily deliver the same plasma deposition at quiescent conditions.
- The kinetic mechanism did not include important plasma/fuel species that can trigger ignition.

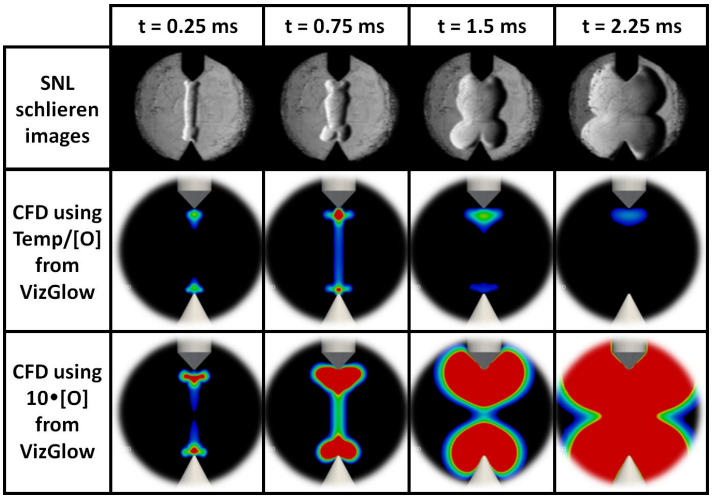

Figure I.8.1 Comparison between optical images and CFD simulation of LTP ignition processes

Multi-Pulse LTP Discharge Simulated and Plasma Properties Evaluated from Pulse to Pulse

The plasma solver VizGlow was used to simulate multiple high-voltage nanosecond pulses in rapid succession. The main challenge for such simulation is represented by the large separation of scales between the time of the nano-pulsed discharge (tens of ns) and the inter-pulse or dwell time between pulses (tens or hundreds of μs). Additionally, the VizGlow tool currently does not possess an implicit time-step solver. An ad-hoc explicit time-step formulation allowed completing a simulation of three subsequent pulses in one-week computational time. The results are shown in Figure I.8.2. At later pulses, the streamer discharge becomes faster, and increased deposition of active species and thermal energy is shown. By capturing the pulse-after-pulse deposition, future CFD results of LTP ignition processes are expected to deliver improved agreement with experiments.

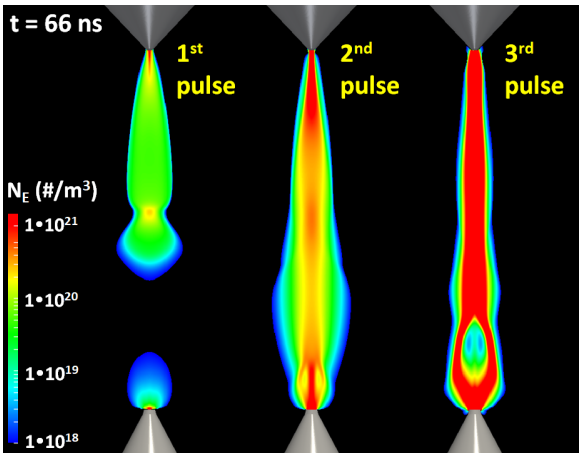

Figure I.8.2 Simulation of three subsequent nano-pulses and impact on plasma properties (electron density, N_E)

In-Depth Analysis of the Impact of Plasma Chemistry on LTP Ignition Performed Using Detailed Kinetics

The analysis of the impact of plasma and fuel kinetics on LTP ignition processes was carried out by a zero-dimensional batch reactor that takes the time-resolved electron density and electric field from VizGlow simulations, calculates electron impact rate coefficient through BOLSIG+, and finally solves for temporal variation in species and temperature. The full non-equilibrium air plasma kinetics from Adamovich et al. [1] and the combustion kinetics from University of California, San Diego [2], were used in Cantera to calculate the reaction coefficient rates. Figure I.8.3 shows the temporal evolution of some of the most significant plasma species that have a relevant impact on ignition processes. Ozone (O_3) and nitrogen oxides (NO) are known to enhance autoignition processes. Fuel radical (C_3H_7) generated during the plasma discharge also enhances ignition. Furthermore, atomic oxygen (O) that does not react with the fuel radicals recombines to produce ozone later during the post-discharge. Future plasma and CFD ignition simulation will have to include all these species in the kinetic model.

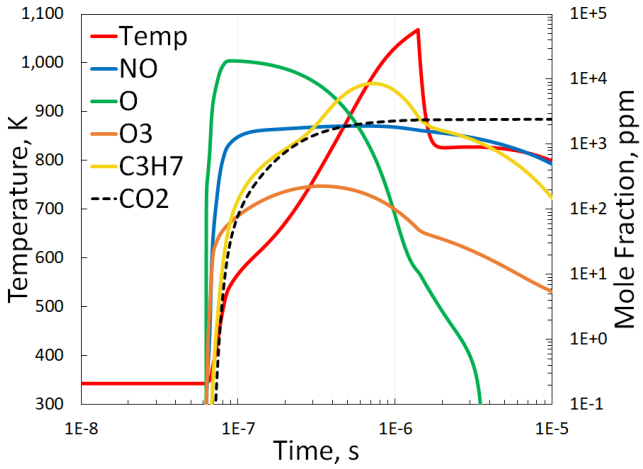

Figure I.8.3 Temporal evolution of plasma species during and after a nano-pulsed discharge

LTP Simulations Extended to Advanced Igniter Geometries Being Evaluated by Industry (GBDI, Corona)

Before FY 2019, all high-fidelity plasma simulations have been performed on a simple, canonical pin-to-pin electrode configuration. However, industry partners are more interested in realistic, advanced LTP igniter

geometries. This year, non-equilibrium plasma calculations have been expanded to simulate two geometries of significant interest to the automotive original equipment manufacturers:

8. The GBDI developed by General Motors and Tenneco

9. The radio-frequency Corona igniter from Tenneco.

The simulation of the GBDI was carried out in collaboration with Sandia. A Sandia in-house made version of GBDI (here referred to as Version 1) was initially modeled using VizGlow. Figure I.8.4 shows a qualitative comparison between simulation results and images from Sandia calorimetry. The surface streamers were covering a large portion of the dielectric barrier and some streamers into air generated at the interface between the power anode and the dielectric insulator. Those streamers could reach the walls of the calorimeter and trigger arcing events. Additional simulations on an advanced GBDI geometry with the power electrode fully covered by dielectric material (GBDI Version 2, not shown here) indicated that the streamers into air could be significantly weakened and the arcing events prevented.

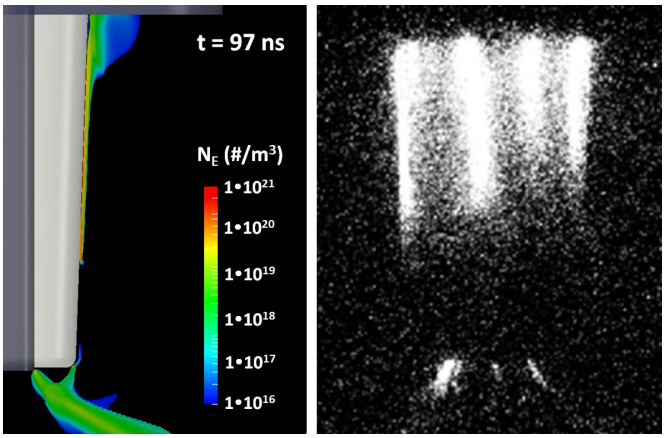

Figure I.8.4 Comparison between simulation (Argonne, left) and optical images (Sandia, right) of LTP discharge from a GBDI

The simulation of radio-frequency Corona discharge was carried out in collaboration with Tenneco and University of Perugia, Italy. The LTP discharge from one of the tips of a Corona igniter was simulated with VizGlow. The main challenge from this series of simulations was imposed by the radio-frequency signal, which stays continuously active for hundreds of microseconds (10^{-6} s), while the simulation computational time-step needs to be low, i.e., on the order of picoseconds (10^{-12} s), to properly resolve the streamer activity. Overcoming the challenge required optimum mesh generation and large computational resources. Finally, it was possible to simulate a few tens of microseconds of Corona discharge, approaching quasi-steady behavior, in a few weeks of computation time. Figure I.8.5 shows the temporal evolution of thermal and chemical plasma properties as a result of a combination of positive and negative streamers from a radio-frequency discharge in a Corona igniter.

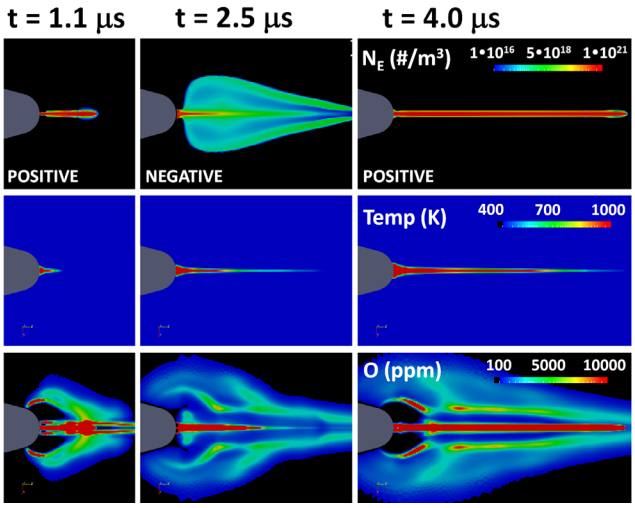

Figure I.8.5 Temporal evolution of LTP discharge and plasma properties from a radio-frequency Corona igniter

Action Items Defined to Continue the Development of Conventional Spark-Ignition Models

In FY 2019, the following progress was also made for conventional and advanced spark-ignition modeling:

- The Lagrangian-Eulerian Spark-Ignition (LESI) model developed at Argonne under this program was fully documented in a conference/journal paper that was awarded as best paper in the numerical simulation track at the 2018 ASME Internal Combustion Engines Fall Conference.
- The LESI model implementation into CONVERGE CFD was awarded under the FY 2019 Technology Commercialization Fund program. As a result of this award, LESI will soon become a new capability of CONVERGE.
- A cooperative research and development agreement with an automotive industry partner (Fiat Chrysler Automobile) is being finalized for FY 2020 and FY 2021, with the goal to further develop and expand the LESI model.
- Pre-chamber ignition modeling studies have been initiated in collaboration with principal investigators at Sandia National Laboratories (Isaac Ekoto) and Argonne National Laboratory (Toby Rockstroh).

Conclusions

- An LTP ignition experiment carried out at Sandia was modeled using VizGlow and then CONVERGE CFD. Simulations were compared with optical data, showing good qualitative agreement, which nevertheless required increasing the amount of atomic oxygen calculated by VizGlow by a factor of 10.
- The simulation of a multi-pulse LTP discharge with VizGlow revealed that the change of mixture properties from one pulse to the next increases the deposition of thermal and chemical energy at later discharges. Fluid dynamics was shown to play an important role in the temporal evolution of the mixture properties.
- Detailed kinetics study using a full batch reactor highlighted the importance of plasma species, such as NO and O_3, as well as fuel radicals. Such species should be included in the mechanism scheme for VizGlow and CONVERGE CFD simulations, as these greatly impact LTP ignition processes.

- Advanced LTP igniter geometries (GBDI, Corona) were simulated with VizGlow, showing good qualitative agreement with experimental data.
- Future work was properly laid out to further improve spark-based ignition models developed by Argonne National Laboratory.

Key Publications

1. Scarcelli, R., et al. 2018. "Numerical Simulation of a Nano-pulsed High-voltage Discharge and Impact on Low-temperature Plasma Ignition Processes for Automotive Applications." 4th International Conference on Ignition Systems for Gasoline Engines (December 6–7), Berlin, Germany.
2. Scarcelli, R., et al. 2018. "Modeling Non-Equilibrium Discharge and Validating Transient Plasma Characteristics at Above-Atmospheric Pressure." *Plasma Sources Sci. Technol.* 27: 124006.
3. Scarcelli, R., et al. 2019. "Development of a Hybrid Lagrangian-Eulerian Model to Describe Spark-Ignition Processes at Engine-Like Turbulent Flow Conditions." *J. Eng. Gas Turb. Power* 141 (9): 091009.
4. Gururajan, V., et al. 2019. "A Computational Study of the Thermodynamic Conditions Leading to Autoignition in Nanosecond Pulsed Discharges." ASME Paper ICEF2019-7260.

References

1. Adamovich, et.al. 2015. Philosophical Transactions of the Royal Society A 373 (2048).
2. Chemical-Kinetic Mechanisms for Combustion Applications (http://combustion.ucsd.edu).

Acknowledgements

The authors wish to acknowledge all the project partners mentioned above in the Approach section. The authors also wish to thank the Laboratory Computing Resource Center folks at Argonne for supporting this project with their cluster Bebop.

I.9 Stretch Efficiency for Combustion Engines: Exploiting New Combustion Regimes (Oak Ridge National Laboratory)

James Szybist, Principal Investigator
Oak Ridge National Laboratory
2360 Cherahala Boulevard
Knoxville, TN 37922
E-mail: szybistjp@ornl.gov

Michael Weismiller, DOE Technology Development Manager
U.S. Department of Energy
E-mail: Michael.Weismiller@ee.doe.gov

Start Date: October 1, 2018 End Date: September 30, 2021
Project Funding (FY19): $450,000 DOE share: $450,000 Non-DOE share: $0

Project Introduction

The overarching goal of this project is to use a thermodynamics-based approach to identify and pursue opportunities for improved efficiency in internal combustion engines. The combustion strategy identified as the most promising approach to improving light-duty engine efficiency is high dilution from exhaust gas recirculation (EGR) for spark-ignited combustion enabled by fuel reforming through thermochemical recuperation. The overall efficiency advantages for high EGR conditions are summarized in a thermodynamic modeling study by Caton [1] and include decreased pumping work, decreased heat transfer, and increased ratio of specific heats (γ). The amount of EGR that can be used is limited due to combustion instabilities, but the dilution limit can be extended for additional efficiency improvements with the use of high flame speed components, namely H_2. This project is pursuing fuel reforming to generate H_2 in an effort to extend the EGR dilution limits for spark-ignited combustion in the most thermodynamically favorable way possible. Ideally, this involves using exhaust heat to drive endothermic reforming reactions to increase the chemical fuel energy to achieve thermochemical recuperation, a form of waste heat recovery.

Efforts in Fiscal Year (FY) 2019 specifically focused on the thermodynamics of consuming reformate in an engine. Unlike the hydrocarbons that are in gasoline, the primary products of reforming, H_2 and CO, have a higher energy content on a 1st Law energy basis (enthalpy) than they do on a 2nd Law basis (exergy). An earlier modeling investigation illustrated that the physical manifestation for the discrepancy between the 1st and 2nd Law bases could be attributed to the molar expansion ratio (MER), or the ratio of product moles to reactant moles [2]. Further, that study showed that the 2nd Law basis was a better indication of the work potential of a fuel, meaning that reformate, which has MER < 1, potentially incurs an efficiency penalty. Developing a better understanding of the relationship between the MER of a fuel and engine efficiency could provide insights into potential efficiency limitations associated with reforming processes. Thus, FY 2019 work was focused on generating and analyzing data to develop a better understanding between MER and efficiency.

Objectives

Overall Objectives

- Identify and characterize the potential of catalytic EGR loop reforming to achieve waste heat recovery through thermochemical recuperation and to extend the dilution limit of an engine
- Perform thermodynamics-focused analysis to determine the efficiency potential of this strategy relative to other emerging combustion strategies.

Fiscal Year 2019 Objectives

- Complete an experimental investigation into the role of MER on 1st and 2nd Law engine efficiency
- Develop a correlation to estimate the change in engine efficiency based on MER and other variables.

Approach

An experimental campaign was conducted to investigate the effect of MER in a spark ignition engine using the four fuels shown in Table I.9.1. These fuels were chosen because they represent a wide range of MER, from 0.852 to 1.058. These fuels were investigated in a single-cylinder version of a Ford 1.6 L Ecoboost engine with a compression ratio of 10.1:1. The liquid fuel (iso-octane) was delivered using the stock centrally mounted direct injection fueling system, whereas the gaseous fuels were fumigated into the intake manifold and were metered using a mass flow controller. The engine was operated at 1,500 rpm at an engine load of 6.5 bar indicated mean effective pressure when the crank angle at 50% mass fraction burned (CA50) combustion phasing was 8 crank angle (CA) degrees after firing top dead center (aTDCf). The engine was operated with constant fueling over a combustion phasing sweep, and under stoichiometric conditions as well as fuel-lean conditions.

Table I.9.1 Fuels Matrix Experimentally Investigated

Fuel	H/C [-]	O/C [-]	MER [-]	Δ MW [%]	AFRstoich [-]	LHV [kJ/g]	Exergy [kJ/g]	Exergy/LHV
Iso-Octane	2.250	0.000	1.058	-0.055	15.052	44.31	46.09	1.040
Propane	2.667	0.000	1.040	-0.039	15.600	46.357	47.45	1.024
Methane	4.000	0.000	1.000	0.000	17.160	50.009	50.44	1.009
95 vol% CO, 5 vol% H_2	0.105	1.000	0.852	0.174	2.297	9.8222	8.9927	0.916

H/C: hydrogen-to-carbon ratio; O/C – oxygen-to-carbon ratio; ΔMW – change in molecular weight; AFRstoich – stoichiometric air–fuel ratio; LHV – lower heating value

In order to help interpret the experimental findings, modeling using Chemkin was performed using a two-zone model for knock assessment. While Chemkin is a modeling tool designed to simulate chemical kinetics, the focus of this study was on the thermodynamic changes with different fuels. In order to focus on the fuel-specific thermodynamics, a Weibe function was specified and kept constant for all fuels to simulate the deflagration event, beginning at -11 to 30 CA degrees aTDCf, which effectively transports mass from the unburned zone to the burned zone at a known rate. The chemical kinetic reactions in the unburned zone were turned off, but the chemical kinetic reactions in the burned zone were on. This allowed the composition of the burned zone to achieve chemical equilibrium, which is important for accounting for the energy of chemical dissociation at the high temperatures.

Results

In order to isolate the thermodynamic difference based on fuel type, efficiency must take into account the gross work produced by the engine, but not the pumping work. This is because, at a constant load, the different fuels require different amounts of pumping work due to the molar flow rate into the intake manifold. Also, it is necessary to correct the results for combustion efficiency. Specifically, the gaseous fuels have better air-fuel mixing and lower hydrocarbon emissions. Thus, to isolate the study to the fuel-specific thermodynamics, only the burned fuel should be considered.

Once calculating the gross efficiency considering only the burned fuel, engine efficiency can be plotted for each fuel type as a function of combustion phasing on both a 1st and 2nd Law basis, as shown in Figure I.9.1. For the hydrocarbon fuels, iso-octane has the highest efficiency on a 1st Law basis, followed by propane and then methane, with a total efficiency difference of approximately 1 percentage point between iso-octane and methane throughout the combustion phasing sweep. The efficiency for the CO/H_2 blend is substantially lower, about 6 percentage points. Throughout all of these fuels, there is a consistent trend of 1st Law efficiency

decreasing as MER decreases, in agreement with the earlier modeling study [2]. On a 2nd Law basis, all of the hydrocarbon fuels produce the same efficiency throughout the combustion phasing sweep. This was the expected result based on the earlier modeling study [2]. However, the CO/H_2 blend continues to exhibit a lower efficiency by approximately 1 to 1.5 efficiency points. This indicates that the majority of the efficiency difference on a 1st Law basis can be attributed to molar expansion ratio effects, but that there are other fuel-specific considerations that need to be taken into account for the CO/H_2 blend.

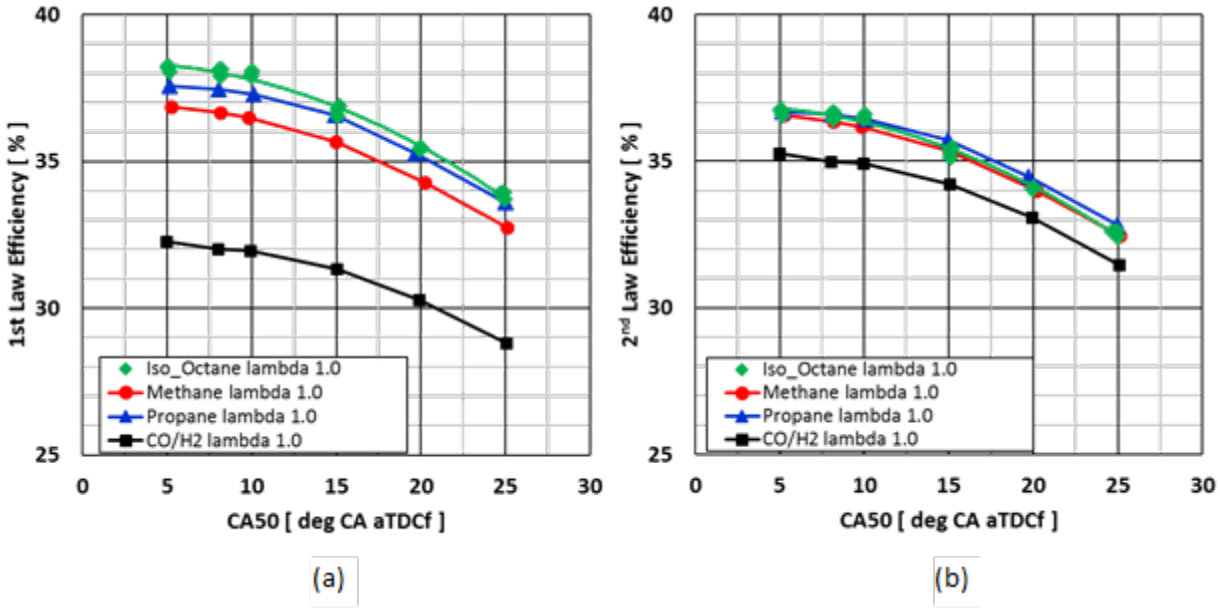

Figure I.9.1 Engine efficiency as a function of CA50 combustion phasing on the basis of (a) 1st Law of Thermodynamics and (b) 2nd Law of Thermodynamics

One of the possible reasons for the lower 2nd Law efficiency for the CO/H_2 blend is the difference in exhaust temperature. Figure I.9.2 shows that while all of the hydrocarbon fuels have nearly identical exhaust temperatures throughout the combustion phasing sweep, the exhaust temperature for the CO/H_2 blend is higher by about 80°C. As a result, heat transfer differences between the fuels cannot be eliminated as a possible source of the efficiency differences. There are a number of other possibilities for these differences, including the fact that combustion analysis also revealed some late-cycle heat release for the CO/H_2 blend that was not observed for the other fuels, and in addition, there are large differences in the thermodynamic gas properties. Thus, modeling can be employed to investigate these fuel-specific thermodynamic differences further.

Using Chemkin to model the thermodynamic processes in the engine had several desirable attributes. First, modeling could be done under adiabatic conditions; thus, the heat transfer differences could be removed and other fuel-specific thermodynamic effects could be isolated. Second, a much wider range of fuels could be investigated than would be feasible to include for an experimental condition. For the modeling study, alkanes included C1 (methane) to C8 (iso-octane), alkenes included C2 (ethene) to C6 (hexene), aromatics included benzene and toluene, alcohols included ethanol and iso-butanol, and acetylene was included as the only alkyne. Additionally, a range of CO/H_2 blends was also included, ranging from 1 mol% CO to 95 mol% CO.

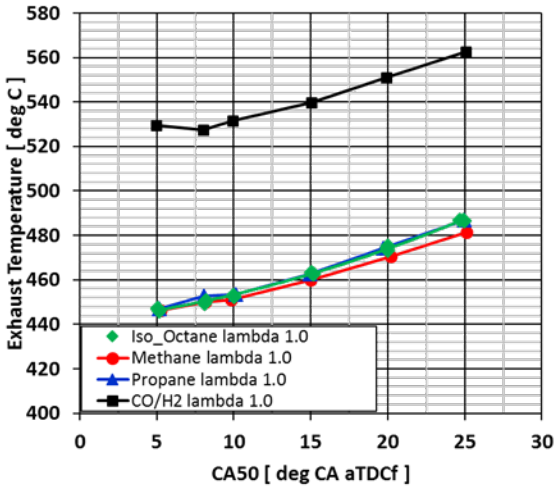

Figure I.9.2 Engine exhaust temperature for each fuel as a function of CA50 combustion phasing

The modeled engine efficiency for the range of fuels investigated is shown in Figure I.9.3 on both a 1st Law and 2nd Law basis as a function of MER. For the 1st Law basis, there is a general trend of increasing efficiency with MER, but the overall correlation is relatively poor ($R^2 = 0.73$). Additionally, there are chemistry-specific trends that are evident. Specifically, the alkanes have higher efficiency than alkenes or aromatics at the same MER. Further, there is a wide range of variability for the reformate blends (CO/H_2) at a constant MER. Relative to the overall spread in the 1st Law differences between fuels, the grouping of efficiency on a 2nd Law basis is significantly tighter, and there is no correlation between 2nd Law efficiency, which would be expected if 2nd Law efficiency already accounted for the molar expansion ratio. Ultimately, though, the reformate blends continue to exhibit a wide spread of efficiency on a 2nd Law basis, meaning that there are factors in this correlation that are not yet accounted for.

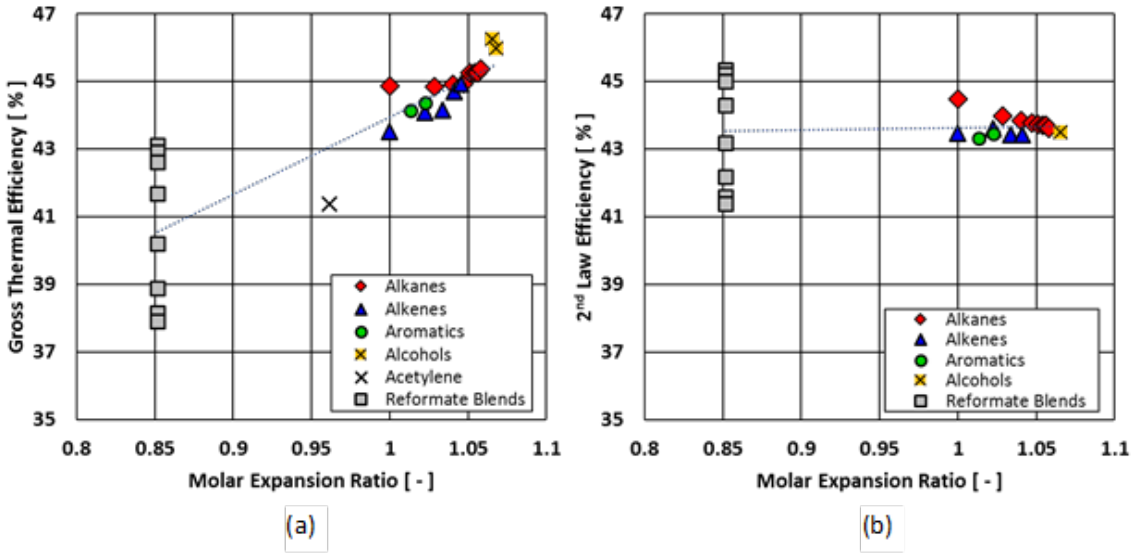

Figure I.9.3 Simulated engine efficiency as a function of MER under stoichiometric conditions: (a) 1st Law of Thermodynamics basis, and (b) 2nd Law of Thermodynamics basis

Further analysis of the total chemical heat release rate from the combustion process reveals two distinct phases of combustion, as shown in Figure I.9.4. The first of these is from the deflagration heat release event, as

defined by the Wiebe function in the simulation. The second phase of the heat release is associated with recombination of water in CO_2 in the burned gas zone. The high temperatures of the burned zone cause chemical dissociation of the water and CO_2. As the combustion chamber cools through the expansion stroke, water and CO_2 recombine in accordance with thermal equilibrium, releasing additional heat. This has the effect of transporting some of the heat release until later in the expansion stroke. This analysis found that the dissociation of these species had to be considered in order to account for the fuel-specific dissociation. The amount of energy associated with CO_2 dissociation and recombination is higher than that of water; at a temperature of 2,300 K, approximately 10% of CO_2 is dissociated, whereas only 3% of water is dissociated. Thus, fuels that have higher concentrations of CO_2 in the combustion products will be expected to transport more of the heat release to later stages of the expansion stroke, thereby reducing thermodynamic efficiency.

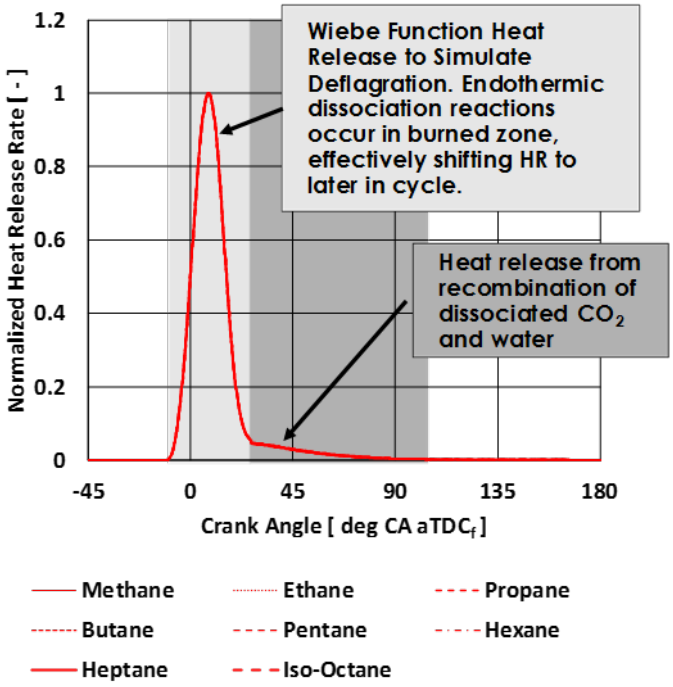

Figure I.9.4 Heat release rate for alkane fuels from the Chemkin two-zone simulations showing the initial deflagration heat release as defined by a Wiebe function, followed by a late-cycle heat release (HR) from the recombination of dissociated CO_2 and water

Based on the Chemkin simulations, an empirical correlation, shown below, was created to be able to predict the relative efficiency change of a fuel relative to a baseline fuel. This correlation considers the change in molecular weight (MW) of the fuel during combustion, as well as the concentrations of CO_2 and H_2O in the exhaust. The change in the molecular weight of the fuel is simply an alternate way to express the MER, since mass is conserved during combustion. Figure I.9.5(a) shows the gross efficiency of the engine as predicted by the correlation vs. the Chemkin simulations, illustrating that this correlation adequately captures the efficiency trend of the reformate fuels, which was not accounted for when considering only MER in Figure I.9.3.

$$Merit = \frac{b * (\Delta MW_i - \Delta MW_{baseline}) \left[\frac{g}{mol}\right] + c * (CO_{2,i} - CO_{2,baseline})[exh\ mol\ frac] + d * (H_2O_i - H_2O_{baseline})[exh\ mol\ frac]}{\eta_{baseline}}$$

b= -0.979; c=-9.342; d=8.167

Figure I.9.5(b) then applies this correlation to the experimental data collected as part of this study, with iso-octane being considered as the baseline fuel. It can be seen that the correlation does a reasonable job of capturing the efficiency trend for methane and propane. The trend with reformate is directionally captured, but there is also room for improvement, which may be possible by considering the trapped residuals when calculating the change in MW, as well as developing the model to consider heat transfer.

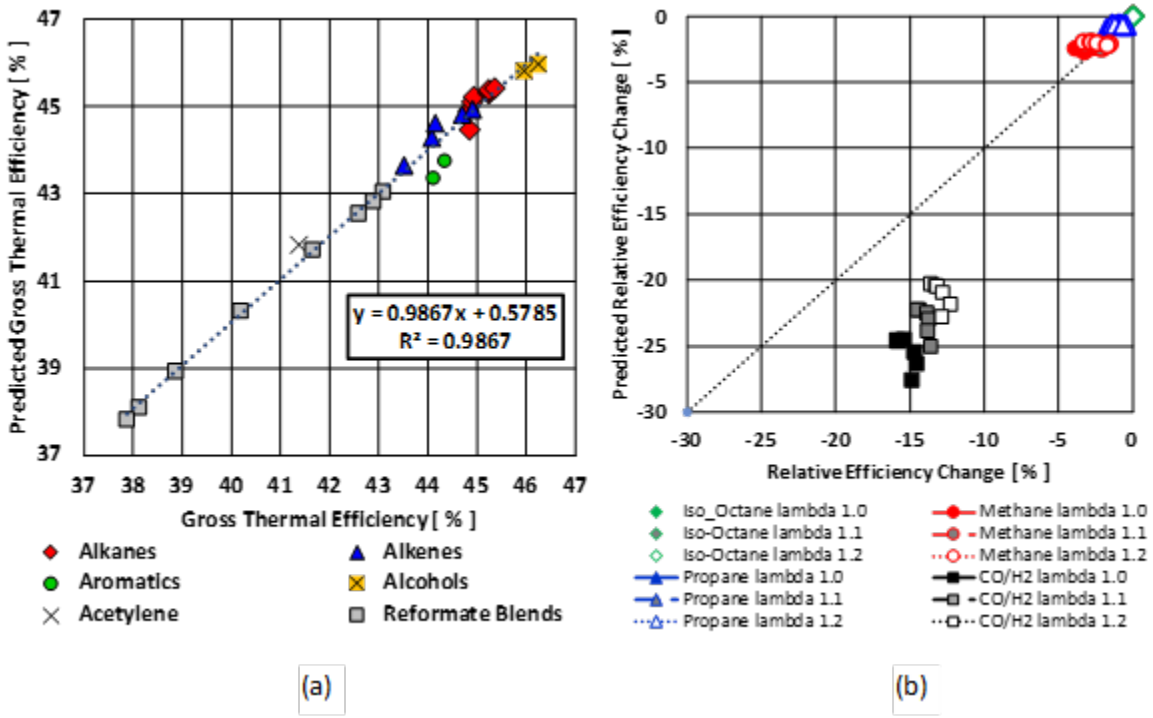

Figure I.9.5 Performance of the empirical efficiency correlation for (a) simulation results from Chemkin and (b) experimental data

Conclusions

In FY 2019, progress was made in developing a better understanding of the role of MER on engine efficiency. This is being studied because reformate is being used in the Oak Ridge National Laboratory EGR-loop catalytic reforming combustion strategy, but reformate also represents a fuel with dramatically reduced MER relative to gasoline and may represent a limit to the potential efficiency increase with this combustion strategy.

- Experimental data showed that 1st Law efficiency decreased as MER decreased.
- On a 2nd Law basis, there were no longer any fuel-specific efficiency differences for the hydrocarbon fuels, supporting the idea that MER is the physical manifestation between 1st and 2nd Law differences.
- However, the 2nd Law basis didn't fully account for the lower efficiency of the reformate fuel blend.
- Modeling investigations showed that in addition to accounting for MER, it is necessary to consider the chemical dissociation of the burned zone, which effectively transports heat release until later stages of the expansion stroke and reduces engine efficiency.

The results from this study will be analyzed further and published during FY 2020.

Key Publications

1. Szybist, J., J. Pihl, S. Huff, and B. Kaul. 2019. "High Load Expansion of Catalytic EGR-Loop Reforming under Stoichiometric Conditions for Increased Efficiency in Spark Ignition Engines." SAE Technical Paper 2019-01-0244, https://doi.org/10.4271/2019-01-0244.

References

1. Caton, J.A. 2013. A Comparison of Lean Operation and Exhaust Gas Recirculation: Thermodynamic Reasons for the Increases of Efficiency. SAE International.

2. Szybist, J.P., K. Chakravathy, and C.S. Daw. 2012. "Analysis of the Impact of Selected Fuel Thermochemical Properties on Internal Combustion Engine Efficiency." Energy & Fuels 26 (5): 2798–2810.

Acknowledgements

Josh Pihl and Tommy Powell of Oak Ridge National Laboratory provided valuable contributions to this project and report.

I.10 Neutron Imaging of Advanced Transportation Technologies (Oak Ridge National Laboratory)

Martin Wissink, Principal Investigator
Oak Ridge National Laboratory
P.O. Box 2008, MS-6472
Oak Ridge, TN 37831
E-mail: wissinkml@ornl.gov

Michael Weismiller, DOE Technology Development Manager
U.S. Department of Energy
E-mail: Michael.Weismiller@ee.doe.gov

Start Date: October 1, 2018 End Date: Project continuation evaluated annually
Project Funding: $188,000 DOE share: $188,000 Non-DOE share: $0

Project Introduction

Neutrons are very sensitive to light elements such as hydrogen and lithium, while at the same time being able to penetrate through common engineering metals such as iron and aluminum alloys (Figure I.10.1a). These two properties make neutrons well suited for probing a variety of automotive components such as particulate filters, exhaust gas recirculation coolers, fuel injectors, oil in engines, oil residues in filters, batteries, and advanced materials. Neutron imaging is based on the interactions of a sample with a neutron beam. The interactions are dependent on sample thickness, density, and elemental composition and result in absorption and scattering of neutrons within the sample. A two-dimensional position-sensitive detector placed behind the sample can measure the transmitted neutron flux (Figure I.10.1b). When combined with a high-precision (~1/100 of a degree) rotational stage, it is possible to perform computed tomography (CT) scans and thus generate three-dimensional images of working fluids inside real devices. Samples can be analyzed at one position, or a complete reconstruction can provide a cross-section of the entire sample at resolutions ranging from 50 to 100 microns.

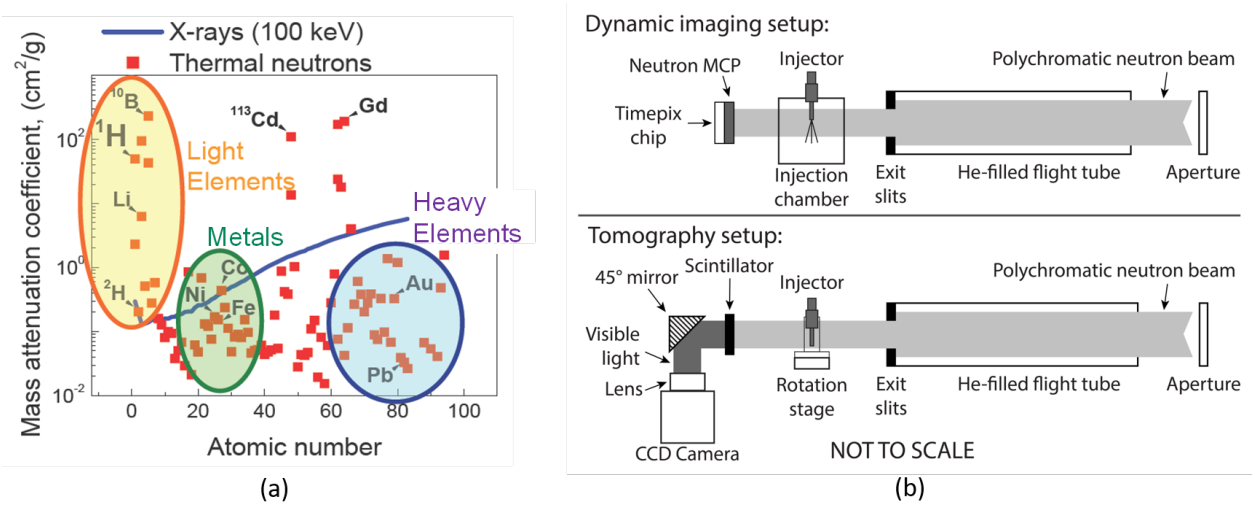

MCP – multichannel plate; CCD – charge coupled device

Figure I.10.1 (a) Mass attenuation coefficients versus atomic number for neutrons and x-rays [1] and (b) schematic of neutron-imaging apparatus for dynamic imaging and CT scans on fuel injectors

Objectives

Overall Objectives

- Implement high-fidelity neutron imaging capabilities using the High Flux Isotope Reactor (HFIR) and Spallation Neutron Source for advanced transportation research. Once fully developed, these capabilities will enable the imaging of a range of processes that occur in advanced vehicle systems.
- Employ neutron diagnostics to aid improved design and control of complex advanced combustion systems and help to guide model validation and input.
- Report findings to the research community and work with industrial partners to ensure research is focused on the most critical topics.

Fiscal Year (FY) 2019 Objectives

- Commission new experimental apparatus to enable dynamic imaging of all internal components of the Engine Combustion Network (ECN) Spray-G-style injector at the HFIR CG-1D imaging beamline.
- Develop an approach for the measurement and quantification of high-speed, sub-pixel displacement of internal components of a gasoline direct injector (GDI) using ensemble neutron imaging of cyclic dynamic operation.
- Design a new spray chamber to enable neutron imaging of spray impingement on a wall at various orientations.

Approach

The project's current focus is to support improved fuel injector and spray models for predictive simulation and to further develop and mature neutron imaging for in situ spray and injector characterization using the Spallation Neutron Source and HFIR at Oak Ridge National Laboratory. Efforts in FY 2019 were aimed at investigating intra-nozzle fuel injector flow and needle dynamics during injector spray events with GDIs. This task also shares resources with a complementary medium/heavy-duty imaging task focused on diesel injectors. These efforts are designed to improve understanding of how external conditions influence internal dynamics, especially as they relate to advanced combustion regimes and injector durability. Dynamic neutron imaging allows internal flow dynamics and needle motion in injectors to be directly visualized, and progress is ongoing in making quantitative measurements to aid in model development and inform future injector design. The physics of the injection process is a key part of the overall combustion system in engines, and the physics is still not adequately understood, particularly as it relates to the influence of internal flow on early spray development and the subsequent impact on combustion and emissions. This is a topic of interest for the ECN, an international collaboration among experimental and computational researchers pursuing better understanding of engine combustion and sprays. Progress has been made in demonstrating the value of dynamic imaging, with current and future efforts focused on improving detector resolution and efficiency and improving spray chamber and experiment design to make relevant and quantifiable measurements of internal flow and needle dynamics that add value to modeling efforts with ECN-specified operating conditions and hardware.

There has been collaboration with researchers from several institutions during this project, including Argonne National Laboratory; General Motors; Bosch; Continental Automotive; the University of Tennessee; the University of California, Berkeley; Boston University; and a Massachusetts Institute of Technology consortium on particulate filters.

Results

Imaging of Spray G Internal Dynamics

A new experimental apparatus to enable dynamic imaging of all internal components of the ECN Spray-G-style GDI was built and commissioned (Figure I.10.2a). The apparatus was installed at the HFIR CG-1D imaging beamline in mid-November 2018 in preparation for a six-day imaging campaign (Figure I.10.2b). Owing to an unscheduled reactor outage at HFIR, the imaging campaign could not be completed as originally scheduled in November 2018, and the experiment remained installed at CG-1D awaiting the reactor restart. The reactor was successfully restarted in October 2019, and the imaging experiments were underway at the time of this writing. Preliminary results will be presented in the FY 2020 first quarter (Q1) quarterly report.

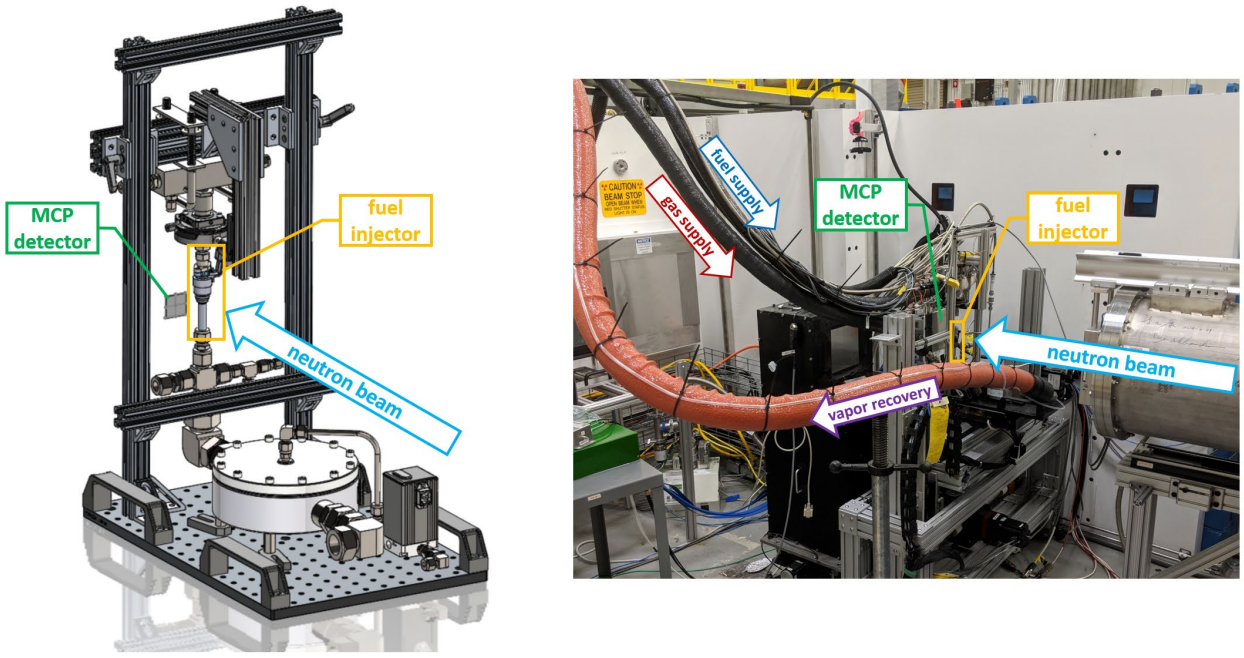

(a) (b)

Figure I.10.2 (a) A model of the new fuel injector apparatus shows that the entire injector can now be exposed to the neutron beam, allowing dynamic imaging to be performed on all internal components. (b) A new GDI dynamic imaging apparatus has been installed at the CG-1D imaging beamline at the HFIR.

A draft manuscript has been prepared on the development of the injector attenuation model to quantify deflection and displacement of the needle during and after injection events. This manuscript features results of both tomographic and dynamic injector imaging (Figure I.10.3) obtained in previous experiments and discusses the development of the filtering and attenuation modeling framework to resolve quantitative displacement data from dynamic imaging (Figure I.10.4).

The manuscript presents an approach to the measurement of high-speed, sub-pixel displacement of the needle in a GDI using ensemble neutron imaging of cyclic dynamic operation. This approach combines a normalization technique that relies on a static reference frame made from the image sequence itself with an analytical neutron attenuation model based on the device's geometry.

The geometry was derived from a neutron CT scan (Figure I.10.3a), and the accuracy obtained by this method was deemed sufficient owing to the large difference in scales between the size of the injector needle and the magnitude of displacement, which was <5% of the needle diameter. For systems in which sub-pixel displacement information is desired for objects that are on the same scale as the displacement, more accurate *a priori* knowledge of the geometry would be required.

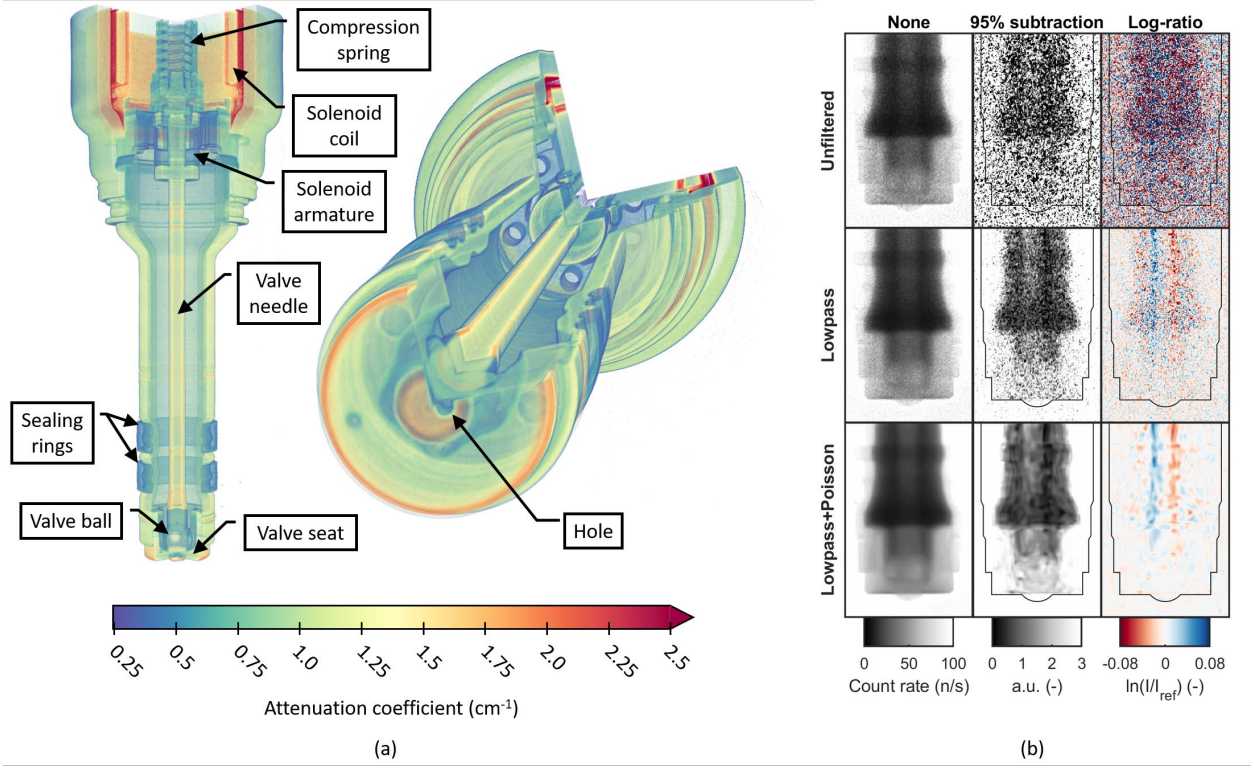

Figure I.10.3 (a) Sectioned volumetric rendering of a neutron CT of the single-hole Spray-G-style GDI shows the internal components of the injector. (b) Various filtering and normalization methods applied to a frame from dynamic imaging with a relatively large needle deflection show the ability to resolve the movement of the injector needle. Rows correspond to the filtering method, while columns correspond to the normalization method. The injector body outline has been overlaid on the normalized images for clarity.

The application of an analytical attenuation model was practical, thanks to the simple geometry of the portion of the injector needle being tracked, which was represented as a cylinder. More complex geometries would likely require a more general numerical model and greater computing resources because of the added computations at each iteration of the displacement fitting process.

The project team performed parametric sweeps of the inputs to the displacement fitting model, including attenuation coefficients, image pixel size, needle radius, reference position, reference position blur, and dynamic position blur. The parameters were estimated using prior knowledge, and except for the attenuation coefficients, all parameters were optimized based on goodness-of-fit metrics.

Two oscillations of the injector needle were observed during injection, with estimated amplitude of 25 µm and 18 µm, respectively (Figure I.10.4). A larger displacement on the order of 55 µm was observed after the needle closing, which was likely induced by needle seating forces. While good agreement was seen in the displacement fits between all data filtering levels, the absolute magnitude and the uncertainty will both largely depend on the values chosen for attenuation coefficients. While these values were not rigorously pursued here, the techniques to do so have been shown in the literature [2] and can be applied in future experiments.

The prospects for this approach to measurement of micron-scale dynamics are encouraging. The field of view and resolution of the current generation of neutron multichannel plate detectors with Timepix readout are sufficient to capture the dynamics of interest in nearly the entirety of a typical automotive GDI, which will be pursued in upcoming work. Oak Ridge National Laboratory is currently developing a new multichannel plate detector with high-bandwidth data-driven Timepix3 readout; this device is expected to enable event centroiding to improve intrinsic spatial resolution by a factor of two or more [3]. Looking farther out, the

subsequent generation of detectors promises to enable an even wider class of measurements, with the four-side buttable Timepix4 architecture enabling the fabrication of arbitrarily large detectors with much higher data throughput capabilities [4].

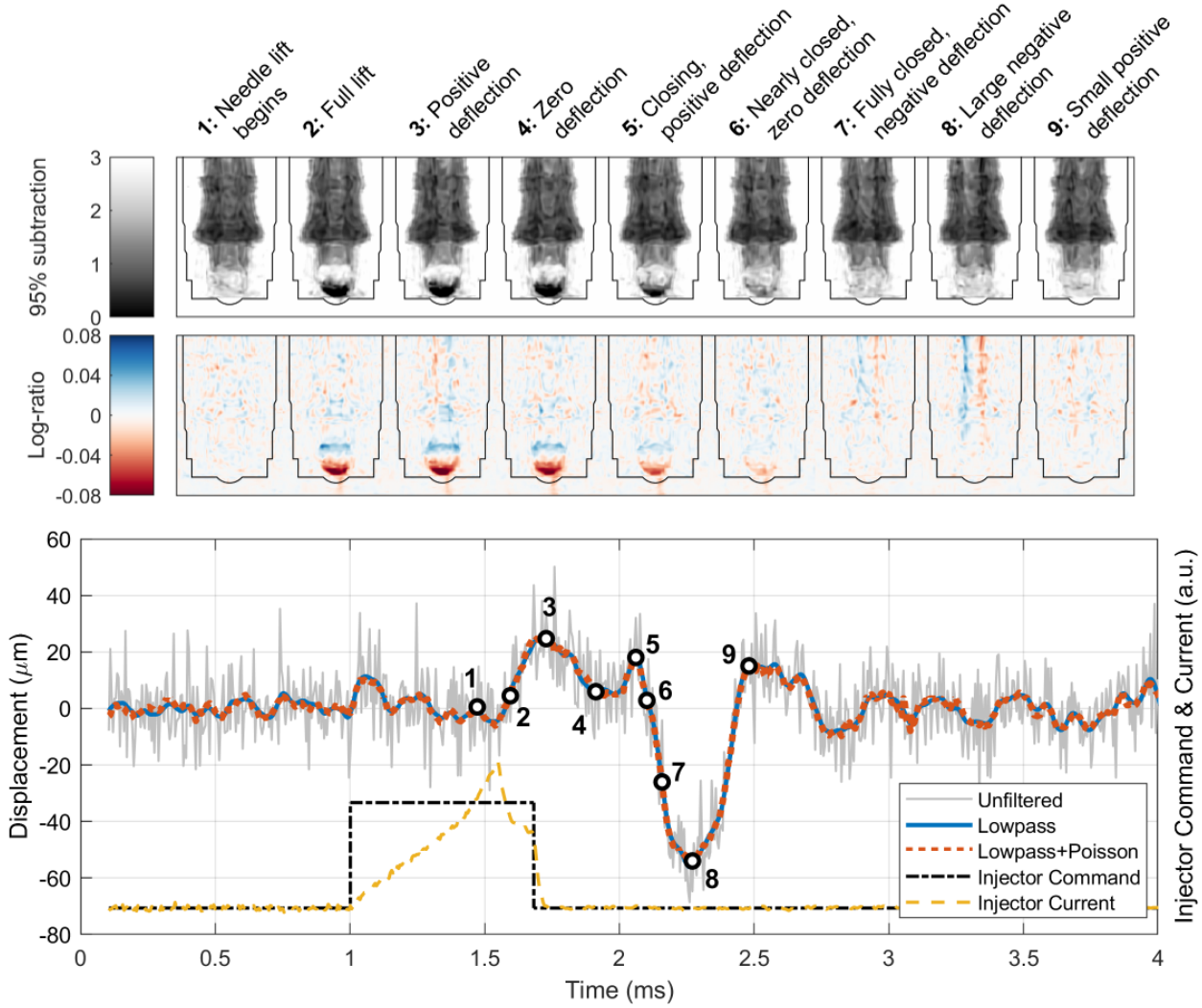

Figure I.10.4 Top: Selected frames from the 95% subtraction and log-ratio normalizations with Lowpass+Poisson filtering highlight visible motion of the injector needle. Bottom: Time-series displacement fits exhibit oscillatory motion of the injector needle both during and after injection and indicate similar results for all three filtering levels.

The manuscript is currently undergoing internal review and will be submitted shortly.

Imaging of Fuel Films

With the formation of the new Combustion Consortium, many of the spray-related tasks have been refocused to problems relevant to cold-start operation, such as the formation and evaporation of fuel films on walls due to spray impingement. Quantifying the thickness of these films in spray chambers or in engines is a problem that appears to be particularly well suited to neutron imaging because of neutrons' ability to penetrate the metal walls while at the same time being sensitive to the hydrogenous fuel.

The project team has modeled the range of film thicknesses that may be measurable with neutron imaging under various approaches, as shown in Figure I.10.5. Attenuation was modeled using the Neutron Imaging Toolbox [5] for film thicknesses ranging from 1 µm to 100 µm, which is representative of the range that may be expected in GDI engines. The baseline scenario is that the neutron beam would be oriented normal to the wall, allowing direct measurement of the fuel film thickness profile from the attenuation measured by neutron imaging. Using isooctane as a gasoline surrogate and 1% attenuation as a cutoff point, the researchers estimated that films as thin as 30 µm may be measured in this baseline configuration. This lower limit can be improved by rotating the wall relative to the neutron beam to increase the path length through the film, as shown in Figure I.10.5. By taking images at multiple angles and using a geometric transform and/or a "sparse" tomographic reconstruction, it should be possible to recover the normal film thickness profile. At angles of 45° and 10° relative to the beam, this may allow measurement of films down to 20 µm and 5 µm, respectively.

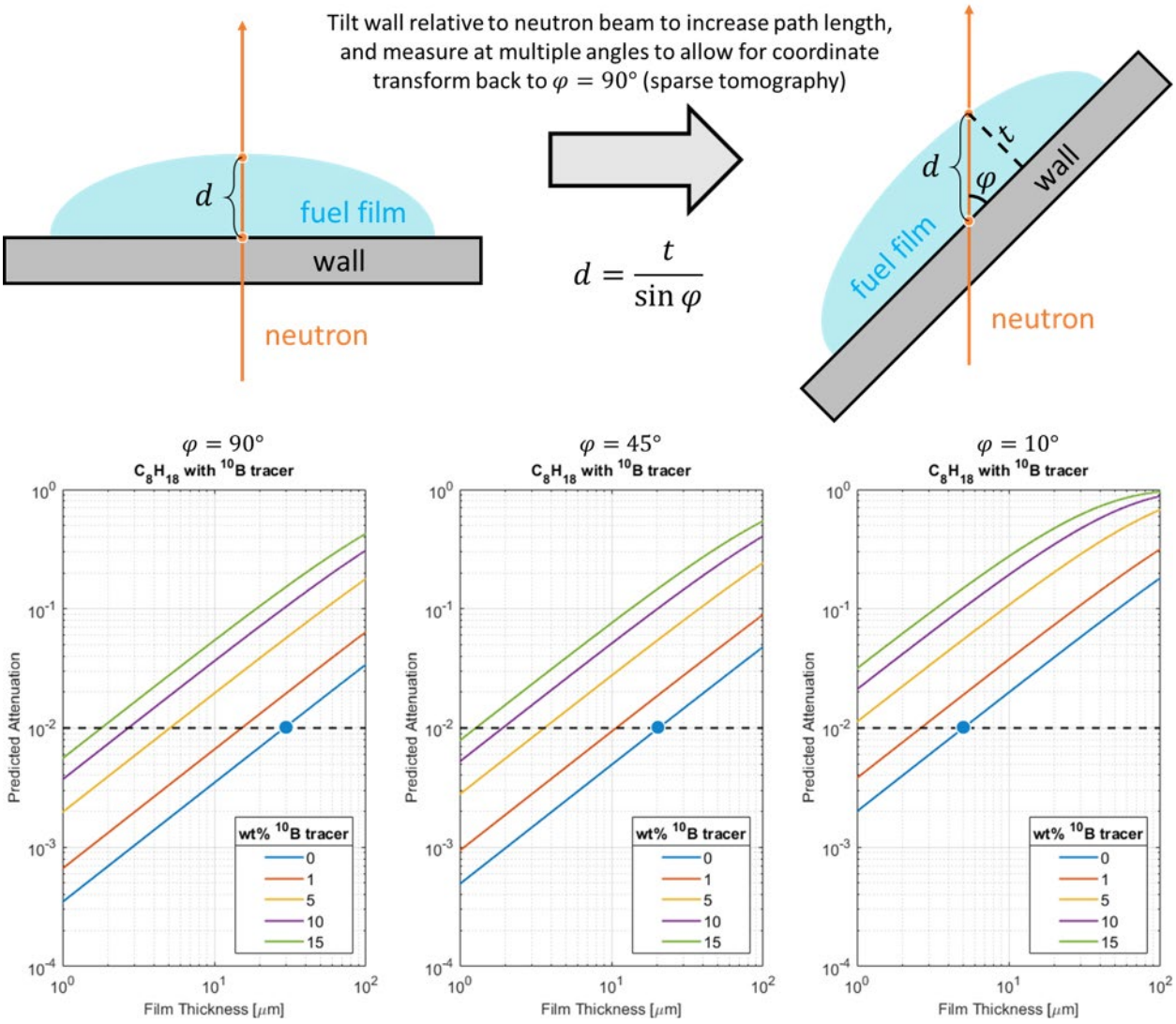

Figure I.10.5 Top: Illustration of tilting wall and film to increase neutron path length through a given section. Multiple projections can be made so that the film profile can be reconstructed from a sparse tomography approach. Bottom: Predicted neutron attenuation as a function of film thickness for various wall orientations and ^{10}B tracer concentrations. Using acute angles of the plate relative to the beam may enable film thickness <10 µm to be measured with neat isooctane. If ^{10}B tracer is used at concentration >5 wt%, it should be possible to measure films <5 µm at any orientation.

Another approach to improving the lower limit of the measurable film thickness would be to add a tracer to the fuel with even higher neutron attenuation, such as isotopically enriched Boron 10 (^{10}B). Simulations with various concentrations of ^{10}B in isooctane are shown in Figure I.10.5; results indicate that 5 µm films could be measured even in the baseline orientation with ^{10}B concentrations >5 wt%. While this approach would greatly simplify the experiments and data reconstruction, it is not initially preferred because of the high cost of ^{10}B. The project team may test very small quantities of ^{10}B compounds to establish their suitability as tracers in terms of solubility and volatility relative to gasoline and isooctane.

Preliminary designs have been completed for a new spray chamber to enable imaging of spray impingement on a wall at various orientations, fulfilling an FY 2019 Q4 milestone. The chamber is inherently modular in design and is based on commercially available vacuum chamber components, which will enable a variety of experimental configurations at relatively low cost. The chamber design, shown in Figure I.10.6, allows the injector to be positioned normal to the wall at varying distances, and the entire assembly will be rotated about the central axis of the wall to enable imaging of the film at different angles. This chamber will be able to operate at the ECN Spray G2 and G3 conditions.

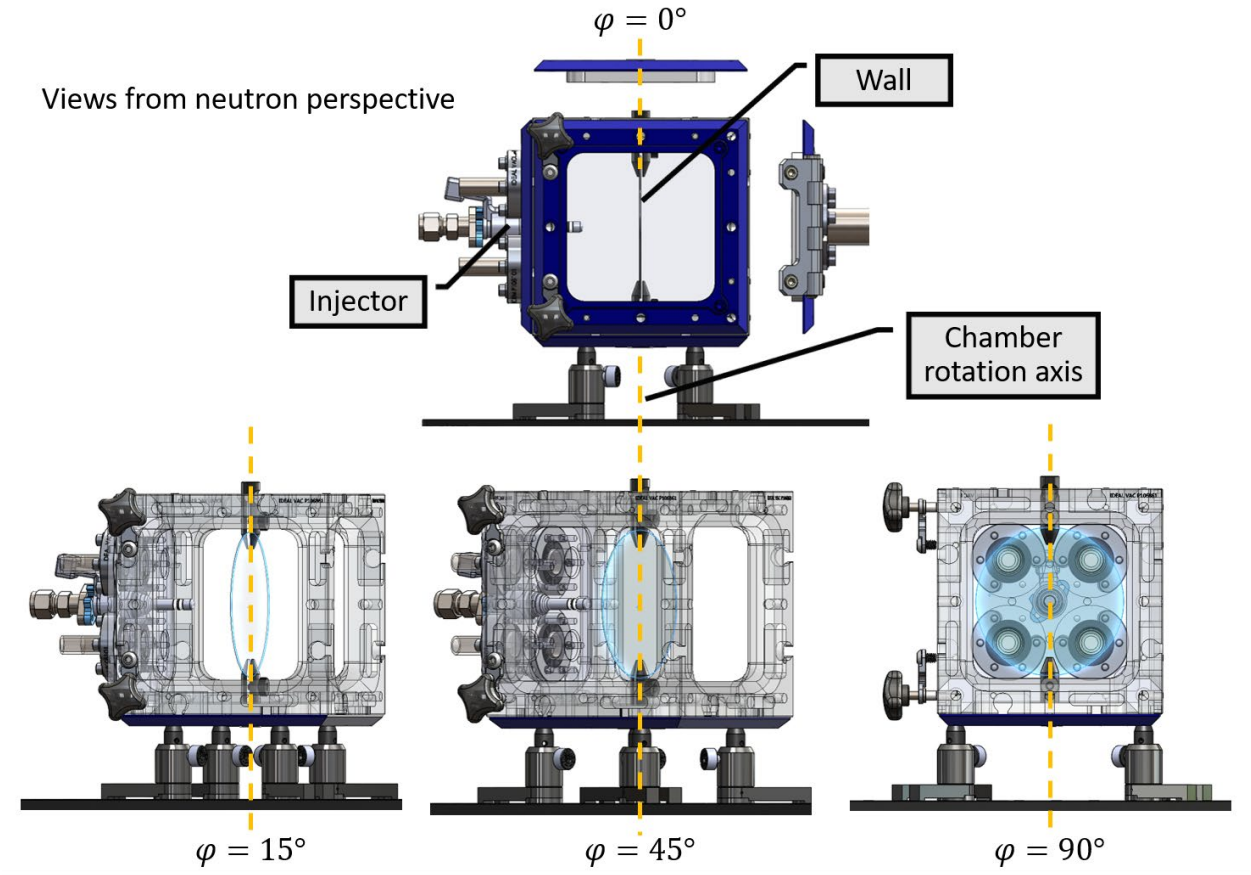

Figure I.10.6 Preliminary design of a wall impingement chamber for neutron imaging. The chamber is constructed entirely of aluminum and fused silica, which are both highly transparent to neutrons and will allow for a good view of the fuel film over a wide angular range.

Conclusions

Neutron imaging is a non-destructive, non-invasive diagnostic approach to improving understanding of advanced vehicle and combustion systems, targeting fuel economy improvements and durability. Efforts to date have focused on fuel injectors and particulate filters:

- Neutron imaging of fuel injection in a dynamic capacity has been demonstrated at the HFIR CG-1D imaging beamline and has shown the ability to both visualize and quantify the internal injector dynamics, including fluid motion and needle deflection/displacement. Dynamic imaging has been performed with several injectors using isooctane at multiple chamber conditions with both single and multiple injections. All injectors exhibited oscillation of the ball and needle during injection, with significant effects seen in cases with multiple injections.

- An approach has been developed to allow for quantitative measurement of "sub-pixel" displacement of the needle in a GDI using ensemble neutron imaging of cyclic dynamic operation. This approach combines a normalization technique that relies on a static reference frame made from the image sequence itself with an analytical neutron attenuation model based on the device's geometry.

- While previous results have focused on the spray and near-nozzle region of the injector, a new experimental apparatus has been developed to enable dynamic imaging of all internal components of the ECN Spray-G-style GDI, and results from this new setup are expected in early in FY 2020.

- Based on modeling of neutron attenuation for various film thicknesses, preliminary designs have been completed for a new spray chamber to enable imaging of spray impingement on a wall at various orientations.

Future directions could include the following:

- A beamtime award of six days on the HFIR CG-1D imaging beamline has been scheduled for October–November 2019. Efforts for this campaign will be focused on needle and fluid motions higher throughout the entire GDI-based injector, including interactions between the needle and the upper stops and solenoid armature. The project team has designed and built a new spray chamber to enable these measurements, as well as operation at more extreme conditions and with higher throughput.

- The project team will construct the newly designed spray chamber to enable neutron imaging of fuel films on walls.

- The project will conduct preliminary experiments to quantify thickness of fuel films on walls.

- A new multichannel plate detector is being commissioned to enable measurements with higher signal-to-noise ratio and improved resolution and data throughput. This detector would be applicable to all currently planned time-resolved experiments involving injectors and sprays.

Key Publications

1. Wissink, Martin, Todd Toops, Charles Finney, Eric Nafziger, Derek Splitter, Hassina Bilheux, Scott Curran, Ke An, and Matt Frost. 2019. "An Update on Neutron Diagnostics of Transportation Technologies." Presentation at AEC Program Review Meeting, The United States Council for Automotive Research (USCAR) (August 14).

2. Wissink, Martin, Todd Toops, Charles Finney, Eric Nafziger, Derek Splitter, Hassina Bilheux, Scott Curran, Ke An, and Matt Frost. 2019. "An Update on Neutron Diagnostics of Transportation Technologies." Presentation at AEC Program Review Meeting, Oak Ridge National Laboratory (January 31).

References

1. Kardjilov, Nikolay, Fabrizio Fiori, Giuseppe Giunta, André Hilger, Franco Rustichelli, Markus Strobl, John Banhart, and Roberto Triolo. 2006. "Neutron Tomography for Archaeological Investigations." *Journal of Neutron Research* 14, no. 1: 29–36.

2. Carminati, Chiara, Pierre Boillat, Florian Schmid, Peter Vontobel, Jan Hovind, Manuel Morgano, Marc Raventos, et al. 2019. "Implementation and Assessment of the Black Body Bias Correction in Quantitative Neutron Imaging." *PloS one* 14, no. 1: e0210300.

3. Tremsin, A.S., J.B. McPhate, J.V. Vallerga, O.H.W. Siegmund, J.S. Hull, W.B. Feller, and E. Lehmann. 2009. "Detection Efficiency, Spatial and Timing Resolution of Thermal and Cold Neutron Counting MCP [Multichannel Plate] Detectors." *Nuclear Instruments and Methods in Physics Research Section A: Accelerators, Spectrometers, Detectors and Associated Equipment* 604, no. 1-2: 140–143.

4. Ballabriga, Rafael, Michael Campbell, and Xavier Llopart. 2018. "Asic Developments for Radiation Imaging Applications: The Medipix and Timepix Family." *Nuclear Instruments and Methods in Physics Research Section A: Accelerators, Spectrometers, Detectors and Associated Equipment* 878: 10–23.

5. Zhang, Y., and J. Bilheux. "Neutron Imaging Toolbox." https://isc.sns.gov/ (accessed October 2018).

Acknowledgements

Todd Toops, Charles Finney, Eric Nafziger, Derek Splitter, Jonathan Willocks, Hassina Bilheux, and Lou Santodonato at Oak Ridge National Laboratory have all contributed to the design and execution of neutron imaging experiments shown in this work.

This research used resources at the High Flux Isotope Reactor, which is a U.S. Department of Energy Office of Science User Facility.

I.11 Chemical Kinetic Models for Advanced Engine Combustion (Lawrence Livermore National Laboratory)

William J. Pitz, Principal Investigator
Lawrence Livermore National Laboratory
P. O. Box 808, L-372
Livermore, CA 94550
E-mail: pitz1@llnl.gov

Michael Weismiller, DOE Technology Development Manager
U.S. Department of Energy
E-mail: Michael.Weismiller@ee.doe.gov

Start Date: October 1, 2018 End Date: September 30, 2023
Project Funding (FY19): $625,000 DOE share: $625,000 Non-DOE share: $0

Project Introduction

Predictive engine simulation models are needed to make rapid progress toward the U.S. Department of Energy's (DOE's) goals of increasing combustion engine efficiency and reducing pollutant emissions. To assess the effect of fuel composition on engine performance and emissions, these engine simulations need to couple to fluid dynamic and fuel chemistry sub-models. Reliable chemical kinetic sub-models representative of conventional and next-generation transportation fuels need to be developed and improved to fulfill these requirements.

Objectives

Overall Objectives

- Develop predictive chemical kinetic models for gasoline, diesel, and next-generation fuels so that simulations can be used to overcome technical barriers to advanced combustion regimes in engines and needed gains in engine efficiency and reductions in pollutant emissions
- Develop detailed chemical kinetic models for fuel components used in surrogate fuels for spark ignition engines, diesel engines, and kinetically controlled compression ignition engines
- Combine component models into surrogate fuel models to represent real transportation fuels. Use them to model advanced combustion strategies in engines that lead to low emissions and high efficiency.

Fiscal Year (FY) 2019 Objectives

Develop fuel surrogate kinetic models with more representative components for real fuels to increase accuracy of autoignition predictions and to cover a range of real fuels. Validate kinetic mechanisms over a range of temperature, pressure, and equivalence ratio relevant to engine combustion.

Approach

Gasoline and diesel fuels consist of complex mixtures of hundreds of different components. These components can be grouped into chemical classes including n-alkanes, iso-alkanes, cyclo-alkanes, alkenes, oxygenates, and aromatics. Since it is not feasible to develop chemical kinetic models for hundreds of components, specific components need to be identified to represent each of these chemical classes. Then, detailed chemical kinetic models can be developed for these selected components. These component models are subsequently merged together to produce a surrogate fuel model for gasoline, diesel, and next-generation transportation fuels. This approach creates realistic gasoline or diesel fuel surrogates that can reproduce experimental behavior of the

practical real fuels that they represent. Detailed kinetic models for surrogate fuels can then be simplified as needed for inclusion in multidimensional computational fluid dynamics simulations of engine combustion.

Results

Key Accomplishments for FY 2019

- Developed more accurate kinetic models for cyclo-alkanes (cyclopentane and cyclohexane)
- Developed kinetic models for more representative olefins (C5 and C6 iso-olefins to characterize this chemical class in gasoline)
- Improved accuracy of the kinetic model for large n-alkanes and tetralin that represent important chemical classes in diesel fuel
- Improved accuracy of the diesel surrogate model to characterize diesel fuel.

Cycloalkanes represent an important chemical class in gasoline fuel because of their effect on ignition behavior under advanced compression ignition conditions and on autoignition in the end gas of a spark ignition engine that lead to engine knock. In FY 2019, the Lawrence Livermore National Laboratory (LLNL) kinetic team developed more accurate models for two cycloalkanes: cyclopentane and cyclohexane. Cyclopentane is an important gasoline surrogate compound because of its high octane sensitivity (research octane number–motor octane number = 18) and its presence in gasoline fuels. It represents the smallest practical surrogate compound to represent cycloalkanes in gasoline fuels. The detailed chemical model for cyclopentane was developed based on the small hydrocarbon (C0 ~ C4) kinetic model from National University of Ireland, Galway [1] and previous kinetic modeling of cyclopentane by Al Rashidi et al. [2]. The cyclopentane, cyclopentene, and cyclopentadiene chemistries in the model were all reviewed and updated with the latest recommendations for reaction paths and associated rate constants. The cyclopentane model was validated against new experimental data from the National University of Ireland, Galway on ignition delays from a shock tube and rapid compression machine (RCM). In these experiments, cyclopentane was mixed with a more reactive compound, dimethyl ether, allowing the study of the blending behavior of an unreactive cyclopentane with a more reactive component. This type of interaction also happens in a gasoline mixture where the chemistry of unreactive components interacts with that of reactive components. The new RCM experimental data was used to improve the kinetic model for cyclopentane. The comparison of the ignition delay times simulated by the kinetic model and measured in the experiments is shown in Figure I.11.1. The simulations agree very well with the experiments. The updated cyclopentane kinetic sub-model has been added to the LLNL gasoline surrogate model, and this has allowed more accurate simulation of gasoline target fuels.

Cyclohexane is another surrogate compound commonly used to represent the cycloalkane chemical class in gasoline. The cyclohexane chemical kinetic model was updated in FY 2019. The kinetic model was based on the previous LLNL 2007 model of Silke et. al [3] but included updated sub-models for the core C0–C4 chemistry [1] and for aromatics [4]. Reaction rates, thermochemistry, and transport properties were improved for cyclohexane and its intermediates, including cyclohexene and cyclohexadiene. Rate constants were taken from the literature or estimated by analogy to similar reactions. The chemical kinetic model was compared to new ignition delay data from the RCM at the University of Connecticut (UCONN). The kinetic model was also compared to speciation data from jet-stirred reactor data available in the literature. The comparison with new RCM experimental data from UCONN is shown in Figure I.11.2. The simulations compare very well with experimental data at high pressure in the RCM for several equivalence ratios (Figure I.11.2[a]). The kinetic model also more accurately simulates the new experimental data than the previous LLNL kinetic model [3], whose ignition delays were too long by about a factor of two (Figure I.11.2[b]).

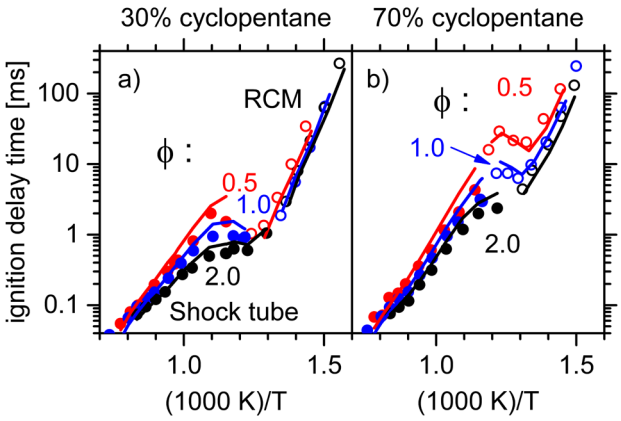

Figure I.11.1 Comparison of the simulated (lines) and measured (symbols) ignition delay times of cyclopentane and dimethyl ether blends. The experiments are from the National University of Ireland Galway shock tube and RCM.

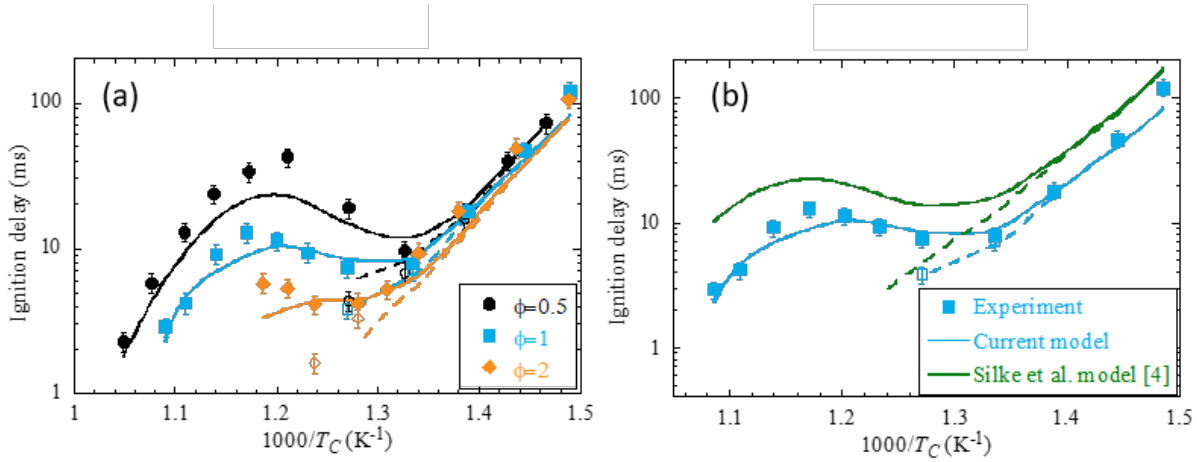

Figure I.11.2 Comparison of simulated (lines) and measured (symbols) ignition delay times in the UCONN RCM. Filled symbols and solid lines correspond to total ignition delay times, and open symbols and dashed lines correspond to first stage ignition delay times. (a) Effect of equivalence ratio on total and first ignition delay times at high pressure for cyclohexane. (b) Comparison of simulations from current model and Silke et al.'s model [3] with the experimental data.

Olefins represent an important chemical class in gasoline so that surrogate compounds are needed to represent them. In the past, the LLNL gasoline surrogate model included straight-chain olefins and not iso-olefins to characterize this chemical class. However, in many gasoline formulations, iso-olefins are also present. Iso-olefins are known to exhibit higher research octane number and higher octane sensitivity than straight-chain olefins. These properties will affect gasoline ignition behavior when iso-olefins are present. In FY 2019, the LLNL kinetic team developed mechanisms for C5 and C6 iso-olefins. The C5 iso-olefins were 2-methyl-1-butene, 2-methyl-2-butene, and 3-methyl-1-butene, and the C6 iso-olefin was 2-methyl-2-pentene. The kinetic model developed incorporates several important reaction pathways that have been proposed in the literature. The rate constant and thermodynamic properties needed for the kinetic model were adopted from recent high-level theoretical chemistry calculations, when available. When such calculations were not available, analogies from isobutene chemistry were used. The kinetic model developed for simulating ignition of these iso-olefins has been validated against ignition delays, flame speeds, pyrolysis data, and jet-stirred reactor data. The model has been found to successfully capture the effect of location of double bond, methyl substitution, and chain length on ignition characteristics of iso-olefins. In Figure I.11.3, ignition delay time

simulations using the iso-olefin kinetic model are compared to measurements in the Argonne National Laboratory RCM with reasonable agreement.

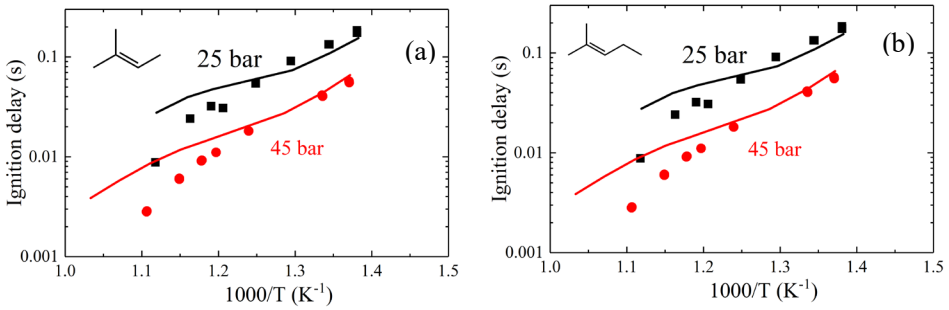

Figure I.11.3 The comparison of simulated (lines) and measured (symbols) ignition delay times of (a) 2-methyl 2-butene and (b) 2-methyl 2-pentene in the Argonne National Laboratory RCM.

Chemical kinetic models for surrogate components and mixtures to represent diesel fuels were also improved in FY 2019. Firstly, surrogate components to represent the n-alkane and naphthenic-aromatic chemical classes were updated. For n-alkanes from C8 to C20, the kinetic model was improved by selecting better reaction rate rules for the low-temperature reaction classes. Figure I.11.4 shows an example of the accuracy of the kinetic model for n-decane. Kinetic model simulations are compared to shock tube ignition delay times from the literature over a wide range of pressure and temperature [5],[6],[7]. The kinetic model simulates the experimental ignition delay times remarkably well. When the improved n-alkane kinetic model is inserted into the diesel surrogate model, the accuracy of the diesel surrogate model is improved as well.

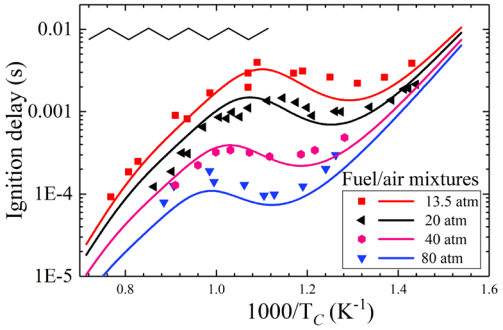

Figure I.11.4 Comparison of simulated (lines) and measured (symbols) ignition delay times for n-decane in shock tubes over an extended temperature and pressure range. The experimental data are from [4],[5],[6],[7].

Secondly, the kinetic model for the diesel-surrogate compound tetralin was significantly improved. This compound represents the naphthenic-aromatic chemical class in diesel, which are compounds that have aromatic and naphthenic rings. Tetralin, a 2-ring naphthenic-aromatic, is the simplest example of this chemical type. Tetralin is also a component on a nine-component diesel surrogate palette designed to provide diesel surrogates that can match target diesel fuel properties [8]. The development of a kinetic model for tetralin was very challenging because of the presence of the aromatic and naphthenic rings. The kinetic model was built using available information on the reaction paths and rate constants of naphthenes and aromatics. The kinetic model was validated by comparing simulated and experimental ignition delay times in an RCM at King Abdullah University of Science and Technology. Since tetralin is very unreactive, it was added to a high-reactivity alkane (3-methyl pentane) to allow the investigation of its behavior at low temperatures important to

diesel ignition processes. This is the first time that the tetralin kinetic model has been validated with experimental data in the low-temperature region. The comparison between the simulated and measured ignition delay times is shown in Figure I.11.5. The kinetic model well simulates experimental data in the low-temperature region from ~700 K to 850 K. When used in a diesel surrogate kinetic model, this improved component kinetic model will allow more accurate simulations of the ignition behavior of target diesel fuels.

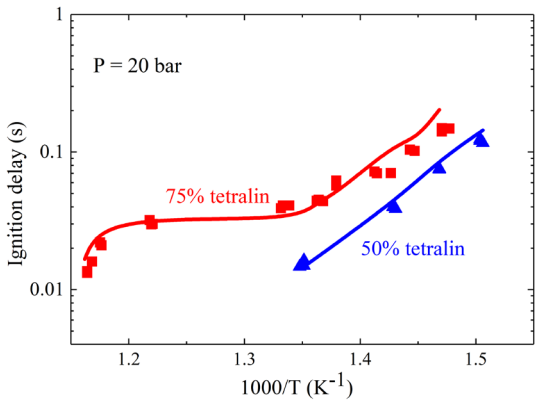

Figure I.11.5 Comparison of simulated (lines) and measured (symbols) ignition delay times of tetralin and 3-methyl pentane blends in an RCM. The experimental measurements are from King Abdullah University of Science and Technology.

The LLNL diesel surrogate kinetic model has sub-models for nine components on the diesel surrogate palette developed by the Advanced Vehicle/Fuel/Lubricants-18 working group under the auspices of the Coordinating Research Council [8]. This surrogate palette was developed to mimic properties of a diesel certification fuel, including distillation curve, density, cetane number, and carbon types. The improved sub-models for n-alkanes and tetralin were inserted into the LLNL diesel surrogate model. Simulations with the improved diesel surrogate model compared well with ignition delay time experiments from the UCONN RCM, as shown in Figure I.11.6. This is a direct comparison of measured and simulated ignition delay times of the diesel surrogate mixture compositions from Mueller et al. [9]. This more accurate and representative diesel surrogate kinetic model is a significant step toward enabling more accurate simulations in multidimensional engine codes.

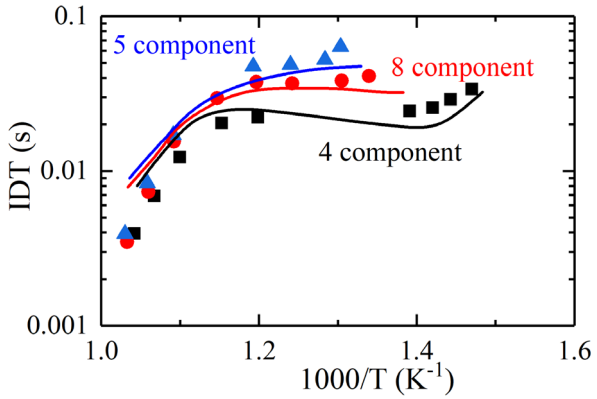

Figure I.11.6 Comparison of a four-, five-, and eight-component diesel surrogate model predictions with experimental measurements of ignition delay time of the same Coordinating Research Council diesel surrogate mixtures [9] in an RCM at UCONN.

Conclusions

- Improved kinetic models to represent cyclo-alkanes in gasoline (cyclopentane and cyclohexane) were developed.
- New kinetic models for iso-olefins were developed that are more representative of olefins found in gasoline than straight-chain olefins.
- Kinetic models to represent the n-alkane and naphthenic-aromatic chemical classes in diesel fuel were improved. These component models include all the C8 to C20 n-alkanes and tetralin to represent the above chemical classes.
- The improved diesel surrogate component models were inserted into the LLNL diesel surrogate kinetic model. The diesel surrogate model well captured the ignition behavior in the UCONN RCM of Coordinating Research Council four-, five-, and eight-component surrogate mixtures used to represent a diesel certification fuel.

Key Publications

1. Malliotakis, Z., C. Banyon, K. Zhang, S. Wagnon, J.J. Rodriguez Henriquez, G. Vourliotakis, C. Keramiotis, M. Founti, F. Mauss, W.J. Pitz and H. Curran. 2019. “Testing the Validity of a Mechanism Describing the Oxidation of Binary n-Heptane/Toluene Mixtures at Engine Operating Conditions.” *Combustion and Flame* 199: 241–248.
2. Fridlyand, A., S.S. Goldsborough, M. Al Rashidi, S.M. Sarathy, M. Mehl and W.J. Pitz. 2019. “Low Temperature Autoignition of 5-Membered Ring Naphthenes: Effects of Substitution.” *Combustion and Flame* 200: 387–404.
3. Zhang, K., C. Banyon, U. Burke, G. Kukkadapu, S.W. Wagnon, M. Mehl, H.J. Curran, C.K. Westbrook, and W.J. Pitz. 2019. “An Experimental and Kinetic Modeling Study of the Oxidation of Hexane Isomers: Developing Consistent Reaction Rate Rules for Alkanes.” *Combustion and Flame* 206: 123–137.
4. Kukkadapu, G., D. Kang, S.W. Wagnon, K. Zhang, M. Mehl, M. Monge-Palacios, H. Wang, S.S. Goldsborough, C.K. Westbrook, and W.J. Pitz. 2019. “Kinetic Modeling Study of Surrogate Components for Gasoline, Jet and diesel Fuels: C7-C11 Methylated Aromatics.” *Proc. Combust. Inst.* 37 (1): 521–529.
5. Davidson, D.F., J.K. Shao, R. Choudhary, M. Mehl, N. Obrecht, and R.K. Hanson. 2019. “Ignition Delay Time Measurements and Modeling for Gasoline at Very High Pressures.” *Proc. Combust. Inst.* 37 (4): 4885–4892.
6. Guzman, J., G. Kukkadapu, K. Brezinsky, and C. Westbrook. 2019. “Experimental and Modeling Study of the Pyrolysis and Oxidation of an Iso-Paraffinic Alcohol-to-Jet Fuel.” *Combustion and Flame* 201: 57–64.

References

1. Li, Y., C.-W. Zhou, K.P. Somers, K. Zhang and H.J. Curran. 2017. “The Oxidation of 2-Butene: A High Pressure Ignition Delay, Kinetic Modeling Study and Reactivity Comparison with Isobutene and 1-Butene.” *Proc. Combust. Inst.* 36 (1): 403–411.
2. Al Rashidi, M.J., M. Mehl, W.J. Pitz, S. Mohamed, and S.M. Sarathy. 2017. “Cyclopentane Combustion Chemistry. Mechanism Development and Computational Kinetics.” *Combustion and Flame* 183: 358–371.

3. Silke, E.J., W.J. Pitz, C.K. Westbrook, and M. Ribaucour. 2007. "Detailed Chemical Kinetic Modeling of Cyclohexane Oxidation." *J. Phys. Chem.* A 111 (19): 3761–3775.

4. Kukkadapu, G., D. Kang, S.W. Wagnon, K. Zhang, M. Mehl, M. Monge-Palacios, H. Wang, S.S. Goldsborough, C.K. Westbrook, and W.J. Pitz. 2019. "Kinetic Modeling Study of Surrogate Components for Gasoline, Jet and Diesel Fuels: C7-C11 Methylated Aromatics." *Proc. Combust. Inst.* 37 (1): 521–529.

5. Pfahl, U., K. Fieweger, and G. Adomeit. 1996. "Self-Ignition of Diesel-Relevant Hydrocarbon-Air Mixtures under Engine Conditions." *Proc. Combust. Inst.* 26: 781–789.

6. Tekawade, A., T. Xie, and M.A. Oehlschlaeger. 2017. "Comparative Study of the Ignition of 1-Decene, trans-5-Decene, and n-Decane: Constant-Volume Spray and Shock-Tube Experiments." *Energy & Fuels* 31 (6): 6493–6500.

7. Zhukov, V.P., V.A. Sechenov, and A.Y. Starikovskii. 2008. "Autoignition of n-Decane at High Pressure." *Combustion and Flame* 153 (1): 130–136.

8. Mueller, C.J., W.J. Cannella, T.J. Bruno, B. Bunting, H.D. Dettman, J.A. Franz, M.L. Huber, M. Natarajan, W.J. Pitz, M.A. Ratcliff, and K. Wright. 2012. "Methodology for Formulating Diesel Surrogate Fuels with Accurate Compositional, Ignition-Quality, and Volatility Characteristics." *Energy & Fuels* 26 (6): 3284–3303.

9. Mueller, C.J., W.J. Cannella, J.T. Bays, T.J. Bruno, K. DeFabio, H.D. Dettman, R.M. Gieleciak, M.L. Huber, C.-B. Kweon, S.S. McConnell, W.J. Pitz, and M.A. Ratcliff. 2016. "Diesel Surrogate Fuels for Engine Testing and Chemical-Kinetic Modeling: Compositions and Properties." *Energy & Fuels* 30 (2): 1445–1461.

Acknowledgements

This work was performed under the auspices of DOE by LLNL under Contract DE-AC52-07NA27344.

I.12 Model Development and Analysis of Clean and Efficient Engine Combustion (Lawrence Livermore National Laboratory)

Russell Whitesides, Principal Investigator
Lawrence Livermore National Laboratory (LLNL)
L-792, 7000 East Avenue
Livermore, CA 94550
E-mail: whitesides1@llnl.gov

Michael Weismiller, DOE Technology Development Manager
U.S. Department of Energy
E-mail: Michael.Weismiller@ee.doe.gov

Start Date: October 1, 2018 End Date: September 30, 2019
Project Funding (FY19): $650,000 DOE share: $650,000 Non-DOE share: $0

Project Introduction

Internal combustion engine design is increasingly driven by computational models used to predict performance metrics, which previously would have been predicted by limited design intuition or expensive and time-consuming physical testing. Improved model capabilities shorten design cycles and enable the production of cleaner and more efficient engines. This project focuses on advancing the state of the art in internal combustion engine simulations. The overarching goal is to enable predictive models and reduced time to solution for simulations that have impacts on combustion engine design.

Objectives

Overall Objective

- Advance the state of the art in engine simulation through development of fast and accurate models
- Work with industry partners to prove capability and impact of combustion software.

Fiscal Year 2019 Objectives

- Investigate the impact of reduced mechanisms on engine simulation results
- Develop fast solvers for one-dimensional diffusion flames
- Release Zero-Order Reaction Kinetics (Zero-RK) software as open-source.

Approach

This project is an ongoing research effort under the Advanced Combustion Engines subprogram, with annual feedback and direction from program managers and memorandum of understanding partners. During the current performance period, this project has focused on three areas: (1) exploring the impact of mechanism reduction on engine simulations, (2) creating new fast solvers for one-dimensional non-premixed flames, and (3) open-source release of the Zero-RK software package.

Results

Impact of Mechanism Reduction on Engine Simulations

Despite continued reduction in computational costs through work in this project and elsewhere, fully detailed reaction models containing thousands of species remain too expensive to include in many engine computational fluid dynamics (CFD) simulations. The constraints on model size result from the high grid resolution necessary in some cases to resolve fine flow structures, or from the short turn-around times required by industrial design cycles. To help understand the impact of mechanism reduction, the project team performed a study in the context of the Engine Combustion Network Spray A condition. Two complementary approaches to mechanism reduction have been developed to research the impact of reduction method and size on CFD simulation results. The first method leverages the directed relation graph (DRG) technique [1],[2] and incorporates the Zero-RK fast chemistry solver [3] to accelerate the process by an order of magnitude. This iterative method produces reaction models of varying size and accuracy. Figure I.12.1 compares mechanism size with the reduction accuracy threshold for reduction of an n-dodecane reaction model. Initially, many species can be removed with small error introduced. Subsequently, the amount of error introduced by further reduction rises quickly, and a plateau is seen at about 200 species, at which point further reduction leads to unacceptably large deviations between the reduced and the fully detailed models. For the current analysis, the smallest acceptable mechanism (with 219 chemical species) was used in the Spray A simulations and is referred to as the DRG mechanism.

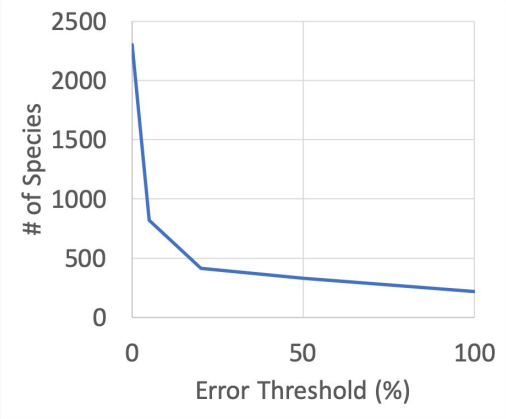

Figure I.12.1 Reduction process for the n-dodecane mechanism using the DRG method. Mechanism size in number of species is reduced according to an error threshold with respect to the fully detailed model.

The project also applied a separate hybrid approach [4] to the n-dodecane reaction model. Briefly, the hybrid model combines a detailed C0-C4 reaction model with a skeletal reaction model for the parent fuel, which is tuned to reproduce the results of the fully detailed mechanism. The hybrid methodology is able to predict the low- and high-temperature ignition with only 65 chemical species. Figure I.12.2 compares the ignition predictions for the full mechanism with the DRG and hybrid mechanisms as well as with the mechanism of Yao et al. [5] (a reduced mechanism that has been used in many reported studies of Spray A). Both of the new reductions capture the overall trend defined by the fully detailed mechanism, including the size and location of the so-called negative temperature coefficient regime. The hybrid mechanism does a slightly better job in matching the location of the extrema for the negative temperature coefficient regime for the first-stage ignition. The Yao mechanism is in worse agreement with the detailed mechanism than with both of the new reductions with respect to its predictions of longer delays at high and low temperatures and shorter ones in the negative temperature coefficient regime.

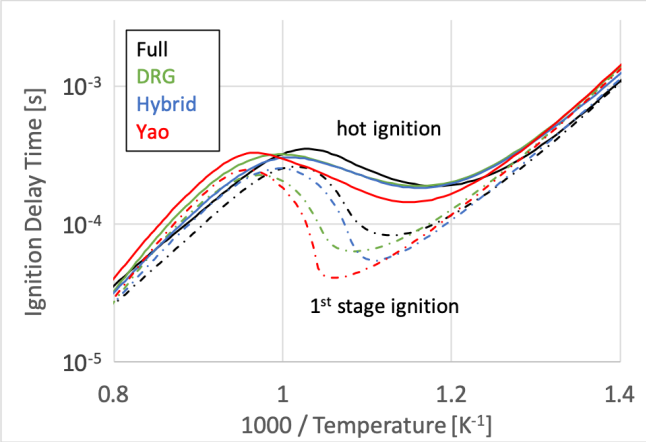

Figure I.12.2 Comparison of predicted ignition delay time as a function of inverse temperature for stoichiometric mixtures of n-dodecane and air at 6 MPa initial pressure for four reaction models

Both of the newly generated mechanisms were used in simulations of the Engine Combustion Network Spray A condition and compared with the fully detailed reaction model and the mechanism of Yao et al. The predicted ignition timings of the spray are shown in Figure I.12.3. All four tested mechanisms capture the overall trend from the experiments; however, the Yao mechanism does not predict ignition at the lowest ambient temperature (750 K). The exact chemical reasons for the differences in predictions are difficult to disentangle in these high-dimensional simulations. Figure I.12.4 shows the distribution of formaldehyde (a common indicator of low-temperature ignition) along a spray co-axial plane during ignition for each of the four mechanisms with ambient temperature set to 900 K. The Yao and hybrid mechanisms agree with the fully detailed mechanism with respect to the shape of the distribution; however, the Yao mechanism does not agree as closely in magnitude of the peak. The DRG mechanism predicts a different shape to the formaldehyde distribution. Based on these results, the project recommends the hybrid mechanism as a good compromise between model complexity/cost and accuracy for engine simulations. The overall comparison is possible because of the fast chemistry solvers for CFD that have been developed in this project [3], as they make the simulations incorporating the fully detailed mechanism feasible.

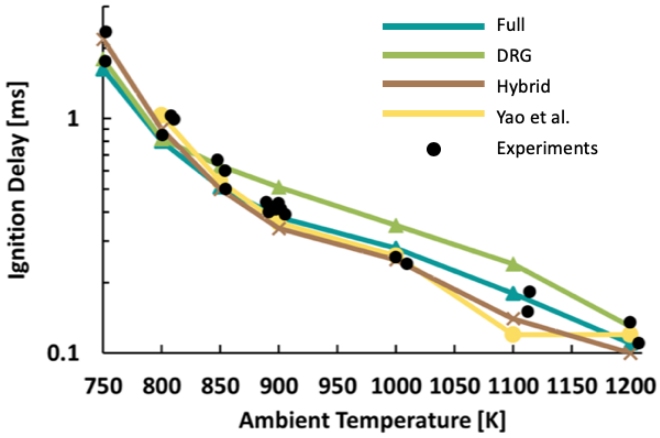

Figure I.12.3 Predicted and measured ignition time for spray combustion of n-dodecane at the Spray A condition as a function of temperature

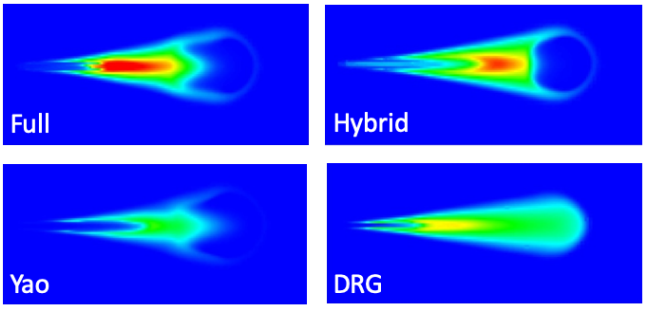

Figure I.12.4 Distribution of formaldehyde over spray co-axial plane during first-stage ignition of n-dodecane at Spray A condition (900 K), compared for four reaction models

Diffusion Flame Solvers for Flamelet Simulations

Simulations of one-dimensional combustion systems using detailed kinetics have many important applications in the study of boosted spark-ignited and multi-mode engine configurations. Premixed flame simulations can be used to generate flame speed correlations used in the study of knock, while non-pre-mixed flames capture important dynamics relevant to multi-mode engines in which the operating regime can transition between well-mixed and diffusion-dominated combustion.

The project has developed fast solvers for simulation of the flamelet equations for non-pre-mixed (or diffusion) flames that are orders of magnitude faster than previously available tools. The flamelet solver extends ideas developed previously in this project [6] to the new non-pre-mixed context and applies a novel numerical technique to reduce the computational cost of solution while maintaining accuracy. Briefly, the method uses an iterative approach, preconditioned by an approximate Jacobian matrix that is factorized into two components (related to chemistry and transport), which can each be further processed efficiently because of the sparsity of each. The resulting simulation cost (in wall time) scales linearly with the number of chemical species included. The linear scaling translates to multiple orders of magnitude reduction in simulation time for mechanisms with greater than 1,000 species when compared with competing solutions such as FlameMaster [7]. Both steady and unsteady solvers have been developed and include central processing unit (CPU) parallelization to further reduce time to solution.

The fast flamelet solver makes it possible to do analyses that were too expensive with previous tools. One of the first applications is investigating the chemical drivers of soot production. The solver has been adapted to predict yield sooting indexes based on the work of Xuan and Blanquart [8]. Figure I.12.5 shows a validation of the solver applied to yield sooting index prediction for a variety of engine-relevant fuels compared with experimental measurements [9]. After validation, the project team applied the solver to computing the sensitivity of soot production to individual reaction rates. This computation requires a solution of the steady flamelet equations for each reaction in the model (of which there can be tens of thousands). It is estimated that FlameMaster (one of the only existing tools for this type of analysis) would require more than 20,000 CPU hours for this computation, while the new fast flamelet solver required only 33 CPU hours. The project team is analyzing the reaction sensitivities in collaboration with Professor Xuan at The Pennsylvania State University. The results will be submitted for publication.

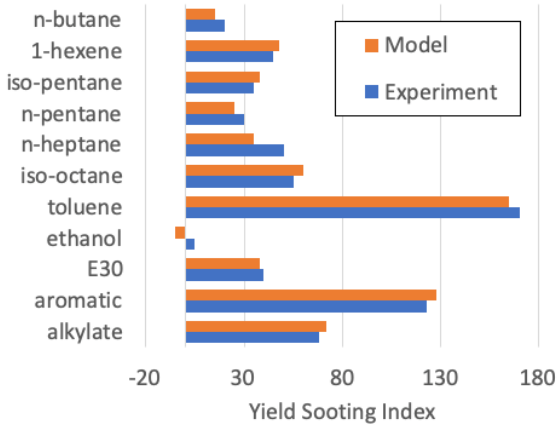

E30 – blend of 30% ethanol with gasoline

Figure I.12.5 Comparison of measured yield sooting index with those predicted with the fast flamelet solver (experimental data from McEnally et al. [9])

Zero-RK Code Release

The Zero-RK fast chemistry solvers developed in this project have significantly improved time to solution for many engine simulation scenarios. However, previously, the tools were limited in use to LLNL researchers and collaborators. The work of these researchers has produced a good set of results in the form of refereed research publications [10],[11],[12],[13],[14] but Zero-RK was not available to industry for direct application to organizations' internal research and design processes. With the help of the Industrial Partnerships Office at LLNL, the Zero-RK code has been released as an open-source package available with a permissive license to combustion researchers throughout the world. The package is available on LLNL's github page (https://github.com/LLNL/zero-rk) and contains the code necessary to run constant-volume, well-stirred reactor models and an interface to couple with reacting flow CFD codes. The wide availability of the code will greatly broaden the impact of the Zero-RK tools on industry problems. Further code releases are planned to include a variable-volume application, flame solvers, and other future developments in this program.

Conclusions

- Developed new understanding of the impact of mechanism reduction on engine CFD and recommended a hybrid approach for mechanism reduction as the best tradeoff between mechanism complexity and accuracy
- Created new fast solvers for one-dimensional diffusion (flamelet) flames that are 10–100 times faster than previous methods and can be used to generate tabulated chemistry for engine CFD and to investigate sensitivity of soot production to chemical reactions
- Released Zero-RK fast chemistry solver as free and open-source software.

Key Publications

1. Lapointe, S., R.A. Whitesides, and M.J. McNenly. 2019. "Sparse, Iterative Simulation Methods for One-Dimensional Laminar Flames." *Combustion and Flame* 204: 23–32. https://doi.org/10.1016/j.combustflame.2019.02.030.

References

1. Lu, T., and C.K. Law. 2005. "A Directed Relation Graph Method for Mechanism Reduction." *Proceedings of the Combustion Institute* 30: 1333–1341. https://doi.org/10.1016/j.proci.2004.08.145.

2. Niemeyer, K.E., C.-J. Sung, and M.P. Raju. 2010. "Skeletal Mechanism Generation for Surrogate Fuels Using Directed Relation Graph with Error Propagation and Sensitivity Analysis." *Combustion and Flame* 157: 1760–1770. https://doi.org/10.1016/j.combustflame.2009.12.022.

3. McNenly, M.J., R.A. Whitesides, and D.L. Flowers. 2015. "Faster Solvers for Large Kinetic Mechanisms Using Adaptive Preconditioners." *Proceedings of the Combustion Institute* 35: 581–587. https://doi.org/10.1016/j.proci.2014.05.113.

4. Lapointe, S., K. Zhang, and M.J. McNenly. 2018. "Reduced Chemical Model for Low and High-Temperature Oxidation of Fuel Blends Relevant to Internal Combustion Engines." *Proc. Combust. Inst.* https://doi.org/10.1016/j.proci.2018.06.139.

5. Yao, T., Y. Pei, B.-J. Zhong, S. Som, T. Lu, and K.H. Luo. 2017. "A Compact Skeletal Mechanism for n-Dodecane with Optimized Semi-Global Low-Temperature Chemistry for Diesel Engine Simulations." *Fuel* 191: 339–349. https://doi.org/10.1016/j.fuel.2016.11.083.

6. Lapointe, S., R.A. Whitesides, and M.J. McNenly. 2019. "Sparse, Iterative Simulation Methods for One-Dimensional Laminar Flames." *Combustion and Flame* 204: 23–32. https://doi.org/10.1016/j.combustflame.2019.02.030.

7. Pitsch, H. 1998. "FlameMaster: A C++ Computer Program for 0D Combustion and 1D Laminar Flame Calculations." Available at http://www.itv.rwth-aachen.de/downloads/flamemaster/.

8. Xuan, Y., and G. Blanquart. 2013. "Numerical Modeling of Sooting Tendencies in a Laminar Co-Flow Diffusion Flame." *Combustion and Flame* 160: 1657–1666. https://doi.org/10.1016/j.combustflame.2013.03.034.

9. McEnally, C.S., Y. Xuan, P.C. St. John, D.D. Das, A. Jain, S. Kim, T.A. Kwan, L.K. Tan, J. Zhu, and L.D. Pfefferle. 2019. "Sooting Tendencies of Co-Optima Test Gasolines and Their Surrogates." *Proceedings of the Combustion Institute* 37: 961–968. https://doi.org/10.1016/j.proci.2018.05.071.

10. Lapointe, S., C.L. Druzgalski, and M.J. McNenly. 2018. "Numerical Study of a Micro Flow Reactor at Engine Pressures: Flames with Repetitive Extinction and Ignition and Simulations with a Reduced Chemical Model." *Combustion and Flame* 197: 102–110. https://doi.org/10.1016/j.combustflame.2018.07.020.

11. Fridlyand, A., M.S. Johnson, S.S. Goldsborough, R.H. West, M.J. McNenly, M. Mehl, and W.J. Pitz. 2017. "The Role of Correlations in Uncertainty Quantification of Transportation Relevant Fuel Models." *Combustion and Flame* 180: 239–249. https://doi.org/10.1016/j.combustflame.2016.10.014.

12. Goldsborough, S.S., A. Fridlyand, R. West, M. McNenly, M. Mehl, and W.J. Pitz. 2018. "Quantifying Uncertainty in Predictions of Kinetically Modulated Combustion: Application to HCCI Using a Detailed Transportation Fuel Model." *WCX World Congr. Exp.* (SAE International). https://doi.org/10.4271/2018-01-1251.

13. Kang, D., A. Fridlyand, S.S. Goldsborough, S.W. Wagnon, M. Mehl, W.J. Pitz, and M.J. McNenly. 2019. "Auto-Ignition Study of FACE Gasoline and Its Surrogates at Advanced IC Engine Conditions." *Proceedings of the Combustion Institute* 37: 4699–4707. https://doi.org/10.1016/j.proci.2018.08.053.

14. Druzgalski, C.L., S. Lapointe, R. Whitesides, and M.J. McNenly. 2019. "Predicting Octane Number from Microscale Flame Dynamics." *Combustion and Flame* 208: 5–14. https://doi.org/10.1016/j.combustflame.2019.06.019.

Acknowledgements

This work was performed under the auspices of the U.S. Department of Energy by Lawrence Livermore National Laboratory under Contract DE-AC52-07NA27344.

LLNL Document Number: LLNL-TR-796965

I.13 Sprays, Flow, Heat Transfer, and Turbulent Mixing (Los Alamos National Laboratory)

David B. Carrington, Principal Investigator
Los Alamos National Laboratory (LANL)
P.O. Box 1663, MS-B216
Theoretical Division, T-3 Fluid Dynamics and Solid Mechanics
Los Alamos, NM 87544
E-mail: dcarring@lanl.gov

Michael Weismiller, DOE Technology Development Manager
U.S. Department of Energy
E-mail: Michael.Weismiller@ee.doe.gov

Start Date: October 1, 2018 End Date: September 30, 2023
Project Funding (FY19): $600,000 DOE share: $600,000 Non-DOE share: $0

Project Introduction

LANL is working with the Partnership on Advanced Combustion Engines (PACE), a U.S. Department of Energy (DOE)-sponsored consortium of National Laboratories supporting research and development (R&D) to create smarter engine design tools for sustainable transportation. Much of that effort is focused on heat, mass, and momentum transfer within an engine. Under PACE in particular, LANL's 2019 focus has been spray modeling, engine mixture formulation, and development of conjugate heat transfer (CHT) analysis (heat transfer to the environment surrounding the combustion chamber). Our efforts rely on LANL's Fast, Easy, Accurate and Robust Continuum Engineering (FEARCE) software, the next generation of engine modeling software for turbulent reactive and multiphase flow (and a 2019 R&D 100 Award winner). This work is relevant to the DOE Vehicle Technologies Office efforts to address national energy security as well. Less dependence on petroleum products leads to greater energy security. By U.S. Environmental Protection Agency standards, some vehicles are now reaching the 42–50 mpg mark. These are conventional gasoline engines. With continued investment and research into new technical innovations, the potential exists to save more than four million barrels of oil, or approximately $200–$400 million, per day. This would be a significant decrease in emissions and use of petroleum and a very large stimulus to the U.S. economy.

Better understanding of fuel injection and fuel–air mixing, thermodynamic combustion losses, and combustion/emission formation processes enhances our ability to minimize fuel use and unwanted emissions. The FEARCE modeling program helps to achieve this understanding by providing state-of-the-art capability for accurately simulating combustion processes, presenting a predictive methodology to help industry and researchers meet national and global goals for fuel usage and emissions. In addition, a predictive, robust, and accurate capability for simulating the engine combustion process helps to minimize time and labor when developing new engine technology.

Objectives

A main LANL project in the PACE consortium helps provide better understanding of engine combustion processes in order to enhance the ability to minimize fuel use and unwanted emissions. LANL works in areas generally related to three broad topics: heat, mass, and momentum transfer in the combustion chamber and surrounding engine metal. LANL is utilizing FEARCE and enhancing particular submodels to have a more predictive methodology than is currently available. Below are project objectives to meet LANL's PACE goals.

Overall Objectives

- Develop mathematical and computer algorithms and software to advance speed, accuracy, robustness, and range of applicability of FEARCE, an internal combustion engine modeling software, to be a more predictive computer code. This is to be accomplished by employing spatially accurate methods for reactive turbulent flow and more predictive spray injection, combined with a robust and accurate actuated parts simulation along with more appropriate turbulence modeling. In addition, researchers seek to understand the effect of heat transfer and the variation of temperatures on the internal combustion engine by using FEARCE's numerical methods that eliminate all usual assumptions about such phenomena, such as assumed heat transfer processes at chamber and part boundaries. The code combines state-of-the-art chemical reaction simulators, such as LANL's parallel version of Chemkin.

- Add models to the software and reduce code development costs into the future via more modern code architecture. In addition, FEARCE is being developed to be commercially available software. DOE and LANL are doing the difficult longer-term research for better modeling software, a task best done using National Laboratory-type capabilities.

- Provide methods in the software capable of producing fast turn-around times needed by industry for general use and in the PACE work, where the simulations are of higher fidelity, requiring more computational resources. FEARCE code not only functions well on small computer platforms but addresses high-performance computing aspects required for high fidelity and more predictive solutions. These objectives require extensive use of high-performance computing, thereby requiring the work to employ modern frameworks and methods that take advantage of computer resources very effectively. FEARCE has accomplished this by scaling to the size of the problem in a superlinear manner, along with employing other efforts to make the process highly scalable.

Fiscal Year 2019 Objectives

- Develop a four-valve direct-injection, spark-ignition (DISI) engine system for validation of FEARCE.

- Validate progress of FEARCE with experimental data of the four-valve DISI engine; collaborate with Dr. Magnus Solberg of Sandia National Laboratories (SNL) on the DISI setup and experimental data.

- Construct systems to use Chemkin reactive chemistry software.

- Continue spray model development for both predictive spray break-up and subsequent droplet transport and droplet fate. This effort includes validating the Kelvin Helmholtz–Rayleigh Taylor (KH-RT) spray model for Engine Combustion Network (ECN) Spray G cases against various data experiments. Another area of work is developing a predictive liquid jet break-up and inputting the large fuel droplets to the KH-RT model for subsequent transport processing of atomization and evaporation.

- Continue the process of commercialization of FEARCE.

Approach

Our approach is founded in designing, inventing, and developing new modeling methods. The design is a finite element method (FEM). Many beneficial and salient attributes of the software stem from the FEM formulation. We invented and developed the following systems to date (details are provided in the referenced publications).

- Developed the FEM predictor-corrector scheme projection method for high accuracy and all the benefits the FEM system brings to computational fluid dynamics (CFD) modeling of engines [1],[2]

- Developed the hp-adaptive system for higher-order accuracy, in which "h-adaptive" is automatic grid refinement and "p-adaptive" is higher-order approximation as driven by the error measure of the simulation [3]

- Invented the local arbitrary Lagrangian-Eulerian (ALE) method for moving bodies [4]; invented a moving marker system to track any chosen interfaces and reconstruct intersected elements to match the interface
- Developed immersed boundary methods for moving bodies [5]
- Developed Menter shear stress transport (k-ϖ) turbulence model based on Reynolds-Averaged Navier-Stokes (RANS) equations, showing improvement over Wilcox's k-ϖ [6]
- Developed a new dynamic large eddy simulation (LES), specifically designed for wall-bounded flows [7]; employed self-damping turbulence at the walls, which negates the need for a law-of-the-wall system or hybrid RANS and LES systems that are most often employed for wall-bounded flows
- Developed the KH-RT spray break-up system in FEARCE, providing accurate spray droplet solution along with FEARCE's in situ droplet evaporation and the aforementioned turbulence modeling
- Invented and developed volume-of-fluid methods in FEM for true multiphase compressible flow
    - Enabled predictive spray modeling to fully represent the spray break-up process [8]
    - Used KH-RT model after volume-of-fluid break-up of ligaments coupling in the Lagrangian particle transport system
- Developed a fast linear solver system that delivers superlinear scalability
    - Developed a parallel solution method [9]; developed implicit solution methods for 10x speed-up over serial parallel for an overall 300x speed-up
    - Added the Trilinos Multigrid matrix solution, further improving solution speed and parallel scaling by an order of magnitude (8x) over the implicit beam-warming system in FEARCE (which delivers 300x speed-up) for a total of 2,400x speed-up over the explicit serial version
    - Adjusted and tweaked the parallel communication for another 2x speed-up, bringing overall speed-up to 4,800x the explicit serial version
- Invented methods for implementing message passing interface (MPI) for today's and future platforms [9]
- Modeling heat transfer from metal engine block and head; engine grid generated with block and combustion chamber—code validation underway.

The project is building models to meet all objectives in an easy-to-maintain software that handles addition of others' submodels. The effort requires careful verification and validation of the methods and code. The development of this technology utilizes many areas of expertise in multispecies turbulent reactive flow modeling with liquid sprays, modeling of immersed moving bodies, and the extensive numerical methods for the solution of the model and governing equations developed in the software.

Results

Efforts this year continued to push toward a comprehensive tool for the future with the accomplishment of more grid generation improvements, validation of immersed moving parts including a four-valve DISI engine, the KH-RT spray model, and algebraic multigrid linear equation solver implementation for even greater computational speed. The project team has also begun the process of commercializing the software to be able to fully support industries and research requirements in simulation software.

Grid Generation

In conjunction with a software development company (GridPro), LANL is working on providing high-quality grids for the engine system with an eye toward ease of use. The overset parts system used in the moving parts algorithm allows for easy grid generation of the cylinders and ports, with the spark and injector modules easily inserted. The pistons and valves are represented as surfaces that are overlaid on the grid, which is easily generated using commercial software. Adding an engine block with cooling water passages is no longer an arduous task, taking only a few hours of effort given computer-aided design. The injector and spark systems are built separately with the idea of making various types of injectors and spark plug modules that are simply connected to the engine cylinder grid. It cannot be overstated: a quality grid is needed to produce reliable simulations. Gridding is a major component of CFD, where researchers seek to provide that quality with a minimum of labor.

Engine Simulation and Continued Validation of Immersed Moving Parts for the Engine System

The project team developed an immersed boundary method and began developing the immersed FEM for moving bodies using FEARCE's surface marker system.

- This effort is partially based on methods used in LANL's local ALE system for moving bodies.
- The moving marker system utilizes track moving boundary interfaces [4].
- The immersed boundary method employs interpolation and projection of the nearest nodal values normal to the surface. The immersed FEM utilizes the shape or basis functions for interpolation and a projection system to place a point along the normal to the surface, from which the nearest node is projected, by which the fluid's motion and thermodynamic state are calculated.
- A four-valve engine test case is functioning as shown in Figure I.13.1 using the immersed boundary methods, showing pressure rise for the motored case as described in the paper by Noah Van Dam et al. [10].

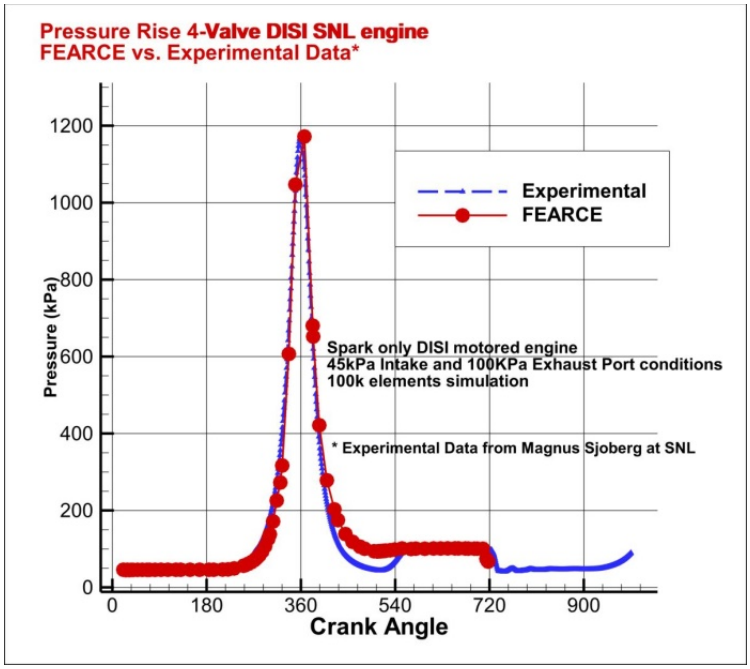

Figure I.13.1 Pressure rise in a four-valve DISI engine as a function of crank angle as compared to experimental data

Spray Modeling

The project has implemented the KH-RT spray model into FEARCE. Researchers have validated the models on Spray A and Spray G ECN test cases. The KH-RT spray model [11] for the Spray G case is based on injection of diesel into quiescent nitrogen at 600 kPa and ambient gas temperature of 573 K, as shown in Figure I.13.2. The isooctane fuel evaporates during the injection and break-up phases of the process. Figure I.13.2a shows the droplets at 1 µs. Figure I.13.2b shows the penetration (mass moment distribution) of the spray droplets and vapor over time compared with experimental data from ECN.

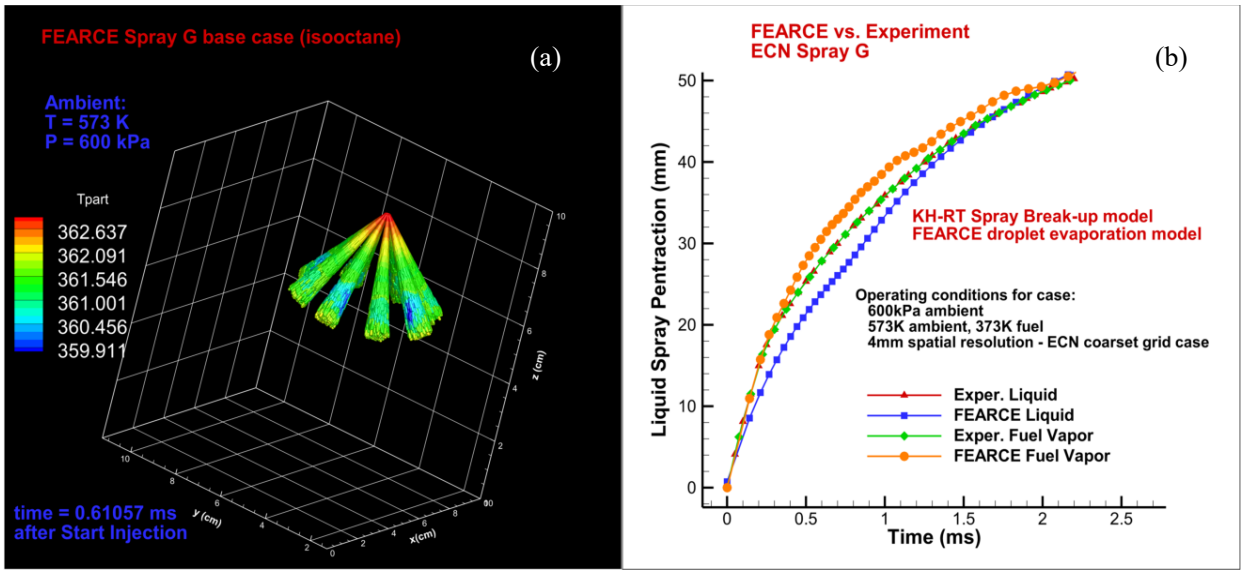

Figure I.13.2 The ECN Spray G case: injection of gasoline in quiescent nitrogen at 600 kPa, with (a) showing the KH-RT spray model and (b) showing the penetration depth of the liquid spray and vapor compared to ECN experimental data

Heat Transfer

A CHT simulation is shown in Figure I.13.3. In Figure I.13.3a, hot gas is flowing (temperature = 600 K) around a cool hollow metal cylinder (pipe) with an interior fixed temperature of 373 K. The gas is cooling as it flows by the cylinder, and the cylinder is warming from the flow. Figure I.13.3b is a validation study using the backward-facing step, as experimentally evaluated by Vogel and Eaton [12]; the study was previously used to validate FEARCE without CHT. Shown is the conduction heating of the air by the heated surface and the cooling of the surface by air flowing quickly over the surface (convection cooling). The unique way FEARCE handles the material, solids and gases, and the heat transfer with its FEM formulation and shared material properties at boundary nodes automatically conserves the flux through the boundary without iteration. In fact, no flux calculation is required; hence, there is no need for assumptions about the efficacy of the heat transfer via a heat transfer coefficient, which is usually an unknown and often a poor assumption in the highly unsteady flow found in engines.

A grid for the four-valve DISI engine having the block surrounding the chamber has been created (shown in Figure I.13.4). This process tests the grid generation for the CHT system, showing it to be a relatively simple addition to the combustion chamber gridding, taking a few hours for an experienced user. The head will be added when LANL has the entire computer-aided design from the metal engine system.

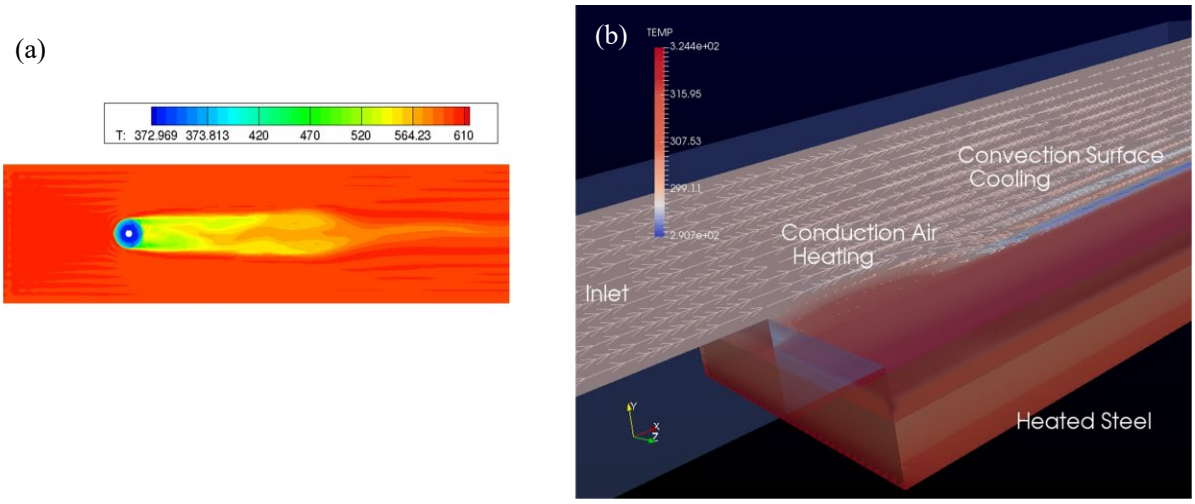

Figure I.13.3 A CHT simulation: (a) highly turbulent flow over a heated cylinder, and (b) turbulent flow over a heated backward-facing step

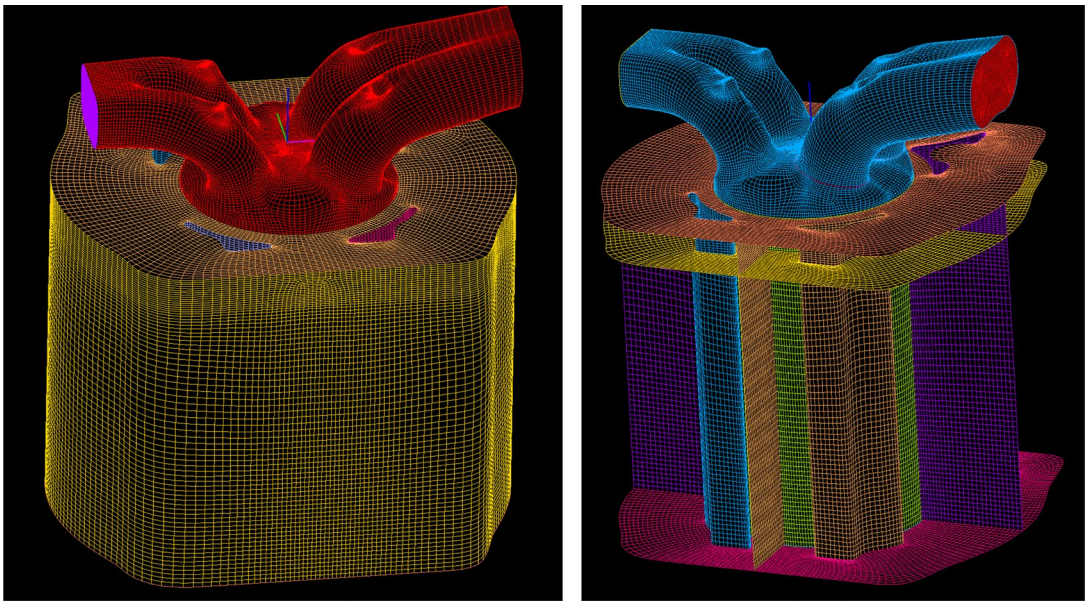

Figure I.13.4 DISI four-valve chamber surrounded by block with water cooling passages

Computational Efficiency

The project continued work on developing a parallel solution method and reducing wall clock time by adding the Trilinos Multigrid preconditioning. Previously, the researchers had achieved a 10x speed-up, with the implicit solution related to increased time-step size. Additionally, the project produced a 30x speed-up over the serial version by implementing a shared-node FEM system that reduces communication cost and produces a superlinear scaling, for a cumulative speed-up of over 300x [9]. The project installed systems to access the Trilinos solver package, where the multigrid preconditioning is providing about 8x speed-up, and researchers tweaked the MPI communication for a factor of 2x, for a total of 4,800x speed-up over the serial version of FEARCE. The Trilinos Multigrid improves the already good parallel scaling when running on a large number of processors. Considering that the parallel version of FEARCE is significantly faster than KIVA-4mpi (the parallel version of KIVA-4), significant strides have been made toward quicker solution.

In addition to the superlinearity of FEARCE, the project has continued to improve communication costs. The communication cost has been cut in half for problems over 1.1 million nodes; communication issues that are not very noticeable in smaller problems become so in larger problems. The project has addressed some handling of the communication to cut the time required.

- The project delivered superlinear scalability, as was demonstrated by Waters and Carrington [9], in a strong scaling experiment on standard CFD benchmark problems such as the backward-facing step or flow over a cylinder. Figure I.13.5 shows the scaling of FEARCE's algorithm (without special linear equation solver treatments such as preconditioning or multigrid) besting the ideal linear scaling on an engine of interest.

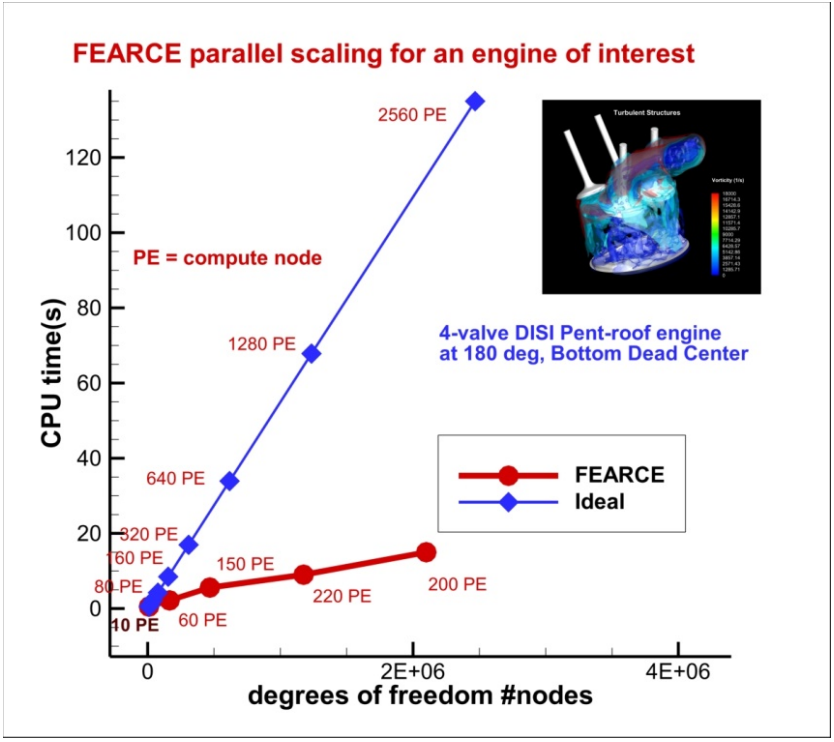

CPU – central processing unit

Figure I.13.5 FEARCE's beam-warming system versus use of the Trilinos Multigrid preconditioned generalized minimal residual method, a weak scaling study

- LANL implemented access to the algebraic multigrid preconditioning and linear equation solvers from Trilinos [13]. Last year, the team improved wall clock times by a factor of eight over the original 300x speed-up, achieving over 2,400x speed-up over the project's explicit serial solver. The project is now encroaching on exceptional high-performance computing. Further gains in wall clock times are expected for the superlinear system through greater vectorization and use of graphics processing units (use of Kukkos with Trilinos).

- FEARCE requires far fewer elements to achieve the same accuracy as older KIVA codes, allowing for much faster solution on the same resolution with higher accuracy. The commercial codes available currently follow the ideal scaling curves, at best, though their clock speeds might be less per time-step than the ideal speeds shown in Figure I.13.5 (speeds based on FEARCE cost). So far, FEARCE has been shown to have flat scaling, is able to solve two million nodes on 200 processors, is faster, uses less resources, and is more accurate.

Conclusions

The KIVA development program at LANL is nearing the objective of having robust state-of-the-art CFD software for turbulent reactive flow, particularly well-suited for combustion modeling in engines or machines that involve immersed moving boundaries, all with an eye toward solutions produced on quality grids created with a minimal amount of labor. Achievements include:

- Fast grid generation for CHT: computer-aided drawing for a complex engine CFD grid
- Four-valve DISI engine experimental data used to validate the robust moving immersed FEM method
- Addition of the RANS model and Menter shear stress transport model, adding to RANS modeling capability
- Continuing KH-RT spray model validation via the ECN test cases, with Spray G cases with evaporation showing good agreement with experimental results, even on the coarse grids
- CHT in the engine system, a system that requires no assumption about the efficacy of the heat transfer process, where the flux is automatically conserved and requires no iterative processing
- A highly scalable parallel solution system, with multigrid preconditioning producing nearly perfect scaling, 4,800x faster than the serial version of FEARCE, 16x faster than the superlinear FEARCE, and more effective than the Krylov generalized minimal residual method linear equation solution; research is now exploring Exascale possibilities using vectorizable Cuda-friendly sections of code for a graphics processing unit nested into the MPI parallel framework
- Addition of LANL's parallel version of Chemkin III for faster, larger, and more robust reactive chemistry.

Key Publications

1. Carrington, D.B., and J. Waters. 2018. "Turbulent Reactive Flow Modeling in Engines: A Robust and Accurate Toolkit/Software for Simulating Engine Dynamics." Proceedings of the ASME 2018 Internal Combustion Fall Technical Conference, ICEF2018, San Diego, CA (November 4–7).
2. Waters, J., and D.B. Carrington. 2019. "Turbulent Reactive Flow Modeling in Engines: A Robust and Accurate Toolkit/Software for Simulating Engine Dynamics." *Journal of Engineering for Gas Turbines and Power* 142 (2): 021006. https://doi.org/10.1115/1.4045340.
3. Waters, J., B. Philipbar, and D.B. Carrington. 2020. "A Finite Element Menter Shear Stress Turbulence Transport Model." Accepted for publication in *Numerical Heat Transfer*, 2020.

References

1. Carrington, D.B. 2009. "A Characteristic-Based Split Hp-Adaptive Finite Element Method for Combustion Modeling in KIVA-hpFE." LANL Scientific Report no. LA-UR-09-06527.
2. Carrington, D.B., X. Wang, and D.W. Pepper. 2014. "A Predictor-Corrector Split Projection Method for Turbulent Reactive Flow." Journal of Computational Thermal Sciences, Begell House Inc., 5 (4): 333–352.
3. Carrington, D.B., X. Wang, and D.W. Pepper. 2014. "An Hp-Adaptive Predictor-Corrector Split Projection Method for Turbulent Compressible Flow." Proceedings of the 15th International Heat Transfer Conference, IHTC-15. Kyoto, Japan. (August 10–15).

4. Carrington, D.B., M. Mazumder, and J.C. Heinrich. 2018. "Three-Dimensional Local ALE-FEM Method for Fluid Flow in Domains Containing Moving Boundaries/Objects Interfaces." *Progress in Computational Fluid Dynamics* 18 (4): 199–215.

5. Waters, J., and D.B. Carrington. 2019. "Engine Modeling with FEARCE Toolkit for Simulating Engine Dynamics and Turbulent Reactive Flow with Sprays." Proceedings of WCX™19: SAE International World Congress Experience (April 9–11), Detroit, MI, USA.

6. Waters, J., B. Philipbar, and D.B. Carrington. 2020. "A Finite Element Menter Shear Stress Turbulence Transport Model." Accepted for publication in *Numerical Heat Transfer*, 2020.

7. Waters, J., D.B. Carrington, and D.W. Pepper. 2016. "An Adaptive Finite Element Method with Dynamic LES for Incompressible and Compressible Flows." Journal of Computational Thermal Sciences, Begell House Inc. 8(1): 57–71.

8. Waters, J., D.B. Carrington, and M.M. Francois. 2017. "Modeling Multi-Phase Flow: Spray Break-Up Using Volume of Fluids in a Dynamic LES FEM method." Numerical Heat Transfer, Part B 72(4): 285–299.

9. Waters, J., and D.B. Carrington. 2016. "A Parallel Large Eddy Simulation in a Finite Element Projection Method for All Flow Regimes." Numerical Heat Transfer, Part A 70(2): 117–131.

10. Van Dam, N., W. Zeng, M. Sjoberg, and S. Som. 2017. "Parallel Multi-Cycles of an Optical Pent-Roof DISI Engine under Motored Operating Conditions." ICEF2017-3603, ASME Proceedings, ICEF (October 5–18).

11. Reitz, R.D. 1987. "Modeling Atomization Processes in High-Pressure Vaporizing Sprays." Atomization and Sprays Technology 3: 309–337.

12. Vogel, J., and J. Eaton. 1985. "Combined Heat Transfer and Fluid Dynamic Measurements Downstream of a Backward-Facing Step." *Journal of Heat Transfer* 107: 922.

13. Trilinos: https://trilinos.org/, Version 12.12. Trilinos is a collection of open-source software libraries generally related to the solution of linear systems of equations.

Acknowledgements

Jiajia Waters is a co-principal investigator on this project. LANL acknowledges Michael Weismiller and Gurpreet Singh of the U.S. Department of Energy's Vehicle Technologies Office as part of the Advanced Combustion Engines and Fuels research portfolio.

I.14 Accelerating Predictive Simulation of Internal Combustion Engines with High-Performance Computing (Oak Ridge National Laboratory)

K. Dean Edwards, Principal Investigator
Oak Ridge National Laboratory (ORNL)
National Transportation Research Center
2360 Cherahala Blvd.
Knoxville, TN 37932
E-mail: edwardskd@ornl.gov

Michael Weismiller, DOE Technology Development Manager
U.S. Department of Energy
E-mail: Michael.Weismiller@ee.doe.gov

Start Date: October 1, 2016 End Date: September 30, 2023
Project Funding (FY19): $400,000 DOE share: $400,000 Non-DOE share: $0

Project Introduction

This project is developing and applying advanced simulation tools and novel techniques to best utilize high-performance computing (HPC) resources and detailed predictive models. These efforts aim to support rapid advancements in engine design, optimization, and control. The project couples ORNL's experimental and modeling expertise in engine and emissions-control technologies with the U.S. Department of Energy (DOE) Office of Advanced Scientific Computing Research's leadership HPC resources and fundamental research tools. Access to these resources is allocated primarily via a competitive process for the Advanced Scientific Computing Research Leadership Computing Challenge program. Specific focus areas evolve according to the needs of industry and DOE, with the project typically supporting one or more tasks in close collaboration with industry partners under the Oak Ridge Leadership Computing Facility Industrial Partnership Program.

During Fiscal Year (FY) 2019, this project primarily supported a multi-year collaborative effort between General Motors, ORNL, Lawrence Livermore National Laboratory (LLNL), and Convergent Science, Inc., which is using HPC resources and graphic processing unit (GPU)-enabled numerical solvers to evaluate the impact of increased simulation detail on the predictive accuracy and computational needs of computational fluid dynamics (CFD) engine simulations. Current commercially available computing resources provide capability for moderately detailed engine simulations when the field of study is relatively narrow and fast turn-around time is not crucial. However, for applications such as virtual engine design and calibration, which require hundreds or thousands of individual simulations with rapid throughput, CFD engine simulations must be overly simplified, resulting in a trade-off between accuracy and speed. Using massively parallel HPC resources and faster, GPU-enabled numerical solvers provides a more favorable trade-off, enabling highly detailed simulations with more acceptable computational times. Under this project, the team is using ORNL's Titan supercomputer and LLNL's Zero-Order Reaction Kinetics (Zero-RK) chemistry solvers to systematically increase the level of simulation detail and add more first-principle, predictive submodels. The resulting impact on simulation accuracy and computational time is then evaluated.

Objectives

Overall Objective

- Use massively parallel HPC resources and GPU-enabled numerical solvers to enable use of CFD engine models with significantly increased levels of detail and predictive submodels

- Evaluate the impact of model refinements on predictive accuracy, computational speed, and extent of operational space covered without further tuning and calibration.

Fiscal Year 2019 Objectives

- Refine the conjugate heat transfer (CHT) modeling approach coupled with Reynolds-Averaged Navier-Stokes (RANS) and large eddy simulation (LES) turbulence submodels
- Evaluate the impact of these model refinements on predictive accuracy and computational requirements
- Adapt modeling tools for use on ORNL's new HPC resource, Summit, and evaluate improvements in computational capabilities for engine simulation.

Approach

As part of a multiyear collaborative effort between General Motors, ORNL, LLNL, and Convergent Science, the project team is using HPC and GPU-enabled numerical solvers to enable increased levels of simulation detail in CFD engine models. The approach involves systematically adding increased detail and first-principles-based submodels to improve the predictive accuracy of combustion performance and emissions formation over more of the engine operating range while reducing the need for tuning and calibration. In this way, the project team can assess the benefits and computational costs of each model refinement. A virtual engine calibration study is being used as a test problem to evaluate the overall approach, as developing a valid calibration requires hundreds or thousands of rapid-throughput engine simulations with sufficient accuracy. The baseline model for this problem on conventional computing resources is a closed-valve, cylinder-sector CFD engine model with skeletal chemistry; this model can simulate combustion performance with reasonable accuracy but fails to accurately predict emissions production. The use of HPC enables use of more detailed models for improved accuracy without compromising throughput. Previous model refinements applied under this multiyear project include transitioning to a full-cylinder, open-cycle model for improved flow and mixing and use of LLNL's Zero-RK chemistry solvers, which take advantage of Titan's GPUs to enable use of highly detailed chemical mechanisms to simulate combustion and emissions formation. A CHT submodel was also added to provide better thermal boundary conditions by solving heat transfer between the combustion gases, the metal cylinder walls, and the engine coolant. During FY 2019, efforts were focused on further refinement of the CHT approach and evaluating performance improvements with both RANS and LES turbulence submodels.

Results

Key model refinements evaluated during FY 2019 include the additions of a CHT submodel to provide spatially and temporally varying thermal boundary conditions and an LES turbulence model for improved resolution of small-scale mixing. Owing to the difficulty of experimentally measuring combustion chamber wall temperatures and heat fluxes, thermal boundary conditions for engine simulations are poorly known and understood. Coupling the combustion model to a CHT model of key solid components (including the piston, cylinder liner, and cylinder head) expands the domain of the model beyond the poorly known conditions at the cylinder walls to boundaries with the cooling jacket where conditions are better known. The transition to an LES turbulence model is expected to provide more accurate small-scale mixing at the flame front, which researchers have previously shown to be crucial for accurately predicting carbon monoxide production.

Using CONVERGE v2.4.20, which includes one- and three-dimensional CHT capabilities, the project constructed a coupled model of the full four-cylinder engine that includes all cylinders (with pistons and liners), the head, and cooling jackets. An iterative approach to solution was used involving separate models for the cooling jacket and the combined combustion gases and solid components. As an initial step, researchers performed a steady-state simulation on the cooling jacket model with imposed constant, uniform wall temperatures at the interface with the solid-gas model at each engine operating point. The resulting heat flux solution from the jacket model was then imposed as boundary conditions on the solid-gas model. To reduce

computational demands, combustion is solved within a single engine cylinder with resulting thermal loads mapped to the remaining cylinders. Heat flux results from the coupled combustion and CHT model are then mapped back to the coolant jacket to complete the iterative loop. Multiple engine cycles must be simulated for solution convergence. Because the solid conduction model converges much more slowly than the combustion model, a supercycling approach is used. At user-defined intervals, the combustion model is paused while the solid heat-transfer model is run to steady state using a full cycle of heat flux data stored in memory. This approach greatly accelerates time to solution, resulting in a converged thermal solution for the water jacket in approximately three engine cycles.

Following this approach, the researchers performed simulations for a down-selected set of eight conditions from the full design of experiments representing some of the more challenging calibration points to accurately capture with simulations. Once the water jacket solution converged, results for each case were used to seed two separate sets of simulations to examine the impact of turbulence model selection. One set simulated additional cycles for each of the eight cases using a RANS turbulence model, coupled CHT models for the piston, liner, head, and coolant jackets, and fully detailed chemistry with Zero-RK. The second set simulated additional consecutive cycles using a similar approach except with an LES turbulence model. Both sets of simulations were then run for as many cycles as our allocation allowed.

Analyses of the results from this effort are underway and have provided some important initial observations.

- The three-dimensional CHT solution with RANS turbulence predicts significantly different thermal boundary conditions within the cylinder than those used in previous studies with higher piston temperatures and lower cylinder head temperatures. Predicted heat losses through these surfaces varied accordingly.
- Considerable spatial and temporal variation in piston and head temperatures were observed.
- LES simulations converged toward steady state at a much slower rate than RANS cases, suggesting lower predicted rates of thermal diffusion. As a result, additional cycles are needed to fully capture the impact of LES on simulation accuracy.
- The resulting impact on predicted performance and emissions varied (see Figure I.14.1). Combustion performance and nitrogen oxide (NO_x) predictions showed little change from previous studies without CHT. Hydrocarbon predictions improved for all cases. Carbon monoxide predictions improved for some cases but worsened for others.

Additional efforts in FY 2019 included transitioning simulation efforts to Summit, Advanced Scientific Computing Research's new flagship HPC platform at ORNL, and the new release of CONVERGE (v3.0) from Convergent Science, which includes improved scaling for HPC environments. The project implemented significant modifications to simulation tools and software for the hardware and software architecture of Summit. Developers at Convergent Science were able to compile CONVERGE v3.0 for the IBM Power9 chipset and the specific version of message passing interface used by Summit. As seen in Figure I.14.2, initial testing on Summit for a motored engine (no fuel spray or combustion) with over one million cells has shown significant improvement in parallel scaling (especially for solving the transport equations), resulting in reductions in total compute time over previous versions. Additional refinements are expected to improve scalability further.

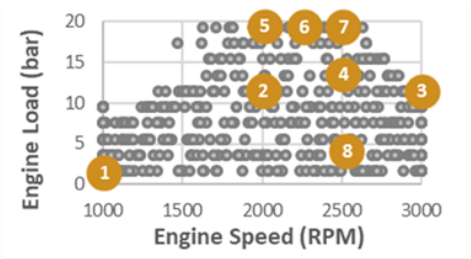

	Baseline	Best Sector	Full-cyl	CHT+RANS
Geometry	Sector	Sector	Cylinder	Engine
Cycle	Closed	Closed	Open	Open
Max # cells	~170k	~1M	~2.5M	~4.5M
# species	47	144	144	144
# reactions	74	900	900	900
NOx	Zel'dovich	GRI 3.0	GRI 3.0	GRI 3.0
Soot	Detailed PSM	Hiroyasu	Hiroyasu	Hiroyasu
Turbulence	RANS	RANS	RANS	RANS
Other changes		Spray and wall-film	Intake swirl vane	CHT
Wall time / cycle	~2 hr	~5 hr	~3.5 days	~2 weeks
Cases	500	602	20	8

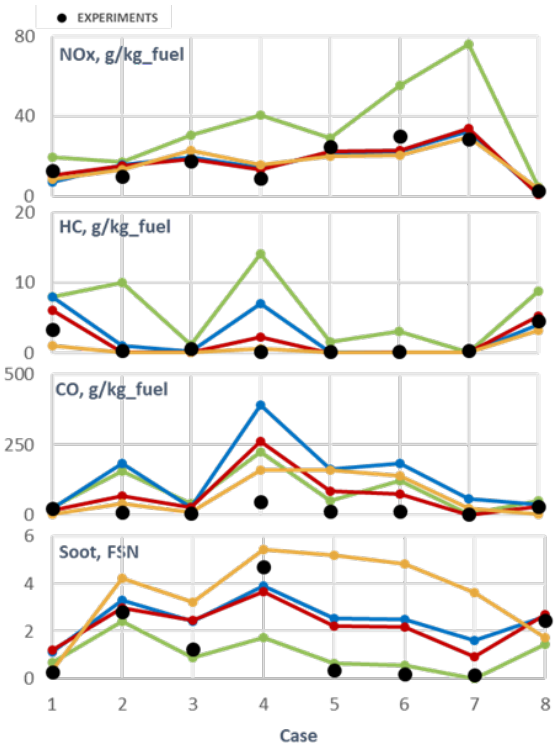

HC – hydrocarbon; FSN – filter smoke number; PSM – particulate size mimic

Figure I.14.1 Comparison of emissions accuracy at eight engine operating points for various levels of model detail including the CHT model with RANS turbulence

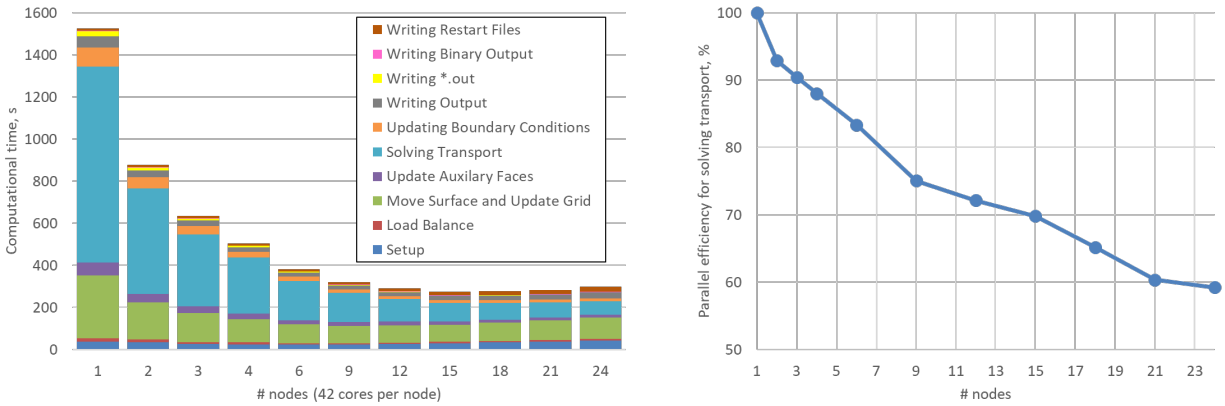

Figure I.14.2 Results of scaling study for portion of a motored engine simulation showing breakdown of computational time and parallel efficiency (ratio of percent speed increase to additional number of cores) for solving transport equations using CONVERGE v3.0 on Summit

Conclusions

- The CHT model predicts significantly different thermal boundary conditions with considerable spatial and temporal variation within the cylinder compared to traditional modeling approaches. Predicted heat losses vary accordingly. Validation of these results will require detailed surface temperature measurements.

- With the LES turbulence submodel, the cylinder thermal solution converged toward steady state at a much slower rate. As a result, additional cycles will need to be run to fully capture the impact of LES on simulation accuracy.

- Initial testing of CONVERGE v3.0 on Summit has shown significant improvements in parallel scalability, especially for solving the transport equations. Combined with the use of Zero-RK to enable use of Summit's GPUs for the chemistry solution, this advancement should greatly improve the level of detail that can be included in engine simulations without having a significant adverse impact on computation time.

Key Publications

1. Edwards, K.D., C.E.A. Finney, W.R. Elwasif, and R.A. Whitesides. 2019. "Using HPC for Detailed Engine Simulations with Coupled CHT." AEC Program Review Meeting, Knoxville, TN (January).

2. Edwards, K.D., C.E.A. Finney, and W.R. Elwasif. 2019. "Accelerating Predictive Simulation of IC Engines with High Performance Computing." DOE Vehicle Technologies Office 2019 Annual Merit Review.

Acknowledgements

The author thanks co-investigators Charles E.A. Finney and Wael R. Elwasif of ORNL. This project was performed in close collaboration with our colleagues and fellow researchers at General Motors (Ron Grover, Jian Gao, Vankatesh Gopalakrishnan, and Ramachandr Diwakar), LLNL (Russell Whitesides), and Convergent Science (Tristan Burton and Nitesh Attal) through the Oak Ridge Leadership Computing Facility Industrial Partnership Program.

Portions of this work used resources of the Oak Ridge Leadership Computing Facility at ORNL, which is supported by the DOE Office of Science under Contract No. DE-AC05-00OR22725.

I.15 Multi-Mode Combustion in Light-Duty Spark-Ignition Engines (Argonne National Laboratory)

Toby Rockstroh, Principal Investigator
Argonne National Laboratory
9700 S. Cass Avenue
Lemont, IL 60439
E-mail: trockstroh@anl.gov

Michael Weismiller, DOE Technology Development Manager
U.S. Department of Energy
E-mail: Michael.Weismiller@ee.doe.gov

Start Date: October 1, 2018 End Date: September 30, 2019
Project Funding (FY19): $600,000 DOE share: $600,000 Non-DOE share: $0

Project Introduction

Numerous advanced compression ignition (ACI) strategies have been previously investigated with gasoline-type fuels, including homogenous charge compression ignition and partially premixed charge compression ignition. However, many challenges constrain commercial implementation of full-time ACI in light-duty engine platforms, such as limited speed-load range and low combustion temperatures, which lead to excessive hydrocarbon and/or carbon monoxide emissions, and difficulties with aftertreatment systems. To address these issues, this study focuses on fundamental understandings that inform ACI's use in a multimode operating strategy.

Objectives

Overall Objectives

- Maximize the thermal efficiency of light-duty gasoline engines by expanding the ACI operating range
- Develop control methodologies for ACI operation using conventional engine control parameters
- Implement alternative ignition systems to control ACI operation and spark-ignition-ACI mode transition.

Fiscal Year 2019 Objectives

- Evaluate ACI control methodologies by utilizing static autoignition data
- Develop an active pre-chamber ignition system for ACI operation.

Approach

Experiments were performed on a single-cylinder gasoline direct injection spark-ignition engine at a compression ratio of 11.3:1, which was found to be a trade-off between enabling low-load ACI and high-load spark ignition when using an anti-knock index (AKI) 87 fuel. The engine was operated at 1,500 rpm and lambda 2.5 without any exhaust gas recirculation. With an intake temperature of 225°C, an intake boost pressure of 1.2 bar absolute was required to maintain a combustion phasing CA50 (crank angle at 50% mass fraction burned) at approximately 14° after top dead center (aTDC).

A collaborating research group at Argonne National Laboratory, led by Dr. Scott Goldsborough, measured the ignition delays for the commercial-grade AKI 87 gasoline using a twin-piston rapid compression machine

(RCM). The RCM tests were conducted at fuel loading and thermodynamic conditions analogous to those obtained in the engine experiments.

The researchers conducted a thorough literature review of pre-chamber ignition systems to design an active pre-chamber ignition system suitable for the planned investigations. The pre-chamber prototype was manufactured in-house at Argonne National Laboratory, and the project team conducted initial scoping tests on the single-cylinder engine in passive mode.

Results

The average pressure-temperature trajectory that the charge undergoes in the engine, shown in blue in Figure I.15.1, was overlaid onto an autoignition delay contour map obtained from RCM experiments. The gas temperature in the engine was estimated using measured cylinder pressure and ideal gas law correlation; the dashed lines indicate trajectories with some uncertainty in estimating the cylinder temperature at intake valve closing. The compression trajectory suggests that autoignition occurs in the intermediate-temperature chemistry range and that start of combustion correlates with an ignition delay of approximately 1.5 ms. To capture the chemical reaction time intervals during the compression process in the engine, researchers applied the Livengood-Wu integral to the autoignition dataset obtained from the RCM experiments. By definition, the start of combustion occurs when the integral reaches unity, which occurred at a cylinder temperature of approximately 1,045 K and 27 bar and corresponded with the constant ignition delay contour of 1.5 ms.

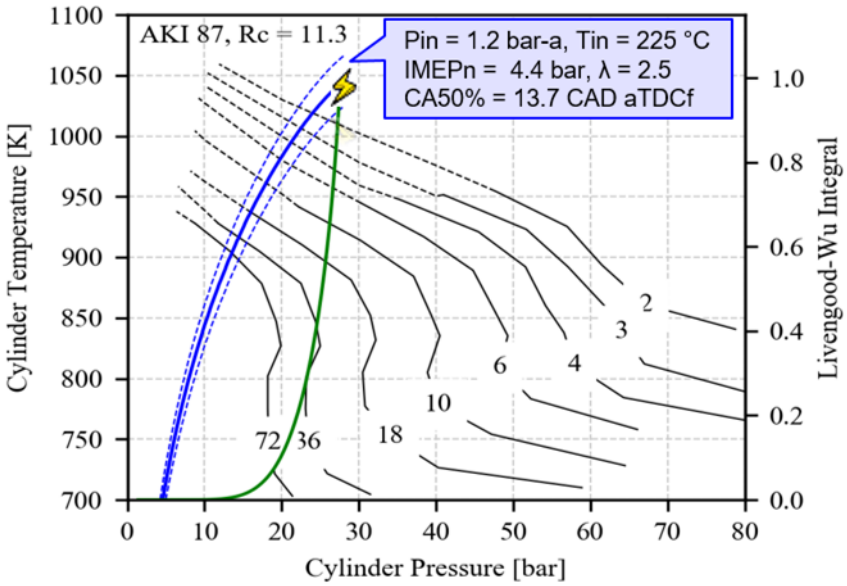

IMEPn – net indicated mean effective pressure; CAD – computer aided drafting; aTDCf – after top dead center firing; Rc – compression ratio

Figure I.15.1 Engine compression trajectory overlaid onto autoignition delay contour map from RCM experiments

However, significant uncertainties are associated with cylinder temperature estimation, which can have a profound effect on the applicability of the Livengood-Wu integral method to predict start of combustion. In addition, there are uncertainties in estimating autoignition delay behavior at engine-relevant conditions, both experimentally and with the aid of kinetic simulations. Efforts are ongoing to assess the application of the autoignition integral method as a combustion phasing control methodology over a wide range of ACI operating conditions.

Researchers conducted a detailed literature review on active pre-chamber ignition systems, with particular emphasis on the work shown by Gussak et al. [1],[2],[3] and Oppenheim et al. [4],[5],[6],[7],[8]. Their work investigated the chemical reactivity of rich auxiliary mixtures in a pre-chamber toward initiating ignition in lean or dilute air-fuel mixtures in the main combustion chamber of a gasoline engine. Pre-chamber design and development was executed with the aim of investigating pre-chamber assisted compression ignition and enabling installation in the existing pent-roof cylinder head of the research engine.

The research team chose a modular design consisting of a pre-chamber head and separate body, as shown in Figure I.15.2. A prototype was manufactured from 4130 alloy steel. The pre-chamber body (shaded in purple) houses the spark plug, piezo electric pressure transducer, and check-valve of the air-fuel supply path. The team designed an external air-fuel mixture supply system consisting of a Bronkhorst® Controlled Evaporator Mixer together with a Coriolis fuel mass flow controller and a digital thermal air mass flow controller. A range of exchangeable pre-chamber bodies (shaded in blue in Figure I.15.2) was designed to allow for a range of pre-chamber volumes and nozzle geometries, as highlighted in Figure I.15.3. The range of pre-chamber volume, configurable from 2 cm^3 to 4 cm^3 (~3%–6.5% of the clearance volume), was constrained by the cylinder head spark plug port design but encompasses the range of pre-chamber volumes that have been reported on in literature. The smallest volume of 2 cm^3 reduces the geometric compression ratio from 15.3:1 to 11.62:1. A range of nozzle geometries (ranging from three to eight nozzles) will be tested; the initial nozzle-diameter-to-pre-chamber-volume correlations were based on previous findings by other researchers [3],[4],[5],[6],[7],[8],[9].

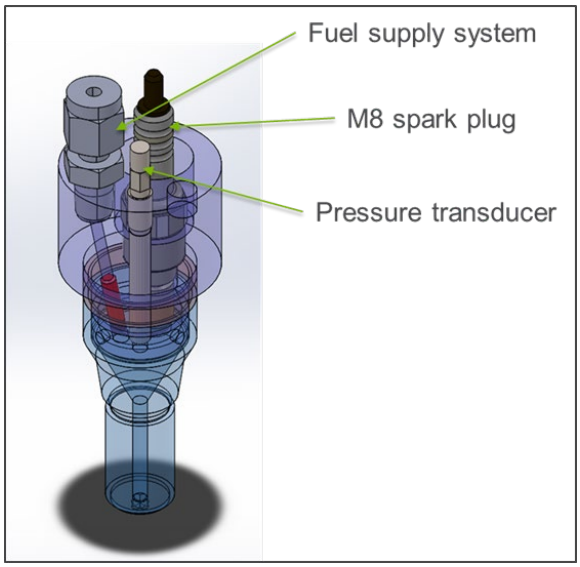

Figure I.15.2 Rendered image of prototype pre-chamber ignition system

The first chosen configuration consisted of 2 cm^3 pre-chamber volume with four nozzles, each with a diameter of 1.5 mm. Preliminary scoping tests were conducted in passive mode (i.e., without external air-fuel supply), as shown in Figure I.15.4. The researchers chose a fairly conservative engine operating condition of 1,500 rpm and 3.2 bar indicated mean effective pressure. It should be noted that the pre-chamber was not designed for passive operation, and the scoping tests were done solely to test the indicating diagnostics and to evaluate the system's general functionality. The external air-fuel supply system is currently being commissioned.

Finally, a three-point analysis model of the single-cylinder engine and the pre-chamber ignitor was developed using GT-Power, as shown in Figure I.15.5. The validation of the model is ongoing.

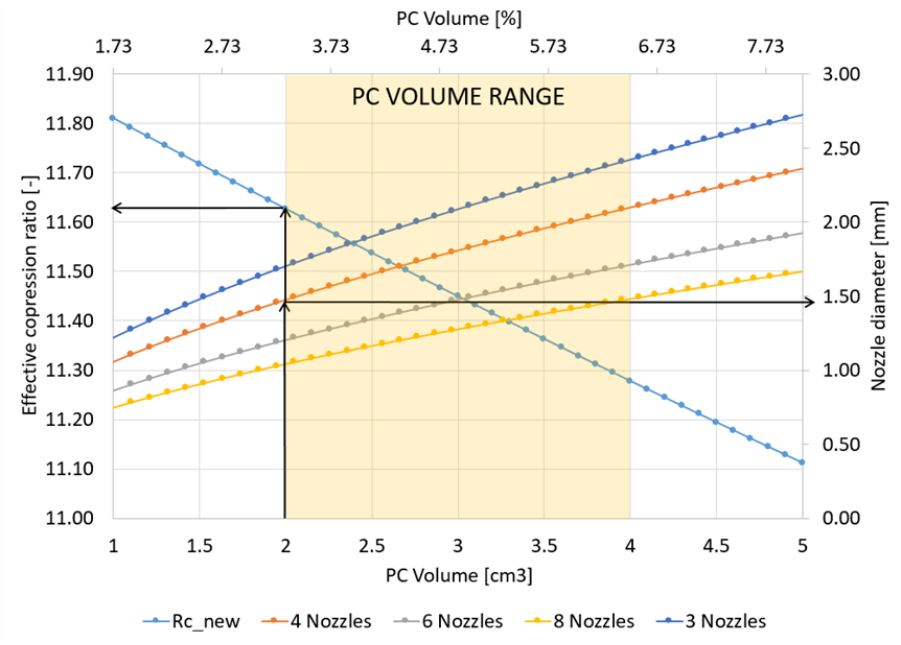

Figure I.15.3 Pre-chamber volume and nozzle design parameters, and effective compression ratio with a base geometric compression ratio of 15.3:1

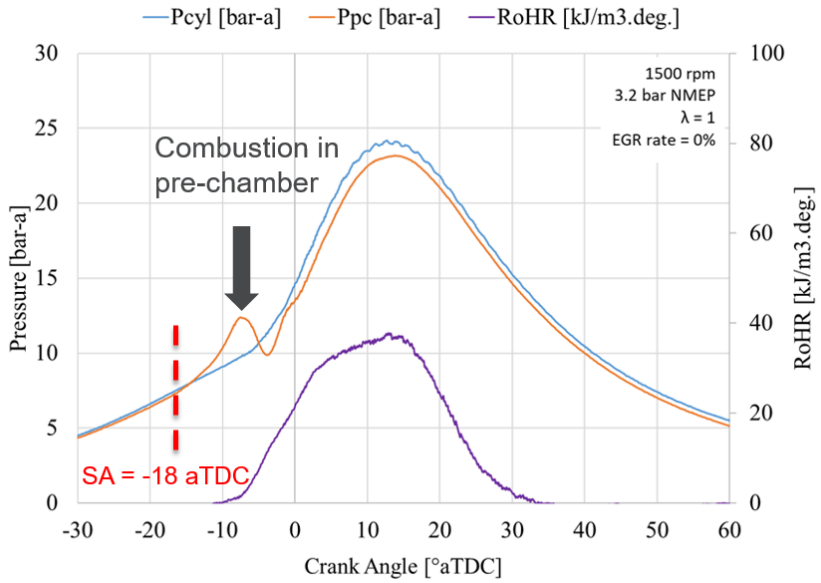

NMEP – net mean effective pressure; EGR – exhaust gas recirculation; GDI – gasoline direct injection

Figure I.15.4 Cylinder pressure (Pcyl), pre-chamber pressure (Ppc), and apparent heat release rate (RoHR) from scoping test conducted with prototype pre-chamber in passive mode

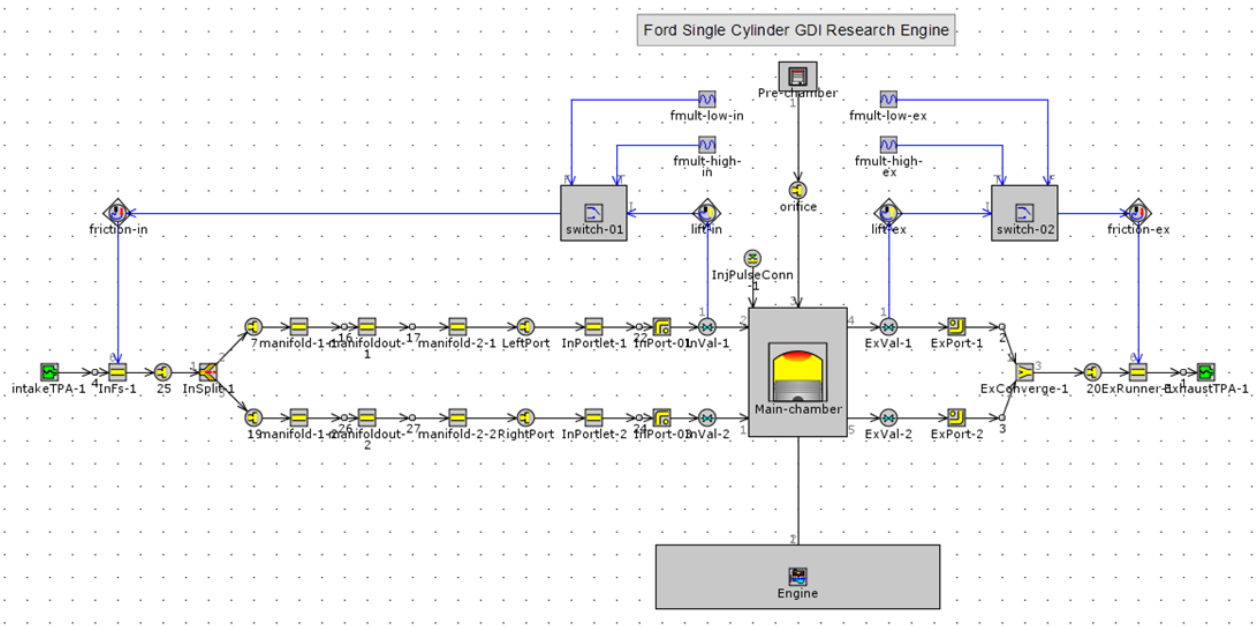

Figure I.15.5 Three-point analysis model of the single-cylinder engine and the pre-chamber ignitor

The major results of this study can be summarized as follows:

- The researchers evaluated ACI operating mode in the gasoline direct injection single-cylinder engine using AKI 87 gasoline and found that a compression ratio of 11.3:1 enables both ACI and spark-ignition operation.
- Combustion phasing prediction may be enabled through the use of static autoignition delay measurements in combination with the Livengood-Wu integral method, although efforts are ongoing to evaluate this procedure over a wider engine operating range and with assessment of uncertainties associated with estimating the thermodynamic conditions in the cylinder.
- The research team designed and manufactured a modular active pre-chamber ignition system and conducted scoping tests in passive mode.

During the course of Fiscal Year 2019, this project realigned its focus areas after a multi-laboratory light-duty engine consortium was established. One of the new focus areas is the investigation of cold-start behavior using pre-chamber ignition systems. As a result, significant engine test cell infrastructure upgrades took place during Fiscal Year 2019 to address the new research priorities.

Conclusions

- Static autoignition delay measurements in combination with the Livengood-Wu integral method are a potentially viable control methodology for combustion phasing control.
- Literature studies suggest that pre-chamber ignition systems have the potential to enable lean and/or dilute gasoline combustion. The mode of combustion in the main chamber is not well understood.
- Realignment of the project tasks will place future research focus on stoichiometric dilute pre-chamber ignition systems and cold start.

References

1. Gussak, L.A. 1983. “The Role of Chemical Activity and Turbulence Intensity in Prechamber-Torch Organization of Combustion of a Stationary Flow of a Fuel-Air Mixture.” SAE Technical Paper 830592.

2. Gussak, L.A. 1975. “High Chemical Activity of Incomplete Combustion Products and a Method of Prechamber Torch Ignition for Avalanche Activation of Combustion in Internal Combustion Engines.” SAE Technical Paper 750890.

3. Gussak, L.A., V.P. Karpov, and Y.V. Tikhonov. 1979. “The Application of Lag-Process in Prechamber Engines.” SAE Technical Paper 790692.

4. Oppenheim, A.K., J. Beltramo, D. Paris, J.A. Maxson, K. Hom, and H.E. Stewart. 1989. “Combustion by Pulsed Jet Plumes–Key to Controlled Combustion Engines.” SAE Technical Paper 890153.

5. Maxson, J.A., and A.K. Oppenheim. 1990. “Pulsed Jet Combustion–Key to a Refinement of the Stratified Charge Concept.” *Proc. Combust. Inst.*: 1041–1046.

6. Murase, E., S. Ono, K. Hanada, J.H. Yun, and A.K. Oppenheim. 1996. “Performance of Pulsed Combustion Jet at High Pressures and Temperatures.” *JSAE Rev.* 17, no. 3: 245–250.

7. Murase, E., S. Ono, K. Hanada, and A.K. Oppenheim. 1994. “Pulsed Combustion Jet Ignition in Lean Mixtures.” SAE Technical Paper 942048.

8. Hensinger, D.M., J.A. Maxson, K. Hom, and A.K. Oppenheim. 1992. “Jet Plume Injection and Combustion.” SAE Technical Paper 920414.

9. Attard, W.P., M. Bassett, P. Parsons, and H. Blaxill. 2011. “A New Combustion System Achieving High Drive Cycle Fuel Economy Improvements in a Modern Vehicle Powertrain.” SAE Technical Paper 2011-01-0664.

Acknowledgements

This work was made possible with the contributions of Ashish Shah and Johannes Rohwer. Furthermore, Timothy Rutter’s technical support and Section Manager Doug Longman’s leadership are greatly appreciated.

I.16 Developing a Framework for Performing High-Fidelity Engine Simulations Using Nek5000 Code for Exascale Computing (Argonne National Laboratory)

Muhsin Ameen, Principal Investigator
Argonne National Laboratory
9700 S. Cass Avenue
Lemont, IL 60439
E-mail: mameen@anl.gov

Michael Weismiller, DOE Technology Development Manager
U.S. Department of Energy
E-mail: Michael.Weismiller@ee.doe.gov

Start Date: July 1, 2018 End Date: Project continuation evaluated annually
Project Funding (FY19): $700,000 DOE share: $700,000 Non-DOE share: $0

Project Introduction

There is a pressing need to develop improved engine designs with high efficiencies and low emissions. The Partnership on Advanced Combustion Engines (PACE), the recently formed U.S. Department of Energy (DOE) light-duty combustion consortium, combines unique experiments with world-class DOE computing and machine-learning expertise to speed discovery of knowledge, improve engine design tools, and enable market-competitive powertrain solutions with potential for best-in-class lifecycle emissions. One of the key requirements in achieving these objectives is the availability of accurate numerical simulation tools that can effectively capture the in-cylinder flow, spray, and combustion phenomena in engines. Engine manufacturers currently use commercial codes that have inherent limitations in predictive capability and massive parallelization. Argonne National Laboratory's massively parallel computational fluid dynamics (CFD) platform, Nek5000 [1], is a leading high-order spectral element, open-source code for accurately modeling fluid turbulence, with more than 400 registered users worldwide. This code already has capabilities that allow moving piston and valve simulations with more advanced turbulence modeling capabilities than current internal combustion engine (ICE) simulation software. DOE's Exascale Computing Project has selected this code as one of the codes that can be run effectively on future exascale platforms, and work is already underway to ensure that the code is scalable on these machines when they come online. As part of this project, the Nek5000 CFD platform is being developed into an accurate scalable numerical platform for performing high-fidelity ICE simulations on the current and upcoming DOE leadership class machines.

In the current year, the project team added several features required for ICE simulation to Nek5000, which led to progress in the ease of mesh generation, study of fluid flow through real engine intake valve geometry, and modeling of reacting flows. High-fidelity large eddy simulation (LES) of the General Motors (GM) transparent combustion chamber (TCC) engine under motored operation was performed with the objective of identifying the root causes of cyclic variability. Cyclic variability mitigation is one of the key PACE objectives, and the conclusions from the current study can help with meeting the consortium goals. Nek5000 was also used to perform LES of a benchmark reacting jet flame to validate the combustion models implemented as part of this project. The validated combustion models will be used in the upcoming years to simulate reacting engine operation. Work is also underway to implement a Lagrangian phase model for modeling engine sprays. These high-fidelity simulations generate abundant, accurate numerical data that can complement experimental measurements, support engineering submodel development, and provide training data for machine-learning tools to develop data-driven models.

Objectives

This project focuses on developing the Nek5000 CFD platform into an effective exascale code for high-fidelity ICE simulations. This involves implementing the state-of-the-art submodels for combustion, spray, and ignition, and validating against several benchmark engine experiments. These efforts will enable high-fidelity ICE simulations with minimal numerical inaccuracies.

Overall Objectives

- Develop an accurate and scalable numerical platform that can capture the in-cylinder flow, spray, and combustion processes
- Determine the root causes of cyclic variability and develop mitigation strategies
- Develop techniques to improve engineering submodels using the data generated from Nek5000.

Fiscal Year 2019 Objectives

- Demonstrate ability to quantitatively predict flow, including variability, under high-load and low-load conditions
- Improve the capability of Nek5000 to model turbulent reacting flows
- Demonstrate the scalability of the engine simulations on leadership class machines.

Approach

The current project is aimed at using an open-source, highly scalable, and accurate numerical platform to understand the complex turbulent flow, spray, and combustion processes in ICEs and devise ways to design engines with high efficiency and low emissions. The simulation platform that will be employed is Nek5000 [1], which is a high-order spectral element code that has been under active development at Argonne National Laboratory and several other institutions. This code has shown excellent scalability on a variety of computing architectures for a variety of flow problems and has been shown to be scalable on up to a million processes [2]. Nek5000 already has capabilities that allow simulations of complex geometries with moving boundaries and has been demonstrated for simulating ICEs [3],[4]. The approach used in the current project is to utilize the overset meshing capability of Nek5000 to allow ease of mesh generation and control of mesh quality and distortion during the simulation. The first stage of the project will involve implementing state-of-the-art spray and combustion models into the code, and leading in to a scalable, open-source platform for engine simulations. The second phase will involve using Nek5000 to simulate the engines selected for the PACE consortium and for which high-fidelity experimental data will be available as part of the consortium research. The accurate data available from these simulations will be shared within the consortium and will be used to complement the experimental measurements and lead to an improved understanding of the combustion process and potential improvements in the engine design.

This project involves strong collaborations with the computational science and Argonne Leadership Computing Facility divisions at Argonne National Laboratory. Collaborations are also underway with the University of Illinois at Urbana-Champaign's Professor Paul Fischer, the chief architect of Nek5000, to obtain guidance on the spectral element solver development. The current project will also leverage the advancements in Nek5000 through the Exascale Computing Project's Center for Efficient Exascale Discretization project, which will enable strong scalability on upcoming exascale architectures at the DOE National Laboratories. The solver team at Lawrence Livermore National Laboratory will be involved in speeding up the chemical kinetics solver development in Nek5000. Computations are being performed on Argonne's Theta supercomputer using an allocation of 40 million core hours from the Advanced Scientific Computing Research Leadership Computing Challenge.

Results

The key accomplishments for Fiscal Year 2019 were in developing an effective mesh generation technique for modeling in-cylinder flows, performing high-fidelity wall-resolved LES of the TCC engine, implementing combustion models into Nek5000, and demonstrating the scalability of the simulations on DOE leadership class machines.

Overset Meshing Strategy for Modeling In-Cylinder Flows

Mesh generation for complex geometries with moving boundaries is challenging. Nek5000 has an overset meshing capability that can be utilized in solving this challenge; however, this capability has not been sufficiently tested for moving meshes. As part of this project, the researchers tested the potential of using the overset mesh capability for modeling a spark-ignition engine flow [5]. The work led to the following key accomplishments:

- Demonstrated the use of an overlapping grid methodology for spark-ignition engines in a spectral element method framework for a two-dimensional (2D) geometry (Figure I.16.1).
- Benchmarked the accuracy of the overset mesh approach by comparing the mean flowfield predicted by the overset approach with a single mesh approach (Figure I.16.2). Demonstrated that the overset

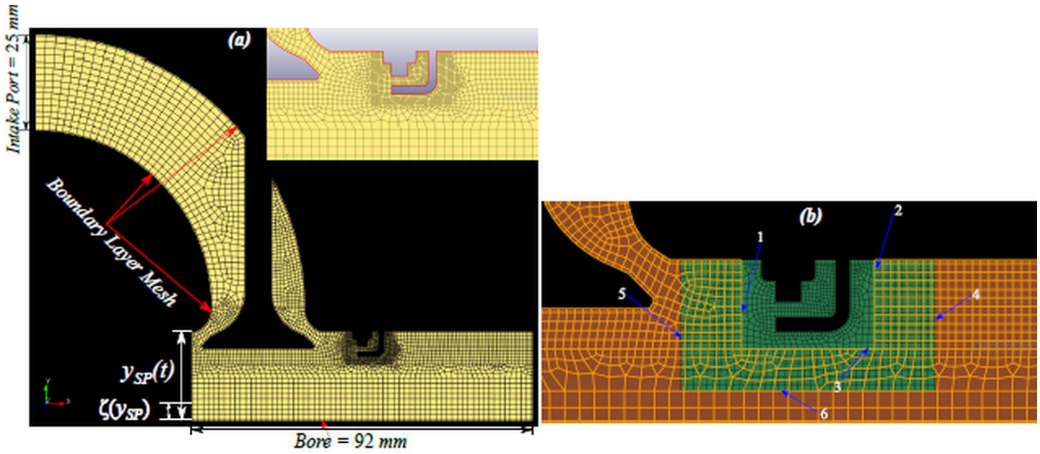

Figure I.16.1 (a) Standard single mesh of 2D engine-like geometry (IA) in the xy plane. Inset: Mesh near the spark plug zoomed, boundary layer mesh region highlighted in red. (b) Overlapping mesh (IB) with the region of overlap zoomed in. Outer domain (orange), outer mesh (yellow lines). Inner domain (green), inner mesh (thin black lines). 1–3: interface of outer domain, 4–6: interface of inner domain. [5]

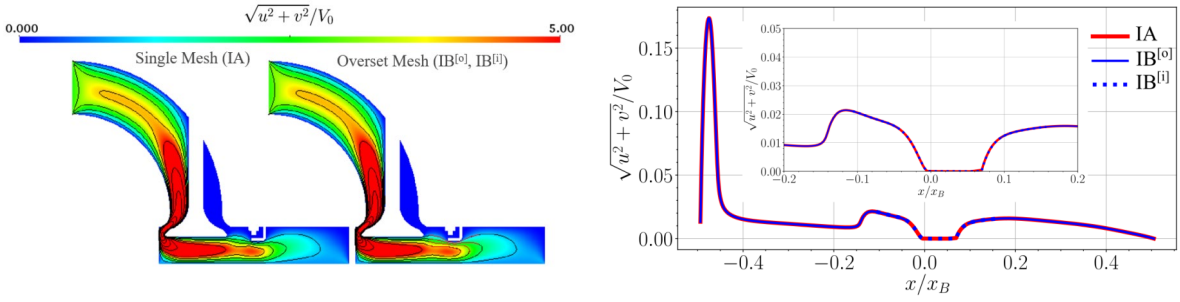

Figure I.16.2 (left) Comparison of the contours of normalized velocity magnitude between the single mesh and overset mesh simulations; (right) line plot of normalized velocity magnitude near the spark plug region for the single mesh (IA) and overset mesh (IB) simulations [5]

mesh approach added only ~10% increased computational expense while providing better mesh size control.

High-Fidelity LES of In-Cylinder Flow

Nek5000, with the overset meshing strategy, was used to perform LES of the in-cylinder flow for the GM TCC engine on the Theta supercomputer. Table I.16.1 shows the grid resolution parameters used for this simulation. The researchers used 38 different spectral element method grids constructed a priori in CUBIT (the Sandia National Laboratory automated mesh generation toolkit) high-order grid-to-grid interpolation to progress the simulation. The project utilized characteristic (semi-Lagrangian) time-stepping for Arbitrary Lagrangian–Eulerian (ALE) [6], which allowed the use of Courant-Friedrichs-Lewy (CFL) numbers of 3.0. Figure I.16.3 shows the instantaneous snapshots of the normalized velocity magnitudes at two different crank angles. The key accomplishments of this work are as follows:

- Demonstrated the workflow to perform realistic three-dimensional engine simulations, including the spark plug geometry using Nek5000.
- Generated high-fidelity numerical data for the in-cylinder flowfield, which will be archived for future use by machine-learning models.

Table I.16.1 Grid Resolution Parameters for the LES of GM TCC Engines Using Nek5000

Resolution Parameters	
Polynomial Order (N)	7
Min # of Elements	135,000 Elements at TDC
Max # of Elements	310,000 Elements at BDC
Min # of Total Points @ TDC	45.7 Million
Max # of Total Points @ BDC	105.3 Million
Element Size (h)	0.08–1.1 mm (TDC → BDC)
Effective Resolution O (h/N)	0.01–0.14 mm

TDC – top dead center; BDC – bottom dead center

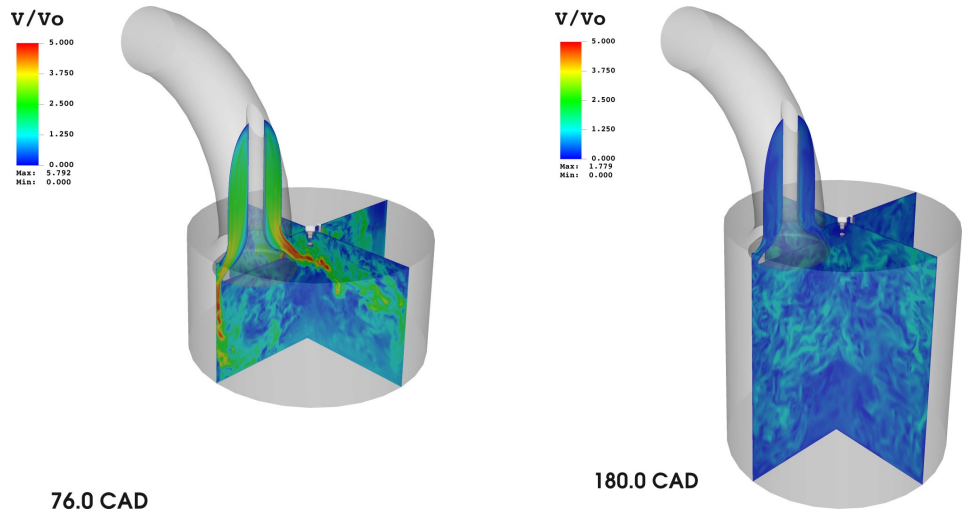

Figure I.16.3 Instantaneous snapshots of the normalized velocity contours along two perpendicular planes through the GM TCC engine during the intake stroke at 76.0 crank angle degrees (CAD) (left) and 180.0 CAD (right)

Combustion Model Implementation into Nek5000

Recent efforts have also involved implementing capabilities into Nek5000 to model reacting flows. Two different combustion models have been implemented: a perfectly stirred reactor combustion model and a tabulated flamelet progress variable (FPV) model. The project validated the FPV model by performing high-fidelity LES of the reacting Cabra jet flame [7]. Figure I.16.4 (left) shows the structure of the flame iso-surface of the statistically steady flame. The following are major accomplishments of this work:

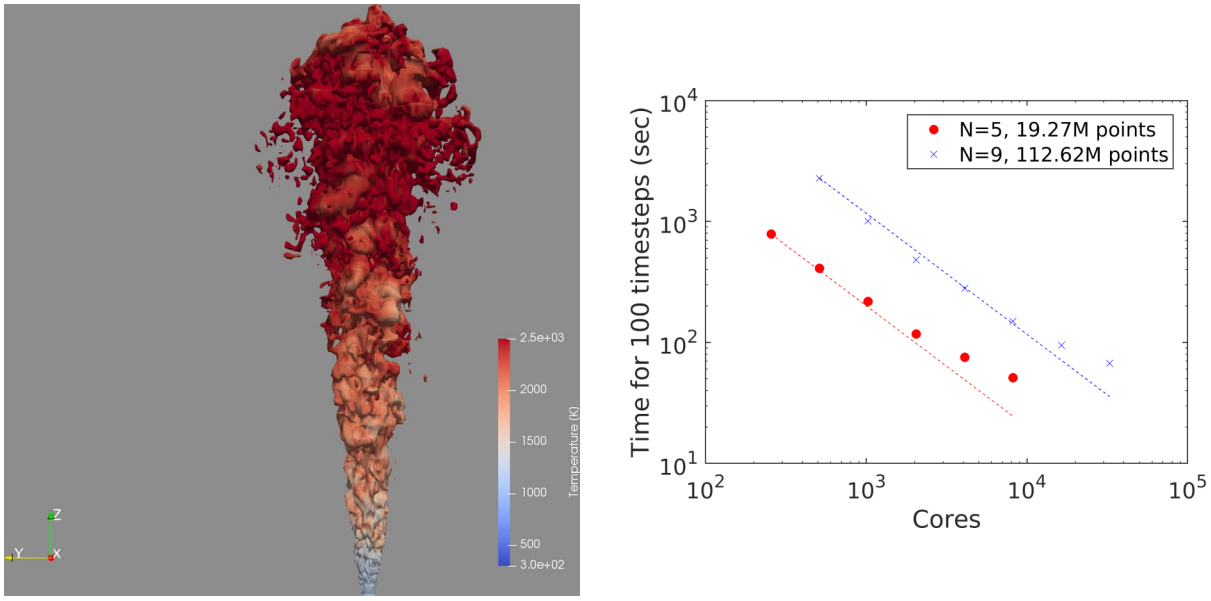

Figure I.16.4 (left) Instantaneous iso-surface of the stoichiometric mixture fraction iso-surface colored by temperature for the Cabra flame at 100 ms after start of injection; (right) strong-scaling results for the Cabra flame simulations on Argonne Leadership Computing Facility Theta

- Demonstrated that ignition occurs in the near-stoichiometric region at locations where the local scalar dissipation rate is low and that ignition kernels grow in time to form the continuous flame front.
- Validated the FPV model implementation by comparing the simulation results with the experimental planar laser-induced fluorescence measurements.
- Demonstrated the strong scalability of the reacting Nek5000 simulations on up to 32,000 processors on Theta (Figure I.16.4 [right]).

Conclusions

The major accomplishments from the work conducted in this year are as follows:

- Demonstrated a workflow to perform high-fidelity engine simulations using an overlapping grid methodology in a spectral element method framework.
- Performed LES of the GM TCC engine and generated high-fidelity numerical data for the in-cylinder flowfield, which will be archived for future use by a machine-learning model.
- Implemented perfectly stirred reactor and FPV combustion models into Nek5000 and performed validation and scalability studies.

Key Publications

1. Chatterjee, Tanmoy, Saumil S. Patel, and Muhsin M. Ameen. 2019. "Towards Improved Mesh-Designing Techniques of Spark-Ignition Engines in the Framework of Spectral Element Methods." U.S. National Combustion Meeting, Pasadena, CA.

2. Chatterjee, Tanmoy, Saumil Patel, and Muhsin Ameen. 2019. "Understanding the Behavior of Large Scale Structures in Highly Scalable Spectral Element Simulations of Internal Combustion Engines in the Framework of Large Eddy Simulation." Bulletin of the American Physical Society.

3. Shudler, Sergei, Nicola Ferrier, Joseph Insley, Michael E. Papka, Saumil Patel, and Silvio Rizzi. 2019. "Fast Mesh Validation in Combustion Simulations through In-Situ Visualization." Eurographics Symposium on Parallel Graphics and Visualization, EGPGV 2019, Porto, Portugal (June 3–4).

References

1. NEK5000 Version 19.0 rc1. 2019. Argonne National Laboratory, Illinois. https://nek5000.mcs.anl.gov.

2. Fischer, Paul F. 2015. "Scaling Limits for PDE-Based Simulation." 22nd AIAA Computational Fluid Dynamics Conference, p. 3049.

3. Giannakopoulos, G.K., Christos E. Frouzakis, Konstantinos Boulouchos, Paul F. Fischer, and A.G. Tomboulides. 2017. "Direct Numerical Simulation of the Flow in the Intake Pipe of an Internal Combustion Engine." *International Journal of Heat and Fluid Flow* 68: 257–268.

4. Giannakopoulos, G.K., C.E. Frouzakis, P.F. Fischer, A.G. Tomboulides, and K. Boulouchos. 2019. "LES of the Gas-Exchange Process inside an Internal Combustion Engine Using a High-Order Method." *Flow, Turbulence and Combustion*: 1–20.

5. Chatterjee, Tanmoy, Saumil S. Patel, and Muhsin M. Ameen. 2019. "Towards Improved Mesh-Designing Techniques of Spark-Ignition Engines in the Framework of Spectral Element Methods." U.S. National Combustion Meeting, Pasadena, CA.

6. Patel, Saumil, Paul Fischer, Misun Min, and Ananias Tomboulides. 2019. "A Characteristic-Based Spectral Element Method for Moving-Domain Problems." *Journal of Scientific Computing* 79, no. 1: 564–592.

7. Cabra, R., T. Myhrvold, J.Y. Chen, R.W. Dibble, A.N. Karpetis, and R.S. Barlow. 2002. "Simultaneous Laser Raman-Rayleigh-LIF Measurements and Numerical Modeling Results of a Lifted Turbulent H_2/N_2 Jet Flame in a Vitiated Coflow." *Proceedings of the Combustion Institute* 29, no. 2: 1881–1888.

Acknowledgements

The work was performed jointly by Tanmoy Chatterjee, Saumil Patel, and Muhsin Ameen from Argonne National Laboratory. The support from Joe Insley and Silvio Rizzi for visualization is acknowledged. Technical guidance and support from Paul Fischer and Ketan Mittal from the University of Illinois at Urbana–Champaign is also acknowledged. The Argonne Laboratory Computing Resources Center and Argonne Leadership Computing Facility provided computing resources.

I.17 High-Efficiency Gasoline Compression Ignition for Heavy-Duty Engines (Argonne National Laboratory)

Christopher P. Kolodziej, Principal Investigator
Argonne National Laboratory
9700 S. Cass Avenue
Lemont, IL 60439
E-mail: ckolodziej@anl.gov

Michael Weismiller, DOE Technology Development Manager
U.S. Department of Energy
E-mail: Michael.Weismiller@ee.doe.gov

Start Date: October 1, 2018 End Date: September 30, 2019
Project Funding (FY19): $950,000 DOE share: $950,000 Non-DOE share: $0

Project Introduction

Diesel is the main fuel of industry (goods transport, construction, agriculture, etc.). However, the future demand for diesel fuel is predicted to increase and be higher than the demand for gasoline [1]. This could lead to gasoline costing significantly less than diesel and becoming an interesting fuel option for medium-duty (MD) and heavy-duty (HD) engines [2]. However, the only gasoline engines available currently for MD/HD vehicles use spark-ignition combustion as opposed to more efficient compression-ignition combustion. Therefore, there is a need to develop MD and HD gasoline compression-ignition (GCI) engines that can obtain diesel-like efficiencies, with high robustness and potentially lower emissions than diesel compression-ignition engines.

Several studies have demonstrated the robustness of GCI combustion at high loads when incorporating mixing-controlled compression ignition (MCCI), achieving efficiency similar to that of diesel combustion, as well as reduced emissions [3],[4]. However, little is known about whether the characteristics of the particulate emissions change between diesel and gasoline MCCI combustion at high load. There is also a need for more research to demonstrate robust GCI engine operation at low loads and idle. This project characterized the particulate emissions of diesel and gasoline MCCI combustion at high load and demonstrated spark-ignition combustion as a possible solution to GCI engine combustion stability at low load and idle.

Objectives

Overall Objectives

- Increase the efficient use of gasoline in MD and HD engines
- Improve combustion stability of HD GCI engines at low load
- Characterize the particulate emissions differences between gasoline and diesel compression-ignition combustion.

Fiscal Year 2019 Objectives

- Demonstrate low-load operation of a high-compression-ratio (16:1) HD GCI engine using knock-free spark-ignition combustion with good combustion stability
- Measure the particulate morphology of gasoline and diesel MCCI combustion at high load.

Approach

A 2.4 liter, single-cylinder HD Caterpillar diesel engine with 16.2:1 compression ratio was outfitted with a port fuel injection system and spark plug. As can be seen in Figure I.17.1, the spark plug for this initial testing was located in the available cylinder pressure relief port, above the squish area of the combustion chamber.

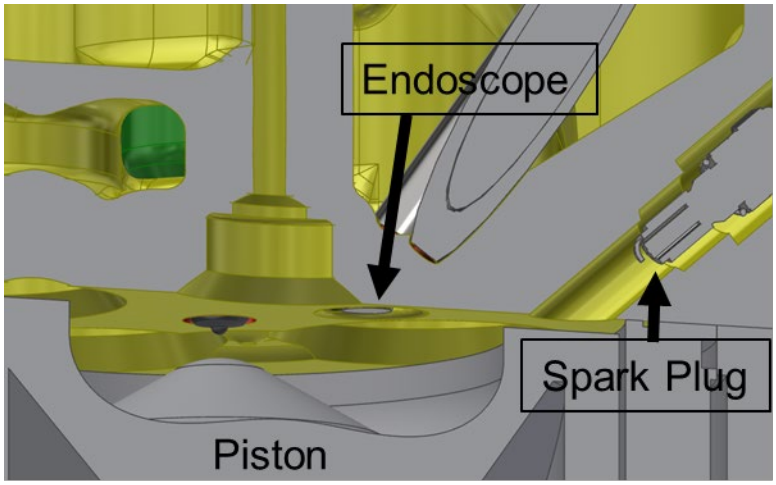

Figure I.17.1 Cross-section view of single-cylinder HD Caterpillar research engine at Argonne National Laboratory

The challenges of spark-ignition combustion in this large-bore quiescent combustion chamber diesel engine come from high knock propensity from a high compression ratio, low flame propagation rates from low turbulence, and a long distance across which the flame must propagate. During Fiscal Year (FY) 2019, Caterpillar and Argonne National Laboratory designed a new cylinder head for the research engine that will allow for a more centrally located spark plug, which can be seen in Figure I.17.2. Testing for this new head design is planned for FY 2020.

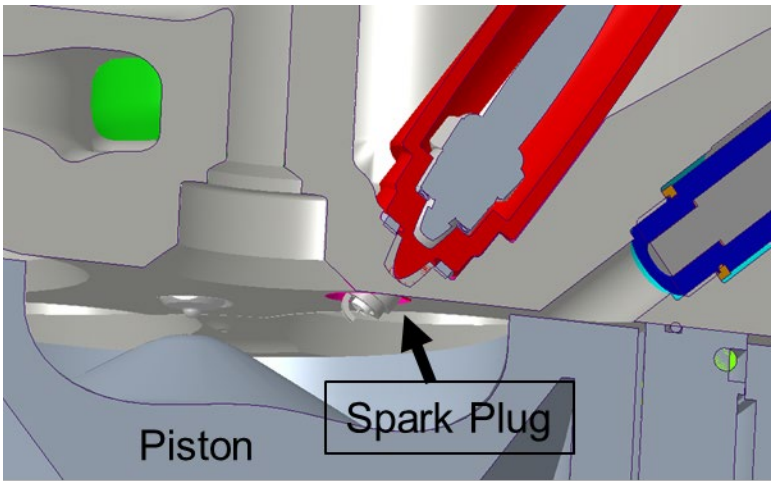

Figure I.17.2 Cross-section view of single-cylinder HD Caterpillar research engine head for FY 2020

Using the cylinder head available in FY 2019 (with the side-mounted spark plug location), spark timing sweeps were performed at 750 rpm engine speed and 3.2 bar gross indicated mean effective pressure (IMEP) for excess air ratios (lambda) of 0.8, 0.9, and 1.0. The range of spark timings available were recorded between

the early knock limit and the late combustion stability limit with 100 vol% ethanol (E100) and E10 87 anti-knock index (AKI) gasoline (gasoline blend containing 10% ethanol). Ethanol was tested as an initial baseline because of its high laminar flame speed and high octane number (and therefore high resistance to knock), followed by the E10 87 AKI gasoline.

For the particulate matter characterization between diesel and gasoline at high load in MCCI combustion, a 12.4 liter, six-cylinder Navistar engine with a 17:1 compression ratio was operated at 1,038 rpm and 14.1 bar brake mean effective pressure. The injection strategy tested was composed of a constant pilot injection start of injection and variable main injection start of injection. The combustion phasing, crank angle degree of 50% mass fraction burned, was held constant for both fuels at 6.3 degrees after top dead center (°aTDC) by adjusting the timing of the main start of injection. The pilot injection quantity was tested at 0%, 5%, 10%, and 15% of total fuel injected. Exhaust gas recirculation (EGR) was also tested at 0%, 9%, and 18%.

Results

Figure I.17.3 shows the spark timing sweeps of E100 and E10 87 AKI gasoline for lambdas of 0.82 (a), 0.9 (b), and 1.0 (c). The spark timing ranges were set by knock (described by the maximum amplitude of pressure oscillations of 0.75 bar) or combustion instability (defined by greater than 3% coefficient of variance of IMEP).

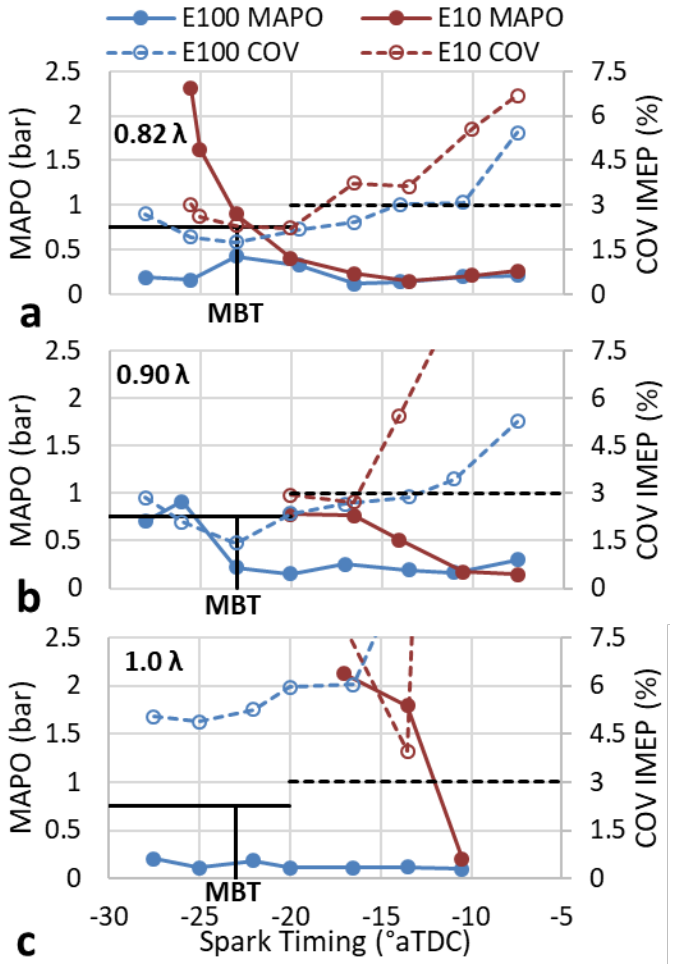

COV – coefficient of variation; MAPO – maximum amplitude pressure oscillation; MBT – maximum brake torque

Figure I.17.3 Spark timing sweeps of E100 (blue) and E10 87 AKI gasoline (red) at lambdas of 0.82 (a), 0.9 (b), and 1.0 (c)

In Figure I.17.3a, the early spark timing limit of ethanol at 0.82 lambda was limited not by knock intensity (solid blue line), but rather by combustion stability (dashed blue line) at approximately -27 °aTDC. The late spark timing limit of ethanol was limited by combustion stability at approximately -11 °aTDC, giving a spark timing range of 16 crank angle degrees (CAD) for ethanol. For the E10 87 AKI gasoline, the early spark timing was limited by knock intensity at approximately -22.5 °aTDC spark timing, and late spark timing was limited by combustion stability at approximately -18 °aTDC, giving a 4.5 CAD range of operable spark timings. This means the operable spark timing range of the engine at near-idle was reduced from 16 CAD with ethanol to 4.5 CAD with E10 87 AKI gasoline. At 0.9 lambda, the operable spark timing range for ethanol was reduced to 12.5 CAD and for E10 87 AKI gasoline to 3.5 CAD, largely because of knock limitations. When the engine was operated at stoichiometry, there was no spark timing for either fuel that allowed both knock-free and stable combustion operation, mostly owing to the reduced combustion stability of both fuels.

Detailed particulate emissions measurements were performed on a 12.4 liter Navistar multi-cylinder engine operating at high load in MCCI combustion. As has been observed by other researchers, gasoline operation generated approximately 30%–50% lower smoke and total particle number emissions at a similar reduced emissions level of oxides of nitrogen (NO_x) [3],[4] compared to diesel operation. Figure I.17.4 shows the particle size distribution measurements of the exhaust of the 12.4 liter Navistar multi-cylinder engine for 0% and 18% EGR rates and several pilot fuel injection quantities. It was observed that the 18% change in EGR rate increased the particle number concentrations and had the largest effect (versus fuel type and pilot injection quantity). At a given EGR rate, gasoline consistently generated fewer exhaust particle numbers than diesel fuel at this high-load, mixing-controlled operating condition. Varying the pilot fuel mass injection quantity from 0% to 15% did not have a significant effect on the particle size distribution measurements for either fuel.

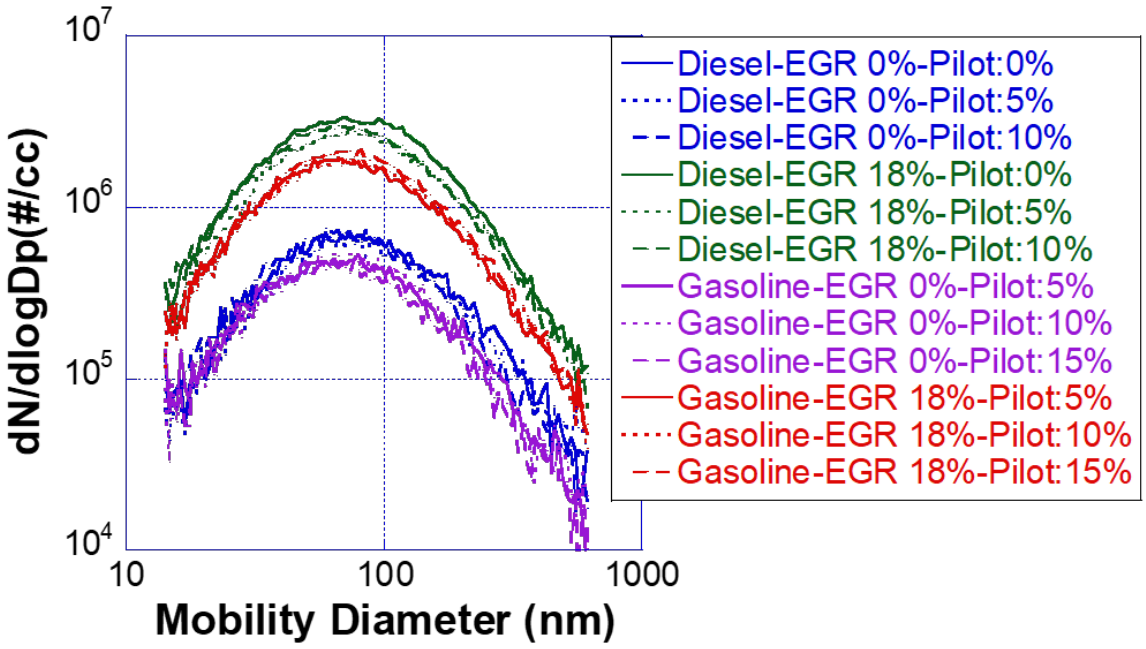

Figure I.17.4 Effects of EGR rate and pilot fuel injection quantity on the particle size distribution measurements of gasoline and diesel high-load GCI operation

During the course of engine testing, soot particles were also sampled on grids to be studied with a transmitting electron microscope. Figure I.17.5a shows an example micrograph of a gasoline soot aggregate and the diameter of one primary particle. This analysis was performed for many aggregates and primary particles for a given engine test point to generate a statistical mean primary particle diameter. The results of the primary particle diameter analysis are shown in Figure I.17.5b. Surprisingly, the mean diameters of the primary

particles of the soot aggregates were not significantly affected under these high-load MCCI combustion conditions for variations in fuel (diesel versus gasoline) or EGR rate (0%, 9%, and 18%). An additional Raman analysis of the crystalline structure revealed that it, too, was not significantly affected by the fuel type or EGR rate.

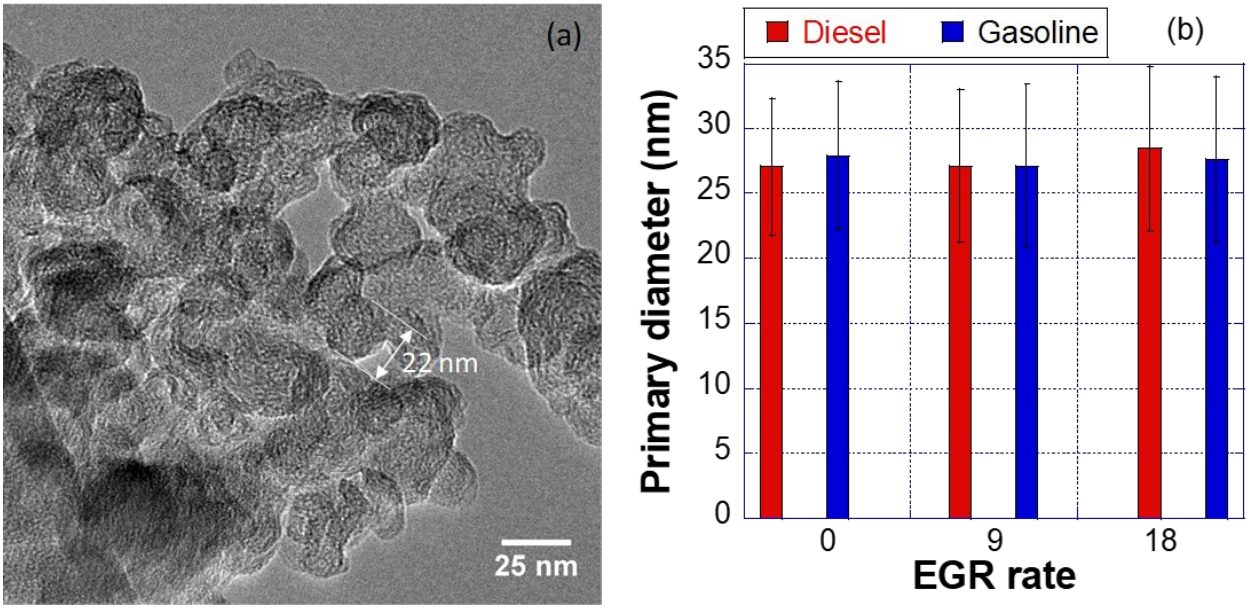

Figure I.17.5 Analysis of primary particle diameters for diesel and gasoline for three levels of EGR (0%, 9%, and 18%) using imaging with a transmitting electron microscope: (a) example micrograph of a gasoline MCCI soot aggregate and (b) the results of the primary particle diameter analysis

Conclusions

- There is a need to develop high-efficiency GCI MD and HD engines based on the projected increased demand and cost of diesel fuel.
- Stable and knock-free spark-ignited gasoline combustion was demonstrated at low load as a proof of concept on a high-compression-ratio (16.2:1) HD engine.
- A wider range of operable spark timings was observed with ethanol versus E10 87 AKI gasoline owing to the former's higher laminar flame speed and resistance to knock.
- Gasoline allowed for a significant reduction of both soot and particle number emissions under MCCI compared to diesel fuel.
- Despite the differences in chemical composition between diesel and gasoline, they produce soot aggregate particles of similar morphology from MCCI: shape of particle size distribution, mean diameter of primary particles, and crystalline structure.

References

1. Organization of the Petroleum Exporting Countries. 2018. 2018 OPEC World Oil Outlook (September). http://www.opec.org.

2. U.S. Energy Information Administration. 2019. Monthly Energy Review (April). www.eia.gov.

3. Zhang, Y., S. Sommers, Y. Pei, P. Kumar, et al. 2017. “Mixing-Controlled Combustion of Conventional and Higher Reactivity Gasolines in a Multi-Cylinder Heavy-Duty Compression Ignition Engine.” SAE Technical Paper 2017-01-0696. doi:10.4271/2017-01-0696.

4. Paz, J., D. Staaden, and S. Kokjohn. 2018. “Gasoline Compression Ignition Operation of a Heavy-Duty Engine at High Load.” SAE Technical Paper 2018-01-0898. doi:10.4271/2018-01-0898.

Acknowledgements

Hee Je Seong is a co-principal investigator on this project. Several people assisted in making this work successful: Jorge Pulpeiro, Clear Flame Engines, Timothy Rutter, Dave Bell, and Doug Longman.

I.18 Simulation Tools for HD Engine Applications (Argonne National Laboratory)

Sibendu Som, Principal Investigator
Argonne National Laboratory
9700 S. Cass Avenue
Lemont, IL 60439
E-mail: ssom@anl.gov

Michael Weismiller, DOE Technology Development Manager
U.S. Department of Energy
E-mail: Michael.Weismiller@ee.doe.gov

Start Date: October 1, 2018 End Date: September 31, 2019
Project Funding (FY19): $300,000 DOE share: $300,000 Non-DOE share: $0

Project Introduction

The focus of this project is to develop predictive computational tools that can guide the design of cleaner and more efficient diesel engines. In particular, significant efforts have been dedicated to advancing the state-of-the-art in multiphase flow and turbulent combustion models. Cavitation-induced erosion continues to be a concern that affects the lifetime and performance of fuel injection systems. To date, modeling tools have not been predictive in providing estimates of the likelihood and severity of erosion within fuel injectors. To address this growing need, the cavitation-induced erosion risk assessment (CIERA) tool was developed. By relating erosion severity to the cumulative energy absorbed by the solid material from repeated hydrodynamic impacts, CIERA provides improved predictions of relative erosion severity, critical erosion locations, and time to material failure over existing tools in the literature. This approach has now been validated over a range of Reynolds and cavitation number conditions, and best practices for predicting cavitation and cavitation-induced erosion using the mixture modeling approach within the CONVERGE computational fluid dynamics code have been outlined. The development and implementation of advanced flamelet models was continued in this part of the work. Improving the predictive capability of tabulated models will lead to significant cost and time reduction. Tabulated models can capture complex turbulence-chemistry effects along with large chemistry mechanisms at low computational costs. However, the simplifications and gaps in traditional tabulated models pose major challenges towards capturing slow-forming species and emissions. The ongoing research activities have led to the development of a hybrid tabulation methodology, representative interactive flamelet—in situ tabulation (RIF-ist). This hybrid method combines the accuracy of unsteady flamelet solvers and efficacy of tabulated models. In-depth model validation was carried out initially against data from a gas jet flame. This was followed by validations against spray flames, the Engine Combustion Network (ECN) [1] Spray A, in a large eddy simulation (LES) framework. The model is able to capture unsteady speciation and flame stabilization accurately. Further, detailed soot models were coupled with this hybrid framework. This involves solving the detailed soot moment equations within the flamelet space. The initial results show that the model was able to capture the overall trends in soot formation.

Objectives

In order to advance the state of the art in cavitation erosion modeling, the CIERA tool was developed to allow for qualitative and quantitative predictions of erosion likelihood and severity. The overall objectives of these efforts are summarized below.

- Develop in-nozzle cavitation erosion model for diesel injectors

- Validate erosion model against data from the literature and new data from the Advanced Photon Source
- Understand and evaluate potential sources of variability in erosion characteristics and injector wear (e.g., variations in injector geometry, needle motion, and fuel properties) and impacts on cavitation and erosion propensity and severity
- Develop "engineering best practices" to expedite internal nozzle flow simulations and enable industry to use the "real geometry" from injectors
- Formulate a hybrid tabulation methodology, RIF-ist, that combines the power of unsteady solvers with tabulated models, leading to higher-fidelity flamelet models
- Implement RIF-ist in CONVERGE code and perform extensive validation against different experiments, conditions, and fuels, and demonstrate reduction in computational costs
- Demonstrate the efficacy of the approach by predicting formation of slow-forming species and soot emissions in spray flames.

Fiscal Year 2019 Objectives

- Develop and implement framework to quantify the incubation period, or time before material removal
- Benchmark predictive capability of CIERA against standard approaches through comparison against available optical data from the literature
- Identify best practices for predicting cavitation and erosion using the mixture modeling approach
- Implement RIF-ist in the CONVERGE code
- Perform extensive quantitative validation against gas jet flames followed by high-pressure spray flames
- Couple RIF-ist approach with detailed soot models and demonstrate prediction of slow-forming species and soot emissions.

Approach

CONVERGE is utilized to model cavitation within the PREVERO Channel "I" geometry from the experimental work of Skoda et al. [2] for diesel fuel with pressure drops ranging from 125 bar to 225 bar. Because the experimental data set quantifies cavitation parameters, critical erosion sites, and incubation period, this case serves as a starting point to validate the fundamental underpinnings of the CIERA model. Key features of the channel geometry include a sharp inlet corner, constant diameter of 304 μm, and channel length of 995 μm. It is important to note that in the experiments of Skoda et al. [2], the channel was constructed from aluminum in order to accelerate the expected incubation period before material erosion. Cavitation and condensation are represented using the homogeneous relaxation model [3]. To represent the progressive damage to the material from repeated impacts, the energy stored by the material, E_{stored}, is calculated as a cumulative sum of all impact energies. In this approach, material failure would then be predicted when E_{stored} exceeds a critical threshold, which is dependent on solid material properties and impact strain rate. Pre-tabulation of flamelet libraries has led to significant cost reduction of computational fluid dynamics simulations. The dimensionality of the flamelet manifolds and the size of the flamelet libraries are constrained due to memory and computational limitations. This limits the applicability and predictive capability of flamelet models. The traditional RIF approach with multiple flamelets, on the other hand, involves online solution of flamelet equations and presumed probability density function integration at each computational cell, making it attractive, but computationally expensive and not suitable for LES with large cell counts. The novel in situ tabulation approach consists of creating a flamelet table at each computational time step using the unsteady

flamelet equations. The flamelets are then integrated based on their respective scalar dissipation rate histories. This approach is capable of including history effects and unsteady chemical kinetic effects as it involves the online solution of unsteady flamelets. Implementation and comprehensive validation of the new framework is carried out against gas jet flames as well as spray flames at high pressures. Due to the offsetting of presumed probability density function integration cost, the proposed framework is shown to be faster than the traditional RIF approach, and the speedup over RIF increases with an increase in the cell count.

Results

In order to identify best practices for modeling cavitation and erosion using the mixture modeling approach within CONVERGE, a numerical study [4] was performed to understand how selected physical and numerical parameters affect predictions of cavitation formation and erosion. Within this study, particular attention was paid to how the selected grid resolution, turbulence model formulation and near-wall treatment, fuel surrogate properties, and non-condensable gas content influence predictions of cavitation and erosion. Selected results from the study are shown in Figure I.18.1(a)–(c) [left], which highlights the influence of the assumed level of non-condensable gas concentration on the predicted peak pressures from cloud collapse events. Increases in the level of non-condensable gas are observed to delay impacts further downstream in the channel, with the strongest impacts predicted near the cavitation cavity length. Additionally, at any axial location along the channel, the number of recorded impacts can be seen to decrease with increased levels of non-condensable gas. In general, the increased concentration of nitrogen gas near the wall effectively "cushions" the hydrodynamic impact and reduces its loading on the wall. Therefore, based on qualitative agreement of impact locations with the experimental observations from Skoda et al. [2] and conservative estimates for solubility of air in iso-octane, a non-condensable gas concentration of Y_{N2} = 2e-05 was selected.

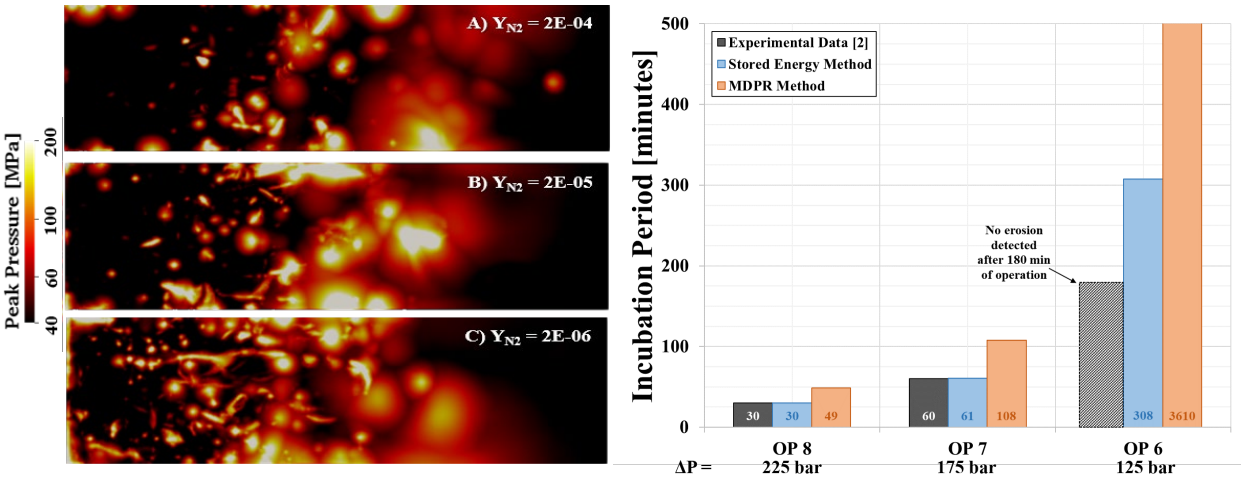

OP – Operating Point

Figure I.18.1 (left) The sensitivity of predicted pressure peaks from cloud collapse events to varying concentrations of non-condensable gas is shown for Y_{N2} levels of (a) 2e-04, (b) 2e-05, and (c) 2e-06. The recorded pressure peaks are shown on the bottom channel surface, where the flow moves from left to right, at t = 348 µs. (right) Comparison of the measured [2] and predicted erosion incubation periods using the stored-energy- and mean depth penetration rate (MDPR)-based methods across the range of flow conditions considered.

Using the best practices for modeling cavitation and erosion, the CIERA tool was further developed to link predictions of multiphase flow development with progress towards material failure. Existing erosion metrics in the literature, such as the MDPR parameter [5], can capture the impact of material properties on cavitation erosion risk. However, the simplified link between cavitation cloud collapse and material damage may limit its ability to predict erosion severity over a wide range of flow conditions. In particular, using the MDPR approach, collapse events with higher impact pressures are predicted to be more erosive than impacts with

lower impact pressures. However, it stands to reason that a smaller load applied for a sufficiently long period of time could be more erosive than a large load applied over a short duration. It is therefore clear that the influence of impact loading time scale on erosion severity cannot be captured by the MDPR approach. By developing a theoretical relationship between energy stored (E_{stored}) in the material and the incubation period, T, or time before first material removal, CIERA can be extended to provide improved predictions of cavitation erosion risk. Integration of the engineering stress-strain curve for a given material can yield an estimate for the total work, W_{total}, required for material failure. Material failure is marked by the local strain reaching the ultimate strain of the material. This calculation includes strain-hardening effects and allows for the erosion severity to be dependent on both fluid and solid material properties. The ratio of W_{total} to E_{stored} represents the number of such impacts that would be required to reach failure. Because E_{stored} quantifies the amount of energy absorbed by the material within a simulated timeframe, τ_{sim}, T is estimated by relating T to the time required for the material to absorb an amount of energy equal to W_{total}. This relationship highlights several key influential factors on erosion severity. First, a material with a high erosion resistance would be characterized by a large W_{total} value and would result in a long incubation period. Additionally, flow conditions that produce highly erosive impacts would yield large E_{stored} values and short incubation periods.

A comparison of the measured and predicted T across the three flow conditions is shown in Figure I.18.1 (right). For the highest pressure drop conditions (“OP 8” and “OP 7”), the incubation periods were experimentally observed to occur at 30 and 60 minutes, respectively. For the lowest pressure drop case (“OP 6”), no erosion was detected within the 180 minutes of operation. For the range of conditions, both the MDPR- and stored-energy-based approaches predict the correct trend of increasing erosion severity with increasing pressure drop. It is clear from Figure I.18.1 (right) that the stored energy metric more accurately represents the sensitivity of T to the change in flow conditions from OP 8 to OP 7, as indicated by the agreement of the model predictions within 2% of the experimentally measured T. When the MDPR-based approach is used to estimate T, the erosion severity is underpredicted, as indicated by the relatively larger T. Although both approaches predict incubation periods in excess of 180 minutes for the OP 6 condition, the sensitivity of T to the change in flow conditions from OP 7 to OP 6 conditions is drastically different for the two approaches. For the stored energy approach, the incubation period is predicted to increase by a factor of 5, whereas for the MDPR-based approach, T is predicted to increase by a factor of 33.

The RIF-ist approach [6] is first validated for a partially premixed methane gas jet flame in a Reynolds-averaged Navier–Stokes (RANS) framework. The modeling approach is then validated against an n-dodecane spray flame (ECN Spray A) at high pressures in a LES framework with a 103-species n-dodecane chemistry mechanism and 22 million cells. The model is able to capture ignition delays and flame liftoff over varying ambient temperature conditions, as shown in Figure I.18.2.

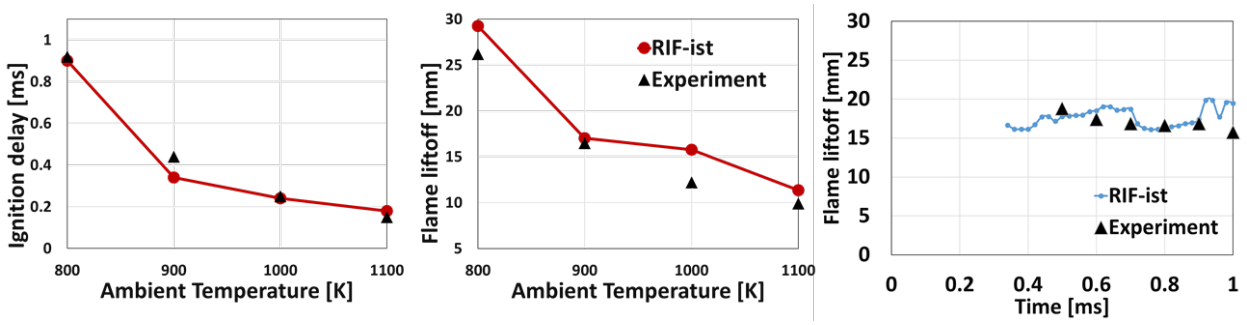

Figure I.18.2 Ignition delay (left) and flame liftoff (middle) for a range of ambient temperatures. (right) Temporal evolution of flame lift-off length at 900 K ambient temperature condition.

The ambient temperature was varied from 800 K to 1,100 K. The unsteady evolution of the flame liftoff and formation of intermediate species was also compared against experimental data. The model is able to predict these unsteady features accurately. Comparative studies showed that the in situ approach recovers the same solution as traditional RIF. Computational costs were reduced by 67% for coarse grid simulations due to the in situ tabulation approach. These results show that LES with unsteady, multi-flamelet RIF approach is now within the realm of engine simulations. Detailed analysis has been presented in [6].

A detailed soot modeling approach was implemented and coupled with the RIF-ist code. The detailed soot equations, i.e., four moment equations, were solved within the flamelet space using an unsteady formulation, along with a polycyclic aromatic hydrocarbon chemistry mechanism. This approach accounts for particle inception, coagulation, and surface growth. The model was tested in a RANS calculation at three ambient temperatures. It is able to capture the initial trends with respect to location of soot formation and time of soot inception over a range of temperature conditions, as shown in Figure I.18.3. The predictions in transient soot mass closely follow the experimental trend up to 1.5 ms. Further validation work will be carried out in future studies. The main findings of the turbulent combustion modeling work with the hybrid tabulation approach can be summarized as follows:

- Hybrid tabulation concept was proposed and implemented for RANS and LES calculations.
- Initial validations were carried out against gas jet flames. The model is able to predict the unsteady evolution of major and minor species in the gas jet flame.
- Detailed soot models were coupled with the RIF-ist framework to demonstrate its predictive capabilities for spray flames at high pressures.

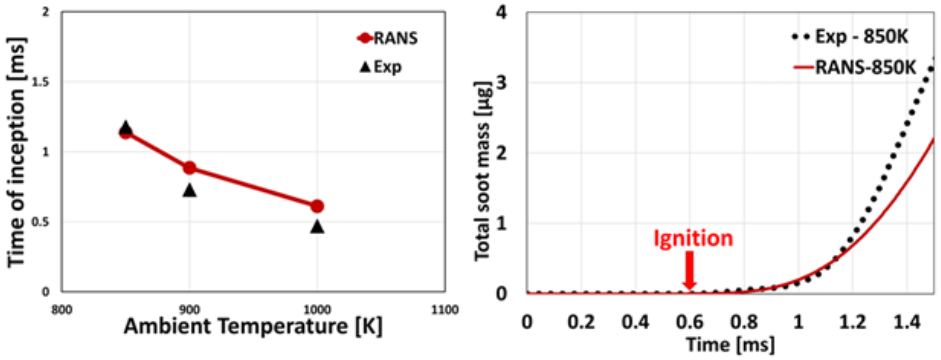

Figure I.18.3 (left) Time of soot inception at different ambient temperatures compared against experiments. (right) Transient soot mass formation at 850 K condition.

Conclusions

To inform best practices for modeling cavitation and erosion using the mixture modeling approach, the sensitivity of cavitation and erosion predictions to selected numerical and physical parameters was studied. In order to extend the predictive capability of CIERA to represent the progress towards material failure and erosion severity, a relationship between E_{stored} and the incubation period, T, was derived and implemented into the CONVERGE code. Comparison of the erosion predictions from the stored energy approach and the MDPR method with available experimental data for critical erosion sites and T revealed the following findings:

- While the MDPR-based approach is able to capture the influence of material properties on erosion progress, it is unable to capture the effect of loading timescale on the cavitation impact strength. In contrast, the stored energy method allows for a more accurate treatment of the cavitation collapse event by considering both the impact load and duration.

- The stored energy distribution was better able to represent the critical erosion sites relative to the peak impact pressure distribution, as well as the response of these locations to changes in the flow conditions.

- For the range of evaluated conditions, the stored energy approach was able to predict the correct sensitivity of T to changes in the flow conditions. Overall, the MDPR approach was found to underpredict the erosion severity.

The hybrid tabulation framework, the RIF-ist model, with multiple flamelets was implemented in the CONVERGE code. It is able to accurately capture the transient species evolution of the lifted gas jet flame. Quantitative comparisons were carried out against experimentally measured species mass fractions and temperatures along the centerline and different radial locations. Quantitative and qualitative results indicate that the flame liftoff is captured accurately. The ECN Spray A is modeled with RIF-ist, using a LES framework with a 60 μm minimum mesh size. The RIF-ist model is able to capture the onset and propagation of low-temperature heat release and transition to high-temperature ignition over a range of conditions. It was also demonstrated that the RIF-ist model predicts the same solution as the traditional RIF model. One of the main advantages of an unsteady solver is the capability to capture slow-forming species like soot precursors. The RIF-ist approach was coupled with a detailed soot modeling approach, where the moment equations were solved within the flamelet space. This approach was demonstrated for constant-volume spray simulations, and it predicted the soot onset time for a range of ambient temperatures. Overall, the RIF-ist approach has been comprehensively validated, and it enables the use of unsteady flamelet solvers for LES calculations. It will now be extended for further validations with respect to soot formation and multiple injections in future developments.

Key Publications

1. Magnotti, Gina M., Michele Battistoni, Kaushik Saha, and Sibendu Som. 2019. “Influence of Turbulence and Thermophysical Fluid Properties on Cavitation Erosion Predictions in Channel Flow Geometries.” *SAE Int. J. Adv. & Curr. Prac. in Mobility* 1, no. 2: 691–705.

2. Magnotti, Gina M., Michele Battistoni, Kaushik Saha, and Sibendu Som. 2019. “Linking Cavitation Collapse Energy with the Erosion Incubation Period.” Paper presented at 29th Conference on Liquid Atomization and Spray Systems, Paris, France (September 2–4).

3. Torelli, Roberto, Gina M. Magnotti, Sibendu Som, Yuanjiang Pei, and Michael L. Traver. 2019. “Exploration of Cavitation-Suppressing Orifice Designs for a Heavy-Duty Diesel Injector Operating with Straight-Run Gasoline.” SAE Technical Paper Series, September. https://doi.org/10.4271/2019-24-0126.

4. Kundu, P., J. Scroggins, and M.M. Ameen. 2018. “A Novel In Situ Flamelet Tabulation Methodology for the Representative Interactive Flamelet Model.” *Combustion Science and Technology*, 1–25.

References

1. Pickett, L., G. Bruneaux, and R. Payri. 2014. Engine Combustion Network, Sandia National Laboratories: Livermore, CA. http://www.ca.sandia.gov/ecn.

2. Skoda, Romuald, Uwe Iben, Alexander Morozov, Michael Mihatsch, Steffen Schmidt, and Nikolaus Adams. 2011. “Numerical Simulation of Collapse Induced Shock Dynamics for the Prediction of the Geometry, Pressure and Temperature Impact on the Cavitation Erosion in Micro Channels.” Paper presented at WIMRC 3rd International Cavitation Forum, University of Warwick, UK (July 4–6).

3. Bilicki, Z., and J. Kestin. 1990. “Physical Aspects of the Relaxation Model in Two-Phase Flow.” *Proc. R. Soc. Lond. A*. 428: 379–397.

4. Magnotti, Gina M., Michele Battistoni, Kaushik Saha, and Sibendu Som. 2019. “Influence of Turbulence and Thermophysical Fluid Properties on Cavitation Erosion Predictions in Channel Flow Geometries.” *SAE Int. J. Adv. & Curr. Prac. in Mobility* 1, no. 2: 691–705.

5. Franc, Jean-Pierre. 2009. “Incubation Time and Cavitation Erosion Rate of Work-Hardening Materials.” *ASME J. Fluids Eng*. 131.

6. Kundu, P., J. Scroggins, and M.M. Ameen. 2018. “A Novel *In Situ* Flamelet Tabulation Methodology for the Representative Interactive Flamelet Model.” *Combustion Science and Technology*, 1–25.

Acknowledgements

This research was funded by DOE's Office of Energy Efficiency and Renewable Energy's Vehicle Technologies Office under Contract No. DE-AC02-06CH11357.

The authors wish to thank Gurpreet Singh, Kevin Stork, and Michael Weismiller, technology managers at DOE, for their support.

The principal investigator gratefully acknowledges the contributions of Dr. Prithwish Kundu on developments related to turbulent combustion modeling and Dr. Gina Magnotti on two-phase flow and cavitation erosion modeling.

We gratefully acknowledge the computing resources provided by the Laboratory Computing Resource Center at Argonne National Laboratory, and Convergent Science, Inc., for providing the software licenses.

II Co-Optimization of Fuels and Engines

II.1 Co-Optima (Oak Ridge National Laboratory)

Robert Wagner, Principal Investigator
Oak Ridge National Laboratory
2360 Cherahala Boulevard
Knoxville, TN 37932
E-mail: wagnerrm@ornl.gov

Robert McCormick, Principal Investigator
National Renewable Energy Laboratory
15013 Denver West Parkway
Golden, CO 80401
E-mail: robert.mccormick@nrel.gov

Daniel Gaspar, Principal Investigator
Pacific Northwest National Laboratory
902 Battelle Boulevard
Richland, WA 99354
E-mail: daniel.gaspar@pnnl.gov

Paul Bryan, Principal Investigator
Sandia National Laboratories
7011 East Avenue
Livermore, CA 94550
E-mail: pfbryan@sandia.gov

Kevin Stork, DOE Technology Development Manager
U.S. Department of Energy
E-mail: Kevin.Stork@ee.doe.gov

Start Date: October 1, 2018 End Date: September 30, 2021
Project Funding (FY19): $8,100,000 DOE share: $8,100,000 Non-DOE share: $0

Project Introduction

The U.S. Department of Energy (DOE) Co-Optima initiative is accelerating the introduction of efficient, clean, affordable, and scalable high-performance fuels and engines. This first-of-its-kind effort is simultaneously tackling fuel and engine research and development to maximize light-duty (LD), medium-duty (MD), and heavy-duty (HD) vehicle fuel economy and performance. It is also mapping lower-cost pathways to reduce emissions, leveraging diverse domestic fuel resources, boosting U.S. economic productivity, and enhancing national energy security. These efforts target solutions with potential to improve today's common fuel and engine types as well as those that could lead to revolutionary technologies.

The importance of this work is emphasized by recent government and industry projections that show a significant role for liquid fuels and internal combustion engines in transportation continuing for many decades to come [1]. The objective scientific outcomes of this initiative are providing American industry and policymakers with the knowledge, data, and tools needed to decide which advances could prove most viable

and beneficial for drivers, businesses, and the environment. The initiative's scope aims to maximize potential impact within available resources and is subject to the following guidelines:

- Focus on liquid fuels only
- Identify candidate blendstocks to blend into petroleum base fuel at up to 30% by volume
- Consider only non-food-based biofuel feedstocks
- Assess well-to-wheel emissions and resource use for bioblendstock options (e.g., CO_2 emissions, water use)
- Consider hybridized and non-hybridized powertrain solutions
- Provide foundational science including data, tools, and knowledge for informed decision making
- Remain technology neutral and avoid "picking winners."

Co-Optima combines the diverse expertise and resources of nine National Laboratories, 14 university-led and one industry-led research activities with numerous additional university and industry partners. It is jointly funded by the DOE Office of Energy Efficiency and Renewable Energy's Vehicle Technologies Office (VTO) and Bioenergy Technologies Office (BETO). This report focuses only on the VTO-funded research performed during Fiscal Year (FY) 2019.

Objectives

Overall Objectives

Co-Optima research under the VTO program is addressing technologies and impact for near-term (2025–2030 target dates) and long-term (beyond 2030) improvements in fuel and engine technologies relative to a 2015 baseline vehicle:

- Identify co-optimized fuel and engine innovations that achieve a 35% increase in LD fuel economy, representing an improvement 10% greater than that expected from engine improvements alone.
- Improve the efficiency and emissions of MD/HD vehicles, including development of low-cost paths to meeting increasingly challenging criteria emissions regulations. A primary technical objective is achieving a 4% increase in MD/HD vehicle fuel economy through fuel and engine innovations capable of delivering brake thermal efficiency of nearly 60%.
- Coordinate with BETO to develop approaches that maximize the cumulative benefits of simultaneously co-optimizing fuel and engine efficiency while displacing petroleum fuels with biofuels.

Although this report focuses on VTO activities, BETO's complementary Co-Optima objectives are included here to better convey the scope of the initiative:

- Identify fuel blendstocks with significantly lower well-to-wheel CO_2 emissions than current fuels, while providing optimal fuel properties.
- Diversify resource base.
- Provide economic options to accommodate projected changing global fuel demand.
- Increase the supply of domestically sourced biofuels by up to 25 billion gallons per year.

In addition to technology-improvement objectives, Co-Optima aims to develop and make available data, tools, and objective knowledge to support informed decision making by stakeholders.

Fiscal Year 2019 Objectives

Co-Optima objectives for FY 2019 included the following:

- Document outcomes from Co-Optima boosted spark-ignition (SI) research in archival journal publications.
- Demonstrate performance of current fuel property metrics and identify promising new fuel property metrics to predict the performance of advanced compression ignition (ACI) combustion in LD engines.
- Complete a sensitivity analysis of ACI impacts on LD fuel economy across various engine speed/load ranges to identify the ranges over which ACI can have maximum impact.
- Characterize the potential of ducted fuel injection (DFI) combined with oxygenated fuels to reduce mixing-controlled compression ignition (MCCI) in-cylinder soot generation by at least one order of magnitude.

Approach

FY 2019 marked the start of Co-Optima's second and final 3-year phase. With boosted SI LD research completed in FY 2018, the initiative focused on LD multimode (MM) approaches that combine SI and other forms of combustion (e.g., ACI) to increase LD vehicle fuel economy. FY 2019 also marked the completion of much of the MD/HD MCCI research and increased focus on ACI combustion research. The MD/HD ACI research includes one focus on gasoline-range fuels and another focus on diesel-range fuels. The gasoline-range research is leveraging strong synergies with LD MM research to dramatically increase fundamental understandings of fuel molecular structure effects on fuel properties, mixing, soot formation, and autoignition. The general approach used successfully with the boosted SI research is being used to address the remaining research areas, with a focus on the following:

- Clarifying fuel property impacts on engine performance through combustion experiments and simulations—and revealing relationships between molecular structure and fuel properties.
- Identifying blendstocks (including but not limited to those sourced from biomass) with fuel properties needed to deliver specific LD or MD/HD improvements in engine efficiency, performance, and engine-out emissions through a tiered screening approach.
- Identifying barriers and opportunities to commercial introduction of new blendstocks, including technical factors of materials compatibility, emissions, and engine knock and performance as well as sustainability, economics, and scalability as determined through lifecycle analysis across a wide spectrum of metrics.

The *Project Introduction* section above lists the guidelines applicable across the Co-Optima approach.

Results

Below is a high-level summary of Co-Optima's three major research directions in FY 2019—LD MM combustion, MD/HD MCCI combustion, and MD/HD ACI combustion—as well as cross-cutting research important to all three. Much of the MD/HD fuels research in FY 2019 focused on fuels production under the BETO program; that research is not covered here but is covered in other publications and a year-in-review document (see *Key Publications* below). Additional VTO reports in this publication detail specific accomplishments from the three Co-Optima thrusts. The initiative had more than 90 milestones in FY 2019 and a go/no-go decision focused on DFI operation for MD/HD MCCI combustion.

Light-Duty Multimode Combustion

LD engine research focused on MM strategies that use boosted SI at high load and other advanced combustion modes, such as ACI, to improve engine efficiency and vehicle fuel economy at part load and thereby achieve high efficiency across a broad range of the vehicle drive cycle. ACI combustion has well-documented potential to improve efficiency and emissions under part-load operation, but it poses challenges that limit its use across an engine's speed/load range. MM SI/ACI combustion is projected to deliver substantial engine efficiency improvements across the speed/load range while maintaining power density and efficiency gains achieved through downsizing.

Co-Optima accomplishments in FY 2019 included the identification of critical fuel properties and expanded fundamental understanding of fuel-property impacts on ACI combustion modes relevant to MM operation through a focus on fuel-dependent autoignition kinetics, flame initiation and propagation, spray development, mixture formation, combustion development, and soot formation processes. Example key accomplishments from FY 2019 include the following:

- An improved understanding of the impact of ACI operational range and efficiency impacts on simulated fuel economy for vehicles with MM engines. Simulations showed that, depending on operational range and engine efficiency, there is a point of diminishing returns that is important for guiding the operational-range focus points of the MM research.

- New insights into critical fuel properties that expand the performance of ACI combustion modes with minimal impact on boosted SI performance. Experiments showed that different approaches may require different fuel properties, the correct properties for predicting ACI performance have not been identified, or both. For example, established fuel properties such as research octane number and octane index showed poor or no correlation with the intake temperature required for autoignition and were not predictive of autoignition under "beyond motor octane number" conditions or across a full range of fuel chemistries. However, research octane number and octane index were good predictors of performance for spark-assisted ACI approaches.

- Significant advances in the development of new fuel properties, characterization of fuel reactivity, and prediction of soot formation for different fuel blends. This included developing new methods for predicting ignition delay and phi-sensitivity from molecular structure to accelerate fuel screening; correlating fuel reactivity in ACI engines based on experiments in a Cooperative Fuel Research engine under homogeneous charge compression ignition conditions; and providing a new understanding of blending effects on autoignition, evaporation, hyper-boosting, and—ultimately—engine performance.

- Novel simulation methods and model improvements for better predicting impacts of fuel and engine technologies on engine performance. This includes improved prediction of fuel-property impacts on soot formation, engine knock, flash boiling, and overall MM performance.

Medium- and Heavy-Duty Mixing-Controlled Compression Ignition Combustion

Diesel-fueled engines using MCCI combustion, which are widely employed for commercial transportation, are extremely efficient but require costly emissions-control technologies. Improved MCCI technologies and low-net-carbon blendstocks hold potential to balance high efficiency with reduced engine-out emissions while maintaining critical fuel characteristics such as high energy density, which is very important for commercial applications.

Major Co-Optima accomplishments in FY 2019 focused on DFI and biofuel candidates with potential to reduce particulate matter emissions. The DFI research had a go/no-go decision in FY 2019 to determine whether, under DFI operation, adding 25% (by volume) of an ether or ester oxygenate to a reference diesel fuel can decrease spatially and cycle-averaged in-cylinder soot incandescence by an order of magnitude relative to the neat diesel reference fuel. The outcome of this decision point was a "go" based on results that showed that combining DFI with oxygenated fuel blends reduced soot formation by two orders of magnitude under

conditions that also lower nitrogen oxides emissions, suggesting a path to the next generation of high-efficiency, cost-effective, high-performance MCCI engines with decreased emissions-control requirements. There is also significant research on bioblendstocks in the MCCI space under the BETO portfolio.

Medium- and Heavy-Duty Advanced Compression Ignition Combustion

ACI combustion may offer further opportunities to balance engine performance with engine-out emissions for MD/HD vehicles. Relevant research includes exploring the potential of gasoline- and diesel-range fuels along with advances in engine technologies to expand stable ACI combustion over a wide speed/load range, controlling engine-out emissions, and ensuring high engine power density. This research is expanding the foundational understanding of fuel properties for advanced combustion modes while leveraging current and ongoing findings from the MCCI and LD MM research. Many of the accomplishments listed under MCCI and LD MM research have direct applicability to the MD/HD ACI combustion research. There is also significant research on bioblendstocks in the MD/HD ACI space under the BETO portfolio.

Crosscutting Research

The Co-Optima team has developed a suite of state-of-the-art facilities and computational tools to advance crosscutting fuel and engine research. This includes broad experimental and simulation capabilities that are unique and complementary across the laboratory complex. The experimental capabilities provide critical data on reaction kinetics for fuel ignition and soot formation, which are used to validate detailed kinetic models and clarify how molecular structure impacts fuel properties. Researchers build on this understanding using computational tools for predicting fuel properties and performance, and that help identify new high-performance blendstocks as well as feasible production routes from biomass. Imaging and characterization tools are used to illuminate how new fuels will change the spray/mixture preparation process, and data on the impact of fuel properties on all engine combustion modes are captured using high-fidelity predictive simulations. Experiments are also performed to understand how new fuel compositions could impact emission-control devices.

Conclusions

The Co-Optima initiative continues to provide critical knowledge on fuel chemistry and the synergies between fuel and engine technologies that can improve engine efficiency while reducing engine-out emissions. This new knowledge has spurred promising research directions and led to unanticipated observations—for example, established fuel properties predict performance for some ACI approaches but not others—that have been important for developing research plans for FY 2020 and beyond. Recent Co-Optima accomplishments have also significantly improved the state of the art in fuel kinetics and engine simulations. To maximize impact to stakeholders and the technical community, the more than 100 Co-Optima researchers regularly publish, present at technical forums, engage with stakeholders through monthly calls, and undergo a rigorous annual merit review.

Key Publications

Co-Optima researchers have continued their strong scientific publication track record with more than 30 peer-reviewed journal articles and peer-reviewed conference papers published during FY 2019. A new publications database has been made available online (https://www.energy.gov/eere/bioenergy/co-optima-publications-library-0) and currently has well over 150 entries. In FY 2019, especially notable publications include the "Top 10 Report," which describes an assessment of 400 biofuel-derived molecules and identifies the top candidates to blend with petroleum fuel to increase boosted SI engine efficiency. In addition, Co-Optima researchers at Lawrence Berkeley National Laboratory and Sandia National Laboratories contributed to a study of high-octane ketone production published in *Nature Communications*. Below are references for these publications and three other representative publications.

1. Gaspar, D., B. West, D. Ruddy, et al. 2019. "Top Ten Blendstocks Derived from Biomass for Turbocharged Spark Ignition Engines: Bio-Blendstocks with Potential for Highest Engine Efficiency." Technical Report. U.S. Department of Energy, Washington, DC. doi:10.2172/1567705.

2. Yuzawa, S., M. Mirsiaghi, R. Jocic, et al. 2018. "Short-Chain Ketone Production by Engineered Polyketide Synthases in *Streptomyces albus*." *Nat Commun* 9: 4569. doi:10.1038/s41467-018-07040-0.

3. Ratcliff, M., B. Windom, G. Fioroni, et al. 2019. "Impact of Ethanol Blending into Gasoline on Aromatic Compound Evaporation and Particle Emissions from a Gasoline Direct Injection Engine." *Applied Energy* 2150: 1618. doi:10.1016/j.apenergy.2019.05.030.

4. Lopez Pintor, D., J. Dec, and G. Gentz. 2019. "Φ-Sensitivity for LTGC Engines: Understanding the Fundamentals and Tailoring Fuel Blends to Maximize This Property." SAE Technical Paper. doi:10.4271/2019-01-0961.

5. Debusk, M., S. Curran, S. Lewis, et al. 2019. "Impacts of Air-Fuel Stratification in ACI Combustion on Particulate Matter and Gaseous Emissions." *Emiss. Control Sci. Technol.* 5: 225. doi:10.1007/s40825-019-00122-5.

References

1. "Annual Energy Outlook 2019 with Projections to 2050." U.S. Energy Information Administration, U.S. Department of Energy, January 2019, https://www.eia.gov/outlooks/aeo/pdf/aeo2019.pdf.

Acknowledgements

The authors gratefully acknowledge the contributions from Alicia Lindauer of DOE's BETO and the more than 100 Co-Optima researchers, technical team leads and their deputies, as well as the Co-Optima steering committee, external advisory board, and board of directors. Team leads and deputies include Anthe George (High Performance Fuels Team Lead), Derek Vardon (High Performance Fuels Team Deputy), Troy Hawkins (ASSERT Team Lead), Avantika Singh (ASSERT Team Deputy), Magnus Sjoberg (Advanced Engine Development Team Lead), Josh Pihl (Advanced Engine Development Team Deputy), Jim Szybist (Fuel Properties Team Lead), Gina Fioroni (Fuel Properties Team Deputy), Sibendu Som (Simulation Toolkit Team Lead), and Ray Grout (Simulation Toolkit Team Lead). The authors also gratefully acknowledge emeritus Co-Optima Leadership Team members John Farrell and Chris Moen, who departed the initiative in FY 2019—we thank you for your leadership.

II.2 Engine Efficiency Potential of High-Octane Renewable Fuels in Multi-Cylinder Engines (Oak Ridge National Laboratory)

C. Scott Sluder, Principal Investigator
Oak Ridge National Laboratory (ORNL)
2360 Cherahala Boulevard
Knoxville, TN 37932
E-mail: sluders@ornl.gov

Kevin Stork, DOE Technology Development Manager
U.S. Department of Energy
E-mail: Kevin.Stork@ee.doe.gov

Start Date: October 1, 2018 End Date: September 30, 2021
Project Funding (FY19): $360,000 DOE share: $360,000 Non-DOE share: $0

Project Introduction

Engine downsizing is an important facet of increasing vehicle fuel efficiency while maintaining performance at a level that customers demand. As the original equipment manufacturers have begun to increase the power density of smaller displacement engines, the onset of knock has emerged as an important challenge that currently limits the degree to which engine displacement (and fuel consumption) can be reduced in a practical automobile. A study by researchers from AVL Powertrain Engineering Inc., BP Products North America Inc., Deere & Company, Ford Motor Company, and ICM Inc. has shown that increasing the fuel octane rating can allow substantial engine efficiency improvements at the knock limit [1]. Improvements were shown to be enabled through both a chemical octane effect as well as a charge-cooling effect derived from the heat of vaporization of the fuel. The charge cooling effect was shown to provide approximately the same order-of-magnitude improvement as the octane increase effect. Other studies have begun to show similar results.

The U.S. certification driving cycles on which fuel economy ratings are based typically result in engines operating well away from their peak efficiency values. Engine downsizing results in engines operating at higher loads more often during normal driving, thus reducing throttling and other losses and moving towards higher efficiency areas of their operating maps. However, in order to satisfy consumer demands, these engines must be able to deliver performance similar to non-downsized engines. These performance demands can cause downsized engines to operate in knock-limited regimes more frequently. In the past, some vehicles have utilized “Premium” fuel for its potential to improve performance, but these engines were not typically downsized to use the added anti-knock capability of the premium-grade fuel to increase efficiency.

One common technique that is used to protect the engine from damage when it reaches the knock limit is to retard the ignition timing. Retarding the timing has the effect of moving the onset of combustion to a cooler, lower pressure point, thus removing the knocking condition. However, this technique also results in a loss in fuel efficiency. Thus, when an engine reaches the knock limit, fuel efficiency is reduced in favor of engine durability. Increasing the knock limit through changes in fuel formulation, such as increasing the octane rating, offers the potential to improve fuel efficiency under these conditions and enable further engine downsizing. This project will study how differing high-octane fuel formulations can be used to enable increased engine efficiency and estimate the magnitude of the effect that increased engine efficiency has on vehicle fuel economy.

Objectives

Overall Objective

Provide assessments of the potential benefits offered by improving gasoline octane ratings to support technoeconomic evaluations of potential future biofuel formulations in the United States. Focus on aspects of high-load, boosted spark ignition operation as a part of a multi-mode combustion strategy that utilizes advanced compression ignition at part-load conditions to improve efficiency.

Fiscal Year 2019 Objectives

- Complete publication of the U.S. DRIVE (United States Driving Research and Innovation for Vehicle efficiency and Energy sustainability) Fuels Working Group High-Octane Fuels Study Report.
- Determine the relationship between fuel properties and the R factor for fuel economy calculation, as this is a critical aspect that may limit successful deployment of future biofuel formulations.
- Initiate study to examine whether boosted spark ignition operation at high loads and speeds is limited by motor octane rating rather than research octane rating.

Approach

ORNL will investigate the potential fuel economy impacts of the use of higher-octane gasoline blends. ORNL is partnering with Ford Motor Company and will make use of an Ecoboost 1.6L engine to examine the potential fuel efficiency benefits of octane improvement in a downsized engine application. Ford has provided ORNL with engine and engineering support for the 1.6L engine. Vehicle modeling using Autonomie will be used to estimate vehicle-level impacts from data gathered during engine-based studies. Hybridization presents opportunities to improve market penetration of engines designed to use high-octane fuels. These opportunities are possible through the use of hybridization strategies that can mitigate the performance penalties that occur when an engine designed for use with high-octane fuels is operated using a fuel with lower octane rating. These strategies will be investigated alongside conventional vehicles using vehicle models to estimate the potential fuel economy benefits that are possible. In the studies for the project, data will be collected using fuel formulations that explore the co-optimization program's central fuel hypothesis: that fuel performance and engine efficiency derive from the measured combustion properties of the fuel. The project will also study fuels blended using the Tier 3 blendstock candidates identified by the program and provide data in support of the Tier 3 evaluations by other teams.

Results

A study begun in previous years with the U.S. DRIVE Fuels Working Group was completed in Fiscal Year 2019 with the publication of three reports detailing the study findings. The first of these reports detailed the experimental and modeling work that established the potential benefits of octane rating on efficiency, tailpipe CO_2 emissions, and fuel economy of the light-duty vehicle fleet for a range of potential future biofuel formulations [2]. The amount of octane improvement that enables a unit increase in compression, or ON/CR, was a significant factor in determining potential benefits that can be obtained. As the ON/CR is reduced from 5.6 to 3.0, higher levels of ethanol blending can simultaneously achieve both reductions in energy use as well as increases in volumetric fuel economy. Non-oxygenated biofuel pathways to high-octane fuels similarly benefit from low ON/CR ratio to reduce the tailpipe CO_2 emissions produced when these fuels are used. All high-octane fuels achieved reductions in energy consumption regardless of the ON/CR level.

The study showed that volumetric fuel economy parity of 20% ethanol blends with the baseline 10% ethanol fuel could be achieved, but that 30% ethanol blends could not achieve parity. Blending higher levels of ethanol improves efficiency, but if the blend fraction is too high, fuel economy losses may still occur. These results provide more certainty about the optimal range of ethanol blending for high-octane fuels to achieve both fuel economy and efficiency improvements.

One critical issue facing the adoption of any new high-octane fuel that uses oxygenate blending is to understand and resolve calculation of fuel economy values that are used for corporate average fuel economy certification by the automotive manufacturers. Blending oxygenates into gasoline typically reduces the volumetric energy content of the fuel, which in turn causes a degradation of fuel economy. This degradation can occur even if engine efficiency increases if the efficiency gain is not high enough to offset the volumetric energy content reduction. The R factor is used in certification fuel economy calculations to describe how vehicle fuel economy responds to marginal changes in volumetric energy content.

Several stakeholders have recently been advocating for an R value of unity, though there have been no studies to date that demonstrate a value of unity is typical for modern vehicles. A brief study was undertaken to provide a greater degree of understanding of the relationship between fuel properties, fuel economy, and R factor value [3].

An R factor of unity means that a vehicle uses the same amount of energy to complete a given drive cycle regardless of what fuel is used to provide the energy. Conducting a sufficiently precise experimental study using a variety of fuels to prove or disprove this hypothesis is nontrivial and may not be possible given the large number of fuel properties that can impact engine efficiency and that all change simultaneously with differences in fuel formulation. Hence, an analytical approach was used. The analytical approach allowed analysis of the energy use of the engine and vehicle in such a way that other fuel property impacts could be considered separately from that of volumetric energy content.

R* was defined as the percent change in engine efficiency divided by the percent change in volumetric heating value at a specific engine condition. R is the cycle-averaged R* value for a given drive cycle. Figure II.2.1 shows how R* varies with engine load for a 1.6-liter spark-ignited engine and considering a change from an ethanol-free certification fuel to one that contains 10% ethanol. The study showed that an R* value of unity is never obtained; it is thermodynamically impossible when the engine load is controlled by throttling. The nonlinear nature of the R* trend with engine load also means that R cannot be generalized, since the cycle-average R* value for a given vehicle depends on the load conditions specific to the drive cycle and the difference in fuel energy content between the test and reference fuels. A more economical and convenient means of determining R factor value for each application was outlined for potential exploration. Alternative approaches to establishing fuel economy values for corporate average fuel economy certification were also proposed.

The Ford EcoBoost 1.6L engine that has been used to support the U.S. DRIVE and other studies was moved to a new cell and re-installed to support a study to investigate conditions where boosted spark ignition engines may be limited by motor octane number rather than research octane number. This situation may emerge at high speeds and loads where spark ignition mode is needed to retain power density in multi-mode engines that use advanced compression ignition at low loads for improved efficiency. Fuels to support the motor octane number study have also been acquired.

Instrumentation upgrades have been completed that will enable a related kinetic modeling task to utilize the data from the motor octane number study to examine conditions beyond those that can be studied experimentally.

Conclusions

- U.S. DRIVE Fuels Working Group reports were published that showed the importance of ON/CR as a factor influencing volumetric fuel economy parity for oxygenated fuels and tailpipe CO_2 emissions parity for non-oxygenated fuels.
- Ethanol blends up to 20% could achieve fuel economy parity with a 10% ethanol blend baseline fuel, but efficiency gains for a 30% ethanol blend were insufficient to prevent fuel economy degradation caused by the reduced energy content of the 30% ethanol blend.

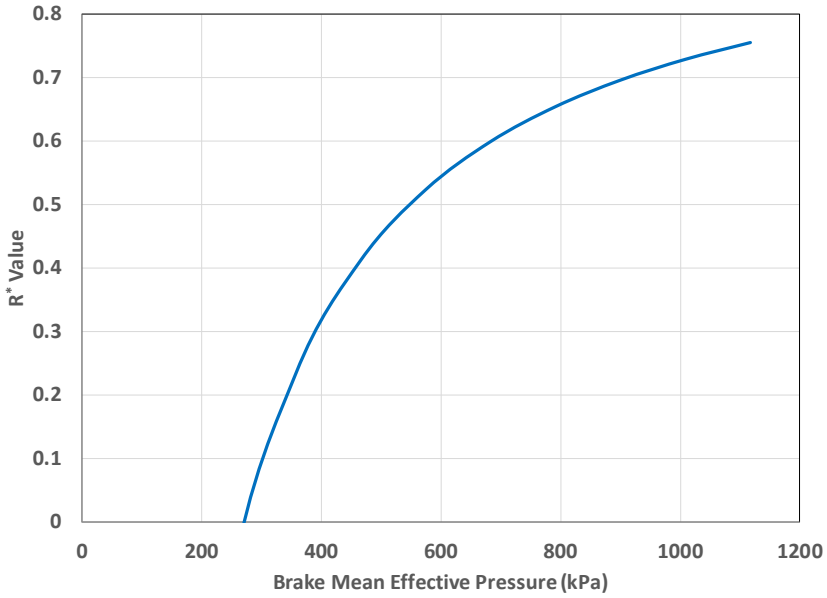

Figure II.2.1 R* values versus engine load (expressed as brake mean effective pressure) for a switch from an ethanol-free certification fuel to a 10% ethanol certification fuel for a 1.6-liter engine

- R factor values of unity are not thermodynamically defensible; R factor is dependent upon the vehicle, drive cycle, and fuel being used and cannot be generalized across the light-duty fleet.

Key Publications

1. Sluder, C. Scott, David E. Smith, James E. Anderson, Thomas G. Leone, and Michael H. Shelby. 2019. "U.S. DRIVE Fuels Working Group Engine and Vehicle Modeling Study to Support Life-Cycle Analysis of High-Octane Fuels." Available online at https://www.energy.gov/eere/vehicles/downloads/us-drive-fuels-working-group-high-octane-reports.

2. Sluder, C. Scott. 2019. "Analytical Examination of the Relationship Between Fuel Properties, Engine Efficiency, and R Factor Values." *SAE Int. J. Adv. & Curr. Prac. in Mobility* 1 (2): 706–716.

References

1. Stein, Robert A., Dusan Polovina, Kevin Roth, Michael Fost, Michael Lynskey, Todd Whiting, James E. Anderson, Michael H. Shelby, Thomas G. Leone, and Steve Vandergriend. 2012. "Effect of Heat of Vaporization, Chemical Octane, and Sensitivity on Knock Limit for Ethanol – Gasoline Blends." *SAE Int. J. Fuels Lubr.* 5 (2), doi: 10.4271/2012-01-1277.

2. Sluder, C. Scott, David E. Smith, James E. Anderson, Thomas G. Leone, and Michael H. Shelby. 2019. "U.S. DRIVE Fuels Working Group Engine and Vehicle Modeling Study to Support Life-Cycle Analysis of High-Octane Fuels." Available online at https://www.energy.gov/eere/vehicles/downloads/us-drive-fuels-working-group-high-octane-reports.

3. Sluder, C. Scott. 2019. "Analytical Examination of the Relationship Between Fuel Properties, Engine Efficiency, and R Factor Values." *SAE Int. J. Adv. & Curr. Prac. in Mobility* 1 (2): 706–716.

II.3 Characterizing BOB Impacts and Limits within Octane Index (Oak Ridge National Laboratory)

James Szybist, Principal Investigator
Oak Ridge National Laboratory (ORNL)
2360 Cherahala Blvd.
Knoxville, TN 37922
E-mail: szybistjp@ornl.gov

Kevin Stork, DOE Technology Development Manager
U.S. Department of Energy
E-mail: Kevin.Stork@ee.doe.gov

Start Date: October 1, 2017 End Date: September 30, 2020
Project Funding (FY19): $375,000 DOE share: $375,000 Non-DOE share: $0

Project Introduction

An organizing principle of the Co-Optimization of Fuels and Engines ("Co-Optima") initiative is the central fuel properties hypothesis, which states that fuel properties provide an indication of the performance of the fuel, regardless of the fuel's chemical composition. By adopting this framework for spark ignition (SI) engines, it was possible to quantify the relative value of the different fuel properties as they relate to potential efficiency improvements through the use of an efficiency merit function, which is discussed in detail in Reference [1]. However, during Fiscal Year (FY) 2018 investigations, it was found that the performance-based fuel properties that are used in the merit function, specifically using research octane number (RON) and octane sensitivity (S) to calculate the octane index (OI), do not enable performance to be predicted in the high-efficiency advanced compression ignition (ACI) combustion strategies. Instead, it was found that there was a much stronger correlation to fuel chemistry, with alkylates and alcohols behaving in accordance with OI, aromatics requiring a higher temperature than is predicted by OI, and olefins requiring a lower temperature than is predicted by OI. One of the confounding issues with the FY 2018 results is that studies were performed using an engine that relied on very high intake manifold temperatures to enable ACI combustion, which while useful in a laboratory setting to study fuels, could be governed by different kinetics than an ACI combustion strategy that relied on high concentrations of trapped residuals. Another confounding issue is that the fuels studied in FY 2018 often had high concentrations of individual chemical components; thus, there remain questions about whether the findings are attributable to individual species or broader chemical classes. To remove these confounding issues, in FY 2019 we partnered with General Motors Company (GM) and Shell Global Solutions (Shell). GM is supporting this work by providing a single-cylinder research engine that is capable of producing an ACI combustion event that is more production-relevant than what was investigated in FY 2018. Shell is supporting this work by producing refinery-relevant fuel blends that are tailored to providing insights on fuel chemistry.

Objectives

Overall Objective of Co-Optima

The overall objective of Co-Optima is to co-develop engines and fuels to accelerate the development of efficient combustion modes and the utilization of diverse fuel sources.

Fiscal Year 2019 Objectives

- Install a new single-cylinder engine to support multimode combustion research for Co-Optima at ORNL that is capable of operating in a production-intent ACI combustion strategy
- Develop a fuel matrix that is representative of fuels that are possible to make in a refinery (rather than using high concentrations of single-component fuels)

- Demonstrate fuel property differences in both ACI and SI combustion strategies using the new single-cylinder engine platform at ORNL.

Approach

This project primarily uses experimental engine investigations combined with supporting chemical kinetic simulations to understand fuel performance and autoignition. Developing an understanding of the fuel autoignition propensity is critical to the development of higher efficiency engines. This is because high efficiency is achieved when the engine pushes the fuel to the autoignition limit, both with SI engines and knock, and with ACI events where autoignition of the fuel is necessary. However, conventional metrics, such as RON and motor octane number (MON), do not fully describe the way that a fuel will behave in an engine. This is because the RON and MON tests represent two distinct pressure-temperature trajectories, and modern engines push beyond these limits. The trajectory of the engine dictates what governing autoignition reactions the fuel will encounter. Thus, fuel A may be more or less prone to autoignition relative to fuel B depending on the operating condition. This is illustrated in Figure II.3.1.

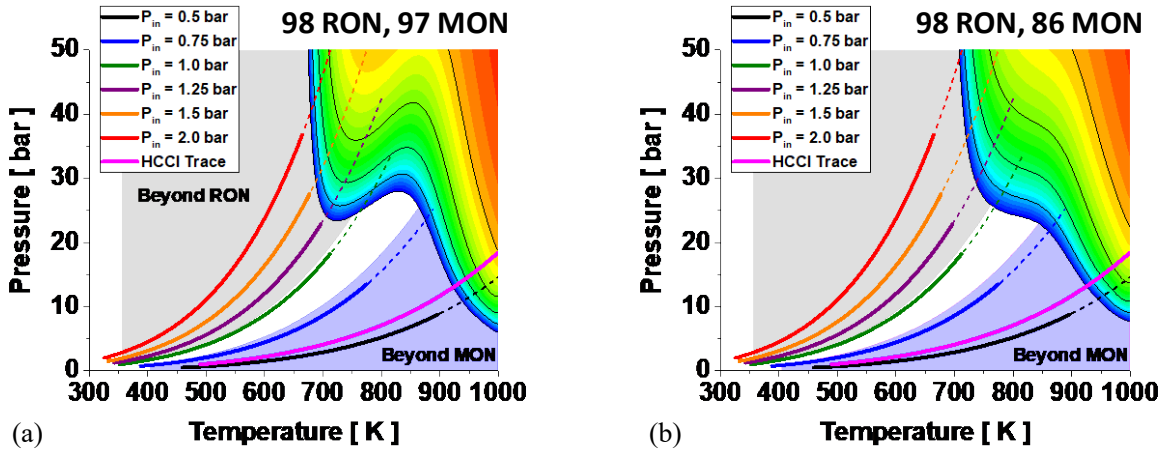

HCCI – homogeneous charge compression ignition

Figure II.3.1 Pressure-temperature trajectories in an engine as a function of intake manifold pressure (P_{in}) overlaid on the constant volume ignition delay contours for two different fuels: (a) an alkylate fuel with RON = 98 and MON = 97, and (b) an aromatic fuel with RON = 98 and MON = 86. More details on the fuels and methodology used to calculate the ignition delay contours can be found in Reference [2].

This project utilizes an experimental single-cylinder research engine from GM to traverse the pressure-temperature domain that includes boosted SI operation, naturally aspirated SI operation, and ACI operation. In doing so, a wide variety of fuels that are of interest to the multimode effort within Co-Optima are investigated to develop a better understanding of where the RON, MON, and OI metrics are insufficient, and to develop an understanding of the extent of a kinetic basis for these metrics. These fuels include the Co-Optima core fuels [3] as well as a series of five refinery-relevant fuels supplied by Shell.

Results

A new single-cylinder engine supported by GM was delivered and installed at ORNL during FY 2019 for investigations into multimode combustion in Co-Optima. The engine is suitable for ACI combustion because of its low charge motion combustion chamber design, combined with a high compression ratio, high authority cam phasing, and centrally mounted direct-injection fuel injection. The engine is equipped with a cylinder pressure transducer for combustion analysis, as well as high-speed pressure transducers in the intake and exhaust manifolds to study the engine breathing. It is equipped with a laboratory air handling system that

allows boost and backpressure to be applied to the engine to simulate a turbocharger. The engine is pictured in Figure II.3.2, and the engine specifications are provided in Table II.3.1.

Figure II.3.2 Picture of the new single-cylinder engine installation at ORNL, supported by GM, to investigate multimode combustion for Co-Optima

Table II.3.1 Engine Specifications

Bore [mm]	86.0
Stroke [mm]	95.1
Displacement [liters]	0.552
Connecting Rod [mm]	166.7
Compression Ratio [-]	12.0:1
Fueling	Bosch 8-hole solenoid-type, central mount direct injection

In addition to installing the new single-cylinder engine at ORNL, fuel blends were acquired from Shell. Similar to the Co-Optima core fuels [3], the fuel blends from Shell include fuels that are high in saturates, olefins, aromatics, and ethanol. However, instead of relying on a small number of individual components, these fuels better represent the mixtures of each chemical family that can be found in a refinery stream. The fuels from Shell are included as part of a fuel matrix that also includes the Co-Optima core fuels, a research grade fuel intended to represent regular grade gasoline with 10% ethanol (RD5-87), and iso-octane. The fuel specifications for the complete test matrix are shown in Table II.3.2.

Table II.3.2 Fuel Specifications

	RON	MON	S_{octane}	Saturates	Aromatics	Olefins	Ethanol
alkylate$_{Co\text{-}Optima}$	98.0	96.6	1.4	100.0	0.0	0.0	0.0
E30$_{Co\text{-}Optima}$	97.4	86.6	10.8	57.1	5.0	8.1	30.6
aromatic$_{Co\text{-}Optima}$	98.1	87.8	10.3	65.0	30.8	4.2	0.0
olefinic$_{Co\text{-}Optima}$	98.2	88.0	10.2	58.1	10.6	31.3	0.0
cyclo-alkane$_{Co\text{-}Optima}$	98.0	87.1	10.9	70.3	28.2	1.5	0.0
BOB$_{Shell}$	87.3	83.3	4.0	79.0	13.3	5.5	0.0
saturate$_{Shell}$	94.6	90.8	4.0	91.5	5.4	2.3	0.0
aromatic$_{Shell}$	94.8	86.8	8.0	56.9	37.4	4.1	0.0
olefinic$_{Shell}$	95.4	86.6	8.8	62.5	10.2	25.6	0.0
ethanol$_{Shell}$	95.0	87.1	7.9	68.5	11.7	4.8	13.1
RD5-87	92.0	84.4	7.6	65.5	19.6	5.0	9.9
Iso-octane	100.0	100.0	0.0	100.0	0.0	0.0	0.0

E30 – gasoline blend with 30% ethanol; BOB – blendstock for oxygenate blending

Engine operating points were selected to span a range of pressure-temperature trajectories in the engine, including both conventional SI as well as ACI combustion. As such, three SI engine operating conditions were selected, all at 1,500 rpm. In addition, two different styles of ACI combustion were chosen to investigate. The first of these is a spark assisted compression ignition operating condition at 1,500 rpm, and the other is a partial fuel stratification condition at 1,200 rpm.

To illustrate some of the fuel effects revealed thus far, two of the SI operating conditions are compared. The first of these, shown in Figure II.3.3, utilized a low intake manifold temperature (35°C) and increased the intake manifold pressure as high as possible to achieve a pressure-temperature trajectory that was in the beyond RON space for the alkylate$_{Co\text{-}Optima}$ and olefinic$_{Co\text{-}Optima}$ fuels. Because of the relatively high compression ratio of this engine configuration (12:1), this load limit was limited to only 12 bar indicated mean effective pressure, which represents only a moderately boosted operating condition. Despite the relatively low load, the alkylate$_{Co\text{-}Optima}$ exhibits pre-spark heat release, whereas the olefinic fuel does not, which agrees with earlier investigations. Additionally, the alkylate$_{Co\text{-}Optima}$ is more knock limited, as exhibited by the additional combustion phasing advance allowed by the olefinic$_{Co\text{-}Optima}$. These same fuels are shown at a higher intake manifold temperature of 152°C in Figure II.3.4, which was chosen to achieve a higher-temperature pressure-temperature trajectory. Expectations from earlier studies dictate that the pre-spark heat release is subdued at this condition and that the alkylate fuel would have comparable or superior knock resistance. This is confirmed in Figure II.3.4, where the alkylate$_{Co\text{-}Optima}$ fuel has a more advanced combustion phasing at the knock limit and there is no detectable pre-spark heat release.

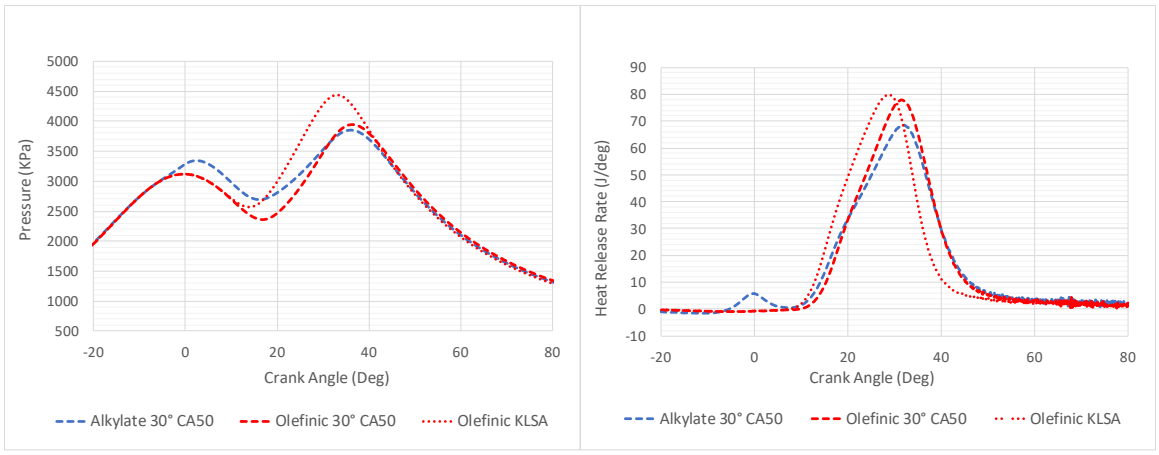

(a) (b)

CA50 – crank angle at 50% mass fraction burned; KLSA – knock limited spark advance

Figure II.3.3 (a) Cylinder pressure and (b) heat release rate for the alkylate and olefinic fuels at the high load SI operating condition at 1,500 rpm. The 30 degrees after top dead center condition is knock limited for the alkylate fuel, but further phasing advance is possible for the olefinic fuel.

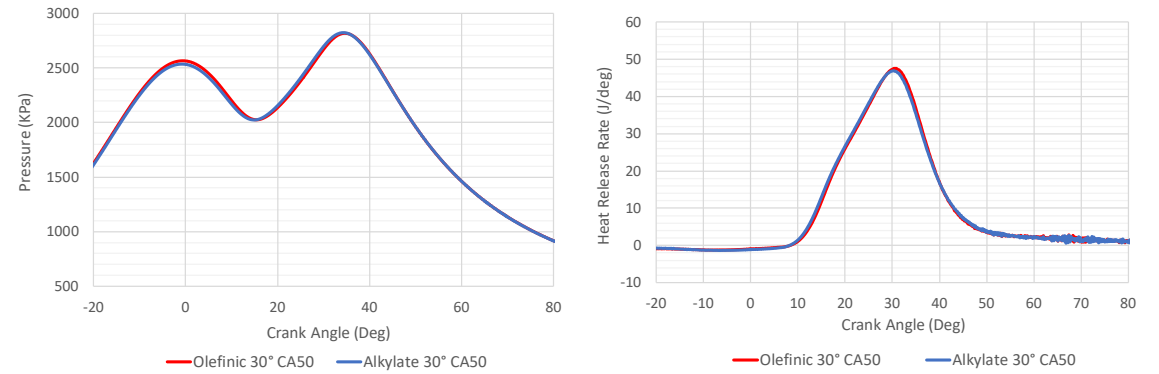

(a) (b)

Figure II.3.4 (a) Cylinder pressure and (b) heat release rate for the alkylate and olefinic fuels at the high intake manifold temperature SI operating condition at 1,500 rpm

The partial fuel stratification ACI operating condition represents a significant fuel effect, shown in Figure II.3.5. Specifically, the alkylate$_{\text{Co-Optima}}$ fuel has a low-magnitude heat release that occurs earlier than the olefinic$_{\text{Co-Optima}}$ fuel, starting before 0 degrees crank angle. This early heat release for the alkylate$_{\text{Co-Optima}}$ attenuates the peak heat release relative to olefinic$_{\text{Co-Optima}}$. This early heat release phenomena is known as intermediate temperature heat release and will be a major focus during the analysis of this data set when trying to explain the autoignition behavior of the fuels.

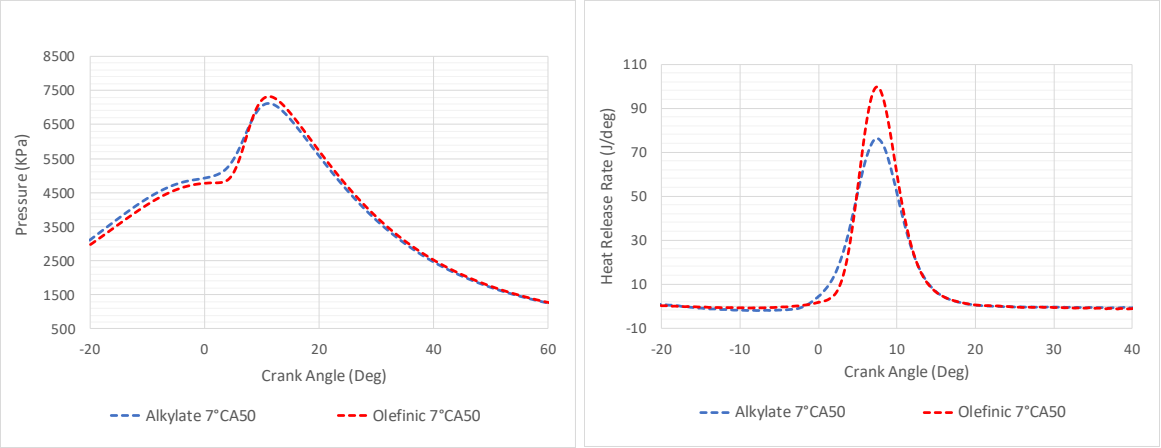

(a) (b)

Figure II.3.5 (a) Cylinder pressure and (b) heat release rate for the alkylate and olefinic fuels at the partial fuel stratification ACI operating condition, which is 6 bar indicated mean effective pressure at 1,200 rpm

The experimental investigation, which was started in FY 2019, will continue into the beginning of FY 2020. Further, the analysis and reporting of this data set will continue in FY 2020.

Conclusions

- The experimental multimode research at ORNL transitioned to a new engine platform in 2019 to allow us to operate with production-intent combustion strategies for ACI operation.
- Working with a major energy company, a fuel matrix was developed that uses refinery-relevant fuel streams.
- An experimental matrix was developed that already enables us to see several fuel-specific differences at various engine operating conditions.

Key Publications

1. Tao, M., P. Zhao, J.P. Szybist, P. Lynch, and H. Ge. 2019. "Insights into Engine Autoignition: Combining Engine Thermodynamic Trajectory and Fuel Ignition Delay Iso-Contour." *Combustion and Flame* 200: 207–218. doi: 10.1016/j.combustflame.2018.11.025.
2. Delvescovo, D., D. Splitter, J. Szybist, and G. Jatana. "Modeling Pre-Spark Heat Release and Low Temperature Chemistry of Iso-Octane in a Boosted Spark-Ignition Engine." Accepted for publication in *Combustion and Flame*. Pub. ID 127047.

References

1. Miles, P. 2018. "Efficiency Merit Function for Spark Ignition Engines: Revisions and Improvements Based on FY16–17 Research." Technical report. U.S. Department of Energy: Washington, DC.
2. Szybist, J.P., et al. 2017. "The Reduced Effectiveness of EGR to Mitigate Knock at High Loads in Boosted SI Engines." *SAE International Journal of Engines* 10 (5): 2305–2318.
3. Fouts, L., et al. 2018. "Properties of Co-Optima Core Research Gasolines." National Renewable Energy Laboratory.

Acknowledgements

The principal investigator thanks Tommy Powell, Flavio Dal Forno Chuahy, and Scott Curran of ORNL for their contributions to this project and report.

II.4 Advanced Light-Duty SI Engine Fuels Research (Sandia National Laboratories)

Magnus Sjöberg, Principal Investigator
Sandia National Laboratories (SNL)
MS 9053, P.O. Box 969
Livermore, CA 94551-0969
E-mail: mgsjobe@sandia.gov

Kevin Stork, DOE Technology Development Manager
U.S. Department of Energy
E-mail: Kevin.Stork@ee.doe.gov

Start Date: October 1, 2018 End Date: September 30, 2019
Project Funding (FY19): $640,000 DOE share: $640,000 Non-DOE share: $0

Project Introduction

This project furthers the science-base needed by industry stakeholders to co-evolve the next generations of highly efficient direct injection spark ignition (DISI) engines and new gasoline-type fuels. Here, the research emphasis is on lean operation, which can provide high efficiency, using fuels that also support traditional non-dilute stoichiometric operation for peak load and power. Lean operation induces challenges with ignition stability, slow flame propagation, and low combustion efficiency. Therefore, techniques that can overcome these challenges are studied. Specifically, fuel stratification is used to ensure ignition and completeness of combustion, but this technique has soot- and NO_x-emissions challenges. For lean well-mixed operation, turbulent deflagration can be combined with controlled end-gas autoignition to render mixed-mode combustion for sufficiently fast heat release. However, such mixed-mode combustion requires an appropriate autoignition reactivity, motivating studies of the octane appetite of lean engine operation.

Objectives

This project provides science-based information needed to understand how emerging alternative gasoline fuels can be co-developed with advanced lean combustion to maximize both engine efficiency and vehicle fuel economy.

Overall Objectives

- Provide the science-base needed to understand how emerging alternative fuels impact highly efficient DISI light-duty engines being developed by industry
- Elucidate how engine design and operation can be optimized for clean and efficient use of future fuels
- Develop and apply advanced optical diagnostics for probing in-cylinder processes.

Fiscal Year 2019 Objectives

- Clarify why particulate matter index fails to predict engine-out soot particulate matter (PM) for boosted stratified-charge spark ignition (SI) engine operation
- Determine the octane requirement of a multimode engine that uses mixed-mode combustion at low to moderate loads
- Quantify the potential of a multimode engine to increase vehicle fuel economy.

Approach

The Alternative Fuels DISI Engine Lab at SNL houses an engine that is capable of both performance testing and in-cylinder optical diagnostics. First, performance testing with an all-metal engine configuration is conducted over wide ranges of operating conditions and alternative fuel blends. This allows quantifying fuel-efficiency, combustion stability, and exhaust emissions behavior. Second, in-cylinder processes are examined with high-speed optical diagnostics, including advanced laser-based techniques. This reveals the mechanisms that govern the combustion process and exhaust-emissions formation. Computer modeling using GT-Power, Chemkin-Pro, and ALPHA extends the studied parameter space and allows estimating the impact of efficient lean combustion on vehicle fuel economy.

To enhance the research in the Alternative Fuels DISI Engine Lab at SNL, several collaborations have been in place. Notably, computational fluid dynamics modeling at Argonne National Laboratory provides insights that are not readily accessible in the experiments, such as mixture and temperature stratification in the end-gas. Furthermore, free-spray experiments conducted in the two spray vessels at SNL provide improved understanding of spray dynamics, which helps interpret the engine results. A collaboration with Technische Universität Darmstadt has also provided valuable insights of the effect of spray-wall interactions and fuel-film formation.

Results

- Assessed reasons for shortcomings of particulate matter index (PMI) for lean boosted stratified-charge SI engine operation
- Further developed in-cylinder soot diagnostics based on diffused back illumination and used them to quantify in-cylinder soot-mass distributions for key operating points
- Used refractive index matching in combination with liquid spray imaging to determine the role of fuel spray dynamics in the formation of piston-top fuel films, including under cold-start conditions
- Developed a modeling methodology with GT-Power and Chemkin-Pro and used it to determine the octane appetite of lean mixed-mode combustion
- Coupled GT-Power and the U.S. Department of Environmental Protection's ALPHA models to quantify the effect of lean operation on vehicle fuel economy for city and highway drive cycles.

Fully Stratified Operation

Spray-guided, stratified-charge SI operation can provide high thermal efficiency for low and mid loads, where a light-duty automotive engine typically spends a large fraction of time. However, while enabling high-efficiency operation, fuel stratification can cause unacceptably high engine-out smoke levels, depending both on the fuel injection and combustion strategy and on the fuel composition. A commonly used metric for a fuel's sooting propensity is the PMI, which originally was developed for port fuel injection engines [1]. Previous years' efforts revealed shortcomings of PMI, which prompted further work to better understand the reasons for PMI's inadequacy for lean stratified operation. Figure II.4.1a shows how the engine-out soot PM varies with fuel type for operation with moderate intake boost at an engine speed of 2,000 rpm. Relative to the trend line, several fuels show large deviations. As a starting point for probing the reasons for these deviations, optical experiments were conducted for the diisobutylene blend and the high olefin and E30 (blend of 30% ethanol and 70% gasoline) core fuels. Together, they exhibit a trend that is opposite to expectations that the engine-out soot PM should increase with increasing PMI. Since the combustion for lean stratified operation is quite different compared to well-mixed stoichiometric operation (for which PMI was developed), it was not obvious if the shortcomings of PMI relate to soot formation or soot oxidation.

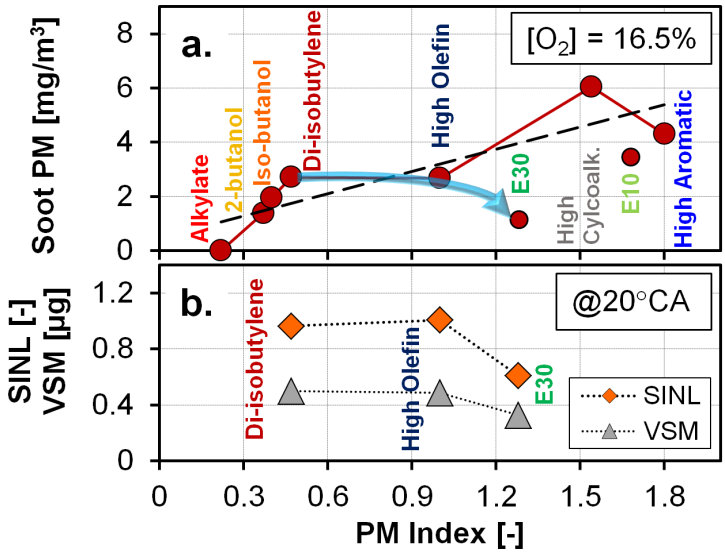

Figure II.4.1 (a) Engine-out soot concentrations of nine test fuels at intake [O_2] = 16.5% and (b) average spatially integrated natural luminosity (SINL) and visible soot mass (VSM) from optical diagnostics at 20 crank angle degrees (°CA). Figure by Namho Kim, SNL.

Figure II.4.2 provides an example of the employed optical diagnostics, using a combination of natural luminosity imaging from below and diffused back illumination extinction imaging (DBI-EI) from the side. Consistent with previous results using a certification gasoline [2], the natural luminosity imaging reveals that a majority of the soot luminosity occurs in the right-hand portion of the combustion chamber. This is a result of a tumble-induced flow asymmetry that places a larger portion of the fuel in that area, creating volumes that are sufficiently rich to support soot formation in the bulk of the gases. The line-of-sight DBI-EI results via the pent-roof are consistent with the natural luminosity results, showing a majority of the soot mass on the right-hand side of the combustion chamber. Ensemble-averaged optical results are presented in Figure II.4.1b, showing that the visible soot mass follows well the engine-out soot PM trend. This indicates that the inability of PMI to rank-order fuels in terms of their engine-out soot PM arises from an incorrect prediction of fuels' soot-formation propensity, as opposed to soot-oxidation differences not captured by the PMI formulation.

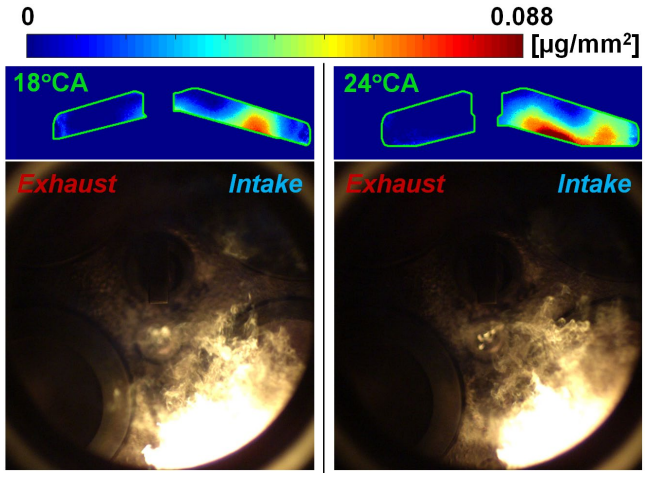

Figure II.4.2 Phase-synchronized DBI-EI and natural luminosity images from operation with the di-isobutylene blend. Figure by Namho Kim, SNL.

For the stratified results presented above, measurements have shown that spray-wall interactions are minimal thanks to a combination of split injections and an elevated in-cylinder density resulting from moderate intake boost. However, other stratified operating conditions can have severe challenges with wall wetting and pool fires, especially for mid-level ethanol blends like E30 [3]. To better understand the role of injection schedules and spray dynamics on the formation of fuel film, a systematic optical-engine study was conducted, involving fuel-film thickness measurements and spray imaging [4]. Figure II.4.3 provides an example of the results.

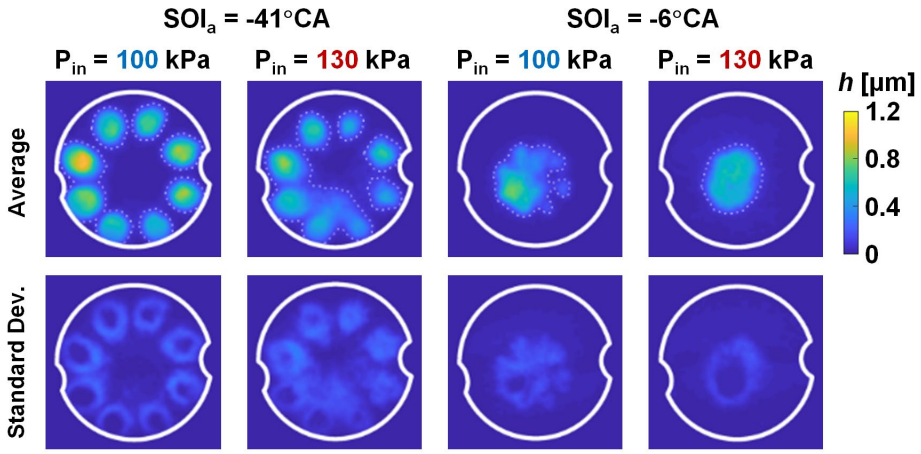

Figure II.4.3 Top: Phase-averaged piston-top fuel-film thickness distributions at crank angle degree of maximum fuel-film area for two intake pressures and two SOI_a (start of injection–actual) timings. Bottom: Standard-deviation maps. P_{in} = 130 kPa used an injection duration of 1,395 µs, and P_{in} = 100 kPa used an injection duration of 1,043 µs, maintaining a supplied ϕ = 0.33 using Co-Optima core E30 fuel. Figure by Carl-Philipp Ding, Technische Universität Darmstadt.

Figure II.4.3 shows that for a relatively early injection timing of SOI_a = -41 °CA, an increased P_{in} reduces the average fuel-film thicknesses somewhat. The reduction is small despite the approximately 30% higher in-cylinder density. This occurs because the overall ϕ was maintained at 0.33, thereby requiring a longer injection duration for the P_{in} = 130 kPa case. It is noteworthy that the fuel-film pattern becomes less distinct for the boosted operation, with merging of the fuel films for some individual sprays. This occurs due to a developing spray collapse for the combination of higher intake pressure and longer injection duration. For injection near top dead center with SOI_a = -6 °CA, the spray plumes quickly merge into one due to the high in-cylinder density. This creates one centrally located fuel film. Furthermore, the standard deviation maps in Figure II.4.3 reveal that cycle-to-cycle variability differs between conditions. The least repeatable fuel films are found for the SOI_a = -41 °CA, P_{in} = 130 kPa case, which represents a borderline spray-collapse condition with occasional merging of individual spray plumes.

Octane Appetite of Mixed-Mode Combustion

Lean or dilute well-mixed SI engine operation can improve thermal efficiency, but a key challenge is to maintain a 10%–90% burn duration shorter than 30 °CA, which is needed to realize efficiency gains of lean combustion [5]. Lean deflagration has a tendency to cause a slow burn-out process. However, a speed-up can be achieved via the use of mixed-mode combustion, which features a combination of turbulent deflagration and end-gas autoignition [6]. In a multimode engine, such mixed-mode combustion can be used at low to moderate engine loads and be combined with boosted stoichiometric SI operation for the highest loads. However, for this to be practical, the fuel property requirements should align as well as possible for the two combustion modes. In addition, it is important to achieve a wide load coverage for the lean operation since such operation provides higher efficiency. As a first step, investigations were undertaken to determine the octane appetite of mixed-mode combustion, also known as spark-assisted compression ignition. Based on experimental observations, a modeling methodology involving GT-Power and Chemkin-Pro was developed to

enable parametric studies of fuel effects on the attainable load range of mixed-mode combustion. Selected results are shown in Figure II.4.4, plotting the upper load limit of mixed-mode combustion against the fuels' anti-knock index (AKI). It can be seen that increasing AKI favors higher loads. It is also clear that increased octane sensitivity (S) is favored, with the S = 10 fuels providing superior load for a given AKI. These results indicate that the octane appetite of lean mixed-mode combustion is well aligned with that of conventional stoichiometric boosted SI, which also favors fuels with high AKI and S. This means that from an octane perspective, there is no conflict for a multimode engine that uses a combination of mixed-mode combustion and stoichiometric boosted SI.

It can be noted that for these experiments, several injections during the intake stroke create a well-mixed fuel-air charge. However, to stabilize flame development for these lean conditions, a small amount of extra fuel (typically ≈0.8 mg) is injected at the time of spark to enrich the mixture near the spark plug, as illustrated in the inset of Figure II.4.4. This injection strategy is called partial fuel stratification.

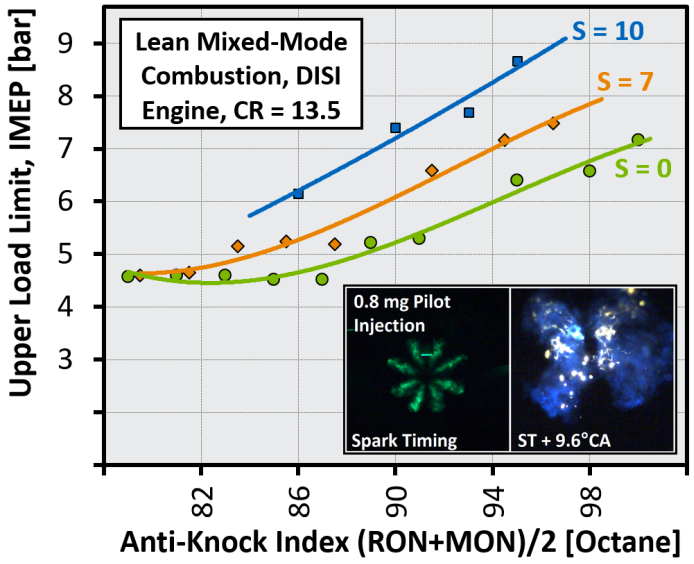

IMEP – indicated mean effective pressure; CR – compression ratio; ST – spark timing; RON – research octane number; MON – motor octane number

Figure II.4.4 Effect of increasing AKI and S on the upper load limit of lean mixed-mode combustion, as predicted by the GT-Power/Chemkin-Pro combination. The inset illustrates the use of a small pilot injection to stabilize the lean combustion. Figure by Magnus Sjöberg, SNL.

Potential of Multimode Engines

Practical implementation of a multimode engine is inevitably more challenging than a conventional boosted SI engine. Therefore, multimode engines only make sense if they can provide substantial fuel savings for practical vehicle operation. To quantify the potential of a multimode engine to increase fuel mileage, a modeling methodology was developed based on engine modeling with GT-Power in combination with the U.S. Environmental Protection Agency's ALPHA vehicle simulation program. Figure II.4.5 shows a scatter plot of the load-speed combinations that the engine traverses during the two drive cycles that are used to determine official light-duty vehicle fuel economy values. With the implemented shift schedule, it can be noted that the engine spends a majority of time near an engine speed of around 1,600 rpm. This suggests that for a multimode engine, it is most important to implement lean combustion at lower engine speeds.

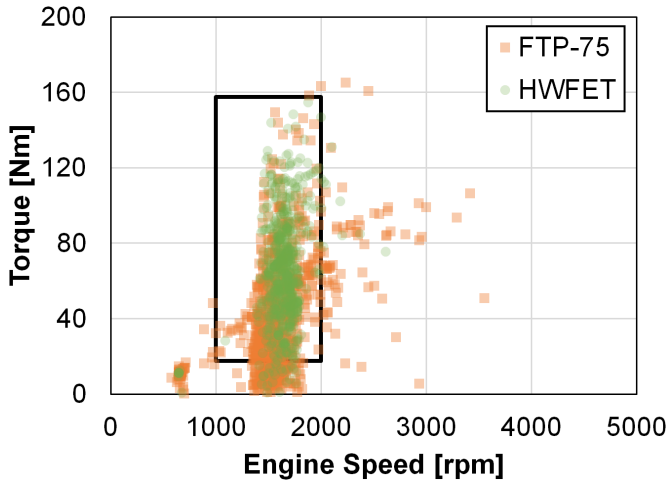

FTP-75 – Federal Test Procedure; HWFET – Highway Fuel Economy Test

Figure II.4.5 Load–speed engine usage for two drive cycles for a standard passenger car with an 8-speed transmission. The black rectangle indicates a hypothetical coverage of lean combustion used in Figure II.4.6. Figure by Colson Johnson and Namho Kim, SNL.

During the earlier phases of the Co-Optima initiative, it has been well established that the efficiency of boosted SI engines can be increased by fuels with higher RON and S [7]. However, to realize these benefits of higher RON and S, the engine has to be designed with a CR that matches the increased autoignition resistance offered by the fuel. Using a combination of GT-Power and ALPHA, the dark-green bars in Figure II.4.6 illustrate this effect. If the CR is increased from 8 to 14 and no other changes are made to the engine, the models predict a relative gain in fuel economy of 8.3% for conventional stoichiometric operation. To estimate an approximate upper boundary for the potential gains offered by a combination of multimode operation and increased CR, the GT-Power modeled was exercised with $\lambda = 2$ operation across a wide torque range, but focusing on lower engine speeds, as illustrated with the black box in Figure II.4.5. The chosen torque range corresponds to a brake mean effective pressure range of 1–9 bar. Figure II.4.6 shows that irrespective of the CR, the lean operation provides a fuel economy (FE) gain of about 15%. Taken together, the results in Figure II.4.4 and Figure II.4.6 make a strong case that fuels with high AKI and S can enable wide load coverage with lean operation at an increased CR, with fuel economy gains greater than 20% being possible.

However, it should be noted that in practice, the fuel economy gains of multimode engines likely will be lower than indicated by Figure II.4.6. There are several reasons for this. First, the lean load coverage might be less than indicated by the black box in Figure II.4.5. Second, mode transitions between lean and stoichiometric operation can lead to efficiency penalties. Third, the need for lean aftertreatment places additional constraints on the engine combustion and may lead to fuel economy penalties that are not considered in this ideal and simplified analysis.

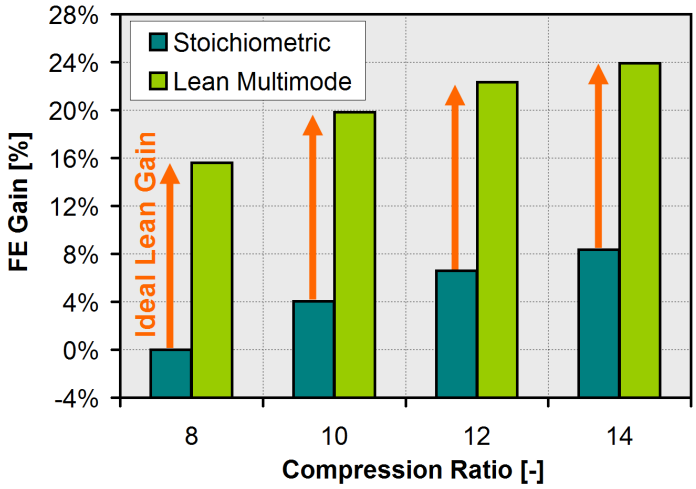

Figure II.4.6 A comparison of the FE gain that stoichiometric and lean multimode operation can offer when the CR is increased. Figure by Magnus Sjöberg, SNL.

Conclusions

The Alternative Fuels DISI Engine Lab has continued to support the Co-Optima initiative with insights that pertain to fuel effects on lean SI operation. Among the findings, it can be noted that:

- For boosted stratified-charge operation, the observed shortcomings of PMI to rank-order fuels in terms of their sooting propensity appears to be caused by an inability of PMI to correctly predict soot-formation tendency.
- Direct injection fuel spray dynamics need to be accounted for when designing a stratified-charge combustion system that has a minimum of wall wetting. Specifically, spray collapse and spray-plume merging are favored by both increased in-cylinder density and longer injection duration, which can lead to the formation of fuel films in the central portion of the piston top.
- The octane appetite of lean mixed-mode combustion (aka spark-assisted compression ignition) is consistent with that of conventional boosted SI, with both combustion systems favoring fuels with increasing AKI (or RON) and S. The synergy goes in the direction of making it more practical to realize a multimode engine that combines spark-assisted compression ignition and boosted SI.
- Simulations of drive cycles show that it is most important to implement lean combustion at low engine speed, where a majority of time is spent. If lean and efficient combustion can be implemented for wide load ranges at an elevated CR, it may be possible for a multimode engine to realize fuel economy gains of around 20%.

Key Publications

1. He, X., Y. Li, M. Sjöberg, D. Vuilleumier, C.P. Ding, F. Liu, and X. Li. 2019. “Impact of Coolant Temperature on Piston Wall-Wetting and Smoke Generation in a Stratified-Charge DISI Engine Operated on E30 Fuel.” *Proceedings of the Combustion Institute* 37 (4): 4955–4963, doi: 10.1016/j.proci.2018.07.073.

2. Ding, C.P., D. Vuilleumier, N. Kim, D.L. Reuss, M. Sjöberg, and B. Böhm. 2019. “Effect of Engine Conditions and Injection Timing on Piston-Top Fuel Films for Stratified Direct-Injection Spark-Ignition Operation Using E30.” *International Journal of Engine Research*, doi: 10.1177/1468087419869785.

References

1. Aikawa, K., T. Sakurai, and J. Jetter. 2010. "Development of a Predictive Model for Gasoline Vehicle Particulate Matter Emissions." *SAE Int. J. Fuels Lubr.* 3 (2): 610–622, doi: 10.4271/2010-01-2115.

2. Zeng, W., M. Sjöberg, D.L. Reuss, and Z. Hu. 2017. "High-Speed PIV, Spray, Combustion Luminosity, and Infrared Fuel-Vapor Imaging for Probing Tumble-Flow-Induced Asymmetry of Gasoline Distribution in a Spray-Guided Stratified-Charge DISI Engine." *Proceedings of the Combustion Institute* 36 (3): 3459–3466, http://doi.org/10.1016/j.proci.2016.08.047.

3. He, X., Y. Li, M. Sjöberg, D. Vuilleumier, C.P. Ding, F. Liu, and X. Li. 2019. "Impact of Coolant Temperature on Piston Wall-Wetting and Smoke Generation in a Stratified-Charge DISI Engine Operated on E30 Fuel." *Proceedings of the Combustion Institute* 37 (4): 4955–4963, doi: 10.1016/j.proci.2018.07.073.

4. Ding, C.P., D. Vuilleumier, N. Kim, D.L. Reuss, M. Sjöberg, and B. Böhm. 2019. "Effect of Engine Conditions and Injection Timing on Piston-Top Fuel Films for Stratified Direct-Injection Spark-Ignition Operation Using E30." *International Journal of Engine Research*, doi: 10.1177/1468087419869785.

5. Ayala, F., and J. Heywood. 2007. "Lean SI Engines: The Role of Combustion Variability in Defining Lean Limits." SAE Technical Paper 2007-24-0030, doi: 10.4271/2007-24-0030.

6. Sjöberg, M., and W. Zeng. 2016. "Combined Effects of Fuel and Dilution Type on Efficiency Gains of Lean Well-Mixed DISI Engine Operation with Enhanced Ignition and Intake Heating for Enabling Mixed-Mode Combustion." *SAE Int. J. Engines* 9 (2): 750–767, doi:10.4271/2016-01-0689.

7. Miles, P. 2018. "Efficiency Merit Function for Spark Ignition Engines: Revisions and Improvements Based on FY16–17 Research." Technical Report. U.S. Department of Energy, Washington, DC. DOE/GO-102018-5041.

Acknowledgements

This work was performed at the Combustion Research Facility, Sandia National Laboratories, Livermore, California, with scientific contributions from Namho Kim, David Vuilleumier, Carl-Philipp Ding, Xu He, Colson Johnson and Eshan Singh. Sandia National Laboratories is a multi-mission laboratory managed and operated by National Technology and Engineering Solutions of Sandia, LLC., a wholly owned subsidiary of Honeywell International, Inc., for the U.S. Department of Energy's National Nuclear Security Administration under contract DE-NA0003525.

II.5 Effect of Properties/Injection Schedule on Fuel Spray Mixing (Sandia National Laboratories)

Lyle M. Pickett, Principal Investigator
Sandia National Laboratories
P.O. Box 969, MS 9053
Livermore, CA 94551-9053
E-mail: LMPicke@sandia.gov

Kevin Stork, DOE Technology Development Manager
U.S. Department of Energy
E-mail: Kevin.Stork@ee.doe.gov

Start Date: October 1, 2018 End Date: September 30, 2019
Project Funding (FY19): $275,000 DOE share: $275,000 Non-DOE share: $0

Project Introduction

An overall goal of the Co-Optimization of Fuels and Engines project is to identify fuels and engine hardware that have the potential for the greatest efficiency and lowest fuel consumption. Because all future high-efficiency engines will have fuel directly sprayed into the engine cylinder, the effect of advanced, renewable fuels on direct-injection sprays must be considered. Gasoline direct-injection engines must be tolerant to a range of fuels, and there must be an understanding of how specific fuel properties affect the spray mixing and evaporation processes to intentionally create better fuels and better injectors. Computational fluid dynamics models for the spray need to be developed and proven to be accurate for different fuels and operating conditions. More predictive spray combustion models for all renewable fuels will enable rapid design and optimization of future high-efficiency engines, providing more affordable vehicles and also saving fuel.

Objectives

Overall Objectives

- Facilitate improvement of engine spray combustion modeling, accelerating the development of cleaner, more efficient engines
- Determine how fuel properties affect fuel spray mixing and combustion, for both early injection during the intake stroke as well as late, controlled injection for mixed-mode combustion.

Fiscal Year 2019 Objectives

- Identify differences in fuel spray mixing, evaporation, plume interaction, droplet atomization, and liquid film formation with respect to selected candidate fuels
- Using a new high-throughput spray chamber, develop and implement a three-dimensional spray diagnostic for multi-hole gasoline direct-injection sprays, including liquid penetration and plume direction under cold-start, flash-boiling operation, and late injection
- Identify sources of fuel film deposition on injector surfaces, including fuel property effects.

Approach

Experiments are performed in a new spray chamber capable of reproducing the thermodynamic conditions at the time of injection in engines, while offering high-throughput capability. A schematic of the vessel is shown in Figure II.5.1. The chamber is rated for gas pressures as high as 150 bar and temperatures as high as 1,100 K, but it also operates in vacuum to mimic throttled engine operation. Gas flows through heaters at the bottom of the vessel to an optically accessible spray test section with large optical ports. Hot gases are isolated/insulated from the cold pressure vessel and then cooled at the top exhaust. Fresh gases with uniformity in temperature continuously flow to the spray section such that injections may be repeated rapidly. The high rate of data acquisition facilitates experiments with a wide range of Co-Optima fuels, injector designs, and injector and gas conditions.

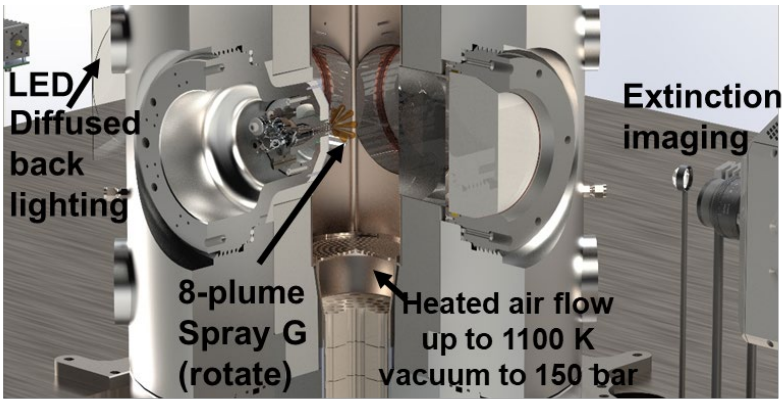

LED – light-emitting diode

Figure II.5.1 Heated flow through spray chamber and optical setup for extinction imaging

The fuel injector chosen for this work is the Engine Combustion Network (ECN) gasoline "Spray G" injector. Many past computational fluid dynamics studies and datasets exist for this injector [1], making the study of new fuels and operating conditions of interest. The Spray G injector is an 8-hole injector. Although current multi-hole fuel injectors are designed to widely disperse and mix fuel, interaction between plumes may cause "collapse" into a single jet, resulting in poor mixing, over-penetration, and impingement, leading to a source of particulate matter and inefficiency. How fuel properties affect the plume interaction and overall liquid penetration is of critical importance for engine and injector design.

Results

Utilizing the high-throughput chamber, a new diagnostic was developed to understand the motion of each plume throughout injection. Figure II.5.1 shows the optical setup for high-speed extinction imaging, with diffused backlighting of the multi-plume spray. Example extinction measurements and processing are shown in Figure II.5.2. The upper left of the figure shows a raw extinction measurement at a given time after the start of injection (aSOI). One can see that the collected extinction is the result of multiple plumes along the line of sight, which may not reveal much information about the separation or growth of individual plumes. However, by rotating the injector to different positions and quantifying the measured extinction at each time aSOI with an ensemble-average of hundreds of injections at each rotation, a three-dimensional map of the liquid distribution is obtained via computed tomography [2]. This technique also relies on droplet optical properties that were obtained using separate measurements for the ECN [3]. The resulting three-dimensional liquid volume fraction (LVF) is indicated in two planes at the bottom of the figure. Data at an axial plane of 30 mm shows the distribution of all eight plumes at that position. A Y-Z cut-plane shows the spacing between Plumes 3 and 7 at a particular timing aSOI. Three-dimensional data like this is resolved in time during and after injection to describe the plume center, width, and liquid concentration, or if plumes merge or bend together.

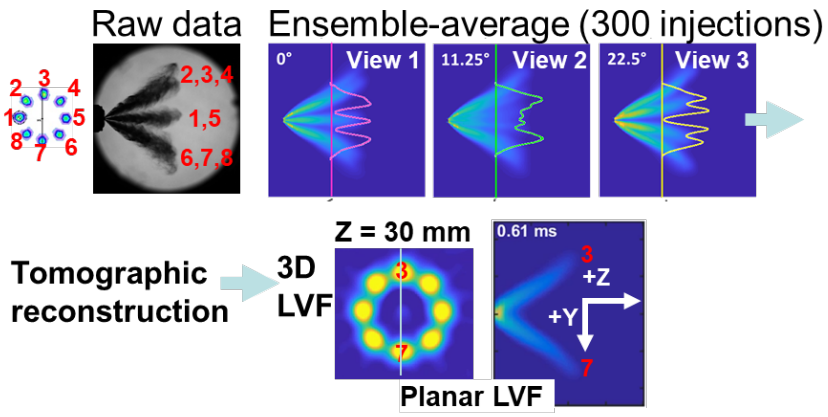

Figure II.5.2 Method for extinction imaging at different injector rotations and using computed tomography for local three-dimensional liquid volume fraction

While over a dozen different fuels were investigated for this research using different injection durations and operating conditions, four primary fuels will be reviewed in this report. Three of the fuels are Tier-3-selected candidates from past Co-Optima research, including a five-component surrogate with di-isobutylene, a refinery distillate with olefin molecular structure, and a refinery distillate with 30% ethanol. The fourth is a single-component reference fuel, iso-octane, used for past ECN research with Spray G. Differences in the distillation characteristics for each of these fuels are shown in Figure II.5.3. Note that the full-range distillates have a fraction of both light and heavy components, while iso-octane and the di-isobutylene blend have a relatively flat distillation curve. E30, containing 30% ethanol, has the lightest distillate fraction compared to any of the other fuels, but it also contains significant heavy fraction with the highest boiling point temperatures.

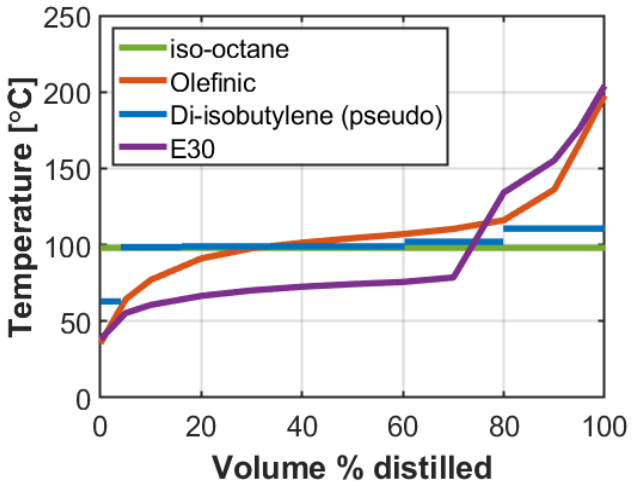

Figure II.5.3 Distillation curve (D86) for four fuels of study

Ensemble-average LVF distributions for iso-octane and E30 are shown in Figure II.5.4 at a condition typical of a warm engine with injection during the intake stroke. While plumes remain separate for iso-octane, allowing rapid mixing and vaporization, the E30 plumes collapse together, creating a poorly mixed core that is slow to vaporize, with a repeatable toroidal vortex at the spray head. The collapsed spray quickly penetrates and is likely to impinge upon engine surfaces. Analysis shows that the ethanol (78°C boiling point) and other lighter components lead to larger individual plume growth, contributing to overall spray collapse.

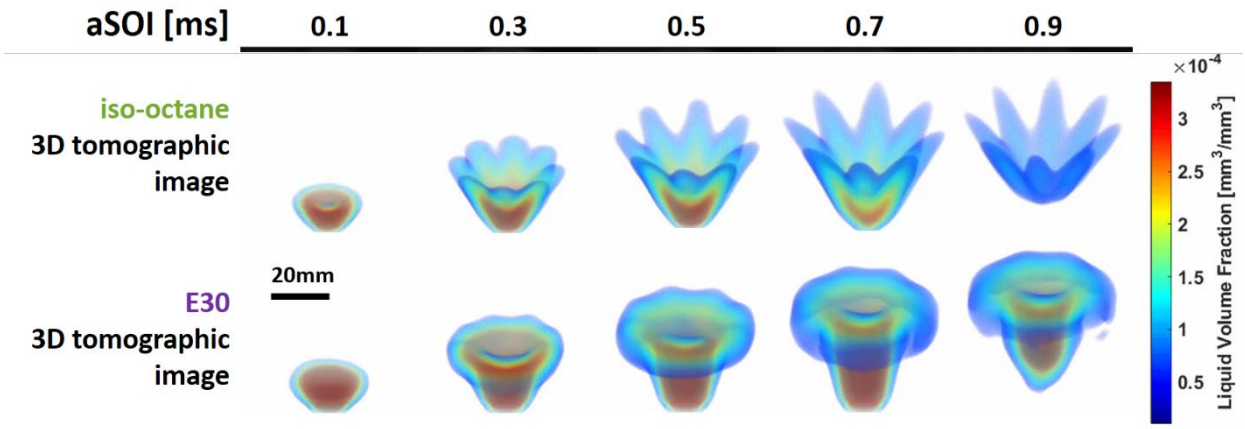

Figure II.5.4 Three-dimensional (3D) rendering of ensemble-average LVF for iso-octane (top) and a 30% ethanol gasoline (bottom) at time aSOI. Fuel injector conditions: ECN 8-hole Spray G, 90°C, 200 bar, injection duration 0.78 ms. Ambient conditions: 60°C, 0.5 bar.

The effect of the four representative fuels on the plume interaction and spray development is illustrated graphically in Figure II.5.5, at the same operating conditions as Figure II.5.4. The liquid volume fraction contour in the Y-Z plane is defined with a liquid volume fraction threshold of $5 \cdot 10^{-3}$. The nozzle drill angle is presented for reference as dotted grey lines. The liquid contours for iso-octane and di-isobutylene are quite similar, but the slightly longer liquid penetration length and wider liquid width of di-isobutylene are indicated during injection. Note that the direction of penetration for each plume does not match the drill angle. Aerodynamic interactions, which are encouraged by larger plume growth at vacuum, flash-boiling conditions, tend to pull plumes together toward the centerline even if the plumes do not collapse completely. The departure from the drill angle direction is especially pronounced at the end of injection.

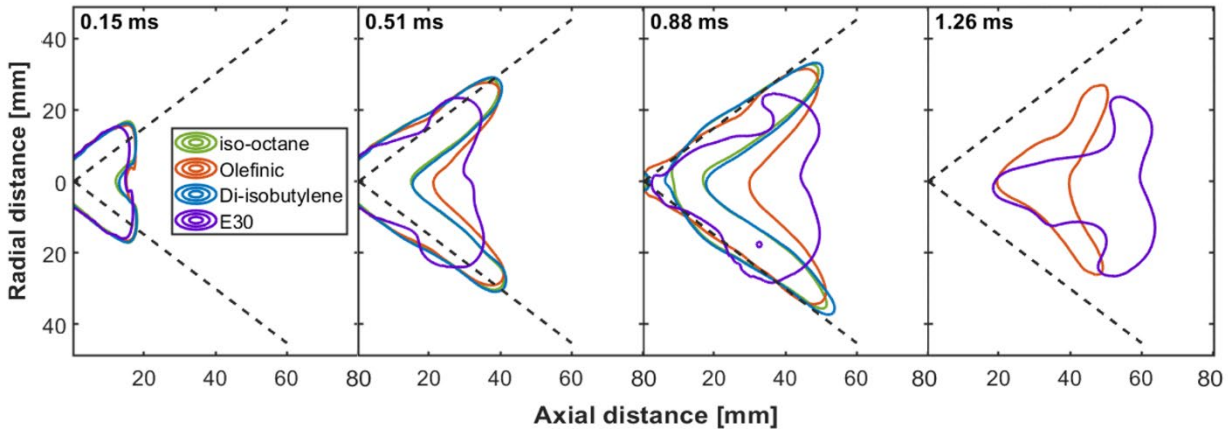

Figure II.5.5 Boundary of liquid spray for iso-octane, olefinic, di-isobutylene surrogate, and E30 blend at Y-Z plane enabled by 3D tomographic reconstruction. The boundary was determined with a liquid volume fraction threshold of $0.5 \cdot 10^{-3}$. Conditions are the same as in Figure II.5.4.

As suggested in Figure II.5.4, the plume movement to much smaller angles than the hole drill angle is most pronounced for E30, to the point of complete merging or collapse of plumes. But the wide-range distillate olefinic blend also shows a tendency for plume collapse. The complete collapse occurs nearly from the start of injection with the E30 blend, leaving specific vortical structures in the head of the jet. Spray collapse occurs at a later timing with the olefinic fuel, but a significant amount of liquid fuel is drawn toward the spray core

region. By 1.26 ms, remaining liquid has dropped below the LVF threshold of $5 \cdot 10^{-3}$ for both iso-octane and the di-isobutylene blend. Liquid persists for the olefinic and E30 fuels because of their heavier distillate fractions, but also because of poor air–fuel mixing resulting from plume collapse. This long, persistent liquid fuel penetration might be a source of liquid films on in-cylinder surfaces in an engine.

Investigation of different operating conditions for a single fuel (iso-octane) showed that the flash-boiling condition at 0.5 bar pressure had an approximately 2° smaller plume direction angle compared to the condition at 1.0 bar pressure, when analyzed 30 mm downstream of the injector during the steady period of injection at 0.5 ms aSOI. This difference increases to approximately 5° after the end of injection at 1.0 ms aSOI. A stronger redirection of the plume direction relative to the hole drill angle has consequences on overall penetration and mixing. For example, even without complete collapse, the plumes directed toward the central axis of the injector will exhibit longer axial liquid penetration and smaller liquid plume width, thus changing the overall mixing of the fuel spray.

Conclusions

To understand the effect of future renewable fuels on sprays, temporally and spatially resolved liquid volume fraction measurements of liquid plume position and dynamics have been acquired for a range of fuels. The understanding provided by these unique datasets motivates the design and optimization of gasoline direct-injection systems that respond well to a wide variety of future renewable fuels. The experimental data provided is also available to improve computational fluid dynamics models that will be used to optimize future engine designs. Key activities for Fiscal Year 2019 included:

- Development of a high-throughput facility and diagnostics for ensemble-average liquid volume fraction from computed tomography of high-speed extinction imaging.
- Completion of a large database (on the bullet above) including more than a dozen fuels and operating conditions spanning intake flash-boiling to late injection.
- Measurement of end-of-injection dribble and liquid film deposits on the injector for a range of conditions.

Future work includes autoignition, combustion, and soot formation for injections at mixed-mode conditions.

Key Publications

1. Hwang, J., L. Weiss, L.M. Pickett, and S.A. Skeen. 2019. “The Influence of Ambient Conditions and Fuel Type on Gasoline Spray Plume Direction.” ILASS-Americas 2019.
2. Three other manuscripts are currently under review.

References

1. Engine Combustion Network data archive < https://ecn.sandia.gov/ >, 2019.
2. Hwang, J., L. Weiss, L.M. Pickett, and S.A. Skeen. 2019. “The Influence of Ambient Conditions and Fuel Type on Gasoline Spray Plume Direction.” ILASS-Americas 2019.
3. Fouts, L., G.M. Fioroni, E. Christensen, M. Ratcliff, R.L. McCormick, B.T. Zigler, S. Sluder, J.P. Szybist, J.E. Dec, P.C. Miles, S. Ciatti, J.T. Bays, W. Pitz, and M. Mehl. 2018. “Properties of Co-Optima Core Research Gasoline.” National Renewable Energy Laboratory, Report No. NREL/TP-5400-71341.

Acknowledgements

Scott A. Skeen is a coauthor of this report. We thank Hyung Sub Sim, Joonsik Hwang, Noud Maes, Koji Yasutomi, Naoki Watanabe, Shane Daly, Emre Cenker, Julien Manin, Lukas Weiss,

Ioannis Karathanassis, Foivos Koukouvinis, Nathan Harry, Aaron Czeszynski, Tim Gilbertson, Alberto Garcia, Chris Ingwerson, Laurie Bell, David Cicone, and Nathan Prisbrey for their devoted research and support. Studies were performed at the Combustion Research Facility. Sandia National Laboratories is a multi-mission laboratory managed and operated by National Technology and Engineering Solutions for Sandia LLC, a wholly owned subsidiary of Honeywell International, Inc., for the U.S. Department of Energy's National Nuclear Security Administration under contract DE-NA0003525.

II.6 Low-Temperature Gasoline Combustion Engines: Fuel Effects and Fuel Co-Optimization (Sandia National Laboratories)

John E. Dec, Principal Investigator
Sandia National Laboratories
MS 9053, P.O. Box 969
Livermore, CA 94550
E-mail: jedec@sandia.gov

Kevin Stork, DOE Technology Development Manager
U.S. Department of Energy
E-mail: Kevin.Stork@ee.doe.gov

Start Date: October 1, 2018 End Date: September 30, 2019
Project Funding (FY19): $240,000 DOE share: $240,000 Non-DOE share: $0

Project Introduction

Engines using low-temperature gasoline combustion (LTGC), including homogeneous charge compression ignition (HCCI), have a strong potential to reduce fuel costs and CO_2 emissions by 30% or more over current spark ignition (SI) engines, as LTGC engines have high thermal efficiencies and very low NO_x and particulate emissions. Because the LTGC combustion process is largely controlled by the chemical kinetics of autoignition, the fuel properties are closely coupled to engine performance, and co-optimization of LTGC engines and their fuels has a strong potential to improve performance. Toward this larger goal, it is critical to understand the effects of fuel properties on autoignition under LTGC-like conditions, including the temperatures, pressures, and high dilution levels (either lean or dilute with exhaust gas recirculation/residuals) typical of these engines. It is also of interest to investigate how this understanding of fuel characteristics can be applied to design a fuel blend with the potential to improve LTGC performance, the low-temperature combustion in multimode LTGC-SI engines, and other advanced compression ignition (ACI) concepts.

Early studies of LTGC/HCCI showed that the classic methods of rating the autoignition propensity of gasoline, the research octane number (RON) and the motor octane number (MON), do not work for LTGC. This is perhaps not surprising since the RON and MON were designed to avoid knock (i.e., the autoignition of the end gas) in near-stoichiometric SI engines. Subsequently, Kalghatgi and co-workers proposed that the octane index (OI) could be used to rate the autoignition reactivity of different fuels in LTGC engines [1]. OI is calculated using the formula OI = RON – K*S, where S = RON – MON, and K is an empirical constant that depends on operating conditions. Although OI has shown some potential, it did not perform well in many studies. In particular, recent studies have shown that the OI does not work well for fuels that have significant differences in composition, such as the Co-Optima core fuels [2]. Accordingly, a systematic study was conducted in Fiscal Year (FY) 2019 to determine the reasons why OI performs poorly for correlating fuel reactivity of naturally aspirated LTGC/HCCI combustion, which is an important step toward the development of an appropriate autoignition metric for LTGC/HCCI engines. Additionally, studies were conducted to experimentally evaluate the performance of a new fuel blend that was computationally designed to improve LTGC performance and also to have a higher RON and S than regular E10 gasoline (gasoline containing 10% ethanol) for improved performance at boosted-SI conditions.

Objectives

Overall Objectives

- Provide fundamental understanding of fuels' autoignition behavior at conditions relevant to LTGC/ACI operation to support the co-development of LTGC/ACI engines and fuels that optimize their performance:

  - Develop an autoignition metric for LTGC engines.
  - Determine the fuel properties required for co-optimization of LTGC for medium to low loads, as would be used in multimode strategies that switch to boosted SI at high loads.
  - Determine the fuel properties required for co-optimization of full-time LTGC for medium- and heavy-duty applications.
- Provide data for a chemical-kinetic model and computational surrogate development and validation.

Fiscal Year 2019 Objectives

- Identify the reasons why the OI is not an adequate autoignition metric for naturally aspirated LTGC engine operation.
  - Evaluate the ability of single-zone CHEMKIN internal combustion engine simulations to reproduce experimentally measured autoignition timing for a wide range of fuels.
  - Systematically investigate each of the differences between LTGC engine operating conditions and the conditions for the RON and MON tests to determine the effect of each difference on the ability of the OI to correlate LTGC autoignition.
- Experimentally evaluate a custom fuel blend (CB#1) that was computationally designed to improve LTGC performance compared to regular gasoline and to have a higher RON and higher octane sensitivity (S) for improved performance in boosted-SI engines.
  - Acquire well-premixed LTGC (i.e., HCCI) data at naturally aspirated conditions for CB#1 and for a regular-grade E10 gasoline, and compare performance.
  - Acquire data with various amounts of partial fuel stratification (PFS) for both CB#1 and regular E10 gasoline to determine whether CB#1 increases the equivalence ratio (ϕ)-sensitivity, an important fuel property for LTGC, compared to regular E10 gasoline.
  - Obtain actual measurements of the RON and MON of CB#1 and compare to those of regular E10 gasoline.

Approach

Experimental studies were conducted in the Sandia LTGC Engine Laboratory using the all-metal single-cylinder LTGC research engine (displacement = 0.98 liters) derived from a Cummins B-series diesel. This engine is equipped with a custom LTGC piston that provides an open combustion chamber with a broad, shallow bowl. The compression ratio was 14:1 for all data presented in this report. This facility allows operation over a wide range of conditions, and it has been designed to provide precise control of virtually all operating parameters, allowing well-characterized experiments. The engine is equipped with two fueling systems. (1) For fully premixed operation, the fuel is injected into an electrically heated vaporizing chamber and mixed with the intake air well upstream of the engine. (2) For the PFS operation, the fuel is supplied by a centrally located gasoline-type direct injector (supplied by General Motors) capable of 300 bar injection pressures. When operated in a well-mixed LTGC mode (i.e., HCCI), the engine provides an excellent platform for determining the differences in autoignition characteristics between fuels. The base gasoline used for comparison with CB#1 was a research-grade E10 gasoline (called RD5-87) that is representative of regular-grade gasolines sold in the United States.

For the investigations of OI, the engine was operated with fully premixed fueling using eight different fuels, and for each fuel, the intake temperature was adjusted to sweep the 50% burn point (CA50) over a wide range, from knocking to near-misfire. CHEMKIN single-zone internal combustion engine simulations that accounted for heat transfer and utilized the Lawrence Livermore National Laboratory detailed mechanism were also

conducted and validated against the experimental data. This simulation approach was then applied to other conditions to determine the reasons for the poor performance of the OI for correlating the autoignition reactivities of the various fuels. For the second project task, single-zone CHEMKIN simulations had previously been applied to screen components to make a new fuel blend (CB#1) designed to simultaneously increase ϕ-sensitivity, RON, and octane sensitivity (S), compared to RD5-87 [3]. The increased ϕ-sensitivity offers several benefits for LTGC, and the higher RON and S can improve performance for boosted-SI operation, making CB#1 a good potential fuel for multimode LTGC-SI engines, as well as for single-mode LTGC or single-mode SI engines. In FY 2019, CB#1 was experimentally evaluated at both well-premixed and partially stratified LTGC conditions and compared to RD5-87 to determine CB#1's ability to improve LTGC engine operation. The RON and MON of CB#1 were also experimentally measured to evaluate its potential for boosted-SI conditions.

Results

A metric is needed to rank the autoignition reactivity of various gasolines at LTGC engine conditions. The OI has been suggested as being such a metric [1], but evaluation against experimental data has met with limited success. Figure II.6.1 shows the OI fitted to experimental data for the 10% burn point (CA10) acquired in the Sandia LTGC research engine for well-premixed, naturally aspirated operation. The same intake temperature (T_{in} = 154°C, which corresponds to a bottom dead center temperature [T_{BDC}] of 441.4 K) and equivalence ratio (ϕ = 0.4) were used for all fuels, so the CA10 values are affected only by differences in the autoignition reactivities of the fuels. Note that the CA10 values are crank angle degrees (CAD) after top dead center (TDC) intake. As the figure shows, the best fit to the data is obtained with K = 1.561, but the correlation is poor with an R^2 of only 0.447. It is important to understand why the OI metric fails in order to design a metric that includes all the relevant parameters.

Also shown in Figure II.6.1 are CHEMKIN single-zone internal combustion engine simulations using computationally tractable seven- to nine-component fuel surrogates that have been carefully designed based on matching the detailed hydrocarbon analyses of the fuels as closely as possible [4]. As evident in the figure, each of the simulated points falls close to its respective experimental point, giving confidence in the computational results. Fitting the OI to these points gives K = 1.533, which is very close to the K for the experimental data, with a slightly worse correlation (R^2 = 0.364).

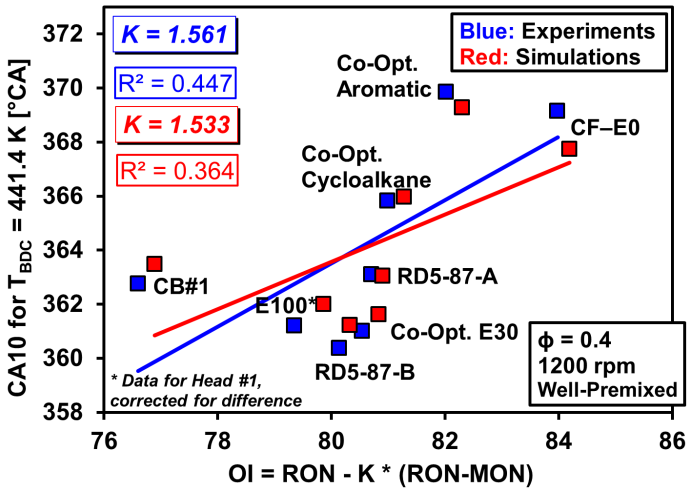

Figure II.6.1 OI = RON – K*S correlation fitted to the CA10 for eight different fuels for naturally aspirated well-mixed LTGC (i.e., HCCI). The blue data points show experimental results, and the red points show the results of simulations using the CHEMKIN internal combustion engine model, corrected for heat transfer and using the Lawrence Livermore National Laboratory detailed Co-Optima mechanism from December 2017. Intake pressure (P_{in}) = 1.0 bar; T_{in} = 154°C; T_{BDC} = 441.4 K; ϕ = 0.4; 1,200 rpm.

To understand why the OI gives a poor correlation, the project researchers conducted CHEMKIN simulations using these same fuels for a series of conditions to evaluate the effect of each difference between naturally aspirated LTGC operation (the conditions in Figure II.6.1) and the conditions of the MON test, for which the OI should work very well since MON is a defining point for the OI. First, simulations were conducted for conditions representative of the MON test ($\phi = 1.0$ and compression of the charge along a pressure-temperature [P-T] trajectory representative of the MON test). The results of this pseudo-MON test showed that for these conditions, the OI correlated the data very well with an $R^2 = 0.931$, and it gave a $K = 1.07$, which is very close to the value of 1.0 for true MON conditions. Next, the compression P-T trajectory was changed from piston compression followed by more rapid flame compression (as in the MON test) to piston-only compression to the same peak pressure and temperature as reached in the MON test (LTGC compression). As shown in the stacked bar graph in Figure II.6.2 (blue section), this reduced the R^2 to 0.889. Then, changing the engine speed from 900 rpm for the pseudo-MON test to 1,200 rpm for the LTGC data further reduced the R^2 to 0.871 (gray section). Next, the initial temperature was increased to match that of the LTGC test. Because this temperature is significantly hotter than that specified for the MON test, it is commonly referred to as a "beyond MON" condition, and as the stacked bar graph shows, this reduced quality of the OI correlation to an $R^2 = 0.823$ (orange section). These results indicate that these three factors (LTGC compression, engine speed, and hotter T_{in}) each moderately reduce the effectiveness of the OI, but that the OI still gives a fairly good correlation. However, switching from $\phi = 1.0$ (representative of MON tests) to $\phi = 0.4$, as used for the LTGC tests, caused a large reduction in the quality of the OI correlation, with the R^2 falling to 0.472 (green section).

Further analysis of the results shows that this large degradation in the OI correlation occurs because of differences in the ϕ-sensitivity of the various fuels used to fit the OI, and these differences are particularly large for the beyond-MON conditions of naturally aspirated LTGC. For example, neat ethanol (E100) has no ϕ-sensitivity, and CA10 is unchanged as ϕ is reduced from 1.0 to 0.4, whereas other fuels, such as CB#1 (discussed below), have a relatively high ϕ-sensitivity, and CA10 shifts as much as 5 CAD. Thus, this study shows that the OI does not provide a good correlation for naturally aspirated LTGC data mainly because LTGC engines operate at lean or highly dilute conditions (e.g., $\phi = 0.4$), whereas the RON and MON tests, from which the OI is derived, are conducted at near-stoichiometric ($\phi \sim 1.0$) conditions, and the OI does not account for differences between fuels in the changes in autoignition reactivity with changes in ϕ (i.e., the ϕ-sensitivity).

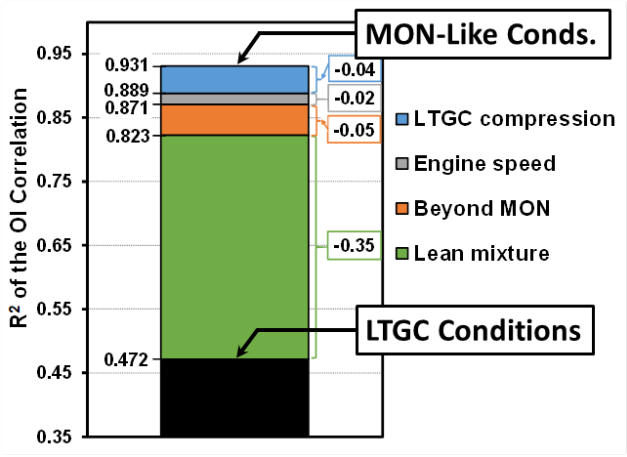

Figure II.6.2 Stacked bar graph showing the effect of each of the four main differences between MON-like conditions, for which OI gives a good correlation ($R^2 = 0.931$), and LTGC conditions, for which the OI gives a poor correlation ($R^2 = 0.472$)

Co-optimization of fuels and engines offers the potential to improve LTGC engine performance by developing a fuel with properties that are beneficial to this combustion process. Toward this goal, CHEMKIN simulations had previously been conducted to design a new fuel blend, called CB#1, with the potential to increase the ϕ-sensitivity at naturally aspirated and low-boost conditions compared to regular E10 gasoline (RD5-87) [3].

For a ϕ-sensitive fuel, autoignition times vary with the local ϕ within a stratified charge, and this effect can be exploited through appropriate charge stratification to provide several benefits for LTGC, such as CA50 control, increased efficiency, reduced noise, and facilitation of higher loads. It is also important that when the ϕ-sensitivity is increased, the RON and octane sensitivity must not be reduced and preferably are increased; these improvements ensure good performance in multimode LTGC-SI engines and in SI and boosted-SI engines so the same fuel can be used in all gasoline engines. Although the computational results indicated that CB#1 should simultaneously increase ϕ-sensitivity, RON, and S (octane sensitivity) compared to RD5-87, these results had not previously been experimentally verified.

During FY 2019, experimental testing of CB#1 was initiated, and the results are shown in Figure II.6.3 and Figure II.6.4. First, the Sandia LTGC engine was run with CB#1 using fully premixed fueling for naturally aspirated (P_{in} = 1.0 bar) conditions with a fuel rate corresponding to ϕ = 0.4, and the T_{in} was adjusted to obtain a ringing intensity (RI) of 5 MW/m^2 [5]. These results were then compared to RD5-87 data acquired in the same manner, and the results are shown in the second set of bar graphs in Figure II.6.3. As the figure shows, the T_{in} required for RI = 5 MW/m^2 for RD5-87 was 147.2°C, while CB#1 required T_{in} = 147.6°C. This very close match of intake temperatures indicates that CB#1 would be no more difficult to autoignite than RD5-87 under naturally aspirated conditions, which are typically the most difficult autoignition conditions for LTGC/HCCI engines. This bar graph also shows that the experimentally measured T_{in} for CB#1 is very close to the T_{in} = 146.7°C predicted by the CHEMKIN simulations, validating the simulation method at this condition.

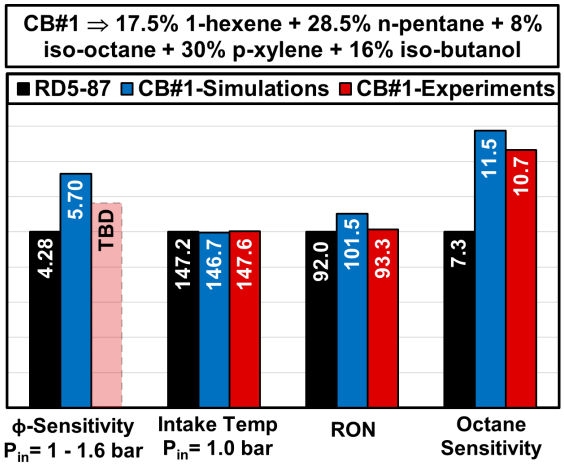

Figure II.6.3 Bar graph comparing various performance characteristics of CB#1 (dark red) with RD5-87 (black) and the values for CB#1 predicted by simulations (blue)

Next, a sample of CB#1 was sent to a reputable external testing laboratory to determine its RON and MON values. These tests showed that CB#1 has both a higher RON and higher octane sensitivity than RD5-87, as desired, so CB#1 should work better in boosted-SI engines than RD5-87. These results are shown in the third and fourth groups of bar graphs in Figure II.6.3, respectively. The RON of CB#1 was found to be 93.3 compared to 92.0 for RD5-87, and the octane sensitivity was 10.7 compared to only 7.3 for RD5-87. Simulations of the RON and octane sensitivity of CB#1, also shown in the bar graph, had suggested that the improvements in RON and octane sensitivity might be even greater than the measured values, but the simulations were based on a linear blending model, so it is not surprising that they are not particularly accurate.

Increasing the ϕ-sensitivity was the leading motivation for developing CB#1. The first bar graph set in Figure II.6.3 shows that simulations predicted CB#1 to have a significantly higher ϕ-sensitivity than RD5-87. Since these simulations are based on CHEMKIN computations using the detailed Lawrence Livermore National Laboratory Co-Optima kinetic mechanism, they should be fairly accurate. However, an experimental

method of quantifying the ϕ-sensitivity is not straightforward because wall and residual temperatures change when varying the ϕ of well-mixed charge [6], which makes measurements of autoignition times under well-mixed conditions not representative of autoignition times within a stratified or partially stratified charge.

For these reasons, an indirect method based on the effects of charge stratification was used to estimate the ϕ-sensitivity of CB#1 relative to RD5-87. With a ϕ-sensitive fuel, stratifying the charge will advance the combustion timing (CA50) because richer regions autoignite faster, and the CA50 advancement with increased stratification will be greater for a fuel with greater ϕ-sensitivity. Figure II.6.4 compares the CA50 advancement of CB#1 and RD5-87 as stratification is increased for operation at a global ϕ = 0.36 using PFS. With PFS, a gasoline-type direct injector supplies the majority of the fuel early in the intake stroke so it is relatively well mixed, and a second injection supplies the remainder of the fuel at a variable time during the compression stroke (referred to as SOI2) to vary the amount of stratification. When SOI2 = 200 CAD (early in the compression stroke), the charge is fairly well mixed, but as SOI2 is delayed beyond about 280–300 CAD, stratification begins to increase rapidly. Figure II.6.4 shows the CA50 relative to the CA50 for SOI2 = 200 CAD (ΔCA50) as SOI2 is retarded from 280 to 340 CAD (i.e., 80 to 20 CAD before TDC compression). For SOI2 = 280 to 320 CAD, both fuels show similar moderate CA50 advancement. Then, as SOI2 is retarded beyond 320 CAD, stratification increases rapidly, causing rapid CA50 advancement for both fuels. However, CB#1 shows significantly more CA50 advancement for the same SOI2, indicating that it is more ϕ-sensitive than RD5-87, in agreement with the simulations (see Figure II.6.3).

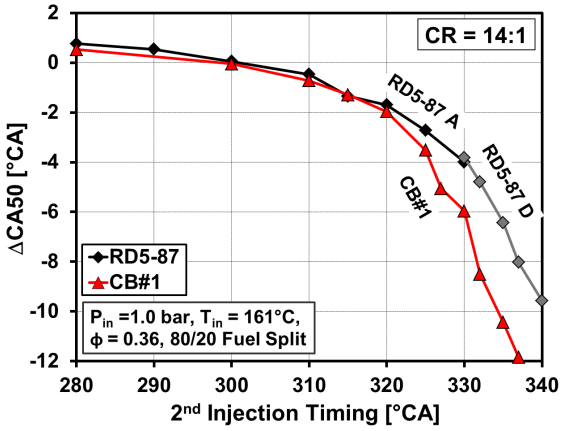

Figure II.6.4 ΔCA50 (CA50 – CA50 for SOI2 = 200 CAD) as a function of the second injection timing (SOI2) for CB#1 and RD5-87 using PFS with 80% of the fuel injected early and 20% injected at SOI2 (80/20 fuel split). P_{in} = 1.0 bar; T_{in} = 161°C; ϕ = 0.36; 1,200 rpm.

A quantitative metric for comparing the ϕ-sensitivity of CB#1 and RD5-87 is being developed, and additional tests comparing the performance of CB#1 and RD5-87 are underway.

Conclusions

- An evaluation of eight different fuels under well-premixed LTGC (i.e., HCCI) conditions with the same intake temperature shows that the OI gives a very poor correlation for the autoignition timing (CA10) of naturally aspirated LTGC, with an R^2 of only 0.447.
- CHEMKIN simulations for these eight fuels using seven- to nine-component surrogates based on the measured composition of the fuels showed very good agreement with the experimental data and a similar poor correlation with OI.
- Applying the CHEMKIN analysis at conditions representative of the MON test showed an excellent correlation against OI, with R^2 = 0.931 and a K value of 1.07, which is very close to the theoretical

value of 1.0, verifying that the CHEMKIN analysis method and the OI work well at MON-like conditions.

- Evaluation of each of the four differences between MON and LTGC/HCCI conditions (piston-only compression, higher engine speed, higher temperatures, and lean mixture) showed that the lean mixtures used for LTGC were the biggest factor in causing the OI to perform poorly for LTGC/HCCI combustion. This is because differences in ϕ-sensitivity between the various fuels cause a shift in their relative reactivities as ϕ is changed from ϕ ≈ 1 for the RON and MON tests, which are the basis for the OI, to the lean conditions used for LTGC (e.g., ϕ = 0.4).
- Experimental evaluations of a new custom fuel blend (CB#1) designed to improve LTGC performance compared to regular gasoline (RD5-87) showed that CB#1 performed well, as predicted by previous simulations.
    - For naturally aspirated operation, CB#1 required essentially the same intake temperature as RD5-87, indicating that CB#1 would be no more difficult to autoignite than regular gasoline.
    - CB#1 has a higher RON than RD5-87: 93.3 vs. 92.0, respectively.
    - CB#1 has a significantly higher octane sensitivity than RD5-87: 10.7 vs. 7.3, respectively.
    - PFS data show that for the same amount of fuel stratification, CB#1 advances CA50 more than RD5-87, indicating that CB#1 has a higher ϕ-sensitivity, which has several benefits for LTGC operation.
- These findings suggest that a fuel with properties similar to CB#1 would be a better fuel than regular gasoline for LTGC, SI, boosted-SI, or multimode LTGC-SI engines.

Key Publications, Presentations, and Awards

1. Dec, J., G. Gentz, R. Grout, A. Hoth, R. King, C. Kolodziej, D. Lopez Pintor, P. Pal, J. Pulpeiro Gonzalez, M. Ratcliff, T. Rockstroh, S. Schneider, A. Shah, and S. Som. 2019. "Autoignition in MM/ACI Combustion, Part 3." Team Report for the DOE Annual Merit Review, Office of Vehicle Technologies, FT072 (June).
2. Lopez-Pintor, D., J.E. Dec, and G.R. Gentz. 2019. "Evaluating a Custom Gasoline-Like Blend Designed to Improve ϕ-Sensitivity, RON and S." Advanced Engine Combustion Working Group Meeting (August).
3. Lopez-Pintor, D., J.E. Dec, and G.R. Gentz. 2019. "Understanding and Quantifying the Reasons RON, MON, and OI are Not Adequate for LTGC Engines." GM/Sandia Working Group Meeting (April).
4. Lopez-Pintor, D., J.E. Dec, and G.R. Gentz. 2019. "Understanding and Quantifying the Reasons OI is Not Adequate for LTGC Engines – Extension to Beyond RON Conditions." GM/Sandia Working Group Meeting (August).
5. Lopez-Pintor, D., J.E. Dec, and G.R. Gentz. 2019. "Understanding the Relationship Between Octane Index and ϕ-Sensitivity for LTGC Engines." Advanced Engine Combustion Working Group Meeting (January).
6. Lopez-Pintor, D. 2019. **Excellence in Oral Presentation Award** for SAE International Congress presentation of SAE Technical Paper 2019-01-0961 (April).

References

1. Risberg, P., G. Kalghatgi, and H.-E. Ångstrom. 2003. "Autoignition Quality of Gasoline-Like Fuels in HCCI Engines." SAE Technical Paper 2003-01-3215. doi:10.4271/2003-01-3215.

2. Dec, J.E. 2017. "Autoignition Fundamentals of Fuels for Multi-Mode Boosted SI and LTGC Engines." DOE Vehicle Technologies Office, Advanced Combustion Systems and Fuels, 2017 Annual Progress Report, report II.14. https://www.energy.gov/eere/vehicles/annual-progress-reports.

3. Lopez Pintor, D., J.E. Dec, and G.R. Gentz. 2019. "Φ-Sensitivity for LTGC Engines: Understanding the Fundamentals and Tailoring Fuel Blends to Maximize this Property." SAE Technical Paper 2019-01-0961. doi:10.4271/2019-01-0961.

4. Dec, J.E. 2018. "Low-Temperature Gasoline Combustion (LTGC) Engines: Fuel Effects and Fuel Co-Optimization." DOE Vehicle Technologies Office, Advanced Combustion Engines and Fuels, 2018 Annual Progress Report, report II.7. https://www.energy.gov/eere/vehicles/annual-progress-reports.

5. Eng, J.A. 2002. "Characterization of Pressure Waves in HCCI Combustion." SAE Technical Paper 2002-01-2859. doi:10.4271/2002-01-2859.

6. Dec, J.E., and M. Sjöberg. 2004. "Isolating the Effects of Fuel Chemistry on Combustion Phasing in an HCCI Engine and the Potential of Fuel Stratification for Ignition Control." SAE Technical Paper 2004-01-0557. *SAE Transactions* 113, no. 4: 239–257.

Acknowledgements

The author would like to thank post-doctoral researchers Dario Lopez-Pintor and Gerald Gentz for their significant contributions to the research reported here. The author is also grateful to Tim Gilbertson, Keith Penney, Aaron Czeszynski, and Alberto Garcia for their dedicated support of the LTGC Engine Laboratory.

This work was performed at the Combustion Research Facility, Sandia National Laboratories, Livermore, California. Sandia National Laboratories is a multi-mission laboratory managed and operated by National Technology and Engineering Solutions of Sandia, LLC, a wholly owned subsidiary of Honeywell International, Inc., for the U.S. Department of Energy's National Nuclear Security Administration under contract DE-NA0003525.

II.7 Multi-Mode SI/ACI: Stratification/Fuel/Dilute (Oak Ridge National Laboratory)

Scott Curran, Principal Investigator
Oak Ridge National Laboratory
2360 Cherahala Boulevard
Knoxville, TN 37932
E-mail: curransj@ornl.gov

Kevin Stork, DOE Technology Development Manager
U.S. Department of Energy
E-mail: Kevin.Stork@ee.doe.gov

Start Date: October 1, 2018 End Date: September 30, 2019
Project Funding (FY19): $200,000 DOE share: $200,000 Non-DOE share: $0

Project Introduction

This project has an overall goal of quantifying the role of fuel properties on enabling advanced compression ignition (ACI) performance and what impact is seen on spark-ignition (SI) performance using a single-cylinder, center-mount, boosted gasoline direct injection engine platform. This project aims to bridge foundational DOE Co-Optima research into fuel property impacts on SI mode efficiency, ACI mode efficiency, and multi-mode impacts. Co-evolution of these emerging technologies and biofuels represents an opportunity to reduce petroleum consumption in future engines and vehicles in a mutually beneficial way. Further understanding of fuel property impacts on maximizing ACI operation with additional requirements of being able to run in SI mode part-time is important to the objectives within the DOE Co-Optimization of Fuels and Engines initiative. This project seeks to use single-cylinder engine experiments to characterize potential fuel consumption benefits of various multi-mode ACI operating modes over state-of-the-art SI engines. This includes determining which fuel properties enable larger load ranges to maximize ACI system fuel consumption improvements with multi-mode operational constraints. Knowledge discovery and additional insights through modeling in collaboration with the Co-Optima Toolkit development team are key to furthering these goals.

Objectives

Overall Objectives

- Quantify fuel effects on multi-mode constraints and impact of range/location of ACI mode
- Understand fuel property impacts on achieving ACI with requirements of being able to run in SI mode part-time as part of a multi-mode strategy
- Characterize the impacts of ACI range and location on potential improvements to fuel economy.

Fiscal Year 2019 Objectives

- Quantify the impact of fuel chemical function characteristics on spark-assisted and kinetically controlled compression ignition strategies focused on multi-mode operation
- Demonstrate performance of ACI strategies on a 12:1 compression ratio (CR) engine and the effect of the fuel choice on the maximum SI achievable load
- Quantify the trade-off between ACI and SI performance due to fuel chemistry effects on the required intake pressure and temperatures at a relatively low CR.

Approach

To achieve the stated project goals, this project focuses on metal engine experiments using a single-cylinder research engine provided by General Motors and developed for multi-mode ACI research with unique enabling capabilities (valve authority, advanced fuel injection and ignition system, etc.) to bookend fuel property effects on expanding ACI operation range and location to maximize multi-mode fuel consumption improvements. The engine configuration used for these experiments is shown in Figure II.7.1. The engine features an 86 mm bore, a 94.6 mm stroke, a displacement of 0.55 L/cylinder, and a CR of 12:1. This unique General Motors single-cylinder metal engine research platform equipped with enabling technologies for a multi-mode combustion strategy will allow for further control over the pressure-temperature space. Special consideration in the design of the air handling system included advanced intake heating for beyond motor octane number conditions needed for ACI operation. The ability of this engine to navigate the pressure-temperature trajectories for achieving stable ACI is important to the objectives of this project.

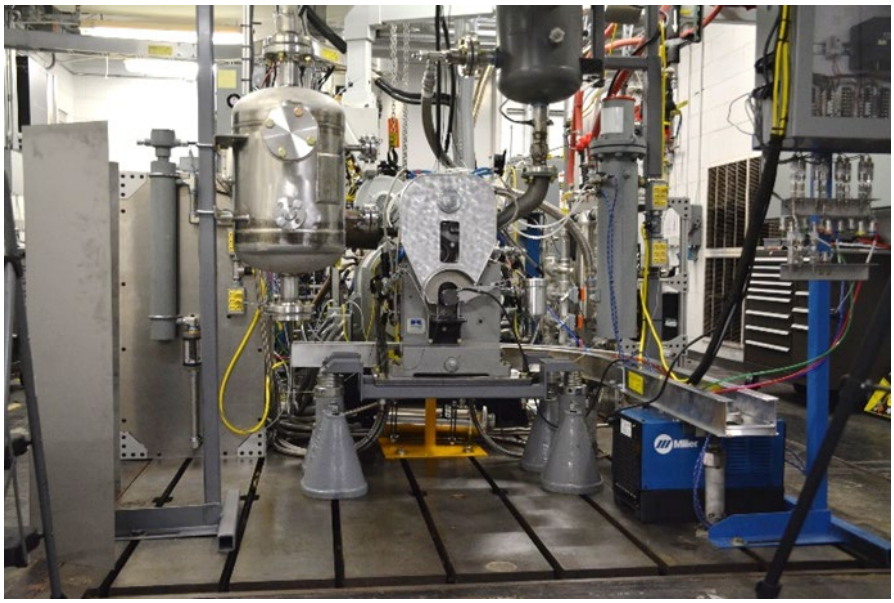

Figure II.7.1 Multi-mode metal single-cylinder engine

Experiments using the Co-Optima core fuels and custom blends will focus on characterizing the effects of fuel properties such as research octane number and octane sensitivity on improving ACI range with the advanced ignition system and valve phasing of the new engine platform to explore the limitations of the fuels to achieve stable, low-load ACI operability, highest-load ACI, and SI high load across possible levels of stratification. A custom fuel delivery system was installed, allowing rapid fuel changes across the range of fuels investigated in these experiments, which included both Co-Optima core fuels and custom blends targeted at isolating chemical functional group property impacts on ACI performance. Table II.7.1 shows the primary combustion mode and fuel set used for these experiments. A spark-assisted compression ignition (SACI) point was added to explore the transition mode between ACI and SI. A partial fuel stratification (PFS) gasoline compression ignition mode was the primary ACI mode explored in this year's experiments. In addition, the ability to run in a moderate or heavy fuel stratification gasoline compression ignition mode was investigated. Additional thermodynamic analysis was performed using information from kinetics modeling to understand the pressure-temperature trajectory effects of the various fuel and combustion mode strategies.

Table II.7.1 Matrix of Fuels and Combustion Strategies

Fuel	SI	SACI	PFS
Alkylate	●	●	●
Olefinic	●	●	●
Cycloalkane	●	●	●
E30	●	●	●
Aromatic	●	●	●
RD5-87	●	●	●
CB1 -Surrogate	●	●	●

E30 – blend of 30% ethanol and 70% gasoline; RD5-87 – research-grade regular gasoline with 10% ethanol

Results

The main objective of the experiments performed in this fiscal year was to quantify the performance of ACI strategies in a 12:1 CR engine and the effect of the fuel choice on the maximum SI achievable load. Experiments were designed to investigate the trade-off between ACI and SI performance due to fuel chemistry effects on the required intake pressure and temperatures (pressure-temperature trajectory effects) at a relatively low CR.

Both SACI and PFS gasoline compression ignition ACI mode points were investigated along with high-load SI. For the SI point, the load is maximized at a combustion phasing of 30 crank angle degrees after top dead center with the same fuel. The matrix of fuels is shown in Table II.7.1. An experimental procedure was created to accommodate the larger range in research octane number for the fuels that were added in addition to the Co-Optima core fuels.

SACI represents a transition mode for multi-mode operation and can also be used for engine speed and load points outside of the ACI window. For the SACI case, an equivalence ratio (ϕ) of 0.51 was maintained, and a dual injection strategy was used with ~20% of the fuel energy on second direct injection. The main direct injection was early in the cycle, around 180° before top dead center, and the second direct injection was commanded at a few degrees before spark. For the SACI experiments, the focus was on understanding the control authority from spark timing on combustion phasing. Figure II.7.2 shows the heat release rate as a function of spark timing with an intake temperature of 65°C and an intake pressure 125 kPa.

The PFS experiments were conducted with $\phi = 0.35$ at a similar load to the SACI points. A dual injection strategy with 80% fuel energy in the first injection and 20% fuel energy in the second injection was used. The focus of the PFS experiments was to assess the combustion phasing control authority as a function of injection timing of the second injection, which alters the in-cylinder fuel and air stratification at the time of ignition (Figure II.7.3).

At the time of this report, the results of the experimental campaign were ongoing with the other fuels, and those results will be summarized in an upcoming manuscript and a presentation at the Advanced Engine Combustion Program Review.

Building off the foundational pressure-temperature analysis by Szybist and Splitter [1], an ACI pressure-temperature analysis framework using partially stratified ACI combustion data was developed to understand any additional requirements. These results are under further analysis.

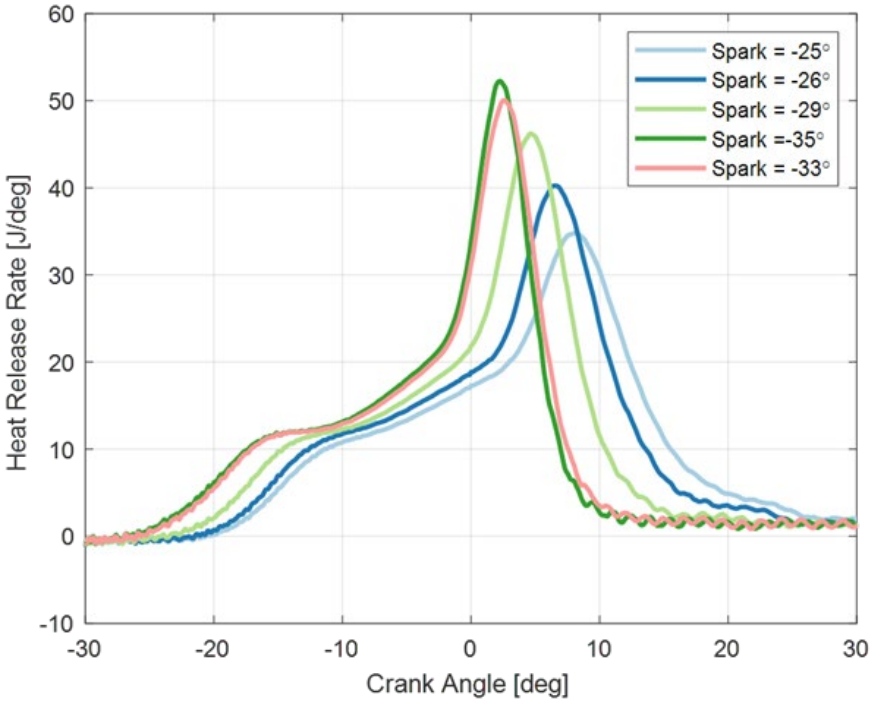

Figure II.7.2 SACI spark timing sweep with the alkylate Co-Optima core fuel

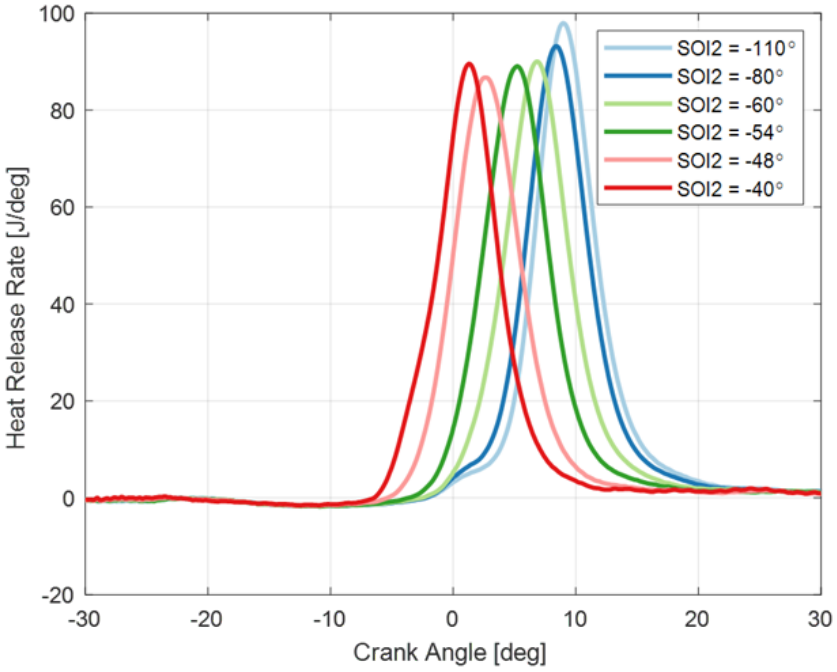

SOI2 – start of second injection

Figure II.7.3 PFS second injection timing sweep with the alkylate Co-Optima core fuel

Key accomplishments for Fiscal Year 2019 included the following:

- Quantified impact of fuel chemical function characteristics on spark-assisted and kinetically controlled compression ignition strategies focused on multi-mode operation
- Demonstrated the performance of ACI strategies on a 12:1 CR engine and the effect of the fuel choice on the maximum SI achievable load
- Quantified the trade-off between ACI and SI performance due to fuel chemistry effects on the required intake pressure and temperatures at a relatively low CR with a wide range in Co-Optima core fuels.

Conclusions

In Fiscal Year 2019, the ACI/SI project worked at quantifying the role of fuel properties in enabling ACI performance and what impact is seen on SI performance to accelerate the development of multi-mode strategies enabled by fuel properties. A unique single-cylinder was engine used to support these goals. The ability of multi-mode strategies to improve fuel economy was better understood using modeling and analysis.

Key Publications

1. Drallmeier, J., M. Wissink, S. Curran, and R. Wagner. 2018. "Ignition Delay in Low Temperature Combustion." SAE Technical Paper 2018-01-1125. DOI:10.4271/2018-01-1125.

2. Wissink, M., S. Curran, C. Kavuri, and S. Kokjohn. 2018. "Spray–Wall Interactions in a Small-Bore, Multicylinder Engine Operating with Reactivity-Controlled Compression Ignition." *ASME. J. Eng. Gas Turbines Power* 140 (9): 092808. DOI:10.1115/1.4039817.

References

1. Szybist, J., and D. Splitter. 2017. "Pressure and Temperature Effects on Fuels with Varying Octane Sensitivity at High Load in SI Engines." *Comb and Flame* 177: 49–66. DOI: 10.1016/j.combustflame.2016.12.002.

Acknowledgements

Flavio Chuahy, Tommy Powell, and Jim Szybist of Oak Ridge National Laboratory provided valuable contributions to this project and report. The authors also gratefully acknowledge General Motors for providing a specialized research platform for the project and the Co-Optima leadership team for guidance.

II.8 Fuel Effects on Low Speed Pre-Ignition (Oak Ridge National Laboratory)

Derek Splitter, Principal Investigator
Oak Ridge National Laboratory (ORNL)
2360 Cherahala Boulevard
Knoxville, TN 37922
E-mail: splitterda@ornl.gov

Kevin Stork, DOE Technology Development Manager
U.S. Department of Energy
E-mail: Kevin.Stork@ee.doe.gov

Start Date: October 1, 2018 End Date: September 30, 2019
Project Funding (FY19): $100,000 DOE share: $100,000 Non-DOE share: $0

Project Introduction

Downsized and turbocharged spark-ignited engines are being increasingly used by engine manufacturers to improve vehicle efficiency while reducing CO_2 emissions [1],[2]. While greatly effective at improving fuel economy, the increased specific outputs of these engines make them more prone to damaging phenomena such as pre-ignition. Although pre-ignition is not a novel process or unique to downsized boosted engines [3], the high-load, low-speed operating conditions of these engines result in a particularly intense pre-ignition process, which is typically referred to as low-speed pre-ignition (LSPI). LSPI events often consist of very strong knock event(s) that can cause significant damage to engine hardware, including catastrophic engine failure.

LSPI typically occurs during very-high-load operation at engine speeds around 2,000 r/min or below, wherein, the flame initiates before the spark is fired and leads to flame propagation at a significantly advanced combustion phasing. The increased pressure rise due to the advanced combustion phasing often causes violent end-gas knock or even 'super-knock' for events that transition to developing detonation [4], all of which can result in catastrophic engine damage. The fundamental causes of LSPI still remain poorly understood, and there is a lack of firm consensus on the underlying mechanisms that promote LSPI, but recent findings by Splitter et al. highlight that fundamental fuel properties are important to LSPI event occurrence [5], and previous findings by Jatana et al. [6] highlighted that there are fuel property effects on LSPI beyond those of fuel distillation alone. Although there has been significant recent work to understand LSPI processes, a gap still exists in the understanding of the impact of fuel properties, both physical and chemical, on LSPI behavior. This project aims to provide more clarity on the relationship between fuel properties and LSPI, with fuel properties being specifically studied.

Objectives

- Quantify the relationship between fuel properties and LSPI frequency with respect to fuel distillation and molecular properties
- Determine if specific fuel properties affect LSPI intensity.

Approach

This project is transitioning between engines in Fiscal Year (FY) 2019. Results will be presented on the exiting platform, while FY 2019 activity is transitioning to a new platform. The existing engine used in this study is based on a 1.6 L Ford Ecoboost engine equipped with the production center-mounted direct injection fueling system. The engine was converted to a single-cylinder engine by disabling Cylinders 2, 3 and 4, where Cylinder 1 is closest to the crank snout and Cylinder 4 is closest to the flywheel. The combustion chamber

geometry and camshaft profiles on Cylinder 1 were unchanged from the stock configuration. The platform to which the project is transitioning is a GM LNF engine, which is a side-mounted injector engine. The engine also is being converted to a single-cylinder engine, but unlike the Ford 1.6 L Ecoboost, the oiling system of the LNF will also be converted from a wet sump to a dry sump oiling system. The dry sump is a necessary change to adapt laser-induced fluorescence diagnostics to the engine to get real-time monitoring of fuel-wall impingement. With the laboratory currently in transition stage for FY 2019, all results presented herein are based on the Ford Ecoboost platform.

The LNF engine will be operated in the same manner that the existing Ford Ecoboost engine was, using standalone laboratory fueling and air handling systems. The engine is controlled through a custom DRIVVEN-based engine controller, with automatic engine controls developed at ORNL with calibration based on manual engine mapping. The controller uses a mass airflow-based control feedback enabled tabular based engine map for fully automatic control of fuel, air, spark timing, and camshaft phasing. All measurements presented in this study were acquired in automated operation using time-varying load square-wave segments at 2,000 r/min. Each segment consists of 5 min of operation at low load (5 bar gross indicated mean effective pressure [IMEPg]), followed by 25 min of high-load (13–16 bar IMEPg) operation. Note that these loads are typically lower than those of previous LSPI work, as the fuel used in the present work is of a reduced research octane number (RON) of 70. This fuel obtains pre-ignition and heavy knock retard at reduced loads. The first 5 min of each 25-min high-load segment were thermally transient in boundary conditions and were discarded from the analysis such that only the last 20 min of data (20,000 cycles) of each high-load segment were used for the study of LSPI behavior. Finally, 8–10 such consecutive low-high-low load square-wave segments were run for each experiment to ensure sufficient LSPI event count for consistent statistical analysis. Fresh engine oil was used for each experiment, and the lubricant pressure was monitored to verify fuel-oil dilution was occurring. To reproduce fuel-oil dilution, the injector was oriented such that the fuel-linear impingement could be increased or decreased to maintain similar fuel-oil dilution for various fuels/load throughout the LSPI segments.

The fuels used were based on a reduced octane number gasoline acquired from Haltermann products. One fuel was baseline fuel from previous high-load experiments: product code HFO437 (hereby referred to as EEE). The other fuels used were lower octane number and operated at reduced load (hereby referred to as 70RON). Two lots of 70RON were used, with various fuel distillation points, which differed in distillation as determined by the ASTM D86 test by approximately 20°F for most of the fuel distillation.

A cycle was identified as LSPI if the peak recorded cylinder pressure and 4% of mass fraction burned (CA04) were both more than 3.85 standard deviations greater than the median maximum cylinder pressure of all the cycles. The approach is similar to that described in detail by Mansfield et al. [7].

Results

- Confirmed that LSPI number count is highly correlated to fuel-wall interaction
- Illustrated that lubricant effects are independent of only fuel-wall interaction, a critical aspect for fuel property formulations
- Developed new engine platform to investigate fuel property effects on fuel-wall interactions relevant to LSPI.

The fuels tested in this project are carryover from FY 2018 and are reported in Table II.8.1, which highlights that the distillation of fuels based on 70 RON gasoline were very similar, and the distillation of EEE and the low-volatility 70 RON fuel were very similar. The EEE gasoline was used as a reference fuel for a baseline comparison for the reduced octane fuels, which are the major focus of the work for this year. The reduced octane fuels were used because they have similar fuel kinetics at reduced engine load, and thus reduced engine damage potential, increasing the repeatability of the experiments. The approach resulted in additional discoveries that revealed information on the fundamentals of LSPI.

Table II.8.1 Tested Fuels

Fuel Name	EEE	70 RON low vol.	70 RON high vol.
Blended molecule	-	-	-
Blended (% vol.)	100%	100%	100%
RON (ASTM D2699)	96.3	71.0	71.2
MON (ASTM D2700)	88.8	67.7	66.9
IBP (°F) (ASTM D86)	87	100	96
T5 (°F) (ASTM D86)	114	143	132
T10 (°F) (ASTM D86)	127	162	146
T20 (°F) (ASTM D86)	148	185	167
T30 (°F) (ASTM D86)	171	202	184
T40 (°F) (ASTM D86)	200	216	199
T50 (°F) (ASTM D86)	220	227	211
T60 (°F) (ASTM D86)	231	238	222
T70 (°F) (ASTM D86)	241	251	233
T80 (°F) (ASTM D86)	257	269	246
T90 (°F) (ASTM D86)	315	293	271
T95 (°F) (ASTM D86)	340	309	298
FBP (°F) (ASTM D86)	411	335	331

MON – motor octane number; IBP – initial boiling point;
Tx – temperature at x percent fuel boiled; FBP – final boiling point

As shown in Figure II.8.1, the oil pressure drop as a function of LSPI segment number for the 70RON fuel (black data in Figure II.8.1) at the reduced load (13 bar IMEPg) operating condition was similar to that for the EEE fuel (red data in Figure II.8.1) at high load (20 bar IMEPg). The similar oil pressure drop was used as a surrogate to determine fuel-oil dilution, and at the lower load condition, injector orientation was required to increase fuel-linear impingement to replicate oil pressure drop.

The oil pressure drop measured from the LSPI testing was used as a coarse measurement for fuel dilution of the sump oil. Interestingly, for a given injector orientation at the 13 bar IMEPg operating condition, it was found that the increased oil pressure drop with the 120° injector orientation (circle marker data in Figure II.8.1) also correlated to statically significant increase in the number count of LSPI events, approximately double the events, as shown in Figure II.8.2.

Using these findings as a baseline, in FY 2019 a new engine platform was developed to directly investigate fuel-wall interaction on LSPI. The engine was converted to a dry sump, which reduces the lubricant residence time in the sump. Therefore, the lubricant supplied to the engine is evacuated quickly and is not diluted with the lubricant in the engine oil sump. The approach enables coupling of the ORNL-developed fuel in oil diagnostic to measure fuel oil dilution directly. The low residence time of the lube in the engine reduces the uncertainty of when fuel dilution occurs, as the measurement is made from scrape-down that is close-coupled in time to LSPI operation and LSPI-prone conditions. The fuel in oil diagnostic uses a spectral-based laser-induced fluorescence (LIF) signal from attenuation of laser light with dye. The concept is presented in Figure II.8.3, where the LIF diagnostic is coupled with the dry sump system for quantification of fuel retention by fuel-wall interaction. This approach will be used to explore fuel-specific properties and interactions on LSPI with direct quantification measurements of fuel retention.

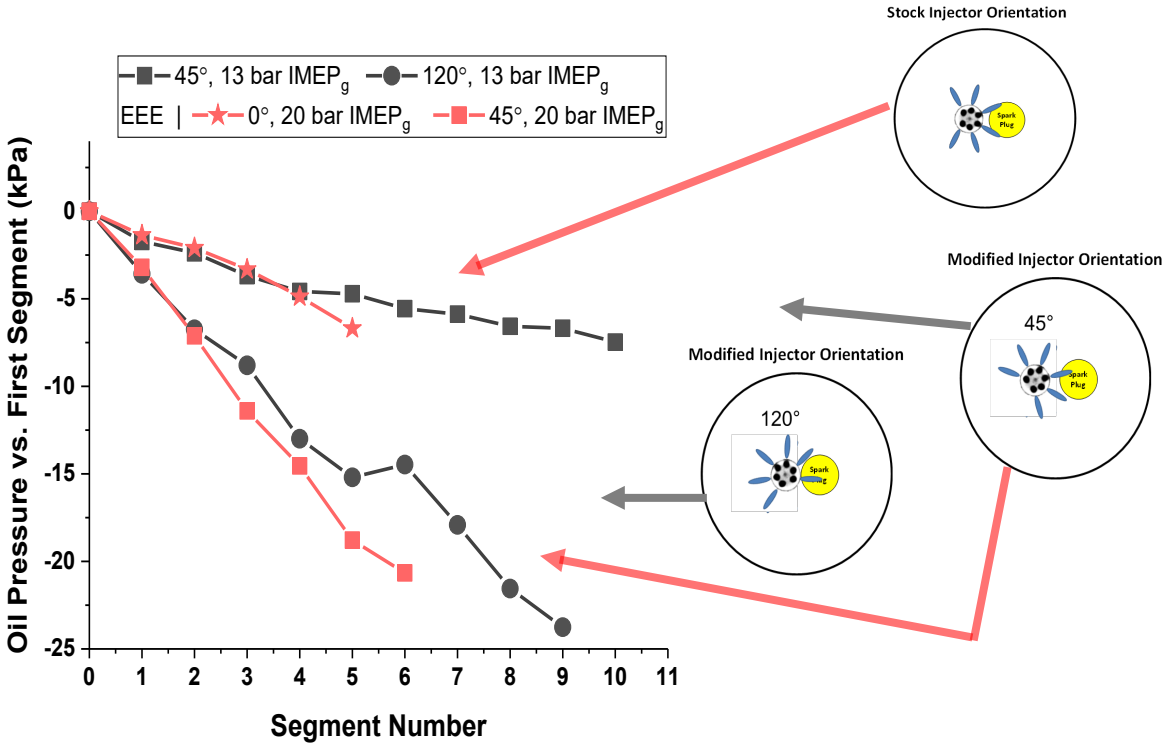

Figure II.8.1 Engine oil pressure reduction as a function of LSPI segment for various engine loads and injector orientations. The reduced engine load conditions required increased fuel-wall targeting to match oil pressure drop present at higher engine load operation.

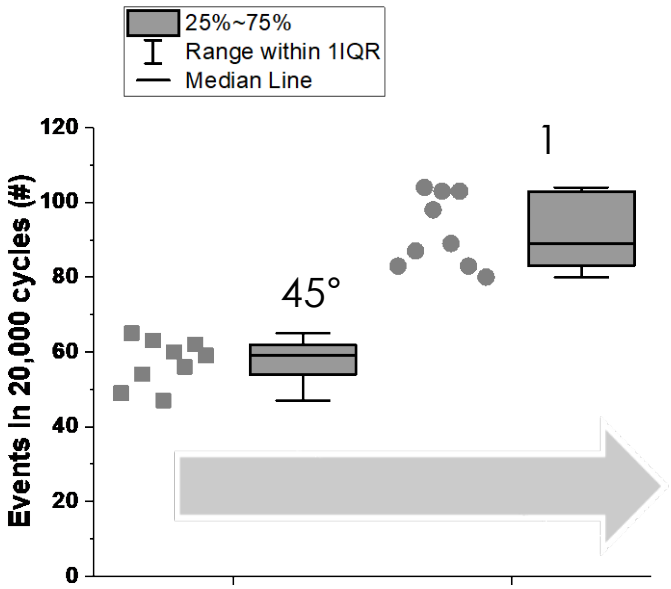

IQR – interquartile range

Figure II.8.2 Recorded LSPI events per segment for matched load, varied injector orientation operation

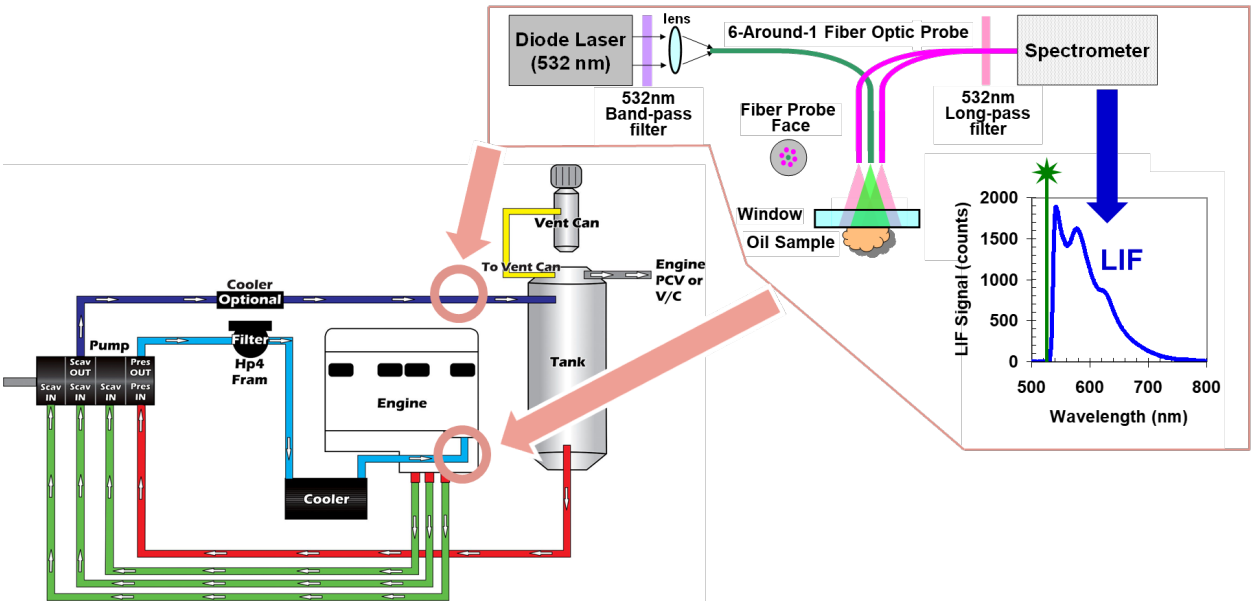

PCV – positive crankcase ventilation; V/C – volume/control

Figure II.8.3 Schematic of LNF dry sump conversion and fuel in oil diagnostic installation points in test cell. Dry sump figure from supplier used in dry sump conversion [8].

The installation on the dry sump converted system is depicted in Figure II.8.4.

Figure II.8.4 Dry sump single-cylinder LNF engine installation and conversion

Conclusions

- Confirmed that LSPI number count is highly correlated with fuel distillation and fuel retention in the top ring zone
- Developed experimental approach to directly test fuel-wall interactions and correlate fuel effects to LSPI in real time.

Key Publications

1. Splitter, D., B. Kaul, and J. Szybist. 2019. "Update on Stochastic Pre Ignition Work at ORNL." AEC/MOU meeting (January 30), Oak Ridge National Laboratory, Oak Ridge, TN.
2. Splitter, D., B. Kaul, and J. Szybist. 2019. "Investigations into Stochastic Pre Ignition Causes." SAE World Congress Experience, Invited Panel Discussion (April 10), Detroit, MI.
3. Splitter, D., B. Kaul, J. Szybist, L. Speed, B. Zigler, and J. Luecke. 2019. "Fuel-Lubricant Interactions on the Propensity for Stochastic Pre-Ignition." SAE Technical Paper No. 2019-24-0103.

References

1. Pawlowski, Alexander, and Derek Splitter. 2015. "SI Engine Trends: A Historical Analysis with Future Projections." SAE Technical Paper No. 2015-01-0972.
2. Splitter, Derek, Alexander Pawlowski, and Robert Wagner. 2016. "A Historical Analysis of the Co-Evolution of Gasoline Octane Number and Spark-Ignition Engines." *Frontiers in Mechanical Engineering* 1: 16.
3. Chapman, Elana M., and Vincent S. Costanzo. 2015. "A Literature Review of Abnormal Ignition by Fuel and Lubricant Derivatives." *SAE International Journal of Engines* 9, No. 2015-01-1869: 107–142.
4. Wang, Zhi, Yunliang Qi, Xin He, Jianxin Wang, Shijing Shuai, and Chung K. Law. 2015. "Analysis of Pre-Ignition to Super-Knock: Hotspot-Induced Deflagration to Detonation." *Fuel* 144: 222–227.
5. Splitter, Derek, Brian Kaul, James Szybist, and Gurneesh Jatana. 2017. "Engine Operating Conditions and Fuel Properties on Pre-Spark Heat Release and SPI Promotion in SI Engines." *SAE International Journal of Engines* 10, No. 2017-01-0688.
6. Jatana, Gurneesh S., Derek A. Splitter, Brian Kaul, and James P. Szybist. 2018. "Fuel Property Effects on Low-Speed Pre-Ignition." *Fuel* 230: 474–482.
7. Mansfield, Andrew B., Elana Chapman, and Kenneth Briscoe. 2016. "Impact of Fuel Octane Rating and Aromatic Content on Stochastic Pre-Ignition." SAE Technical Paper No. 2016-01-0721.
8. Figure from Armstrong Race Engineering, www.drysump.com, accessed December 2019.

II.9 Fuel Properties Enhancing Multi-Mode ACI/SI Engine Operation (Argonne National Laboratory)

Toby Rockstroh, Principal Investigator
Argonne National Laboratory
9700 S. Cass Avenue
Lemont, IL 60439
E-mail: trockstroh@anl.gov

Kevin Stork, DOE Technology Development Manager
U.S. Department of Energy
E-mail: Kevin.Stork@ee.doe.gov

Start Date: October 1, 2017 End Date: September 30, 2019
Project Funding (FY19): $245,000 DOE share: $245,000 Non-DOE share: $0

Project Introduction

The potential efficiency benefits of advanced compression ignition (ACI) in multi-mode gasoline engines as well as the complexities associated with controlling the ACI combustion mode and mode switching are well documented [1],[2],[3].

The gasoline fuel for a multi-mode engine needs to fulfill two seemingly contradicting requirements. For ACI operation at low load, a fuel with a moderate autoignition propensity is desired, while the high-load spark ignition (SI) operation demands a fuel with high autoignition resistance in order to prevent knock. Historically, gasoline knock resistance (or conversely, the autoignition propensity) has been described by the research octane number (RON) and the motor octane number (MON). It has since been shown that octane number does not adequately describe knock resistance in modern SI engines [4],[5],[6] or autoignition behavior in ACI operation [7],[8].

For the purpose of this investigation, five Co-Optima gasolines with RON of 98 were investigated. One of the test fuels had a low octane sensitivity of S = 3, while the remaining fuels had a high sensitivity of S = 10, albeit utilizing different chemical classes to generate the octane sensitivity. The aim of the study was to characterize the ignition delay behavior of the fuels over a range of engine-relevant conditions using experimental data from a rapid compression machine (RCM) and chemical kinetic simulation. Furthermore, correlations between the engine control parameters and the thermodynamic state at the time of autoignition were investigated. Finally, an analysis was conducted to characterize the effect of engine control parameters and geometric compression ratio on the autoignition propensity under ACI operation for three of the RON 98 fuels.

Objectives

Overall Objectives

- Quantify the effects of advanced fuel properties towards expanding the ACI operating envelope using a SI engine platform
- Optimize the engine control parameters to take advantage of the enhanced fuel properties
- Demonstrate the ability to implement an enhanced multi-mode combustion strategy on a light-duty SI engine platform to improve fuel efficiency.

Fiscal Year 2019 Objectives

- Characterize the effects of octane sensitivity and fuel chemistry on multi-mode engine operation in a light-duty SI engine
- Utilize the engine compressed gas conditions and fundamental autoignition delay trajectories to characterize the engine control parameters
- Identify the constraints imposed by the SI engine hardware and fuel properties towards enabling multi-mode engine operation.

Approach

All Co-Optima RON 98 fuels were tested on a single-cylinder direct injection SI engine at a compression ratio of 15.3:1. The engine was operated at 1,500 rpm and two fuel loading conditions, lambda 3.6 and 2.6, respectively. The injection timing was maintained at 300 degrees before top dead center (°bTDC), and three intake temperatures of 100°C, 135°C, and 170°C were tested while the intake pressure was used to maintain the combustion phasing CA50 (crank angle at 50% mass fraction burned) at 12 degrees after top dead center (°aTDC).

The ignition delays were measured by a collaborating group at Argonne National Laboratory, led by Dr. Scott Goldsborough, using a twin-piston RCM, and kinetic simulations were done using the Zero-Order Reaction Kinetics (Zero-RK) solver and a detailed kinetic mechanism for transportation fuels developed by Lawrence Livermore National Laboratory.

Details of the core fuels are listed in Table II.9.1 below.

Table II.9.1 Co-Optima Fuel Properties

Property	Method	O30[e]	E30[f]	A30[g]	ALK[h]	N30[i]
PHYSICAL PROPERTIES						
RON (R)	D2699	98.2	97.4	98.1	98.0	98.0
MON (M)	D2700	88.0	86.6	87.8	96.6	87.1
S[a]	R-M	10.2	10.8	10.3	1.4	10.9
LHV[b]	D4809	44.071	38.170	42.952	44.524	43.208
HoV[c]		337	565	412	309	393
COMPOSITION ANALYSIS						
Aromatic[d]	D1319	10.6	8.1	30.8	0	28.2
Olefin[d]	D1319	31.3	5	4.2	0	1.5
Saturate[d]	D1319	58.1	57.1	65	100	70.3
Ethanol[d]	D5599	<0.1	30.59	<0.1	<0.1	<0.1

[a]S = Octane Sensitivity, [b]LHV [MJ/kg] = Lower Heating Value, [c]HoV [kJ/kg] = Heat of Vaporization, [d]Volume fraction, [e]O30 = Co-Optima gasoline blend containing 30% olefins by volume, [f]E30 = Co-Optima gasoline blend containing 30% ethanol by volume, [g]A30 = Co-Optima gasoline blend containing 30% aromatics by volume, [h]ALK = predominantly alkylate-containing Co-Optima gasoline blend, [i]N30 = Co-Optima gasoline blend containing 30% naphthenes by volume

In order to investigate the effect of engine control parameters and compression ratio on ACI operation in a multi-mode SI engine, the Taguchi design of experiments approach was utilized to define a test matrix of 27 test points using the operating parameters outlined in Table II.9.2. The experiments were conducted using the ALK, E30, and O30 test fuels. Three levels were chosen for each engine control parameter, and the intake pressure was used to maintain the combustion phasing CA50 at 10 °aTDC. The lowest compression ratio was chosen to enable ACI operation without misfire while the highest compression ratio was constrained by knock-limited SI operation at high load.

Table II.9.2 Engine Test Operating Parameters According to Design of Experiments

Level	CR[a] [-]	N[b] [rpm]	T_{in}[c] [°C]	EGR[d] [-]	Φ[e] [-]	EOI[f] [°bTDC]
-1	11.3	1,000	180	0	0.2	30
0	12	1,500	230	20	0.28	50
1	12.7	2,000	280	40	0.35	300

[a]CR = Compression Ratio, [b]N = Engine Speed, [c]T_{in} = Intake Temperature,
[d]EGR = Exhaust Gas Recirculation, [e]Φ = Equivalence Ratio, [f]EOI = End of Injection

Results

The autoignition behavior of the Co-Optima core fuels was characterized in the engine, and the thermodynamic conditions at the end of compression were replicated in the RCM. It was found that the intake boost requirements could be correlated to the compressed pressure in the RCM, as shown in Figure II.9.1. Here the boost pressure and compressed pressure were normalized over the requirements of the ALK fuel. The behavior appeared to be consistent over a range of intake temperatures and the equivalence ratios tested.

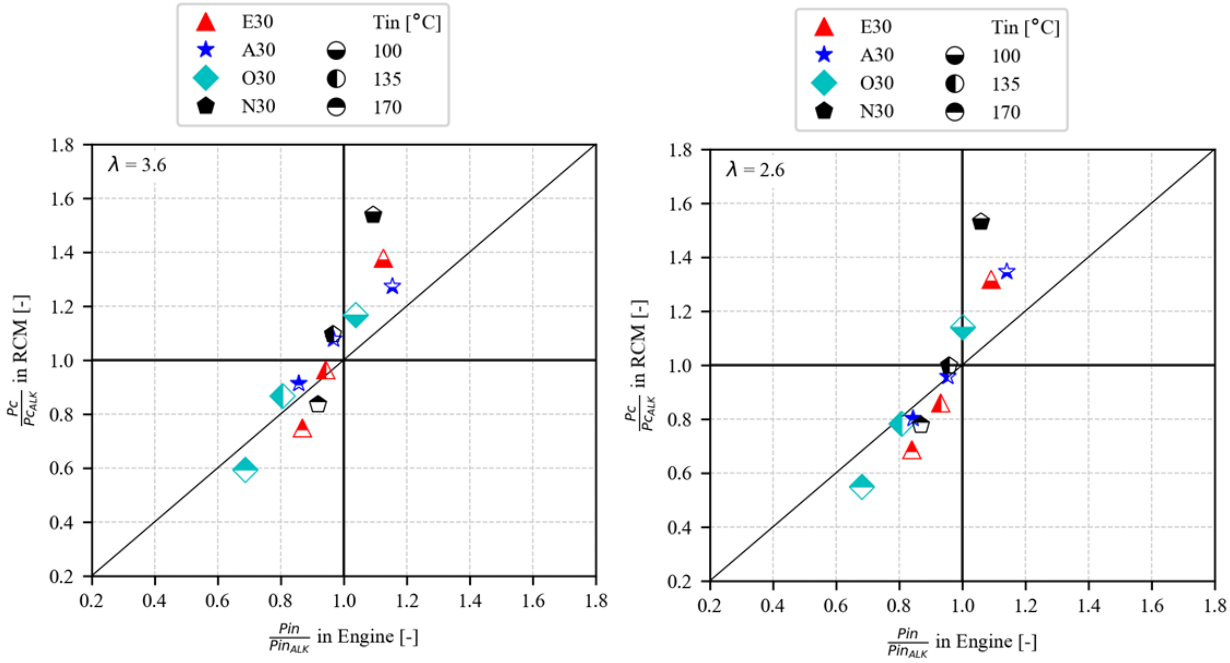

Figure II.9.1 Comparison between required intake pressure (P_{in}), at various T_{in}, in the engine experiments to achieve identical combustion phasing, normalized over ALK's requirements; and compressed pressure (P_c) required for a given compressed temperature (T_c) to achieve τ_{main} = 4 ms in RCM experiments, at lambda 3.6 and 2.6

A similar trend was observed when using chemical kinetic simulations, although some discrepancies in the autoignition behavior were noted between model and experimental results, as shown in Figure II.9.2 for a fuel load of lambda 2.6. It should be noted that a recently updated kinetic mechanism showed results that were more consistent with the RCM experiments.

In principle, validated kinetic mechanisms are a useful tool to generate reactivity maps using isopleths (i.e., constant ignition delay contours) over a range of engine-relevant conditions (e.g., pressure and temperature), which can be implemented in control methodologies for ACI engine operation.

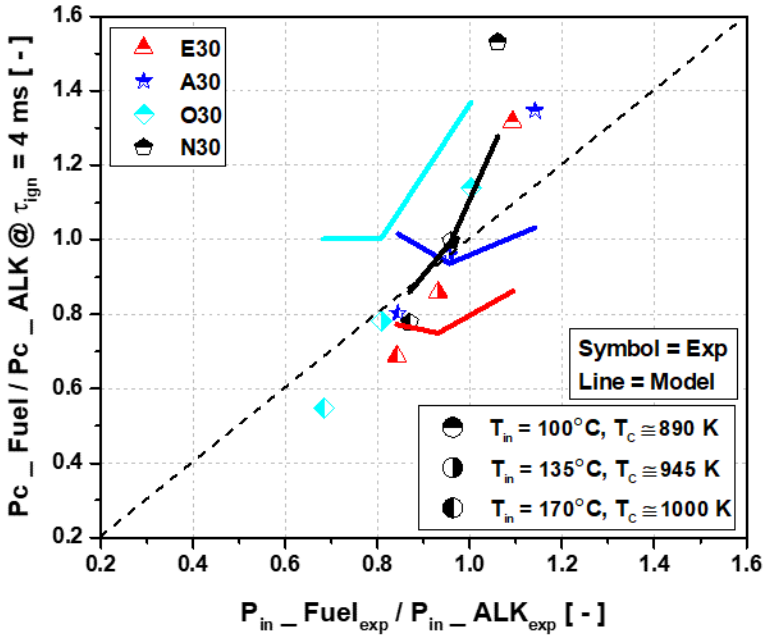

Figure II.9.2 Comparison between required P_{in}, at various T_{in}, in the engine experiments to achieve identical combustion phasing, normalized over ALK's requirements; and P_c required for a given T_c to achieve τ_{main} = 4 ms in RCM experiments and kinetic model simulation, at lambda 2.6

The impact of the engine control parameters on the intake pressure requirements can be highlighted by comparing the coefficients of a linear regression analysis, as depicted in Figure II.9.3. Since intake pressure was used as a control strategy to maintain a constant combustion phasing, this comparison provides a qualitative analysis of the influence of the remaining engine control parameters on the reactivity of the charge. Intake temperature and compression ratio have the highest negative standardized coefficients, implying that an increase in either parameter resulted in a strong reduction of the required intake pressure, i.e., an increase in the reactivity of the charge at the end of compression. The remaining control parameters have a smaller effect on the inlet pressure. The equivalence ratio and engine speed are shown to marginally decrease the required intake pressure, while EGR has the opposite effect. Mixture stratification due to later injection phasing is shown to have almost negligible effect on boost pressure required to maintain constant combustion phasing.

In order to gain a better understanding of the thermodynamic conditions to which the air/fuel mixtures were subjected at the end of compression, the compressed pressure and temperature for each operating condition were plotted, as shown in Figure II.9.4. The cylinder gas temperature was estimated using the measured cylinder pressure and ideal gas law correlations. The 0.5 ms and 4 ms constant volume ignition delay isopleth lines were computed for two equivalence ratios of 0.38 and 0.28 (lambda 2.6 and 3.6) with 18.5% oxygen concentration; they are provided for reference. The effectiveness of utilizing static autoignition delay characteristics of a fuel to determine the intake air pressure and temperature required to control the combustion phasing for ACI operation was shown and discussed in Figure II.9.1 and Figure II.9.2.

However, the ACI operating envelope is also constrained by combustion noise and stability, which will be assessed in more detail here.

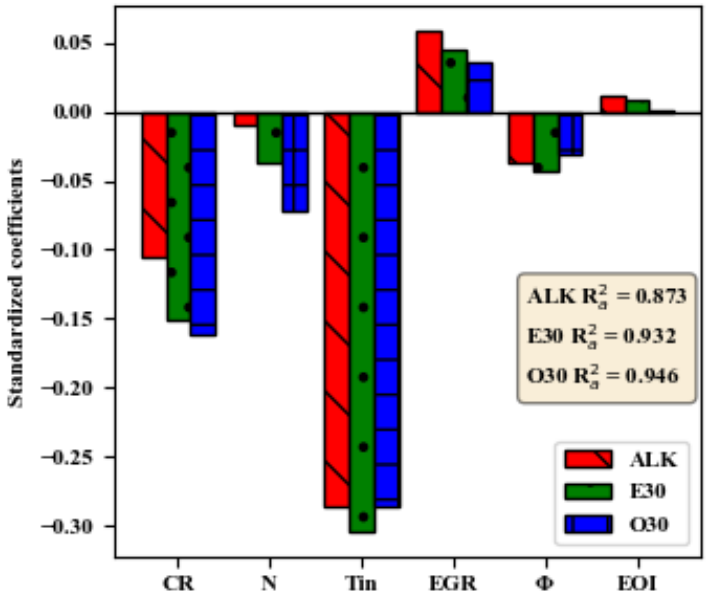

Figure II.9.3 Impact of engine control parameters on the intake pressure requirements over all test conditions

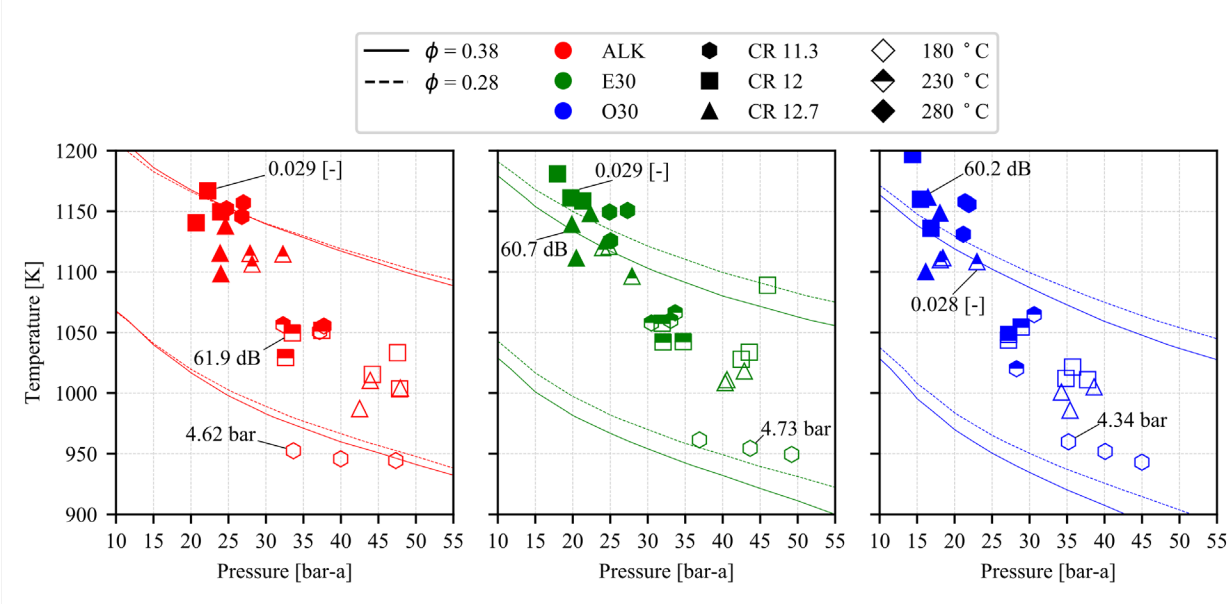

Figure II.9.4 Comparison of the cylinder pressure and temperature conditions at top dead center in engine experiments against constant ignition delay isopleths of 0.5 ms and 4 ms at two equivalence ratios

It is apparent that the operating conditions resulted in intermediate- to high-temperature autoignition regimes from approximately 950 K to 1,200 K. The highest indicated mean effective pressure (IMEP) was found to occur at the low compressed temperature and the high compressed pressures, as discussed previously. Combustion noise varied at the different compressed conditions, while the highest combustion stability appeared to be at the high compressed temperatures. The three intake air temperature and compression ratio set points resulted in three compressed gas temperature regions, which will be defined as “low-temperature,” “mid-temperature,” and “high-temperature” based on their respective intake air temperature. Distribution diagrams of IMEP, cycle-to-cycle standard deviation of IMEP (IMEPst), and combustion noise for the

operating points in those temperature regions were drawn, as shown in Figure II.9.5, Figure II.9.6, and Figure II.9.7. Each distribution diagram was divided into low (L), medium (M), and high (H) response parameters, as outlined in Table II.9.3.

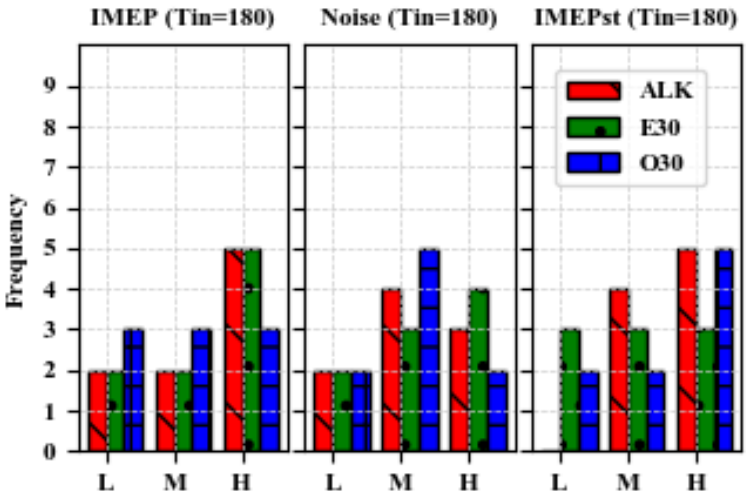

Figure II.9.5 Distribution of IMEP, combustion noise, and IMEPst in the low-temperature region (T_{in} = 180°C)

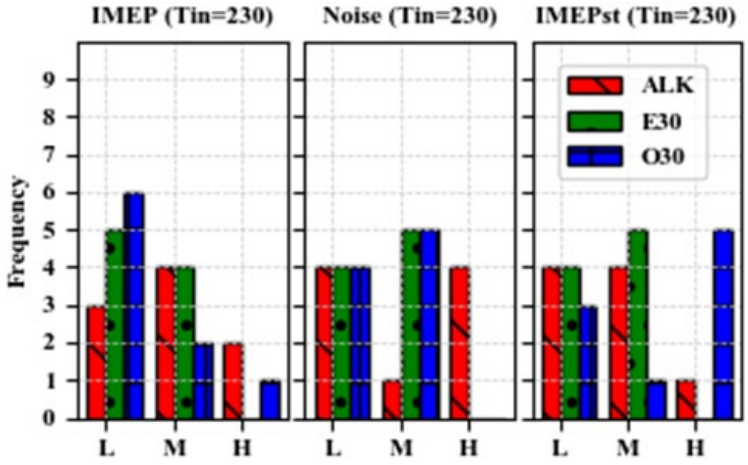

Figure II.9.6 Distribution of IMEP, combustion noise, and IMEPst in the mid-temperature region (T_{in} = 230°C)

It is evident that higher IMEP was obtained in the low-temperature region than the other regions. This behavior was consistent for each of the fuels and was expected since the intake manifold pressure needed to be increased at lower intake temperatures in order to maintain constant combustion phasing. Conversely, the IMEP was the lowest in the high-temperature region. ALK exhibited the highest IMEP in the high-temperature region, while E30 and O30 required a lower boost pressure, thereby resulting in lower IMEP. In the low-temperature region, E30 behaved more akin to ALK, requiring a higher intake manifold pressure than O30. The temperature-dependent reactivity of E30 and O30 agree with the findings outlined earlier.

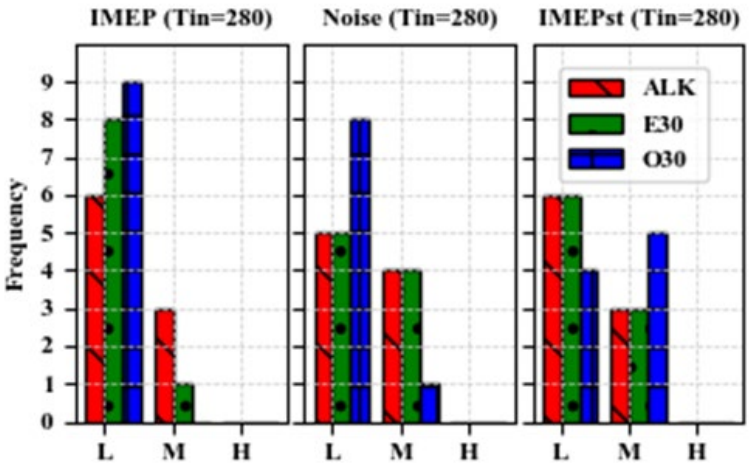

Figure II.9.7 Distribution of IMEP, combustion noise, and IMEPst in the high-temperature region (T_{in} = 280°C)

Table II.9.3 Response Parameters Used for the Distribution Diagram

	Low (L)	Medium (M)	High (H)
IMEP [bar]	x < 1.5	1.5 ≤ x < 2.5	x ≥ 2.5
IMEPst [-]	x < 0.075	0.075 ≤ x < 0.125	x ≥ 0.125
Noise [dB]	x < 70	70 ≤ x < 80	x ≥ 80

Some fuel differences were found when investigating the combustion instability (IMEPst). The ALK fuel exhibited the highest instability in the low-temperature region, while O30 was found to display more unstable operating points in the mid-temperature region. E30, on the other hand, was found to exhibit the highest combustion stability in the different temperature regions amongst the fuels, with the least stable operating points appearing in the low-temperature region.

The combustion noise was found to be the highest in the low-temperature region for all of the fuels, due to the highest load. O30 exhibited a lower number of operating points with high combustion noise, which can be linked to its higher reactivity, thereby requiring a lower intake air pressure to maintain the combustion phasing. Conversely, the lower intake pressure (due to increased reactivity) also resulted in a lower IMEP. The high-intake-temperature region displayed the lowest combustion noise for all of the fuels, with O30 exhibiting the most operating points with low combustion noise. E30 displayed similar combustion noise behavior as ALK in the low-temperature region while behaving similar to O30 in the intermediate-temperature region.

The accomplishments can be summarized as follows:

- Correlated engine boost requirements to compressed pressure in an RCM over a range of intake temperatures and two equivalence ratios.
- Demonstrated the use of static autoignition delay data to generate fuel reactivity maps, which can be implemented in ACI engine control strategies for combustion phasing control in a multi-mode SI engine.
- Completed a design of experiments study to correlate the engine control parameters on the ACI operating range in a multi-mode engine platform to distinguish fuel-specific effects on operating parameters.

Conclusions

- Static autoignition delay measurements or simulations from validated mechanisms can provide guidance on the intake manifold conditions required to control combustion phasing.
- Disparate autoignition characteristics were observed between the Co-Optima fuels despite similar RON and sensitivity. O30 fuel was found to be most reactive, requiring lower intake air boosting.
- The design of experiments study resulted in a range of compressed gas conditions, spanning the intermediate-temperature chemistry to high-temperature chemistry from approximately 950 K to 1,200 K.
- IMEP, combustion noise, and stability varied for the compressed temperature regions at which the engine was operated.
- This study warrants further investigation into the development of fuel-specific empirical models to characterize the effect of engine operating parameters for ACI operation.

Key Publications

1. Shah, A., D. Kang, S. Goldsborough, and T. Rockstroh. 2019. "Utilizing Static Auto-Ignition Measurements to Estimate Intake Air Condition Requirements for Compression Ignition in a Multi-Mode Engine – Engine and RCM Experimental Study." SAE 2019-01-0957.
2. Kang, D., A. Shah, T. Rockstroh, and S. Goldsborough. 2019. "Utilizing Static Autoignition Measurements to Estimate Intake Air Condition Requirements for Compression Ignition in a Multi-Mode Engine – Application of Chemical Kinetic Modeling." SAE 2019-01-0955.
3. Rohwer, J., A. Shah, and T. Rockstroh. 2019. "Analytical Approach to Characterize the Effect of Engine Control Parameters on the ACI Operating Envelope in a Multi-Mode GDI Engine." Technical paper under review for SAE WCX 2020.

References

1. Koopmans, L., H. Ström, S. Lundgren, O. Backlund, and I. Denbratt. 2003. "Demonstrating a SI-HCCI-SI Mode Change on a Volvo 5-Cylinder Electronic Valve Control Engine." SAE Technical Paper 2003-01-0753. Also in *Homogeneous Charge Compression Ignition (Hcci) Combustion*.
2. Kulzer, A., A. Christ, M. Rauscher, C. Sauer, G. Würfel, and T. Blank. 2006. "Thermodynamic Analysis and Benchmark of Various Gasoline Combustion Concepts." SAE Technical Paper 2006-01-0231.
3. Milovanovic, N., D. Blundell, S. Gedge, and J. Turner. 2005. "SI-HCCI-SI Mode Transition at Different Engine Operating Conditions." SAE Technical Paper 2005-01-0156.
4. Kalghatgi, G.T. 2001. "Fuel Anti-Knock Quality - Part I. Engine Studies." SAE Technical Paper 2001-01-3584.
5. Kalghatgi, G.T. 2001. "Fuel Anti-Knock Quality- Part II. Vehicle Studies - How Relevant is Motor Octane Number (MON) in Modern Engines?" SAE Technical Paper 2001-01-3585.
6. Kalghatgi, G.T. 2005. "Auto-Ignition Quality of Practical Fuels and Implications for Fuel Requirements of Future SI and HCCI Engines." SAE Technical Paper 2005-01-0239.
7. Kalghatgi, G.T., K. Nakata, and K. Mogi. 2005. "Octane Appetite Studies in Direct Injection Spark Ignition (DISI) Engines." SAE Technical Paper 2005-01-0244.

8. Prakash, A., et al. 2016. “Understanding the Octane Appetite of Modern Vehicles.” *SAE Int. J. Fuels Lubr.* 9 (2): 2016-01–0834.

Acknowledgements

This work was made possible with the contributions of Ashish Shah and Johannes Rohwer. Furthermore, the technical support of Timothy Rutter and the leadership by section manager Doug Longman is greatly appreciated.

II.10 X-Ray Imaging of GDI Sprays with Alcohol Blends (Argonne National Laboratory)

Christopher F. Powell, Principal Investigator
Argonne National Laboratory
9700 S. Cass Avenue
Lemont, IL 60439
E-mail: powell@anl.gov

Kevin Stork, DOE Technology Development Manager
U.S. Department of Energy
E-mail: Kevin.Stork@ee.doe.gov

Start Date: October 1, 2018 End Date: September 30, 2019
Project Funding (FY19): $200,000 DOE share: $200,000 Non-DOE share: $0

Project Introduction

The introduction of new cleaner-burning fuels into the marketplace must overcome several hurdles. One of these is the fuel's impact on the injection and mixing of fuel and air. It is well known that changing the physical properties of the fuel has an impact on injector performance and combustion [1]. However, the link between engine performance and the fuel's density, viscosity, volatility, and other properties is not well understood. This project aims to determine how the physical properties of the fuel affect the mixture preparation.

The mixture formation will be studied in a spray chamber under conditions that mimic a gasoline direct-injection (GDI) engine. The fuel distributions will be measured for several different operating conditions, including low-load conditions that cause flash-boiling and possibly spray collapse. Studies of mixing under these extreme cases will help in the development and validation of computational spray models that establish a scientific link between the fuel properties and the injection, combustion, and engine performance.

Objectives

Overall Objectives

- Studies of mixture formation will quantify the link between the physical properties of the fuel and the spray breakup. X-ray diagnostics will be used to quantify the fuel distribution as the spray first emerges from the nozzle and in the primary breakup region. These measurements will be performed with several fuel blends that cover a range of physical properties.
- Results of the measurements will be shared with the toolkit team and with simulations groups worldwide to speed the development and validation of predictive models for spray atomization.
- The experimental measurements will include a focus on GDI injection under throttled, part-load engine operating conditions, where standard spark ignition combustion suffers from poor efficiency. Under these conditions, spray collapse and flash-boiling are a particular challenge for simulations, and quantitative measurement data will help to develop models that capture these phenomena.

Fiscal Year 2019 Objectives

- Perform three-dimensional X-ray tomography measurements that quantify the near-nozzle fuel distributions under flash-boiling conditions for three alcohol fuel blends

- With these same fuel blends, perform ultra-small-angle X-ray scattering measurements to determine two-dimensional distributions of the near-nozzle surface area
- Combine near-nozzle density and surface area to build a map of the Sauter mean diameter (SMD) in the near-nozzle spray atomization region.

Approach

A detailed understanding of the impact that fuel properties have on the fuel injection process and the mechanisms of spray atomization is needed to spur the adoption of low-carbon fuels. Near-nozzle measurements of sprays using visible light are difficult because of strong scattering from the high number of droplets in this region. For this reason, X-ray diagnostics will be used for these studies. X-rays are highly penetrative and can generate quantitative, unambiguous measurements of useful spray properties, even in the optically opaque region very near the nozzle [2]. These measurements are performed at the Advanced Photon Source at Argonne National Laboratory. This source provides a very high flux beam of X-rays, enabling quantitative, time-resolved measurements of sprays with very high spatial resolution.

Quantitative X-ray measurements of the near-nozzle fuel distribution from GDI injection will be performed. Alcohol fuel blends will be used to vary the physical properties of the fuel, such as density and viscosity, in order to assess the effect of these properties on the mixture preparation. The first series of measurements will be done under non-vaporizing conditions, so that phase change does not impact the results and the physical properties are specifically isolated. In this way, the effect that the fuels have on the fuel/air mixing can be quantified and understood based on the physical properties of the fuels.

In addition to the non-vaporizing studies, a second series of measurements will quantify the near-nozzle fuel distributions under flash-boiling conditions. Flash-boiling and spray collapse cause a very abrupt change in the fuel/air mixing and are a big challenge for GDI engines at low loads. The measurements will study phenomena such as spray collapse across a range of fuels and assess how the properties of the fuels impact the mixture preparation and the initial conditions of combustion.

The measurements will quantify features of the near-nozzle fuel distribution using several alcohol blends. Specifically, this year researchers investigated three fuel blends: neat iso-octane, iso-octane with 20% ethanol, and iso-octane with 20% n-butanol. Together, these fuels give a broad span of density and viscosity and allow the impact of those properties on the fuel/air mixing to be assessed. These measurements will be done under non-vaporizing conditions so that the chemistry of the fuels doesn't matter, and the measurements will specifically focus on the physical properties.

Results

Ultra-small-angle X-ray scattering is a highly accurate technique to determine particle shapes and sizes in the nanometer to micrometer range using X-ray scattering [3]. In order to quantify the morphology of the near-nozzle sprays, ultra-small-angle X-ray scattering was applied to GDI sprays of alcohol fuel blends. X-ray scattering curves were collected for the three fuel blends using the Engine Combustion Network (ECN) "Spray G" injector. In Figure II.10.1, measurements in the ECN "Primary" view are shown. The curves resolve three plumes and are a measurement of the total surface area in the line-of-sight volume that is illuminated by the X-ray beam. The absolute values for specific surface area vary greatly between the different fuels and as a function of axial distance within a given fuel. It is noted that the mean value for surface area remains the most consistent for iso-octane as the scans progress in axial distance, whereas, for the n-butanol blend, the near-nozzle measurements are very low, suggesting that there are likely large, unbroken ligaments of liquid that do not contribute to the scattering signal as much as smaller droplets. Progressing downstream, though, the n-butanol blend has a marked rise in surface area at 2 mm, and then a lower absolute signal at 5 mm, where the spray has also widened. In contrast, the surface area values for the ethanol blend are one to two orders of magnitude higher than the other fuel cases at Z=1 mm. This could be caused by significant disintegration of

the liquid into many particles with interfacial boundaries contributing to the scattering signal. At the 2 mm and 5 mm locations, this signal has decreased, suggesting that those droplets have either coalesced or evaporated.

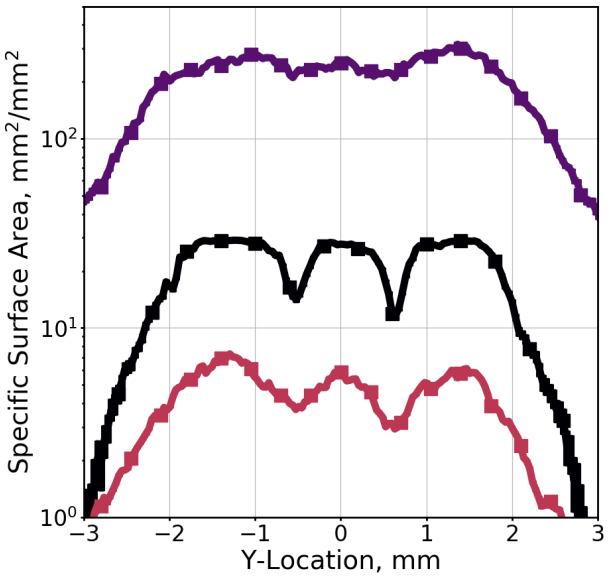

Figure II.10.1 The surface area of fuel droplets as a function of position for three fuel blends at a distance 1 mm from the fuel injector. The peaks and troughs in the plot show the separate plumes of the multi-hole spray.

The specific surface area measurements can be combined with the measurement of liquid volume in the probe region by X-ray radiography to yield the SMD of the droplets. This computation was performed by Sforzo et al. [4] using transverse ultra-small-angle X-ray scattering scans taken 1 mm downstream of the nozzle and the corresponding radiography projections for each fuel condition. These SMD profiles are plotted in Figure II.10.2 on a semi-log scale to highlight the variability between the conditions.

When plotted as SMD, the characteristic plume separations are suppressed, which may be caused by the relatively large cross section of the beam or may result from the fact that the measurements are line-of-sight projections through the spray. The plot of SMD also highlights the differences in the atomization of the different fuel blends. The observation of larger droplets from the n-butanol (BuOH) blend is supported by the higher viscosity and surface tension, which cause resistance to breakup. The higher boiling temperature for n-butanol may also contrast with the other two cases, possibly suppressing the effect of flashing in this blend. Conversely, for the ethanol (EtOH) blend, the previously discussed mass distribution and spray surface area, and here, the derived SMD, point to a flash-boiling-promoted breakup and fast fragmentation of the liquid iso-octane.

X-ray radiography from many lines of sight was used to make a tomographic reconstruction of the density distributions for the three fuels. The resulting tomography slices are presented in Figure II.10.3 for the three fuels, time-averaged over the steady portion of the spray (0.6–0.8 ms after command). The profiles are depicted in the ECN “Primary” view.

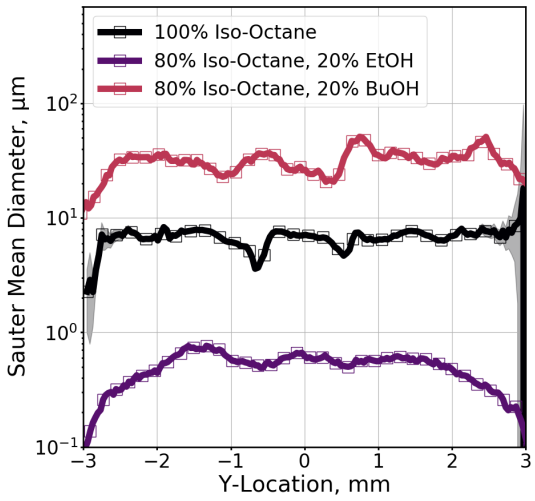

Figure II.10.2 SMD distribution across the spray for the three fuel blends measured 1 mm downstream. The SMD increases with the boiling point of the mixture.

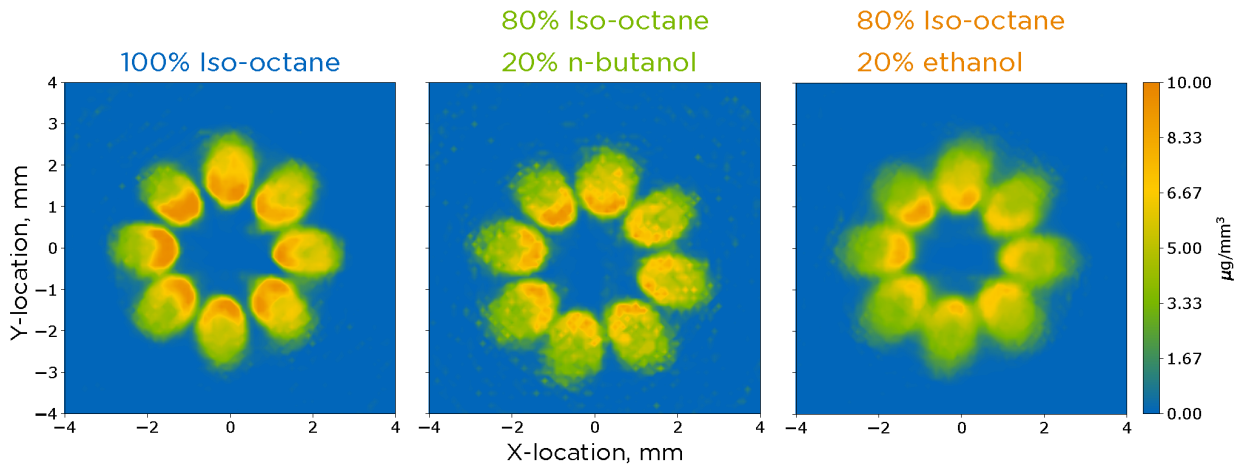

Figure II.10.3 Tomographic reconstructions of X-ray spray radiography, revealing the density distributions in slices through the spray from a gasoline injector measured 1.0 mm downstream of the injector. The measurements quantify the differences in spray breakup between the three fuel blends.

These profiles provide a transverse slice of the fuel mass per volume for each condition. Comparing each case, there is consistency in the asymmetry of the fuel distribution; for example, higher peak densities are measured for the holes at the upper left for all three fuels. The distribution of mass for these peak values is more concentrated for the neat iso-octane, potentially indicating a continued breakup and distribution of a more cohesive liquid jet at this downstream location. Furthermore, the separation between the plumes is more distinct for the neat iso-octane and the blend with n-butanol than in the ethanol blend. This is an indication of enhanced expansion and plume collapse.

The physical property that appears to be most significant for the spray dispersion for these fuel blends is the boiling temperature for the constituents, with the boiling point of ethanol (78.4°C) well below the 90°C operating temperature of the injector. The iso-octane and n-butanol constituents have boiling temperatures above the operating temperature, though vaporization is enhanced by the sub-atmospheric chamber pressure. Since the hot pressurized conditions within the injector cause the ethanol to be in a superheated state as it emerges from the nozzle, a rapid expansion takes place during injection, which could enhance the jet velocity

above that of the other two blends. This hypothesis is supported by the collapsing plume and homogeneous mass distribution within the plumes visible for the ethanol case in Figure II.10.3.

Conclusions

Experiments have quantified the near-nozzle fuel density distribution, surface area, and SMD of flash-boiling sprays for the first time and have done so across a range of fuel properties. The precise measurements will provide other Co-Optima researchers with data for validating computational models that predict the links among fuel properties, fuel density distribution, engine conditions, and combustion characteristics.

Key Publications

1. Sforzo, B.A., A. Tekawade, K.E. Matusik, A.L. Kastengren, J. Ilavsky, and C.F. Powell. 2019. "X-ray Characterization and Spray Measurements of ECN Spray G Using Alternative Fuels at Flashing Conditions." ILASS–Europe 2019, 29th Conference on Liquid Atomization and Spray Systems (September).

2. Matusik, Katarzyna E., Brandon A. Sforzo, Hee Je Seong, Daniel J. Duke, Alan L. Kastengren, Jan Ilavsky, and Christopher F. Powell. 2019. "X-Ray Measurements of Fuel Spray Specific Surface Area and Sauter Mean Diameter for Cavitating and Non-Cavitating Diesel Sprays." *Atomization and Sprays* 29 (3): 199–216, doi:10.1615/AtomizSpr.2019030112 (June).

3. Sforzo, B.A., A. Tekawade, K.E. Matusik, A.L. Kastengren, J. Ilavsky, K. Fezzaa, and C.F. Powell. 2019. "X-ray Characterization and Spray Measurements of ECN Spray G Using Alternative Fuels Under Flashing Conditions." 30th Annual Conference on Liquid Atomization and Spray Systems, Tempe, AZ (May).

References

1. Lešnik, L., B. Vajda, Z. Žunič, L. Škerget, and B. Kegl. 2013. "The Influence of Biodiesel Fuel on Injection Characteristics, Diesel Engine Performance, and Emission Formation." *Applied Energy* 111: 558–570.

2. Kastengren, L., and C.F. Powell. 2014. "Synchrotron X-Ray Techniques for Fluid Dynamics." *Experiments in Fluids* 55: 1686.

3. Ilavsky, J., P.R. Jemian, A.J. Allen, F. Zhang, L.E. Levine, and G.G. Long. 2009. "Ultra-Small-Angle X-ray Scattering at the Advanced Photon Source." *J. Appl. Cryst.* 42: 469–479.

4. Sforzo, B.A., A. Tekawade, K.E. Matusik, A.L. Kastengren, J. Ilavsky, and C.F. Powell. 2019. "X-ray Characterization and Spray Measurements of ECN Spray G Using Alternative Fuels at Flashing Conditions." ILASS–Europe 2019, 29th Conference on Liquid Atomization and Spray Systems (September).

Acknowledgements

The authors acknowledge Alan L. Kastengren, Brandon A. Sforzo, and Aniket Tekawade for their efforts as part of this work. Measurements were performed at the 7BM, 9ID, and 32ID beamlines of the Advanced Photon Source at Argonne National Laboratory. Use of the Advanced Photon Source is supported by the U.S. Department of Energy under Contract No. DEAC0206CH11357.

II.11 Fuel Properties Effects on Auto-Ignition in Internal Combustion Engines (Argonne National Laboratory)

Christopher P. Kolodziej, Principal Investigator
Argonne National Laboratory (ANL)
9700 S. Cass Avenue
Lemont, IL 60439
E-mail: ckolodziej@anl.gov

Kevin Stork, DOE Technology Development Manager
U.S. Department of Energy
E-mail: Kevin.Stork@ee.doe.gov

Start Date: October 1, 2018 End Date: September 30, 2019
Project Funding (FY19): $243,000 DOE share: $243,000 Non-DOE share: $0

Project Introduction

The Cooperative Fuel Research (CFR) octane rating engine is the standard apparatus used to rate the research octane number (RON) and motor octane number (MON) of gasoline [1],[2]. The unique attributes of this engine include its variable compression ratio (4:1 to 18:1) and robust design, able to withstand harsh combustion conditions. It is also the most common and widely distributed fuels research engine in the world, with more than 2,000 units currently in service [3]. These features make the CFR octane rating engine an attractive apparatus on which to base new fuels rating methods. The CFR octane rating engine installed at ANL has been highly instrumented to develop new fuels rating metrics but also gain a better understanding of the current RON and MON rating methods.

In September 2019, Mazda was the first vehicle manufacturer to launch a multi-mode engine in production that operates in advanced compression ignition (ACI) combustion in addition to spark ignition (SI) combustion [4]. Research within the U.S. Department of Energy (DOE) Co-Optimization of Fuels and Engines program (Co-Optima) has shown that RON and MON ratings of gasoline are not able to predict fuel reactivity in lean ACI combustion [5],[6]. This project has utilized the widely disseminated CFR octane rating engine to help develop a new fuel reactivity rating metric for lean ACI combustion, which has shown a high degree of correlation ($R2 > 0.9$) with fuel reactivity measurements on modern multi-mode ACI engines.

Low-temperature heat release (LTHR) is caused by fuel chemical reactions before the start of the main autoignition event and is especially prevalent for highly paraffinic fuels and boosted engine operating conditions. In the past, LTHR has been characterized in homogeneous charge compression ignition (HCCI) engines operating under lean conditions. Operation of HCCI engines at stoichiometry leads to harsh rates of heat release and often engine damage. In stoichiometric SI engines, the heat release from flame propagation overshadows the LTHR in the end gas, and it is not possible to characterize the low-temperature chemistry, which can have a significant effect on end-gas autoignition and knock. Taking advantage of the variable compression ratio mechanism of the CFR engine, a new test methodology has allowed for experimental measurement of stoichiometric LTHR for a given fuel and intake conditions. With a better understanding of the role fuel low-temperature chemistry plays under stoichiometric conditions, it may be possible to design SI fuels and engines for higher compression ratios and efficiency with improved knock limitations.

Objectives

Overall Objective

The overall objective of this project is to identify the effects of fuel composition and engine intake conditions on combustion, autoignition, and knocking characteristics.

Fiscal Year 2019 Objectives

- Develop a better understanding of the synergistic octane blending behavior of prenol in different base fuels
- Investigate the correlation of a lean ACI fuels rating metric on the CFR octane rating engine compared to modern ACI multi-mode engines
- Create a new test methodology to experimentally characterize the low-temperature chemistry of stoichiometric mixtures.

Approach

A standard CFR octane test engine was installed at ANL and instrumented in a similar way as other modern single-cylinder research engines. Instruments installed on the CFR engine include cylinder pressure transducer, high-speed intake and exhaust pressure transducers, fuel flow meter, wideband lambda sensor, emissions bench exhaust sampling port, etc. The approach allows for a deeper understanding of how fuel properties affect the engine operation and combustion characteristics during RON and MON testing. A compressed air intake system was also installed on the engine, allowing operation with the standard carbureted fueling system and boosted intake pressures. In knocking SI combustion, the knock propensity of fuels are rated based on their knock intensity. In lean HCCI test conditions, the fuel's reactivity is rated based on the compression ratio required to maintain a constant combustion phasing of three crank angle degrees after top dead center (°aTDC). In order to characterize the low-temperature chemistry of stoichiometric mixtures, the spark timing was delayed to 20 °aTDC and the compression ratio was increased until the LTHR was centered at top dead center. A strong collaboration has developed with CFR Engines, Inc., the manufacturer of the engine, to give a better understanding of the ASTM test methods and engine design. Collaboration with Prof. Bengt Johansson, the originator of the CFR HCCI fuel rating method, has helped develop the HCCI fuels rating research and stoichiometric LTHR characterization.

Results

Researchers from the Co-Optima program have identified prenol as having a strong synergistic octane blending behavior, to the point that mid-level blends (20–50 vol% prenol) can have higher RON ratings than both the base fuel and neat prenol [7]. It has also been observed that the level of synergistic octane blending of other alcohols—ethanol and isobutanol, for instance—is reduced when aromatic components are present in the base fuel. To assist the Co-Optima investigation, prenol was splash-blended into three base fuels having the same RON (85.2) but varying in aromatic composition (0, 38.9, and 66 vol% toluene). At 20 vol% prenol, the highly isoparaffinic base fuel (Primary Reference Fuel 85.2 [PRF85.2]) showed a 7 RON higher increase in octane number than the highly aromatic base fuel (Toluene Standardization Fuel 85.2 [TSF85.2]), with the mid-level aromatic base fuel (four-component surrogate fuel [4Comp]) falling in between the others (Figure II.11.1). The peak RON rating of the prenol/PRF85.2 blends, 30–40 vol% prenol, was 4 RON higher than the RON rating of neat prenol, while the peak RON rating of the prenol/TSF85.2 blends, 60 vol% prenol, was only 0.8 RON higher than neat prenol. This data shows that the peak synergistic octane blending effect of prenol into a highly isoparaffinic fuel (PRF85.2) is highest and occurs at lower prenol levels than the peak synergistic octane blending effect of prenol into a highly aromatic fuel (TSF85.2).

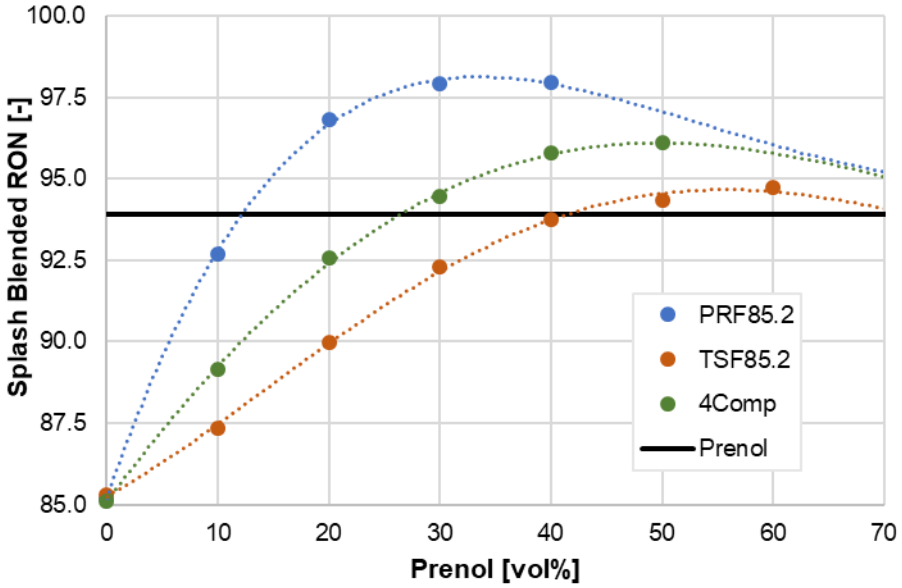

Figure II.11.1 RON of prenol splash-blending into RON 85.2 base fuels with varying aromatic content: PRF85.2 (0 vol% aromatic), 4Comp (38.9 vol% aromatic), and TSF85.2 (66 vol% aromatic)

Researchers within Co-Optima have demonstrated that RON, MON, and octane index are not able to describe the reactivity of gasoline fuels under lean ACI conditions [5],[6]. For the same octane index, they observed high aromatic fuels to be relatively less reactive and high olefinic and ethanol fuels to be relatively more reactive. Lopez-Pintor and Dec showed that the biggest reason for this discrepancy was the lean ACI conditions compared to the near-stoichiometric conditions of the RON and MON test methods [6]. This shows that a new fuels rating method is needed for lean ACI conditions. In recent years, Lund University and Chevron used the variable compression ratio CFR octane rating engine to develop a series of fuel ratings in lean HCCI combustion [8]. Table II.11.1 shows the original four Lund-Chevron HCCI number test conditions. At each combination of engine speed and intake temperature, the compression ratio is adjusted to maintain a constant combustion phasing, crank angle degree of 50% mass fraction burned (CA50), with a lambda of 3. The engine speeds and intake temperatures were derived from those used on the CFR engine in the RON and MON test methods. In this research, the intake temperature was swept from an unheated condition (30°C) to the maximum capability of the CFR engine intake air heater (200°C), and the intake pressure was swept from 0.9 bara to 1.3 bara with the specially installed compressed air boosting system.

Table II.11.1 Operating Conditions of Original Lund-Chevron HCCI Number Test Methods

Parameter	HCCI #1	HCCI #2	HCCI #3	HCCI #4
Speed (RPM)	600	600	900	900
Intake Temperature (°C)	52	149	52	149
Lambda (-)	3	3	3	3
CA50 (°aTDC)	3	3	3	3
Compression Ratio (-)	Control Variable	Control Variable	Control Variable	Control Variable

The fuels test matrix contained 19 gasolines and surrogate blends, covering 70 to 100 RON, which three fellow Co-Optima researchers also measured on their modern HCCI engines: Dr. Jim Szybist (nine fuels), Dr. Toby Rockstroh (five fuels), and Dr. John Dec (four fuels). Figure II.11.2 shows the fuels tested in common with these other researchers and the critical compression ratios required to operate each fuel at a combustion phasing (CA50) of 3 °aTDC for intake mixture air temperatures (MAT) between 100°C and 200°C. For this data set, the fuels were tested at 900 RPM, 1.0 bara manifold air pressure (MAP), and lambda of 3. Generally, all fuels required lower compression ratio (CR) as temperature increased. However, the ordering of the fuels' reactivity changed between 100°C, 150°C, and 200°C. It is also interesting to see that the compression ratio separation between the primary reference fuels decreased with increased temperature, but the compression ratio separation between the Co-Optima RON 98 gasolines remained more or less the same.

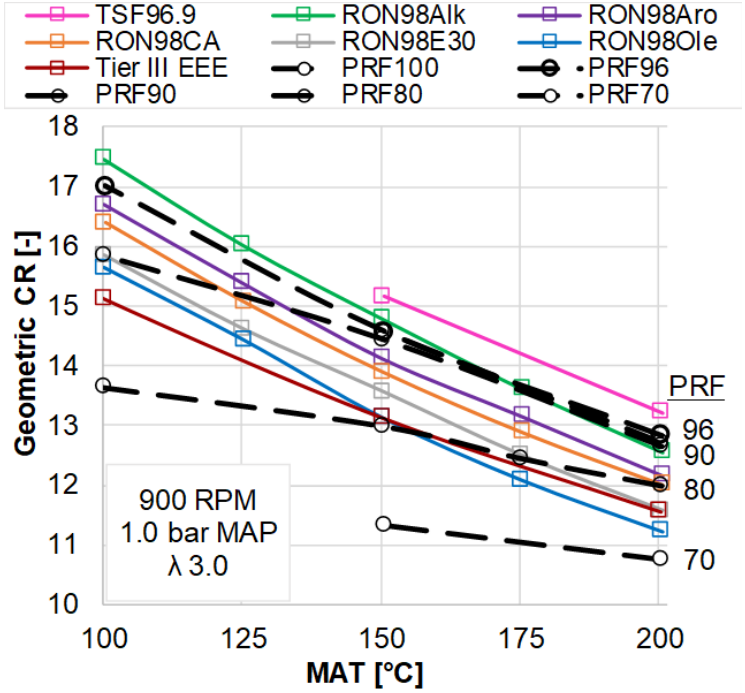

Figure II.11.2 Critical compression ratios of 12 test fuels over a range of intake air temperatures at 900 RPM, 1.0 bara manifold air pressure (MAP), and lambda of 3

Figure II.11.3 shows the correlation of the CFR HCCI critical compression ratios of the fuels (x-axis) to the fuel reactivity metric measured on each of the modern HCCI engines (y-axis). In Figure II.11.3a, the single-cylinder gasoline direct injection (GDI) multi-mode engine at ANL adjusted intake air temperature to operate all of the fuels at a constant combustion phasing (CA50) of 12 °aTDC with a fixed 15:1 compression ratio. Other operating condition parameters of the ANL GDI engine are shown in the figure. The intake temperatures from the ANL GDI engine (y-axis) correlated best (R2 = 0.90) with the CFR HCCI critical compression ratios (x-axis) with the intake air conditions of 1.0 bara and 150°C. Other CFR HCCI intake air temperature and pressure test conditions were evaluated; however, they had a lower correlation to the ANL GDI engine data. The same approach was followed in Figure II.11.3b to correlate intake air temperature (y-axis) from a single-cylinder GDI multi-mode engine at Oak Ridge National Laboratory (ORNL) to CFR HCCI critical compression ratios (x-axis) for nine fuels. Due to the higher engine speed (2,000 RPM), reduced compression ratio (13.7:1), and advanced combustion phasing (CA50) of 5°aTDC of the ORNL engine, the intake air temperature range necessary was higher than that of the ANL engine (240°C–300°C vs. 150°C–185°C). Thus, the CFR HCCI intake conditions which gave the highest critical compression ratio correlation (R2 = 0.96) to the ORNL engine data were 1.0 bara and 200°C. In Figure II.11.3c, the reactivity of four fuels was observed by comparing the combustion phasing (CA50) of each fuel while operating at a set intake temperature of

154°C on the low-temperature gasoline combustion (LTGC) engine at Sandia National Laboratory (SNL). In that case, the CFR HCCI critical compression ratios correlated best with the LTGC engine's CA50 values when the CFR engine was operated with intake conditions of 1.0 bara and 150°C.

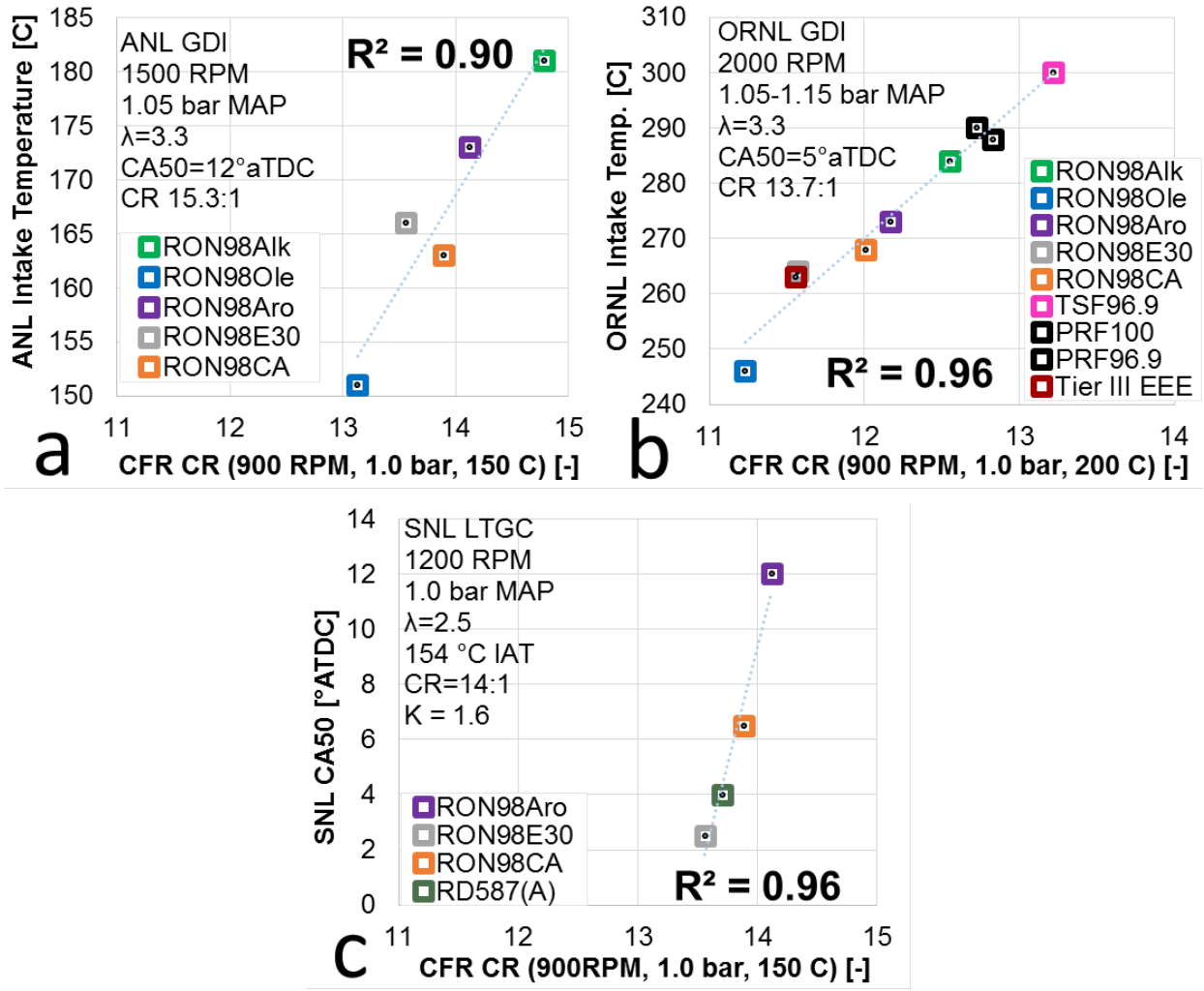

Figure II.11.3 Correlation of CFR HCCI critical compression ratios with fuel reactivity levels measured on modern multi-mode engines operating in HCCI combustion

As a result, the CFR HCCI critical compression ratio fuel rating metric was found to have a high degree of correlation (R^2 = 0.9–0.96) with the fuel reactivity levels measured in modern multi-mode engines operating in HCCI combustion. This demonstrates an HCCI fuels rating method that gives significantly improved accuracy over SI knocking-based RON, MON, and octane index metrics.

Normally the LTHR of a fuel is characterized experimentally in an engine under lean or dilute stoichiometric HCCI conditions, and this information is used to test and build up chemical kinetic models of engine combustion. However, there is very limited experimental engine data available for the LTHR of fuels under stoichiometric conditions due to harsh combustion conditions usually causing damage to the engine. Stoichiometric LTHR is believed to be present in, and contribute to, end-gas autoignition and knock in stoichiometric SI combustion. Thus, it is highly valuable to characterize the LTHR of a stoichiometric mixture in an engine. A new experimental method was developed in this project to characterize the LTHR of a stoichiometric mixture by retarding the spark timing to 20° aTDC on the CFR engine and increasing the compression ratio until the maximum of LTHR occurs at top dead center. Figure II.11.4 shows a

characterization of experimental LTHR of a stoichiometric mixture of Primary Reference Fuel (PRF) 90 with increasing intake air pressure (0.9–1.3 bara) at a constant intake air temperature of 52°C on the CFR engine. The duration and quantity of LTHR can be experimentally measured before the spark timing (20 °aTDC) and the start of flame propagation.

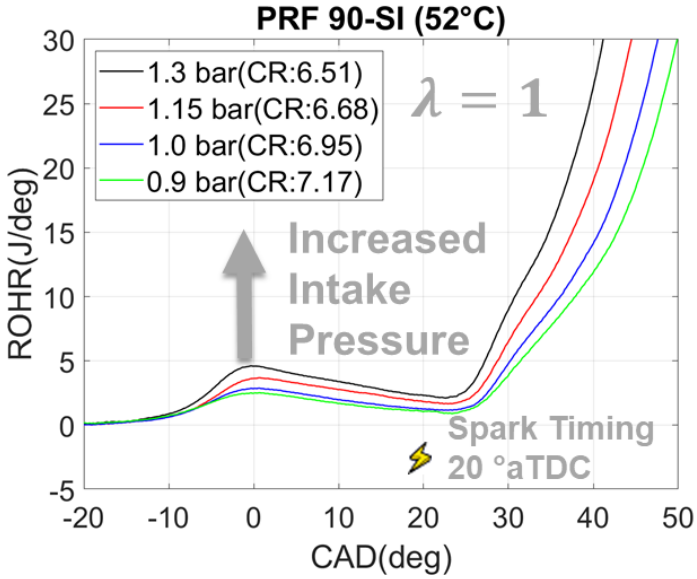

ROHR – rate of heat release; CAD – crank angle degrees

Figure II.11.4 Experimentally measured LTHR of a stoichiometric mixture of PRF 90 with increasing intake pressure

Conclusions

- Blending prenol with base fuels of increased aromatic content decreases the level of synergistic octane blending and shifts the maximum octane level to higher prenol blends.
- The original Lund-Chevron HCCI fuel rating method was tested over a wider range of intake temperatures and pressures and showed high correlation (R2 = 0.9–0.96) with modern multi-mode engines operating in HCCI combustion with relatively high intake air temperatures.
- A new experimental methodology was developed, taking advantage of the CFR engine variable compression ratio to characterize the LTHR of stoichiometric mixtures with varied intake conditions.

Key Publications

1. Salih, Saif, Daniel DelVescovo, Christopher P. Kolodziej, Toby Rockstroh, and Alexander Hoth. 2018. “Defining the Boundary Conditions of the CFR Engine under RON Conditions for Knock Prediction and Robust Chemical Mechanism Validation.” Proceedings of the ASME 2018 Internal Combustion Engine Division Fall Technical Conference, Volume 1: Large Bore Engines; Fuels; Advanced Combustion. San Diego, CA, USA. November 4–7, 2018. V001T02A005.

2. Hoth, A., J.P. Gonzalez, C.P. Kolodziej, and T. Rockstroh. 2019. “Effects of Lambda on Knocking Characteristics and RON Rating.” SAE Technical Paper 2019-01-0627, doi:10.4271/2019-01-0627.

3. Gonzalez, J.P., A. Shah, A. Hoth, T. Rockstroh, et al. 2019. “Statistical Analysis of Fuel Effects on Cylinder Conditions Leading to End-Gas Autoignition in SI Engines.” SAE Technical Paper 2019-01-0630, doi:10.4271/2019-01-0630.

4. Waqas, M.U., A. Hoth, C.P. Kolodziej, T. Rockstroh, J.P. Gonzalez, and B. Johansson. 2019. "Detection of Low Temperature Heat Release (LTHR) in the Standard Cooperative Fuel Research (CFR) Engine in Both SI and HCCI Combustion Modes." *Fuel* 256: 115745.

5. Waqas, M.U., A. Hoth, C.P. Kolodziej, T. Rockstroh, J.P. Gonzalez, and B. Johansson. 2019. "Introduction of Homogeneous Charge Compression Ignition (HCCI) Engine Combustion Mode in the Standard Cooperative Fuel Research (CFR) Engine." *SAE Int. J. Engines* 12 (5): 597–610.

References

1. ASTM International. 2015. "Standard Test Method for Research Octane Number of Spark-Ignition Engine Fuel." ASTM D2699-15a.

2. ASTM International. 2016. "Standard Test Method for Motor Octane Number of Spark-Ignition Engine Fuel." ASTM D2700-16.

3. CFR Engines, Inc., personal communication, October 31, 2019.

4. Mazda, "Fiscal Year March 2020 - Second Quarter Financial Results," 2019.

5. Szybist, J., et al. 2019. "MM: Fuel Property Impacts and Limitations on Combustion – Spark Ignition Focus." DOE Vehicle Technologies Office Annual Merit Review, Washington, D.C., June 10, 2019.

6. Kolodziej, C.P., et al. "MM: Autoignition in MM/ACI Combustion, Part 3." DOE Vehicle Technologies Office Annual Merit Review, Washington, D.C., June 10, 2019.

7. Monroe, E., J. Gladden, K.O. Albrecht, J.T. Bays, R. McCormick, R.W. Davis, and A.F. George. 2019. "Discovery of Novel Octane Hyperboosting Phenomenon in Prenol Biofuel/Gasoline Blends." *Fuel* 239: 1143–1148. doi:10.1016/j.fuel.2018.11.046.

8. Truedsson, I. 2014. "The HCCI Fuel Number – Measuring and Describing Auto-Ignition for HCCI Combustion Engines." PhD Dissertation, Lund University.

Acknowledgements

Several people assisted in making this work successful, including Alexander Hoth, Jorge Pulpeiro, Dr. Muhammad Waqas, Dr. Toby Rockstroh, Dr. James Szybist, Dr. John Dec, Timothy Rutter, Dave Bell, and Doug Longman.

II.12 Rapid Compression Machine for Kinetic Mechanism Development (Argonne National Laboratory)

S. Scott Goldsborough, Principal Investigator
Argonne National Laboratory
9700 S. Cass Avenue
Lemont, IL 60439
E-mail: Scott.Goldsborough@anl.gov

Kevin Stork, DOE Technology Development Manager
U.S. Department of Energy
E-mail: Kevin.Stork@ee.doe.gov

Start Date: October 1, 2018 End Date: September 30, 2019
Project Funding (FY19): $180,000 DOE share: $180,000 Non-DOE share: $0

Project Introduction

Fuel performance in modern spark-ignition (SI), advanced compression-ignition (ACI), and multimode engines depends on many fuel properties. Although autoignition chemistry is a primary driver, heat of vaporization and flame speed, as well as chemical kinetic sensitivities to thermal and compositional stratification, are also important. Furthermore, the development and propagation/amplification of pressure waves after localized autoignition events leading to structural damage can also depend on the fuel. The capability to model, and thus predict, fuel performance based on fundamental measurements could significantly reduce the costs and time associated with co-optimizing fuels and engines.

This project focuses primarily on acquiring experimental autoignition data that will (1) support the development, validation, and improvement of robust chemical kinetic mechanisms for real and surrogate fuels; and (2) provide insight into the chemical effects of fuel performance in boosted SI and ACI engines.

Objectives

Overall Objectives

- Acquire autoignition data for a variety of conventional and potential high-performance fuels using Argonne National Laboratory's (ANL's) rapid compression machine (RCM) facilities, at conditions relevant to boosted SI and ACI engines. The autoignition data is necessary for the development/ validation of chemical kinetic models and the interpretation of fuel-engine interactions.
- Investigate fuel-dependent chemical kinetic processes that influence fuel performance.

Fiscal Year 2019 Objectives

- Acquire autoignition data for select high-performance fuels (i.e., isoalcohols) blended into a research-grade gasoline, covering a range of thermodynamic conditions and a range of blending levels.
- Acquire autoignition measurements for a representative ether (methylpropyl ether [MPE]) covering a range of thermodynamic conditions. Collaborate with National Renewable Energy Laboratory and Massachusetts Institute of Technology on model development for this prototypical ether.
- Acquire screening measurements for isoolefins produced by ANL's high-performance fuel team at conditions comparable to those used previously to acquire data for C4 and C5 isoolefins 2-methyl 2-butene and 2-methyl 2-pentene.

- Conduct investigations of methods to quantify phi-sensitivity of fuels with future validation against experimental measurements in an internal combustion engine operating on advanced compression ignition.

Approach

The work pursued for this project seeks to address challenges associated with measuring the autoignition properties of potential future fuels and fuel blends, interpreting their performance in combustion engines (in terms of knock and combustion phasing), and properly modeling their behavior in zero- and multi-dimensional simulation frameworks. The approach used in this project is based on ANL's RCM, which is able to access experimental conditions that are directly relevant to modern SI and ACI engines, e.g., T = 650 K–1,100 K, P = 10–100 bar, O_2 = 10%–21%, and ϕ = 0.2–2.0+. ANL's RCM typically uses 10–20 ml of fuel to conduct tests covering a wide range of conditions, with the autoignition chemistry studied over the low-, NTC (negative temperature coefficient), and intermediate-temperature regimes. Smaller volumes can be used to explore focused operating regimes.

RCMs have been used for nearly 100 years to investigate autoignition phenomena at engine-relevant conditions, and they have continually become more sophisticated [1],[2]. They are capable of creating and maintaining well-controlled, elevated temperature and pressure environments in which the chemically active period preceding autoignition can be decoupled from physical interactions that occur in an engine and some combustion vessels, e.g., spray breakup, turbulent fuel–air mixing, and thermal/compositional stratification. Furthermore, the operating conditions, e.g., T, P, ϕ, and O_2, can be independently varied, unlike in internal combustion engines, and this provides necessary insight. The ability to utilize wide ranges of fuel and oxygen concentrations within RCMs, from ultra-lean to over-rich, and spanning dilute to undiluted regimes, offers specific advantages relative to other laboratory apparatuses such as shock tubes and flow reactors, where complications can arise under such conditions. ANL's twin-piston RCM is utilized in this project where ignition times are measured and heat release rates are quantified.

Results

Key accomplishments for Fiscal Year (FY) 2019 include the following:

- Acquired autoignition data for select high-performance fuels (i.e., isoalcohols) blended into a research-grade gasoline, covering a range of thermodynamic conditions and a range of blending levels. Collaborated with Lawrence Livermore National Laboratory to model the chemical kinetics of the RCM experiments to interpret the measurements.

- Acquired autoignition measurements for a representative ether (MPE), covering a range of thermodynamic conditions. Collaborated with National Renewable Energy Laboratory and Massachusetts Institute of Technology on model development for this prototypical ether.

Alcohols possess generally advantageous characteristics as fuels for internal combustion engines, including systems such as conventional SI, compression-ignition, and advanced combustion concepts such as spark-assisted compression ignition. While ethanol is in widespread use as a gasoline additive, there are technical and economical disadvantages associated with it. Many alcohols can be blended directly with petroleum-derived gasoline, but fuels containing three- and four-carbon molecules maintain beneficial knock suppression capability similar to methanol and ethanol. Larger alcohols (C3–C4) also possess physical and chemical properties, such as energy density, water absorptivity, miscibility, and corrosivity, closer to conventional gasoline.

A tiered screening approach within the Co-Optima Initiative identified branched alcohols, or isoalcohols, as promising. A more comprehensive understanding of the fundamental autoignition characteristics is required to effectively design modern and advanced internal combustion engines that use isoalcohols. Existing models do not adequately capture their blending effects in petroleum-derived full-boiling-range gasolines. To meet these needs, work in FY 2019 utilized ANL's RCM facility to acquire data, where isopropanol and isobutanol were

blended into a research-grade gasoline. Measurements were conducted at engine-relevant conditions (P = 20–40 bar, T = 700 K–1,000 K) using a dilute, stoichiometric fuel loading. Researchers employed the Co-Optima chemical kinetic model for gasoline, incorporating isoalcohol chemistry, to simulate the RCM experiments and provide insights into the relevant chemical interactions.

The ignition delay data shown in Figure II.12.1 suggest that isoalcohol blending effects, like those of ethanol, can be segregated into two temperature regimes: low-temperature/NTC (Tc = 700 K–850 K) and intermediate-temperature (Tc = 850 K–1,000 K). At low-temperature/NTC conditions, the six blended fuels exhibit two-stage ignition behavior in which ignition resistance, for both τ_1 and τ, is significantly increased as the isoalcohol content increases. Isopropanol (iPrOH) was found to be more potent than isobutanol (iBuOH). At the highest blending fraction (30% vol./vol., i.e., iPrOH30, iBuOH30), first-stage reactivity through ketohydroperoxide chain branching pathways is suppressed such that there is no discernable staged heat release at Tc > 780 K. Furthermore, the NTC characteristics of the "neat" gasoline are nearly flattened with increasing isoalcohol content, where iPrOH again displays greater perturbative characteristics than iBuOH. In the intermediate-temperature regime, all test fuels exhibit single-stage ignition with typical Arrhenius behavior. However, unlike at lower temperatures, the influence of both isoalcohols on fuel reactivity is almost negligible; similar ignition times are measured for all test fuels. iBuOH is found to increase fuel reactivity only slightly at these conditions.

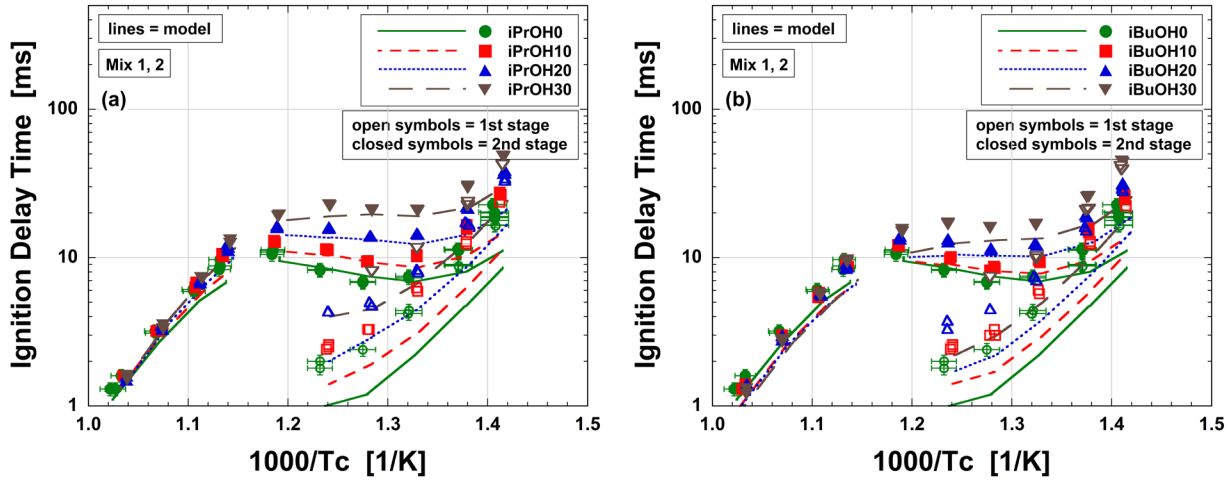

Figure II.12.1 Experimental and modeled ignition delay times for (a) FACE-F/iPrOH and (b) FACE-F/iBuOH blends at Pc = 40 bar, presented as functions of inverse temperature. Symbols indicate data from experiments (open – first-stage; closed – main), and lines indicate model results.

The chemical kinetic model for FGF-LLNL (Fuels for Advanced Combustion Engines – Gasoline F [FACE-F] – Lawrence Livermore National Laboratory) in general captures the overall reactivity of the "neat" FACE-F at the experimental conditions, but the low-temperature reactivity is somewhat overpredicted with consistently shorter τ_1 and τ (simulated τ_1 and τ are within factors of ~0.5 and ~0.8, respectively, of the measurements). In addition, the model reasonably captures the blending effects of iPrOH and iBuOH, though there are discrepancies in extents of reactivity suppression in both low-temperature/NTC and intermediate-temperature regimes. Finally, when comparing the current results to those for FACE-F/EtOH (ethanol) blends, it is evident that the perturbative influences of the three alcohols can be ranked as EtOH > iPrOH > iBuOH. When compared on a molar basis as shown in Cheng et al. [3], however, the reactivity suppression characteristics seem to be more consistent.

Another topic investigated in FY 2019 was the autoignition behavior of a prototypical ether. Ethers have been identified as promising oxygenates to reduce in-cylinder soot formation within mixing-controlled

compression-ignition engines by altering kinetic pathways, diluting soot-forming hydrocarbon species, and enhancing fuel–air mixing. Many oxygenated species derived from bio-feedstocks offer kinetic pathways that can improve the ignition characteristics important for optimal mixing-controlled compression-ignition operation, such as high cetane number (CN), relative to their petroleum counterparts. Furthermore, cost-competitive production pathways have been identified where ethers can be produced from alcohols derived from lignocellulosic biomass, and these advanced ether biofuels demonstrate >50% greenhouse gas reduction compared to conventional diesel.

Being able to predict CN and other combustion properties based upon the structures of ethers can help reduce the development time of these biofuels by focusing efforts on the molecules with the most favorable properties. Existing compilations of ether CN show that ethers have a wide range of CNs that are difficult to predict accurately. For instance, straight-chain alkyl ethers have CNs ranging from 55 for dimethyl ether to over 110 for dipentyl ether; these CNs are significantly higher than the U.S. minimum CN of commercial diesel fuel (CN = 40). Oxymethylene ethers, which are essentially polymers of CH_2O, are also of interest and can have high CN. For instance, the tetramer has a CN = 90. Quantum and kinetic modeling can be used to develop a quantitative understanding of combustion properties of biofuels. This work investigated the low-temperature oxidation chemistry of a small ether, MPE ($CH_3CH_2CH_2OCH_3$), which has an alkyl chain long enough for the intramolecular hydrogen transfer reactions important in autoignition.

The RCM tests covered a wide temperature range, Tc = 600 K–935 K, at compressed pressures of Pc = 10, 15, and 20 bar using diluted, stoichiometric mixtures [4]. Alterations to the compression ratio, diluent composition, and initial temperature were used to sweep from low to high temperature. The lowest temperatures facilitate evaluation of trends in τ_1 and low-temperature heat release, as these occur before the end of compression when Tc > 700 K. The fuel is very reactive with short ignition delays; low pressure and low temperature are required to observe first-stage ignition.

Figure II.12.2 presents summaries of τ_1 and τ plotted as functions of inverse temperature. Two test shots are included at each condition, and excellent shot-to-shot consistency can be observed across the entire span of experimental conditions. It can be seen that at the experimental conditions, the MPE/O_2/diluent mixtures exhibit low-, NTC, and intermediate-temperature behavior, where the measurement results are noticeably influenced by the test compression ratio and diluent composition. Pressure appears to have little influence on τ_1 but significant influence on ignition delay at intermediate temperatures. Results from a preliminary model are also shown; no observable first-stage ignition or NTC behavior is present in the model, while the model exhibits much less pressure sensitivity than observed in the measurements. These discrepancies are currently under investigation, with improvements being made in the individual reaction parameters.

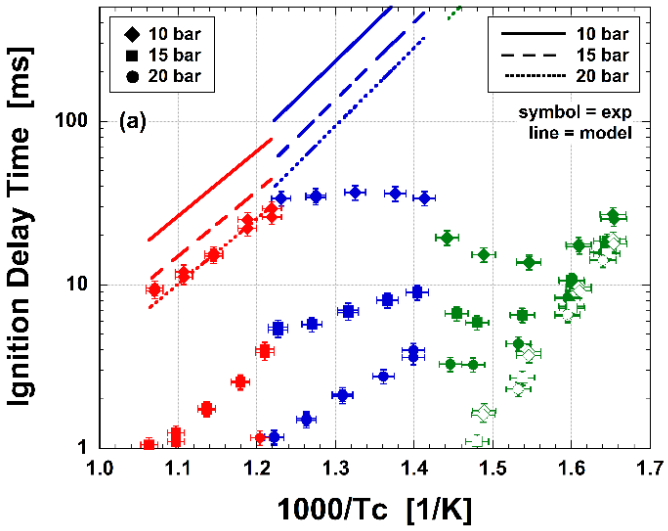

Figure II.12.2 Experimental and modeled ignition delay times for stoichiometric mixtures of MPE at Pc = 10, 15, and 20 bar, presented as functions of inverse temperature. Symbols indicate data from experiments (open – first-stage; closed – main), and lines indicate preliminary model results.

Conclusions

- The project acquired data for select high-performance fuels (i.e., isoalcohols) blended into a research-grade gasoline, covering a range of thermodynamic conditions and a range of blending levels. Results demonstrate that, on a liquid volume basis, the perturbative influences of the alcohols can be ranked as EtOH > iPrOH > iBuOH.

- The project acquired autoignition measurements for a representative ether (MPE), covering a range of thermodynamic conditions. Results indicate substantial low-temperature heat release across a very wide range of temperature (Tc = 600 K–935 K). The preliminary model requires improvements to properly represent many low-temperature chemical pathways.

- Screening measurements for isoolefin mixes produced by ANL's high-performance fuel team indicated reactivity, as well as phi-sensitivities, similar to C4 and C5 isoolefins 2-methyl 2-butene and 2-methyl 2-pentene .

Key Publications

1. Laich, A.R., E. Ninnemann, S. Neupane, R. Rahman, S. Barak, W.J. Pitz, S.S. Goldsborough, and S.S. Vasu. "High-Pressure Shock Tube Study of Ethanol Oxidation: Ignition Delay Time and CO Time-History Measurements." *Combustion and Flame*. In press.

2. Goldsborough, S.S., D. Kang, B. Wagner, K. Zhang, and W.J. Pitz. 2019. "Autoignition Behavior of Iso-Olefins." 17th International Conference on Numerical Combustion, Aachen, Germany.

3. Goldsborough, S.S., D. Kang, B. Wagner, K. Zhang, and W.J. Pitz. 2019. "Autoignition Behavior of Iso-Olefins." 11th U.S. Combustion Meeting, Pasadena, CA.

4. Nimlos, M.R., L. Bu, M.S. Johnson, D. Kang, G.M. Fioroni, R.L. McCormick, S. Kim, T.D. Foust, S.S. Goldsborough, and W.H. Green. 2019. "Low Temperature Oxidation of Methylpropyl Ether." 11th U.S. Combustion Meeting, Pasadena, CA.

5. Kang, D., and S.S. Goldsborough. 2019. "Autoignition Characteristics of Relevant Fuels: Iso-Olefins, Alcohol-Blended Gasolines, and an Ether." AEC Winter Review Meeting, Knoxville, TN.

6. Shah, A., D. Kang, T. Rockstroh, and S.S. Goldsborough. 2019. "Autoignition Behavior of High Octane Full Boiling Range Gasolines." AEC Winter Review Meeting, Knoxville, TN.

7. Saggese, C., S.W. Wagnon, G. Kukkadapu, S. Cheng, S.S. Goldsborough, and W.J. Pitz. 2019. "An Improved Detailed Chemical Kinetic Model for Butanol Isomers and Their Blends with Gasoline for Engine-Relevant Conditions." Submitted to International Symposium on Combustion, Adelaide, Australia.

8. Cheng, S., D. Kang, S.S. Goldsborough, C. Sagasse, S. Wagnon, and W.J. Pitz. 2019. "Autoignition Behavior of Isoalcohol-Blended Gasoline: FACE-F + Isopropanol, Isobutanol." Submitted to International Symposium on Combustion, Adelaide, Australia.

9. Cheng, S., D. Kang, S.S. Goldsborough, C. Sagasse, S. Wagnon, and W.J. Pitz. 2019. "Experimental and Modeling Study of C2–C4 Saturated Alcohol Autoignition at Intermediate Temperature Conditions." Submitted to International Symposium on Combustion, Adelaide, Australia.

References

1. "Basic Research Needs for Clean and Efficient Combustion of 21st Century Transportation Fuels." U.S. Department of Energy, Office of Science (website). Accessed 2019. http://science.energy.gov/~/media/bes/pdf/reports/files/ctf_rpt.pdf.

2. Goldsborough, S.S., S. Hochgreb, G. Vanhove, M.S. Wooldridge, H.J. Curran, and C.-J. Sung. 2017. "Advances in Rapid Compression Machine Studies of Low- and Intermediate-Temperature Autoignition Phenomena." *Prog. Energy Combust. Sci.* 63: 1–78.

3. Cheng, S., D. Kang, S.S. Goldsborough, C. Sagasse, S. Wagnon, and W.J. Pitz. 2019. "Autoignition Behavior of Isoalcohol-Blended Gasoline: FACE-F + Isopropanol, Isobutanol." Submitted to International Symposium on Combustion, Adelaide, Australia.

4. Nimlos, M.R., L. Bu, M.S. Johnson, D. Kang, G.M. Fioroni, R.L. McCormick, S. Kim, T.D. Foust, S.S. Goldsborough, and W.H. Green. 2019. "Low Temperature Oxidation of Methylpropyl Ether." 11th U.S. Combustion Meeting, Pasadena, CA.

Acknowledgements

ANL performed this work under the auspices of the U.S. Department of Energy under Contract DE-AC02-06CH11357. Dongil Kang, Song Cheng, Jake Tracey, and Monica Viz assisted with experimental measurements and analysis. Scott Wagnon, Goutham Kukkadapu, William Pitz and Russell Whitesides (Lawrence Livermore National Laboratory), and Matt Johnson and William Green (Massachusetts Institute of Technology) assisted with chemical kinetic modeling.

II.13 Mixing-Controlled CI Combustion and Fuel-Effects Research (Sandia National Laboratories)

Charles J. Mueller, Principal Investigator
Sandia National Laboratories
7011 East Ave., MS 9053
Livermore, CA 94550-9517
E-mail: cjmuell@sandia.gov

Kevin Stork, DOE Technology Development Manager
U.S. Department of Energy
E-mail: Kevin.Stork@ee.doe.gov

Start Date: October 1, 2018 End Date: September 30, 2019
Project Funding (FY19): $640,000 DOE share: $640,000 Non-DOE share: $0

Project Introduction

This project is focused on developing advanced combustion strategies for mixing-controlled compression-ignition (i.e., diesel-cycle) engines that are synergistic with renewable and/or unconventional fuels in a manner that enhances domestic energy security, economic competitiveness, and environmental quality. During this reporting period, the focus was on ducted fuel injection (DFI), a technology that differs from conventional diesel combustion (CDC) in that it involves injecting fuel along the axis of one or more small cylindrical ducts within the combustion chamber. Each duct performs a function similar to the tube on a Bunsen burner, helping to premix the fuel with the charge-gas before ignition, creating a stable flame that forms little to no soot. The purpose of the work conducted during Fiscal Year (FY) 2019 was to begin determining the extent to which the use of oxygenated fuels, when combined with DFI and charge-gas dilution, can simultaneously lower the soot and nitrogen-oxides (NO_x) emissions from mixing-controlled compression-ignition engines, and what the corresponding impacts on other regulated emissions and efficiency are likely to be.

Objectives

The **overall objectives** of this project are to provide:

- new technologies like DFI to increase the performance per unit cost, mass, and volume of future high-efficiency engine/fuel systems;
- high-quality experimental data for computational fluid dynamics model development to facilitate the accurate, rapid, and cost-effective computational optimization of new technologies; and
- a fundamental understanding of fuel composition and property effects by formulating and studying the performance of chemically and physically well-characterized reference fuels made from blending stocks as well as pure compounds.

The **specific objectives** of research **in FY 2019** were to:

- conduct optical-engine experiments at two levels of charge-gas dilution to compare DFI with CDC using two oxygenated blends as well as conventional diesel fuel;
- determine the extent to which DFI and oxygenated fuels can reduce in-cylinder soot formation, as indicated by soot incandescence; and

- quantify the effects of DFI on engine-out emissions of soot, NO_x, hydrocarbons (HC), carbon monoxide (CO), and fuel-conversion efficiency.

Approach

This project aims to deliver an improved understanding of mixing-controlled compression-ignition combustion and fuel effects through experimental observation employing optical and conventional diagnostics, combined with careful analysis of the results. DFI research conducted before FY 2019 [1],[2],[3] used non-oxygenated, conventional diesel fuel and a surrogate thereof in constant-volume combustion-vessel and optical-engine experiments to show that DFI is a promising soot-attenuation technology for mixing-controlled compression-ignition applications. Building from these results, efforts in FY 2019 were focused on obtaining an improved understanding of the effects of oxygenated fuels on in-cylinder soot formation, engine-out emissions, and efficiency for DFI relative to CDC. To achieve this, high-speed in-cylinder imaging of natural luminosity was combined with measurements of efficiency, cylinder pressure, and engine-out emissions for two dilution levels: intake-oxygen (O_2) mole fractions of 21% and 16%.

Results

A schematic showing the DFI concept is provided in Figure II.13.1a. This concept was first implemented in the optical engine in FY 2018. The presence of the duct curtails soot formation, apparently by lowering equivalence ratios in the autoignition zone. A rendering of the two-duct holder as installed in the engine and used in the FY 2019 experiments is provided in Figure II.13.1b. Each stainless-steel duct has an inner diameter, length, and standoff distance from the injector-orifice exit of 2.0 mm, 12.0 mm, and 3.0 mm, respectively. This configuration was used to acquire all of the data presented in this report.

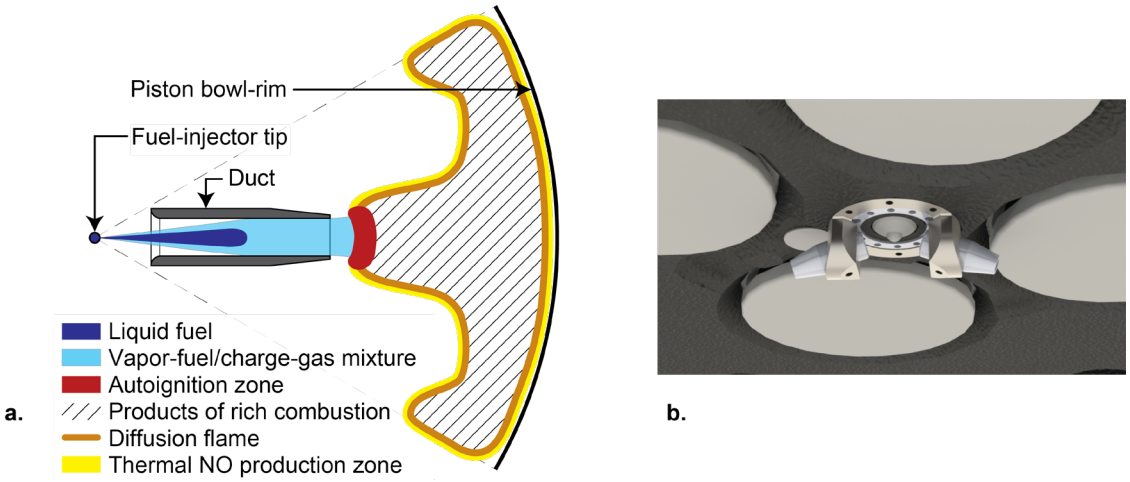

Figure II.13.1 (a) Schematic of DFI with a single duct. (b) Rendering of the two-duct assembly installed in the optical engine.

The two oxygenated blendstocks that were tested are methyl decanoate (an ester) and tri-propylene glycol mono-methyl ether. The molecular structures of these compounds are shown in Figure II.13.2. Each oxygenate was separately blended at 25% (by volume) into a baseline No. 2 S15 emissions-certification diesel fuel denoted CFB. The resulting ester and ether blends are denoted MD25 and T25, respectively. The 25 vol% blend level for the oxygenates was selected because it is representative of biodiesel blend levels that are currently commercially available in the United States.

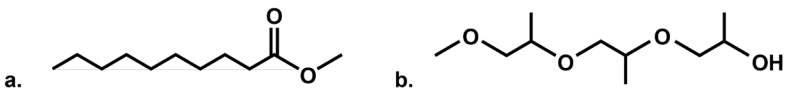

Figure II.13.2 Molecular structures of (a) methyl decanoate and (b) one isomer of tri-propylene glycol mono-methyl ether

Spatially integrated natural luminosity (SINL) is an indicator of the amount of hot soot within the combustion chamber. It is obtained from high-speed movies of in-cylinder natural luminosity. Measurements of SINL as a function of engine crank angle for the three fuels (CFB, MD25, and T25) under both CDC and DFI operating conditions are shown in Figure II.13.3. The figure shows that DFI with either oxygenated blend lowered the peak SINL by approximately two orders of magnitude relative to CDC with the non-oxygenated CFB baseline diesel fuel. Switching from CDC to DFI with diesel fuel accounted for one order of magnitude (see Figure II.13.3a), and switching from diesel fuel to an oxygenated blend under DFI conditions accounted for the second order of magnitude (see Figure II.13.3b). Oxygenate blending produced a larger relative SINL reduction under DFI conditions than under CDC conditions, and changing from CDC to DFI lowered SINL more than oxygenate blending under CDC conditions. The results were essentially the same regardless of the intake-mixture dilution level. Results at 16 mol% O_2 are shown because at this condition, there is not only a substantial soot-reduction benefit from DFI, there is also a simultaneous NO_x-reduction benefit from dilution.

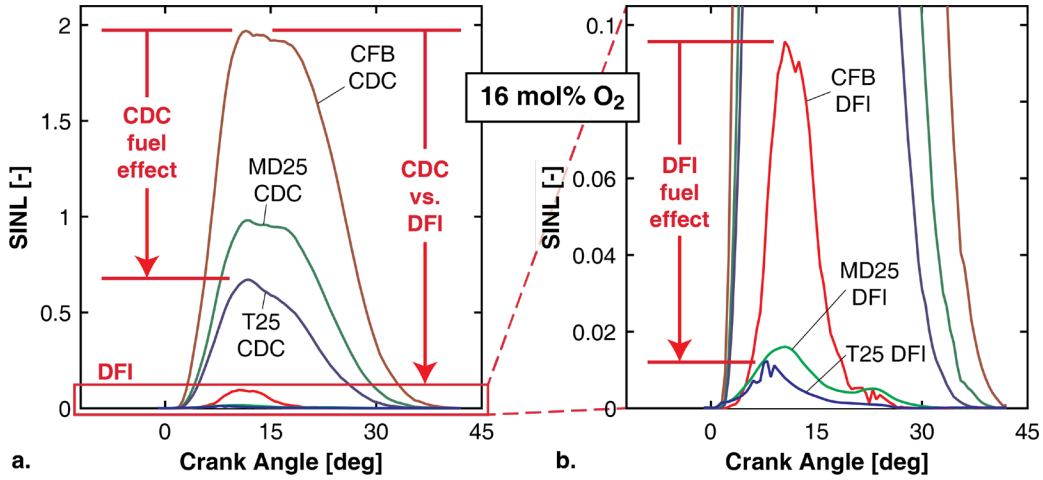

Figure II.13.3 Spatially integrated natural luminosity (SINL)—an indicator of the amount of hot, in-cylinder soot—as a function of crank angle and fuel type for CDC and DFI operation. In all cases, the intake mixtures have been diluted such that the O_2 mole fraction is 16%, to enable the simultaneous attenuation of both soot and NO_x. Note: The data plotted in (b) are the same as those plotted in (a), but the y-axis scale has been magnified in (b) to show the very low SINL levels associated with DFI.

To provide a more comprehensive summary of the effects of DFI with oxygenated fuels, Figure II.13.4 shows cycle-integrated SINL (ΣSINL); indicated-specific engine-out emissions of soot, NO_x, HC, and CO; and gross indicated fuel-conversion efficiency (η_f) for CDC and DFI at both 21 mol% and 16 mol% O_2. These data show that ΣSINL is reduced by at least two orders of magnitude when changing from CDC with diesel fuel to DFI with an oxygenated blend, regardless of dilution level. In all DFI cases, the engine-out soot is below the 0.002 g/kWh detection limit of the smoke meter used to make the measurements, precluding precise quantitative comparisons. Nevertheless, engine-out soot emissions for DFI with an oxygenated blend appear to be at least an order of magnitude smaller than those for CDC with diesel fuel. NO_x emissions are approximately an order of magnitude lower with dilution, regardless of the combustion strategy employed. HC emissions are typically maintained or improved by fuel oxygenation and DFI. Although CO emissions

typically increase with DFI, the levels are low enough to be controlled easily by an oxidation catalyst. Fuel-conversion efficiencies are typically 1%–2% lower for DFI with an oxygenated fuel. This adverse effect diminishes with increasing dilution, which is where DFI is likely to be used, due to the beneficial effect of dilution on NO_x emissions. A manuscript describing all of the preceding results is currently in preparation [4].

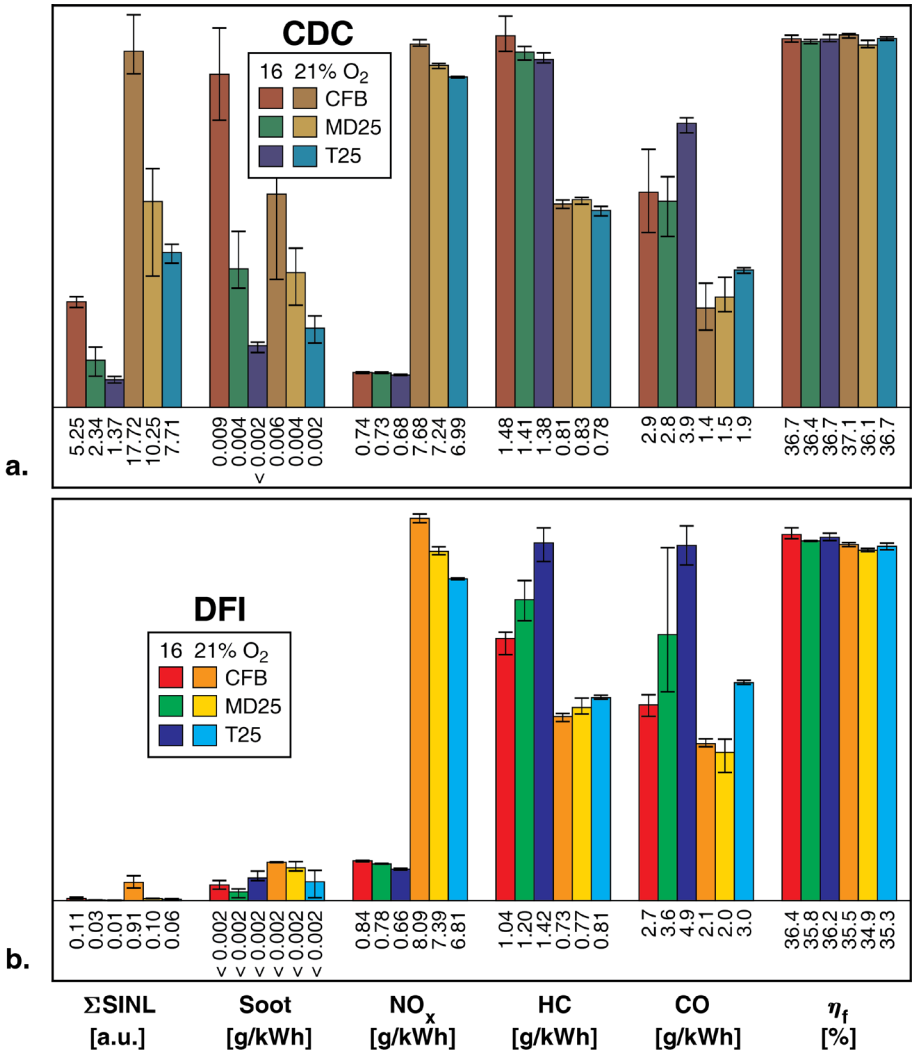

Figure II.13.4 Cycle-integrated SINL (ΣSINL); indicated-specific engine-out emissions of soot, NO_x, HC, and CO; and gross indicated fuel-conversion efficiency (η_f) for (a) CDC and (b) DFI at both 21 mol% and 16 mol% O_2. The vertical scales are the same in (a) and (b).

Conclusions

Employing DFI in combination with only 25 vol% of an oxygenated fuel can curtail in-cylinder soot incandescence by approximately two orders of magnitude for the two-duct configuration employed in this study. One order of magnitude comes from using DFI, and the second comes from blending with the oxygenated fuel. This benefit is achieved in a combustion system that is easy to control and maintains low HC and CO emissions as well as high efficiency. By virtue of its dramatic soot attenuation, DFI with an oxygenated fuel provides the additional benefit of enabling operation at low-NO_x conditions (achieved via dilution) that are not feasible with CDC due to excessive soot emissions. Given that many renewable fuels are oxygenated, the combination of DFI, fuel oxygenation, and dilution is a promising path to high-efficiency, cost-effective, clean, and sustainable engines and fuels for the future.

Key Publications

1. Nilsen, C.W., D.E. Biles, and C.J. Mueller. 2019. "Using Ducted Fuel Injection to Attenuate Soot Formation in a Mixing-Controlled Compression-Ignition Engine." *SAE Int. J. Engines* 12 (3): 309–322, doi:10.4271/03-12-03-0021, https://saemobilus.sae.org/content/03-12-03-0021/.

2. Mueller, C.J. 2018. "Ducted Fuel Injection with Ignition Assist." U.S. Patent #10,138,855; issued November 27, 2018.

3. Mueller, C.J. 2018. "Ducted Fuel Injection." U.S. Patent #10,161,626; issued December 25, 2018.

4. Mueller, C.J. 2018. "Mixing-Controlled Compression-Ignition Combustion and Fuel-Effects Research: Ducted Fuel Injection." U.S. Dept. of Energy: *Vehicle Technologies Office FY 2018 Annual Progress Report, Advanced Combustion Systems and Fuels*, https://www.energy.gov/eere/vehicles/downloads/advanced-combustion-engines-and-fuels-fy2018-annual-progress-report-0.

5. Mueller, C.J. 2019. "Ducted Fuel Injection Enables Simultaneously Lower Diesel Soot and Nitrogen Oxides Emissions." *2018 U.S. DRIVE Highlights of Technical Accomplishments* (March), https://www.energy.gov/eere/vehicles/downloads/us-drive-2018-technical-accomplishments-report.

6. Mueller, C.J. 2019. "Ducted Fuel Injection Dramatically Decreases Diesel Soot and NO_x Emissions." *Co-Optimization of Fuels & Engines FY18 Year in Review* (April), https://content.govdelivery.com/accounts/USEERE/bulletins/24d3a05.

7. Cline, E., and C.J. Mueller. 2019. "TCF Project: Ducted Fuel Injection." *Sandia FY2018 Partnerships Annual Report* (April), https://www.sandia.gov/news/publications/partnerships/index.html.

8. Mueller, C.J. 2019. "Sandia National Laboratories R&D 100 Award Video: Ducted Fuel Injection." Sandia Release SAND2019-4135V (April), https://youtu.be/1dijtRUZeLw.

References

1. Mueller, C.J., C.W. Nilsen, D.J. Ruth, R.K. Gehmlich, L.M. Pickett, and S.A. Skeen. 2017. "Ducted Fuel Injection: A New Approach for Lowering Soot Emissions from Direct-Injection Engines." *Applied Energy* 204: 206–220, doi:10.1016/j.apenergy.2017.07.001.

2. Gehmlich, R.K., C.J. Mueller, D.J. Ruth, C.W. Nilsen, S.A. Skeen, and J. Manin. 2018. "Using Ducted Fuel Injection to Attenuate or Prevent Soot Formation in Mixing-Controlled Combustion Strategies for Engine Applications." *Applied Energy* 226: 1169–86, doi:10.1016/j.apenergy.2018.05.078.

3. Nilsen, C.W., D.E. Biles, and C.J. Mueller. 2019. "Using Ducted Fuel Injection to Attenuate Soot Formation in a Mixing-Controlled Compression-Ignition Engine." *SAE Int. J. Engines* 12 (3): 309–322, doi:10.4271/03-12-03-0021, https://saemobilus.sae.org/content/03-12-03-0021/.

4. Mueller, C.J., C.W. Nilsen, and D.E. Biles. 2019. "Effects of Fuel Oxygenation and Ducted Fuel Injection on the Performance of a Mixing-Controlled Compression-Ignition Optical Engine Equipped with a Two-Orifice Fuel Injector." Manuscript in preparation for *SAE Int. J. Fuels Lubr.*

Acknowledgements

The principal investigator gratefully acknowledges major contributions to FY 2019 research efforts from interns Christopher W. Nilsen (University of California, Davis), Drummond E. Biles (University of New Hampshire), and Boni F. Yraguen (Georgia Institute of Technology). This research was conducted at the Combustion Research Facility, Sandia National Laboratories, Livermore, California. Sandia National

Laboratories is a multi-mission laboratory managed and operated by National Technology and Engineering Solutions of Sandia, LLC, a wholly owned subsidiary of Honeywell International, Inc., for the U.S. Department of Energy's National Nuclear Security Administration under contract DE-NA-0003525. SAND2020-2398 R

II.14 Fuel Autoignition Behavior (National Renewable Energy Laboratory)

Brad Zigler, Principal Investigator
National Renewable Energy Laboratory
15013 Denver West Parkway
Golden, CO 80401
E-mail: brad.zigler@nrel.gov

Kevin Stork, DOE Technology Development Manager
U.S. Department of Energy
E-mail: Kevin.Stork@ee.doe.gov

Start Date: October 1, 2018 End Date: September 30, 2019
Project Funding: $550,000 DOE share: $550,000 Non-DOE share: $0

Project Introduction

Co-development of new high-performance chemistries and high-efficiency internal combustion engines requires fast, accurate numerical simulations of critical processes to evaluate the interaction between fuel ignition behavior and advanced combustion strategies. These numerical simulations rely on accurate computational fluid dynamics (CFD) linked with fuel chemical kinetic mechanisms to model ignition and combustion performance during the engine cycle. Since fuel composition is complex, chemical kinetic mechanisms are based on surrogate compounds in representative blends. Simulation efficiency also typically requires the use of significantly reduced versions of kinetic mechanisms.

Development of these reduced, yet accurately representative, chemical kinetic mechanisms is enabled by experimental input data and validation through a range of devices, including shock tubes, rapid compression machines, flow reactors, and constant-volume combustion chambers (CVCCs). Experimental measurements are especially important for highlighting and validating ignition kinetic performance when combining kinetic mechanisms for different chemical classes to represent a fuel blend. Novel fuel blending components can affect ignition performance in non-linear and varying antagonistic or complementary degrees over temperature, pressure, and equivalence ratio space. Fuel kinetic mechanism development and validation therefore benefits from experimental mapping of ignition delay (ID) performance of fuel blends over engine-relevant parametric space. These experimental parametric maps of ID may also be used in simplified engine simulations to provide rapid screening predictions of engine performance with complex fuel blends for which kinetic mechanisms have not yet been developed. The ID studies span fuel autoignition under the collaborative multilaboratory Co-Optimization of Fuels and Engines (Co-Optima) program for avoiding end-gas autoignition for spark-ignition (SI) engines as well as for control of advanced compression-ignition (ACI) strategies, including sensitivity to fuel–air equivalence ratio (ϕ) and multimode SI/ACI operation.

Objectives

Overall Objectives

- Develop experimental and simulation tools to characterize fuel ignition behavior in support of advanced combustion engine development, including SI, ACI, and multimode operation
- Support development of research fuels, surrogates, and blends, as well as related reduced kinetic mechanisms, to further enable co-development of advanced combustion engines and high-performance fuels

- Link bench-scale CVCC-based fuel ignition measurements to single-cylinder research engine studies to enable rapid predictive feedback of engine performance for complex fuel blends
- Develop understanding of fuel chemical and physical properties that enable furtherance of the Co-Optima research and development program for co-optimization of high-performance fuels and high-efficiency engines.

Fiscal Year 2019 Objectives

- Develop CVCC-based ID measurements to quantify ϕ-sensitivity for fuels showing ϕ-sensitivity in published engine combustion studies
- Support development of a ϕ-sensitivity metric to apply to fuel screening for ACI and multimode strategies.

Approach

The National Renewable Energy Laboratory (NREL) has adapted the Advanced Fuel Ignition Delay Analyzer (AFIDA) [1] as a flexible CVCC research platform, with greater capability for fuel ignition kinetics ID studies than NREL's Ignition Quality Tester [2] and Fuel Ignition Tester. The AFIDA covers a broader range of pressures (up to 5 MPa) and temperatures (up to 1,000 K) with a high-pressure (up to 2,000 bar) fuel injection system that significantly reduces the spray physics effects timescales compared to the Ignition Quality Tester, enabling greater focus on the chemical kinetics portion of ID. In Fiscal Year (FY) 2018, NREL extensively characterized internal chamber conditions for the AFIDA, and in FY 2019, the project team continued development of a CFD model for the AFIDA to utilize with experimental data as part of the feedback loop for chemical kinetic mechanism development.

In addition to standard indicated cetane number (ICN) measurements of diesel-range fuels for which the AFIDA was originally designed [3], NREL developed techniques to conduct ID studies over temperature sweeps at various fixed pressures and global ϕ. The focus on gasoline-boiling-range fuels supported SI engine development, as well as other advanced strategies such as ACI and multimode operation. Inherently longer ID times typical of gasoline-range fuels allowed better mixing, reduced spray physics to affect only a small portion of the overall ID (focusing more on chemical-kinetics-dominated ID), and enabled studies at higher pressures relevant to engine operation. As a result, NREL's flexible AFIDA produced engine-relevant ignition kinetic data for gasoline-range compounds and blends, filling data voids and overlapping some conditions covered by rapid compression machines and shock tubes. Experimental ID studies of ϕ-sensitivity at various pressures over temperature sweeps were conducted to focus on ACI where ϕ stratification may be used as a control strategy. Zero-dimensional (0D) and CFD simulations were developed and evaluated to enable the AFIDA to be used in validation in support of kinetic mechanism development, as well as to provide insight for studies of fuel structure effects on ignition performance.

Results

NREL completed characterization, adaptation, and modeling of the AFIDA for a wide range of fuel autoignition kinetics studies, and utilized it for a range of ID studies under Co-Optima. The research resulted in a journal article documenting experimental and numerical investigations of the AFIDA as a research platform for fuel chemical kinetic mechanism validation [4]. As reported in FY 2018, air mixture amounts, fuel delivery, and global ϕ limits were mapped over a range of temperatures and pressures. Critically, interior chamber temperature stratification was mapped in support of developing both CFD and simplified 0D simulations. Experiments measuring ID with ranges of primary reference fuels were conducted and validated against CFD and 0D simulations. As illustrated in Figure II.14.1, 0D simulation with a 127-species primary reference fuel reduction of the Co-Optima 2017 kinetic mechanism [5] is presented (blue line) along with full CFD simulation with the same mechanism (red squares), showing good agreement with experimental data (black circles, with experimental error bars) through the negative temperature coefficient region at around 100 ms. Results with Co-Optima study compounds in blends provide critical feedback to mechanism

development, especially with the ability to evaluate mechanisms against experimental data using simple 0D simulations.

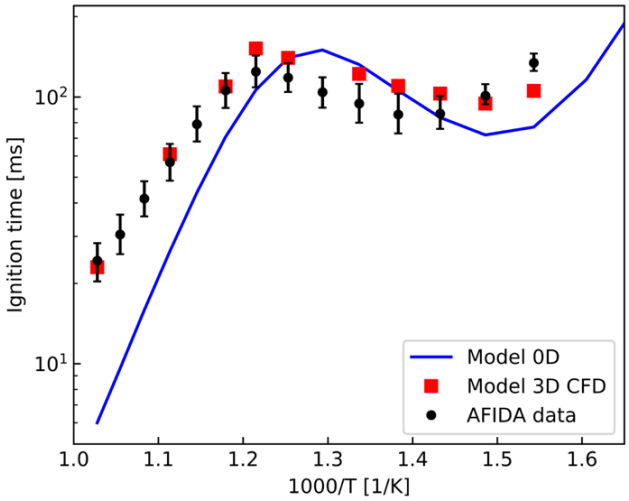

Figure II.14.1 Arrhenius plot of ID (log scale) versus inverse temperature (1,000/K) showing experimental versus numerical ignition delay results for 10 bar iso-octane over the temperature range (973–648 K) and global ϕ (1.2–0.8). (Figure: Mohammad Rahimi, NREL; adapted from Leucke, et al. [4])

AFIDA experiments involve injecting liquid fuel into the heated and pressurized CVCC, producing an ID measurement (derived from a pressure trace) resulting from a combination of physical mixing and chemical kinetic processes, a complexity which makes the development of complementary numerical models necessary for the development and validation of chemical kinetic mechanisms [4]. Fortunately, spray mixing timescales in the AFIDA result in a quasi-homogenous state that enable 0D simulations with homogenous approximations under a range of engine-relevant conditions, as illustrated in Figure II.14.2. The homogenous approximation error is greatest for conditions with short IDs and the system is not sufficiently mixed (<30 ms), providing guidance to select a 0D simulation versus CFD modeling approach based on desired accuracy [4]. The combination of AFIDA experiments and simulations provides a useful tool for kinetic mechanism development, complementing shock tubes, rapid compression machines, and flow reactors.

NREL applied AFIDA experiments and 0D simulations to investigate ϕ-sensitivity in support of a published journal article proposing a new definition of ϕ-sensitivity as a fuel quality metric that may be applied to predicting fuel performance for ACI strategies [6] (see Figure II.14.3). NREL developed novel AFIDA experiments to measure ϕ-sensitivity in terms of ID over a range of temperatures, pressures, and ϕ in a manner that may provide a new and rapid experimental measurement of this fuel property. The AFIDA experiments were used in collaboration with other NREL colleagues who derived a new definition for ϕ-sensitivity that is much less dependent on the values of ϕ or ID and is thus more universally applicable [6]; that definition is $\eta \equiv -(d\log(\tau))/(d\log(\phi))$, where τ is ID in milliseconds.

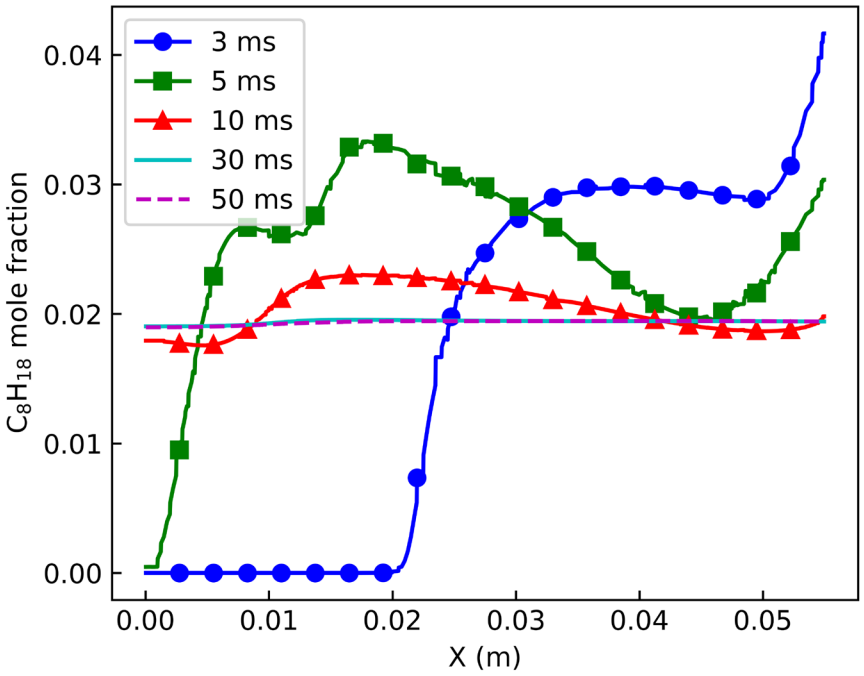

Figure II.14.2 Simulated iso-octane mole fraction concentration starting from the center (X = 0) and moving radially outward from the AFIDA's centerline for ϕ = 1.2, 973 K, 10 bar conditions with a 4 ms, 0.169 mL injection, centered in the middle of the AFIDA chamber. (Figure: Mohammad Rahimi, NREL; adapted from [4].)

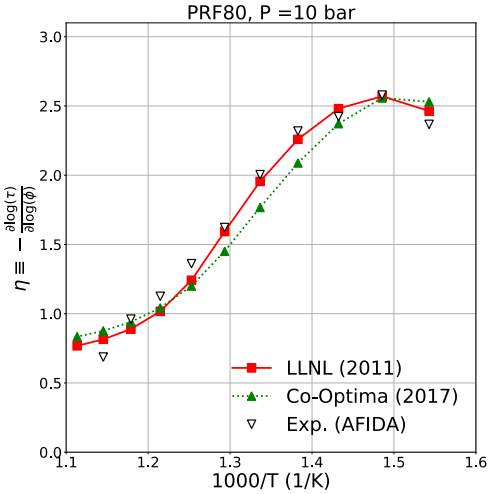

Figure II.14.3 Comparison of ϕ-sensitivity AFIDA experimental results with 0D simulation results using Lawrence Livermore National Laboratory (LLNL) 2011 [7] and Co-Optima 2017 [5] kinetic mechanisms for PRF80 (primary reference fuel 80) at P = 10 bar. (Figure: Richard Messerly, NREL; adapted from [6].)

The experimental data supported validation of detailed kinetic simulations revealing additional key reactions that are the physical basis for ϕ-sensitivity. In ACI engines, these findings can be used to create sequential autoignition, reducing pressure rise rate and maximum pressure and allowing the engine to achieve higher loads while retaining the efficiency and emissions benefits of ACI. The AFIDA experiments, along with flow reactor experiments, enable study of molecular structure effects on ϕ-sensitivity and examine underlying reaction kinetics in greater detail.

Conclusions

- AFIDA ignition kinetics experiments quantify fuel component, surrogate blend, and full-boiling-range gasoline ignition performance over engine-relevant parametric space.
- Unique AFIDA data complement data from other devices such as shock tubes and rapid compression machines and provide additional perspective beyond research octane number or motor octane number values alone.
- Integrated 0D and CFD simulations of AFIDA experiments provide validation for development of accurate full and reduced kinetic mechanisms.
- Experiments and simulations targeting ϕ-sensitivity provide another fuel metric that may enable early-stage screening of fuels for ACI strategies using mixture stratification with cascading autoignition for control.
- AFIDA experiments and simulations enable study of molecular structure effects on ϕ-sensitivity and examine underlying reaction kinetics in greater detail.

Key Publications

1. Luecke, J., M.J. Rahimi, B.T. Zigler, and R.W. Grout. 2020. "Experimental and Numerical Investigation of the Advanced Fuel Ignition Delay Analyzer (AFIDA) Constant-Volume Combustion Chamber as a Research Platform for Fuel Chemical Kinetic Mechanism Validation." *Fuel* 265: 116929, ISSN 0016-2361. https://doi.org/10.1016/j.fuel.2019.116929.
2. Messerly, R.A., M.J. Rahimi, P.C. St. John, J.H. Luecke, J.W. Park, N.A. Huq, T.D. Foust, T. Lu, B.T. Zigler, R.L. McCormick, and S. Kim. 2020. "Towards Quantitative Prediction of Ignition-Delay-Time Sensitivity on Fuel-to-Air Equivalence Ratio." *Combustion and Flame* 214: 103–115, ISSN 0010-2180. https://doi.org/10.1016/j.combustflame.2019.12.019.

References

1. Seidenspinner, P., M. Härtl, T. Wilharm, and G. Wachtmeister. 2015. "Cetane Number Determination by Advanced Fuel Ignition Delay Analysis in a New Constant Volume Combustion Chamber." SAE Technical Paper 2015-01-0798. https://doi.org/10.4271/2015-01-0798.
2. Bogin Jr., G.E., J. Luecke, M.A. Ratcliff, E. Osecky, and B.T. Zigler. 2016. "Effects of Iso-Octane/Ethanol Blend Ratios on the Observance of Negative Temperature Coefficient Behavior within the Ignition Quality Tester." *Fuel* 186 (December 15): 82–90, ISSN 0016-2361. http://dx.doi.org/10.1016/j.fuel.2016.08.021.
3. ASTM D8183-18. 2018. "Standard Test Method for Determination of Indicated Cetane Number (ICN) of Diesel Fuel Oils using a Constant Volume Combustion Chamber—Reference Fuels Calibration Method." *ASTM International*, West Conshohocken, PA. www.astm.org.
4. Luecke. J., M.J. Rahimi, B.T. Zigler, and R.W. Grout. 2020. "Experimental and Numerical Investigation of the Advanced Fuel Ignition Delay Analyzer (AFIDA) Constant-Volume Combustion Chamber as a Research Platform for Fuel Chemical Kinetic Mechanism Validation." *Fuel* 265: 116929. ISSN 0016-2361. https://doi.org/10.1016/j.fuel.2019.116929.
5. Mehl, M., S. Wagnon, K. Tsang, G. Kukkadapu, W. Pitz, C. Westbrook, Y. Tsang, H. Curran, N. Atef, M. Rachidi, M. Sarathy, and A. Ahmed. 2017. "A Comprehensive Detailed Kinetic Mechanism for the Simulation of Transportation Fuels." 10th U.S. National Combustion Meeting, LLNL–CONF–725343.

6. Messerly, R.A., M.J. Rahimi, P.C. St. John, J.H. Luecke, J.W. Park, N.A. Huq, T.D. Foust, T. Lu, B.T. Zigler, R.L. McCormick, and S. Kim. 2020. "Towards Quantitative Prediction of Ignition-Delay-Time Sensitivity on Fuel-to-Air Equivalence Ratio." *Combustion and Flame* 214: 103–115. ISSN 0010-2180. https://doi.org/10.1016/j.combustflame.2019.12.019.

7. Mehl, M., W.J. Pitz, C.K. Westbrook, and H.J. Curran. 2011. "Kinetic Modeling of Gasoline Surrogate Components and Mixtures under Engine Conditions." *Proceedings of the Combustion Institute* 33, Issue 1: 193–200. ISSN 1540-7489. https://doi.org/10.1016/j.proci.2010.05.027.

Acknowledgements

NREL would like to thank Kevin Stork for his support of this research under the Co-Optima program. NREL would also like to thank Philipp Seidenspinner at Analytik-Service Gesellschaft MbH for continued collaboration in expanding the AFIDA as a flexible research platform. Jon Luecke led NREL's AFIDA-based experimental studies, and Mohammad Rahimi conducted AFIDA simulations within the broader Co-Optima project simulation activities. Seonah Kim and Richard Messerly collaborated to include AFIDA experimental data in ϕ-sensitivity theoretical chemistry fuel ignition kinetics studies.

II.15 Flow Reactor Autoignition Kinetic Mechanism Development and Validation (National Renewable Energy Laboratory)

Gina Fioroni, Principal Investigator
National Renewable Energy Laboratory
15013 Denver West Parkway
Golden, CO 80401
E-mail: gina.fioroni@nrel.gov

Kevin Stork, DOE Technology Development Manager
U.S. Department of Energy
E-mail: Kevin.Stork@ee.doe.gov

Start Date: October 1, 2018 End Date: September 30, 2019
Project Funding (FY19): $750,000 DOE share: $750,000 Non-DOE share: $0

Project Introduction

This project is a continuation of flow reactor work that was performed in Fiscal Year (FY) 2017 and FY 2018 and builds on prior kinetic mechanism validation and soot precursor formation work [1]. The concept is to use a simple, straight quartz tube flow reactor connected to a dual gas chromatograph system to analyze autoignition products and soot precursor molecules to gain insight into skeletal reaction mechanisms. The yield sooting index (YSI) is a metric that describes a molecule's sooting tendency and has been found to vary widely for different isomers of certain molecules (same chemical makeup, but different arrangement of atoms). Understanding how the arrangement of atoms affects the sooting tendency of different isomers is of great interest. Flow reactor results can be compared to quantum mechanical simulations to elucidate the species responsible for varying values of YSI. This project is jointly funded by DOE's Vehicle Technologies Office and Bioenergy Technologies Office.

Objectives

Fiscal Year 2019 Objectives

- Test the ability of the flow reactor to observe phi sensitivity using heptane and primary reference fuels by varying phi and residence time at low temperatures
- Measure methylpropyl ether autoignition in the flow reactor to validate the kinetic mechanism
- Investigate the YSI differences between the isomers of phenylethanol (PE) (1-PE and 2-PE) and ethylphenols (EP) (2-, 3-, and 4-EP) across a wide temperature range and high phi (phi = 3).

Approach

The flow reactor consists of a straight quartz tube that is heated inside a ceramic furnace from 600 K up to 1,200 K. Helium is used as the dilution gas and is fed at the inlet of the reactor along with oxygen and fuel, which is delivered via a syringe pump. The effluent reactor gas is sampled directly into a dual gas chromatograph analysis system that contains five different detectors, which are used to measure a wide range of autoignition products. A mass spectrometer is used to provide identification of unknown species, and dual flame ionization and thermal conductivity detectors provide quantification of light-molecular-weight gases (methane, ethane, etc.), carbon monoxide, carbon dioxide, and molecules up to about carbon number 14 in size.

Results

Use of Flow Reactor to Observe Phi Sensitivity

Phi sensitivity is an important parameter that has been measured in engine studies [2] and is observed as a significant change in ignition delay with relatively small changes in phi. Fuels such as Primary Reference Fuel 80 (PRF80) (a blend of 20% heptane and 80% isooctane) and isooctane itself have been shown to demonstrate phi sensitivity. Our investigation began looking at heptane conversion across the low to intermediate temperature range (550 K to 900 K) and various values of phi (0.25 to 1.0) at atmospheric pressure in the flow reactor. An obvious difference in reactivity (conversion of heptane) was observed when phi was changed from 0.25 to just 0.35, and conversion was completely non-existent at a phi of 0.5. In addition, PRF80 and isooctane were run in this temperature region at three values of phi: 0.25, 0.35, and 0.45. Unfortunately, changes in reactivity of these compounds were not as clearly defined as was the case with heptane. The difficulty in observing differences in reactivity for these fuels is most likely attributable to the lower pressure of the flow reactor experiments compared to engine experiments. Therefore, a key conclusion of this work is that the flow reactor must be upgraded to operate at elevated pressures to observe phi sensitivity for PRF80 and isooctane. Plans for the upgrade are underway, and the upgrade is expected to be completed in the second quarter of FY 2020.

Methylpropyl Ether Mechanism Validation

Ethers have been identified as promising oxygenates for blending into diesel fuel because of their high cetane number and low sooting propensity. Having a better understanding of the chemistry of ether autoignition can assist researchers in better predicting cetane numbers for ethers, which is currently not straightforward. Thus, the autoignition of methylpropyl ether (MPE) was studied, as it serves as a surrogate for higher-molecular-weight ethers that are experimentally and computationally more challenging to study. Flow reactor experiments in combination with kinetic simulations were analyzed. Flow reactor experiments were conducted from 700 K up to 1,000 K at a phi of 1 and two different residence times: 2 s and 5 s. Figure II.15.1 shows the experimental flow reactor data for MPE and one of the key intermediate species, propanal, in comparison to simulation results. The current model underpredicts the conversion of MPE while overpredicting the formation of propanal. Current research efforts are underway to adjust the model to more accurately predict the conversion of MPE.

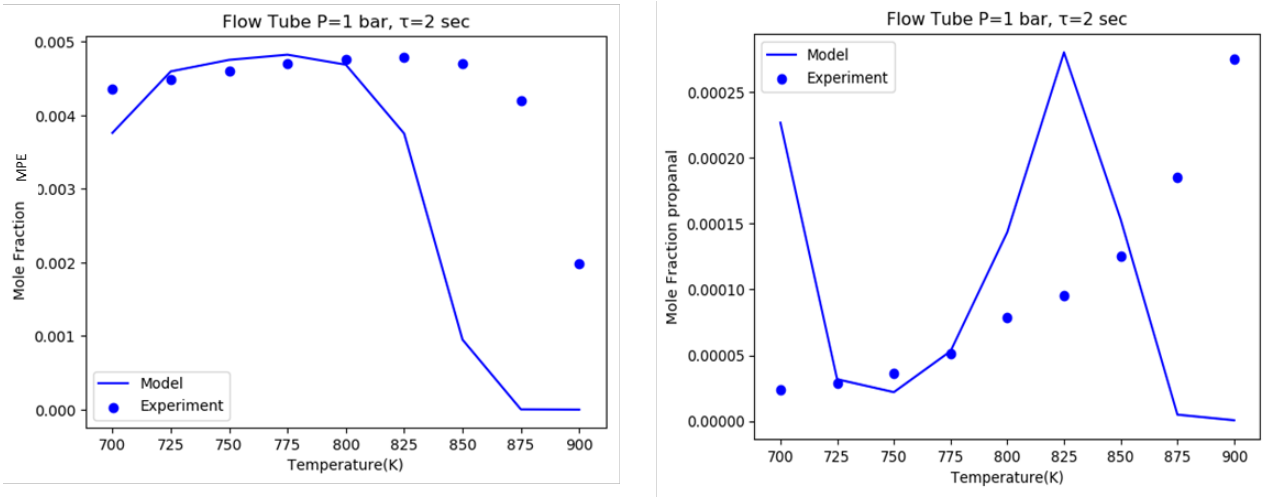

Figure II.15.1 Model versus experimental results for MPE conversion and propanal formation

Yield Sooting Tendency of Phenyl Ethanols and Ethylphenols

YSI is an experimentally measured parameter for the sooting tendency of a molecule. In past work [1], we have noted that the YSI values for methylcyclohexene isomers varied vastly depending on their chemical

structure. Flow reactor experiments in combination with quantum mechanical calculations were able to explain the differences in YSI values based upon the intermediate structures observed in experiments and the calculated bond dissociation energies, which showed which intermediates were more favorable. To continue to expand our knowledge of molecular structure effects on soot formation, in FY 2019 we pursued additional isomers that have produced widely varied YSI values. These compounds include 1- and 2-PE and 2- and 3-EP. (4-EP was also of interest but is a solid at room temperature and was therefore not researched at this time.)

Figure II.15.2 shows the chemical structures for 1-PE (YSI = 142) and 2-PE (YSI = 207). The two structures vary based on the position of the alcohol functionality relative to the ring. Flow reactor experiments were run under rich conditions (phi = 3) and across a wide temperature range (800 K to 1,200 K) and were compared to quantum mechanical results. Figure II.15.3 shows the reaction of the PE isomers along with the area percent observed for the major reaction products formed. The rate of reaction of 1-PE was much faster than that of 2-PE, which can be explained by the lower bond dissociation energies determined for the substituent chain of 1-PE versus 2-PE.

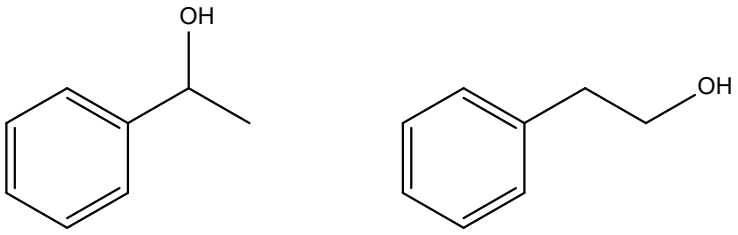

1-phenylethanol 2-phenylethanol

Figure II.15.2 Chemical structures of 1- and 2-phenylethanol

YSI measurements have shown that oxygenated aromatic compounds (OACs) typically have a lower YSI than their aromatic hydrocarbon (AHC) counterparts. For example, the OACs benzaldehyde and acetophenone have YSIs of 119 and 131, respectively, while the AHCs toluene and styrene have YSIs of 171 and 174, respectively. In Figure II.15.3, graphs b and c present a comparison of the OACs and AHCs formed from both PE isomers. 1-PE shows a higher concentration of OACs versus 2-PE across the entire temperature range, indicating oxygen functionality is maintained upon decomposition, lowering the YSI of 1-PE. Formation of AHCs for 1-PE (graph c) is initially higher than that for 2-PE due to the faster decomposition rate of 1-PE (shown in panel a); however, once the temperature reaches 1,000 K, 2-PE decomposes into significantly more AHCs than 1-PE. The AHCs produced by 2-PE result from loss of the oxygen functionality and increase the YSI of 2-PE. Also noted in graph d, previously proposed mechanisms of OAC consumption [3] produce benzene, carbon monoxide, and carbon dioxide; all three of these compounds are produced in higher concentrations for 1-PE versus 2-PE. While quantum mechanical results are not shown, they are in good agreement with flow reactor results and further explain the higher YSI value observed for 2-PE versus 1-PE through elucidation of primary unimolecular and bimolecular decomposition mechanisms.

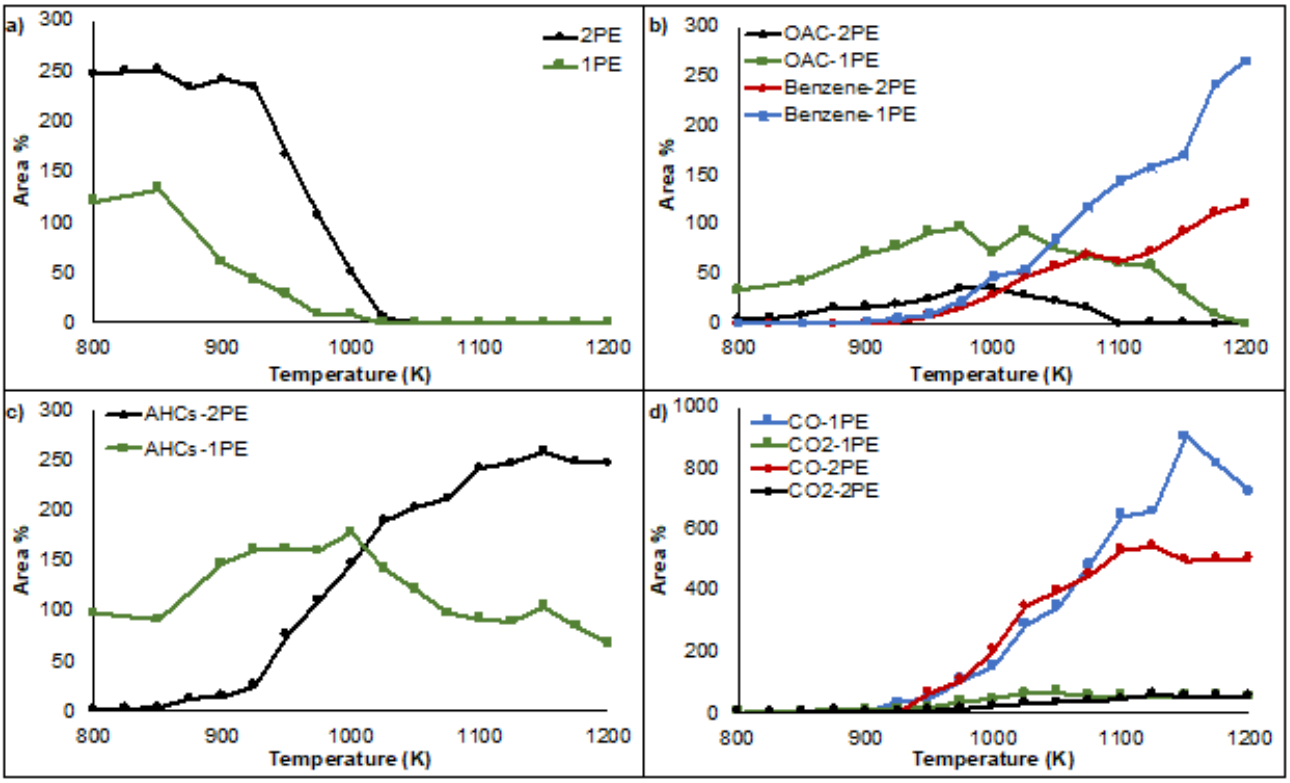

Figure II.15.3 (a) Area percent from the reactant fuels: 1-PE (green) and 2-PE (black). (b) Primary OACs produced from 1 PE (green) and 2-PE (black), and formation of benzene for both isomers (1-PE – blue, 2-PE – red). (c) Primary AHCs produced from 1-PE (green) and 2-PE (black). (d) Formation of carbon monoxide (blue and red) and carbon dioxide (green and black) from 1-PE and 2-PE, respectively. (Figure courtesy of Brian Etz)

Ethylphenol isomers were also investigated in the flow reactor using identical conditions to those run for 1-PE and 2-PE. The differences in YSI for the three isomers are not as significant as those discussed in the PE case; however, investigation into the positional effect of secondary aromatic substituents gives further insight into how to design alternative aromatic fuel additives. The YSIs for 2-EP (YSI = 120) and 4-EP (YSI = 128) are lower than that of 3-EP (YSI=138), indicating that the position of the ethyl substituent with respect to the alcohol is important in soot formation. Flow reactor results for 2-EP and 3-EP are shown in Figure II.15.4. For these isomers, the 2-EP was consumed more rapidly than 3-EP. The formation of the lower-sooting OACs was observed to be higher for 2-EP versus 3-EP until about 1,100 K, where the OACs produced began to decompose into benzene and carbon monoxide as already discussed. Formation of AHCs is comparable for both isomers and is in agreement with the similar YSI for the two isomers. The difference in YSI is attributed to the higher yields of OACs for 2-EP than for 3-EP. Our hypothesis is that the resonance (i.e., position of the substituent) is resulting in more OACs, but further investigation is needed to confirm the reasons for the difference in OACs.

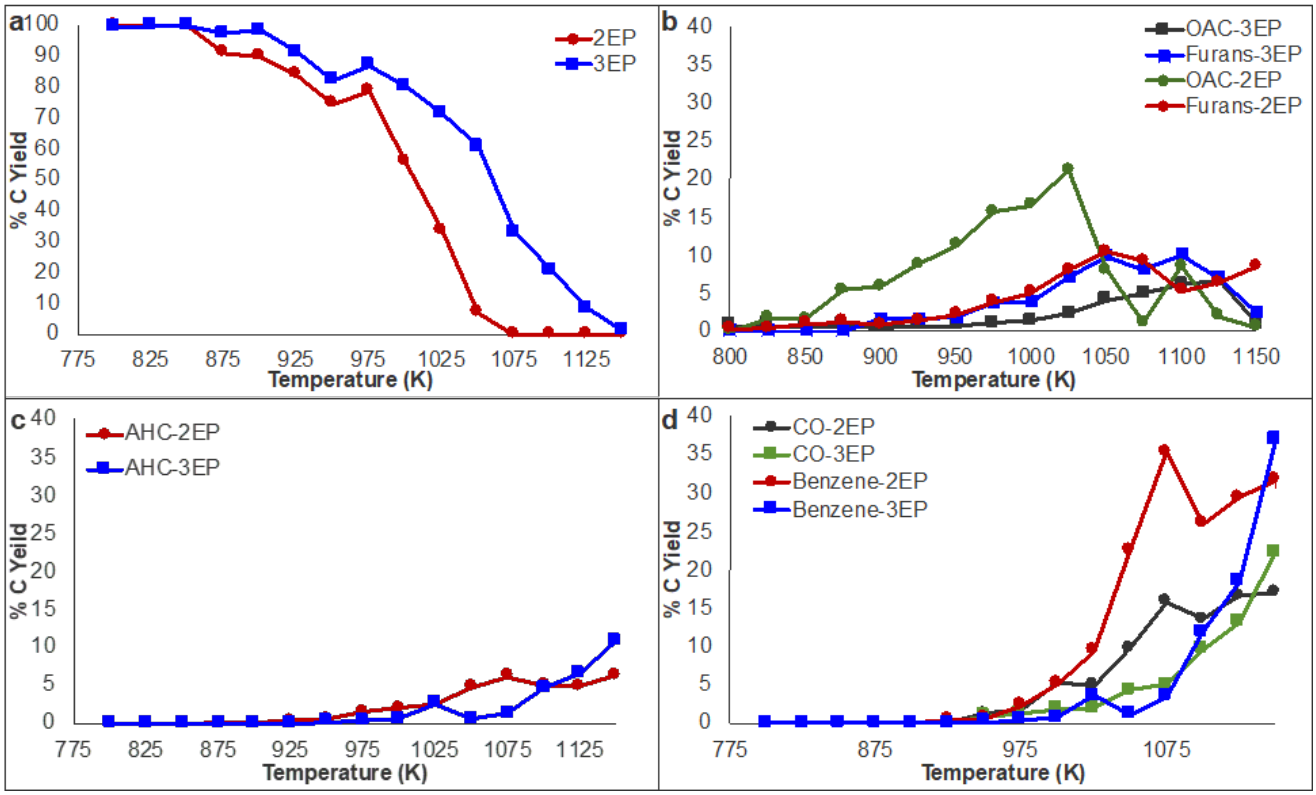

Figure II.15.4 (a) Carbon percent from the reactant fuels: 2-EP (red) and 3-EP (blue). (b) Primary OACs produced from 3-EP (green) and 2-EP (black), and formation of benzofurans for both isomers (3-EP – blue, 2-EP – red). (c) Primary AHCs produced from 2-EP (red) and 3-EP (blue). (d) Formation of carbon monoxide (green and black) and benzene (blue and red) from 2-EP and 3-EP, respectively. (Figure courtesy of Brian Etz)

Conclusions

- The ability to observe phi sensitivity for phi-sensitive fuels was investigated in the flow reactor. It was determined that operation at elevated pressures is required to clearly observe phi sensitivity. Work is underway to increase operational pressure up to 10 bar.
- Methylpropyl ether autoignition was studied in the flow reactor at two residence times. These data were used to improve the kinetic model that was developed at the Massachusetts Institute of Technology.
- Flow reactor results in combination with quantum mechanical calculations were used to explain the differences in YSI values from the different isomers: 1-PE and 2-PE, and 2-EP and 3-EP.

Key Publications

1. Nimlos, M.R., L. Bu, M.S. Johnson, D. Kang, G.M. Fioroni, R.L. McCormick, S. Kim, T. Foust, S.S. Goldsborough, and W.H. Green. 2019. “Low Temperature Oxidation of Methylpropyl Ether.” Presented at the 11th U.S. National Combustion Meeting (March).

2. St. John, P.C., G.M. Fioroni, N. Hug, X. Huo, B.D. Etz, Y. Xuan, C.S. McEnally, L. Pfefferle, D.R. Vardon, R.S. Paton, R.L. McCormick, and S. Kim. 2019. “Predicting the Sooting Tendencies from Chemical Structure with Experimental and Theoretical Insight.” Presented at the 11th U.S. National Combustion Meeting (March).

3. Etz, B.D., G.M. Fioroni, R.A. Messerly, M.J. Rahimi, P.C. St. John, E.D. Christensen, C.S. McEnally, L.D. Pfefferle, Y. Xuan, S. Vyas, R.S. Paton, R.L. McCormick, and S. Kim. "Elucidating the Chemical Pathways of Soot Formation during Combustion of 1- and 2-Phenylethanol." Submitted to the 38th International Symposium on Combustion.

4. Kim, Y., B.D. Etz, P.C. St. John, G.M. Fioroni, R. Messerly, S. Vyas, C.S. McEnally, L.D. Pfefferle, R.L. McCormick, and S. Kim. "Investigation of Structural Effects of Aromatic Compounds on Sooting Tendency with Mechanistic Insight into Ethylphenol Isomers." Submitted to the 38th International Symposium on Combustion.

References

1. Kim, S., G.M. Fioroni, J. Park, D. Robichaud, D.D. Das, P.C. St. John, T. Lu, C.S. McEnally, L.D. Pfefferle, R.S. Paton, T. Foust, and R.L. McCormick. 2018. "Experimental and Theoretical Insight into the Soot Tendencies of the Methylcyclohexene Isomers." Proceedings of the Combustion Institute, pp 1–8.

2. Lopez Pintor, D., J.E. Dec, and G.R. Gentz. 2019. "Φ-Sensitivity for LTGC Engines: Understanding the Fundamentals and Tailoring Fuel Blends to Maximize This Property." SAE Technical Paper 2019-01-0961.

3. Vasiliou, A.K., J.H. Kim, T.K. Ormond, K.M. Piech, K.N. Urness, A.M. Scheer, D.J. Robichaud, C. Mukarakate, M.R. Nimlos, J.W. Daily, Q. Guan, H. Carstensen, and G.B. Ellison. 2013. "Biomass Pyrolysis: Thermal Decomposition Mechanisms of Furfural and Benzaldehyde." *J Chem Phys,* pp. 104310.

Acknowledgements

The principal investigator gratefully acknowledges the contributions of Seonah Kim (co-Principal Investigator), Lisa Fouts, Peter St. John, Brian Etz, Mohammad Rahimi, Mark Nimlos, Matt Johnson, Bill Green, and Robert McCormick to this report.

II.16 Scenario Co-Optimizer (Lawrence Berkeley National Laboratory)

Juliane Mueller, Principal Investigator
Lawrence Berkeley National Laboratory
1 Cyclotron Road
Berkeley, CA 94720
E-mail: JulianeMueller@lbl.gov

Kevin Stork, DOE Technology Development Manager
U.S. Department of Energy
E-mail: Kevin.Stork@ee.doe.gov

Start Date: October 1, 2018 End Date: September 30, 2019
Project Funding: $195,000 DOE share: $195,000 Non-DOE share: $0

Project Introduction

This research is part of the simulation toolkit team in Co-Optima. In this research, the scenario co-optimization software has been further developed, and new optimization capabilities have been included that enable solving a wider class of problems than was previously possible. The overarching goal of developing the co-optimizer is to give experimentalists and computational scientists an easy-to-use optimizer that enables them to autonomously steer their laboratory experiments and to optimize the parameters in their simulation models, respectively.

The new capabilities include bi-level optimization, constrained optimization, and the use of different types of surrogate models that steer experimentation and can be used to quantify the uncertainty of experimental outcomes across the experimental domain. Bi-level optimization is a type of leader-follower approach in which at the upper level ('leader problem'), a fuel composition is chosen and its efficiency is computed by optimizing over the engine operation conditions at the lower level ('follower problem'). Then, at the upper level, a new fuel is chosen and the lower level problem is solved again, etc. This enables not only identifying the most efficient fuel but also the best engine operation conditions for that fuel. The surrogate models are used in this context to approximate input-output relationships, e.g., fuels and their efficiency. This allows the prediction of the output and its associated uncertainty over the whole parameter domain without having to try thousands of different inputs.

Objectives

Overall Objectives

- Develop new optimization capabilities targeted at Co-Optima relevant applications (experimentation and simulation)
- Demonstrate efficiency and effectiveness of previous and new methods on fast-to-compute synthetic problems (proof of concept) and on selected experimental data and simulations.

Fiscal Year 2019 Objectives

- Assess effectiveness and efficiency of the developed capabilities on synthetic problems
- Demonstrate the effectiveness and efficiency on engine data from Oak Ridge National Laboratory (ORNL) and National Renewable Energy Laboratory (NREL)

- Perform preliminary exploration of the effectiveness and efficiency of the methods on Zero-RK (Zero-Order Reaction Kinetics combustion software package) simulations from Lawrence Livermore National Laboratory (LLNL) or on a small-scale problem.

Approach

One of the main tools used in this research is response surface models (i.e., surrogate models). These models are widely used in the black-box optimization context when objective and constraint functions are computationally expensive and when derivatives are not available. Surrogate models are used to approximate the true underlying response that can only be obtained by querying a computationally intensive simulation model or by conducting a time-consuming lab experiment. If any kind of analysis such as sensitivity analysis, uncertainty quantification, or optimization of the response is required, a large number of these queries would be needed, which is intractable computationally as well as from a resource perspective.

Surrogate models are trained on known input-output data pairs, e.g., fuel-efficiency pairs or engine operation-efficiency pairs. They are cheap to build, and making predictions of the response at an untried input is also cheap. Thus, surrogates provide a good approximation of the expensive-to-obtain response in analysis and optimization. Different types of surrogate models exist. In this research, radial basis functions and Gaussian process models are employed. These models have the advantage that they can model nonlinearities well, and in the case of Gaussian process models, they provide an uncertainty estimate together with the response prediction.

The surrogate models are used in this research within an iterative optimization scheme in which an acquisition function is optimized on the surrogate, and the result of this optimization determines which input should be tried next in the experiment or simulation. After the new input-output pair has been obtained, the surrogate model is updated. This adaptive sampling approach saves a significant number of expensive queries during optimization and analysis. The developed methods were tested on experimental data (from Szybist, ORNL [3]) as well as on optimizing simulation models (McNenley and Lapointe, LLNL [4],[5]).

Results

- Developed, verified, and demonstrated new bi-level optimization capabilities with surrogate modeling
- Demonstrated efficiency and effectiveness of the methods on real engine data provided by ORNL and NREL and simulation model from LLNL
- Extended surrogate modeling capabilities to radial basis functions
- Demonstrated that surrogate model predictions are sensitive to outlier data, indicating that expert knowledge is needed when selecting data for training the surrogate
- Released updated version of the co-optimizer on bitbucket.

Bi-Level Optimization

The bi-level approach optimizes fuel properties at the upper level and engine operation conditions at the lower level to achieve optimized fuel-engine performance. This approach was taken because experimental data were provided with different parameters (upper level: fuel properties only; lower level: fuel properties and engine operation conditions). The objectives were to maximize the merit function (MMF) as defined by Miles [1] and the net mean effective pressure (NMEP) as measured in Ratcliff et al. [2] simultaneously and to identify tradeoffs between the two. Figure II.16.1 shows the tradeoff between the two objectives; the color bar indicates the corresponding values of heat of vaporization (HOV) for each tradeoff solution. The figure shows clearly that there is a tradeoff between the two objectives and that lower HOV values will lead to higher NMEP but lower MMF in this setting. This bi-level approach is straight-forwardly generalizable to other types of objective functions (simulation objective, experiments, analytic expressions) and to more than two objective functions.

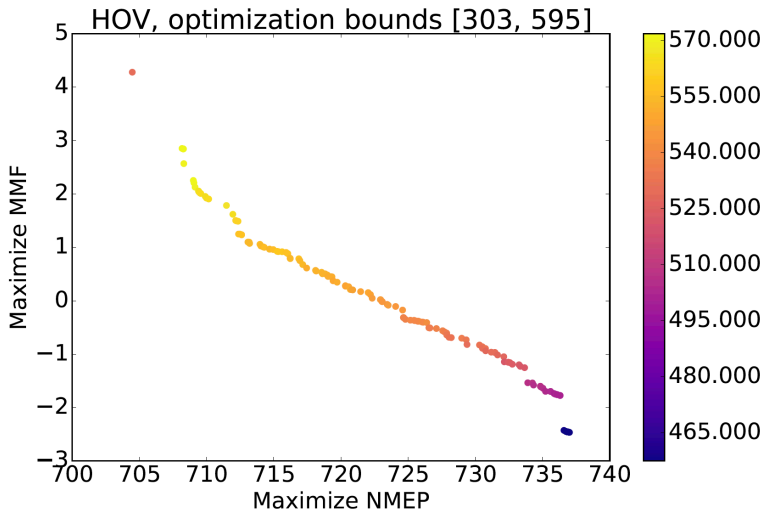

Figure II.16.1 Tradeoff curves between bi-level-optimized MMF and NMEP as approximated with a surrogate model. The range of HOV that corresponds to the tradeoff solutions is shown in the colored bar. High HOV leads to better NMEP and worse MMF.

Multi-Objective Optimization on Experimental Data

The applicability of the multi-objective optimization tools in the optimization software was demonstrated on fuel-engine data provided by J. Szybist (ORNL) [3]. It was found that 'outlier' fuels have an impact on the predication and uncertainty of the surrogate models. A multi-objective optimization for maximizing the fuel efficiency while minimizing the uncertainty of the predictions shows that about 40% efficiency could be attainable, which is in agreement with the experimentalists' intuition (see Figure II.16.2 and Figure II.16.3). When using the outlier fuel in the training of the surrogate model, it was found that the uncertainty of the predicted performance was higher (compare Figure II.16.2 and Figure II.16.3). This may be related to the fact that the outlier fuel is furthest away from all other sample data (in the Euclidean norm), and a single data point in an otherwise sparsely sampled region of the parameter space that in addition has higher efficiency than any other data point may induce higher uncertainty in that area of the parameter space. Sensitivity analyses suggest that oxygenates, olefins, and fuel sensitivity are the most important parameters that influence fuel efficiency with and without outlier fuels.

Constrained Optimization of Simulations

Lastly, preliminary work has been conducted for treating constrained optimization problems where both the objective function and the constraint function are computed by computationally expensive simulations, as in the Zero-RK model from McNenly and Lapointe (LLNL). A small dimensional test case was considered. Both the objective and the constraint were approximated by separate surrogate models, and the objective was only evaluated if the constraints were satisfied (objective and constraint values are outcomes from two separate calculations). The optimizer led to fast convergence and has the potential to reduce the computational demand for finding near-optimal solutions as compared to commonly used genetic algorithms. Follow-on research work in this area is underway addressing scalability, improved constraint handling, and additional objective functions.

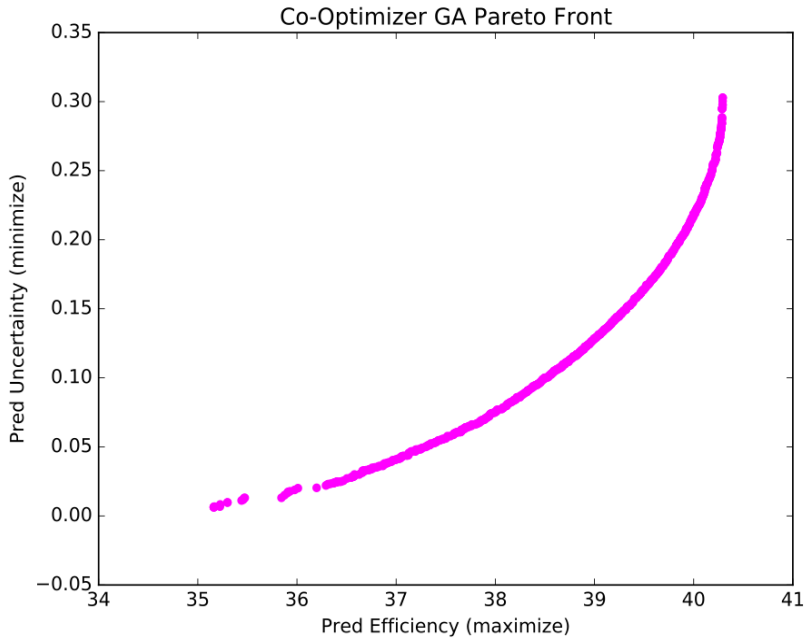

Figure II.16.3 Tradeoff curve between predicted efficiency and predicted uncertainty for Szybist data when outlier fuel is included. Higher efficiency leads to higher uncertainty. Efficiency of over 40% may be attainable, but with high uncertainty.

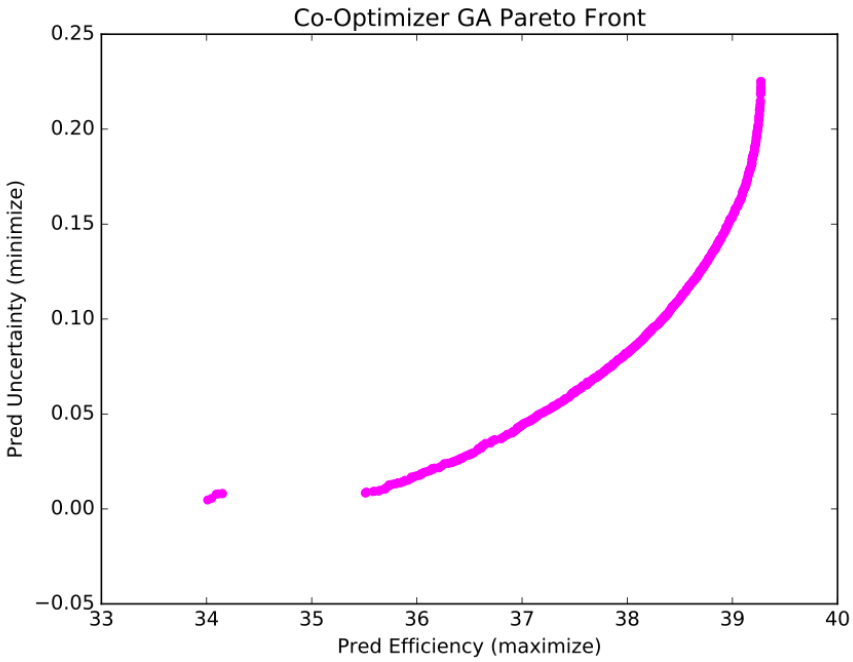

Figure II.16.2 Tradeoff curve between predicted efficiency and predicted uncertainty for Szybist data when outlier fuel is **not** included. Higher efficiency leads to higher uncertainty.

Conclusions

- Surrogate-model-based optimization leads to efficient and effective solution of otherwise time- and resource-consuming experiments.
- Bi-level optimization readily lends itself to co-optimizing fuels and engine operation conditions.
- Optimization through adaptive sampling guided by surrogate models enables autonomous experimentation and should be employed by experimentalists as well as computer scientists (rather than trial-and-error methods).
- Tight collaboration with experimentalists as well as computer scientists is necessary to identify opportunities where automated computational optimization and analysis tools will improve current approaches to accelerate scientific discovery.

Key Publications

1. Co-optimizer release, including graphical user interface and user manual: https://bitbucket.org/julianem/co-optima-summer/. Available to Co-Optima collaborators upon request.

References

1. Miles, Paul. 2018. "Efficiency Merit Function for Spark Ignition Engines: Revisions and Improvements Based on FY16–17 Research." Technical Report. U.S. Department of Energy, Washington, DC. DOE/GO-102018-5041.

2. Ratcliff, Matthew A., Jonathan Burton, Petr Sindler, Earl Christensen, Lisa Fouts, and Robert L. McCormick. 2018. "Effects of Heat of Vaporization and Octane Sensitivity on Knock-Limited Spark Ignition Engine Performance." WCX18: SAE World Congress Experience (April 10–12), Detroit, MI.

3. Szybist, James, and Derek Splitter. 2018. "Impact of Engine Pressure-Temperature Trajectory on Autoignition for 19 Fuels: From Boosted SI (beyond RON) to HCCI (beyond MON)." Presentation at the AEC Program Review Meeting (August 16), USCAR, Southfield, MI.

4. McNenly, M.J., R.A. Whitesides, and D.L. Flowers. 2015. "Faster Solvers for Large Kinetic Mechanisms Using Adaptive Preconditioners." *Proceedings of the Combustion Institute* 35 (1): 581–587.

5. Zero-RK code repository: https://github.com/LLNL/zero-rk.

Acknowledgements

The application of the developments to simulation optimization is joint work with Matthew McNenly and Simon Lapointe from LLNL. Fuel and engine performance data for data-informed surrogate modeling, optimization, and sensitivity analysis has been provided by James Szybist from ORNL and Matthew Ratcliff from NREL.

II.17 Fuel Property Blending Model (Pacific Northwest National Laboratory)

J. Timothy Bays, Principal Investigator
Pacific Northwest National Laboratory
902 Battelle Blvd., MS K2-44
Richland, WA 99352
E-mail: tim.bays@pnnl.gov

Kevin Stork, DOE Technology Development Manager
U.S. Department of Energy
E-mail: Kevin.Stork@ee.doe.gov

Start Date: October 1, 2018 End Date: September 30, 2019
Project Funding (FY19): $150,000 DOE share: $150,000 Non-DOE share: $0

Project Introduction

This project is focused on connecting the effects of molecular-level solution structures, such as clustering, hydrogen-bonding networks, and crystallization, to fuel properties in a finished fuel. Understanding and leveraging the effects of oxygenate clusters as a function of concentration and oxygenate-fuel interactions may yield new approaches to favorably influencing fuel properties in automotive applications. In doing so, this project seeks to facilitate the successful co-optimization of fuels and advanced combustion engines by providing an understanding of changes in properties resulting from the incorporation of potential renewable fuel feedstocks and unconventional hydrocarbon fuels into the domestic fuel supply. This would enhance domestic energy security and economic competitiveness and improve environmental quality.

Objectives

Overall Objectives

- Advance an understanding of the role of molecular-level solution structures, such as clustering, hydrogen-bonding networks, and crystallization, within a fuel on fuel properties (important to current and future engine-combustion strategies)
- Develop predictive models based upon analytical approaches correlating molecular-level solution structures within fuel components to fuel properties and performance.

Fiscal Year 2019 Objectives

- Relate nuclear magnetic resonance (NMR) spectroscopic measurements and molecular dynamics simulations of alcohol clusters in model fuel systems to engine performance properties, specifically, research octane number (RON) and motor octane number (MON), using data from Foong and Kolodziej, as well as heat of vaporization (HOV) measurements from National Renewable Energy Laboratory
- Submit one publication documenting chemical methods for the separation of ethanol from gasoline onboard a vehicle.

Approach

This project uses NMR spectroscopy and molecular dynamics simulations to identify and quantify temperature-dependent, molecular-level solution structures within gasoline and model fuels. NMR diffusion measurements, obtained through a technique called diffusion-ordered spectroscopy, are used to identify oxygenate clustering and hydrogen-bonding network formation. Ethanol clustering in gasoline has previously

been observed using this technique, but the reported results provided conflicting information without explanation and provided no links to the impacts that molecular-level clustering might have on fuel properties [1],[2]. Previously, Reid vapor pressure was selected as an important fuel property likely to be influenced by molecular aggregation or clustering, but during Fiscal Year 2019, RON, MON, and HOV were explored. To probe cluster formation at shorter time scales than available using NMR, molecular dynamics simulations were undertaken for systems parallel to those used in the NMR studies. These simulations provide a great deal of information, including computation of diffusion coefficients, hydrogen-bonding networks, cluster size distributions, and lifetimes. Together, these experiments provide synergistic data and allow researchers to observe molecular clusters and hydrogen-bonding networks in gasoline surrogates consisting of oxygenates in model fuels like *n*-heptane or isooctane, in higher complexity surrogate fuels, and in the case of NMR, in authentic gasoline samples.

Results

- Alcohol clusters and hydrogen-bonding networks for C1–C4 alcohols have been observed in single-component surrogate fuels, as well as in gasoline.
- Alcohol concentration, identity of the alcohol, identity of the fuel, and temperature influence the balance between cluster size and population and the extent of hydrogen-bonding network formation.

NMR diffusion measurements, specifically diffusion-ordered spectroscopy, yielded diffusion coefficients for alcohols in single-component gasoline surrogates, gasoline, and diesel. Alcohol diffusion coefficients were then correlated with alcohol cluster weights and the average number of molecules per cluster in gasoline surrogates for the following alcohol-surrogate combinations: ethanol in isooctane and methanol (MeOH), ethanol (EtOH), isopropanol (i-PrOH), *n*-butanol, and isobutanol (i-BuOH) in *n*-heptane. Also tested were concentrations of ethanol in a certification gasoline (Haltermann Solutions, Tier III EEE U.S. Federal Emission Certification Gasoline) and concentrations of tri(propylene glycol) methyl ether (TPGME) in a Chevron-Phillips diesel emissions certification fuel known as CFA. As shown in Figure II.17.1, the average alcohol cluster size was found to increase with increasing alcohol concentration, to a maximum of approximately six alcohol molecules per cluster. The results for four alcohols in *n*-heptane, plotted in Figure II.17.1(a), show that as the size of the alcohol increases from one carbon to four carbons, the maximum alcohol cluster size is achieved at successively higher alcohol concentrations. Figure II.17.1(b) shows that the maximum cluster size for ethanol was found to occur at 40 mole percent ethanol in isooctane and 50 mole percent ethanol in gasoline. While TPGME appears to interact with the molecules in the CFA diesel fuel, as suggested by a maximum cluster size of 1.5, clustering was not considered to occur. The effects of increased temperature on isobutanol clustering in *n*-heptane are shown in Figure II.17.1(c). The maximum isobutanol cluster size in *n*-heptane decreased on average from about 5.5 to about 2 when temperature was increased from 25°C to 80°C. Similar decreases in cluster size with increasing temperature were observed regardless of the alcohol, although the maximum cluster sizes achieved differed, depending upon the alcohol. These experiments demonstrate that the alcohol, nature of the fuel, and temperature affect the maximum cluster size and concentration of maximum cluster size observed in these systems.

In these experiments, increasing cluster size occurred as a result of increasing alcohol concentration, but only to a point. After that point, where the maxima occurred, continued increases in alcohol concentration resulted in apparently decreasing alcohol cluster sizes. These apparent decreases were attributed to the increasing presence and influence of hydrogen-bonding networks. In the NMR diffusion experiments, the increasing alcohol cluster size resulted in slower diffusion of the clusters through the fluid. When the clusters became sufficiently large, the diffusion rate was too slow to be observed in these NMR experiments. This condition was attributed to the increasing influence of hydrogen bonding with the higher concentration of alcohol within the fuel, leaving fewer alcohol molecules available to form clusters, thereby resulting in smaller cluster sizes available to diffuse. The balance between alcohol clustering and hydrogen-bond network formation is

determined by each of the factors mentioned previously that influence clustering, e.g., the properties of the alcohol, the properties of the fuel, and the temperature.

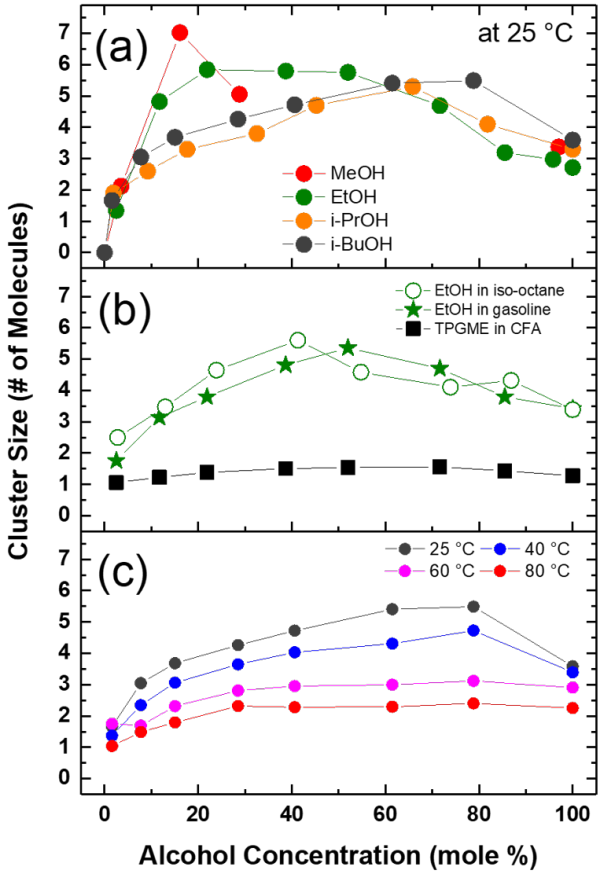

Figure II.17.1 Alcohol cluster size as a function of alcohol, concentration, fuel, and temperature. (a) MeOH, EtOH, *i*-PrOH, and *i*-BuOH in *n*-heptane at 25 °C show different alcohol concentrations for maximum cluster size. (b) EtOH in isooctane and EtOH in gasoline at 25 °C show a close resemblance for peak cluster size; TPGME in CFA diesel shows a maximum average cluster size of about 1.5; (c) *i*-BuOH in *n*-heptane at various temperatures shows that cluster size decreases with increasing temperature. (Credit: Kee Sung Han)

Previously, molecular dynamics (MD) simulations of gasoline surrogate mixtures (methanol, ethanol, *n*-propanol, and *n*-butanol in *n*-heptane) were performed to visualize cluster formation of alcohols in these mixtures and calculate the average number of hydrogen bonds per alcohol molecule, as well as determine an alcohol-cluster size distribution. This work showed that the number of hydrogen bonds per alcohol molecule tended to increase rapidly up to 20% alcohol by volume (nearly 50 mole percent for methanol and 30 mole percent for *n*-butanol) and then gradually increase above 20% alcohol. The number of hydrogen bonds per alcohol molecule tended to decrease with the length of the alcohol carbon chain, although that of *n*-propanol is consistently slightly less than that for *n*-butanol. A continuous, broad distribution of ethanol cluster sizes is observed up to 10% ethanol in *n*-heptane. After 10% ethanol in *n*-heptane, the small-cluster distribution attenuates and a large-cluster (much larger, network clusters) distribution appears.

Further analysis of molecular cluster size in the MD simulations was subsequently used to shed light on the effects of alcohol clustering resulting from hydrogen bonding and van der Waals forces in simple surrogate fuel mixtures. The use of both MD simulation and NMR diffusion measurements to understand the influence of intermolecular forces on physical properties of fuel mixtures with oxygenates was a first-of-its-kind investigation. These experiments and MD simulations were employed to show molecular-level correspondence

between hydrogen-bonded/van der Waals clustering of alcohols in *n*-heptane and in isooctane and thermodynamic quantities such as Reid vapor pressure. Beyond the NMR diffusion experiments, MD simulations show the extent of large-scale, alcohol-clustering networks for higher-percentage alcohol compositions in fuel surrogates (Figure II.17.2). Corresponding with the solution experiments, small clustering peaks at around 20 mole percent ethanol in the *n*-heptane case and tapers off with increasing percentage of ethanol. In the case of ethanol in isooctane, small clustering peaks at the low percentages of ethanol and then peaks (at a lower peak) around 60 mole percent, which qualitatively fits the trend seen in the NMR experiments. The balance between populations of discrete clusters and large-scale clustering networks was found to be dependent upon fuel/fuel surrogate composition, temperature, alcohol concentration, and identity of the alcohol, and for ethanol, shows correspondence with Reid vapor pressure. Both NMR diffusion experiments and MD simulations are shown to be useful tools in understanding and predicting the molecular-level structure and dynamics of oxygenated fuel mixtures, which directly tie into the macroscopic physical properties of these fuel mixtures.

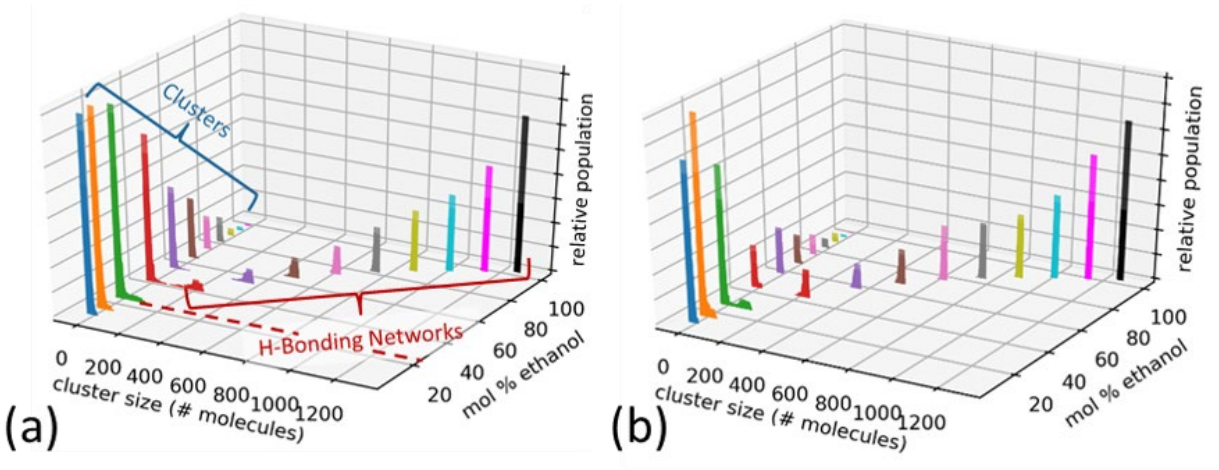

Figure II.17.2 Molecular clustering analysis. Relative populations and sizes for ethanol clusters and hydrogen-bonding networks as a function of (a) ethanol in *n*-heptane and (b) ethanol in isooctane. (Credit: Amity Andersen)

While these studies have proven to be fruitful, offering a reasonable correlation and explanation for the trends observed in the Reid vapor pressure for ethanol-fuel combinations, they have not yet been sufficiently extended to show the influence on RON, MON, and HOV. Initial efforts to link the molecular-level inhomogeneities to RON and MON using literature data from Foong, Kolodziej, Sarathy, Anderson, and their colleagues proved to be flawed [3],[4],[5],[6]. The critical aspect that makes these literature studies inappropriate for studying inhomogeneities in fuel is that they use ASTM D2699 and ASTM D2700 to obtain RON and MON, respectively [7],[8]. These standards use a naturally aspirated engine, which, ideally, vaporizes the fuel prior to entering the combustion chamber. Any residual fuel that remains in droplet form constitutes a small portion of the fuel, reducing the influence of the liquid droplets. Effects from liquid-state inhomogeneities, such as clustering, aggregation, and hydrogen-bonding networks, are lost after the fuel has been vaporized, with the possible exception of HOV, which has been discussed in the context of charge cooling by both Foong and Kolodziej, and their coworkers [3],[4],[9]. Work by Fioroni and coworkers examining the influence of alcohols on the instantaneous HOV promises to be a better direction of exploration because of the observed changes in HOV as the alcohol-fuel mixtures evaporate [10]. Considerable work in the literature has explored the evaporation of liquid droplets containing mixtures of alcohol and a fuel or fuel surrogate. These modeling efforts empirically describe non-ideal vapor-liquid equilibria observed during the evaporation of the liquid components and the partitioning of the components between the liquid and vapor phases (examples are referenced) [11],[12],[13],[14],[15]. With these last works in mind, the observed non-ideal evaporative behavior of alcohol-fuel mixtures, and the changes reported in fuel injector spray

characteristics, as well as correlations with soot formation, suggest that continued work in understanding the interplay between solution inhomogeneities and fuel evaporation/distillation will provide fundamental insights into the origins of some fuel properties.

Conclusions

- Synergistic information from molecular diffusion studies and molecular dynamics simulations show cluster development and hydrogen-bond network formation, which have previously been tied to changes in Reid vapor pressure with increasing ethanol concentration.
- Solution inhomogeneities, like alcohol clusters and hydrogen-bonding networks, are affected by alcohol concentration, the nature of the alcohol, the nature of the fuel or fuel surrogate, and by temperature.
- These behaviors have been observed in single-component surrogate fuels, like n-heptane and isooctane, using C1–C4 alcohols, and in gasoline using ethanol, but not convincingly in diesel fuel using the polyether alcohol, TPGME.

Key Publications

1. Grubel, K., W. Chouyyok, D.J. Heldebrant, J.C. Linehan, and J.T. Bays. 2019. "Octane-On-Demand: Onboard Separation of Oxygenates from Gasoline." *Energy & Fuels* 33, no. 3 (March): 1869–1881. doi: https://doi.org/10.1021/acs.energyfuels.8b03781.
2. Bays, J.T., K. Grubel, D.J. Heldebrant, and J.C. Linehan. 2018. On-Board Separation of Oxygenates from Gasoline. Edited by U.S. Patent and Trademark Office. United States: Battelle Memorial Institute. Original edition, 62/746,899.
3. Bays, J.T., et al. 2018. "Fuel Property Blending Model." In Advanced Combustion Systems and Fuels, 2018 Annual Progress Report, edited by G. Singh, K.C. Howden, R.M. Gravel, K. Stork, and M. Weismiller. U.S. Department of Energy, Energy Efficiency & Renewable Energy, Vehicle Technologies Office, https://www.energy.gov/sites/prod/files/2019/04/f62/fy2018_adv-comb-sys_and_fuelsb.pdf.

References

1. Turanov, A., and A.K. Khitrin. 2014. "Proton NMR Characterization of Gasoline-Ethanol Blends." *Fuel* 137 (December): 335–338. doi: https://doi.org/10.1016/j.fuel.2014.08.018.
2. Turanov, A., and A.K. Khitrin. 2016. "Ethanol Clusters in Gasoline-Ethanol Blends." *Industrial & Engineering Chemistry Research* 55, no. 37 (September): 9952–9955. doi: https://doi.org/10.1021/acs.iecr.6b02569.
3. Anderson, J.E., U. Kramer, S.A. Mueller, and T.J. Wallington. 2010. "Octane Numbers of Ethanol- and Methanol-Gasoline Blends Estimated from Molar Concentrations." *Energy & Fuels* 24, no. 12 (December): 6576–6585. doi: https://doi.org/10.1021/ef101125c.
4. Badra, J., A.S. AlRamadan, and S.M. Sarathy. 2017. "Optimization of the Octane Response of Gasoline/Ethanol Blends." *Applied Energy* 203 (July): 778–793. doi: https://doi.org/10.1016/j.apenergy.2017.06.084.
5. Foong, T.M., K.J. Morganti, M.J. Brear, G. da Silva, Y. Yang, and F.L. Dryer. 2014. "The Octane Numbers of Ethanol Blended with Gasoline and Its Surrogates." *Fuel* 115 (January): 727–739. doi: https://doi.org/10.1016/j.fuel.2013.07.105.

6. Hoth, A., C.P. Kolodziej, T. Rockstroh, and T. Wallner. 2018. "Combustion Characteristics of PRF and TSF Ethanol Blends with RON 98 in an Instrumented CFR Engine." *SAE Technical Paper* 2018-01-1672. doi: https://doi.org/10.4271/2018-01-1672.

7. Standard Test Method for Motor Octane Number of Spark-Ignition Engine Fuel. 2017. In *ASTM D2700*: ASTM International.

8. Standard Test Method for Research Octane Number of Spark-Ignition Engine Fuel. 2017. In *ASTM D2699*: ASTM International.

9. Foong, T.M., K.J. Morganti, M.J. Brear, G. da Silva, Y. Yang, and F.L. Dryer. 2013. "The Effect of Charge Cooling on the RON of Ethanol/Gasoline Blends." *SAE International Journal of Fuels and Lubricants* 6 (1): 34–43. doi: https://doi.org/10.4271/2013-01-0886.

10. Fioroni, G.M., E. Christensen, L. Fouts, and R. McCormick. 2019. "Heat of Vaporization and Species Evolution during Gasoline Evaporation Measured by DSC/TGA/MS for Blends of C1 to C4 Alcohols in Commercial Gasoline Blendstocks." *SAE Technical Paper* 2019-01-0014. doi: https://doi.org/10.4271/2019-01-0014.

11. Bader, A., P. Keller, and C. Hasse. 2013. "The Influence of Non-Ideal Vapor–Liquid Equilibrium on the Evaporation of Ethanol/iso-Octane Droplets." *International Journal of Heat and Mass Transfer* 64 (September): 547–558. doi: https://doi.org/10.1016/j.ijheatmasstransfer.2013.04.056.

12. Burke, S.C., M. Ratcliff, R. McCormick, R. Rhoads, and B. Windom. 2017. "Distillation-Based Droplet Modeling of Non-Ideal Oxygenated Gasoline Blends: Investigating the Role of Droplet Evaporation on PM Emissions." *SAE International Journal of Fuels and Lubricants* 10 (1): 69–81. doi: https://doi.org/10.4271/2017-01-0581.

13. Cordier, M., L. Itani, and G. Bruneaux. 2019. "Quantitative Measurements of Preferential Evaporation Effects of Multicomponent Gasoline Fuel Sprays at ECN Spray G Conditions." *International Journal of Engine Research* (March). doi: https://doi.org/10.1177/1468087419838391.

14. Corsetti, S., R.E.H. Miles, C. McDonald, Y. Belotti, J.P. Reid, J. Kiefer, and D. McGloin. 2015. "Probing the Evaporation Dynamics of Ethanol/Gasoline Biofuel Blends Using Single Droplet Manipulation Techniques." *Journal of Physical Chemistry A* 119, no. 51 (December): 12797–12804. doi: https://doi.org/10.1021/acs.jpca.5b10098.

15. Storch, M., S. Erdenkäufer, M. Wensing, S. Will, and L. Zigan. 2015. "The Effect of Ethanol Blending on Combustion and Soot Formation in an Optical DISI Engine Using High-speed Imaging." *Energy Procedia* 66 (May): 77–80. doi: https://doi.org/10.1016/j.egypro.2015.02.041.

Acknowledgements

The work necessary to reach the goals of this project was conducted primarily by this project's co-contributors, Kee Sung Han, Amity Andersen, Kristen B. Campbell, Katarzyna Grubel, Molly J. O'Hagan, and John C. Linehan. PNNL clearance number: PNNL-29399.

II.18 Fuel Impacts on Emissions Control Performance and Durability (Oak Ridge National Laboratory)

Josh A. Pihl, Principal Investigator
Oak Ridge National Laboratory
2360 Cherahala Boulevard
Knoxville, TN 37932
E-mail: pihlja@ornl.gov

Kevin Stork, DOE Technology Development Manager
U.S. Department of Energy
E-mail: Kevin.Stork@ee.doe.gov

Start Date: October 1, 2018 End Date: September 30, 2019
Project Funding (FY19): $340,000 DOE share: $340,000 Non-DOE share: $0

Project Introduction

The overall objective of the Co-Optimization of Fuels and Engines Initiative (Co-Optima) is to cooperatively develop emerging high-performance fuels and advanced engines to bring these technologies to the market sooner to realize a reduction in petroleum consumption. This project aims to investigate the compatibility of Co-Optima fuel candidates with emissions control systems and to identify opportunities for alternative emissions control strategies based on novel fuel chemistry. Specifically, this project is investigating the following questions:

1. Is the catalytic reactivity of Co-Optima candidate blendstocks sufficient to allow continued use of current emissions control technologies?

2. Do the Co-Optima candidate blendstocks create opportunities for reducing tailpipe emissions and/or aftertreatment system costs based on their reactivities over emissions control catalysts?

Objectives

Overall Objectives

- Measure the effects of Co-Optima candidate blendstocks on the performance of emissions control catalysts relevant to the various combustion strategies under investigation in the Co-Optima initiative

- Identify and evaluate potential alternative emissions control strategies that exploit the unique chemistry of Co-Optima blendstock candidates.

Fiscal Year 2019 Objectives

- Explain why fuel blends containing up to 30% of several different Co-Optima blendstocks all show similar catalyst light-off performance even though the pure blendstocks have substantially different catalytic reactivity

- Measure the catalyst light-down of Co-Optima blendstock candidates under conditions relevant to spark ignition/advanced compression ignition (SI/ACI) multimode engine operation.

Approach

This project utilizes targeted flow reactor studies to evaluate the compatibility of Co-Optima candidate blendstocks with emissions control catalysts and identify opportunities for alternative emissions control strategies that make use of novel fuel chemistry. The synthetic exhaust gas flow reactor systems are designed

to offer maximum flexibility to mimic exhaust conditions expected in vehicle applications and further allow the exploration of the boundary conditions associated with the candidate emissions control systems. Great care has been taken to ensure the results from the flow reactors will correlate well with engine-based studies.

In modern gasoline-fueled light-duty vehicles with stoichiometrically operated SI engines, three-way catalysts (TWC) are very efficient at reducing the emissions of deleterious pollutants such as non-methane organic gases, oxides of nitrogen, and carbon monoxide (CO) to enable compliance with stringent emissions regulations. Most of the non-methane organic gases, oxides of nitrogen, and CO emissions occur during cold-start, when the TWC is below a critical temperature known as the catalyst light-off temperature. Engine operating strategies adopted to rapidly heat up the catalyst, such as injecting additional fuel and delaying spark timing, incur a fuel penalty, as the engine is not operating at its optimum efficiency during the cold-start period [1],[2],[3]. Cold-start strategies must be carefully optimized to minimize both the time to achieve catalyst light-off as well as the emissions released during the cold-start period. Prior work at Oak Ridge National Laboratory and elsewhere has shown that TWC light-off performance depends on the chemical composition of the organic species in the exhaust, which change with fuel composition. In prior years, this project has been focused on measuring the potential impacts of Co-Optima blendstocks on TWC light-off.

Keeping with the overarching goals of the Co-Optima initiative, this project shifted focus to emissions control for SI/ACI multimode engines in Fiscal Year 2019. Such engines will operate with stoichiometric air/fuel ratios at high engine loads and during cold-start, and they will still rely on TWCs for emissions control under those conditions. Thus, the prior work on TWC light-off under stoichiometric conditions is still relevant. However, the benefit of SI/ACI multimode engines derives from the use of advanced lean-burn combustion strategies to increase efficiency under part-load operation, introducing additional emissions control challenges beyond stoichiometric cold-start. One of these challenges is handling the elevated non-methane organic gases emissions and low exhaust temperatures during ACI operation. Under real-world operation, an SI/ACI multimode engine would regularly transition back and forth between stoichiometric and lean operation. During a switch from stoichiometric to lean, the TWC catalyst would start at a high temperature and gradually cool under the lower-temperature lean ACI exhaust. Some of the experiments for Fiscal Year 2019 focused on measuring the so-called catalyst “light-down” using a decreasing temperature ramp under lean exhaust mixtures.

Results

Fiscal Year 2019 Accomplishments

- Measured catalyst light-off for a series of binary, ternary, and quaternary blends of Co-Optima blendstocks and surrogate blendstock for oxygenate blending (BOB) components
- Determined that aromatic constituents inhibit the catalytic reactivity of other fuel components, resulting in similar catalyst light-off temperatures for fuel blends containing similar levels of aromatics
- Measured catalyst light-down and light-off for six pure fuel components, including both Co-Optima blendstocks and petroleum-derived constituents, under lean conditions relevant to ACI operation in a multimode SI/ACI engine: ethanol, iso-propanol, iso-butanol, di-iso-butylene, toluene, and iso-octane.

Two different sets of experiments were conducted in Fiscal Year 2019. The first set focused on the light-off behavior of a series of simple fuel blends under stoichiometric conditions. The second set measured the lean light-down behavior of several pure Co-Optima blendstocks. All of the measurements were carried out under synthetic engine-exhaust conditions on an automated flow reactor system. A vapor delivery module was used to vaporize the liquid fuels. The gas compositions, summarized in Table II.18.1, were based on the United States Driving Research and Innovation for Vehicle efficiency and Energy sustainability (U.S. DRIVE) Low-Temperature Oxidation Catalyst Test Protocol [4]. For stoichiometric experiments, λ (ratio of actual air/fuel ratio to stoichiometric air/fuel ratio) was kept constant at 0.999 by adjusting the O_2 concentration to account

for the different C, H, and O contents of the fuels. Each measurement with a specific fuel was repeated at least three times to make sure that the light-off or light-down behavior was reproducible. The catalyst used in these measurements was a dual-zone TWC from a Model Year 2009 Chevrolet Malibu partial zero-emission vehicle. The catalyst was hydrothermally aged as per industry guidelines delineated in the U.S. DRIVE Low-Temperature Oxidation Catalyst Test Protocol for 50 h under neutral/rich/lean cycles at 800°C [4].

Table II.18.1 Synthetic Exhaust Compositions

Component	Stoichiometric (S-GDI)	Lean (LTC-G)
O_2	varied to achieve $\lambda = 0.999$	12%
CO_2	13%	6%
H_2O	13%	6%
CO	0.5%	0.2%
H_2	0.17%	0.07%
NO	0.1%	0.01%
HC (C_1 basis)	0.3%	0.3%

S-GDI – stoichiometric gasoline direct injection; LTC-G – low-temperature combustion – gasoline; HC – hydrocarbon

Figure II.18.1 summarizes stoichiometric light-off temperatures for blends containing up to 30% of four different Co-Optima candidate blendstocks mixed with a surrogate BOB that consisted of 55% iso-octane, 25% toluene, 15% n-heptane, and 5% 1-hexene. The plot also shows the light-off temperatures for the pure blendstocks (not mixed with the surrogate BOB), which vary significantly for the different blendstocks. However, all the blend light-off temperatures fall within a narrow window of ~15°C, as indicated by the gray rectangle.

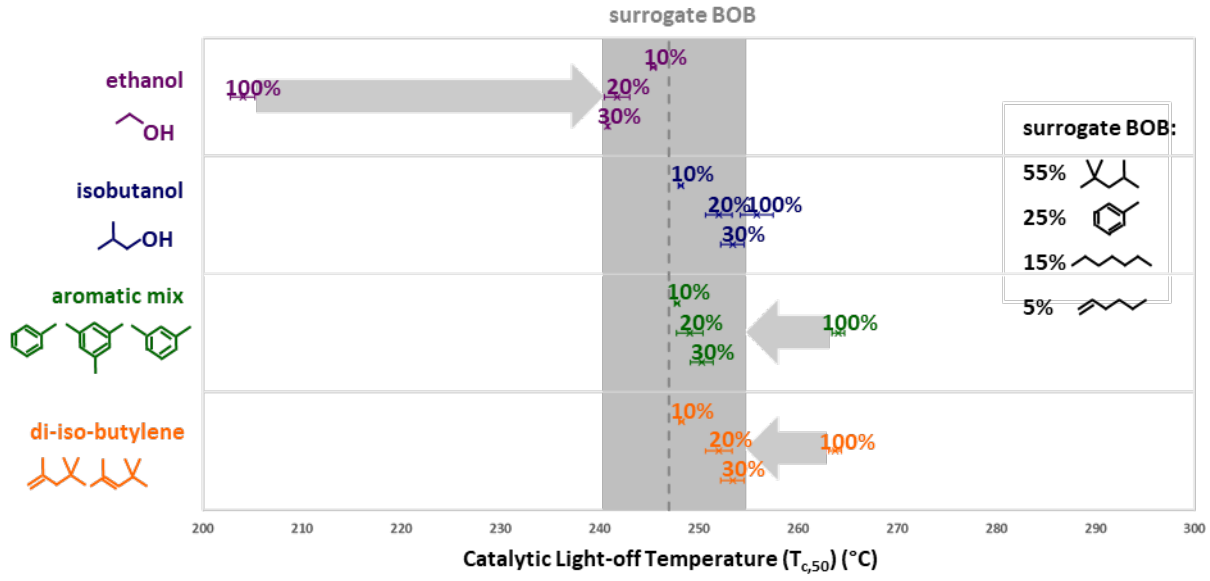

Figure II.18.1 $Tc_{,50}$ measured with stoichiometric synthetic exhaust mixtures over a TWC for a surrogate BOB (dashed vertical line); 10%, 20%, and 30% ethanol blended into the BOB; unblended (100%) ethanol; 10%, 20%, and 30% iso-butanol blended into the BOB; unblended (100%) iso-butanol; 10%, 20%, and 30% of an aromatic mixture blended into the BOB; unblended (100%) aromatic mixture; 10%, 20%, and 30% di-iso-butylene blended into the BOB; and unblended (100%) di-iso-butylene.

To understand why blendstocks with very different catalytic reactivities would have very similar light-off characteristics when blended into a surrogate BOB, an extensive series of experiments was conducted with binary and ternary mixtures of fuel components. Figure II.18.2 shows the results of a few of those experiments.

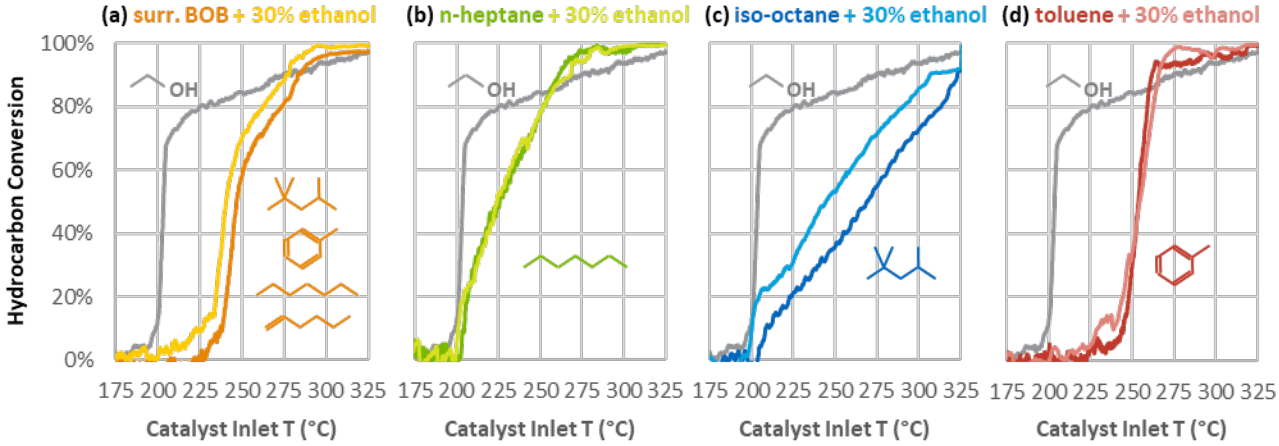

Figure II.18.2 Hydrocarbon conversion vs. TWC inlet temperature under stoichiometric synthetic exhaust conditions for pure fuel components (dark lines) and 30% ethanol blends (light lines) with (a) a surrogate BOB containing 55% iso-octane, 25% toluene, 15% n-heptane, and 5% 1-hexene; (b) n-heptane; (c) iso-octane; and (d) toluene. The conversion of pure ethanol is denoted by the gray line in each chart, and the chemical structures of the fuel components in each experiment are shown within their respective charts.

Figure II.18.2(a) shows the stoichiometric light-off curves for pure ethanol, the surrogate BOB, and a blend of 30% ethanol with the surrogate BOB. Ethanol is one of the most catalytically reactive blendstocks evaluated; it begins to react over the TWC at around 200°C. Adding ethanol to the BOB does shift the light-off curve to slightly lower temperatures, but the low-temperature reactivity of ethanol is gone in the presence of the BOB. The remaining panels in Figure II.18.2 show the light-off curves of three of the BOB components (n-heptane, iso-octane, and toluene) by themselves and blended with 30% ethanol. Both n-heptane (Figure II.18.2(b)) and iso-octane (Figure II.18.2(c)) still exhibit low-temperature reactivity, indicating that the ethanol is still reacting over the TWC in the presence of these hydrocarbons. However, when blended with toluene, the low-temperature reactivity of ethanol completely disappears. Thus, the toluene inhibits the reactivity of ethanol. This is likely due to the delocalized electrons in the aromatic ring of toluene; they allow toluene to adsorb strongly to the catalyst surface, blocking the active sites and preventing other species from adsorbing, but the delocalized electrons also stabilize the resulting adsorbed species and prevent further oxidation until higher temperatures.

Additional experiments were conducted to further quantify the catalytic inhibition effects of toluene. Figure II.18.3 shows light-off curves collected under stoichiometric synthetic exhaust conditions for a series of binary blends containing 0%, 5%, 10%, 25%, 50%, and 100% toluene mixed with n-heptane. Pure n-heptane begins reacting at roughly 200°C. Adding increasing levels of toluene to n-heptane progressively shifts the initial light-off to higher temperatures, indicating that the toluene is inhibiting the reactivity of the n-heptane. With each increase in toluene, the concentration of toluene is roughly doubled, but the low-temperature light-off only shifts by about 5°C. These results lead to two conclusions: (1) even catalytically reactive blendstocks will have a minimal effect on emissions control system performance during cold-start if they are blended into typical petroleum-based fuels containing aromatic components; (2) taking advantage of catalytically reactive blendstocks to improve cold-start emissions performance would require removing significant amounts of the aromatic content from market fuels.

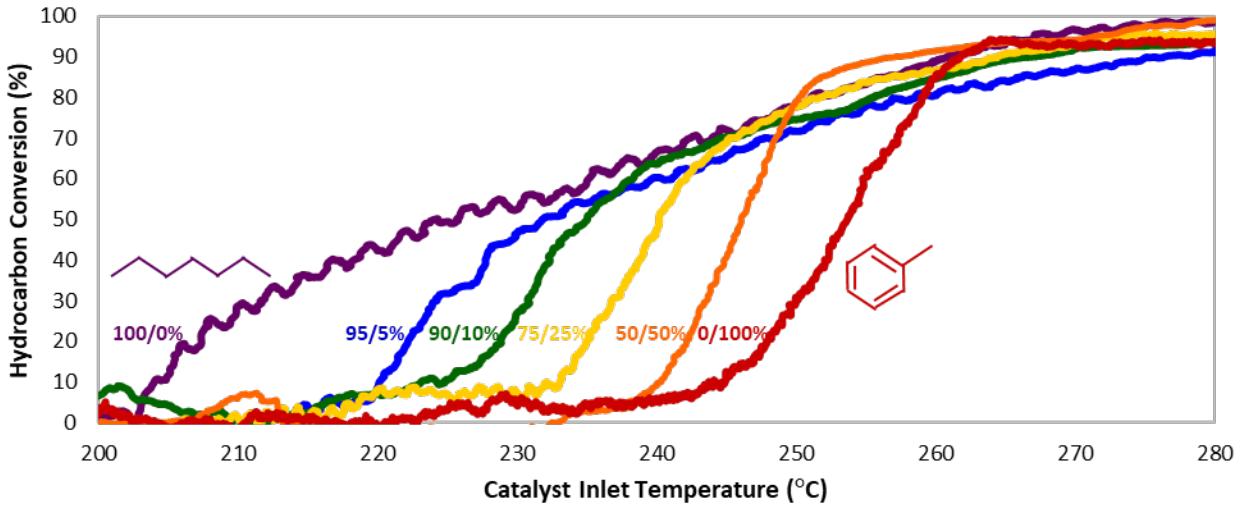

Figure II.18.3 Hydrocarbon conversion as a function of TWC temperature under stoichiometric exhaust conditions for a series of binary fuel blends containing n-heptane and toluene at: 100%/0%, 95%/5%, 90%/10%, 75%/25%, 50%/50%, and 0%/100% by volume

In addition to investigations into TWC light-off with fuel blends under stoichiometric conditions, a new effort on lean light-down was started in Fiscal Year 2019. Preliminary results from these experiments are summarized in Figure II.18.4, which shows previously measured light-off temperatures under stoichiometric conditions in Figure II.18.4(a) and the new measurements of lean light-down in Figure II.18.4(b). Interestingly, there are marked differences in catalytic reactivity between stoichiometric and lean conditions. Among the alcohols, ethanol and isopropanol both shift to higher temperatures under lean conditions, while isobutanol shifts to lower temperatures to become the most reactive alcohol under lean conditions. Di-iso-butylene is more reactive under lean conditions, while the lean light-down temperature for iso-octane is nearly 150°C higher than its stoichiometric light-off. Additional experiments to further characterize lean light-down trends with fuel chemical structure are underway.

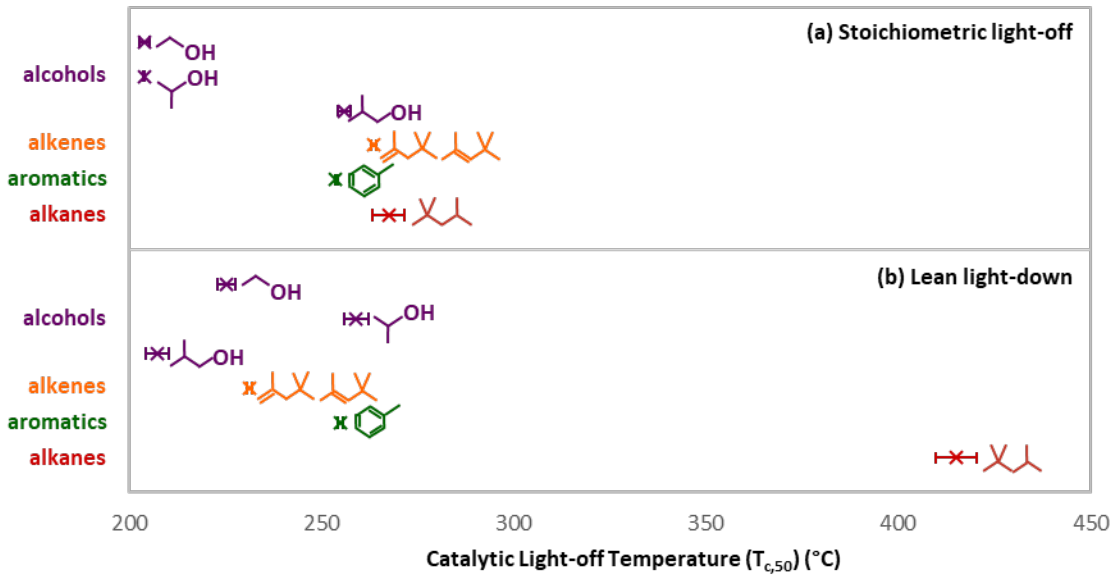

Figure II.18.4 (a) Stoichiometric light-off temperatures and (b) lean light-down temperatures measured over a TWC with ethanol, iso-propanol, iso-butanol, di-iso-butylene, toluene, and iso-octane

Conclusions

- Blends of 10%–30% (by volume) of various Co-Optima blendstocks mixed with a surrogate BOB show very similar TWC light-off behavior because the aromatic component of the BOB inhibits the low-temperature reactivity of the more reactive blendstocks.
- Taking advantage of more catalytically reactive blendstocks to improve cold-start performance will require removing a significant fraction of the aromatic content from market fuels.
- Pure blendstocks show very different behavior under lean light-down conditions as opposed to stoichiometric light-off; some react at lower temperatures under lean light-down, while others react at higher temperatures. Further experiments to characterize the trends with chemical structure are underway.

Key Publications

1. Majumdar, S.S., J.A. Pihl, and T.J. Toops. 2019. "Reactivity of Novel High-Performance Fuels on Commercial Three-Way Catalysts for Control of Emissions from Spark-Ignition Engines." *Applied Energy* 255: 113640.

References

1. Anderson, J., E. Rask, H. Lohse-Busch, and S. Miers. 2014. "A Comparison of Cold-Start Behavior and its Impact on Fuel Economy for Advanced Technology Vehicles." *SAE Int. J. Fuels Lubr.* 7 (2). doi:10.4271/2014-01-1375.
2. Kessels, J.T.B.A., D.L. Foster, and W.A.J. Bleuanus. 2010. "Fuel Penalty Comparison for (Electrically) Heated Catalyst Technology." *Oil & Gas Science and Technology – Rev. IFP*, Vol. 65, No. 1: 47–54.
3. Pihl, Josh, John Thomas, Sreshtha Sinha Majumdar, Shean Huff, Brian West, and Todd Toops. 2018. "Development of a Cold Start Fuel Penalty Metric for Evaluating the Impact of Fuel Composition Changes on SI Engine Emissions Control." SAE Technical Paper Series.
4. U.S. DRIVE ACEC Tech Team Low Temperature Aftertreatment Working Group. 2016. "Aftertreatment Protocols for Catalyst Characterization and Performance Evaluation: Low Temperature Oxidation Catalyst Test Protocol." https://cleers.org/acec-lowt/.

Acknowledgements

Sreshtha Sinha Majumdar and Todd J. Toops provided valuable contributions to this project and report.

II.19 Impact of Fuel Chemistry on PM Emissions across ACI Modes with the Multimode Operating Space (Oak Ridge National Laboratory)

Melanie Moses-DeBusk, Principal Investigator
Oak Ridge National Laboratory
2360 Cherahala Boulevard
Knoxville, TN 37932
E-mail: mosesmj@ornl.gov

Kevin Stork, DOE Technology Development Manager
U.S. Department of Energy
E-mail: Kevin.Stork@ee.doe.gov

Start Date: October 1, 2018 End Date: September 30, 2019
Project Funding (FY19): $225,000 DOE share: $225,000 Non-DOE share: $0

Project Introduction

To enable new and emerging Co-Optima fuels to displace petroleum, it is critical to evaluate their impact on emissions and compatibility with vehicle technologies. This effort investigates the effects of fuel properties on emissions and the functionality of the emissions control systems to identify potential challenges as well as opportunities created by new fuel compositions. The Co-Optima multimode strategy for light-duty vehicles targets the use of spark ignited/advanced compression ignition (ACI) multimode engines. While changes to fuel properties are being considered across the Co-Optima program to maximize engine efficiency during both spark ignited and ACI operating modes, the impact of changes to the fuel properties on emissions is not well understood, especially in ACI mode. The goal of this project is to expand the understanding of different fuel properties' influence on ACI particulate matter (PM) and gaseous emissions. Since the operating maps for ACI combustion strategies have not been fully established, a second goal of this project is to understand how fuel property changes impact emissions across the potential range of ACI air–fuel stratification modes.

Objectives

Overall Objectives

- Quantify the impact of fuel properties on PM and gaseous emissions from multimode engine operation
- Demonstrate the effect of different ACI operating modes within the multimode operating space on PM and gaseous emissions.

Fiscal Year 2019 Objectives

- Quantify the impact of fuel aromatic content and fuel distillation curve on ACI PM mass emissions
- Demonstrate how changes in the level of air-fuel stratification during ACI combustion influence all forms of hydrocarbon (HC) emissions, including PM and both oxygenated and non-oxygenated gaseous species
- Quantify the changes in HC emission speciation as air-fuel stratification varies from fully premixed to highly stratified within potential ACI modes of the multimode operating space.

Approach

A modified 2007 General Motors direct injection (DI) 1.9 L multi-cylinder light-duty diesel engine was used for studying emissions over a range of ACI operating modes while maintaining constant combustion timing.

For this work, the ACI approaches investigated were gasoline compression ignition modes that are relevant to light-duty, medium-duty, and heavy-duty multimode strategies. Three air–fuel stratification modes, using a combined premixed/DI fueling strategy, went from a mode with 100% premixed fuel (designated 100/0 SOI -), often referred to as homogeneous charge compression ignition, to highly stratified mode (designated 70/30 SOI 3), with an additional mode that fell in-between with only partial air–fuel stratification (70/30 SOI 46). The number appearing after start of injection (SOI) designates the crank angle degree before top dead center at which injection starts. A second highly stratified mode was studied that used only a single DI fueling strategy (0/100 SOI 15). The air–fuel stratification levels were varied by changing the SOI of the DI fraction of the fuel, but the combustion timing, as designated by CA50, the crank angle at which 50% of the fuel is burned, was maintained constant for all four conditions studied along with the speed and load (2,000 rpm, 4–5 bar). Global equivalence ratio and fuel energy were kept constant, and the intake temperature was adjusted for each fuel to achieve the desired CA50 at the homogeneous charge compression ignition condition.

The impact of these four ACI operating modes on the speciation of HC gaseous emissions, including oxygenated HCs, and mass, size, and composition of PM emissions was studied and quantified. The influence of two fuel properties, aromatic content and distillation range, was investigated by studying the emissions at these four modes from three different fuels with research octane number of 90. Two fuels maintain a similar low aromatic content, but different distillation ranges: low aromatic-low distillation (LA-LD) and low aromatic-high distillation (LA-HD). The third fuel was high aromatic-high distillation (HA-HD) fuel. The low and high terms are relative to the distillation temperatures and aromatic content of ethanol-free (E0) certification gasoline.

Results

FY 2019 Accomplishments

- Demonstrated that improvements in combustion efficiency for ACI operating mode/fuel combinations tracked a decrease in brake specific PM and total hydrocarbon (THC) emissions
- Determined that the fuel's aromatic content had a greater impact on HC-based emissions than the fuel's distillation range, for the fuels studied
- Showed that changes in air–fuel stratification mode, at a constant CA50, had little impact on emissions unless all the fuel was direct-injected at high air–fuel stratification.

There were two major objectives of the 2019 engine study. The first objective was to quantify how changes to fuel aromatic content and fuel distillation range impact HC-based emissions during ACI operation when the fuel research octane number is held constant. The second objective was to demonstrate how the carbon-based emissions change when the ACI air–fuel stratification mode changes. The engine study was successfully completed and emissions samples were collected at four different ACI air–fuel stratification modes with three different fuels. Chemical analyses of the gaseous HC emissions and the PM from the different conditions and data analysis are ongoing. Detailed HC and aldehyde (oxygenated HCs) speciation and identification of elemental carbon/organic carbon composition of the particulate matter were completed using a variety of extraction and analytical (i.e., gas chromatography, mass spectrometry) techniques on physical samples collected during engine operation. Early data analysis of different types of emissions is showing a strong influence from fuel chemical composition.

Figure II.19.1 shows how the ACI combustion efficiency changed as a function of increasing levels of air–fuel stratification and fuel property changes. The ACI modes change the fraction of fuel in the first and second injections and vary SOI of the second DI injection to transverse the air–fuel stratification range while maintaining CA50. The 100/0 SOI - mode has 100% premixed fuel (homogeneous charge compression ignition), and the 0/100 SOI 15 mode is 100% direct-injected fuel; these provide the bookends of air–fuel stratification. The other two ACI modes provide air–fuel stratification by premixing 70% of the fuel in an early injection in addition to a late injection containing 30% of the fuel such that a range of air–fuel stratifications

can be achieved; the 70/30 SOI 46 mode would be considered to have partial fuel stratification, while the 70/30 SOI 3 mode delays the injection time to reach a high fuel stratification. The combustion efficiency varies little across the air–fuel stratification range when a combined premix/DI fueling strategy is used. However, changes to the fuel properties do influence the combustion efficiency within these modes. Increasing the distillation range of the fuel without changing the aromatic content (LA-LD vs. LA-HD) results in a small drop in combustion efficiency, while an increase in the aromatic content shows a more significant drop in the combustion efficiency (LA-HD vs. HA-HD), likely due to the fuel's chemical characteristics. The best combustion efficiency, regardless of fuel properties, is obtained when all the fuel is direct injected, but as expected, 100% DI comes with significantly more NO_x emissions.

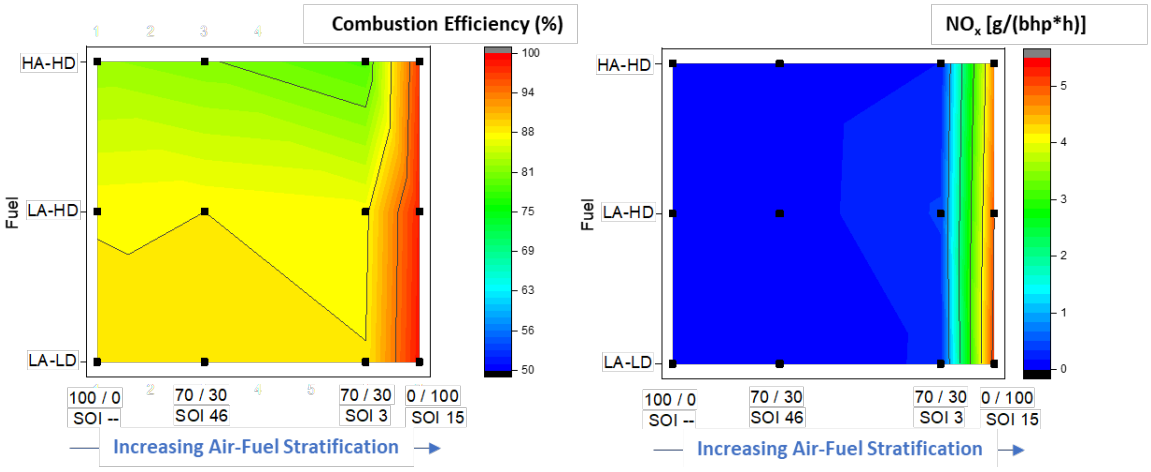

Figure II.19.1 Combustion efficiency and NO_x emissions as the air–fuel stratification is varied for three fuels with research octane number 90 and varied aromatic content and distillation curve, in reference to E0 certification fuel

Both total HC (THC flame ionization detector data) emissions, on a C1 basis, and total carbon PM mass strongly correlate with the combustion efficiency results and are shown in Figure II.19.2. The lower combustion efficiency of the HA-HD fuel, seen in Figure II.19.1, correlates to higher THC emissions, due to unburned or partially burned fuel. In keeping with the combustion efficiency, little to no impact on THC was seen when the fuel distillation property was changed (LA-LD vs. LA-HD) for a given fuel across the air–fuel stratification ranges unless all the fuel is direct injected. Similar to the dramatic increase in combustion efficiency when all the fuel is direct injected, the THC emissions drop dramatically. While the 0/100 SOI 15 ACI mode has dramatically lower THC emissions than the other fuel/mode combinations studied, the fuel aromatic content still impacts the THC emissions, with the HA-HD fuel producing nearly double that of LA-HD. The LA-LD and LA-HD generated about the same THC emissions at this mode. Figure II.19.2 also shows that the PM mass increases significantly for the HA-HD fuel, following the same fuel/mode trends as those discussed for combustion efficiency and THC emissions. As reported in the literature [1], under low-temperature ACI combustion modes with low combustion efficiency, the PM emissions are comprised predominantly of organic carbon, with little to no elemental carbon. Of particular significance was the difference in PM emissions between the LA-HD and HA-HD, and conversely, the similarity between the LA-LD and LA-HD PM emissions. Due to the organic nature of the PM, an assumption could be made that the less volatile fuel would lead to more PM. Instead, these experiments demonstrate that the *aromatic* content of the fuel contributed more to the creation of the organic PM than the volatility of the fuel. Continued efforts to speciate the ACI PM may provide a better understanding of the formation mechanisms during ACI combustion.

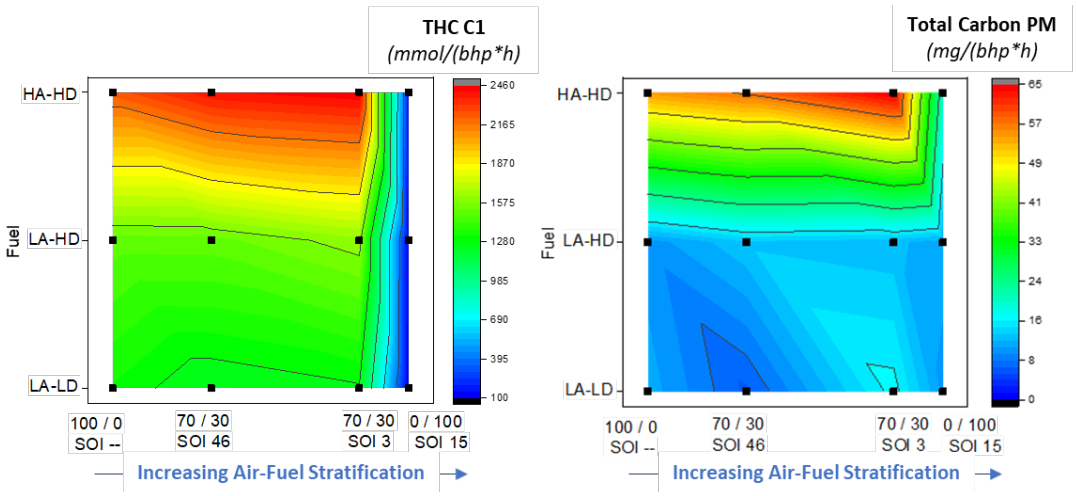

Figure II.19.2 THC (left) and total carbon PM (right) emissions as a function of fuel and air-fuel stratification mode

While ACI operation offers higher thermal efficiency, the low combustion efficiency of most modes results in increased THC and aldehyde emissions. The increased carbon-based gaseous emissions caused by the lower combustion efficiency, which occurs when at least a fraction of the fuel is premixed, result in the PM being predominately organic carbon. The high fuel stratification mode (70/30 SOI 3) had about 5x more PM than the other stratification modes, regardless of fuel properties, but the PM was still >96% organic carbon.

Conclusions

- Fuel properties impact emissions regardless of fueling strategy and air–fuel stratification.
- Fuel aromatic content has a significant impact on carbon-based emissions, while fuel distillation range has little to no impact for the fuels studied.
- Fueling strategy influences emissions more than air–fuel stratification alone. Emissions changed little across the combined premix/DI fueling, stratification modes for a single fuel, but a significant change in emissions was seen for high fuel stratification modes between the two fueling strategies: combined premix/DI and 100% DI.
- A combined premix/DI fueling strategy with a high air–fuel stratification mode significantly increases carbon-based emissions, both PM and gaseous.

Key Publications

1. Moses-DeBusk, M., S.J. Curran, S.A. Lewis, Sr., R.M. Connatser, and J.M.E. Storey. 2019. "Impacts of Air-Fuel Stratification in ACI Combustion on Particulate Matter and Gaseous Emissions." *Emiss. Control Sci. Technol.* 5: 225. https://doi.org/10.1007/s40825-019-00122-5.

References

1. Storey, J.M.E, S.J. Curran, S.A. Lewis, A. Dempsey, T.L. Barone, M. Moses-DeBusk, R.M. Hanson, V.Y. Prikhodko, and W.F. Northrop. 2017. "Evolution and Current Understanding of Physicochemical Characterization of Particulate Matter from Reactivity Controlled Compression Ignition Combustion on a Multicylinder Light-Duty Engine." *Int. J. Eng. Res.* 18 (5–6): 505–519. https://doi.org/10.4271/2017-01-1005.

Acknowledgements

John Storey, Sam Lewis, Maggie Connatser, Jim Szybist, Scott Curran, and Flavio Dal Forno Chauhy provided valuable contributions to this research.

II.20 Kinetic Mechanism Development (Lawrence Livermore National Laboratory)

William J. Pitz, Principal Investigator
Lawrence Livermore National Laboratory (LLNL)
P. O. Box 808, L-372
Livermore, CA 94550
E-mail: pitz1@llnl.gov

Kevin Stork, DOE Technology Development Manager
U.S. Department of Energy
E-mail: Kevin.Stork@ee.doe.gov

Start Date: October 1, 2018 End Date: September 30, 2021
Project Funding (FY19): $708,000 DOE share: $708,000 Non-DOE share: $0

Project Introduction

Predictive chemical kinetic models are needed to represent high-performance fuels and their mixtures with conventional fuels (e.g., gasoline and diesel fuels) for Co-Optima. These kinetic models can be used in computational fluid dynamics simulations of advanced combustion engines to predict the behavior of these fuel blends. Enabled by kinetic models, computational fluid dynamics simulations can be used to co-optimize fuel formulations and engines so that goals for engine efficiency, fossil-fuel displacement, and minimizing harmful emissions can be achieved.

Objectives

Overall Objectives

- Develop and improve chemical kinetic models for high-performance fuels and base fuels (e.g., gasoline and diesel) so that the kinetic models accurately predict fuel behavior at engine conditions
- Use chemical kinetic models to simulate combustion properties at boosted spark ignition, advanced compression ignition, and mixing-controlled compression ignition engine conditions.

Fiscal Year (FY) 2019 Objectives

- Develop and improve chemical kinetic models for 5–7 high-performance fuels and base fuels (e.g., gasoline and diesel) for multimode, advanced compression ignition, and mixing-controlled compression ignition engine conditions so that the kinetic models accurately predict fuel behavior at engine conditions
- Predict sooting propensity behavior of mixing-controlled compression ignition blendstocks when blended into a diesel base fuel.

Approach

To develop chemical kinetic models for blends of high-performance fuels and conventional transportation fuels, chemical kinetic models for each fuel of interest are developed and improved, as needed. These fuel component models are developed by identifying the reaction paths and assembling the associated rate constants, thermodynamic data, and transport data. Next, the kinetic models for high-performance fuels are combined with kinetic models for conventional fuels to represent blends of high-performance fuels and conventional transportation fuels. The models are validated by comparison of computed results to fundamental experimental data from rapid compression machines (RCMs), shock tubes, jet-stirred reactors, flow reactors, and premixed laminar flames. Then, the kinetic models are reduced and used in multidimensional engine

simulation codes to assess fuel property effects in engines. These simulation results can guide and inform efforts to co-optimize fuels and engines for best performance and engine efficiency and to reduce harmful emissions.

Results

Key Accomplishments for FY 2019

- Developed and improved kinetic models for prenol, di-isobutylene, and iso-butanol for downsized, high-compression-ratio, spark ignition engines [1]
- Developed and validated a new kinetic model for polycyclic aromatic hydrocarbons (PAHs) to enable more accurate soot predictions in engines.

The LLNL kinetic team developed and improved detailed chemical kinetic models for high-performance fuels on the Co-Optima top 10 fuel list [1]. The top 10 fuel list contains fuels that have high research octane number (RON) and high octane sensitivity, which are advantageous for maximizing the performance of highly efficient, boosted, high-compression-ratio spark ignition engines. One of these fuels is prenol, an important fuel because Co-Optima researchers have previously identified it as a hyperboosting blendstock [2], meaning that the RON of prenol/gasoline blends is higher than that of either the neat prenol or gasoline. In FY 2019, LLNL researchers continued their development of a kinetic model for prenol and iso-prenol by obtaining improved estimates of thermodynamic properties of prenol-related species and of prenol-associated reaction rate constants. They validated the model by comparing simulated results with new experimental data from a shock tube, an RCM, and a flow reactor. Experimental data were obtained from Co-Optima researchers; the National University of Ireland, Galway; and existing literature. Figure II.20.1 shows the close agreement between model predictions and experimental measurements in the National University of Ireland, Galway shock tube and RCM. The LLNL kinetic team examined the chemical pathways of prenol and found that its short alkyl chains and highly olefinic nature suppress traditional low-temperature reactivity-enhancing pathways (oxygen addition to fuel radicals and subsequent isomerization), while its hydroxyl group leads to the increased formation of relatively unreactive hydroperoxyl (HO_2) radicals. These structural features inhibit reactivity during combustion at low temperatures for neat prenol and likely contribute to the observed hyperboosting effect on RON in blends. However, additional studies of prenol in binary and multi-component mixtures of gasoline surrogate compounds are required to further resolve the fundamental chemistry and physics behind prenol's hyperboosting effect on RON.

In FY 2019, the LLNL kinetic modeling team improved kinetic models for iso-butanol and n-butanol, where iso-butanol is one of the top 10 Co-Optima fuels. Updates to H-atom abstraction rates, low-temperature reaction classes, and thermochemistry improved the ability of the model to simulate autoignition at low temperatures and high pressure. The kinetic model reproduces well the ignition delay times of both butanol isomers. Variations in reactivity over a wide range of temperatures and other operating conditions are well predicted. Recent ignition delay time measurements of neat iso-butanol [3] and blends with a research-grade gasoline [4] at elevated pressure (20–40 bar) and intermediate temperatures (780–950 K) were obtained from an RCM and used to demonstrate the accuracy of the current kinetic model at conditions relevant to boosted spark ignition engines. Figure II.20.2 shows the agreement between neat iso-butanol and its blends with a research-grade gasoline compared to ignition delays from an RCM at Argonne National Laboratory. The kinetic model captures the suppression of reactivity in the low-temperature and negative-temperature-coefficient region when iso-butanol isomer is added to a gasoline fuel (Figure II.20.2b).

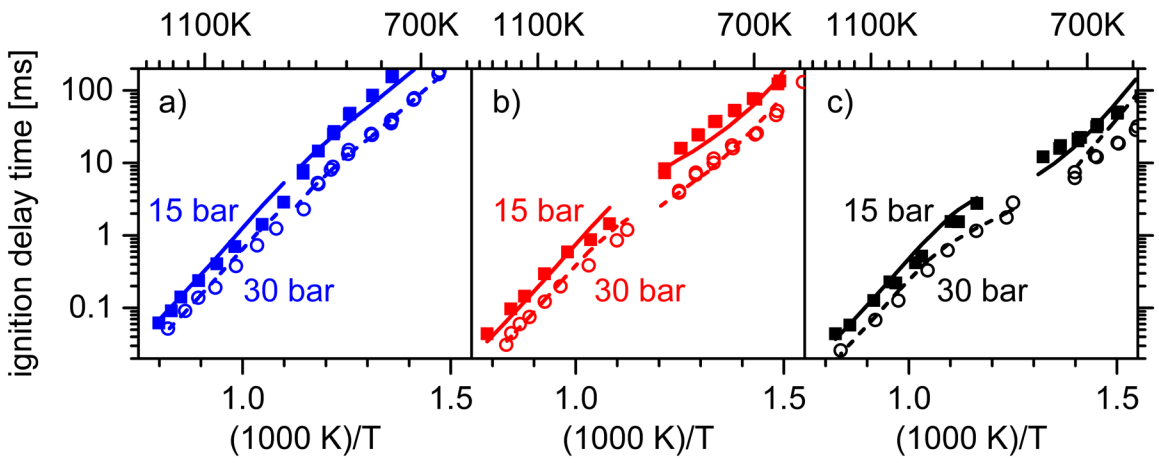

Figure II.20.1 Simulations (lines) using the prenol kinetic model and measurements (symbols) of ignition delay times for mixtures of neat prenol with O_2/N_2 in a shock tube and RCM. The filled symbols and solid lines are at 15 bar, and the open circles and dashed lines are at 30 bar. (a) Fuel-lean mixture. (b) Near-stoichiometric mixture. (c) Fuel-rich mixture. The experimental measurements are from National University of Ireland, Galway.

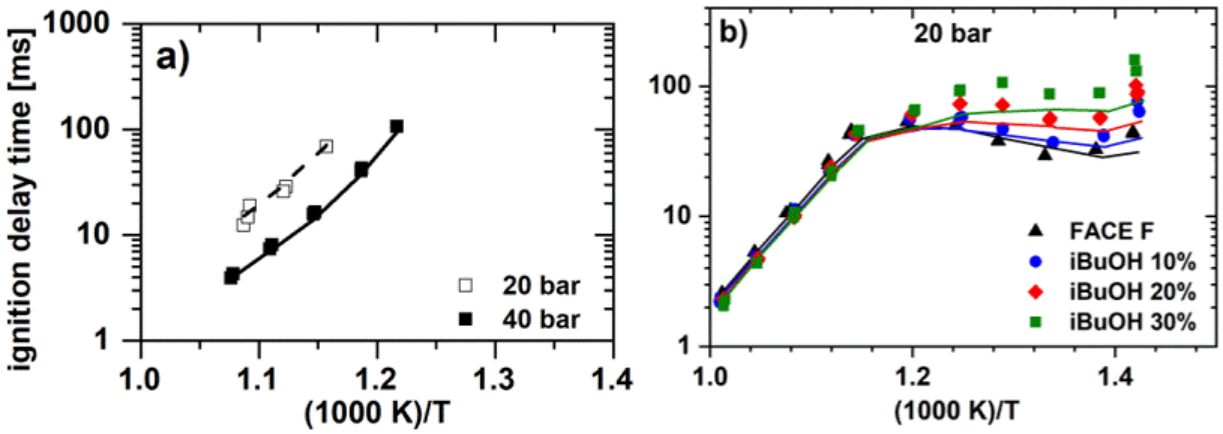

Figure II.20.2 Measured (symbols) and simulated (lines) ignition delay times for iso-butanol and its blends with a research-grade gasoline in the Argonne National Laboratory RCM for stoichiometric mixtures: (a) neat iso-butanol with O_2 in Ar and N_2 [3]; (b) iso-butanol (iBuOH) blended with Fuels for Advanced Combustion Engines F (FACE F) gasoline with O_2 in Ar and N_2 [4]

Another high-performance fuel on the top 10 list whose kinetic model was updated was di-isobutylene. Several significant improvements were made. Firstly, much more accurate estimates were made for thermochemistry of di-isobutylene-related species. Thermochemistry of species can have a profound effect on chemical kinetic modeling predictions. Secondly, rate constants for low-temperature chemistry of di-isobutylene were evaluated, and improved estimates were made. Also, new and important reaction paths were added. Finally, in collaboration with National University of Ireland, Galway, an updated isobutene sub-model was developed that greatly improved the prediction of flame speeds for di-isobutylene. Flame speeds are an important fuel property that controls early flame development in spark ignition engines, and they are used in engine simulations to enable prediction of turbulent flame speeds.

Co-Optima researchers are investigating promising mixing-controlled compression ignition blendstocks that can be produced from biomass and that have favorable properties as diesel blendstocks [5]. In FY 2019, the LLNL kinetic modeling team developed new detailed kinetic models for high-temperature combustion for two

promising blendstocks: 2-nonanol and di-pentyl ether. These blendstocks contain oxygen, whose presence is known to often reduce soot compared to non-oxygen-containing blendstocks. The high-temperature mechanism for these mixing-controlled compression ignition blendstocks has been developed using reaction pathways and associated rates from chemistry of n-alkanes, butanols, and di-butyl ether. Preliminary validation of the di-pentyl ether mechanism has been conducted against pyrolysis data obtained from shock tube experiments. These high-temperature kinetic models can be combined with a kinetic model for PAHs to predict possible reduction in soot formation when the blendstocks are blended with a diesel fuel.

The LLNL kinetic team also developed and validated a new kinetic model for PAHs to help enable accurate soot predictions in engine simulations. Developing a kinetic model that accurately predicts concentrations of PAHs—soot precursors that form during combustion—has been a longstanding challenge for the combustion research community. LLNL kinetic team researchers helped fill this gap by incorporating recently available PAH-formation reaction rates and product channels into a new PAH model, which also captures formation of PAHs from aromatic components when they are present in the fuel. The LLNL kinetic team validated the model for PAH sizes up to seven rings by comparing experimental results to simulated results for the pyrolysis of acetylene, ethylene, propene, cyclopentene, cyclopentadiene, n-dodecane, and a three-component gasoline surrogate mixture (n-heptane/iso-octane/toluene). Overall, the experimental and simulated results agreed closely. Figure II.20.3 shows kinetic model predictions for PAHs compared to measurements in a flow reactor for the pyrolysis of a gasoline surrogate [6]. The researchers also linked this PAH model to a soot sectional model that enables comparison of preliminary soot predictions with measured soot data from fundamental combustion devices. This is a significant step toward an improved sub-model to predict soot for use in multidimensional engine simulations.

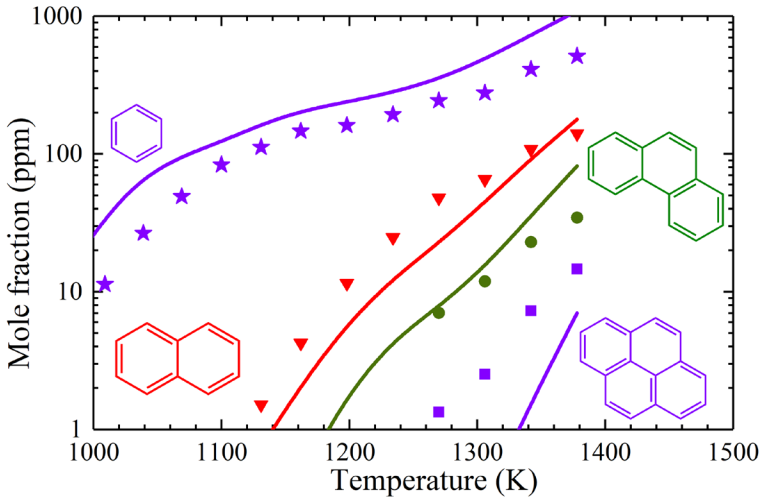

Figure II.20.3 Concentrations of major PAHs during pyrolysis of a three-component gasoline surrogate mixture in a flow reactor, showing close agreement between literature experimental data (symbols) [6] and PAH model predictions (lines)

Conclusions

- Developed and validated an improved kinetic model for prenol, a hyperboosting blendstock. Found its short alkyl chain, olefinic nature, and hydroxyl group suppress low-temperature chemistry.
- Updated and validated the kinetic model for iso-butanol, one of the top 10 Co-Optima fuels. Demonstrated that it could reproduce the ignition behavior in the Argonne National Laboratory RCM when blended into a gasoline fuel.
- Developed an improved chemical kinetic model for PAHs, which is an important step toward a more predictive soot model for use in engine simulations.

Key Publications

1. Ahmed, A., W.J. Pitz, C. Cavallotti, M. Mehl, N. Lokachari, E.J.K. Nilsson, J.-Y. Wang, A.A. Konnov, S.W. Wagnon, B. Chen, Z. Wang, S. Kim, H.J. Curran, S.J. Klippenstein, W.L. Roberts, and S.M. Sarathy. 2019. "Small Ester Combustion Chemistry: Computational Kinetics and Experimental Study of Methyl Acetate and Ethyl Acetate." *Proceedings of the Combustion Institute* 37 (1): 419–428.
2. Zhang, K., N. Lokachari, E. Ninnemann, S. Khanniche, W.H. Green, H.J. Curran, S.S. Vasu, and W.J. Pitz. 2019. "An Experimental, Theoretical, and Modeling Study of the Ignition Behavior of Cyclopentanone." *Proceedings of the Combustion Institute* 37 (1): 657–665.
3. Kim, G., B. Almansour, S. Park, A. Terracciano, S. Vasu, K. Zhang, S. Wagnon, and W. Pitz. 2019. "Laminar Burning Velocities of High-Performance Fuels Relevant to the Co-Optima Initiative." *SAE Int. J. Adv. & Curr. Prac. in Mobility* 1 (3): 1139–1147.
4. Ninnemann, E., G. Kim, A. Laich, B. Almansour, A.C., Terracciano, S. Park, K. Thurmond, S. Neupane, S. Wagnon, W.J. Pitz, and S.S. Vasu. 2019. "Co-Optima Fuels Combustion: A Comprehensive Experimental Investigation of Prenol Isomers." *Fuel* 254: 115630.
5. Fioroni, G., L. Fouts, J. Luecke, D. Vardon, N. Huq, E. Christensen, X. Huo, T. Alleman, R. McCormick, M. Kass, E. Polikarpov, G. Kukkadapu, and R.A. Whitesides. 2019. "Screening of Potential Biomass-Derived Streams as Fuel Blendstocks for Mixing Controlled Compression Ignition Combustion." SAE Technical Paper 2019-01-0570.

References

1. Gaspar, D.J., B.H. West, D. Ruddy, T.J. Wilke, E. Polikarpov, T.L. Alleman, A. George, E. Monroe, R.W. Davis, D. Vardon, A.D. Sutton, C.M. Moore, P.T. Benavides, J. Dunn, M.J. Biddy, S.B. Jones, M.D. Kass, J.A. Pihl, J.A. Pihl, M.M. Debusk, M. Sjoberg, J. Szybist, C.S. Sluder, G. Fioroni, and W.J. Pitz. 2019. "Top Ten Blendstocks Derived from Biomass for Turbocharged Spark Ignition Engines: Bio-Blendstocks with Potential for Highest Engine Efficiency." Pacific Northwest National Laboratory, Richland, WA (United States), PNNL-28713 United States 10.2172/1567705 PNNL English, https://www.osti.gov/servlets/purl/1567705.
2. Monroe, E., J. Gladden, K.O. Albrecht, J.T. Bays, R. McCormick, R.W. Davis, and A. George. 2019. "Discovery of Novel Octane Hyperboosting Phenomenon in Prenol Biofuel/Gasoline Blends." *Fuel* 239: 1143–1148.
3. Cheng, S., D. Kang, S.S. Goldsborough, C. Saggese, S.W. Wagnon, and W.J. Pitz. "Experimental and Modeling Study of C2-C4 Alcohol Autoignition at Intermediate Temperature Conditions." Submitted to *Proc. Combust. Inst.* (2020).

4. Goldsborough, S.S., S. Cheng, D. Kang, C. Saggese, S.W. Wagnon, and W.J. Pitz. "The Effect of Iso-Alcohol Blending with Gasoline on Autoignition Behavior in a Rapid Compression Machine: Iso-Propanol and Iso-Butanol." Submitted to *Proc. Combust. Inst.* (2020).

5. Fioroni, G., L. Fouts, J. Luecke, D. Vardon, N. Huq, E. Christensen, X. Huo, T. Alleman, R. McCormick, M. Kass, E. Polikarpov, G. Kukkadapu, and R.A. Whitesides. 2019. "Screening of Potential Biomass-Derived Streams as Fuel Blendstocks for Mixing Controlled Compression Ignition Combustion." SAE International, https://doi.org/10.4271/2019-01-0570.

6. Shao, C., H. Wang, N. Atef, Z. Wang, B. Chen, M. Almalki, Y. Zhang, C. Cao, J. Yang, and S.M. Sarathy. 2019. "Polycyclic Aromatic Hydrocarbons in Pyrolysis of Gasoline Surrogates (n-Heptane/iso-Octane/Toluene)." *Proc. Combust. Inst.* 37 (1): 993–1001.

Acknowledgements

This work was performed under the auspices of the U.S. Department of Energy by Lawrence Livermore National Laboratory under Contract DE-AC52-07NA27344.

II.21 Virtual Properties, Reduced Mechanism, Blending of Kinetics Properties, and Modeling of Fuel Properties (Lawrence Livermore National Laboratory)

Matthew J. McNenly, Principal Investigator
Lawrence Livermore National Laboratory
7000 East Avenue
Livermore, CA 94550
E-mail: mcnenly1@llnl.gov

Kevin Stork, DOE Technology Development Manager
U.S. Department of Energy
E-mail: Kevin.Stork@ee.doe.gov

Start Date: October 1, 2018 End Date: September 30, 2019
Project Funding (FY19): $250,000 DOE share: $250,000 Non-DOE share: $0

Project Introduction

The Central Fuel Hypothesis (CFH) is one of the major hypotheses around which the Co-Optima program is organized. It states that if one identifies target values for the critical fuel properties that maximize efficiency and emissions performance for a given engine architecture, then fuels that have properties with those values (regardless of chemical composition) will provide comparable performance. During the performance period, the main purpose of this project is to experimentally validate the Fiscal Year (FY) 2018 simulation results on high-performance fuels mixed into blendstocks for oxygenate blending (BOBs). FY 2018 simulations suggested that the CFH cannot predict blending performance from the base BOB octane rating alone and that a molecular composition property may be needed.

Validating the simulation results creates an opportunity to optimize the BOB using the missing composition property for a given blendstock. Uncovering this fundamental knowledge could allow the BOB to be designed to maximize the research octane number (RON) and octane sensitivity (RON minus motor octane number [MON]) for a given blendstock. Cost information could also be included to optimize for the best octane rating per dollar for a given engine configuration. The understanding will allow for more accurate evaluation of BOB and blendstock combinations using the boosted spark ignition (SI) merit function [1]. This research demonstrates new Co-Optima tools for stakeholders to evaluate a blendstock's potential with respect to their market estimates. Successful experimental validation of the simulation results will open the door for model-based fuel optimization, which could help refiners save money and energy designing a BOB for new blendstocks.

Objectives

Overall Objectives

- Create new simulation tools to search for fuel blends that offer unique performance characteristics and the potential to optimize engine performance
- Accelerate the simulation-based, fuel/engine performance models to allow for millions of blend combinations to be evaluated on modest computer clusters
- Validate model performance and recommend interesting blends for engine testing that explore the CFH and demonstrate the potential for co-optimization of fuels and engines.

Fiscal Year 2019 Objectives

- Assess the validity of the CFH with respect to using the octane rating of a BOB to capture its blending performance with oxygenates and bio-derived hydrocarbons
- Quantify the potential to optimize the BOB and finished fuel performance using a chemical kinetic model for the inputs to the boosted SI merit function, specifically, the RON and the octane sensitivity
- Coordinate with the Co-Optima Fuel Properties Team to test the BOB and blendstock combinations found in the virtual fuel search to have the largest variation in the boosted SI merit score
- Validate the model octane predictions using new test data collected using the ASTM standard measurements for RON (D2699) and MON (D2700).

Approach

The project takes advantage of the latest gasoline surrogate mechanism developed for the Co-Optima program at Lawrence Livermore National Laboratory [2]. This fuel model contains over 2,800 reacting species to resolve ignition phenomena—including 23 hydrocarbon blendstocks commonly found in gasoline. It also contains 20 oxygenates and bio-derived blendstocks, including all those tested in the BOB blending study by McCormick et al. [3] as promising candidates for use in advanced SI engines. The blending performance of the BOBs considered here is evaluated by the change in the boosted SI merit function score [1] due to the change in RON and octane sensitivity. The kinetic-based model RON and model MON are computed using a neural network architecture that takes ignition delay calculations, heat of vaporization, and other readily available fuel properties as inputs [4]. To accelerate the octane prediction model, the ignition delay times are computed using the high-performance combustion solver, Zero-RK, developed at Lawrence Livermore National Laboratory [5].

The CFH for oxygenate blending is tested with virtual BOBs created to have the same octane rating (90.3 RON and 84.7 MON) as the four-component BOB surrogate tested previously for the Co-Optima program [3]. The BOBs are considered "virtual fuels" because the octane blending behavior is simulated using the neural network model. It is not possible to test every possible molecular composition of a BOB to verify that the blending performance is independent. Instead, a small, but diverse, set of BOB compositions is considered, which have widely varying concentrations of the different hydrocarbon functional groups. To achieve this diversity, five virtual BOBs are created such that the volume fraction is maximized for each of the PIONA molecular classes while still matching the octane rating of the four-component Co-Optima BOB. Here PIONA stands for paraffins (P), iso-paraffins (I), olefins (O), naphthenes (N), and aromatics (A).

These five virtual blends are then actually created by Co-Optima partners on the Fuel Properties Team at National Renewable Energy Laboratory and tested using the ASTM 2699 and ASTM 2700 standards for RON and MON by an independent fuel testing lab. The real-world blend compositions are then adjusted and retested, if needed, until the RON and MON are within 0.7 of a common target octane rating. Six high-performance blendstocks (ethanol, iso-butanol, methylacetate, 3-pentanone, 2-methylfuran, and diisobutylene) that exhibit the largest simulated change in the merit score are blended at the 10%, 20%, and 30% (by volume) levels into the five real-world BOBs that have each PIONA class maximized. RON and MON are measured experimentally for the 90 new high-performance fuel blends, and the merit score spread across the BOBs is compared against the reproducibility accuracy to see if there is a significant variation.

Results

There are five key outcomes from FY 2019:

- Five BOBs were created to maximize each of the PIONA molecular classes and were tested to be within 0.7 octane number of a common rating, RON = 90.5 and MON = 85.3.

- Ninety mixtures have been created using six high-performance blendstocks (ethanol, iso-butanol, methylacetate, 3-pentanone, 2-methylfuran, and diisobutylene) blended into the five BOBs at the 10%, 20%, and 30% (by volume) levels; the mixtures were then sent for octane tests.
- Seventy-two mixture tests (80%) have been completed and analyzed for their blending performance (all blends with the max iso-paraffin, max olefin, max naphthene, and max aromatic BOBs).
- The neural network octane predictions for these 72 previously untested mixtures have a mean absolute error in RON of 1.3 and in MON of 1.4.
- The available experimental results suggest that variation in merit score across BOBs is smaller than predicted via simulation and that the Central Fuel Hypothesis may ultimately hold to within a prescribed tolerance for all high-performance fuels tested except 3-pentanone.

Five virtual BOBs were created in FY 2018 [6] to match the model-based octane rating of the Co-Optima BOB while maximizing the volume fraction of each of the PIONA classes of molecules. In this performance period, one-liter samples of each BOB were prepared by Co-Optima partners on the Fuel Properties Team at National Renewable Energy Laboratory and tested for RON and MON by the standard ASTM measurement using a Cooperative Fuel Research engine. The first round of BOB development (Phase 1a) had two samples of each BOB, one with the original target octane rating (RON = 90.3 and MON = 84.7) and one with a model-predicted RON two points lower. From this round, the max olefin, max naphthene, and max aromatic BOB compositions were found to form a sufficiently tight cluster around the target octane rating. The max paraffin and max iso-paraffin BOBs in Phase 1a were found to have too-low and too-high RON, respectively. The composition of these two BOBs was further adjusted by their paraffin levels in a second round of testing (Phase 1b), with a satisfactory match found for the max iso-paraffin BOB with an increased amount of n-pentane. A third round of testing (Phase 1c) was needed to improve the octane sensitivity of the max paraffin BOB, yielding the final, real-world compositions given in Figure II.21.1.

If the CFH is generally applicable for oxygenate blending, then the five BOBs should have similar octane ratings when an oxygenate, or any blendstock, is added to them. The change in merit score is used to quantify how similar the octane ratings are across the BOBs. Based on the merit function formula [1], the change in merit score due to the octane rating is computed as $\Delta Merit = 0.625\ \Delta RON + 0.781\ \Delta S$, where S is the octane sensitivity. The change in the merit score is scaled so that a value of one represents the potential for a 1% efficiency gain in an engine optimized for the fuel. The reproducibility error of the ASTM standard RON and MON tests produces an uncertainty in ΔMerit of 1.2 (95% confidence). Differences in the merit score across the BOBs are considered negligible below this level. To provide a sense of scale, differences in the merit score on the order of 5.7 are considered substantial, corresponding to the change that occurs switching from 87 AKI (anti-knocking index) gasoline to 93 AKI (98 RON) gasoline [7].

In FY 2018, the RON and MON were computed using the neural network model for the Co-Optima BOB and the five virtual BOBs. Specifically, the octane ratings of 17 high-performance blendstocks studied in McCormick et al. [3] were calculated for blending levels between zero and 30% (by volume). From these results, the change in the merit score [1] from the zero blending level was computed to assess the validity of the CFH. The maximum difference between the largest and smallest merit score was then found for each blendstock across the six BOBs. For 11 out of the 17 blendstocks, the maximum merit score change between BOBs was greater than 3.0. A value greater than 3.0 represents more than 50% of the engine efficiency gain possible when switching from 87 AKI to 93 AKI gasoline. If validated experimentally, this would be strong evidence that the CFH does not apply to the octane rating of a BOB when used to predict the blending performance of a finished fuel.

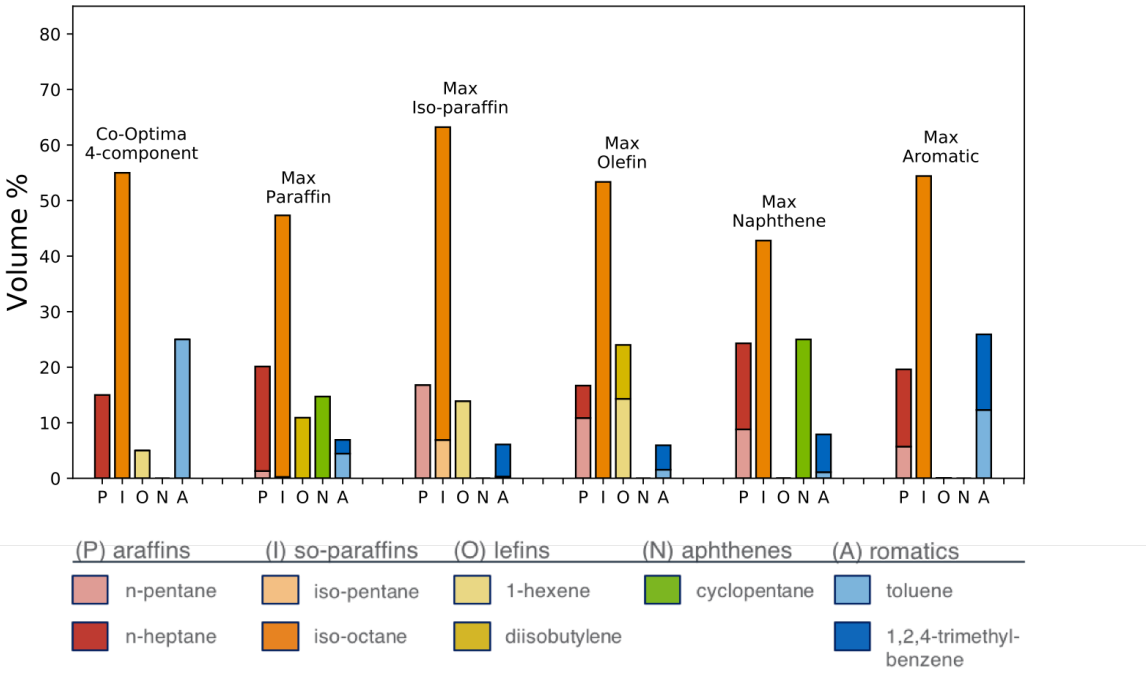

Figure II.21.1 Composition of the four-component Co-Optima BOB and the five BOBs that maximize the volume fraction of each of the PIONA classes. The octane numbers measured by the ASTM standard tests are within 0.7 of a target RON of 90.5 and target MON of 85.3.

Eight blendstocks were found to have a maximum merit score change of 3.5 or greater. Of these, six were recommended for experimental validation by the Co-Optima Fuel Properties Team at National Renewable Energy Laboratory. These include ethanol, iso-butanol, methylacetate, 3-pentanone, 2-methylfuran, and diisobutylene. These blendstocks were selected because they represent a broad range of functional groups and carbon numbers.

The neural network octane model had some difficulty predicting the adjustment to the max paraffin BOB to better match the octane rating of the other BOBs (see Figure II.21.2a). To improve the prediction, and the confidence of obtaining a match in the Phase 1c round of testing, a Bayesian approach was used to construct a local blending model with an uncertainty estimate based on the previous tests. With a budget of five test samples planned for Phase 1c, perturbations to the max paraffin composition were computed to maximize the probability that at least one test sample is within 0.7 octane numbers of the cluster center. The results of this round of testing, along with the 95% confidence interval (C.I.) of the five model predictions, are also shown in Figure II.21.2a. The approach yielded three compositions inside the octane rating cluster of the other BOBs, with the ultimate octane rating shown as a solid red circle.

The accuracy of the neural network octane model [4] is shown in Figure II.21.2b for the max iso-paraffin, max olefin, max naphthene, and max aromatic BOBs blended with the six high-performance blendstocks. These 76 blends have never been tested before and represent blind predictions for the octane model. The mean absolute error in RON is 1.3 octane numbers and in MON is 1.4 octane numbers. For comparison, the 95% confidence interval for simultaneous RON and MON target with the ASTM measurement is shown with a solid line in Figure II.21.2b. For the higher RON measurements obtained in this study (100 < RON < 104), the standard deviation increases nearly three-fold, as shown by the dashed line.

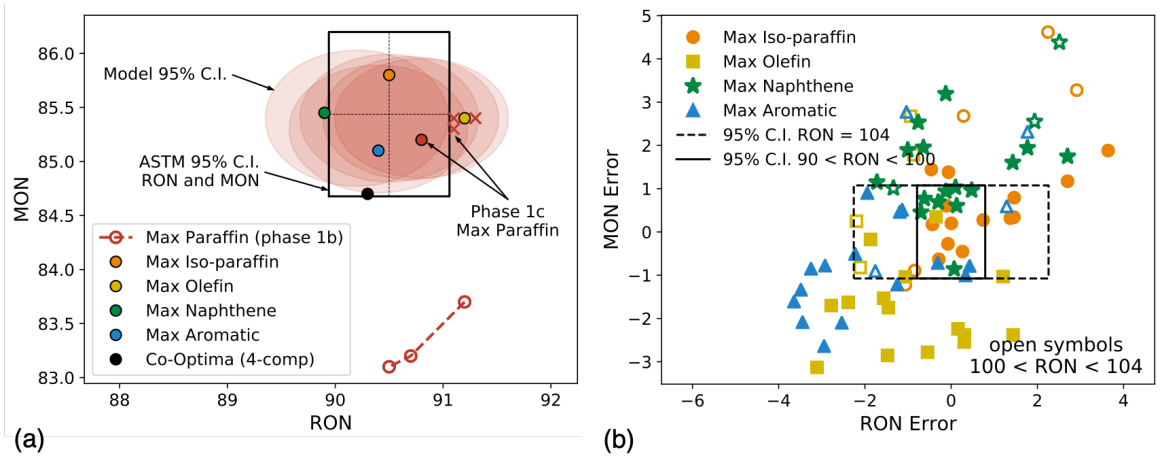

Figure II.21.2 ASTM octane test results: (a) the final octane ratings (solid circles) of the five new BOBs considered in this investigation along with the modeled 95% confidence interval for each of the max paraffin blends tested in Phase 1c; (b) the model error in the octane rating of the new blends tested in this study compared to the ASTM reproducibility error.

For the four BOBs that were tested in this performance period, the merit score spread across the BOBs was much less than originally predicted [6]. Only the blends with 3-pentanone produced merit score spreads greater than two (i.e., $2.3 < \Delta\text{Merit} < 3.2$), which is the test result most consistent with the model predictions. The measured blending performance of the max paraffin BOB has not been analyzed yet. However, it is predicted by the model to have the most antagonistic blending performance of the five new BOBs, which would increase the merit score spread. As a consequence, the final assessment of the CFH for using the BOB octane ratings to predict blending behavior must wait until all the test results are completed.

Conclusions

This project conducted experiments to validate a simulation-based approach to assess the applicability of the Central Fuel Hypothesis when using BOB octane ratings to predict blending performance. Once the validation is complete, the results of this project will improve the accuracy of non-linear octane models, which opens the door for model-based fuel optimization for boosted SI and multi-mode engine performance. There are five key accomplishments from FY 2019:

- Five BOBs were created and tested to be within 0.7 octane numbers of a common rating, RON = 90.5 and MON = 85.3, while maximizing each of the PIONA molecular classes.
- Ninety mixtures were created and sent for octane tests using six high-performance blendstocks (ethanol, iso-butanol, methylacetate, 3-pentanone, 2-methylfuran, and diisobutylene) blended into the five BOBs at the 10%, 20%, and 30% (by volume) levels.
- Seventy-two mixture tests (80%) were completed and analyzed for their blending performance (all blends with the max iso-paraffin, max olefin, max naphthene, and max aromatic BOBs).
- The neural network octane predictions for these 72 previously untested mixtures were found to have a mean absolute error in RON of 1.3 and in MON of 1.4.
- The available experimental results suggest that variation in merit score across BOBs was smaller than predicted via simulation and that the Central Fuel Hypothesis may ultimately hold to within a prescribed tolerance for all high-performance fuels tested except 3-pentanone.

Key Publications

1. McNenly, Matthew, Geoffrey Oxberry, Ahmed Ismail, Nicholas Killingsworth, and Daniel Flowers. 2019. "Ultra-Compact System for Characterization of Physical, Chemical and Ignition Properties of Fuels." U.S. Patent 10,371,689.

References

1. Miles, Paul. 2018. "Efficiency Merit Function for Spark Ignition Engines: Revisions and Improvements Based on FY16–17 Research." Technical Report. U.S. Department of Energy, Washington, DC. DOE/GO-102018-5041.

2. Mehl, Marco, Scott Wagnon, Kuiwen Zhang, Goutham Kukkadapu, William Pitz, Charles Westbrook, Yingjia Zhang, et al. 2017. "A Comprehensive Detailed Kinetic Mechanism for the Simulation of Transportation Fuels." 10th U.S. National Combustion Meeting (April 23–26), paper 1A17, College Park, MD.

3. McCormick, Robert, Gina Fioroni, Lisa Fouts, Earl Christensen, Janet Yanowitz, Evgueni Polikarpov, Karl Albrecht, Daniel Gaspar, John Gladden, and Anthe George. 2017. "Selection Criteria and Screening of Potential Biomass-Derived Streams as Fuel Blendstocks for Advanced Spark-Ignition Engines." *SAE International Journal of Fuels and Lubricants* 10 (2): 442–460. https://doi.org/10.4271/2017-01-0868.

4. Whiteside, Russell. 2018. "Prediction of RON and MON of Gasoline Surrogates by Neural Network Regression of Ignition Delay Times and Fuel Properties." AEC Working Group Meeting (January 29–February 1), Lemont, IL.

5. McNenly, Matthew, Russell Whitesides, and Daniel Flowers. 2015. "Faster Solvers for Large Kinetic Mechanisms Using Adaptive Preconditioners." *Proceeding of the Combustion Institute* 35: 581–587. https:/doi.org/10.1016/j.proci.2014.05.113.

6. McNenly, Matthew. 2018. "Virtual Properties, Reduced Mechanism, Blending of Kinetics Properties, and Modeling of Fuel Properties (LLNL)." Advanced Combustion Engines and Fuels, 2018 Annual Progress Report. DOE Vehicle Technologies Office.

7. Farrell, John, John Holladay, and Robert Wagner. 2017. "Fuel Blendstocks with the Potential to Optimize Boosted Spark-Ignition Engine Performance: Identification of Five Chemical Families for Detailed Evaluation." Technical Report. National Renewable Energy Laboratory.

Acknowledgements

The principal investigator would like to thank the Co-Optima Fuel Properties Team at National Renewable Energy Laboratory. It would have been impossible to validate the simulation results in this study without the extensive help from Lisa Fouts to develop a reliable blending process that could handle volatile components and prepare more than 100 one-liter test samples. Further, this study would not have been successful without the guidance of Gina Fioroni and Robert McCormick.

II.22 Engine Simulations in Support of Co-Optima (Argonne National Laboratory)

Sibendu Som, Principal Investigator
Argonne National Laboratory
9700 S. Cass Avenue
Lemont, IL 60439
E-mail: ssom@anl.gov

Kevin Stork, DOE Technology Development Manager
U.S. Department of Energy
E-mail: Kevin.Stork@ee.doe.gov

Start Date: October 1, 2018 End Date: September 30, 2019
Project Funding (FY19): $650,000 DOE share: $650,000 Non-DOE share: $0

Project Introduction

Towards the goal of multi-mode combustion strategy, it is essential to accurately control the engine operating conditions that may require rapid combustion mode change, e.g., from boosted spark ignition (SI) mode at high loads to advanced compression ignition (ACI) mode at low loads. To better understand the fuel-engine interaction under different operating conditions, this project has developed computational fluid dynamics (CFD) models for four engine platforms that cover the full spectrum of multi-mode combustion, using commercial software CONVERGE.

For high-load boosted SI mode, knock is a major bottleneck to achieving higher thermal efficiency, and the impacts of fuel properties other than research octane number (RON) and motor octane number (MON) require further investigation. In this task, an efficient knock model has been developed and was leveraged to study the fuel effects on knock-limited spark advance (KLSA) and indicated thermal efficiency (ITE) with knock constraint. The numerical results were further used to validate and improve the Co-Optima efficiency merit function for boosted SI engine.

For low-load ACI operation, accurate control of intake charge thermodynamic state is necessary to ensure rapid mode switch from SI to ACI; hence, the reactivity of employed gasoline fuel can be adjusted thermodynamically to enable combustion phasing control. To this end, it is important to gain fundamental insight into the auto-ignition process with regards to fuel–air mixture stratification and thermal wall boundary condition. In this task, a CFD study has been carried out to facilitate revealing the correlation between mixture/thermal stratification and cylinder wall temperature and their impact on combustion phasing control.

Lean mixed-mode combustion or spark-assisted compression ignition combines conventional SI and ACI modes and has the potential to realize mode transition and improve engine efficiency and performance under a range of operating conditions. Understanding the mechanisms of spark-assisted compression ignition multi-mode operation as well as the relationships between fuel properties and combustion characteristics is critical. In this task, a computational framework utilizing a hybrid combustion modeling strategy in CFD was developed for lean mixed-mode engine operation and was demonstrated to be able to capture pressure and heat release rate traces, as well as cyclic variability with confidence. The new computational model was then leveraged to investigate effects of NO_x chemistry and different fuel properties through sensitivity analysis. It was found that fuel properties could strongly affect flame propagation and/or end-gas auto-ignition, and thus the engine efficiency.

Objectives

Overall Objectives

- Develop and validate CFD models for full multi-mode combustion
- Develop a robust and efficient knock model incorporating fuel effects
- Quantify the fuel property effects on multi-mode combustion using sensitivity analysis
- Investigate the impact of fuel–air mixture and thermal stratification under ACI conditions
- Investigate the sensitivity of auto-ignition tendency to fuel composition under ACI conditions.

Fiscal Year 2019 Objectives

- Develop and validate the knock model for KLSA prediction
- Develop numerical models that capture mixed-mode combustion
- Characterize the degree of mixture and thermal stratification under ACI mode of combustion
- Investigate fuel-engine interactions under both beyond-RON and beyond-MON homogeneous charge compression ignition conditions.

Approach

A CFD model was developed for the Oak Ridge National Laboratory engine to investigate the fuel property impacts on engine knock propensity and thermal efficiency under boosted SI condition. The spark-ignited flame propagation was modeled using the level-set G-equation combustion model. A transported Livengood-Wu integral approach considering sub-grid fluctuation in mixture fraction and temperature was used to indicate auto-ignition in the unburnt region. The engine model was validated against experiments performed by Scott Sluder [1] at Oak Ridge National Laboratory and was shown to give good predictions for in-cylinder pressure, heat release rate, indicated mean effective pressure (IMEP), and combustion phasing. A criterion using the peak auto-ignition volume was identified to predict KLSA by comparing against experiments, which provides accurate prediction of KLSA at multiple operating conditions of interest. Sensitivity analysis on fuel properties such as heat of vaporization (HoV) and laminar flame speed (LFS) was performed wherein +/–50% and +/–30% of baseline values were tested in the simulations. The corresponding changes in KLSA and combustion performance were quantified and analyzed.

A computational framework with three-dimensional CFD was developed for lean, mixed-mode combustion of an E30 fuel in a direct injection spark ignition engine operated at Sandia National Laboratories. A fuel surrogate matching RON and MON of E30 was first developed using neural-network-based non-linear regression model developed by Russell Whitesides [2] and Matthew McNenly [3] at Lawrence Livermore National Laboratory. A 164-species skeletal reaction mechanism incorporating NO_x chemistry was derived from a detailed chemical kinetic model in collaboration with Prof. Tianfeng Lu at University of Connecticut. A hybrid combustion modeling approach that incorporates the G-equation model and the well-stirred reactor model with a multi-zone approach was developed to predict mixed-mode combustion. The developed computational framework was validated against measured in-cylinder pressure and heat release rate traces from Magnus Sjöberg at Sandia National Laboratories. The validated computational model was finally leveraged to quantify effects of NO_x chemistry and fuel properties, including HoV and LFS, on performance of mixed-mode combustion engine operation through sensitivity analysis.

For ACI combustion modeling, three-dimensional full engine open cycle simulations have been conducted and validated against experiments on the Argonne single-cylinder gasoline direct injection engine platform. The test engine was modified to run with high compression ratio, CR = 15.3, and the low-load ACI operation was successfully achieved through intake air heating. The engine speed was kept constant at 1,500 rpm, and two

excess-air ratios were considered, λ = 2.6 and 3.6, respectively. Two sets of fuel were tested, namely alkylate and E30. The injection event begins early enough (e.g., start of injection at 300 degrees crank angle before top dead center) to obtain a relatively well-mixed fuel–air mixture charge at the end of compression. Numerical simulations were performed using re-normalization group (RNG) k-ε model with wall functions and the well-stirred reactor model with a multi-zone approach for accelerating chemical kinetics computation.

Another effort for ACI modeling was performed with the virtual Cooperative Fuel Research (CFR) engine model. The CFD model was adapted to simulate homogeneous charge compression ignition combustion using the well-stirred reactor model with a multi-zone approach. In addition, a piston crevice was added to the CFR engine geometry. The CFD model was validated against in-house CFR engine experiments performed by Chris Kolodziej under two representative operating conditions (at 600 rpm) corresponding to beyond-RON (boosted intake pressure of 1.3 bar and intake temperature of 52°C) and beyond-MON (intake pressure of 1.0 bar and intake temperature of 150°C) pressure-temperature trajectories. Three binary fuel blends were simulated: iso-octane/n-heptane, toluene/n-heptane, and ethanol/n-heptane blends, with the same RON of 90. The MON was 10 for the toluene/n-heptane and ethanol/n-heptane blends. The numerical results were validated against experimental data for in-cylinder pressure, ignition timing, and combustion phasing. In addition, the level of in-cylinder thermal stratification was quantified in terms of standard deviation of temperature. Subsequently, a numerical study was performed to investigate the impact of fuel composition, RON, and MON on ACI combustion using the validated CFR engine model. Compression ratio sweeps were conducted for each of the three binary blends mentioned above, and critical compression ratio was determined under both beyond-RON and beyond-MON conditions, based on the criterion of CA50 (the crank angle at 50% mass fraction burned) = 3 crank angle degrees (CAD) after top dead center (aTDC). The critical compression ratios for different blends were compared and the numerical results were analyzed to understand fuel composition and chemistry effects.

Results

- A new approach of KLSA prediction using the transported Livengood-Wu integral was developed, which provides 3~10 times faster simulation turn-around time than a maximum amplitude pressure oscillation based approach.
- Sensitivity analysis quantified the effects of HoV and LFS on KLSA and ITE at multiple operating loads.
- Good agreement was found between the Co-Optima efficiency merit function and the current simulation results for the HoV effects, and a new merit function term quantifying LFS effects under stoichiometric condition was proposed based on this study.

Figure II.22.1 (left) shows a contour plot of the peak auto-ignition (AI) volume normalized by the cylinder displacement (4E-4 m3) in the dimensions of IMEP and spark timing by performing a spark timing sweep at each condition. It is seen that the normalized peak AI volume increases as the spark timing is advanced, although a decrease is also observed with extreme early spark timing at high load condition. The black symbols mark the experimental KLSA, which was defined as the crank angle before a significant increase in the knock meter reading was observed while gradually advancing the spark timing. An iso-line of 1E-4, as shown by the red line, is identified to correlate with the KLSA locations very well, and thus is used as the threshold in normalized peak AI volume to predict KLSA in CFD. This threshold gives a root mean square error of 1.94 CAD in KLSA prediction for the medium to high load conditions, which is comparable to the errors in the predictions of CA10 (crank angle at 10% mass fraction burned) and CA50.

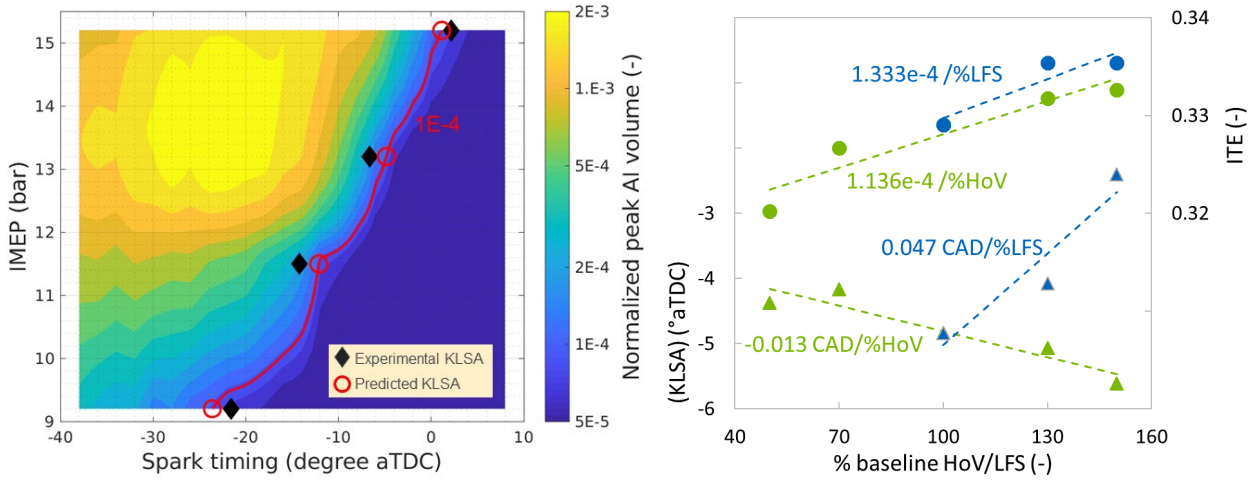

Figure II.22.1 (left) Contour of normalized peak auto-ignition volume predicted by the Livengood-Wu integral model. Black diamonds mark the experimental KLSA locations; red line is the iso-line of 1E-4, and the circles mark the CFD-predicted KLSA. (right) Impacts of HoV (green) and LFS (blue) on KLSA (triangles) and ITE (circles). Symbols are CFD predictions. Lines are linear curve fittings with slopes labeled. Operating condition at 2,000 rpm, 120 ft·lbs.

Figure II.22.1 (right) shows the sensitivity analysis of HoV and LFS effects on KLSA and ITE at 2,000 rpm, 120 ft·lb condition. HoVs were varied by ±30% / ±50%, and LFSs were varied by 30% / 50% independently. It was found that the HoV cooling effect on knock mitigation is only marginal, and the efficiency benefit with higher HoV is mainly attributable to reduced heat loss. Higher LFS increases knock tendency and requires delayed KLSA, but ITE is found to increase with LFS due to the reduced combustion duration. The CFD-generated data showed good agreement with the Co-Optima efficiency merit function in terms of HoV effects. A new merit term for LFS effect under stoichiometric condition is proposed based on the CFD prediction as $M = (LFS \ -46[cm/s])/12.6$.

- Developed a new computational framework utilizing hybrid combustion modeling for lean mixed-mode engine operation.
- Demonstrated the good accuracy of the developed computational model in predicting in-cylinder pressure and heat release rate traces, as well as cyclic variability.
- Quantified the effects of HoV and laminar flame speed using the new model through local sensitivity analysis, showing larger sensitivity of mixed-mode combustion characteristics to laminar flame speed than HoV.

Figure II.22.2 shows the pressure (left panel) and apparent heat release rate (AHRR, center panel) traces obtained from experiment (500 cycles) and simulation (13 cycles). Good agreement is observed between simulation and experimental data, with the predicted mean pressure being slightly higher than the measured mean pressure. A moderate level of cycle-to-cycle variation is also captured by CFD. Two types of combustion cycles are observed in both experiment and simulation. The first type of cycles features low in-cylinder pressure and heat release rate, resulting in a single AHRR peak. This type of combustion cycle is similar to those observed in conventional SI engines. The other type of cycles shows higher in-cylinder pressure and heat release rate and exhibits two AHRR peaks. The first and second peaks correspond to the early flame propagation and the subsequent end-gas auto-ignition processes, respectively. This type of cycles is referred to as mixed-mode cycles, and the right panel of Figure II.22.2 shows the flame structure of a representative mixed-mode cycle where premixed fronts and auto-igniting pockets are present simultaneously.

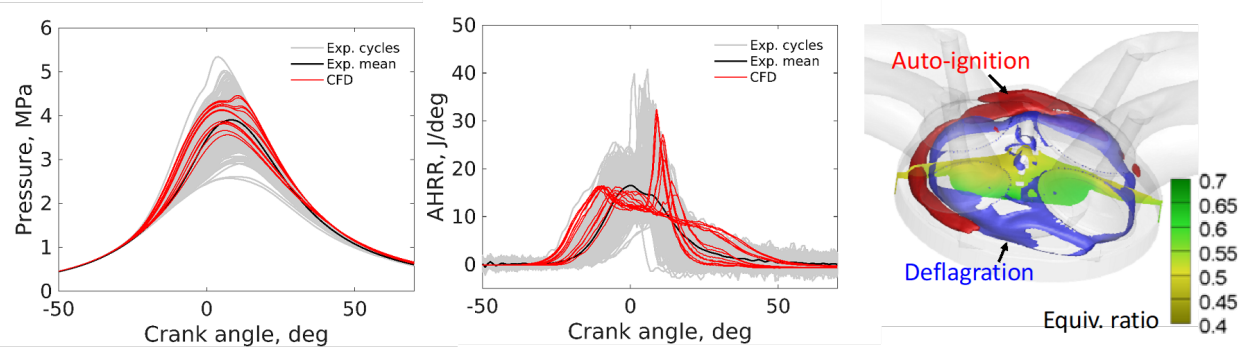

Figure II.22.2 Predicted pressure (left) and apparent heat release rate (AHRR, center) compared with experiment, along with the flame structure of a representative mixed-mode cycle (right) showing deflagrative flame fronts (blue) and auto-ignition fronts (red). The gradient across the center represents equivalence ratio.

Effects of physical and chemical properties of the E30 fuel, including HoV and LFS, on mixed-mode combustion characteristics are examined in Figure II.22.3. A 30% perturbation is applied to the nominal values of HoV and LFS, respectively. As seen, a perturbation on HoV has a negligible effect on initial flame propagation, while a lower HoV enhances the auto-ignition-induced heat release rate since a lower HoV indicates reduced evaporative cooling, which induces a smaller reduction in in-cylinder temperature far before combustion occurs. In contrast, the effect of LFS has a much larger impact on mixed-mode combustion. Large LFS accelerates the turbulent flame propagation speed and thus advances the combustion phase and increases the first peak of heat release rate associated with deflagration. Compared with the case with nominal flame speed, the mean heat release rate at the first peak decreases by 23% for -30% LFS, and increases by 22% for +30% LFS. The enhanced deflagrative heat release rate leads to the increased pressure and temperature and thus further promotes autoignition.

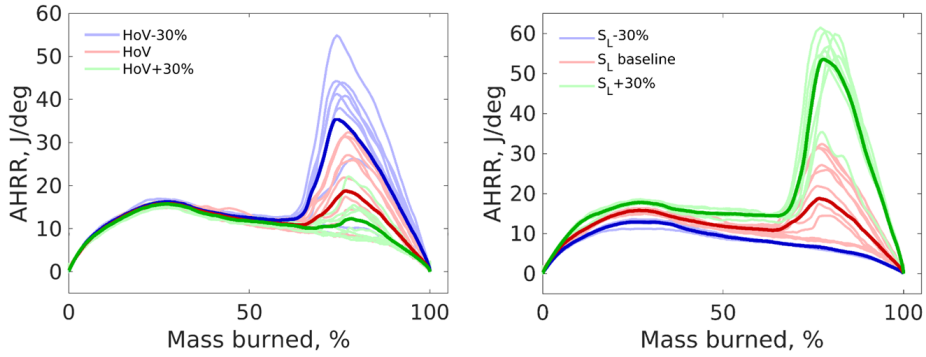

Figure II.22.3 Sensitivity of predicted heat release rate in the mass burned space to heat of evaporation (left) and laminar flame speed (right). Dark thick lines represent the mean values.

- Assessment of the employed CFD model setup is made against Argonne's experimental engine data across a broad range of ACI engine conditions.
- Impact of thermal wall boundary condition is investigated.
- Mixture/thermal stratification impact is addressed in terms of auto-ignition process.

Simulations were performed to obtain multi-cycle repetitions over 10 cycles with properly selected wall temperature boundary conditions and validated against Argonne experiments as shown Figure II.22.4. Due to the intrinsic nature of Reynolds-averaged Navier–Stokes formulation with artificial turbulent viscosity term, the simulations exhibit a very narrow, and almost negligible, band of cyclic variation. Nevertheless, the current

approach of modeling ACI provides good accuracy with properly chosen wall temperature setup. The same wall temperature conditions consistently apply across two different Co-Optima fuels, e.g., alkylate and E30.

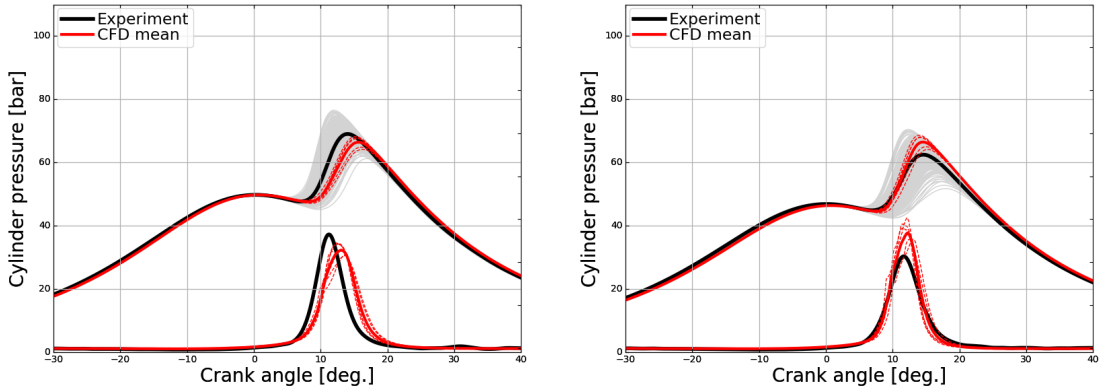

Figure II.22.4 Measured and calculated in-cylinder pressure and heat release rate for alkylate (left) and E30 (right), at λ=2.6 and intake temperature (T_{int}) of 135 °C, using the following wall boundary temperature values: T_{liner} = 425 K, T_{piston} = 475 K, and T_{head} = 455 K.

Figure II.22.5 illustrates the degree of mixture and thermal stratification prior to auto-ignition. Despite the early injection timing, the mixture state barely shows complete homogeneity in space. Such a heterogeneous mixture may be due to incomplete fuel–air mixing and non-homogenous fuel evaporation due to relatively cold walls and spray wall interaction. It is interesting to find out that the major temperature gradient is found near the chamber walls. While mixture stratification appears to be larger than thermal stratification, it was found that the latter plays a more significant role in determining the actual combustion phasing.

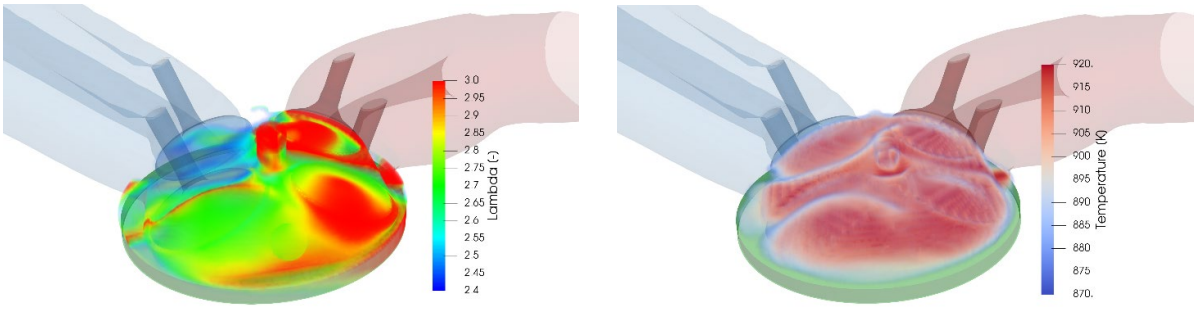

Figure II.22.5 Excess ratio (λ, left) and temperature (right) distribution in combustion chamber shortly before the ignition begins; the quantities are evaluated under λ=2.6 and intake temperature of 135 °C and captured at 15 CAD before top dead center.

- Developed a modeling approach to predict homogeneous charge compression ignition combustion in the CFR engine.
- Validated the CFD model against experimental data with regard to in-cylinder pressure and combustion phasing (within the uncertainty of 1 CAD) for different fuel blends and operating conditions.
- Characterized the degree of thermal stratification in the CFR engine under homogeneous charge compression ignition conditions.
- Achieved the goal of investigating fuel composition effects under beyond-RON and beyond-MON ACI conditions.

Conclusions

- CFD models have been developed and validated for multiple engine platforms that cover the multi-mode operations, e.g., Oak Ridge National Laboratory engine (boosted SI), Sandia engine (mixed-mode), Argonne CFR (ACI), and Argonne single-cylinder gasoline direct injection engine (ACI).
- A new efficient knock model in CFD simulation has been proposed to provide accurate prediction of KLSA and to provide 3~10 times faster simulation compared to maximum amplitude pressure oscillation based approach.
- The impacts of HoV and LFS have been studied in both boosted SI and mixed-mode condition using sensitivity analysis. Increasing LFS or decreasing HoV is found to enhance end-gas auto-ignition, while LFS shows a more profound impact on the mixed-mode combustion intensity or knock tendency in boosted SI.
- In ACI study, despite the larger degree of variability of mixture homogeneity compared to thermal stratification, the latter more significantly affected the CFD results.
- The ACI simulations showed a strong sensitivity to the temperature imposed at the boundaries; therefore, cylinder wall temperature needs to be properly determined.
- Mixture/thermal stratification impact needs to be relevantly addressed in ACI engine design strategy, as indicated by the numerical results.
- Numerical study of fuel-engine interactions revealed fuel composition effects to be more dominant under boosted beyond-RON ACI conditions compared to beyond-MON ACI operation.

Key Publications

1. Yue, Z., and S. Som. 2019. “Fuel Property Effects on Knock Propensity and Thermal Efficiency in a Direct-Injection Spark-Ignition Engine.” *Applied Energy*: 114221.
2. Xu, C., P. Pal, X. Ren, S. Som, M. Sjöberg, N. Van Dam, Y. Wu, T. Lu, and M. McNenly. 2019. “Numerical Investigation of Fuel Property Effects on Mixed-Mode Combustion in a Spark-Ignition Engine. Proceedings of the ASME 2019 Internal Combustion Engine Division Fall Technical Conference, ICEF2019-7265, Chicago, IL, October 2019.
3. Kim, Sayop, Joohan Kim, Ashish Shah, Pinaki Pal, Riccardo Scarcelli, Toby Rockstroh, Sibendu Som, Yunchao Wu, and Tianfeng Lu. 2019. “Numerical Study of Advanced Compression Ignition and Combustion in a Gasoline Direct Injection Engine.” Proceedings of the ASME ICEF2019-7281, October 20-23, Chicago, IL.
4. Kalvakala, K., P. Pal, Y. Wu, G. Kukkadapu, C. Kolodziej, J.P. Gonzalez, M. Waqas, T. Lu, S.K. Aggarwal, and S. Som. 2020. “Analysis of Fuel Effects on Advanced Compression Ignition using a Virtual CFR Engine Model.” ASME ICEF 2020 (in preparation).

References

1. Sluder, C.S., J.P. Szybist, R.L. McCormick, M.A. Ratcliff, and B.T. Zigler. 2016. “Exploring the Relationship between Octane Sensitivity and Heat-of-Vaporization.” *SAE International Journal of Fuels and Lubricants* 9 (1): 80–90.
2. Xu, C., P. Pal, X. Ren, S. Som, M. Sjöberg, N. Van Dam, Y. Wu, T. Lu, and M. McNenly. 2019. “Numerical Investigation of Fuel Property Effects on Mixed-Mode Combustion in a Spark-Ignition Engine.” ASME 2019 Internal Combustion Engine Division Fall Technical Conference (October 20–23).

3. Pal, P., K. Kalvakala, Y. Wu, M. McNenly, S. Lapointe, R. Whitesides, T. Lu, S.K. Aggarwal, and S. Som. 2019. "Numerical Investigation of a Central Fuel Property Hypothesis under Boosted Spark-Ignition Conditions." ASME 2019 Internal Combustion Engine Division Fall Technical Conference (October 20–23).

Acknowledgements

This research was funded by DOE's Office of Vehicle Technologies and Office of Energy Efficiency and Renewable Energy under Contract No. DE-AC02-06CH11357.

The principal investigator gratefully acknowledges the contributions of Dr. Pinaki Pal for the CFR engine simulations, Dr. Zongyu Yue for Oak Ridge National Laboratory engine simulations, Dr. Chao Xu for Sandia National Laboratories direct injection spark ignition engine simulations, and Dr. Riccardo Scarcelli and Dr. Sayop Kim for Argonne National Laboratory single-cylinder gasoline direct injection engine under the Co-Optima project.

The authors wish to thank Gurpreet Singh, Kevin Stork, Michael Weismiller, and Alicia Lindauer, technology managers at DOE, for their support. This research was conducted as part of the Co-Optimization of Fuels & Engines (Co-Optima) project sponsored by the DOE Office of Energy Efficiency and Renewable Energy, Bioenergy Technologies and Vehicle Technologies Offices.

The authors would also like to acknowledge the high-performance computing center at the National Renewable Energy Laboratory for computing time on the Peregrine cluster as well as the Laboratory Computing Resource Center at Argonne National Laboratory for computing time on the Bebop and Blues cluster, which were used in this research.

II.23 Characterization of Biomass-Based Fuels and Fuel Blends for Low-Emissions, Advanced Compression Ignition Engines (The University of Alabama)

Ajay K. Agrawal, Principal Investigator
The University of Alabama
Box 870279, 3047 H.M. Comer, 247 7th Ave.
Tuscaloosa, AL 34587
E-mail: aagrawal@eng.ua.edu

Michael Weismiller, DOE Technology Development Manager
U.S. Department of Energy
E-mail: Michael.Weismiller@ee.doe.gov

Start Date: May 1, 2017 End Date: April 30, 2020
Project Funding (FY19): $201,690 DOE share: $180,642 Non-DOE share: $21,048

Project Introduction

The ultimate goal of this project is to accelerate deployment of co-optimized fuels and engines that will reduce fuel consumption, criterion pollutants, and greenhouse gas emissions. Specifically, we will acquire combustion measurements in a constant pressure flow rig (CPFR) with optical access and develop models to predict combustion characteristics based on known fuel and ambient conditions. We are targeting prediction of properties relevant to lean lifted flame combustion, a mixing-controlled low-temperature combustion strategy to reduce soot production in advanced compression ignition engines. Unlike other low-temperature combustion strategies that rely upon chemical kinetics, the combustion or heat release rate in lean lifted flame combustion can be controlled by the fuel injection timing.

Objectives

Overall Objectives

- Experimentally investigate fuel–air mixing and subsequent ignition and combustion processes and properties in different fuel injection regimes, with particular focus on supercritical fuel injection when the surface tension is no longer present.
- Identify synergistic opportunities offered by biofuels and their blends with conventional fuels. We seek to analyze the relationship between fuel physical/chemical properties and combustion properties to co-optimize fuels and advanced compression ignition engines.
- Perform experiments in a flexible, modular, and optically accessible flow rig (available at The University of Alabama) with a continuous supply of preheated compressed air to attain the desired pressure and temperature within the chamber volume. The ability to rapidly rinse the test chamber permits acquisition of statistically significant experimental sample sizes and will allow us to collect extensive data sets for a range of test conditions and biofuel blends.
- Utilize a suite of time-resolved (TR) optical diagnostics techniques: TR rainbow schlieren deflectometry (RSD) technique to examine fuel–air mixing and turbulent flame speed, TR OH* chemiluminescence to quantify turbulent flame structure, and TR two-color pyrometry (2CP) to characterize the soot production.

- Develop a neural network to model functional relationships between fuels' physical/chemical properties and ignition/combustion characteristics. The models will be validated against secondary sets of data not used for the initial development.

Fiscal Year 2019 Objectives

- Integrate TR diagnostics systems to the test facility
- Acquire simultaneous data at diesel conditions using over 400 injections in quick succession
- Analyze RSD, OH* chemiluminescence, and 2CP data to describe the flame evolution process.

Approach

The project is systematically investigating fuel–air mixing and subsequent ignition and combustion processes in a CPFR with a continuous supply of preheated compressed air to attain the desired pressure and temperature within the chamber volume. In this CPFR, the time between tests is greatly reduced (~0.2 Hz) by upstream control of the ambient conditions to create bulk air (or inert gas) flow rates that are minimal compared to the fuel jet velocity. High-fidelity data are acquired simultaneously by three different optical diagnostics techniques at high temporal and spatial resolutions. These techniques focus on different regions of the jet/flame and not only provide the time-averaged measurements, but also help delineate the instantaneous flow and chemical features. Phenomena such as autoignition, flame stabilization, and soot formation can be observed simultaneously in real time to improve our understanding and to provide benchmark data for computational fluid dynamics code development. The fuel property prediction model will be developed as a neural network.

Results

- Developed a new optical design for the 2CP system to improve spatial resolution of the measurements
- Performed over 400 injections in quick succession to acquire statistically relevant data simultaneously using RSD, OH* chemiluminescence, and 2CP
- Analyzed test results to describe flame evolution instantaneously and on average basis.

Novel Two-Color Pyrometer: 2CP has long been used to measure flame temperature and soot concentration from radiative emission in flames. While 2CP is not an absolute measurement in non-axisymmetric flames (such as diesel spray combustion), it is a desirable diagnostic for semi-quantitative or qualitative measurements since it requires minimal optical access and can utilize high-speed imaging to attain exceptional temporal and spatial resolutions. We have developed an improved optical configuration of 2CP that (1) eliminates optical errors inherent in other designs and (2) uses off-the-shelf optics and a single camera. In particular, this work analyzes the impact of parallax and path length differences on the 2CP measurement and exemplifies how the present design eliminates associated errors by design rather than in post-processing. The theoretical range of measurements was generated a priori and overlaid with experimental data to illustrate the dynamic range over which 2CP can determine the soot concentration and temperature in theory and in practice.

The two-color pyrometer design presented in Figure II.23.1 provides a cost-effective solution using off-the-shelf optics and a single camera to resolve parallax, path length, and demosaicing issues associated with previous designs. The setup uses a beamsplitter for light collection, and it is oriented at a 45 degree angle with respect to the camera sensor, thereby dividing the image symmetrically about the axis of the camera lens. Bandpass filters are attached to the beamsplitter to pass the light at the desired wavelengths. Filters with 550 nm and 650 nm central wavelengths are used, as reported in the literature. A pair of turning mirrors reflects the two signals toward a right-angle prism mirror, which directs the signals toward the high-speed camera (Phantom v7.3) for imaging on the same but separate portions of the sensor.

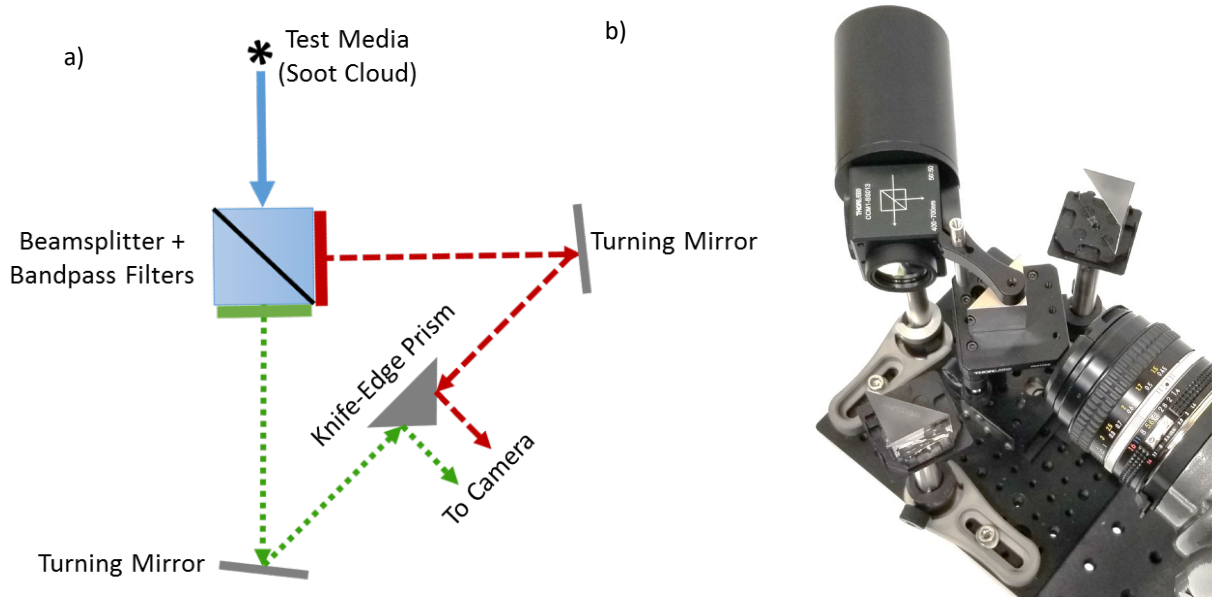

Figure II.23.1 (a) Schematic of optical configuration for the new two-color pyrometer; (b) photograph of the two-color pyrometer

The beamsplitter in the new two-color pyrometer design records the flame emissions from the same point of view for both wavelengths with equal path lengths; therefore, the intensity characteristics of the two images can be precisely correlated at each pixel location, which is crucial to achieve accurate pixel-to-pixel mapping with high spatial resolution. The spatial resolution and precise pixel mapping abilities of the current setup are assessed by recording a spatial calibration target, Siemens star, using the two-color pyrometer. The calibration target was printed on a high-resolution 35 mm slide film, the film was placed in front of the uniform illumination sphere light source, and the target was recorded with the complete two-color pyrometer setup, including the bandpass filters. The acquired image was focused, and no difference in the focal length of the two wavelengths was evident.

The recorded frame with the two images (Figure II.23.2a) was binarized (1 for bright, 0 for dark for the right image and 2 for bright, 0 for dark for the left image) after applying an intensity threshold to remove low-level noise. The binarized images were combined to create the image in Figure II.23.2b with four discrete values: 0 for spatially matching dark pixels (blue color), 3 for spatially matching bright pixels (red color), and 1 or 2 if the pixels in the two images do not match spatially (yellow or dark blue colors). The combined image shows over 92% spatially matching pixels (40% blue or 0 and 52% red or 3). The mismatch in 8% of the pixels occurred mainly at the edges of the Siemens star and can mainly be attributed to the difficulty in prescribing an accurate intensity threshold to binarize the images. Overall, results show that images at the two different wavelengths are accurately mapped in spatial coordinates.

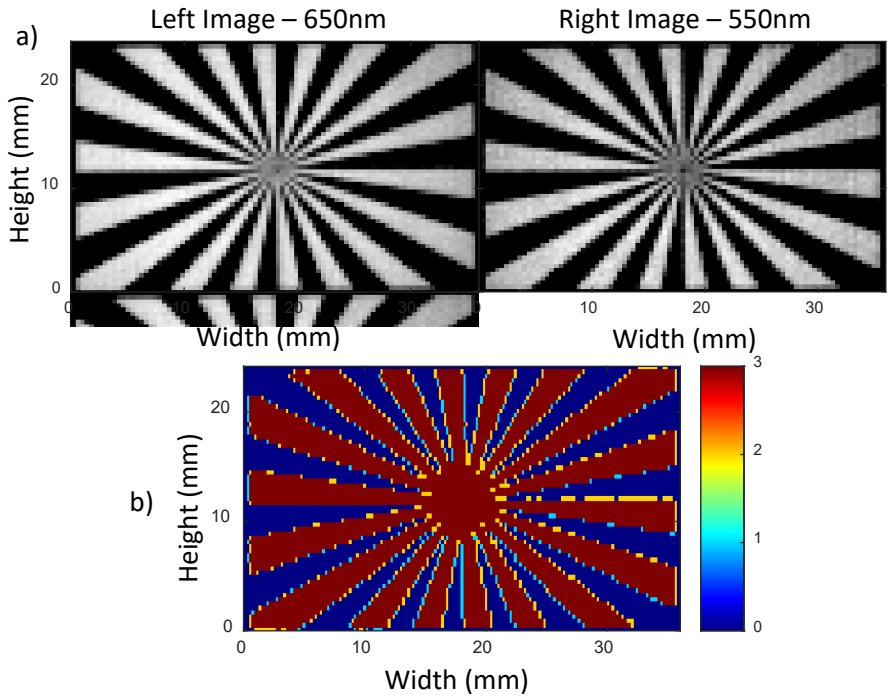

Figure II.23.2 (a) A spatial calibration target (Siemens star) was placed in front of the uniform illumination sphere and recorded by the two-color pyrometer; (b) The right and left images were binarized and overlaid on top of one another to distinguish pixel mapping between images

Simultaneous Optical Diagnostics: We investigated a diesel spray flame to gain unique insight into the transient fuel–air mixing, cool-flame behavior, ignition, flame stabilization, combustion, and soot formation and oxidation processes in n-heptane spray at diesel-like conditions. The study combined two major experimental advancements: (1) a CPFR allowing for the largest number of fuel injection experiments at high-pressure and high-temperature test conditions to collect statistically significant data; and (2) the first application of combined RSD, OH* imaging, and 2CP to simultaneously measure line-of-sight ray deflection angle, OH* concentration, and soot temperature and concentration across the whole field. These diagnostics provide insight into fuel–air mixing, cool-flame development, ignition, flame propagation and stabilization, and combustion.

Figure II.23.3(a) shows the CPFR with two parallel 100 mm diameter quartz windows to provide optical access. Electrically heated air enters the bottom of the rig at a speed of about 0.5 m/s through a flow conditioning device with a fine metal mesh to break down large vortical structures, align the flow, and uniformly disperse flow to create a nearly homogeneous temperature distribution across the chamber. The air exits at the top of the rig through four 3 mm diameter holes placed symmetrically around the injector tip. The air supply pressure is controlled by an upstream dome regulator, and the air flow rate is regulated by a downstream control valve. The temperatures near the injector tip, near the chamber wall, and on the injector tip are monitored by thermocouples to confirm steady operation with minimal variations in the air flow. Steady-state temperature is reached in about three hours when the air temperature at the center of the rig is within 50 K of that at the chamber wall. A Bosch CRIN3-18 fuel injector, modified to have a single, 100 µm orifice at the tip, injects n-heptane fuel from the top of the chamber for an actual duration of 2.1 ms at a supply pressure of 990±8 bar.

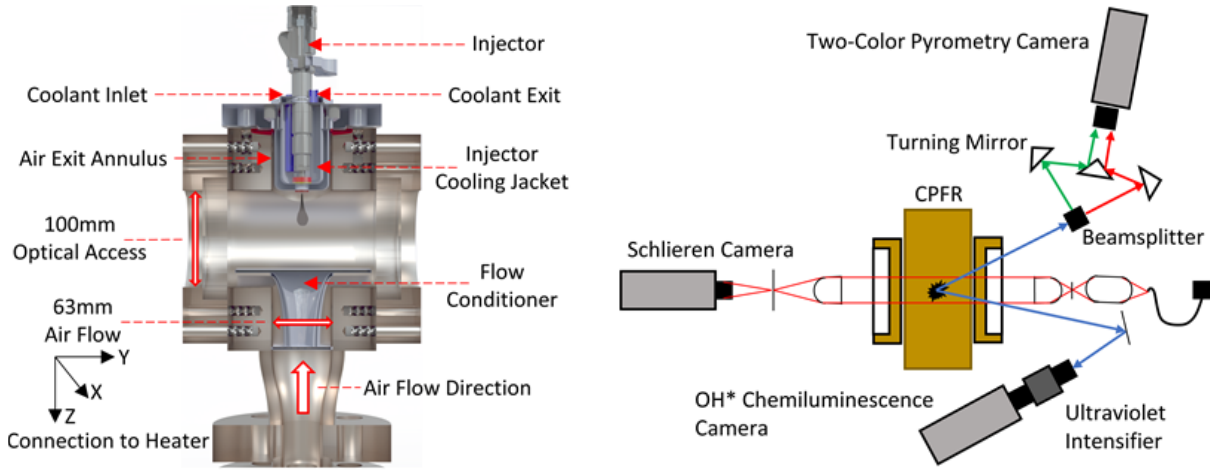

Figure II.23.3 (a) Constant pressure flow rig schematic; (b) Layout of the optical diagnostics

Figure II.23.3(b) shows the layout of the three simultaneous optical diagnostics used for data acquisition: RSD and OH* chemiluminescence, or OH* CH, and 2CP. RSD is orthogonal to the chamber while OH* CH and 2CP are viewed at an angle. A Photron Nova S9 color camera (1) with 512 x 784 pixel resolution is placed directly behind the filter plane to acquire the RSD images at 20 kHz with 4 µs exposure time. The camera is outfitted with a Nikon Nikkor 50 mm lens to provide a spatial resolution of 90 µm per pixel. In the OH* CH system, incoming light is filtered by a 310 nm bandpass filter with a 10 nm full-width half-peak value. The light is collected by a 105 mm lens and focused onto an Invisible Vision ultraviolet intensifier with a 70 µs gate time. The intensifier output goes through a 50 mm lens to a monochrome, 16-bit Photron SA5 camera operated at 10 kHz. The effective resolution of the resulting image is 158.7 µm/pixel. For 2CP, the incoming soot radiation is split by a beamsplitter, and the two spatially identical images are filtered at 550 nm and 650 nm, respectively. Mirrors redirect both images into the camera lens with equal path lengths, ensuring equal focus and size on the camera sensor. The two images from the same viewpoint (a unique feature of this optical setup) appear side by side on a single monochrome camera sensor (Phantom v7.3) at a bit depth of 14 bits. For this experiment, a 105 mm lens with f-stop of 2, providing spatial resolution of 241.9 µm/pixel, is used. The images are acquired at 10 kHz with an exposure time of 98 µs and are stored with no gain or gamma correction.

Cool-flame behavior was identified by visual observation of the RSD images and experimental data for liquid/vapor penetration and cone angles. Results supported previous findings showing cool-flames along the jet periphery, much earlier and with a much longer induction time than that between ignition and combustion. Once developed, the cool-flame spreads inward into the jet core and downward to the jet head, where ignition ultimately occurs. Planar profiles of refractive index difference demonstrate quasi-steady fuel–air mixing conditions, enabling identification of the cool-flame pathway both spatially and temporally. The cool-flame reactions decreased the quasi-steady fuel–air mixing duration at the downstream locations. The planar contours of OH* intensity revealed ignition and combustion occurring close to each other and at nearly the same location. At the end of injection, OH* intensity contours revealed a bimodal distribution, indicating distinct upstream (near lift-off length) and downstream reaction zones. At later times, the upstream zone decayed while reactions continued in the downstream zone.

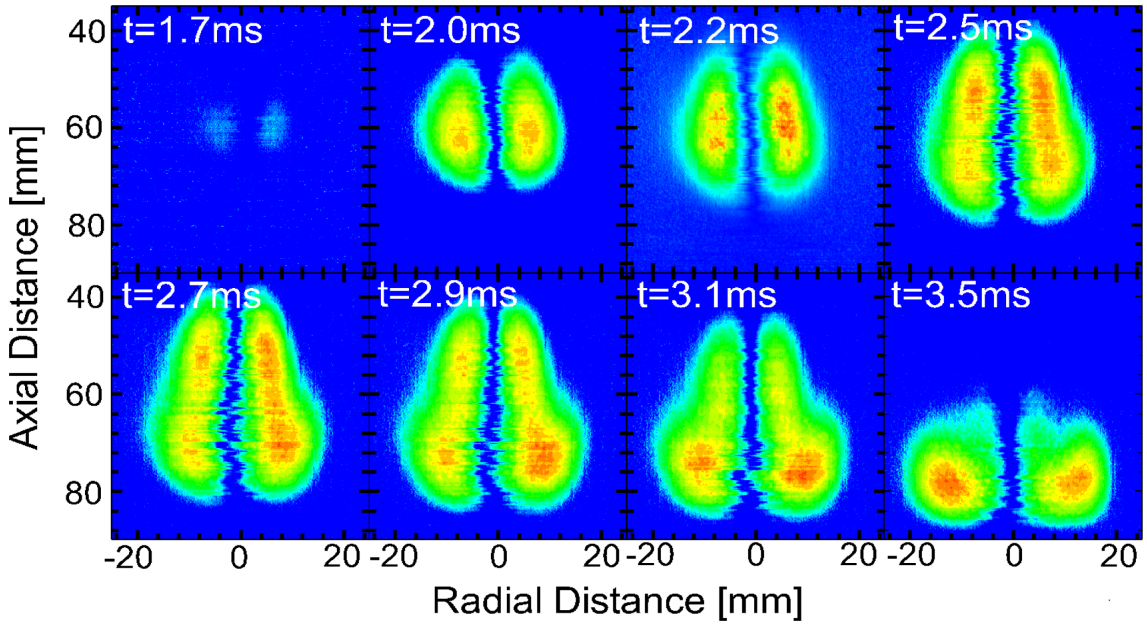

Figure II.23.4 Ensemble average (over 400 injections) planar OH* intensity contours are shown at eight different times

Figure II.23.4 shows the ensemble averaged planar OH* intensity contours for eight different times after start of injection to quantify the time and spatial location (axial and radial) of ignition observed via RSD. On average, the ignition kernels first appear at t = 1.7 ms at z = 60 mm. The radial location of main ignition, r = 8 mm, is precisely the region of cool-flame development following RSD visualizations. By t = 2 ms, the ignition region has broadened, with peak OH* intensity at approximately the same location as the previous plot. At t = 2.2 ms, the flame has stabilized at the lift-off length. After t = 2.2 ms, the OH* intensity contour reveals that the peak reaction zone has shifted radially inward. The next time reveals the bimodal shape observed in the instantaneous images, where OH* concentrations peak at both upstream and downstream locations. Beyond this time, the upstream radical pool diminishes (t = 2.7 ms) and the reactions persist downstream between
t = 3.1 and 3.5 ms.

Figure II.23.5 presents 2CP data at five different times after start of injection to depict the transient flame evolution. The contours are grouped into three categories: Figure II.23.5a and Figure II.23.5b show an instantaneous T and KL (soot concentration) contour plots, while Figure II.23.5c and Figure II.23.5d show mean and root-mean-square (RMS) T plots and Figure II.23.5e and Figure II.23.5f show mean and RMS KL plots, respectively, each based on 413 injections; the reaction zone boundary identified from OH* is shown by white curves.

Conclusions

We have expanded capabilities of the CPFR facility to operate at higher pressures than previously possible. A two-color pyrometry system has been developed with a much refined optical setup. The three time-resolved optical diagnostic techniques have been applied independently, and their integration to acquire simultaneous images has been demonstrated. We acquire high-speed data simultaneously using three different diagnostics at diesel conditions using over 400 consecutive injections to obtain statistically relevant measurements.

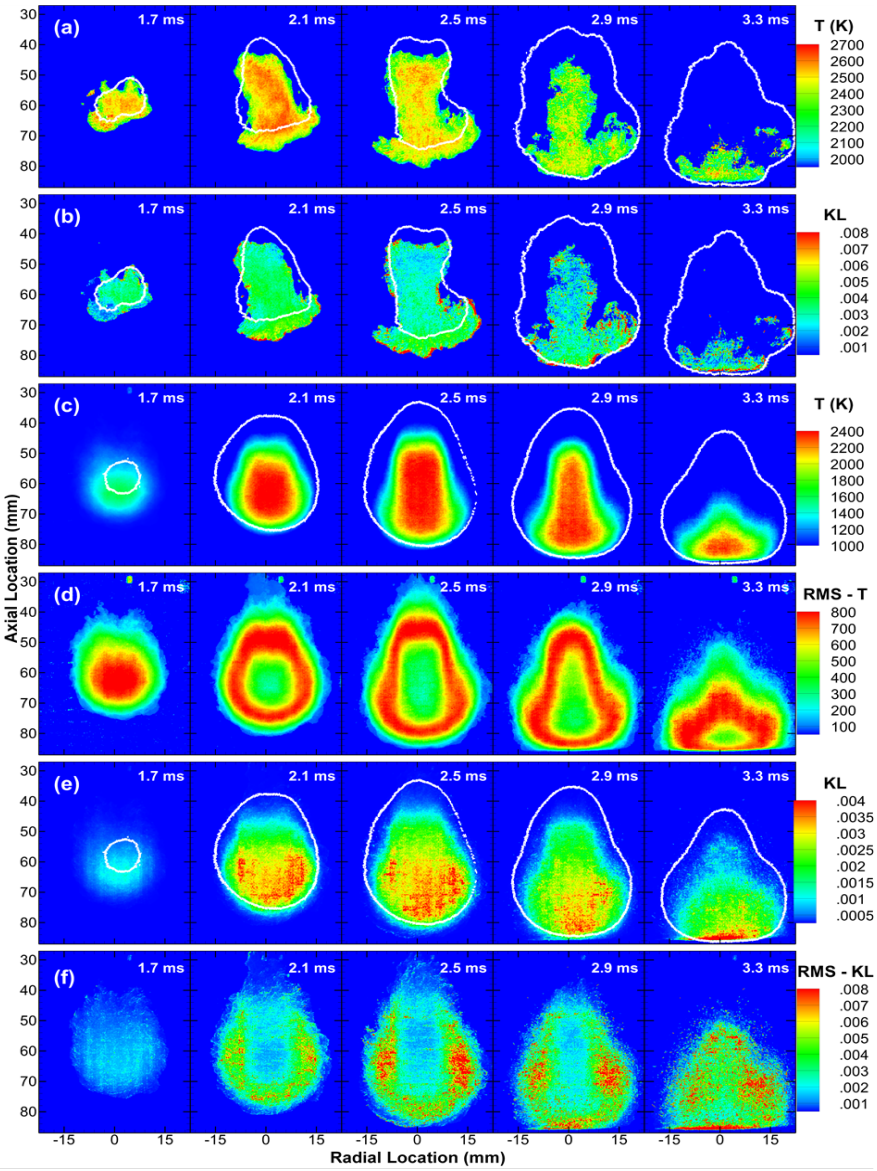

Figure II.23.5 (a) Soot temperature from a single injection with the outline of OH* detection shown in white. (b) KL measurement from a single injection. (c) Ensemble averaged (411 consecutive injections) soot temperature with the outline of OH* detection in white. (d) Standard deviation of soot temperature. (e) Ensemble averaged KL. (f) Standard deviation of KL.

Acknowledgements

Professor Joshua Bittle of The University of Alabama is a co-principal investigator on this project. We would like to thank Chuck Mueller of Combustion Research Lab at Sandia National Laboratories for technical guidance and input on various aspects of this project.

II.24 Dynamic Species Reduction for Multi-Cycle CFD Simulations (University of Michigan)

Robert J. Middleton, Principal Investigator
University of Michigan (UM)
Department of Mechanical Engineering
1231 Beal Avenue
Ann Arbor, MI 48109-2133
E-mail: rjmidd@umich.edu

Kevin Stork, DOE Technology Development Manager
U.S. Department of Energy
E-mail: Kevin.Stork@ee.doe.gov

Start Date: April 17, 2017 End Date: January 31, 2021
Project Funding: $480,000 DOE share: $432,000 Non-DOE share: $48,000

Project Introduction

Full-cycle, full-chemistry computational fluid dynamics (CFD) simulations form a key part of the Co-Optima program effort of developing suitable fuels for future advanced engines. While full-cycle CFD simulations can capture the flow phenomena associated with the intake and exhaust events, single-cycle simulations with chemistry are sensitive to the choice of initial conditions and are inadequate to capture prior-cycle chemical and/or thermal feedback. Meanwhile, the autoignition and compression ignition combustion modes present in both the virtual Cooperative Fuel Research (CFR)/spark ignition engine and advanced compression ignition (ACI) engine configurations are known to be highly sensitive to these effects. Multi-cycle CFD simulations can capture this cyclic feedback but are prohibitively expensive computationally. The existing species reduction methods of reducing this cost rely on user intervention to define the species of interest and suffer from potentially large errors if important intermediate species are erroneously removed from the computation. This project proposes new methods of increasing computational efficiency for multi-cycle simulations while maintaining accuracy by dynamic species reduction (DSR) during open valve events, thereby retaining the species of greatest importance to cyclic feedback effects.

Objectives

The goal of this project is to provide CFD tools that will reduce the computational expense of a full-engine-cycle simulation with chemistry by 80% relative to the state of the art and enable the Co-Optima team to efficiently perform multi-cycle simulations to capture prior-cycle compositional and thermal effects while improving numerical accuracy. Co-Optima's Simulation Toolkit team is developing engine CFD simulation tools for use in several areas of the program, including facilitating the development of fuel surrogates for bio-fuels and gasoline/bio-fuel blends in a virtual CFR engine, modeling the research octane number and motor octane number tests, and providing insight for the development of advanced ACI engines.

Overall Objectives

- Develop a method of dynamically reducing the number of species fluxed during gas exchange to reduce the computational expense of the transport equations by 90% while the valves are open
- Improve multi-zone chemistry binning methods to enhance computational efficiency during the expansion stroke, where temperatures are high and the charge composition contains primarily product species.

Fiscal Year 2019 Objectives

- Complete baseline ACI and CFR multi-cycle simulations with chemistry active throughout the cycle, using new ACI conditions from current National Lab efforts
- Finalize implementation of DSR routines into CONVERGE
- Identify CFR and ACI conditions with cyclic coupling
- Validate the DSR model and refine as needed
- Develop and implement a new multi-zone binning method, Product Directed Remapping (PDR), for post-combustion chemistry.

Approach

Starting with prior work in species reduction and multi-zone binning in the open source KIVA framework, the approach here is to develop improved methods and to incorporate them into the CONVERGE CFD code with active collaboration with Convergent Sciences. This is intended to ensure broad accessibility for the computational community, including the Co-Optima fuels project. Collaboration is also ongoing with the computational group at Argonne National Laboratory (ANL), which is providing baseline information on detailed CFD simulations of CFR and ACI engines, which will be used as a baseline to validate the new computational approaches.

Results

- Baseline simulations for DSR have been completed using a CFR engine mesh and operating conditions provided by ANL [1],[2].
- The DSR algorithm initially developed in KIVA has been successfully converted to the CONVERGE platform.
- The DSR algorithm was validated using the CFR engine mesh in a configuration relevant for boosted spark ignition engine operation and previously studied by ANL.
- The new DSR implementation was shown to provide improved agreement with full-chemistry simulations relative to a similar manual procedure available in CONVERGE.
- Provisional ACI operating conditions have been identified to explore cyclic coupling and to develop improved burned-gas binning procedures.

Baseline three-dimensional CFD simulations have been conducted in CONVERGE to enable development of both the DSR and the improved burned-gas binning models. Open-cycle Reynolds-averaged Navier–Stokes simulations of a CFR engine were conducted using a mesh provided by ANL. The simulations were consistent with conditions studied extensively by ANL. ACI engine simulation conditions were developed using a direct injection spark ignition engine mesh from ANL previously used to model experimental boosted spark ignition results from Oak Ridge National Laboratory. The valve events and boundary conditions were configured to replicate homogeneous charge compression ignition operating conditions previously studied at UM and used to develop the initial version of DSR in KIVA.

Two separate versions of DSR were implemented in CONVERGE. When executed, the model considers the local concentrations in every cell and boundary in the simulations to determine which species to retain during the accelerated portion of the simulation. Any species with a local concentration above a user-specified threshold is retained. The first version was implemented as a calculation external to CONVERGE and leveraged a similar method in CONVERGE called “Skip Species” to execute the removal of the species from the mesh. The second version was implemented in situ in CONVERGE using a usermodel interface provided

by Convergent Science and is consistent with the proof-of-concept model previously developed in KIVA. In this version, the retained hydrocarbon species are adjusted to maintain the mixture heating value after species removal, while the major combustion products (CO_2 and H_2O) are adjusted to maintain the atomic balances of carbon and hydrogen.

Simulation results comparing the baseline configuration with all species retained throughout the simulation to the CONVERGE 'Skip Species' model with manual species selection and the two DSR implementations are shown in Figure II.24.1. Both DSR versions replicate the full-chemistry simulations well while retaining fewer species than the manually configured Skip Species model. The major difference in the species retained between the models is the inclusion of NO by the automatic selection in DSR, providing for the ignition advance observed. Performance gains for these models were modest, with roughly 10% improvement over the baseline simulation. This is due to a combination of factors that have changed from the initial proof-of-concept studies. In this case, the baseline suspends kinetics calculations during the open cycle. It is also configured with a large mesh of more than one million cells while using a small mechanism of 48 species. The proof-of-concept simulations were conducted with a smaller mesh, on the order of 100,000 cells, and a larger mechanism of 314 species and exhibited larger computational efficiency gains.

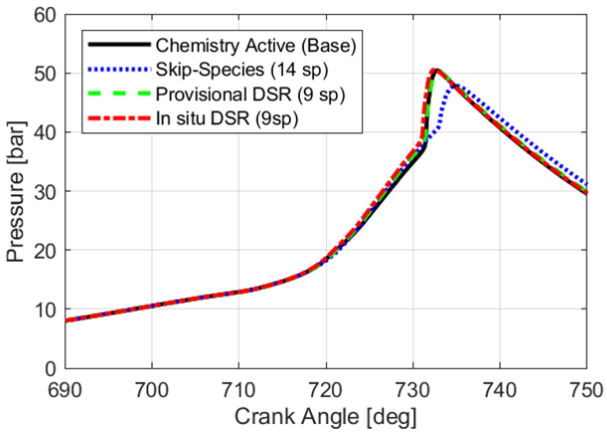

Figure II.24.1 Second-cycle predictions for the CFR engine baseline conditions comparing several methods of reducing gas exchange computational cost. UM's DSR implementations provide excellent agreement with detailed simulations without requiring manual selection of retained species.

Figure II.24.2 shows the configuration of the initial ACI simulations, indicating the negative valve overlap (NVO) region and valve events. A 2,000 rpm low load (5 bar indicated mean effective pressure) condition was developed based on previous UM homogeneous charge compression ignition studies. Two consecutive cycles were simulated and the second-cycle predictions with DSR compared to the baseline predictions without species reduction. For these initial baselines, the chemical kinetics was disabled during both gas exchange and NVO for all configurations. Figure II.24.3 shows the second-cycle predictions for two configurations of DSR. Good replication of the baseline results are observed with DSR, while a 30% computational cost savings occurs. The increased savings relative to the CFR engine case are attributed to the increased mechanism size of 312 species [3] and the smaller computational mesh of approximately 200,000 cells.

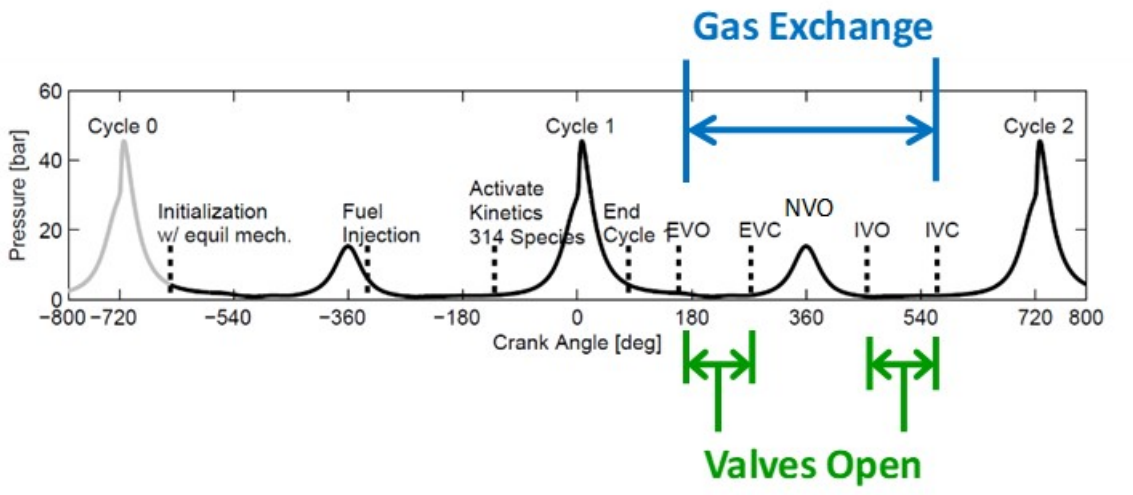

EVO – exhaust valve opening; EVC – exhaust valve closing; IVO – intake valve opening; IVC – intake valve closing

Figure II.24.2 Cycle diagram showing gas exchange and open valve periods for the ACI simulations. Dynamic species reduction was applied for the entire gas exchange period.

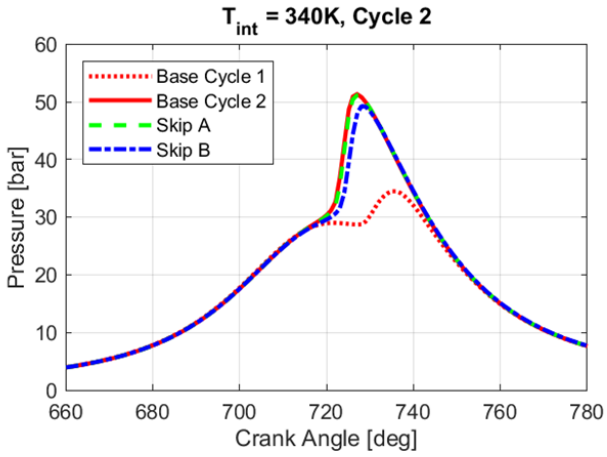

Figure II.24.3 Second-cycle predictions for an ACI engine operating condition, showing two configurations of DSR replicating the detailed baseline predictions

The results of the ACI simulations are currently being used to develop improved multi-zone binning methods for the post-combustion period. Additional simulations are underway to refine the computational efficiency gains and account for computer run-time variability.

Conclusions

- Implementation of UM's dynamic species reduction model in CONVERGE has been completed and demonstrated for both CFR and ACI engine conditions. Good agreement with detailed baseline simulations is observed.
- Sensitivity in the computational improvement available to the mesh and mechanism sizes has been identified.
- Full DSR validation and timing studies are expected to be completed shortly.
- Development of new burned-gas binning methods is underway.

References

1. Pal, P., Y. Wu, T. Lu, S. Som, Y.C. See, and A. Le Moine. 2017. "Multi-Dimensional CFD Simulations of Knocking Combustion in a CFR Engine." Proceedings of the ASME 2017 Internal Combustion Engine Division Fall Technical Conference (October 15–18), Seattle, WA, USA, Paper ICEF2017-3599.

2. Pal, P., et al. 2018. "Development of a Virtual CFR Engine Model for Knocking Combustion Analysis." SAE Paper No. 2018-01-0187.

3. Mehl, M., W.J. Pitz, C.K. Westbrook, and H.J. Curran. 2011. "Kinetic Modeling of Gasoline Surrogate Components and Mixtures under Engine Conditions." *Proceedings of the Combustion Institute* 33 (1): 193–200.

Acknowledgements

Initial simulation configurations and predictions from ANL were provided by Sibendu Som, Pinaki Pal (CFR engine), and Zongyu Yue (direct injection engine). Convergent Sciences has provided software licenses and technical support to integrate new models into CONVERGE. Integral contributions to this project were provided by George A. Lavoie, Vansh Sharma, Amber Smith, and Nicole Sitek of the UM Department of Mechanical Engineering.

II.25 Micro-Liter Fuel Characterization and Property Prediction (Louisiana State University)

Ingmar Schoegl, Principal Investigator
Louisiana State University (LSU)
Mechanical & Industrial Engineering
3261 Patrick F Taylor Hall
Baton Rouge, LA 70803
E-mail: ischoegl@lsu.edu

Shyam Menon, Principal Investigator
Louisiana State University (LSU)
Mechanical & Industrial Engineering
3261 Patrick F Taylor Hall
Baton Rouge, LA 70803
E-mail: smenon@lsu.edu

Eric Petersen, Principal Investigator
Texas A&M University (TAMU)
Department of Mechanical Engineering
3123 TAMU
College Station, TX 77845
E-mail: epetersen@tamu.edu

Tianfeng Lu, Principal Investigator
University of Connecticut (UConn)
Department. of Mechanical Engineering
191 Auditorium Rd. U-3139
Storrs, CT 06269
E-mail: tianfeng.lu@uconn.edu

Michael Weismiller, DOE Technology Development Manager
U.S. Department of Energy
E-mail: Michael.Weismiller@ee.doe.gov

Start Date: March 1, 2017 End Date: February 28, 2020
Project Funding: $1,574,444 DOE share: $1,359,544 Non-DOE share: $214,900

Project Introduction

The DOE Co-Optima initiative seeks to accelerate the introduction of affordable, scalable, and sustainable high performance fuels for use in high-efficiency, low-emission engines. Co-optimized fuels and engines offer the opportunity to build on long-term research in both fuels and engines, where advances over the last ten years have identified combustion engine strategies that, especially if optimized to run on new fuels, would offer higher gas mileage and produce less engine-out pollutants than current engines.

This project addresses DOE's stated interest in enabling small-volume (<20 µl), high-throughput (>100 tests per device per month) measurements of transportation fuels and blends that are relevant to co-optimized fuels and engines. In this context, the ability to quantify the performance of a fuel in terms of autoignition metrics

(e.g., octane number/sensitivity), combustion properties (e.g., flame speed), and physical properties (e.g., volatility and viscosity) is of significant interest. Predictions of fuel performance in a combustion engine require a link to be made between small-volume measurements and combustion behavior of a fuel blend at engine-relevant conditions.

Objectives

The project seeks to establish a foundation for small-volume, high-throughput fuel testing, where relevant fuel metrics are quantified in a micro-combustion experiment.

Overall Objectives

- Quantify combustion metrics of transportation fuels (e.g., octane number, flame speed)
- Construct an experimental prototype that can operate at elevated pressures
- Develop prediction models linking small-volume measurements to engine-relevant conditions
- Demonstrate small-volume, high-throughput testing capabilities in blind tests.

Fiscal Year 2019 Objectives

- Demonstrate capability to operate at elevated pressure (continued from Fiscal Year 2018)
- Validate core assumptions for existence of essential combustion modes at elevated pressure
- Document physical property measurements.

Approach

The approach for micro-liter fuel characterization relies on cyclical combustion events within a heated micro-tube. This combustion mode is known as FREI (Flames with Repetitive Extinction and Ignition) and relies on self-excited instabilities that are sensitive to fuel properties. A total sample volume of 20 ml is stored on a disposable microfluidic chip, dispensed via a MEMS (micro-electromechanical systems) droplet generator, and mixed with air to create desired stoichiometry and mass flow rate. Within the micro-tube, a temperature profile (300–1,400 K) is established by external heating, whereas the desired operating pressure (25–30 bar) is regulated by a pressure controller downstream of the micro-tube. The time required to capture individual data points lies in the order of 10–20 s, which allows for high-throughput testing. FREI characteristics are evaluated for sweeps of mass flow rates and/or pressure. Image analysis provides information on ignition, extinction, and flame propagation, which have been shown to be sensitive to fuel octane numbers.

The overall approach aligns with Sub-Topic 5 of the original funding opportunity announcement, i.e., “Small-volume, high-throughput fuel testing.” The main objective is to demonstrate the feasibility of micro-liter fuel characterization as a method with smaller sample volumes and higher throughput than conventional approaches (I. Schoegl/LSU). A broadened scope includes engine-relevant physical fuel metrics (S. Menon/LSU) and thus encompasses Sub-Topic 1 (“Fuel characterization and fuel property prediction”). The approach further needs to be validated against data from established experimental methods (E. Petersen/TAMU), whereas numerical analyses require reduced kinetic models (T. Lu/UConn).

Results

Key Accomplishments for Fiscal Year 2019

- Documented micro-combustion phenomena up to 10 bar
- Obtained new results showing the loss of an unstable combustion regime at diluted conditions, creating new pathways for fuel testing at high pressures
- Quantified droplet oscillation to measure surface tension and viscosity with 20% accuracy
- Obtained new shock tube data for DOE reference blendstocks.

Micro-Combustion Experiment (Principal Investigator: I. Schoegl, LSU)

The project is built around a micro-combustion setup at LSU. For measurements, the fuel to be tested is premixed with combustion air and introduced into an externally heated micro-channel. Due to the strong coupling of gas and wall temperatures, multiple combustion regimes are supported, which allows for the characterization of fuel-dependent ignition, flame propagation, and extinction events.

Figure II.25.1 shows current results from an experiment seeking to probe inherent pressure and dilution effects. The results are novel in multiple ways. (i) At 10 bar peak pressure, the LSU setup achieved the second highest documented pressure for this type of experiment. (ii) Measurements involve a thin filament pyrometry approach that has not been previously used in comparable setups. The pyrometry technique developed at LSU involves high dynamic range imaging with conventional machine vision cameras. Notably, the low-temperature limit of 800 K significantly improves upon comparable work with conventional cameras that are typically used for substantially higher temperatures. (iii) Most importantly, the results show, for the first time, the loss of an intermediate unstable combustion regime due to dilution effects. In particular, the last finding is essential for the final steps of the research project, where multiple fuel-dependent combustion zones will be investigated at pressures of 15–25 bar.

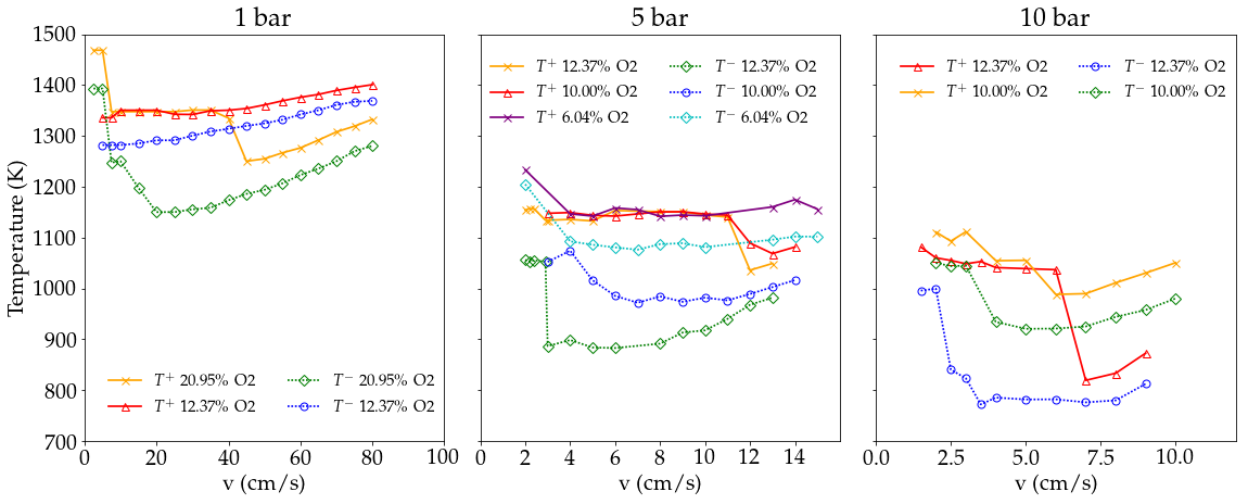

Figure II.25.1 Current results for pressure and dilution effects

With pressures up to 10 bar, the intermediate-pressure setup at LSU operates beyond conditions that are documented for comparable micro-combustion experiments in the literature. A significant portion of efforts in this reporting period focused on obtaining data that are needed to understand the impact of operating parameters of the experiment for simple fuels, where ethane serves as a benchmark for characterization tests. Experimental results showed good correspondence with the predictive analytical model developed in Fiscal

Year 2018. Next steps involve tests for a range of fuel blends at diluted conditions in the 10 bar setup, as well as tests with a newly implemented high-pressure setup (30 bar peak pressure).

Droplet Delivery (Principal Investigator: S. Menon, LSU)

A commercial off-the-shelf piezoelectric droplet generator was implemented as a micro-liter fuel delivery device. The ability to control droplet size in a range of 20–70 µm while independently varying fuel flow rate through adjustment of the operating frequency (1–1,200 Hz) creates flow rates required for the micro-combustor setup (0.5–4 µl/min). Operation of the droplet generator was verified for high-vapor-pressure fuels at operating pressures of up to 7 bar and room temperature (323 K) by implementing the setup in a chamber with controlled pressure and temperature. To extend the range of operation, a new high-pressure delivery apparatus, designed to operate at up to 30 bar and at a temperature of 423 K, has been fabricated and pressure-tested to 35 bar. Ongoing work involves integrating the droplet generator into the high-pressure manifold, upgrading all fluid connections in the system to operate at up to 35 bar, and beginning efforts on high-pressure fuel droplet generation and visualization.

In Fiscal Year 2019, measurements of surface tension and viscosity using micro-liter quantities of fuel at atmospheric pressure were completed for a variety of fuels. This includes primary reference fuels (PRFs) (iso-octane and n-heptane) as well as functional group molecules representative of biofuels, including ketones, esters, alcohols, and furans, from the Tier II selection of Co-Optima fuels. Measurement of surface tension and viscosity involves the observation of droplet dynamics post-injection from a piezoelectric droplet generator. Stroboscopic measurements are illustrated in Figure II.25.2. Tests were conducted to determine optimal strobe operation time for imaging the droplets as well as to find the best edge-tracking algorithm for droplet shape detection. Preliminary results for viscosity and surface tension lie within 20% of literature-reported values. Given that measurements require only about 5 µl of fuel within 500 µs per sample, the approach has the capability to be further improved to provide a high-throughput, low-cost, small-volume property measurement tool.

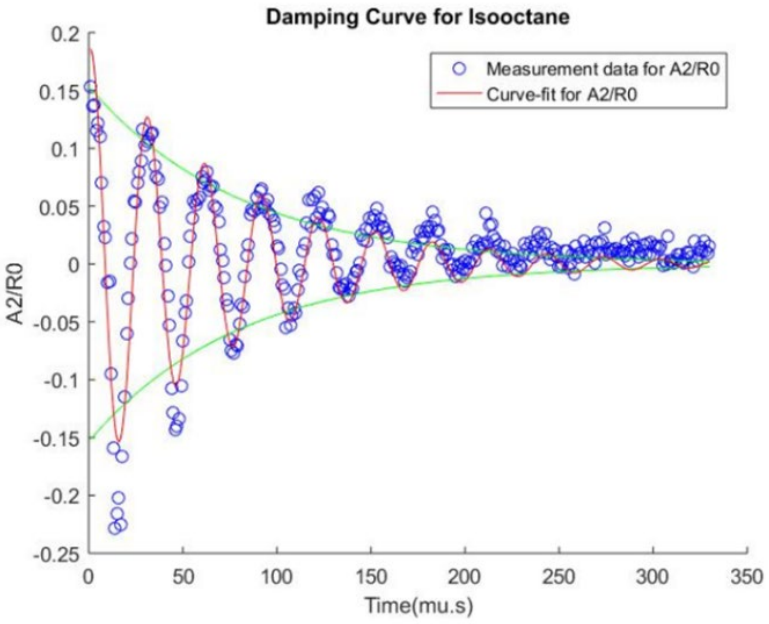

Figure II.25.2 Sample damping curve for iso-octane. Data are used for physical property measurements, e.g., viscosity and surface tension.

Reference Measurements (Principal Investigator: E. Petersen, TAMU)

Ignition delay times of a gasoline surrogate (iso-octane/toluene/n-heptane/1-hexene at 55%/25%/15%/5% by liquid volume, developed by McCormick et al. [1]) with high-level bioblendstock–gasoline surrogate blends (50% and 85% biofuel by liquid volume each of ethanol and methyl acetate) were collected behind reflected shock waves. Post-reflected-shock temperatures ranged from 968 K to 1,361 K at pressures of about 4, 10, 25, and 50 atm. Data were collected for real fuel–air mixtures at fuel-lean and stoichiometric conditions (ϕ = 0.5, 1.0), with focus on the more practical fuel-lean conditions. Ignition delay times were measured from OH* chemiluminescence around 307 nm using an endwall diagnostic. Figure II.25.3 shows some of the new data, namely for stoichiometric conditions and for 25 atm. The research octane number and motor octane number of the surrogate were 90.3 and 84.7, respectively, which places the surrogate within the range of standard U.S. gasoline. Ethanol was chosen due to its wide use in flex-fuel vehicles and availability, while also providing an increased octane rating. Methyl acetate was chosen for its especially high octane rating to investigate the effect of an extreme case.

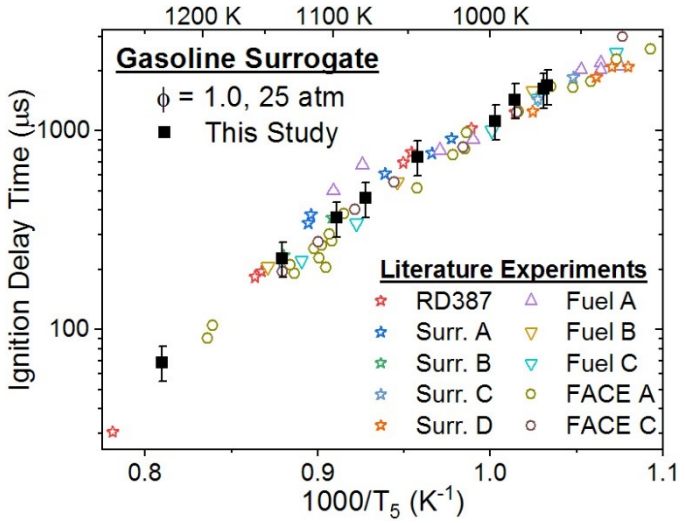

FACE – Fuels for Advanced Combustion Engines

Figure II.25.3 T_{ign} data for the gasoline surrogate from this study at 25 atm and stoichiometric conditions compared to literature results. Pressure adjusted to 25 atm using the reported pressure exponent for each fuel.

To validate the gasoline surrogate, the data were compared to real gasoline (RD387) and several gasoline surrogate experiments from the literature. Using the wide range of pressures studied, the gasoline surrogate's pressure dependence was quantified to account for test-to-test variations using regression analysis. Similarly, a global correlation for gasoline and its surrogates was developed using all available data from the literature. Two modern chemical kinetics models targeting gasoline and its surrogates are compared to the ignition delay time measurements. Each model predicts ignition delay time values slower than those observed from experiment for virtually all mixtures, with better agreement occurring at higher temperatures and bioblendstock content. Significant disagreement between the models in the negative temperature coefficient region shape and location is also observed. These new high-pressure, high-bioblendstock concentration tests provide required chemical kinetic data for optimizing fuel and engine design.

During this reporting period, much progress was made on the development of the laminar flame speed experiment to perform repeatable tests on liquid fuels with reduced uncertainty. Efforts for the characterization phase focused on decane to perfect the techniques. Experiments using the McCormick blend were begun.

Reduced Mechanisms (Principal Investigator: T. Lu, UConn)

To obtain compact and accurate skeletal and reduced mechanisms for gasoline surrogate fuels with the working conditions relevant to the Co-Optima applications, different skeletal mechanisms were generated for individual fuels as detailed in the following.

The reduction tasks were performed based on reaction states sampled within a pressure range of 1–80 atm; equivalence ratio of 0.8–1.2; initial temperature of 600–1,600 K for autoignition, including the negative temperature coefficient regime; and inlet temperature of 300 K for a perfectly stirred reactor for high-temperature flames. It was found that reduced mechanisms developed based on both autoignition and perfectly stirred reactor can be readily extended to other flame types and conditions [2]. The starting detailed mechanism was developed by Lawrence Livermore National Laboratory [3] and consisted of 2,878 species. The reduction process involved the directed relation graph, directed relation graph-aided sensitivity analysis, and linearized quasi steady-state approximations [2],[4],[5]. Furthermore, the stiff chemistry solver LSODES was implemented with sparse analytical Jacobian to speed up the iterative ignition delay time evaluations in the sensitivity analysis. Substantial reduction in computational cost was achieved for the reduction process.

Twelve skeletal mechanisms and three reduced mechanisms were developed for selected target fuels as summarized, with the specified error threshold values listed in Table II.25.1. The mechanisms were extensively validated for ignition delay time, perfectly stirred reactor extinction profiles, and laminar flame speed. Selected validation results of BOB-alk and air mixtures are shown in Figure II.25.4. Based on the validation results, these skeletal and reduced mechanisms are suitable for capturing autoignition at different initial temperatures and end-gas autoignition, as well as flame propagation characteristics in both compression ignition and spark ignition engines.

Table II.25.1 Cases for Skeletal and/or Reduced Mechanism Development

Case NO.	Target fuels	ERROR Threshold	# of species (skeletal)	# of species (reduced)
1	EXPERT	0.3	128	
2	TPRF-E30	0.2	149	
3	TPRF-Anisole 20%	0.2	129	
4	TPRF-Isobutanol10%	0.2	121	
5	BOB-alk	0.3	116	80
6	BOB-aro	0.3	140	105
7	BOB-E30	0.3	138	96
8	Ethanol 75%/n-heptane 25%	0.2	130	
9	Toluene 75%/n-heptane 25%	0.2	181	
10	TPRF-DIB30%	0.2	150	
11	PRF90	0.15	182	
12	TPRF-Anisole 30%	0.3	112	

TPRF – toluene primary reference fuel; E30 –30% ethanol, 70% gasoline blend; BOB – blendstock for oxygenate blending; alk – alkane; aro – aromatic; DIB30% – 30% diisobutylene

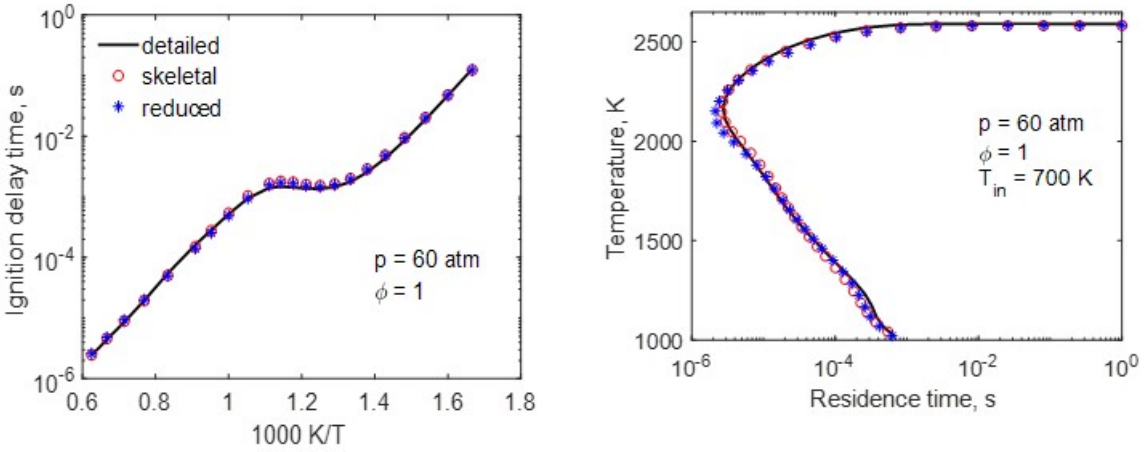

Figure II.25.4 Selected ignition delay time and perfectly stirred reactor validations for BOB-alk and air mixtures.

Conclusions

The following conclusions are derived for the final phase of the project "Micro-Liter Fuel Characterization and Property Prediction:"

- Micro-combustion tests in an intermediate pressure demonstrate the existence of relevant combustion phenomena up to 10 bar. Results illustrate the loss of an unstable combustion regime, which holds substantial promise for tests at high pressure.
- Experimental data show good correspondence to predictions from a simplified analytical model for variations of both dilution and pressures up to 10 bar.
- The newly developed pyrometry allows for accurate measurements above 800 K, which is a significant improvement over comparable techniques working in the near-infrared regime.
- Nanoliter fuel delivery via piezoelectric droplet generation was demonstrated at intermediate pressure. Stroboscopic droplet imaging allows for measurements of viscosity and surface tension.
- Reference shock tube measurements for blendstocks and fuel surrogates have shown some discrepancies between predictions from chemical kinetics and experimental data.
- Kinetic model reduction efforts have produced a series of skeletal mechanisms that are used for predictive modeling.

Key Publications

1. Schoegl, I., V.M. Saue, and P. Sharma. 2019. "Predicting Combustion Characteristics in Externally Heated Microtubes." *Combustion and Flame* 204: 33–48.
2. Sauer, V.M., and I. Schoegl. 2019. "Numerical Assessment of Uncertainty and Dynamic Range Expansion of Multispectral Image-Based Pyrometry." *Measurement* 145: 820–832.
3. Pinzón, L.T., O. Mathieu, C.R. Mulvihill, I. Schoegl, and E.L. Petersen. 2019. "Ignition Delay Time and H_2O Measurements During Methanol Oxidation Behind Reflected Shock Waves." *Combustion and Flame* 203: 143–156.

4. Pinzón, L.T., O. Mathieu, C.R. Mulvihill, I. Schoegl, and E.L. Petersen. 2019. "Ethanol Pyrolysis Kinetics Using H_2O Time History Measurements Behind Reflected Shock Waves." *Proceedings of the Combustion Institute* 37: 239–247.

References

1. McCormick, R., G. Fioroni, L. Fouts, E. Christensen, et al. 2017. "Selection Criteria and Screening of Potential Biomass-Derived Streams as Fuel Blendstocks for Advanced Spark-Ignition Engines." *SAE Int. J. Fuels Lubr.* 10: 442–460.

2. Lu, T., and C.K. Law. 2009. "Toward Accommodating Realistic Fuel Chemistry in Large-Scale Computations." *Prog. Energy Combust. Sci.* 35: 192–215.

3. Mehl, M., K. Zhang, S. Wagnon, G. Kukkadapu, C.K. Westbrook, W.J. Pitz, Y. Zhang, H. Curran, M. Al Rachidi, N. Atef, and M.S. Sarathy. 2017. "A Comprehensive Detailed Kinetic Mechanism for the Simulation of Transportation Fuels," in 10th U.S. Natl. Combust. Meet., pp. 1–6.

4. Lu, T., and C.K. Law. 2006. "Systematic Approach to Obtain Analytic Solutions of Quasi Steady State Species in Reduced Mechanisms." *J. Phys. Chem. A.* 110: 13202–13208.

5. Luo, Z., T. Lu, and J. Liu. 2011. "A Reduced Mechanism for Ethylene/Methane Mixtures with Excessive NO Enrichment." *Combust. Flame* 158: 1245–1254.

Acknowledgements

The principal investigators would like to thank the DOE Vehicle Technologies Office leadership—Michael Berube, Gurpreet Singh, Kevin Stork, Ralph Nine, and Michael Weismiller—as well as the DOE project mentor, Matthew McNenly, for their guidance and support.

II.26 The Development of Yield-Based Sooting Tendency Measurements and Modeling to Enable Advanced Combustion Fuels (Yale University)

Lisa Pfefferle, Principal Investigator
Yale University
305 Mason Laboratory
New Haven, CT 06511
E-mail: lisa.pfefferle@yale.edu

Yuan Xuan, Principal Investigator
The Pennsylvania State University (PSU)
105 Research East Building
University Park, PA 16802
E-mail: yux19@engr.psu.edu

Kevin Stork, DOE Technology Development Manager
U.S. Department of Energy
E-mail: Kevin.Stork@ee.doe.gov

Start Date: May 1, 2017 End Date: April 30, 2020
Project Funding: $1,452,787 DOE share: $1,307,505 Non-DOE share: $145,282

Project Introduction

Biofuels can benefit society by reducing emissions of carbonaceous soot particles from motor vehicles. Soot emissions are the second largest source of climate change [1], and they contribute to ambient fine particulate matter that causes over three million deaths worldwide each year [2]. As a consequence of these issues, particulate emissions are regulated, and engine companies frequently have to install particulate filters, which cost thousands of dollars and require periodic cleaning to remove noncombustible ash [3].

The amount of soot formed in an engine depends strongly on the chemical structure of the fuel; therefore, as biomass-derived fuels begin to replace petroleum-derived fuels, an opportunity exists to achieve lower emissions at lower costs. Biofuels normally contain oxygenated hydrocarbons, and the oxygen atoms in these molecules can hinder the formation of aromatic species that serve as precursors to soot particles [4].

To fully exploit this opportunity, stakeholders need information that describes the effects of biofuel composition on soot formation. This information includes: (1) lists of possible biofuel components ranked by their soot-forming propensities; (2) empirical models and simulations that can extend these rankings to potentially interesting biofuel components that have not yet been synthesized and tested; (3) engineering metrics that combine sooting tendencies with other fuel properties—volatility, cetane number, etc.—to predict emissions from specific engine configurations; and (4) validated chemical kinetic models that enable computational fluid dynamics (CFD) simulations of soot formation in engines. Major challenges are that these items need to be available from laboratory-scale research in advance of direct engine testing, they need to cover the broad range of biofuel compositions being considered as possible blendstocks, and they need to cover the wide variety of engine configurations available for current and future use (spark ignition, compression ignition, multimode, etc.), each of which has its own unique mixing conditions.

Objectives

Overall Objectives

- Produce a database of measured soot-forming propensities for hydrocarbons from the chemical families that constitute petroleum-derived fuels and possible biomass-derived blendstocks. This database will enable stakeholders to rationally select the biofuels that offer the lowest cost path to meeting emissions regulations.

- Develop engineering metrics that combine the database of laboratory-scale sooting tendencies with other fuel properties (volatility, heat of vaporization, cetane number, viscosity, etc.) to predict the soot emissions from real combustion engines. These metrics will allow a single sooting tendency database to be applied to a wide range of engine configurations, including spark ignition, compression ignition, and advanced concepts such as multimode.

- Test the ability of detailed chemical kinetic mechanisms to reproduce the measured sooting tendencies. Once these mechanisms have been validated, they can be used in CFD simulations to optimize engine designs to emit the least possible particulates.

Fiscal Year 2019 Objectives

- Measure the sooting tendencies of at least 25 commercially available hydrocarbons and 25 bio-blendstock samples that have been produced by researchers at DOE National Laboratories who are part of the Co-Optimization of Fuels and Engines (Co-Optima) High Performance Fuels Team.

- Use the sooting tendency defined in this work to produce engineering metrics for spark ignition fuels that account for the impact of ethanol and other oxygenated components.

- Validate a detailed chemical kinetic mechanism for 15 spark ignition blendstocks and perform sensitivity analysis to identify the key soot formation pathways from these blendstocks.

Approach

This project has defined a fundamental fuel property called yield sooting index (YSI) that quantifies the tendency of fuels to form particulates in combustion systems. YSI is determined by adding a small amount of the test fuel to a laboratory-scale methane/air flame and then measuring the flame's maximum soot concentration. The underlying idea is that if the test fuel has a lesser propensity to form soot than another fuel, then it will form less soot when added to the flame and a smaller soot concentration will be measured.

The YSI methodology offers several benefits:

- Each measurement requires a small volume of the test fuel (0.1 ml). For perspective, the ASTM International smoke point test requires 100 times as much (10 ml) [5]. This difference allows a wider range of biofuels to be studied, since they are typically produced in milliliter or smaller quantities during the research phase.

- The YSI approach enables a large number of samples to be processed in a short time. Over 50 fuel samples were tested during Fiscal Year 2019.

- The YSI flames are well defined and can be computationally simulated with perturbation methods that reduce the computational expense of large kinetic mechanisms. Thus, the YSI data can be used to test kinetic mechanisms of soot formation, even mechanisms that include thousands of species.

Results

The soot-forming characteristics of over 50 novel biofuels were studied experimentally and numerically. The total uncertainty in the experiments is typically ±5%. The results of these studies enable the development of new fuels that will offer a lower cost pathway to meeting emissions regulations, and they contribute to CFD

simulations that can optimize engines for low emissions early in the design stage. To make the measured data accessible to all stakeholders, it is being posted to the Co-Optima Fuel Properties Database [6], an online YSI database [7], and a YSI prediction tool developed at the National Renewable Energy Laboratory (NREL) [8]. Some of the key results are listed here:

- Furans were demonstrated to have better sooting properties than conventional gasolines. For example, Figure II.26.1 shows that the YSI of 2-methylfuran (41.5) is lower than those of the four Co-Optima test gasolines (TGs; YSI = 60.9 to 114.9). 2-Methylfuran constitutes 40 weight percent of the furan mixture that was selected as one of the Co-Optima top ten spark ignition bio-blendstocks [9]. The TGs are refinery-derived fuels with enhanced concentrations of alkanes, olefins, cycloalkanes, and aromatics [10]; they serve as a useful benchmark because they bracket the compositions of gasolines currently on the market. While 2-methylfuran has favorable soot emissions properties, Figure II.26.1 shows that some other carbohydrate-derived molecules with the same number of carbon atoms have even lower sooting tendencies. In particular, cyclopentanone, which is another of the top ten bio-blendstocks [9], has a YSI of only 22.0.

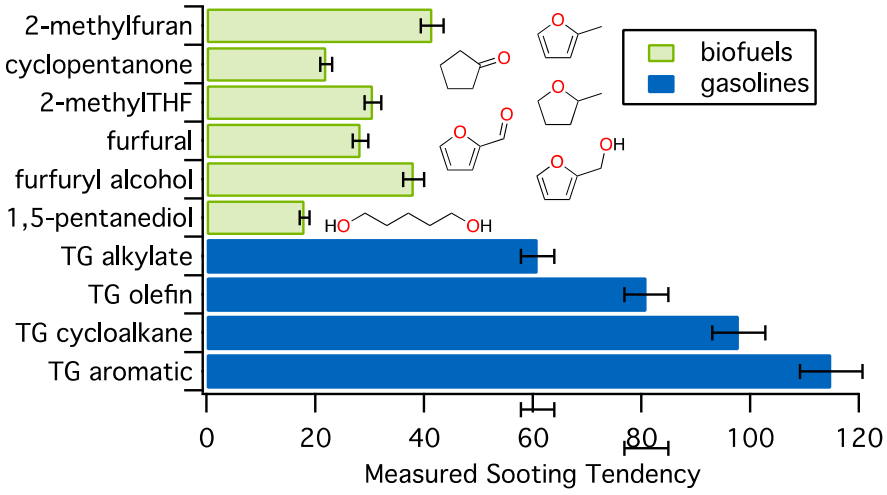

Figure II.26.1 Sooting tendencies measured for several carbohydrate-derived biofuel molecules and for the Co-Optima test gasolines. A larger value corresponds to a sootier fuel. THF = tetrahydrofuran; TG = Co-Optima Test Gasoline. (Figure: Charles McEnally, Yale)

- This project assessed the sooting behavior of dozens of advanced fuel samples generated by researchers at DOE National Laboratories. As an example, Figure II.26.2 shows data for a mixture of camphorane isomers synthesized by researchers at Los Alamos National Laboratory. The camphorane was synthesized by cyclodimerization and hydrogenation of myrcene, a terpene that can be produced at industrial scale by fermentation of lignocellulosic carbohydrates using metabolically engineered microorganisms. The left side of the figure shows the four isomers of camphorane; with a molecular formula of $C_{20}H_{40}$, it contains enough carbon to be a suitable diesel fuel, and it has a high energy density due to the central cyclohexyl ring. The YSI measurements show that while the ring increases soot relative to n-alkanes, the overall sooting tendency is still less than diesel fuel. The right side of the figure shows that adding camphorane to diesel fuel linearly decreases soot production from the blend.

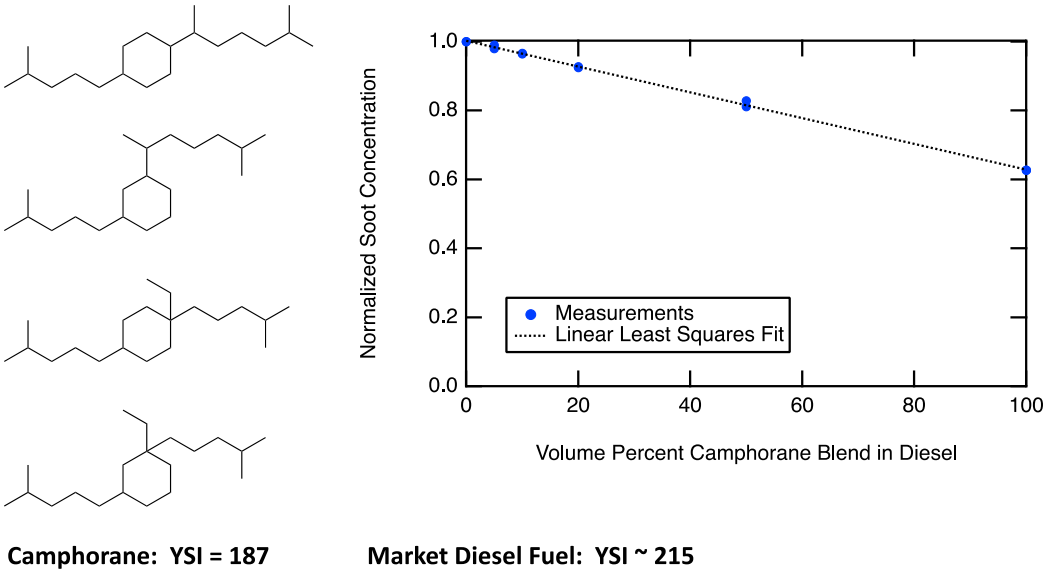

Figure II.26.2 Left: The four isomers of camphorane. Right: Normalized soot concentration measured in the YSI flame for mixtures of a camphorane blend and a summer blend market diesel fuel purchased in the Albuquerque, New Mexico, area. The mixtures were injected at a fixed volumetric flow rate of 100 µL/h. The soot concentrations were normalized to the pure diesel fuel. (Figure: Charles McEnally, Yale)

- The empirical sooting tendency measured in this work (YSI) was demonstrated to better capture the effects of oxygen on soot formation than double bond equivalent (DBE). DBE serves as the sooting tendency parameter in the particulate mass index (PMI) model [11], which is widely used in the automotive industry to capture the effects of fuel properties on soot emissions from direct injection spark ignition engines. Figure II.26.3 compares the measured YSI with DBE for the 500+ hydrocarbons that have been measured in this project. In general, the two parameters correlate. However, the YSI can vary by up to a factor of 10 for a given DBE (note the log scale on the vertical axis). Furthermore, oxygenated species, such as the furans highlighted in the figure (green triangles), fall below the correlation, which shows that DBE systematically overpredicts their sooting tendency. The primary advantage of DBE over YSI is that it can be trivially calculated for any hydrocarbon; however, researchers at NREL have developed a predictive tool for YSI [8], which allows YSI to be calculated as easily as DBE for most fuel-relevant hydrocarbons. Given this model, the researchers have been able to formulate sooting indices analogous to PMI that use YSI instead of DBE and offer improved correlations with measured engine emissions [12].

- This project has validated and improved a detailed chemical kinetic mechanism for 20 promising spark ignition bio-blendstocks identified by the Co-Optima program. The mechanism was initially developed by researchers at Lawrence Livermore National Laboratory [13]. The YSI of each bio-blendstock was simulated using a one-dimensional flamelet-based solver, and then a modified sensitivity coefficient formulation was used to identify the most important reaction pathways. The predicted YSIs agree well with measurements for all fuels except 2,5-dimethylfuran (25DMF). The sensitivity analysis identified the reactions shown in Figure II.26.4 as the most important fuel consumption pathways for 25DMF; these reactions are currently being re-evaluated to improve the prediction. Once the mechanism is fully validated, it can be used to accurately predict soot concentrations in engine CFD simulations.

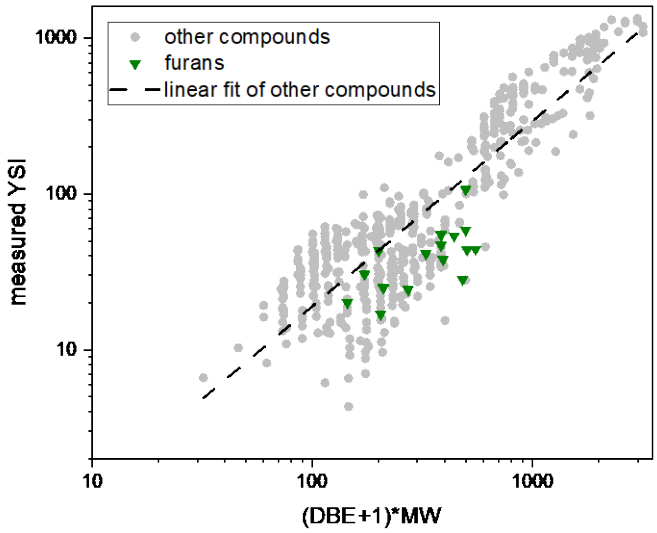

Figure II.26.3 Empirical YSIs compared with DBE for over 500 hydrocarbons. The specific quantity plotted on the horizontal axis is (DBE+1)*MW, where MW is molecular weight. This functional form was chosen to match the PMI model [11], which is based on the weight percent of each fuel component (not mole percent), and which adds 1 to DBE since fuels with DBE = 0 also produce soot.
(Figure: Junqing Zhu, Yale)

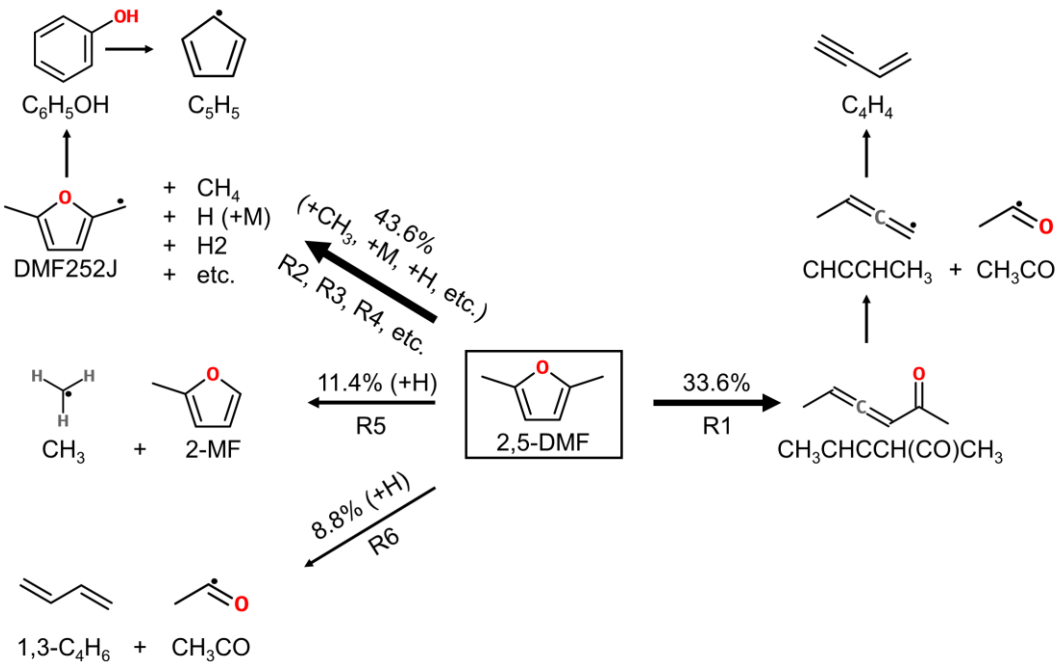

Figure II.26.4 The major consumption pathways of 25DMF. (Figure: Hyunguk Kwon, PSU)

- A molecular dynamics methodology was developed to predict YSIs of fuels with novel chemical structures. These fuels cannot be studied with CFD simulations because their chemical kinetic mechanisms are unknown. Furthermore, their sooting tendencies cannot be estimated from empirical methods such as the NREL model [8] because their structures differ from the species in the training dataset. The molecular dynamics simulations track the motion of a random assembly of fuel and oxidizer molecules as they move around in the force field created by all of the atoms in the system. The force field used in this work, ReaxFF [14], allows the species to react and form new products. As an example, Figure II.26.5 shows results for dicyclopentylmethane (DCPM), a potential biofuel that has a large energy density due to its pair of strained C5 rings (see the chemical structure on the top left). The products are mostly ethylene and other small alkenes (see right panel)—not dehydrogenation products of the cyclopentyl rings—which indicates that DCPM has a low sooting tendency.

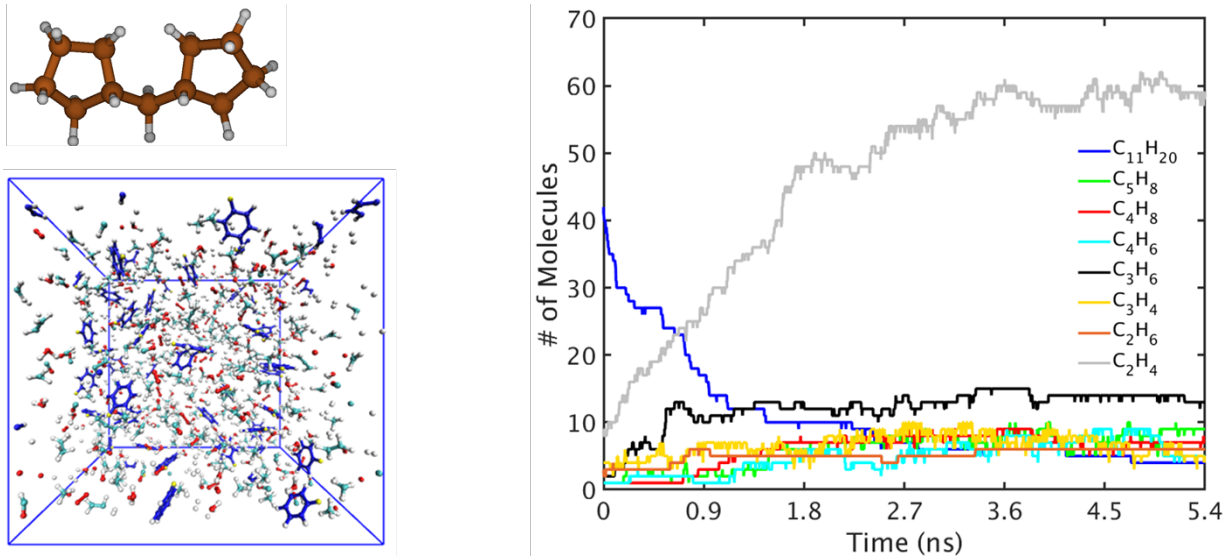

Figure II.26.5 Top left: The chemical structure of DCPM. Bottom left: Visualization of the computational domain during a ReaxFF molecular dynamics simulation. Right: The products formed from DCPM as a function of time. (Figure: Yuan Xuan, PSU)

Conclusions

The sooting tendency parameter developed in this project, YSI, is a valuable method for assessing the sooting behavior of novel biofuels. The key advantage of YSI is that it enables high-throughput measurements with low sample volumes (<0.1 mL), which allowed over 50 biofuels to be tested in Fiscal Year 2019, including many that had been custom-synthesized at DOE National Laboratories. These measurements showed that properly chosen biofuels have the potential to reduce soot formation in internal combustion engines. Since YSI employs a well-defined laboratory-scale flame, the results can be simulated numerically. Simulations in Fiscal Year 2019 validated detailed chemical kinetic mechanisms, identified key reaction pathways, and provided insight into the emissions characteristics of hypothetical fuels that have not yet been synthesized.

Key Publications

1. McEnally, C.S., et al. 2019. "Sooting Tendencies of Co-Optima Test Gasolines and Their Surrogates." *Proc. Combust. Inst.* 37: 961–968.

2. Jain, A., D.D. Das, C.S. McEnally, L.D. Pfefferle, and Y. Xuan. 2019. "Experimental and Numerical Study of Variable Oxygen Index Effects on Soot Yield and Distribution in Laminar Co-Flow Diffusion Flames." *Proc. Combust. Inst.* 37: 859–867.

3. Montgomery, M.J., D.D. Das, C.S. McEnally, and L.D. Pfefferle. 2019. "Analyzing the Robustness of the Yield Sooting Index as a Measure of Sooting Tendency." *Proc. Combust. Inst.* 37: 911–918.

4. Kim, S., et al. 2019. "Experimental and Theoretical Insight into the Soot Tendencies of the Methylcyclohexene Isomers." *Proc. Combust. Inst.* 37: 1083–1090.

5. Staples, O., J.H. Leal, P.A. Cherry, C.S. McEnally, L.D. Pfefferle, T.A. Semelsberger, A.D. Sutton, and C.M. Moore. 2019. "Camphorane as a Renewable Diesel Blendstock Produced by Cyclodimerization of Myrcene." *Energy Fuels* 33: 9949–9955.

6. Kwon, H., A. Jain, C.S. McEnally, L.D. Pfefferle, and Y. Xuan. 2019. "Numerical Investigation of the Pressure-Dependence of Yield Sooting Indices for *n*-Alkane and Aromatic Species." *Fuel* 254: article 115574.

7. Huo, X., et al. 2019. "Tailoring Diesel Bioblendstock from Integrated Catalytic Upgrading of Carboxylic Acids: A "Fuel Property First" Approach." *Green Chem.* 21: 5813–5827.

References

1. Bond, T.C., et al. 2013. "Bounding the Role of Black Carbon in the Climate System: A Scientific Assessment." *J. Geophy. Res. Atmos*. 118: 5380–5552.

2. Stanaway, J.D., et al. 2018. "Global, Regional, and National Comparative Risk Assessment of 84 Behavioural, Environmental and Occupational, and Metabolic Risks of Clusters of Risks for 195 Countries and Territories, 1990–2017: A Systematic Analysis for the Global Burden of Disease Study 2017." *Lancet* 392: 1923–1994.

3. Ou, L., et al. 2019. "Co-Optimization of Heavy-Duty Fuels and Engines: Cost Benefit Analysis and Implications." *Environ. Sci. Technol*. In press. DOI: 10.1021/acs.est.9b03690.

4. Westbrook, C., W. Pitz, and H. Curran. 2006. "Chemical Kinetic Modeling Study of the Effects of Oxygenated Hydrocarbons on Soot Emissions from Diesel Engines." *J. Phys. Chem. A* 110: 6912–6922.

5. ASTM International. 2018. *D1322-18: Standard test method for smoke point of kerosene and aviation turbine fuel*. ASTM International: West Conshohocken, PA.

6. Fioroni, G.M. 2019. "Co-Optimization of Fuels & Engines: Fuel Properties Database." https://fuelsdb.nrel.gov/fmi/webd/FuelEngineCoOptimization.

7. McEnally, C.S., D.D. Das, and L.D. Pfefferle. 2017. "Yield Sooting Index Database Volume 2: Sooting Tendencies of a Wide Range of Fuel Compounds on a Unified Scale." Harvard Dataverse. https://doi.org/10.7910/DVN/7HGFT8.

8. St. John, P.C., and Seonah Kim. 2019. "YSI Estimator." https://ysipred.herokuapp.com.

9. Gaspar, D. 2019. "Top Ten Blendstocks for Turbocharged Gasoline Engines: Bio-Blendstocks with Potential to Deliver the Highest Engine Efficiency." *PNNL-28713*. Pacific Northwest National Laboratory: Richland, WA.

10. Vuilleumier, D., and M. Sjöberg. 2017. "Significance of RON, MON, and LTHR for Knock Limits of Compositionally Dissimilar Gasoline Fuels in a DISI Engine." *SAE Int. J. Engines* 10: 938–950.

11. Aikawa, K., T. Sakurai, and J.J. Jetter. 2010. "Development of a Predictive Model for Gasoline Vehicle Particulate Matter Emissions." *SAE Int. J. Fuels Lubr*. 3: 510–522.

12. St. John, P.C., S. Kim, and R.L. McCormick. 2019. "Development of a Data-Derived Sooting Index Including Oxygen-Containing Fuel Components." *Energy Fuels* 33: 10290–10296.

13. Mehl, M., et al. 2017. "A Comprehensive Detailed Kinetic Mechanism for the Simulation of Transportation Fuels." 10th U.S. Combustion Meeting. Available at http://hdl.handle.net/10754/627140.

14. van Duin, A.C.T., S. Dasgupta, F. Lorant, and W.A. Goddard III. 2001. "ReaxFF: A Reactive Force Field for Hydrocarbons." *J. Phys. Chem. A* 105: 9396–9409.

Acknowledgements

Co-Principal Investigator: Charles McEnally (Yale). We are very proud of our students and want to acknowledge their hard work: Patrick Cherry, Facheng Guo, Rafael Gottlieb, Binhang Hu, Amy Kolor, Matthew Montgomery, Suheyla Tozan, Junqing Zhu (Yale); Hungyuk Kwon, Karthigeyan Mohhan (PSU). External collaborators: Courtney Ryan Ford, Cameron Moore, Andrew Sutton (Los Alamos National Laboratory); Simon Lapointe, William Pitz, Scott Wagnon, Kuiwen Zhang (Lawrence Livermore National Laboratory); Brian Etz, Gina Fioroni, Thomas Foust, Xiangchen Huo, Nabila Huq, Seonah Kim, Robert McCormick, Peter St. John, Derek Vardon (NREL); Adri van Duin (PSU).

III Alternative Fuel Engines

III.1 Expanding the Knock/Emissions/Misfire Limits for the Realization of Ultra-Low Emissions, High Efficiency Heavy Duty Natural Gas Engines (Colorado State University)

Daniel B. Olsen, Principal Investigator
Colorado State University (CSU)
Mechanical Engineering Department
Fort Collins, CO 80523-1374
E-mail: daniel.olsen@colostate.edu

Hui Xu, Principal Investigator
Cummins Inc.
1900 McKinley Avenue
Columbus, IN 47201
E-mail: hui.xu@cummins.com

Gregory Hampson, Principal Investigator
Woodward, Inc.
1081 Woodward Way
Fort Collins, CO 80524
E-mail: Greg.Hampson@woodward.com

Kevin Stork, DOE Technology Development Manager
U.S. Department of Energy
E-mail: Kevin.Stork@ee.doe.gov

Start Date: October 1, 2018 End Date: September 30, 2019
Project Funding: $577,027 DOE share: $463,242 Non-DOE share: $113,785

Project Introduction

The Vehicle Technologies Office is funding early-stage, high-risk research to develop technology upon which industry can implement innovative transportation energy technologies that increase efficiency, decrease cost, and expand use of domestic energy sources, such as natural gas (NG). To improve the viability of medium- and heavy-duty vehicles, the NG engine efficiency must be closer to that of diesel. This work is addressing fundamental limitations to achieving diesel-like efficiencies in heavy-duty on-road NG engines. Engine knock and misfire are barriers to pathways leading to higher-efficiency engines. The problem is further complicated by low emissions limits and the wide range of chemical reactivity in pipeline-quality NG.

This study includes three research areas focused on enabling technologies for development of high-efficiency stoichiometric engines with cooled exhaust gas recirculation (EGR) and three-way catalysts. The research areas are (1) fundamental combustion studies to characterize chemical reactivity, flame speed, and end-gas autoignition (EGAI) at elevated pressures and temperatures for $CH_4/C_2H_6/C_3H_8$/EGR gas blends; (2) design strategies for fast and stable combustion and higher dilution tolerance; and (3) advanced control methodologies to maintain stable operation between expanded knock and misfire limits with realistic constraints (e.g., variability in fuel reactivity and transient load conditions) and to explore controlled EGAI strategies.

Objectives

The overarching goal of this research is to address fundamental limitations to achieving diesel-like efficiencies in heavy-duty on-road NG engines. The focus is on the Cummins 15-liter heavy-duty engine platform, which has a baseline diesel efficiency of 44% at peak torque. The baseline NG engine with baseline technology of open chamber spark ignition (SI), cooled EGR, stoichiometric air/fuel ratio, and a three-way catalyst is estimated to have an efficiency of 39%. Thus, the main project goal is to increase the peak torque efficiency of a 15-liter NG engine by 5.0 efficiency points (13% relative change) from 39% to 44%.

Overall Objectives

To achieve the main project goal, the following four key project objectives are identified:

- Characterize EGAI phenomena for NG/air/EGR mixtures of varying reactivity under engine-like conditions
- Validate/refine tools for closed-cycle engine combustion design with detailed chemical kinetics (CHEMKIN), three-dimensional (3-D) computational fluid dynamics (CFD, CONVERGE), and cycle simulation (GT-Power)
- Optimize combustion chamber design as informed by experiments and validated models
- Develop advanced real-time control algorithms to facilitate expansion of EGR, knock, and misfire limits; tolerance and adaptation to variable fuel reactivity (methane index from 65 to 90); and controlled EGAI.

Fiscal Year 2019 Objectives

Project objectives for Fiscal Year 2019 are:

- Design, assemble, and test EGR cart for cooperative fuel research (CFR) engine testing
- Demonstrate effect of EGR on flame speed and EGAI in the CFR engine and rapid compression machine (RCM)
- Validate reduced chemical kinetic mechanism (~50 species) for use in engine and RCM modeling
- Complete CONVERGE and GT-Power models of CFR engine and validate with blind tests.

Approach

This work is being conducted with a combined experimental and computational approach with fundamental experiments utilizing (1) a one-of-a-kind RCM and laser ignition system that enables measurement of flame speed and EGAI at engine relevant conditions; (2) a variable compression ratio CFR engine to examine knock propensity, EGR limits, emissions tradeoffs, and the relationship between EGAI heat release fraction and knock intensity; and (3) a Cummins single cylinder 2.5-liter engine to develop advanced control algorithms under realistic operating conditions. The RCM and CFR experiments are used to systematically validate computational modeling with detailed chemical kinetics using GT-Power, CONVERGE, and CHEMKIN, which facilitate the development of fully validated and predictive models. Modeling of the 2.5-liter Cummins platform informs advanced control strategies via a better understanding of the underlying combustion phenomena. A 2.5-liter single cylinder engine (SCE) based on the Cummins X15 diesel engine platform is designed, fabricated, and supplied to CSU for this research by Cummins Inc. Real-time combustion controls to facilitate controlled EGAI are an integral part of this work. This will be accomplished using the large engine control module manufactured by Woodward, Inc.

Results

Key accomplishments for Fiscal Year 2019 are listed below:

- Demonstrated functionality of the EGR cart for the CFR engine, supplying EGR rates well beyond the engine EGR limit, exceeding the 40% EGR requirement
- Evaluated the effect of EGR on flame speed and EGAI in the CFR engine and RCM
- Developed and validated a reduced chemical kinetic mechanism (~50 species) within 5% accuracy for use in engine and RCM modeling
- Completed CONVERGE and GT-Power models of the CFR engine and validated with blind tests
- Designed, fabricated, and installed Cummins X15 SCE at CSU.

RCM Ignition Delay. The RCM test results contribute to objectives related to the impact of EGR and fuel reactivity on combustion and the development of the reduced chemical kinetic mechanism. The change that EGR substitution has on pipeline quality NG mixtures from a chemical kinetic standpoint was explored using the RCM. The RCM uses dual horizontally opposed pistons to maintain symmetrical compression, an Nd:YAG (neodymium-doped yttrium aluminum garnet) laser as the ignition system, and Schlieren imaging to observe flame propagation rates. Three different fuel compositions were tested, indicated as dry, mid, and wet, with dry having the highest CH_4 mole fraction and wet having the lowest. Flame propagation rate is very sensitive to EGR substitution. As EGR substitution increases, the flame speed of the mixture decreases, as shown in Figure III.1.1. The rate at which the flame speed decreases is unique to each fuel blend. This indicates that EGR substitution could impact the same engine in different ways if the fuel reactivity changes. This would be important in mobile SI NG engines. As fuel reactivity increases, the fraction of EGAI also increases. As EGR substitution increases, the fraction of EGAI also increases due to slower flame speeds consuming less fuel in more time, allowing more fuel to be ignited as an end-gas.

Reduced Chemical Kinetic Mechanism. Aramco 3.0 [1] was selected based on its ignition delay and flame speed performance compared to published NG combustion data. The original Aramco 3.0 mechanism was reduced to 51 species. Mechanism reduction is often required to make CFD analysis feasible with a reasonable computation cost. This reduction was performed using ANSYS Reaction Workbench. The reduction was done using ignition delay as the tuning parameter with the target points being predicted by the original Aramco 3.0 mechanism. The reduced mechanism is used in a zero-dimensional (0-D) model to predict the ignition delay time. The 0-D modeling and the reduced mechanism were used extensively to predict the ignition delay time over a wide range of conditions. Figure III.1.2 summarizes the comparison between RCM measured ignition delay and 0-D model predicted ignition delay. The target is <15%, and the predictions are better than 5%. The range of ignition delay times investigated in the experiments is about 5 ms. This is equivalent to the time of 36 crank angle degrees (CADs) of engine rotation at 1,200 RPM. The range of 36 CADs covers the expected range of EGAI occurrence.

CFR Engine Combustion. The CFR engine work supports the objective to determine the impact of EGR on combustion and engine performance. The impact of EGR was examined in the CFR engine to understand the impact of EGR on stoichiometric, SI NG engines. This was implemented using a custom EGR cart that controlled the EGR rate independent of engine conditions. Engine efficiency and combustion statistics were utilized to evaluate performance. The addition of EGR to baseline CFR operating points initially increased efficiency until 23% EGR rate, then decreased efficiency values for any greater EGR rate. The knock intensity values decreased with increasing EGR rates, allowing for the knock threshold to be expanded. Operating at higher critical compression values compared to that of 0% EGR allowed for a 3.4% efficiency gain. In the absence of design or operating parameter adjustments, increased EGR reduces performance due to slower combustion rates. This is illustrated by the mass fraction burn curves presented in Figure III.1.3. Operating at the new critical output power of 1,250 kPa indicated mean effective pressure instead of 800 kPa allowed for a 4.5% efficiency gain at 22% EGR rate. The optimal operational window for the CFR engine with EGR was found to be between 15% and 20% EGR rate with a compression ratio around 10.5.

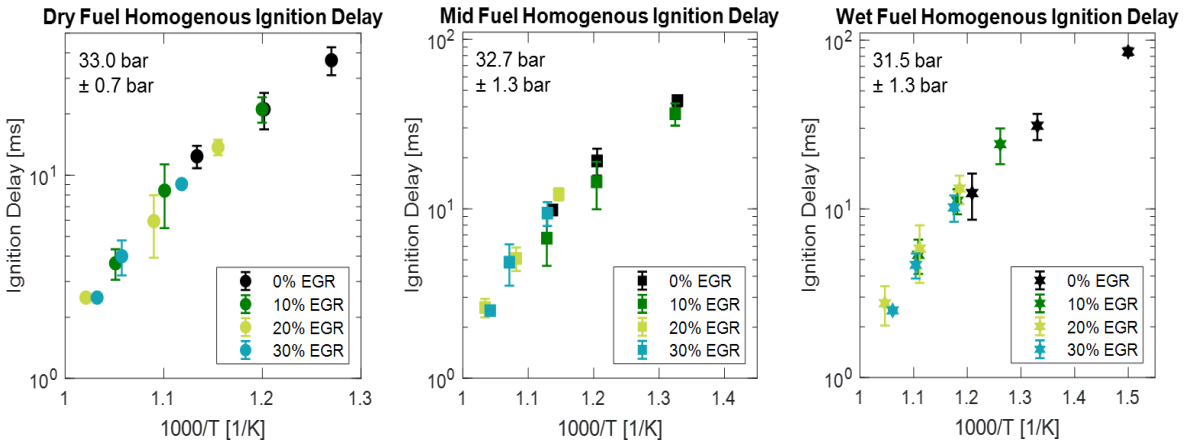

Figure III.1.1 Homogenous ignition delay results of fuel blends with standard (contains NO, CO) EGR substitution. Ignition delay is defined as time from the RCM pistons reaching top dead center to time of maximum heat release rate.

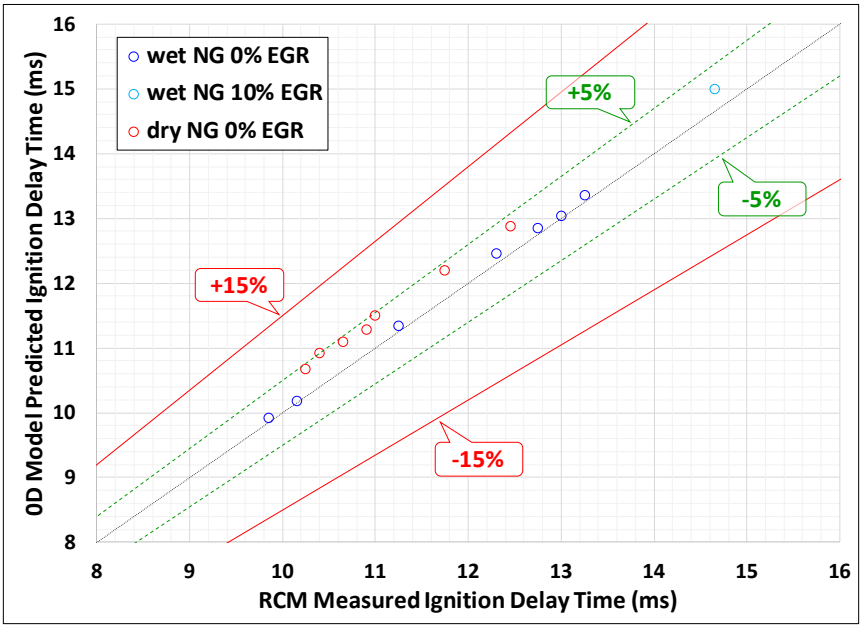

Figure III.1.2 Ignition delay comparison between 0-D model prediction and RCM measurement

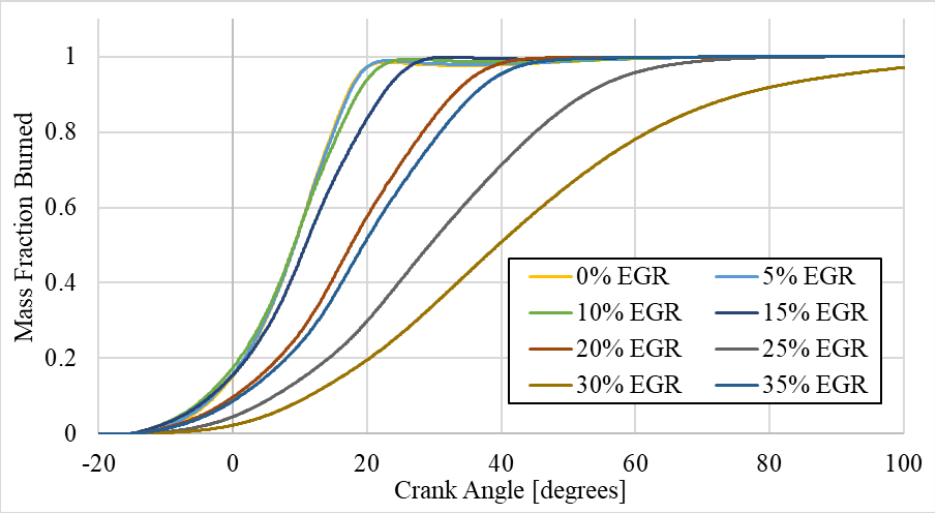

Figure III.1.3 Mass fraction burned for the CFR engine from 0% to 35% EGR rate

Engine Simulation. A 3-D CFD model of the CFR engine was developed and calibrated to predict NG combustion and knocking behavior, a Fiscal Year 2019 objective. The model was developed using a Reynolds-averaged Navier–Stokes turbulence model, a combined G-Equation and SAGE approach in the combustion model, and was used to simulate both non-knocking and knocking cases. The CFR engine geometry was provided by Argonne National Laboratory [2] and updated to better match the in-house CFR engine at CSU. Additionally, a one-dimensional GT-Power model of the CFR engine was used to compute the appropriate boundary and initial conditions. The model is capable of predicting cylinder pressures, heat releases, and combustion phasing satisfactorily well for both non-knocking and knocking cases, including different knocking intensity levels. Figure III.1.4 shows the mass fractions of OH and CH_2O for crank angles of 11° and 11.5° after top dead center, illustrating conditions just before and after EGAI, or knock. An iso-surface of 2,200 K is used to show the flame front, and the cylinder pressure trace has a vertical bar to better visualize its location. Despite discrepancies in the initial kernel growth in the non-knocking case and the knock onset in the knocking cases, if one is interested in predicting peak cylinder pressures and their crank-angle of occurrence as well as combustion phasing, the model is suitable for such simulations with reasonably good agreement with the experimental data. The model can be used to study the effects of engine operating conditions and NG fuel reactivity/composition on engine knock.

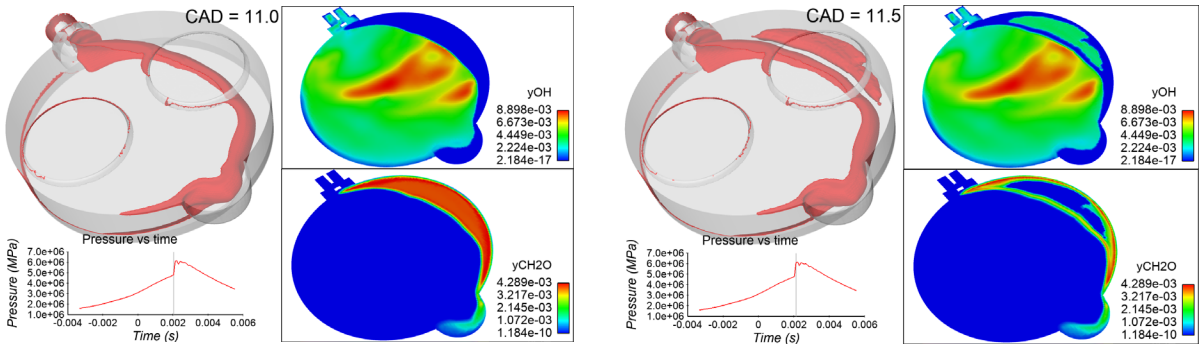

Figure III.1.4 Flame front and OH and CH_2O mass fractions at 11° after top dead center, right before EGAI occurs (left). Flame front and OH and CH_2O mass fractions at 11.5° after top dead center, when EGAI is occurring (right).

2.5-Liter Single Cylinder Engine. The development of a heavy-duty single cylinder NG engine is necessary to achieve our project goal, which is to demonstrate diesel-like efficiencies for a similarly sized NG engine. A GT-Power model was developed for the X15 SCE to support initial engine design and future design optimization simulations. The design and development of the X15 SCE took place at Cummins. This effort included base-engine configuration selection, engine design modifications, unique-component designs, and SCE GT-Power model development. The general approach was to convert a six cylinder engine to a single cylinder engine by enabling combustion for Cylinder 6 and deactivating Cylinders 1–5. A spark plug adaptor was designed for Cylinder 6, and diesel injectors were removed for Cylinders 1–5. Sealing of all cylinders and cooling to the Cylinder 6 spark plug were considered to ensure safe and reliable SI operation. For Cylinder 6, a baseline piston bowl shape was designed for NG SI operating condition. An adaptor was needed for proper fitment of the spark plug. Pistons 1–5 were modified to eliminate compression due to the piston movement.

The piston mass was adjusted to match the mass of the firing cylinder piston. A piston ring combination to minimize the piston movement friction was selected. A new camshaft design was produced for NG SI engine operating conditions. Swirl plates were designed for the Cylinder 6 head, and various configurations were characterized on a flow bench. The SCE was delivered to CSU in July 2019.

Conclusions

- The use of EGR expands the knock limit while reducing NO_x emissions and increasing engine efficiency as much as 4.5% through increased compression ratio and power density. The highest EGR rate that demonstrates beneficial gains on the CFR engine is 23%; the optimal EGR rate is 19%.
- As EGR substitution increases, the flame speed of the mixture decreases. The rate at which the flame speed decreases varies with fuel composition.
- The reduced chemical kinetic mechanism (~50 species) for use in engine and RCM modeling is shown to predict ignition delay within 5% accuracy.
- The 3-D CFD model of the CFR engine predicts NG combustion satisfactorily well for both non-knocking and knocking cases, including different knocking intensity levels.

Key Publications

1. Zdanowicz, Andrew, Jeffrey Mohr, Jessica Tryner, Kara Gustafson, Bret Windom, Daniel Olsen, and Anthony J. Marchese. 2019. “End-Gas Autoignition Fraction and Flame Propagation Rate in Laser-Ignited Primary Reference Fuel Mixtures at Elevated Temperature and Pressure.” 11th U.S. National Combustion Meeting (March).
2. Bestel, Diego, Bret Windom, Daniel Olsen, Scott Bayliff, and Hui Xu. 2019. “3-D Modeling of the CFR Engine for the Investigation of Knock on Natural Gas.” 11th U.S. National Combustion Meeting (March).
3. Mohr, Jeffrey, Andrew Zdanowicz, Jessica Tryner, Kara Gustafson, Juan Venegas, Bret Windom, Daniel Olsen, and Anthony Marchese. 2019. “Ignition, Flame Propagation, and End-Gas Autoignition Studies of Natural Gas/EGR Blends in a Rapid Compression Machine.” WSSCI Fall Technical Meeting (October).
4. Zdanowicz, Andrew, Jeffrey Mohr, Jessica Tryner, Kara Gustafson, Bret Windom, Daniel B. Olsen, Gregory Hampson, and Anthony J. Marchese. 2019. “Effect of Fuel Reactivity and End-Gas Temperature on Autoignition and Flame Propagation Rate in Primary Reference Fuel Mixtures at Elevated Temperature and Pressure.” WSSCI Fall Technical Meeting (October).

5. Bayliff, Scott, Anthony Marchese, Bret Windom, and Daniel Olsen. 2019. “The Effect of EGR on Knock Suppression, Efficiency, and Emissions in a Stoichiometric, Spark Ignited, Natural Gas Engine.” WSSCI Fall Technical Meeting (October).

6. Bestel, Diego, Bret Windom, Daniel Olsen, Anthony Marchese, Scott Bayliff, and Hui Xu. 2019. “3-D Modeling of the CFR Engine for the Investigation of Knock on Natural Gas.” WSSCI Fall Technical Meeting (October).

References

1. Zhou, C-W., Y. Li, U. Burke, C. Banyon, K.P. Somers, S. Khan, J.W. Hargis, T. Sikes, E.L. Petersen, M. AlAbbad, A. Farooq, Y. Pan, Y. Zhang, Z. Huang, J. Lopez, Z. Loparo, S.S. Vasu, and H.J. Curran. 2018. “An Experimental and Chemical Kinetic Modeling Study of 1,3-Butadiene Combustion: Ignition Delay Time and Laminar Flame Speed Measurements.” *Combustion and Flame* 197: 423–438.

2. Pal, P., Y. Wu, T. Lu, S. Som, Y.C. See, and A. Le Moine. 2017. “Multi-Dimensional CFD Simulations of Knocking Combustion in a CFR Engine.” ASME 2017 Internal Combustion Engine Division Fall Technical Conference.

Acknowledgements

Anthony J. Marchese and Bret Windom of CSU were Co-Principal Investigators on this study.

III.2 On-Demand Reactivity Enhancement to Enable Advanced Low-Temperature Natural Gas Internal Combustion Engines (University of Minnesota)

William Northrop, Principal Investigator
University of Minnesota Twin Cities
111 Church Street SE
Minneapolis, MN 55455
E-mail: wnorthro@umn.edu

Kevin Stork, DOE Technology Development Manager
U.S. Department of Energy
E-mail: Kevin.Stork@ee.doe.gov

Start Date: May 1, 2018 End Date: June 30, 2021
Project Funding (FY19): $430,539 DOE share: $339,136 Non-DOE share: $91,403

Project Introduction

On-road natural gas (NG) engines occupy a growing share of the medium- and heavy-duty engine market owing to low fuel cost and the potential for lower criteria emissions. NG engines have been developed for many years as alternatives to diesel engines. Two primary categories of combustion technology are used in commercial NG engines: dedicated spark-ignition (DSI) and dual-fuel compression-ignition. Dual-fuel compression-ignition engines have been shown to achieve higher efficiency than lean-burn DSI engines but require the storage of two fuels on board a vehicle. Onboard fuel reforming, the conversion of a fuel to hydrogen and carbon monoxide (i.e., syngas), has been studied as a means of decreasing the reactivity of diesel fuel for dual-fuel diesel engines or of increasing the lean-burn/dilute limit of gasoline-fueled spark-ignition engines. Reforming has also been studied to enable highly lean or dilute DSI NG engines. However, reforming has largely failed commercially because NG reforming requires a higher temperature and more energy than gasoline or diesel reforming, resulting in low catalyst conversion and poor overall system efficiency.

This research project takes a novel approach by converting a small portion of the incoming methane-containing NG to more reactive, higher-molecular-weight hydrocarbons using a catalytic reaction called oxidative coupling of methane (OCM). These more reactive hydrocarbons created by the OCM process can influence combustion at low (<10%) concentrations in the intake air and can enable highly efficient NG engine combustion modes.

Objectives

The research project goal is to overcome the reactivity barrier of NG as an engine fuel by developing catalytic fuel pretreatment technology to control lean and dilute NG engine combustion modes. The project seeks to determine whether OCM, a catalytic process that converts methane to ethylene and ethane, can be used in NG engines to enhance NG reactivity. Although industrially relevant for polymer synthesis from natural gas, OCM has not previously been studied for vehicular applications. In the proposed work, the project team will refine OCM and methane oxidation catalysts, develop short-contact-time reactors that allow greater selectivity to desired products with lower carbon formation, and demonstrate a thermally integrated reactor. Beyond proving that the novel OCM fuel pretreatment developed in the project can enable low-temperature compression-ignition combustion in a variable-compression-ratio single-cylinder research engine, this project will prove that the overall system can achieve 10% indicated thermal improvement over lean-burn DSI engines through one-dimensional simulation of a multicylinder NG engine.

Overall Objectives

The specific overall goals of the project are as follows:

- Develop an OCM catalyst and metal wash-coating formulation suitable for use in vehicular applications and for reactants and conditions not commonly found in industrial OCM applications
- Simulate and demonstrate that OCM fuel pretreatment technology can enable higher NG reactivity, providing a pathway to 10% higher indicated thermal efficiency compared to lean-burn DSI engines
- Develop and demonstrate a reactor for a single-cylinder engine that combines OCM and exhaust oxidation. This reactor concept will serve as the starting point for scale-up development in follow-on research.

Fiscal Year 2019 Objectives

Fiscal Year (FY) 2019 project objectives were to:

- Determine whether a unique short-contact-time reactor developed in earlier research work is a good candidate for the OCM reaction when compared to traditional premixed monolith or pelleted catalyst beds
- Achieve a milestone to reach 10% methane conversion and 20% selectivity to C2 hydrocarbon products that may consist of ethane, ethylene, and acetylene
- Quantify the performance of wash-coated OCM catalysts, and identify a catalyst material for further use in the project.

Approach

The project includes investigators from two world-class research universities, the University of Minnesota (UMN) and Carnegie Mellon University, in partnership with Johnson Matthey Inc. (JM). Together, they are working to develop onboard OCM reactor technology for enabling highly efficient NG engines. The project team has a unique set of skills and capabilities for developing the proposed novel fuel pretreatment reactor technology. Both UMN and JM have microreactor systems and bench-scale reactors, along with the analytics necessary to develop new reactor technology needed to meet the project objectives.

UMN has developed short-contact-time reactors for fuel-reforming reactions in the past and will determine whether similar technology is appropriate for the OCM reaction. With catalyst wash-coating technology developed by JM for metal substrates, the project will develop a compact, engine-scale reactor using either the short-contact-time concept or a more traditional premixed long-residence-time configuration. The project team will decide which reactor concept is most appropriate for transportation applications where compactness, durability, and high performance are required.

Results

In FY 2019, the team developed a bench-scale reactor and tested OCM catalysts at UMN and in a traditional microreactor setup located at JM facilities. Simulations were conducted to validate literature chemical pathways for the OCM catalysts and to evaluate engine-scale reactor concepts appropriate for single-cylinder engine experiments to be conducted later in the project. A summary of the main results are as follows:

- Selected a Sr/La_2O_3 catalyst for all future project work based on its selectivity and conversion at low temperatures.
- Evaluated the short-contact-time reactor concept in both experiments and simulation. A decision was made to use more traditional monolith-supported catalysts for bench and engine experiments in future budget periods.

- Achieved the first budget period go/no-go milestone of greater than 10% methane conversion and 20% selectivity to C2 hydrocarbon products that may consist of ethane, ethylene, and acetylene.

The project conducted a full range of microreactor experiments with two candidate OCM catalysts, as shown in Figure III.2.1. The catalysts were tested in a microreactor setup at JM research facilities. Both SrLa/CaO and Sr/La_2O_3 catalysts were evaluated in the study over two molar oxygen-to-carbon (O/C) ratios and three temperatures. It is clear from the figure that the Sr/La_2O_3 material had superior methane conversion at all temperatures and space velocities and maintained high conversion at lower temperatures. The selectivity of the Sr/La_2O_3 catalyst was lower at high temperatures but higher at low temperatures than that of the SrLa/CaO catalyst at low gas hourly space velocity. Based on these data, the Sr/La_2O_3 catalyst was chosen for future project research. Furthermore, the SrLa/CaO catalyst encountered permanent deactivation at high molar carbon-to-oxygen (C/O) ratios and high temperatures, deeming it unsuitable for the engine-scale reactor work to be conducted during the project.

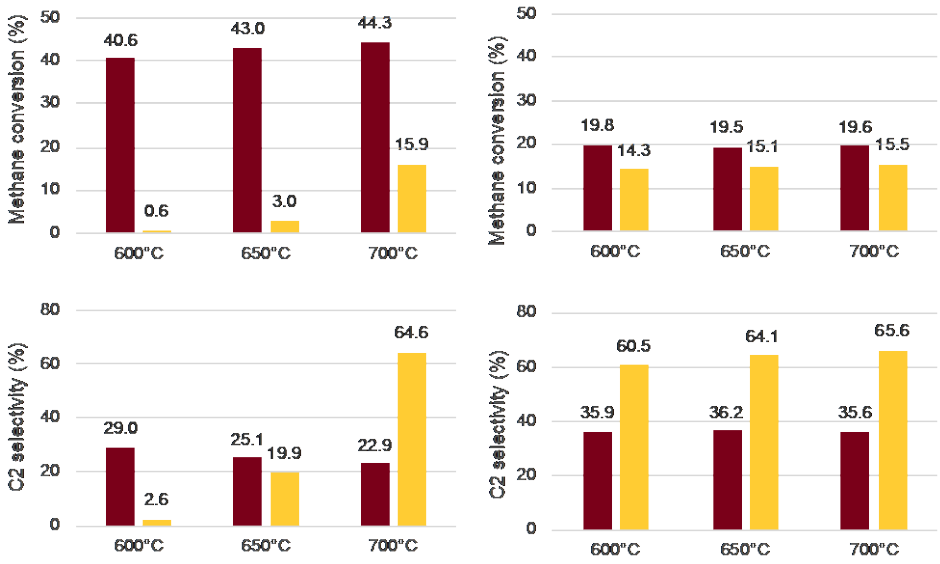

Figure III.2.1 Methane conversion and C_2 selectivity for Sr/La_2O_3 (maroon) and SrLa/CaO (yellow) OCM catalysts at two gas hourly space velocities and three catalyst temperatures: 50,000 h^{-1} gas hourly space velocity (left); 100,000 h^{-1} gas hourly space velocity (right)

During FY 2019, the project team developed and tested a bench-scale short-contact-time reactor based on prior research conducted under a separate federal award. This reactor was also simulated using computational fluid dynamics models. Reaction kinetics from the literature were used for reacting experiments [1]. The original concept proposed in the project was to use a short-contact-time reactor that combined fuel and air from opposing fluid manifolds, as shown in Figure III.2.2. This reactor was expected to increase selectivity to C_2 hydrocarbon products during the OCM reaction. However, in experiments with Sr/La_2O_3 catalysts provided by JM, the reactor was unable to achieve even 1% methane conversion. Additional experiments were conducted using an oxidation catalyst installed prior to the OCM catalyst to heat the latter to a high enough temperature, as shown in Figure III.2.1.

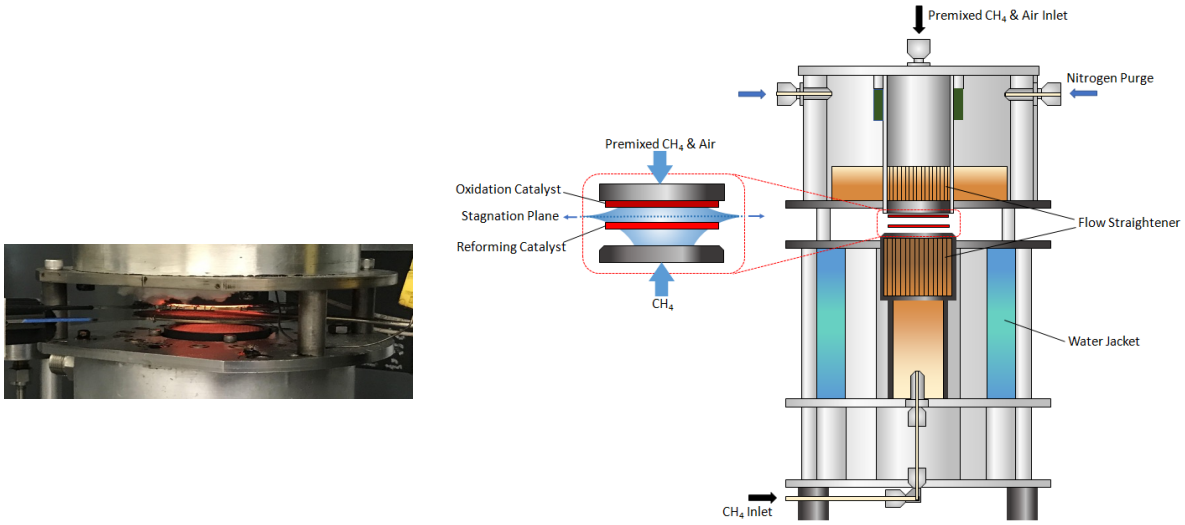

Figure III.2.2 Opposed-flow short-contact-time bench-scale reactor used in initial OCM experiments. Inset shows flow direction and location of catalyst. Photo shows catalyst heated using an oxidation catalyst stage.

Through experiments and modeling, the researchers concluded that the OCM catalysts are not active enough, nor is the reaction exothermic enough, to allow conversion at the short residence times (<1 ms) tested in the short-contact-time reactor. Furthermore, the OCM reaction required longer residence time than reforming reactions such as partial oxidation; the longer duration is due to relatively slow gas-phase reactions that convert methane and ethane to ethylene. These can be accomplished only in more traditional longer-residence-time reactors. Based on this research, the project team decided to focus efforts on premixed catalytic reactors using ceramic or metal monolith substrates.

In parallel with the bench-scale short-contact-time reactor, the project conducted non-reactive computational fluid dynamics modeling with an engine-scale opposed-flow reactor wrapped into a cylindrical geometry, as shown in Figure III.2.3. Here oxidizer and fuel enter one end of the cylinder in separate manifolds and emerge radially in opposition to each other near an interstitial catalytic mesh. Non-reacting simulations were conducted to determine the flow distribution and mixture stoichiometry at the mesh location. The right panel of Figure III.2.3 shows that the axial distribution of O_2 and CH_4 are visually similar along the length of the reactor. Although the stoichiometry of the opposed-flow reactor could be kept constant, prior experiments showing poor conversion for short contact time required that the research team place future focus on more traditional premixed monolith reactor styles.

Experiments with coated metal mesh catalysts were conducted in FY 2019 to meet the go/no-go milestone for the first budget period. These experiments were conducted at UMN in a tubular reactor within a tube furnace. Figure III.2.4 shows that the supported Sr/La_2O_3 provided by JM met the 10% conversion and 20% selectivity target at the lowest C/O ratio and highest inlet temperature. Experiments are continuing into FY 2020 to improve catalyst performance and to determine the impact of exhaust gas products such as CO_2 and H_2O as reactants to the OCM reaction.

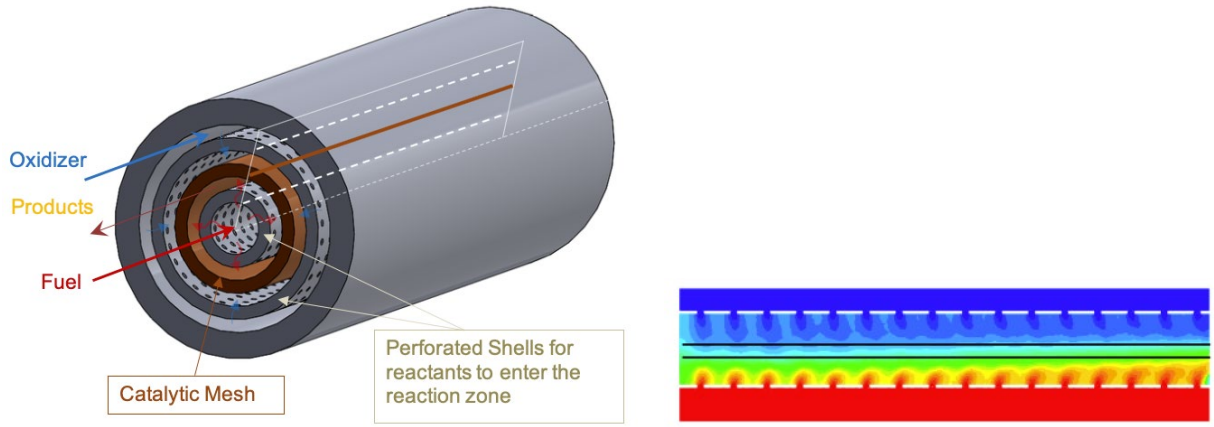

Figure III.2.3 Cylindrical geometry for opposed flow OCM reactor for engine-scale reactor (left). Oxygen (blue) and methane (red) mole fraction contours for a sector of the geometry at O/C = 5.0 (right).

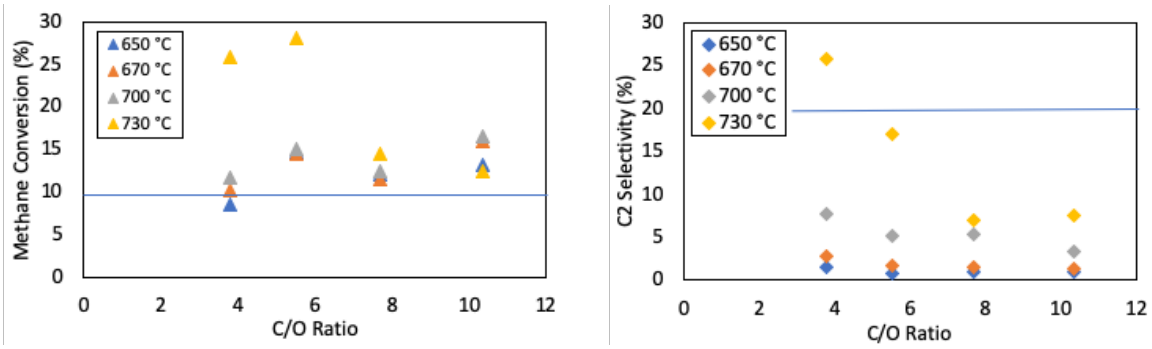

Figure III.2.4 Conversion (left) and selectivity (right) for plug-flow bench-scale reactor at different temperatures. Coated meshes from JM were used in the experiments. The go/no-go milestone for the first budget period was met at the highest temperature and lowest C/O ratio point.

Conclusions

The following conclusions can be made regarding this project through FY 2019:

- Catalytic OCM still appears to be a promising technology for converting abundant NG in the United States to a more reactive fuel for NG engines. This more reactive fuel can enable lean/dilute combustion or can potentially allow alternative compression-ignition modes with potential for significant efficiency gains over traditional engines.
- Supported Sr/La_2O_3 catalysts have effectively the same catalytic activity for the OCM reaction as pelleted catalysts used in industrial applications per unit catalyst mass. These catalysts can be coated onto automotive monolith substrates for use in transportation applications.

References

1. Sun, Jianjun, Joris W. Thybaut, and Guy B. Marin. 2008. "Microkinetics of Methane Oxidative Coupling." *Catalysis Today* 137: 90–102. https://doi.org/10.1016/j.cattod.2008.02.026.

Acknowledgements

The team members at Johnson Matthey and Carnegie Mellon University are gratefully acknowledged for their strong contributions to this project.

III.3 Reduced Petroleum Use through Easily Reformed Fuels and Dedicated Exhaust Gas Recirculation (Southwest Research Institute)

Thomas E. Briggs, Jr., Principal Investigator
Southwest Research Institute
6220 Culebra Road
San Antonio, TX 78238
E-mail: thomas.briggs@swri.org

Kevin Stork, DOE Technology Development Manager
U.S. Department of Energy
E-mail: Kevin.Stork@ee.doe.gov

Start Date: October 2014 End Date: November 2019
Project Funding (FY19): $285,188 DOE share: $220,722 Non-DOE share: $64,466

Project Introduction

This project is focused on improving the efficiency of a gasoline engine by using advanced petroleum and bio-derived fuels in a dedicated exhaust gas recirculation (D-EGR) engine. The D-EGR engine uses one or more of the cylinders to recirculate exhaust gas back to the intake of the engine. This increases the efficiency of the engine by itself, but also allows running those cylinders in such a way that they produce hydrogen as one of the byproducts of combustion. Hydrogen enhances combustion so that the compression ratio of the engine can be increased and so it can be optimized to run in a more efficient manner.

Running such an engine on regular gasoline provides significant benefits but becomes limited in how much hydrogen can be produced due to fuel chemistry. By adjusting the chemistry of the fuel, an even more efficient version of the engine can be built that will support the DOE goal of a 25% improvement in vehicle fuel economy for a typical passenger car.

Objectives

Overall Objectives

- Quantify the impact of fuel chemistry and formulation on D-EGR hydrogen production
- Optimize the operation of a D-EGR engine with purpose-developed fuel
- Demonstrate >25% reduction in petroleum usage for a mid-sized passenger car.

Fiscal Year 2019 Objectives

- Quantify the impact of refinery fuel blending on hydrogen production in the dedicated cylinder of a D-EGR engine
- Demonstrate 25% reduction in petroleum consumption through a combination of D-EGR engine operation, optimized refinery fuel blending, and bio-derived fuel component addition.

Approach

An existing engine is modified to function as a D-EGR engine. The operation of the engine on gasoline is then optimized to ensure that the fuel injection approach and intake/exhaust valve timings are optimal for producing hydrogen using a known fuel. The fuel chemistry is adjusted using a combination of refinery products which are

already made (though potentially not used in gasoline) and bio-derived fuel products. The potential improvement in hydrogen production is demonstrated using these fuels. Learnings from the engine optimization study are used to demonstrate an updated engine configuration that can maximize hydrogen production (and hence enable maximized compression ratio and engine efficiency) when using optimized fuels.

Results

Fuels were blended to reflect key property variations identified in testing in the previous fiscal year. The fuel hydrogen-to-carbon (H/C) ratio and the fuel octane numbers were varied to yield four fuel blends, as noted in Table III.3.1. The primary metric of interest was the H/C ratio, as that can be reasonably expected to impact the ratio of H_2 to CO production in the D-EGR dedicated cylinder. The research octane number (RON) and motor octane number (MON) values were also of interest, as there was some indication that fuels with similar H/C ratios but different RON and MON values also showed different responses to enriched operation.

Table III.3.1 Fuel Properties of Refinery Blend Fuels

Fuel	A	B	C	D
RON	97.0	107.0	91.1	95.7
MON	86.2	96.0	82.1	92.5
H/C Ratio	1.85	1.40	1.90	2.26

The fuels were initially tested in their as-delivered state. The test matrix considered three speed-load operation points, as used in all previous testing:

1. 2,000 rpm, 4 bar indicated mean effective pressure (IMEP)
2. 2,000 rpm, 12 bar IMEP
3. 4,000 rpm, 12 bar IMEP

At each test condition, the fuel was run at equivalence ratios of 1.0, 1.2, 1.4, and the maximum stable equivalence ratio. This was similar to the protocol used for previous fuel testing. The primary equivalence ratio of interest was the phi = 1.4 case; this is generally a stable operating equivalence ratio, generates significant H_2 in the combustion process, and has not been found to lead to hydrocarbon fouling of exhaust gas recirculation (EGR) components. Previous testing at up to phi = 1.8 showed higher H_2 production rates but also significant fouling of EGR coolers, which rapidly degraded engine performance.

The testing was performed on a 1.6 L spray-guided gasoline direct injection engine. This was a platform shift from previous testing. The engine had been extensively characterized in the HEDGE III combustion research consortium and was available for testing in a time window that was suitable for the program. The engine was configured with a low pressure EGR loop rather than in a D-EGR configuration, so for the initial screening tests all four cylinders were operated rich in order to determine the H_2/CO production rates for the four fuels under test. The engine specifications are listed in Table III.3.2, and a diagram of the engine and EGR layout is shown in Figure III.3.1.

Table III.3.2 Test Engine Specifications

Compression ratio	10.5:1
Bore	77 mm
Stroke	86 mm
Max Power	135 kW at 5,500 rpm
Max Torque	240 Nm at 1,600–5,000 rpm

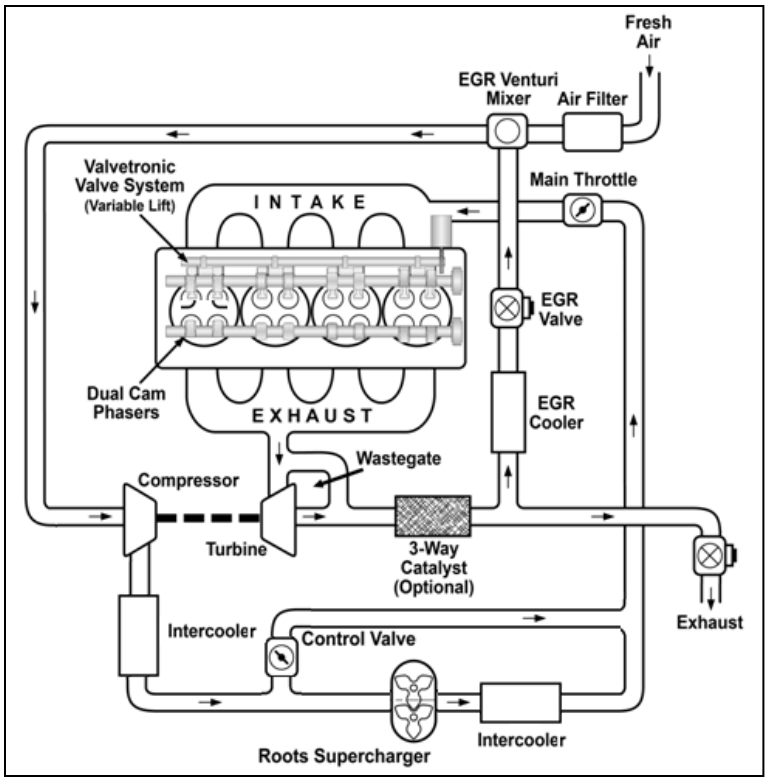

Figure III.3.1 Test Engine EGR System Configuration

The best-performing fuel was found to be Fuel C, as it generated the highest concentration of H_2 in the exhaust of the engine. Analysis of the results from these fuel tests is ongoing to understand the impact of the fuel properties on the measured H_2 production rates.

Based on these results, the 56B fuel will be blended with butanol (not bio-derived, but with the same physical and chemical properties as bio-derived iso-butanol) at a 10% by volume level. The engine then will be run with 25% EGR and with bottled H_2 and CO gases to mimic the behavior of a D-EGR engine. This will allow for final validation of the target 25% reduction in petroleum use from the combination of the fuel and D-EGR combustion system.

Conclusions

The results to date indicate the potential to increase the H_2 yield of rich combustion with proper selection of fuel properties, even when restricted to refinery output streams for blending. The final results are anticipated to yield at least a 25% reduction in petroleum consumption relative to the base engine and fuel combination used in this research.

Acknowledgements

The project's Principal Investigator gratefully thanks Ken Hardman at Fiat Chrysler Automobiles and Nicolas Obrecht at Total for their engineering and in-kind support for this project.

III.4 Improving the Fundamental Understanding of Opportunities Available from Direct Injected Propane in Spark Ignited Engines (Oak Ridge National Laboratory)

James Szybist, Principal Investigator
Oak Ridge National Laboratory
2360 Cherahala Boulevard
Knoxville, TN 37922
E-mail: szybistjp@ornl.gov

Derek Splitter, Principal Investigator
Oak Ridge National Laboratory
2360 Cherahala Boulevard
Knoxville, TN 37922
E-mail: splitterda@ornl.gov

Michael Weismiller, DOE Technology Development Manager
U.S. Department of Energy
E-mail: Michael.Weismiller@ee.doe.gov

Start Date: October 1, 2017 End Date: September 30, 2019
Project Funding (FY19): $243,000 DOE share: $243,000 Non-DOE share: $0

Project Introduction

Spark ignition engine efficiency and operation are fundamentally limited by knock, a process observed via cylinder-pressure measurements as early as the late 1910s [1]. Knock is an unwanted and uncontrolled autoignition of the fuel, which if not avoided can lead to engine damage, and therefore is impermissible in almost all engine applications. It is well known that knock can be reduced through use of fuels with increased octane number. Propane is a high-octane-number fuel; however, to date, the intake fumigation or port fuel injection processes used for propane have displaced engine intake air and thus limited the potential of propane as a motor fuel. The goal of this project is to expand the understanding of propane as a motor fuel using direct injection (DI) in advanced spark ignition engines. The results are analyzed by comparing propane to conventional fuels and assessing the efficiency potential that the fuel properties of propane enable relative to conventional fuels.

Objectives

Overall Objective

The overall objective of this project is to utilize the unique properties of propane to enable higher efficiency in DI engines.

Fiscal Year 2019 Objectives

- Understand unique opportunities of propane for high compression ratio (rc) and dilution tolerance in stoichiometric spark ignition operation with increased stroke and overexpansion
- Quantify products and enthalpy balance of propane catalytic reforming over a range of temperature and space velocity conditions
- Develop a high-pressure fueling system to supply DI fuel rail pressure to the multi-cylinder engine.

Approach

Subtask 1: Single-Cylinder Research: Two single-cylinder engine configurations are being explored with DI propane. The first will be with the conventional engine geometry. This will serve as a calibration baseline, where efficiency results with direct-injected propane will be compared to existing Oak Ridge National Laboratory data with conventional and alternative fuels. In the stock configuration, the engine will have r_c = 9.2:1 and a 1:1 stroke-to-bore ratio and is based on a 2.0 L GM LNF Ecotec engine equipped with the production side-mounted DI fueling system. The engine was converted to a single-cylinder engine by disabling Cylinders 1, 2, and 3, where Cylinder 1 is closest to the crank snout and Cylinder 4 is closest to the flywheel. The camshaft profiles on Cylinder 4 were unchanged from the stock configuration, and two different engine piston geometries were used: the stock 9.2:1 and a modified 13.6:1 r_c (obtained by a modified piston). The engine was operated using standalone laboratory fueling and air handling systems. The engine was controlled through an open setpoint engine controller. The second single-cylinder engine configuration is an advanced engine design with diesel-like r_c and a high stroke-to-bore ratio. It achieves r_c = 13.6:1 through a modified 1.5:1 stroke-to-bore ratio while retaining the stock combustion chamber geometry. The unique aspect of the advanced single-cylinder engine design is that the top dead center engine geometry is identical between the two single-cylinder engine configurations, so there is minimal alteration to the top dead center fluid mechanic scales and quenching effects, minimizing losses typical of conventional reduced clearance volume high r_c approaches. Moreover, the advanced engine design is specifically oriented towards increased dilution tolerance, where high levels of exhaust gas recirculation (EGR) are possible (greater than 30% cooled external EGR). Using this approach, the work will explore the possibility of achieving diesel engine efficiency parody with stoichiometric dilute DI propane spark ignition combustion. Regardless of the single-cylinder engine configuration, a hydraulic valve train will be used, which has near-infinite control authority, enabling high-efficiency opportunities.

Subtask 2: Multi-Cylinder EGR-Loop Reforming: On the multi-cylinder platform, a catalytic EGR-loop reforming strategy will be investigated. This engine operating strategy has been developed at Oak Ridge National Laboratory with liquid fuels. Prior work has demonstrated that high-efficiency fuel reforming and engine operation is possible, achieving an overall fuel consumption decrease of 10% over a range of engine loads. An isolated cylinder feeds a Rh-based reforming catalyst with a small amount of O_2 present to make the reforming process robust against coking and sulfur deactivation. To guide the engine experiments, a synthetic exhaust flow reactor is being used to define the reforming catalyst boundary conditions suitable for good performance with favorable thermodynamics, including thermochemical recuperation (TCR). High-efficiency engine operation is enabled by the reformate extending the dilution limit, which is largely due to the high flame speed of the H_2 in the reformate. This was achieved previously with iso-octane and gasoline, where the H/C ratio of the fuel was 1.85–2.125. For propane, the H/C ratio is 2.67, so the H_2 yield, dilution tolerance extension, and efficiency benefits are potentially higher. In addition, the initially high octane number of propane combined with the high dilution levels will enable an increase in the r_c for an even higher engine efficiency.

Results

Subtask 1: Single-Cylinder Research: Experiments with propane and two gasolines (91 RON E10 and 99 RON E0, where RON is research octane number, E10 is a gasoline blend containing 10% ethanol, and E0 is ethanol-free gasoline) were conducted with the custom engine over a range of loads from low to full load. Full load was determined by knock-limited combustion phasing. The findings in Figure III.4.1 show that even with a 13.3:1 r_c, there is significant load range extension with propane compared to regular-grade and a beyond-premium-grade gasoline with EGR and late intake valve closing (LIVC), technologies to reduce knocking.

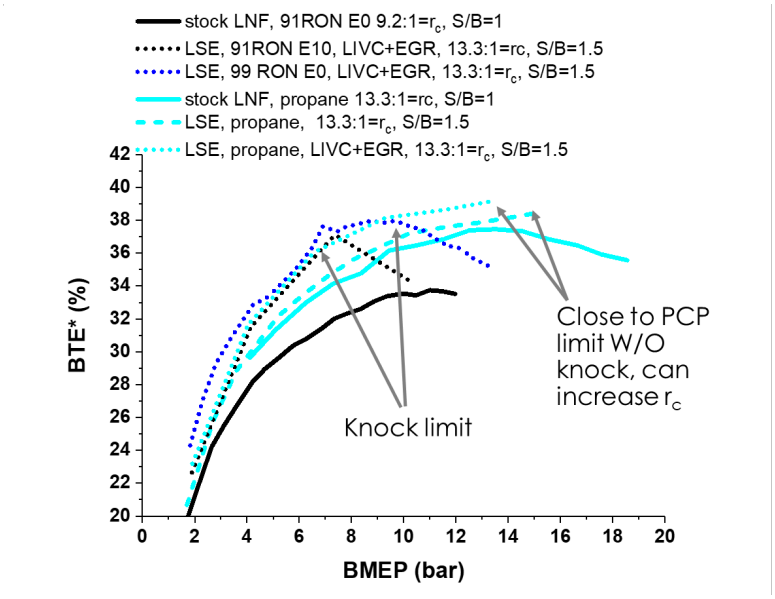

BMEP – brake mean effective pressure; S/B – stroke-to-bore ratio

Figure III.4.1 Brake thermal efficiency (BTE) and load range at 2,000 r/min of regular-grade E10 certification gasoline and high-octane E0 gasoline with high rc and LIVC+EGR for knock mitigation relative to the stroke engine (black) and propane. Note that propane reaches the peak cylinder pressure (PCP) with 13.3:1 rc but is not knock-limited before that. LNF is the stock GM engine, LSE is the long-stroke engine.

To explore the differences between propane and gasoline, zero-dimensional ignition delay simulations were used. Figure III.4.2 shows the ignition delay of each fuel defined as a 50 K rise in temperature, overlaid with in-cylinder experimental pressure-temperature trajectories during compression. With gasoline, the engine was knock-limited without EGR or LIVC at a load of 9 bar gross indicated mean effective pressure ($IMEP_g$) using 13.3:1 r_c. However, with propane, the ignition delay contours are much further away, and the r_c and load can be increased all the way to 14 bar $IMEP_g$ using 16.8:1 r_c before knock is observed. Note the similarity in the propane case at that condition relative to the ignition delay contours.

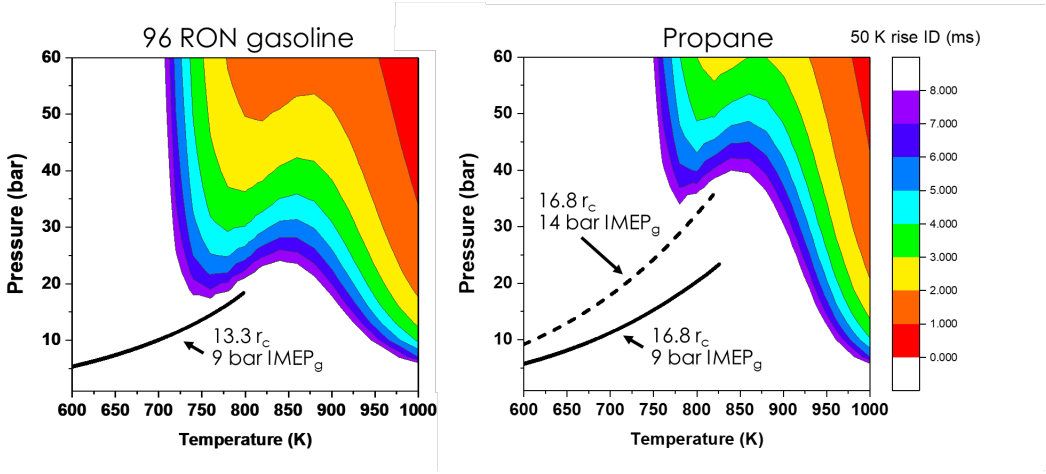

Figure III.4.2 In-cylinder compression history plotted on top of contours of constant-volume ignition delay (ID) simulation for gasoline (left) and propane (right). Note the significant increase in loaf (50%) with simultaneous 3.5 point increase in rc for propane at matched knock condition. Note: 16.8 rc, 9 bar IMEP case with propane is not knock-limited but inserted for reference.

From the high-load and high-r_c findings with propane, the load sweep, with r_c increased from 13.3:1 to 16.8:1, was conducted. The results, shown in Figure III.4.3, illustrate that with nearly 17:1 r_c, propane was operable to high loads before knock was encountered. In fact, the knock limit with propane with nearly 17:1 r_c was approximately the same as that exhibited by the production LNF engine on which the long-stroke research engine was based with 9:1 r_c and gasoline [2]. Moreover, the efficiency increase with DI propane was over eight points absolute efficiency gain, over a 25% efficiency improvement compared to the stock engine. These results are under further analysis, but the initial findings are significant and show pathways for achieving high efficiency with stoichiometric spark ignition engine operation.

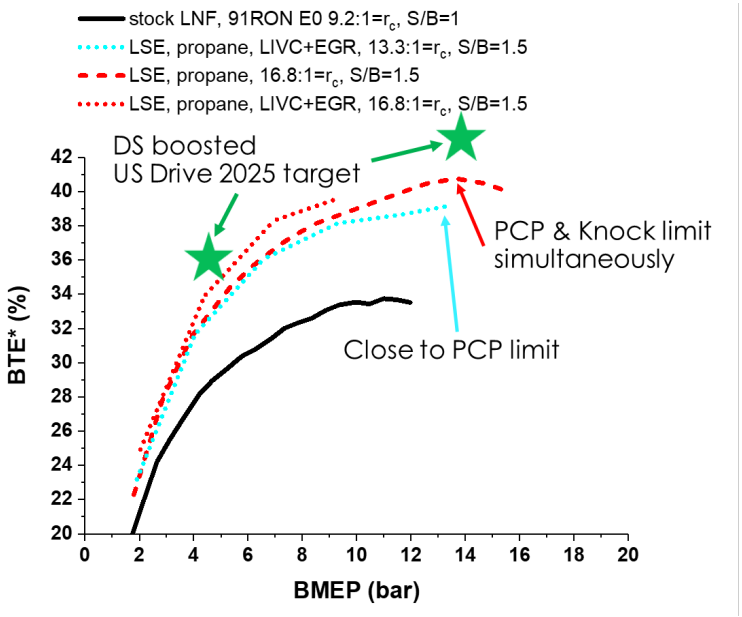

Figure III.4.3 BTE estimates for propane relative to the stock LNF engine with gasoline (black). Note the stars that indicate the U.S. DRIVE (United States Driving Research and Innovation for Vehicle efficiency and Energy sustainability) targets for efficiency in downsized, down speed (DS) engines. The propane data is approaching these targets with r_c and known technologies like EGR and LIVC.

Subtask 2: Multi-Cylinder EGR-Loop Reforming: There were two primary efforts in 2019 associated with this subtask. The first was to evaluate the reforming thermodynamics and performance on a synthetic exhaust flow reactor experiment. This was done using a core sample from a Rh-based reforming catalyst and controlling the feed gas composition, flow rate, and catalyst inlet temperature using a series of mass flow controllers, a water injection system, and a tube furnace. The reforming products were then analyzed and speciated using a series of gas analyzers, including a flame ionization detector hydrocarbon analyzer, a Fourier-transform infrared spectrometer, and a mass spectrometer, which enables the measurement of both H_2 and O_2 in addition to higher concentrations of CH_4 and C_3H_8. This system has been used in the past to measure fuel reforming thermodynamics and performance with liquid fuels [3]. Importantly, for this study, we spanned a wider range of inlet conditions (composition, flow rate, and temperature) to emulate engine operation over a wider range of engine load conditions, spanning from idle to boosted operation. Preliminary results for this effort were collected in 2018, but experiments were repeated in 2019 after a number of experimental issues were resolved.

Figure III.4.4 shows the ratio of enthalpy in the reforming products relative to the total fuel enthalpy fed to the catalyst in the synthetic exhaust flow reactor as a function of inlet O_2 concentration and target catalyst equivalence ratio for three different space velocity and temperature conditions, which emulated three different engine operating conditions. The 800°C condition replicates a high-load exhaust condition of 2,000 rpm, 14.0 bar BMEP; the 580°C condition replicates a moderate exhaust condition of 2,000 rpm, 4.0 bar BMEP; and the 450°C condition replicates a high-speed idle condition of 1,500 rpm, 0.8 bar BMEP. It is interesting

and encouraging that the highest enthalpy fraction recovered occurs at the middle condition, which best represents frequently-visited operating conditions on a real vehicle. A significant range of operating conditions have an enthalpy fraction recovered of greater than unity for this inlet temperature and space velocity combination, which indicates that TCR is being achieved. It was expected that the higher-temperature conditions would be more favorable for TCR, but the results indicate that there are other factors, perhaps the higher space velocity or higher heat losses to ambient, that are resulting in lower overall enthalpy recovery.

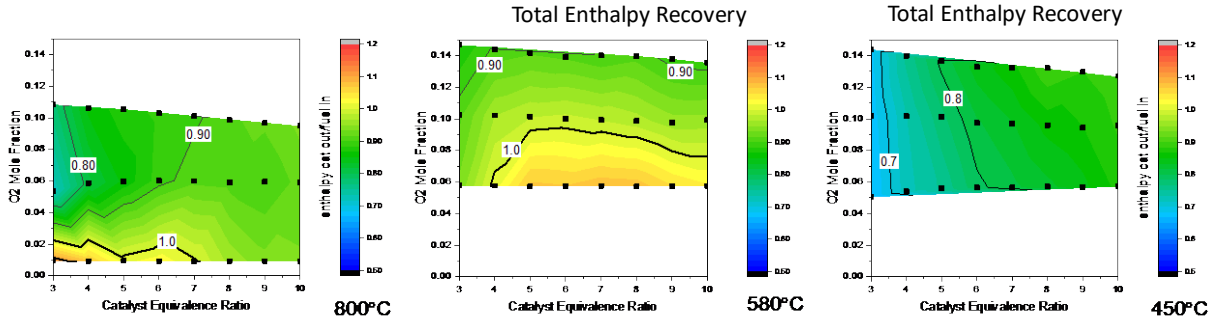

Figure III.4.4 Enthalpy fraction recovered after reforming for three different inlet temperature and space velocity conditions over the reforming catalyst as functions of O_2 mole fraction and catalyst equivalence ratio. The space velocities for the 800°C, 580°C, and 450°C conditions are 3,300 h^{-1}, 8,500 h^{-1}, and 23,500 h^{-1}, respectively.

Another unexpected finding was the amount of methane that was formed. Earlier studies into fuel reforming from Oak Ridge National Laboratory have shown that methane can be an equilibrium reforming product, and the concentration of methane can be significant [3],[4],[5], but those studies were with gasoline and iso-octane fuels. Experimental results with propane show that the methane formation can be even higher. Figure III.4.5 illustrates that methane concentrations are highly dependent on the catalyst boundary conditions, and that at the 800°C condition, the amount of methane was relatively low, with only two operating conditions showing more than 10% of the fuel energy, and 0% methane over much of the operating map. However, an increase was seen at the moderate exhaust condition, and at the high-speed idle condition, methane exceeded 60% of the fuel energy in the reforming products. Methane formation is undesirable when trying to achieve TCR because the reactions leading to H_2 and CO are more endothermic. Additional analysis to better understand the reaction pathways and conditions that lead to methane formation is ongoing.

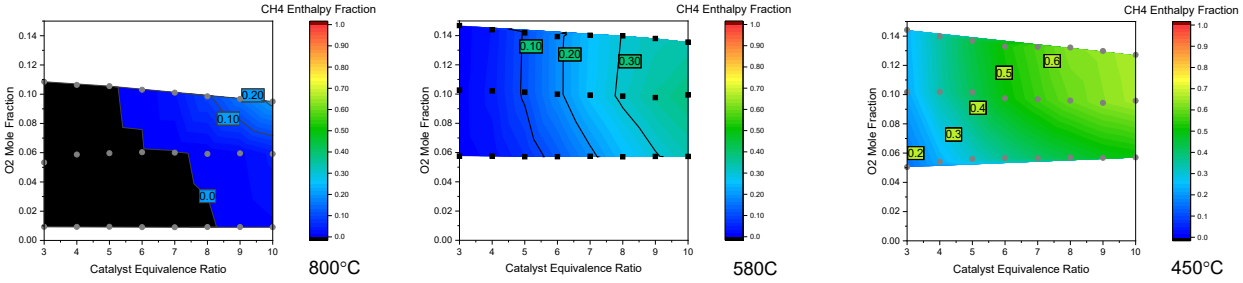

Figure III.4.5 Methane formed in the reforming catalyst as a fraction of the total fuel energy for each of the temperature and space velocity conditions

Lastly, the multi-cylinder engine is currently operational using DI propane. In order to accomplish this, a positive displacement piston-style pump, controlled with a variable-speed drive, pumps the liquid propane from the tank pressure (~150 psi, depending on the room temperature) directly to DI rail pressure (up to 100 bar). In order to pump the liquid propane, it is necessary to use a chiller to cool the propane to 0°C at the inlet of the pump. Thus, while the multi-cylinder engine work has been delayed, this issue has been resolved, and the engine experiments will be completed early in Fiscal Year 2020. Photographs of the pump and pump controller are shown in Figure III.4.6.

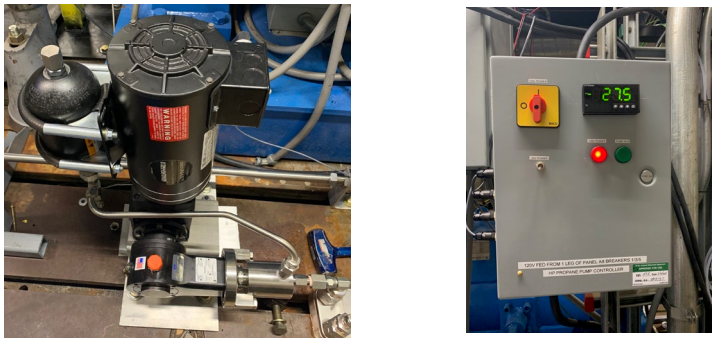

Figure III.4.6 Liquid propane pump and pump controller capable of pumping liquid propane from the tank pressure to DI rail pressure

Conclusions

- Propane is significantly more knock-resistant than gasoline, enabling significant improvements in engine efficiency by raising the compression ratio.
- The highest level of TCR was achieved at the middle temperature/space velocity condition investigated. This indicates that there are likely competing reactions or time scales for the most beneficial endothermic reactions.
- Methane can be a favored product of propane reforming, particularly with low catalyst inlet temperatures. This is not a desired product to achieve TCR. Additional analysis to understand methane formation pathways and conditions is ongoing.

Key Publications

1. Boronat, V., D. Splitter, F. Chuahy, and J. Storey. 2019. “Update on ORNL High Stroke-to-Bore SI Research.” Presented at the AEC/MOU meeting (August 15), Southfield, MI.

References

1. Splitter, D., A. Pawlowski, and R. Wagner. 2016. *Frontiers in Mechanical Engineering* (1), https://doi.org/10.3389/fmech.2015.00016.
2. Splitter, D., and J. Szybist. 2014. “Intermediate Alcohol-Gasoline Blends, Fuels for Enabling Increased Engine Efficiency and Powertrain Possibilities.” *SAE International Journal of Fuels and Lubricants* 7 (1): 29–47.
3. Brookshear, D.W., J.A. Pihl, and J.P. Szybist. 2018. “Catalytic Steam and Partial Oxidation Reforming of Liquid Fuels for Application in Improving the Efficiency of Internal Combustion Engines.” *Energy Fuels* 32 (2): 2267–2281. DOI: 10.1021/acs.energyfuels.7b02576.
4. Chang, Y., J.P. Szybist, J.A. Pihl, and D.W. Brookshear. 2018. “Catalytic Exhaust Gas Recirculation-Loop Reforming for High Efficiency in a Stoichiometric Spark-Ignited Engine through

Thermochemical Recuperation and Dilution Limit Extension, Part 1: Catalyst Performance." *Energy Fuels* 32 (2): 2245–2256. DOI: 10.1021/acs.energyfuels.7b02564.

5. Chang, Y., J.P. Szybist, J.A. Pihl, and D.W. Brookshear. 2018. "Catalytic Exhaust Gas Recirculation-Loop Reforming for High Efficiency in a Stoichiometric Spark-Ignited Engine through Thermochemical Recuperation and Dilution Limit Extension, Part 2: Engine Performance." *Energy Fuels* 32 (2): 2257–2266. DOI: 10.1021/acs.energyfuels.7b02565.

Acknowledgements

The principal investigators gratefully acknowledge the valuable contributions of Melanie Debusk, Josh Pihl, and Vicente Boronat Colomer to this project.

III.5 Fundamental Advancements in Pre-Chamber Spark Ignition and Emissions Control for Natural Gas Engines (Argonne National Laboratory, National Renewable Energy Laboratory, Oak Ridge National Laboratory, and Sandia National Laboratories)

Brad Zigler, Principal Investigator
National Renewable Energy Laboratory
15013 Denver West Parkway
Golden, CO 80401
E-mail: brad.zigler@nrel.gov

Doug Longman, Principal Investigator
Argonne National Laboratory
9700 S. Cass Avenue
Lemont, IL 60439
E-mail: dlongman@anl.gov

Scott Curran, Principal Investigator
Oak Ridge National Laboratory
1 Bethel Valley Road
Oak Ridge, TN 37830
E-mail: curransj@ornl.gov

Mark Musculus, Principal Investigator
Sandia National Laboratories
7011 East Avenue
Livermore, CA 94550
E-mail: mpmuscu@sandia.gov

Kevin Stork, DOE Technology Development Manager
U.S. Department of Energy
E-mail: Kevin.Stork@ee.doe.gov

Start Date: October 1, 2017 End Date: September 30, 2020
Project Funding: $3,000,000 DOE share: $3,000,000 Non-DOE share: $0

Project Introduction

Medium-duty (MD) and heavy-duty (HD) natural gas (NG) vehicles have benefited from significant recent growth in NG production, with relatively low and stable NG prices. Growing compressed NG and liquefied NG refueling capability and growing interest in renewable NG pathways align with increasing MD/HD NG engine options and vehicle availability to further strengthen the market. Additionally, growing interest by the California Air Resources Board and U.S. Environmental Protection Agency in potential regulations requiring ultra-low levels of oxides of nitrogen (NO_x) emissions may encourage MD/HD NG vehicle adoption since NG engine and aftertreatment technology may help meet those ultra-low NO_x levels more cost-effectively than diesel. However, current MD/HD NG engine technology, with stoichiometric spark ignition (SI), exhaust gas recirculation (EGR), and three-way catalyst aftertreatment, is less efficient than current diesel technology.

Therefore, early-stage research to significantly increase MD/HD NG engine efficiency is of interest for supporting better utilization of NG resources.

A 2017 U.S. Department of Energy workshop on NG vehicle research helped identify key MD/HD NG engine efficiency and emissions control research needs [1],[2]. Additional industry input from the annual Natural Gas Vehicle Technology Forum also helped form project objectives [3]. Industry feedback showed interest in low-technology-readiness-level (TRL) research focused on barriers to enable diesel-like efficiency in MD/HD NG engines, including understanding of ignition chemistry, flame speed, and mixing. Industry feedback also cited the need for fundamental catalysis research for methane conversion in response to the challenge of methane activation. Argonne National Laboratory (ANL), the National Renewable Energy Laboratory (NREL), Oak Ridge National Laboratory (ORNL), and Sandia National Laboratories (SNL) designed this collaborative research project to investigate fundamental combustion processes for pre-chamber spark-ignition (PCSI) concepts to enable diesel-like efficiency in MD/HD NG engines. By extending the lean dilution limit and/or the EGR dilution limit, as well as shortening the burn duration, PCSI has already demonstrated efficiency improvements of up to 20% in light-duty gasoline engines at low load, achieving diesel-like efficiencies [4]. This project involves early-stage research focusing on low-TRL PCSI to achieve diesel-like efficiency in MD/HD NG engines by extending the lean dilution limit and/or EGR dilution limit, as well as shortening burn duration, with integrated aftertreatment.

Objectives

Overall Objectives

This project integrates experimental and simulation-based tasks to address four key barriers to market penetration of PCSI for MD/HD NG engines:

- Inadequate science base and simulation tools to describe/predict the fluid–mechanical and chemical–kinetic processes governing PCSI to enable industry engineers to optimize designs for efficiency, noise, reliability, pollutant formation, emissions control integration, and drivability [5]
- Limited ability to extend EGR and/or lean dilution limits at higher loads [6]
- Increased propensity for PCSI hot-spot pre-ignition at high loads relative to conventional spark ignition [6]
- Ineffective methane catalysts for the high engine-out unburned fuel concentrations coupled with low exhaust temperatures (<<400°C) of high-efficiency engines [7].

Fiscal Year 2019 Objectives

- Design a modular PCSI system, sharing key design parameters and maintaining as much commonality as possible across ANL, NREL, ORNL, and SNL bench-scale, single-cylinder engine (SCE), and multi-cylinder research engine platforms
- Quantify the performance improvements in engine efficiency with unfueled and fueled PCSI systems in a metal SCE
- Evaluate Reynolds-averaged Navier–Stokes (RANS) models used by industry to simulate pre-chamber (PC) ignition in MD/HD NG engines
- Validate computational fluid dynamics (CFD) results against engine data at a wide range of PCSI operating conditions
- Conduct PCSI NG bench-scale ignition studies across a parametric range of globally lean and variable PC conditions with integrated zero-dimensional (0D) and CFD simulations using a modified Advanced Fuel Ignition Delay Analyzer (AFIDA)

- Modify an existing optically accessible HD SCE for PSCI, and conduct experiments over a range of operating conditions with high-speed laser and/or chemiluminescence imaging diagnostics
- Modify a multi-cylinder HD metal engine with a PCSI system with characteristics matched to PCSI systems used in other bench-scale and SCE studies
- Synthesize novel methane oxidation catalysts (MOCs) designed to overcome the underlying physical and chemical processes that limit the reactivity of methane over traditional precious metal catalysts
- Evaluate MOCs in realistic synthetic mixtures (including water).

Approach

This project integrates experiments and simulations spanning bench-scale to SCE to multi-cylinder research engine studies for combustion and aftertreatment. The work leverages strong collaboration and unique capabilities from ANL, NREL, ORNL, and SNL.

ANL performed SCE simulations with CONVERGE CFD. A number of RANS combustion models were preliminarily tested. The research team selected two conceptually different models for the validation effort: the multizone well-stirred reactor (MZ-WSR) model to represent the direct chemistry approach and the G-Equation (G EQN) model to represent the "flamelet" approach. The team compared modeling results with experimental data from the ANL metal SCE, for both unfueled and fueled PC operation, to validate the models. A single-cylinder NG research MD engine (1.8 L) was retrofitted with a modular in-house PCSI system. This relatively simple design accommodated an igniter (M8 spark plug), pressure transducer, and medium to introduce fuel into the PC via a check valve. The design also allowed PC volume and nozzle geometry, number, and orientation variations with relative ease. Both SNL and NREL adopted variations of the PC design to have similar simulated operating conditions to help with combustion investigations.

NREL modified the AFIDA to adapt a PCSI module in place of the existing piezoelectric diesel injector. Lean main chamber conditions were filled with gas cylinders, with PC fueling via gasoline direct injection (GDI). Multiple piezoelectric pressure transducers and thermocouples monitored conditions, and a spark plug fitted within the PC controlled initial ignition timing. Parametric ignition studies were conducted to span global air–fuel equivalence ratio, lambda (λ), for both the main chamber and PC, along with variable effects of temperature, pressure, and spark timing. AFIDA PCSI simulations were also conducted with 0D, multi-zone 0D, and full CFD models to elucidate experimental results. Specifically, PCSI composition output was used to explore main chamber ignition sensitivity to identify key controlling radical species. PC λ sweeps replicating experimental conditions were studied to understand competing effects between radical species production and PC jet strength into the main chamber.

SNL modified an existing direct-injection HD optical SCE for PCSI of NG to study PC output penetration to the main chamber and characterize flame propagation versus sequential autoignition. Figure III.5.1 shows a cross-sectional schematic of the engine, with the PC installed in the cylinder head on the cylinder axis, where the diesel fuel injector would otherwise be located. As shown in the photograph in the top right of Figure III.5.1, the GDI injector is mounted in the top of the PC to provide the option for active NG fueling of the PC. A "Rimfire" miniature spark plug and piezoelectric pressure transducer are also mounted in the PC top. The project installed a side-mounted GDI injector in a port in the cylinder wall to fuel the main chamber with a premixed, fuel-lean charge of NG; the injector is modified to have a single 1 mm hole and is operated at 100 bar NG supply pressure. For the optical diagnostics, a large window in the crown of the extended piston provides imaging access to the piston bowl (Figure III.5.1). A high-speed intensified complementary metal oxide semiconductor camera captures images of hydroxyl radical (OH*) chemiluminescence, which generally indicates the location of high-temperature combustion. Additionally, infrared emission imaging from carbon–hydrogen bond excitation is used to infer temperature gradients in unburned fuel distribution.

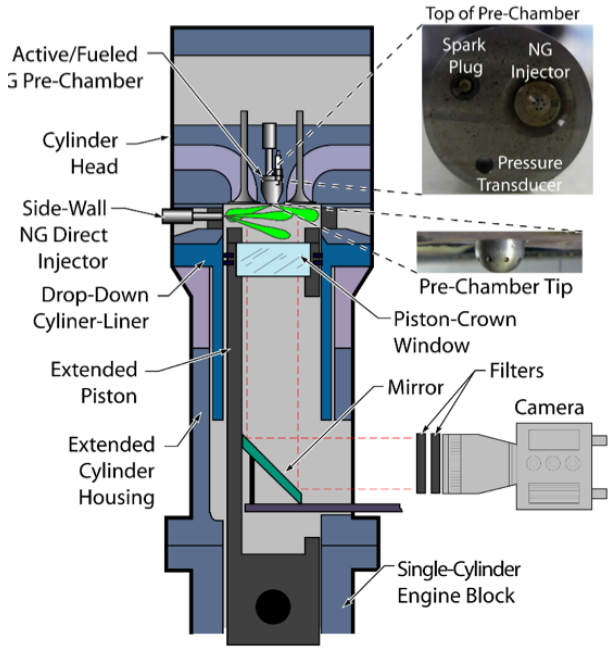

Figure III.5.1 Schematic showing the side-wall NG direct injector and PC that were installed on the existing HD optical diesel engine. The photographs show a bottom view of the top internal surface of the PC (top right) and a side view of the tip of the PC protruding below the firedeck (middle right). (Figure: Mark Musculus, SNL)

Two tasks are interlinked for the work at ORNL. The first task involves the use of a multi-cylinder HD engine outfitted with PCSI modules to explore a focused dilution tolerance investigation. The aim is to characterize the engine thermodynamics to provide insight on how PCSI shifts the thermodynamic balances and to understand what additional opportunities there may be for improved efficiency. A collaboration with MAHLE Powertrain resulted in the design of a multi-cylinder PCSI system with key characteristics matched to the PCSI system for the other collaborative PCSI tasks. The second task focused on the development of a new MOC for lower-temperature conversion. Different palladium/chabazite (Pd/SSZ-13) catalysts were synthesized by adjusting the post-ion-exchange treatments. A microreactor was used to measure oxidation of methane on powder catalysts with the simulated exhaust relevant for a lean NG engine. This required a modification to the U.S. DRIVE (United States Driving Research and Innovation for Vehicle efficiency and Energy sustainability) low-temperature oxidation catalyst protocol for lean GDI exhaust to account for differences in NG engine exhaust (CH_4 as hydrocarbon, higher H_2O). The catalytic methane oxidation activity was studied using a microscale synthetic exhaust flow reactor for simulating lean NG engine exhaust with 12% water and 3,000 ppm methane along with oxygen, carbon dioxide, carbon monoxide, and nitric oxide.

Results

ANL CFD Simulations

Simulation results showed that all the tested models required significant tuning to match experiments. Q-EQN appeared to be a superior model because of the capability to account for both large and small turbulent scales. It was shown that small turbulent scales are generated into the PC at the time of the spark, unlike typical large turbulent scales in conventional SI operation (i.e., open chamber). Model tuning compensated for specific challenges in describing PCSI combustion, as illustrated in Figure III.5.2. In all CFD calculations, at any operation, it was shown that the flame regime was rapidly shifting across the Borghi–Peters diagram [8] between thin reaction zone and the flamelet regions. The Damkohler number (Da) was changing rapidly across the PC orifice, where strong turbulence–chemistry interaction is expected, thus decoupling the combustion events in the PC and main chamber, respectively. It was also shown that lean conditions in the PC were posing

a serious challenge for the models at unfueled PC operation, while less tuning was required at fueled PC operation since the PC mixture was close to stoichiometric conditions.

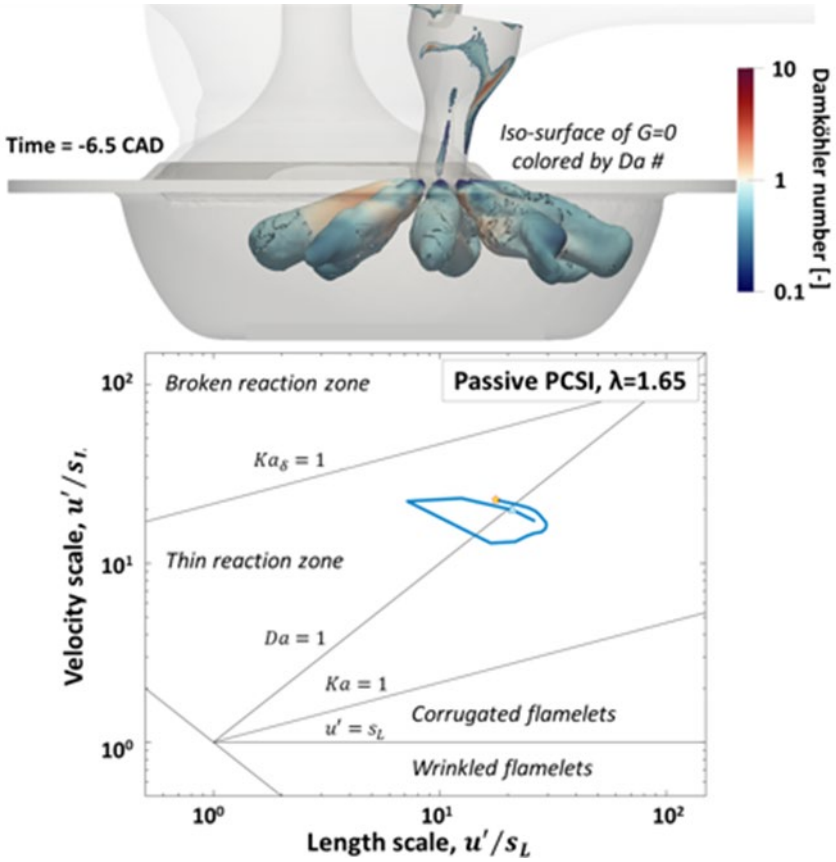

u' – turbulent velocity fluctuation; s_L – laminar flame velocity; Ka – Karlovitz number

Figure III.5.2 Da distribution at the PC exit and corresponding flame regime on the Borghi–Peters diagram (Figure: Joohan Kim, ANL)

ANL SCE Experiments

Unfueled PC ignition extended the lean operating limit from λ ~ 1.5 to 1.6, as shown in Figure III.5.3, allowing an increase in thermal efficiency. Lean limit extension beyond λ ~ 1.8 required a fuel-rich mixture in the PC. Fuel-rich jets, which are "rich" in radicals, react with the ultra-lean charge in the main chamber. Additionally, fueled PC ignition with a fuel-rich mixture in the PC allowed even further efficiency improvement by extending lean limit vis-a-vis λ ~ 2.3.

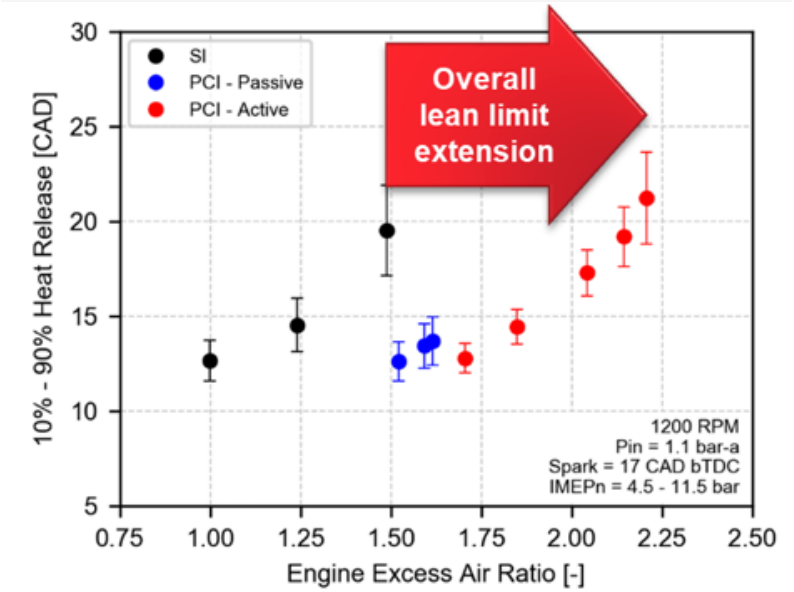

CAD – crank angle degrees; PCI – pre-chamber ignition; bar-a – bar absolute; bTDC – before top dead center; IMEPn – net indicated mean effective pressure

Figure III.5.3 Combustion instability under lean conditions (Figure: Ashish Shah, ANL)

NREL Bench-Scale Experiments and Simulations

Initial simulations were conducted to build a computational model approximating the AFIDA with a PC, validate that the model captures trends in ignition delay with air–fuel ratio successfully, use the model to infer the flux between the chambers, and finally study the impact on the main chamber. The simulations showed that the combination of temperature plus key species transferring into the main chamber results in an order-of-magnitude reduction in ignition delay beyond temperature only. Critically, transfer of non-equilibrium products from incomplete combustion in the PC is desirable. PC variable effects on main chamber ignition were then experimentally studied in the AFIDA over a range of lean main chamber conditions. Variables included temperature effects, SI timing with respect to PC fueling with the GDI injector, and most importantly, PC λ controlled by GDI injector duration. Figure III.5.4 illustrates that, for a given lean main chamber charge, a sweep of richer (evidently near-stoichiometry) conditions in the PC resulted in an optimal combination of competing effects—a point where transfer of desirable radical species from increasingly rich conditions were evidently offset by jet output from higher initial peak PC pressures with decreasingly rich conditions. Recent CFD and multi-zone 0D simulations match the experimental trends, and calculated main chamber ignition delay times matched experiments for main chamber λ = 1.4–1.9. The conditions most recently studied in AFIDA experiments and simulations closely match optical SCE studies conducted by SNL, and results are presently being compared.

SNL Optical SCE Experiments

The optical engine is operated at a relatively low engine speed of 600 rpm because of flow limits of the main-chamber direct injector. (Future experiments will use a higher-flow fumigation injector to allow higher-speed operation.) The experiments presented in this report utilize main-chamber injection only, with zero PC fueling, which is akin to a passive PC configuration. The load is approximately 5 bar gross indicated mean effective pressure (IMEPg) for all conditions reported here. Across the tests, λ is varied across a range of fuel-lean conditions from λ = 1.5 to λ = 1.9, while the spark advance is held at 343 CAD. Depending on the value of λ, the injection duration is 20–25 ms, with injection starting 40º crank angle (CA) into the intake stroke.

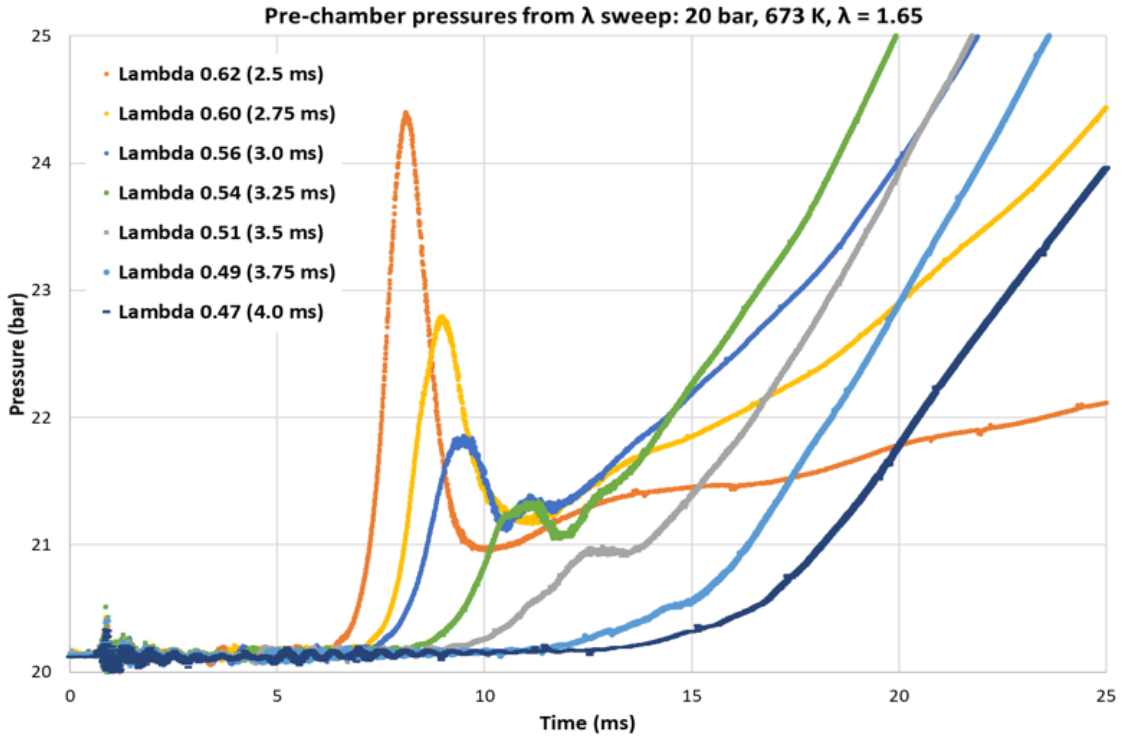

Figure III.5.4 PC combustion pressure curves as functions of PC λ. Main charge–air mixture at 20 bar, 673 K, λ =1.65. Note that curves are not smoothed; the pressure data acquisition rate was 250 kHz up to 40.4 ms, then 25 kHz thereafter. (Figure: Matt Ratcliff, NREL)

Figure III.5.5 shows three selected images taken from the high-speed OH* chemiluminescence movies, one for each of λ = 1.5, 1.7, and 1.9. The PC is located in the center of the image, and the outer dark circle represents the piston bowl. Above each image are the 10-cycle averages of the measured cylinder (main chamber) and PC pressure, as well as the combined apparent heat release rate (AHRR) derived from those pressure data. For all three conditions, the PC pressure rises above the main-chamber pressure after the spark at 343 CAD, indicating combustion in the PC. Comparing the three conditions, which have constant spark timing, the combustion duration increases with increasing λ. For $\lambda \leq 1.7$, the cycle-to-cycle coefficient of variation of IMEPg is less than 2%, but for $\lambda > 1.7$, the combustion becomes less stable, with 20% and 60% misfires at $\lambda = 1.8$ and $\lambda = 1.9$, respectively. Even for the conditions with low coefficient of variation of IMEPg, cycle-to-cycle variation in the timing of individual jet emergence from the PC and luminosity from the subsequent combustion in the main chamber are quite large. Furthermore, the luminosity fluctuates on and off for some of the jets, resembling repeated extinction and re-ignition. Such stochastic variations and phenomenological characteristics will be important to understand and resolve in simulations.

The optical data also show that the combustion luminosity decreases with increasing λ, which is consistent with a decreasing flame temperature at higher dilution. Importantly, the jets emerging from the PC for $\lambda \geq 1.7$ generally have no detectable OH* chemiluminescence emission until ignition in the main chamber. This suggests that the mechanism of ignition changes from $\lambda < 1.7$ to $\lambda \geq 1.7$. The main-chamber gas may be ignited by a flame emerging from the PC for the less fuel-lean conditions, while either thermal or chemical–radical effects from the hot PC jets may ignite the main-chamber gases under more fuel-lean conditions. Future work with other laser/imaging diagnostics, as well as complementary experiments and modeling in the other facilities of this project, will build further understanding of chemical and physical processes for these and other conditions using active (fueled) PC conditions.

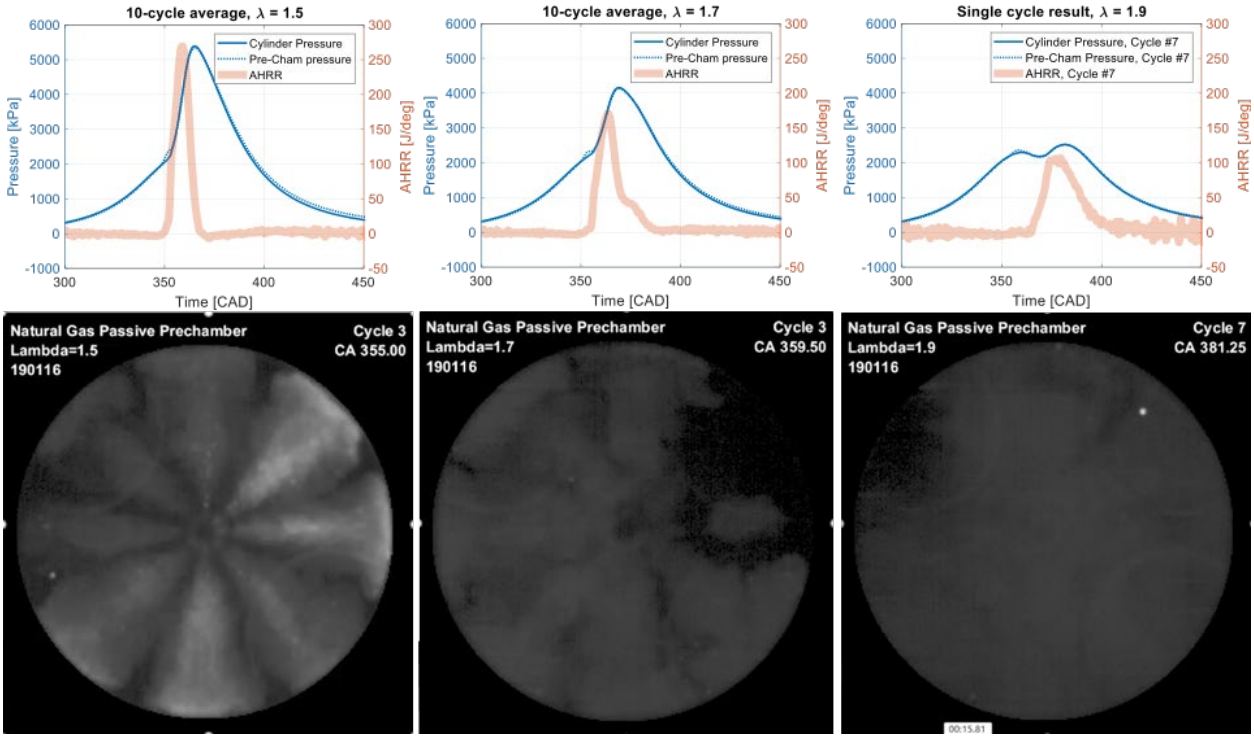

Figure III.5.5 Top: 10-cycle averages of the measured cylinder (main chamber) and PC pressure, as well as the AHRR derived from those pressure data, as indicated in the legend, at λ = 1.5, 1.7, and 1.9 from left to right. Bottom: Selected images of OH* chemiluminescence for each of the three λ values, as viewed through the large piston window shown in Figure 215. (Figure: Mark Musculus, SNL)

ORNL Multi-Cylinder PCSI

The multi-cylinder PCSI design was matched to have overlapping characteristics with the other National Laboratory PCSI systems. The active PC was designed around the mixture preparation requirements for the multi-cylinder DD13 HD engine. Figure III.5.6 shows the four PC bodies that have been designed. ORNL completed and delivered the PCSI system and the modified head for the multi-cylinder engine experiments during the previous quarter.

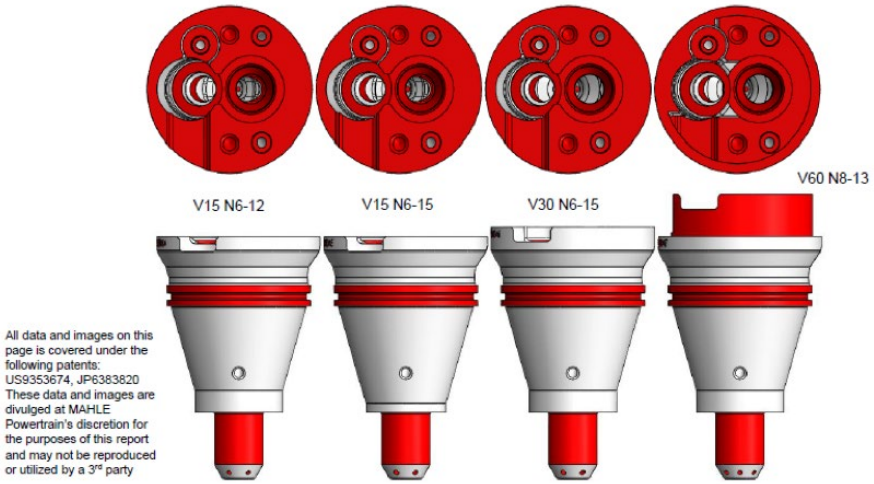

Figure III.5.6 Multi-cylinder PCSI modules (Figure: Scott Curran, ORNL, shared from MAHLE Powertrain)

ORNL MOC

Catalytic activities of Pd ion-exchanged SSZ-13 catalysts with a variety of post-ion-exchange treatments were studied for the conversion of methane under synthetic exhaust conditions (see Figure III.5.7). The researchers selected the ion-exchanged catalyst with the highest low-temperature methane conversion, along with a series of non-ion-exchanged supported Pd catalysts, for addition of magnesium. The addition of magnesium is expected to facilitate the hydrogen abstraction of methane at a lower temperature, leading to lower-temperature light-off of a methane oxidation catalyst for use in an emissions control solution for lean PCSI engines.

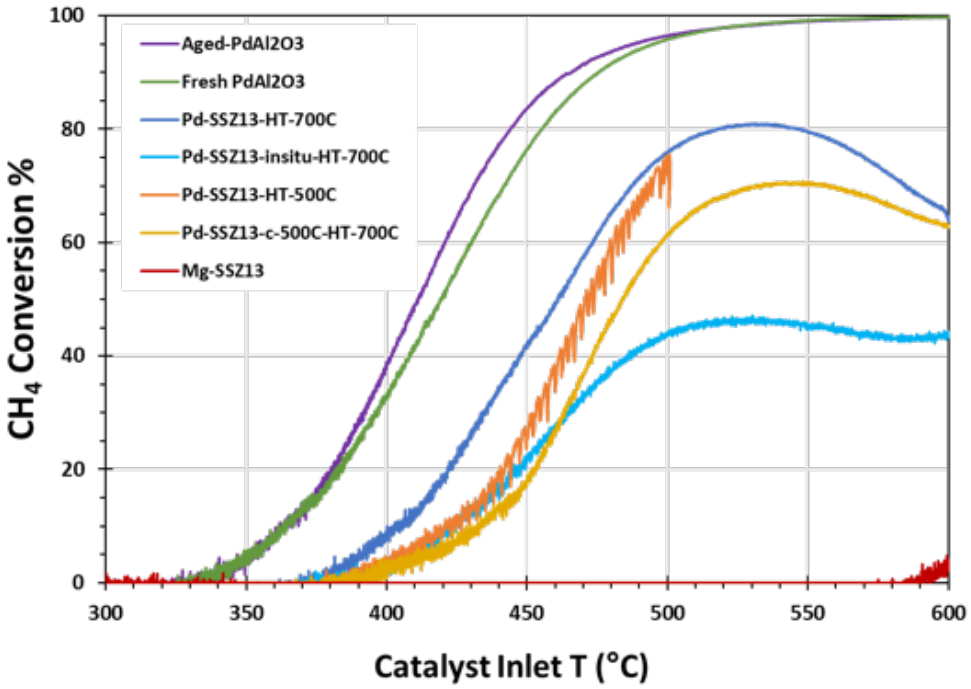

Figure III.5.7 MOC light-off curve (Figure: Melanie Debusk, ORNL)

Conclusions

- A modular PCSI system, sharing key design parameters and as much commonality as possible, has been adapted across ANL, NREL, ORNL, and SNL bench-scale, SCE, and multi-cylinder research engine platforms.
- CFD simulations could match ANL engine data; nevertheless, the models needed some tuning. Tuning compensated for the intrinsic challenges of simulating PCSI combustion, consisting of a multi-regime combustion process and ultra-lean conditions for ignition in the PC.
- Both passive and active PC modes extended the lean ignition limit, with significant improvement under fuel-rich conditions in the PC. The next suite of tests will include study of PC volume, nozzle area, and mixture strength effects on efficiency and emissions under dilute conditions.
- Bench-scale simulations examining species and enthalpy transfer from PCSI into the main chamber showed that the combination of temperature plus key species transferring into the main chamber results in an order-of-magnitude reduction in ignition delay beyond temperature only. Critically, transfer of non-equilibrium products from incomplete combustion in the PC is desirable.

- AFIDA experiments showed that for a given lean main chamber charge, a sweep of richer (evidently near-stoichiometry) conditions in the PC resulted in an optimal combination of competing effects—a point where transfer of desirable radical species from increasingly rich conditions was evidently offset by jet output from higher initial peak PC pressures with decreasingly rich conditions. Recent CFD and multi-zone 0D simulations match the experimental trends, suggesting that the main chamber ignition process may be changing based on PC output.

- Optical SCE experiments show that the combustion luminosity decreases with increasing λ, which is consistent with a decreasing flame temperature at higher dilution. For $\lambda \geq 1.7$, the jets emerging from the PC generally have no detectable OH* chemiluminescence emission until ignition in the main chamber. This suggests that the mechanism of ignition may be changing, where the main chamber may be ignited by a flame emerging from the PC for the less fuel-lean conditions, and either thermal or chemical–radical effects from the hot PC jets may ignite the main chamber gases under more fuel-lean conditions.

- Multi-cylinder implementation of HD PCSI is possible without having to recast the engine head and will be well suited for the dilution and thermodynamic studies planned.

- Initial results for MOC studies have been positive.

Key Publications

1. Zigler, B., D. Longman, S. Curran, and M. Musculus. "Fundamental Advancements in Pre-Chamber Ignition and Emissions Control for Natural Gas Engines." 2019 DOE Vehicle Technologies Office Annual Merit Review and Peer Evaluation Meeting. https://www.energy.gov/sites/prod/files/2019/06/f64/ft080_%20zigler_2019_o_4.30_4.02pm_jl.pdf.

2. Kim, J., R. Scarcelli, S. Som, A. Shah, M. Biruduganti, and D. Longman. "Assessment of Turbulent Combustion Models for Simulating Pre-Chamber Ignition in a Natural Gas Engine." ASME Paper ICEF2019-7278, 2019. https://doi.org/10.1115/ICEF2019-7278.

3. Musculus, M., et al. 2019. "Fundamental Advancements in Pre-Chamber Spark-Ignition and Emissions Control for Lean-Burn Natural-Gas Engines." Poster presented at International Energy Agency – Task Leader meeting, Montreux, Switzerland (November 3–8).

References

1. U.S. Department of Energy, Vehicle Technologies Office. Natural Gas Vehicle Research Workshop, July 25, 2017. https://www.nrel.gov/transportation/ngv-research-workshop.html.

2. U.S. Department of Energy, Vehicle Technologies Office. Natural Gas Vehicle Workshop Summary and Key Observations. July 25, 2017. https://www.nrel.gov/transportation/assets/pdfs/ngv_workshop_summary.pdf.

3. U.S. Department of Energy, Office of Energy Efficiency and Renewable Energy. "Natural Gas Vehicle Technology Forum." Clean Cities Coalition Network website. Accessed 2019. https://cleancities.energy.gov/natural-gas-forum/.

4. Attard, W., M. Bassett, P. Parsons, and H. Blaxill. 2011. "A New Combustion System Achieving High Drive Cycle Fuel Economy Improvements in a Modern Vehicle Powertrain." SAE Technical Paper 2011-01-0664. https://doi.org/10.4271/2011-01-0664.

5. Roethlisberger, R. P., and D. Favrat. 2003. "Investigation of the Prechamber Geometrical Configuration of a Natural Gas Spark Ignition Engine for Cogeneration: Part II. Experimentation."

International Journal of Thermal Sciences 42 (3): 239–253. ISSN 1290-0729. https://doi.org/10.1016/S1290-0729(02)00024-8.asdf.

6. Shah, A., P. Tunestal, and B. Johansson. 2012. "Investigation of Performance and Emission Characteristics of a Heavy Duty Natural Gas Engine Operated with Pre-Chamber Spark Plug and Dilution with Excess Air and EGR." *SAE Int. J. Engines* 5 (4). doi:10.4271/2012-01-1980.

7. Xi, Y., N. Ottinger, and Z. Liu. 2016. "Effect of Reductive Regeneration Conditions on Reactivity and Stability of a Pd-Based Oxidation Catalyst for Lean-Burn Natural Gas Applications." SAE Technical Paper 2016-01-1005. doi:10.4271/2016-01-1005.

8. Peters, N. 2000. *Turbulent Combustion*. Cambridge University Press, United Kingdom.

Acknowledgements

ANL, NREL, ORNL, and SNL researchers would like to thank Kevin Stork and the U.S. Department of Energy's Vehicle Technologies Office for support of this high-efficiency NG engine research. The principal investigators for this project wish to thank all of their colleagues at their respective laboratories who have conducted this research and so effectively collaborated with each other. ANL, NREL, ORNL, and SNL wish to thank Altronic for supporting all four laboratory experiments with NGI-1000 flexible NG engine SI systems. ANL wishes to thank the Laboratory Computing Resource Center at ANL for supporting this project with the Center's cluster Bebop. NREL wishes to thank Philipp Seidenspinner at Analytic-Service Gesellshaft MbH for support in modifying AFIDA controls to adapt a PCSI module. ORNL wishes to thank Daimler Trucks North America and MAHLE Powertrain for support of this project.

Sandia National Laboratories is a multi-mission laboratory managed and operated by National Technology and Engineering Solutions of Sandia, LLC, a wholly owned subsidiary of Honeywell International, Inc., for the U.S. Department of Energy's National Nuclear Security Administration under contract DE-NA0003525.

III.6 Direct Injection Propane for Advanced Combustion (National Renewable Energy Laboratory)

Brad Zigler, Principal Investigator
National Renewable Energy Laboratory (NREL)
15013 Denver West Parkway
Golden, CO 80401
E-mail: Brad.Zigler@nrel.gov

Michael Weismiller, DOE Technology Development Manager
U.S. Department of Energy
E-mail: Michael.Weismiller@ee.doe.gov

Start Date: July 1, 2017 End Date: September 30, 2019
Project Funding (FY19): $500,000 DOE share: $500,000 Non-DOE share: $0

Project Introduction

For on-road transportation, propane, also known as liquefied petroleum gas (LPG) or propane autogas, is primarily used in spark-ignition (SI) engines adapted from existing original equipment manufacturer (OEM) gasoline engines in cars, light-duty trucks, and medium-duty trucks. Similar to natural gas, dual-fuel adaptations of propane fumigated in the intake air stream of a compression-ignition (CI) heavy-duty (HD) truck engine have also been attempted but are not currently common in the United States. In light- and medium-duty SI engines, propane is commonly used in a bi-fuel strategy in which gasoline is used for the cold start with OEM controls, switching over to propane through additional port fuel injection (PFI) injectors added to the intake manifold, controlled by a piggy-back slave engine control unit using OEM gasoline injector signal inputs after the engine is warmed up. Monofuel propane SI engines have also been available but are less common.

Since most propane engines are based on production OEM SI gasoline engines and vehicles, the industry trend for those engines toward direct injection (DI) represents a technology challenge for propane. The combustion strategy enabled by high pressure, direct fuel injection, and unique piston geometries does not adapt well with propane added on with PFI for bi-fuel operation. Converting to monofuel operation and flowing propane through the OEM gasoline direct injection (GDI) fuel system is also not a simple engineering problem. Beyond adapting propane to GDI technology, a longer-term strategy for propane could involve leveraging injection benefits possible with DI to use propane in advanced CI strategies for higher efficiency with low emissions. Expanded transportation use of propane could be enabled, possibly in LPG blends with other similar molecules, in medium-duty and HD trucks with advanced CI engines. These truck applications will require high efficiency, could build off current fueling infrastructure technology, and may offer low emissions without some of the complex aftertreatment necessary with diesel. This project focuses on early-stage research to understand fundamental challenges and potential for propane blends to support advanced CI using DI.

Objectives

Overall Objectives

- Provide guidance to industry regarding potential for propane blends to enable advanced CI combustion strategies for increased engine efficiency
- Understand technical challenges regarding propane flow through high-pressure direct injectors that support increased engine efficiency.

Fiscal Year 2019 Objectives

- Develop bench-scale experiments to address technical challenges and characterize injection behavior for controlling propane injection through existing OEM DI fuel injectors
- Adapt NREL's constant-volume combustion chamber research facilities to quantify ignition behavior of propane blends under conditions relevant to advanced CI engine operation.

Approach

The research NREL is conducting under this project has a low-technology-readiness-level focus to explore DI of propane with more advanced combustion engine strategies, focusing on increasing efficiency and identifying potential future technology paths leveraging LPG blends. This project builds on recent gasoline direct injection compression ignition (GDCI) advances by Argonne National Laboratory, Delphi, Mazda, and Sandia National Laboratories [1],[2],[3],[4],[5],[6]. Multi-cylinder engine research and development has been demonstrated for variations of GDCI strategies with gasoline-range fuels operating with research octane numbers (RONs) as high as 91–92 [2],[3],[4], but higher efficiencies have been demonstrated with lower RONs (~80) [3]. Fundamental challenges for DI of propane under an advanced low-temperature-combustion, advanced CI strategy include fuel spray penetration/breakup/evaporation behavior [7], ignition properties, and fuel system handling issues [8] that are significantly different from those associated with gasoline.

Leveraging propane system knowledge gained from a prior higher-technology-readiness-level project, NREL previously conducted scale experiments in Fiscal Year (FY) 2018 to understand how propane behaves with the high-pressure DI fuel injector types required for injecting fuel during the compression stroke. FY 2019 research expanded these bench-scale injection control studies to span a range of fuel properties, including propane. In FY 2018, NREL also conducted computational fluid dynamics simulations to model propane injection behavior through DI fuel injectors originally designed for diesel or gasoline-range fuels. Since existing kinetic mechanisms do not cover propane blends of interest, NREL continued adapting the Advanced Fuel Ignition Delay Analyzer (AFIDA) constant-volume combustion chamber platform to conduct experiments on propane blend ignition delay performance under advanced CI-relevant conditions [9]. These ignition kinetics studies build on other related research NREL is performing, as reported in another FY 2019 Annual Progress Report chapter, "Fuel Autoignition Behavior." These bench-scale experiments and simulations were integrated in FY 2019 and will be completed in FY 2020.

NREL's approach involves collaboration, including an undergraduate student intern, Jacob Barson from Colorado School of Mines. NREL has also been reviewing this project with industry for technical guidance, including meetings with the propane industry, engine OEMs, and key engine component suppliers.

Results

NREL's prior related research studying gasoline-range ignition kinetics in the AFIDA highlighted issues with flowing low-boiling-range, low-viscosity fuels through a diesel piezoelectric fuel injector. This type of fuel injector is used in the AFIDA, and a similar injector is used in NREL's new advanced CI research single-cylinder engine, which is based on the Ford 6.7 L Power Stroke diesel engine. While a DI injector is needed to inject fuel at sufficient pressure to provide adequate mixing during the compression stroke in an advanced CI strategy, it was not yet certain whether propane blends would need to be injected at very high pressures typical of diesel (~2,000 bar) or moderate pressures typical of GDI (~200 bar). While GDI injection pressures may be sufficient, bench studies are still valuable because newer-generation GDI injectors include piezoelectric actuation (instead of a solenoid) that may be necessary to provide multiple discrete injection events. Earlier NREL research has shown that gasoline-boiling-range fuels do not allow the internal hydraulic flow control valving in a piezoelectric diesel injector to function properly; propane was expected to be worse. Those earlier qualitative studies indicated the piezoelectric injector internal valving did not sufficiently seal to provide adequate injection control when fuel samples were progressively stepped from diesel to higher volatility with various blends of iso-octane and pentane.

In FY 2019, NREL designed and fabricated a new bench-scale system to characterize injection of liquid propane and liquid propane/higher hydrocarbon mixtures through a piezoelectric diesel injector (and/or a solenoid or piezoelectric gasoline injector), as shown in Figure III.6.1. In that figure, the green cylinder in the top right is a housing for the liquid-phase propane fuel mixture supplied to the injector. At the center of the bench system is a syringe pump that supplies fuel to the injector at 10,000 psi. The Bosch piezoelectric diesel injector used was from a Ford 6.7 L Power Stroke engine, common to the platform used for NREL's new advanced fuels research single-cylinder engine. The injector is located in the sectioned production OEM cylinder head on the left, and it fires into a simulated cylinder collection vessel below. Once it has passed through the injector, gaseous fuel is pulled through the remainder of the system via a vacuum pump, shown at the bottom right. After injection, the fuel passes through a liquid catch and a mass flow meter before being vented into the hood. This flow meter is used to quantify fuel flow over a number of injection events. The system was designed to ensure the injected liquids flash to gas-phase after injection in order to measure the flow of fuel injected with a mass flow meter. Data collection includes volumetric totals of injected fuel, as a function of injection pressure, injector pulse width and frequency, and the amount of fuel bypassing the injector. The bypassed fuel normally returns to the high-pressure fuel pump. However, low-viscosity and low-lubricity fuels can increase the rate of bypass flow, potentially leading to degraded peak injector flow rate and increased fuel heating. Collection and analysis of these data will aid in validating the use of these piezoelectric injectors in future DI propane engines.

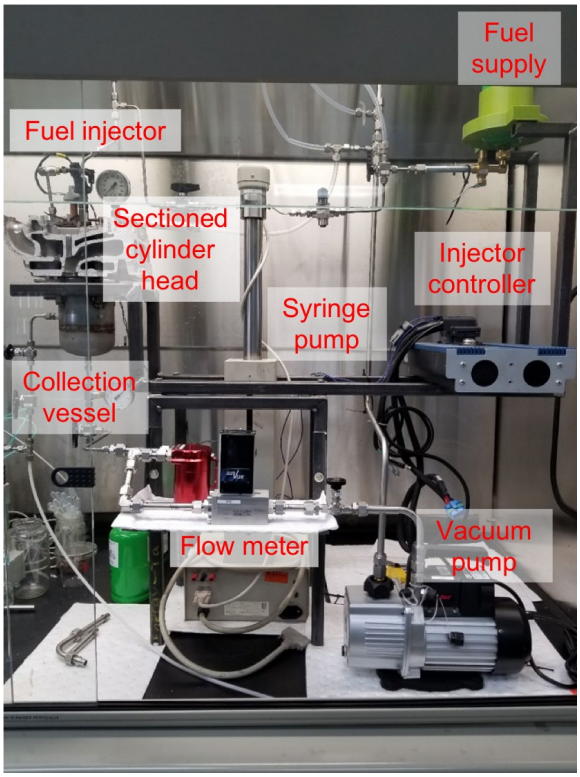

Figure III.6.1 Bench-scale fuel injector flow measurement experimental apparatus (figure: Jacob Barson, NREL)

The experimental validation centered around documenting injector behavior during operation while flowing propane and propane–liquid hydrocarbon mixtures through the injector. Past experiments designed to validate injector behavior when flowing dry liquid fuels such as iso-pentane and iso-octane were successful, indicating that injector operation with propane and propane fuel mixtures may be possible. However, when working with these propane fuel mixtures, it is expected that the use of lubricity additives will be required to achieve injector performance comparable to operation with diesel fuel. Prior research has shown that dosing gasoline-range

fuels with Infineum R655 lubricity additive on the order of 1,000 parts per million by volume (ppmv) restored injector performance comparable to operation with diesel fuel [1],[9]. Experiments in FY 2019 included preliminary trials for the fuels listed in Table III.6.1. Experimental studies are currently underway, including with lubricity additive doping. These bench-scale injector studies will be completed and published in FY 2020 with remaining carryover funding.

Table III.6.1 Range of Fuel Properties Studied in Bench-Scale Injector Control Experiments

Fuel	Boiling Point (or range, °C)	Viscosity Level (cP)
Diesel	150–370	2.40
Iso-octane	99	0.5
Iso-octane/iso-pentane mixtures	28–99	0.23–0.5
Iso-pentane	28	0.023
Iso-pentane/propane mixtures	-42–99	Not known
Propane	-42	0.198 @ 1 bar / -41°C 0.1117 @ 100 bar / 27°C

In FY 2019, NREL continued preparing the AFIDA for propane and LPG blend ignition delay studies to enable advanced CI operation, guided by the bench-scale injector flow studies previously noted. The HD-5 transportation fuel specification [10] for LPG will serve as a starting point, but its high pump octane anti-knock index (AKI) rating (~104–112) [11] and minimum RON (108.2) [12] will likely prevent its direct use for advanced CI strategies. In FY 2020, NREL will study ignition behavior of HD-5 LPG and various propane blends to provide guidance on blends that will lower ignition resistance, realizing that current metrics of RON or octane sensitivity may not be sufficient. The propane blend components must maintain LPG-like physical properties, and researchers continue to gather industry feedback to understand potential impacts on transportation LPG fueling infrastructure. Propane blends for this GDCI-like study include propane blended with natural gasolines (~C5–C6), which have RON ~68–72 with very low octane sensitivity [13],[14]. Initial linear blend calculations for propane (estimated RON = 110) blended with natural gasoline (estimated RON = 70) provide blends as shown in Table III.6.2.

Table III.6.2. Estimated Volumetric Blending for Propane/Natural Gasoline

Estimated RON	Propane Volume %	Natural Gasolline Volume %
98	70	30
94	60	40
90	50	50
86	40	60
82	30	70

NREL previously reached out to industry to understand more about GDCI studies with naphtha-range blends, as light naphtha has a RON in the range of ~68 and heavy naphtha in the range of <40 [15]. Other researchers have evidently also investigated CI of propane blended with cetane improvers, but their recent published work focuses on propane blends with diesel fuel [16],[17]. NREL will follow up with those researchers to

understand how cetane improvers blended directly with propane were studied and whether this is relevant to GDCI-like combustion.

Conclusions

- A new bench-scale experimental apparatus has been constructed to quantify fuel injection flow control with propane-range fuels that may challenge piezoelectric DI injectors.
- Preliminary experiments have been conducted to determine whether lubricity additives may enable LPG to operate with a piezoelectric DI injector, and more experiments are in progress.
- The AFIDA is being prepared for a series of studies mapping propane blend ignition in support of advanced CI engine strategies.

References

1. Kolodziej, C., J. Kodavasal, S. Ciatti, S. Som, et al. 2015. "Achieving Stable Engine Operation of Gasoline Compression Ignition Using 87 AKI Gasoline Down to Idle." SAE Technical Paper 2015-01-0832. doi:10.4271/2015-01-0832.

2. Sellnau, M., W. Moore, J. Sinnamon, K. Hoyer, et al. 2015. "GDCI Multi-Cylinder Engine for High Fuel Efficiency and Low Emissions." *SAE Int. J. Engines* 8 (2). doi:10.4271/2015-01-0834.

3. Cho, K., E. Latimer, M. Lorey, D. Cleary, et al. 2017. "Gasoline Fuels Assessment for Delphi's Second Generation Gasoline Direct-Injection Compression Ignition (GDCI) Multi-Cylinder Engine." *SAE Int. J. Engines* 10 (4). doi:10.4271/2017-01-0743.

4. Kolodziej, C., M. Sellnau, K. Cho, and D. Cleary. 2016. "Operation of a Gasoline Direct Injection Compression Ignition Engine on Naphtha and E10 Gasoline Fuels." *SAE Int. J. Engines* 9 (2). doi:10.4271/2016-01-0759.

5. Fujiwara, K. n.d. "Briefing on Mazda's Long-Term Vision for Technology Development Technical Overview of SKYACTIV-X." Mazda Motor Corporation. Accessed September 2017. https://www.scribd.com/document/355807597/mazda-zoom-zoom-2030-skyactiv-x-fujiwara-presentation.

6. Gentz, G., J. Dernotte, C. Ji, D.L. Pintor, et al. 2019. "Combustion-Timing Control of Low-Temperature Gasoline Combustion (LTGC) Engines by Using Double Direct-Injections to Control Kinetic Rates." SAE Technical Paper 2019-01-1156. doi:10.4271/2019-01-1156.

7. Lacey, J., F. Poursadegh, M. Brear, P. Petersen, et al. 2016. "Optical Characterization of Propane at Representative Spark Ignition, Gasoline Direct Injection Conditions." SAE Technical Paper 2016-01-0842. doi:10.4271/2016-01-0842.

8. Krieck, M., M. Günther, S. Pischinger, U. Kramer, et al. 2016. "Future Specification of Automotive LPG Fuels for Modern Turbocharged DI SI Engines with Today's High Pressure Fuel Pumps." *SAE Int. J. Fuels Lubr.* 9 (3). doi:10.4271/2016-01-2255.

9. Luecke, J., M.J. Rahimi, B.T. Zigler, and R.W. Grout. 2020. "Experimental and Numerical Investigation of the Advanced Fuel Ignition Delay Analyzer (AFIDA) Constant-Volume Combustion Chamber as a Research Platform for Fuel Chemical Kinetic Mechanism Validation." *Fuel* 265 (April 1): 116929, ISSN 0016-2361. https://doi.org/10.1016/j.fuel.2019.116929.

10. Gas Processors Association. 1997. Liquefied Petroleum Gas Specifications and Test Methods, Designation 2140. Tulsa, OK.

11. Alternative Fuels Data Center. n.d. “Propane Benefits and Considerations.” Accessed 2019. https://www.afdc.energy.gov/fuels/propane_benefits.html.

12. da Silva, G., K. Morganti, T.M. Foong, M.J. Brear, Y. Yang, and F. Dryer. 2013. “The Research and Motor Octane Numbers of Liquefied Petroleum Gas (LPG).” *Fuel* 108: 797–811. 10.1016/j.fuel.2013.01.072.

13. Alleman, T.L., and J. Yanowitz. 2016. “Property Analysis of Ethanol−Natural Gasoline−BOB Blends to Make Flex Fuel.” Technical Report NREL/TP-5400-67243 (November).

14. Alleman, T.L., R.L. McCormick, and J. Yanowitz. 2015. “Properties of Ethanol Fuel Blends Made with Natural Gasoline.” *Energy & Fuels* 29 (8): 5095–5102. doi: 10.1021/acs.energyfuels.5b00818.

15. Viollet, Y., J. Chang, and G. Kalghatgi. 2014. “Compression Ratio and Derived Cetane Number Effects on Gasoline Compression Ignition Engine Running with Naphtha Fuels.” *SAE Int. J. Fuels Lubr.* 7 (2). doi:10.4271/2014-01-1301.

16. Mancaruso, E., R. Marialto, L. Sequino, B. Vaglieco, et al. 2015. “Investigation of the Injection Process in a Research CR Diesel Engine Using Different Blends of Propane-Diesel Fuel.” SAE Technical Paper 2015-24-2477. doi:10.4271/2015-24-2477.

17. Cardone, M., E. Mancaruso, R. Marialto, L. Sequino, et al. 2016. “Characterization of Combustion and Emissions of a Propane-Diesel Blend in a Research Diesel Engine.” SAE Technical Paper 2016-01-0810. doi:10.4271/2016-01-0810.

Acknowledgements

NREL would like to thank Mike Weismiller for his support of this research. Matt Ratcliff led this research effort and mentored intern Jacob Barson from Colorado School of Mines, who designed and constructed the experimental apparatus. Matt Viele from Vieletech provided invaluable assistance with fuel injector controls. NREL greatly appreciates Ford Motor Company’s support in sharing design information to base NREL’s new advanced CI research single-cylinder engine on the Ford 6.7 L combustion chamber and architecture, including the fuel injector used in this project. NREL would also like to acknowledge valuable feedback provided to date from various meetings with the propane industry, engine OEMs, and key engine component suppliers.

IV Emission Control R&D

IV.1 Joint Development and Coordination of Emission Control Data and Models: Crosscut Lean Exhaust Emissions Reduction Simulations (CLEERS) Analysis and Coordination (Oak Ridge National Laboratory)

Josh Pihl, Principal Investigator
Oak Ridge National Laboratory (ORNL)
2360 Cherahala Boulevard
Knoxville, TN 37931
E-mail: pihlja@ornl.gov

Ken Howden, DOE Technology Development Manager
U.S. Department of Energy
E-mail: Ken.Howden@ee.doe.gov

Start Date: October 1, 2018 End Date: September 30, 2021
Project Funding (FY19): $600,000 DOE share: $600,000 Non-DOE share: $0

Project Introduction

Catalytic emissions control devices will play a critical role in deployment of advanced high-efficiency engine systems by enabling compliance with increasingly stringent emissions regulations. High-efficiency diesel and lean gasoline engines, for example, will require NO_x reduction catalysts with very high conversion efficiencies to meet the U.S. Environmental Protection Agency's Tier 3 NO_x emissions standard. Low-temperature combustion strategies, on the other hand, significantly reduce engine-out NO_x, but they generate a challenging combination of high hydrocarbon and carbon monoxide concentrations at low exhaust temperatures that will likely demand novel approaches to emissions control. Design of progressively more complex engine/aftertreatment systems will rely increasingly on advanced simulation tools to ensure that next-generation vehicles maximize efficiency while still meeting emissions standards. These simulation tools will, in turn, require accurate, robust, and computationally efficient component models for emissions control devices. Recognizing this need, the U.S. Department of Energy (DOE) Advanced Engine Crosscut Team initiated the Crosscut Lean Exhaust Emissions Reduction Simulations (CLEERS) activity to support development of improved computational tools and data for simulating realistic full-system performance of high-efficiency engines and associated emissions control systems. DOE provides funding to ORNL to perform two complementary roles that support this goal: (1) coordination of CLEERS activities that provide a consistent framework for sharing information and supporting precompetitive collaborative interactions among the emissions control community, and (2) focused measurement, analysis, and modeling activities aimed at developing the strategies, data sets, and device parameters needed for better models of catalytic emissions control devices through collaborations with other National Laboratories and partners in academia and industry.

Objectives

Overall Objective

The overall objective of this project is to support industry in the development of accurate simulation tools for the design of catalytic emissions control systems that will enable advanced high-efficiency combustion engines to meet emissions regulations while maximizing fuel efficiency.

Fiscal Year 2019 Objectives

- Coordinate the CLEERS activity for the DOE Advanced Engine Crosscut Team
- Support precompetitive collaborative interactions, and provide a consistent framework for sharing information among the emissions control research and development community
- Identify emissions control research and development needs and priorities
- Collaborate with Pacific Northwest National Laboratory to develop mechanistic insights, modeling strategies, benchmark data sets, and representative device parameters for catalytic emissions control devices
- Utilize the CLEERS framework to share the resulting insights, strategies, data sets, and parameters with the emissions control community.

Approach

In its administrative role, ORNL coordinates the CLEERS Planning Committee, the CLEERS Focus Group teleconferences, CLEERS public workshops, the biannual CLEERS industry priorities survey, and the CLEERS website (www.cleers.org). ORNL acts as a communication hub and scheduling coordinator among these groups and as the spokesperson and documentation source for CLEERS information and reports. The latter role involves preparing and presenting status reports to the Advanced Engine Crosscut Team, responding to public requests and inquiries about CLEERS, and developing summary reports from the biannual industry surveys.

Measurement, analysis, and modeling activities are conducted in collaboration with Pacific Northwest National Laboratory. These activities include identifying reaction mechanisms occurring over catalytic devices under relevant operating conditions, developing modeling strategies that represent key catalyst processes in a computationally efficient manner, generating benchmark data sets for model calibration and validation, and measuring critical device parameters needed for model development. The results of these activities are disseminated through the CLEERS information-sharing apparatuses and through publications and presentations. Research directions are guided by the DOE Advanced Engine Crosscut Team, which collectively oversees CLEERS, and by regular CLEERS industry participant priority surveys. ORNL's CLEERS research activities are currently focused on low-temperature aftertreatment technologies such as passive NO_x adsorbers and hydrocarbon traps.

Results

Below is a summary of Fiscal Year (FY) 2019 accomplishments:

- Organized the 2019 DOE Crosscut Workshop on Lean Emissions Reduction Simulation (CLEERS Workshop) in Ann Arbor, Michigan, September 17–19, 2019
- Facilitated CLEERS Focus Group teleconferences, which continue to have strong domestic and international participation (typically over 40 participants, a majority of which are from industry)
- Provided regular update reports to the DOE Advanced Combustion Engine Crosscut Team
- Supported the Advanced Combustion and Emissions Control Tech Team's Low-Temperature Aftertreatment Team in developing evaluation protocols for low-temperature catalysts and identifying future research directions
- Conducted extensive experiments to measure the impacts of exhaust gas composition and temperature on the storage and release of NO on a Pd-exchanged zeolite passive NO_x adsorber material.

Developed a revised a conceptual mechanism to explain trends in both NO storage capacity and uptake rates.

ORNL's CLEERS coordination work during FY 2019 continued to focus on activities that CLEERS industrial participants identified as high priorities, including the CLEERS Workshop, teleconferences, and the CLEERS website.

The 2019 (22nd) CLEERS Workshop was held September 17–19, 2019, in Ann Arbor, Michigan. The workshop was open to participants from any organization or institution, and workshop registrations once again reached full capacity. Figure IV.1.1(a) illustrates the broad cross-section of organizations represented at the event. The workshop agenda included 4 invited speakers, 35 contributed presentations, 19 posters, and an industry panel discussion on "PGM [Platinum Group Metal] Utilization and Replacement." Additional details, including many of the workshop presentations, can be found on the CLEERS website (https://cleers.org) under the 2019 Workshop heading.

ORNL continued hosting CLEERS Focus Group technical teleconferences in FY 2019. The presentations covered a wide range of research results in emissions control experimentation, modeling, and simulation by members of the CLEERS Focus Group as well as outside experts. Presenters included Jason Lupescu (Ford Motor Co.), Eric Hruby (John Deere), Ameya Joshi (Corning), Paul Ragaller (CTS Corp.), and Professor Raj Gounder (Purdue University). Teleconference attendance was between 40 and 60 participants, with industry representing well over half of them (Figure IV.1.1[b]).

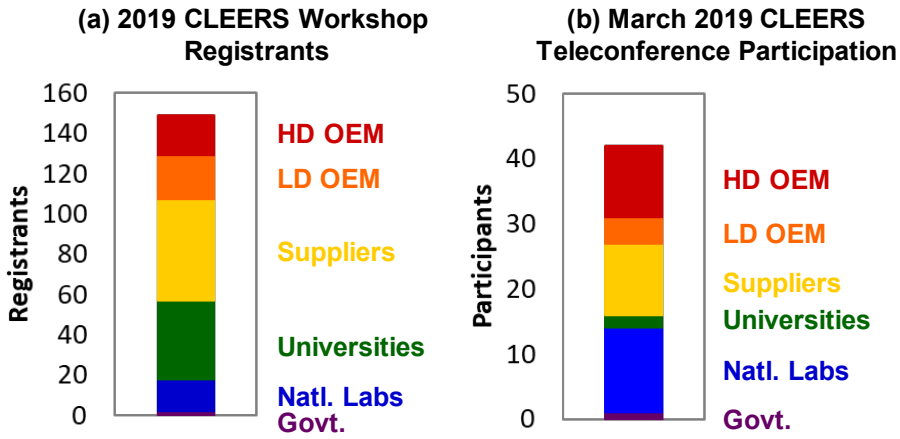

HD – heavy-duty; LD – light-duty; OEM – original equipment manufacturer

Figure IV.1.1 (a) 2019 CLEERS Workshop registrations and (b) March 2019 CLEERS teleconference participants by type of organization

ORNL also continued to work closely with Pacific Northwest National Laboratory and the industry members of the Advanced Combustion and Emissions Control Tech Team's Low-Temperature Aftertreatment Working Group to support development of new low-temperature catalyst laboratory evaluation protocols. The protocols for oxidation catalysts, three-way catalysts, low-temperature storage materials, and urea selective catalytic reduction catalysts are all available for download from the CLEERS website.

During FY 2019, ORNL's CLEERS measurement, analysis, and modeling activities continued to focus on NO storage and release on a passive NO_x adsorber catalyst. Johnson Matthey provided a Pd-exchanged ZSM-5 (Zeolite Socony Mobil–5) core sample that was used in a series of synthetic exhaust flow reactor experiments designed to measure the impacts of exhaust composition and temperature on NO storage capacity and release temperatures. Much of the effort during FY 2019 focused on repeating experiments from FY 2018 at a higher temperature (150°C instead of 100°C); the purpose was to get a better understanding of the interactions

between NO, H_2O, and CO on the Pd storage sites. Figure IV.1.2 shows the impact of changing H_2O concentration during NO adsorption at both 100°C and 150°C. The dashed vertical lines, which indicate the time at which 10% of the inlet NO concentration slips from the catalyst, show that increasing H_2O concentration decreases the rate of NO uptake (leading to faster breakthrough) at 100°C, but increasing H_2O has no effect at 150°C. Other experiments showed that increasing CO concentration increases the rate of NO uptake at 100°C but has no effect at 150°C, implying that the benefit of CO comes from mitigation of the impacts of H_2O at 100°C.

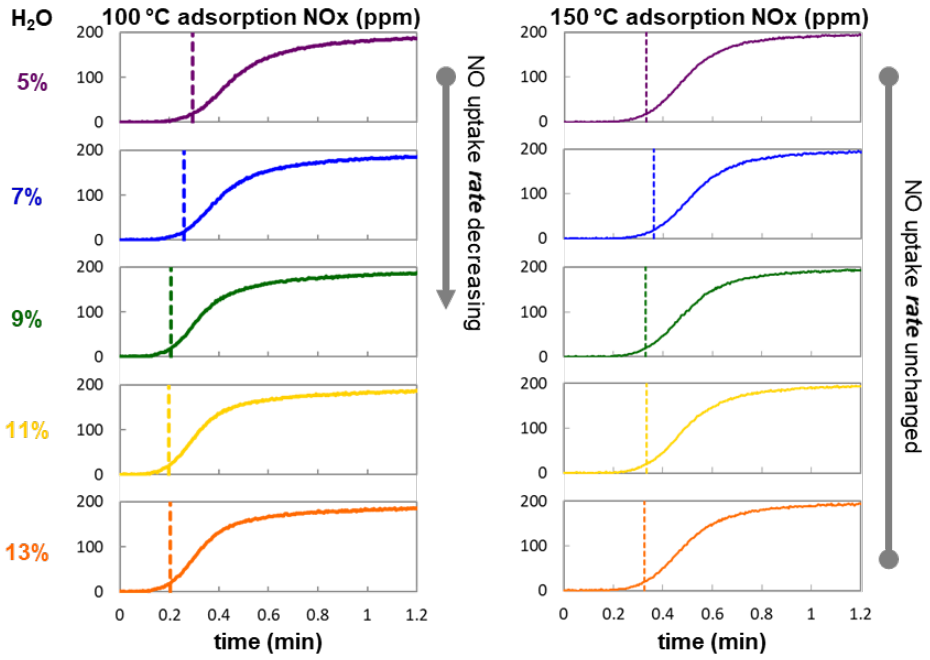

Figure IV.1.2 Effects of H_2O concentration on isothermal NO uptake profiles over a Pd/ZSM-5 passive NO_x adsorber at 100°C and 150°C. Synthetic exhaust mixtures included 200 ppm NO, 200 ppm CO, 10% O_2, and 5%–13% H_2O at a space velocity of 30,000 h^{-1}.

Figure IV.1.3 shows another set of data that looked at how the order of exposure of CO and NO affects the rate of NO uptake and the total NO storage capacity. Exposing the catalyst to CO first results in much faster NO uptake (and longer time to breakthrough), while exposing the catalyst to NO and CO at the same time or NO first results in a much lower rate of NO uptake. However, the order of exposure has no impact at all on the total amount of NO stored, as illustrated by the identical NO release profiles.

In summary, the experimental results show that:

- Increasing H_2O decreases the rate of NO uptake at 100°C.
- Increasing CO increases the rate of NO uptake at 100°C.
- Neither H_2O nor CO impacts the rate of NO uptake at 150°C.
- Changes in H_2O and CO concentration do not have a major impact on the total NO storage capacity; they affect just the uptake rate.

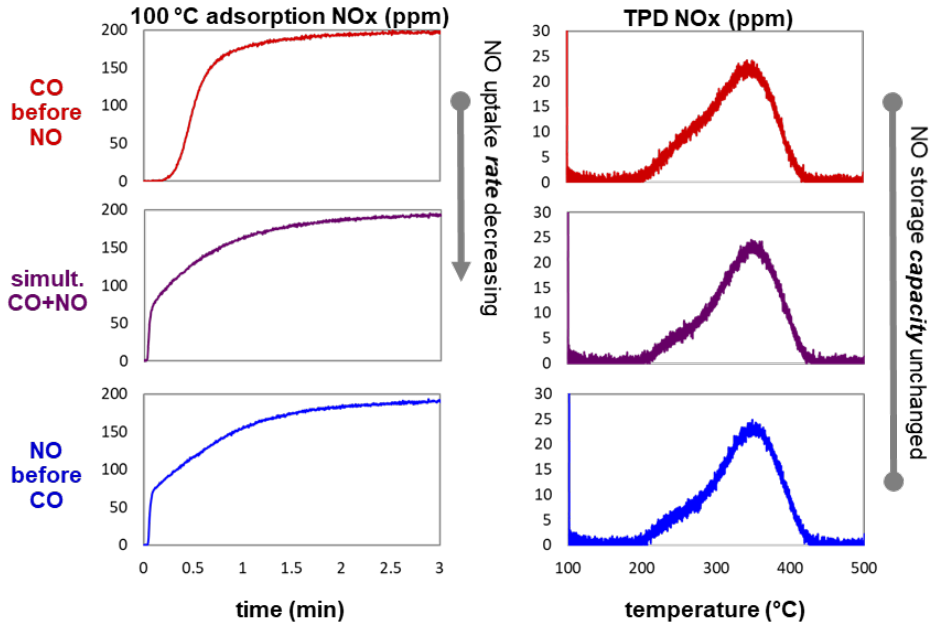

Figure IV.1.3 Effects of order of exposure of NO and CO on isothermal NO uptake at 100 °C and temperature programmed desorption (TPD) profiles for a Pd/ZSM-5 passive NO_x adsorber. Synthetic exhaust mixtures included 200 ppm NO, 200 ppm CO, 10% O_2, and 7% H_2O at a space velocity of 30,000 h^{-1}.

One potential explanation for these observations is that H_2O blocks access to the Pd sites by forming hydrated complexes at low temperatures, and CO displaces some of the H_2O surrounding the Pd sites when it adsorbs on the Pd. At higher temperatures, the hydrated Pd complexes are less prevalent since there is less H_2O adsorbed in the zeolite pores. These observations, combined with prior conclusions from FY 2018 work, have been incorporated into a conceptual model for NO adsorption and desorption that is summarized in Figure IV.1.4. ORNL is currently collaborating with Professor William Epling at the University of Virginia to further refine this conceptual model, which will be used to guide development of simulation tools for predicting passive NO_x adsorber performance and behavior.

Conclusions

- CLEERS continues to be a valuable resource for the aftertreatment development community, based on the high level of participation in the CLEERS Workshop and Focus Group teleconferences.
- NO storage and release on a Pd-exchanged ZSM-5 passive NO_x adsorber material depend on the exhaust gas composition (particularly H_2O and CO concentrations) and exposure temperature. A conceptual model has been proposed to account for the key observed trends in NO uptake. After further refinement, this conceptual model will guide the development of simulation tools for passive NO_x adsorbers.

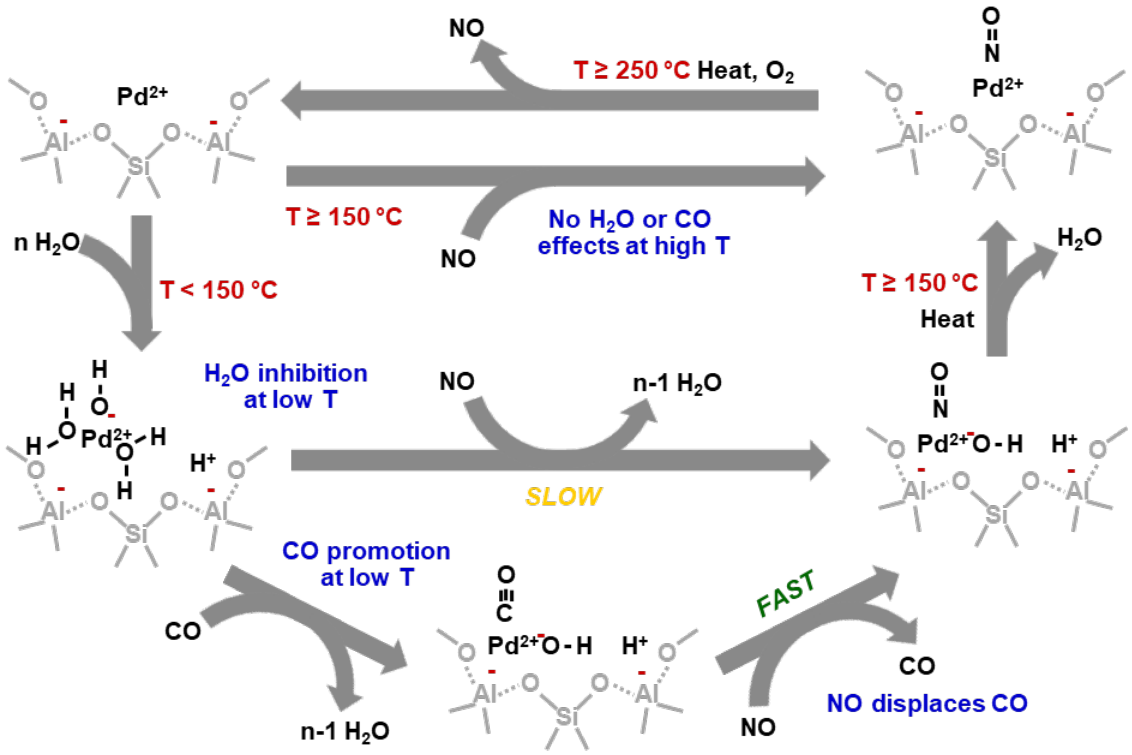

Figure IV.1.4 Conceptual model of NO adsorption and desorption on a Pd-exchanged zeolite passive NO_x adsorber that accounts for the interacting effects of temperature, H_2O, and CO

Key Publications

1. Gao, Z., D. Deter, D. Smith, J.A. Pihl, C.S. Daw, and J.E. Parks II. 2019. "Engine-Aftertreatment in Closed-Loop Modeling for Heavy Duty Truck Emissions Control." SAE Technical Paper 2019-01-0986.

Acknowledgements

Coauthors of this report include Vitaly Prikhodko, Sreshtha Sinha Majumdar, Calvin Thomas, Todd Toops, Charles Finney, and Zhiming Gao of ORNL. The authors gratefully acknowledge Haiying Chen of Johnson Matthey for providing catalyst samples and technical guidance for this work.

IV.2 CLEERS Aftertreatment Modeling and Analysis (Pacific Northwest National Laboratory)

Yong Wang, Principal Investigator
Pacific Northwest National Laboratory (PNNL)
P.O. Box 999, MS K2-12
Richland, WA 99354
E-mail: yong.wang@pnnl.gov

Ken Howden, DOE Technology Development Manager
U.S. Department of Energy
E-mail: Ken.Howden@ee.doe.gov

Start Date: October 1, 2018 End Date: September 30, 2019
Project Funding (FY19): $1,150,000 DOE share: $1,150,000 Non-DOE share: $0

Project Introduction

The Crosscut Lean Exhaust Emissions Reduction Simulations (CLEERS) initiative is a research and development focus project of the Diesel Crosscut Team, funded by the U.S. Department of Energy's (DOE's) Vehicle Technologies Office. The overall objective is to promote the development of improved computational tools for simulating realistic full-system performance of lean-burn engines and the associated emissions control systems. Through CLEERS, PNNL supports fundamental research projects in four topic areas: selective catalytic reduction (SCR), passive NO_x (oxides of nitrogen) adsorbers (PNAs), multifunctional devices, and low-temperature aftertreatment (LTAT). Resources are shared among these efforts to allow for active response to current industrial needs.

Objectives

- Promote the development of improved computational tools for simulating realistic full-system performance of lean-burn engines and the associated emissions control systems
- Provide the practical and scientific understanding and analytical base required to enable the development of efficient, commercially viable emissions control solutions for ultra-high-efficiency vehicles
- Lead and contribute to the CLEERS activities, e.g., lead technical discussions, invite distinguished speakers, maintain an open dialogue on modeling issues, and work closely with the Advanced Combustion and Emission Control (ACEC) LTAT team to actively respond to current industrial needs.

Approach

This project builds off PNNL's strong base in fundamental sciences by effectively leveraging capabilities from the Institute for Integrated Catalysis and the Environmental Molecular Sciences Laboratory. The Institute is the largest non-industrial catalysis organization in the United States, and the Laboratory is a DOE scientific user facility located at PNNL. The project team collaborates closely with the private sector (BASF, Cummins, General Motors, Johnson Matthey, and Kymanetics) to address science-based questions of import and broad interest to industry. The CLEERS project is strongly oriented toward addressing fundamental issues with broad impacts on applications and commercialization, working closely with original equipment manufacturers, Tier 1 suppliers, and project partners and sponsors (e.g., Oak Ridge National Laboratory and the DOE Advanced Engine Crosscut Team).

Results

Key accomplishments for Fiscal Year 2019 include the following:

- Using advanced in situ characterization coupled with theory, for the first time, the researchers provided detailed Cu/SAPO-34 (copper/silicoaluminophosphate zeolite) deactivation pathways during low-temperature moisture treatment and storage.
- The project achieved atomic Pd dispersion with a modified preparation method and selection of the right form of zeolites for Pd/SSZ-13-based PNAs. The researchers also provided more accurate descriptions of Pd sites under practical conditions for simulations under CLEERS.
- PNNL led the LTAT group in completing the Low-Temperature NH_3-SCR Catalyst Test Protocol, which was released to the CLEERS website for review and will be used by the technical community. Parallel to those efforts, the team also captured all four low-temperature catalyst test protocols (Oxidation, Storage/Release, Three-Way Catalyst, and NH_3-SCR) in an open literature publication.
- Researchers discovered that significantly improved oxygen activation via the atom trapping approach to prepare a Pt-based single-atom catalyst leads to enhanced low-temperature CO oxidation activity.
- The team developed a new technique to measure local permeability in multifunctional filters with zoned catalyst coatings and to compare with simulation results, which can then be used for the future device-scale modeling.

SCR

Commercial Cu/SAPO-34 SCR catalysts have experienced unexpected and quite perplexing failure. Understanding the causes at an atomic level is vital for the synthesis of more robust Cu/SAPO-34 catalysts. Using model Cu/SAPO-34 catalysts with homogeneously dispersed, isolated Cu ions, the project shows that Cu transformations resulting from low- and high-temperature hydrothermal aging and ambient-temperature storage (Figure IV.2.1) can be semi-quantitatively probed with two-dimensional pulsed electron paramagnetic resonance. Coupling these results with SCR kinetics, additional material characterizations, and density functional theory simulations, the project team proposes the following catalyst deactivation steps: (1) detachment of Cu(II) ions from catalytically active cationic positions, likely in the form of $Cu(OH)_2$; (2) irreversible hydrolysis of the SAPO-34 framework that forms terminal Al species; and (3) interaction between $Cu(OH)_2$ and terminal Al species to form SCR-inactive, Cu-aluminate-like species. Especially significant is that these reactions are shown to be greatly facilitated by condensed water molecules under wet ambient conditions, causing the “mysterious” low-temperature failure of the commercial Cu/SAPO-34 catalysts. Furthermore, these discoveries explain why the typical hydrothermal aging conditions practiced by industries cannot be used to access these deactivation processes: there is a lack of sufficient concentration of adsorbed water within the zeolite.

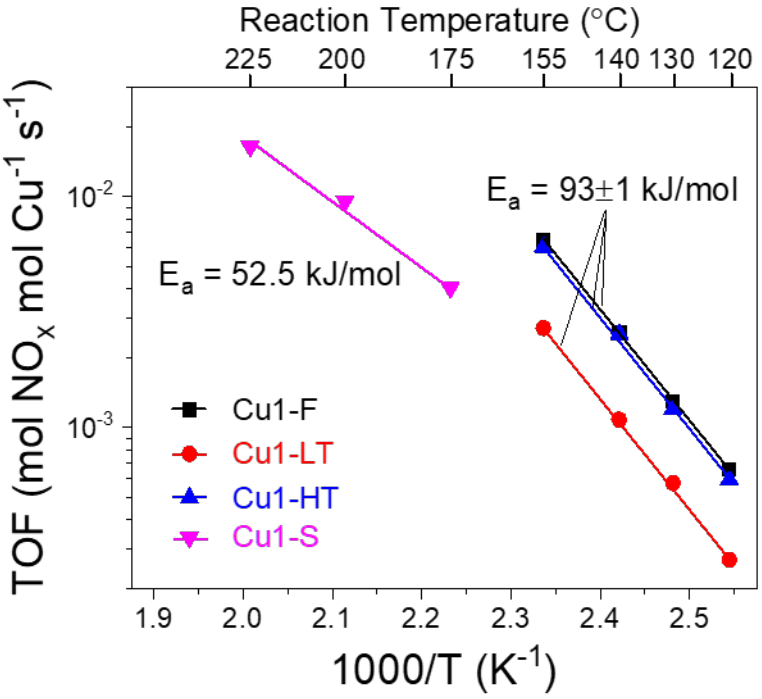

Figure IV.2.1 Arrhenius plots for low-temperature standard NH_3-SCR on 0.71 wt% Cu/SAPO-34 catalysts (Cu1-F: freshly prepared; Cu1-LT: hydrothermally treated at 70°C; Cu1-HT: hydrothermally treated at 800°C; and Cu1-S: stored in ambient conditions for 240 days). The feed gas contained 360 ppm NO, 360 ppm NH_3, 14% O_2, 2.5% H_2O, and balance N_2. The total gas flow was 1,000 sccm, and the gas hourly space velocity was estimated to be ~650,000 h^{-1}. Turnover frequency (TOF) was calculated using pulsed electron paramagnetic resonance active Cu(II) contents in each sample.

PNA

The project developed a direct, simple, and scalable route to highly loaded ionic Pd and Pt in a small-pore siliceous ($3 < Si/Al < 12$) zeolite (Figure IV.2.2). This route utilizes only wet chemistry and does not require the use of expensive organometallic precursors or organic solvents. The key is to use the NH_4-form of the zeolite and the modified incipient wetness impregnation method, not the conventional ion exchange. Furthermore, the researchers reconciled the contradictory literature data, in which the Fourier-transform infrared spectroscopy characterization for high-loaded Pt and Pd species in ZSM-5 and other zeolites always indicates the presence of significant amounts of metallic nanoparticles (not well-dispersed Pd or Pt). The reasons are as follow:

- H-forms of zeolite are often used for ion exchange.
- Si/Al ratios >10 are not able to disperse metals as individual atoms because of the decreased hydrophilicity of the zeolite micropores.
- For Pt, the calcination temperature should not exceed 350°C because of the instability of ionic Pt2+ above this temperature.

These new insights led to the synthesis of Pd/SSZ-13 with up to 2 wt% atomically dispersed Pd for immediate industrial application as CO and passive NO_x adsorbers. These materials are able to abate 180 $\mu moleg^{-1}$ NO_x and simultaneously CO during cold-start of the vehicle while maintaining atomic dispersion. The project achieved complete utilization of each Pd atom, surpassing the best performance of Pd/zeolite adsorbers reported in both patents and open literature.

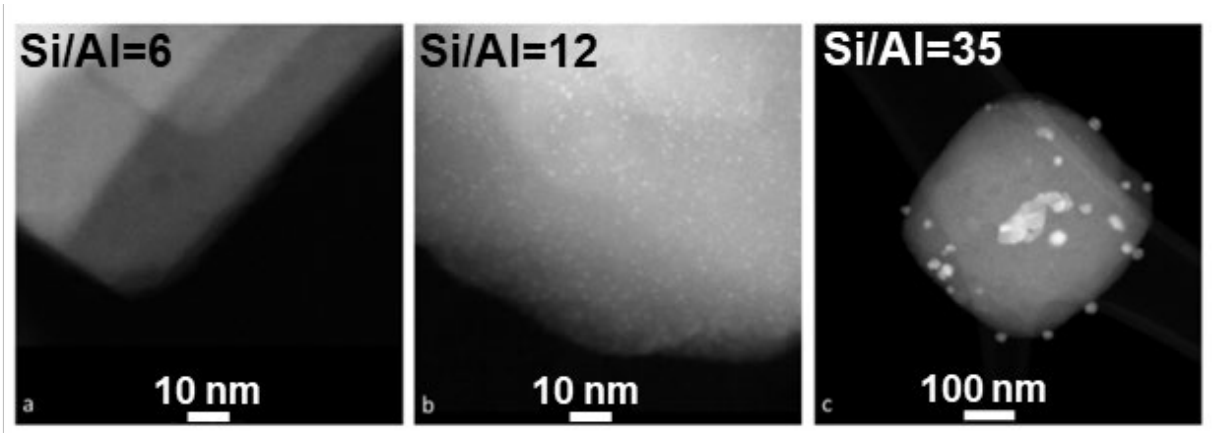

Figure IV.2.2 High-angle annular dark-field scanning transmission electron microscopy (HAADF-STEM) images of 1 wt% Pd/H-SSZ-13: a) Si/Al=6, b) Si/Al=12, c) Si/Al=35

Multifunctional Devices

In previous work, PNNL showed that a commercial SCR-filter brick deployed in the United States exhibited three distinct axial coating zones, each having different loading patterns and quantities of SCR catalyst. To understand the effects of this coating configuration on flow patterns within the device, the research team developed a method for approximately measuring the local permeability of the filter wall. Small sections of the honeycomb filter (four-by-four channels, approximately ½ inch long) were removed from each of the axial zones. Custom-designed manifolds were created using a 3D printer. The manifolds directed flow to the alternating inlet channels, forcing air through the filter walls and allowing it to exit via the outlet channels. By measuring flow and pressure drop, the researchers could calculate permeability values for a number of small samples taken from each axial zone. To better understand the effects of microscale catalyst distribution and washcoat morphology in the three zones, the team made three-dimensional reconstructions from micro X-ray computed tomography (CT) data having a resolution of approximately 1.7 microns. These reconstructions were used for detailed flow simulations, as shown in Figure IV.2.3. A total of twelve simulations were run, four in each of the three axial zones. Both the experiments and the lattice-Boltzmann simulations showed the expected variation in permeability between the three zones. Permeability was highest in the first of the axial zones, closest to the filter inlet, which had a relatively light coating, predominantly on the inlet side of the filter wall. Measured permeabilities were roughly an order of magnitude lower in the second axial zone, which had heavy coatings on both the inlet and outlet filter wall surfaces. The third axial region, which accounted for most of the total filter length, had an intermediate permeability. This region also had an intermediate catalyst loading, primarily on the outlet side of the filter wall. As more multifunctional exhaust filters enter the market, a detailed understanding of catalyst distribution effects may be needed to account for some overall performance characteristics. The methods demonstrated in Fiscal Year 2019 allow details of pore-scale catalyst distribution to be connected to measured filter wall permeabilities, which can then be used in device-scale models.

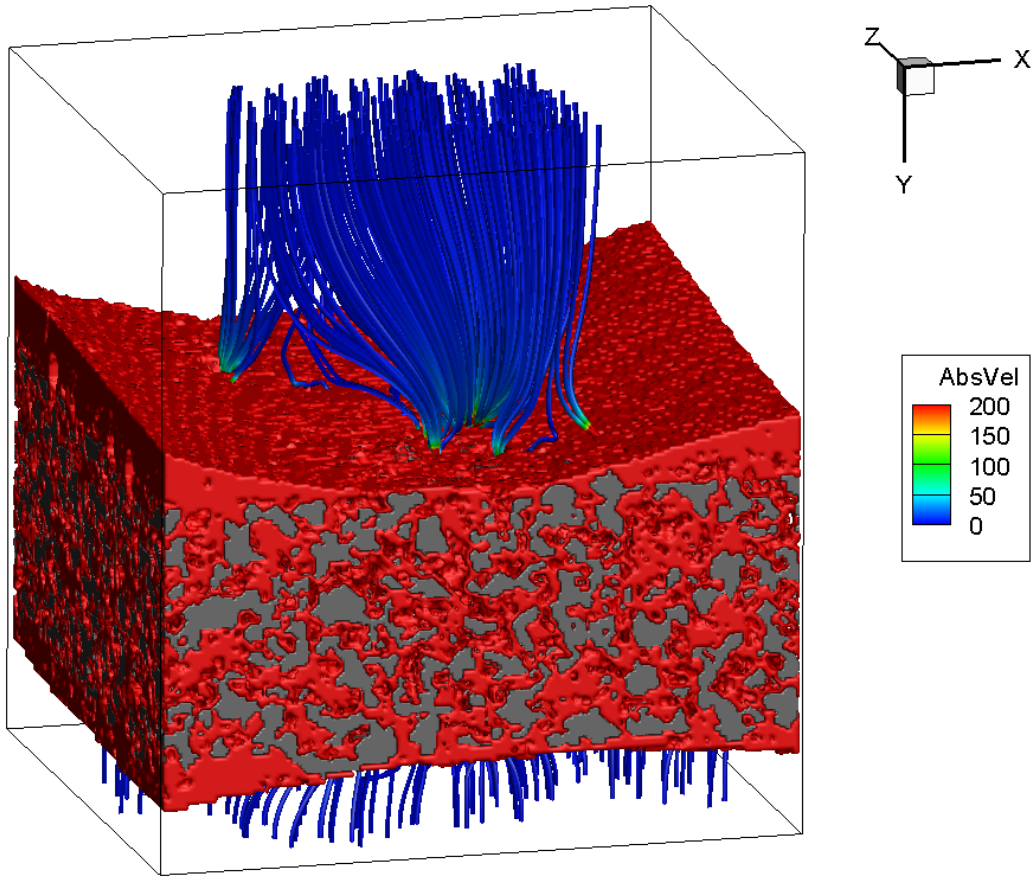

Figure IV.2.3 Microscale simulation of flow through a small section of filter wall in the second axial zone, with relatively thick coatings on both the inlet and outlet wall surfaces

LTAT

In Fiscal Year 2019, PNNL supported the activities and mission of the ACEC Tech Team through participation in the LTAT sub-group. These efforts consisted of (1) routine interaction via bi-weekly LTAT group conference calls and bi-monthly ACEC Tech Team meetings, (2) LTAT catalyst test protocol development, (3) precious group metal (PGM) utilization and replacement roadmap planning, and (4) U.S. DRIVE (United States Driving Research and Innovation for Vehicle efficiency and Energy sustainability) technical highlight preparation. In 2019, the LTAT group completed the Low-Temperature NH_3-SCR Catalyst Test Protocol and released it to the CLEERS website for review and use by the technical community. Parallel to those efforts, the LTAT group also captured all four low-temperature catalyst test protocols (Oxidation, Storage/Release, Three-Way Catalyst, and NH_3-SCR) in an open literature publication with PNNL as lead author. [1] These efforts maximize the visibility of the test protocols to research planning and literature reviews related to aftertreatment catalysis development.

Also in 2019, the LTAT group performed roadmap planning efforts surrounding PGM utilization and replacement and developed the problem statement through (1) projected PGM deficit as predicted by BASF through close comparison of demand to above- and below-ground PGM sources; (2) PGM usage drivers, including global vehicle production and more demand on aftertreatment; and (3) the lack of underlying science to enable sustainable aftertreatment solution. This statement also provides a landscape of current DOE-funded research that intersects with PGM utilization and a proposed course of action to have near-term impact on the PGM challenge presented.

Single-atom catalysts have attracted a good deal of interest thanks to the promise of atom efficiency, superior reactivity, and selectivity. However, ionic Pt single atoms on CeO_2 were found to be inactive for low-temperature (<150°C) CO oxidation. Instead, the single-atom catalyst serves as an excellent precursor, evolving into a catalyst that achieves high activity after treatment in a reducing atmosphere. The project investigated the factors responsible for improved low-temperature CO oxidation reactivity by using near- ambient-pressure X-ray photoelectron spectroscopy (NAP-XPS), diffuse reflectance infrared Fourier transform spectroscopy (DRIFTS), HAADF-STEM, and temperature-programmed reduction using CO as reducing gas (CO-TPR). The focus was on the calcination temperature during catalyst synthesis. Researchers compared a catalyst prepared via conventional wet chemical synthesis (strong electrostatic adsorption), calcined at 350°C in air, with a catalyst prepared via high-temperature vapor-phase synthesis (atom trapping), calcined at 800°C in air. Both catalysts initially contain atomically dispersed Pt species. Reduction of the catalyst in CO at 275°C leads to enhanced reactivity for both catalysts, but the atom-trapping catalyst exhibited much higher CO oxidation activity than the strong electrostatic adsorption catalyst, achieving 100% CO conversion below 70°C (T_{100} < 70°C) at a gas hourly space velocity of 232,500 ml g_{cat}^{-1} h^{-1}. The high reactivity can be related to the absence of CO poisoning of Pt and the fact that the CeO_2 support is able to readily provide oxygen to the active sites at lower temperatures (Figure IV.2.4). High-temperature vapor-phase synthesis provides a novel approach for tuning the reactivity of the CeO_2 support.

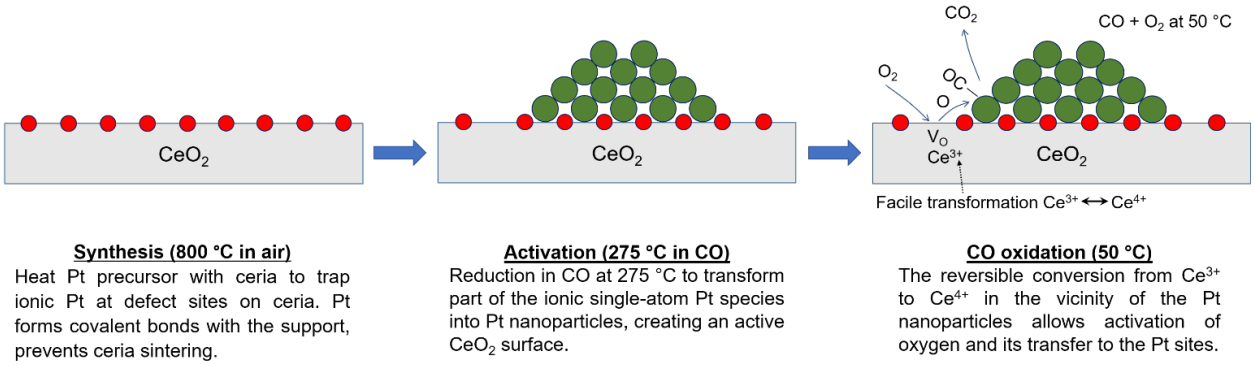

Figure IV.2.4 Transforming the Pt single-atom catalyst into nanoparticles creates active sites on the ceria support (red: ionic Pt, green: metallic Pt)

Conclusions

- Provided molecular insight toward the "mysterious" deactivation of Cu/SAPO-34 SCR catalysts
- Achieved atomic Pd dispersion for Pd/SSZ-13-based PNAs.
- Published four low-temperature catalyst test protocols (Oxidation, Storage/Release, Three-Way Catalyst, and NH_3-SCR) in open literature
- Discovered an approved method to enhance oxygen activation for improved low-temperature CO oxidation activity
- Developed a new technique to measure local permeability in multifunctional filters with zoned catalyst coatings.

Key Publications

1. Stewart, Mark L., Carl Justin Kamp, Feng Gao, Yilin Wang, and Mark H. Engelhard. 2018. "Coating Distribution in a Commercial SCR Filter." *Emission Control Science and Technology* 4: 260–270. (Emission Control Science and Technology – Best Paper Award 2018)

2. Wang, Aiyong, Yilin Wang, Eric D. Walter, Nancy M. Washton, Yanglong Guo, Guanzhong Lu, Charles H.F. Peden, and Feng Gao. 2019. "NH_3-SCR on Cu, Fe and Cu+Fe Exchanged Beta and SSZ-13 Catalysts: Hydrothermal Aging and Propylene Poisoning Effects." *Catal. Today* 320: 91–99.

3. Chen, Hai-Ying, Marton Kollar, Zhehao Wei, Feng Gao, Yilin Wang, János Szanyi, and Charles H.F. Peden. 2019. "Formation of NO^+ and Its Possible Roles during the Selective Catalytic Reduction of NO_x with NH_3 on Cu-CHA Catalysts." *Catal. Today* 320: 61–71.

4. Khivantsev, Konstantin, Nicholas R. Jaegers, Libor Kovarik, Sebastian Prodinger, Miroslaw A. Derewinski, Yong Wang, Feng Gao, Aiyong Wang, Ying Chen, Eric D. Walter, Nancy M. Washton, Donghai Mei, Tamas Varga, Yilin Wang, János Szanyi, Yong Wang, Charles H.F. Peden, and Feng Gao. 2019. "Unraveling the Mysterious Failure of Cu/SAPO-34 Selective Catalytic Reduction Catalysts." *Nat. Comm.* 10: 1137.

5. Cui, Yanran, and Feng Gao. 2019. "Cu Loading Dependence of Fast NH_3-SCR on Cu/SSZ-13." *Emission Control Science and Technology*, in press. DOI 10.1007/s40825-019-00117-2.

6. Cui, Y., Y. Wang, E.D. Walter, J. Szanyi, Y. Wang, and F. Gao. 2019. "Influences of Na^+ Co-Cation on the Structure and Performance of Cu/SSZ-13 Selective Catalytic Reduction Catalysts." *Catal. Today*, in press. DOI: 10.1016/j.cattod.2019.02.037.

7. Khivantsev, K., F. Gao, L. Kovarik, Y. Wang, and J. Szanyi. 2018. "Molecular Level Understanding of How Oxygen and Carbon Monoxide Improve NO_x Storage in Palladium/SSZ-13 Passive NO_x Adsorbers: The Role of NO^+ and Pd(II)(CO)(NO) Species." *J. Phys. Chem. C* 122: 10820−10827.

8. Khivantsev, K., N.R. Jaegers, L. Kovarik, J.C. Hanson, F. Tao, Y. Tang, X. Zhang, I. Koleva, H.A. Aleksandrov, G.N. Vayssilov, Y. Wang, F. Gao, and J. Szanyi. 2018. "Achieving Atomic Dispersion of Highly Loaded Transition Metals in Small-Pore Zeolite SSZ-13: High Capacity and High-Efficiency Low-Temperature CO and Passive NO_x Adsorbers." *Angewandte Chemie-International Edition* 57, no. 51: 16672–16677.

9. Mei, D., F, Gao, Y. Wang, and J. Szanyi. 2019. "Mechanistic Insight into the Passive NO_x Adsorption in the Highly Dispersed Pd/H-Beta Zeolite." *Applied Catalysis A-General* 569: 181–189.

10. Khivantsev, K., N.R. Jaegers, L. Kovarik, S. Prodinger, M. Derewinski, Y. Wang, F. Gao, and J. Szanyi. 2019. "Palladium/Beta Zeolite Passive NO_x Adsorbers (PNA): Clarification of PNA Chemistry and the Effect of CO and Zeolite Crystallite Size on PNA Performance." *Applied Catalysis A-General* 569: 141–148.

References

1. Rappé, K.G., C. DiMaggio, J.A. Pihl, et al. 2019. "Aftertreatment Protocols for Catalyst Characterization and Performance Evaluation: Low-Temperature Oxidation, Storage, Three-Way, and NH_3-SCR Catalyst Test Protocols." *Emiss. Control Sci. Technol*. 5: 183. https://doi.org/10.1007/s40825-019-00120-7.

Acknowledgements

The principal investigator thanks Feng Gao, Jamie Holladay, Donghai Mei, Ken Rappe, Mark Stewart, Janos Szanyi, and Yilin Wang for their contributions to this project and report.

IV.3 Low-Temperature Emission Control to Enable Fuel-Efficient Engine Commercialization (Oak Ridge National Laboratory)

Todd J. Toops, Principal Investigator
Oak Ridge National Laboratory (ORNL)
2360 Cherahala Boulevard
Knoxville, TN 37932
E-mail: toopstj@ornl.gov

Ken Howden, DOE Technology Development Manager
U.S. Department of Energy
E-mail: Ken.Howden@ee.doe.gov

Start Date: October 1, 2018 End Date: September 30, 2021
Total Project Cost: $1,500,000 DOE share: $1,500,000 Non-DOE share: $0

Project Introduction

Removing the harmful pollutants in automotive exhaust has been an intense focus of the automotive industry over the last several decades. In particular, the emissions regulations for fuel-efficient diesel engines that were implemented in 2007 and 2010 have resulted in a new generation of emissions control technologies. These catalysts usually reach 90% conversion of pollutants between 200°C and 350°C, but below these temperatures, the catalysts are relatively inactive. Consequently, more than 50% of pollutant emissions occur in the first 2–3 min of the transient drive cycle required for certification and under cold-start or idling conditions. Thus, as emissions regulations become more stringent, meeting the emissions regulations will require increased activity during this warm-up period. To further complicate matters, the increased corporate average fuel economy (CAFE) standards that will be implemented over the next decade will result in the introduction of more fuel-efficient engines. Higher fuel efficiency will result in less heat loss to exhaust and lower exhaust temperatures, which further necessitates increased emissions control activity at low temperatures. With these challenges in mind, the United States Driving Research and Innovation for Vehicle efficiency and Energy sustainability (U.S. DRIVE) Advanced Combustion and Emission Control Tech Team has set a goal of achieving 90% conversion of carbon monoxide (CO), hydrocarbon (HC), and oxides of nitrogen (NO_x) at 150°C. Higher Pt and Pd loadings may help to increase the catalytic efficiency, but such methods are too expensive for long-term success. Thus, this project focuses on developing new catalytic materials that are active at lower temperatures. In addition, other options to meet the emissions standards, such as hydrocarbon traps and NO_x adsorbers, are being pursued; these adsorber materials can trap the pollutants at low temperature for later release and conversion at higher temperatures where catalysts are active.

Objectives

- Develop emissions control technologies that achieve >90% reduction of pollutants at low temperatures (<150°C) to enable fuel-efficient engines with low exhaust temperatures to meet new U.S. Environmental Protection Agency Tier 3 emissions regulations that require ~80% less NO_x and hydrocarbon emissions than current standards
- Identify advancements in technologies that will enable commercialization of advanced combustion engine vehicles
- Understand fundamental surface chemistry mechanisms that either enable or limit low-temperature emissions control.

Approach

To reach the goal of 90% conversion at 150°C, a multi-functional approach will be pursued. We are actively synthesizing materials at ORNL that have the potential to meet this goal, including novel materials not currently being used in automotive applications and also new high-surface-area materials that serve as a support for platinum group metals (PGMs). With these new support materials, we aim to stabilize the PGM particles while also enhancing their low-temperature activity. Additionally, there are researchers across the world focused on studying catalysts with very high activity regardless of the specific application. We initiate contact with these researchers to investigate their catalysts in the harsh conditions that are present in automotive exhaust, e.g., H_2O, CO_2, CO, HC, NO_x, and hydrothermal aging above 800°C [1],[2]. Often, these catalysts show exceptional activity in single-component exhaust streams, but there is significant inhibition from other exhaust species. With this in mind, we are aiming to understand the limitations of each system but also look for synergistic opportunities when possible. This includes using traps to limit exposure of inhibiting species to active catalysts until temperatures are more amenable to reaction. Also, mixing catalytic components where the catalysts are limited by different species will be explored. Our efforts aim to understand the processes at a fundamental level and illustrate any benefits or shortcomings of each catalyst we study, while striving to find compositions that will achieve the very challenging goal of 90% conversion of CO, NO_x, and HC at 150°C. Improving this understanding of the potential advantages and limitations of catalysts will guide the reformulation of new catalysts.

Results

ORNL established two new collaborations. The first one is with the Wyss Institute at Harvard University, which has shown promising results from an oxidation catalyst. ORNL evaluated their samples under the rigorous conditions outlined in the U.S. DRIVE protocols [1],[2], including hydrothermal aging to 800°C for 50 h. This evaluation was performed on relatively simple formulations: Pt/alumina, Pd/alumina, and a physical mixture of the two materials. The materials showed excellent reactivity under the low-temperature diesel combustion conditions. Of the materials evaluated, the physical mixture showed the highest reactivity after hydrothermal aging (Figure IV.3.1), with a temperature of 90% conversion (T90) of 186°C–187°C for CO and 219°C–222°C for all of the hydrocarbons combined. Although the material did not meet the target of 150°C, the exceptionally steep light-off behavior shows a lot of promise, and there are several approaches that can be attempted with the goal of finding improvements.

ORNL established an additional collaboration with the University at Buffalo. This effort builds on ORNL's core@shell support technique [3], which has shown significant promise in improving the reactivity and durability of PGMs that are supported on these materials. A goal of this collaboration was to expand beyond the SiO_2@ZrO_2 core@shell support that has been the foundation of ORNL's low-temperature oxidation catalyst research (Figure IV.3.2a). Synthesis of a wide range of materials has been successfully accomplished, with the micrographs in Figure IV.3.2b–Figure IV.3.2d showing the following new materials: SiO_2@CeO_2, SiO_2@CeO_2-ZrO_2, and CeO_2@ZrO_2. Figure IV.3.2d also employs an energy dispersive X-ray spectroscopy elemental mapping technique to highlight the location of the Zr and Ce phases. Pt and Pd will be dispersed on these materials, and their activity will be evaluated under a wide range of exhaust conditions.

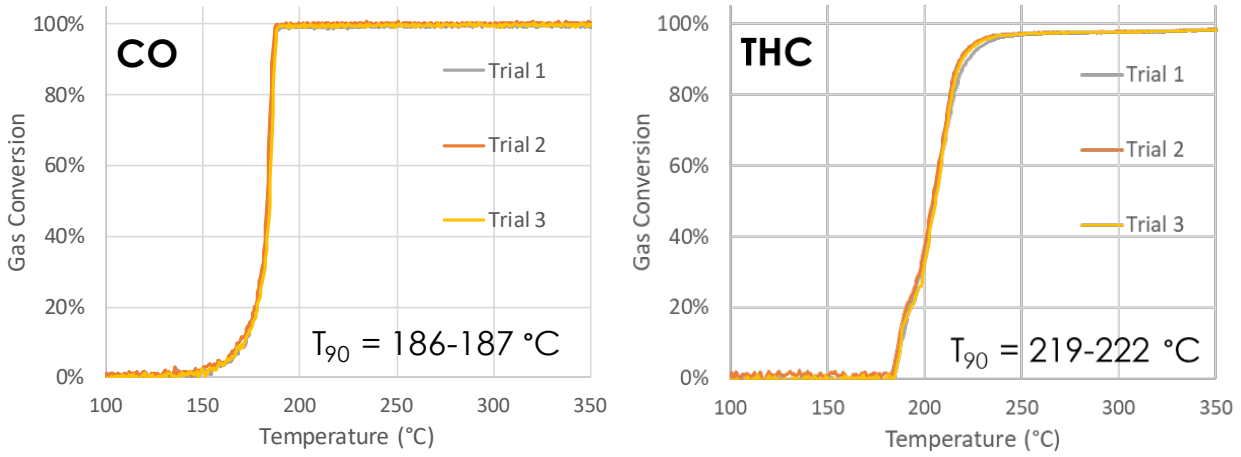

Figure IV.3.1 Light-off curves for (a) CO and (b) total hydrocarbon (THC) under simulated exhaust conditions for 0.57% Pd/Al_2O_3 after aging at 800 °C for 50 h under reactants stream. Reaction conditions: weight hourly space velocity (WHSV) = 200 L/g/h; 12% O_2; 6% H_2O; 6% CO_2; 100 ppm NO; 2,000 ppm CO; 250 ppm C_2H_4; 100 ppm C_3H_6; 33 ppm C_3H_8; 210 ppm $C_{10}H_{22}$; Ar balance. Ramp rate = 5 °C/min.

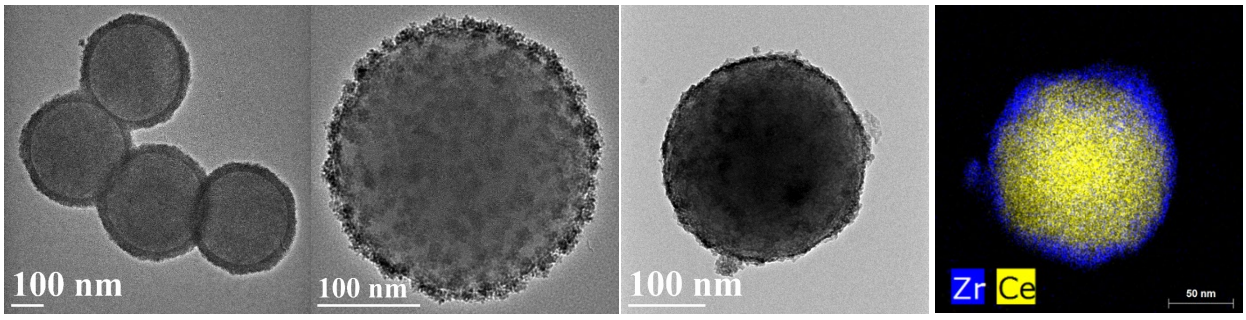

(a) (b) (c) (d)

Figure IV.3.2 Core@shell materials synthesized at the University at Buffalo. Materials are made of (a) $SiO_2@ZrO_2$, (b) $SiO_2@CeO_2$, (c) $SiO_2@CeO_2$-ZrO_2, and (d) $CeO_2@ZrO_2$.

In addition to oxidation catalysts, ORNL initiated synthesis and evaluation of Pd-free hydrocarbon traps, including unexchanged and Ag-exchanged zeolites. Under the low-temperature diesel combustion gas mixture described above, both unexchanged zeolites, zeolite beta (BEA) and Zeolite Socony Mobil–5 (ZSM-5), were able to store significant hydrocarbons at 90°C (Figure IV.3.3a and Figure IV.3.3b). The primary hydrocarbon adsorbed in this unexchanged case is decane (0.7–1.0 mmols C_1/g_{cat}), with only a small amount of propylene and ethylene being adsorbed. The addition of Ag leads to a higher uptake of 1.0–1.2 mmols C_1/g_{cat} (Figure IV.3.3c and Figure IV.3.3d). These materials show promise and appear to be stable from Trial 1 to Trial 4.

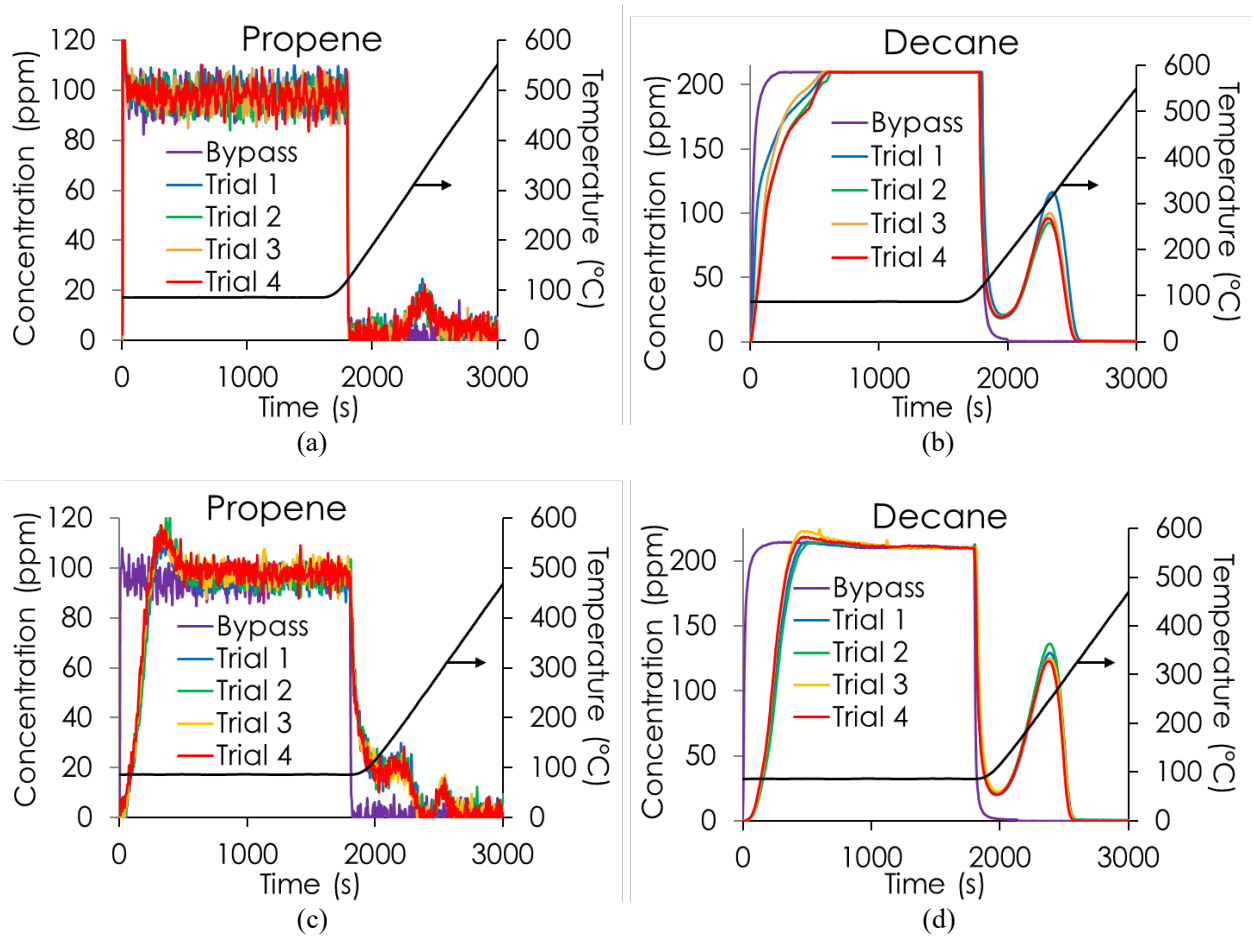

Figure IV.3.3 Hydrocarbon adsorption and desorption for (a) propene and (b) decane on BEA, as well as (c) propene and (d) decane on Ag/BEA. Reaction conditions: WHSV = 200 L/g/h; 12% O_2; 6% H_2O; 6% CO_2; 100 ppm NO; 2,000 ppm CO; 250 ppm C_2H_4; 100 ppm C_3H_6; 33 ppm C_3H_8; 210 ppm $C_{10}H_{22}$; Ar balance. Storage temperature = 90°C; ramp rate = 20°C/min.

To aid in the capture of NO_x at low temperatures, passive NO_x adsorbers (PNAs) have been studied. The most effective trap materials for NO_x are Pd-exchanged zeolites [4],[5], and the most durable zeolite for high-temperature applications is chabazite (CHA). With this in mind, ORNL synthesized Pd/CHA to evaluate. As above, low-temperature diesel combustion was the gas mixture chosen for this evaluation. Figure IV.3.4 shows the initial evaluations while storing at 90°C and heating to 600°C at 20°C/min; the data is shown as a function of NO:Pd, with a theoretical maximum uptake of 1 mole of NO to 1 mole of Pd. The initial hold time at 600°C was 1 h (Trials 1–4); however, the observation of declining adsorption and release with each trial, 0.22 to 0.18 mol NO/mol Pd, led ORNL to increase the high-temperature hold time to 4 h (Trials 5–8). This appeared to slow down the trial-to-trial decline, but as shown in Figure IV.3.4, there is still some decrease in adsorption, 0.18 to 0.16 mol NO/mol Pd. Following these initial evaluations, the Pd/CHA was heated to 800°C for 25 h to perform hydrothermal aging. The amount of uptake increased significantly to 0.32 mol NO/mol Pd, indicating that additional adsorption sites were formed during this process. However, after four subsequent trials, NO_x adsorption decreased to 0.27 mol NO/mol Pd (Trials 9–12). Also interesting to note is that the temperature of peak NO_x release decreased from 300°C to 258°C upon heating to 800°C for 25 h. An additional 25 h at 800°C did not result in additional NO_x adsorption or change the release temperature, and once again a systematic decrease in uptake was observed (Trials 13–15). The precise mechanism of this deactivation is not well understood at this point, but this deactivation is a significant concern in employing this technology going forward, and efforts will be focused on understanding and then remedying this deactivation in future research.

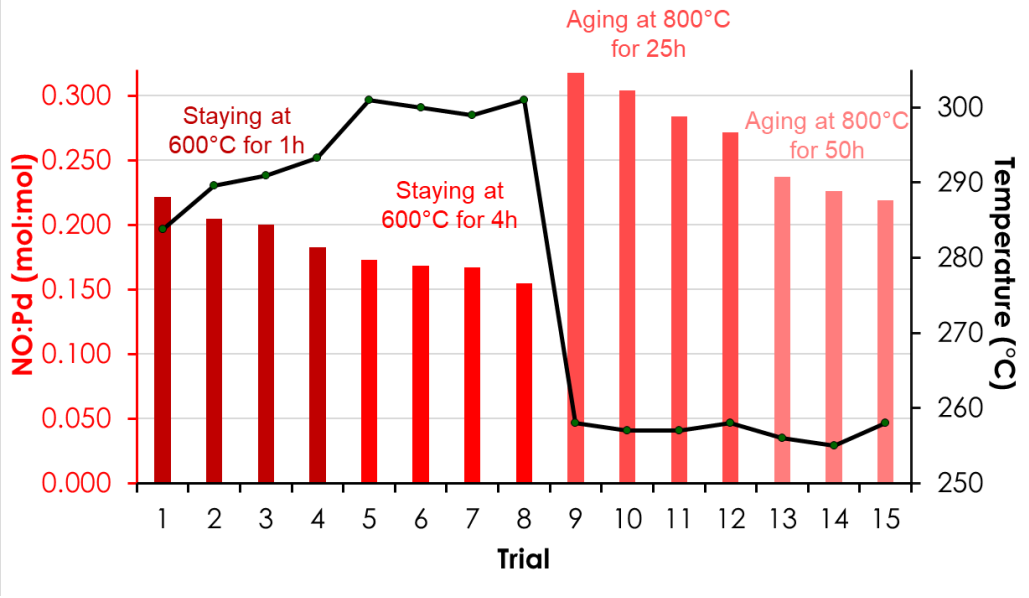

Figure IV.3.4 PNA activity obtained using Pd/CHA catalyst under different conditions, with temperature of peak desorption also shown. Reaction conditions: WHSV = 200 L/g/h; 12% O_2; 6% H_2O; 6% CO_2; 100 ppm NO; 2,000 ppm CO; 250 ppm C_2H_4; 100 ppm C_3H_6; 33 ppm C_3H_8; 210 ppm $C_{10}H_{22}$; Ar balance. Storage temperature = 90°C; ramp rate = 20°C/min.

Understanding how these two trapping materials work together is important, as that is the expected approach to be used in the field. Thus, ORNL prepared a catalyst bed with both PNA (Pd/CHA) and hydrocarbon trap (Ag/BEA) functionalities. This was a physical mixture with equal masses of the two components, and the gas mixture and temperature profiles were the same as in previous studies (low-temperature diesel combustion gas mixture). The results of this study are shown in Figure IV.3.5. The hydrocarbon trap functionality was significantly higher than observed in the one-component studies, with 4.3–5.2 mmols C_1/g_{cat}, and both the adsorption and desorption were very stable after repeated measurements, as shown in Trials 1–11 in Figure IV.3.5a. Hydrothermal aging at 800°C for 25 h led to a ~25% decrease in uptake, but 3.4–3.8 mmols C_1/g_{cat} could still be adsorbed, as shown in Trials 12–15 in Figure IV.3.5a. PNA adsorption was also observed to be significantly higher in the two-component system, with an initial uptake of 0.70 mol NO/mol Pd, twice as much as for Pd/CHA-only (Figure IV.3.5b). Although the trial-to-trial rate of deactivation was slower in the two-component system, there were still notable losses in Trials 1–11. The uptake decreased from 0.70 to 0.48 mol NO/mol Pd. Aging at 800°C for 25 h did not have a significant impact, as the NO_x uptake had stabilized at ~0.45 mol NO/mol Pd. Once again, this trial-to-trial decrease in activity is not ideal, and future investigations will aim to mitigate this through new material research.

Conclusions

- Established new collaborations with University at Buffalo and Harvard University
- Synthesized a new class of novel supports to be investigated for improved durability and low-temperature oxidation
- Demonstrated hydrocarbon trap functionality and durability of PGM-free zeolite
- Evaluated Pd/SSZ-13 (aluminosilicate zeolite) for passive NO_x adsorption and discovered a deactivation mechanism that occurs during evaluation as a single component
- Demonstrated the potential and durability of combining a non-PGM zeolite, Pd/SSZ-13 PNA, and an oxidation catalyst to treat low-temperature emissions.

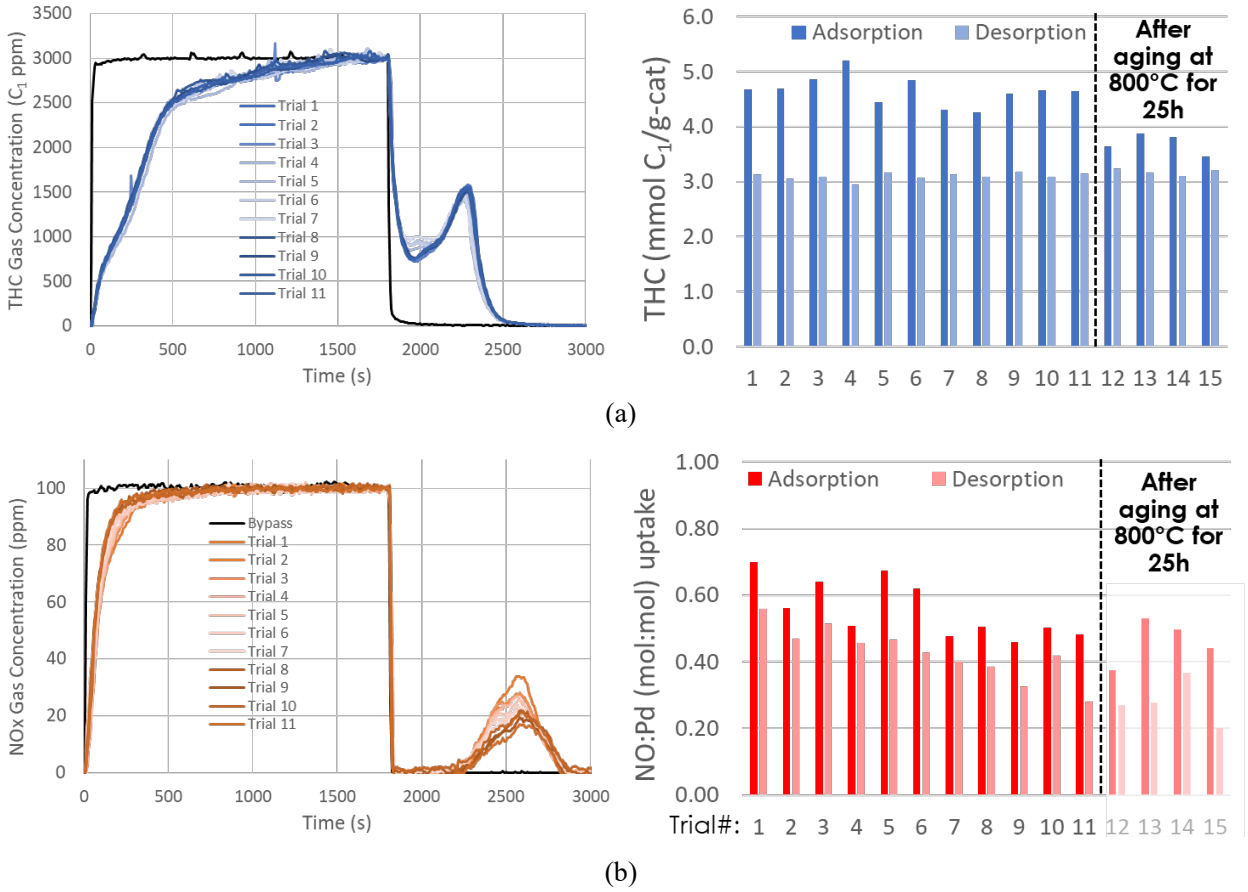

Figure IV.3.5 (a) Hydrocarbon trap and (b) PNA activity for two-component reactor bed comprised of Ag/BEA and Pd/SSZ-13. Reaction conditions: WHSV = 200 L/g/h; 12% O_2; 6% H_2O; 6% CO_2; 100 ppm NO; 2,000 ppm CO; 250 ppm C_2H_4; 100 ppm C_3H_6; 33 ppm C_3H_8; 210 ppm $C_{10}H_{22}$; Ar balance. Storage temperature = 90°C; ramp rate = 20°C/min.

Key Publications

1. Vuong, Hung, Andrew J. Binder, Jonathan E. Sutton, Todd J. Toops, and Aditya Savara. 2019. "Experimental Data Based Combinatorial Kinetic Simulations for Predictions of Synergistic Catalyst Mixtures." *Catalysis Today* 338: 117–127; https://doi.org/10.1016/j.cattod.2019.04.026.

2. Chen, Junjie, Benjamin D. Carlson, Jae-Soon Choi, Zhenglong Li, Todd J. Toops, and Eleni A. Kyriakidou. 2019. "Complete Methane Combustion over $Ni/Ce_xZr_{1-x}O_2$ Catalysts." Submitted to *Applied Catalysis A* (September 2019).

3. Hoang, Son, Yanbing Guo, Xingxu Lu, Wenxiang Tang, Sibo Wang, Shoucheng Du, Chang-Yong Nam, Yong Ding, Andrew J. Binder, Eleni V. Kyriakidou, Ji Yang, Todd J. Toops, Wen Xiao, Jun Ding, and Pu-Xian Gao. 2019. "Enhanced Mass Transport and Strong Metal-Support Interactions in Mesoporous Titania Nanoarray Supported Pt Nanoparticles." Submitted to *Angewandte Chemie* (September 2019).

4. Kyriakidou, Eleni A., Jungkuk Lee, Jae-Soon Choi, Michael Lance, and Todd J. Toops. 2019. "A Comparative Study of ZSM-5 and BEA Zeolites for Low Temperature Passive Hydrocarbon and NO Adsorption." Resubmitted to *Applied Catalysis B* (August 2019).

5. Hoang, Son, Yanbing Guo, Andrew J. Binder, Wenxiang Tang, Sibo Wang, Jingyue Liu, Tran D. Huan, Yu Wang, Xingxu Lu, Yong Ding, Eleni V. Kyriakidou, Ji Yang, Todd J. Toops, Thomas J. Pauly,

Rampi Ramprasad, and Pu-Xian Gao. 2019. "Activating Low-Temperature Diesel Oxidation by Single-Atom Pt on TiO_2 Nanowire Array." Resubmitted to *Nature Materials* (August 2019).

6. Gremminger, Andreas, Josh A Pihl, Maria Casapu, Jan Dierk Grunwaldt, Todd J. Toops, and Olaf Deutschmann. 2019. "PGM Based Catalysts for Exhaust-Gas After-Treatment under Typical Diesel, Gasoline and Gas Engine Conditions with Focus on Methane and Formaldehyde Oxidation." Submitted to *Applied Catalysis B: Environmental* (January 2019).

References

1. U.S. DRIVE, Aftertreatment Protocols for Catalyst Characterization and Performance Evaluation: Low-Temperature Oxidation Catalyst Test Protocol, www.cleers.org, 2015.

2. Rappe, Kenneth G., Craig DiMaggio, Josh A. Pihl, Joseph R. Theis, Se H. Oh, Galen B. Fisher, Jim Parks, Vencon G. Easterling, Ming Yang, Mark L. Stewart, and Kenneth C. Howden. 2019. "Aftertreatment Protocols for Catalyst Characterization and Performance Evaluation: Low-Temperature Oxidation, Storage, Three-Way, and NH_3-SCR Catalyst Test Protocols." *Emiss. Control Sci. Technol.* 5 (2): 183–214.

3. Kyriakidou, Eleni, Todd J. Toops, Jae-Soon Choi, Michael J. Lance, and James E. Parks II. 2018. "Exhaust Treatment Catalysts with Enhanced Hydrothermal Stability and Low Temperature Activity." U.S. Patent Number 10,427,137. Publication number: US 2018 / 0250659 A1, US Patent App. #15/ 906,606 filed February 27, 2018, published September 6, 2018, issued October 1, 2019.

4. Chen, Hai-Ying, Jillian E. Collier, Dongxia Liu, Loredana Mantarosie, Desirée Durán-Martín, Vladimír Novák, Raj R. Rajaram, and David Thompsett. 2016. "Low Temperature NO Storage of Zeolite Supported Pd for Low Temperature Diesel Engine Emission Control." *Catal. Lett.* 146 (9): 1706–1711.

5. Lee, Jaeha, Young-Seok Ryou, Sungha Hwang, Yongwoo Kim, Sung June Cho, Hyokyoung Lee, Chang Hwan Kim, and Do Heui Kim. 2019. "Comparative Study of the Mobility of Pd Species in SSZ-13 and ZSM-5, and Its Implication for Their Activity as Passive NO_x Adsorbers (PNAs) after Hydro-Thermal Aging." *Catal. Sci. Technol.* 9: 163.

Acknowledgements

Pranaw Kunal and James E. Parks II provided valuable contributions to this project and report.

IV.4 Dilute Lean Gasoline Emissions Control (Oak Ridge National Laboratory)

Vitaly Y. Prikhodko, Principal Investigator
Oak Ridge National Laboratory
2360 Cherahala Boulevard
Knoxville, TN 37932
E-mail: prikhodkovy@ornl.gov

Ken Howden, DOE Technology Development Manager
U.S. Department of Energy
E-mail: Ken.Howden@ee.doe.gov

Start Date: October 1, 2018 End Date: September 30, 2021
Project Funding: $1,500,000 DOE share: $1,500,000 Non-DOE share: $0

Project Introduction

Currently, the U.S. passenger car market is dominated by gasoline engine powertrains that operate at stoichiometric air-to-fuel ratios (sufficient fuel is mixed in air such that all of the oxygen in the air is consumed during combustion). Stoichiometric combustion leads to exhaust conditions suitable for three-way catalyst (TWC) technology to reduce oxides of nitrogen (NO_x), carbon monoxide (CO), and hydrocarbon (HC) emissions to extremely low levels. Operating gasoline engines at lean air-to-fuel ratios (excess air) enables more efficient engine operation and reduces fuel consumption; however, the resulting oxygen in the exhaust prevents the TWC technology from reducing NO_x emissions. It is relatively straightforward to operate an engine lean over a significant portion of the load and speed operating range; so, the largest challenge preventing fuel-saving lean combustion in gasoline applications is the control of emissions, primarily NO_x. This project addresses the challenge of reducing emissions from fuel-saving lean gasoline engines in a cost-effective and fuel-efficient manner to enable their market introduction. "Passive SCR" [1],[2],[3] is one potential strategy for NO_x control in lean gasoline engines. In the passive SCR approach, where SCR stands for selective catalytic reduction, ammonia (NH_3) is generated over the TWC under slightly rich engine operation and then stored on a downstream SCR catalyst. After the engine returns to lean operation, the stored NH_3 reduces NO_x that is not converted over the upstream TWC. In this manner, the TWC controls NO_x during stoichiometric and rich operation of the engine, and the SCR catalyst controls NO_x during lean engine operation. Utilizing passive SCR, this project has demonstrated NO_x emission reduction efficiencies over 99.8% on a four-cylinder lean gasoline engine. In addition, experiments have been conducted to identify catalyst material compositions that minimize the fuel penalty associated with NH_3 generation, and accelerated aging studies have been conducted to understand the durability of the catalysts used in the passive SCR approach.

Objectives

Overall Objectives

- Assess and characterize catalytic emission control technologies for lean gasoline engines
- Identify strategies for reducing the costs, improving the performance, and minimizing the fuel penalty associated with emission controls for lean gasoline engines
- Identify a technical pathway for a lean gasoline engine to meet U.S. Environmental Protection Agency Tier 3 emissions regulations with minimal fuel consumption and cost

- Demonstrate the fuel efficiency improvement of lean operation over stoichiometric operation of a modern gasoline engine with reduced NO_x emissions during lean operation.

Fiscal Year 2019 Objectives

- Demonstrate a pathway for higher fuel efficiency with an improved passive SCR aftertreatment system architecture while meeting U.S. Environmental Protection Agency Tier 3 emissions levels
- Identify potential strategies to reduce CO emissions during rich engine operation
- Procure and install a MAHLE Jet Ignition engine as the engine platform for this project.

Approach

This project utilizes a wide range of capabilities available at Oak Ridge National Laboratory's National Transportation Research Center, including a lean gasoline engine on an engine dynamometer, simulated exhaust flow reactors for detailed catalyst evaluations under carefully controlled operating conditions, and material characterization tools for catalyst analysis. The combination of catalyst studies on flow reactor and engine platforms is a key component of the project approach. Prototype catalyst formulations are first studied on flow reactors to understand catalytic function and establish operating parameters in a controlled setting; then, select catalyst combinations are studied on the engine platform to characterize performance under realistic exhaust conditions. The engine studies also enable direct measurement of fuel consumption benefits from lean gasoline engine operation as well as measurement of "fuel penalties" imposed by the emission control system to function properly.

The engine platform for the project is from a model year 2008 BMW 120i vehicle sold in Europe. The four-cylinder, direct-injection, naturally aspirated engine operates in multiple modes, including lean (excess air) and stoichiometric combustion. The BMW 120i employs both a TWC for stoichiometric operation and a lean NO_x trap catalyst for NO_x reduction during lean operation. Although this engine and aftertreatment combination met the relevant emissions regulations in Europe, as configured, its emissions are well above the current U.S. emissions standards. Furthermore, the lean NO_x trap catalyst contains high levels of platinum group metals, which add significantly to the overall cost of the vehicle. The goal for this project is to identify emission control technologies that can meet the U.S. Environmental Protection Agency Tier 3 emissions standards. In addition to the emissions goal, the project aims to maximize the fuel efficiency benefit from lean gasoline engine operation and minimize system cost.

The catalysts studied in the project were either supplied or recommended by collaborating partner Umicore, a major catalyst supplier to the automotive industry. Other collaborating partners include General Motors (GM) for project guidance and the University of South Carolina for research on catalyst aging and durability.

Results

The Fiscal Year 2018 report for this project described experiments that demonstrated a 5.9% improvement in fuel economy relative to stoichiometric-only operation, with emissions nearly achieving the Tier 3 limits while the BMW engine was operated over a simplified transient drive cycle using the passive SCR approach. During Fiscal Year 2019, efforts focused on using a five-function passive SCR emission control system architecture to improve fuel economy and further reduce tailpipe emissions. The emission control system, as shown in Figure IV.4.1, consisted of a Pd-only TWC, a TWC containing oxygen storage (OSC) and NO_x storage (NSC) components, an uncatalyzed gasoline particulate filter (GPF), a small-pore Cu-zeolite SCR catalyst, and a clean-up catalyst (CUC) with high amounts of OSC. Description and functionality of each catalyst are listed in Table IV.4.1. All of the catalysts, with the exception of the SCR, were aged using a lean-rich-stoich aging protocol defined by the Advanced Combustion and Emission Control Technical Team [4]. The aging protocol is intended to simulate catalyst performance up to full useful life, which is important since current regulations require emission control durability to 150,000 miles for light-duty vehicles. Future research will focus on SCR durability under conditions relevant to passive SCR conditions.

To enable emissions and fuel economy measurement under realistic operating conditions, a pseudo-transient drive cycle provided by GM was employed. This cycle is a simplified modal engine test cycle intended to be representative of the engine operating conditions encountered during the Federal Test Procedure (FTP) driving cycle. It consists of a compilation of six speed and load points with constant acceleration during speed and load transitions. The BMW lean gasoline engine utilized in this project is a purpose-built multimode engine. The engine employs lean combustion modes during part-load operation. At higher speeds and loads, when the demanded speed and load fall outside the lean operating range, the engine transitions to a stoichiometric combustion mode. Over the pseudo-transient FTP cycle, the multimode (lean + stoichiometric) operation exhibited 9.6% fuel economy improvement relative to stoichiometric-only operation, which is the maximum fuel economy improvement the engine can achieve under these conditions and serves as the baseline for comparing fuel penalties of different aftertreatment system architectures.

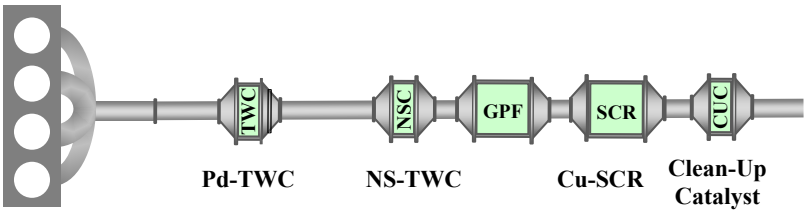

Figure IV.4.1 Schematic of a five-function passive SCR emission control system

Table IV.4.1 Passive SCR System Catalyst Details

Catalyst ID	Description	Pt (g/l)	Pd (g/l)	Rh (g/l)	OSC/NSC (Yes/No)	Volume (l)
Pd-TWC	Pd-only TWC utilized for NH_3 generation	0	7.3	0	No/No	0.62
NS-TWC	TWC with oxygen and NO_x storage components utilized for NH_3 generation and lean NO_x storage	2.47	4.17	0.05	Yes/Yes	0.82
GPF	Uncatalyzed GPF utilized as a heat sink and particulate matter control	-	-	-	-	2.47
Cu-SCR	Small-pore Cu-zeolite SCR utilized for lean NO_x reduction	-	-	-	-	2.47
CUC	High-OSC-containing catalyst utilized for rich CO and HC control and NH_3 slip	0	6.5	0	Yes/No	1.00

With the five-function passive SCR system, multimode engine operation generated an 8.3% fuel economy improvement over stoichiometric-only operations, as compared to 5.9% with a two-catalyst system (TWC + SCR) evaluated last year. The sum of NO_x and non-methane organic gas (NMOG) emissions over the pseudo-transient drive cycle was below Tier 3 levels (sum of NO_x+NMOG emissions for Tier 3 Bin 30 standard = 0.03 g/mi), although it should be noted that this evaluation was not the fully transient FTP cycle and did not include cold start. The inclusion of the TWC with a NO_x storage component offered two benefits. First, by storing NO_x during lean phase, it enabled longer lean operation by releasing less lean NO_x to consume NH_3 stored on the SCR catalyst. Second, by converting some of the stored NO_x to NH_3, shorter rich times were needed to produce the required levels of NH_3. Both longer lean times and shorter rich times resulted in a lower fuel penalty. The CO emissions (primarily from rich operation) significantly exceeded the U.S. Environmental Protection Agency Tier 3 levels, and thus, more research is needed to further control CO emissions. Additionally, NH_3 was observed to slip from the SCR, indicating a potential for higher fuel efficiency with further optimization of the control strategy and catalyst system architecture. The emissions performance of the two passive SCR system architectures is compared in Figure IV.4.2.

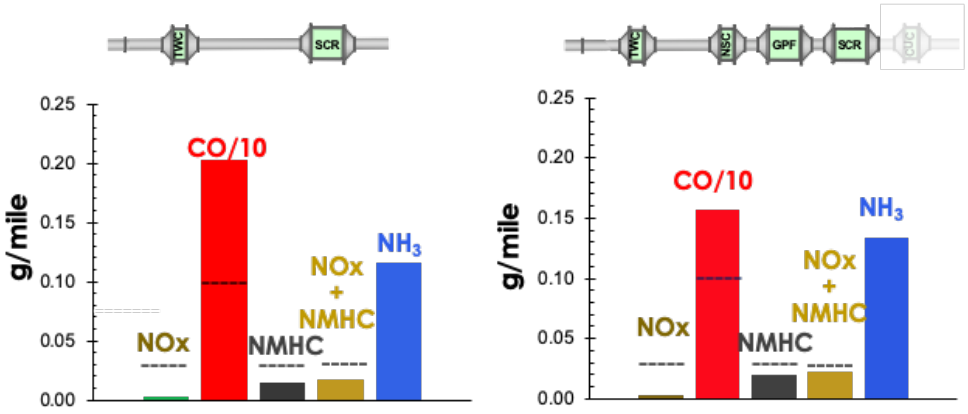

NMHC – non-methane hydrocarbons

Figure IV.4.2 Emissions from a two-catalyst passive SCR system that consisted of a Pd-only TWC and a Cu-zeolite (left); and emissions at SCR outlet from a five-function emission control system (right) over a six-mode pseudo-transient FTP cycle

Rich CO emission control remains challenging. Potential solutions currently under consideration include a downstream clean-up catalyst with either significant oxygen storage and excellent water-gas shift activity, or secondary air injection to directly oxidize the CO. The five-function catalyst system included a platinum-group-metal-based catalyst with high OSC downstream of the SCR. As depicted in Figure IV.4.3, the CUC catalyst decreases CO and HC emissions and helps with NH_3 slip, but some of the NH_3 is converted back to NO_x. Rich CO emissions were still high. Future research will focus on solutions for rich CO control that do not increase NO_x emissions, including newly obtained CUC technologies supplied by Umicore. To date, engine catalyst system research was conducted on the Model Year 2008 BMW 120i lean gasoline engine, and the results demonstrated that NO_x emissions from a lean gasoline engine can effectively be controlled by a passive SCR approach. This year, a new downsized boosted gasoline direct injection platform equipped with a MAHLE pre-chamber ignition system has been procured. The MAHLE Jet Ignition engine enables ultra-lean homogeneous combustion with improved fuel efficiency and provides more flexibility in controlling exhaust composition and temperatures to better represent state-of-the-art lean gasoline engine technology, which makes it a more relevant research platform to employ for future lean gasoline emission control research at Oak Ridge National Laboratory.

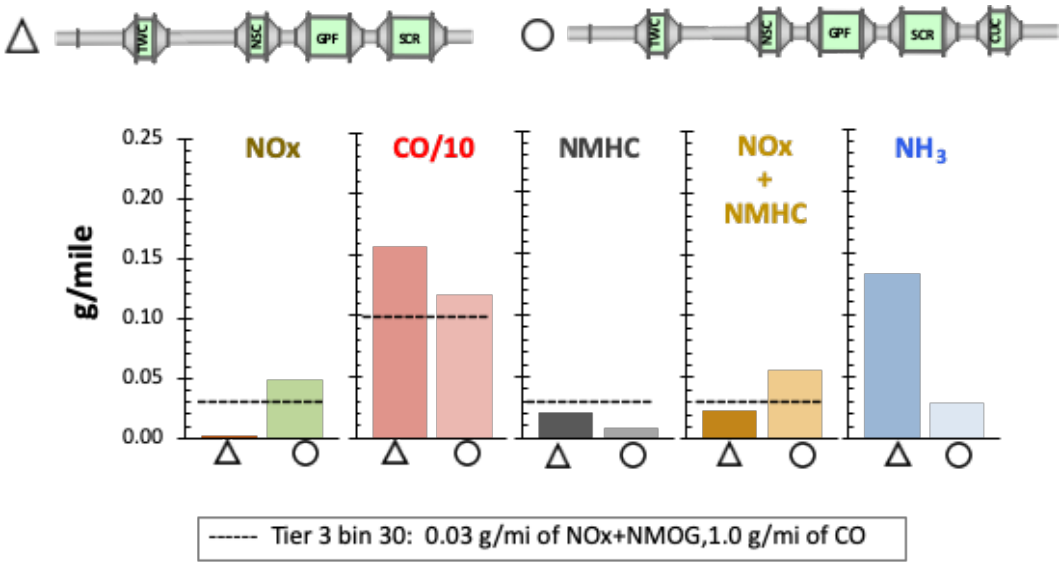

Figure IV.4.3 Emissions from a five-function emission control system before and after the CUC over a six-mode pseudo-transient FTP cycle

Conclusions

- Demonstrated 8.3% fuel economy benefit on the lean gasoline engine platform using a five-function emission control system with NO_x + NMOG emissions below Tier 3 levels (0.03 g/mi) over a pseudo-transient FTP cycle, compared to 5.9% fuel economy improvement demonstrated last year with a two-catalyst passive SCR system
- Improved rich CO and HC emissions with a clean-up catalyst; additional clean-up catalysts provided by Umicore are under investigation
- Procured MAHLE Jet Ignition gasoline engine platform for future lean gasoline emission control research.

Key Publications

2. Prikhodko, Vitaly, Josh Pihl, Todd Toops, and James Parks II. 2019. "Passive SCR Performance under Pseudo-Transient Cycle: Challenges and Opportunities for Meeting Tier 3 Emissions." *Emiss. Control Sci. Technol*. 5: 253. https://doi.org/10.1007/s40825-019-00126-1.

References

1. Li, W., K. Perry, K. Narayanaswamy, C. Kim, et al. 2010. "Passive Ammonia SCR System for Lean-Burn SIDI Engines." *SAE Int. J. Fuels Lubr.* 3 (1): 99–106. doi:10.4271/2010-01-0366.
2. Kim, C., K. Perry, M. Viola, W. Li, et al. 2011. "Three-Way Catalyst Design for Urealess Passive Ammonia SCR: Lean-Burn SIDI Aftertreatment System." *SAE Technical Paper 2011-01-0306*. doi:10.4271/2011-01-0306.
3. Guralp, O., G. Qi, W. Li, and P. Najt. 2011. "Experimental Study of NO_x Reduction by Passive Ammonia-SCR for Stoichiometric SIDI Engines." *SAE Technical Paper 2011-01-0307*. doi:10.4271/2011-01-0307.
4. "Aftertreatment Protocols for Catalyst Characterization and Performance Evaluation: Low-Temperature Oxidation Catalyst Test Protocol." The Advanced Combustion and Emission Control (ACEC) Technical Team Low-Temperature Aftertreatment Group, 2015, https://cleers.org/wp-content/uploads/2015_LTAT-Oxidation-Catalyst-Characterization-Protocol.pdf.

Acknowledgements

Todd J. Toops, Josh A. Pihl, Calvin R. Thomas, and James E. Parks II of Oak Ridge National Laboratory coauthored this report. The authors thank their colleagues Wei Li, Patrick Szymkowicz, Paul Battiston, Arun Solomon, and Paul Najt of General Motors for technical guidance and Ken Price, David Moser, Ryan Day, and Tom Pauly of Umicore for providing catalyst samples and valuable discussion in this project.

IV.5 Cummins-ORNL Catalyst CRADA: NO_x Control and Measurement Technology for Heavy-Duty Diesel Engines (Oak Ridge National Laboratory)

Bill Partridge, Principal Investigator
Oak Ridge National Laboratory (ORNL)
2360 Cherahala Boulevard
Knoxville, TN 37932
E-mail: partridgewp@ornl.gov

Ken Howden, DOE Technology Development Manager
U.S. Department of Energy
E-mail: Ken.Howden@ee.doe.gov

Start Date: October 1, 2018 End Date: September 30, 2021
Project Funding (FY19): $900,000 DOE share: $450,000 Non-DOE share: $450,000 (in-kind)

Project Introduction

A combination of improved technologies for control of oxides of nitrogen (NO_x) and particulate emissions is required to efficiently meet increasingly stringent emission regulations. This cooperative research and development agreement (CRADA) section focuses on catalyst technologies. Improved catalyst-system efficiency, durability, and cost can be achieved through advanced control methodologies based on continuous catalyst-state monitoring. The overarching goal of this CRADA section is to enable self-diagnosing or smart catalyst systems; these are enabled by basic and practical insights into the transient distributed nature of catalyst performance, improved catalyst models, insights suggesting control methodologies, and instrumentation for improved control. Development and application of enhanced diagnostic tools are required to realize these technology improvements.

Objectives

Fiscal Year 2019 objectives focus on assembling and preparing the modeling, material, and hardware resources necessary for determining selective catalytic reduction (SCR) kinetic parameters and mechanistic impacts of ageing and formulation.

Overall Objectives

- Understand the fundamental chemistry of automotive catalysts
- Identify strategies for enabling self-diagnosing catalyst systems
- Address critical barriers to market penetration.

Fiscal Year 2019 Objectives

- Determine detailed model structure for fitting Cu-redox half-cycle kinetic parameters
- Assemble SCR catalyst samples for analysis
- Build reactor for performing transient response experiments.

Approach

The CRADA applies the historically successful approach of developing and applying minimally invasive advanced diagnostics to resolve spatial and temporal function and performance variations within operating

catalysts. Diagnostics are applied to study the detailed nature and origins of catalyst performance variations, including spatial and temporal variations unique to each catalyst function during operation and how these vary with ageing. Measurements are used to assess and guide model development. A combination of measurements and modeling is applied to understand how catalysts function and degrade, develop device and system models, and develop advanced control strategies.

Results

SCR catalysts for NO_x-emissions control in lean combustion environments experience SCR-onset transients indicative of the underlying kinetic parameters. In some cases, as shown in Figure IV.5.1e, conversion inflection (CI) occurs at SCR onset (SCR-on), where a super-steady-state conversion is momentarily achieved in a step-like transient, followed by slow conversion degradation to the steady-state (SS) value. The CI has been observed to vary with catalyst age, space velocity, and feed composition; it thus provides a pathway for investigating the mechanistic impacts of these important parameters. Figure IV.5.1 shows a conceptual model for how the initially imbalanced Cu-redox half cycles (RHC: reduction half cycle, and OHC: oxidation half cycle) and their progressive balancing produce the SCR-onset CI.

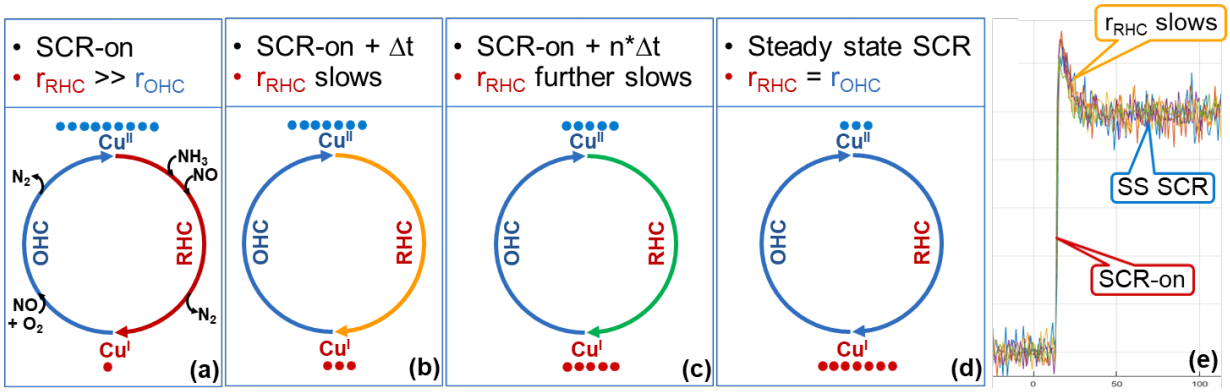

Figure IV.5.1 Conceptual model of Cu-SCR CI origin [1]

A kinetic model was formulated, as shown in Figure IV.5.2, and exercised to assess its transient performance relative to experimentally observed CI trends. The conceptual model shows how CI occurs when RHC is initially faster than OHC, and the half-cycle rates progressively converge as SS is approached, primarily via RHC slowing. Figure IV.5.3 shows how the r-ratio (ratio of the RHC and OHC rates) increases with temperature and how CI becomes more distinct with increasing r-ratio; combined, these demonstrate consistency between the model and measurements in that CI is more apparent at higher temperatures. Via spatially resolved capillary inlet mass spectrometry measurements on commercial SCR catalysts, CI has been observed to become progressively less distinct along the catalyst axis with increasing NO conversion, as shown in Figure IV.5.4 (left). The kinetic model results of Figure IV.5.4 (right) match these experimentally observed trends. Other consistencies between the kinetic model CI predications and experimental observations have been documented [1], suggesting that indeed the conceptual and kinetic models provide a faithful representation of the kinetic origins of CI and thus that CI can be used to determine the half-cycle kinetic parameters and their impact by field and other ageing processes and catalyst formulation changes.

Standard SCR

RHC: $Cu^{II}(OH)(NH_3) + 2{\cdot}NH_3 + NO \rightarrow Cu^{I}(NH_3)_2 + N_2 + 2H_2O$

$r_{RHC} = k_{RHC} \cdot [Cu^{II}] \cdot [NO] \cdot (\theta_{NH3})^{\sim 0} \cong k_{RHC} \cdot [Cu^{II}] \cdot [NO]$

OHC: $2{\cdot}Cu^{I}(NH_3)_2 + O_2 + 2{\cdot}NO \rightarrow 2{\cdot}\ Cu^{II}(OH)(NH_3) + 2{\cdot}N_2 + 2{\cdot}H_2O$

$r_{OHC} = k_{OHC} \cdot [Cu^{I}]^2 \cdot [O_2] \cdot [NO]$

Net Standard SCR: $4{\cdot}NO + 4{\cdot}NH_3 + O_2 \rightarrow 4{\cdot}N_2 + 6{\cdot}H_2O$

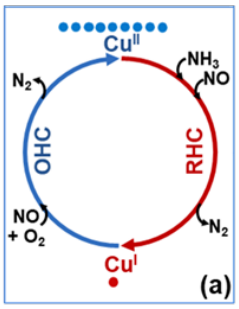

Figure IV.5.2 Kinetic model of transient Cu-SCR based on RHC and OHC Cu-redox half cycles [1]

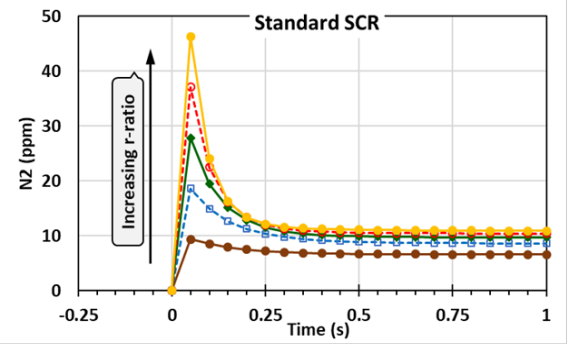

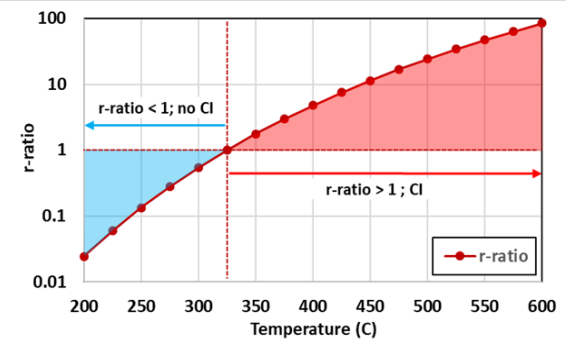

Figure IV.5.3 Variation in predicted CI with r-ratio (left) and r-ratio with temperature (right) as predicted by the Cu-redox half-cycle kinetic model [1]

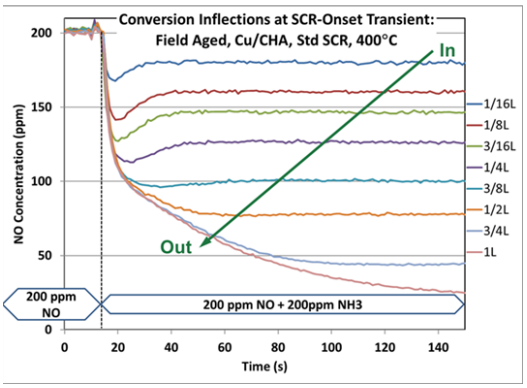

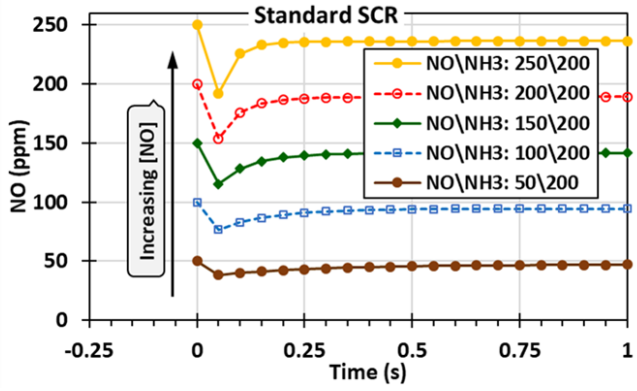

CHA –chabazite

Figure IV.5.4 Experimentally observed CI variation along the catalyst axis at SCR onset (left), and model-predicated variation in CI with increasing NO (right) [1]

In preparation for this research to study the mechanistic origins of ageing and formulation impacts on commercial SCR performance, the necessary modeling, material, and hardware resources are being assembled. The Cu-redox detailed-model structure will be based on that described in our Cu-redox half-cycle publication [1]. Cummins will code this new model in AVL BOOST for use with the transient protocol data to determine kinetic parameters. The research will be based on a Cu-SSZ-13 (copper aluminosilicate zeolite) SCR catalyst,

which is the current commercial product in use with Cummins automotive diesel systems. Cummins has provided fresh and field-aged versions of this catalyst sample. In addition to specifying catalyst sample core locations, degreening, and hydrothermal ageing details, the team has finalized the initial experimental matrix for performing the transient-response five-step protocol; this will provide the experimental data for kinetic parameter determination using the detailed model. Transient-response experiments require an improved catalyst reactor; this reactor has been designed and is currently being assembled. Initial applications will be to the degreened catalyst sample and will be used to validate Cummins' proprietary SCR models at relevant space velocity values greater than those available thus far, and with respect to spatial reaction evolution. Insights to the catalyst ageing process will be made by analyzing how the catalyst kinetic parameters vary with ageing; this has applicability to improving catalyst formulation and durability as well as catalyst-state assessment for on-board diagnostics and control. The general results will be shared with the community.

Conclusions

This project has demonstrated that transient CI at SCR onset is caused by the initial imbalance between the Cu-redox RHC and OHC rates and progressive balancing as SS is approached. Conceptual and kinetic models have been applied to demonstrate numerous consistencies between experimental observations and the Cu-redox half-cycle model, thus demonstrating the kinetic origins of CI and appropriateness of the proposed model. Using measured CI transients and a detailed Cu-redox model, the half-cycle kinetic parameters can be determined. The basic structure for this model has been decided, the catalyst materials have been assembled, and an improved transient reactor for making the required five-step protocol measurements is being constructed and assessed. With this new transient response methodology, the impact of ageing, formulation, and other catalyst and operation parameters on the kinetic parameters can be quantified, and thus the mechanistic origins of their impact on catalyst performance studied. This will be the focus of follow-on CRADA research.

Key Publications and Presentations

1. Partridge, W.P., S. Joshi, J.A. Pihl, N. Currier, K. Kamasamudram, and A. Yezerets. 2018. "Using Transient Response to Study Half-Cycle Rates of the NO SCR Cu-Redox Cycle." Invited presentation at University of Houston, Department of Chemical & Biomolecular Engineering, Houston, TX (October 19). (PTS Pub ID# 119240)

2. Partridge, W.P., J.A. Pihl, S. Joshi, N. Currier, A. Yezerets, and K. Kamasamudram. 2019. "NO_x Control & Measurement Technology for Heavy-Duty Diesel Engines." 2019 DOE Vehicle Technologies Program Annual Merit Review, Arlington, VA (June 12). (PTS Pub ID# 125516)

3. Partridge, W.P., S. Joshi, J.A. Pihl, N. Currier, K. Kamasamudram, and A. Yezerets. 2019. "Using Transient Response to Study Half-Cycle Rates of the NO SCR Cu-Redox Cycle." Invited presentation at Queen's University Belfast, School of Chemistry & Chemical Engineering, Belfast, Northern Ireland (May 29). (PTS Pub ID# 126905)

4. Partridge, W.P., S. Joshi, J.A. Pihl, N. Currier, K. Kamasamudram, and A. Yezerets. 2019. "Using Transient Response to Study Half-Cycle Rates of the NO SCR Cu-Redox Cycle." 26th North American Catalysis Society Meeting, Chicago, IL (June 23–28). (PTS Pub ID# 127950)

5. Partridge, W.P., S. Joshi, J.A. Pihl, N. Currier, K. Kamasamudram, and A. Yezerets. 2019. "Using Transient Response to Study Half-Cycle Rates of the NO SCR Cu-Redox Cycle." Invited presentation at Cummins Post-NAM Symposium, Columbus, IN (June 29). (PTS Pub ID# 127952)

6. Partridge, Bill. 2019. "Diagnostics Development & Application for Advancing Engine Catalyst System Technology." Invited presentation at ORNL Tech Day, Cummins Technical Center, Columbus, IN (August 7). (PTS Pub ID# 130127)

References

1. Partridge, W.P., S.Y. Joshi, J.A. Pihl, and N.W. Currier. 2018. "New Operando Method for Quantifying the Relative Half-Cycle Rates of the NO SCR Redox Cycle over Cu-Exchanged Zeolites." *Applied Catalysis B: Environmental* 236: 195–204. doi.org/10.1016/j.apcatb.2018.04.071. (PTS Pub ID# 105708)

Acknowledgements

The principal investigator gratefully acknowledges the contributions of Saurabh Joshi, Rohil Daya, Neal Currier, Krishna Kamasamudram, and Alex Yezerets of Cummins, Inc., and Josh Pihl of ORNL.

IV.6 Next-Generation Ammonia Dosing System (Pacific Northwest National Laboratory)

Abhi Karkamkar, Principal Investigator
Pacific Northwest National Laboratory
902 Battelle Boulevard
Richland, WA 99352
E-mail: abhi.karkamkar@pnnl.gov

Ken Howden, DOE Technology Development Manager
U.S. Department of Energy
E-mail: Ken.Howden@ee.doe.gov

Start Date: October 1, 2018 End Date: September 30, 2019
Project Funding (FY19): $160,000 DOE share: $160,000 Non-DOE share: $0

Project Introduction

Selective catalytic reduction (SCR) offers a number of advantages, including excellent NO_x reduction efficiency over a wide range of temperatures and overall lower system cost. Currently, SCR is being used to meet the NO_x emission standards for diesel engines in Europe and North America, and it is being considered for meeting future NO_x emission standards for lean-burn gasoline engines. Aqueous urea solutions (e.g., Diesel Exhaust Fluid and AdBlue) are currently used as ammonia storage compounds for mobile applications. When the aqueous urea solution is sprayed into the exhaust gas stream, urea is decomposed to release ammonia, which then reduces NO_x over the downstream SCR catalyst. Although aqueous urea solution technology has enabled automakers and engine manufacturers to meet the current NO_x emission requirements, the process requires a hot exhaust gas and sufficient mixing, creating challenges for low-temperature NO_x emissions control and aftertreatment system packaging.

For these reasons, alternative materials and technologies have been developed as ammonia sources (e.g., solid urea, ammonium carbamate, and metal ammine chloride) during the past few years [1],[2],[3]. These technologies promise more convenient handling and distribution of ammonia sources, help maximize the low-temperature performance of SCR catalysts, and reduce overall system volume and weight. However, none of these alternative technologies can be successfully implemented without industry consensus.

Objectives

Overall Objectives

- Increase engine efficiency by minimizing the energy requirement for dosing ammonia
- Synthesize novel materials that can store and release ammonia in the solid state
- Quantify the gravimetric ammonia capacity of the materials
- Quantify the strength of ammonia binding to tune the ammonia release temperature
- Demonstrate the ability to tune the ammonia release temperature to 100°C–180°C.

Fiscal Year 2019 Objectives

- Identify halide-free compositions that can store greater than 25 wt% ammonia
- Use synthetic modifications to optimize the ammonia storage capacity of oxidic materials

- Use theoretical calculations to down-select compositions that show moderate ammonia binding energies.

Approach

Pacific Northwest National Laboratory is developing protocols in collaboration with United States Council for Automotive Research to improve or optimize the properties of solid-state ammonia storage materials based on the information collected during the prior years. This fiscal year, the project focused on ways to develop experimental protocols to synthesize and quantify novel non-halide-containing materials to eliminate corrosive HCl generation observed in the metal halide ammine complexes. The novel materials were synthesized by a combination of co-precipitation, ion-exchange techniques, and solid-state synthesis. The project focused on the following three classes of materials:

1. Zeolite-based materials: Researchers synthesized and modified several zeolites, including Beta zeolite and Y zeolite. Various metal cations were impregnated in the zeolites to modify the capacity and acid strength.

2. Amorphous oxides: The project evaluated the ammonia storage capacity of several high-surface oxides of silica, titania, and alumina. Researchers utilized a combination of sol-gel and co-precipitation approaches to synthesize a large variety of materials.

3. Crystalline oxides: The project synthesized layered cesium titanates (CTO) based on literature protocols and modified them with metal ions such as nickel, magnesium, iron, and cobalt.

The synthesized materials were characterized using X-ray diffraction before and after ammonia capture to determine the structure and formation of a new material. The ammonia storage and release behaviors were studied using calorimetric and gravimetric studies using simultaneous thermogravimetric analysis–differential scanning calorimetry coupled with mass spectrometry. The project utilized ammonia temperature-programmed desorption to characterize the ammonia release behavior. Researchers used ab initio and molecular dynamics calculations to computationally screen materials. Utilizing a combination of experimental and modeling tools, the project will down-select the most promising materials.

Results

- Completed synthesis of three classes of materials and evaluated ammonia uptake on 10 materials
- Achieved 10–15 wt% ammonia storage capacity in zeolite-based materials
- Used a combination of metal doping and the Si/Al ratio to successfully decrease the temperature of ammonia release from 250°C to 150°C without loss of capacity
- Used ab initio and molecular dynamics simulations to identify the energetics of silicate, titano-silicate, and aluminosilicate materials.

Zeolite-Based Materials

The initial set of materials was based on zeolite Y with an Si/Al ratio of 5 [4]. The materials adsorbed ammonia rapidly (in a few seconds). However, the materials were left in an ammonia environment for four hours to ensure maximum adsorption. The ammonia-loaded materials were then characterized using thermogravimetric–mass spectrum analysis to evaluate their ammonia adsorption capacities. Figure IV.6.1(a) shows the ammonia release profile as a function of temperature. Figure IV.6.1(b) shows the corresponding mass spectrum signal for ammonia gas. Table IV.6.1 shows the ammonia uptake capacities of various aluminosilicate materials.

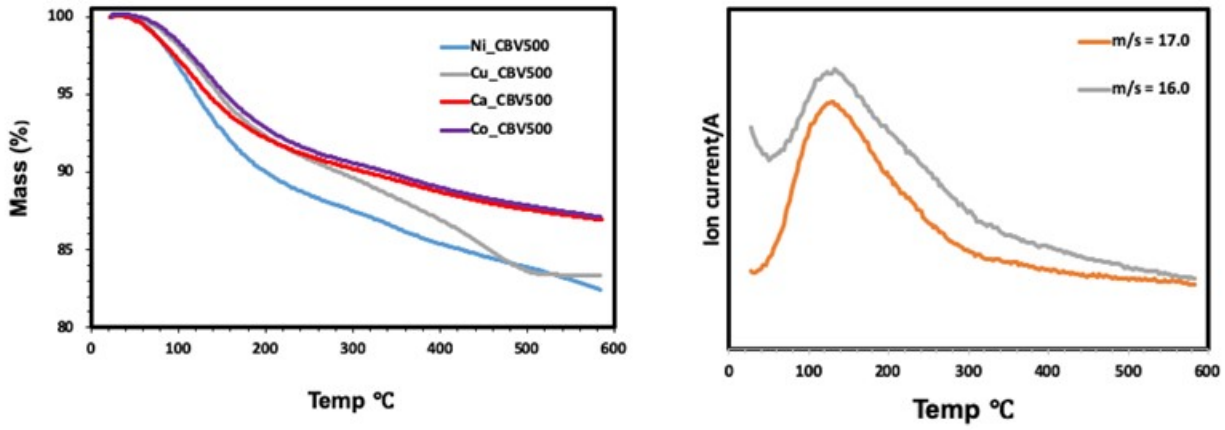

Figure IV.6.1 (a) Thermogravimetric analysis of metal-modified zeolite Y. The weight loss corresponds to ammonia stored in the zeolites. (b) The graph shows the mass spectrum signal associated with ammonia being released for Cu-Y.

Table IV.6.1 Ammonia Uptake Capacities of Various Aluminosilicate Materials

Material	Ammonia Capacity (wt%)	Impregnation Method
MCM-41*	4.55	
Al-MCM-41	5.55	Incipient wetness
Zeolite Y CBV 500	9.55	
2% Ca_zeolite Y CBV 500	12.13	Incipient wetness
Cu_zeolite Y CBV 500	16.68	Ion exchange

* MCM-41 – Mobil Composition of Matter No. 41

Metal-Modified CTO Materials

CTO-based materials were synthesized using solid-state synthesis followed by ion exchange to replace cesium in the framework with nickel [5]. These materials showed promising uptake in the initial cycles. These materials are not very stable upon ammonia cycling and slowly fall apart, as can be seen in the first two cycles. They also have much higher affinity for water over ammonia. Figure IV.6.2(a) shows the ammonia release profile as a function of temperature for CTO materials. Figure IV.6.2(b) shows the corresponding mass spectrum signal for ammonia gas.

Computational Modeling for Screening Materials

The project utilized a density functional theory (DFT)-based screening approach to identify the materials with ideal compositions for optimum binding of ammonia. Materials that bind ammonia too strongly or weakly are not ideal. According to project calculations, pure silica materials bind ammonia very weakly and will release ammonia at very low temperatures, hence not providing the desired stability. Silica materials doped with aluminum will bind ammonia very strongly, hence releasing the ammonia at temperatures >250°C. This is highly undesirable. Based on an initial screening, silica materials doped with titanium have an intermediate binding strength for ammonia. Table IV.6.2 summarizes the binding energy of ammonia to these three materials.

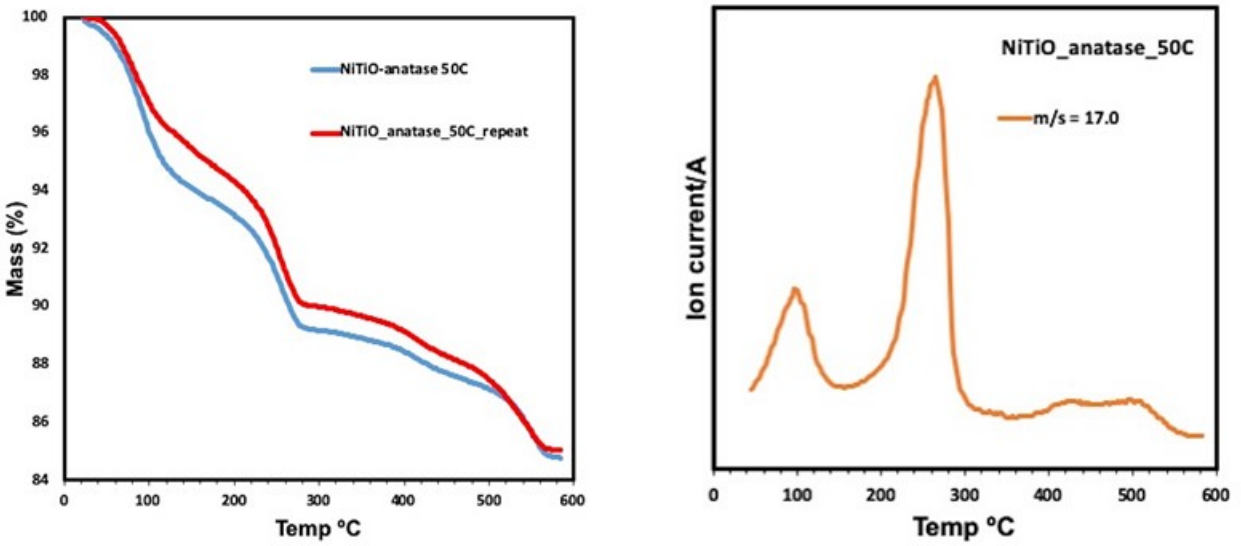

Figure IV.6.2 (a) Thermogravimetric analysis of metal-modified CTO. The weight loss corresponds to ammonia stored in the zeolites. (b) The graph shows the mass spectrum signal associated with ammonia being released for NiTiO.

Table IV.6.2 Energetics of Ammonia Binding to Silica and Doped Silica

E (kJ/mol)	Silica	Ti-Doped	Al-Doped
DFT(B3LYP)	-6.0	-8.0	-28.0
SAPT0	2.0	2.0	-23.0

Conclusions

- Zeolite-based materials have shown 15–20 wt% ammonia capacity.
- Metal-modified zeolites provide the ability to decrease the temperature of ammonia release from 250°C to 150°C without loss of capacity.
- Initial DFT simulations identified that the energetics of titano-silicate materials is more desirable than that of silicate and aluminosilicate materials.

References

1. Liu, Chun Yi, and Ken-ichi Aika. 2004. "Ammonia Absorption into Alkaline Earth Metal Halide Mixtures as an Ammonia Storage Material." *Ind. Eng. Chem. Res.* 43: 7484–7491.
2. Jensen, Peter Bjerre, Steen Lysgaard, Ulrich J. Quaade, and Tejs Vegge. 2014. "Designing Mixed Metal Halide Ammines for Ammonia Storage Using Density Functional Theory and Genetic Algorithms." *Phys.Chem. Chem.Phys.* 16: 19732–19740.
3. Johannessen, T. 2016. "Emissions Solutions for Optimal $DeNO_x$ in Real Driving Conditions." Integer Emissions Summit Asia Pacific.
4. Liu, Chun Yi, and Ken-ichi Aika. 2003. "Ammonia Adsorption on Ion Exchanged Y-Zeolites as Ammonia Storage Material." *Journal of the Japan Petroleum Institute* 46 (5): 301–307.

5. Yokosawa, Kazuki, Takahiro Takei, Sayaka Yanagida, Nobuhiro Kumada, and Ken-ichi Katsumata. 2018. “Ion Exchange of Layered Titanate with Transition Metal and Application to Ammonia Storage.” *Journal of the Ceramic Society of Japan* 126 (10): 808–813.

Acknowledgements

Pacific Northwest National Laboratory acknowledges the contributions of Shari Li, Yongsoon Shin, and Vassiliki-Alexandra Glezakou.

IV.7 Development and Optimization of a Multi-Functional SCR-DPF Aftertreatment System for Heavy-Duty NO_x and Soot Emission Reduction (Pacific Northwest National Laboratory)

Kenneth G. Rappé, Principal Investigator
Pacific Northwest National Laboratory (PNNL)
P. O. Box 999
Richland, WA 99354
E-mail: ken.rappe@pnnl.gov

Ken Howden, DOE Technology Development Manager
U.S. Department of Energy
E-mail: Ken.Howden@ee.doe.gov

Start Date: June 15, 2016 End Date: June 14, 2020
Project Funding (FY19): $600,000 DOE share: $300,000 Non-DOE share: $300,000 (in-kind)

Project Introduction

SCR-on-DPF (i.e., the integration of selective catalytic reduction [SCR] catalytic and diesel particulate filter [DPF] filtration technologies) combines NO_x reduction and soot filtration in a single two-way device by loading an SCR catalyst into the porous wall microstructure of a DPF. Its development is motivated by the need to comply with emissions regulations in a manner that reduces aftertreatment system volume and cost, increases packaging flexibility, and enables a pathway towards improved low-temperature (and overall) NO_x reduction performance. The challenges faced for successful application of SCR-on-DPF technology to heavy-duty diesel vehicles are (i) achieving the necessary soot filtration and SCR catalytic performance, (ii) achieving the necessary SCR durability requirements, and (iii) retaining the ability to oxidize soot (filtered by the DPF) passively using NO_2. The first two challenges have been addressed through the development of advanced ultra-high-porosity substrates and catalyst coating and imaging techniques, and through the development of small-pore chabazite (CHA) or CHA-like zeolite-based SCR catalysts with superior thermal durability; thus, there is a clear path to overcoming these challenges [1],[2],[3]. The third challenge is significant because oxidation of soot by NO_2 (i.e., passive soot oxidation) is a cost-effective strategy to oxidize soot in heavy-duty diesel applications and significantly reduces the fuel penalty for managing soot emissions versus active DPF regeneration.

Passive soot oxidation becomes challenging with SCR-on-DPF technology because of reduced NO_2 availability to drive the reaction due to the fast SCR reaction. Fast SCR consumes NO and NO_2 in equimolar amounts and is kinetically dominating in the SCR and soot oxidation reaction network in the temperature range of interest. Thus, the integration of current state-of-the-art SCR catalyst technology on a DPF results in significantly reduced passive soot oxidation activity due to preferential depletion of the NO_2 by the SCR catalyst. This work is focused on the development of a novel active SCR phase that, when employed in the SCR-on-DPF configuration, will enable improved passive soot oxidation capacity versus current SCR catalysts while retaining the necessary NO_x reduction performance efficiency to be attractive for the heavy-duty diesel application.

Objectives

Overall Objectives

- Develop an SCR-SCO binary catalyst system, consisting of an SCR catalyst combined with a selective catalytic oxidation (SCO) phase, that improves the availability of NO_2 versus current SCR technology

while retaining comparably high NO_x reduction efficiency and minimizing the parasitic oxidation of NH_3 (with O_2)

- Demonstrate the successful integration of DPF technology with the SCR-SCO binary catalyst that enables increased passive soot oxidation (i.e., with NO_2) within the integrated device versus SCR-on-DPF technology
- Develop the fundamental understanding of the interaction of SCR and SCO catalyst phases that will lead to an optimized binary catalyst system, identifying the necessary engineering requirements and system limitations for their integration, with a view to proper function and optimal integration
- Develop models that incorporate the SCR-SCO catalyst system that can accelerate the optimization of SCR-on-DPF technology by providing operational insight while simultaneously minimizing experimental testing
- Develop the necessary understanding to potentially lead to the design and optimization of four-way devices, which will address particulate matter, hydrocarbons, CO, and NO_x in a single unit.

Fiscal Year 2019 Objectives

- Inform on critical catalyst design parameters for a ZrO_2-based SCO phase combined with a Cu-CHA SCR phase, forming an SCR-SCO binary catalyst system, in relation to NO_x reduction performance and SCR durability
- Understand the impact of secondary oxide or heteroatom additives to ZrO_2, employed to improve NO oxidation (to NO_2), on binary catalyst NO_x reduction performance and SCR durability
- Inform on the optimized pathway towards SCO impact on fast SCR contribution to NO_x reduction.

Approach

The work is tasked with developing a novel active SCR catalyst phase that enables superior passive soot oxidation activity and comparable NO_x reduction performance when employed in the SCR-on-DPF configuration in comparison to current state-of-the-art SCR catalyst technology. This is to be accomplished by the integration of an SCO phase to the SCR catalyst, forming an SCO-SCR binary catalyst active phase. The intent of the SCO phase is to increase the NO oxidation (to NO_2) capacity of the active SCR phase, thus generating NO_2 in situ, while retaining or improving upon the NO_x reduction efficiency and SCR durability. The result of a successful SCO-SCR binary catalyst integration will be greater availability of NO_2 to drive passive soot oxidation without compromising durable and efficient NO_x reduction performance. The SCO phase is building off of a ZrO_2-base structure, with potential variations in its chemistry to enhance reducibility and/or oxygen storage (e.g., inclusion of CeO_2), improve NO oxidation capacity (e.g., inclusion of Mn and/or Co), and enable other benefits such as improved activity or durability. The targets for a successful binary catalyst active phase are (i) high NO oxidation capacity to drive passive soot oxidation performance, (ii) without oxidizing NH_3 reductant at unacceptably high levels, thus retaining high NO_x reduction performance and selectivity, and (iii) without inflicting unacceptable damage on the SCR active phase, thus retaining high SCR durability.

PNNL utilizes an extensive suite of standard and specialty analytical tools and test reactors to support steady-state and transient testing that are necessary to provide information on critical catalyst design parameters, enablers, and limitations with the binary catalyst system. PNNL is focused on fundamental understanding of the pathway towards high NO oxidation (to NO_2) capacity of the binary catalyst system that retains highly efficient and selective NO_x reduction and a durable SCR catalyst phase. PNNL utilizes resources associated with PNNL's Exhaust Emissions Science Lab and leverages the capabilities within the Environmental Molecular Science Laboratory, Institute for Interfacial Catalysis, and Emissions Chemistry & Aerosol

Research facility. PACCAR is providing input on preferential direction for SCO phase chemistry and is leading efforts associated with catalyst coating on cores and scaling to the device level.

Results

Initial work in Fiscal Year 2019 was focused on optimizing the SCO phase chemistry to be the area of focus for SCR-SCO binary catalyst optimization. ZrO_2 is the bulk oxide of most significant interest due to its enhanced durability demonstrated in vehicle emission applications. However, CeO_2 is also considered for its reducibility and oxygen storage function, which can each add attractive catalytic function. Thus, each was considered in preliminary SCO phase development. Due to its proclivity in advanced NO oxidation formulations as well as other reasons, Mn was chosen as the active metal component for focused SCO phase development.

Coprecipitation of Mn with ZrO_2 or CeO_2 was demonstrated as a preferred method of SCO-phase synthesis for NO oxidation activity versus Mn impregnation (on ZrO_2 or CeO_2) or physical mixing of MnO_2 (with ZrO_2 or CeO_2). Figure IV.7.1 shows the NO oxidation activity versus temperature for 30 wt% Mn combined with ZrO_2, comparing coprecipitation, impregnation, and physical mixing preparation techniques as well as the individual components MnO_2 and ZrO_2 (both deposited on SiO_2 in analogous weight ratios). The coprecipitated Mn/ZrO_2 sample demonstrated far superior NO oxidation activity to those prepared using impregnation or physical mixing, lighting off at lower temperature ($T_{50} < 250°C$) and thus reaching higher peak NO conversion before being limited by $NO \leftrightarrow NO_2$ thermodynamics. Additionally, the coprecipitated Mn/ZrO_2 sample was shown to exhibit NO oxidation activity that is far superior to the sum of those of the individual MnO_2 and ZrO_2 components. Similarly, the coprecipitated Mn/CeO_2 sample demonstrated superior NO oxidation activity to the samples prepared with impregnation or physical mixing (data not shown) and exhibited activity that was greater than the sum of the individual MnO_2 and CeO_2 components. X-ray diffraction data (data not shown) indicated that NO oxidation activity was correlated to extent of dispersion of Mn into the bulk oxide lattice. Both the physically mixed and impregnated 30 wt% MnO_2/CeO_2 and MnO_2/ZrO_2 samples exhibited MnO_2 diffraction peaks (in addition to CeO_2 and ZrO_2 diffraction pattern). In contrast, the coprecipitated Mn-CeO_2 sample was void of MnO_2 diffraction features, CeO_2 diffraction was shifted slightly to lower 2Θ, and the coprecipitated Mn-ZrO_2 sample exhibited amorphous (or nanocrystalline) MnO_2 coverage indicative of exceeding the saturated lattice occupancy of Mn in ZrO_2. Collectively, these results indicate that the interface site of Mn and the bulk oxide is the preferred active site for catalyzing the NO oxidation reaction.

From activity measurements and X-ray diffraction and electron paramagnetic resonance (EPR) spectroscopy, 10 wt% Mn coprecipitated with 90% ZrO_2 was found to be a near-optimum Mn content in ZrO_2 for high NO oxidation activity and efficient Mn usage. Figure IV.7.2 shows the NO oxidation activity versus temperature for Mn coprecipitated with ZrO_2, with Mn content ranging from 1 wt% to 30 wt%. The data showed somewhat insignificant improvement of NO oxidation light-off at <350°C for ≤2 wt% Mn. In contrast, significant improvement of NO oxidation activity and light-off was observed for ≥5 wt% Mn up to 20 wt% Mn, above which further improvement in activity was not observed. The corresponding X-ray diffraction data showed that ≤2 wt% Mn coprecipitated with ZrO_2 was not enough to fully transform the ZrO_2 from monoclinic to the preferred tetragonal form, which required ≥5 wt% Mn. Furthermore, ≥20 wt% Mn content exceeded the saturated lattice occupancy of Mn in ZrO_2, as evidenced by amorphous MnO_2 coverage, indicating inefficient use of Mn. EPR results provided further clarity to the optimum Mn/ZrO_2 SCO-phase catalyst, as they allowed for assessment of relative Mn(II) and Mn(III) content. Figure IV.7.3 shows the low-field EPR and the high-field EPR signals of the Mn/ZrO_2 coprecipitated samples arranged into two groups: (i) 1, 2, and 5 wt% Mn; and (ii) 5, 10, and 20 wt% Mn. In Mn-cation-containing materials, the low-field EPR provides information on relative Mn(III) content, and the high-field EPR provides information on relative Mn(II) content. At ≤5 wt% Mn, Mn content was directly proportional to Mn(II) content and indirectly proportional to Mn(III) content. In contrast, at ≥5 wt% Mn, Mn content was indirectly proportional to both Mn(II) and Mn(III) content, indicative of a directly proportional shift to non-isolated Mn species. Collectively, these results indicate that the preferred active catalytic center for promoting NO oxidation in Mn/ZrO_2 catalysts is the interface site of Mn-dimers and

ZrO_2. This herein provides a technique for rapid optimization of Mn-based SCO-phase materials for the SCR-SCO binary catalyst system.

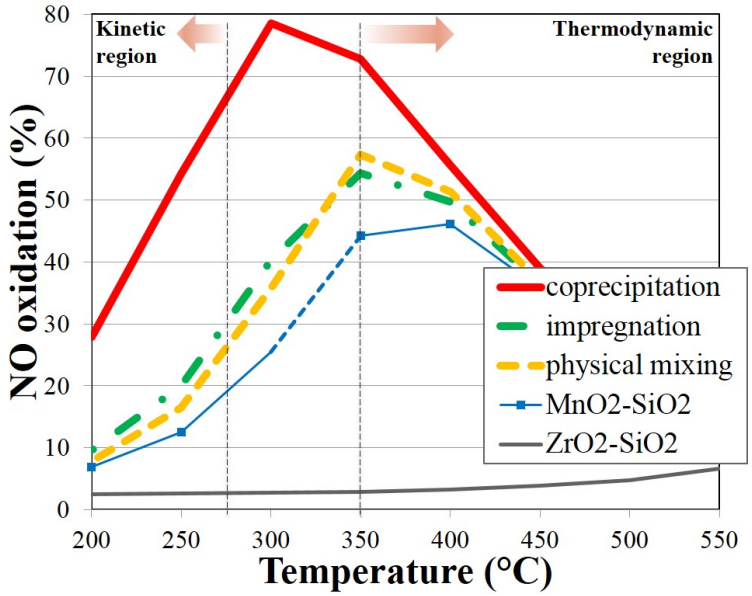

Figure IV.7.1 NO oxidation activity of different preparations of 30 wt% Mn/ZrO_2 along with activity of the oxide components

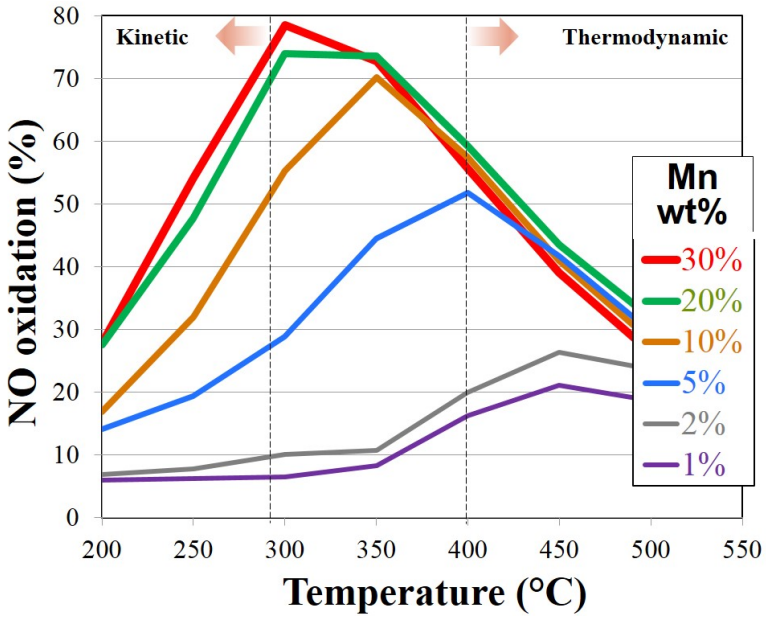

Figure IV.7.2 NO oxidation activity of coprecipitated Mn/ZrO_2 with varying Mn content

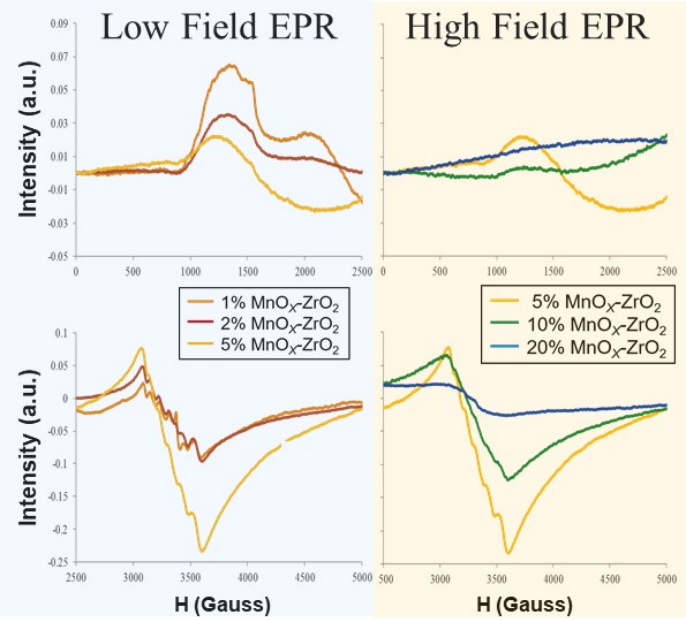

Figure IV.7.3 EPR activity of coprecipitated Mn/ZrO_2 with varying Mn content

SCO-phase activity measurements combined with results from previous studies provide evidence of three separate pathways for SCR rate enhancement from inclusion of an SCO phase: (i) direct SCR activity of the SCO phase, (ii) sequential oxidation of NO to NO_2 on the SCO phase and classical fast SCR contribution on the SCR phase, and (iii) oxidation of NO on the SCO phase contributing to fast SCR contribution on the SCR phase in a manner that circumvents the requirement for NO_2 desorption on the SCO phase. Figure IV.7.4 shows the SCO-phase performance under standard SCR reaction conditions (i.e., without NO_2 in the feed), with the concentrations of NO, NO_2, N_2O, and NH_3 presented together with the N-balance in the system, which correlates SCR activity to the offset of the N-balance from 100%. The results show that, for this composition, the SCO phase exhibited dominant SCR behavior below ~225°C, characterized by direct SCR contribution from the SCO phase, and dominant oxidation behavior above 225°C, characterized by NH_3 elimination and NO_2 production. The high-temperature oxidation regime of SCO behavior will contribute to the classical fast SCR reaction pathway for NO_x reduction when coupled with an SCR catalyst. Evidence suggests that a third pathway exists for SCR rate enhancement of SCR-SCO binary catalyst systems, which is the participation of a surface active oxidized NO intermediate formed on the SCO phase and reduced on the SCR phase via a fast-SCR-type reaction mechanism. This reaction pathway circumvents the rate-limiting NO_2-desorption requirement from the SCO phase for contribution to the classical fast SCR reaction pathway and will be discussed further below.

An SCR-SCO binary catalyst system consisting of 30% SCO phase physically mixed with 70% SCR phase demonstrated improved low-temperature SCR performance and significantly increased NO_2 availability under SCR reaction conditions versus the SCR catalyst alone. The SCO phase consisted of 10 wt% Mn/ZrO_2 coprecipitated, and the SCR phase was a current state-of-the-art Cu-SSZ-13 (aluminosilicate zeolite) SCR formulation. Figure IV.7.5 shows the results of testing the SCO-SCR binary catalyst under standard SCR reaction conditions and compares performance to the SCR catalyst alone. The low-temperature NO_x reduction performance of the binary catalyst was improved >20% at 150°C and ~8% at 200°C. Furthermore, the SCO did not add additional NH_3 oxidation activity at high temperature (>300°C) above what was observed with the SCR phase alone. The SCO phase also significantly shifted the NO_2 balance in the system under the conditions tested. The NO_x in the effluent from the binary catalyst system contained a significantly greater fraction of NO_2 versus the SCR catalyst, as indicated by the data in Figure IV.7.5, and was predominantly NO_2 (i.e., $NO_2/NO > 1$) between 290ºC and 360°C. Interestingly, the NO_x reduction performance improvement of the

binary catalyst is greater than that explained by SCR contribution from the SCO phase and NO oxidation activity of the binary catalyst (data not shown), which is negligible (<1%). This can be explained by either increased NO oxidation activity of the SCO phase under SCR conditions due to rapid local consumption of NO_2, or the participation of a surface active oxidized NO intermediate. In any case, it speaks to a synergistic effect of the SCO and SCR catalyst phases of the system.

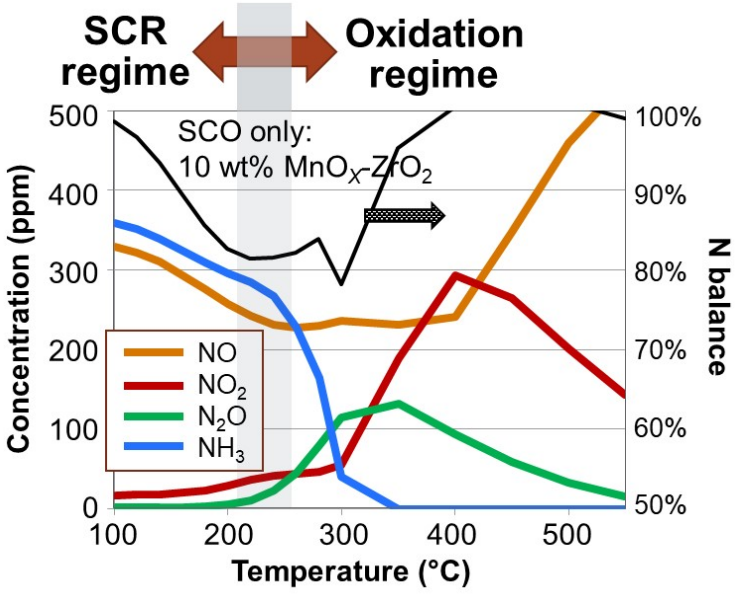

Figure IV.7.4 Activity of coprecipitated 10 wt% MnO_2-ZrO_2 under standard SCR reaction conditions

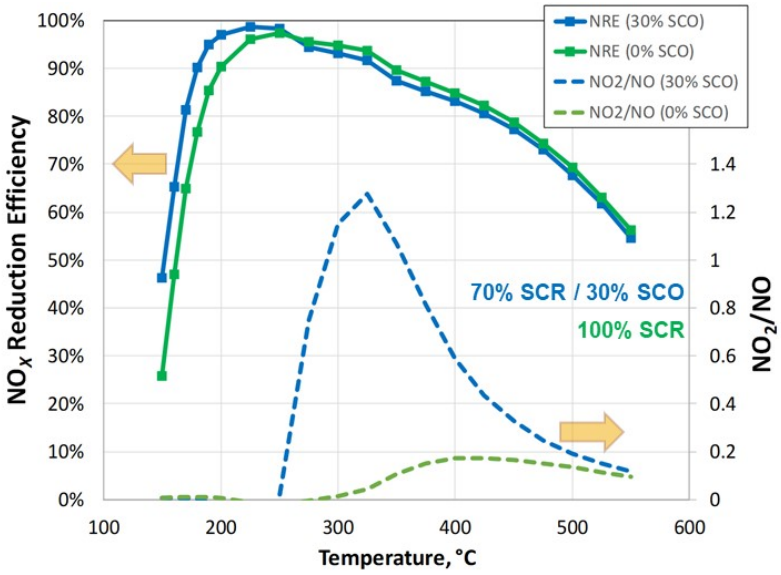

Figure IV.7.5 NO_x reduction efficiency (NRE) and NO_2/NO ratio in the effluent of the SCR-SCO and SCR-only catalysts

Proper engineering on an SCO-SCR binary catalyst system must consider multiple and potentially unique aging mechanisms not observed on the SCO and SCR phases alone. Achieving a closer proximity of SCO and SCR catalyst phases introduces potential risk of Mn entering into charge-balancing position in the zeolite. This was observed by H_2 temperature-programmed reduction (data not shown), which indicated that achieving a closer proximity of the SCO and SCR phases via coprecipitation of the MnO_2 and ZrO_2 onto the SCR catalyst resulted in a portion of the Mn entering the zeolite structure. Additionally, a unique aging mechanism was observed with the SCO-SCR binary catalyst. As shown in Figure IV.7.6, hydrothermal aging at 800°C for 16 h resulted in significant reduction of SCR activity across the full operating window, whereas hydrothermal aging at 650°C for 100 h had very little impact on SCR activity. The NH_3 oxidation behavior of these aged samples (data not shown) suggested a significant loss of SCR-active Cu centers. This suggests that the SCR-SCO binary catalyst system is susceptible to a new aging mechanism that reduces the quantity of active Cu centers in the SCR catalyst, which must be considered in designing accelerated aging protocols to match on-engine aging results.

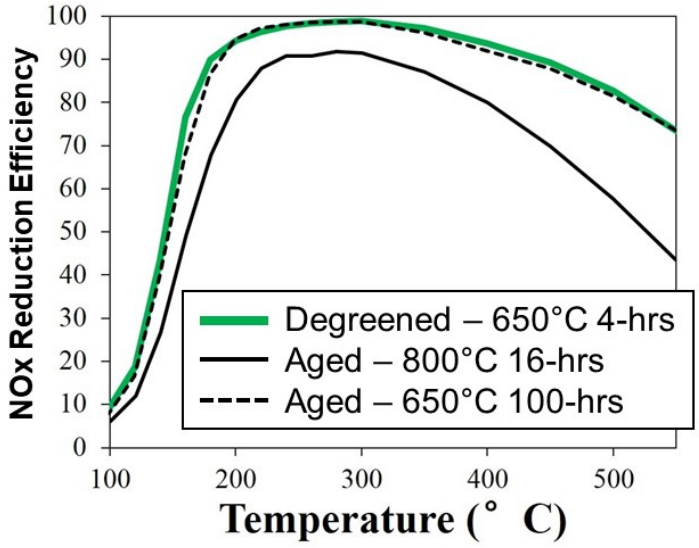

Figure IV.7.6 NO_x reduction efficiency of the SCR-SCO binary catalyst following hydrothermal aging at 800°C for 16 h and 650°C for 100 h versus degreened at 650°C for 4 h

Conclusions

- Demonstrated that coprecipitation of Mn with ZrO_2 or CeO_2 bulk oxide is the optimum method of SCO-phase synthesis, as it maximizes the density of preferred interface sites of Mn and the bulk oxide
- Demonstrated that 10 wt% Mn coprecipitated with 90% ZrO_2 is the near-optimum SCO-phase chemistry for NO oxidation activity and efficient Mn usage
- Discovered via EPR spectroscopy that the active site for NO oxidation is the interface of Mn-dimer and ZrO_2, enabling a technique for rapid optimization of alternate Mn-based SCO-phase chemistries
- Demonstrated evidence of three separate pathways for SCR rate enhancement from inclusion of an SCO phase: (i) direct SCR activity of the SCO phase, (ii) sequential oxidation of NO to NO_2 on the SCO phase and classical fast SCR contribution on the SCR phase, and (iii) oxidation of NO on the SCO phase contributing to fast SCR contribution on the SCR phase in a manner that circumvents the requirement for rate-limiting NO_2 desorption from the SCO phase

- Demonstrated improved low-temperature SCR performance and significantly increased NO_2 availability on the binary catalyst under SCR reaction conditions versus the SCR catalyst alone, the former of which arises from a synergistic effect of the coupling of the SCO and SCR phases

- Discovered a unique ion-exchange aging mechanism that must be considered for accurate replication of field aging at the bench scale for SCR-SCO binary catalyst systems.

Key Publications

1. Peng, B., K.G. Rappé, Y. Cui, F. Gao, J. Szanyi, M.J. Olszta, E.D. Walter, Y. Wang, J.D. Holladay, and R.A. Goffe. 2019. "Enhancement of High-Temperature Selectivity on Cu-SSZ-13 towards NH_3-SCR Reaction from Highly Dispersed ZrO_2." *Applied Catalysis B: Environmental*, doi:https://doi.org/10.1016/j.apcatb.2019.118359.

References

1. Melscoet-Chauvel, I., C. Remy, and T.H. Tao. 2005. "High Porosity Cordierite Filter Development for NO_x/PM Reduction." *Develop Adv Ceram Compos* 26 (8): 11–19.

2. van Setten, B.A.A.L., M. Makkee, and J.A. Moulijn. 2001. "Science and Technology of Diesel Particulate Filters." *Catal Rev: Sci Eng* 43 (4): 489–564.

3. Beale, A.M., F. Gao, I. Lezcano-Gonzalez, C.H.F. Peden, and J. Szanyi. 2015. "Recent Advances in Automotive Catalysis for NO_x Emission Control by Small-Pore Microporous Materials." *Chem Soc Rev* 44: 7371–7405.

IV.8 Cold-Start Hydrocarbon Emissions from Light-Duty Gasoline Direct Injection Vehicles (Oak Ridge National Laboratory)

Melanie Moses-DeBusk, Principal Investigator
Oak Ridge National Laboratory
2360 Cherahala Blvd.
Knoxville, TN 37931
E-mail: mosesmj@ornl.gov

Ken Howden, DOE Technology Development Manager
U.S. Department of Energy
E-mail: Ken.Howden@ee.doe.gov

Start Date: October 1, 2018 End Date: September 1, 2021
Project Funding (FY19): $500,000 DOE share: $500,000 Non-DOE share: $0

Project Introduction

To enable advanced combustion engines to achieve cost-effective compliance with current and future U.S. emissions regulations, this effort will address the barriers/challenges associated with emission control compliance during vehicle cold start and transients encountered as a result of hybridization or low-temperature combustion.

This project's key focuses include measuring the detailed exhaust chemistry during cold start of boosted spark-ignition, diesel, and hybrid spark-ignition engine platforms at engine out (EO) and downstream of relevant emission control systems, including but not limited to three-way catalysts (TWCs) and hydrocarbon (HC) traps. Previous research has shown that, for modern vehicles, the majority of emissions downstream of the emission control catalysts occurs during the first 250 seconds of the federal test procedure (FTP-75) certification cycle—i.e., the start of the cold-start portion of the test—when the engine, oil, and catalyst systems are all still cold [1]. A true cold start requires that the vehicle be shut off for at least 12 hours before it is keyed on for the test. This fiscal year (FY), the research will focus on characterization of gasoline direct injection (GDI) cold-start emissions using market-available vehicles. A special focus will be placed on HC speciation upstream and downstream of the HC trap to study how different HC chemistry (e.g., functional group) affects the HC trap's effectiveness during cold start. Since HC traps are not currently in commercial use, the project collaborated with a catalyst supplier to procure the HC traps for this project. While the detailed speciation is of specific interest for the development of emission control solutions for HC emissions, it is also beneficial to the development of low-temperature oxidation catalyst striving to meet the U.S. Department of Energy's 150°C Challenge, since different HCs have been shown to have different impacts on catalyst light-off temperatures.

Objectives

Overall Objectives

- Develop an understanding of how particulate matter and HC chemistry change during cold start
- Determine what HC species can be trapped on HC traps during cold start as opposed to what species must be converted by low-temperature catalyst formulations.

Fiscal Year 2019 Objectives

- Quantify HC cold-start emissions from current GDI vehicles during the first 250 seconds of the cold-start cycle

- Provide detailed speciation of HC emissions compositions during the first 250 seconds of the cold-start cycle.

Approach

Cold-start emissions were measured from two Model Year 2018 GDI light-duty pick-ups in Oak Ridge National Laboratory's chassis dynamometer laboratory. The project targeted emissions during the first 250 seconds of the FTP-75 test cycle under cold-start conditions, as literature reports indicate that it takes at least that long for the commercial TWC to fully light off and control emissions. Standard cold-start testing requires that the engine be off for at least 12 hours prior to the test. Therefore, each truck could be tested only once per day; one truck was left on the chassis rolls overnight for testing, and the second truck was rolled onto the chassis rolls so that the engine was not keyed on until the start of the test. Truck A had a 2.7 L turbocharged GDI engine, and Truck B had a 5.3 L naturally aspirated GDI engine. Both trucks had between roughly 25,000 and 30,000 miles of consumer driving on them. The dual original engine manufacturer (OEM) close-coupled TWCs in the OEM split-bank, y-configuration were left on during cold start during tests, but the resonators and mufflers were removed from both exhaust systems. Additionally, Truck B had an underbody clean-up catalyst that was removed. An exhaust slipstream, upstream from one of the close-coupled TWCs (passenger cylinder bank), was used to study EO exhaust properties, while the full exhaust was sampled from the tailpipe for the combined dual-TWC-out exhaust. Researchers used specialty sampling techniques to study the speciation of C3–C18 hydrocarbons and aldehydes produced over the first 250 seconds of the FTP-75 cycle. The detailed HC speciation and particulate matter samples were taken from dilute exhaust using an in-house-designed dilution tunnel for the EO location and from a constant-volume sampling tunnel for the full TWC-out exhaust. Time-resolved analysis was performed on thermally denuded particulate size/number (Engine Exhaust Particle Sizer™), soot particulate matter mass (Micro Soot Sensor™), and gaseous emissions using a Fourier-transform infrared (FTIR) spectroscope from MKS Instruments for the entire 505 seconds of the FTP-75 Bag 1 (cold-LA4, used for light-duty vehicle testing).

Results

FY 2019 Accomplishments

- Measured detailed gaseous emissions generated in the first 250 seconds of the cold-start FTP-75 drive cycle on modern GDI vehicles
- Determined the specific key molecular species (aromatics, paraffins, olefins, and aldehydes) contributing to total HC emissions
- Prepared both vehicle exhaust systems for underbody dual exhaust HC trap and/or gasoline particulate filter emission control studies.

Two types of cold-start emission studies were conducted in FY 2019. The first type targeted GDI EO HC species, and the second focused on close-coupled TWC-out emissions species. The majority of modern vehicle emissions occur during cold start, when the engine is cold and the aftertreatment catalyst(s) has not reached light-off temperatures. Therefore, it is beneficial to know what specific HC species are present in the exhaust in order to develop low-temperature oxidation catalysts and/or other emission control solutions for mitigating cold-start HC emissions. To further this knowledge, the project took time-resolved emissions concentrations using an MKS FTIR spectrometer. While the infrared vibrations for some smaller HCs are unique, making identification possible, other larger HCs are harder to differentiate; thus, FTIR spectroscopy provides only a more general functional group identification, like aromatics, for larger HCs. To help identify the specific HCs present in the emissions, the researchers used a range of other integrated sampling and analysis techniques to collect and analyze the HC species cumulatively present in the first 250 seconds of the FTP-75 cycle. The TWC-out samples were taken from the constant-volume sampling dilution tunnel, maintaining an accurate species-to-species ratio over the 250-second sampling duration. However, EO sampling options were limited, as dual close-coupled TWCs could not be removed because of feedback controls affecting vehicle performance/operation. Only slipstream sampling upstream of one catalyst was taken for EO data. Therefore,

the integrated samples taken for detailed HC speciation data from the EO study provided data only on the species present but did not maintain an accurate species-to-species ratio.

Figure IV.8.1 presents the time-resolved FTIR results for both EO (left) and TWC out (right) on both Truck A (top) and Truck B (bottom). Using the time-resolved total vehicle exhaust flow rate during the FTP test (black dashed lines), the FTIR concentrations for the MKS-software-identified HCs were first converted to mass (mg) on a C1-basis as a function of time; then, for simplicity, they were summed according to functional group. Increased HC emissions for both trucks were seen to correspond to increased exhaust flow, likely associated with increased fuel flow. While Truck A had higher EO HCs, both vehicles showed significant reduction in the TWC-out tailpipe exhaust. Truck A had lower HC emissions for the TWC out in the first 50 seconds but then had additional breakthrough in the 150–200 second window, while Truck B had notable HC emissions only in the first 50 seconds.

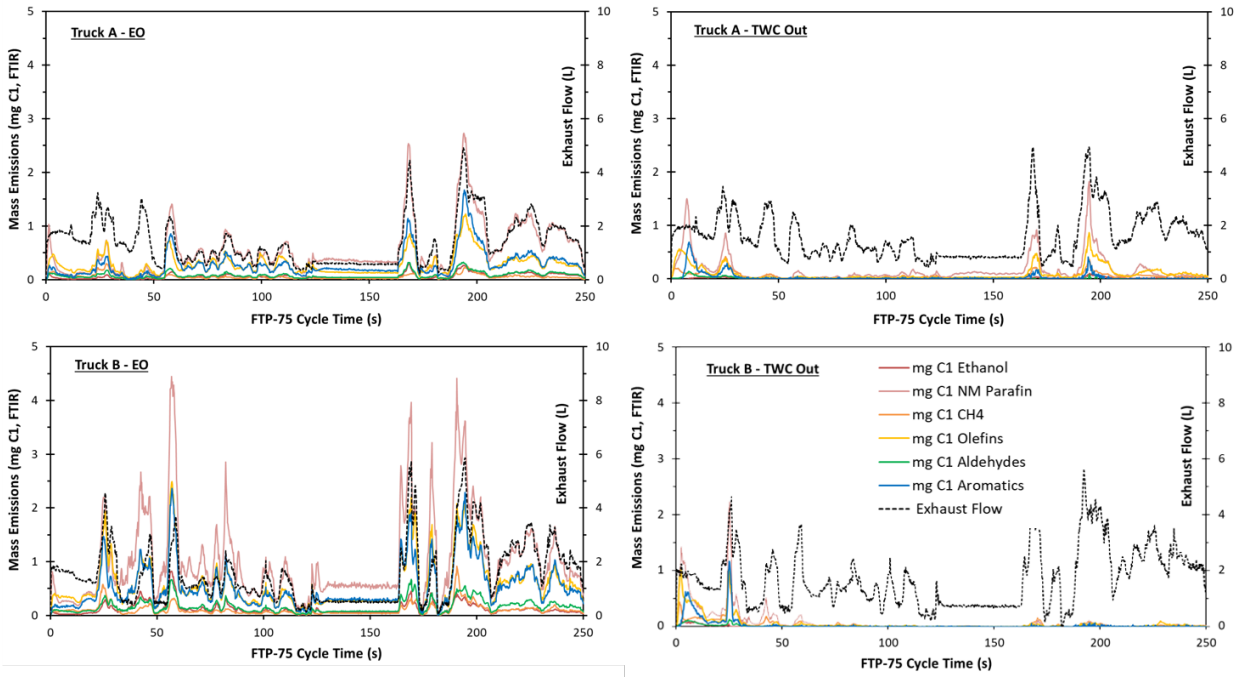

Figure IV.8.1 Time-resolved hydrocarbon mass emissions derived from FTIR concentrations for EO and TWC out of Truck A (top) and Truck B (bottom). Plots of mass emissions are on a C1 basis as a function of the FTP-75 cycle time (left y-axis), and total vehicle exhaust flow as a function of time (right, y-axis) is also shown on each plot.

The time-resolved FTIR C1 mass emissions are further summarized as a cumulative fractional distribution in Figure IV.8.2. Detailed speciation of the HCs was done on a cumulative basis over the first 250 seconds. The smaller HCs (C5–C9) were sampled by gaseous collection into Tedlar bags and stored in stainless steel canisters before analysis using a gas chromatograph – mass spectrometer (GC-MS). The C5–C9 HCs included paraffins, olefins, and small aromatics. A wide range of paraffins was present, but pentane and octane were the only ones in significant individual quantities. The individual olefins in significant mass quantity during this 250-second cold start were 1-pentene and 1-hexene. As expected, the researchers identified typical BTEX aromatics (benzene, toluene, ethylbenzene, and xylene), but two C9 aromatics, ethyl methyl benzene and trimethyl benzene, were also identified. A second sampling technique was used for collecting larger C9–C18 HCs during the same 250-second cold start (cumulatively). This technique employs a polytetrafluoroethylene membrane disk supporting a solid phase extraction material (Empore® styrene divinyl benzene); the solvent is extracted and analyzed by liquid injection onto a GC-MS [2]. Only aromatics were identified in this C9–C18 carbon range, and they included the two C9 aromatics also identified by the gas-sampled GC-MS techniques. Table IV.8.1 lists all of the C9–C18 HCs identified by this Empore® technique, in either the EO or TWC-out

emissions; however, the table includes only the fractional distribution of the larger HCs identified by this method for the TWC-out emissions, as the EO sampling method did not allow accurate ratio quantification comparisons for the cumulative 250 seconds. In addition to the two C9 aromatics, seven more aromatic compounds were identified, but no large paraffins or olefins were detected. The seven additional aromatics included five C10 substituted benzene compounds, one C10 di-substituted styrene compound, and a C11 mono-substituted naphthalene.

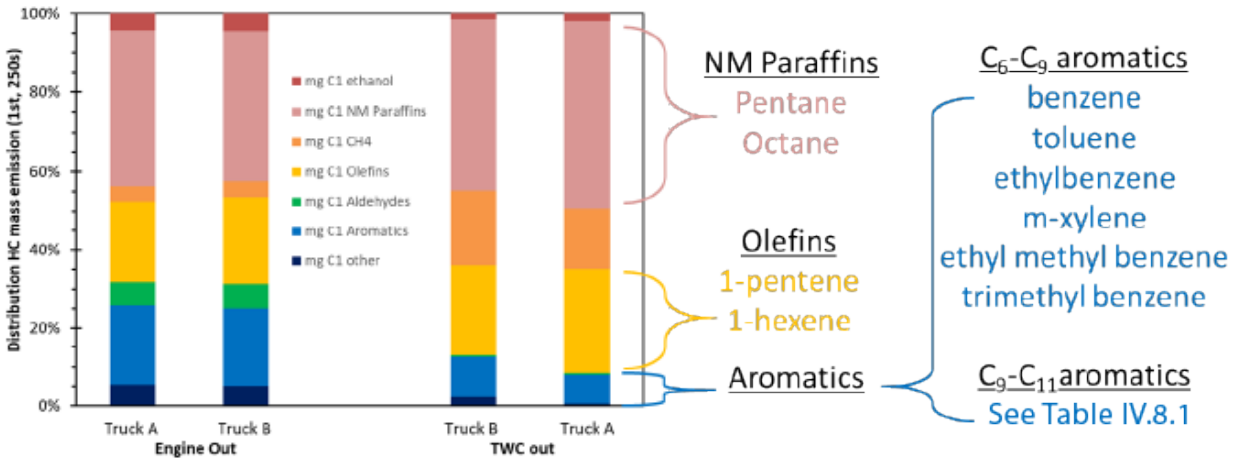

Figure IV.8.2 The bar graph shows the C1 mass distribution from FTIR concentrations cumulatively over the first 250 seconds of the cold-start FTP-75. The major non-methane (NM) paraffin, olefin, and aromatic species were specifically identified by gaseous or liquid GC-MS analyses. Two different types of capture and speciation were used to identify all aromatics; C6–C9 aromatics identified (gaseous sampled GC-MS) are listed, and C9–C11 aromatics (liquid sampled GC-MS) are specified in Table IV.8.1

Table IV.8.1 Distribution of Aromatic HCs Identified by Empore® Membrane Extraction and Analysis*

	TWC out	
	Truck A	Truck B
ethyl methyl benzene	27%	24%
trimethyl benzene	7%	13%
methyl propyl benzene	10%	9%
ethyl dimethyl benzene	32%	28%
methyl methylethyl benzene	11%	9%
tetramethyl benzene	0%	0%
dimethyl styrene	12%	15%
methyl naphthalene	0%	3%

*Listed HCs were all found in EO emissions, but fractional distribution is only for TWC-out emissions.

Conclusions

- Detailed speciation of EO and TWC-out emissions during the first 250 seconds of the cold start identified a larger range of HCs than could be isolated by the time-resolved FTIR analyses.
- Time-resolved sampling by the FTIR provided an understanding of which HC functional types were emitted over the first 250 seconds of an FTP cold start, while detailed analytical techniques provided identification of specific HC species.

- Using a variety of techniques, the project measured reduction in HC emissions for TWC out, detecting reductions for all species except methane from Truck A.

- Specific speciation and general HC distribution in EO and TWC-out emissions from the turbocharged GDI engine (Truck A) and the naturally aspirated GDI engine (Truck B) were very similar.

Key Publications

1. Moses-DeBusk, M., J.M. Storey, S.A. Lewis, Jr., R.M. Connatser, S. Mahurin, L. Moore, and S. Huff. 2019. "Hydrocarbon Speciation of GDI Cold-Start Exhaust Emissions on Current Light-Duty Trucks." DOE 2019 CLEERS Workshop, Ann Arbor, MI (September 17–19).

References

1. Lupescu, J., L. Xu, H.-W. Jen, A. Harwell, et al. 2018. "A New Catalyzed HC Trap Technology that Enhances the Conversion of Gasoline Fuel Cold-Start Emissions." SAE Technical Paper 2018-01-0938. https://doi.org/10.4271/2018-01-0938.

2. Storey, J.M.E., N. Domingo, S. Lewis, and D. Irick. 1999. "Analysis of Semivolatile Organic Compounds in Diesel Exhaust Using a Novel Sorption and Extraction Method." SAE Technical Paper 1999-01-3534. https://doi.org/10.4271/1999-01-3534.

Acknowledgements

The principal investigator thanks John Storey, Shannon Mahurin, Sam Lewis, Maggie Connatser, Shean Huff, and Larry Moore of Oak Ridge National Laboratory for their contributions to this project and report.

V High Efficiency Engine Technologies

V.1 Volvo SuperTruck 2: Pathway to Cost-Effective Commercialized Freight Efficiency (Volvo Group North America)

Pascal Amar, Principal Investigator
Volvo Group North America
7900 National Service Rd.
Greensboro, NC 27409
E-mail: pascal.amar@volvo.com

Ken Howden, DOE Technology Development Manager
U.S. Department of Energy
E-mail: Ken.Howden@ee.doe.gov

Start Date: October 1, 2016 End Date: September 30, 2021
Project Funding (FY19): $11,080,168 DOE share: $5,430,928 Non-DOE share: $5,649,241

Project Introduction

Volvo's SuperTruck 2 continues to build on the success of the SuperTruck project that demonstrated vehicle freight efficiency improvements in excess of the program goals. Many SuperTruck technologies with customer-acceptable payback (e.g., aerodynamics, powertrain components, tractor lightweighting) are now used in commercial trucks, thereby reducing national energy consumption.

Federal data on truck utilization shows that a majority of Class 8 long-haul trucks operate at or below 65,000 lbs gross combined weight, much lower than the maximum combined vehicle weight of 80,000 lbs. This implies that most trucks are under-utilized and are overdesigned, i.e., heavier and with more powerful engines than needed to meet their actual operational requirements. Volvo's SuperTruck 2 will therefore demonstrate an all new complete vehicle concept designed with an integrated approach to maximize freight efficiency.

The project consists of three work packages organized in four sequential phases, as illustrated in Figure V.1.1. During Fiscal Year 2019, the focus shifted from concept selection to technology development and integration.

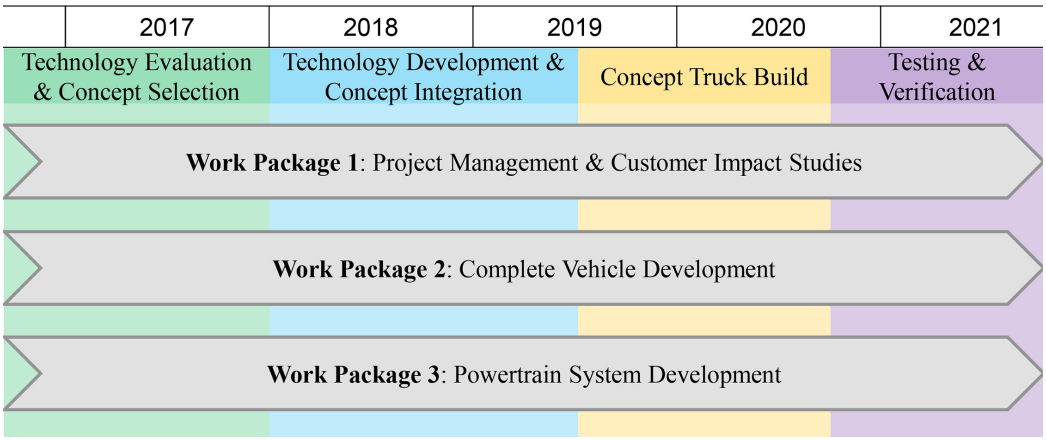

Figure V.1.1 Project schedule and phasing (Volvo)

Objectives

Overall Objective

- Demonstrate >100% improvement in vehicle ton-miles per gallon compared with a "best in class" 2009 truck, with a stretch goal of 120%
- Demonstrate 55% brake thermal efficiency (BTE) on an engine dynamometer
- Develop technologies that are commercially cost effective in terms of a simple payback.

Fiscal Year 2019 Objectives

- Finalize new cab interior concept design
- Complete component and sub-system studies
- Complete aerodynamic optimization of the complete vehicle.

Approach

Volvo's vision is to develop a super-efficient vehicle optimized for 65,000 lbs and designed for the long-haul drivers of the future. The truck has therefore been redesigned from the ground up to ensure that each component contributes to maximizing payload capacity and fuel economy of the complete vehicle.

The powertrain research in this project is guided by two goals: to demonstrate over 100% freight efficiency increase in a vehicle and to demonstrate 55% BTE of the engine in a test cell. These goals differ not only in the level of efficiency required by the powertrain solution but also in the size of the design space. Consequently, the team is taking a two-pronged approach and will deliver one powertrain shaped as part of a total vehicle optimization toward maximum freight efficiency and another focused on demonstrating 55% BTE. Though the dual-path approach may yield two different system-level approaches, significant synergies exist in the fundamental areas of internal combustion efficiency improvement.

Results

Volvo leverages its big data platforms for customer analytics as well as complete vehicle simulation tools. The team also works with fleet partners to analyze their operations in more detail. This work has yielded virtual duty cycles capturing the unique characteristics of each customer, which we will use to evaluate the impact of the technologies selected for SuperTruck 2 in each of these real-world fleet operating environments. These duty cycles will also aid in the optimization of our complete vehicle energy management system.

Powertrain System Development

The multiple ongoing 55% BTE engine concept studies are on track with many achievements to date. University of Michigan modified a Volvo six-cylinder 11L with a Delphi F3 injection system that is operating on Cylinder Number 6 only. During the budget period, this research engine was equipped with a variable valve control system with independent authority over each valve. The engine was used to evaluate multiple in-cylinder thermal barrier technologies. Based on earlier results, the team is now testing modifications of surface coatings to reduce surface roughness and optimize the impacts of the thermal barrier coated pistons.

The main objective of Oak Ridge National Laboratory's contribution to this project is to evaluate exhaust aftertreatment system architectures, component formulations, and control strategies that would enable the 55% BTE engine and SuperTruck 2 demonstrator engine to achieve applicable U.S. emission levels. The key challenge is that engines operating at high BTE will have low exhaust temperatures downstream of the final expansion, requiring aftertreatment components optimized for low-temperature operation or placement of aftertreatment components upstream of the final expander.

In Fiscal Year 2018, Oak Ridge National Laboratory developed a synthetic exhaust flow reactor capable of operating at elevated pressures typical of pre-expander exhaust aftertreatment system conditions. The

experiments performed during this budget period covered a wide range of exhaust compositions, flows, temperatures, and pressures, selected based on Volvo engine simulation results, to represent a range of engine loads. We found that for commercial selective catalytic reduction (SCR) catalysts, elevated pressures had no significant impact on NO_x conversion and increased NH_3 conversion.

To reduce the weight of exhaust aftertreatment components, the diesel particulate filter was coated on a thin wall substrate, and the length of the filter was reduced to lower the weight. The length of the SCR catalyst and ammonia slip catalyst was also reduced, but the cell density of the substrates was increased to compensate for any loss in performance as a result of the reduced length. Johnson Matthey produced samples of a modified diesel particulate filter, SCR catalyst, and ammonia slip catalyst, which were hydrothermally aged to simulate the performance of a full-life-aged catalyst. The diesel particulate filter catalysts and reduced-length SCR and SCR/ammonia slip catalyst substrates were canned and tested on an engine in order to validate the impacts of reduced weight, thermal mass, and backpressure, with encouraging results.

A detailed analysis and development of a new low-pressure drop cooling system were performed because low air-side pressure drop of the cooling package is a key enabler for a compact and lightweight cooling system design as well as to minimize cooling fan power consumption. More than five complete packages were analyzed in simulations, with over 20 iterations of each configuration. Cooling package design was completed before summer, and final drawings were sent to suppliers. Pipes and hoses have been designed, and routing for the circuits is finalized.

Aerodynamics

Aero simulation iterations progressed at a good pace during Fiscal Year 2019 as the virtual complete vehicle model was continuously evaluated and refined to ensure that it achieved aerodynamic improvement targets while still meeting manufacturing feasibility. Recent iterations focused on the front end of the vehicle in order to optimize the shape of the hood while maximizing heat rejection and incorporating styling characteristics. Our final demonstrator is still on track to meet or exceed the final target of 15% aero drag reduction versus Volvo's SuperTruck 1.

Advanced Lightweight Concepts

During Fiscal Year 2019, Metalsa completed the design of the lightweight frame, developed a method for flexible roll forming and joining technologies, and maximized component integration opportunities to achieve their target weight reduction of 35% lower than the standard steel frame assembly of an equivalent wheelbase. A complete lightweight frame assembly was delivered to Greensboro by the end of August.

The team also investigated additive manufacturing processes and design in order to minimize the weight of the front engine mount. Weight reductions of more than 25% are possible according to this design concept study.

Low Rolling Resistance Tires

During this reporting period, Michelin evaluated the tire improvements developed earlier in the project on a 22.5 inch tire size, which led to the finalization of the 19.5 inch tire technologies this summer. Michelin has now completed designs of the advanced SuperTruck 2 tires and produced prototypes to support the next phase of complete vehicle validation testing.

Hotel Mode

Bergstrom completed the design of the heating, ventilation, and air conditioning system. All final mounting and detail work is now complete, and build/assembly is expected to be complete by the end of the fiscal year. The team is currently focusing on air distribution tuning, system performance optimization, and minimizing power consumption.

An energy storage system was designed and fabricated for bench testing. It will be a key part of the vehicle's 48 V micro-hybrid system and will provide power to all truck loads, both when driving and when parked for longer rest periods.

Complete Vehicle Energy Management

Hardware and low-level controller designs have been reviewed to ensure the ability to support high-level energy management controller inputs and to enable the energy management features targeted for this demonstrator. Work is ongoing to develop a representative model to begin controller development and simulation efforts.

Bench testing of the energy storage system was completed on schedule in September and confirmed the performance of the system in terms of charge/discharge capabilities and thermal management.

Concept Trailer Development

The Wabash team completed its concept trailer development, which includes aerodynamic devices and lightweighting. The work focused on optimizing the geometry of commercially available aerodynamic devices through complete vehicle aerodynamic simulations and road testing in order to match the performance of Volvo's SuperTruck 1 idealized trailer configuration.

Demonstrator Vehicle Assembly

Major chassis components such as the front and rear suspensions as well as the axles were delivered to Greensboro during the summer. They were installed on the prototype chassis delivered by Metalsa in August, and we had a "rolling chassis" by the end of September. Next steps in the assembly process will include installation of the pneumatic and electrical components on the frame. By the end of the reporting period, the chassis will be ready for the first functional powertrain, followed by the cab, and finally hood and fairings.

Conclusions

Development and integration of the technologies selected in the previous project phase of Volvo's SuperTruck 2 project progressed on schedule during Fiscal Year 2019. The work has been divided between validation of prototype components on test benches and assembly of systems and sub-systems. The project is on track to deliver a complete prototype vehicle ready for initial road tests by mid 2020.

V.2 Cummins/Peterbilt SuperTruck II (Cummins Inc.)

Jonathan Dickson, Principal Investigator
Cummins Inc.
P.O. Box 3005
Columbus, IN 47201-3005
E-mail: jon.a.dickson@cummins.com

Ken Howden, DOE Technology Development Manager
U.S. Department of Energy
E-mail: Ken.Howden@ee.doe.gov

Start Date: October 1, 2016 End Date: September 30, 2021
Project Funding (FY19): $13,600,000 DOE share: $4,500,000 Non-DOE share: $9,100,000

Project Introduction

The trucking industry is faced with numerous challenges to reduce petroleum consumption while meeting stringent criteria emissions regulations and providing customer value. The United States has approximately 3.5 million Class 8 vehicles on the road, consuming 4.5 million barrels of petroleum per day. If only half of the fleet implemented half of the benefits proposed, at $3.85/gal, the nation would see a fuel savings over $30 billion annually and reduce petroleum consumption by over 0.5 million barrels per day. This reduction would have a positive impact on the environment by eliminating 200,000 metric tons of CO_2 emissions per day.

The goals of the Cummins-led SuperTruck II project are to design, develop, and demonstrate a very high efficiency engine that is optimized around the drive cycle, yielding a substantial increase in vehicle freight efficiency compared to the baseline 2009 vehicle. The demonstration will be conducted with vehicle specifications similar to those of the baseline vehicle. The engine will maintain compliance with the current heavy-duty diesel emission regulation for line haul vehicles, while the vehicle system will remain compliant with the current greenhouse gas regulatory requirements.

Objectives

- Demonstrate a minimum of 55% brake thermal efficiency (BTE) using 65 mph cruise conditions on an engine dynamometer test
- Utilize the same engine system demonstrated on dynamometer in vehicle and operating on real world drive cycles
- Achieve a minimum of 125% freight ton efficiency (FTE) over a relevant drive cycle (FTE = MPG * Tons of Freight)
- Track, promote, and report on cost-effective solutions, prioritizing solutions that have a payback period of approximately three years and utilizing a relevant customer counsel for understanding customer acceptance and expectations.

Approach

The approach for meeting the 55% BTE target involves careful dissection of the diesel cycle and reduction of losses via waste heat recovery (WHR). The engine will be tuned to take advantage of ideal conditions for the aftertreatment effectiveness, therefore reducing the inefficiency of the exhaust gas recirculation (EGR) and injection timing systems. The closed cycle efficiency will be optimized for high expansion ratio via rapid heat release and insulated surfaces. The open cycle will be optimized by using low pressure EGR, ideal valve

events, and a fixed geometry turbocharger with the ultimate in tip clearance and efficiency. The mechanical efficiency of the engine system will be developed to use low viscosity oil with variable lube and cooling pumps, all while running the engine at a low enough speed to minimize spin and pumping losses. The WHR system will be a two-loop system harvesting both low quality heat from the coolant and charge cooler and high quality heat from the EGR coolers and tailpipe boiler. The WHR system will be the primary cooling system for the engine under the cruise operating conditions; a small radiator will provide additional cooling for sustained high load conditions.

The powertrain will integrate the WHR system and an energy recovery system (motor/generator [M/G]) onto the Eaton automated transmission for compactness and efficiency reasons. During flat-road and uphill operations, this system can input power to the system to reduce fuel consumption. As the vehicle operates downhill, the engine can be decoupled from the powertrain, leaving the controls to apply power from the WHR system as needed and/or to recover energy from the system through the M/G, to be stored in an onboard battery.

The vehicle will achieve the high FTE with the combination of low motive resistance and lightweighting. Bridgestone will supply tires that can meet customer requirements for longevity yet reduce rolling resistance well beyond the current commercially available tires via compound development and siping design. The vehicle structure will include a new weight-saving composite design that will incorporate a kneeling suspension that will aid in the reduction of aerodynamic load. The vehicle design will incorporate aerodynamic features to improve drag in all wind conditions via moving surfaces that react to changing winds detected by the onboard Lidar system. Finally, the drive axle will incorporate an advanced control system that will ensure good low speed traction with state-of-the-art low parasitic, high speed operation.

Results

The following list shows the key accomplishments for Fiscal Year 2019. The accomplishments listed below are fundamental steps required to complete the objectives of the project.

The team has:

- Demonstrated 50.3% BTE (engine only) of the new platform
- Upfit the transmission integral 48 V, P2.5 mild hybrid system into the powertrain mule development truck, including the electrification thermal management, electric power steering, and electric heating, ventilation, and air conditioning systems
- Developed and calibrated software to control the 6x4 Disconnect axle system
- Finalized and procured the powertrain mule WHR cooling system with integral WHR/air conditioning condensers, topping radiator, active fan louvers, and electric fans
- Fit engine WHR system components (dual loop EGR and mixed charge cooler) onto the 55% BTE development engine and begun test cell development of the system
- Completed initial build and begun rig testing of the transmission integral WHR expander system, including the turbine, gearbox, lube system, and feed pump
- Identified a pathway to 55% BTE, considering the losses of the 50% BTE (engine only) system
- Performed the first round of friction assessment of the 55% BTE engine system in the Mechanical Efficiency Lab
- Completed initial calibration of the adjustable ride height system used on the powertrain mule vehicle

- Finalized the demonstrator vehicle outer body (body-in-white, outer fairings, hood) and begun procurement
- Confirmed the exceedance of the aerodynamic drag target via computational fluid dynamics for the demonstrator vehicle
- Confirmed via rig testing that the demonstrator vehicle's tire Crr (rolling resistance coefficient) reduction will exceed the target
- Confirmed the weight target analytically for the demonstrator vehicle.

The 50% BTE (engine only) system made use of the following technologies to achieve success:

- A high heat release rate combustion system with increased compression ratio
- Reduced friction via improvements to the power cylinder, variable flow oil pump, and piston cooling nozzles
- Air handling improvements, including a low heat transfer exhaust system and a high efficiency turbocharger.

The 48 V mild hybrid system tested in 2018 at Oak Ridge National Laboratory's Vehicle Systems Integration Lab was successfully installed into the powertrain mule vehicle. This integration included the electrification thermal management system to manage battery and M/G temperatures during operation. Additionally, key accessories have been electrified in preparation for engine-off-coasting to enable higher energy recapture and up to 4% fuel economy benefit for the system.

The 6x4 Disconnect axle system was successfully demonstrated. This system is expected to yield 2.4% efficiency gain while maintaining traction capabilities required in the marketplace.

Significant progress has been made on the WHR system in Fiscal Year (FY) 2019. Successful integration of this system into the vehicle and onto the engine and transmission will be key to the team's plans to bring the 55% BTE engine system out of the test cell and into the vehicle. Figure V.2.1 shows the transmission integration of the Cummins Energy Recovery Drive and WHR expander system.

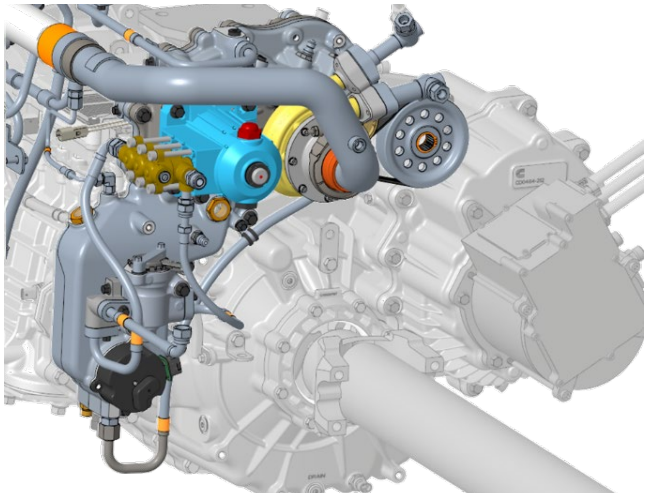

Figure V.2.1 Transmission integral WHR turbine expander system. This system has begun rig testing and will be developed further in the test cell in the fourth quarter of 2019, with integration into the mule vehicle in the first quarter of 2020.

Once WHR is fully integral in the powertrain mule vehicle, primary cooling of the engine system will be done via the WHR condenser; see Figure V.2.2. A topping radiator (mounted below the WHR condenser) provides peak cooling during extended operation at high loads. Louvers are utilized to maximize fan-off performance of the system. While the demonstrator vehicle system will be adjusted for the aerodynamic characteristics of that vehicle, the module will be similar to that of the mule vehicle.

Figure V.2.2 Powertrain mule WHR cooling module with integral electric fans and louvers

The 55% BTE pathway has been set based upon the remaining opportunities of the 50% BTE (engine only) system. The primary focus is on low heat transfer technology, including in cylinder, through the head, and in the exhaust system; improved turbocharger efficiency and matching; and further friction reduction via a superfinished crankshaft with match fit bearings and low viscosity oil.

The demonstrator vehicle outer body and interior designs have progressed well. Early in FY 2019, the aerodynamic design of the cab shape was finalized. The body-in-white was finalized in the second quarter of 2019, enabling the kick-off of its production. The remaining outer body shapes of the hood, bumper, fairings, and extenders have also been finalized. The full aerodynamic package, including the adjustable ride height system and active yaw control surfaces, has yielded drag reductions greater than the 56% target from the 2009 baseline system.

Bridgestone has completed the build of the demonstration vehicle tires. Testing of the drive and steer tires has been completed, with results exceeding the target of 30% reduction in rolling resistance. Testing on the trailer tires will be completed in the fourth quarter of 2019.

Given the improvements in aerodynamic and tire loss, along with the contributions of engine efficiency and the hybrid system, the freight efficiency objective of greater than 125% is on plan. The vehicle weight is being tracked and is on plan to yield >3,800 lbs reduction.

Additionally, the Advanced Cycle Efficiency Manager (ACEM) features have been selected and are expected to yield >5% fuel savings; see Figure V.2.3. Those features include:

- Predictive cruise control, utilizing speed limits, traffic, weather, grade, and yaw wind direction

- Look-ahead control of the transmission gear shifting
- Engine-off coasting for reduced engine cycle work and improved engine BTE
- Predictive mild hybrid regeneration and torque assist.

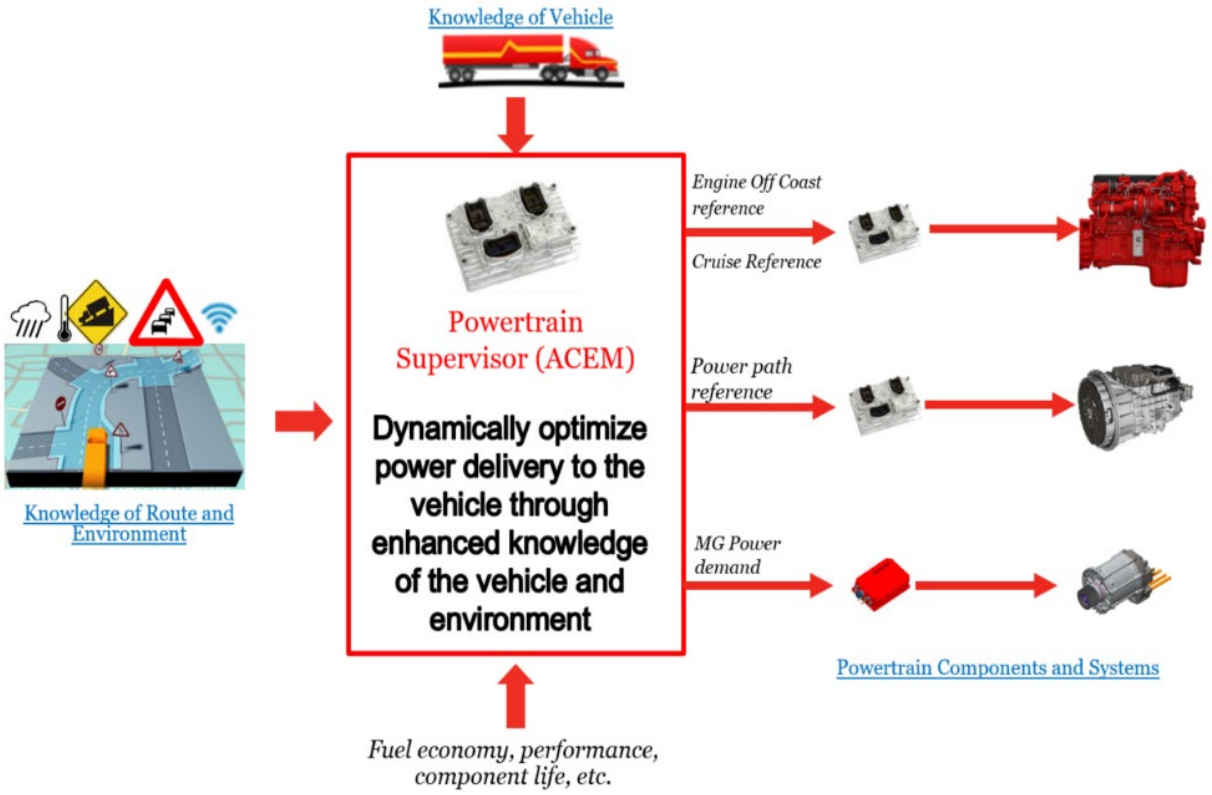

Figure V.2.3 ACEM feature selection was finalized in FY 2019

Conclusions

The Cummins-led SuperTruck II team has completed the third year of the planned five-year project. In the first three years, the team has concluded many goals and set direction for the remainder of the project. The conclusions are summarized as follows:

- Development activities for the powertrain mule vehicle have prepared the hybrid system for integration into the demonstrator vehicle. Preparation of the dual loop EGR and WHR systems is planned for 2020.
- Successful vehicle and powertrain integration of the WHR system is on plan to enable bringing the 55% BTE engine system to the final demonstration vehicle.
- The path-to-target for the 55% BTE engine has been identified and is being executed. Testing of the initial phase of this development activity is underway. Work continues on additional technologies to be added in the remainder of 2019 and early 2020 as they are available in support of the June demonstration.
- The aerodynamics package is on target to over-deliver against the targets.

- The tire build has been completed, with validation of target complete on the steer and drive tires.
- Due to the successes of engine, axle, and transmission efficiency gains, reductions in tire and aerodynamic loss, and reduced mass of the vehicle system, the freight efficiency improvement target of >125% is on plan.

Key Publications

1. DOE quarterly progress report, Q9 – January 30, 2019.
2. Mohr, D., T. Shipp, and X. Lu. 2019. "The Thermodynamic Design, Analysis and Test of Cummins' Supertruck II 50% Brake Thermal Efficiency Engine System." SAE Technical Paper 2019-01-0247.
3. DOE quarterly progress report, Q10 – April 30, 2019.
4. 2019 Annual Merit Review – June 13, 2019.
5. DOE quarterly progress report, Q11 – July 30, 2019.
6. DOE quarterly progress report, Q12 – October 30, 2019.

Acknowledgements

Ken Damon (Peterbilt), Nicole Downing (Eaton), Reubin Close (Bridgestone), Ralph Nine (National Energy Technology Laboratory Program Manager)

V.3 Development and Demonstration of a Fuel-Efficient Class 8 Tractor and Trailer SuperTruck (Navistar, Inc.)

Russell Zukouski, Principal Investigator
Navistar, Inc.
2701 Navistar Drive
Lisle, IL 60531
E-mail: russ.zukouski@navistar.com

Ken Howden, DOE Technology Development Manager
U.S. Department of Energy
E-mail: Ken.Howden@ee.doe.gov

Start Date: October 1, 2016 End Date: November 1, 2021
Project Funding (FY19): $11,600,000 DOE share: $3,900,000 Non-DOE share: $7,700,000

Project Introduction

The objective of the SuperTruck 2 engine project is to research, develop, and demonstrate a heavy-duty engine that can meet 2010 federal emission standards and can achieve 55% brake thermal efficiency (BTE) demonstrated in an operational engine at a 65-mph cruise point on a dynamometer. In addition, the technologies applied to this engine should be commercially cost-effective.

Objectives

Overall Objectives

- Attain greater than or equal to 55% BTE demonstrated in an operational engine at a 65-mph cruise point on a dynamometer
- Develop engine technologies that are commercially cost-effective
- Contribute to greater than 100% improvement in vehicle freight efficiency relative to a 2009 baseline.

Fiscal Year 2019 Objectives

- Evaluate cylinder deactivation (CDA) technology for fuel economy
- Improve air system efficiency for SuperTruck 2 engine
- Investigate novel fuel-system configuration to increase combustion burn rates
- Identify organic Rankine cycle waste heat recovery system that contributes to achieving 55% BTE
- Continue gasoline compression ignition investigation at Argonne National Laboratory.

Approach

The work will include component and system-level consideration of base engine architecture, air system, combustion and fuel system, advanced aftertreatment, thermal management, and waste heat recovery. It will involve analysis, development, testing, and down-selection of individual and system-level engine technologies, as well as integration of the final selected technologies into a prototype engine.

Results

Cylinder Deactivation

In previous work, a cylinder deactivation system was installed on an engine for testing. During the deactivation of a cylinder, the opening of its intake and exhaust valves was disabled, and the fuel injection was turned off. The brake mean effective pressure for the remaining active cylinders increased to maintain the power for a specified condition, resulting in an increase in exhaust temperature. In addition to the increase in exhaust temperatures, test results showed significant improvement of brake specific fuel consumption (BSFC) at very light load.

Initial engine calibration and control implementation for cylinder deactivation were completed. This cylinder deactivation system was then installed on a vehicle for fuel economy testing. Due to uncertainty of traffic and weather conditions, the vehicle testing was carried out in a chassis dyno at Navistar. Prior to the chassis dyno, the vehicle was sent to Navistar Proving Ground at New Carlisle, Indiana, to collect the coast-down coefficients for chassis dyno testing setup.

An urban drive cycle was selected for fuel economy testing at the chassis dyno (Figure V.3.1). Two vehicle weights, 42,000 lbs (42k) and 72,000 lbs (72k), were tested. A baseline-CDA-baseline test sequence with four runs each was completed. The results show a significant 6.7% fuel saving for the 42k vehicle weight with the CDA; however, there is no measurable fuel saving for the vehicle weight of 72k. Analysis showed that, due to the higher torque demand with 72k, it has much less CDA engagement occurrence than in the 42k case.

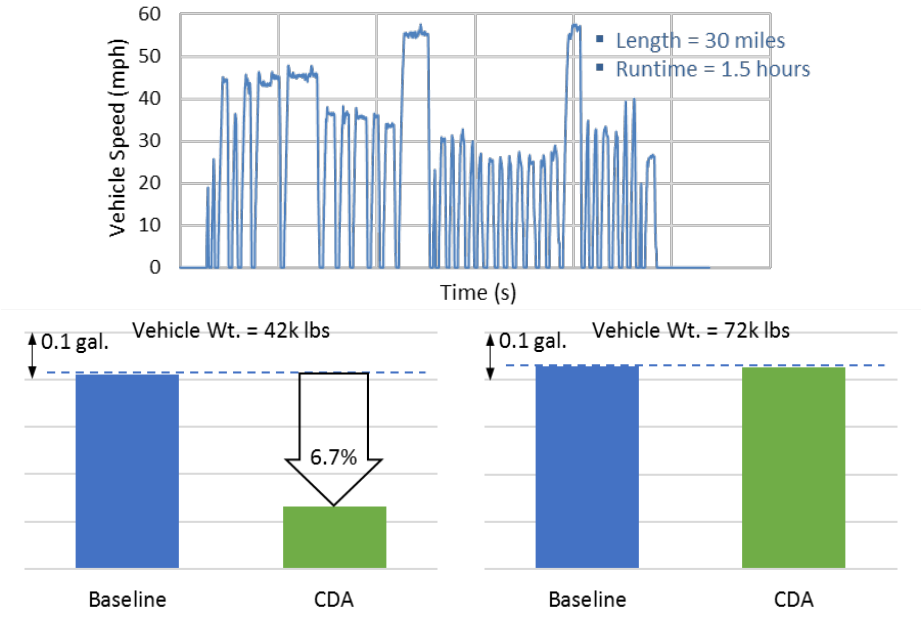

Figure V.3.1 Comparison of average fuel consumption over an urban drive cycle

Air System

Turbocharger performance has a direct impact on the air/fuel ratio (AFR), which affects BTE greatly. The performance of a turbocharger is usually described by its compressor and turbine maps, which are obtained from a gas stand. Although it is accepted practice for such maps to represent turbocharger performance and efficiency, the maps can underpredict performance versus testing with on-engine conditions with strong exhaust pulsation, such as low speeds and high loads. This is especially true for the turbine performance. In

addition to the engine speed and load, the geometry/volume of the exhaust system could affect the exhaust pulsation. Therefore, an engine test was conducted to investigate the effect of exhaust system volume on exhaust pulsation.

The exhaust system volume includes both the exhaust manifold and the exhaust gas recirculation (EGR) system. Due to the long lead time of a prototype exhaust manifold, this test focused on changing the EGR system volume. Three EGR block-off locations were selected to effectively change the system volume before the turbo. Blocking off EGR ports on the exhaust manifold creates a minimum system volume before the turbo. The maximum system volume is achieved by blocking off the EGR on the cold side of the EGR cooler. Blocking the system at the pre-EGR cooler, where the EGR valve is typically installed on this engine family, represents an intermediate exhaust system volume.

The engine testing was carried out at A75. Due to the divided exhaust manifold (front and rear banks), two pressure transducers were installed at each turbine volute inlet to monitor and record the crank-angle-resolved exhaust pulsation of both banks. The measurement shows an increase of exhaust pulse amplitude with the decrease of EGR system volume (Figure V.3.2). The average expansion ratio of the turbine increases. Engine test data show an increase of turbine efficiency with the decrease of EGR system volume. The AFR correlates with the increase of turbine efficiency, as does engine BTE. These test data were provided to the turbocharger supplier for the next iteration of design.

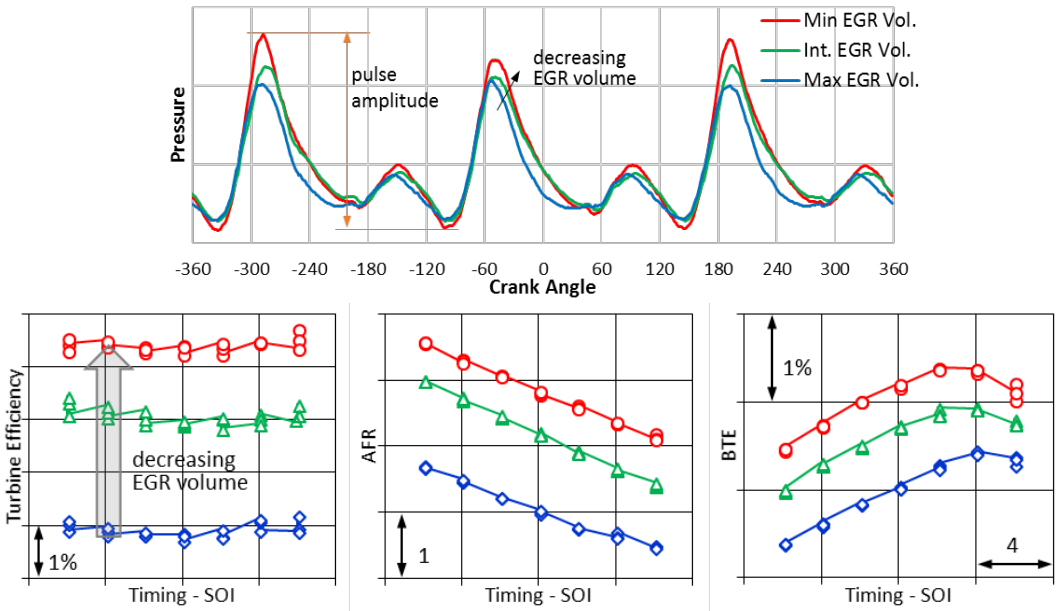

SOI – start of injection

Figure V.3.2 Effects of EGR volumes on turbocharger and engine performance

Combustion System

The focus of combustion optimization was on nozzle configurations such as nozzle flow rates and number of holes. In addition to the nozzle configuration, the hydraulic characteristics of an injector affect the rate of injection. Figure V.3.3 shows the rate of injection profiles of two injectors with difference hydraulic characteristics, Hyd_1 and Hyd_2. With the same nozzle configuration, the Hyd_2 injector has a faster rise rate of injection than the Hyd_1 injector. Consequently, the Hyd_1 injector requires a longer energizing time to deliver the same quantity of fuel than does the Hyd_2 injector. Engine testing of these two injectors was carried out at 1,000 rpm, 75% load conditions. Figure V.3.3 shows the preliminary results of a variable geometry turbocharger sweep at a constant start of injection. The Hyd_2 injector yields better BSFC than the

Hyd_1 injector. It is interesting to note that the Hyd_1 injector resulted in higher AFR yet worse BSFC. Analysis indicates that this phenomenon is due to the longer injection duration of the Hyd_1 injector. The longer injection duration resulted in an extended combustion duration, which generated more heat rather than useful work. As a result, a higher exhaust manifold temperature was observed with the Hyd_1 injector.

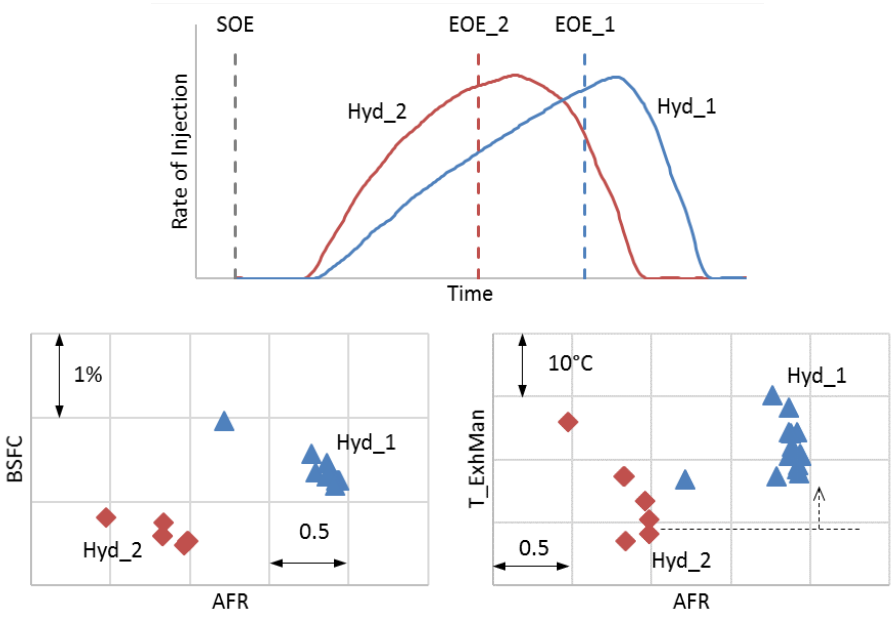

SOE – start of energizing; EOE – end of energizing

Figure V.3.3 Effects of two injector hydraulic characteristics on engine performance

Waste Heat Recovery – Organic Rankine Cycle (ORC)

To achieve 55% BTE, waste heat recovery plays a critical role. Navistar has selected ORC technologies as the prime path for waste heat recovery. To maximize ORC system efficiency, energy recovery from all available waste heat was considered. Based on the temperature characteristics of the heat sources, the ORC system was separated into high-temperature (HT) and low-temperature (LT) loops. After analyzing various possible configurations, an intent ORC system was selected for the dyno demonstration. Based on the assumptions of boundary conditions and component efficiency, the initial simulation showed a 2.9% BTE gain of the system. A detailed analysis indicated that the system could deliver more than 3.1% BTE gain by changing the charge air cooler (CAC) heat exchanger design to achieve two-phase flow at its outlet (Figure V.3.4).

The identified configuration is being supplied by Borg Warner, with controls supplied by AVL, both aided by Clemson University. Testing and calibration for the system will be carried out at Clemson University. All subsystem components have been received, and the integration of both HT and LT loops in the dyno was completed. The commission of the system is underway.

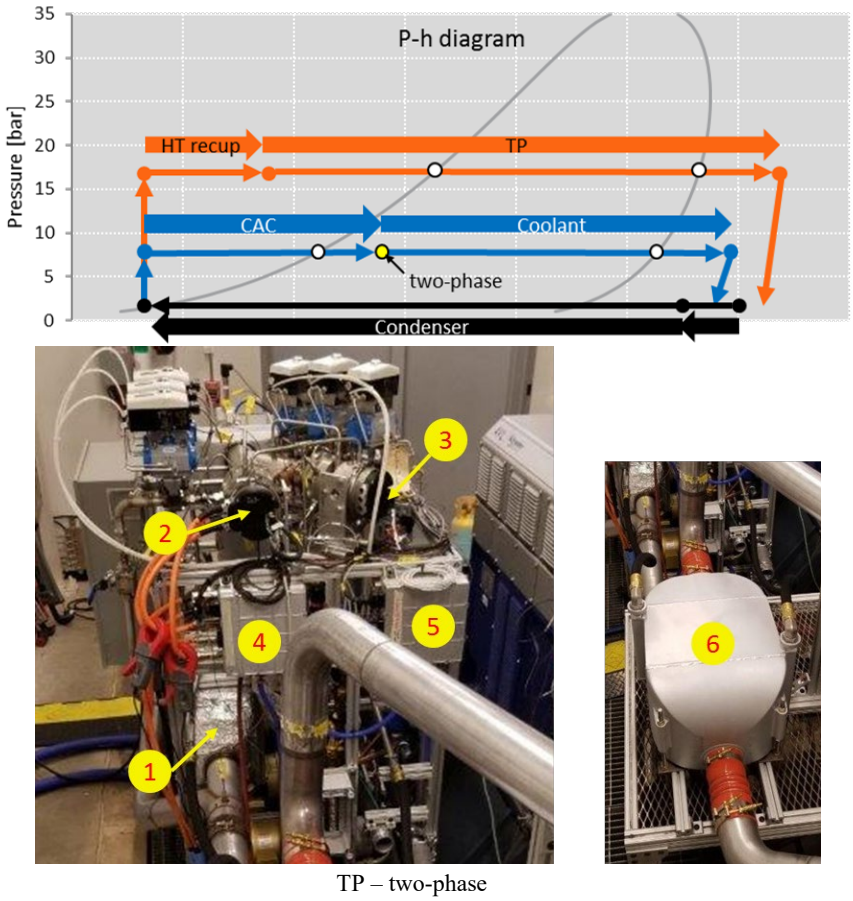

Figure V.3.4 (top) Pressure enthalpy (P-h) diagram for the intent ORC system; (bottom) integrated ORC system in dyno at Clemson University: (1) exhaust boiler, (2) HT expander, (3) LT expander, (4) HT power electronics, (5) LT power electronics, (6) CAC boiler

Gasoline Compression Ignition at Argonne National Laboratory

Gasoline compression ignition is a combination of two advanced combustion strategies: partial fuel stratification and partially premixed combustion. A key factor in gasoline compression ignition is to increase the premixed combustion portion. Two fuel-injection strategies can be used to increase the portion of premixed combustion: early/late pilot injection and port fuel injection (PFI)/direct injection (DI) strategy. The gasoline fuels selected for investigation were U.S. Environmental Protection Agency Tier II certification gasoline (EEE) and E85 gasoline, which was blended in-house with 85 vol% dry ethanol and 15 vol% EEE. A lubricity improver was blended into the gasoline fuels to protect the high-pressure diesel-injection system.

Various tests were carried out. Five sets of test data were selected for detailed analysis: diesel baseline, EEE with late pilot injection, EEE with PFI/DI, E85 with PFI/DI, and diesel/E85 dual fuel. The analysis was based on thermodynamics principles to understand the energy distribution within the engine and allow for further efficiency improvements. An adiabatic constant-volume combustion at top dead center, with the real unburned- and burned-gas properties from test data, was used to calculate ideal efficiency. The combustion-phasing loss, combustion-duration loss, unburned-fuel loss, and heat-transfer loss were determined accordingly.

Figure V.3.5 shows that the ideal efficiency was about 60.5% for all fuels except E85. E85 operation exhibited a smaller specific heat ratio during the compression and combustion attributed to its largest PFI mass fraction. Thus, a lower peak pressure after the constant-volume combustion at top dead center resulted in a low ideal efficiency. Since the crank angle at 50% mass fraction burned (CA50) was maintained close to top dead center,

the combustion-phasing loss was very low, less than 0.6%. However, the obvious diffusion combustion in tests extended the combustion duration, leading to a combustion-duration loss of up to 3.9%. Among the tests, E85 exhibited the largest premixed combustion and, therefore, showed the lowest combustion-duration loss. Different from traditional low-temperature combustion concepts, the unburned-fuel loss was low, less than 0.2%, especially for the late pilot strategy. The PFI/DI strategy exhibited the lowest heat-transfer loss, which can be attributed to the reduction in local richness and combustion temperatures due to the significant portion of port-injected fuel compared to diesel and EEE with late pilot injection.

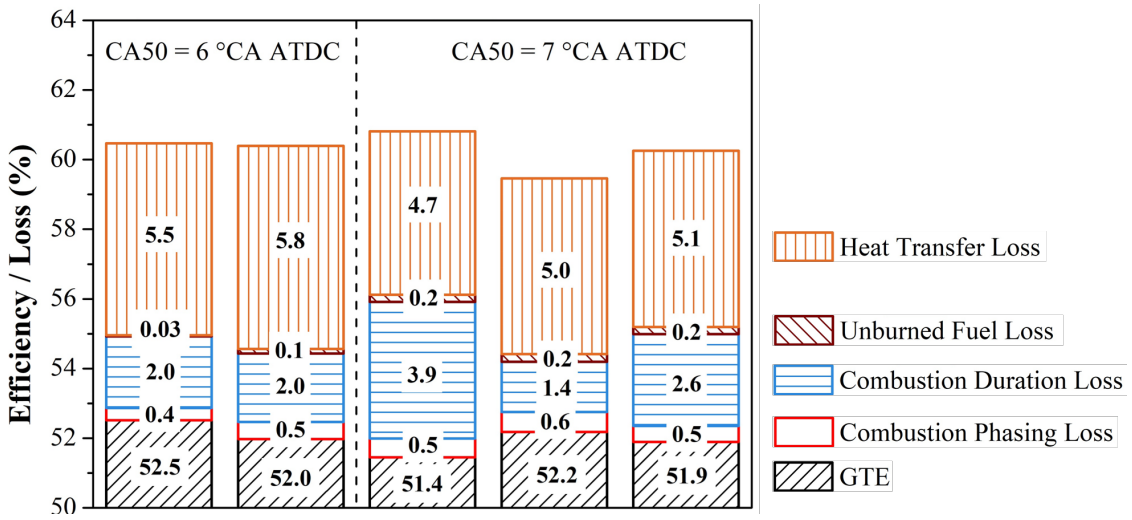

°CA – crank angle degrees; ATDC – after top dead center; GTE – gas turbine efficiency

Figure V.3.5 The ideal efficiency and losses for the operation with diesel baseline, EEE late pilot injection (EEE-LP), EEE PFI/DI (EEE-PD), E85 PFI/DI, and diesel/E85 dual fuel

Conclusions

- A cylinder deactivation system was installed on a vehicle for fuel economy testing in a chassis dyno at Navistar over an urban drive cycle. Two vehicle weights were tested. A fuel saving of 6.7% was measured for the lighter vehicle weight, but no benefit was observed for the heavier vehicle weight with the installed CDA system as calibrated.

- Improvement/optimization work for both air system and combustion system were continued throughout this fiscal year. Testing showed a BTE improvement with the decrease of exhaust system volume. In addition, a modification in injector hydraulic characteristics leads to a shorter injection duration, which results in an improvement in BSFC at 1,000 rpm, 75% load conditions.

- A detailed analysis of the intent ORC system indicated more than 3% BTE gain. The integration of all subsystem components in the dyno was completed. The commission of the system is in progress.

- Gasoline compression ignition investigation continued at Argonne National Laboratory. Five sets of test data were selected for detailed analysis based on thermodynamics principles. Among these tests, E85 showed the lowest combustion-duration loss.

Key Publications

1. Pamminger, Michael, Buyu Wang, Carrie M. Hall, Ryan Vojtech, and Thomas Wallner. 2019. “The Impact of Water Injection and Exhaust Gas Recirculation on Combustion and Emissions in a Heavy-Duty Compression Ignition Engine Operated on Diesel and Gasoline.” *International Journal of Engine Research* (January 8). https://doi.org/10.1177/1468087418815290.

2. Wang, B., M. Pamminger, and T. Wallner. 2019. “Optimizing Thermal Efficiency of a Multi-Cylinder Heavy Duty Engine with E85 Gasoline Compression Ignition.” SAE 2019 World Congress and Exhibition, SAE Technical Paper 2019-01-0557. https://doi.org/10.4271/2019-01-0557.

3. Pamminger, Michael, Carrie Hall, Buyu Wang, Thomas Wallner, and Raj Kumar. 2019. “A Framework for Heat Release Predictions in Compression Ignition Engines with Multiple Injection Events.” 2019 IEEE Conference on Control Technology and Applications (CCTA).

4. Wang, B., M. Pamminger, and T. Wallner. 2019. “Impact of Fuel and Engine Operating Conditions on Efficiency of a Heavy Duty Truck Engine Running Compression Ignition Mode Using Energy and Exergy Analysis.” *Applied Energy* 254 (November). https://doi.org/10.1016/j.apenergy.2019.113645.

5. Pamminger, Michael, Carrie Hall, Buyu Wang, Thomas Wallner, and M. Rajkumar. 2019. “Zero-Dimensional Heat Release Modeling Framework for Gasoline Compression-Ignition Engines with Multiple Injection Events.” ICE 2019 - 14th International Conference on Engines and Vehicles, SAE Technical Paper 2019-24-0083.

6. Kumar, Raj, Yan Wang, Ryan Vojtech, and James Cigler. 2019. “Effect of Fuel Injection Parameters on Performance and Emissions for High Efficiency Engines.” Technical Paper Publication, ICEF2019-7221.

V.4 Improving Transportation Efficiency through Integrated Vehicle, Engine and Powertrain Research – SuperTruck 2 (Daimler Trucks North America)

Darek Villeneuve, Principal Investigator
Daimler Trucks North America
4555 N Channel Ave
Portland, OR 97217
E-mail: Darek.Villeneuve@daimler.com

Ken Howden, DOE Technology Development Manager
U.S. Department of Energy
E-mail: Ken.Howden@ee.doe.gov

Start Date: January 1, 2017 End Date: January 1, 2022
Project Funding: $40,000,000 DOE share: $20,000,000 Non-DOE share: $20,000,000

Project Introduction

The objective of the SuperTruck 2 (ST2) project is to develop and demonstrate a greater than 100% improvement in overall freight efficiency on a heavy-duty Class 8 tractor-trailer measured in ton-miles per gallon. In addition, an engine capable of achieving 55% brake thermal efficiency (BTE) will be designed and demonstrated. Daimler Trucks North America will achieve these targets through the application of several advanced vehicle system technologies and advanced engine technologies.

The ST2 project is broken into five phases (Figure V.4.1), of which we are coming toward the end of Phase 3. There have been three parallel activities in Phase 3. The first activity has been the final design and

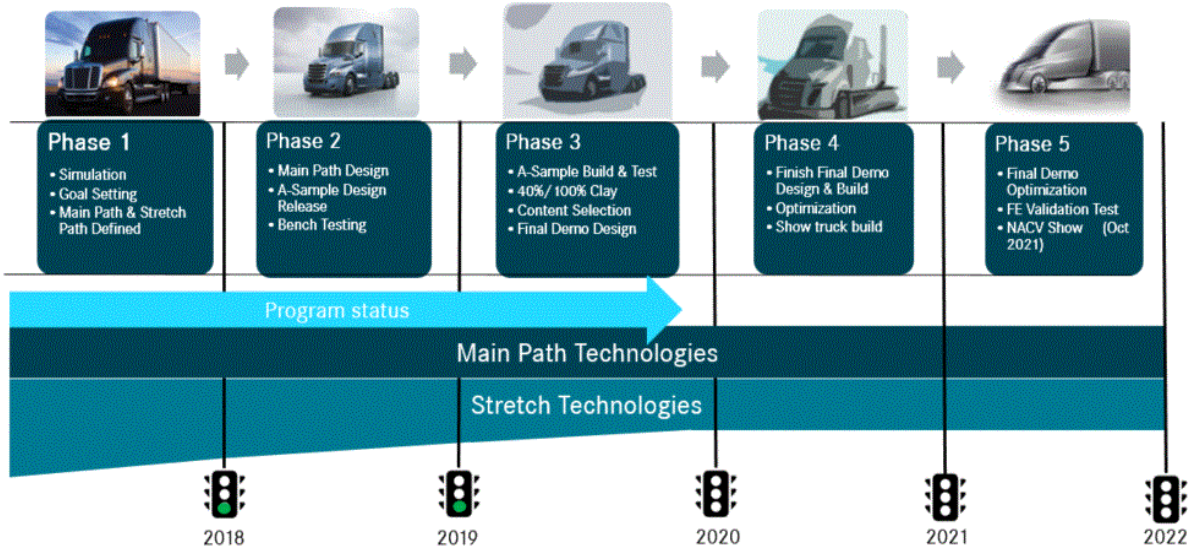

NACV – North American Commercial Vehicle

Figure V.4.1 Phases of the SuperTruck 2 project

physical build of the integration vehicle called A-sample. The second activity has been the production of a SuperTruck 2 theme that improved aerodynamics while being developed in the design studio. The last activity has been moving from learnings during the A-sample development and build to creating the final demonstrator design and content.

Objectives

Overall Objective

There are two main objectives for the ST2 project:

- Meet or exceed the vehicle freight efficiency target for the ST2 project, specified as a 100% freight efficiency improvement over a baseline vehicle (same vehicle as used in SuperTruck 1, a 2009 Cascadia). Daimler Trucks North America has specified that they will exceed the target with a vehicle that demonstrates 115% freight efficiency.
- Demonstrate an engine that meets or exceeds a 55% BTE rating in a test cell.

Fiscal Year 2019 Objectives

- Build and then test the A-sample integration vehicle on the road
- Progress from a 40% clay model into a single theme full-scale model in the design studio
- Build and place in test cell an engine with a two-stage turbocharger and intercooled air system
- Procure parts for waste heat recovery and set up parts into test cell
- Select concept for major systems such as split cooling and the boost recoup motor location.

Approach

In Phase 3 of the ST2 project, individual system simulations were used to define fuel consumption reduction benefits of each potential item and will then be used in a freight efficiency calculator.

- Oak Ridge National Laboratory and university partners aided in engine componentry development.
- National Renewable Energy Laboratory aided in an optimized air-conditioning system.
- Computational fluid dynamics simulations optimized the low temperature cooling system and aerodynamics performance of an evolving studio surface.
- Vehicle computer-aided design model balanced space claims for the individual components.

Validating the individual component impact to vehicle or engine performance will be the focus of the remainder of the SuperTruck project. Freight efficiency calculator development is in process for the next fiscal year based upon vehicle mass saving content and performance improvements of individual items.

Results

Vehicle Development

Further refinement of the initial ST2 workstream targets for freight efficiency are in process. The teams have focused on determining how to meet those project goals with the current expected vehicle mass savings. Ideation, simulation, and design development have led to the following simulated performance results.

- Base vehicle improvement: measured 61% freight efficiency
- Engine (in vehicle): simulated 9% freight efficiency

- Tractor aerodynamics: simulated 11% freight efficiency
- Split cooling: simulated 3% freight efficiency
- Powertrain: simulated 7% freight efficiency
- Tractor tires: simulated 5% freight efficiency
- Energy management: simulated 3% freight efficiency
- Vehicle controls: simulated 1% freight efficiency
- Trailer aero and tires: calculated 15% freight efficiency.

Figure V.4.2 shows a summary of the simulation results. In Phase 4 of the project, the team will be validating the simulation results by updating physical measurements and feeding the knowledge gained back into the design for the final demonstrator. Some designs will be tested independently on a tinker truck, while the aero components will be tested on a closed track. The closed track is necessary when measuring very small improvements in aerodynamic performance.

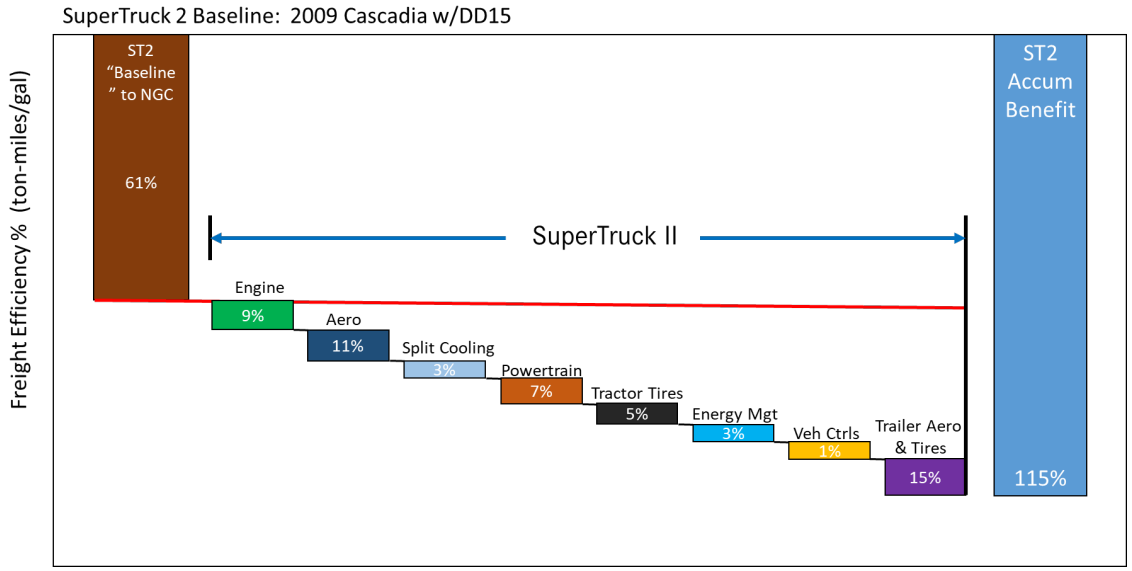

DD15 – baseline 15 liter engine; NGC – 2017 production new Cascadia tractor

Figure V.4.2 Daimler Trucks North America updated pathway to reach 115% freight efficiency target

Significant progress was made on integrating all available technologies into our running vehicle called A-sample. The cooling system was split into a low temperature circuit with the air conditioning condenser moved from the main stack. Studio surfaces and the condenser design were all updated. A-sample design and build now reflects this change, and control software integration into the 48 V system was completed. The A-sample vehicle made its initial trip in late June and has since accumulated over 6,000 miles.

Some content, such as a new battery pack and position of the boost recoup motor, is being developed on another vehicle. This enables A-sample to resolve control integration issues with the existing hardware installed. In addition, this allows mileage accumulation to break in many of the new hardware components before the fuel efficiency evaluation, which is scheduled before the end of this year.

Engine Development

Year 3 of the project saw the experimental implementation of a number of fuel economy measures listed in the 55% BTE engine roadmap. The roadmap, which was developed and refined during Years 1 and 2 of the project, is shown below in Figure V.4.3. It is the result of extensive one-dimensional and three-dimensional analytical work conducted in-house and by teams at Oak Ridge National Laboratory as well as Clemson University.

The design and analysis work led to procurement of critical engine components in this reporting period. As a result, the ST2 engine in its near final configuration was built and put on test in the third quarter in the Detroit test cell. It features a two-stage turbocharger, intercooled air system that enables further engine down-speeding and high brake mean effective pressure compared to today's production engines. It also includes a split cooling system that enables lower exhaust gas recirculation and intake charge temperatures. The aftertreatment system, with close-coupled selective catalytic reduction, was evaluated under transient conditions. A low pressure exhaust gas recirculation system was also tested. A majority of the waste heat recovery components were procured, leading to an estimated start of test in the first quarter (Q1) of 2020. The team at the University of Michigan demonstrated measureable improvement in thermal management resulting from receding-horizon predictive control of the engine and aftertreatment system. Several low-friction prototype components (plasma-sprayed liners, diamond-like carbon coated piston pins, and low-friction piston rings) were also procured and are being put on test.

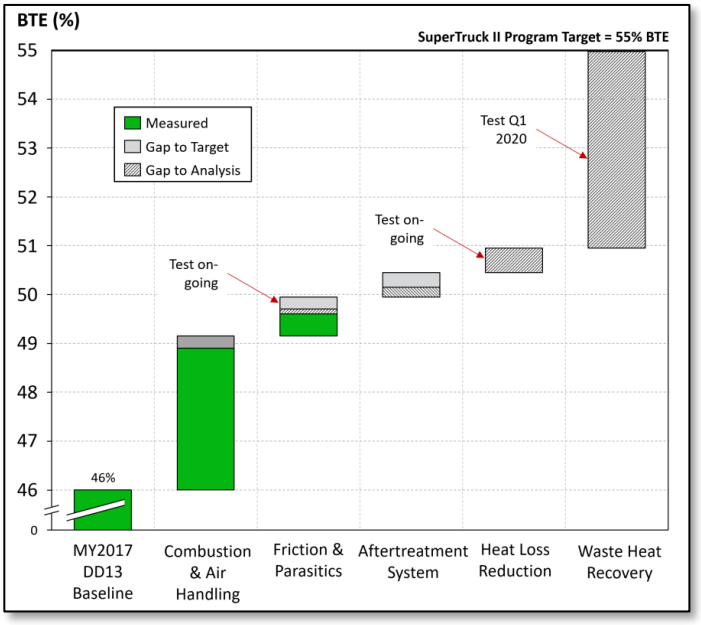

MY2017 – Model Year 2017; DD13 – baseline 13 liter engine

Figure V.4.3 Detroit SuperTruck 2 engine roadmap

Conclusions

The ST2 project is on a successful path towards meeting the fuel efficiency target of 115% freight efficiency improvement over a 2009 Cascadia, and the engine team is on schedule to meet their goal of a 55% BTE demonstrator engine.

- Content scope meets performance objectives.
- Further freight efficiency improvement is possible through additional mass reduction or aerodynamic enhancements.

- The project plan provides sufficient time for execution of the remaining work.
- Collaboration with key partners is in place:
    - Oak Ridge National Laboratory
    - National Renewable Energy Laboratory
    - University of Michigan
    - Michelin Tire Corporation.

ST2 technology development finds solutions that, while not currently economically feasible, have a pathway towards future production. Investigation of the implementation issues up front allows us to stretch the organization to look at solutions we would otherwise not have considered. Funding this research in the early stages is of large importance due to the high risk of the technologies.

Key Publications

1. Duraiarasan, S. (University of Michigan). 2019. “Control Oriented Physics Based NO_x Emission Model for a Diesel Engine with Exhaust Gas Recirculation.” ASME 2019 Dynamic Systems and Control Conference.

2. Salehi, R. (University of Michigan). 2019. “Reduced-Order Long-Horizon Predictive Thermal Management for Diesel Engine Aftertreatment Systems.” 2019 American Controls Conference.

Acknowledgements

Thanks to Jeff Girbach, principal investigator of engine research, of Daimler Detroit Diesel Corporation, for integral contributions to the project.

V.5 Development and Demonstration of Advanced Engine and Vehicle Technologies for Class 8 Heavy-Duty Vehicle – SuperTruck II (PACCAR Inc.)

Carl Hergart, Ph.D., Principal Investigator
PACCAR Inc.
12479 Farm to Market Road
Mount Vernon, WA 98273
E-mail: Carl.Hergart@paccar.com

Ken Howden, DOE Technology Development Manager
U.S. Department of Energy
E-mail: Ken.Howden@ee.doe.gov

Start Date: October 1, 2017 End Date: September 30, 2022
Project Funding (FY19): $40,000,000 DOE share: $20,000,000 Non-DOE share: $20,000,000

Project Introduction

PACCAR Inc., through Kenworth Truck Company, PACCAR Technical Center, and PACCAR Engine Company, together with its partners (National Renewable Energy Laboratory, AVL NA, and Eaton Corp.), is collaborating in the design and development of a very high efficiency engine with advanced combustion, reduced friction, advanced air management, and waste heat recovery. A mild hybrid powertrain enhanced through accessory electrification and advanced controls is also under development. The powertrain will be incorporated into a highly aerodynamic and lightweight tractor-trailer combination. The vehicle concept includes advancements in rolling resistance, thermal management, and auxiliary components. Representative customer driving routes have been selected and will be used for development and optimization of the integrated vehicle controls package. Testing of engine, powertrain, and vehicle will demonstrate that project goals have been met.

The combination of technologies is forecasted to provide greater than 100% improvement in vehicle freight efficiency at an affordable cost and with a short payback time. This level of fuel efficiency improvement, applied over the entire Class 7 and Class 8 vehicle fleet in the United States, will have a tremendous positive impact on the operating efficiency of truck fleets and significantly reduce fossil fuel energy dependency.

Objectives

The objective of this project is to research, develop, and demonstrate a Class 8 long-haul tractor-trailer combination that meets prevailing federal emission standards and applicable safety and regulatory requirements while achieving the following goals:

Overall Objectives

- Greater than 100% improvement in vehicle freight efficiency (on a ton-mile-per-gallon basis) with a stretch goal of 120% relative to a 2009 baseline
- 55% engine brake thermal efficiency (BTE) demonstrated in an operational point representative of cruise conditions
- Same or improved vehicle performance (acceleration and gradeability) relative to a 2009 baseline
- Cost-effectiveness as expressed in terms of a simple payback to foster rapid market adoption of new technologies.

Fiscal Year 2019 Objectives

- Finalize design for vehicle cab and trailer aerodynamics
- Complete vehicle design for chassis and components
- Define the control system for hardware-in-loop and model-in-loop testing
- Define powertrain architecture
- Continue investigation of combustion recipe
- Finalize engine design and combustion recipe and select suppliers.

Approach

The project has been approached in three distinct but related areas: vehicle, powertrain, and engine. The vehicle design includes significant aerodynamic improvements such as tractor wheel-well close outs, camera-based mirrors, optimized windshield curvature and A-pillars, as well as reduced tractor-trailer gap, among other things. The tractor and trailer are also undergoing significant lightweighting along with reduced energy use for auxiliary loads.

The powertrain portion incorporates the successful PACCAR Automated Transmission, seamlessly integrated with the MX-11 engine and configured in a 4x2 axle architecture. The truck will feature low rolling resistance tires, hybrid electric power for accessories with energy storage capability, and predictive powertrain management.

The engine portion will use a PACCAR MX-11 engine (produced at PACCAR's state-of-the-art plant in Columbus, Mississippi) as a baseline. The team is optimizing the combustion system, including the fuel injection parameters and the piston bowl geometry, in order to maximize the combustion efficiency. Revisions to the air handling system, including port geometry, manifold design, and turbocharger, are also underway. Furthermore, methods to reduce parasitic loads are being investigated. Recognizing that a significant portion of the heat generated during combustion is expelled with the exhaust, waste heat recovery will be used to extract energy from multiple sources around the engine.

Results

Vehicle Design

In 2019, the PACCAR team accomplished several tasks in the area of vehicle design, including the following:

- Proof of concept chassis design has been completed; parts have been procured to assemble a mule vehicle.
- Advanced no-idle solution has been defined, including insulation and modular heat pump assembly for the cabin. All key systems have been designed, tested, and delivered for vehicle-level assembly. Cooling and heating targets have been exceeded.
- Electrical architecture, controls, and electrified accessories have been defined. Hardware has been procured for mule vehicle assembly. Hardware bench level testing with developed controls is complete.
- Styling theme has been defined in concert with aerodynamic studies, exceeding aerodynamic performance target. Cab mockup is complete to evaluate and gather customer feedback on driving position, visibility, accessibility, interior content, and layout.
- Trailer construction and aerodynamic treatment concept have been defined. Trailer design is in progress. Tail construction concepts are in progress.

The new chassis concept design is complete, leveraging system design and integration to achieve weight saving goals. This concept developed in parallel with structure and aerodynamics enables architecture changes to the vehicle for efficiency. Design completion this year includes tailored solutions for frame rails, cross-members, suspension (front and rear), and powertrain systems. Vehicle level simulation models developed to analyze component and system behavior enabled the team to build confidence prior to prototype part procurement. Chassis assembly is in progress this budget period.

An aerodynamics packaging including tractor and trailer features supports significant improvement to the freight efficiency goal. Tractor shape started as an ideal form, which was morphed to an actual theme through collaboration between design and engineering teams with customer feedback. Similarly, trailer design and construction is in progress following extensive computational fluid dynamics work on a novel approach to skirts and tail, which are co-optimized for minimal drag. Design and optimization work on the aerodynamics package this budget period has resulted in greater than 60% drag reduction compared to the baseline.

Development on the cab and sleeper has progressed with a full-scale mockup of the driving and living spaces, used to review the concept with several large fleet-oriented customers. Key takeaways include alignment to, and agreement with, the general design direction and content of the vehicle. Accessibility, driving position, visibility, and interior layout are some examples of cab and sleeper properties reviewed. The current concept attributes are foreseen to accommodate the needs of a future market and operations where fleets will run more regional routes, with drivers away from home for shorter periods of time.

Powertrain Design

Highlights of the work performed by the powertrain team include the following:

- All mild hybrid drivetrain components were selected based on freight efficiency optimization studies.
- Hardware is under development for the power take-off (PTO)-based 30 kW e-motor/generator, two-speed e-motor gearbox, and power electronics (Figure V.5.1).
- Overall vehicle-level energy management controller and dual-loop cooling system were developed.
- System components were integrated with the Predictive Adaptive Cruise Controller in order to maximize freight fuel efficiency in real-time (Figure V.5.2).
- First vehicle software was released for model-in-loop and hardware-in-loop testing.

In Figure V.5.1, the proposed architecture of the SuperTruck II advanced powertrain is shown. The belt-driven accessories are all replaced by a 48 V electrical system, which is supplemented by the e-Machine on the PTO. The primary requirements of the motor/generator are high power regeneration and the engine cranking function to start the engine (1,000 Nm for cold crank torque at the flywheel). The motor/generator suppliers under consideration have provided torque and efficiency predictions for their machines. Using this information, the team has co-optimized the system so that the motor is running in an area of acceptable efficiency during coasting operation with the selected gearing. In a cruising mode, the motor can charge efficiently at low current levels to maintain battery voltage.

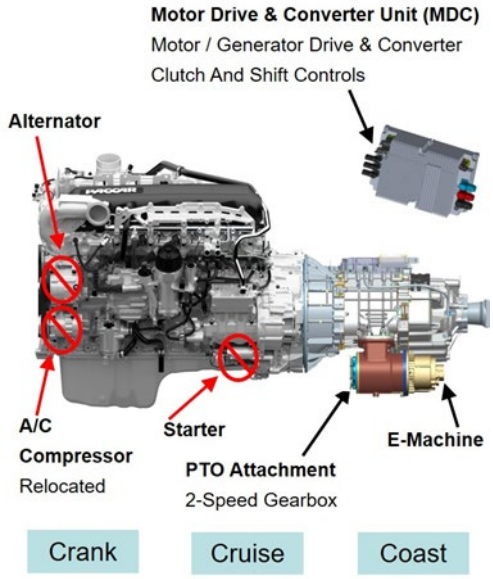

A/C – air conditioning

Figure V.5.1 Sample architecture for powertrain configuration

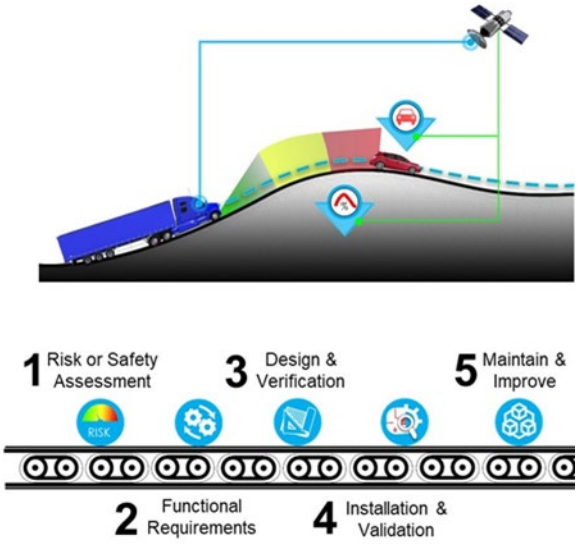

Figure V.5.2 Predictive cruise control operation

Powertrain control state requests and actuator demands will be centrally managed by the Vehicle Energy Management Controller and executed by the transmission, the engine, and the auxiliary braking control module. The Vehicle Energy Management Controller handles energy demands and limits at a tactical level, based on strategic guidance provided by the Predictive Adaptive Cruise Controller.

Engine Design

The roadmap for selecting engine technologies required to meet the 55% BTE goal is shown in Figure V.5.3. The baseline engine was measured to achieve a peak of 47% BTE. The technologies selected to achieve the 55% BTE goal include improved combustion efficiency (where in Figure V.5.3 CAC denotes charge air cooler, CR denotes compression ratio, and PFP denotes peak firing pressure), improved air management, reduced friction and parasitic losses, and the use of an organic Rankine cycle waste heat recovery system. Engine simulations and supporting engine test results have produced a recipe viewed as feasible in meeting the BTE goal for the engine. The team has noted several accomplishments toward the achievement of 55% BTE. In Fiscal Year 2019, the engine team made advancements in:

- Combustion System
  - Computational optimization of injector configuration.
  - Experiments with high-flow injectors on single- and multi-cylinder engines.
- Air Management System
  - Miller Cycle engine tests.
  - Modeling comparison of single vs. two-stage turbocharger BTE potential.
  - Cylinder head flow analysis for port and valve geometry development.
  - Exhaust gas recirculation pump development.
- Heat Rejection: Increased engine coolant temperatures to explore heat transfer reduction.
- Waste Heat Recovery: Supplier selection and system analysis is complete, demonstrating feasibility of achieving 55% BTE. System design is ongoing.

Modeling has been carried out to investigate the impact of nozzle inclusion angle and nozzle-hole diameter variation on combustion systems featuring higher compression ratio and high injector flow rates. The model was created using a revised piston bowl design, with the optimization algorithm programmed to maximize gross indicated thermal efficiency in the SuperTruck II road load point. Maximum gross indicated thermal efficiency is obtained with large nozzle holes, wide nozzle inclusion angles, moderate rail pressure, and a moderate start of injection timing.

As shown in Figure V.5.4, both the standard valve timing and the Miller valve timing results show sensitivity to turbocharger efficiency. The peak efficiency also moves toward higher inlet boost as the efficiency increases, i.e., the peak shifts to the right as the efficiency improves from 70% to 80%. In addition, for the multi-cylinder engine test results, the break-even point between standard and Miller valve timing is at a turbo efficiency of roughly 66%, as shown in Figure V.5.4.

Two rapid prototype models of the SuperTruck II cylinder head, including valve and seat hardware, were created to investigate flow characteristics of the new port geometry. The baseline geometry from the MX-11 was compared to the modified design (seen in Figure V.5.5), which was created with input from multiple iterations of prior computational fluid dynamics simulation work. The results suggest a 10% improvement in exhaust mass flow allowed by the modified geometry relative to the baseline.

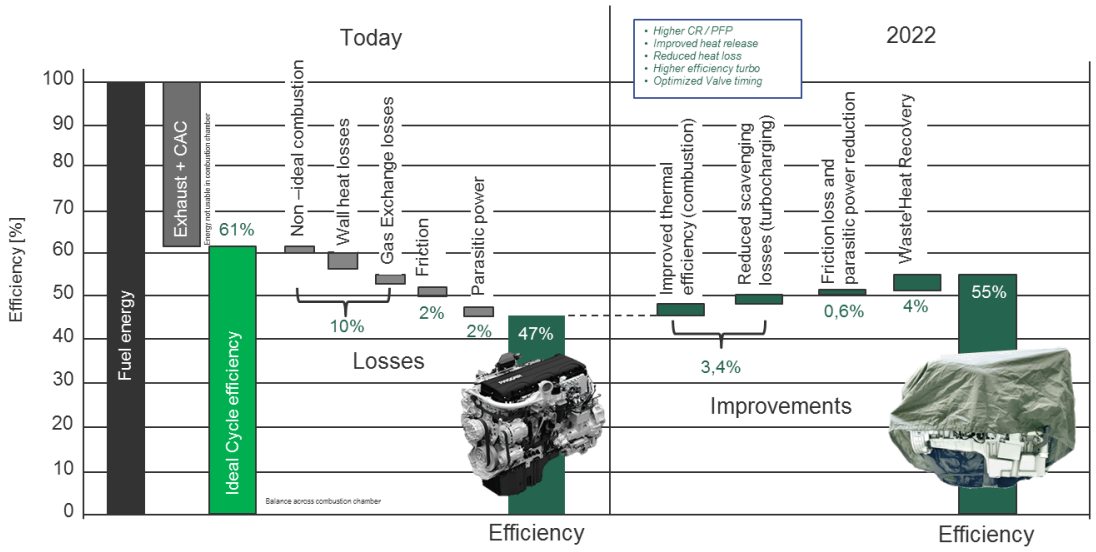

Figure V.5.3 Engine technology roadmap to 55% BTE

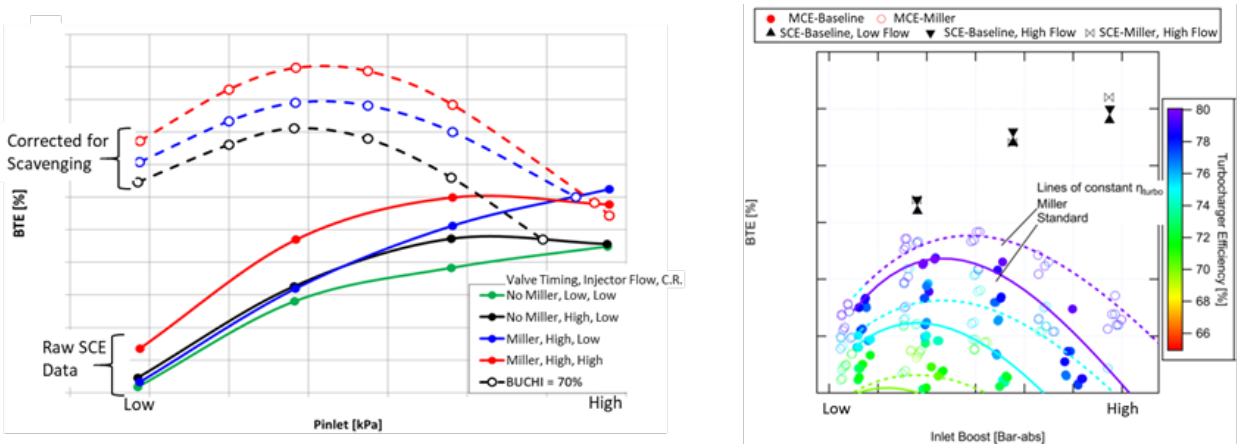

Figure V.5.4 Single-cylinder engine (SCE) and multi-cylinder engine (MCE) hardware testing results

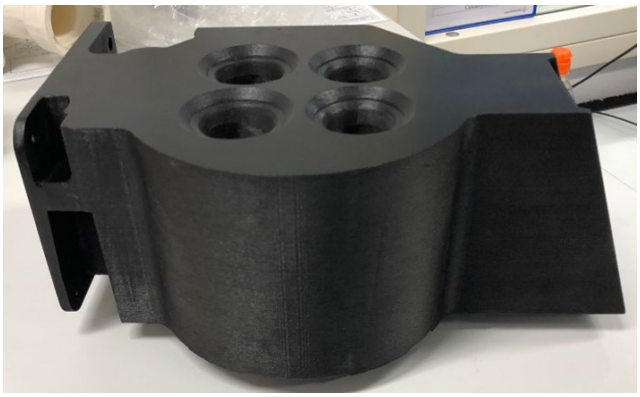

Figure V.5.5 Example of MX-11 3-D printed cylinder head for flow testing

Conclusions

The PACCAR-led team has used simulation, testing, and analysis to develop recipes for engine, powertrain, and vehicle to meet the project objectives. This includes:

- Vehicle improvements
  - Significantly improved aerodynamics of the tractor and trailer.
  - Lightweighting of the tractor and trailer to maximize freight efficiency.
  - Advanced electronics and driver assistance.
- Powertrain technology improvements
  - 48 V mild hybrid system selected based upon a variety of factors to maximize both energy and freight efficiency.
  - Electrified accessories enable maximum flexibility of the mild hybrid.
- Engine technologies to reach 55% BTE
  - High flow injectors and optimized piston bowl shape to improve combustion efficiency.
  - SCE and MCE experimental validation of simulation for effectiveness of Miller Cycle.
  - Evaluation of engine operation at elevated coolant temperature to enhance waste heat recovery operation.
  - Evaluation of new manifold design and turbocharger.

Key Publications

2019 Annual Merit Review Presentation, June 13, 2019.

Acknowledgements

Ralph Nine, National Energy Technology Laboratory Project Manager

V.6 A High Specific Output Gasoline Low Temperature Combustion Engine (General Motors)

Hanho Yun, Principal Investigator
Propulsion System Research Lab., General Motors
30565 William Durant Boulevard
Warren, MI 48092-2031
E-mail: Hanho.yun@gm.com

Ken Howden, DOE Technology Development Manager
U.S. Department of Energy
E-mail: Ken.Howden@ee.doe.gov

Start Date: January 1, 2017 End Date: December 31, 2019
Project Funding (FY19): $696,044 DOE share: $334,101 Non-DOE share: $361,943

Project Introduction

In this project, we are developing and demonstrating a downsized, boosted, lean, low temperature combustion (LTC) engine system capable of achieving 15%–17% fuel economy improvement relative to a contemporary naturally aspirated, stoichiometric combustion engine consistent with relevant emissions constraints. The project is focused on the integration and development of the engine as well as demonstration of the overall engine system performance potential over the Federal Test Procedure (FTP) drive cycles as well as the harsh conditions associated with real-world driving. Testing is conducted on a transient engine dynamometer using a fully functional multi-cylinder engine.

The project is focused on maximizing internal combustion engine fuel economy potential by combining (1) lean LTC over the majority of the drive cycle to maximize work extraction while minimizing NO_x emissions with advanced cylinder-pressure based controls for precise in-cylinder composition control, (2) downsizing and turbocharging for reduced parasitic losses, and (3) a novel plasma-based ignition technology to enhance combustion robustness and controllability through in-cylinder reactive species generation.

The project is currently in Budget Period 3.

Objectives

The objective of this project is the development of a high output, gasoline LTC engine system demonstrating 15%–17% fuel economy improvement relative to a contemporary stoichiometric combustion engine.

Overall Objectives

- Develop a gasoline combustion engine system demonstrating 15%–17% fuel economy improvement relative to a contemporary stoichiometric combustion engine using marketplace gasoline (RD5-87)
- Be consistent with relevant emissions constraints (target: Super Ultra-Low Emission Vehicle [SULEV] 30 regulation)
- Integrate the enabling technologies (gasoline LTC combined with downsizing and boosting technology; low temperature plasma ignition; physics-based, model-based control; Protection of Aftertreatment Systems from Sulfur [PASS] lean aftertreatment system) synergistically.

Fiscal Year 2019 Objectives

- Develop and demonstrate LTC engine calibration and control algorithms necessary for robust transient operation and LTC/spark ignition (SI) combustion mode shifts with prototype controller
- Develop and demonstrate LTC engine calibration and control strategies necessary for robust operation over the hot FTP drive cycle consistent with stability objectives
- Develop and demonstrate LTC engine calibration and control strategies necessary for robust operation over the hot FTP drive cycle consistent with fuel economy, engine-out emissions, and stability objectives
- Develop and demonstrate LTC engine calibration and control strategies necessary for robust operation over the cold FTP drive cycle consistent with fuel economy, engine-out emissions, and stability objectives.

Approach

Budget Period 1: Multi-cylinder engine and prototype controller design, build, and testing

Design modification and procurement activities for the LTC multi-cylinder engine and prototype controller including build and installation of the baseline engine into a dynamometer test cell.

Go/No-Go Decision #1 approval required to continue to Phase 2

Budget Period 2: LTC combustion and controls development – steady-state condition

LTC multi-cylinder engine combustion and controls development and testing using the low temperature plasma ignition system.

Go/No-Go Decision #2 approval required to continue to Phase 3

Budget Period 3: Development/demonstration of full integrated engine, combustion, and controls capability

Final integration and demonstration phase. This phase will turn to refining the transient controls and calibration packages. All dynamometer-based multi-cylinder testing will have been completed and a 100% verified dynamometer-based calibration developed.

Results

- Completed the refinement of steady-state LTC calibrations for a smooth transient operation.
- Developed an overall control architecture for LTC operation (Figure V.6.1).

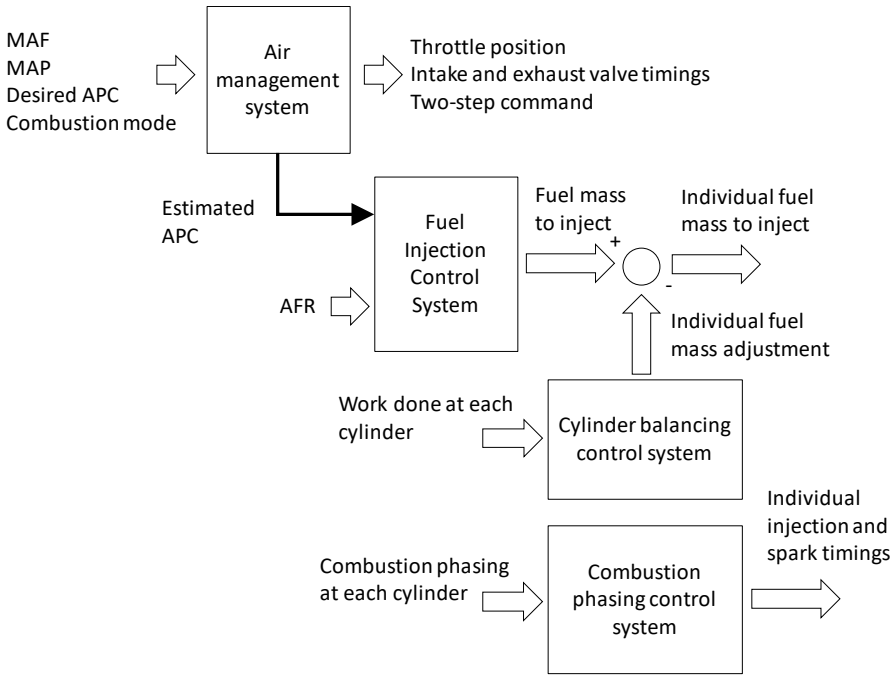

MAF – mass air flow; MAP – manifold absolute pressure; APC – air per cylinder; AFR – air-fuel ratio

Figure V.6.1 Overall structure of LTC engine controller

- **Simulation Results** – The functionality of the LTC controller has been validated with an LTC engine model (Figure V.6.2). APC and torque models developed for the LTC engine were combined to simulate the response of the LTC engine. The controller was closed-loop with the LTC engine model, and a step change in torque demand was given to the controller. At the beginning of simulation, the LTC engine was in negative valve overlap (NVO) mode. As torque demand increased, the controller triggered a two-step system such that the combustion mode switched to positive valve overlap (PVO) mode and eventually to SI mode as the torque demand further increased.

- **Cylinder Balancing Control** – To maintain balanced combustion in individual cylinders, fuel mass injected in each cylinder must be closely matched to the desired value. As individual cylinders may have different thermal conditions due to imbalance in wall temperature and air and exhaust gas recirculation (EGR) maldistributions, it is critical to maintain combustion timing during transient operation and in steady state.

- **Individual Combustion Timing Control Strategy** – Combustion timing for each cylinder in the LTC engine can vary significantly due to differences in the thermal conditions of the individual cylinders. Throttle and EGR valve positions have global effects on combustion phasing for all cylinders; therefore, they cannot be used for individual combustion phasing control. Besides, combustion timing may not be as sensitive to spark timing as in conventional SI combustion, as combustion modes such as NVO and PVO rely on autoignition even though they are assisted by spark. Thus, individual combustion timings are calculated based on cylinder pressure traces at every engine event, and individual injection timing as well as spark timing are tied and adjusted together by a combustion timing controller until the all combustion timings are equal to the desired value (Figure V.6.3).

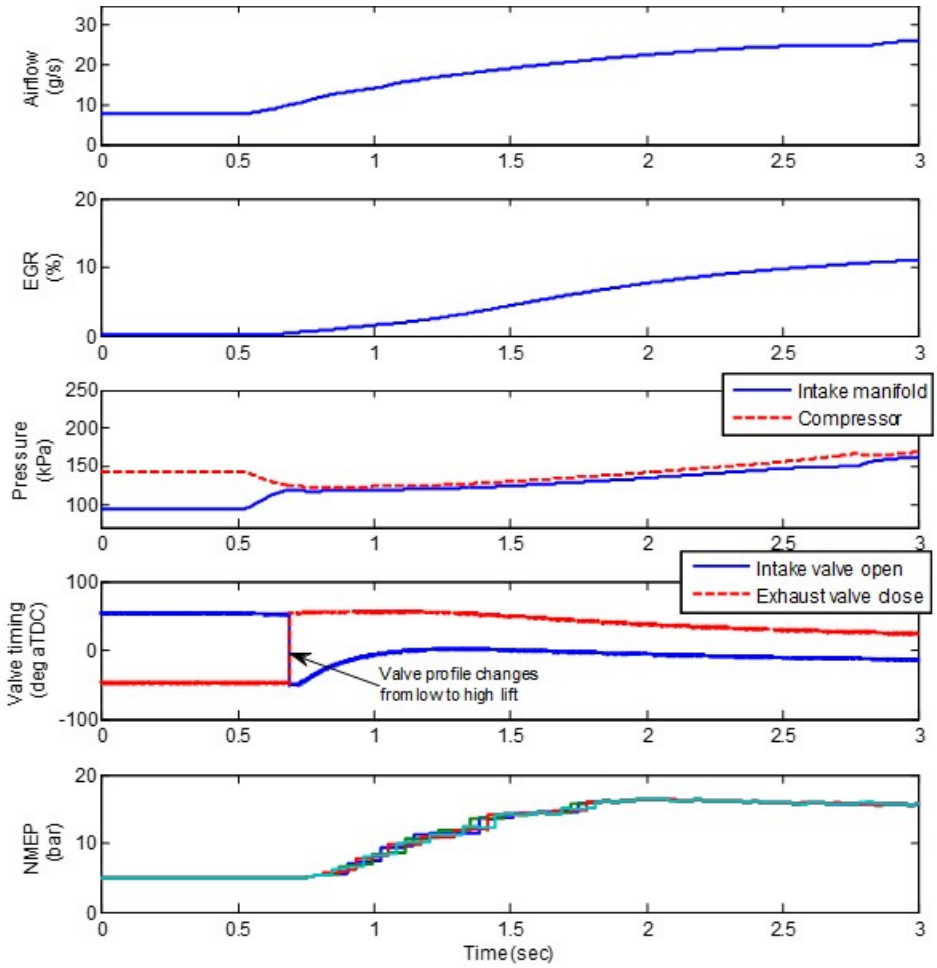

deg aTDC – degrees after top dead center; NMEP – net mean effective pressure

Figure V.6.2 Closed-loop simulation of LTC engine controller

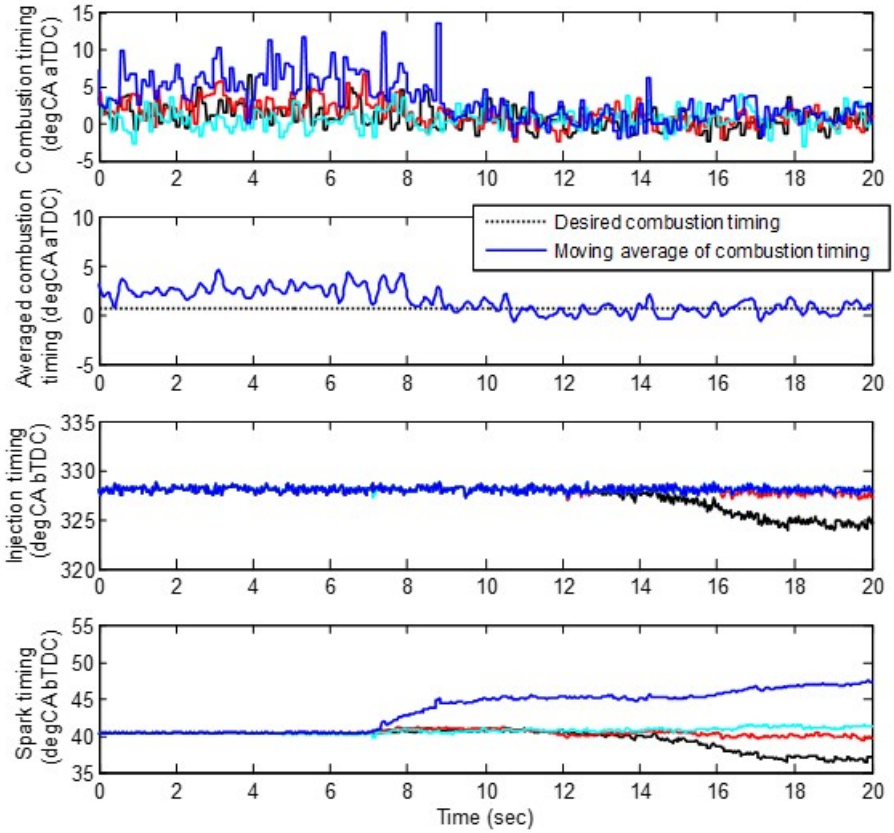

deg CA aTDC – degrees crank angle after top dead center;
deg CA bTDC – degrees crank angle before top dead center

Figure V.6.3 Combustion timing control in PVO mode at 1,000 rpm

- **Individual Fuel Mass Balancing Strategy** – The LTC engine is equipped with individual cylinder pressure sensors and linear oxygen sensor at the exhaust manifold to measure air–fuel ratio. Thus, given air charge, the level of imbalance of fuel masses injected in the individual cylinders can be obtained using indicated mean effective pressures (IMEPs) and combustion timing calculated from measured cylinder pressure traces, while the mean of fuel mass deviations from the desired can be obtained from the oxygen sensor (Figure V.6.4).

- **Mode Transition Control** – The LTC engine is equipped with a two-step valve lifter that can instantaneously switch low-lift valve profiles (for NVO mode) to high-lift valve profiles (for PVO and SI modes) and vice versa. When intake and exhaust valve timings with the low-lift valve profiles reach minimum NVO, desired mode changes from NVO to PVO. The cam lobes of low-lift and high-lift profiles are designed such that geometrical cylinder volumes are closely matched before and after mode change from NVO to PVO and vice versa so that cylinder charge has minimal disruption during mode transitions (Figure V.6.5).

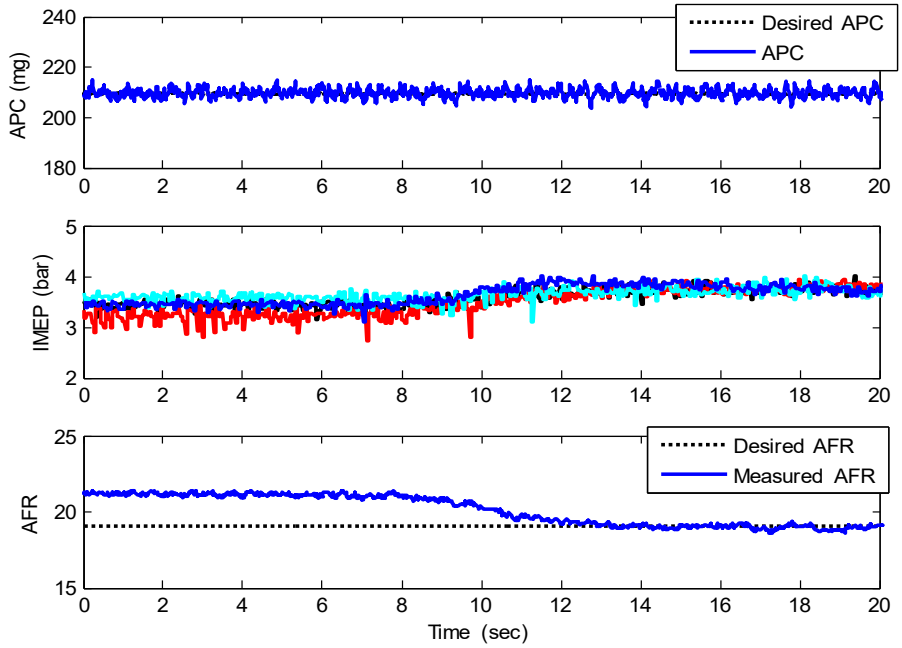

Figure V.6.4 Fuel mass balancing control in NVO mode at 2,000 rpm

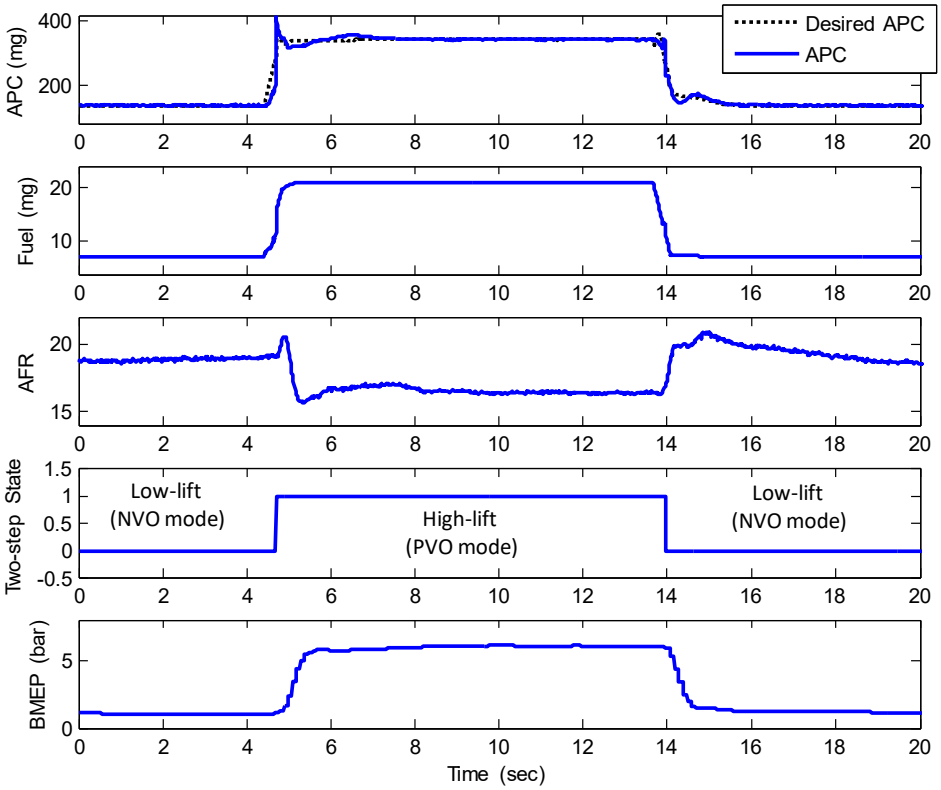

BMEP – brake mean effective pressure

Figure V.6.5 Load transient at 2,000 rpm

Variable Injection Strategy for Combustion Noise Control during Mode Transition – To reduce the combustion noise during mode transitions, an extra amount of fuel is temporarily injected at around spark timing immediately after mode switching from NVO to PVO until exhaust gas reaches the intake manifold through the EGR pipe, while the total amount of fuel injected in the cylinder is still maintained at the desired value to meet the torque demand. The extra fuel helps combustion to slow down by fortifying spark-assisted autoignition, but at the cost of NO_x emissions as cylinder charge is more stratified. Thus, the amount of extra fuel must be optimized to decrease emissions while maintaining combustion stability during mode transitions (Figure V.6.6).

- Re-firing Strategy with Fuel Reforming after Deceleration-Fuel-Cut-Off – It is challenging to initiate LTC combustion after deceleration-fuel-cut-off or engine stop as hot residual gas is not available. In the LTC engine, re-firing is initiated in NVO mode where recompression occurs before the intake valve opens. During the recompression, a small amount of fuel is injected near top dead center, and spark is used to trigger consistent reforming process of the fuel. The heat and reformates such as hydrogen generated from the reforming process support succeeding combustion after the intake stroke. After a successful re-firing, combustion continues in the following engine cycles as hot residual gas is available afterwards (Figure V.6.7).

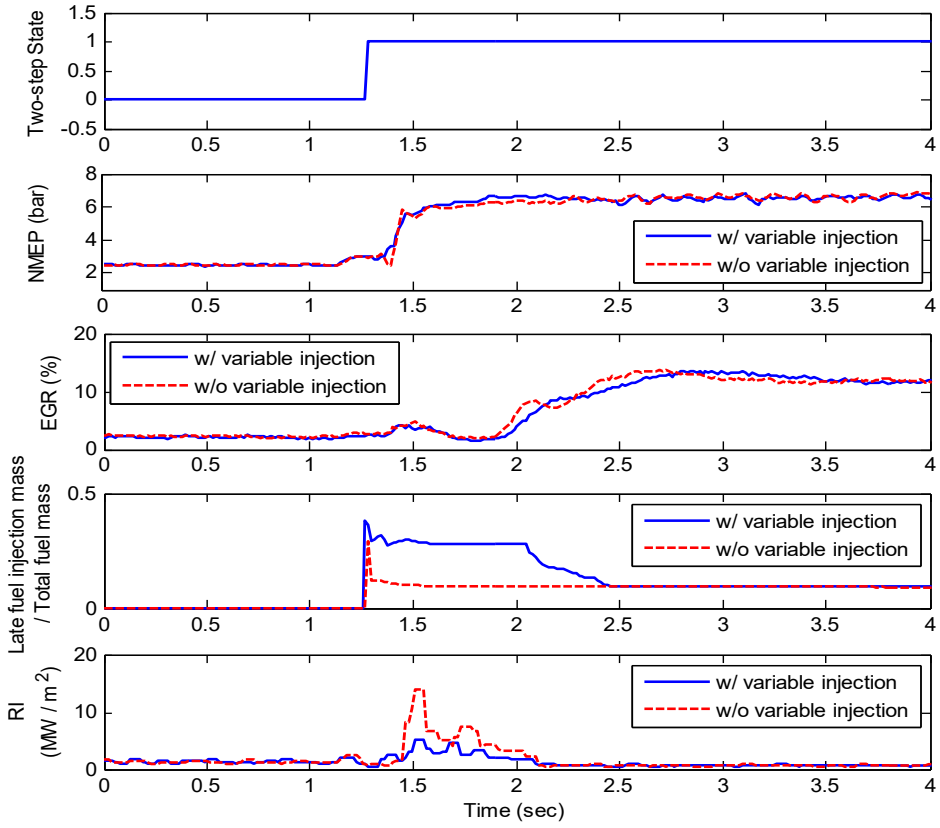

RI – ringing intensity

Figure V.6.6 Variable injection strategy for combustion noise reduction during mode transition

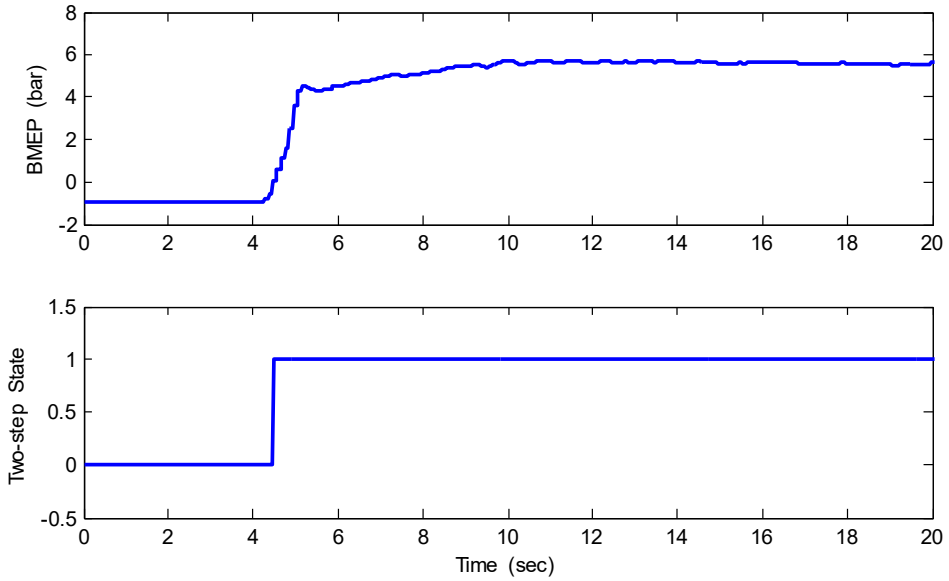

Figure V.6.7 Load transient after re-firing at 1,000 rpm

- FTP Test Results – The APC and torque model calibrated with a wide range of experimental data has been implemented to operate the LTC engine to follow the load demand from FTP driving cycles (UDDS is the Urban Dynamometer Driving Schedule, and HWFET is the Highway Fuel Economy Test). Engine speed is controlled by a dynamometer (dyno) controller to follow the engine speed trajectory of the targeted driving cycle, while the engine controller controls the engine to generate desired torque trajectory. For each sub-driving cycle, the dyno test was repeated three times for each engine, and experimental data collected from the engine are averaged for consistency (Table V.6.1).

Table V.6.1 Summary of FTP Driving Cycle Test Results of 2.2 L SI and 1.4 L LTC Engines

	Engine	2.2 L SI	1.4 L LTC
UDDS	Fuel (g)	569.63	476.89
	MPG - work compensated	***37.24***	***44.31***
	MPG gain (%) - work compensated	0.00	***18.97***
HWFET	Fuel (g)	574.69	514.37
	MPG - work compensated	***51.04***	***56.87***
	MPG gain (%) - work compensated	0.00	***11.44***

MPG – miles per gallon

- Achieved 19% fuel economy improvement from UDDS drive cycle and 11% fuel economy improvement from HWFET drive cycle.

Conclusions

- Completed the development of the overall control architecture for LTC transient operation
- Successfully verified control system using simulation

- Developed the methodology of combustion noise reduction during transient operation
- Developed the re-firing strategy after deceleration-fuel-cut-off
- Developed individual cylinder balancing strategy
- Successfully achieved 19% fuel economy improvement from hot FTP cycle test (both UDDS and HWFET) compared with homogeneous stoichiometric SI operation, which is higher than the project target.

Acknowledgements

The author would like to thank Ralph Nine, Ken Howden, and Gurpreet Singh for support of this project.

V.7 Solenoid Actuated Cylinder Deactivation Valve Train for Dynamic Skip Fire (Delphi Technologies, PLC)

Richard B. Roe, Principal Investigator
Delphi Technologies, PLC
5500 W. Henrietta Road
W. Henrietta, NY 14586
E-mail: Richard.B.Roe@delphi.com

Robert Wang, Principal Investigator
Tula Technology, Inc.
2460 Zanker Road
San Jose, CA 95131
E-mail: wangr@tulatech.com

Ken Howden, DOE Technology Development Manager
U.S. Department of Energy
E-mail: Ken.Howden@ee.doe.gov

Start Date: January 1, 2017 End Date: June 30, 2019*
Project Funding (FY19): $1,645,705* DOE share: $822,853 Non-DOE share: $822,853

*A six-month project period extension has been requested for an end date of December 31, 2019.

Project Introduction

Delphi Technologies, PLC, and Tula Technology, Inc., are developing an advanced combustion strategy known as dynamic skip fire (DSF). The basis of this strategy is to selectively deactivate cylinders based on engine load and speed to minimize fuel consumption. Cylinder deactivation requires intake and exhaust valve as well as fuel injector deactivation to reduce engine pumping work and improve efficiency. Existing hydraulically actuated valve train hardware has been used on development engines and vehicles to prove out the fuel economy benefits of DSF. Hydraulic actuation has proven difficult to implement for production level programs due to the complexity of adding four independent hydraulic circuits to an existing cylinder head for a 4-cylinder engine.

The purpose of this project is to develop solenoid actuated valve train hardware that will allow DSF technology to be more easily commercialized with current overhead cam production engines. Additional benefits expected from this project include a faster and more repeatable switching response, leading to improved system reliability as well as a larger operating window for DSF.

Objectives

The objective of this project is to improve engine fuel efficiency by developing a production-feasible electrically actuated cylinder deactivation valve train that will enable internal combustion engines to employ this combustion strategy.

The project is expected to enable the realization of 8% to 10% fuel economy improvement above stock operation of a non-cylinder-deactivation 4-cylinder engine, while maintaining production-level noise, vibration, and harshness targets and emissions.

This project will enable DSF technology to be more easily implemented into production engines by eliminating the complex hydraulic circuit packaging that is currently required to individually deactivate cylinders. This will allow broader market adaptations, especially on overhead cam engines.

The Fiscal Year 2019 objective is verification motored cylinder head testing of the hardware of the actuation system, confirming the deactivation and reactivation of the engine valves. After completion of the verification testing, the cylinder head will be transferred to a firing dynamometer engine, documenting the steady-state fuel economy of the engine, and the data will be compared to the baseline data from 2018 for fuel economy improvement. This testing will confirm that the deactivation system meets the modeled switching speed requirements on a motored cylinder head and effectively deactivates cylinders as planned.

Approach

Delphi is responsible for all the physical testing of the switchable valve train on a motored cylinder head and on the firing dynamometer engine. The deactivation roller finger follower (RFF) and electrical actuators manufactured in Fiscal Year 2018 are to be assembled on three cylinder heads for motored cylinder head testing, and this testing is the responsibility of the Valve Train Engineering department. The first cylinder head was used for dynamic performance testing, and the second was used for durability testing. The third cylinder head was for verification testing of the system, and the complete head was to be transferred to the Engine Management Systems department, which is responsible for the dynamometer firing engine testing. Once installed on the engine, the actuation system will be confirmed to function correctly, then engine performance will be documented through testing at various engine conditions.

Once the firing dynamometer engine data is collected, comparisons will be made at the various engine conditions, comparing the baseline engine without the deactivation system to the engine with the deactivation system.

Results

Major Accomplishments

- Verification of the deactivation RFF and electrical actuators on a cylinder head function as expected.
- Completion of dynamics testing, which demonstrated that the dynamic behavior of seating velocity did not exceed -1,000 mm/s, which is an industry guideline to avoid valve seating (closing) noise. See Figure V.7.1.
- Rocker arm load is another critical dynamic performance measurement that is evaluated in order to determine if the valve train is close to having the rocker arm separate from the cam. Figure V.7.2 shows force at 6,000 engine revolutions per minute (erpm) was in control and did not go below 0 N.
- Durability testing successfully completed 400 h at speeds varying from 700 erpm to 6,000 erpm. Figure V.7.3 shows the cylinder head test configuration.

Firing Dynamometer Testing

- Used emission test (Federal Test Procedure [FTP]) data from a DSF equipped vehicle to generate dyno testing points. Key data used to determine the best dyno test points were the time spent at given engine speeds, torque output, and firing fraction from INCA (Integrated Calibration and Application tool) data. Data from three emission tests were used.
- Speed/loads (test points) used to test the electronic deactivation (eDEAC or EDEAC) hardware on the dynamometer were selected based on durations in a speed/load zone and higher rates of fuel used. The baseline engine was also operated at these same torque and engine speed points. See Figure V.7.4.

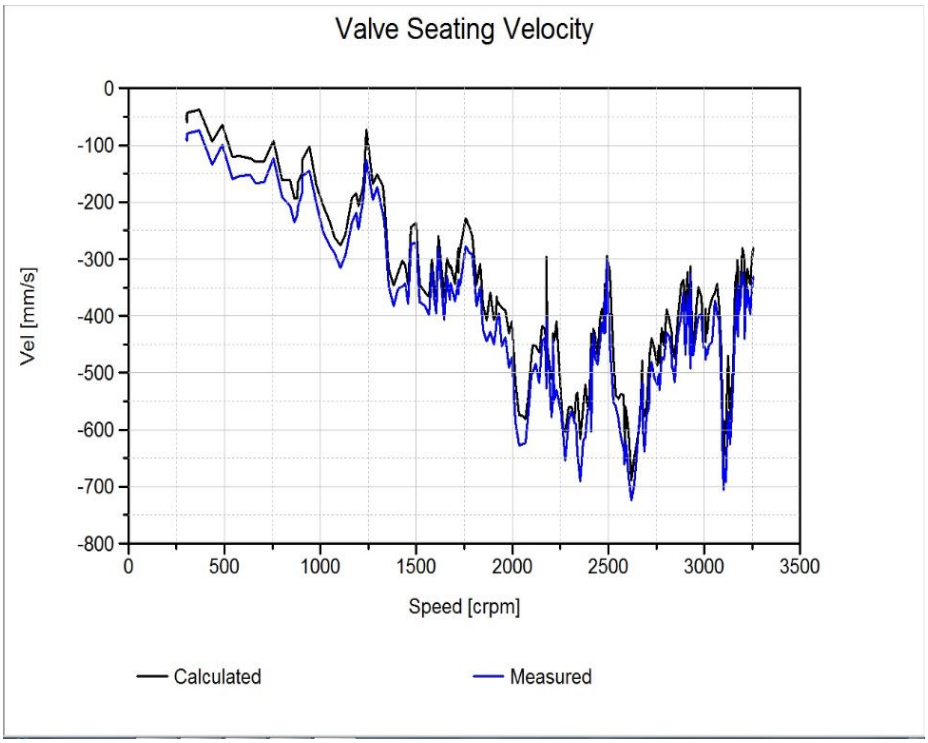

Figure V.7.1 Valve seating velocity from dynamics testing

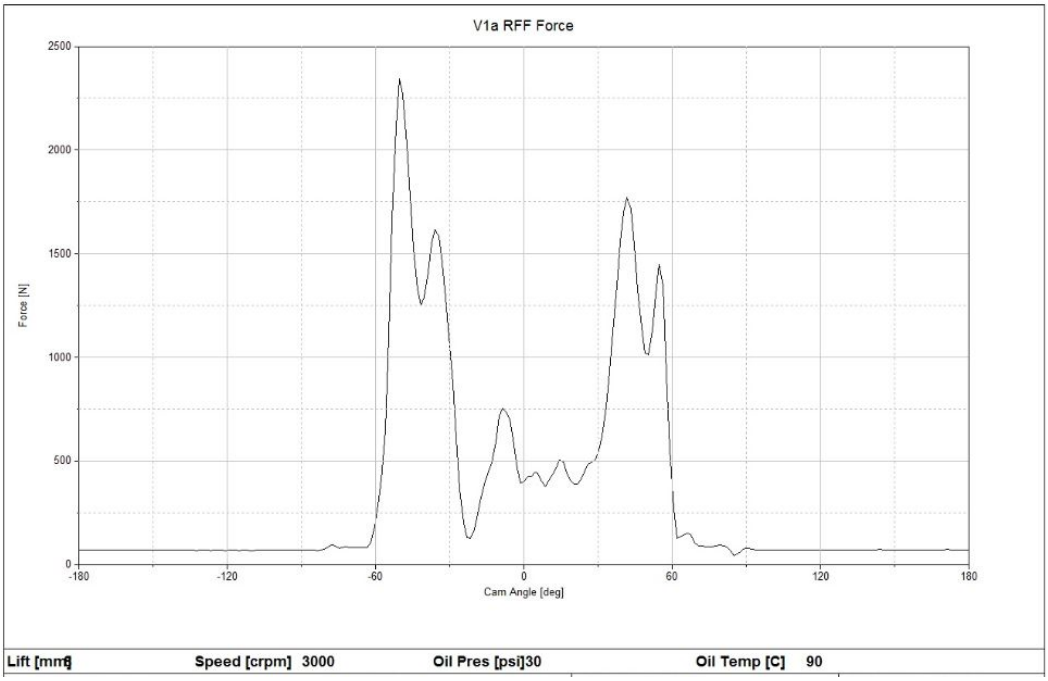

Figure V.7.2 Rocker arm load at 6,000 erpm

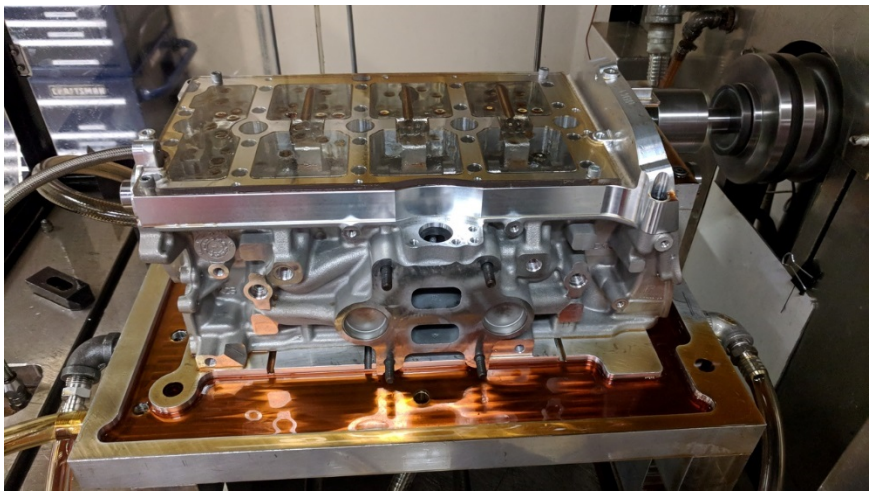

Figure V.7.3 Durability test configuration

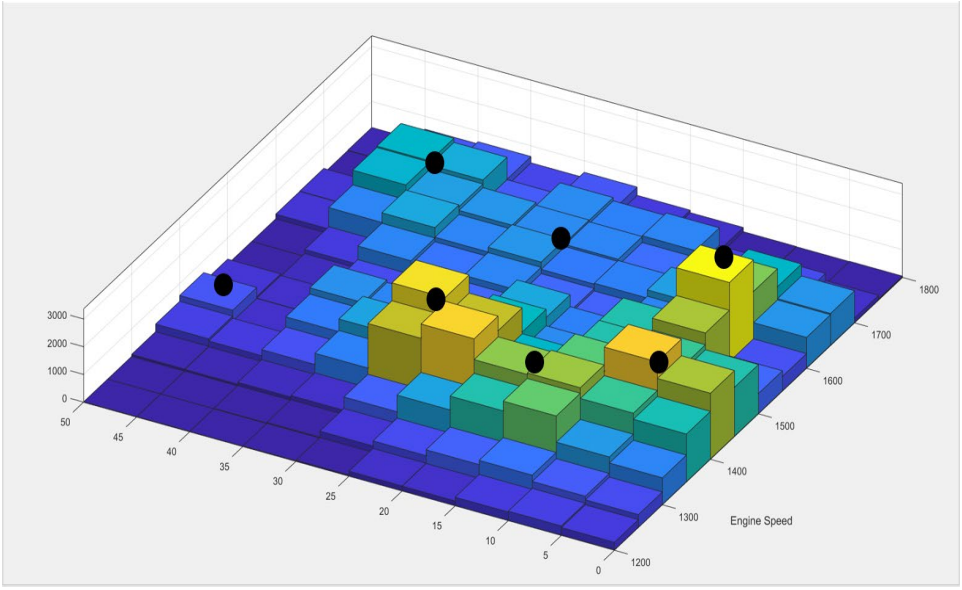

Figure V.7.4 Dynamometer test points are shown as black dots

- Determined the duration of each firing fraction (FF) used in each speed/load zone of vehicle test data that is covered by the seven selected speed/load test conditions for dynamometer testing. The result of the data analysis of three emission tests was a defined test matrix for dynamometer testing that could be used to determine a level of benefit from eDEAC DSF. See Table V.7.1.

- The results of steady-state brake specific fuel consumption (BSFC) or fuel rate were calculated for each test point comparing the test point where the firing fraction is equal to one (EDEAC FF 1). See Table V.7.2 and Figure V.7.5.

Table V.7.1 Test Matrix for Dynamometer Testing

Top table shows the full map in time base; the blue shaded boxes indicate test points of interest for the dynamometer test. The bottom table shows the points of interest in percent base of the test points of interest.

Entire Test Points of Interest		Time at .8 FF	Time at .75 FF	Time at .66 FF	Time at .6 FF	Time at .5 FF	Time at .4 FF	Time at .33 FF	Time at .25 FF	Total Time at Speed and Load	Percentage of actual DSF time vs possible time	Delta Time Lost
Engine Speed	Torque	Time in Seconds for sum of 3 Emissions tests										
1400 (+-50)	5 (+-5)	3.5	0.1	0.2	0.0	6.4	1.6	66.3	0.3	101.4	77.22%	23.1
1350 (+-50)	15 (+-5)	29.5	1.9	3.5	0.0	39.4	7.2	3.5	0.0	114.7	74.01%	29.81
1400 (+-50)	25 (+-5)	25.2	18.4	44.6	0.0	19.1	0.3	0.6	0.0	134.7	80.32%	26.51
1550 (+-50)	7 (+-5)	2.1	0.3	0.5	0.0	7.5	2.3	17.0	33.3	90.3	69.64%	27.41
1650 (+-50)	25 (+-5)	0.2	0.2	0.1	0.0	27.3	14.5	0.6	0.0	51.0	83.97%	8.18
1700 (+-50)	40 (+-5)	0.0	0.5	0.1	0.0	46.6	0.0	0.0	0.0	55.0	86.08%	7.66
1400 (+-50)	45 (+-5)	10.6	0.6	0.1	0.2	0.1	0.0	0.0	0.0	64.1	17.79%	52.72
							Total Time		435.9	611.3		

Entire Test Points of Interest		.8 FF	.75 FF	.66 FF	.6 FF	.5 FF	.4 FF	.33 FF	.25 FF	Time Total in DSF
Engine Speed	Torque	Percentage of time in each firing fraction vs total DSF time per speed and load								Sec
1400 (+-50)	5 (+-5)					8.1%		84.6%		78.3
1350 (+-50)	15 (+-5)	34.7%				46.4%	8.4%			84.9
1400 (+-50)	25 (+-5)	23.3%	17.0%	41.2%		17.7%				108.2
1550 (+-50)	7 (+-5)					11.9%		27.0%	52.9%	62.9
1650 (+-50)	25 (+-5)					63.6%	33.9%			42.9
1700 (+-50)	40 (+-5)					98.5%				47.4
1400 (+-50)	45 (+-5)	92.7%								11.4

- The final prediction of 5.92% fuel economy (FE) gain compared to the baseline non-deactivation engine is made. Compared to hydraulic deactivation DSF, eDEAC DSF has an additional 0.46% FE gain. Additional adjustment of the fuel savings for variables not accounted for on the steady-state dynamometer testing are included. These include fuel saved at selected speed points not tested in the dynamometer engine, fuel not consumed by fuel cut-off O2 depletion maneuvers, and fuel saved by being able to utilize deactivation earlier compared to a hydraulic system deactivation, which requires a minimum oil temperature. See Table V.7.3.

- A technical review with Ralph Nine and Ken Howden from the U.S. Department of Energy was held on June 19, 2019, at Delphi Technologies' Technical Center in Rochester, New York. During the review of this data and the project, it was mentioned that two subtasks, 5.1.2 and 5.4.4, to simulate vehicle FTP testing, were not completed, and it was acknowledged that Delphi was not capable to make these simulations. At the suggestion of the DOE representatives, Delphi has requested a time period continuation of six months to actually perform FTP measurements on a vehicle chassis dynamometer. The continuation request has not yet been approved as of the writing of this report.

Table V.7.2 BSFC and Fuel Rate Percent Increase

BSFC percent increase is shown in the top table. Fuel rate percent increase is shown in the bottom table.

Brake Specific Fuel Consumption Percentage increase										
Entire Test Points of Interest		**EDEAC FF 1**	**.8 FF**	**.75 FF**	**.66 FF**	**.6 FF**	**.5 FF**	**.4 FF**	**.33 FF**	**.25 FF**
Engine Speed (rpm)	Torque (Nm)	BSFC (g/kWh)	BSFC %	BSFC %	BSFC %	BSFC %	BSFC %	BSFC %	BSFC %	BSFC %
1400	5	648.9		11.0%			26.8%		34.6%	
1350	15	415.9	7.6%	10.8%			21.2%	21.9%		
1400	25	340.1	6.1%	8.3%	8.7%		16.8%			
1550	7	555.5		10.9%			25.0%		30.9%	38.4%
1650	25	345.7		8.7%			16.4%	16.0%		
1700	40	298.1	3.7%	6.6%			10.9%			
1400	45	284.4	3.4%							

Fuel Rate Percentage Increase										
Entire Test Points of Interest		**EDEAC FF 1**	**.8 FF**	**.75 FF**	**.66 FF**	**.6 FF**	**.5 FF**	**.4 FF**	**.33 FF**	**.25 FF**
Engine Speed (rpm)	Torque (Nm)	Fuel Rate (g/s)	Fuel Rate %	Fuel Rate %	Fuel Rate %	Fuel Rate %	Fuel Rate %	Fuel Rate %	Fuel Rate %	Fuel Rate %
1400	5	0.264		12.9%			26.8%		35.0%	
1350	15	0.343	7.7%	11.4%			21.9%	21.5%		
1400	25	0.436	5.4%	8.1%	8.3%		16.5%			
1550	7	0.315		11.2%			25.3%		30.7%	37.6%
1650	25	0.504		9.6%			16.5%	15.4%		
1700	40	0.637	3.8%	5.2%			11.0%			
1400	45	0.586	3.3%							

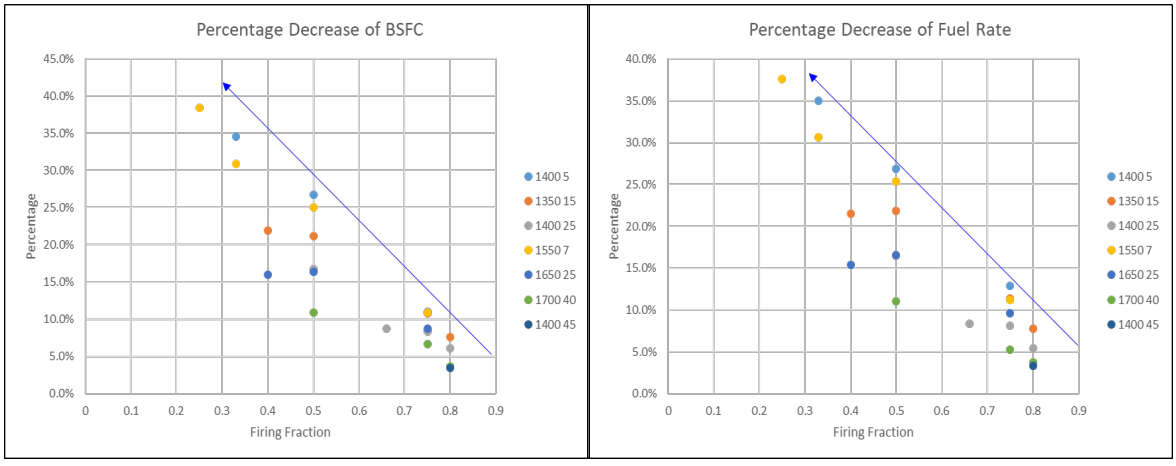

Figure V.7.5 Graphical representation of the table data in Table V.7.2

Table V.7.3 Final Analysis of Fuel Economy Gain after the Additional Adjustments for Variables Not Accounted for on the Steady-State Dynamometer Testing

Inidividual Results and Conclusion				
	Phase 1,2	Phase 3	Average	
I4 Mode	708.0	287.7	**995.7**	
Hydraulic DSF	672.3	272.2	**944.5**	
Percentage decrease from fuel consumption From data comparisons (INCA fuel data from FTP)				**5.14%**

EDEAC Data analyzed		
Description	**fuel (g)**	**% FE FTP**
Sum of grams fuel saved at selected speed load points	**11.83**	1.19%
Sum of grams fuel saved when applied (extrapolated) to all FTP test points	**30.42**	3.00%
Adjustments for other conditions (that are not accounted for above)		
Fuel Consumption benefit from DCCO (No O2 depletion)	**12.90**	1.30%
45 Sec more of DCCO	**11.62**	1.17%
Ability to enable earlier in cycle 1	**4.60**	0.46%
Estimated FE benefit from eDEAC DSF for comparison to Hydraulic DSF		**5.46%**
Estimated eDEAC benefit if enabled in cycle 1		**5.92%**

DCCO – deceleration cylinder cut-off

Conclusions

- The final analysis estimates a 5.92% fuel economy gain compared to the baseline non-deactivation engine. Compared to hydraulic deactivation DSF, eDEAC DSF has an additional 0.46% fuel economy gain (5.46% vs 5.92%).
- Compared to the initial project stated goal of 8% to 10% fuel economy gain, this testing does not show this level of gain.

V.8 Temperature-Following Thermal Barrier Coatings for High-Efficiency Engines (HRL Laboratories, LLC)

Tobias Schaedler, Principal Investigator
HRL Laboratories, LLC
3011 Malibu Canyon Road
Malibu, CA 90265
E-mail: taschaedler@hrl.com

Ken Howden, DOE Technology Development Manager
U.S. Department of Energy
E-mail: Ken.Howden@ee.doe.gov

Start Date: January 1, 2018 End Date: January 31, 2020
Project Funding (FY19): $568,000 DOE share: $284,000 Non-DOE share: $284,000

Project Introduction

HRL Laboratories, with the support of General Motors, is pursuing this effort to dramatically increase the efficiency of internal combustion engines by 4% to 8% by developing and implementing temperature-following thermal barrier coatings (TBCs) to decrease heat loss from the combustion chamber. HRL developed microshell TBCs based on hollow high-temperature alloy spheres with average diameter of 50 µm and wall thickness ~1 µm (microshells) that achieve unprecedented low thermal conductivity and heat capacity (10X lower than the state of the art) while offering exceptional environmental and mechanical resistance.

In current internal combustion engines, approximately 29% of the fuel's energy is lost to the cooling system, and about 22% goes into moving the car. By limiting heat losses from the combustion chamber with insulating coatings, fuel energy can be redirected into additional piston work and into the exhaust stream. The additional energy that goes into the exhaust stream can be turned into useful work through the use of an exhaust energy recovery device, such as turbo-compounding, and/or through driving a turbocharger to increase the power density of the engine, allowing downsizing.

Insulating coatings for piston crowns have been pursued in the past, but previous materials—typically ceramics—exhibited low thermal conductivity but retained high heat capacity. Such materials reduce heat losses but stabilize at a high surface temperature. The high surface temperature heats the incoming gases, which lowers volumetric efficiency and increases propensity for knock, resulting in degraded engine performance.

This project is developing an innovative new material that combines low thermal conductivity with low heat capacity. These unique properties allow it to follow rapid changes in gas temperature during each combustion cycle. A metallic microshell TBC has been demonstrated that exhibits increased surface temperature during the combustion period, resulting in reduced heat transfer losses, while still returning to a low surface temperature during the gas exchange period. A 10X lower thermal conductivity and heat capacity than state-of-the-art TBCs has been demonstrated. These unprecedented thermal properties are achieved through the coating architecture, which consists of closed pores on the microscale and exhibits a total porosity of 90% to 95%. By selecting a high-temperature nickel alloy as the coating material, the ductility and strength of metals can be harnessed to achieve much better durability and damage tolerance than brittle ceramic coatings can ever achieve.

Objectives

The objective of this project is to increase the efficiency of internal combustion engines by 4% to 8% with temperature-following TBCs that add less than ~$250 in cost to a 4-cylinder engine. This project includes work to develop, implement, and test TBCs that will decrease heat loss from the combustion chamber. TBCs with extremely low thermal conductivity and heat capacity will be developed based on high-temperature alloy microshells. Approaches to apply these TBCs to valve faces, piston crowns, and exhaust port liners will be developed. Coated engine parts will then be tested in single-cylinder engine tests to quantify coating durability and efficiency benefits.

Overall Objectives

- Increase internal combustion engine efficiency by 4% to 8% with temperature-following TBCs
- Develop temperature-following TBCs with extremely low thermal conductivity and heat capacity based on high-temperature alloy microshells
- Develop methods to apply TBCs to valve faces, piston crowns, and exhaust port liners that add less than ~$250 in cost to a 4-cylinder engine.

Fiscal Year 2019 Objectives

- Demonstrate scalable low-cost processes to coat valves, pistons, and port liners
- Optimize temperature-following TBC properties, including surface roughness, surface sealing, thermal conductivity, and heat capacity
- Demonstrate durability of temperature-following TBCs in engine tests
- Quantify efficiency gains achieved with TBCs by simulation and experimental engine testing.

Approach

HRL is fabricating the metal microshells in house and is then processing the microshells into coatings on engine parts. Different coating approaches are used for valve faces, piston crowns, and exhaust port liners. Steel valves are used, and the microshells can be directly sintered onto the valve face and then sealed with a metal foil or ceramic plasma spray coating. Aluminum pistons were pursued initially, but the melting point of aluminum alloy is lower than the sintering temperature required for the microshells. Therefore, the microshells were sintered on a copper sheet first, and the copper sheet was then brazed to the aluminum piston crown or inserted during the piston casting. Both approaches have been successful, but the copper sheet with the TBC came off during engine testing. After multiple iterations leading to repeated premature coating failure during engine testing, it was decided to pursue steel pistons instead, which allow sintering the microshells directly to the crown. The repeated coating failures have delayed the project because each iteration takes at least six months, involving coating piston blanks at HRL, machining the blanks into pistons at a vendor, and testing the piston at General Motors R&D. General Motors is conducting all engine testing in a fully instrumented single-cylinder research engine. Post-test characterization including scanning electron microscopy is performed at HRL.

Results

Key Accomplishments for Fiscal Year 2019

- Improved model fidelity and simulated efficiency gains in detail as shown below
- Optimized thermal and mechanical properties of temperature-following thermal barrier coating
- Developed two sealing methods for microshell-based TBCs with differing applicabilities: Monel/Inconel foil and alumina-based ceramic

- Fabricated TBC-coated valves and demonstrated durability of TBC for >50 h in test engine
- Fabricated TBC-coated steel pistons; delays and difficulties at the supplier have confounded testing
- Developed exhaust port liner insulated with nickel microspheres and demonstrated durability during casting process as well as feasibility of cost-effective insertion during casting.

Modeling

Two different engine configurations were simulated with a GT Power thermodynamic model coupled to a custom MatLab thermal model including temperature-swing thermal barrier material (TBM) coating model. The engines modeled were a modern 1.9-liter four-cylinder light-duty turbodiesel and a 1.1-liter two-cylinder supercharged, piston-compounded spark ignition (SI) engine, both with maximum outputs of ~110 kW. These were chosen to examine the effects of different dilution and exhaust energy recuperation levels. Performance of the engines was simulated at a number of operating points typical in a drive cycle, with various configurations of in-cylinder insulation. While more insulation configurations were modeled, with results presented in the quarterly reports, they have been simplified for this document to the four configurations presented below in Table V.8.1. The diesel engine only had power cylinder components and exhaust ports—the transfer ports and expander cylinder components were unique to the piston-compounded engine. Configuration 1 was the baseline with conventional materials used. Configuration 4, plotted as blue throughout this document, had insulation based on our exhaust port liners in the exhaust ports and other components downstream of the power cylinders. Configuration 5 (orange) extended this insulation into the power cylinders as well, covering the piston and head surfaces with a highly insulating coating, but with a very thick sealing layer that would prevent temperature swing. Finally, Configuration 9 (green) has the same insulation downstream of the power cylinders but uses what we believe to be a good representation of the temperature-swing coating with ceramic sealing layer, adjusted to account for the observed disparity between modelled and measured temperature swing. Notably, the total steady-state insulating potential of Configuration 5 in the power cylinder is roughly 12 times that of the temperature-swing insulation in Configuration 9, due primarily to the much thicker Ni microsphere layer.

Table V.8.1 Insulation Configurations for Turbodiesel and Piston-Compounded Engines

Config #	Power Cylinders' Piston & Head	Power Cylinders' Valve Faces	Transfer Ports	Expander Cylinders' Piston, Head, Valves	Exhaust Ports
1	Aluminum	Stainless Steel	Conventional	Al & Stainless Steel	Conventional
4	Aluminum	Stainless Steel	200 µm Inconel, 1 mm Ni Microspheres, 1 mm porous ceramic	200 µm Inconel, 1 mm Ni Microspheres, 1 mm porous ceramic	200 µm Inconel, 1 mm Ni Microspheres, 1 mm porous ceramic
5	200 µm Inconel, 1 mm Ni Microspheres, 1 mm porous ceramic	200 µm Inconel, 1 mm Ni Microspheres	Same as 4	Same as 4	Same as 4
9	5 µm Alumina, 20% $Depth_{1\%}$ (93 µm) Ni Microspheres, 0.5 mm Copper, with 130% Adjusted Temperature-Swing	5 µm Alumina, 20% $Depth_{1\%}$ (93 µm) Ni Microspheres, with 130% Adjusted Temperature-Swing	Same as 4	Same as 4	Same as 4

The impacts of these insulation configurations on the two engines is shown in Figure V.8.1, with solid lines for the piston-compounded engine and dashed lines for the diesel engine. Exhaust port insulation had minimal effect on the diesel engine's efficiency since the only path to recover this energy was through the turbocharger, but it could improve the piston-compounded engine's performance by up to 1%. Simultaneously, exhaust temperatures increased by up to 20°C in the diesel and by up to 100°C in the piston-compounded engine. The vast difference

mostly comes down to the hotter gas leaving the power cylinders in the SI piston-compounded engine, and the much greater surface area over which it could cool as it passes through the transfer ports, expander cylinder, and exhaust ports, all of which received some insulation. Adding either of the insulation configurations to the power cylinders improved brake specific fuel consumption (BSFC) by another 3%–5%, but the temperature-swing Configuration 9 ("Temp-Swing Power Cyl + Ports") has less than half the effect over the ports (and expander cylinder, if so equipped) alone on exhaust temperature as Configuration 5 ("High Cp Power Cyl + Ports"). These two forms of insulation accomplish their gains in efficiency in a much different manner.

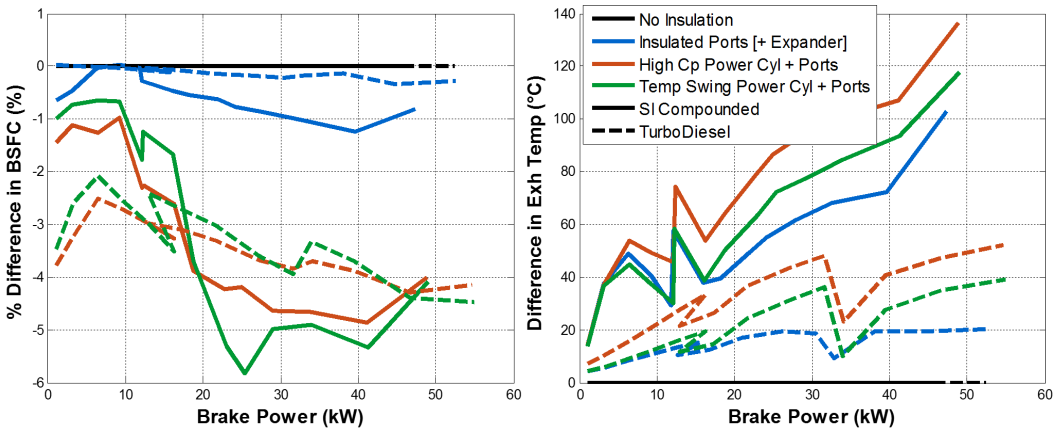

Figure V.8.1 BSFC and exhaust temperature improvements due to insulation configurations

Looking at the point at 21 kW brake power, the differences in these approaches can be seen clearly for all configurations of insulations and engines. The piston surface temperature is plotted to the left in Figure V.8.2, which shows the difference in response between the temperature-swing and high-Cp configurations. Also worth noting is the absolute difference in surface temperature between engine types; primarily this is due to the temperature of the combustion gasses because the SI piston-compounded engine operates stoichiometrically and only has two firing cylinders, while the diesel is leaner and at a lower cylinder-specific power because it is a 4-cylinder engine. This leads to a much greater thermal loading SI piston-compounded engine. However, the temperature-swing behavior allows both engines to recover just about the same amount of energy as brake work as an insulation with 12 times the steady-state thermal resistance because it does not affect the volumetric efficiency, nor does it heat the gas during compression with constantly hot walls. Both of these loss mechanisms require more crank work during the compression stroke to get to top dead center, which is shown by the negative portions of the instantaneous firing cylinder power from -180 to 0 crank angle degrees for the High Cp coating.

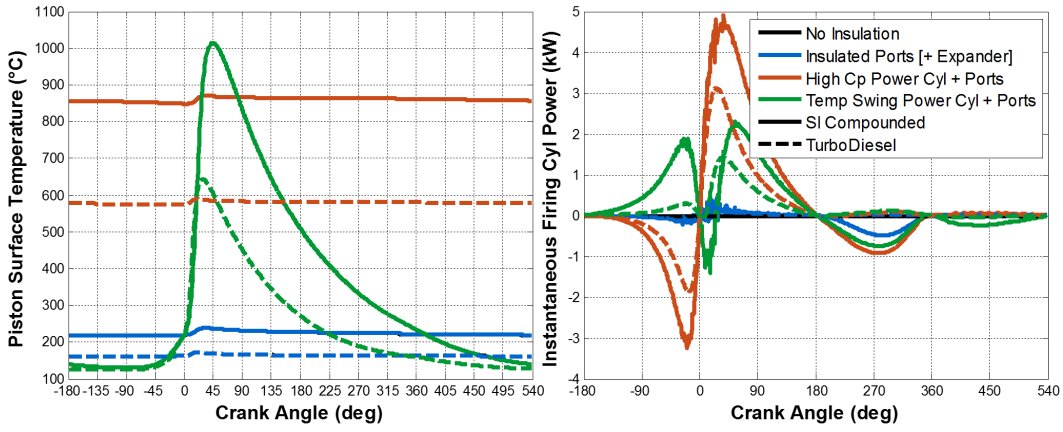

Figure V.8.2 Insulation configuration effects on piston surface temperature and instantaneous power for both engines

Beyond top dead center, the initial pressure for combustion is higher, and, thus, the final pressure after combustion is also higher, which compensates for the compression losses but ultimately does not redirect energy from the coolant to brake work as effectively. This is why the exhaust temperature with the High Cp coating is just about double—it prevents about 50% more heat losses from the power cylinder than the temperature-swing coating, but only recovers the same amount as brake work, so the rest of the energy redirected from the coolant ends up as an increase in exhaust temperature. These findings also neglect the impact of increased gas and wall temperatures on knock for the SI engine, which is expected to be significant since most of the points examined were knock-limited, or on mixing and combustion for the diesel engine, which could impact NO_x formation. Furthermore, most current engines are limited by the capabilities of their boosting devices, so any increases in volumetric efficiency could negatively impact the performance envelope of these engines. To summarize the modeling findings:

- Port insulation alone could effectively raise exhaust gas temperature, but could only appreciably improve efficiency when coupled with exhaust compounding.
- Theoretically, power cylinder insulations could increase engine brake efficiency, but temperature-swing coatings could do so without impacting volumetric efficiency or incurring penalties with hotter walls or gas prior to combustion (such as knock, diesel jet flame penetration and mixing).
- This application of thermal barrier materials allowed an overall reduction in heat losses to the coolant of up to 15% at the points tested, which additionally could be recovered as brake work through reducing the coolant flow capacity or total engine thermal mass for warm-up.
- The expander piston was able to recover approximately 10%–18% of the thermal energy that was kept in the gas from upstream (transfer port and power cylinder) insulation, enabling a recovery mechanism for any type of insulation applied to the power cylinder or port.
- Temperature-swing insulation was only important in the power cylinders; the expander and ports had the most benefit with conventional insulation because they do not experience the wide range of gas temperatures.
- Between 50% and 65% of the energy prevented from leaving the gas with temperature-swing coatings could be recovered in gross indicated work within the power cylinders.

Valve Fabrication and Testing

Experimental testing of several variations of TBC-coated and sealed valves has been completed. The purpose of these tests was to evaluate the coating durability resulting from changes in microsphere layer compression, microsphere selective filtering and layering, sealing foil thickness, and other processing variables. These tests were conducted on single exhaust valves installed in the single-cylinder engine with otherwise conventional metal components. Exhaust valves were chosen because they are by far the hottest component in the engine and should provide the most rigorous testing environment for these coatings. Figure V.8.3 shows a selection of the valves before and after testing. The majority of the second generation foil sealing layers show minimal punctures in the center of the coated region. However, all of the valves do exhibit edge erosion to various degrees. Maintaining the sealing layer across the step transition from the stainless steel valve surface around the periphery of the coating pocket to the microsphere surface is a challenge due to the potential for different thermal expansion rates of the solid steel versus the microsphere matrix, post-sintering heights (if the microsphere structure stands proud of the pocket, or is compressed to be below the lip of the pocket), and material compositions to which the Ni foil must sinter.

Figure V.8.3 Pre-test (top) and post-test (bottom) condition of coated valves

As an alternative to metal foil sealing, a ceramic sealing layer was investigated. This potential path was enabled by the improvements to the microsphere layer discussed above—the smoother, more consistent top surface and underlying structure of the microsphere matrix would enable another material to penetrate the topmost layer of cavities between microspheres, which could then be better supported by those microspheres. Furthermore, moving to a ceramic sealing layer interspersed between microspheres would reduce the specific heat of the sealing layer, allowing a thicker and potentially more durable layer to be applied without negatively impacting the temperature-swing effects, while still relying on the ductility of the microspheres for protection against repetitive thermal stresses. In order to create such a coating, sample disks coated with a microsphere layer were sent to an outside supplier to add a ceramic sealing layer. An alumina-based ceramic composition was downselected from this initial test round for application to a set of six exhaust valves, as shown in Figure V.8.4. Ceramic-sealed valves #2 and #3 were run in the engine to evaluate how well the sealing layer survived the in-cylinder environment. In both cases, no significant differences in engine performance were noted, as was expected based on the total amount of coated surface area. Multiple small pock-marks are visible across the surface after running the valve and generally appear to be surrounded by greater discoloration, indicative of higher local temperatures. However, no notable cracking or surface penetration was noted around the perimeter of the coated area, which is encouraging for future tests of parts with greater ceramic-sealed surface areas.

Figure V.8.4 Ceramic sealing layer exhaust valve images and thicknesses; far right: valve #2 after 18 h engine testing

Steel Piston Fabrication

Steel pistons with TBC applied to the piston crown were fabricated, with selected pistons shown in Figure V.8.5. The microsphere-based TBCs were sealed by Inconel and Monel foils with different thicknesses, as well as delivered without sealing layers with the intent of sealing with ceramic coatings through a second supplier. HRL has delivered 15 coated pistons to a supplier for machining and finishing, after a long and arduous process of attempting to quench and temper the steel pistons to attain the harness within the specifications requested by the supplier. However, machining problems attributable to the hardened specification that they requested have delayed shipment of the completed pistons to General Motors for testing;

apparently the quenching and tempering hardening process has prevented successful machining, despite achieving the desired surface harness requested by the supplier. Further information from the supplier concerning the status of some pistons is still outstanding, but a few of the machined pistons have been delivered and will be tested. A plan to recover many of the other pistons has been formulated; they will be annealed to remove any residual stresses and the effects of the prior hardening process and will be re-machined and coated to allow a more broad test matrix that aligns with the discoveries made through the recent modeling work.

Figure V.8.5 Insulating and sealing layer configurations on steel pistons: top view and underside machined view

Exhaust Port Liner Fabrication

Figure V.8.6 summarizes the fabrication process for the exhaust port liners. Once the completed port liner was created following the steps delineated in this figure, the port liner was packed with ceramic media and cast within aluminum. No damage, shrinking, or warping was detected in the port liner as a result of the aluminum casting. A cross section was taken at the middle of the part and polished to obtain scanning electron microscopy imaging and energy dispersive spectroscopy analysis. The results of this imaging, shown in Figure V.8.7, show the interface between the aluminum and the protective ceramic layer over the microspheres. The casting process was successful, and the aluminum did not cause any damage to or degradation of the ceramic coating or underlying thermal microsphere coating. Additionally, Figure V.8.7 shows that the spraying and curing process of the ceramic caused significant void fractions within the ceramic, which will further decrease the effective thermal conductivity of the port liner to make it more effective.

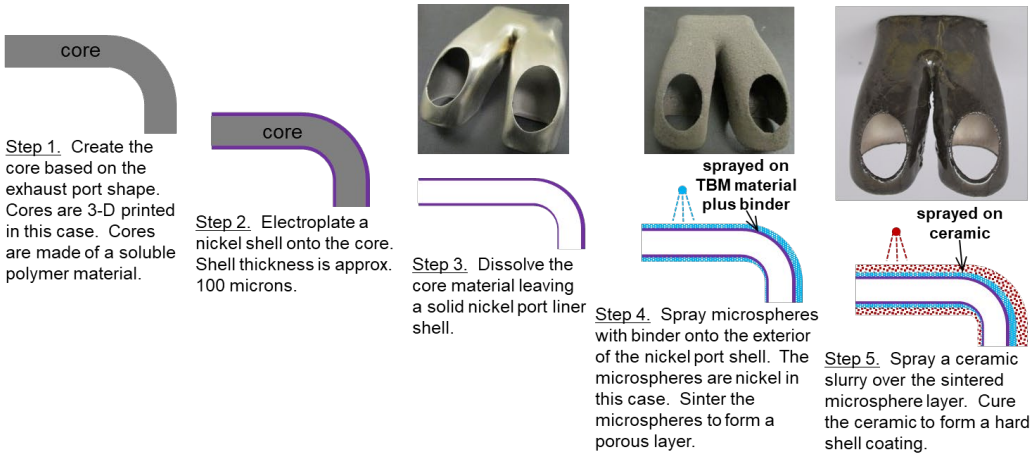

3-D – three dimensional

Figure V.8.6 Exhaust port fabrication process

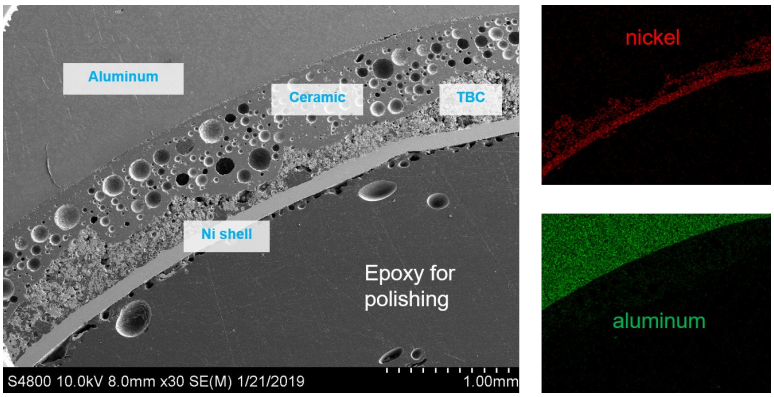

Figure V.8.7 Scanning electron microscopy and energy dispersive spectroscopy of port liner cross-section showing aluminum casting success

Conclusions

- Optimized temperature-following TBC, including thermal conductivity, heat capacity, and mechanical durability with input from thermal and thermodynamic modelling
- Improved microsphere matrix surface smoothness, consistency, packing density, and re-optimized microsphere properties to maintain temperature-swing performance
- Developed two non-dependent sealing methods for microsphere TBC coatings enabled by the above microsphere matrix improvements with different applicabilities and traits
- Improved methods to apply TBC to valve faces, piston crowns, and exhaust port liners
- Fabricated coated valves, steel pistons and exhaust port liners.

Next steps:

- Evaluate permeability of current sealing layer technologies with fuel contaminant intrusion evaluation
- Test coated steel pistons and quantify efficiency gains, durability, and permeability
- Evaluate different TBC and sealing layer properties and analyze performance in the engine
- Cast cylinder heads with TBC-coated exhaust port liners and conduct engine tests.

V.9 CERC-TRUCK – U.S.-China Clean Energy Research Center (CERC), Truck Research Utilizing Collaborative Knowledge (TRUCK) (Argonne National Laboratory)

Vincent Freyermuth, Principal Investigator
Argonne National Laboratory
9700 S. Cass Avenue
Lemont, IL 60439
E-mail: vfreyermuth@anl.gov

Gurpreet Singh, DOE Program Manager
U.S. Department of Energy
E-mail: Gurpreet.Singh@ee.doe.gov

Start Date: April 1, 2018 End Date: September 31, 2019
Project Funding: $26,338,760 DOE Share: $12,500,000 Non-DOE Share: $13,838,760

Project Introduction

The project is a collaboration between U.S. and China partners to develop technologies that will lead to the commercialization of clean vehicle solutions for medium-duty (MD) and heavy-duty (HD) trucks. The project research efforts are divided into five topic areas with an overall goal of increasing freight efficiency by 50% over a 2016 baseline.

Topic Area 1 is divided into two tracks focusing on MD and HD applications. In the MD track, Cummins, as the lead partner, is developing a new natural gas engine that will be integrated in a MD range extender powertrain solution for a delivery van. In the HD track, the University of Michigan is developing a low-temperature combustion system using low-life-cycle carbon fuels. The main objective of Topic Area 2 is to maximize fleet efficiency through advanced energy management at the vehicle, multivehicle, and fleet levels. Topic Area 3 focuses on all aspects of powertrain electrification and architectures. Topic Area 4 considers reductions in weight, drag coefficient, and tire rolling resistance to further improve efficiency. Finally, Topic Area 5 integrates the technologies from the other prior topic areas into a vehicle to demonstrate the freight efficiency improvement.

Objectives

The overall objective is to demonstrate technologies on a vehicle that will achieve a 50% increase in freight efficiency over a 2016 baseline. Detailed objectives for Fiscal Year 2019 are as follows:

- To explore the ignition behavior of potential low-life-cycle greenhouse gas fuels to assess fuel properties;
- To define the engine requirements;
- To determine the choice and location of air-handling actuators and sensors;
- To explore the electrified MD powertrain architectures for a pickup and delivery van;
- To test the baseline vehicle over selected duty cycles;
- To develop MD and HD route prediction algorithms; and

- To develop technologies for lightweight components, reduced aerodynamic drag, and low-rolling-resistance tires.

Approach

The project is large in scope and covers many areas of expertise, each necessary to reach the goal of 50% freight efficiency improvement. Several partners are involved in the project. Cummins, the main industrial partner, focuses on the development of a new natural gas engine suitable for MD range extender applications. Cummins also leads the vehicle demonstration. The University of Michigan, working along with Aramco Services Company, studies the suitability of low-life-cycle carbon fuels as replacements in HD engines. Purdue University focuses on specific controls, actuators, and sensors for the new natural gas engine developed by Cummins. Argonne National Laboratory and Oak Ridge National Laboratory work on modeling and hardware testing of vehicle communication (vehicle-to-infrastructure and vehicle-to-vehicle), automation, and other vehicle-level technology that will help reduce fuel consumption. The Ohio State University focuses on selection of the appropriate powertrain architecture for the pickup and delivery demonstration vehicle and on the development of battery systems that integrate different battery chemistries. Finally, Freightliner Custom Chassis Corporation focuses on the reduction of component weight, aerodynamic drag, and tire rolling resistance.

Results

Baseline Vehicle

A Class 5 walk-in van was chosen as the vehicle of choice for the MD research and for the vehicle demonstration. The baseline vehicle is an MT55 Freightliner truck with a GM 6L gasoline engine. Three drive cycles were selected and will be used to evaluate fuel consumption and freight efficiency of the baseline vehicle and of the demonstration vehicle. The freight efficiency demonstration will occur on a cycle that is developed using portions of the FTP-75 (Federal Test Procedure), and the two additional cycles will be used to understand the impact on criteria emissions for future certification strategies. Cummins completed the fuel economy testing of the baseline vehicle at the HD chassis dynamometer at The Ohio State University. Cummins also performed standard noise measurement tests of the baseline vehicle. Both fuel economy and noise tests will be performed again with the demonstration vehicle. The baseline vehicle will not be modified so that further testing, including on-road testing, will be possible later in order to compare results with those for the demonstration vehicle. The data from the baseline testing were used to validate the models used for predicting fuel economy.

The partners have developed a path to target for meeting the 50% freight efficiency goal. Figure V.9.1 highlights the benefits of the different technical solutions. The vehicle provides a 135+% improvement compared to the baseline gasoline vehicle and a 70+% improvement in freight efficiency compared to the conventional diesel powertrain. The hybrid component provides significant fuel economy savings, but when the hybrid is evaluated for freight, the savings decline because of the added weight from the battery, machines, and other power electronics.

Engine Development

Cummins has modified a current diesel engine platform to make it suitable for natural gas. The design takes into consideration the potential use of gasoline, natural gas, and propane. The attributes of the engine design are shown in Figure V.9.2. Cummins has completed the design and design analysis. The concept layout incorporates the complete engine system, including the crank/bearings, block, head, head gasket, lube and cooling, gear train, valve train, air handling, fuel system, integration, and control unit/electronics/wiring. The design further includes extensive three-dimensional modeling of flows, combustion, and stress for the engine structure and will include mule engine testing to guide and validate analyses.

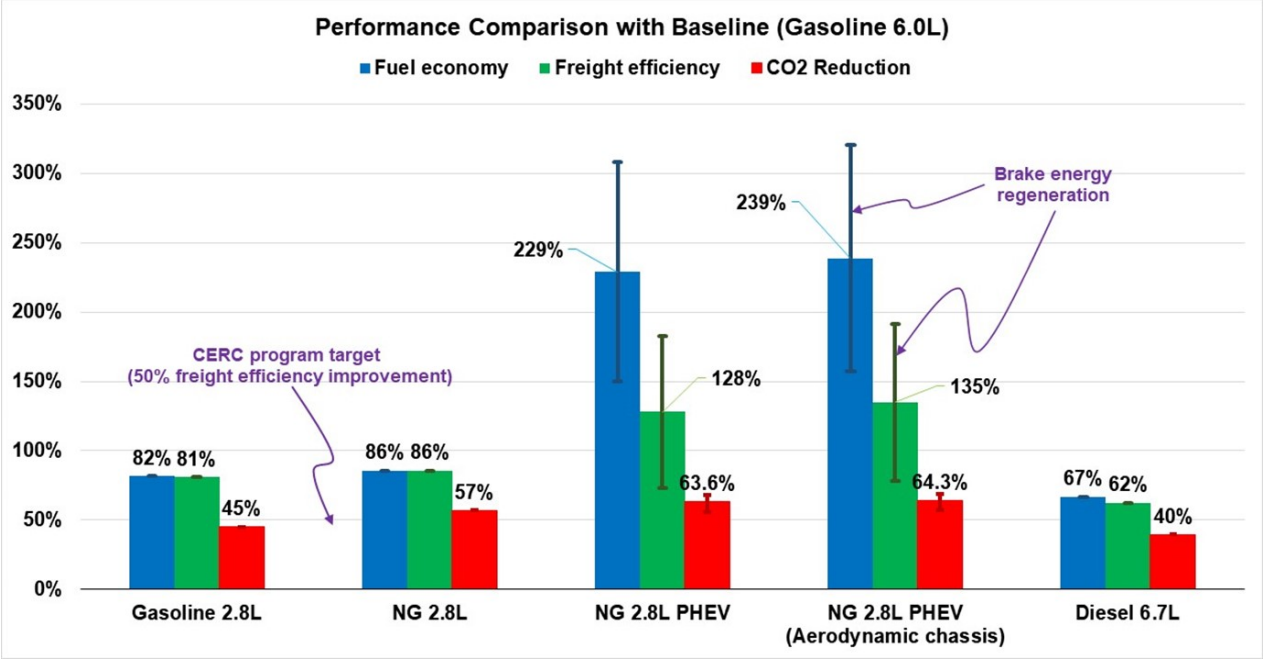

NG – natural gas; PHEV – plug-in hybrid electric vehicle

Figure V.9.1 Path to target for meeting the 50% freight efficiency improvement

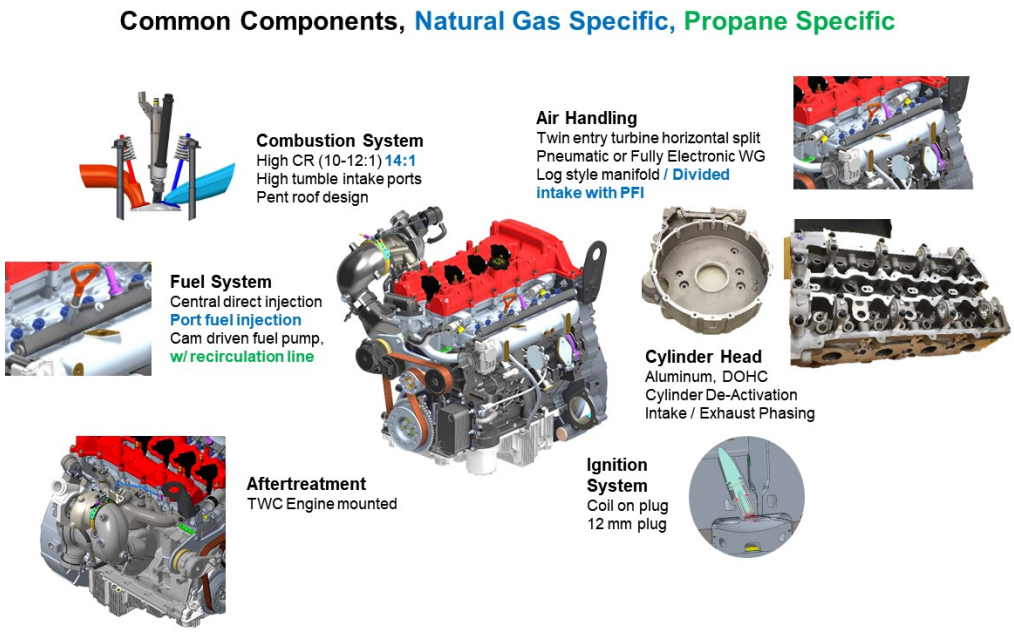

CR – compression ratio; WG – water gauge; PFi – port fuel injection; DOHC – dual overhead camshaft; TWC – three-way catalyst

Figure V.9.2 Engine design considerations

All components successfully completed design reviews and are now in the procurement phase. A major accomplishment has been the delivery of the prototype of the cylinder and head and valve cover, shown in Figure V.9.3. The overall requirements for the engine subsystem are detailed in Table V.9.1.

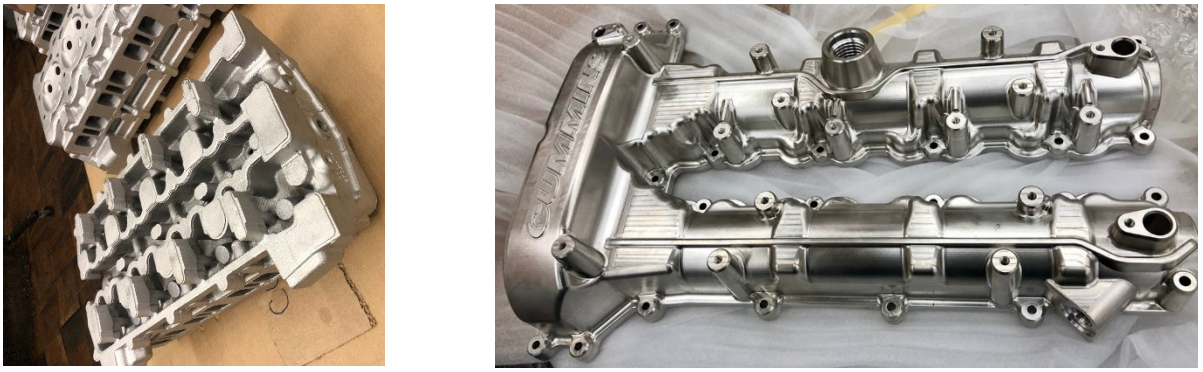

Figure V.9.3 Prototype cylinder head and valve cover

Table V.9.1 Engine Subsystem Requirements

Peak Torque	460 Nm @ 2,000–3,600 rpm
Rated Power	173 kW / 3,600 rpm
Vehicle Performance (% grade @ vehicle speed)	25% @ 13 kph, 10% @ 48 kph, 1.25% @ 105 kph
Certification (emissions/on-board diagnostics)	U.S. Environmental Protection Agency 2027+
Freight Efficiency	50% improvement from baseline
All-Electric Range	40 miles all-electric range

Purdue University has led an analysis for the selection and placement of sensors and actuators. A nonlinear physics-based engine model was developed and validated with GT-Power software. Two frameworks were developed to design sensing strategies for engine air-handling systems to reduce brute-force experimentations and calibrations. The first framework computes the optimal sensor sets and their Kalman-filters based on sensor characteristics to best estimate the intake manifold oxygen fraction. The results indicate that the exhaust gas recirculation delta pressure sensor is the best single sensor set for the estimation among five candidate sensors. The optimal two-sensor set is exhaust gas recirculation delta pressure and inlet air flow sensor, which is better than any other combinations and reduces the error by 15%. This framework can also be used to select optimal signals and design observers for other non-measurable key parameter estimations in future work. The second framework simultaneously co-designs the robust sensing and controlling strategies to meet the performance requirements. Three different sensing scenarios are analyzed and the corresponding controllers are designed by this framework to maintain cylinder air-to-fuel ratio and track desired torque curve.

Purdue also developed a physics-based model for engine cylinder charge air flow estimations. This work is to directly calculate the air flow into the cylinder at steady-state and transient operations based on measurable parameters. This model is being validated with GT-Power truth-reference model. The deliverables of this work can be used as a virtual charge air flow sensor that is robust across vehicle configurations.

On the HD side, the University of Michigan has completed studies on gasoline compression ignition fuel formulation and explored the fuel composition effects of gasolines that lead to the widest range of operability, as defined by a multidimensional optimization function. A gasoline with an intermediate octane number but some amount of octane sensitivity provides optimum merit values not only at low-load but also at high-load

conditions. High octane sensitivity can increase operable range at entire load conditions since high-sensitivity fuel is more reactive at low-load, high-intake-temperature conditions and less reactive at high-load boosted conditions than low-sensitivity fuel.

Vehicle-Level Improvements

Freightliner Custom Chassis Corporation, through multiple iterations of computational fluid dynamic modeling, developed new concepts showing reduction of aerodynamic drag losses of up to 60% (Figure V.9.4). Vehicle front-end optimization contributes to the major share of the air drag benefit with up to a 46% reduction. Underbody flow optimization contributes to a vital 7% air drag benefit. The addition of a boat tail reduces the rear wake separation considerably, and the converging guide surfaces into the rear wake bring another 7% reduction.

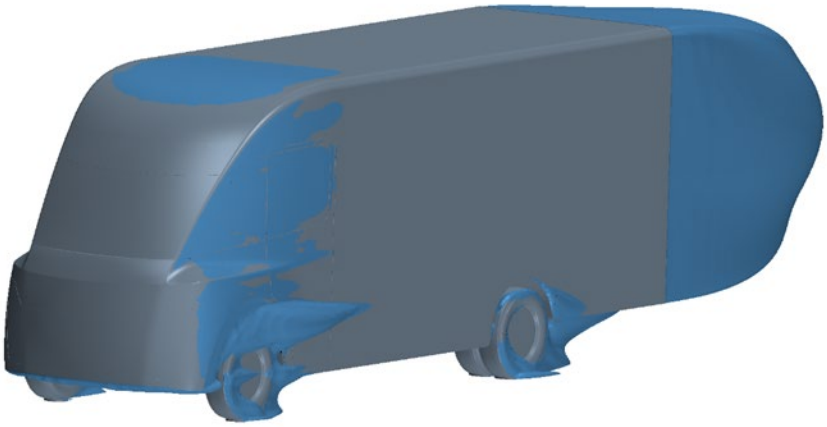

Figure V.9.4 Stylized representation of truck shape based on aerodynamic studies

In order to reduce component weights, traditional steel is being replaced by aluminum in rails and cross members. The design was finalized, and prototypes of the components are now being developed by suppliers. Work is also continuing on the use of carbon fiber to reduce weight in the front axle and suspension. New joining techniques using riveted connections are showing great potential for weight reduction when compared to traditional screw fastener options. A 60% reduction has been demonstrated, but the absolute impact is minimal at 3.64 kg.

Freightliner, working along with Michelin, developed a new low-resistance tire. The tire prototype phase is finished, and homologation testing is underway. The measured rolling resistance of the new tire is 5.1 kg/T.

Hybrid Powertrain Architecture Selection

The Ohio State University developed a methodology to evaluate a variety of powertrain solutions. The powertrain design space is defined using several powertrain architectures, limited to series plugin with a range extender engine, battery pack, and various component sizes. Powertrains with and without transmissions were considered, including fully automatic transmissions with and without torque converter; automated transmissions; and E-axles with two-, three-, and four-speed transmissions (Zhao et al. 2018; Jung, Ahmed, and Rizzoni 2018; Jung, Ahmed, Zhang, and Rizzoni 2018).

The best fuel economy was achieved with an E-axle with a two-speed transmission. The single-speed E-axle has 6% better fuel economy because of the reduced gearing losses, but the grade requirement cannot be met.

Route Prediction Algorithm

Argonne National Laboratory has developed an MD version of Stochastic Vehicle Trip Prediction (SVTRIP), a software tool that can predict vehicle speed traces given origin/destination information. SVTRIP requires a large amount of vehicle data to construct the probability matrices used to predict vehicle speed. SVTRIP was originally designed for passenger cars, and the process was built using a large amount of passenger car duty cycles. The process has been adapted using data provided by Cummins to represent MD truck applications. Origin/destination information is sent to a mapping software such as HERE or Google Maps to gather route information, including speed limits, global positioning system information, and locations of stop signs and red lights. The information is then used along with the probability matrices to develop a 1-Hz speed profile of a vehicle along that route.

Conclusions

The following research was completed this year:

- A Freightliner MT55 pickup and delivery van was selected as the demonstration vehicle.
- The method for measuring freight efficiency gain was defined, and three duty cycles were selected.
- The fuel economy and noise characteristics of the baseline vehicle were measured.
- The design of the natural gas engine for the vehicle demonstration was successfully completed.
- A two-speed E-axle range extender powertrain with a 74 kWh battery was selected as the powertrain of choice for the demonstration vehicle.
- A speed prediction algorithm based on origin/destination was developed for MD trucks.

Key Publications

1. Zhao, T., Q. Ahmed, and G. Rizzoni. 2018. “Influence of Battery Charging Current Limit on the Design of Range Extender Hybrid Electric Trucks.” Paper presented at Vehicle Power and Propulsion Conference, Chicago, IL.
2. Jung, D., Q. Ahmed, and G. Rizzoni. 2018. “Design Space Exploration for Powertrain Electrification Using Gaussian Processes.” Paper presented at American Control Conference, Milwaukee, WI.
3. Jung, D., Q. Ahmed, X. Zhang, and G. Rizzoni. 2018. “Mission-Based Design Space Exploration for Powertrain Electrification of Series Plugin Hybrid Electric Delivery Truck.” SAE Technical Paper 2018-01-1027.

Acknowledgements

Thomas Wallner of Argonne National Laboratory contributed to this research and coauthored this report.

Argonne National Laboratory thanks its partners in this project: Cummins Inc., Freightliner Custom Chassis Corporation, Aramco Services Company, Ohio State University, Purdue University, University of Michigan, and Oak Ridge National Laboratory.

VI Lubricant Technologies

VI.1 Power Cylinder Friction Reduction through Coatings, Surface Finish, and Design (Ford Motor Company)

Dr. Arup K. Gangopadhyay, Principal Investigator
Ford Motor Company
2101 Village Road
Dearborn, MI 48121
E-mail: agangopa@ford.com

Dr. Ali Erdemir, Principal Investigator
Argonne National Laboratory
9700 S. Cass Avenue
Lemont, IL 60439
E-mail: erdemir@anl.gov

Michael Weismiller, DOE Technology Development Manager
U.S. Department of Energy
E-mail: Michael.Weismiller@ee.doe.gov

Start Date: January 1, 2015 End Date: December 31, 2019
Project Funding (FY19): $1,070,000 DOE share: $820,000 Non-DOE share: $250,000

Project Introduction

About 7%–10% of the total energy input in a vehicle is lost due to mechanical friction [1]. In an engine, about 60% of the total frictional losses occur at the interface between the cylinder and pistons and piston rings, and about 30% at the bearings [2]. The goal of this study is to demonstrate friction reduction potential using advanced high porosity (HP) plasma transfer wire arc (PTWA) coatings, surface finish, and design on the power cylinder system containing cylinder bore, piston rings, piston skirt, bearings and crankshaft, and advanced engine oils. Experience through years of research in this area leads us to believe that full benefit potential can be realized only by considering a systems approach.

This project developed (a) a process for depositing and honing HP PTWA coatings to achieve different porosity levels with improved surface finish on free-standing cylinder liners [3] and engine blocks [4]; (b) various techniques for characterizing coatings, including porosity area percent, porosity size distribution, oxide content, etc. [3]; (c) a method for achieving micro-polishing crankshaft journals [3]; (d) a technique for depositing nano-composite vanadium nitride (VN)-Cu and VN-Ni coatings on piston rings and piston skirts [3]; (e) a method for laboratory friction and wear assessment for generating Stribeck curve [3]; (f) a method for evaluating friction reduction potential of PTWA coatings and micro-polished journals using a motored cranktrain rig [4]; and (g) a method for evaluating wear (durability) of PTWA coatings and ring coatings using radiotracer method.

Objectives

Overall Objectives

- Demonstrate deposition of PTWA coatings at various porosity levels on liners and engine blocks with improved surface finish
- Develop and demonstrate deposition of nano-composite coatings on piston rings and skirts

- Demonstrate friction benefits of micro-polished crank journals
- Demonstrate friction benefits through laboratory bench, motored cranktrain and engine, fired single cylinder engine, and chassis roll dynamometer (vehicle) tests
- Demonstrate durability of PTWA coatings using radiotracer technique.

Fiscal Year 2019 Objectives

- Demonstrate friction benefit of ring face coating technologies in laboratory bench, motored single cylinder, and motored engine cranktrain tests
- Demonstrate friction benefit in motored engine tests
- Demonstrate wear performance of HP PTWA coating
- Demonstrate fuel economy benefits in chassis roll dynamometer tests.

Approach

The project goal of delivering 4% fuel economy improvement over current (2014) technologies can be achieved through a technology bundle comprising (a) deposition of low friction coating (HP PTWA) on cylinder bores, (b) low friction nano-composite and other thin film coatings on piston rings, (c) improved surface finish on cylinder bores and crankshaft, and (d) novel engine oil formulation (polyalkylene glycol), an outcome of a previously DOE-funded project.

Achieving the project goals necessitated partnering with key suppliers including (a) Comau for deposition of bore coatings, (b) Gehring for cylinder bore honing of PTWA coatings, (c) Future Tools for mechanical roughening treatment prior to coating deposition, (d) NETZSCH for assessment of coating thermal properties, (e) Mahle and KS for low friction piston skirt and piston ring coatings, (f) Southwest Research Institute for single cylinder fired engine tests, and (g) Dow Chemical Company for novel polyalkylene glycol engine oil.

Results

It was indicated in the last report [5] that although the engine blocks had high porosity levels, they were lower than the target values. A significant effort was put to resolve the issue. The initial focus was on identifying a plasma torch with the correct flame spray characteristics. Several plasma torches were tried but were not able to produce the desired high porosity level. Therefore, the focus was shifted to identifying suitable honing conditions to reach targeted porosity levels. Using a design matrix, appropriate honing conditions were identified to reach high porosity levels. This is an important step in generating HP PTWA coating on (a) cast iron liners for single cylinder fired engine friction evaluation and (b) aluminum engine blocks for wear measurements on HP PTWA coating and piston rings using radiotracer method.

Motored Cranktrain Friction Assessment

Cranktrain friction was evaluated using a block from an I-4 engine. The friction contributions on this rig are from the bearings (main and connecting rod), piston skirt, and piston rings in contact with cylinder bore. GF-5 SAE 5W-20 engine oil was used at 40°C, 60°C, 100°C, and 120°C. The blocks were carefully assembled to maintain a fixed piston-to-bore clearance and nominal bearing clearance to avoid confounding factors affecting friction results. Engine blocks with HP PTWA coatings having various porosity levels were evaluated against current production piston rings, and the results were reported last year [5]. This year, the efforts were focused on friction evaluation in contact with various ring face coatings. Figure VI.1.1 shows friction torque at 120°C oil temperature for engine blocks with cast iron liner and HP PTWA 3 coating in contact with production, nitride, diamond-like carbon (DLC), and physical vapor deposition (PVD) piston rings. The results indicate HP PTWA 3 block offered 10% friction reduction over cast iron liner block at 1,500 RPM with production rings. Nitride, PVD, and DLC rings offered friction advantage over production rings with cast iron liner at engine

speeds greater than 1,500 RPM. These rings offered additional friction advantage with HP PTWA 3 coating, and specifically, DLC rings offered 22% lower friction compared to cast iron liner with production rings.

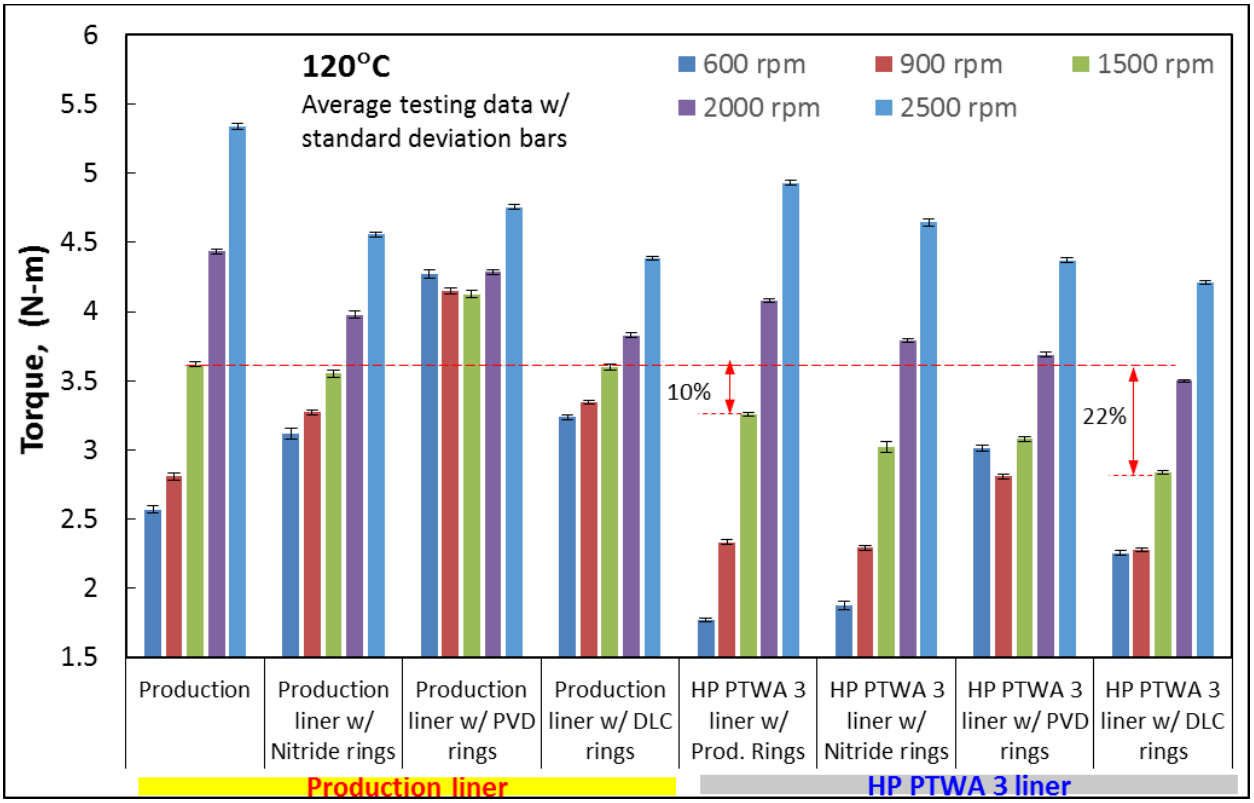

Figure VI.1.1 Cranktrain friction as a function of crankshaft speed at 120°C oil temperature for HP PTWA 3 coating and cast iron liner in contact with production, nitride, DLC, and PVD piston rings

Motored Single Cylinder Friction Assessment

Friction force measurements were conducted under unpressurized conditions using the motored single cylinder rig. The rig measures friction force at piston (and piston ring) and cylinder liner contact. The measurements were completed with both current production cast iron liner and HP PTWA coated liners in contact with different ring face coatings at various temperatures. Results in Figure VI.1.2 show friction force measured as a function of crank angle at 500 RPM and 100°C oil temperature using GF-5 SAE 5W-20 oil. Crank angles 0 to 180 represent piston motion in one direction, while crank angles 180 to 360 represent motion in the opposite direction. The area under the curve represents friction force for one complete rotation of the crankshaft. In the case of cast iron liner, the nitride rings showed a distinct friction advantage. The friction advantage of HP PTWA 3 coating with production rings can be clearly seen. The combination of HP PTWA 3 coated block in contact with nitride rings showed a significant friction benefit over cast iron liner with production rings.

Motored Engine Friction Assessment

Figure VI.1.3 shows motored engine friction results obtained using various HP PTWA coatings compared with production cast iron block with production piston rings using GF-5 SAE 5W-20 oil at 100°C. HP PTWA 3 showed an average (over engine speed range investigated) 5.2% lower friction.

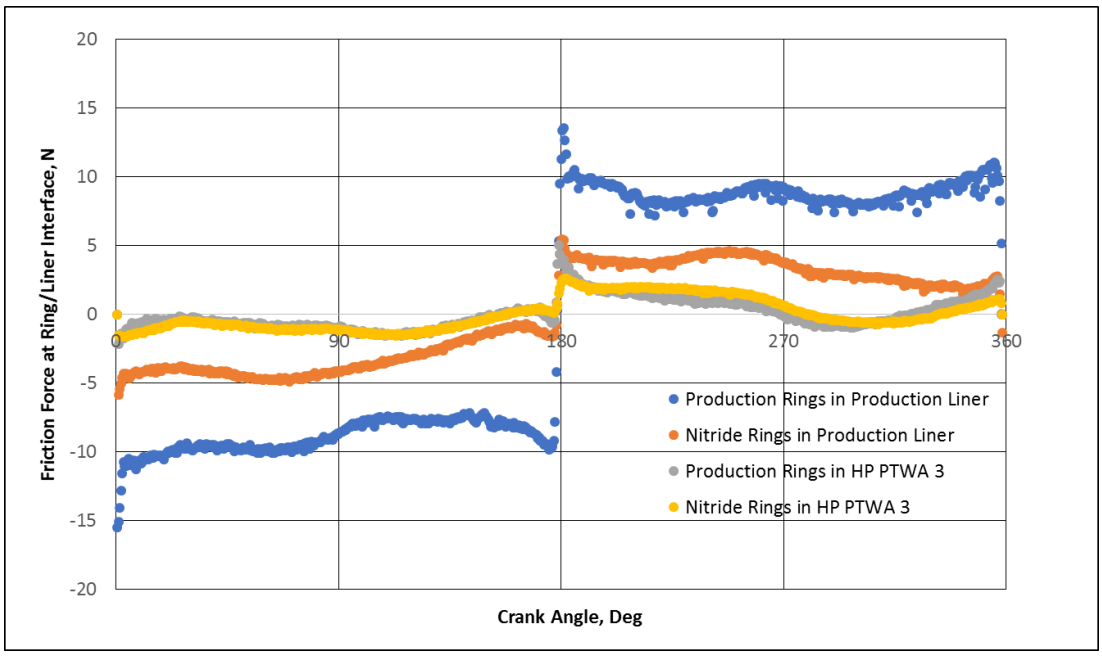

Figure VI.1.2 A comparison of friction force as a function of crank angle at piston and liner contact between production ring and liner with HP PTWA 3 coating and nitride rings at 500 RPM engine speed and 100°C oil temperature

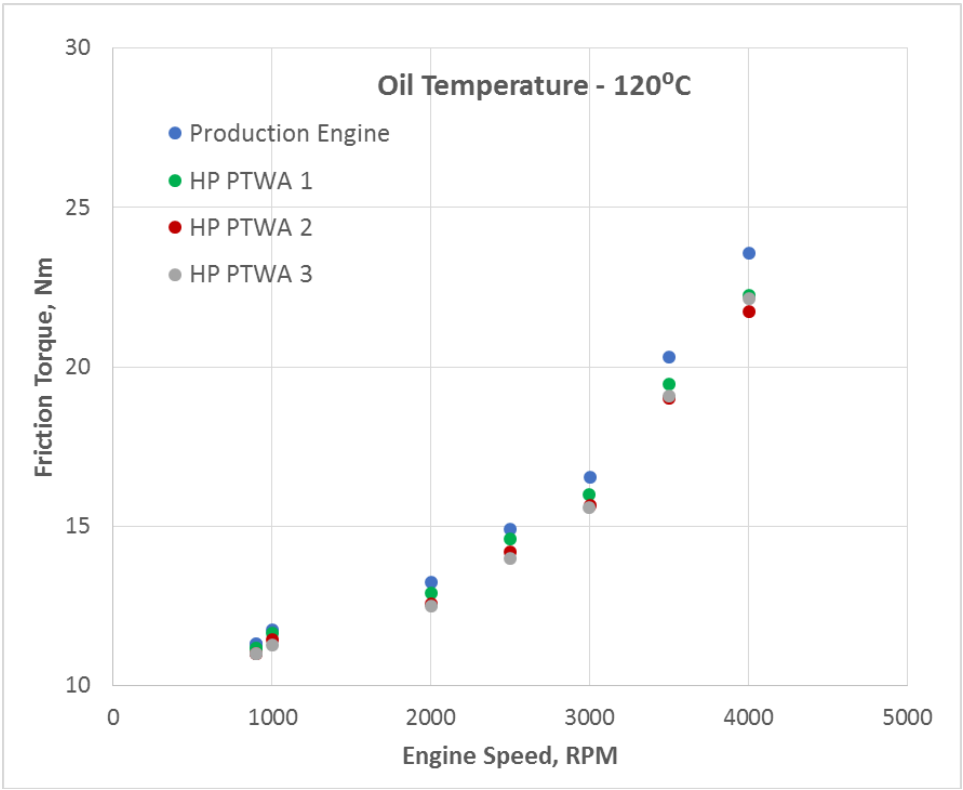

Figure VI.1.3 Motored engine friction torque as a function of engine speed at 120°C oil temperature for three variants of HP PTWA coatings

Motored Cranktrain Wear Assessment

Cylinder bore wear measurements were conducted using a motored cranktrain rig where the top dead center area of one of the four cylinders was activated to Co^{56} using proton beam. Wear measurements were done with current production, PVD, and DLC rings with one engine block with cast iron liner and another block with HP PTWA 3 coated block using GF-5 SAE 5W-20 oil at 100°C. The radioactive wear debris generated from wear was circulated in a closed circuit through a radiation detector. The intensity of radioactivity in engine oil was translated into wear rate as mass loss per hour. The engine speed was quickly ramped from 1,000 RPM to 3,500 RPM in less than a minute to allow more transient conditions to promote wear. Due to the long test duration (about 140 hours), two tests were run on production cast iron liner with production rings and the wear rate was found to be within 20%. Figure VI.1.4 shows that the wear rate of HP PTWA 3 coated block is similar to cast iron block with production and PVD rings while DLC rings showed lower wear rate with cast iron block. However, the wear rate of HP PTWA 3 coated block was lower with DLC rings than cast iron liner with production rings.

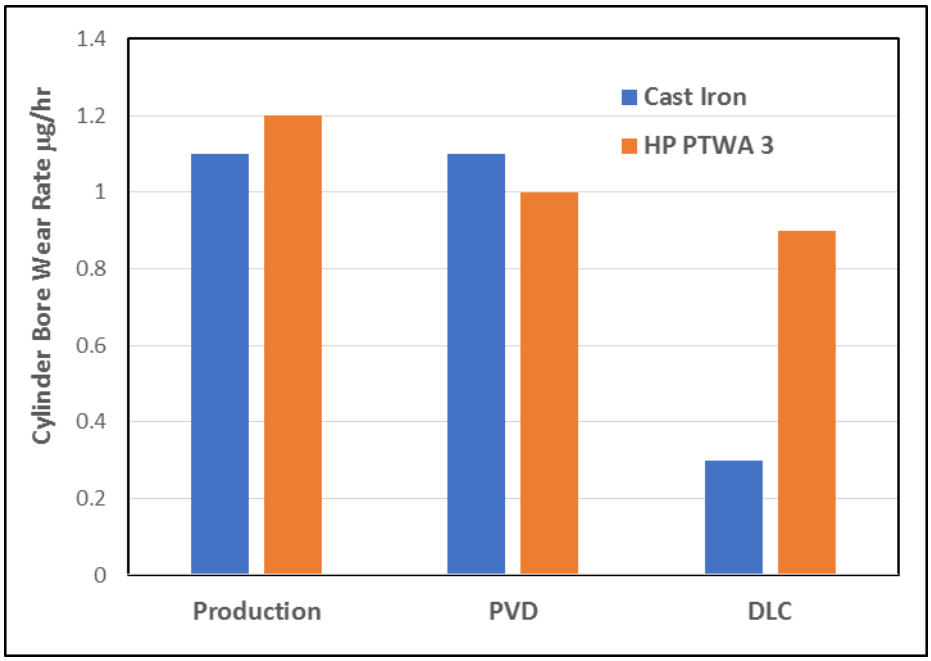

Figure VI.1.4 A comparison of cylinder bore wear rate between cast iron liner and HP PTWA 3 coating in contact with production, PVD, and DLC ring coatings

Conclusions

- HP PTWA 3 coating showed an average 5.2% friction benefit over cast iron liner block in motored engine friction tests.
- Ring face coatings offer additional (up to 12%) friction benefit with HP PTWA 3 coating.
- HP PTWA 3 coating showed similar wear rate to cast iron liner material.

References

1. Pinkus, O., and D.F. Wilcock. 1977. “Strategy for Energy Conservation through Tribology.” New York, ASME.
2. Kiovsky, T.E., N.C. Yates, and J.R. Bales. 1994. “Fuel Efficient Lubricants and the Effect of Base Oils.” *Lubrication Engineering* 50 (4): 307.

3. Gangopadhyay, A., and A. Erdemir. 2017. “Power Cylinder Friction Reduction through Coatings, Surface Finish, and Design.” Fuel and Lubricant Technologies 2016 Annual Report, U.S. Department of Energy, Vehicle Technologies Office, Washington, DC.

4. Gangopadhyay, A., A. Erdemir, G. Ramirez, and O. Eryilmaz. 2018. “Power Cylinder Friction Reduction through Coatings, Surface Finish, and Design.” Advanced Combustion Systems and Fuels 2017 Annual Progress Report, U.S. Department of Energy, Vehicle Technologies Office, Washington, DC.

5. Gangopadhyay, A., and A. Erdemir. 2019. “Power Cylinder Friction Reduction through Coatings, Surface Finish, and Design.” Advanced Combustion Engines and Fuels 2018 Annual Progress Report, U.S. Department of Energy, Vehicle Technologies Office, Washington, DC.

Acknowledgements

Dr. Osman Eryilmaz of Argonne National Laboratory also contributed to this research and coauthored this report.

VI.2 Integrated Friction Reduction Technology to Improve Fuel Economy without Sacrificing Durability (George Washington University)

Stephen Hsu, Principal Investigator
George Washington University
323C Exploration Hall, 20101 Academic Way
Ashburn, VA 20147
E-mail: stevehsu@gwu.edu

Tim Cushing, Principal Investigator
GMC
GM Technical Center
Warren, MI 48090
E-mail: timothy.cushing@gm.com

Gefei Wu, Principal Investigator
Valvoline New Product Development Lab
251 Yorkshire Blvd.
Lexington, KY 40509
E-mail: gwu@valvoline.com

Michael Weismiller, DOE Technology Development Manager
U.S. Department of Energy
E-mail: Michael.Weismiller@ee.doe.gov

Start Date: October 1, 2014 End Date: December 30, 2019
Project Funding: $2,000,000 DOE share: $1,000,000 Non-DOE share: $1,000,000

Project Introduction

The use of petroleum-based fuels to propel vehicles to transport people and goods is the major oil use in the United States, resulting in yearly oil imports of about 10 million barrels of oil per day in 2016. Improving the fuel economy of cars and trucks will reduce U.S. dependence on foreign oil. The new Corporate Average Fuel Economy standard has raised fuel economy of cars and light trucks from 27.5 mpg in 2012 to 54.5 mpg by 2025. This project supports the energy independence goal.

In a worldwide effort to improve fuel economy, Japanese automakers have introduced a new class of ultra-low viscosity lubricants to reduce drag, hence improving fuel economy. This new class has three viscosity grades: 0W-16 (defined by 2.3 mPa.s high temperature high shear viscosity at 150ºC), 0W-12 (2.0 mPa.s), and 0W-8 (1.7 mPa.s). The technical concern for these ultra-low viscosity oils is that the resultant thin oil film thickness may cause wear. This project aims to (1) develop a prototype 0W-20 low viscosity oil and demonstrate that it can improve fuel economy by 2%, the oil is backward compatible, and it is suitable for use by current cars and light trucks; (2) develop a prototype 0W-16 ultra-low viscosity oil and demonstrate that it can improve fuel economy by 2% against current commercial oils for future cars; and (3) develop surface materials technologies to maintain current durability for future engines using ultra-low viscosity oils.

Objectives

Overall Objectives

- Develop 0W-20 and 0W-16 low viscosity lubricants that will improve fuel economy by 2%
- Conduct ASTM standard engine tests at the time of development to verify their fuel efficiency
- Measure engine durability using ultra-low viscosity lubricants
- Assess the effects of surface textures, coatings, and microcapsules on fuel economy.

Fiscal Year (FY) 2019 Objectives

- Complete fabrication of surface textures on the new 2018 platform engine for fuel economy testing
- Complete engine testing on surface textures and microencapsulated friction modifiers.

Approach

1. Establish a vertically integrated research team with engine manufacturer, oil marketer, and additive companies to develop the low viscosity lubricants and conduct engine tests to assess fuel economy.
2. Valvoline and GM are partners in this project. They provide formulation assistance and engine testing on ultra-low viscosity lubricants and subsequent engine durability testing.
3. George Washington University conducts basic and applied research in additive evaluation, additive interactions, and microencapsulation of additives, surface texture (design and fabrication techniques).

The team was organized in 2014 at the initialization of this project. During the past 5 years, many industrial and research organizations have contributed over 120 samples of base oils and additives to the effort. For the GF-6A category, several 0W-20 formulations were developed and tested in ASTM Sequence test VI-E and achieved 2.4% fuel economy improvement against current commercial lubricants, meeting the key DOE program goals. For future vehicles, four generations of GF-6B 0W-16 formulations were developed and achieved 2.1% fuel economy improvement in ASTM Sequence VI-E. For future vehicles, a 2018 platform engine with modern fuel-efficient technologies was used to measure vehicle performance and fuel efficiency. The new engine also has many new materials technologies, which pose challenges to surface texture fabrication. To overcome these challenges, the team requested extensions (2017 and 2018). This report describes vehicle testing results.

Results

For FY 2019, the key objectives are to (1) complete surface texture designs and fabrication of most of the sliding components of the new engine for testing, and (2) conduct engine testing on textured engine and microencapsulated friction modifiers.

Key Accomplishments

- Completed the design and fabrication of surface textures on the 2018 platform engine with fuel efficient technologies incorporated. The textured parts were installed into the engine and tested on an engine dynamometer test to evaluate engine efficiency improvement using the 5W-30 baseline oil.
- Microencapsulated friction modifiers were incorporated into a 0W-16 formulation and tested in an engine chassis dynamometer in a vehicle. This test is ongoing due to the need to accumulate miles to measure long drain properties.

DOE Technical Targets and Objective

The DOE technical target is to attain 2% fuel economy improvement for cars and light trucks (the legacy fleet) via advanced lubricants without sacrificing engine durability. We have fulfilled this target.

Technical Details

The research team has developed three generations of 0W-16 oil formulations. Some were tested in the ASTM Seq. VI-E Engine Dynamometer fuel economy tests and compared to the baseline oil (GF-5 5W-30 commercial oil). We have engine test data on the baseline oil (GF-5 5W-30), GF-6A 0W-20 formulation, and the GF-6B 0W-16 formulations. The 0W-20 oil achieved 2.4% fuel economy improvement in Seq. VI-E, while the 0W-16 showed 2.1% fuel economy improvement. Both test results met the DOE target of 2% fuel economy improvement.

At the same time, the auto industry has gone through rapid change to improve fuel economy. Engine designs and new materials were introduced into vehicles at an unprecedented pace. The 2019 vehicles and engines are very different from the 2009 Cadillac engine used in the ASTM Seq. VI test engine. To fulfill the DOE target of future engines and vehicle fuel economy targets, the project team decided to change the test engine from the 2009 Cadillac engine to the 2018 platform engine, a V-8 engine with advanced fuel-efficient technologies. The new test engine used is the Gen-V 5.3-liter V-8 L-83 engine, which has incorporated most of the modern fuel-efficient technologies, such as direct injection, active fuel management (cylinder deactivation), and dual-equal camshaft phasing (variable valve timing), that support an advanced combustion system. Advanced coatings also have been introduced into the bearings, rings, and other sliding components, and directionally aligned shallow grooves on some of the bearings.

The fuel efficiency test procedure used consists of five tests, one per day for five days. Each day, the test starts with a cold-start FTP-75 (Federal Test Procedure, a U.S. Environmental Protection Agency city driving cycle) followed by a double FFE (U.S. Environmental Protection Agency highway driving cycle). Summary test results are shown in Table VI.2.1. This new generation of low viscosity potential GF-6B oils does show fuel economy improvements when compared to the baseline oil, 5W-30 GF-5 current commercial premium oil. We have tested three George Washington University (GW) 0W-16 oil formulations. They show improvement in cold start city driving cycle but much less improvement in highway test cycle (still showing improvements). GW G3 formulation has the best overall fuel economy results by balancing the city driving cycle and the highway cycle.

Table VI.2.1 Percent Improvement of Fuel Efficiency of 0W-16 Formulations

	FTP City cycle mpg	FFE Highway mpg	Combined mpg
Baseline GF-5 5W-30	23±0.05	36±0.04	27.5±0.04
GW G1 “GF-6A” 0W-20	+1.11%	+0.39%	+0.87%
GW G1 “GF-6B” 0W-16 (A)	+1.33%	+0.47%	+0.99%
GW G2 “GF-6B” 0W-16 (B)	+1.66%	+0.08%	+0.95%
GW G3 “GF-6B” 0W-16 (C)	+1.05%	+0.92%	+1.16%
Top Tier com. 0W-16 oil	+1.16%	-0.02%	+0.76%

These engine test results conclude the fuel economy improvement effort of this project. The remaining work focuses on the materials technology and durability issues and potential technology evaluation of surface textures and microencapsulated friction modifiers to ensure long-lasting friction reduction.

Surface Texture Fabrication

The fabrication of surface textures on engine components has been presented in detail in the 2017 annual report [1]. We are using a once-through soft mask to couple with electrochemical etching on engine parts. The one-step soft mask was developed in 2017, and many of the engine parts have not been textured due to additional interference from existing coatings and surface textures (simple shallow grooves in the direction of sliding). The soft mask can be used to impart complex location-specific texture for smooth surface. The presence of micro-grooves and organic/inorganic coatings tends to increase the overall surface roughness; this

tends to create air bubbles trapped between the mask and the surface when the mask is applied to bearings and other concave surfaces. After much research and trials, small jigs were designed and used to put the soft mask on the surface, which is pre-coated with a monolayer of either hydrophilic or hydrophobic molecular layer. This approach has proven to be effective, and all the engine parts were successfully textured.

Engine Test Protocols to Evaluate the Effect of Surface Texture

An engine dynamometer test stand was chosen to conduct the L-83 engine. The engine was tested with a protocol before the textured parts were installed to generate the baseline comparison test results. The test protocol consists of fired wide open throttle engine operation at specified rpm set points of the engine; the torque output and engine power were recorded. To measure friction resistance force as a function of rpm set points, an in-line torque meter was installed to measure friction resistance at that rpm set point. The rpm set points ranged from 1,200 to 5,600 rpm.

Large amounts of data were generated since duplicate, sometimes triplicate runs were conducted to improve the test precision confidence limits. We are currently analyzing the data and will report detailed analysis and conclusions when completed. In general, for wide open throttle power runs, the textured engine tends to deliver higher torque and power. For motored engine runs, the torque necessary to maintain a certain speed tends to be lower. This indicates that textured engine is more efficient. The exact magnitude of the difference will be reported in the final project report.

Engine Tests on Microencapsulated Friction Modifiers

This is the first time that encapsulated additives have been tested in an engine, so a new test procedure had to be created. The test procedure that was developed is a three-phase test: (1) fuel economy test using a chassis engine dynamometer test with the same L-83 engine installed to measure initial fuel economy using U.S. Environmental Protection Agency cycles; (2) miles accumulation procedure to obtain at least 3,000 miles; (3) repeat of fuel economy test to measure the fuel efficiency to assess the extended life of additional friction modifiers released from the capsules.

The test is ongoing, and we will report the final test results in the project report.

Conclusions

Based on the work accomplished this year, the following conclusions can be drawn:

- Surface textured engine has been evaluated using a new test protocol to measure friction reduction of the textures. It appears that the texture provides more efficient engine operation with no adverse effects.
- Microencapsulated friction modifiers are being evaluated currently using a newly developed test protocol. The capsules appear to provide better fuel economy under highway operating conditions. No adverse effect was noted.

References

1. Hsu, S., G. Wu, and T. Cushing. 2018. “Integrated Friction Reduction Technology to Improve Fuel Economy Without Sacrificing Durability.” Published in *Advanced Combustion Systems and Fuels 2017 Annual Progress Report*, pp. 547. U.S. Department of Energy, Office of Energy Efficiency and Renewable Energy, Vehicle Technologies Office, Washington, DC.

VII System-Level Efficiency Improvement

VII.1 Advanced Non-Tread Materials for Fuel Efficient Tires (PPG Industries, Inc.)

Lucas Dos Santos Freire, Principal Investigator
PPG Industries, Inc.
440 College Park Dr.
Monroeville, PA 15146
E-mail: dossantosfreire@ppg.com

Ken Howden, DOE Technology Development Manager
U.S. Department of Energy
E-mail: Ken.Howden@ee.doe.gov

Start Date: October 1, 2016 End Date: March 30, 2020
Project Funding: $1,143,464 DOE share: $914,771 Non-DOE share: $228,693

Project Introduction

Precipitated silica is an amorphous particle produced commercially by the acid neutralization of a sodium silicate solution. It is primarily used as a reinforcing filler for synthetic rubber tires. Amorphous silica is known to provide a variety of benefits in tire rubber compounds, including the capability to significantly reduce rolling resistance when compared to carbon black (CB). Much emphasis has been placed on incorporating fuel-efficient silicas into tire tread compounds since the tread is often the single largest contributor to fuel consumption. However, although approximately 50% of the fuel efficiency impact of a tire is ascribed to the tread, the remaining 50% is attributed to the energy dissipation of non-tread components. Of the non-tread tire components, roughly 20% of the energy losses are attributed to the sidewall, in many cases making it the next largest contributor to fuel efficiency after the tread. For this reason, the sidewall is an excellent candidate to evaluate new reinforcing materials for non-tread compounds.

Agilon® silicas are a new generation of pre-treated silicas that can overcome the problem of mixing silicas with natural rubber (NR), the main rubber in non-tread compounds. These silicas have been shown to provide dramatic improvements in rolling resistance compared to carbon black in NR-based compounds. The work in this area has been published and presented in industry magazines, conferences, and the 2017 and 2018 DOE Annual Merit Reviews, and has been well received [1],[2],[3],[4],[5]. In this work, we are developing sidewall compounds containing non-treated and treated silica fillers. While the main objective is to improve rolling resistance, performance parameters relevant to non-tread components have to be taken into account. Ozone resistance, additives migration, and conductivity are some of the parameters that are taken into account in this project.

Objectives

The objective of the project is to develop a new silica filler that can increase tire fuel efficiency by 2% while maximizing key performance properties in non-tread tire components compared to current CB-filled sidewall compounds. To achieve these goals, the developed compounds will be required to maintain or improve resistance to degradative forces while reducing compound hysteresis by approximately 25%.

Overall Objectives

- Develop a predictive model that maps reinforcing filler characteristics to trends in sidewall performance

- Model a sidewall compound that exhibits at least a 25% reduction in energy loss compared to carbon black, with no more than a 5% loss of resistance to degradative forces (targeting better performance).

Fiscal Year 2019 Objectives

- Develop a database with custom-made silica fillers to enable statistical analysis of the results
- Identify optimal silica fillers and optimize sidewall compound formulation using selected silica prototypes
- Analyze compound formulation, varying fillers and curatives, to demonstrate key characteristics where a reduction in energy loss is reached with no more than a 5% loss of resistance to other degradative forces.

Approach

The first steps of the project were to understand the tradeoffs in performance of different commercially available materials in model sidewall compounds and identify trends toward improved fuel efficiency indicators and resistance to degradative forces. These steps were performed by systematically selecting representative commercial silica and carbon black fillers to provide a significant range in filler morphology and surface chemistry and evaluating their performance in a model sidewall formulation. The top silica prototypes were selected based on the improvements seen in a model CB sidewall formulation. The selected silica prototypes were used in additional compounding studies with variations in the loadings of sulfur, CB, and silica to continue optimization of the rubber formulation. Akron Rubber Development Lab facilities were used to perform certain sidewall-specific tests, such as ozone resistance and antioxidants migration.

Results from several studies were used to perform a statistical analysis to determine the best balance of rubber properties to create an optimized sidewall formulation. These results will be used in a final study with a complete analysis on the impact on energy loss (i.e., tan δ, loss modulus, and Goodrich heat build-up) and degradative processes (i.e., Monsanto fatigue to failure, tear strength, ozone resistance, and antioxidant migration) to achieve the final project goal of developing a compound with 25% reduction in energy loss while maintaining other compound properties similar to the carbon black control compound.

Results

Two silica prototypes were selected based on previous data as the optimum silica fillers to be compounded, tested, and compared for their rubber properties. Of the two prototypes, LD0690-1 has a lower surface area for both cetyl trimethyl ammonium bromide (CTAB) and Brunauer-Emmett-Teller (BET) testing, and LD0721-1 has a higher surface area. The two silicas compare well for carbon, sulfur, and water content. Rubber compounds with these two silicas were tested and optimized. The rubber performance will be compared to complete the final studies. Table VII.1.1 contains the properties of the two silica prototypes being evaluated.

Table VII.1.1 Silica Prototypes Characterization Data

	LD0690-1	LD0721-1
CTAB (m^2/g)	97	115
BET (m^2/g)	48	66
Carbon (%)	4.54	4.58
Sulfur (%)	1.48	1.55
H_2O (%)	4.4	4.8
pH	7.1	7.7

Compounding studies were performed using various loadings of sulfur, carbon black, and silica to optimize the rubber formulation. The first set of studies performed during this year focused on varying sulfur and silica

loadings while maintaining CB loading constant. Table VII.1.2 shows the rubber formulations and results for the lower surface area silica (LD0690-1). For all batches, tan δ and elongation show improvement versus CB, with other performance indicators comparable to the CB control. Three batches met or exceeded the tan δ goal. Table VII.1.3 shows a similar study for the higher surface area silica (LD0721-1). The low surface area silica provides the highest improvement in tan δ at the expense of tear strength. The higher surface area silica loses some tan δ improvements but gains in tear strength.

Table VII.1.2 Compound Study Varying Sulfur and Silica Loadings with the Low Surface Area Silica Prototype

Filler	LD0690-1									CB N-550
Silica	27	32	37	27	32	37	27	32	37	-
CB N-550	20	20	20	20	20	20	20	20	20	50
RM Sulfur	1.50	1.50	1.50	1.60	1.60	1.60	1.70	1.70	1.70	1.25
TBBS	0.96	0.96	0.96	1.02	1.02	1.02	1.09	1.09	1.09	0.80
ML (1+4)	36	38	41	36	35	39	36	39	38	37
S'_{max} (in-lbs)	7.2	7.2	7.6	7.8	7.2	7.8	8.0	8.3	8.6	8.2
S'_{min} (in-lbs)	1.0	1.0	1.2	1.0	1.0	1.1	1.0	1.1	1.1	1.1
MH-ML (in-lbs)	6.2	6.2	6.5	6.8	6.3	6.7	7.0	7.2	7.5	7.1
TC50	4.6	4.7	4.6	4.7	4.5	4.4	4.3	4.2	4.3	5.8
TC90	9.2	9.1	9.1	9.0	8.4	8.4	8.1	8.1	8.4	11.7
Tensile, MPa	18.4	18.2	18.4	18.4	18.0	18.3	19.1	18.8	18.5	18.8
Elongation, %	618	616	609	585	601	581	591	584	571	546
Modulus @ 100%, MPa	1.2	1.2	1.4	1.3	1.3	1.4	1.4	1.5	1.5	1.8
Modulus @ 300%, MPa	5.8	5.8	6.7	6.2	6.1	7.1	6.7	7.0	7.0	8.7
300/100 % Modulus ratio	4.7	4.9	4.8	4.7	4.6	4.9	4.7	4.8	4.8	5.0
Hardness @ 23°C	51	50	53	50	51	52	52	53	53	53
Tan δ at 5% DMA	0.149	0.151	0.162	0.131	0.141	0.161	0.143	0.144	0.151	0.172
Tan δ at 5% ARES	0.122	0.128	0.135	0.108	0.113	0.122	0.104	0.115	0.123	0.148
G' at 0.2 strain @ 30°C Mpa	0.94	1.01	1.09	0.96	0.96	1.07	0.90	1.03	1.11	1.02
Strebler @ 100°C	155	167	190	122	148	166	101	129	146	208
Heat Build-up (°F)	27	36	35	21	29	36	22	27	27	24
Permanent Set (%)	6.5	9.5	9.6	4.3	7.6	8.9	5.4	5.8	5.4	5.4

RM – rubber-maker; TBBS – N-t-butyl-2-benzothiazole sulfenamide; ML – minimum torque; S'_{max} – maximum torque from rheometer cure test; S'_{min} – minimum torque from rheometer cure test; MH–ML – torque difference (maximum torque minus minimum torque); TC50 – time at which 50% of cure has taken place; TC90 – time at which 90% of cure has taken place; DMA – dynamic mechanical analysis; ARES – a rotational rheometer; G' – dynamic stiffness

Table VII.1.3 Compound Study Varying Sulfur and Silica Loadings with the Higher Surface Area Silica Prototype

Filler	LD0721-1									CB N-550
Silica	27	32	37	27	32	37	27	32	37	
CB N-550	20	20	20	20	20	20	20	20	20	50
RM Sulfur	1.50	1.50	1.50	1.60	1.60	1.60	1.70	1.70	1.70	1.25
TBBS	0.96	0.96	0.96	1.02	1.02	1.02	1.09	1.09	1.09	0.80
ML (1+4)	38	39	41	37	40	42	38	42	43	37
S'_{max} (in-lbs)	6.6	7.0	7.0	7.0	7.3	7.2	7.6	7.7	8.1	7.6
S'_{min} (in-lbs)	1.0	1.1	1.1	1.0	1.1	1.1	1.0	1.1	1.2	1.1
MH-ML (in-lbs)	5.6	5.9	5.9	6.0	6.2	6.1	6.6	6.5	6.9	6.5
TC50	5.5	5.8	5.7	5.5	5.3	5.2	5.3	4.9	5.1	6.7
TC90	10.5	11.3	11.5	10.4	10.5	10.1	9.9	9.2	9.9	12.8
Tensile, MPa	18.6	18.2	18.0	18.3	18.7	18.5	18.7	19.4	18.0	17.5
Elongation, %	777	748	753	769	747	743	706	726	687	711
Modulus @ 100%, MPa	1.0	1.0	1.1	1.0	1.1	1.1	1.2	1.2	1.3	1.1
Modulus @ 300%, MPa	4.1	4.4	4.6	4.1	4.4	4.6	4.8	5.1	5.5	5.7
300%/100% Modulus ratio	3.9	4.2	4.0	4.0	4.1	4.1	4.1	4.2	4.2	5.0
Hardness @ 23°C	50	50	53	48	52	53	52	52	54	54
Tan δ at 5% DMA	0.156	0.168	0.183	0.149	0.162	0.173	0.143	0.155	0.162	0.197
Tan δ at 5% ARES	0.124	0.128	0.139	0.113	0.127	0.134	0.114	0.116	0.127	0.179
G' at 0.2 strain @ 30°C Mpa	0.90	0.94	1.01	0.88	0.93	1.09	0.94	0.99	1.06	0.99
Strebler @ 100°C	158	172	223	124	174	202	122	130	151	235
Heat Build-up (°F)	30	28	31	25	29	32	17	22	24	33
Permanent Set (%)	8.1	7.8	9.9	6.3	6.5	9..3	5.2	6.1	6.1	7.4

Regarding the parameters related to the resistance of the compounds to degradation, previous studies have shown that all silica compounds have better flex fatigue resistance than the CB control. The hardness after aging remains slightly higher than the CB control. Furthermore, the mechanical properties measured before and after different aging protocols have been applied are slightly better than the CB control. Because of this, there are no concerns that any of these silica prototypes would provide any significant deficiencies after aging. Therefore, not all of the compound work was tested for aging due to the time it takes to complete the aging tests. However, the final optimization will be performed with a complete set of testing.

Table VII.1.3 shows results for a similar study with the higher surface area silica (LD0721-1). For all batches, the tan δ was close to the 25% improvement goal compared with the CB control. Heat build-up and elongation also showed improvement versus CB, with other performance indicators comparable to CB. Hardness is closest to CB for the higher silica loadings. The compound with 37 parts per hundred rubber (phr) of silica and 1.5 phr of sulfur has the lowest improvement in tan δ (22%), while maintaining other properties comparable

with the CB control. On the other side, the compound with 27 phr of silica and 1.7 phr of sulfur has the best improvement in tan δ (36%), but tear strength is deficient. The best balance of performance is somewhere in between these two compounds.

The studies completed to date have been evaluated using statistical analysis software to determine the best balance of these loadings to achieve the 25% improvement in tan δ while maintaining other performance properties. The analysis shown in Figure VII.1.1 shows the effect of fillers and sulfur loadings and silica surface area on key rubber performance properties. Silica surface area has little effect on hardness but slightly increases tan δ and tear strength. CB, silica, and rubber-maker silica (RMS) create a stiffer compound as the loadings increase. RMS loadings decrease tan δ and tear strength, where CB and silica loadings increase both. Higher surface area silica allows the compound to reach the tan δ goal while maintaining good tear strength. Based on this model, the ideal formulation contains 24 phr of N-550 carbon black, 27 phr of high surface area silica, and 1.5 phr of sulfur. The final study performed will be based on these results.

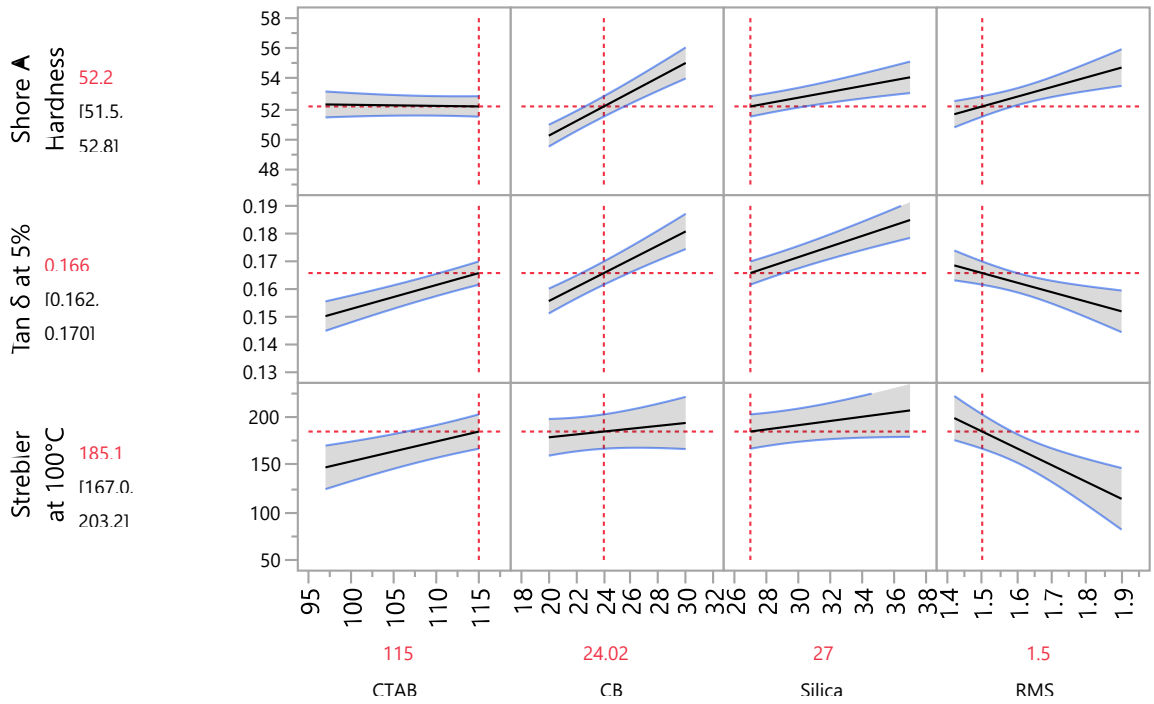

Figure VII.1.1 Statistical evaluation of compounds filled with silica prototypes

The final study will place emphasis on testing the high surface area silica prototype (LD0721-1) with CB N-550. Slight modifications to the formulation, silica, or CB will also be tested to obtain the rolling resistance goal with several variations. The study will be completed with all the testing shown in Table VII.1.2 and Table VII.1.3 as well as the addition of aging studies.

Conclusions

Two optimized silica prototypes were prepared, based on previous results, and tested in sidewall rubber compounds made with different variations of filler and curative loadings. Traditional performance parameters were determined, as well as parameters related to resistance to compound degradation. The experimental plan allowed the project team to:

- Identify the optimal sidewall formulation to meet the wide range of required sidewall performance metrics

- Meet the 25% decrease in rolling resistance
- Maintain or improve other performance properties
- Develop a database with custom-made silica fillers and their compound performance
- Develop and evaluate different tools to determine compound degradation performance.

The data generated showed that functionalized silica technology can deliver the project goals by producing an improved overall compound performance balance, with lower hysteresis than the carbon black control compound, while maintaining the resistance to degradation.

References

1. Okel, Tim, and Justin Martin. 2014. "Innovating the Silica Surface for Improved NR Truck Tire Vulcanisates." Tire Technology International, Cologne, Germany (February).

2. Okel, Tim, and Justin Martin. 2014. "Functionalized Silicas for Improved NR Truck Tire Vulcanizates." *Rubber World* 249 (2), 19–24.

3. Okel, Tim, and Justin Martin. 2013. "Bringing Innovation to the Surface: Functionalized Silicas for Improved Natural Rubber Truck Tire Vulcanizates." 184th Technical Meeting of the American Chemical Society Rubber Division, Paper #33 (October).

4. Okel, Tim, et al. 2011. "Agilon Performance Silicas in Natural Rubber Truck Tire Tread Compounds." 180th Technical Meeting of the American Chemical Society Rubber Division, Paper #70 (October).

5. Dos Santos Freire, Lucas, and Tiffany Brenner. 2019. "Silica Development for Sidewall Compounds." 196th Technical Meeting of the International Elastomer Conference, Paper #C12 (October).

Acknowledgements

The authors would like to acknowledge Akron Rubber Development Lab for their rubber mixing and characterization work performed in this project and David Ollett of National Energy and Technology Laboratory.

VII.2 High-Performance Fluids and Coatings for Off-Road Hydraulic Components: Coatings, Advanced Fluids, and Fluid–Surface Interactions (Argonne National Laboratory)

George Fenske, Principal Investigator
Argonne National Laboratory
9700 S. Cass Avenue
Lemont, IL 60439
E-mail: gfenske@anl.gov

Michael Weismiller, DOE Technology Development Manager
U.S. Department of Energy
E-mail: Michael.Weismiller@ee.doe.gov

Start Date: June 1, 2018 End Date: May 30, 2020
Project Funding: $1,081,000 DOE share: $1,081,000 Non-DOE share: $0

Project Introduction

This project is part of a multilaboratory effort (Argonne National Laboratory, lead; Oak Ridge National Laboratory; and Pacific Northwest National Laboratory) in response to the U.S. Department of Energy (DOE) Vehicle Technologies Office Advanced Engine and Fuel Technologies Program's request for research on technologies to improve the energy efficiency of fluid power systems of off-road vehicles. A recent DOE analysis [1] indicates that the off-road fluid power sector consumes 0.36–1.8 quads of energy per year, representing 1.3%–6.5% of the total energy consumed in 2016 for the transportation sector. Of the 0.36–1.8 quads consumed, approximately 70% is parasitic losses in the engine and hydraulic fluid components (pumps, bypass/idle, valves, hoses, and actuators). The overall focus of this multilaboratory, low-technology-readiness-level research is to develop high-performance hydraulic fluids and wear-resistant coatings to improve the efficiency, durability, and environmental compatibility of off-road hydraulic components.

The Argonne activity includes three major tasks: one focusing on development of composite base fluids (synthetics and bioderived components) that provide high viscosity index (VI) characteristics with minimal use of compounds with high-mass polymers that modify VI, another task focusing on advanced catalytically doped nitride coatings that are wear-resistant and promote formation of low-friction tribofilms, and a third focusing on development of a low-volume fluid power test facility (FPTF) that can measure hydraulic system performance with small volumes (<2 gal) of experimental fluids.

Objectives

The overall objective of the multilaboratory (Argonne, Oak Ridge National Laboratory, Pacific Northwest National Laboratory) project is the development of low-technology-readiness-level fluid, additive, and material/coating technology platforms that, when properly integrated on a systems level, can impart significant improvements in energy efficiency, durability, reliability, and environmental compliance.

The overall objectives of the Argonne tasks are as follows:

- Quantify and optimize the tribological and rheological performance of composite fluids consisting of mixtures of polyalphaolefin and bioderived esters
- Develop and optimize the tribological performance of catalytically doped nitride coatings

- Design and fabricate a benchtop FPTF capable of evaluating the impact of advanced hydraulic fluids and materials of construction on system efficiency.

Task 1 Composite Fluids

Objective and Approach

The primary objective of this subtask is the development of shear-stable base stock with optimized pertinent properties for energy-efficient hydraulic fluid formulation. Key physical properties of hydraulic fluids governing overall fluid system efficiencies include viscosity, VI, and bulk modulus. Similarly, traction behavior of the fluid and boundary regime behavior are important for efficiency, reliability, and durability of the fluid power system. Another important requirement for hydraulic fluids is biodegradability, or environmental friendliness.

Task 1 used an approach to developing composite base fluids with optimized physical and rheological properties that is analogous to composite material formulation. Binary, ternary, and quaternary base fluids can be blended from bioderived ester, synthetic ester, polyalphaolefin, and polyalkylene glycol fluids with low viscosity, high VI, and high bulk modulus. Comprehensive rheological properties, density, bulk modulus, traction behavior, friction, and wear behavior of the composite base fluids will be compared to those of the commercial project baseline hydraulic fluid.

Results

Binary and ternary composite fluids were blended from polyalphaolefin and different types of bioderived ester fluids in a range of different compositions to the International Organization for Standardization Grade 32 hydraulic fluid properties target. The rheological properties in terms of viscosity, VI, and traction were measured. The density and bulk modulus of the fluids were also measured. The boundary friction of the fluids was measured with prototypical hydraulic pump materials, namely, cast iron, bronze, and 52100 hardened steel. The wear and scuffing protection capabilities of the composite fluids were also evaluated. All the properties and performance attributes evaluated for the composite fluids were also measured for three fully formulated commercially available International Organization for Standardization Grade 32 hydraulic fluids. These are the project benchmark fluids: mineral oil monograde (FF-MO-mono), mineral oil multigrade (FF-MO-multi), and synthetic multigrade (FF-Synth-multi).

The traction coefficient of the unformulated composite fluid is substantially lower than that of the fully formulated commercial fluid. Similarly, the friction coefficients for the composite fluids are substantially lower than those of the three fully formulated fluids under all lubrication regimes, as indicated on the Stribeck curve shown in Figure VII.2.1. A common concern about bioderived fluids is their viscosity at low temperatures. The cold crank viscosity for the composite base fluid was compared with that of the fully formulated fluids down to −40°C; the results are shown in Figure VII.2.2. Indeed, the composite fluid viscosity at low temperatures is comparable to that of the synthetic fluid and much lower than that of both monograde and multigrade mineral-oil-based fluids. Both the boundary friction and the wear in various pump materials are substantially lower with composite fluids than with fully formulated commercial fluids. Furthermore, the composite fluids prevented occurrence of scuffing in different pump materials.

A comprehensive summary of the various properties and performance attributes of two unformulated composite fluids in comparison with the three benchmark fully formulated commercial hydraulic fluids is shown in Table VII.2.1. Even without any performance-enhancing additives, both composite fluids exhibit superior properties and performance compared to all the fully formulated commercial benchmark fluids. Hence, the new composite base fluid will be an excellent platform on which to build advanced energy-efficient hydraulic fluid technology.

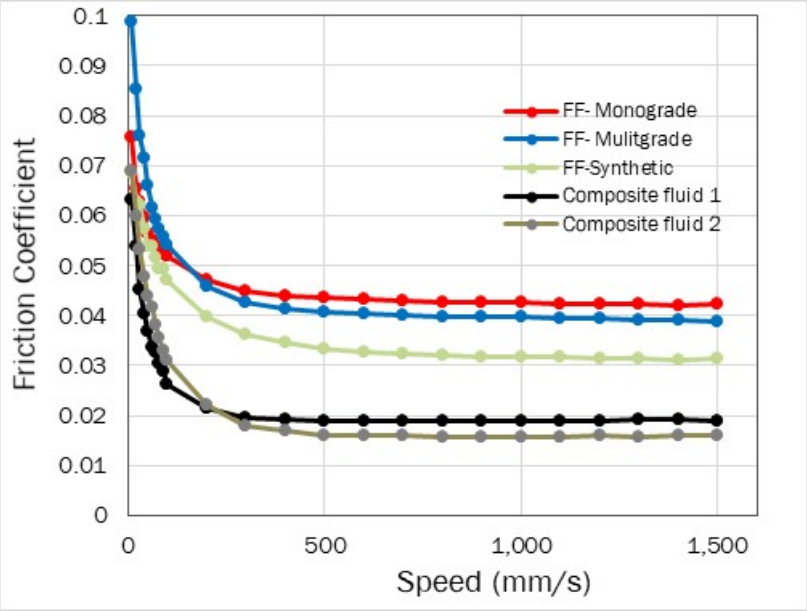

Figure VII.2.1 Stribeck curve for commercial and composite fluids

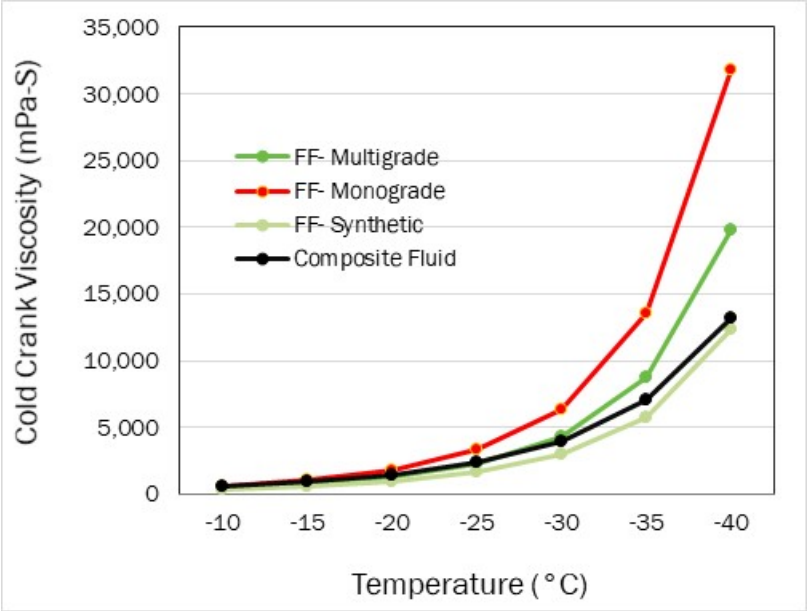

Figure VII.2.2 Cold crank viscosity for different fluids

Table VII.2.1 Summary of Properties and Performance for Composite Base Fluids and Commercial Fluids

Fluid	Viscosity 40°C (cSt)	Viscosity 100°C (cSt)	Viscosity Index	Max Traction (75°C)	Boundary friction (75°C)	Bulk Modulus (GPa) at 70°C	Wear Volume Bronze-CI (μm³)	Wear Volume Steel- CI (μm³)	Scuffing Load (N)
FF-MO-mono	32.2	5.48	105.9	0.057	0.076	1.355	68045	3976	175
FF-MO-multi	**33.43**	**6.51**	**152.2**	**0.060**	**0.098**	**1.338**	**31333**	**1098**	**325**
FF-Synth-multi	32.50	6.78	173.7	0.051	0.077	1.316	40010	3808	400
Exptal. Fluid #1									
25% BioE-1	39.43	7.45	158.3	0.037	0.060	1.315	21939	664	No scuffing
50% BioE-1	30.40	6.14	155.3	0.037	0.068	1.326	14525	1430	No scuffing
75% BioE-1	18.76	4.63	175.1	0.036	0.070	1.327	12692	567	No scuffing
100% BioE-1	12.69	3.42	153.2	0.033	0.081	1.336	92209	1572	No scuffing
Exptal. Fluid#2									
25% BioE-2	49.58	8.36	143.8	0.037	0.048	1.332	18743	2071	No scuffing
50% BioE-2	39.14	7.70	170.5	0.036	0.055	1.347	39446	648	No scuffing
75% BioE-2	30.31	6.82	194.7	0.033	0.063	1.371	42764	1233	No scuffing
100% BioE-2	23.81	5.28	163.8	0.037	0.070	1.412	61645	683	No scuffing

Task 2 Catalytically Doped Coatings

Objective and Approach

The aim of the proposed coating activities is to design, develop, and optimize novel super-hard and low-friction coatings to reduce friction, wear, and scuffing failures in fluid power components. Specifically, the project will develop a new breed of catalytically active nanocomposite coatings to achieve in situ formation of highly protective tribofilms providing superior friction, wear, and scuffing properties over current state-of-the-art materials and coatings. This transformational coating technology uses catalytically active hard nitrides and a suite of catalyst metals (such as nickel, silver, cobalt, copper, and the like) in a nanocomposite coating architecture to convert lubricant and additive molecules in hydraulic fluids into highly protective tribofilms directly on the contact spots where friction, wear, and scuffing take place. These higher-performance coatings may also enable higher power density in fluid power systems with downsized and more compact designs.

The approach to developing catalyst coatings included the use of a production-scale magnetron sputtering system and several rounds of coating trials in order to optimize the deposition conditions that yielded truly nanocomposite coatings with the right amount of catalyst metal, mechanical hardness, surface roughness, and chemical composition. Specifically, by controlling and further optimizing the deposition parameters, researchers produced a series of composite coatings consisting of molybdenum, vanadium, and copper with controlled composition and crystalline phases. These coatings were fully characterized by using a suite of surface and mechanical tools to measure their surface smoothness, uniform thickness, hardness, and adhesion. Overall, most of the coatings produced were high-quality and suitable for tribological testing using the baseline oils supplied by an industrial partner.

Results

This project's systematic studies have shown that the most favorable catalyst metal content in coating composition is about 5 wt%. Copper, rather than nickel, appeared to provide lower friction, but both catalysts were equally effective in reducing wear. The composite coating hardness was between 18 and 22 GPa at a 5 wt% catalyst metal loading. All the coating products met our target adhesion value of HF1 (which is the best) in the Rockwell C ball indentation adhesion test. This may have been due to the use of metal ion etching of the substrate surfaces, employing a high-power impulse magnetron sputtering mode in the beginning of the deposition process. This type of etching is expected to provide an ultraclean substrate surface and even some intermixing between the atoms of substrate material and the coating ingredients. The surface roughness of nanocomposite coatings varied between 20 nm and 50 nm and appeared to be very desirable for both the

friction and wear performance, even under severe loading conditions of more than 1 GPa. For comparison, when uncoated steel test pairs were tested in commercial-grade hydraulic oils, the friction was very unsteady and the amount of wear on both sides was excessive, as shown in Figure VII.2.3.

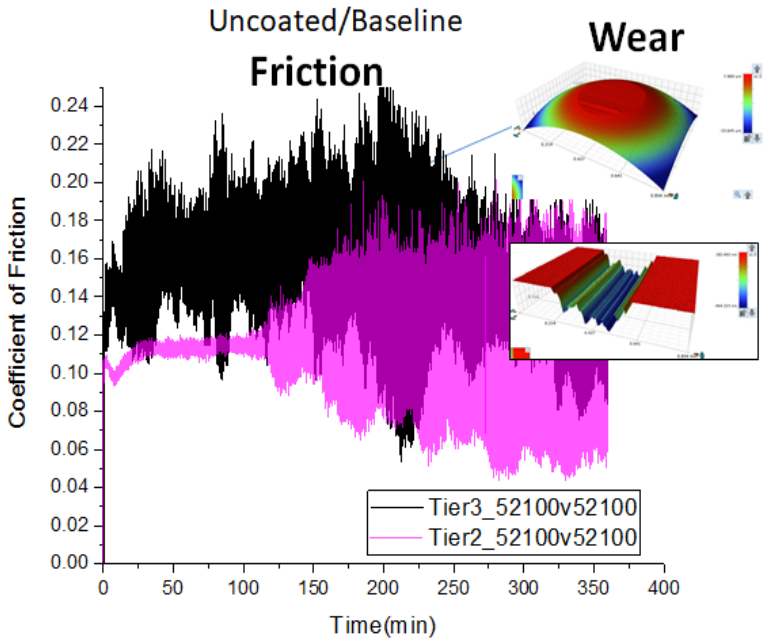

Figure VII.2.3 Friction and wear performance of uncoated/baseline steel test pair in two kinds of hydraulic fluids. Friction was very unsteady and the amount of wear on both the ball and flat sides was severe.

When researchers repeated the same tests with a highly optimized catalyst coating, the results were different in such a way that the friction coefficients were much lower and very steady, as shown in the friction-versus-time graph in Figure VII.2.4. Further, little measurable wear was observed on either the ball or flat samples. Compared to that for uncoated samples, the friction was reduced by 50% in some samples, while the wear was reduced to unmeasurable levels. Overall, the nanocomposite coatings developed under this project dramatically reduced wear losses under extreme conditions, even with the use of unformulated base oils. Friction was also much lower compared to the baseline steel samples; therefore, the coatings developed under this project hold great promise for the demanding fluid power applications of off-road vehicles.

Overall, the catalyst coatings developed under this project have met all the stated objectives by demonstrating extreme resistance to wear under severe boundary conditions and significantly reducing friction over the uncoated test samples. Even without the use of any additive (i.e., base oils), these coatings were able to afford very low friction and wear to sliding surfaces.

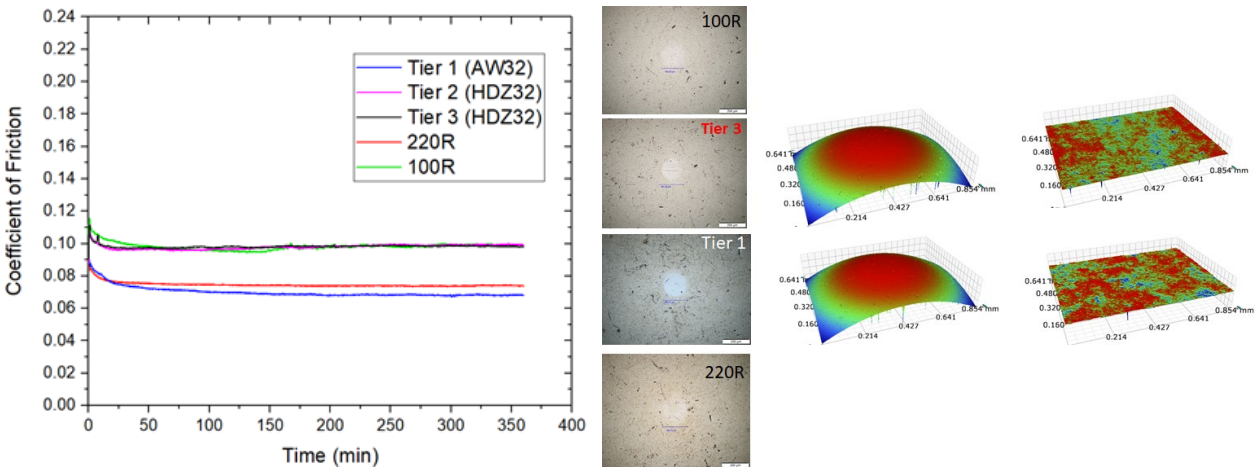

Figure VII.2.4 Friction (left) and wear (right) performance of an optimized nanocomposite coating during tests in base and formulated hydraulic fluids

Task 3 Fluid Power Test Facility

Objective and Approach

Properties of the working fluid play an important role in the efficiency of a fluid power system. Experimental testing is one research technique for assessing and comparing the performance of different working fluids. Experimental testing can simulate operational situations of a working fluid in a fluid power system; therefore, the testing results can be directly used to predict the performance of the tested fluid in its practical application conditions. Various commercial fluid power test systems have been developed. However, these test systems usually require a large volume (approximately 40 gal or more) of the tested fluid. There is a huge gap between this fluid volume requirement and the available fluid volume (generally limited to approximately 5 gal) at the research and development stage. Therefore, there is an urgent need for a fluid power test system with a much lower fluid volume requirement.

The main focus of Task 3 is to develop an FPTF for testing hydraulic fluids at their research and development stage with a testing fluid volume requirement of 2 gal or less. The FPTF will have various controls on experimental parameters, including test system pressure, test fluid temperature, test fluid flow rate, and test system component (mainly hydraulic pump and hydraulic motor) shaft torque. The FPTF will directly measure system-level and component-level efficiencies under various fluid flow rates, pressures, and temperatures. It is expected that successful development of the FPTF will provide a laboratory capacity for evaluating the hydraulic performance of baseline fluids and their modifications, and this will accelerate the development of new and improved hydraulic fluids for meeting DOE research targets. The FPTF will be used for performance comparison of experimental fluids with their baseline fluids.

Results

Figure VII.2.5 shows the concept design of the FPTF. The facility includes the two main hydraulic components (hydraulic pump and hydraulic motor) of fluid power systems, an electric motor as the power source, and a dynamometer for torque measurements. The experimental test facility is instrumented to evaluate both volumetric and mechanical efficiencies for each hydraulic component as well as the overall efficiency of each component and the system. The key measurements include flow rate, rotating speed, pressure gain, and shaft torque for the hydraulic pump; flow rate, rotating speed, pressure drop, and shaft torque for the hydraulic motor; and input torque, input rotating speed, output torque, and output rotating speed for the overall test system loop.

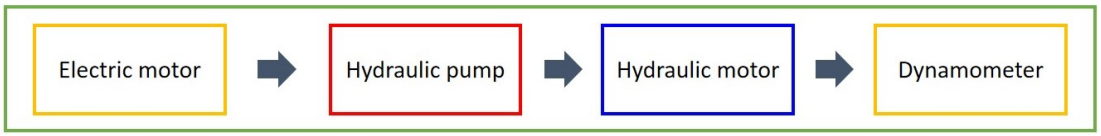

Figure VII.2.5 Main components of the fluid power test facility

The completed experimental test loop is shown in Figure VII.2.6. The key features of the FPTF's hardware, software, and overall system are as follows:

- Test fluid volume requirement of <2 gal
- Temperature range of 20°C–80°C controlled by the heater and the cooler
- Pressures of up to 2,000 psi controlled by the dynamometer setting
- Flow rate range of 0.3–0.9 gal/min
- Rotating speed ranges of 375–1,000 rpm for the hydraulic pump and 750–2,000 rpm for the hydraulic motor
- Torques of ≤62 lb-in. for the hydraulic pump and ≤31 lb-in. for the hydraulic motor controlled by the dynamometer setting.

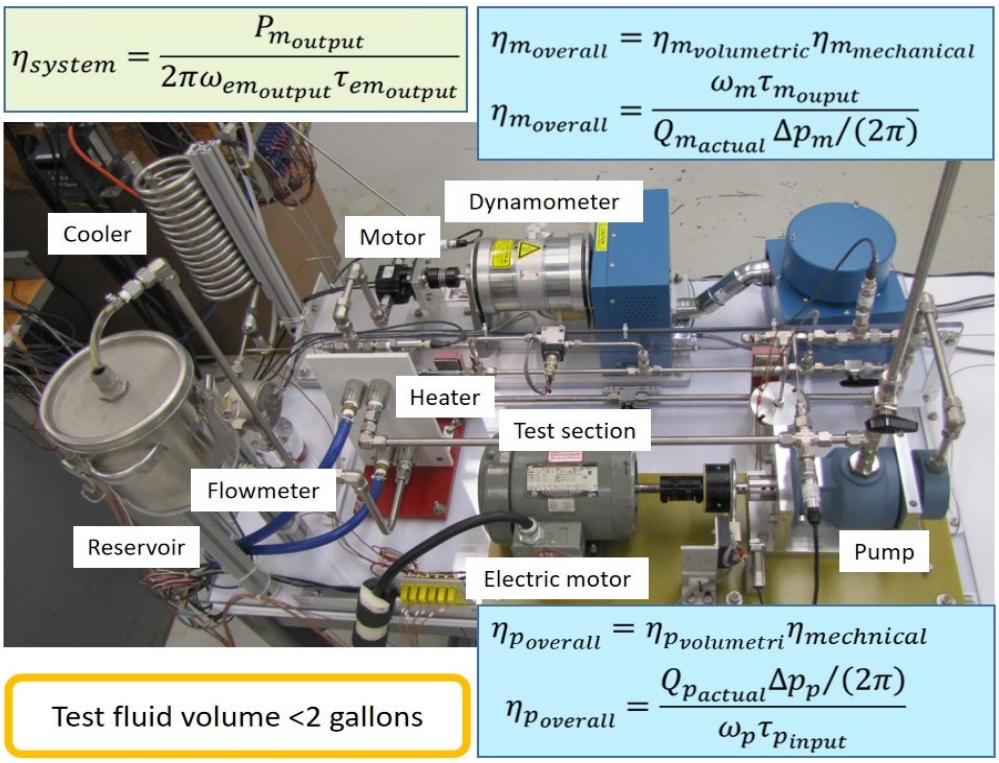

Figure VII.2.6 Test loop of the FPTF

Conclusions

For Task 1, composite fluids, the project team successfully developed binary and ternary composite base fluids from polyalphaolefin and different bioderived esters. The composite fluids exhibit superior rheological and frictional properties, as well as wear and scuffing protection capabilities, compared to fully formulated, commercially available fluids. The new composite fluids will be excellent base stock for the development of new-generation energy-efficient hydraulic fluids.

For Task 2, catalytic coatings, the project team successfully developed catalyst coatings that met all the stated objectives by demonstrating extreme resistance to wear under severe boundary conditions and significantly reducing friction over the uncoated test samples.

For Task 3, FPTF, the project team completed the concept design, engineering design, and construction of an experimental fluid power test loop, as well as the integration of the loop with a data acquisition and control system.

Key Publications

1. Lorenzo-Martin, C., O.A.J. Nguyen, and G. Fenske. 2019. “Tribological Performance of Composite Basefluid for Hydraulic Systems.” Slide presentation at the 74th Society of Tribologists and Lubrication Engineers Annual Meeting and Exhibition, Nashville, TN (May 19–23).

2. Lorenzo-Martin, C., O. Ajayi, G. Fenske, S. Lum, G. Bantchev, G. Biresaw, and R. Harry-O'kuru. 2019. “Scuffing Performance of Brass-Cast Iron Contact Pair in Hydraulic Fluid.” Slide presentation at the 74th Society of Tribologists and Lubrication Engineers Annual Meeting and Exhibition, Nashville, TN (May 19–23).

3. Lorenzo-Martin, C., M. De La Cinta, O. Ajayi, G. Biresaw, G. Bantchev, and R.H. O'kuru. 2019. “A Peculiar Observation of ‘Gelling’ in Bio-Derived Phosphonate Ester.” Slide presentation at the 74th Society of Tribologists and Lubrication Engineers Annual Meeting and Exhibition, Nashville, TN (May 19–23).

4. Fenske, G. 2019. “High-Performance Fluids and Coatings for Off-Road Hydraulic Components.” Oral presentation at the 2019 DOE VTO Annual Merit Review (June).

5. Erdemir, A. 2019. “Surface and Interface Engineering for Ultra-Low Friction and Wear.” Presented at the Special Frontiers of Tribology Session of the 74th Annual Meeting of the Society of Tribologists and Lubrication Engineers, Nashville, TN (May 19–23).

6. DaSilva, V., O.L. Eryilmaz, and A. Erdemir. 2019. “Development of Catalytically Active Nano-Composite Coating for Severe Boundary Lubricated Conditions of Hydraulic Fluids.” Presented at the 46th International Conference on Metallurgical Coatings and Thin Films, San Diego, CA (May 20–24).

Reference

1. Lynch, L.A., and B.T. Zigler. 2017. “Estimating Energy Consumption of Mobile Fluid Power in the United States.” National Renewable Energy Laboratory.

Acknowledgements

The principal investigator thanks coinvestigators and coauthors Oyelayo Ajayi, Cinta Lorenzo-Martin, Ali Erdemir, Osman Eryilmaz, Robert Erck, Dileep Singh, Wenhua Yu, and David France of Argonne National Laboratory. The authors acknowledge the valuable assistance and guidance provided by David Gray, OEM Manager/Technical Liaison for Evonik–North America.

VII.3 High Performance Fluids and Coatings for Off-Road Hydraulic Components - Development of Environmentally-Friendly Additives for Hydraulic Fluids (Oak Ridge National Laboratory)

Jun Qu, Principal Investigator
Oak Ridge National Laboratory (ORNL)
P.O. Box 2008, MS 6063
Oak Ridge, TN 37831-6063
E-mail: qujn@ornl.gov

Michael Weismiller, DOE Technology Development Manager
U.S. Department of Energy
E-mail: Michael.Weismiller@ee.doe.gov

Start Date: June 1, 2018 End Date: June 30, 2020
Project Funding (FY19): $230,000 DOE share: $230,000 Non-DOE share: $0

Project Introduction

This project is part of a multi-lab effort (Argonne National Laboratory, ORNL, and Pacific Northwest National Laboratory) responding to DOE's Vehicle Technologies Office's Advanced Engine and Fuel Technologies Program request for research on technologies to improve the energy efficiency of fluid power systems for off-road vehicles. A recent DOE analysis [1] indicates the off-road fluid power sector consumes 0.36–1.8 quads of energy per year, representing 1.3%–6.5% of the total energy consumed in 2016 for the transportation sector. Of the 0.36–1.8 quads consumed, approximately 70% is lost to parasitic losses in the hydraulic fluid components (pumps, bypass/idle, valves, hoses, and actuators). The overall focus of this multi-lab, low-technology-readiness-level research is to develop high-performance hydraulic fluids and wear-resistant coatings to improve the efficiency, durability, and environmental compatibility of off-road hydraulic components.

This particular project, led by ORNL, focuses on development of eco-friendly additives for hydraulic fluids. Environmentally acceptable lubricants (EALs) have seen increasing demand in hydraulic systems. Current hydraulic fluids are typically mineral-oil-based, which have low biodegradability and often are toxic to environmental receptors. There are four types of Environmental Protection Agency-approved EALs: water, vegetable oil, synthetic ester, and polyalkylene glycol (PAG). However, there is a lack of eco-friendly, effective additives available for EALs. Specifically, many conventional anti-wear additives used in hydraulic fluids, such as zinc dialkyldithiophosphates (ZDDPs) or sulfur-based additives, are not allowed in EALs due to their adverse eco-impact. Ashless (metal-free) organic phosphorus-containing additives may have lower toxicity, but their wear protection is often inferior.

Objectives

Overall Objectives

- Develop candidate eco-friendly ionic liquids as novel additives for hydraulic fluids
- Demonstrate low toxicity and superior friction/wear reduction for candidate ionic liquids
- Understand the friction/wear-reduction mechanisms of eco-friendly ionic liquids and their compatibilities with wear-resistant coatings.

Fiscal Year 2019 Objectives

- Design and synthesize candidate ionic liquids as eco-friendly additives for PAG
- Demonstrate reduced toxicity of candidate ionic liquids and improved lubricating performance benchmarked against conventional additives.

Approach

This study develops a new class of eco-friendly ionic liquids (ILs) as multi-functional additives, including but not limited to anti-wear and friction-reducing, for EALs with a focus on PAG. ORNL has previously developed oil-soluble ILs for automotive engine and gear lubrication and demonstrated significantly improved efficiency and durability [2],[3],[4],[5],[6]. In this work, the focus is to minimize toxicity and maximize lubricating performance of the ILs by tailoring their molecular structures. The physicochemical properties, aquatic toxicity, and tribological behavior of candidate ILs will be compared with those of selected commercial anti-wear additives for hydraulic fluids. Tribofilm characterization will be carried out to reveal the wear protection mechanism. The potential impacts include friction reduction and superior wear protection to allow lower-viscosity hydraulic fluids for higher mechanical efficiency, reduction of start-up friction to enable system downsizing, and reduction of environmental impact.

Results

Key accomplishments for Fiscal Year 2019 include the following:

- A series of candidate ionic liquids have been developed as eco-friendly lubricant additives, and ORNL Invention Disclosure #20190449 [7] has been filed.
- Candidate ionic liquids have demonstrated low/no toxicity by increasing the survival rate of Ceriodaphnia dubia from 0% to 100% and reproduction rate from 0 to >40 per week in comparison to a conventional additive.
- Candidate ionic liquids have demonstrated superior lubricating characteristics with additional 20%–30% friction reduction and 80%–90% wear reduction in comparison to a conventional additive.

Materials and Experimental

More than a dozen candidate ILs from four different groups have been designed and synthesized, and the detailed molecular structures are protected by the ORNL Invention Disclosure #20190449 [7]. A commercial lubricant anti-wear additive, a primary ZDDP, was provided by Lubrizol as a reference. A TGA-2950 (TA Instruments) was used to conduct the thermogravimetric analysis of the candidate ILs at a 10°C/min heating rate in air.

Three base oils chosen for this study were PAG, oil-soluble PAG (OSP), and mineral blend oil. The PAG (UCONTM Lubricant 50-HB-170) and OSP (UCONTM Lubricant OSP-32) were provided by Dow Chemical Company. The viscosity values at 40°C of these two polar base oils measured on a PertroLab Minivis II viscometer were 33.0 cSt and 30.4 cSt, respectively. The mineral blend oil is mixed by Chevron Neutral Oil 100R and Chevron Neutral Oil 220R (Chevron Corporation) to reach the target viscosity (32.0 cSt) at 40°C based on the Refutas equation [8]. The solubility of ILs in base oils was determined by direct observation after centrifuge test at 13,000 rpm for 5 min.

Aquatic toxicity tests were conducted on selected ILs in the Aquatic Ecology Lab at ORNL. *Ceriodaphnia dubia* (Daphnia), a model organism as shown in Figure VII.3.1, was used in the toxicity tests due to its fast reproduction rate and high sensitivity to environment change. The laboratory-bred, less-than-24-hours-old Daphnia neonates were used in this test, which were all born within eight hours of each other. Acute and chronic toxicity tests were conducted with six PAG-based lubricants diluted to 0.001% (10 ppm) with dilute mineral water. The six lubricants are neat PAG base oil, PAG + 5 wt% ZDDP, PAG + 5 wt% [P8888][DEHP] (a previously developed IL for engine [6] and gear [4] lubrication), PAG + 5 wt% [N888H][DEHP] (another

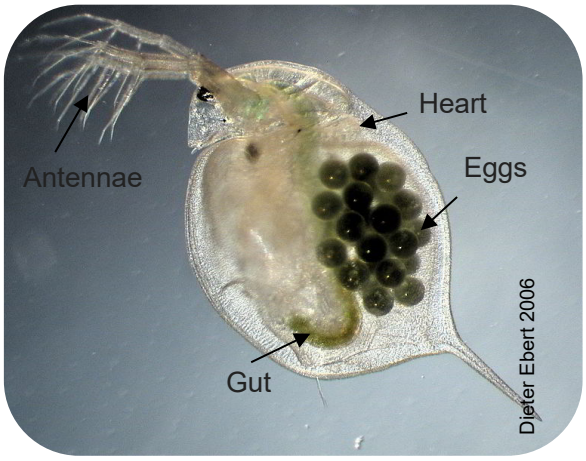

Figure VII.3.1 *Ceriodaphnia dubia* (Daphnia), a model organism in aquatic toxicity tests

previously developed IL [9]), PAG + 5 wt% IL-1 (a new candidate IL synthesized in this work), and PAG + 5 wt% IL-2 (another new candidate IL). The additive concentration in the diluted water solution was 0.5 ppm. The solution renewal period was 24 hours. The temperature for all tests was controlled at 25.0°C. In acute toxicity tests, four neonates were put in each chamber, and three replicates were performed per treatment. The five-day period tests used survival rate as the criterion to assess the toxicity. In chronic toxicity tests, each chamber contained one neonate, and ten replicates were performed per treatment. The toxicity is assessed with respect to the survival rate and reproduction rate in a seven-day period experiment.

Test lubricants were prepared by adding candidate ILs into the base oils at 0.5 wt%, and their tribological behavior was tested under boundary lubrication with a reciprocating ball-on-flat configuration on a Plint TE 77 tribometer. The flat was a M2 tool steel with a roughness of 60–70 nm. An AISI 52100 bearing steel ball (10 mm diameter) was used as the counterface, which has a roughness of 20–50 nm. Tests were performed with a constant load of 100 N, at an oscillation frequency of 10 Hz with a stroke of 10 mm, for 1,000 m of sliding at 180°F (82°C, a typical operation temperature of hydraulic fluids). The ratio of lubrication film thickness to the composite roughness, known as λ ratio, was calculated based on the Hamrock and Dowson formula [10] to be <1, ensuring boundary lubrication.

The friction force was measured in situ during the test, and the wear volume was measured using a three dimensional optical profilometer (Wyko NT9100). Wear scars were examined using scanning electron microscopy and energy-dispersive spectroscopy (EDS) on a JEOL 6500F scanning electron microscope equipped with an EDAX system. A Thermal Scientific K-Alpha XPS system was used to conduct the X-ray photoelectron spectroscopy (XPS) analysis. The depth profile measurements of the tribofilms were obtained by using an argon-ion sputter gun at 10.0 keV. Focused ion beam-aided cross-sectional scanning transmission electron microscopy nanostructural examination and EDS chemical analysis were conducted on selected tribofilms.

Toxicity Results

All candidate ILs are fully soluble in the two polar base oils, PAG and OSP. Some ILs have lower solubility (<1%) in the mineral oil blend. Thermogravimetric analysis results showed that all candidate ILs have decomposition temperatures above 120°C, and some are higher than 200°C.

Table VII.3.1 and Table VII.3.2 summarize the results of the acute and chronic toxicity tests. The water with the PAG base oil (without any additive) had a 100% survival rate in either the five-day acute or seven-day chronic toxicity tests. All Dephnia died by the end of the tests of the conventional ZDDP and previously developed ILs, [P8888][DEHP] and [N888H][DEHP], though [N888H][DEHP] seems slightly less toxic. In

contrast, the two new candidate ILs did not cause any death in either survival test. Table VII.3.2 presents the reproductions in the seven-day chronic toxicity test. The reproduction rate indicates the long-term effect on Daphnia neonates. In the water containing the neat PAG base oil, the neonates successfully reproduced and had a total of 428 offspring. When the conventional ZDDP or a previously developed IL, [P8888][DEHP] or [N888H][DEHP], was added, there was no reproduction at all. In contrast, neither of the new candidate ILs stopped or reduced the reproduction. Interestingly, the number of offspring slightly increased when they were introduced. Results clearly demonstrated that the newly developed candidate ILs are much more eco-friendly than the conventional ZDDP and previously developed ILs, which confirmed our development approach.

Table VII.3.1 Survivals of Daphnia in Acute Toxicity Test (5 Days)

Days	Neat PAG	IL-1	IL-2	[N888H][DEHP]	[P8888][DEHP]	ZDDP
1	12	12	12	12	12	12
2	12	12	12	12	0	0
3	12	12	12	2	0	0
4	12	12	12	1	0	0
5	12	12	12	0	0	0

Table VII.3.2 Reproductions of Daphnia in Chronic Toxicity Test (7 Days)

Days	Neat PAG	IL-1	IL-2	[N888H][DEHP]	[P8888][DEHP]	ZDDP
1	0	0	0	0	0	0
2	0	0	0	0	0	0
3	32	36	45	0	0	0
4	2	0	13	0	0	0
5	91	98	82	0	0	0
6	128	159	141	0	0	0
7	175	201	172	0	0	0
Grand total	428	494	453	0	0	0

Tribological Results

The friction and wear results for two new candidate eco-friendly ILs, IL-1 and IL-2, are compared to those of a conventional ZDDP and a previously developed IL, [N888H][DEHP], as shown in Figure VII.3.3. Both IL-1 and IL-2 significantly reduced both friction and wear in all three base oils, both polar and non-polar. Particularly, IL-1 provided 20%–30% friction reduction and 70%–90% wear reduction, in comparison with the conventional ZDDP.

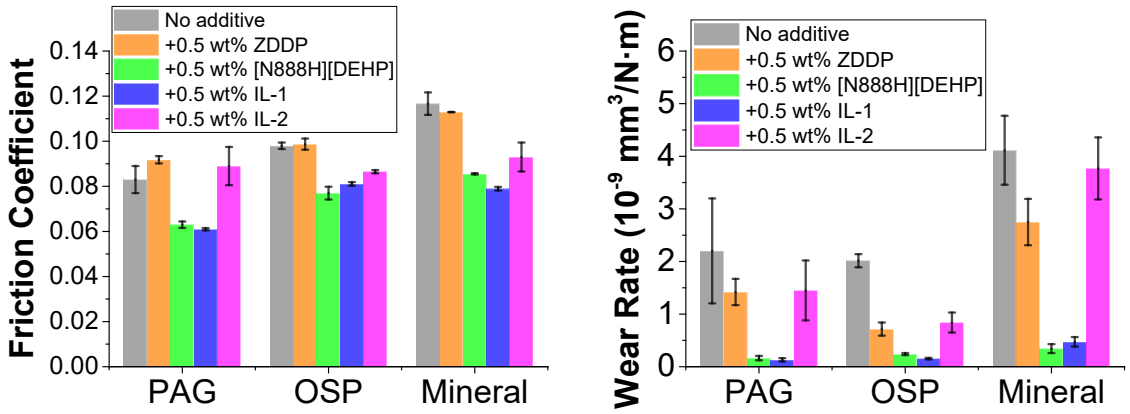

Figure VII.3.3 Comparison of steady-state friction coefficient and wear rate

Worn surface morphology examination and compositional analysis provided insights for the superior lubricating performance of the top-performing IL-1. Figure VII.3.2 (top) shows the scanning electron microscopy images and EDS spectra of the wear scars on the steel ball surfaces. The IL-1 produced smoother tribofilms in PAG and OSP than in the mineral oil blend. This correlates well with the trend of tribological behavior: PAG + 0.5% IL-1 and OSP + 0.5% IL-1 produced lower friction and wear than mineral oil + 0.5% IL-1. Figure VII.3.2 (bottom) shows the XPS composition-depth profiles, which clearly suggest a thinner tribofilm grown in a more polar base oil, due to higher competition against the polar base oil for surface adsorption. Lower wear in a polar base oil with IL is likely a combined protection from the polar base oil and IL. Focused ion beam-aided cross-sectional scanning transmission electron microscopy/EDS characterization results are shown in Figure VII.3.4. The thickness of the IL-1 tribofilm is around 20 nm in the PAG but 300 nm in the mineral blend. EDS elemental mapping indicates Fe, P, and O contents in the tribofilm, consistent with the top-surface EDS and XPS analyses in Figure VII.3.2.

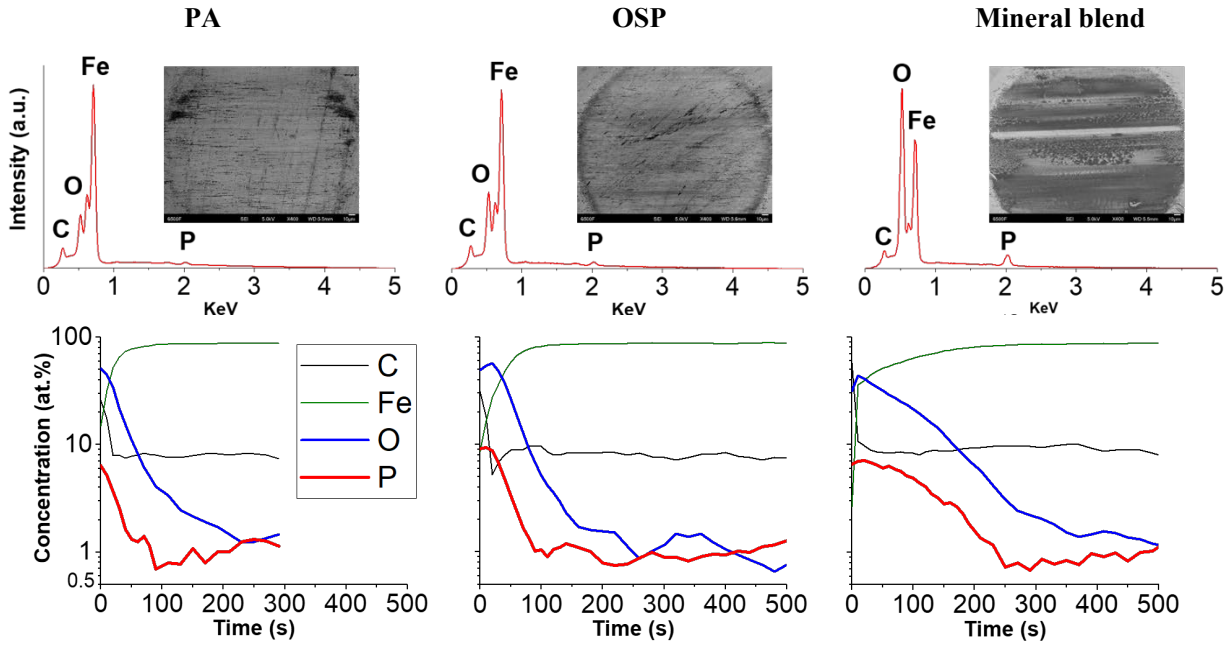

Figure VII.3.2 Morphology and composition of the worn surfaces produced by oils containing IL-1

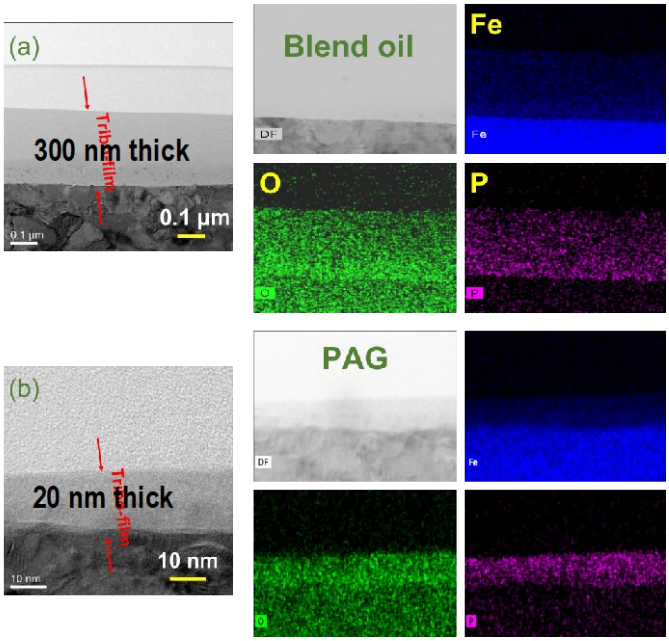

Figure VII.3.4 Cross-sectional scanning transmission electron microscopy images and EDS elemental maps of the IL-1 tribofilms on the steel ball surfaces

Conclusions

New eco-friendly ionic liquids have been developed as candidate EAL additives. Top-performing ionic liquids have demonstrated low/no toxicity and superior friction- and wear-reducing characteristics: (1) Daphnia survival rate increased from 0 to 100% and reproduction rate increased from 0 to >40 per week, and (2) friction was reduced by 20%–30% and wear was reduced by 80%–90% compared to ZDDP in boundary lubrication.

Key Publications

1. Qu, J., H. Luo, and X. He. 2019. "Eco-Friendly Ionic Liquids as Lubricant Additives." ORNL Invention Disclosure #201904491.

2. Duan, H., W. Li, C. Kumara, Y. Jin, H. Meyer, H. Luo, and J. Qu. 2019. "Ionic Liquids as Oil Additives for Lubricating Oxygen-Diffusion Case-Hardened Titanium." *Tribology International* 136: 342–348.

3. He, X., H. Luo, and J. Qu. 2019. "Ionic Liquid Additized Environmentally-Friendly Hydraulic Fluids." *74th STLE Annual Meeting & Exhibition*, Nashville, May 19–23.

References

1. Lynch, Lauren A., and Bradley T. Zigler. 2017. "Estimating Energy Consumption of Mobile Fluid Power in the United States." National Renewable Energy Laboratory.

2. R&D 100 Award, jointly among ORNL, General Motors, Shell, and Lubrizol. 2014. "Ionic Liquid Anti-Wear Additives for Fuel-Efficient Engine Lubricants." R&D Magazine.

3. Qu, J., and H. Luo. 2018. "Ionic Liquids Containing Symmetric Quaternary Phosphonium Cations and Phosphorus-Containing Anions, and Their Use as Lubricant Additives." U.S. Patent #9,957,460.

4. Stump, B.C., Y. Zhou, H. Luo, D.N. Leonard, M.B. Viola, and J. Qu. 2019. "A New Functionality of Ionic Liquids as Lubricant Additives: Mitigating Rolling Contact Fatigue." *ACS Applied Materials & Interfaces* 11: 30484–30492.

5. Qu, J., W.C. Barnhill, H. Luo, H.M. Meyer, D.N. Leonard, A.K. Landauer, B. Kheireddin, H. Gao, B.L. Papke, and S. Dai. 2015. "Synergistic Effects between Phosphonium-Alkylphosphate Ionic Liquids and ZDDP as Lubricant Additives." *Advanced Materials* 27: 4767–4774.

6. Qu, J., D.G. Bansal, B. Yu, J. Howe, H. Luo, S. Dai, H. Li, P.J. Blau, B.G. Bunting, G. Mordukhovich, and D.J. Smolenski. 2012. "Anti-Wear Performance and Mechanism of an Oil-Miscible Ionic Liquid as a Lubricant Additive." *ACS Applied Materials & Interfaces* 4: 997–1002.

7. Qu, J., H. Luo, and X. He. 2019. "Eco-Friendly Ionic Liquids as Lubricant Additives." ORNL Invention Disclosure #201904491.

8. Maples, R.E. 2000. *Petroleum Refinery Process Economics*. Pennwell Books.

9. Barnhill, W.C., H. Luo, H.M. Meyer, C. Ma, M. Chi, B.L. Papke, and J. Qu. 2016. "Tertiary and Quaternary Ammonium-Phosphate Ionic Liquids as Lubricant Additives." *Tribology Letters* 63: 22.

10. Hamrock, B.J., and D. Dowson. 1981. *Bearing Lubrication: The Elastohydrodynamics of Elliptical Contacts.* New York: A Wiley-Interscience Publication, John Wiley & Sons.

Acknowledgements

Co-authors: Xin He, Huimin Luo, Teresa J. Mathews, Harry M. Meyer III, and Chanaka Kumara, ORNL.

VII.4 High Performance Fluids and Coatings for Off-Road Hydraulic Components – Shear Stable Viscosity Index Improvers (Pacific Northwest National Laboratory)

Lelia Cosimbescu, Principal Investigator
Pacific Northwest National Laboratory (PNNL)
908 Battelle Blvd. MSIN K2-44
Richland, WA 99354
E-mail: lelia.cosimbescu@pnnl.gov

Michael Weismiller, DOE Technology Development Manager
U.S. Department of Energy
E-mail: Michael.Weismiller@ee.doe.gov

Start Date: May 1, 2018 End Date: May 31, 2020
Project Funding (FY19): $175,000 DOE share: $175,000 Non-DOE share: $0

Project Introduction

This multi-lab effort (Argonne National Laboratory [ANL], Oak Ridge National Laboratory, and PNNL) is responding to the DOE Vehicle Technologies Office Advanced Engine and Fuel Technologies Program's request for research on technologies to improve the energy efficiency of fluid power systems for off-road vehicles. The project focuses on low technology readiness level research to develop shear-stable high viscosity index (VI) hydraulic fluids and robust, wear-resistant material and coating processes to improve the efficiency, durability, and environmental compatibility of off-road hydraulic components. The project will identify fluids, additives, VI modifiers (VMs), and coatings with enhanced tribological properties that improve efficiency, productivity, and reliability. Barriers specifically related to fluids and materials that are addressed in the project include current fluids that do not have sufficient shear-stable high-VI (temperature–viscosity) properties to maintain volumetric and mechanical efficiencies during the oil's lifetime. The project takes advantage of diverse, complimentary capabilities at Argonne (simulation, characterization, coatings, and modeling), Oak Ridge (additives and characterization), and PNNL (base fluids, additives, and VMs) to perform low technology readiness level research on fluids and coatings that will improve hydraulic fluid system efficiency. Improvements in fuel consumption (5%–6%), and more importantly, productivity (15%), can be achieved with high-VI and shear-stable hydraulic fluids, which is the focus of this work.

Objectives

The research encompasses the development and evaluation of stable, energy-efficient fluids and additives that increase the efficiency and durability of components (pumps, valves, actuators, and motors) used in hydraulic fluid systems in off-road vehicles. Fluid activities address the development of shear-stable, high-VI, low-viscosity, multi-grade fluids and viscosity index improvers (VIIs) to reduce viscous losses, reduce fluid heating, and increase volumetric efficiency. In addition, additive activities address the development of compounds that reduce boundary friction losses and wear while increasing reliability, durability, and tolerance to contaminants (wear debris).

Overall Objective

The overall objective of this project is to demonstrate the feasibility of the approach and generate at least one VII candidate with superior performance versus the benchmark.

Fiscal Year 2019 Objectives

- Complete characterization of dendritic polymers for enhanced shear stability

- Evaluate the viscosity index and shear stability of these polymers
- Design and develop low molecular weight functional polymers for increased shear stability and reduced wear and friction
- Develop a fundamental understanding of the effects of polymer polarity on the friction and wear performance of a base oil.

Approach

Fluid power research was performed collaboratively at three national laboratories with industrial stakeholder input and feedback. Due to the complexity of the work proposed, and complementary approaches pursued by each laboratory, the work presented herein is focused on the development of VIIs, which impart durability and life to the hydraulic fluid and, in turn, efficiency to the system as a whole. Specifically, the design, synthesis, and rheological/tribological characterization of multifunctional VIIs as additives in hydraulic fluid are addressed here. Two separate strategies are described.

Task 1. A major consideration for VII design in applications that encounter shear is permanent shear loss of the polymer. The focus of this work was to investigate the effects of the chain composition and architecture on the shear stability of nearly dendritic polymers based on poly(dodecyl)methacrylates and poly(ethylhexyl)methacrylates containing 16, 32, and 64 arms, with and without caprolactone segments. In addition, the influence of topology and composition on viscosity index was studied due to its relevance in hydraulic fluid applications. Rheology and shear stability are important parameters in hydraulic fluid design and have a critical impact on its performance and durability. Multiple analogs with hyperbranched architectures were prepared via the core-first strategy from commercially available hydroxyl-terminated hyperbranched cores MPA_{16}, MPA_{32}, and MPA_{64}.

Task 2. Typically, efficient VIIs have a viscosity index above 200, even 250; however, they suffer from permanent viscosity losses under mechanical shear. In contrast, friction modifiers and anti-wear additives are small molecules that are resistant to mechanical cleavage. Hence, our approach was to target lower molecular weight (M_w) polymers around 150 kDa with modest VIs that would have an enhanced shear stability versus regular VIIs, while introducing polarity in the molecule for added benefits, such as friction or wear resistance. As such, homopolymers and co-polymers of one or two methacrylates were generated via controlled radical polymerizations.

Results

Fiscal Year 2019 Key Accomplishments

- Prepared a series of dendritic polymers that display good shear stabilities for their respective high Mw
- Demonstrated polymers' superior VI when a semi-crystalline segment is present (VI is 1.5x higher than benchmark)
- Demonstrated the efficient synthesis of polar co-polymers via controlled radical polymerization
- Achieved a multifunctional VII that displayed comparable shear losses to the benchmark, but 5–7 times greater anti-wear properties.

Task 1. It is well accepted that hyperbranched polymeric architectures enhance shear stability while having a minimal influence on the viscosity or thickening power. Viscosity measurements were performed on 2% (w/w) polymer solutions in a base oil composed of 70% 100R/30% 220R. To evaluate the thickening abilities and viscosity index of the polymer solutions, the dynamic viscosities of the samples were measured at 40ºC and 100°C. This effect is supported by the data, particularly for systems that do not possess a semi-crystalline segment, as in compounds P-7 through P-12. Regardless of the branching increasing from 16 to 64, the VIs are not increasing at all, particularly for dodecylmethacrylate (DMA) analogs, despite the substantial increase in

M_w. It appears that 2-ethylhexylmethacrylate (EHMA), the shorter chain monomer, may actually have a positive effect on VI. Only polymers P-2 and P-6 show a VI boost, bringing the VI up to 230. The pair of compounds that illustrates this effect best is P-2 and P-10; both polymers contain EHMA, both had similar conversions (95% and 93%, respectively), both had the same number of arms (32), yet their VIs are very different. The differing behavior of the EHMA and DMA can potentially be attributed to the branched structure of the EHMA, which prevents ordering of the alkyl side chains (as will be the case for DMA analogs) and potentially increases the polymer solubility. Ultimately, this would lead to more expanded polymer coils that are more efficient viscosity improvers simply because of their larger hydrodynamic volume. Table VII.4.1 includes the roughly normalized kinematic viscosities at 100°C (KV100) for the 2% (w/w) blends. The polymers whose kinematic viscosities were very high were adjusted to bring them within +/- 0.5 cSt at 100°C so the blends could be more accurately compared. The shear stability of the polymer-oil solutions was evaluated via KRL (a test method for determination of mechanical shear stability) at 100°C. Shear stability does not appear to be influenced by the M_w of the polymers (the expected M_w should be considered and not the values measured by size-exclusion chromatography). Even the high molecular weight analogs with 64 arms tend to have a lower viscosity loss than the linear benchmarks used for comparison (Benchmarks 2 and 3). Therefore, hyperbranching appears to offset M_w differences and is shown to increase shear stability for a given molecular weight. Note that the number of arms reported in the table is calculated via ^{1}H nuclear magnetic resonance and deviates from theoretical (16, 32, 64).

Table VII.4.1 Viscosity and Shear Stability Performance of Normalized Blends at KV100 of [additive]/[70% 100R/30% 220R] Benchmark

Polymer	KV100	# arms	Composition	VI	Viscosity loss (%)
P-1	6.83	11.3	MPA_{16}-CL-EHMA	172	26
P-2	7.02	25.6	MPA_{32}-CL-EHMA	180	26
P-3	6.95	54	MPA_{64}-CL-EHMA	173	22
P-4	6.81	11.3	MPA_{16}-CL-DMA	161	19.2
P-5	6.67	25.6	MPA_{32}-CL-DMA	162	15.4
P-6	6.29	54	MPA_{64}-CL-DMA	151	23.5
P-7	6.88	14.3	MPA_{16}-DMA	167	18.6
P-8	6.88	29	MPA_{32}-DMA	167	16.5
P-9	6.69	56	MPA_{64}-DMA	165	14.2
P-10	7.07	14.3	MPA_{16}-EHMA	174	23
P-11	7.14	29	MPA_{32}-EHMA	184	20
P-12	6.87	56	MPA_{64}-EHMA	172	16
Benchmark 1	5.64	–		160	2.5
Benchmark 2	13.40	linear	DMA	235	33
Benchmark 3	7.01	linear	PCL-DMA	219	17.5
Benchmark 4 (1.7%)	7.69	–	–	238	31

MPA_{16} – hyperbranched bis-MPA polyester-16-hydroxyl, generation 2;
bis-MPA – 2,2-Bis(hydroxymethyl)propionic acid;
MPA_{32} – hyperbranched bis-MPA polyester-32-hydroxyl, generation 3;
MPA_{64} – hyperbranched bis-MPA polyester-64-hydroxyl, generation 4;
CL – caprolactone; PCL – polycaprolactone

Task 2. Random copolymers having both polar and nonpolar functionality were also prepared via reversible addition−fragmentation chain-transfer polymerization and contained about 16% polar co-monomer based on feed ratio. DMA, the more lipophilic of the two non-polar monomers used, was efficient in providing required solubility of the resulting co-polymer in oil. EHMA, with a shorter chain-length, in contrast, provided oil-insoluble co-polymers; those compounds could not be fully evaluated and therefore are not reported here. The synthesis of the polar co-monomers and the co-monomers used for our study is shown in Figure VII.4.1.

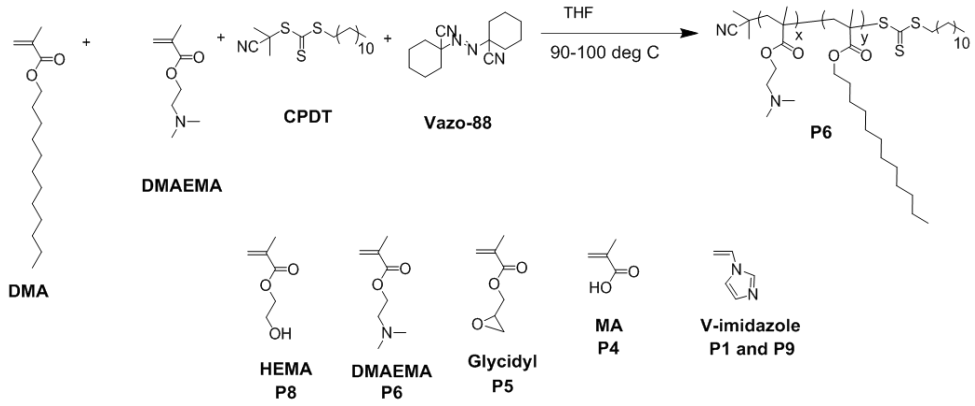

DMAEMA – 2-(dimethylamino)ethyl methacrylate;
CPDT – S-(2-cyanoprop-2-yl)-S-dodecyl trithiocarbonate; MA – methacrylic acid;
HEMA – hydroxyethyl methacrylate; THF – tetrahydrofuran

Figure VII.4.1 Synthesis of polar co-polymers as multi-functional viscosity index improvers

Viscosity measurements were performed on 2% (w/w) polymer solutions in a base oil composed of 70% 100R/30% 220R. To evaluate the thickening abilities and viscosity index of the polymer solutions, the dynamic viscosities of the samples were measured at 40°C and 100°C. The benchmark used is a commercial product of unknown concentration at a minimum concentration of 60% in a neutral base oil; this polymer was diluted to 2% with the above base oil assuming a concentration of 60% of the polymer. The samples were roughly normalized with respect to the KV100 value of the benchmark by further dilution with base oil. A list of all the normalized blends, their respective VIs, and viscosity losses under KRL can be found in Table VII.4.2. All blends have a higher VI than the base oil and comparable or higher VI than the benchmark.

Table VII.4.2 Viscosity and Shear Stability Performance of Normalized Blends at KV100 of [additive]/[70% 100R/30% 220R] Versus Benchmark

Polymer	KV100	M_w^{app} (kg/mol)	Composition	VI	Viscosity loss (%)
P1	6.00	45.6	Poly(DMA-co-Vimidazole)	162	4.9
P2	5.99	151	Poly(EHMA)	159	11.1
P3	5.96	126	Poly(DMA)	149	3.5
P4	5.52	137	Poly(DMA-co-MA)	144	2.5
P5	5.95	171	Poly(DMA-co-glycidyl)	160	6.8
P6	6.00	156	Poly(DMA-co-DMAEMA)	148	9.2
P7	5.95	150	Poly(DMA-co-boronate)	149	7.3
P8	5.75	124	Poly(DMA-co-HEMA)	167	4.4
P9	5.89	59.6	Poly(DMA-co-Vimidazole)	145	5.6
Base Oil	4.80			116	
Benchmark 1	5.64		unknown	147	2.5

P1 is different than P9; they have the same composition but have different M_w.

Since the focus of this work was to provide high shear stability, the modest VIs (~140–170) were expected. Despite their relatively low M_w, these polymers can be used at low concentrations from 2% (w/w) to 1.2% (w/w) and still maintain a moderate VI. The highlighted rows emphasize those analogs that have comparable shear stability to the benchmark; these are considered promising analogs for scale-up and further study.

The other research facet of this class of compounds is to evaluate their friction and wear and probe the hypothesis that they would provide surface protection benefits. Base oil solutions of all polymers, including Benchmark 1, were subjected to tribological measurements, conducted at Argonne by Dr. Erck. A modified Plint reciprocating tribometer (ball on flat geometry) was used to obtain friction measurements of the test oils. The test temperature was 100°C, and the test duration was 1 h. The data is illustrated in Figure VII.4.2.

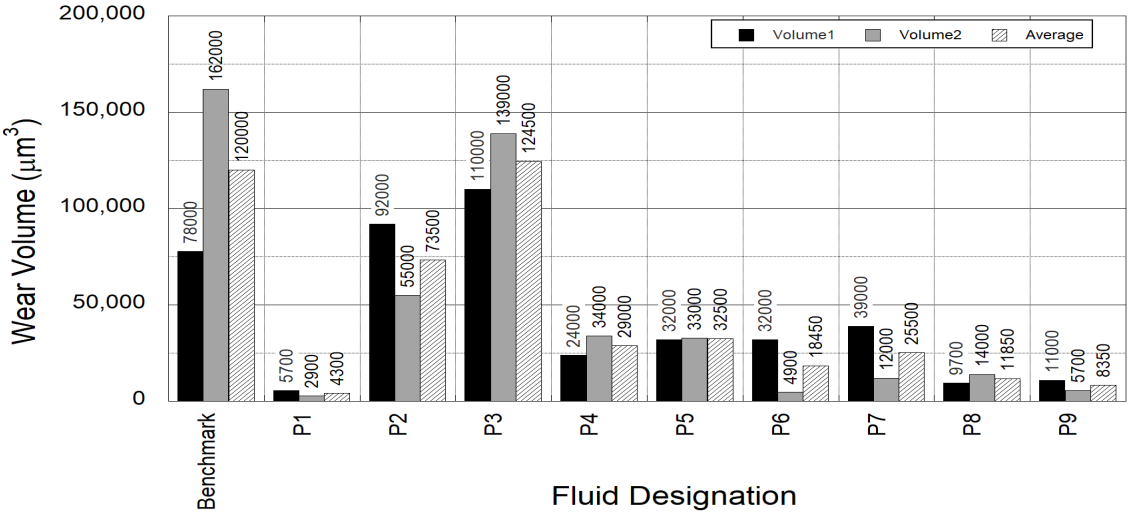

Figure VII.4.2 Wear volume averages for each co-polymer, homo-polymer, and benchmark. Averages are shown in gray.

All polar co-polymers performed better with respect to wear than the non-polar co-polymers as well as the benchmark. P3 and the benchmark had similar wear volume averages, while P2 had a lower wear volume. P2 was comprised of a shorter chain, a C6-ethyl (EHMA), compared to P3. A C12 is slightly less hydrophobic, which could explain the lower wear volume of P2, hence the better wear behavior. The most polar compounds, P1, P8, and P9, containing imidazole and alcohol pendants, have the lowest volume of wear. In addition, P1, P8, and P9 had the lowest M_w, which could further contribute to their wear reducing properties. Notably, the least amount of wear occurred in P1 at 4.3 x 10^3 µm. The data suggests that imidazole (P1 and P9), alcohol (P8), and amine (P6) may have the highest affinity for the metal surface.

Conclusions

Both strategies implemented for the VII development were successful in generating a fundamental understanding of structure-properties correlations. Furthermore, the low M_w analogs have shear stabilities comparable to the commercial benchmark but provide superior VIs and added anti-wear benefits.

Key Publications

1. Cosimbescu, L., D. Malhotra, K. Campbell, M. Swita. 2019. “Molecular Design Strategies to Achieve a Shear Stable Polymer.” 74th STLE Annual Meeting & Exhibition, Nashville, TN (May).

2. Cosimbescu, L, D. Malhotra, K. Campbell, M. Swita, and Z. Kennedy. 2019. “Molecular Design and Shear Stability Correlations of Dendritic Polymethacrylates.” *Molecular Systems Design & Engineering*. Accepted.

3. Cosimbescu, L. 2019. “Additives (VIIs) and Base Fluid Design for Enhanced Mechanical Efficiency of Hydraulic Fluids.” Center for Compact and Efficient Fluid Power, Madison, WI (October).

Acknowledgements

Many thanks go to contributors who made this work possible: K. Campbell (PNNL); D. Malhotra (PNNL); Robert Erck (ANL); G. Fenske (ANL); M. Swita (PNNL).

VII.5 Efficient, Compact, and Smooth Variable Propulsion Motor (University of Minnesota)

James D. Van de Ven, Principal Investigator
University of Minnesota
111 Church Street SE
Minneapolis, MN 55455
E-mail: Vandeven@umn.edu

Michael Weismiller, DOE Technology Development Manager
U.S. Department of Energy
E-mail: Michael.Weismiller@ee.doe.gov

Start Date: May 1, 2018 End Date: April 30, 2020
Project Funding (FY19): $479,777 DOE share: $398,691 Non-DOE share: $81,086

Project Introduction

In this project, a highly efficient hydraulic motor is being developed for the propulsion of off-highway vehicles. The motor uses an adjustable mechanism to vary the displacement of the pistons, resulting in a variable displacement linkage motor (VDLM). The VDLM uses rolling element bearings for low friction, which is especially important in the demanding low-speed, high-torque conditions experienced by off-highway vehicles. In addition to high mechanical efficiency, the volumetric efficiency of the VDLM is high due to a small unswept volume (reducing compressible energy loss) and low piston side-loading. These attributes result in a motor that exceeds 90% efficiency across a wide operating range. The VDLM has high torque capabilities for its size due to the radial piston packaging and use of a multi-lobe cam. A novel benefit of the VDLM is the ability to design the cam profile such that torque ripple through a revolution of the motor is minimized. Torque ripple at low speed is a critical metric for traction motors; poor performance in this area often requires oversizing the motor, resulting in decreased efficiency. The combination of high motor efficiency and expanded system flexibility through the motor variability enables a reduction in vehicle fuel consumption of 30%.

The first year of the project focused on developing mathematical models of the VDLM for the purpose of optimizing the motor parameters. The models developed captured the mechanism kinematics (motion), kinetics (forces due to motion), friction in all of the bearing types, fluid dynamics throughout the motor, and system dynamics of the motor operating in a vehicle through a drive cycle. These models were used in multi-objective optimization to maximize efficiency, minimize motor size, and minimize torque ripple. The parameters from the selected optimal solution were used in the detailed design of a single-cylinder prototype. This prototype will be fabricated and tested in the coming year with the purpose of validating the developed models. The validated models will then be used to design a multi-cylinder prototype in the final year of the project. The project team consists of the University of Minnesota, Milwaukee School of Engineering, Poclain Hydraulics, and Bobcat.

Objectives

Overall Objective

The objective of this project is to improve the efficiency of off-highway vehicles by developing an efficient, compact, and smooth variable displacement propulsion motor. The technology will be demonstrated with the design, construction, and testing of a single-cylinder prototype and a multi-cylinder concept demonstration prototype for the application of a compact track loader. Hardware-in-the-loop testing will be used to demonstrate the performance of the drive train when operating through a standard drive cycle. The performance targets for the motor are to demonstrate:

- A peak total efficiency of 93% and total efficiency >90% at displacements above 50%
- An improvement in vehicle efficiency of 30% through a compact track loader drive cycle
- A torque ripple less than 5% of the mean output torque at maximum displacement
- A power density of 5 kW/kg
- A cost of $4/kW for medium-volume production.

Fiscal Year 2019 Objectives

The objectives for Fiscal Year 2019 were to:

- Model the motion and forces in the adjustable cam-linkage mechanism that couples translation of the pistons to the rotation of the cam
- Quantify the energy losses of the motor, including joint friction, leakage, and valve throttling
- Optimize the motor parameters for the objectives of maximizing efficiency, minimizing size, and minimizing torque ripple
- Design a single-cylinder prototype of the motor for the purpose of experimentally validating the mathematical models.

Approach

The research approach to date has focused on constructing a dynamic model of the motor and designing and optimizing a single-cylinder prototype that will be used to validate the models. In the third budget period of the project, the validated models will be used to design a multi-cylinder prototype to demonstrate the performance targets.

The comprehensive dynamic model of the motor captures the kinematics, dynamic forces, bearing friction, and fluid dynamics. The submodels were combined into an automated design code that selects bearings to handle the joint forces, estimates link masses, and detects interference between components. The models were used in an optimization of the motor parameters with the objectives of maximizing efficiency, minimizing the size, and minimizing the torque ripple. The parameters of a motor selected from the Pareto optimal set were used in the detailed design of a single-cylinder motor. The model results from this motor were also used to simulate the operation of the variable displacement propulsion motor in both hydrostatic and series hybrid architectures of a compact track loader performing a standard skid steer loader drive cycle provided by our original equipment manufacturer industry partner Bobcat Doosan. A detailed business case was constructed for the VDLM through interviews with our industry partners to better align the technology with the market needs. Once the single-cylinder prototype is fabricated, it will be tested on the pump/motor dynamometer at Milwaukee School of Engineering in order to validate the models.

Results

The key accomplishments for Fiscal Year 2019 were the development of a comprehensive dynamic model of the VDLM, vehicle system simulations, preparation of a preliminary business plan, and detailed design of a single-cylinder VDLM prototype. Highlights of the results from each of these areas will now be presented.

The kinematics model of the VDLM mechanism, illustrated in Figure VII.5.1, generates the cam curve and linkage geometry for a set of geometric parameters. The kinematics model uses an inverse design approach to first specify the desired piston trajectory (which defines the motor torque ripple) with a sixth-order periodic B-spline and then solve for the resulting cam profile. To solve for the motion when the pump displacement changes, a new kinematic formulation was created that solves for the intersection of the cam profile and linkage coupler curve.

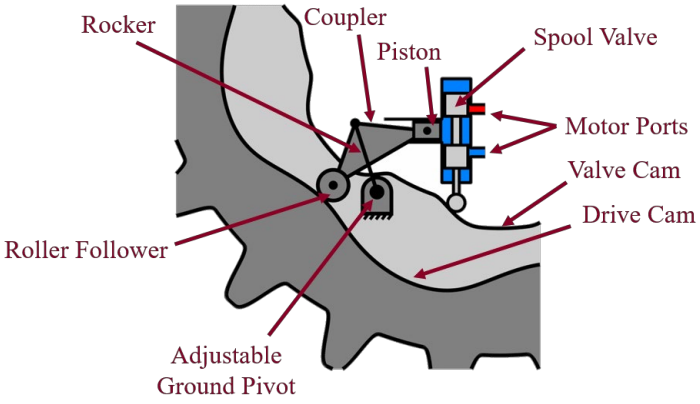

Figure VII.5.1 Diagram of the VDLM mechanism

The kinetics model, illustrated in Figure VII.5.2, is used to predict the joint forces and mechanical energy losses in the motor. First, a static analysis force analysis of the mechanism is performed based on the applied cylinder pressure. The model then selects bearings from a look-up table and sizes links for the applied loads. Finally, a dynamic force balance is performed that includes the friction force in all of the bearings. The bearing friction model uses the applied loads and velocities as inputs to predict the fluid film thicknesses in the bearings and the effective coefficient of friction. As the bearing force model is highly non-linear, iteration is needed in the dynamic force analysis to converge on joint forces and torques.

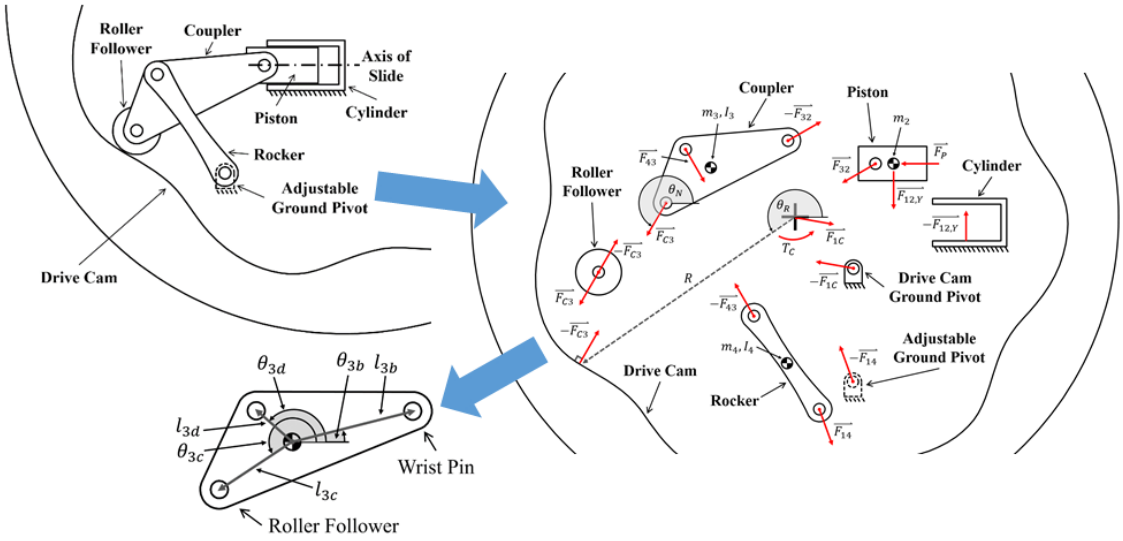

Figure VII.5.2 Overview diagram of the kinetics model used to predict the torques and forces at each joint

The fluid mechanics model predicts the flow rate through the valves and the pressure in the piston-cylinder. By exploring the influence of valve timing on the motor efficiency at varying operation conditions, it was determined that variable valve timing offered negligible efficiency improvement as long as the unswept volume in the cylinder was minimal. The fluid mechanics model was also used to evaluate hydraulic pilot versus mechanical valve actuation. The results of this study were that the motor efficiency with the hydraulically piloted valve decreased as the motor speed varied, while the efficiency with the mechanically actuated valve remained nearly constant. This drove the design decision to use a cam-driven spool valve for the prototype.

The models were used in a multi-objective optimization of the motor parameters, illustrated in the flowchart in Figure VII.5.3. An optimal solution with seven pistons and five cam lobes was selected. As predicted by the model, the select motor:

- Achieved a total efficiency of 97% for displacements above 15%, exceeding the target of over 90% efficiency
- Achieved a torque ripple at maximum displacement of 2.8%, exceeding the performance target of less than 5% ripple.

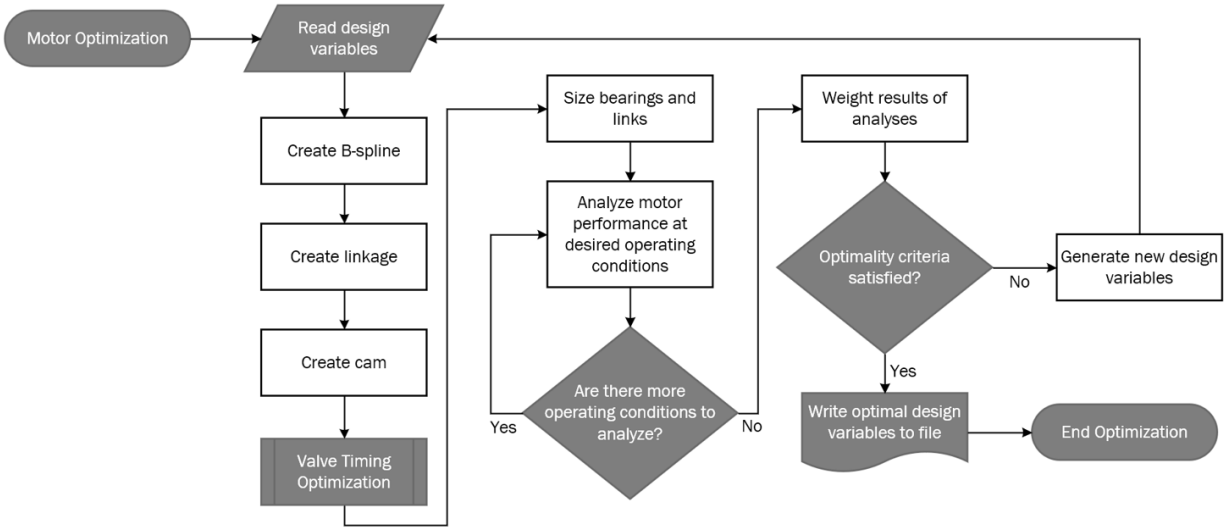

Figure VII.5.3 Flowchart of the optimization algorithm

From the optimal parameter set, the detailed design of a single-cylinder prototype was performed. Highlights of the design are bilateral symmetry of the linkage mechanism to avoid out-of-plane deflection, needle roller bearings in most of the joints, and a straddled bearing configuration for high moment capability. As the purpose of the prototype is model validation, the displacement will be manually varied through discrete points to ensure repeatable test results. Renderings of the linkage and full motor are presented in Figure VII.5.4.

A vehicle system simulation was constructed to evaluate the influence of the VDLM on vehicle performance. Models were constructed of the baseline vehicle with a hydrostatic transmission with variable pumps and fixed motors as well as a hydrostatic transmission that includes the VDLM. The baseline system sizing was based on the schematic of the Bobcat T770 compact track loader provided by the original equipment manufacturer partner Bobcat Doosan. Experimentally developed pump and motor models for existing components were provided by project partners Milwaukee School of Engineering and Poclain. The model has been simulated with a duty cycle provided by the original equipment manufacturer. The results of the simulation study are that including the variable motor allows the pump size to be dramatically reduced from the baseline size of

46 cc/rev to 25 cc/rev, saving cost and reducing pump energy losses by 10%. Furthermore, the results indicate that the minimum useful motor fractional displacement is 50%. These findings drove the team to revise the specification for the single-cylinder prototype.

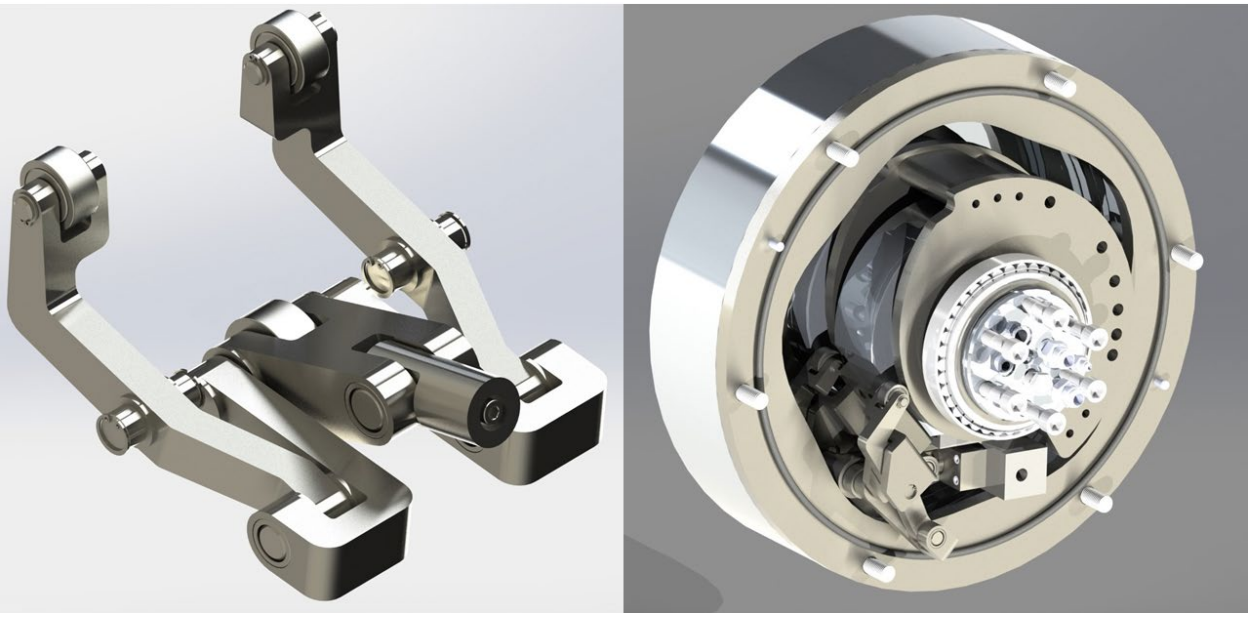

Figure VII.5.4 Rendering of the single-cylinder linkage and full motor assembly

Conclusions

In conclusion, during Fiscal Year 2019 the project team:

- Constructed a comprehensive dynamic model of the VDLM that predicts all major energy losses and the torque ripple
- Developed a novel kinematic model using an inverse cam design that prescribes the follower motion to generate the cam profile
- Developed a motor design code that constructs the motor geometry from a given set of parameters, sizes links and bearings for the applied loads, and detects interference between components
- Utilized a multi-objective genetic algorithm to explore the design trade-offs between motor efficiency, size, and torque ripple, resulting in a solution with over 97% efficiency across the displacement range and 2.8% torque ripple at maximum displacement
- Performed a detailed design of a single-cylinder prototype for the purpose of validating the mathematical models
- Constructed a vehicle system model to evaluate the benefits of utilizing a variable hydraulic motor, resulting in the ability to downsize the pump and significantly reduce fuel consumption
- Constructed a preliminary business plan.

Key Publications

1. Fulbright, Nathan, Grey Boyce-Erickson, Thomas R. Chase, Perry Y. Li, and James D. Van de Ven. 2019. “Automated Design and Analysis of a Variable Displacement Linkage Motor.” FPMC2019-1677. Paper presented at the ASME/Bath Symposium on Fluid Power and Motion Control, Sarasota, FL (October 7–9).

2. Boyce-Erickson, Grey, Nathan Fulbright, John Voth, Thomas R. Chase, Perry Y. Li, and James D. Van de Ven. 2019. “Mechanical and Hydraulic Actuation Strategies for Mainstage Spool Valves in Hydraulic Motors.” FPMC2019-1687. Paper presented at the ASME/Bath Symposium on Fluid Power and Motion Control, Sarasota, FL (October 7–9).

Acknowledgements

The U.S. Department of Energy Project Officer for this project is John Terneus and Contract Specialist is Jodi Collins. The co-Principal Investigators for the project are Dr. Perry Li (University of Minnesota), Dr. Thomas Chase (University of Minnesota), and Paul Michael (Milwaukee School of Engineering). The project manager is Michael Gust (University of Minnesota). Industry partners include Gilles Lemaire (Poclain), Clement Recoura (Poclain), Adam Frey (Poclain), Douglas Kallas (Bobcat), Eric Zabel (Bobcat), and Charles Young (Bobcat). Project consultants include Dr. Shawn Wilhelm and Marvin Flachenriem.

VII.6 Hybrid Hydraulic–Electric Architecture for Mobile Machines (University of Minnesota)

Perry Y. Li, Principal Investigator
University of Minnesota
111 Church Street SE
Minneapolis, MN 55455
E-mail: lixxx099@umn.edu

Michael Weismiller, DOE Technology Development Manager
U.S. Department of Energy
E-mail: Michael.Weismiller@ee.doe.gov

Start Date: September 1, 2018 End Date: August 31, 2021
Project Funding: $1,890,766 DOE share: $1,504,677 Non-DOE share: $386,089

Project Introduction

The majority of off-road mobile machines, such as excavators, wheel loaders, and agricultural combines, are powered using hydraulics. Hydraulics are used because of their ability to deliver high power using small components. They are typically an order of magnitude more powerful than electric machines of the same size. Nevertheless, conventional hydraulically driven machines are not efficient; the average efficiency from the engine output to the useful work is only 21% [1]. Some reasons for this low efficiency are the use of throttling valves that use flow resistance for control and the inability to capture and reuse energy from over-running loads. Yet mobile hydraulic machines consume an important portion (0.4%–1.3%) of the total energy consumed in the United States. Thus, improving energy efficiency of such machines is important.

Similar to the on-road automotive sector, there is also a trend for mobile hydraulic machines to be electrified in some way to take advantage of the potential benefits of better efficiency and faster and more precise control. A common approach is to control the work circuits (e.g., to control the arm of the wheel loader instead of using the propulsion function) using electric motors and drives via the electro–hydraulic actuators. This approach is quite feasible for lower-power machines, but for high-power machines, the cost, size, and weight of the electric motors, drives, and batteries can be prohibitive, as the electric components need to provide the full power required of the machine.

The project goal is to develop a methodology for improving the efficiency of high-power off-road mobile machines that takes advantage of electrification without the need for very high power or costly electric components. The general idea is to develop a system architecture that marries the comparative advantages of hydraulic actuation and electrical actuation. In particular, most of the power would be delivered by the power-dense hydraulic, which would then be modulated by small but highly controllable electrical actuation.

Objectives

Overall Objectives

- Develop an actuation system architecture that combines the benefits of hydraulic and electric actuations and that is applicable to a wide range of multi-degree-of-freedom mobile machines
- Develop a tightly integrated, efficient, powerful, and compact electric–hydraulic power conversion machine for use with the architecture

- Demonstrate that the proposed system architecture can achieve a target efficiency of greater than 65% in a typical off-road machine platform while maintaining or surpassing the control performance expected of current machines.

Fiscal Year 2019 Objectives

The overall objective of the first year is to establish the feasibility of the approach. Specific objectives are to:

- Evaluate the energy savings potential of the proposed system architecture for at least three select machine platforms, and demonstrate that the target efficiency of 65% or energy savings of at least 40% (compared to a baseline) can be achieved for at least one of these platforms
- Develop a control methodology suitable for the proposed system architecture, and validate it in simulation
- Select electric motor and hydraulic pump/motor topologies for tight integration that have the potential of achieving the target conversion efficiency of 85% and the gravimetric density of 5 kW/kg.

Approach

The proposed hybrid hydraulic–electric architecture (HHEA) is shown in Figure VII.6.1. It makes use of a set of common pressure rails at different pressure levels that serve all degrees of freedom of the system. Each degree of freedom is controlled by a hydraulic–electric control module (HECM) that combines hydraulic power from the common pressure rails and electric power from the electric direct current (DC) bus or battery. The HECM consists of a set of on/off valves that select which pressure rails to use for a given time and a tightly integrated electric motor and hydraulic pump/motor that serve to modulate the hydraulic power. This architecture does not use throttling for control, can regenerate energy from overrunning loads, and thus is potentially efficient. Moreover, electric components are needed only to modulate the total power for each degree of freedom; they do not need to be capable of very high power and thus are reasonably small and cost-effective.

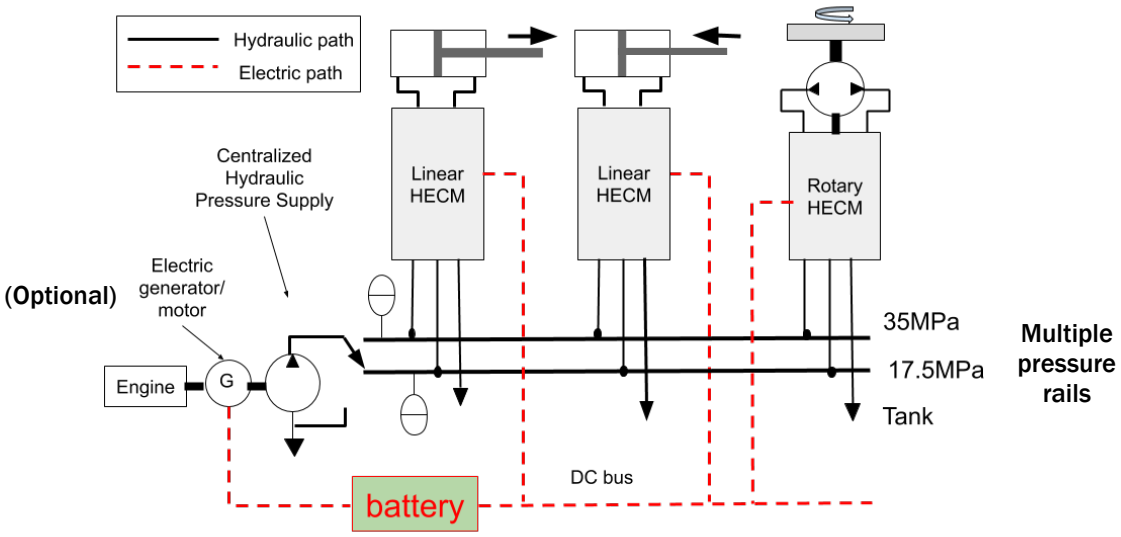

Figure VII.6.1 Hybrid hydraulic–electric architecture (HHEA)

The project researchers selected the platforms to evaluate in terms of energy savings potential based on the platforms' import for various sectors, whether the platforms were representative of other machines, and how much machine and duty cycle information was available for investigation. The research team consulted industry original equipment manufacturer (OEM) partners (CNH Industrial, JCB, and Toro) when selecting the various platforms. To evaluate the energy savings potential, researchers developed an algorithm that

determines the most efficient operating strategy for each design using a computationally efficient Lagrange multiplier optimization method. Static system models for the baseline load-sensing architecture and for the proposed HHEA were then developed for each selected platform. Energy savings potential was then evaluated for each selected platform using representative duty cycles provided by OEM partners.

Control algorithms were developed for two scenarios: (1) the short duration when the selected pressure rails are switching and (2) the times between those switches. The controller for the in-between-switching scenario was developed using a nonlinear, passivity-based backstepping approach [2] that has been shown to be robust and of high performance. The controller for pressure rail switching was designed to minimize the adverse effect on position and velocity tracking error of the actuator due to the near-instantaneous pressure changes with the assumption that the electric motor torque has physical limitations.

The topologies for the electric motor and the hydraulic pump/motor to be tightly integrated within the HECM were selected by modeling, exploring the design space, and analyzing the various electric linear and rotary motor and hydraulic pump/motor design principles. Attributes such as rotor inertia, power density, and energy efficiencies were considered in the selection process. The project team selected the topologies that most likely satisfy or exceed the target performance merits.

Results

Energy savings potential: Three machine platforms were analyzed in Fiscal Year 2019: a wheel loader, a 5-ton mini-excavator, and a 22-ton medium-sized excavator. These machines are representative of equipment used in construction and agriculture. OEM partners provided drive cycles for analysis. Energy consumption was analyzed for the baseline load-sensing architecture and for the proposed HHEA. For fair comparison, the same pump/motor efficiency map, taken from the literature, is assumed for both the load-sensing and HHEA systems after appropriate displacement scalings. The results for the three platforms are shown in Table VII.6.1, Table VII.6.2, and Table VII.6.3. Here, efficiency is defined as the ratio of positive output work to input energy, which can be greater than 100% when regenerative energy is used effectively (such as in the HHEA case). Table VII.6.1–Table VII.6.3 show that, for all three platforms that have been analyzed, the proposed HHEA has the potential of reducing energy consumption by over 60% compared to the baseline. In all but one duty cycle, efficiencies exceed the target of 65%. With most cycles, efficiency as defined here even approaches or exceeds 100%.

Table VII.6.1 Efficiency and Energy Input for the Wheel-Loader

	Cycle 1: Efficiency/energy input	Cycle 2: Efficiency/energy input
Load sense (baseline)	41.3%/19.9 MJ	47.6%/24.0 MJ
HHEA	107.2%/7.7 MJ	96.2%/11.9 MJ

Table VII.6.2 Efficiency and Energy Input for the Mini-Excavator

	Cycle 1: Efficiency/energy input	Cycle 2: Efficiency/energy input	Cycle 3: Efficiency/energy input
Load sense (baseline)	29.7%/1.64 MJ	19.5%/1.94 MJ	31.4%/1.39 MJ
HHEA	101.8%/0.48 MJ	58.5%/0.65 MJ	86.1%/0.51 MJ

Table VII.6.3 Efficiency and Energy Input for the 22-Ton Excavator

	Cycle 1: Efficiency/energy input	Cycle 2: Efficiency/energy input	Cycle 3: Efficiency/energy input
Load sense (baseline)	38.3%/14.2 MJ	22.7%/12.5 MJ	35.1%/13.1 MJ
HHEA	121.4%/4.48 MJ	103.2%/2.75 MJ	103%/4.46 MJ

- **Electrical component downsizing:** It was found that the required sizes of the electrical components can be significantly reduced compared to using a direct electro–hydraulic actuator approach, with more and more common pressure rails. For example, for the 22-ton excavator application, a direct electro–hydraulic actuator approach for electrification would require electric motors and drives capable of ~100 kW corner power (product of maximum torque capability and maximum speed). Using the HHEA and four common pressure rails, the corner power requirements are reduced to the 20–30 kW range.
- **Control algorithm:** A control algorithm was designed using the backstepping principle. In the absence of pressure rail switching events, the controller is able to track a desired trajectory accurately. In the presence of pressure rail switching, and when the electric motor torque capability is limited, position error of as much as 7 mm is incurred when the backstepping controller is used without modification. By applying the controller designed to mitigate the adverse effect of pressure rail switching, the position error is reduced to 0.5 mm, which is deemed acceptable.
- **Selection of integration topologies:**
    - Various hydraulic pump/motor topologies, including internal gear, external gear, gerotor, axial piston, and radial piston, have been compared for their appropriateness for the proposed HHEA. It was found that the radial ball piston topology is the most appropriate given its potential for high efficiency (especially at relatively low differential pressure), high operating speed, and compact packaging.
    - Various electric motor topologies, linear and rotary configurations, and radial and axial flux configurations have been compared for their appropriateness for the proposed HHEA. It was found that rotary configurations have much higher power density than linear configurations and that an axial flux configuration offers more compatible integration with the radial ball piston pump/motor and has lower rotor inertia, which is advantageous for fast control performance.
    - A conceptual topology of an axial flux rotary electric machine integrated with a radial ball piston has therefore been created, as shown in Figure VII.6.2.
    - The axial flux electric machine has been modeled and analyzed using finite element analysis. The design space has been explored. Through multi-objective optimization using a genetic algorithm, the Pareto optimal front mapping the design parameters to motor performance has been determined. Figure VII.6.3 is an example showing the tradeoff between motor efficiency and power density. In particular, a sample design for a 20 kW electric motor with an efficiency of 91.85% and a weight of 1.65 kg has been shown to be feasible.
    - A dynamic model of the radial ball piston hydraulic pump/motor has also been developed to determine how various parameters are mapped to efficiency, power density, and torque and flow ripples. Using the dynamic model, the researchers explored the design space and performed a preliminary multi-objective optimization to maximize power density and efficiency. In particular,

a sample design for a 20 kW hydraulic pump/motor operating at 15,000 rpm with an efficiency of 94.16% and with a weight of 1.01 kg has been shown to be feasible.

- Analysis of the efficiency and power density of the combination of the sample electric motor design and the sample hydraulic pump/motor design, accounting for the weight of compatible power electronics, shows that the target efficiency of 85% and power density of 5 kW/kg are indeed feasible.

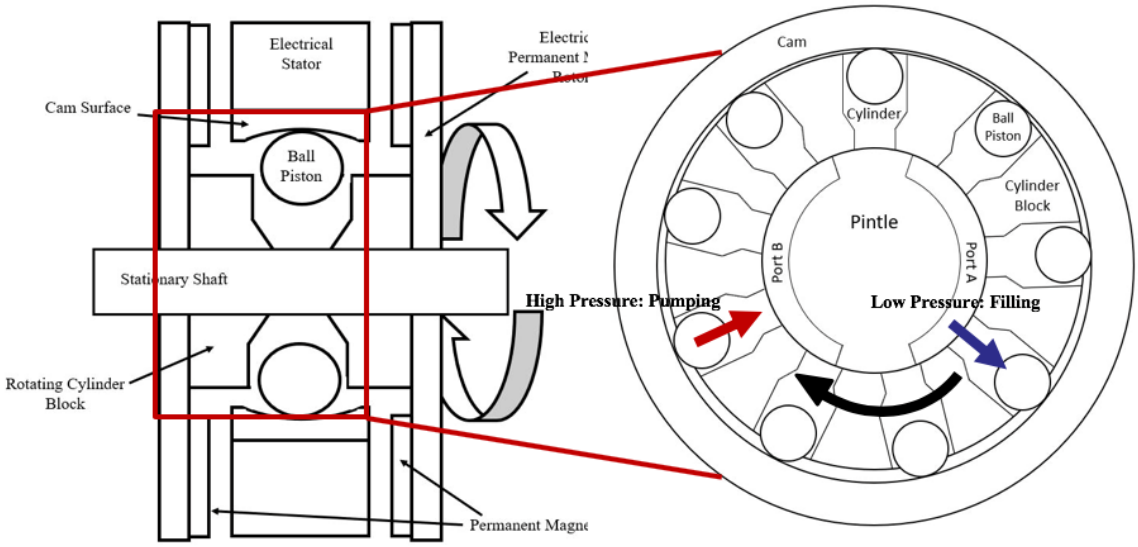

Figure VII.6.2 An axial flux electric motor integrated with a radial ball piston pump/motor

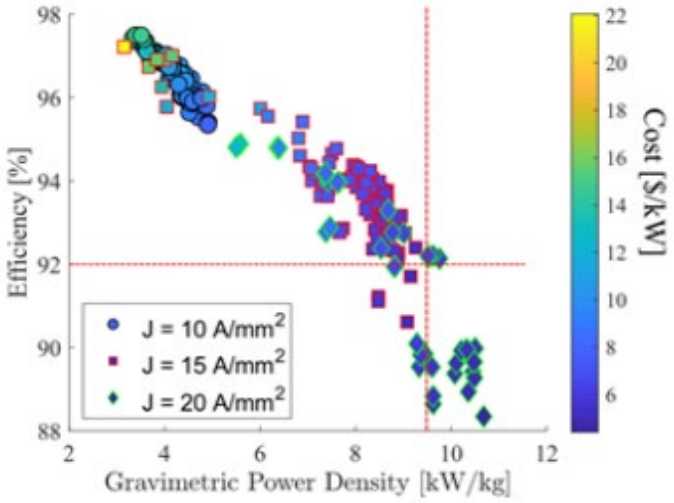

Figure VII.6.3 Sample efficiency–power density trade-off for an axial flux electric machine

Conclusions

In its first year, this project established the feasibility of the proposed HHEA to significantly improve efficiency for off-road mobile machines. For all three representative machine platforms, the proposed system architecture can increase efficiency by approximately three times, meeting the project target. A control

algorithm has been developed that provides good position tracking despite switching in the pressure rails. A concept of tightly integrating an axial flux rotary electric motor with a radial ball piston pump/motor has been developed for use with the proposed system architecture. Preliminary analysis shows that this combination offers designs that can meet the desired efficiency and power density.

Key Publications

1. Li, Perry Y., Jacob Siefert, and David Bigelow. 2019. “Hybrid Hydraulic-Electric Architecture for Mobile Machines.” 2019 ASME/Bath Symposium on Fluid Power and Motion Control, Sarasota, FL (October 7–9).

2. Bohach, Garret, Nishanth, Eric Severson, and James Van de Ven. 2019. “Modeling and Optimization Study of a Tightly Integrated Rotary Electric Motor-Hydraulic Pump.” 2019 ASME/Bath Symposium on Fluid Power and Motion Control, Sarasota, FL (October 7–9).

3. Nishanth, Garrett Bohach, James Van de Ven, and Eric Severson. 2019. “Design of a Highly Integrated Electric-Hydraulic Machine for Electrifying Off-Highway Vehicles.” IEEE Energy Conversion Congress and Exposition (ECCE-2019), Baltimore, MD (September 29–October 3).

4. Li, Perry Y. 2019. “Hybrid Hydraulic-Electric Actuation Architecture Hybrid.” U.S. Provisional Patent, Serial No. 62/801,137, filed on February 5, 2019.

References

1. Love, Lonnie, Eric Lanke, and Pete Alles. 2012. “Estimating the Impact (Energy, Emissions and Economics) of the US Fluid Power Industry.” Oak Ridge National Laboratory, Oak Ridge, TN. Love,

2. Li, Perry Y., and Meng Rachel Wang. 2013. “Natural Storage Function for Passivity-Based Trajectory Control of Hydraulic Actuators.” IEEE/ASME Transactions on Mechatronics 19 (3): 1057–1068.

VII.7 Individual Electro-Hydraulic Drives for Off-Road Vehicles (Purdue University)

Andrea Vacca, Principal Investigator
Purdue University
Maha Fluid Power Research Center
1500 Kepner Drive
Lafayette, IN 47905
E-mail: avacca@purdue.edu

Michael Weismiller, DOE Technology Development Manager
U.S. Department of Energy
E-mail: Michael.Weismiller@ee.doe.gov

Start Date: May 1, 2018 End Date: August 31, 2020
Project Funding (FY19): $646,095 DOE share: $498,445 Non-DOE share: $147,650

Project Introduction

Energy consumed by off-road vehicles represents about 8% of the total energy consumption in the U.S. transportation sector [1]. Typically, these vehicles heavily rely on fluid power (FP) technology for both the propulsion and the main actuation systems. Despite the low cost and favorable power-to-weight ratio of FP, the energy efficiency of these drive systems is very low, usually in the order of 20% [2].

The goal of this project is to introduce a new electro-hydraulic (EH) technology that drastically changes the current design approach of FP systems for off-road machines. This novel technology is based on a radical vehicle electrification, and it introduces a novel EH hybrid solution that benefits from both electric (ease of control) and FP (high power density) technologies.

Off-road vehicle FP systems typically use a centralized architecture, which implies design complexity and, most importantly, significant energy loss due to throttling of the fluid supplied to the different hydraulic functions. Instead, the proposed technology pushes a more elegant concept based on hydraulic individualization, which eliminates power losses due to load interference between different functions. The electrification of the hydraulic functions also allows recovery of the energy consumed during overrunning load conditions (for example, a lowering of the boom). Such energy is normally dissipated in current state-of-the-art technology.

The proposed layout architecture is based on new flexible and modular electro-hydraulic actuators (EHAs), which minimize the cost of the hydraulic components. In this way, the extra cost of the electric components relative to the state-of-the-art solution can be compensated by a (potentially) lower cost of the hydraulic components, and, most importantly, by a much higher fuel economy.

The use of an EHA enables utilizing an electrical distribution system with battery energy storage. Therefore, compared with current state-of-art solutions, the proposed system can:

- Lower power consumption of the hydraulic system up to 70% by eliminating most energy losses resulting from fluid throttling and by employing energy recuperation strategies
- Reduce the design complexity of mobile FP systems by proposing designs of independent EH modules that are scalable to the power level of each application
- Allow for a zero-emission mode for hydraulic functions

- Enable smart connectivity among hydraulic functions with independent EH modules
- Reduce chances of oil leakage by utilizing sealed, electrically connected EH units instead of fluid pipes
- Reduce vibration and noise by replacing a large central pump with smaller and quieter EH units.

The project team is composed of Purdue University (Dr. Vacca and Dr. Sudhoff), a fluid power manufacturer (Bosch-Rexroth, Dr. Uwe Neumann), and an off-road vehicle original equipment manufacturer (Case New Holland, Gary Kassen).

Objectives

In order to develop and demonstrate the proposed individualized EH technology applied to off-road vehicles, efforts are conducted on the following project objectives, with an approach that includes simulations, fabrication of prototypes, and experimentation.

Overall Objectives

- Objective 1 (O1). Four-quadrant EH hydraulic unit. O1 addresses the core element of the system, the main energy conversion unit (electric-hydraulic) capable of working in multiple quadrants of operation.
- Objective 2 (O2). Individualized EH system. O2 identifies and develops the layout and control architecture for the usage of the EH unit to realize an individualized hydraulic drive.
- Objective 3 (O3). Technology demonstration. O3 is aimed at demonstrating the proposed technology on an actual off-road vehicle application.

Fiscal Year 2019 Objectives

- Design the four-quadrant hydraulic unit, including both the hydraulic machine and the electric machine (O1)
- Evaluate the performance of the EH unit in simulation (O1)
- Define the layout architecture of the complete EH module that utilizes the four-quadrant EH unit; the circuit should allow throttleless regulation as well as energy recuperation (O2)
- Define the methods for energy recuperation, involving the use of hydraulic accumulators as well as electric generators (O2)
- Define a reference vehicle as well as the hydraulic functions to be considered as the baseline for the project (O3)
- Determine the energy consumption of the hydraulic system of the reference vehicle as a baseline against which to evaluate the relative performance of the proposed solution (O3)
- Define the electric system suitable for a hybrid architecture that uses the EH modules. (O3)

Approach

Activities in Fiscal Year 2019 included simulations aimed at design considerations for O1 and O2, while experimentation was already performed on the reference vehicle as pertains to O3. Activities were performed at the Maha Fluid Power Research Center of Purdue University (design of the hydraulic machine, hydraulic system layout, tests on the reference vehicle) and at the Grainger Labs of Purdue University (design of the electric machine and of the electric system), with close collaboration of the industry partners Case New

Holland (support on the reference vehicle tests and duty cycle definition) and Bosch Rexroth (support on both the hydraulic and the electric machine design).

As pertains to both the hydraulic machine and the electric machine that compose the four-quadrant EH unit (O1), a complex numerical optimization procedure was formulated and implemented during Fiscal Year 2019. The procedure involves the main fluid dynamic aspects and the micro-motions of the mechanical parts for the hydraulic unit, as well as winding configuration, motor shell mass, motor rotor geometry, cogging torque, and motor design map for the electric machine. The overall optimum Pareto front was used for the unit to be prototyped in the following Budget Period 2. For the electric motor design, a power electronic inverter was also designed, built, and tested to convert direct current into alternating current for the electric machine.

The layout for the individualized hydraulic drive system was analyzed through a lumped parameter simulation approach able to capture the main dynamic features of the actuation system as well as the energy flow in the reference vehicle (O2). The most energy-efficient drive solution was selected for further prototyping in Budget Period 2.

Regarding O3, a reference off-road vehicle was selected based on the following criteria: (i) manufacturing in United States, (ii) suitability for lab tests in a university environment, and (iii) typically low energy efficiency of the state-of-the-art hydraulic system. The selected vehicle was then instrumented and tested for generating baseline measurements of energy consumption. Experimental results served also to validate the lumped parameter model.

Results

During Fiscal Year 2019, the project accomplished significant results towards achieving the overall project objectives. The following list outlines the main results according to each project objective (O1, O2, O3).

- O1. An optimization procedure was successfully developed for designing a four-quadrant EH unit that combines an external gear pump and a permanent magnet electric motor for a power lever of about 15 kW. At the expected point of operation (representative of actuator lifting/lowering in the reference machine), the overall energy efficiency is above 80%, as shown in Figure VII.7.1. The hydraulic machine is an external gear pump/motor. The electric machine is a permanent motor design focusing on minimizing cogging torque and refining the machine's back electromagnetic frequency waveform. The geometry of the electric machine is depicted in Figure VII.7.2.

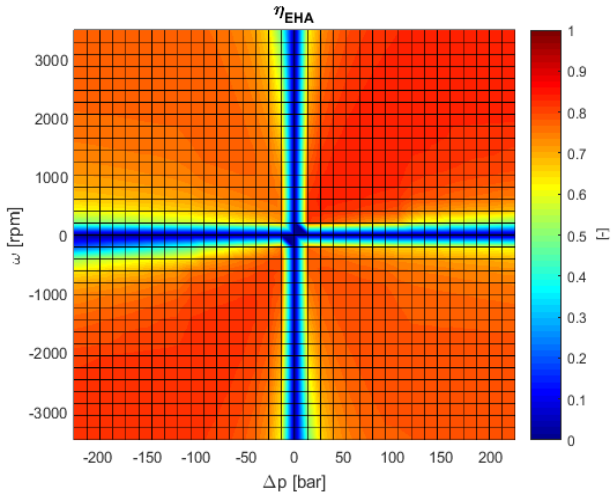

Figure VII.7.1 Efficiency of the combined electric machine and hydraulic machine in the four quadrants

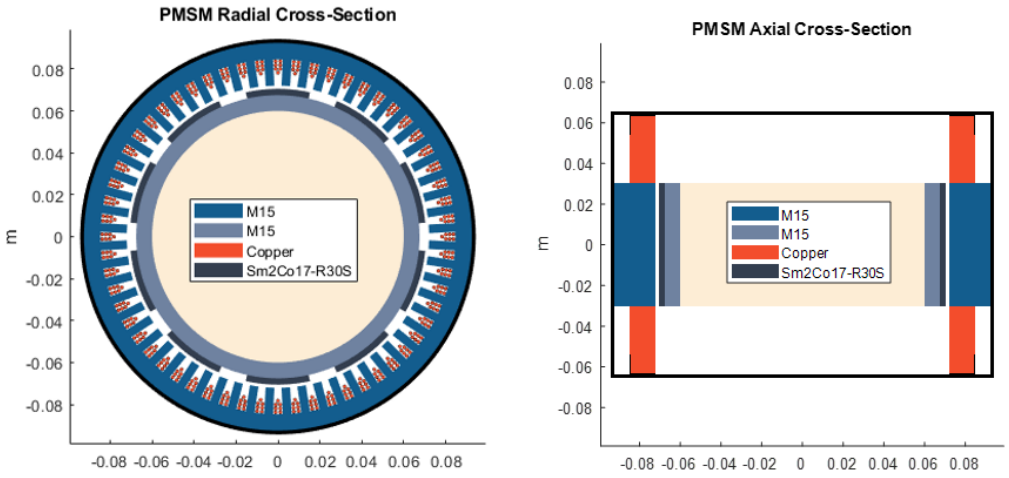

PMSM – permanent magnet synchronous motor

Figure VII.7.2 Design parameters and materials for the electric machine

- O1. A prototype suitable for EHA implementation on the reference off-road vehicle was formulated and proposed for testing in Budget Period 2. The design is shown in Figure VII.7.3.

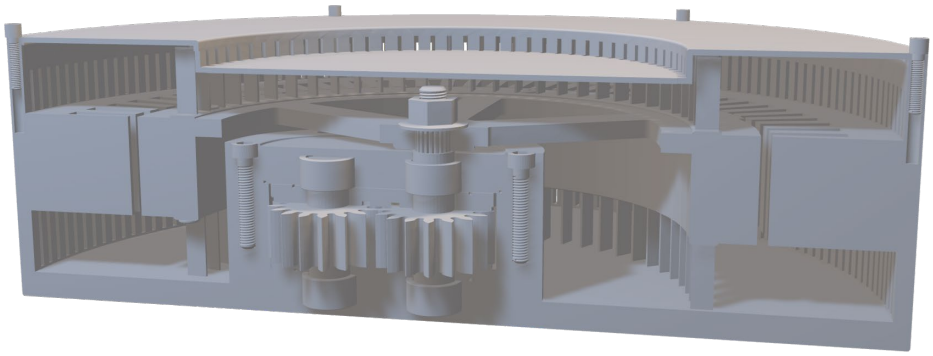

Figure VII.7.3 Computer-aided design image of the integrated external gear machine and electric machine (1st generation prototype)

- O2. Two hydraulic circuit layouts were proposed for the EH unit suitable for the hydraulic drive according to the principle of individualization. Both systems have the capability of energy recuperation during overrunning loads and allow for fine regulation of actuator velocity by using a fixed displacement hydraulic machine. The two layouts are proposed in Figure VII.7.4.

- O2. The energy efficiency of the complete EH module of Figure VII.7.4 using the EH unit of Figure VII.7.3 was estimated based on a lumped parameter model, which was validated by tests performed on the reference machine. On a significant digging cycle suggested by Case New Holland, the energy savings with respect to the baseline hydraulic system were quantified to be up to 75%, as shown in Figure VII.7.5.

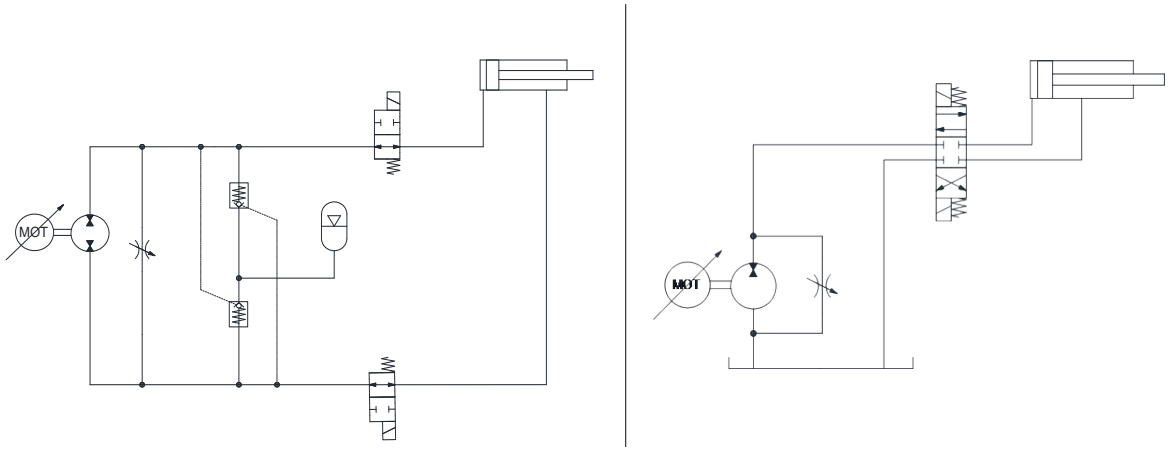

Figure VII.7.4 Proposed layouts for the EH system: closed center with accumulator (left); open center (right)

- O3. A 90 kW skid steer produced by Case New Holland (model TV380, see detail of Figure VII.7.5) was selected as the baseline vehicle. The vehicle was delivered to Purdue and fully instrumented to allow detailed measurements on the hydraulic control system. A simulation model created in Siemens.PLM.Amesim environment was validated based on experiments. The simulation model allowed estimation of the energy savings shown in Figure VII.7.5.

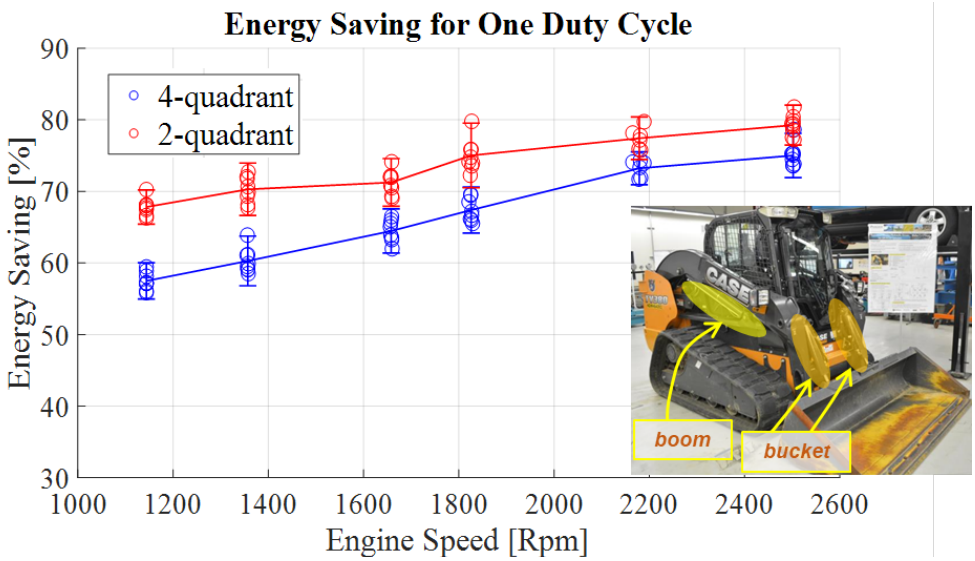

Figure VII.7.5 Estimated energy savings compared to the baseline hydraulic systems for the two proposed architectures

Conclusions

- A technology based on individual hydraulic supplies based on EHA was proposed. The technology promotes machine electrification, and in Fiscal Year 2019, it was found that the technology can save up to 75% of the energy in the actuation of the boom and bucket of a reference compact wheel loader.

- The project formulated a design of a combined electric and hydraulic machine suitable for 15 kW actuation. The overall efficiency of the machine is above 80% in the range of typical application.

- The presented results are based on measurements on an off-road vehicle instrumented during the project. The vehicle allowed validating the simulation model over the typical duty cycles of typical machine operation.

- The proposed system is suitable for an electric hybridization of off-road vehicles, and it is scalable to different power sizes. It allows for improved fuel economy, but it also has potential for additional features such as zero-emission mode of operation, improved controllability, and integrated diagnostic.

Key Publication

1. Ransegnola, Thomas, X. Zhao, and A. Vacca. 2019. "A Comparison of Helical and Spur External Gear Machines for Fluid Power Applications: Design and Optimization." *Mechanism and Machine Theory* 142: 103604.

References

1. Davis, S.C., S.E. Williams, and R.G. Boundy. 2017. *Transportation Energy Data Book: Edition 36*. Oak Ridge, TN: Oak Ridge National Laboratory.

2. Love, L.J., E. Lanke, and P. Alles. 2012. "Estimating the Impact (Energy, Emissions and Economics) of the US Fluid Power Industry." Oak Ridge National Laboratory. doi:10.2172/1061537.

Acknowledgements

The team would like to acknowledge John R. Terneus at National Energy Technology Laboratory and Michael R. Weismiller at the Vehicle Technologies Office of DOE for the technical feedback provided during the project.

(This page intentionally left blank)

U.S. DEPARTMENT OF
ENERGY

Office of
ENERGY EFFICIENCY &
RENEWABLE ENERGY

For more information, visit:
energy.gov/vehicles

DOE/EE-1992 • May 2020